A Thesis submitted for the degree of Doctor of Philosophy

The Application of Surface Effect Ships to Freight Transport

P.J. Minty

April 29, 2020

Department of Mechanical Engineering
The University of Melbourne

Contents

Acknowledgements xix

Abstract xx

1. Introduction 1
1.1. Motivation . . . 1
1.2. Research aims . . . 1
1.3. Thesis structure . . . 1

2. A practical application for Surface Effect Ships 4
2.1. Introduction . . . 4
2.2. Description of Surface Effect Ships . . . 4
2.3. Characteristics of environments that suit AMVs . . . 8
2.4. Southeast Asia natural environment . . . 11
2.5. Maritime freight in Southeast Asia . . . 16
2.6. Applications for Advanced Marine Vehicles . . . 17
2.7. Pugh Selection . . . 21
2.7.1. Background . . . 22
2.7.2. Surface Effect Ships . . . 27
2.7.3. Catamarans . . . 28
2.7.4. SWATH . . . 31
2.7.5. Trimarans . . . 32
2.7.6. Hydrofoils . . . 34
2.7.7. Selection analysis . . . 36
2.8. Concluding remarks . . . 37

3. Systematic identification of Surface Effect Ship research questions 38
3.1. Introduction . . . 38
3.2. The Surface Effect Ship characteristics . . . 39
3.3. Resistance . . . 44
3.4. Sea-keeping . . . 44
3.5. Parameters for Conceptual Design Tools . . . 45
3.6. House of Quality . . . 49
3.7. Failure Mode Effect Analysis . . . 52
3.8. Fault Tree Analysis . . . 52
3.9. Concluding remarks . . . 58

4. Dynamic Motions of Surface Effect Ships 59
4.1. Introduction . . . 59
4.2. Overview of the literature on SES dynamics . . . 60
4.3. Empirical observations of ship motions on SESs . . . 61

4.4. Analysis of SES air cushion pressure . . . 65
4.4.1. The Reynolds model assuming incompressible air flow . . . 65
4.4.2. Compressible Air Flow . . . 66
4.5. Other aspects of SES dynamics . . . 70
4.5.1. Rigid body mechanics . . . 70
4.5.2. Air supply to the cushion . . . 73
4.5.3. Air flows exiting the cushion . . . 75
4.5.4. Air Cushion Boundary Conditions . . . 76
4.5.5. Hydrostatic and Hydrodynamic Forces . . . 77
4.6. Design of practical automatic feedback control systems to regulate SES vertical accelerations . . . 77
4.6.1. The Kaplan et al. system . . . 78
4.6.2. The Sorensen and Egeland system . . . 78
4.6.3. The Auestad et al. system . . . 79
4.6.4. Observations . . . 79
4.7. Critical examination of the Kaplan model . . . 79
4.7.1. Rigid Body Equations of Motion . . . 80
4.7.2. Continuity of Air Mass in the Air Cushion . . . 80
4.7.3. Solution for natural frequency . . . 84
4.8. Questions arising from the literature review . . . 85
4.9. Concluding remarks . . . 86

5. Experimental Design **87**
5.1. Introduction . . . 87
5.2. Preliminary Experiment . . . 88
5.2.1. Aims . . . 88
5.2.2. Method . . . 88
5.2.3. Results . . . 89
5.2.4. Discussion . . . 90
5.2.5. Concluding remarks . . . 92
5.3. Research Questions and Hypotheses . . . 93
5.3.1. Experimental factors, resultants and measurands . . . 94
5.4. Physical analogue of a typical SES . . . 96
5.4.1. Overview . . . 96
5.4.2. Air cushion . . . 97
5.4.3. Water waves . . . 99
5.4.4. Air exit area . . . 100
5.4.5. Vessel heave motions . . . 100
5.4.6. Buoyancy . . . 101
5.4.7. Sealing . . . 102
5.4.8. Air supply . . . 103
5.4.9. Hydrodynamic forces . . . 104
5.4.10. Summary . . . 104
5.5. Experimental rig . . . 105
5.6. Mathematical model of the experimental rig . . . 114
5.6.1. Heave deck equation of motion . . . 114
5.6.2. Continuity of air mass through the plenum . . . 120

5.6.3. Air volume flow rate into the plenum . . . 120
5.6.4. Air volume flow rate exiting the plenum . . . 121
5.6.5. Air compressibility . . . 122
5.6.6. Variations in plenum volume . . . 124
5.6.7. Combined effect of density and volume changes . . . 125
5.6.8. System model adopted for experiment . . . 126
5.7. Environmental and random factors . . . 128
5.8. Measurement system . . . 128
5.9. Numerical solution of the mathematical model . . . 129
5.10. Coupled oscillation and steady decline motions . . . 136
5.11. Concluding remarks . . . 138

6. Experimental results and analysis **139**
6.1. Introduction . . . 139
6.2. Experimental rig parameter values—part one . . . 140
6.2.1. Spring stiffness . . . 140
6.2.2. Heave deck rotational inertia . . . 141
6.3. Experimental rig dynamic characteristics . . . 144
6.3.1. Estimating system damped frequency . . . 148
6.3.2. Estimating settling time . . . 152
6.3.3. Estimating falling time . . . 154
6.4. Experimental rig parameter values—part two . . . 156
6.4.1. Dry (Coulomb) friction . . . 156
6.4.2. Parasitic leakage . . . 158
6.4.3. Plenum stiffness . . . 159
6.4.4. Velocity-dependent heave deck resistance . . . 159
6.4.5. Summary of experimental rig parameter values . . . 161
6.5. Main experimental results with forced plenum oscillations . . . 163
6.5.1. Reconfiguration of experimental rig to enable forced oscillations of the plenum volume . . . 165
6.5.2. Frequency of the forcing . . . 165
6.5.3. Experimental analysis . . . 166
6.5.4. Principal experimental results . . . 168
6.5.5. Direct comparison of flapper and supported mass time-series . . . 181
6.6. Concluding remarks . . . 194

7. Conclusions and recommendations **196**
7.1. Introduction . . . 196
7.2. Research questions and hypotheses . . . 197
7.3. Novel contributions . . . 198
7.4. Applicable range of the experimental findings . . . 198
7.5. Practical applications of this research . . . 199
7.6. Further work . . . 199
7.7. Concluding remarks . . . 200

Bibliography **201**

Appendices **207**

Appendix A. Significant Wave Height Data **208**

Appendix B. Conceptual design tool data **213**

Appendix C. Failure Mode and Effects Analyses **235**

Appendix D. MATLAB code **237**
D.1. Setup experimental rig properties . . . 237
D.2. Step change experiment results . . . 240
D.3. Simulink model . . . 248
D.4. Parametric curve fitting to step change experimental data . . . 253
D.5. Experimental data analysis for oscillating plenum volume . . . 259
D.6. Theoretical predictions . . . 269

Appendix E. Decomposed signal results **275**
E.1. Experimental condition one . . . 277
E.2. Experimental condition two . . . 278
E.3. Experimental condition three . . . 280
E.4. Experimental condition four . . . 282
E.5. Experimental condition five . . . 283
E.6. Experimental condition six . . . 284
E.7. Experimental condition seven . . . 286
E.8. Experimental condition eight . . . 289
E.9. Experimental condition nine . . . 291
E.10. Experimental condition ten . . . 293
E.11. Experimental condition eleven . . . 295
E.12. Experimental condition twelve . . . 297
E.13. Experimental condition thirteen . . . 298
E.14. Experimental condition fourteen . . . 299
E.15. Experimental condition fifteen . . . 300
E.16. Experimental condition sixteen . . . 301
E.17. Experimental condition seventeen . . . 303
E.18. Experimental condition eighteen . . . 304
E.19. Experimental condition nineteen . . . 305
E.20. Experimental condition twenty . . . 309
E.21. Experimental condition twenty-one . . . 313
E.22. Experimental condition twenty-two . . . 314
E.23. Experimental condition twenty-three . . . 316
E.24. Experimental condition twenty-four . . . 318
E.25. Experimental condition twenty-five . . . 324
E.26. Experimental condition twenty-six . . . 325
E.27. Experimental condition twenty-seven . . . 326
E.28. Experimental condition twenty-eight . . . 329
E.29. Experimental condition twenty-nine . . . 330
E.30. Experimental condition thirty . . . 331

Appendix F. Experimental Rig Parameter Estimation Through Curve Fitting **333**

Appendix G. The construction, testing and modelling of a concept rig 364
G.1. Purpose . . . 364
G.2. Construction images of the Concept Rig . . . 364
G.3. Concept Rig geometric parameters used for modelling . . . 372
G.4. Basis of analysis: . . . 373
G.4.1. Approach to numerical solution using Excel spreadsheet . . . 373
G.5. Result of sample run with Concept Rig . . . 374
G.6. Predicted vibration period for an idealised mass / spring oscillator . . . 376
G.7. Results of Excel simulations of sample run . . . 376
G.7.1. Simulation one: data as for sample run . . . 376
G.7.2. Simulation two: larger exit hole diameter (44 mm) . . . 378
G.7.3. Simulation three: reduced air flow ($0.01 m^3 s^{-1}$) . . . 379
G.7.4. Simulation four: add Coulomb Friction to 44 mm hole (10 N friction) 380
G.7.5. Simulation five: add extended outlet volume represented by a 300 m long tube . . . 382
G.7.6. Simulation six: add flexibility to plenum volume . . . 383
G.8. Sensitivity study . . . 384
G.8.1. Sensitivity Study one: Hole size from 0 to 60 mm . . . 384
G.8.2. Sensitivity study two: Reduced spring deflection (and increased air flow to compensate) . . . 387
G.8.3. Sensitivity study three: altering the discharge coefficient of the leakage hole from 0.8 . . . 388
G.8.4. Sensitivity study four: Altering the speed at which the input flap closes . . . 389
G.8.5. Sensitivity study five: Altering the drag coefficient on the deck . . . 390
G.9. Conclusions from concept rig trials . . . 390

Appendix H. Extended experimental results 392
H.1. Power spectrum analysis of experimental results . . . 392
H.2. Input and output time series of experimental results . . . 402
H.2.1. Condition One . . . 405
H.2.2. Condition Two . . . 419
H.2.3. Condition Three . . . 438
H.2.4. Condition Four . . . 460
H.2.5. Condition Five . . . 477
H.2.6. Condition Six . . . 497
H.2.7. Condition Seven . . . 515
H.2.8. Condition Eight . . . 547
H.2.9. Condition Nine . . . 563

List of Figures

2.1. Typical Surface Effect Ship (SES) ferry 'Ponza Jet', ©John Gilbey 6
2.2. Skjold-class naval Surface Effect Ship (SES), ©Marco McGinty 6
2.3. Map of Southeast Asia 12
2.4. Sheltered waters of Southeast Asia 13
2.5. Significant wave height February 1999 (Jet Propulsion Laboratory, 1999) . 14
2.6. Significant wave height August 1999 (Jet Propulsion Laboratory, 1999) . . 15
2.7. Typical displacement hull container ship, public domain 23
2.8. Roll-On Roll-Off (RORO) detail, public domain 24
2.9. Detail of RORO container unloading, ©Clement Philippe 25
2.10. Typical catamaran, bow view, Creative Commons ©Ivan T. 29
2.11. Typical wave piercing catamaran, ©Incat Australia Pty Ltd 30
2.12. SWATH type pilot boat, Creative Commons ©Ra Boe 31
2.13. Contemporary naval trimaran, forward quarter view, ©Austal 32
2.14. Contemporary naval trimaran, rear quarter view, ©Austal 33
2.15. U.S. Navy hydrofoil, public domain 34

3.1. Schematic of a typical Surface Effect Ship. 40
3.2. SES bag and finger seal schematic 41
3.3. SES triple lobe seal schematic 42
3.4. House of Quality analysis for Surface Effect Ships in general. 50
3.5. Failure Space for SES 53
3.6. FTA part 1 for the 'uncomfortable accelerations in moderate sea states' failure mode 55
3.7. FTA part 2 for the 'uncomfortable accelerations in moderate sea states' failure mode 56
3.8. FTA part 3 for the 'uncomfortable accelerations in moderate sea states' failure mode 57

4.1. Ship translations, public domain 71
4.2. Ship rotations, public domain 71

5.1. Schematic of the preliminary rig. 89
5.2. Forced oscillation magnitude from preliminary experiment. 90
5.3. Mean of forced oscillations from the preliminary experiment 91
5.4. Experimental rig analogue to SES 97
5.5. Experimental rig 106
5.6. Air exit area 107
5.7. Heave deck from above 108
5.8. Heave deck from below 109
5.9. Air supply 110
5.10. Volume step-change mechanism 111

5.11. Volume oscillating change mechanism 112
5.12. Volume oscillating flap detail 113
5.13. Volume oscillating change mechanism installed 113
5.14. Experimental rig heave deck schematic 115
5.15. Simulink model of experimental rig 130
5.16. Simulink model of supported mass equation of motion 132
5.17. Simulink model of air mass continuity 133
5.18. Simulink model of air density and plenum volume rates of change 134
5.19. Supported mass motion time series 137

6.1. Initial displacement of supported mass time-series 143
6.2. Decomposed transient response 145
6.3. The mass-plenum system damped frequency plotted against the plenum height. 151
6.4. Settling time of the experimental rig 153
6.5. Experimental rig falling time 155
6.6. Example of curve fitting to a commissioning test result 157
6.7. Velocity-dependent heave deck resistance 160
6.8. Flapper sensor position. 166
6.9. Example analysis of main experiment data 167
6.10. Icon representing main experiment conditions 169
6.11. Results for main experiment at Condition Five 170
6.12. Results for main experiment at Condition Six 174
6.13. Results for main experiment at Condition Four 175
6.14. Results for main experiment at Condition Eight 177
6.15. Results for main experiment at Condition Two 179
6.16. Power spectrum analysis of main experiment run 126 182
6.17. Power spectrum analysis of main experiment run 128 183
6.18. Power spectrum analysis of main experiment run 131 184
6.19. Power spectrum analysis of main experiment run 135 186
6.20. Power spectrum analysis of main experiment run 146 188
6.21. Power spectrum analysis of main experiment run 125 189
6.22. Power spectrum analysis of main experiment run 136 191
6.23. Power spectrum analysis of main experiment run 147 192

A.1. Significant wave height January 30-February 9 1999 (Jet Propulsion Laboratory, 1999) 208
A.2. Significant wave height June 18-28 1999 (Jet Propulsion Laboratory, 1999) 208
A.3. Significant wave height June 28-July 8 1999 (Jet Propulsion Laboratory, 1999) 209
A.4. Significant wave height July 8-17 1999 (Jet Propulsion Laboratory, 1999) . 209
A.5. Significant wave height July 17-27 1999 (Jet Propulsion Laboratory, 1999) 209
A.6. Significant wave height July 27-August 6 1999 (Jet Propulsion Laboratory, 1999) 210
A.7. Significant wave height August 6-16 1999 (Jet Propulsion Laboratory, 1999) 210
A.8. Significant wave height August 16-26 1999 (Jet Propulsion Laboratory, 1999) 210

A.9. Significant wave height September 15-20 1999 (Jet Propulsion Laboratory, 1999) . . . 211
A.10. Significant wave height January 11-22 2000 (Jet Propulsion Laboratory, 1999) 211
A.11. Significant wave height January 23-February 2000 (Jet Propulsion Laboratory, 1999) . . . 212

D.1. Appendix copy of Simulink model of experimental rig . . . 249
D.2. Appendix copy of Simulink model of supported mass equation of motion . 250
D.3. Appendix copy of Simulink model of air mass continuity . . . 251
D.4. Appendix copy of Simulink model of air density and plenum volume rates of change . . . 252

E.1. Decomposition of run 88. . . . 277
E.2. Decomposition of run 89. . . . 278
E.3. Decomposition of run 95. . . . 279
E.4. Decomposition of run 90. . . . 280
E.5. Decomposition of run 97. . . . 281
E.6. Decomposition of run 91. . . . 282
E.7. Decomposition of run 92. . . . 283
E.8. Decomposition of run 93. . . . 284
E.9. Decomposition of run 94. . . . 285
E.10. Decomposition of run 55. . . . 286
E.11. Decomposition of run 63. . . . 287
E.12. Decomposition of run 65. . . . 288
E.13. Decomposition of run 57. . . . 289
E.14. Decomposition of run 62. . . . 290
E.15. Decomposition of run 59. . . . 291
E.16. Decomposition of run 69. . . . 292
E.17. Decomposition of run 56. . . . 293
E.18. Decomposition of run 66. . . . 294
E.19. Decomposition of run 58. . . . 295
E.20. Decomposition of run 68. . . . 296
E.21. Decomposition of run 60. . . . 297
E.22. Decomposition of run 107. . . . 298
E.23. Decomposition of run 100. . . . 299
E.24. Decomposition of run 102. . . . 300
E.25. Decomposition of run 105. . . . 301
E.26. Decomposition of run 106. . . . 302
E.27. Decomposition of run 104. . . . 303
E.28. Decomposition of run 103. . . . 304
E.29. Decomposition of run 118. . . . 305
E.30. Decomposition of run 124. . . . 306
E.31. Decomposition of run 128. . . . 307
E.32. Decomposition of run 134. . . . 308
E.33. Decomposition of run 120. . . . 309
E.34. Decomposition of run 125. . . . 310
E.35. Decomposition of run 130. . . . 311

E.36. Decomposition of run 135. . . . 312
E.37. Decomposition of run 132. . . . 313
E.38. Decomposition of run 119. . . . 314
E.39. Decomposition of run 129. . . . 315
E.40. Decomposition of run 121. . . . 316
E.41. Decomposition of run 131. . . . 317
E.42. Decomposition of run 123. . . . 318
E.43. Decomposition of run 126. . . . 319
E.44. Decomposition of run 127. . . . 320
E.45. Decomposition of run 133. . . . 321
E.46. Decomposition of run 136. . . . 322
E.47. Decomposition of run 137. . . . 323
E.48. Decomposition of run 110. . . . 325
E.49. Decomposition of run 112. . . . 326
E.50. Decomposition of run 115. . . . 327
E.51. Decomposition of run 116. . . . 328
E.52. Decomposition of run 109. . . . 329
E.53. Decomposition of run 111. . . . 330
E.54. Decomposition of run 113. . . . 331
E.55. Decomposition of run 114. . . . 332

F.1. Curve fitting for condition 1 . . . 335
F.2. Curve fitting for condition 2 . . . 336
F.3. Curve fitting for condition 3 . . . 337
F.4. Curve fitting for condition 4 . . . 338
F.5. Curve fitting for condition 5 . . . 339
F.6. Curve fitting for condition 6 . . . 340
F.7. Curve fitting for condition 7 . . . 341
F.8. Curve fitting for condition 8 . . . 342
F.9. Curve fitting for condition 9 . . . 343
F.10. Curve fitting for condition 10 . . . 344
F.11. Curve fitting for condition 11 . . . 345
F.12. Curve fitting for condition 12 . . . 346
F.13. Curve fitting for condition 13 . . . 347
F.14. Curve fitting for condition 14 . . . 348
F.15. Curve fitting for condition 15 . . . 349
F.16. Curve fitting for condition 6 . . . 350
F.17. Curve fitting for condition 7 . . . 351
F.18. Curve fitting for condition 8 . . . 352
F.19. Curve fitting for condition 9 . . . 353
F.20. Curve fitting for condition 20 . . . 354
F.21. Curve fitting for condition 21 . . . 355
F.22. Curve fitting for condition 22 . . . 356
F.23. Curve fitting for condition 23 . . . 357
F.24. Curve fitting for condition 24 . . . 358
F.25. Curve fitting for condition 26 . . . 359
F.26. Curve fitting for condition 27 . . . 360

F.27. Curve fitting for condition 28 . . . 361
F.28. Curve fitting for condition 29 . . . 362
F.29. Curve fitting for condition 30 . . . 363

G.1. Concept rig carcass . . . 365
G.2. Concept rig plenum internal detail . . . 366
G.3. Concept rig input flap . . . 367
G.4. Concept rig heave deck . . . 368
G.5. Concept rig air exit area . . . 369
G.6. Concept rig suspension spring . . . 370
G.7. Concept rig instrumentation . . . 371
G.8. Concept rig schematic . . . 372
G.9. Concept rig test data . . . 375
G.10. Concept tests simulation one sample run . . . 377
G.11. Concept test simulation two sample run . . . 378
G.12. Concept rig simulation three sample run . . . 379
G.13. Concept rig simulation four sample run . . . 380
G.14. Concept rig extended-time sample run . . . 381
G.15. Concept rig simulation five sample run . . . 382
G.16. Concept rig simulation six sample run . . . 383
G.17. Sensitivity run 1(a) . . . 384
G.18. Sensitivity run 1(b) . . . 385
G.19. Plot of leakage area vs air speed . . . 386
G.20. Sensitivity run two . . . 387
G.21. Sensitivity run three . . . 388
G.22. Sensitivity run four . . . 389
G.23. Sensitivity run four . . . 390

H.1. Icon representing main experiment conditions . . . 393
H.2. Results for main experiment at Condition One . . . 394
H.3. Results for main experiment at Condition Two . . . 395
H.4. Results for main experiment at Condition Three . . . 396
H.5. Results for main experiment at Condition Four . . . 397
H.6. Results for main experiment at Condition Five . . . 398
H.7. Results for main experiment at Condition Six . . . 399
H.8. Results for main experiment at Condition Seven . . . 400
H.9. Results for main experiment at Condition Eight . . . 401
H.10. Results for main experiment at Condition Nine . . . 402
H.11. Experimental trial data for Condition 62 . . . 405
H.12. Experimental trial data for Condition 63 . . . 406
H.13. Experimental trial data for Condition 64 . . . 407
H.14. Experimental trial data for Condition 65 . . . 408
H.15. Experimental trial data for Condition 66 . . . 409
H.16. Experimental trial data for Condition 67 . . . 410
H.17. Experimental trial data for Condition 68 . . . 411
H.18. Experimental trial data for Condition 69 . . . 412
H.19. Experimental trial data for Condition 70 . . . 413

H.20.Experimental trial data for Condition 71 414
H.21.Experimental trial data for Condition 72 415
H.22.Experimental trial data for Condition 95 416
H.23.Experimental trial data for Condition 105 417
H.24.Experimental trial data for Condition 73 419
H.25.Experimental trial data for Condition 74 420
H.26.Experimental trial data for Condition 75 421
H.27.Experimental trial data for Condition 76 422
H.28.Experimental trial data for Condition 77 423
H.29.Experimental trial data for Condition 78 424
H.30.Experimental trial data for Condition 109 425
H.31.Experimental trial data for Condition 80 426
H.32.Experimental trial data for Condition 81 427
H.33.Experimental trial data for Condition 82 428
H.34.Experimental trial data for Condition 83 429
H.35.Experimental trial data for Condition 97 430
H.36.Experimental trial data for Condition 99 431
H.37.Experimental trial data for Condition 104 432
H.38.Experimental trial data for Condition 107 433
H.39.Experimental trial data for Condition 108 434
H.40.Experimental trial data for Condition 109 435
H.41.Experimental trial data for Condition 114 436
H.42.Experimental trial data for Condition 84 438
H.43.Experimental trial data for Condition 85 439
H.44.Experimental trial data for Condition 86 440
H.45.Experimental trial data for Condition 87 441
H.46.Experimental trial data for Condition 88 442
H.47.Experimental trial data for Condition 89 443
H.48.Experimental trial data for Condition 90 444
H.49.Experimental trial data for Condition 91 445
H.50.Experimental trial data for Condition 92 446
H.51.Experimental trial data for Condition 93 447
H.52.Experimental trial data for Condition 94 448
H.53.Experimental trial data for Condition 96 449
H.54.Experimental trial data for Condition 100 450
H.55.Experimental trial data for Condition 101 451
H.56.Experimental trial data for Condition 102 452
H.57.Experimental trial data for Condition 103 453
H.58.Experimental trial data for Condition 106 454
H.59.Experimental trial data for Condition 110 455
H.60.Experimental trial data for Condition 111 456
H.61.Experimental trial data for Condition 112 457
H.62.Experimental trial data for Condition 113 458
H.63.Experimental trial data for Condition 115 460
H.64.Experimental trial data for Condition 116 461
H.65.Experimental trial data for Condition 117 462
H.66.Experimental trial data for Condition 118 463

H.67.Experimental trial data for Condition 119 464
H.68.Experimental trial data for Condition 120 465
H.69.Experimental trial data for Condition 121 466
H.70.Experimental trial data for Condition 122 467
H.71.Experimental trial data for Condition 123 468
H.72.Experimental trial data for Condition 124 469
H.73.Experimental trial data for Condition 125 470
H.74.Experimental trial data for Condition 148 471
H.75.Experimental trial data for Condition 153 472
H.76.Experimental trial data for Condition 157 473
H.77.Experimental trial data for Condition 158 474
H.78.Experimental trial data for Condition 163 475
H.79.Experimental trial data for Condition 167 476
H.80.Experimental trial data for Condition 126 477
H.81.Experimental trial data for Condition 127 478
H.82.Experimental trial data for Condition 128 479
H.83.Experimental trial data for Condition 129 480
H.84.Experimental trial data for Condition 130 481
H.85.Experimental trial data for Condition 131 482
H.86.Experimental trial data for Condition 132 483
H.87.Experimental trial data for Condition 133 484
H.88.Experimental trial data for Condition 134 485
H.89.Experimental trial data for Condition 135 486
H.90.Experimental trial data for Condition 136 487
H.91.Experimental trial data for Condition 150 488
H.92.Experimental trial data for Condition 152 489
H.93.Experimental trial data for Condition 154 490
H.94.Experimental trial data for Condition 156 491
H.95.Experimental trial data for Condition 160 492
H.96.Experimental trial data for Condition 162 493
H.97.Experimental trial data for Condition 164 494
H.98.Experimental trial data for Condition 166 495
H.99.Experimental trial data for Condition 137 497
H.100Experimental trial data for Condition 138 498
H.101Experimental trial data for Condition 139 499
H.102Experimental trial data for Condition 140 500
H.103Experimental trial data for Condition 141 501
H.104Experimental trial data for Condition 142 502
H.105Experimental trial data for Condition 143 503
H.106Experimental trial data for Condition 144 504
H.107Experimental trial data for Condition 145 505
H.108Experimental trial data for Condition 146 506
H.109Experimental trial data for Condition 147 507
H.110Experimental trial data for Condition 149 508
H.111Experimental trial data for Condition 151 509
H.112Experimental trial data for Condition 155 510
H.113Experimental trial data for Condition 159 511

H.114 Experimental trial data for Condition 161 . . . 512
H.115 Experimental trial data for Condition 165 . . . 513
H.116 Experimental trial data for Condition 1 . . . 515
H.117 Experimental trial data for Condition 2 . . . 516
H.118 Experimental trial data for Condition 3 . . . 517
H.119 Experimental trial data for Condition 4 . . . 518
H.120 Experimental trial data for Condition 5 . . . 519
H.121 Experimental trial data for Condition 6 . . . 520
H.122 Experimental trial data for Condition 7 . . . 521
H.123 Experimental trial data for Condition 8 . . . 522
H.124 Experimental trial data for Condition 9 . . . 523
H.125 Experimental trial data for Condition 10 . . . 524
H.126 Experimental trial data for Condition 11 . . . 525
H.127 Experimental trial data for Condition 12 . . . 526
H.128 Experimental trial data for Condition 13 . . . 527
H.129 Experimental trial data for Condition 14 . . . 528
H.130 Experimental trial data for Condition 15 . . . 529
H.131 Experimental trial data for Condition 16 . . . 530
H.132 Experimental trial data for Condition 17 . . . 531
H.133 Experimental trial data for Condition 18 . . . 532
H.134 Experimental trial data for Condition 19 . . . 533
H.135 Experimental trial data for Condition 43 . . . 534
H.136 Experimental trial data for Condition 44 . . . 535
H.137 Experimental trial data for Condition 45 . . . 536
H.138 Experimental trial data for Condition 46 . . . 537
H.139 Experimental trial data for Condition 49 . . . 538
H.140 Experimental trial data for Condition 51 . . . 539
H.141 Experimental trial data for Condition 53 . . . 540
H.142 Experimental trial data for Condition 54 . . . 541
H.143 Experimental trial data for Condition 55 . . . 542
H.144 Experimental trial data for Condition 56 . . . 543
H.145 Experimental trial data for Condition 59 . . . 544
H.146 Experimental trial data for Condition 61 . . . 545
H.147 Experimental trial data for Condition 20 . . . 547
H.148 Experimental trial data for Condition 21 . . . 548
H.149 Experimental trial data for Condition 22 . . . 549
H.150 Experimental trial data for Condition 23 . . . 550
H.151 Experimental trial data for Condition 24 . . . 551
H.152 Experimental trial data for Condition 25 . . . 552
H.153 Experimental trial data for Condition 26 . . . 553
H.154 Experimental trial data for Condition 27 . . . 554
H.155 Experimental trial data for Condition 28 . . . 555
H.156 Experimental trial data for Condition 29 . . . 556
H.157 Experimental trial data for Condition 30 . . . 557
H.158 Experimental trial data for Condition 42 . . . 558
H.159 Experimental trial data for Condition 48 . . . 559
H.160 Experimental trial data for Condition 52 . . . 560

H.161 Experimental trial data for Condition 58 561
H.162 Experimental trial data for Condition 31 563
H.163 Experimental trial data for Condition 32 564
H.164 Experimental trial data for Condition 33 565
H.165 Experimental trial data for Condition 34 566
H.166 Experimental trial data for Condition 35 567
H.167 Experimental trial data for Condition 36 568
H.168 Experimental trial data for Condition 37 569
H.169 Experimental trial data for Condition 38 570
H.170 Experimental trial data for Condition 39 571
H.171 Experimental trial data for Condition 40 572
H.172 Experimental trial data for Condition 41 573
H.173 Experimental trial data for Condition 50 574
H.174 Experimental trial data for Condition 60 575

List of Tables

2.1. A comparison of transportation modes 20
2.2. Surface Effect Ship advantages and disadvantages 27
2.3. Catamaran advantages and disadvantages 28
2.4. SWATH advantages and disadvantages 31
2.5. Trimaran advantages and disadvantages 32
2.6. Hydrofoil advantages and disadvantages 35
2.7. Pugh selection analysis 36

3.1. Count of parameters found in source texts by category 47
3.2. Count of Engineering Attributes found in the analysed texts 48
3.3. Prioritised EAs as indicated by the HoQ analysis 51

5.1. Parameters for the air flow into the plenum 121
5.2. Experimental rig parameters 127
5.3. Laser interferometer values 128

6.1. Spring stiffness experimental results 140
6.2. Spring properties 140
6.3. Heave deck parameters and values 142
6.4. Falling time results 154
6.5. Experimental rig parameter values used for main experiment 162
6.6. The nine conditions of the main experiment 169

B.1. Engineering Attributes, Customer Requirements and Failure Modes sourced and categorised. 213

C.1. Surface Effect Ship Bow Seal Fingers FMEA 235
C.2. Surface Effect Ship Stern Bag Seal FMEA 236

E.1. Experimental conditions for finding experimental rig dynamic properties . 276

F.1. Experimental rig parameter values 334

G.1. Data from concept rig varying air exit area sensitivity test 385

H.1. The nine conditions of the main experiment 392
H.2. Main experiment conditions and runs 403

Nomenclature

$\ddot{\theta}$	angular acceleration of the rotating object, $\mathrm{rad\,s^{-2}}$
Δl_o	spring extension when the spring fully suports the experimental rig mass
Δp	changes in air cushion gauge pressure, relative to the hover pressure
γ	Adiabatic gas coefficient
μ	a non-dimensional form of the instantaneious air cushion pressure **??**
μ	non-dimensional air cushion pressure, defined in Eq. (5.14)
∇	displacement corresponding to the design waterline in $\mathrm{m^3}$
ρ	instantaneous density of the air in the air cushion
ρ_a	atmospheric air density
σ	Laplace variable
θ	the rigid body pitch angle, bow up positive
$\triangle A_{waves}$	Forced change to the air cushion exit area due to the direct action of water waves
A	horizontal cross sectional area of the air cushion, assumed constant throughout the air cushion
A_e	Air exit area on experimental rig
A_{L0}	total area through which air exits the air cushion
A_L	Instantaneous area through which air exits the air cushion
C_c	Coulomb friction factor
c_n	orifice air flow coefficient, dependent on orifice geometry, values for which are in standard Fluid Mechanic reference works
d_θ	rigid body pitch damping constant
F_c	force on the experimental rig suported mass due to Coulomb friction
g	gravitational acceleration
h	Instantaneous air cushion height

h_0	Air cushion height at static equilibrium (hover)
h_b	Air cushion height (superseded US nomenclature)
I	moment of inertia of the rotating object, $\mathrm{kg\,m^{-2}}$
I_y	rigid body moment of inertia for the pitch motion
k	The spring constant in Newtons per metre
k	spring stiffness, $\mathrm{m\,N^{-1}}$
K_θ	rigid body pitch stiffness constant
m	mass of the rigid body
m_b	mass of air in the cushion
M_{waves}	the moment induced on a rigid body by water wave action
p	dynamic gauge air pressure in the air cushion or plenum
p	instantaneous air cushion gauge pressure
p_0	the gauge air pressure of the air cushion at static equilibrium (hover)
p_a	atmospheric air pressure
p_h	air cushion or plenum pressure at static equilibrium (undisturbed hover), gauge pressure in Pa
Q_0	volume flow rate of air into, and out of, the cushion at static equilibrium (hover)
Q_{in}	air volume flow rate into the air cushion
Q_{out}	air volume flow rate out of the air cushion
T	torque applied to the rotating platform carrying the supported mass, N m
V	volume of the air cushion
V_s	Air supply duct centreline air velocity
V_{waves}	Forced changes to the air cushion volume due to the direct action of water waves
x_{cp}	distance between the axis of pitch rotation and the centre of effort of the air cushion
y_s	vertical displacement of the experimental rig supported mass at the point where the supporting spring is attached
z	rigid body axis of motion, vertically up, through the centre of gravity

A	area of the heave deck, upon which the air cushion or plenum air pressure acts
AMV	Advanced Marine Vessels
Q	air volume flow rate through the air supply fan
RORO	Roll-On-Roll-Off

Acknowledgements

This research was supervised Associate Professor C.R. Burvill, of the Department of Mechanical Engineering, The University of Melbourne. Experiments were conducted thanks to Professor J. Monty, Department of Mechanical Engineering, The University of Melbourne who gave generous access to the required laboratory space. Use of several sensors was provided by Professor Vincent Rouillard, Institute for Sustainable Industries and Liveable Cities, Victoria University. A piece of very stiff and light Nida-core honeycomb panel was supplied by Chris Kasapis of CKAS Mechatronics Pty. Ltd. Further advice and guidance was received from Associate Professor Bruce Field and Associate Professor William Lewis. This research was made possible by financial support of several personal friends, including Mr A. Deans. Early parts of the research were supervised by Dr Peter Milner and impetus for selecting the field of research was due to the efforts of Mr R.W.G. MacDonald: both of the Mechanical Engineering Department of the University of Melbourne. The author is extremely grateful to the support of his wife, Naomi Swindon, and daughter, Chloe: most people would have a doctorate if they were blessed with such support.

MATLAB and Simulink are registered trademarks of The MathWorks, Inc. See http://www.mathworks.com/trademarks for a list of additional trademarks.

Abstract

The research project was conducted in two phases. The first phase, a policy-based investigation of the application of a suitable technology to commercial freight transport in Southeast Asia, concluded that the candidate technology that best met the sought objectives was a hybrid catamaran hovercraft configuration, or Surface Effect Ship (SES). In the second phase, a specific physical issue associated with the Surface Effect Ship (SES) reported in the available literature was investigated, specifically, the control of water-wave induced ship motions caused by air pressure resonance in the SES air cushion. Air pressure resonance was investigated experimentally using a custom designed and fabricated air chamber apparatus and associated numerical simulation validation studies. The novel phenomenon of increase in time-wise mean air cushion pressure at higher frequency oscillations of an air cushion volume was predicted using numerical simulation. Experimental observations were in agreement with the predicted behaviour. It was concluded that some dynamic characteristics of the SES that could inhibit the wider use of this type of craft were able to be replicated in laboratory apparatus and predicted with a numerical model, thereby facilitating future design tools for practical SESs.

1. Introduction

1.1. Motivation

The 'Surface Effect Ship' (SES) is a hybrid of a catamaran and a hovercraft, in that it employs a pair of rigid narrow hulls and an air cushion to support the vessel. Unlike hovercraft, SESs are not amphibious. The rigid hulls are always in contact with the water and allow the use of conventional propulsion and steering systems. Surface Effects Ships can experience high vertical accelerations when travelling over small water waves, due to the effect of air compressibility in the air cushion, a phenomenon commonly known as the 'cobblestone effect' (Doctors, 2018).

The SES competes against other Advanced Marine Vessel (AMV) concepts in a variety of practical applications (Faltinsen, 2005b; Lavis & Spaulding, 1991; Steen & Faltinsen, 1995). Identifying a suitable practical application, and then comparing the SES with competing types of AMV enables the development of research questions that have a link to practical outcomes. In this thesis, conceptual design tools are used to compare the SES concept to other AMV concepts and analyse the engineering characteristics of the SES, indicating that continued research into the cobblestone effect has the potential to contribute towards new practical applications of the SES.

1.2. Research aims

The broad research aim is to investigate whether it would be practical for the Surface Effect Ship (SES) concept to be used for moving freight in suitable geographic regions. More specifically:

Research Aim 1: To investigate how a policy of improvement of the SES dynamic response to the motions of water waves could benefit the selection of the SES over competing concepts when designing practical freight-carrying systems in South East Asia.

Research Aim 2: To investigate changes in hover height and vibration of a SES when the SES air cushion volume is oscillated by incoming water waves – phenomena that could adversely affect SES performance if left uncontrolled.

1.3. Thesis structure

In Chapter 2, the question of whether AMVs can be applied usefully for freight transport is investigated. The topics considered are: the natural environment; the economic trends in sea-borne freight; and the characteristics of various types of advanced marine vehicles. A set of possible user requirements for advanced marine vehicles is derived from a survey of the technical and industrial literature. The Pugh selection criterion (Pugh, 1991) is applied to the types of advanced marine vehicles and the SES is selected for further investigation.

The author[1] concluded that the open waters in South East Asia provide a favourable opportunity for SESs.

In Chapter 3, the strengths and deficiencies of the SES are investigated in detail, with aims to identify practical issues that would benefit from further research, and to select a research topic of practical significance. The conceptual design tools Quality Functional Deployment (QFD), Failure Mode and Effect Analysis (FMEA) and Fault Tree Analysis (FTA) (Dieter & Schmidt, 2009) were used to select, for experimental investigation, the effect of air compressibility on vertical accelerations.

Chapter 4 presents a critical review of the available literature associated with SESs. The topics reviewed include: sea-keeping, ship habitability and seasickness; wave-making drag of SESs; and vertical motion dynamics of air-lift systems. Chapter 4 includes a critical derivation of the mathematical model of SES heave dynamics published in Kaplan et al. (1981). Several assumptions published in the available literature are identified as candidates for further investigation.

Chapter 5 includes a report of a preliminary, qualitative experiment (Preliminary Experiment), demonstrating that there may be a change in hover height when the air cushion volume is oscillated by incoming water waves. The results of the Preliminary Experiment, together with the conclusions drawn from the critical literature review of Chapter 4, resulted in five research questions, with associated hypotheses. The design and development of a novel experimental apparatus (the 'Experimental Rig') is reported. The experimental apparatus has three novel features:

1. The apparatus is sufficiently large to make air compressibility significant in the study of SES air cushions
2. The effect of air compressibility is isolated from other air cushion characteristics that may lead to whole-ship vertical accelerations
3. The experimental apparatus facilitates the investigation of hover height phenomena

The Experimental Rig was capable of being reconfigured so that two distinct types of experiment could be conducted: a step change to the air cushion volume and; forced oscillations of the air cushion volume.

Several other topics concerning the experimental method are presented in Chapter 5: the derivation of a mathematical model of the experimental apparatus; the formulation of the mathematical model to make it suitable to be solved numerically, using Simulink and; the programme of experiments.

Chapter 6 reports on experimental results. The first set of experiments used a step change in the air cushion volume to determine parameters specific to the Experimental Rig, which are then used in the mathematical model adopted for the Experimental Rig. The second set of experiments used a forced oscillation of the air cushion volume, representing uniform water waves, to investigate the change in hover height and also to investigate whether an air cushion system could be forced to resonate. The results are critically discussed as they are presented.

Chapter 7 contains the conclusions and recommendations arising from this research project. The findings are discussed with respect to the hypotheses postulated in Chapter 5. The readiness for SESs for practical application to the carrying of freight is addressed and

[1]In this thesis, 'the author' is used only to refer to the author of this thesis. Other authors referred to in this thesis will always be named.

some recommendations for further research, arising from the experimental investigation are proposed.

2. A practical application for Surface Effect Ships

2.1. Introduction

Significant research has been undertaken, with respect to Surface Effect Ships (SESs), in high speed military applications (Butler, 1985; Kaplan et al., 1981). While SESs have also been considered for civil applications (Lavis & Spaulding, 1991), recent research into SES related phenomena is not as prolific (Doctors, 2018). In order to select research topics that may stimulate further research and practical development of the SES, it is useful to pose four questions:

1. what are the characteristics of the environment that suits AMVs?
2. is there a natural environment conducive to the operation of small, high-speed ships?
3. is there a need to use advanced marine vehicles rather than conventional ships?
4. is it reasonable to further investigate the type of advanced marine vehicle known as Surface Effect Ships?

In this chapter, after a brief description of SESs, these four questions are addressed using the available literature. Firstly, the nature and quantification of the marine environment that impacts the performance of AMVs is reviewed. Secondly, Southeast Asia is considered as a potential physical and economic environment for the operation of AMVs. Thirdly, the needs of current ship operators are reviewed in order to investigate whether AMVs are potentially useful. Lastly, the needs of ship operators are used to formulate a list of requirements and constraints against which AMV concepts can be compared using the Pugh selection criteria (Pugh, 1991).

2.2. Description of Surface Effect Ships

The SES uses two hulls and an air cushion to support the ship's mass (Fig. 2.1). Unlike hovercraft from which they are derived, the SES is not capable of amphibious operation. The air cushion is created by blowing air into the void between the two hulls. The void is partially sealed at bow and stern by flexible skirts. The flexible skirts are designed to follow the surface of any water waves the SES travels over, maintaining sealing and avoiding the drag of impacting the water surface or becoming immersed in the water.

The motivation for using an air cushion for the SES is to reduce the resistance to forward motion. The raising of the hulls from the water reduces the wetted area, reducing frictional resistance. The contact between the air inside the air cushion and the water is frictionless. The reduction in frictional resistance leads to propulsive power savings greater in magnitude than the increase in power required to both provide propulsion and create the air cushion. The primary type of resistance experienced by the SES is

wave-making drag, caused by the air cushion displacing water. A detailed description of the forms of resistance experienced by the SES can be found in Kaplan et al. (1981). The primary practical interest in SESs is therefore their capability of high speeds at reasonable operating cost.

In comparison to hovercraft, the inclusion of the rigid side-hulls gives the SES two advantages. Firstly, the rigid side-hulls provide lateral forces, which counteract yaw and sway. Secondly, the rigid side-hulls also provide accommodation for propellers or water-jets, both more efficient means of propulsion than the airscrews used on hovercraft. Therefore, while the hovercraft shares the low resistance characteristic of the SES, the SES is the more practical choice when amphibious operation is not required. An SES can reduce its draft by employing the air cushion, making it capable of transiting shallow water. The SES's ability to change the altitude of its decks may also have practical advantages in ports with limited infrastructure.

SESs are capable of travelling at very high speeds; several SESs are operating in speeds in excess of 50 kn (93 km h^{-1}) (Phillips, 2007) and an experimental SES, the Bell 100B built in 1972, has reached 94 kn (174 km h^{-1}) (Lavis & Spaulding, 1991). A large SES was built in 2005 to demonstrate the concept operating as an ocean-going high-speed cargo vessel (Phillips, 2007). The 'Super Liner Ogasawara' is 140 m long, can carry a payload of 210 t, has a maximum speed (confirmed during sea trials) of 42.8 kn and a claimed range of 1.200×10^3 M. A typical SES is the 'Ponza Jet', (Fig. 2.1), built by the Norwegian company Ulstein Technology in 1992 as the Santa Elorana, which is 39 m long, can carry 342 passengers and is capable of operating at 46 kn (Phillips, 2007).

Surface Effects Ships are in current use with Scandinavian navies, (Fig. 2.2), Phillips (2007) reports they are used primarily as patrol vessels (the 55.2 m Oskøy class and 47.5 m Skjold class) and mine-sweepers (the 55.2 m Alta class). A claimed advantage of SES in military applications is the lower susceptibility to underwater explosions (such as from mines) due to the energy absorption through the air cushion (Lavis & Spaulding, 1991).



Figure 2.1. Typical Surface Effect Ship (SES) ferry 'Ponza Jet' in Naples July 2017, ©John Gilbey / Alamy Stock Photo.



Figure 2.2. A contemporary naval application of the Surface Effect Ship (SES) type, the 47.5 m long KNM Skudd (P962), a Skjold-class coastal patrol vessel operated by the Norwegian Navy, passing Greenock in 2015, ©Marco McGinty / Alamy Stock Photo.

In summary, the defining feature of the SES is the use of an air cushion, the primary motivation for which is efficient operation at high speeds. A more complete discussion of the SES primary characteristics will be presented in Sec. 3.2.

2.3. Characteristics of environments that suit AMVs

The scientific study of water waves occurring in the ocean has three distinct historical periods. Kinsman (1965) produced a summary of the early work, when simplified mathematical models of wave forms were applied and the first few years of the post-1952 period, when the mathematics of power spectral density (also known as 'spectral energy density') were applied, following the work of Pierson (Kinsman, 1965). Massel (1996) provides a summary of work done after Kinsman's book appeared in 1965, following the introduction of satellite altimetry (late 1980s), which gave a large volume of water wave height observational data (Massel, 1996). Holthuijsen (2007) provides a general overview of ocean water waves suitable for engineering purposes, covering a similar scope to Kinsman, but updated with current developments in the field of oceanography.

The most common type of water wave found in the ocean is produced by the action of wind on the surface of the water (Holthuijsen, 2007). Waves that are under the ongoing influence of wind are called 'wind waves' and waves that are no longer under the influence of wind are called 'swells' (Boccotti, 2000).

An early and simple theory for the development of waves was formulated by Sverdrup and Munk in 1943 (Kinsman, 1965). The Sverdrup-Munk theory proposed that the height of water waves depended on the wind force (or speed), the duration (in terms of time) and the 'fetch' (or distance over which the wind interacts with the water. This theory of wave development is still accepted for idealized conditions, but to predict the development of waves in more realistic, arbitrary ocean conditions, the 'spectral energy balance' (a form of the power spectral density) is used instead of the fetch and duration (Holthuijsen, 2007).

The concept of a significant wave height was introduced by Sverdup and Munk in 1947 (Massel, 1996). This significant wave height (H_s or $H_{1/3}$) is the average height of the highest one-third of wave heights Eq. (2.1) (Massel, 1996), (Holthuijsen, 2007). In this context, significant wave height is determined from observation of water waves in the time domain. The subscript j inEq. (2.1) refers to the rank of the wave height, where $j = 1$ denotes the largest observed wave height.

$$H_{1/3} = \frac{1}{N/3} \sum_{j=1}^{N/3} H_j \tag{2.1}$$

It is possible to represent an observed sequence of waves using a Fourier analysis (Holthuijsen, 2007). This enables the geometry of an observed sequence of waves to be represented mathematically, which is useful for engineering design purposes Eq. (2.2).

$$\eta(t) = \sum_{i=1}^{N} a_i \cos(2\pi f_i t + \alpha_i) \tag{2.2}$$

where $\eta(t)$ = surface elevation at one point as a function of time

a_i = amplitude of the periodic component

α_i = phase of the periodic component

f_i = frequency of the periodic component

with $f_i = \dfrac{i}{D}$

where $i = 1, 2, 3 \ldots$

D = duration of the original observation of the waves

For a series of up to twelve waves in sequence, the wave geometry and behaviour can be predicted using classical mechanics and described using the Fourier analysis (Holthuijsen, 2007). For large sequences of waves, stochastic (statistical) methods must be used. The complexity of the seaway increases greatly as a greater number of waves in the sequence are considered, as stated by Shaw (1982):

> "...the real sea conditions create a whole spectrum of waves of different heights, periods and directions. This situation arises because waves, once created, dissipate very little energy and, unless they encounter head-winds, they continue over considerable distances (perhaps thousands of miles) for long periods (perhaps several days). Any given location may therefore receive waves which have been generated at many different places by winds blowing in many different directions." ' Shaw (1982)

If the observation of a sequence of waves is repeated under identical conditions, a different record of sea surface elevation at a given point will be obtained. This is because water waves in the ocean are chaotic in nature. Holthuijsen (2007) states it is necessary to use stochastic approaches to describe ocean waves usefully:

> "The aim of describing ocean waves with a spectrum is not so much to describe in detail one observation of the sea surface (i.e., on time record), but rather to describe the sea surface as a stochastic process, i.e., to characterise all possible observations (time records) that could have been made under the conditions of the actual observation. An observation is thus formally treated as one realisation of a stochastic process." Holthuijsen (2007, p. 31)

The wave spectrum is determined by considering the amplitude and phase of the components of a Fourier analysis as random variables. The frequency of incidence of various amplitudes gives the wave amplitude spectrum: similarly for the phase.

It is possible to calculate significant wave height for a wave spectrum (Massel, 1996). Significant wave height calculated in this way is slightly greater than significant wave height calculated from observations (Massel, 1996). Knowing the significant wave height calculated from the wave spectrum allows the calculation of the probability of waves of various heights occurring (Holthuijsen, 2007).

Publicly available data exists for the significant wave height in all regions of the ocean over various time periods. This data is based on satellite observations, such as from the TOPEX/POSEIDON or GEOSAT satellite missions (Figs. 2.5 and 2.6), (Young & Holland, 1996). Processed data from the year 1999 is publicly available and is presented here. More recent data from similar satellite missions is only available in raw form, requiring expert analysis to produce results applicable to this thesis. The satellite observations use a radar altimeter system (Holthuijsen, 2007). In this system, a small area of the ocean is 'illuminated' by energy in the radio wave frequency. The reflected energy is sensed by the satellite. A rough surface reflects the energy back over a small time period, whereas a flat surface reflects all the energy back simultaneously. This principle enables the radar altimeter system to determine the roughness of the surface under observation. This roughness is expressed as a significant wave height.

The motion of a vessel over a water wave is not just dependent on the height of the water wave. The *encounter frequency* (ω_e) is the frequency with which the vessel passes over wave peaks and is likely to be significant if resonant motions of the vessel in response to water waves is of interest. The wave steepness may also be significant as the mechanics of striking a 'wall' of water is different to the mechanics of floating over a rising surface of water. Encounter frequency and steepness may be inferred from significant wave height data Eq. (2.2) but for practical design purposes, care should be taken to not assume that a series of water waves of unusual height, ω_e and steepness cannot be encountered. Designing for performance may make use of statistical treatments of water waves, but designing for safety should always consider failure modes when operating at full speed in normal seagoing conditions (International Maritime Organization, 1995, section 4.2 point 1, p.176).

2.4. Southeast Asia natural environment

Southeast Asia is the region "... bounded by India, China, and the Pacific Ocean, and comprising Burma, Thailand, Malaysia, Cambodia, Laos, Vietnam, Philippines, Singapore, and Indonesia" (Southeast Asia, 2008) (Fig. 2.3). Southeast Asia lies to the north of the region of 'Australasia', which is a "... name used to describe Australia and the islands of the south-west Pacific Ocean, including New Zealand and New Guinea" (Australasia, 2014). The Association of Southeast Asian Nations (ASEAN) has ten member nations: Brunei Darussalam, Cambodia, Indonesia, Lao PDR, Malaysia, Myanmar, Philippines, Singapore, Thailand, and Viet Nam (ASEAN, 2015).



Figure 2.3. Map of Southeast Asia, the region under consideration in this thesis. The shaded area is added by the author (Central Intelligence Agency, 2009a).

In this thesis, the word 'sea' refers to a body of open water bound at least in part by land. The seas of Southeast Asia include: South China Sea, Andaman Sea, Java Sea, Celebes Sea, Banda Sea, Timor Sea, Arafura Sea, Molucca Sea and Sulu Sea. The region of ASEAN in 2012 had 2,708 domestic ports and 457 international ports (AJTP Information Centre, 2012).

The feature of the ocean most relevant to the operation of AMVs is water waves. In particular, waves that occur frequently enough to be considered a normal part of a ship's operating environment and are of sufficient size to affect the motions of a ship. The seas

in Southeast Asia are sheltered from water waves originating in the Indian Ocean by the archipelagos of Indonesia and from water waves originating in the Pacific Ocean by the Philippines (Fig. 2.4). The land masses of Australia and mainland Asia shelter the seas of Southeast Asia from large ocean waves originating elsewhere. The seas of Southeast Asia are smaller than the Indian Ocean and the Pacific Ocean.



Figure 2.4. Sheltered waters of Southeast Asia.
The waters of Southeast Asia are sheltered from the effects of large waves. Waves from the Indian Ocean are blocked by the islands of Indonesia. Waves from the Pacific Ocean are blocked by the islands of the Philippines. Approximate locations of sheltering geographic features added by author, (Central Intelligence Agency, 2009b).

Examination of the available satellite data for significant wave height (Figs. 2.5 and 2.6, further data sets are included in Appendix A) shows that the significant wave height in Southeast Asia is less than 3 m for most of the year. Due to the features of the natural geography, this is likely to be the case for the foreseeable future. Bodies of open water with smaller significant wave heights are generally conducive to the operation of a broad range of marine vehicles, the specifics of which will be discussed in Sec. 2.7.

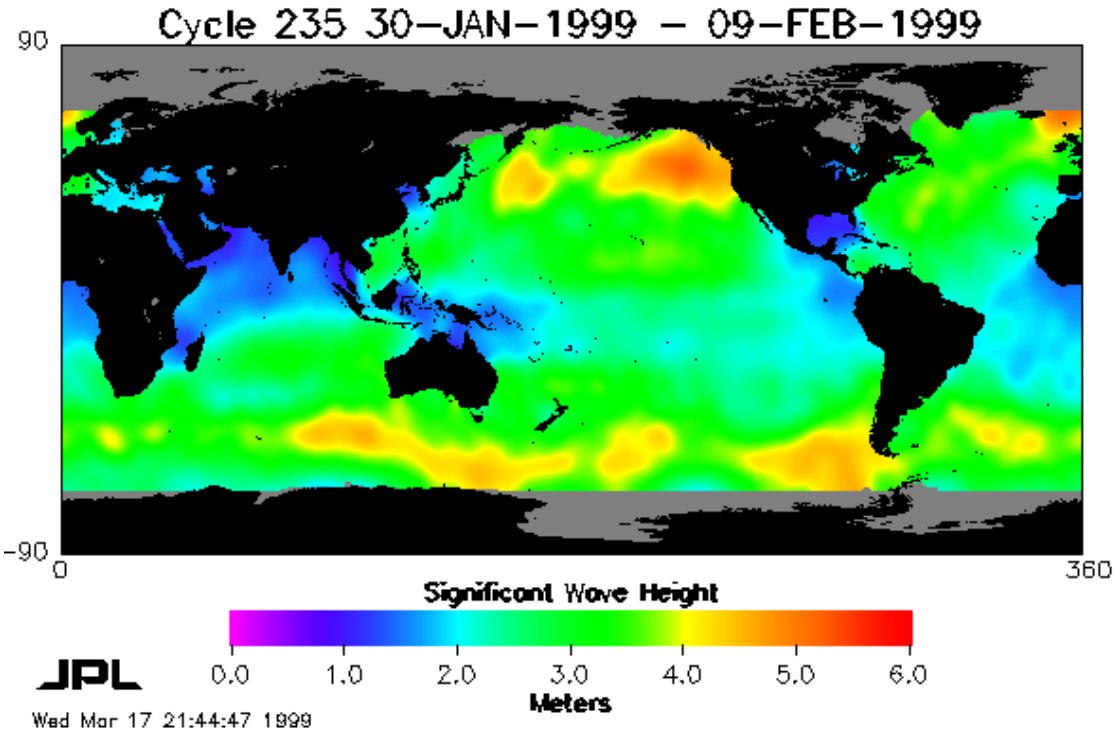


Figure 2.5. Significant wave height February 1999 (Jet Propulsion Laboratory, 1999)

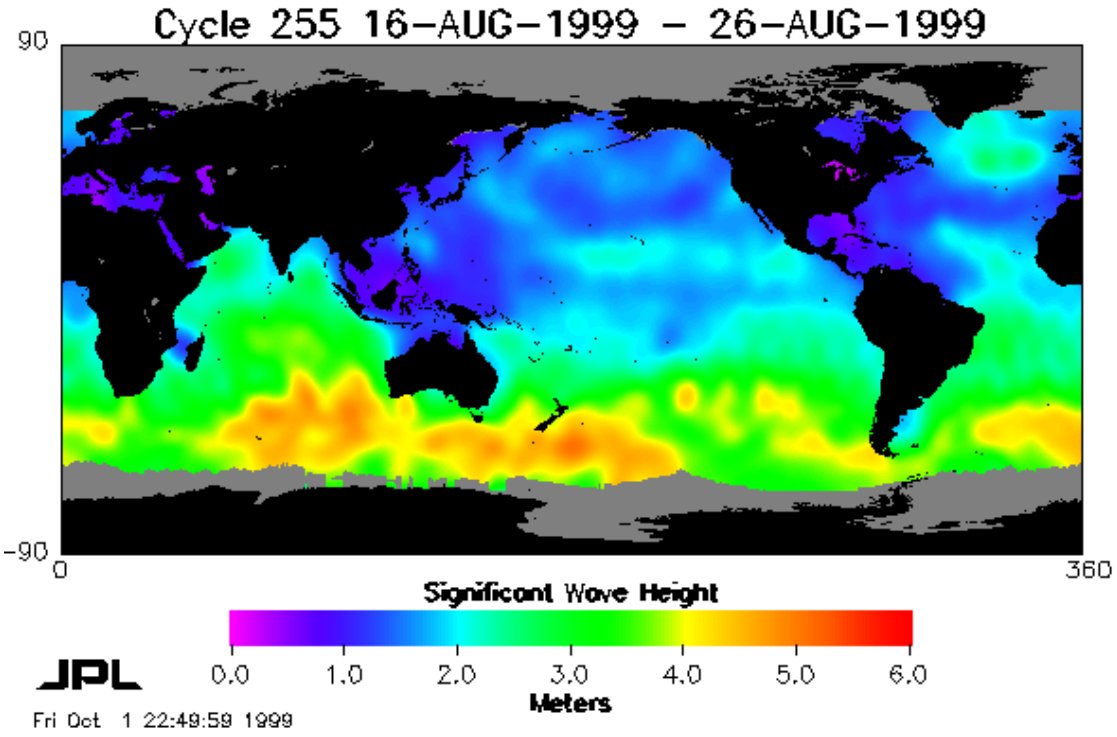


Figure 2.6. Significant wave height August 1999 (Jet Propulsion Laboratory, 1999)

2.5. Maritime freight in Southeast Asia

The open waters of Southeast Asia may be conducive to the operation of Advanced Marine Vehicles (AVM), but significant design and manufacture of AVMs will not occur without a practical use for them. This research is particularly concerned with larger AVMs, which are rarely found in practice and are likely to have issues worth researching, so the use of AVMs to carry freight will be considered, rather than the carrying of passengers which is typically done with smaller vessels.

Freight moves in large volumes when significant populations of people engage in significant economic activity. Southeast Asia is home to over 617 million people (the most recent complete statistics was for 2013) which is a significant number of people (ASEAN, 2013). In economic terms, ASEAN as an entire region has a GDP per capita of US $3,761, with GDP growing at 5.7% per annum in 2013 (ASEAN, 2013). The GDP per capita is significantly lower than for developed countries, but the growth rate is significant and indicates growing economic activity.

The natural geography of Southeast Asia, with a large number of bodies of open water spread spread between many population centres, suggests that water-borne trade should be significant. Statistics published by ASEAN affirms that water-borne freight is a significant activity in the region. The ASEAN-Japan Transport Partnership asserts that in 2012 there were 2,708 domestic ports in Southeast Asia (of which 2,187 were in Indonesia) and 457 international parts in Southeast Asia (of which 141 were in Indonesia) (Partnership, 2012).

Southeast Asia has significant water-borne freight moving every year, providing opportunities for novel AVMs to be adopted for practical reasons.

2.6. Applications for Advanced Marine Vehicles

In general, this thesis investigates 'suitability' and as such, requires some assessment of Customer Requirements (CRs). A review of the available engineering literature shows that detailed CRs are not available for applications of SESs. Eggington and Kobitz (1975) discusses possible applications of SESs. Lavis and Spaulding (1991) discuss actual applications of SESs, from which some indication of CRs can be inferred. Butler (1985) discusses the characteristics of SESs and their potential naval applications. However, these papers do not present detailed CRs for using SESs in a freight carrying application. This is not surprising as the engineering science literature primarily deals with technical issues. Furthermore, detailed requirements gathered by shipbuilders will be kept confidential for commercial reasons.

In this section, the author will establish a rigorous basis for a relevant set of CRs by reviewing the available literature describing the commercial needs of potential high speed ship owners, and deriving a set of desired attributes for the ships by a process of inductive reasoning.

In this thesis, transport is considered to be the movement of goods. Transport is carried out by specialist businesses called 'carriers', which may be within a larger organisation, within a larger business that specialises in services of a logistical nature or be independent businesses (Coyle et al., 2009). The carrier's customer is known as the 'shipper' (Coyle et al., 2009).

From an economic perspective, transport adds 'place utility value' and 'time utility value' to goods (Bowersox et al., 2007, p. 46; Coyle et al., 2009, pp. 37-9). In non-specialist terms, place utility value means that an item is more useful (and probably worth more money) when it has been moved to the desired location, for example, an appliance is more useful to the customer if it in the customer's home rather than a shop. Similarly, time utility value means that an item is more useful if it is available at the right time, for example, food is useful to the customer when the customer wishes to eat and of less value when the customer does not wish to eat.

Within business, transport is an element of the logistics function, which also includes warehousing, inventory management and related activities (Bowersox et al., 2007; Coyle et al., 2009). In recent decades, logistics has become part of a larger grouping of business activities known as 'supply chains' (Christopher, 2004). A supply chain is a functional grouping of business activities, across multiple enterprises, which cover the supply of goods from the origin of materials to final interactions with the customer (Christopher, 2005). An important element of supply chains is that information from the customer is available to all business functions within the supply chain.

Trends in supply chains influence trends in logistics and trends in transportation. Carriers within the transportation industry are the customers for Advanced Marine Vehicles. Therefore, reviewing trends in transportation, logistics and supply chains is the logical method for deducing the likely needs of carriers and hence the likely CRs for Advanced Marine Vehicles.

A significant trend in supply chains is the creation of 'agile' (sometimes known as 'responsive') supply chains (Bowersox et al., 2007; Christopher, 2000; Coyle et al., 2009; Lagoudis et al., 2002). Agile supply chains are a business strategy for the delivery of high-value goods with a time-dependent demand (Christopher, 2000, 2006). The agile supply chain aims to meet the needs of a volatile market while reducing the risks of running out

of stock and stock obsolescence (Harrison & van Hoek, 2008; Jonsson, 2008). Christopher (2005) states that agility is the capability to 'respond in shorter time-frames both in terms of volume change and variety change'. Methods to achieve agility include simplification of business process and synchronisation across different businesses (Christopher, 2005; Harrison & van Hoek, 2008).

Another significant attribute of agile supply chains is flexibility (Christopher, 2001). One important method by which supply chains can be made more flexible is through postponement of final assembly or configuration of the product (Christopher, 2005; Coyle et al., 2009; Harrison & van Hoek, 2008; Jonsson, 2008). Bowersox et al. (2007) distinguish between 'form postponement', in which the product is assembled as late as possible and 'geographic postponement' in which the final good is stored in a large central warehouse for as long as possible (as distinct from warehousing small inventories of product close to the final customer). Both types of postponement require small amounts of products or components to be transported rapidly.

Lagoudis (2006) surveyed major ocean transportation carriers in order to determine the trends in carrier operations in comparison to trends in supply chains. Lagoudis (2006) found that ocean transport carriers did not place a high priority on speed in contrast to the trend towards speed amongst supply chains. Lagoudis (2006) asserts that this is because current carriers are maximising the use of their conventional ships, which are not suited to applications within agile supply chains. By considering the trends in supply chains, it becomes apparent that a new kind of transportation mode is necessary.

From the perspective of logistics, transportation planning becomes a choice between modes and carriers (Coyle et al., 2009). The basic transportation modes are: road, rail, air, water and, pipe.

Of these, only air and water are viable modes for transoceanic transportation of goods. Road and rail must operate on land and pipes are suitable for commodities, such as oil or gas.

Coyle et al. (2009, p. 423) state that 'a critical transportation management issue is modal selection; it affects how fast and economically product will flow across portions of the supply chain.' Coyle et al. (2009, pp. 423-7) identify factors that are important to the shipper when selecting the appropriate mode of transport. The desirable characteristics a transportation mode suitable for an agile supply chain, as described in the available literature were analysed. When considering which mode of transport to use, the shipper in an agile supply chain requires:

- high accessibility, to enable flexibility in destination and origin
- low transit time
- high reliability, as there are limited time frames within which to deliver goods
- moderate to high product safety, as most goods suitable for agile supply chains have low durability

The product characteristics when they are packaged up as a shipment, such as weight, volume, density and shape of the goods, should also be considered (Coyle et al., 2009) when selecting a mode of transport. A shipper in an agile supply chain has products:

- of variable size
- of moderate to light weight
- that occupy low volumes

- of low density
- that are packaged into standard shapes (containerised)

The durability of the goods to be shipped should also be considered when selecting a mode of transport (Coyle et al., 2009, p. 427). Durability can be analysed by considering the fragility, temperature sensitivity and perishability. In this context, perishability includes any dependency of the value upon time, such as goods becoming out of date or out of fashion. In agile supply chain, the shipper has goods:

- that are fragile
- may be sensitive to temperature
- that are perishable (such as fresh food and magazines)

In an agile supply chain, the shipper has goods of higher than average value. Higher freight costs can be acceptable, but lower prices allow a larger range of goods to transported cost-effectively – which increases flexibility.

Most of the available literature discussing transportation modes from a logistics perspective assumes that the modes are fixed. However, Lagoudis et al. (2002) considers several variations of the water transport mode and which may suit a shipper best in the context of an agile supply chain.

Lagoudis et al. (2002) argue that where flexibility is the most important need of the shipper, a 'high speed vessel' transportation mode is the best choice when compared to common existing transportation modes: conventional vessel, container vessel, RORO [1], air and road. Lagoudis et al. (2002) compares the transportation modes on the basis of six factors: supply volume, cost of transported product, distance of trip, frequency of service, transit time and, product types. The factors used by Lagoudis et al. (2002) are consistent with the factors presented by Coyle et al. (2009), but extend them to include factors describing the route and the supply chain. Lagoudis et al. (2002) assumes the high-speed vessel mode to have an 'operational speed' of 30 kn to 45 kn (55 km h^{-1} to 83 km h^{-1}), whereas the conventional vessel operational speed is considered to be 12 kn to 15 kn (22 km h^{-1} to 28 km h^{-1}), compared to the assumed road operational speed of 40 km h^{-1}. Operational speed is taken to mean the average speed over the duration of the journey. In this thesis, the term 'Fast Ship' is used instead of the term 'high-speed vessel'. Therefore Lagoudis et al. (2002) have argued that agile supply chains need a new kind of transportation mode, the Fast Ship transportation mode. The characteristics of the Fast Ship transportation mode given by Lagoudis et al. (2002) are:

- as flexible as container ships and RORO
- suitable for high-cost products, similar to air, RORO and road
- flexible in terms of distance as they are suitable for short and long journeys
- service frequency is high, similar to container, RORO, air and road
- transit times are short, similar to air
- capable of transporting both commodities and finished goods

The development of air as a transportation mode provides a model for the possible exploitation of the high speed capabilities of Advanced Marine Vehicles as a commercial

[1] RORO refers to 'Roll On Roll Off', a ship that has ramps allowing wheeled vehicles to move between the dock and cargo holds.

Table 2.1. A comparison of transportation modes, completed by the author. The attributes of a transportation mode that are required in an Agile Supply Chain are identified. The attributes of the existing conventional ships and aircraft transportation modes are compared to the requirements and found to be lacking. The attributes of a possible 'Fast Ship' transportation mode that takes advantage of the high speed capabilities of Advanced Marine Vehicles is listed and found to be a good match to the requirements of an Agile Supply Chain.

Agile Supply Chains		Transportation Mode		
Attribute	Value Required	Conventional Ships	Aircraft	Fast Ship
Transit speed	Moderate-Fast	Slow	Fast	Moderate
Cost	Flexible	Cheap	Expensive	Moderate
Cargo flexibility	High	High	Low	High
Destination flexibility	High	Low	Moderate	High
Volume capacity per trip	Moderate	High	Low	Moderate
Mass capacity per trip	Moderate	High	Low	Moderate
Handles containers	Capable	Capable	Not Capable	Capable
Product safety	Moderate-High	Low	High	Moderate
Reliability	High	High	High	Moderate

transportation mode. Initially, air was predominantly used as a passenger transport mode, with some freight carried in the hold of the aeroplane (belly cargo) (Coyle et al., 2009, pp. 48-9). Over time, as air freight services were established, dedicated air freight carriers were established (Coyle et al., 2009, pp. 412-3). A similar trend could occur in the Advanced Marine Vehicle transportation mode, i.e. initially passenger ships operating at high speeds will carry some cargo, leading to an eventual development of dedicated freight services: the Fast Ship transportation mode. An example of this starting to occur is the building of several fast ferries that have an intentional capability to carry cargo as well as passengers, a situation that is similar to the carrying of belly cargo in aeroplanes. If ships follow a similar development to aeroplanes, the eventual commercial demand for dedicated freight carrying ships capable of high speed operation is plausible: the Fast Ship transportation mode.

A Fast Ship transportation mode would better meets the needs of agile supply chains, compared to the existing conventional modes of transport. To illustrate this, the author has reviewed the relevant attributes of common existing transportation modes, based on Coyle et al. (2009, pp. 424-426), Bowersox et al. (2007, p. 183) and Lagoudis et al. (2002). The attributes of the conventional ships, aircraft, and Fast Ship transportation mode given by these sources are analysed on a three-level scale (e.g. low, moderate, high) and structured against the list of required attributes. This analysis is summarised in Table 2.1.

2.7. Pugh Selection

This investigation aims to assess whether the SES has any merit as a concept to be considered for application as a Fast Ship. This is done for two reasons: first, to present the SES in comparison to other types of Fast Ship; second, to ensure that the SES has been correctly identified as a concept of interest for use in Southeast Asia in the context of responsive supply chains.

This preliminary investigation was limited to general requirements – applicable to all Fast Ship applications – and the inherent engineering characteristics of each type of Fast Ship that was considered. Only types of Fast Ship that offered sufficient real data were considered.

The method followed made use of Pugh's Concept Selection Method (Pugh, 1991) to compare abstractions of Fast Ship types. The abstractions were generated by reviewing existing real designs and abstracting them. Some parametric analysis was used to create abstractions.

The initial data for real ships was drawn from academic reviews of the relevant technology (e.g. a review of SES development by Lavis and Spaulding (1991)), supplemented by available reports of operating ships from ship brokerage websites, the International Maritime Organisation and other marine transport industry information sources. This was done to make sure that abstractions are based on real world observations.

The size of the selected vessels was guided by the requirements set out in the U.S. Navy's 'Fast Sealift Project' (Butler, 1985; Kaplan et al., 1981) and the Japanese Government's 'Technosuperliner' project (Matsumura et al., 2006; Sugai & Yamaguchi, 1991a). These provide a realistic size of vessel, considered by the respective project sponsors as being suitable for useful operation. This is not necessarily the same size as that suitable for use in Southeast Asia in a responsive supply chain, but it is taken as a useful indicator of size for Fast Ships in general.

The abstraction process was done by application of parametric analysis (Clausing, 1994) to the real world examples to derive a concept suitable for the general customer requirements for Fast Ships. This ensured a sound basis for comparison.

The abstracted Fast Ship concepts constituted the data in this preliminary investigation. This data was analysed using the Pugh Concept Selection Method. The Pugh Concept Selection Method compares competing concepts against a datum concept, on the basis of various criteria. For brevity, the analysis is tabulated using symbols (Pugh, 1991):

\+ The considered concept has an advantage compared to the datum concept
= The considered concept has neither an advantage nor a disadvantage compared to the datum concept
− The considered concept has a disadvantage compared to the datum concept

The advantages and disadvantages are counted. Where the advantages outweigh the disadvantages, the concept is considered suitable. The tabulated advantages and disadvantages will be presented in Table 2.7.

2.7.1. Background

The International Maritime Organisation defines 'high-speed craft' as marine vehicles capable of speeds equal to or exceeding a speed related to the displacement of the vessel as per Eq. (2.3) (International Maritime Organization, 1995, p. 9).

$$v = 3.7\nabla^{0.1667} \tag{2.3}$$

where v = maximum speed in $\mathrm{m\,s^{-1}}$

∇ = displacement corresponding to the design waterline in $\mathrm{m^3}$

This discussion follows de Osés and Castells (2008) by defining Fast Ships as those ships travelling faster than 23 kn ($\approx$43 $\mathrm{km\,h^{-1}}$, $\approx$12 $\mathrm{m\,s^{-1}}$). According to Eq. (2.3), a craft that displaces less than $1.0507 \times 10^3\,\mathrm{m^3}$ of water and is capable of speeds greater than $11.8\,\mathrm{m\,s^{-1}}$ ($43\,\mathrm{km\,h^{-1}}$), is defined as a high-speed craft. Following de Osés and Castells (2008) facilitates a more convenient comparison of the current work with publications in the logistics field.

For comparison purposes, a conventional ship is defined within this thesis as a ship that is supported above the water surface by the displacement of water by its hull. A conventional container ship is defined as a conventional ship that carries cargo entirely in standard containers, stacked until the cargo is well above deck level (Fig. 2.7). A variation of a conventional container ship is the added capability for road vehicles to drive on and off the vessel (Roll On – Roll Off or 'RORO', Fig. 2.8). This allows trucks carrying containers to embark and disembark very quickly (Fig. 2.9). Each container needs to be accompanied by a prime mover and trailer. A conventional cargo ship with RORO capability will be used as a datum concept in this thesis.



Figure 2.7. Typical container ship with a displacement monohull. MSC Valencia: built 2006; carrying capacity approximately 102.000×10^3 t; length 334 m. Ship data from 'Vessel Finder' https://www.vesselfinder.com/vessels/MSC-VALENCIA-IMO-9301471-MMSI-255805558 accessed November 2019. Public domain image photographed by Flickr user 'pete' via Wikimedia Commons https://commons.wikimedia.org/wiki/File:MSC_Valencia_at_Hong_Kong.jpg accessed November 2019.



Figure 2.8. 'Weser Highway' is a conventional monohull displacement ship with Roll-On Roll-Off (RORO) capability. This photograph, taken in May 2008, shows cars leaving the vessel via the built-in ramp. The Weser Highway is approximately 100 m long with a carrying capacity of approximately 3.222×10^3 t (source Vessel Finder https://www.vesselfinder.com/vessels/WESER-HIGHWAY-IMO-9065417-MMSI-355390000 accessed November 2019). Public domain image photographed by Wikimedia Commons user 'Pujanak' https://commons.wikimedia.org/wiki/File:Weser_Highway_Roro.jpg accessed November 2019.



Figure 2.9. Containers being unloaded from the stern of the Roll On – Roll Off (RORO) ship MV Bore Song, Zeebrugge, Belgium in September 2016. Photograph ©Clement Philippe, Arterra Picture Library / Alamy Stock Photo, used with permission.

Tupper (2004) lists several types of vessel used as 'high speed craft': monohulls (especially hard chine forms), Surface Effect Ships (by which Tupper means Air Cushion Vehicles in general), hydrofoils, multihull ships (including catamarans, SWATH[2] and trimarans) and 'rigid inflatable boats' (only suitable for very small vessels).

Monohulls suitable for high speeds can be further classed as being displacement hulls or planing hulls, with some ships using a hybrid known as a semi-planing (semi-displacement) hull. A displacement hull supports the ship weight solely by hydrostatic forces (the displacement of water). A planing hull supports the ship weight solely by hydrodynamic lift. A semi-planing hull supports the ship weight by a combination of hydrostatic and hydrodynamic forces. Large displacement monohulls can operate at speeds greater than 23 kn (43 km h^{-1}), however only smaller vessels (which are more flexible in their port and harbour needs) are considered in this thesis.

This analysis compares several concepts against the datum concept, to support the selection of one concept for further investigation as a Fast Ship. The concepts considered are:

- SESs
- high speed catamarans
- SWATH
- hydrofoils
- high speed trimarans

[2]Small Waterplane Area Twin Hull

Each concept being considered is described in the following sections and the salient points for consideration tabulated. Only concepts with significant data available are considered. The characteristics of each type of AVM is sourced from Tupper (2004), Lavis and Spaulding (1991) and Faltinsen (2005a).

2.7.2. Surface Effect Ships

A description of SES was given in Sec. 2.2. A summary of the advantages and disadvantages of the SES is given in Table 2.2.

Table 2.2. Surface Effect Ship advantages and disadvantages

Advantages	Disadvantages
At high speeds, require less installed power than an equivalent catamaran	Extra complexity of air cushion system
The air cushion absorbs the shock of hitting large water waves	Resonance in the air cushion may lead to sea-keeping issues
Can operate both cushion-borne and hull-borne for greater flexibility	Extra expense of installing the air cushion system
Wide deck for flexible cargo carrying and work platform	Extra expense of maintaining the air cushion system
Less roll in a seaway due to a wide beam	

2.7.3. Catamarans

A catamaran is any ship with two hulls (Fig. 2.10). The hulls may be of different forms: displacement, semi-displacement and planing.

Displacement hulls have narrower hulls compared to the equivalent displacement monohull, leading to less form resistance compared to the equivalent displacement monohull. Because the two hulls can be spaced apart, the deck above the hulls is a wider (greater beam) than for the equivalent monohull, allowing for easier accommodation of the payload. In general, the greater beam reduces wave-induced roll motions, except in the case of water waves approaching the catamaran from the side, in which case the catamaran may have greater roll motions than the equivalent monohull.

Semi-displacement hulls are capable of greater speeds compared to displacement, though at the expense of reduced transport efficiency . A 'wave-piercing' catamaran uses semi-displacement hulls, with a pronounced extension of the hull and very fine lines at each bow. These bows have little buoyancy and will become immersed in a wave, rather than float over the top. The wave-piercing hull acts to reduce the pitching motion of catamarans. To prevent the main deck slamming into waves, an extra hull is mounted under the deck; this provides buoyancy when the wave is big enough to reach it (Fig. 2.11).

Planing hulls reach high speeds. This type is not usually applied to ships, but is used for small, recreational, water-craft as they are susceptible to hull slamming which leads to involuntary speed reductions when encountering water waves.

Table 2.3 summarises the advantages and disadvantages of catamarans.

Table 2.3. Catamaran advantages and disadvantages

Advantages	Disadvantages
Low resistance	Complex structure
Minimal hull slamming	Wet deck slamming
Space to accommodate power systems	Requires light weight construction
Broad beam for roll stability	



Figure 2.10. Front view of a typical catamaran used as a ferry. Adriana docked in the port of Split March 2013. Image ©Ivan T., used under Creative Commons http://creativecommons.org/licenses/by-sa/3.0) via Wikimedia Commons, https://commons.wikimedia.org/wiki/File:Adriana_(ship,_1992)_IMO_9042104,_Split,_2012-04-28.jpg accessed November 2019.



Figure 2.11. Typical wave piercing catamaran, Incat hull 068 'Akane' during sea trials. The vessel was built in 2015, the overall length (centre hull) is 85 m, speed approximately 37 kn when loaded with 470 t of cargo (Incat Australia https://www.incat.com.au/wp-content/uploads/2018/02/hull-068-85m-mini-spec.pdf accessed November 2019. Image ©Incat Australia Pty Ltd. https://www.incat.com.au/vessel-gallery/068/ accessed November 2019.

2.7.4. SWATH

The 'Small Water-plane Area Twin Hull' (SWATH) type of vessel supports the ship's weight by displacement. The displacement is provided by hulls that are big in volume under the water, but have very little volume at the waterline, with the aim of making the hulls very long and narrow (Fig. 2.12). This reduces wave making drag and also increases stability. Table 2.4 summarises the advantages and disadvantages of SWATHs.



Figure 2.12. Small Water-plane Area Twin Hull (SWATH) type ship 'Borkum' in service as a pilot boat in the harbour of Cuxhaven, Lower Saxony, Germany, Winter 2008. Image ©Ra Boe used under Creative Commons http://creativecommons.org/licenses/by-sa/3.0) via Wikimedia Commons, https://commons.wikimedia.org/wiki/File:SWATH_Pilot_Borkum_06.jpg accessed November 2019.

Table 2.4. SWATH advantages and disadvantages

Advantages	Disadvantages
Low resistance	Complicated structure
Minimal hull slamming	Small volume available for power systems
Minimal motions in water waves	Deep draft
	Speed limited by form drag

2.7.5. Trimarans

Trimarans are defined here as a vessel with three hulls. Recent, important, trimarans have little displacement in the sidehulls and their builders prefer the term 'stabilised monohulls' (Ellery, 2009).

The Austal Littoral Combat Ship is used here as an example of Trimarans for the purposes of this thesis. The vessel supports most of the ship's mass on a central hull, stabilised for excessive roll motions by two smaller side-hulls (Fig. 2.13). A wide deck is built across all three hulls (Fig. 2.14). Table 2.5 summarises the advantages and disadvantages of trimarans.

Table 2.5. Trimaran advantages and disadvantages

Advantages	Disadvantages
Low resistance	Complicated structure
Conventional power system arrangement	Some hull slamming
Minimal motions in water waves	
Capable of high speeds	



Figure 2.13. Contemporary naval trimaran, Austal Ships Littoral Combat Ship on sea trials 2009, forward quarter view, showing the very slender centre hull with bulbous bow typical of this type of vessel. Image ©Austal http://www.austal.com accessed October 2018, cropped by the author.



Figure 2.14. Trimaran, Austal Ships Littoral Combat Ship on sea trials 2009, rear quarter view, showing the width of deck typical of this type of vessel. Image ©Austal http://www.austal.com accessed October 2018.

2.7.6. Hydrofoils

The hydrofoil is supported by immersed foils (wings) and driven by either propellers or a waterjet mounted near the foils (Fig. 2.15). The foils have much less wetted surface area and operate without causing waves, and thus have much less resistance than a displacement hull. The form resistance is much higher than for a conventional hull.

The hydrofoil is experiences less wave-induced motions as the main hull travels above the waves and the foils travel below the waves. The hydrofoil can descend from its foil-borne mode to its hull-borne mode quickly, aiding in slowing the ship and providing a safer mode of motion when circumstances warrant it. The hydrofoils may be retractable, reducing resistance and draft when in the hull-borne mode. The hydrofoil cannot transition from foil-borne mode to hull-borne mode unless there is sufficient depth of water to accommodate the depth of the foils. Table 2.6 summarises the advantages and disadvantages of hydrofoils.



Figure 2.15. U.S.S. Taurus travelling foil-borne circa 1983, with the foils visible under water. U.S.S. Taurus was a Pegasus class hydrofoil built by Boeing: displacement approximately 231.000×10^3 kg; length 40.5 metre; top speed approximately 48 knot; commissioned October 10, 1981; decommissioned July 30, 1993. Public domain image from U.S. Navy archives, https://www.navysite.de/pboats/phm3.htm accessed November 2019.

Table 2.6. Hydrofoil advantages and disadvantages

Advantages	Disadvantages
Higher speeds	Extra cost of foils
Less wave-induced motion	Greater draft off-foil
Minimal motions in water waves	Complexity of foils
	High structural loads on foils, greater risks of failure

2.7.7. Selection analysis

The types of AMV were compared to a datum concept, a conventional cargo vessel with RORO capability. The datum concept is a small ship, compared to the world container fleet average, suitable for flexible operations. The first two factors are the power required to travel at 30 kn (56 km h^{-1}) and the power required to travel at 50 kn (93 km h^{-1}). The SES concept is assumed to be free of sea-keeping issues, the particulars of reported SES sea-keeping issues are investigated experimentally in later chapters. The comparison is presented in Table 2.7, in the form of a Pugh selection analysis. Under the Pugh selection criteria, the concept that has the most advantages is selected. In this case, the SES, with four positive comparisons, is selected for further investigation.

Table 2.7. Pugh selection analysis: conventional container ship with RORO capability as datum concept (Pugh, 1991). The types of AMV described in the text are compared to the datum concept. A positive comparison is denoted +, an equal comparison is denoted = and a negative comparison is denoted −. The concept with the most number of positive comparisons is selected for further design effort.

Factor	Fast Monohull	SESs	ACVs	Trimarans	Catamarans	Hydrofoils
Power at 30 kn	+	+	+	+	+	+
Power at 50 kn	=	+	+	=	=	+
Flexibility	=	+	+	=	=	-
Capital Cost	−	−	−	−	−	−
Transport Efficiency	−	−	−	−	−	−
Sea-keeping	=	+	−	+	+	+
Reliability	=	−	−	=	=	−
Number of '+'	1	**4**	3	2	2	3
Number of '='	4	0	0	3	3	0
Number of '−'	2	3	4	2	2	4

2.8. Concluding remarks

Southeast Asia contains both a physical and an economic environment that is conducive to AMVs operating as freight transporters, especially if they can operate at higher speeds than conventional ships.

The trend towards Agile Supply Chains has the potential to create demand for a novel freight carrying mode, Fast Ships. Various types of AMV could be practically applied as Fast Ships.

Quantified comparisons between types of AMVs, especially using agreed parameters, were not found in the available literature. In the absence of quantified comparisons, the abstracted concepts analysed here offer a practical basis for comparison.

All AMV concepts display some advantages over the datum concept (conventional displacement monohull ships), but all concepts have some disadvantages over the datum concept.

SES sea-keeping has been left aside, as there are some gaps in understanding of this concept. Even so, the SES has enough advantages to potentially outweigh any disadvantages when compared to the datum concept. SESs are favourable or equivalent compared to other concepts. The analysis indicates that SESs are of interest for fast ship applications. Further comparison must include a complete understanding of the SES sea-keeping characteristics. As such, it is reasonable to select the SES for further investigation.

3. Systematic identification of Surface Effect Ship research questions

3.1. Introduction

The practical application of Advanced Marine Vehicles (AMVs) was described in Chapter 2 and the AMV type Surface Effect Ship (SES) was selected for further investigation. The practical application itself was termed 'Fast Ships' in the context of an agile supply chain. To progress the investigation, the question is now posed: what needs to be done to the SES type of vessel to make it ready for practical application as a 'Fast Ships' in the context of an agile supply chain in Southeast Asia? This chapter investigates this question in a systematic way.

An overview of the Customer Requirements (CRs) of a fast freight transporter in Southeast Asia were listed in Sec. 2.6. Assessing the SES type of vessel against the CRs will proceed by assessing the SES capabilities and then assessing the possible failures of the SES to meet the CRs.

Conceptual design tools are analytical tools used during the concept phase of an engineering design project (Dieter & Schmidt, 2009). Conceptual design tools to be considered are:

- Quality Function Deployment (QFD), specifically using the "House of Quality" (HoQ)
- Root cause analysis of failures, specifically using the Failure Mode Effect Analysis (FMEA)
- Weighted objectives method, specifically the Fault Tree Analysis (FTA)

All of these rely on a plausible set of user requirements, which are thoroughly researched, validated and understood for the current research.

The QFD aims to identify the relationship between features of a concept and the user requirements. For example, the colour of a car may both affect the aesthetic requirements and the safety requirements, although brighter colours will enhance safety but may detract from aesthetics. The relationship between and research outcomes and features of a designed product are usually straight forward: in the above case research on paint that looks black to casual observers but looks fluorescent orange to approaching drivers could be considered a desirable research outcome.

The QFD is inductive by nature, going from minor known facts to more general suppositions. It may be used to systematically and rationally form hypotheses that can be tested by market research or entrepreneurial activity. Some deductive reasoning may be used to form the magnitude and direction of the impacts that features have on requirements.

If the feature impacts and directions are accepted, then research can be directed to better realise those features.

The analysis of root causes of failures helps to identify specific physical phenomena that warrant further research. Understanding a root cause is very important to preventing the failure. The investigation of root causes should be done in great depth to identify questions for which answers are not known. A comprehensive and flexible analytical tool for the analysis of failure root causes is the Fault Tree Analysis (FTA) (Vesely et al., 2002), which allows the ready analysis of multiple causal factors and unlimited depth of analysis.

For the SES, several failure modes can be analysed: the overall failure known colloquially as 'sea-keeping'; the more specific issue of 'cobblestoning'; the instance of air ingestion into the propulsion system; wear of skirts; and speed loss in a speedway.

Necessary background will be presented first:

- SES technical details
- Resistance to vehicles passing across a water surface at high speed
- Sea-keeping, especially at high speeds

3.2. The Surface Effect Ship characteristics

The SES has five major systems:

- air lift system
- propulsion system
- navigation system
- structural system
- buoyancy system.

Of these, only the air lift system is peculiar to the SES; the other subsystems are similar to the systems of a high speed catamaran.

The air lift system on an SES uses an 'air cushion' contained by the rigid hulls and flexible bow and stern seals, the underside of the hull (the wet deck) and the sea surface (Fig. 3.1). The air in the cushion is at a pressure slightly greater than atmospheric pressure and thus acts to lift the hull up and push the sea surface down. Air is drawn into the system through an air intake, typically located on the SES deck. The air passes into a fan, usually mounted quite close to the air intake. The fan is usually driven by a dedicated diesel engine, though other arrangements can be found in practice. The fan itself is typically of the centrifugal type; air thus passes through it from its axis to the periphery where it enters the ductwork. The main cushion duct takes air from the fan through to the air cushion. Sometimes the air is passed into a large volume, known as a plenum chamber. The plenum chamber is meant to absorb small variations in the air cushion pressure and volume flow. From the plenum chamber, the air passes, usually through a number of small holes in the wet deck, into the main air cushion space. The air passes out from the air cushion through gaps under the bow and stern seals.

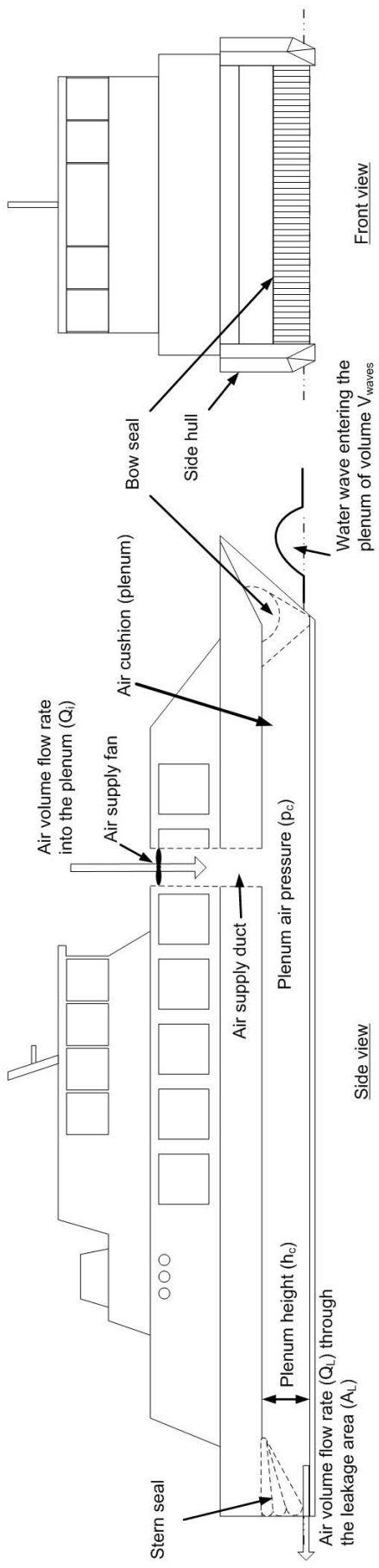


Figure 3.1. Schematic of a typical Surface Effect Ship.

There are two broad types of seals used in practice: flexible seals inflated by air and rigid seals mounted with hinges. Both types are designed to constrict the airflow out of the air cushion whilst minimizing contact with the sea surface. The flexible seals are favoured on commercial ships, though they have been prone to fatigue failure. The rigid seals are attractive because they don't have the fatigue problems inherent in flexible seals; but they have not won acceptance on commercial ships.

Flexible bow and stern seals are inflated by air that may be fed to them either directly from the main fan, by air bled from the air cushion or by air that is fed via small booster fans that maintain a slightly higher pressure in the seals than in the main air cushion.

The bow seal is typically of the 'bag and finger' type (Lavis & Spaulding, 1991) where the air is fed to a plenum bag from the air supply system (Fig. 3.2). Holes in the bag direct air into the scoop shaped fingers, inflating them so that they touch each other on each side. The fingers are prevented from blowing out forward under the air cushion pressure by cables running to the wet deck.

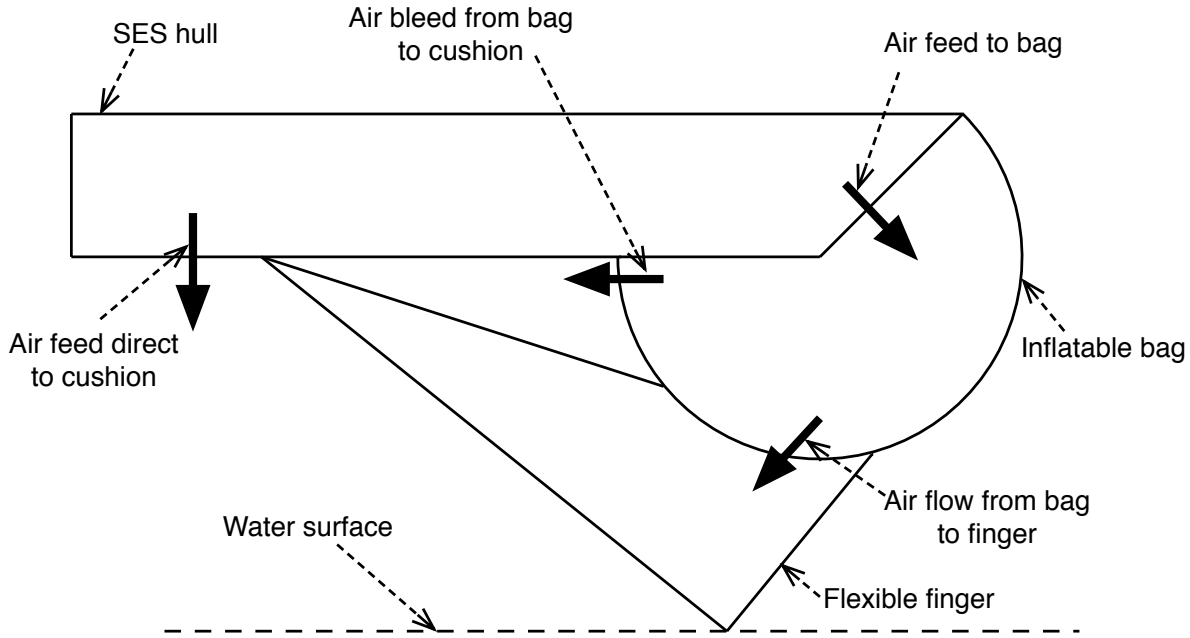


Figure 3.2. SES bag and finger seal schematic showing air flow paths.

The stern seal is typically of the 'triple lobe' type (Lavis & Spaulding, 1991). In this arrangement air is fed to a series of bags (Fig. 3.3). After passing from each bag to the next through small holes, the air escapes into the gap between the seal and the water surface. Each lobe can collapse partially and thus the seal as a whole moves away from the water surface to minimize contact.

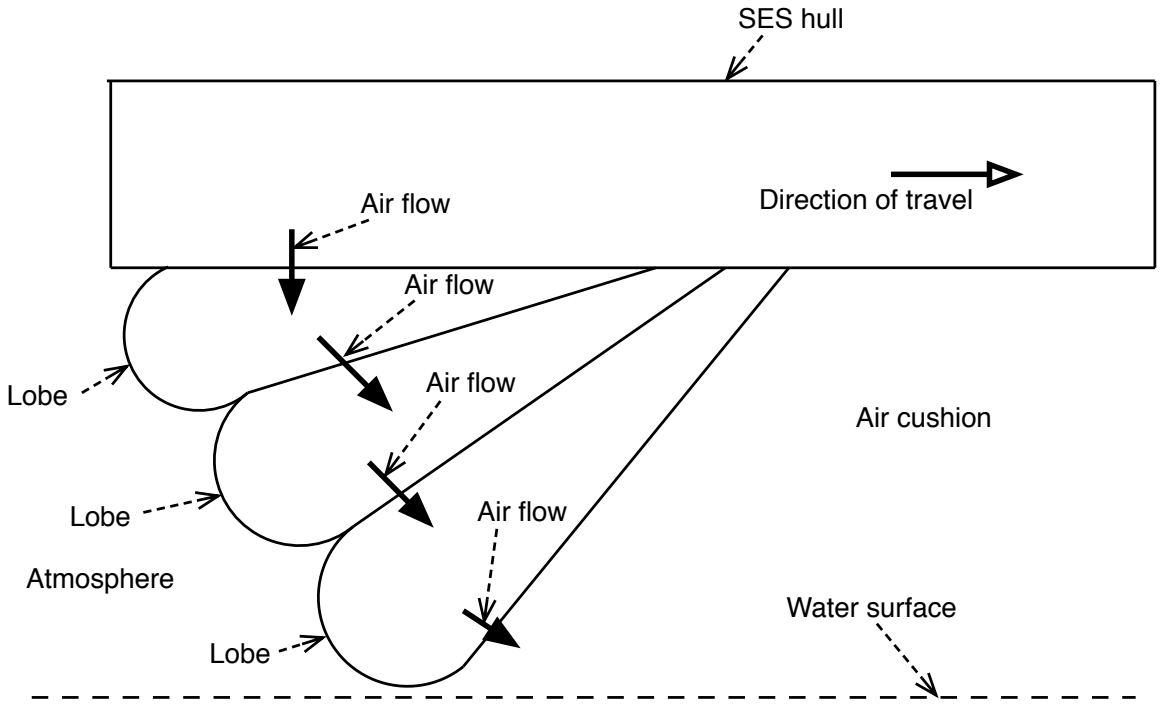


Figure 3.3. SES triple lobe seal schematic showing air flow paths.

The pressure in the air cushion is dependent on the net flow of air through the air cushion space and the instantaneous volume of the air cushion space.

The airflow into the cushion is dependent on the characteristics of the air supply fan, the ductwork, the plenum chamber and the instantaneous air cushion pressure.

The airflow out of the air cushion is dependent on the size and shape of the gap under the bow and stern seals and the instantaneous air cushion pressure. The size and shape of the gap under the bow and stern seals is dependent on the air pressure in the gap, the pressure of the air inflating the seals, the characteristics of the flexible material used to construct the seals, any contact between the water surface and the seals and the motion of the hull to which the seals are attached.

The air cushion volume is directly affected by changes in the sea surface height relative to the hull. This varies across the water surface under the air cushion space. The bow and stern seals can impinge slightly on the air cushion space as they move. The average width of the air cushion space can change as the depth of the air cushion space changes due to the shape of the side-hulls

The side-hulls are partially submerged at all times and thus there is an associated buoyancy force. The volume submerged at any time is related to the cross-sectional area and the depth of the submerged portion. The cross-sectional area is dependent on the geometry of the side-hull. This may be used by SES designers to give extra buoyancy at certain displacements.

The inclusion of side-hulls on the SES — whilst they are responsible for an increase in drag for an SES over a conventional, hovercraft — gives four advantages to the SES over a conventional hovercraft. Firstly, the side-hulls are typically designed so that hydrodynamic forces caused by the side-hulls passage through the water enhance roll stability during

turning (Lavis & Spaulding, 1991). Secondly, the lateral hydrodynamic forces generated by the side-hulls passage through the water provide directional stability. Thirdly, the side-hulls provide accommodation for water-jets which is advantageous due to the water-jets' efficiency compared to the air propellers which are typically used to propel conventional hovercraft. Fourthly, the side-hulls seal the air cushion along both sides. As this leads to less air volume flow from the cushion and hence less air volume flows into the cushion: less installed power is required by the air lift system. The value of these key advantages needs to be preserved by any solution the cobblestoning problem with SESs.

3.3. Resistance

In order to discuss Fast Ships, it is necessary to introduce some terms and concepts regarding resistance (drag). Resistance is the reaction to forward motion and is caused by a number of phenomena (Comstock, 1967; Tupper, 2004):

1. Wave making resistance: due to the ship making waves in the water
2. Frictional resistance: due to the passage of a viscous fluid over the ship's surface
3. Form resistance: due to the creation of eddies in the water behind features of the hull
4. Air resistance: due to the passage of the ship through the air

It is conventional to separate the form resistance of appendages (such as fins, probes, mounting brackets) from the form resistance of the main hull, the separated resistance is called appendage resistance (Tupper, 2004).

The frictional resistance accounts for approximately 80% of the total resistance at slower speeds, and approximately 50% at higher speeds (Comstock, 1967). Wave-making resistance contributes the next largest proportion of total resistance and is the most significant factor in determining the maximum operational speed of a hull form.

The frictional resistance is proportional to the wetted surface area and the Reynolds number. It may be reduced by making the wetted surface area smooth (creating laminar flow) or by reducing the wetted surface area.

The wave-making resistance varies exclusively with Froude number for any specific hull form. The interference of the wave system created by the motion of the ship with various features of the ship's hull creates important characteristics of the wave-making drag (Comstock, 1967). The most important of these for discussing Fast Ships is the 'primary hump' and 'secondary hump'.

The primary hump forms when the bow wave of a ship is twice the length of the ship (Comstock, 1967). This occurs at a particular Froude number for a specific hull form, and thus at a specific speed for a specific length of a specific hull form. At this speed, the trough of the bow wave lies under the stern of the ship; leading to high resistance. It is impractical for a conventional hull form to be accelerated past this speed.

The secondary hump occurs when the bow wave is the same length as the ship, where the ship is mainly supported by wave peaks at the bow and stern. At this speed, the immersion of the stern causes eddies to form at the stern, greatly increasing the resistance. Some hull forms that can accelerate through the primary hump speed cannot be practically accelerated through the secondary hump speed.

3.4. Sea-keeping

Sea-keeping is the term applied to the ability of a water-borne vessel maintaining a desired speed when encountering water waves (Korvin-Kroukovsky, 1961). A vessel's sea-keeping ability is subject to: the nature of sea waves; the hydrodynamic forces arising from the interaction of the sea waves and the vessel hull; and the response of a vessel to those forces. The most common phenomena that adversely affect a ship's sea-keeping are: excessive rolling motions of the ship (Conolly, 1974); excessive vertical accelerations of the ship (Sariöz & Narli, 2005); the ship's hull striking the water surface after broaching the water

surface (hull slamming) (Comstock, 1967); and partial submergence of the ship, leading to large amounts of water arriving on the deck (deck wetness) (Faltinsen, 1993). Comstock (1967) gives the direct causes of a vessel's undesired reduction in speed as: increased resistance to forward motion; survivability (the risk of mechanical failure of the vessel's structure and critical systems); operability; and habitability (the ability of the ship to provide a safe environment for humans and an appropriate level of comfort, given the crew and passenger expectations and desire to perform tasks).

The increased resistance in a seaway is primarily due to hydrodynamic effects of the relative motion of the ship hull and surrounding water. The vertical oscillations of an air cushion vehicle may increase its wave making drag (Tatinclaux, 1975).

Survivability refers to the integrity of ship structures affected by the overall acceleration of the ship as a rigid body, and bending moments induced on the ship by wave action and extreme localized loading caused by deck wetness or hull slamming. This is not to be confused with the survivability of military ships, which depends on explosions and such.

Operability issues include the ability of machinery to carry out assigned tasks whilst subject to wave induced motion. This is largely dependent on overall vessel acceleration, though displacement and velocity may have some effect. Deck wetness may affect some machinery.

Habitability is the ability of the vessel to be a safe and comfortable environment for human activity. The primary cause of unsatisfactory habitability is vertical accelerations (mainly caused by heave motions, with contributions from roll and pitch motions) (Sariöz & Narli, 2005). The effect of vertical accelerations on humans has been investigated in depth and an international standard exists for the relationship between exposure to vertical accelerations and the debilitation of humans (Standards Australia, 2001). O'Hanlon and McCauley (1975) used laboratory experiments to find that that ship vertical motion was the only ship motion that contributed to motion sickness (Bles et al., 1998). However, Wertheim et al. (1998) investigated the effect of roll and pitch on seasickness and concluded that roll and pitch can worsen the effect of heave on human discomfort.

Two other significant causes of habitability issues are hull slamming and deck wetness. Hull slamming may have a subjective psychological effect on the ship's controlling officer, leading them to choose to slow the vessel to reduce hull slamming, even though structural considerations don't warrant it Conolly (1974). Deck wetness (typically caused by a wave striking the ship, or the ship plunging into a wave) affects habitability by impeding people travelling across deck as well as potentially making living quarters uninhabitable.

3.5. Parameters for Conceptual Design Tools

The practical method for applying the Conceptual Design Tools (Sec. 3.1)) used published accounts of real SES performance and failures. A series of papers were identified as being useful sources of data. To be useful, the data needed to be based on real observations, but applicable to the general SES concept, not restricted to a specific design or prototype. The three main papers were reviews of the SES technology; as such they were all much longer than a normal peer-reviewed paper (Butler, 1985; Eggington & Kobitz, 1975; Lavis & Spaulding, 1991). Only one was peer reviewed in a journal, the others being book chapters. To complement these three major papers, a further five relevant papers were identified. The complementary papers were chosen to update the information or to cover gaps. The

gaps to be covered were the Royal Norwegian Navy use of SESs (Instefjord et al., 1996), recent studies on the Japanese Techno Super Liner project (Matsumura et al., 2006; Sugai & Yamaguchi, 1991b) and investigations conducted in the USSR that were not available to Western researchers until the end of the cold war (Lavis & Forstell, 2008; Pustoshny & Rusetsky, 2006).

Each paper was analysed and every time an author used a word or phrase that was useful, the source was quoted in a simple database along with the source paper, the page name and any notes to aid categorisation. Preliminary categories were assigned as the data was recorded; these were then revised for errors of understanding or data entry errors. The data table's format allowed the data to be sorted or filtered by field.

The categories used are in two groups: categorising the entries by general type and categorising within their type. Types of entries were:

CRs Customer Requirements
EAs Engineering Attributes
FMs Failure Modes

The CRs did not require any further categorisation. The EAs needed two further categories, the system and sub-system on the SES that they pertained to (unless they describe the SES in its entirety) and the type of EA. The research distinguished between Performance Measures (PMs), Design Variables (DVs), Design Parameters (DPs) and Constraints (CTs) (Dieter & Schmidt, 2009). PMs describe the behaviour of the SES in quantifiable terms. DVs are attributes that can be directly controlled by the SES designer. DPs are attributes that can be indirectly modified by the SES designer. Constraints are limits on design freedom.

The data was further analysed by identifying entries that meant the same thing (either suggested by different authors or repeated by an author within the source), a final title was given to each field, enabling the frequency of CRs, EAs and PMs to be counted. The original data was preserved whilst categorisation was applied, allowing the sources to be checked, or the categorisation to be undertaken by an independent researcher. The analysed data is reproduced in full in Table B.1.

- Lift System: Fan; Control; Duct; Plenum
- Propulsion System: Engine; Drive Train; Propulsor; Control
- Hull System: Side-hulls; Centre Body; Structure; Accomodation

In summary, the method followed was:

1. Read through papers describing the design and operation of SESs
2. Note the parameters, with source, page number. Only quote parameters specifically referred to, and try to quote author's own words, to minimize inference.
3. Categorise the parameter as an Engineering Attribute (EA), Customer Requirement (CR) or Failure Mode (FM)
4. Categorize which system the parameter is associated with (see list below)
5. Extract parameters in this way from all relevant papers – do not skip or infer from previous papers
6. Use categories to identify possible synonyms used by the authors
7. Identify overlapping parameters (usually general versus specific parameters)

8. Reconcile overlapping parameters into convenient single parameters
9. Count the frequency that parameters are used and rank them in importance accordingly
10. Analyse the most important CRs and EAs using the House of Quality tool
11. Categorise FMs according to type: component-specific or general
12. Analyse the most important component-specific FMs using the FMEA tool
13. Analyse the most important top-level FMs using the FTA tool

A total of 707 fields of various kinds were recorded from the source material (Table 3.1). The majority are EAs. The EAs used in the HoQ analysis were all mentioned more than twice and were also either PMs or were ship related DVs and DPs (Table 3.2).

Table 3.1. Count of parameters found in source texts by category

Category	Count
CR	135
EA	506
FM	66
Total	**707**

Table 3.2. Count of Engineering Attributes found in the analysed texts

Engineering Attribute	Count
Heave motion attenuation	13
Side-hull Drag	11
Installed Power	11
Pitch motion attenuation	9
Total resistance	8
Length	8
Cushion Wave-making Drag	7
Lightship Weight	7
Static Stability	6
On-Cushion Draft	6
L/B Ratio	6
Lift Power	6
Deck Area	5
Roll motion attenuation	5
Cushion Height	5
Roll Stability	4
Propulsive Efficiency	4
Machinery Accommodation volume	4
Cushion Pressure	4
Off-Cushion Draft	3
Beam	3
Yaw Stability	3
Side-hull Displacement	3
Fuel Load	3
Cushion Air Flow Rate	3
Full Load Displacement	3
Cushion Width	3
Producibility	3
Total	156

3.6. House of Quality

The House of Quality (HoQ) is a tool within the Quality for Deployment (QFD) framework. It compares the CRs to the EAs. The CRs are assigned priorities relative to each other, target values for EAs are set and provision is made to compare the engineering artefact to similar artefacts (Dieter & Schmidt, 2009).

The elements of the House of Quality that can be determined within the scope of the current research are: Customer Requirements (CR), Engineering Characteristics (EC), Relationship matrix and Correlation matrix

The other elements require access to information that is specific to a manufacturer and customer and are outside the scope of the current research.

The data was prepared for analysis using the HoQ. EAs that were categorised as belonging to the SES as a whole were used for subsequent analysis; other EAs were filtered out at this stage. The frequency of the EAs in the sources was counted and EAs with more than two entries were identified. CTs were filtered out at this stage as they are not relevant to a HoQ analysis. This data was then used as the EAs for the HoQ analysis.

The CRs for the HoQ was sourced from the literature review in Chapter 2 describing trends in transportation within the context of agile supply chains in Southeast Asia. These CRs were compared to the CRs mentioned in the source papers and found to be compatible. The source material contained some irrelevant CRs (such as those pertaining to military applications) and mostly had CRs that were too generalised or had been expressed in quantified terms, as is typical when adapted for use by engineers. These CRs had been used in a preliminary investigation using the Pugh Concept Selection Method.

The HoQ analysis was carried out (Fig. 3.4), with priorities assigned to the CRs, direction of improvement and units were assigned to EAs, relationships (low, medium, high) assigned to the EA-CR relationship and correlations between EAs quantified (low, medium, high). In both the relationship and correlation matrix, the relationship was identified as direct or inverse (Leary & Burvill, 2007). The ranking of the EAs was calculated (using the absolute value of the correlation matrix) and the most important EAs were identified (Table 3.3).

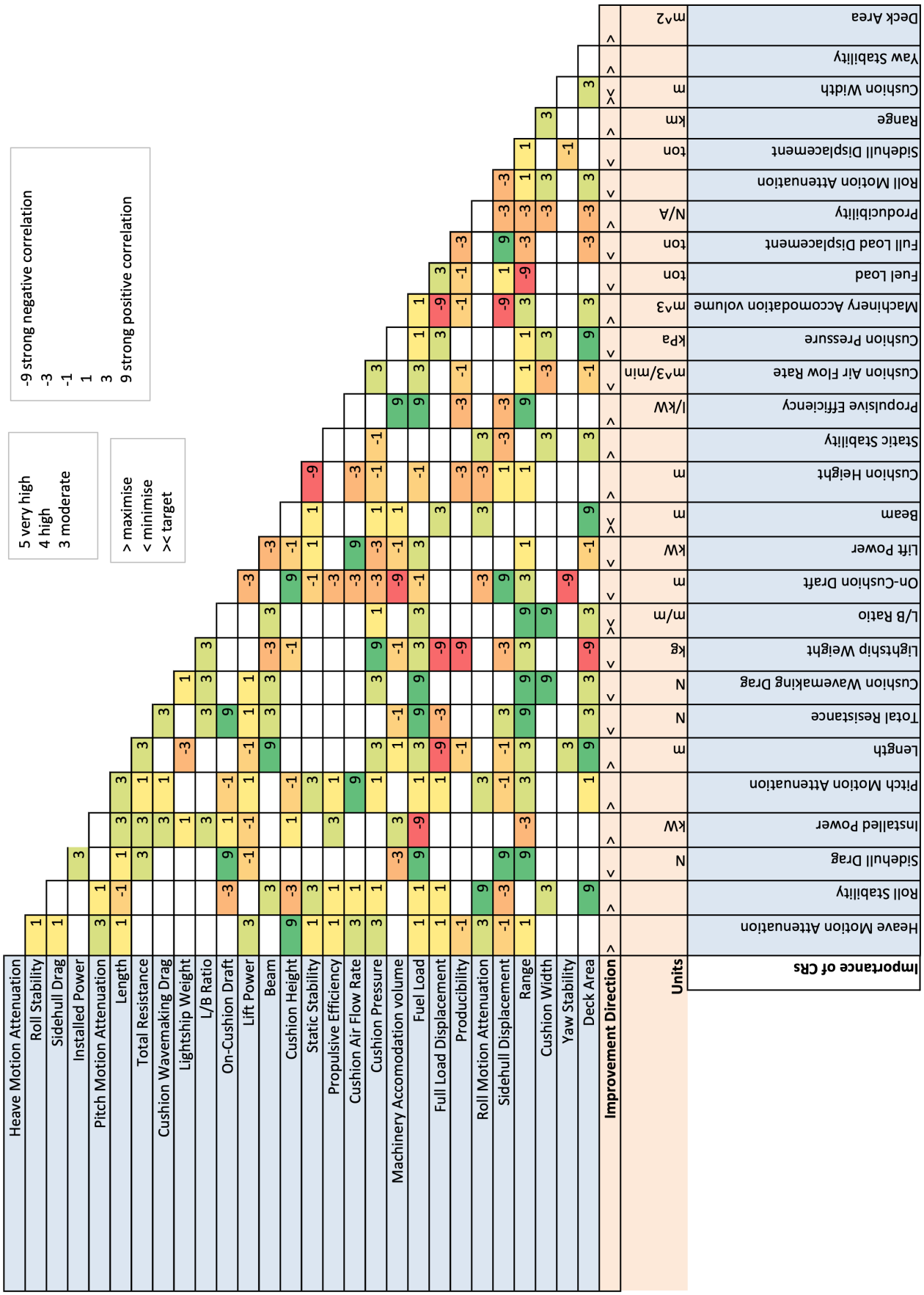


Figure 3.4. House of Quality analysis for Surface Effect Ships in general.

Table 3.3. Prioritised EAs as indicated by the HoQ analysis

Rank	EA
1	Pitch Motion Attenuation
2	Cushion Height
3	Deck Area
4	Heave Motion Attenuation
5	Yaw Stability

3.7. Failure Mode Effect Analysis

The Failure Modes (FMs) were categorised by the component they pertained to, if any. The ones that pertained to a component formed the basis of a Failure Mode Effect Analysis (FMEA) and the others formed the basis of a Fault Tree Analysis (FTA).

The components were identified in the categories and source material generally identified the mode of failure and the subsequent effect. The source material often described the mitigations that were undertaken in practice, allowing a mitigation and relevant 'Risk Priority Number' (RPN) to be entered. The ratings for Severity (S), Occurrence likelihood (O) and Detection likelihood (D) were assigned based on the source material. The RPNs were then calculated and the most important failure modes thus identified. The results of the analyses are given in Appendix C.

The component with the most failure modes was the bow seal fingers. The mitigation measures reported in the available literature were effective in lowering the RPN to non-critical values. Based on the successful mitigation of this failure mode and the absence of subsequent reports of this type of failure occurring in more recent SESs, it is likely that this failure mode can be prevented in practice.

Based on this analysis, there are no failure modes currently known that would prevent the further practical application of SESs. The International Code of Safety for High-Speed Craft (International Maritime Organization, 1995) recommends that FMEA is used in the design of high-speed craft and be reported as part of the safety certification process.

3.8. Fault Tree Analysis

The Fault Tree Analysis (FTA) was used to study SES ship-level failures. The FTA is a type of logic diagram that shows the relationship between failure mechanisms, failure modes and failure effects in increasing levels of detail (Vesely et al., 2002). Ship-level failures affect the entire SES and may be caused by a combination of root causes. The FTA shows the sequence and combination of root causes that may lead to a specific ship-level failure. Studying the SES ship-level failures contributes to studying the suitability of the SES for use in carrying freight in Southeast Asia.

The FTA was applied in a methodical and rigorous way. The data analysed in the FTA was sourced from the survey of relevant literature as previously described. During that survey, several failure modes were classified as 'ship-level'. These were assessed for the importance of the failure by placing them in a 'failure space', as described by Vesely et al. (1981, pp. III-1 to III-3). Failure modes that exceeded the maximum tolerable failure were considered for further study using the FTA (Fig. 3.5). FTA diagrams were created by methods described by Vesely et al. (1981, pp. V-8 to V-11). Some other failure modes identified in the original survey were found to be contributing mechanisms to the failures modes being studied. In this way, most of the failure modes identified in the survey were also identified by application of the FTA. In this way, the FTA was applied to data that was present in the available literature in a systematic and repeatable way.

Of the four failure modes that exceeded the maximum tolerable failure were considered for further analysis; only the 'uncomfortable accelerations in moderate sea states' failure mode was of interest for further investigation. The 'capsize whilst turning' failure mode is based on one reported capsize event, which was found to be caused by design inadequacies

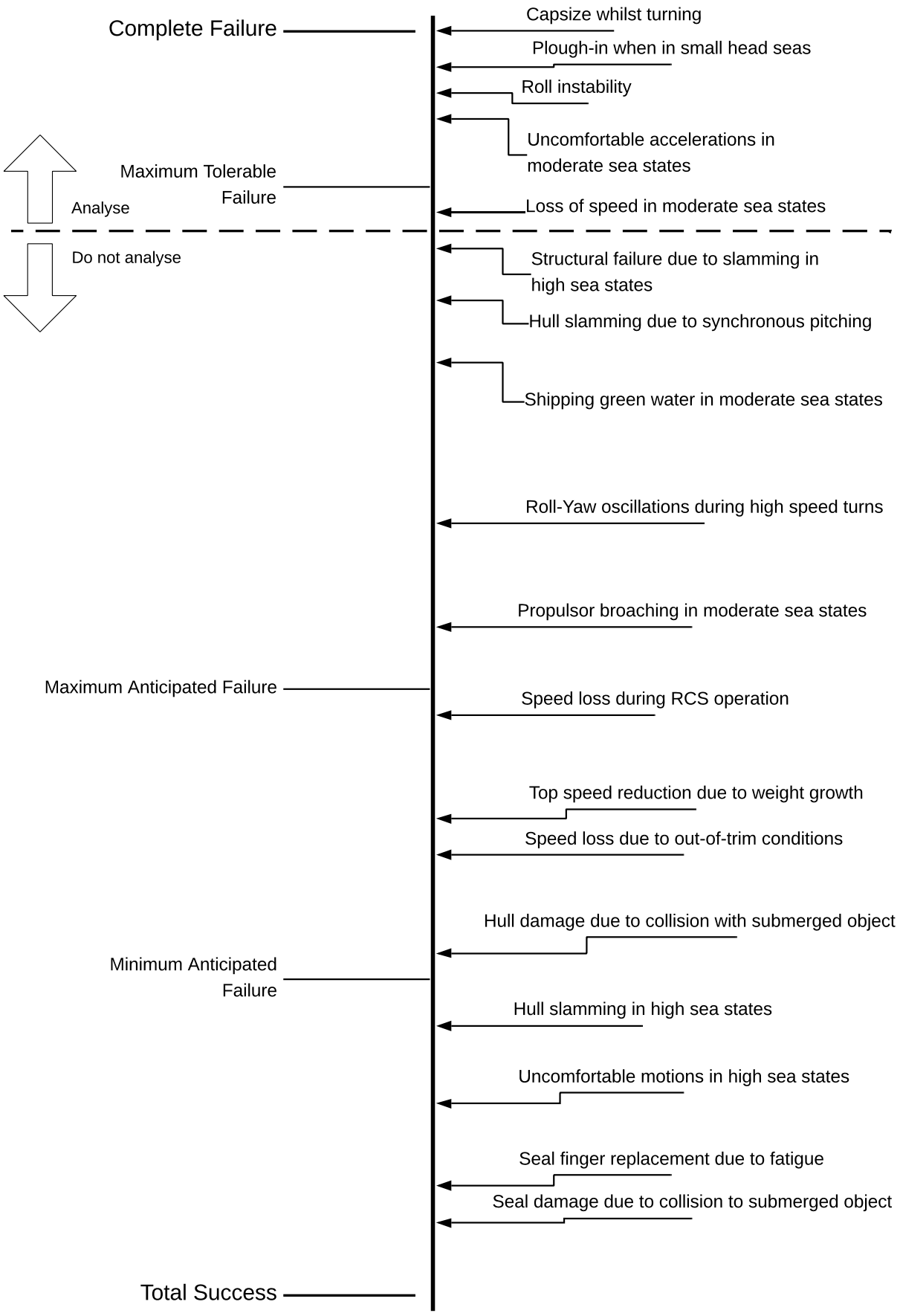


Figure 3.5. Failure Space for SES

which were corrected (Butler, 1985; Eggington & Kobitz, 1975; Lavis & Spaulding, 1991). As no publicly available publications indicate that this failure mode is a problem for current SES designs, it is not investigated further. The 'plough-in' in small head seas failure mode has also been rendered very unlikely by new designs of SES bow seals; therefore, this failure mode is not investigated at this time (Eggington & Kobitz, 1975). Roll instability was reported for an early prototype of the SES. Since the instability was corrected through design changes (Eggington & Kobitz, 1975), roll instability is not investigated. Only the 'uncomfortable accelerations in moderate sea states' failure mode was of interest for further investigation.

A Fault Tree Analysis was undertaken of the 'uncomfortable accelerations in moderate sea states' failure mode. Three main causes were identified: excessive forces due to water-hull interactions (Fig. 3.6), failure of air cushion pressure regulator mechanisms (Fig. 3.7), and excessive forces due to air cushion pressure (Fig. 3.8).

The root causes of the excessive heave accelerations are of interest and practical importance.

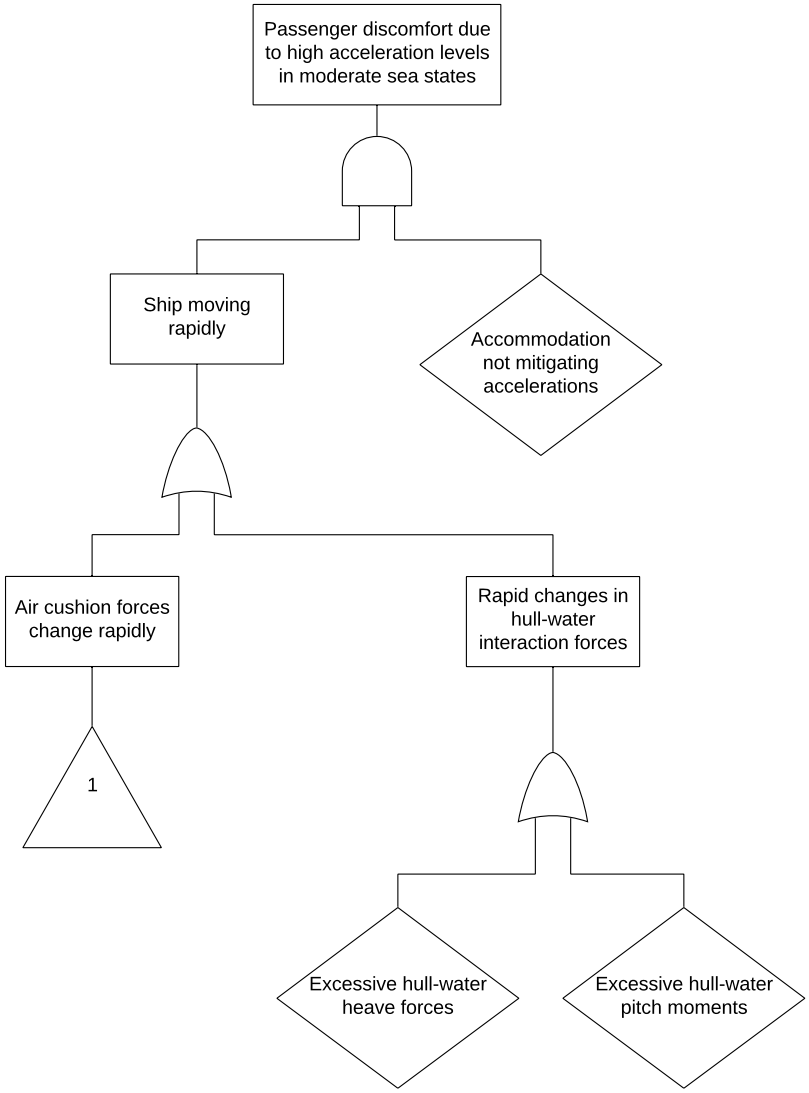


Figure 3.6. FTA part 1 for the 'uncomfortable accelerations in moderate sea states' failure mode

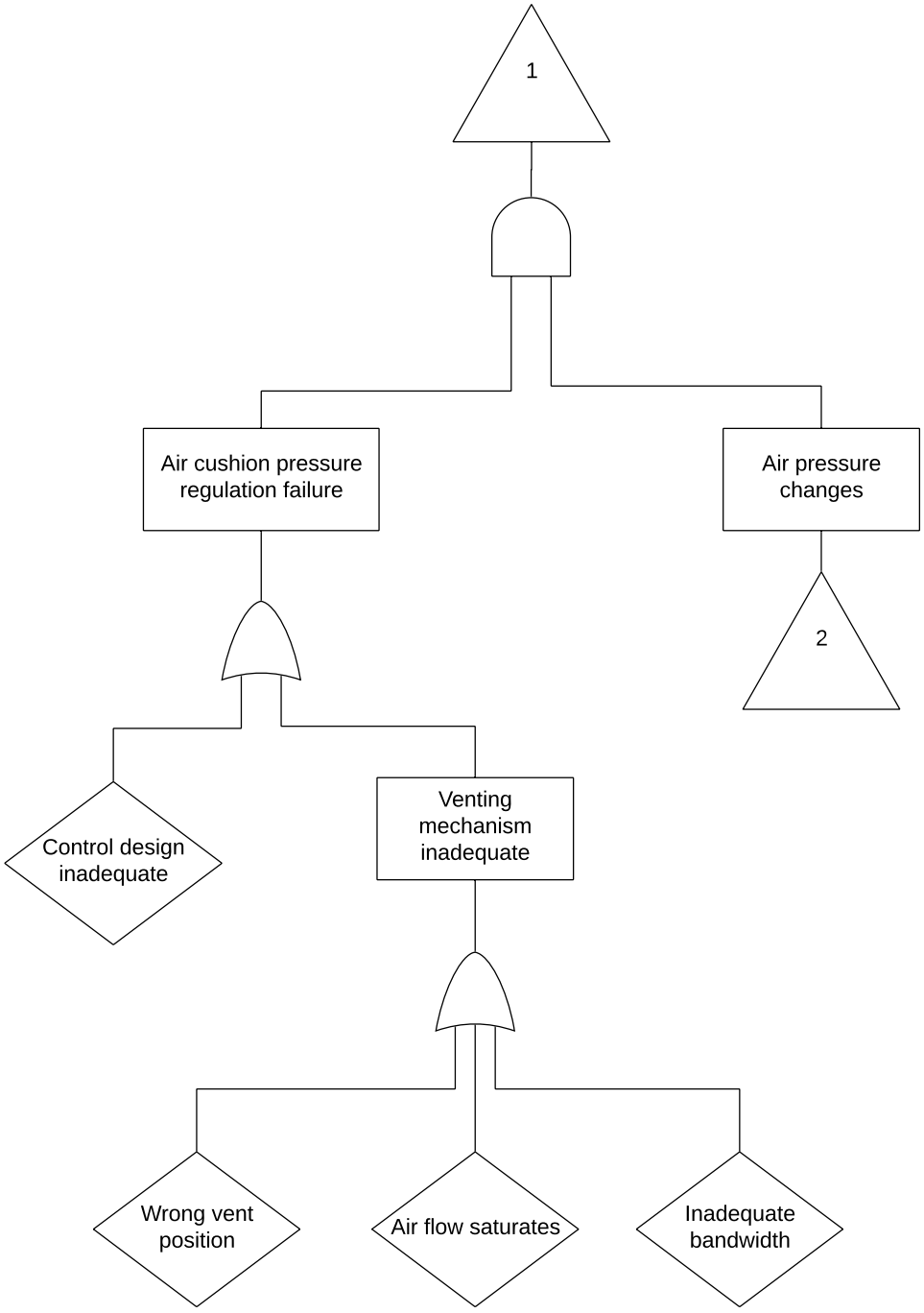


Figure 3.7. FTA part 2 for the 'uncomfortable accelerations in moderate sea states' failure mode

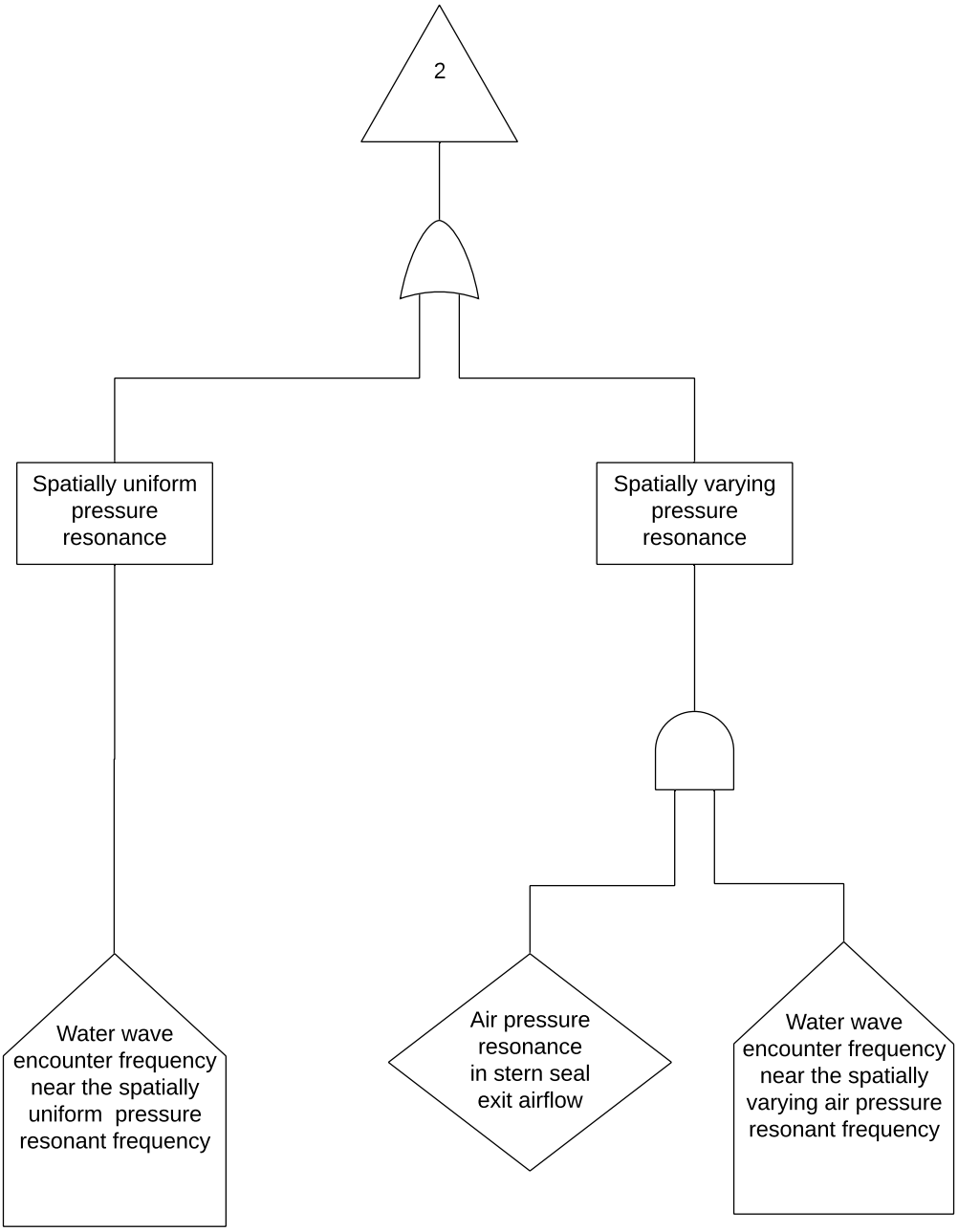


Figure 3.8. FTA part 3 for the 'uncomfortable accelerations in moderate sea states' failure mode

3.9. Concluding remarks

After a review of the characteristics of the SES performance, a series of analyses was conducted using conceptual design tools. The House of Quality, Failure Mode Effects Analysis and the Fault Tree Analysis tools were useful to gain insight into the question as to the viability of the SES as a practical concept.

There is no evidence that the SES cannot be designed to meet the CRs to a satisfactory level of quality.

There is no evidence that component-level failures would prevent the SES concept being applied to carrying freight in Southeast Asia.

The top-level failure mode that is worthy of further study is the 'uncomfortable accelerations in moderate sea states' failure mode. Several failure mechanisms that contribute to the 'uncomfortable accelerations in moderate sea states' failure mode are worthy of further investigation.

- The uniform pressure dynamics in the air cushion
- The spatially varying pressure dynamics in the air cushion
- The design of a air cushion pressure regulator
- The air flow dynamics under the stern cushion seal

4. Dynamic Motions of Surface Effect Ships

4.1. Introduction

In Chapter 2, design parameters that are important to the successful design of Surface Effect Ships (SESs) were identified. In Sec. 3.6, the House of Quality tool (HoQ) was used to show that attenuation of heave accelerations will be important to designing a SES of satisfactory functionality. The investigation in Section 3.8, found that failure to attenuate the accelerations caused by interactions with water waves could lead to 'passenger discomfort due to high acceleration levels in moderate sea states'. Therefore, the current chapter investigates the attenuation of vertical accelerations.

Regulating the accelerations that affect passengers, crew, cargo and the SES hull and machinery is an important consideration when designing a SES. The term 'regulating' comes from the field of control system engineering and refers to 'keeping a system output steady while the system is experiencing unknown disturbances' (Franklin et al., 2010, p.0)[1]. In this thesis, the system output corresponds to the accelerations of the SES, and the unknown disturbances are forces caused by the SES interacting with water waves. The desired accelerations of the SES are less than the level that will discomfort passengers; however, some acceleration is necessary for the SES to manoeuvre. It is claimed that SES have good sea-keeping in large amplitude water waves, due to attenuation of vertical motions through the action of the air cushion (Butler, 1985; Lavis & Spaulding, 1991; Matsumura et al., 2006; Sorensen & Egeland, 1994). However, Faltinsen (1993, 2005b) suggests that uncomfortable vertical accelerations of SESs result from 'resonant compressible effects in the air cushion'. Faltinsen (1993) uses the term 'cobblestone oscillations' to describe this phenomenon. This thesis reports into research into the origin of cobblestone oscillations.

A comprehensive review of available literature relevant to the regulation of SES accelerations is presented in this chapter. Literature was reviewed on the following relevant topics: dynamics and hydrodynamics of SESs, airflow through air cushion systems, the effect of whole-body accelerations on human comfort and, the design of air pressure regulation systems for air cushion vehicles. The aim of this literature review was to study the current knowledge concerning the regulation of SES accelerations. For brevity, the word 'ship motions' will be adopted to mean a physical phenomenon that causes whole-body accelerations of the SES.

This literature review is organised into the following sections:

- Sec. 4.2 an overview of the literature
- Sec. 4.3 empirical observations of ship motions on SESs
- Sec. 4.4 analysis of air cushion pressure

[1] Franklin et al. (2010) has a page zero.

- Sec. 4.5 other aspects of SES dynamical analysis
- Sec. 4.6 control system design of acceleration regulators
- Sec. 4.7 a detailed review of the principal mathematical model from the available literature

4.2. Overview of the literature on SES dynamics

Of the available literature, three papers specifically address the design of SES acceleration regulators. Kaplan et al. (1981) discusses 'Ride Control System' (RCS) design as part of a more general discussion of SES dynamics and hydrodynamics. Sorensen and Egeland (1995)[2] present a method for designing a RCS using dissipative control. Bertin et al. (2000) presents a method for designing a RCS using a method of decoupling. Kaplan et al. (1981) is cited by Sorensen and Egeland (1995) and also by Bertin et al. (2000).

Reviewing literature more broadly resulted in additional papers of some relevance being identified. These papers do not focus on SES or RCSs but are concerned with issues such as: air cushion vehicle (ACV) heave motions, ACV heave stability, dynamics of air cushion systems and motions of other types of advanced marine vehicles. In total, 53 papers of relevance were identified. Of these, 28 papers were arranged into three principal groups according to research initiatives and left 25 papers ungrouped. The three principal groups had direct links between researchers within each group and a clear research focus. The ungrouped papers are relevant to the current research program, but had no direct link to one of the three principal research initiatives. The groups were named after the related research program or institution: the U.S. Navy group (spanning work done by the Joint Surface Effect Ship Project Office, the Surface Effect Ship Project Office and NavSea PMS 304); the UTIAS group (University of Toronto, Institute for Aerospace Studies, Toronto, Canada); and the NIMT group (Norwegian Institute of Marine Technology, Trondheim, Norway).

The U.S. Navy group was primarily concerned with designing SESs for maximum speed and size (Lavis & Spaulding, 1991). Problems of static stability, cornering stability and ride comfort were addressed. This group was active from the 1960s through to the early 1980s. Much of the group's work is not publicly available, but three review papers make some of the research outcomes publicly available (Butler, 1985; Eggington & Kobitz, 1975; Kaplan et al., 1981).

The NIMT group is based at the Trondheim maritime research facility in Norway. Their concern was seakeeping on SESs of moderate size (around 35 m in length) and operating at moderate speeds (40 kn to 60 kn)[3] (Faltinsen, 1991, 1993). This group researched cobblestone oscillations , with an emphasis on spatially varying cushion pressure (Sorensen & Egeland, 1994) and the effects of flexible bag stern seal (Hirata & Faltinsen, 2000; Steen & Faltinsen, 1995).

The UTIAS group addressed the static heave and pitch stability of hovercraft (not SESs) operating over land and water using laboratory experiments of air cushion systems constrained to one degree of freedom of motion, i.e. vertical or heave (Graham et al.,

[2]The spelling in Norwegian is Sørensen. However, as many citations and databases of academic literature use the anglicised spelling 'Sorensen', the anglicised spelling is used in this thesis.

[3]The conventional nautical unit of speed is the 'knot', which is 1 nautical mile per hour, it is abbreviated kn and is equal to $1.852\,\mathrm{km\,h^{-1}}$.

1985; Hinchey, 1982, 1983; Hinchey & Sullivan, 1981; Sullivan et al., 1993). The research emphasis reflects the Canadian interest in ACVs as amphibious utility vehicles in the Arctic regions of Canada. The UTIAS group formulated a mathematical model to investigate the effects of ducts (Hinchey & Sullivan, 1977, 1981; Sullivan et al., 1982). The model was later extended to include the effects of skirts (Graham & Sullivan, 2002; Graham et al., 1985) and the interaction with the water surface (Sullivan et al., 1993). The analysis is compared to empirical observations gathered using heave table apparatus (Graham et al., 1983; Hinchey & Sullivan, 1981; Sullivan et al., 1994; Sullivan et al., 1982). The UTIAS group investigated hovercraft and used heave table apparatus to make empirical observations of small models, so some of their conclusions may be inapplicable to SES. However, the assumptions made by the group were tested against empirical observations. It was concluded that the work of the UTIAS group must be considered in any SES investigation.

One of the ungrouped papers directly addresses the design of SES RCS (Bertin et al., 2000). Another covered the resistance of SES (Oehlmann, 1991). Several papers cover the stability of air cushion systems used as suspensions on tracked vehicles (Hrovat & Margolis, 1981; Hullender et al., 1972; Margolis et al., 1975; Sweet & Richardson, 1976; Sweet et al., 1975). Two papers covered similar dynamics of other types of high speed ship (Davis et al., 2004; Vassalos et al., 2007). Four papers are from early British researchers into hovercraft dynamics (Reynolds, 1971, 1974; Reynolds & Brooks, 1977; Reynolds et al., 1972). Two papers were reviewed from the Japanese 'Techno Super Liner' program, reporting on simulations, model tests and sea trials of large (70 m to 140 m) and moderately fast ($\approx$ 40 kn) SESs (Matsumura et al., 2006; Sugai & Yamaguchi, 1991b). Several papers dealt with ship motions (not necessarily SES) that cause discomfort to humans (e.g. Davis et al., 2004; Fang & Chan, 2007). Other papers from individual researchers dealt with the dynamics of hovercraft (e.g. Pozzi et al., 1993).

4.3. Empirical observations of ship motions on SESs

This section reviews empirical observations of ship motion phenomena on SESs. In this thesis:

- Empirical observations are taken to mean observations done with instruments in controlled conditions and reported in a way that enables others to replicate the results.
- Ship motion phenomena on SESs are taken to mean any periodic SES whole-body motions that are related to accelerations experienced by passengers, crew, cargo and machinery on-board the SES. Accelerations caused by machinery vibrations are excluded, only ship motions caused by the SES's interaction with water waves are considered.

Sorensen and Egeland (1994) report on an empirical study that is important to the current research. The paper:

- is directly concerned with damping of heave accelerations on a SES
- reports empirical observations of the accelerations on board a prototype SES in real sea conditions

- reports some aspects of the experimental method and presents results in a form that are sufficient for qualitative comparison

No other paper in the available literature has this combination of direct relevance, empirical method and detailed reporting of the experimental method. Sorensen and Egeland (1994) present three important results:

- the presence of resonance in the SES heave accelerations
- the presence of resonance at multiple frequencies
- evidence that the air pressure in the air cushion varies across the volume i.e. 'spatially varying'

Sorensen and Egeland (1994) used a single accelerometer mounted 5 m aft of the SES centre of gravity to observe the whole-body acceleration of a 35 m long prototype SES. The output of the accelerometer is reported in the form of spectral power density. Sorensen and Egeland (1994) reported resonance at 2 Hz, 5 Hz and 8 Hz at the position 5 m aft of the SES centre of gravity. A pressure sensor was mounted 10 m forward of the SES centre of gravity, a power spectrum of excess pressure shows resonance at 2 Hz and around 5 Hz. Sorensen and Egeland (1994) report that the sea states were estimated to be in the range 300×10^{-3} m to 600×10^{-3} m. The resonance at 2 m is attributed to the 'resonance of the dynamic uniform pressure'. Similarly, Kaplan et al. (1981) reported that a 40 m prototype SES experiences resonance in the heave accelerations at a frequency of 1.8 m. However, the precise source of Kaplan's data is unclear. Sorensen and Egeland (1994) did not report: the method of determining the SES centre of gravity; the type of sensors used; the precise mounting position; or, any means of isolating the instruments from other sources of vibration — making it possible that other forms of resonance (such as resonance of structural members or vibrations caused by machines on board the SES) were observed instead of whole-body SES ship motions. While not conclusive, the evidence presented by Sorensen and Egeland (1994) and Kaplan et al. (1981) does support the hypothesis that SESs experience resonance in the air cushion system in small water waves.

Sorensen and Egeland (1994) reported resonance in the SES whole-body accelerations and cushion pressure at several frequencies, whereas Kaplan et al. (1981) assumed that only spatially invariant pressure is present in the air cushion and did not report any observations of acceleration or pressure variations above a frequency of 4 Hz. Kaplan's experimental data is sourced from a number of model tests in tow tanks, small prototype tests in real sea conditions, and observations of a 100 ton (90.7 t) SES in real sea conditions, these were smaller than the prototype SES described in Sorensen and Egeland (1994) and therefore they may not have experienced resonance at multiple frequencies. The available literature contains no empirical evidence refuting that resonance was observed at multiple frequencies, as published in Sorensen and Egeland (1994).

Sorensen and Egeland (1994) conducted an experiment to test the hypothesis that the resonance observed at high frequencies (5 Hz and 8 Hz) were due to spatially varying pressure. The prototype SES had an air cushion vent (a louvre mechanism) located near the air cushion pressure sensor 10 m forward of the SES centre of gravity. A second air cushion pressure sensor was located 10 m aft of the SES centre of gravity. A RCS was configured so that either of the pressure sensors, in combination with the accelerometer, could be used to control the air cushion vent. The results show that when the pressure sensor and the vent were collocated, the resonance was attenuated; however, when the

sensor and the vent were not collocated, the resonance at 5 Hz and 8 Hz worsened (the resonance at 2 Hz was still attenuated). Sorensen and Egeland (1994) suggests that this is because the air cushion pressure is spatially varying, meaning that the pressure sensed at the non-collocated sensor was different to the pressure at the vent. Results for the pressure observations at the two locations were not reported. No other paper in the available literature presented empirical (or theoretical) evidence to confirm or refute this claim.

Sorensen and Egeland (1994) demonstrated a good match between a theoretical prediction of the resonant frequencies and the experimental observations. The small discrepancy in the predicted frequencies is attributed to the effect of the flexible stern seal, but no empirical evidence is presented to support this assertion.

The theoretical prediction of the effect of the spatially varying air cushion pressure indicates that positioning the air feed fan at one end of the air cushion would have a positive effect on the damping of air pressure resonance (Sorensen & Egeland, 1994). This prediction is not tested empirically.

A notable theoretical outcome reported by Sorensen and Egeland (1994) is that the spatially varying pressure does not contribute directly to the heave motion of the SES as it is symmetrical about the geometric centre of the cushion . Vertical motions of the SES are also caused by pitching motions, which the spatially varying air cushion pressure does have an effect on through its odd modes.

Kaplan et al. (1981) presented important studies which included empirical observations made by other researchers. Kaplan et al. (1981) describes a numerical simulation in six degrees of freedom (the motions of the SES as a rigid body) and compared the results with various empirical observations from several sources. The experimental data referenced in Kaplan et al. (1981) was sourced from tests on a 1/7 scale model of the XR-1C test craft in regular-wave conditions made by the David Taylor ship basin and from prototype tests made on the XR-3 test craft and a variant of the XR-1B test craft. The availability of the data through the US Navy public access program was checked, but it was not available. The sources referenced by Kaplan et al. (1981) are reputable and the appropriate use of the data is confirmed in the peer reviews of their work, published alongside the paper. The validation process described in Kaplan et al. (1981) supports the hypothesis that a resonant frequency is present for SES heave accelerations. The results also support the hypothesis that a ride control system can positively affect the damping of SES heave accelerations. The work described in Kaplan et al. (1981) is of limited use as it does not report the original experiments in full. The models used were of varying configurations and may not represent the mechanical systems used on current SESs, particularly the designs of the various seals used. The behaviour of the air cushion depends on absolute pressure (Kaplan et al., 1981; Sorensen & Egeland, 1994). As the model results are scaled using a Froude number, but the atmospheric pressure stays constant, phenomena affecting prototype SESs may not affect models called in this way.

Matsumura et al. (2006) report on the simulations, model tests and sea trials of a 140 m SES designed and built by the Japanese 'Techno Super Liner' program. Their paper reports that a ride control system (RCS) was used on the prototype design. The research did not consider spatially carrying air cushion pressure, but the authors do cite the research into spatially varying air cushion pressure reported in Sorensen and Egeland (1994). The paper also cites Kaplan as a source for the modelling of the SES motions. This paper presents some illustrative results of model tests that may support the presence of resonance in the air cushion system, but the results lack full quantification and are

therefore inconclusive. Matsumura et al. (2006) asserts that the prototype SES did not experience excessive vertical accelerations during sea trials and the RCS had some effect in reducing vertical accelerations. This paper provides some support for the hypothesis that resonance occurs in a prototype SES air lift system, but is inconclusive.

Several researchers assert that the inlet fan can act to damp cushion resonance (Butler, 1985; Kaplan et al., 1981; Sorensen & Egeland, 1994) and that the fan characteristic must have a negative slope for damping to occur (Kaplan et al., 1981; Matsuo & Matsuo, 1980; Sorensen & Egeland, 1994). However, the available literature contains no empirical studies of unsteady flow through SES inlet fans.

Resonance in the ducts leading from the fan to the air cushion may have an effect on heave stability (Sullivan et al., 1982). Sullivan et al. (1982) reports the use of a model hovercraft on a heave table apparatus with the air cushion supplied with air from a fan through a duct. Sweet et al. (1975) also observed duct effects using a heave table apparatus. The available literature does not report any investigation of duct effects on SESs, or large prototypes of ACVs.

Sullivan et al. (1994) suggested that bag-and-finger skirts (this type of seal design is current practice on SESs) have an effect on the heave stiffness of a hovercraft. Sullivan et al. (1994) describes the use of a heave table apparatus to empirically observe the effect of varying the bag and finger geometry on the heave stiffness of the air cushion system.

Sullivan et al. (1993) report observations of Kelvin-Helmholtz wave generation beneath the skirts of a hovercraft. The observations were made using a model skirt suspended above the water surface and introducing airflow underneath the skirt. Unstable water waves were generated, which could have an adverse effect on air cushion stability. There is no evidence in the available literature that this phenomenon has been studied on a SES.

Several researchers studied air cushion suspensions for use on tracked air cushion vehicles, (e.g. Hrovat & Margolis, 1981; Margolis et al., 1975). These researchers used heave table apparatus to simulate dynamic motions of the vehicles in laboratory conditions. The tracked air cushion vehicle uses a channel as a track to guide the vehicle and a air cushion to support the vehicle within the channel. The tracked air cushion vehicle uses a thinner air cushion (a few centimetres thick) than used on the SES (metres thick). There is no evidence in the available literature that these studies have been applied to SESs.

The heave table apparatus used by the UTIAS group and by researchers in the tracked air cushion vehicle field employs a moving surface (the table), which is oscillated vertically. A model hovercraft is suspended above the heave table, constrained to move only vertically. The heave table can be used to activate a single seal, a cross-section of a hovercraft or an entire model hovercraft (Sullivan et al., 1994). Any empirical observations made using heave table apparatus must consider several factors which may make the results inapplicable to prototype SESs:

- The atmospheric pressure does not scale, therefore the model may experience phenomena that the prototype does not and vice versa
- Models constrained in one degree of freedom (heave motion) will not experience pitch motions, therefore spatially varying air cushion pressure may not be observable
- The types of seals used on early hovercraft may have very different effects on the cushion dynamics in comparison with seals used on prototype SESs
- Heave table apparatus cannot show the effect of rigid sidehulls on cushion sealing nor their contribution to supporting the SES

Further experimental work under controlled conditions is warranted to extend the knowledge in this field.

4.4. Analysis of SES air cushion pressure

This section critically reviews the available literature on the topic of analysing SES air cushion pressure, with the emphasis being air cushion resonance. Nineteen of the reviewed papers were concerned with airflow through the cushion. The analysis of SES rigid-body motions, airflow into the cushion, airflow out of the cushion and contribution of hydrostatic and hydrodynamic forces are discussed in Sec. 4.5.

Air in the SES air cushion is disturbed by the encroachment of water waves into the cushion space; for example, a decrease in cushion volume results in an increase in cushion pressure. Since the air cushion pressure supports around 80% of the SES weight (Butler, 1985; Eggington & Kobitz, 1975; Kaplan et al., 1981), variations in air cushion pressure have a significant effect on the SES dynamics.

4.4.1. The Reynolds model assuming incompressible air flow

Reynolds (1971) theoretically investigated the heave dynamics of an ACV travelling over sea. The work is theoretical, comprising only mathematical analysis, with no empirical investigations. The ACV studied was a hovercraft with no sidehulls and a cushion system that differed from SESs in having an extra chamber between the air supply fans and the air cushion. A brief chronology of Reynolds' work follows.

- Reynolds (1971) formulated a linear model of the ACV heaving response moving over regular water waves.
- Reynolds et al. (1972) considered pitching motions as well as heave.
- Reynolds (1974) extended the model to include two nonlinearities: the collapse of the seals against the water surface; and large variations from equilibrium conditions.
- Reynolds and Brooks (1977) further extended the model to include realistic air cushion planforms and seal deflection.

The Reynolds model of hovercraft heave motions in response to water waves assumes that air flow through the cushion is incompressible (Reynolds, 1971, 1974; Reynolds & Brooks, 1977; Reynolds et al., 1972). The assumption of incompressible air flow is based on assuming that the variations in air cushion volume are sufficiently slow so that the pressure is uniform throughout the air cushion and therefore the air density is constant. It is common to assume that gas flows with a Mach number of less than 0.3 may be treated as incompressible, as the maximum density variation is less than 5% (Fox & McDonald, 1998, p.38). In contrast, the other research groups reviewed assumed that the air is compressible (Hinchey & Sullivan, 1984; Kaplan et al., 1981; Sorensen & Egeland, 1995). The UTIAS research group present empirical evidence that is in good agreement with their analytical models. Sorensen and Egeland (1994) also present some empirical evidence from a SES prototype showing the effects of air compressibility. It was concluded that the Reynolds model is deficient because it neglects air compressibility. Reynolds conceded that air compressibility is a significant phenomenon:

> "In the interests of simplicity, we have neglected compressibility, but Doctors found that it has a marked influence on response for high wave-encounter frequencies." (Reynolds & Brooks, 1977)

4.4.2. Compressible Air Flow

This section will discuss the hypotheses of the UTIAS group, the US Navy group and the NIMT group with regards to compressibility of the air in the air cushion. It will be shown that all the groups that the compression of the air in the air cushion has a significant effect on the ACV dynamics and that the air compression is adiabatic[4]. The groups differ in how they treat air compressibility mathematically and their assumptions concerning other properties of the airflow. The following sections will critically review each group in chronological order: the UTIAS group, the US Navy group then the NIMT group.

4.4.2.1. Lumped Capacitance model

The UTIAS group formulated a mathematical model using a 'lumped capacitance approach' to model the effects of air compressibility. The lumped capacitance approach is normally used to model the effects of air compressibility on the flow of gases in pneumatic systems[5] (Ogata, 1990, p.192). The pressure of a gas within a pipe will vary along the length (a distributed parameter). To reduce the distributed parameter to a lumped parameter, the compressibility is used to form a 'capacitance' term Eq. (4.1). This approach is applicable when the diameter of the pipe is small compared to the length.

$$C_c = \frac{V_{ce}}{\rho a^2} \tag{4.1}$$

where C_c lumped capacitance
V_{ce} volume of the air cushion
ρ nominal density
$a = \sqrt{\gamma RT}$
γ ratio of specific heats
R ideal gas constant
T temperature of the gas

The UTIAS group assumed that a hovercraft air cushion could be considered pipe-like and used a lumped capacitance approach to model the hovercraft air cushion: the 'Lumped Capacitance Model' (LC model). The LC model assumes the air flow through the hovercraft air cushion is compressible and unsteady Eq. (4.2), p_c is the cushion gauge pressure, Q_c is the airflow into the cushion, Q_a is the flow through the hover-gap from the cushion to the atmosphere, $S_a \frac{dh}{dt}$ models the change in cushion volume, where h is the hover-gap between the skirt and the ground, S_a is the area acted on by the pressure in the vertical direction.

[4] An adiabatic process is one in which no heat is transferred to or from the fluid (in this case the fluid is the air in the air cushion) (Fox & McDonald, 1998).

[5] The lumped capacitance approach is sometimes referred to as 'transmission line analysis'

$$C_c \frac{dp_c}{dt} = (Q_c - Q_a) - S_a \frac{dh}{dt} \tag{4.2}$$

The use of a lumped capacitance model may not be valid. The lumped capacitance model is only justified when the effects of internal flows are negligible; this is most likely to apply when the cross-section of the air cushion is small compared to its length. The UTIAS group do present empirical observations that are in good agreement with their analytical results. However, the group uses small models which may not adequately replicate the behaviour of a prototype. The NIMT group present evidence that internal flows do have a significant effect on prototype SESs (Sorensen & Egeland, 1994), but their work is restricted to a single set of observations on a prototype SES in uncontrolled conditions. The lumped capacitance approach does provide a mathematical model in a linear form that is conducive to control engineering techniques. For control engineering purposes, a linear model need not be very accurate to be useful because a control mechanism could normally accommodate inaccuracies in the underlying model (Franklin et al., 2010).

4.4.2.2. Linearised Adiabatic Model

The US Navy group used a different approach to modelling the compressibility of the air in the air cushion. As with the UTIAS group, the US Navy group assumed that internal flows in the air cushion have a negligible effect: in other words, the air cushion pressure is spatially uniform (Kaplan et al., 1981). However, the US Navy group linearised the adiabatic gas law about the operating point Eq. (4.3) and combined it with the continuity equation for mass flow in and out of the air cushion, giving a 'Linearised Adiabatic' model (LA model). The LA model is in terms of absolute pressure, which cannot be readily scaled under laboratory conditions, whereas the LC model is in terms of cushion gauge pressure.

$$\frac{p}{(p_0 + p_a)} = \left(\frac{\rho_c}{\rho_a}\right)^{\gamma} \approx \left(1 + {}^{1}\!/\!_{\gamma} \frac{(\mu(t) p_0)}{(p_0 + p_a)}\right) \tag{4.3}$$

where p = dynamic cushion pressure (differential)
p_0 = equilibrium pressure in the air cushion (gauge)
p_a = atmospheric pressure (absolute)
ρ_c = dynamic air density
ρ_a = air density at equilibrium conditions
$\mu(t)$ = variations of gauge cushion pressure

The LA model was accepted by independent researchers. Sorensen and Egeland (1994) used the LA model to predict the spatially uniform cushion pressure without further investigation of its validity. Bertin et al. (2000) used the LA model for the spatially uniform pressure in a theoretical study of the control of air cushion pressure resonance in a large SES. Faltinsen (2005b) presented the LAS model as a means of estimating the frequency of spatially uniform pressure resonance for all SESs. Matsumura et al. (2006) used the LA model to model spatially uniform pressure resonance for a prototype SES. None of the available papers contain experimental validation of the LA model.

Validating the LA model is difficult. To validate the LA model properly, the model must be compared to a significant set of empirical observations. This may have been done

within the US Navy group, but validation results have not been made publicly available (as discussed in Sec. 4.3). Because the adiabatic expression is in terms of absolute pressure, and atmospheric pressure cannot be easily scaled for laboratory tests, using scale models to predict the behaviour of prototypes is, at the very least, a difficult exercise. The most scientifically robust means of validating the LA model is through experimentation on large models under controlled conditions. However, the available literature does not contain any report of such experiments. Furthermore, there is no evidence in the available literature that the linearisation of the adiabatic expression has been validated. It is concluded that the applicability of the LA model to SES dynamics is an open question.

4.4.2.3. Velocity Potential Model

The NIMT group extends the LA model by including the effects of spatially varying air cushion pressure. The NIMT group used the LA model for the spatially uniform component of air cushion pressure (Sorensen & Egeland, 1994). However, the NIMT group introduced a spatially varying component into the cushion pressure (Hirata & Faltinsen, 2000; Sorensen & Egeland, 1994; Steen & Faltinsen, 1995). The spatially varying air cushion pressure takes the form of pressure waves that travel up and down the cushion, where the changes in pressure are caused by the change in cushion volume. The spatially varying air cushion pressure is modelled using a potential function for the velocity field in the air cushion: the Velocity Potential model (VP model). The air inlet flows, air outlet flows, rigid cushion walls, rigid wet-deck, and the moving water surface are formulated as boundary conditions for the velocity potential (ϕ), where c is the speed of sound, x, y and z are the three dimensions of the air cushion void and t is time Eq. (4.4).

$$\frac{\partial^2\phi}{\partial x^2} + \frac{\partial^2\phi}{\partial y^2} + \frac{\partial^2\phi}{\partial z^2} - \frac{1}{c^2}\frac{\partial^2\phi}{\partial t^2} = 0 \tag{4.4}$$

Empirical evidence of spatially varying air pressure is required to validate the VP model. Sorensen and Egeland (1994) used the VP model to predict the resonant frequency of a prototype SES operating in real operating conditions. A small discrepancy between the predicted resonant frequency and the measured resonant frequency was attributed to the effects of the flexible stern seal, which had been assumed rigid in the analysis. Steen and Faltinsen (1995) extended the VP model to include the effects of a flexible stern seal, and achieved a good agreement with the empirical results of Sorensen and Egeland (1994). Hirata and Faltinsen (2000) used the VP model to formulate a Computational Fluid Dynamics (CFD) model of the spatially varying air cushion pressure, but did not investigate the VP model empirically. Therefore, the validation of the VP model is based on a single set of empirical observations of a prototype SES in real operating conditions. The empirical observations of Sorensen and Egeland (1994) are not statistically significant and therefore, are not sufficient to exclude the possibility of random occurrences influencing the test results. Neither were the empirical observations of Sorensen and Egeland (1994) conducted in controlled conditions to eliminate the possibility that a phenomena other than spatially varying air cushion pressure caused the observed pressure resonance, as discussed in Sec. 4.3. While there is no evidence in the available literature to refute the applicability of the VP model, it was concluded that further validation of the VP model, based on empirical methods, is desirable.

The VP model can reveal interesting aspects of the spatially varying air cushion pressure. Solutions of the VP model indicate that there are various modes of oscillation (Hirata & Faltinsen, 2000; Sorensen & Egeland, 1994; Steen & Faltinsen, 1995). In the odd modes of oscillation[6] there is no overall effect on the SES, as the mean pressure across the cushion is zero. For even modes of oscillation, the resulting effect is a pitching moment on the SES, for example, the mean pressure forward of the SES centre of gravity is greater than the mean pressure aft of the centre of gravity. Therefore, while the spatially uniform pressure causes a heaving motion of the SES, the spatially varying air cushion pressure causes a pitching moment. The author concluded that this will be a significant factor in determining the appropriate means of SES control system design.

In formulating the VP model, the NIMT group assumed that the airflow through the cushion is one-dimensional (along the SES's direction of travel). For their physical prototype, the cushion length to height ratio was 14:1 and the cushion length to width ratio was 7:2. The airflow exited the cushion through gaps under the bow and stern seals that extend the full width of the cushion. The air entered the air cushion through an inlet in the upper surface, located approximately amidships and on the longitudinal centreline. For this configuration, the air flowed in the vertical direction (from the inlet in the upper surface to the outlet at the lower surface of the air cushion) and in the lateral direction (from the inlet in the centreline of the vessel to the full width of the outlets). The available literature does not contain any investigations of the significance of the lateral or vertical flow. The author concluded that the assumption of one-dimensional flow must be investigated before it can be accepted.

The VP model is a distributed parameter model and cannot be used directly in control system design. A distributed parameter mathematical model takes the form of a partial differential equation and may be reduced to a lumped parameter model by integration across one of the independent variables or by mathematical manipulation. The lumped parameter model, expressed as an ordinary differential equation, can be readily formulated in a way that is suitable for the control system design techniques based on time-domain (classical), frequency-domain or state-space analytical techniques. It is desirable to determine a means of transforming the VP model so that it can be used for control system design.

The significance of spatially varying air pressure remains an open question as there is limited empirical evidence for its significance. The VP model is a reasonable model for a spatially varying air cushion pressure, provided that turbulence is negligible and the airflow is one-dimensional. The VP model cannot be used directly as a linear model suitable for control system design, but it can be integrated, resulting in parameters such as the cushion pressure and centre of effort that are suitable for control system design. Overall, the VP model has merit, while several aspects require further validation.

4.4.2.4. LC, LA and VP models of air cushion compressibility – concluding remarks

The LC model is attractive for modelling the air cushion compressibility as it provides a linear model suited for control system design. There is some empirical evidence that the LC model is valid for small physical models of hovercraft, but it has not been considered by other researchers as a suitable model for SESs.

The available literature lacks sufficient empirical evidence of the LA model validity. The LA model may be linearised into a form suitable for control system design. However, the

[6]The odd modes of oscillation occur when the associated eigenvalue is odd.

LA model will always be dependent on absolute air pressure, which precludes the use of dimensionally similar models being used to investigate spatially uniform cushion pressure.

Despite the limitations, the VP model presents a reasonable model of spatially varying air cushion pressure, but further validation is needed and the VP model cannot be directly used for control system design. The VP model must be investigated further, both to validate the model and to determine a means of using it for practical control system design. This requires access to large SESs for experimental purposes and lies outside of the scope of the current research program.

4.5. Other aspects of SES dynamics

This section reviews aspect of the SES acceleration regulation problem that are not directly concerned with the airflow through the air cushion. While the airflow through the air cushion is the most important aspect, these other aspects are significant and are required when analysing SES ship motions. The following section discusses each important aspect in turn:

1. Rigid body mechanics
2. Air supply to the cushion
3. Air flows exiting the cushion
4. Air cushion boundary conditions of the air cushion control volume analysis
5. Hydrodynamic and hydrostatic forces on the SES

4.5.1. Rigid body mechanics

The acceleration experienced by passengers, crew, cargo and machinery at any point on a SES is important to the current research. The acceleration may be found by formulating the equations of motion of the SES as a rigid body. The rigid body is subject to forces from the air cushion, water-hull interactions and the airflow over the superstructure of the SES. This section discusses how the SES rigid body has been analysed in the available literature.

The first steps in formulating the rigid body equations of motion are to select an appropriate inertial reference system and choose an appropriate formulation of the laws of mechanics. An inertial reference system is one that does not accelerate. While the Newtonian formulation of the laws of mechanics (classical mechanics) is commonly used, the Lagrangian formulation is another possibility[7]. Kaplan et al. (1981) used a reference system with its origin at the SES centre of gravity. However, Sorensen and Egeland (1994) proposed a coordinate system with its origin at the juncture of the nominal waterline, and the two orthogonal, vertical planes running through the vessel centre of gravity. The nominal waterline plane is chosen as a datum plane both to continue a Naval Architecture convention and to simplify the instantaneous cushion volume calculation. This means that there is a moment lever present between the vessel centre of gravity and the origin of the coordinate system and the SES centre of gravity moves around the origin of the coordinate system. The inertial reference system of Sorensen and Egeland (1994) complicates the

[7]The Hamiltonian formulation is another possibility, but is normally only useful when considering quantum effect, which is not relevant to the current research.

equations of motion and only simplifies the analysis when the calculation of hydrodynamic forces is considered significant. In both reference systems, the SES rigid body is free to move in six degrees of freedom, three translational (Fig. 4.1) and three rotational (Fig. 4.2). Both reference systems move with the SES at its average forward speed and average yaw rate, but remain fixed in terms of an earthed reference system. Both Kaplan et al. (1981) and Sorensen and Egeland (1994) describe formulations the equations of motion using Newtonian mechanics. The Lagrangian formulation has the potential to simplify the analysis of the SES motions. No comparison of the Newtonian formulation with the Lagrangian formulation was reported in the available literature. The inertial reference system of Kaplan et al. (1981) and Newtonian formulation of the equations of motion are suitable for the current research.

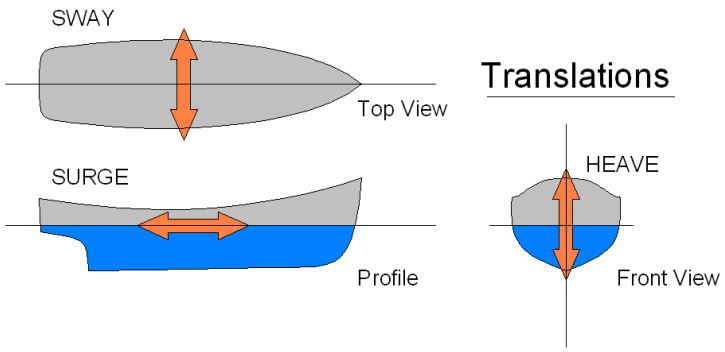


Figure 4.1. Three linear degrees of freedom of a boat or ship. Public domain image created by user 'JMVolc' via Wikimedia Commons https://commons.wikimedia.org/wiki/File:Translations.PNG accessed November 2019.

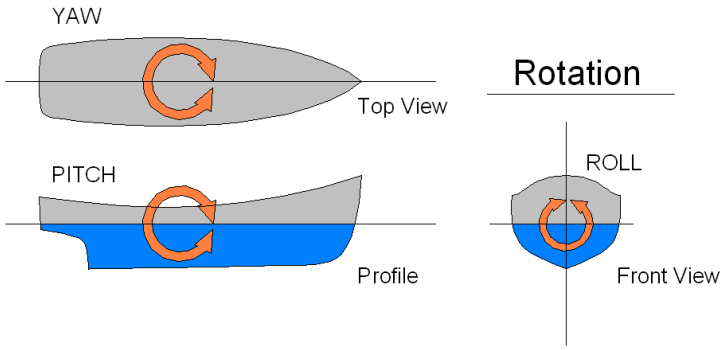


Figure 4.2. Three rotational degrees of freedom of a boat or ship. Public domain image created by user 'JMVolc' via Wikimedia Commons https://commons.wikimedia.org/wiki/File:Rotations.png accessed November 2019.

Kaplan et al. (1981) also proposes a simplified model of the SES motions, assuming that only pitch and heave are significant. Kaplan et al. (1981) used the simplified model for analytical purposes, alongside a numerical simulation based on the equations of motion in

six degrees of freedom. It is commonly assumed that only vertical motions are significant when considering human discomfort (Bos et al., 2007). However, the current research is also concerned with the preservation of high value cargo carried on board SES (Sec. 2.6). Furthermore, some researchers consider that motions in all directions may have a more significant effect on seasickness than is currently assumed (Fang & Chan, 2007). While a six degree of freedom model of the SES motions may be desirable, the heave and pitch motions are still likely to be larger than any other motion. The current research is restricted to heave and pitch, since these are known to be significant.

The equations of motion are normally 'decoupled', but this may not be suitable when considering the needs of both passengers and cargo. The equations of motion can be decoupled by assuming that interactions between the motions are weak. For example, the vertical motions at the bow of the SES are the sum of both the vertical motions of the SES centre of gravity and the vertical component due to the pitching about the centre of gravity. If the pitching influence is considered negligible, the equations of motion are said to be decoupled. For a large SES, the moment arm between the SES centre of gravity and the bow is large, thus the vertical motions caused by pitch are likely to be significant. The available literature does not contain any reports of investigations into the accelerations experience by cargo, particularly at the extremities of a SES. In fact, there are examples of research where only the areas of a high speed ship near the ship centre of gravity are considered, because that is the likely location of passenger accommodation (Fang & Chan, 2007). It is considered that decoupled equations to be appropriate for the current research program, but further investigations into the acceleration experienced by cargo should consider the applicability of decoupling the equations of motion.

In conclusion, the SES rigid body mechanics are important to the analysis of acceleration. A choice of coordinate systems is available in the literature, and the approaches are compatible. Only Newtonian mechanics has been used to form the rigid body equations of motion. Heave and pitch are considered the most significant motions, but the significance of other motions has not been investigated fully. Decoupling the equations of motions may lead to non-conservative estimations of the acceleration levels experienced by cargo located in the extremities of the SES hull.

4.5.2. Air supply to the cushion

All the papers reviewed in the current research acknowledge that the fans feeding the air into the air cushion could have some effect on the SES motions. However, many of the air feed phenomena considered significant by researchers concerned with hovercraft are not considered significant by researchers concerned with SESs. This section will critically review the available literature on air feed phenomena.

First, an overview of the air feed system on SESs (Sec. 3.2). Rotating Diffuser (RD) fans were introduced on early commercial vessels and this is still the conventional design practice (Butler, 1985). An air intake must lie upstream of the fan, bringing the air into the system from the atmosphere and guiding it to the fan. Ducts carry the air from the fan to the air cushion and to the bow and stern seals. Inflated bow and stern seals are generally maintained at a higher pressure to the air cushion and air may feed from the bow seal to the cushion and be taken from the cushion and fed to the stern seal. Earlier designs for hovercraft air supply systems had extra chambers between the fan and the air cushion that were used to damp out variations in air cushion pressure. The precise configuration of the air supply system should be noted when considering research concerning earlier designs of hovercraft.

Fans, including the RD fans in use on SESs, have a long history of being used industrially and have an accompanying body of literature concerning their analysis in industrial applications. In industrial application, the fans operate at a steady-state; in particular, pressure changes downstream of the fan are small and slow. In contrast, fans used on SESs operate dynamically, the pressure downstream of the fan has significant and rapid oscillations, and the fan's rotation speed will typically change as a result. In the papers reviewed for the current research, assuming the fan operates in a quasi-steady state was normal (Bertin et al., 2000; Kaplan et al., 1981; Reynolds & Brooks, 1977; Sorensen & Egeland, 1994; Steen & Faltinsen, 1995; Sullivan et al., 1993). Kaplan et al. (1981) references papers concerning the effect of pressure variations on the operation of fans, however these papers were not accessible for analysis and it is likely that they were not subject to peer review. It is considered that investigating the behaviour of fans in dynamic applications to be important to the SES field. However, such an investigation lies outside the scope of the current research project.

Modelling the fan behaviour is an important part of the SES dynamic analysis. The fan behaviour of interest is the volume flow rate of air through the fan, the power required by the fan and the pressure difference maintained between the upstream and downstream airflows. As the pressure downstream of the fan changes due to variations in the air cushion volume, the air flow rate through the fan is affected, and this may have a further effect on air cushion pressure. Reynolds et al. (1972) used a quadratic approximation of the fan characteristic to model the pressure and flow rate behaviours of a fan. The fan characteristic is a common description of fan behaviour; it plots experimental results for pressure difference versus flow rate for a family of geometrically similar fans. Fan characteristics are usually made available from the fan manufacturer. A quadratic approximation creates an analytical form of the experimental data. In contrast, Kaplan et al. (1981) uses the assumption of a linear approximation of the fan characteristic, stipulating that it must have negative slope so that the air cushion system is stable. Sorensen and Egeland (1994) and Bertin et al. (2000) also describe the use a linear approximation of the fan characteristic, without reporting any validation. The relevance of the fan characteristic is dependent on the validity of assuming

that the fan operates in a quasi-steady manner, and that further empirical investigation of fan behaviour should include an investigation of the fan characteristic in a dynamic environment.

The behaviour of the air as it flows from the fan into the air cushion may also have a significant effect on the SES dynamics. Air flows from the air supply to the air cushion through a duct. Hinchey and Sullivan (1977) show that the flow along the duct has a significant effect on the behaviour of a small hovercraft lift system. However, Kaplan et al. (1981) assumes that the lift fans feed directly into the cushion volume and Sorensen and Egeland (1994) follows the assumption of Kaplan et al. (1981) without further validation. It is possible that large SESs do not have significant duct effects, unlike the small hovercraft considered by Hinchey and Sullivan (1977), however, the available literature does not contain any reports of scientific investigation into this issue. It was concluded that the behaviour of the airflow through ducts on SESs should be investigated further, however, this investigation lies outside the scope of the current research program.

Air flow to the air cushion via the bow seal may be significant to the SES air cushion pressure dynamics. Air is sometimes supplied to the air cushion via the bow seal bag (Butler, 1985). The air flows from the bow seal because the pressure in the bow seal bag is higher than the air cushion pressure. This may become an air flow that is significant to the air cushion pressure in one of two scenarios. The first scenario is when the bow seal bag interacts directly with larger waves (Butler, 1985) and air is forced from the bag into the air cushion, at a time when it is desirable for excess air to be removed from the air cushion. The second scenario is in smaller waves, when the bow seal bag does not interact directly with waves, but interacts with the bow seal fingers that may be undergoing high frequency excited motion (Butler, 1985). Kaplan et al. (1981) assumes the only significant air flow into the air cushion is from the inlet fans, as does Sorensen and Egeland (1994). The available literature does not contain any report of an investigation into the significance of the air flowing into the air cushion from the bow seal bag. Therefore, it was concluded that further investigation of air flow into the air cushion from the bow seal bag could be of value.

The type of airflow into the air cushion has an impact on the validity of using the VP model to describe the airflow through the air cushion. The airflow into the air cushion could be irrotational or rotational. As the air is flowing through fans and ducts prior to entering the air cushion, it is possible that the airflow is significantly rotational as it enters the air cushion. The velocity potential assumes irrotational flow (Fox & McDonald, 1998, p.267), therefore the air flow entering the cushion must either have insignificant rotation, or the transition to irrotational flow must have insignificant effects on the SES dynamics. The papers proposing the VP model do not report any investigation into the type of airflow entering the air cushion. It was concluded that direct observation of the airflow entering the cushion to determine the type of airflow is necessary to completely validate the VP model.

After considering the air feed into the air cushion, it was concluded that there are several topics of further interest. The assumption that the air flow through the fan can be modelled by the conventional fan characteristic should be further investigated. The influence of airflow through the ducts bringing air from the fans to the air cushion should be investigated further. There are sources of air flow into the air cushion, the most obvious of which is the air flow from the bow seal bag, which are assumed insignificant by several of the reviewed papers. However, there is no evidence that this assumption has been

systematically investigated. Further investigation of airflow into the air cushion lies outside the scope of the current research program, but its likely significance indicates that it is imortant for airflow dynamics to be accommodated.

4.5.3. Air flows exiting the cushion

The cushion exit airflow is the air flow from the air cushion to the atmosphere. It mainly occurs under the bow seal and the stern seal, though air may leak from the air cushion through gaps between the seals and the side hulls (Butler, 1985). It is common in the ACV field of research to use the term 'leakage' to refer to all these exit airflows. The exit airflow, specifically the mass flow rate of the exit airflow, has a significant effect on the air cushion pressure (Kaplan et al., 1981; Sorensen & Egeland, 1994), so much so that common type of RCS uses controlled air vents to release air from the air cushion to the atmosphere.

The reviewed papers analyse the air mass flow rate exiting the cushion by assuming the airflow is similar to the airflow through an orifice (Hinchey & Sullivan, 1984; Kaplan et al., 1981; Reynolds, 1971; Sorensen & Egeland, 1994). An orifice is a hole in a barrier to fluid flow; a simple example is a round hole in the side of a water tank. Under this assumption, the exit area (the cross-sectional area normal to the air flow direction), the geometry of the orifice and the pressure difference across the orifice all have significant influence on the mass flow rate through the orifice. Orifice flow is usually considered to be incompressible (if speed of the fluid flow is less than Mach 0.3), irrotational and inviscid (Fox & McDonald, 1998, p.252). None of the reviewed papers reported any validation of the assumption that the cushion exit airflows are similar to gas flow through an orifice.

Further to the assumption that the cushion exit airflow is orifice-like, the LA model and the VP model assume that the exit area is invariant. Kaplan et al. (1981) assumes that the seals follow the water surface perfectly, so that the air leakage area remains constant. Sorensen and Egeland (1994) also assume that the leakage area is invariant. However, some of the reviewed papers suggest that the effect of leakage area variation on the air cushion pressure is significant.

Reynolds (1971) suggested that the leakage area has a significant effect on the air cushion pressure, especially when large variations in the leakage area coincide with large variations in the cushion volume. While Reynolds' work assumes incompressible airflow through the cushion, his suggestion that the leakage area is significant appears reasonable.

Steen and Faltinsen (1995) investigated the influence of the stern bag seal on air cushion pressure analytically, a study which was then progressed by Ulstein and Faltinsen (1998) and Hirata and Faltinsen (2000). The stern seal bag can undergo excited motions under the influence of the airflow passing under it. The exit airflow may be of a lower pressure than the stern seal bag internal pressure, drawing the stern seal bag into the leakage area. The motions of the stern seal bag possibly have a significant effect on the spatially varying air cushion pressure. This line of investigation potentially contradicts the assumption that the leakage area is invariant.

Sullivan et al. (1993) investigated the airflow under a hovercraft seal under laboratory conditions, observing water waves caused by the flow of air across the water surface. The seal was of the bag and finger type, the model was stationary on the water and the model was scaled compared to a prototype hovercraft. If this phenomenon occurs on prototype SESs, the resulting cushion exit airflow will have a varying leakage area (as the generated

water waves will impinge on the leakage area) and could be unsteady (and hence not orifice-like).

In conclusion, the cushion exit airflow could be a significant influence on the air cushion pressure and it is desirable to investigate the SES exit airflow in detail. Current practice when modelling the cushion exit airflows is to assume orifice-like airflow and invariant leakage area. It is desirable to further investigate: the influence of air cushion pressure on the leakage area; resonance of the stern bag seal and its influence on leakage area; and the air-water interaction as the air exits the cushion. These phenomena require laboratory facilities beyond the resources of the current research program and are recommended future research investigations.

4.5.4. Air Cushion Boundary Conditions

The air cushion boundary conditions:

- form the control volume for an integral analysis
- form the boundary conditions for the differential analysis (wave equation)
- assume rigid walls and non-deforming water surface
- assume deflections in seals are significant
- may have to include significant air-water interaction

There are three ways to mathematically model the cushion volume described in the literature. The first is reprted in Reynolds (1971), Kaplan et al. (1981) and Sorensen and Egeland (1995) and assumes that the walls and seals of the cushion do not deflect and that the water surface is unperturbed by the cushion pressure. The cushion volume thus depends on the vertical motion of the SES hull relative to the water surface and on the intrusion of the water surface into the cushion space (known as wave volume pumping).

The second way to derive the cushion volume function is to include the deflections of the flexible rear seal (Hirata & Faltinsen, 2000; Steen & Faltinsen, 1995). Sullivan et al. (1994) also regarded the motions of the seals as being critical to the hovercraft dynamics.

The third approach is to model the deflection of the water surface due to the cushion pressure. Hinchey (1982) considered the effect of air cushion pressure on the water surface for a hovercraft that is stationary over deep water. Sullivan et al. (1993) investigates the action of airflow under hovercraft seals on the water surface, suggesting that unstable water waves can result. The work done by Doctors (1978) on the hydrodynamic power radiated by SES motions indicate that SES cushion pressure has a significant effect on the water surface below the cushion space.

In order to gain more physical insight into the problem, Steen and Faltinsen (1995) found an analytical solution to the Helmholtz equation using a modal solution approach. The spatially varying pressure is given by a modal solution of the Helmholtz equation in two dimensions. The spatially uniform pressure is included in the modal solution as the zero mode. This equation is solved using the boundary conditions along the boundaries of the cushion volume. This was done in two parts. The first part assumes a rigid stern seal and real boundary conditions for the rest of the air cushion, the second part assumes a flexible seal, and all other surfaces are considered rigid. This is primarily done so that Steen and Faltinsen (1995) can examine the effect of the flexible stern seal directly, usually the spatially varying air pressure could be formulated as a single modal solution to the Helmholtz equation.

The Reynolds model predicts large peaks in the cushion pressure when the phase of the three sinusoidal forcing functions for cushion volume, bow exit orifice area and stern exit orifice area are such that reductions in cushion volume due to wave action were accompanied by reductions in the exit areas. Similarly, the US Navy group (Kaplan et al., 1981) and the NIMT group (Hirata & Faltinsen, 2000; Sorensen & Egeland, 1994) take the water surface under the SES to vary with distance along the SES, however, they assume that the exit areas are invariant. In contrast, Hinchey and Sullivan (1984) assumes that the surface under the seals and air cushion are synchronised. However, they do investigate the effect of varying exit area and conclude that it has a significant effect on hovercraft heave dynamics. It was concluded that the synchronisation of the forcing functions may be a significant influence on the SES dynamics and it should be investigated further.

4.5.5. Hydrostatic and Hydrodynamic Forces

The sidehulls interact with the surrounding water, leading to them experience hydrodynamic and hydrostatic forces. The hydrostatic force is given by Archimedes principle: the weight of water displaced is equal to the weight displacing it. This force varies with the depth to which the sidehull is immersed. The hydrodynamic forces include the drag associated with the vertical motion of the sidehull as well as the forces created by the motion of the sidehull horizontally through the water. Discussions of the proportions of the SES weight supported by the sidehull buoyancy compared to the air cushion pressure can be found in Butler (1985), Kaplan et al. (1981), Lavis and Spaulding (1991). Between 0% and 20% of the total weight may be supported by hydrostatic and hydrodynamic forces associated with the sidehulls.

The sidehulls are essentially very thin displacement hulls, with the vertical forces associated with the craft's forward motion assumed to be small (rather than large as for a planing hull). Work done on high speed catamarans shows that the interaction of the water motions set up by the passing twin hulls is small, thus the sidehulls can be regarded as operating in isolation as very thin displacement hulls (Davis & Holloway, 2003; Davis et al., 2004). This kind of physical situation can be described by strip theory, which is the approach taken by both the Kaplan and Ulstein groups.

SES researchers largely ignore the question of added mass, an issue revealed by the brief consideration of the seakeeping field presented in Sec. 3.4. The additions of sidehulls to the system makes added mass an issue to be considered.

SES sidehulls are being designed as semi-planing hulls and therefore generate some hydrodynamic lift (Lavis & Spaulding, 1991). Lift will be affected by vessel speed, the hull angle of attack and the submersion of the hull. These hydrodynamic forces are important for maintaining roll stability during manoeuvres. Another source of hydrodynamic force may be fins used as ride control surfaces (Kaplan et al., 1981; Lavis & Spaulding, 1991).

4.6. Design of practical automatic feedback control systems to regulate SES vertical accelerations

To improve the seakeeping characteristics of the SES, the vertical heave accelerations must be kept under the exposure thresholds defined in Standards Australia (2001), despite the actions of water waves over which the SES must pass. An automatic feedback control

system that keeps a system parameter within a predetermined range despite the effects of environmental 'noise' is called an 'automatic regulating system' or 'governor' Ogata (1990, p. 4). Three such automatic regulating systems for SESs are found in the available literature, and are discussed in turn in the following sections.

- Section 4.6.1 Kaplan et al. (1981)
- Section 4.6.2 Sorensen and Egeland (1994)
- Section 4.6.3 Auestad et al. (2014)

4.6.1. The Kaplan et al. system

The automatic regulating system described in Kaplan et al. (1981) uses a pressure sensor to give the feedback signal and uses a set of vents on the walls of the air cushion plenum to allow air to escape the plenum (under the influence of the instantaneous plenum pressure) and thus reduce the plenum air pressure. The full mathematical model of the SES heave-pressure system is not published in Kaplan et al. (1981), only a simplified (including linearisation) form, and the full mathematical model is not reviewed in detail. The efficacy of the automatic regulating system is supported by a summary of practical trials (apparently beyond a controlled laboratory environment) of a prototype system, which lacks the details of method and the breadth of data to be strong evidence that the automatic regulating system is effective. Kaplan et al. (1981) presents an approximate solution for the system's natural heave frequency and damping ratio that can be used for preliminary design of a practical automatic regulating system (and is subsequently used in Sorensen and Egeland (1994) and Auestad et al. (2014)), but no experimental result is given to support the accuracy of the approximate solution. Investigating this proposed solution using an experimental method is an important step towards the practical design of SES vertical acceleration regulators. A full mathematical model, derived using the assumptions published in Kaplan et al. (1981), has not been experimentally investigated in the available literature. The full mathematical model is not found in the available literature, therefore it has been developed and critically reviewed by the author in Sec. 4.7. One critical aspect of the simplified mathematical model published by Kaplan et al. (1981) is that the 'accumulation of air' Doctors (1976) must be neglected in the mathematical description, with unknown effects on the practical regulation of the SES vertical accelerations.

4.6.2. The Sorensen and Egeland system

The automatic regulating system described in Sorensen and Egeland (1994) uses the same pressure sensing and air venting concept as described in Kaplan et al. (1981). The contribution of Sorensen and Egeland (1994) is to propose that the pressure within the air cushion plenum is spatially varying. The automatic regulating system investigated in Sorensen and Egeland (1994) uses pressure sensors located adjacent to the air vents, compared to locating the pressure sensors some distance from the vents. A summary of results from sea trials of a prototype SES indicates that the collocated sensors and vents are more effective in regulating SES vertical accelerations. Sorensen and Egeland (1994) report on trials without controlled laboratory conditions, providing the opportunity to further investigate the hypothesis of spatially varying air pressure under controlled conditions.

4.6.3. The Auestad et al. system

The automatic regulating system described in Auestad et al. (2014) is for the express purpose of controlling the vertical displacement of the SES at zero forward speed (for the practical purpose of docking with fixed objects such as ocean-located wind turbines). The details of the automatic regulating system reported in Auestad et al. (2014) are not applicable to the scope of this project. The control mechanism again adopts a pressure sensor and air vent concept, and the underlying mathematical model is substantially the same as Sorensen and Egeland (1994). Auestad et al. (2014) explicitly uses the approximate solution for the natural frequency described in Kaplan et al. (1981) as part of the automatic regulating system design.

4.6.4. Observations

This review of automatic regulating systems suggests that four topics should be furthered reviewed or experimentally investigated.

1. The approximate solution for the SES heave-pressure system natural frequency and damping ratio described in Kaplan et al. (1981).
2. The full mathematical model implicit in Kaplan et al. (1981) but not published in its entirety.
3. The hypothesis of Sorensen and Egeland (1994) that the air pressure in the SES plenum is spatially varying.
4. The 'accumulation of air' in the plenum under the influence of rapid volume changes. Doctors (1976)

4.7. Critical examination of the Kaplan model

The mathematical model published in Kaplan et al. (1974) and (with some small corrections and simplifications) in Kaplan et al. (1981) is used in Sorensen and Egeland (1994), later in Bertin et al. (2000), and again in Auestad et al. (2014). The Kaplan mathematical model was published as a summary of research done on behalf of the United States Navy and is largely contained in technical reports outside of the public domain (Kaplan et al., 1981). The mathematical model is important for further research but is not verified via comparison with experimental results in the available literature. In this section, the full Kaplan mathematical model is presented and critically reviewed.

Before presenting the full critical review, a correction to Kaplan et al. (1974) is required. The μ term in Kaplan et al. (1974, equation 4), contains a constant K_3 Eq. (4.5) that is incorrect. The correct form of the equation is Eq. (4.6) and is found in Kaplan et al. (1981). This was verified by the author by substituting into the mathematical derivation reported in Kaplan et al. (1974). The correct form of K_3 will be used without further comment throughout the critical review.

$$K_3 = \frac{K_2 A_{L0}}{2} - \rho_a \left(\frac{\partial Q}{\partial p} \right) p_0 \tag{4.5}$$

$$K_3 = \rho_a \left(\frac{\partial Q}{\partial p} \right) p_0 \tag{4.6}$$

A critical review of the mathematical model presented in Kaplan et al. (1981) will proceed by analysing the derivation of Kaplan et al. (1981), supplemented with reference to Kaplan et al. (1974). Where Kaplan et al. (1981) does not report derivation details, this review will continue with the most logical mathematical steps.

4.7.1. Rigid Body Equations of Motion

The mathematical model begins with the formulation of Newton's second law of motion, applied to the heave, z Eq. (4.7) and pitch, θ Eq. (4.8) motions of the SES. The pressure term μ is defined in Eq. (4.9).

$$m\ddot{z} + Ap_0\mu = 0 \tag{4.7}$$

$$I_y\ddot{\theta} + d_\theta\dot{\theta} + K_\theta\theta - Ap_0x_{cp}\mu = M_{waves} \tag{4.8}$$

The air pressure is formulated as a non-dimensional pressure perturbation, μ Eq. (4.9) using gauge pressure values: p_0 for the air cushion pressure at hover and p for the instantaneous air cushion pressure.

$$\mu = \frac{p - p_0}{p_0} \tag{4.9}$$

The vertical equilibrium state is formulated in Kaplan et al. (1981) as if for a hovercraft with no side hulls contributing buoyancy Eq. (4.10). In general, the vertical equilibrium state requires a term or terms to account for the buoyancy provided by the side-hulls.

$$mg - Ap_0 = 0 \tag{4.10}$$

4.7.2. Continuity of Air Mass in the Air Cushion

The basic continuity equation for the mass of air in the air cushion is given by Eq. (4.11), this follows from the principle of conservation of mass of the air in the cushion. As air is compressible, the relationship between the air cushion volume (V) and the density of the air (ρ) inside the air cushion must be accomodated. The change of air mass in the system is the difference between the mass of air flowing into the air cushion (ρ_aQ_{in}) and the mass of air flowing out of the cushion (ρ_aQ_{out}) is given by the second expression of Eq. (4.11). As the air cushion control volume is defined to include the air supply air intake, the air density for the air entering the system and the air exiting the system can both be taken as ρ_a. The change in air mass in the system must be equal to the change in mass of air inside the air cushion, which will be the time-wise derivative of the product of the air density (ρ) and the air cushion volume (V), which expands to give the final term of Eq. (4.11).

$$\frac{dm_b}{dt} = \rho_a(Q_{in} - Q_{out}) = \frac{d}{dt}(pV) = \rho\frac{dV}{dt} + V\frac{d\rho}{dt} \tag{4.11}$$

In this review, each term in Eq. (4.11) will be expanded in turn. The first term in Eq. (4.11) concerns the air flow in to the air cushion and can be expressed in terms of the equilibrium air flow and the fan characteristic Eq. (4.12). The term Q is the air volume

flow rate through the air supply fan, and is dependent on the downstream air pressure, i.e. the air pressure in the air cushion itself.

$$\rho_a Q_{in} = \rho_a Q_0 + \rho_a \left(\frac{\partial Q}{\partial p}\right) p_0 \mu \tag{4.12}$$

Assuming that the initial air volume flow rate is in equilibrium, $Q_{in} = Q_{out} = Q_0$ and applying a simple model of air volume flow rate through an orifice:

$$Q_0 \quad = \quad A_{L0} c_n \sqrt{(2p_0/p_a)} \tag{4.13}$$

Let:

$$K_2 = \rho_a c_n \sqrt{(2p_0/p_a)} \tag{4.14}$$

Equation (4.14) as it appears here is from Kaplan et al. (1981), Kaplan et al. (1974) used p instead of p_0. Multiplying Eq. (4.17) by ρ_a and then substituting Eq. (4.14) into Eq. (4.17)

$$\rho_a Q_0 = K_2 A_{L0} \tag{4.15}$$

$$\rho_a Q_{in} = K_2 A_{L0} + \rho_a \left(\frac{\partial Q}{\partial p}\right) p_0 \mu \tag{4.16}$$

The second term in Eq. (4.12), describes the air flow out of the air cushion. Again applying the simple model of air volume flow rate through an orifice, this time allowing for instantaneous changes in cushion pressure, μ and changes in instantaneous air exit area, A_L.

$$\rho_a Q_{out} = \rho_a c_n A_L \sqrt{(2p/p_a)} \tag{4.17}$$

The air leakage area (A_L) is given by Kaplan et al. (1974, equation 11), including terms for the variation of A_L by heave and pitch motions and also the forced variations in A_L due to actions of the water wave surface ($\triangle A_{waves}$), reproduced as Eq. (4.18).

$$A_L = A_{L0} + \left(\frac{\partial A_L}{\partial z}\right) z + \left(\frac{\partial A_L}{\partial \theta}\right) \theta + \triangle A_{waves} \tag{4.18}$$

The instantaneous pressure (p), in terms of initial pressure (p_0) and the non-dimensional pressure perturbation, μ Eq. (4.9) is given by Eq. (4.19).

$$p = \mu p_0 + p_0 \tag{4.19}$$

Therefore, Eq. (4.17) can be rewritten as:

$$\rho_a Q_{out} = \rho_a c_n A_L \sqrt{(2(\mu p_0 + p_0)/p_a)} \tag{4.20}$$

Expanding the square root term gives:

$$\rho_a Q_{out} = \frac{\sqrt{2}\sqrt{p_0}\rho_a \sqrt{\mu + 1} c_n A_L}{\sqrt{p_a}} \tag{4.21}$$

Equation (4.21) could alternatively be simplified by assuming that the plenum pressure changes are very small compared to the atmospheric pressure:

$$p \approx p_0 \text{ for } \mu \ll p_0 \tag{4.22}$$

therefore:

$$\rho_a Q_{out} = \rho_a c_n A_L \sqrt{(2p_0/p_a)} \tag{4.23}$$

If pressure changes can be considered small, compared to the air cushion hover pressure, the simplification in Eq. (4.22) can be adopted, in terms of the constant K_2:

$$\rho_a Q_{out} = K_2 A_L \tag{4.24}$$

If air cushion pressure changes are significant, the full expression in Eq. (4.21) should be adopted, this can be expressed in terms of K_2 as:

$$\rho_a Q_{out} = K_2 A_L \sqrt{\mu + 1} \tag{4.25}$$

In both Eq. (4.24) and Eq. (4.25), A_L is a variable and Eq. (4.18) should be substituted. Doing so with Eq. (4.24) gives

$$\rho_a Q_{out} = K_2 \left(A_{L0} + \left(\frac{\partial A_L}{\partial z} \right) z + \left(\frac{\partial A_L}{\partial \theta} \right) \theta + \triangle A_{waves} \right) \tag{4.26}$$

expanding this gives

$$\rho_a Q_{out} = K_2 A_{L0} + K_2 \left(\frac{\partial A_L}{\partial z} \right) z + K_2 \left(\frac{\partial A_L}{\partial \theta} \right) \theta + K_2 \triangle A_{waves} \tag{4.27}$$

substituting the expression for $A_L$into Eq. (4.25) gives

$$\rho_a Q_{out} = \left(K_2 \sqrt{\mu + 1} \right) \times \left(A_{L0} + \left(\frac{\partial A_L}{\partial z} \right) z + \left(\frac{\partial A_L}{\partial \theta} \right) \theta + \triangle A_{waves} \right) \tag{4.28}$$

expanding

$$\rho_a Q_{out} = K_2 \sqrt{\mu + 1} A_{L0} + K_2 \sqrt{\mu + 1} \left(\frac{\partial A_L}{\partial z} \right) z + \\ + K_2 \sqrt{\mu + 1} \left(\frac{\partial A_L}{\partial \theta} \right) \theta + K_2 \sqrt{\mu + 1} \triangle A_{waves} \tag{4.29}$$

The first term of the expanded form of Eq. (4.11), $\rho^{dV}/_{dt}$ can be expanded. The adiabatic pressure-density law is used in Kaplan et al. (1974, equation 8):

$$\frac{p}{\rho^\gamma} = \frac{p + p_a}{\rho^\gamma} = \frac{p_a + p_0}{\rho_a^\gamma} = \text{constant} \tag{4.30}$$

The nonlinear adiabatic gas law is expressed in terms of μ and linearised in several papers: Kaplan et al. (1974), Doctors (1978) and Kaplan et al. (1981):

$$\rho = \rho_0 \left[1 + \frac{1}{1 + (p_a/p_0)}\mu\right]^{1/\gamma} \approx \rho_a \left[1 + \frac{1}{\gamma(1 + (p_a/p_0))}\mu\right] \tag{4.31}$$

Kaplan et al. (1974) also use a relation for the change in cushion volume with time:

$$\frac{dV}{dt} = -A\dot{z} + Ax_{cp}\dot{\theta} + \frac{d}{dt}(V_{waves}) \tag{4.32}$$

therefore

$$\rho\frac{dV}{dt} = \rho_a \left[1 + \frac{1}{\gamma(1 + (p_a/p_0))}\mu\right] \times -A\dot{z} + Ax_{cp}\dot{\theta} + \frac{d}{dt}(V_{waves}) \tag{4.33}$$

multiplying out:

$$\rho\frac{dV}{dt} = -\rho_a A\dot{z} + \rho_a Ax_{cp}\dot{\theta} + \rho_a\dot{V}_{waves} - \\ - \frac{\rho_a\mu A\dot{z}}{\gamma(1 + (p_a/p_0))} + \frac{\rho_a\mu Ax_{cp}\dot{\theta}}{\gamma(1 + (p_a/p_0)} + \frac{\rho_a\mu\dot{V}_{waves}}{\gamma(1 + (p_a/p_0))} \tag{4.34}$$

Kaplan et al. (1981) neglects three terms from Eq. (4.34), implying that these coupled terms are considered to be negligible, although the reason for dropping these terms is not given. Neglecting these three terms necessarily means that any physical phenomena that can't be represented by linear equations is absent from the mathematical model, including asymmetry between the upward acceleration of the SES rigid hull under the influence of plenum air pressure, compared to the downwards acceleration of the SES rigid hull under the influence of gravity. The validity of neglecting these three terms should be further investigated. The three dropped terms are:

$$\frac{\rho_a\mu A\dot{z}}{\gamma(1 + (p_a/p_0))} \tag{4.35}$$

$$\frac{\rho_a\mu Ax_{cp}\dot{\theta}}{\gamma(1 + (p_a/p_0)} \tag{4.36}$$

$$\frac{\rho_a\mu\dot{V}_{waves}}{\gamma(1 + (p_a/p_0))} \tag{4.37}$$

Equation (4.34) then becomes:

$$\rho\frac{dV}{dt} \approx -\rho_a A\dot{z} + \rho_a Ax_{cp}\dot{\theta} + \rho_a\dot{V}_{waves} \tag{4.38}$$

The second term of the expanded form of Eq. (4.11), $V^{d\rho}/_{dt}$ can be expanded. The derivative of Eq. (4.31) (the linearised version):

$$\frac{d\rho}{dt} = \frac{d}{dt}\left[\rho_a + \frac{\rho_a}{\gamma(1 + (p_a/p_0))}\mu\right] = \frac{\rho_a\dot{\mu}}{\gamma(1 + (p_a/p_0))} \tag{4.39}$$

Kaplan et al. (1974) takes the cushion volume as constant, because changes are considered in the first term and the cushion volume is a simple rectangular prism. A practical SES

may have significant changes to the planform dimensions throughout the height of the plenum (Butler, 1985; Lavis & Spaulding, 1991) and the justification for this simplification is not given in Kaplan et al. (1981). This assumption should be considered critically if applied to a practical SES. Following the mathematical derivation published in Kaplan et al. (1974) gives:

$$V = Ah \tag{4.40}$$

therefore the $V\frac{d\rho}{dt}$ term from Kaplan et al. (1981, equation 9) is:

$$V\frac{d\rho}{dt} = \frac{Ah\rho_a\dot{\mu}}{\gamma(1+(p_a/p_0))} = K_1\dot{\mu} \tag{4.41}$$

where

$$K_1 = \frac{\rho_a Ah}{\gamma(1+(p_a/p_0))} \tag{4.42}$$

The resulting combination of the linearised pressure equation and the continuity equation is given by Kaplan et al. (1974) as:

$$\begin{aligned} K_1\dot{\mu} - \rho_a A\dot{z} + \rho_a A x_{cp}\dot{\theta} = \\ = -K_3\mu - K_2\left(\frac{\partial A_L}{\partial z}\right)z + -K_2\left(\frac{\partial A_L}{\partial \theta}\right)\theta - K_2\triangle A_{waves} - \rho_a \dot{V_{waves}}(t) \end{aligned} \tag{4.43}$$

where

$$K_1 = \frac{\rho_a Ah}{\gamma(1+(p_a/p_0))}, \tag{4.44}$$

$$K_2 = \rho_a c_n\sqrt{(2p_0/p_a)}, \tag{4.45}$$

$$K_3 = \frac{K_2 A_{L0}}{2} - \rho_a\left(\frac{\partial Q}{\partial p}\right)p_0 = \frac{\rho_a Q_0}{2} - \rho_a\left(\frac{\partial Q}{\partial p}\right)p_0 \tag{4.46}$$

However, the definition of K_3 given in Kaplan et al. (1974) Eq. (4.46) does not give Eq. (4.43), so there is an error in Eq. (4.46). The correct form of K_3 was derived by the author and is given by Eq. (4.47), assuming that the changes in air cushion pressure are small and that Eq. (4.22) can be used.

$$K_3 = K_2 A_{L0} - \rho_a\left(\frac{\partial Q}{\partial p}\right)p_0 \tag{4.47}$$

4.7.3. Solution for natural frequency

Kaplan et al. (1981) presents[8] a simplified characteristic equation (in terms of the Laplace variable, σ) Eq. (4.48), which they solve to give an equation for heave natural frequency Eq. (4.49) and an equation for heave damping ratio Eq. (4.50).

[8]Kaplan et al. (1981) use the variable h_b for air cushion height, the subscript originating from the term 'bubble' being used for the air cushion.

$$mK_1\sigma^2 + mK_3\sigma + \rho_a A_b^2 p_0 = 0 \tag{4.48}$$

$$\omega_z = \left[\frac{\gamma A_b(p_0 + p_a)}{mh_b}\right]^{1/2} \approx \left[\frac{\gamma g(1 + {}^{p_a}/_{p_0})}{h_b}\right]^{1/2} \tag{4.49}$$

$$\zeta_z = \frac{K_3}{2\omega_z K_1} \tag{4.50}$$

$$\text{where } K_1 = \frac{\rho_a A_b h_b}{\gamma\left(1 + \frac{p_a}{p_0}\right)} \tag{4.51}$$

$$\text{and } K_3 = \frac{\rho_a Q_0}{2} - \rho_a \left(\frac{\partial Q}{\partial p}\right)_0 p_0 \tag{4.52}$$

This system of equations does not have terms for either the variable air exit area, nor the buoyancy force caused by immersed side-hulls. For a mass supported on an air cushion system to hover it is necessary to have either a variable air exit area dependent on vertical displacement or a buoyancy force that is dependent on vertical displacement. Including these two variables potentially modify the natural frequency and damping of a system with a mass supported on an air cushion.

It is necessary to include both air cushion gauge pressure at hover (p_0) and the atmospheric pressure (p_a) as the air compressibility depends on the absolute pressure of the air in the air cushion, whereas the force applied to the supported mass by the air cushion pressure is dependent on the air cushion gauge pressure.

The approximate solution for natural frequency and damping in Eqs. (4.48) to (4.50) neglects higher order terms and is linearised by assuming changes in parameters are small. No experimental evidence is presented to support the simplification, and there is no comparison with the fully developed mathematical model. The fully developed mathematical model is impractical to solve analytically, even with Computer Algebra System (CAS) assistance. It is most feasible to compare the approximate solutions to those calculated using Eq. (4.49) and Eq. (4.50) since those parameters are distinct.

4.8. Questions arising from the literature review

Several topics for further investigation can now be identified. It is important to focus on the dynamics of the plenum air pressure since it creates the principal force affecting SES vertical accelerations. The linearisation and other simplifications of the mathematical model of Kaplan et al. (1981) is the principal focus of further investigation.

Some questions could only be answered by systematic experiments on actual ships - such as the tracking of the sea surface by the flexible seals.

Questions that arose from the literature review, which will be further distilled suitable for further investigation in the current research program:

- Can the SES air lift system be reduced to a fundamental system, able to be observed in controlled conditions?
- Can the effects of the air compressibility be made dominant under controlled conditions?

- Are perturbations to the system sufficiently small to allow the linearisation of the mathematics by application of the small perturbation theorem?
- Can a fundamental air cushion system be forced to resonate under controlled conditions?
- Is the simplified mathematical model from Kaplan et al. (1981) sufficiently accurate for practical design purposes?

These questions arising from the literature review were used to formulate research questions (Sec. 5.3), after further insights were gained from a Preliminary Experiment (Sec. 5.2). The research questions are stated in Sec. 5.3.

4.9. Concluding remarks

There are three novel contributions in this chapter.

- An emphasis on whether the currently available knowledge is sufficient to design and build an effective SES acceleration regulator.
- A detailed comparison of the competing mathematical models for the air flow through an air cushion system.
- An investigation into suitable performance specifications for SES acceleration regulators, considering both the requirement that cargo be undamaged and the comfort of passengers.

A review of the available literature concerning the cobblestone effect and its potential to be controlled was conducted and in Sec. 4.8 several questions were identified for further investigation.

Section 4.7.3 reported on a simplified mathematical model from Kaplan et al. (1981) that is proposed by Kaplan et al. as a useful way of calculating the natural frequency and damping of an air cushion system. The mathematical model does not model flexible air cushion boundaries, variable air exit area or buoyancy forces. The mathematical model does model air compressibility, air cushion height, air cushion planform area, air cushion pressure and atmospheric pressure, the mass supported by the air cushion and the gravitational acceleration, the density of the atmospheric air, the air volume flow rate exiting the air cushion and the air volume flow rate entering the air cushion (dependent on the air cushion pressure). These factors suggest the scope of a simple experimental system that can be used to observe a mass supported on an air cushion in its simplest form.

Chapter 5 contains details of a preliminary experiment completed in response to the questions arising from this literature review, and then continues with the details of the experimental program.

The typical PhD thesis would include a series of Research Questions at the end of the Literature Review chapter. In the current research, the Research Questions were developed from both opportunities found from within the available literature and a preliminary experiment completed by the author. As such, the research questions investigated in the current research are introduced in Sec. 5.3.

5. Experimental Design

5.1. Introduction

In Chapter 4, it was shown that sea-keeping issues are of practical importance to the use of SESs and that air cushion pressure has a significant influence on SES sea-keeping. Four topics were selected for further investigation.

1. The validity of predicting the plenum natural frequency and damping using a mathematical model that neglects higher order terms.
2. The significance of coupled parameters on the plenum natural frequency and damping.
3. The possibility that the plenum air pressure is spatially varying.
4. The accumulation of air in the plenum during plenum volume periodic changes.

In Sec. 5.2, an unexpected and previously unreported phenomenon, observed during a preliminary qualitative experiment, is described. This unexpected observation influenced the research aims of the current research project.

In Sec. 5.3 a summary of the research aims and the set of hypotheses to be tested experimentally is discussed. Three factors influenced the research aims:

1. The background information on SES practical applications presented in Chapters 2 and 3.
2. The critical review of the available literature on SES heave dynamics research reported in Chapter 4.
3. The unexpected result of the preliminary experiment reported in Sec. 5.2.

The remainder of the chapter is structured as follows.

- Section 5.4 reports the development of a novel experimental apparatus, different from any reported in the available literature on the topic of SES dynamics.
- Section 5.5 contains a description of the experimental apparatus.
- Section 5.6 presents the mathematical model adopted for the experimental apparatus.
- Section 5.7 discusses the main environmental parameters and how they were monitored and how the experimental runs were randomised to minimise the impact of environmental parameters on the experimental results.
- Section 5.8 contains a description of the measurement system used.
- Section 5.9 describes how the mathematical model was solved numerically, using the 'Simulink' environment of 'MATLAB'.
- Section 5.10 describes the coupled motions inherent in the functioning of the experimental rig, necessitating extra analysis of the experimental measurements.

5.2. Preliminary Experiment

5.2.1. Aims

A preliminary experiment was conducted to qualitatively observe an air cushion under the action of a periodic forced volume change, with two aims. The first aim of the preliminary experiment was to gain an appreciation of the practical challenges in constructing an experimental air cushion system. The second aim was to make qualitative observations of evidence supporting the hypothesis that the air in the air cushion had significant compressibility. It was reasoned that compressibility of the air would lead to the air cushion behaving like a spring, and hence it was hypothesised that the experimental apparatus would behave like a damped mass-spring system, the damping being due to friction and water dynamics. Following the general understanding of a damped mass-spring system behaviour when undergoing forced oscillations, it could be expected that changes in response magnitude and phase would be observable at different frequencies of periodic forced changes in air cushion volume.

5.2.2. Method

A preliminary rig was designed and built (Fig. 5.1) with an air cushion of approximately $6.3 \times 10^{-3}\,\mathrm{m}^3$. Two pistons, an upper and a lower piston, were inserted into a central vertical cylinder, creating an enclosed plenum. The 150mm diameter cylinder was clear acrylic, allowing the pistons moving within to be easily observed. The pistons were of low mass and sealed with fibre impregnated with oil, running tightly against the inside of the cylinder, some leakage past the cylinders was allowed in the interests of low mechanical resistance. The lower piston was used to force oscillatory changes in plenum volume, by driving it through a simple crank powered by a variable speed electric motor. Because an SES is supported by both air pressure and buoyancy, the upper piston was also supported by both air pressure and buoyancy. The upper piston was connected through a stiff frame to three equispaced floats. The three floats were partially immersed in water in individual containers that prevented the induced water waves from affecting other floats, although the induced water waves were allowed to reflect from the container walls back to the float. A mass was mounted to the upper piston and a visual indicator was placed on the cylinder wall. Air was supplied continuously to the plenum from a laboratory air supply that was minimally dependent on the air cushion pressure. Extra air leakage holes were drilled in the air cushion walls to adjust the overall leakage area and indirectly the air cushion pressure. In the available literature it is generally accepted that the air exit area on a SES is fixed (Sec. 4.5.3), so no attempt was made to allow the air exit area to change due to air pressure or piston movement. In the available literature, it is also generally accepted that the walls, the front seal, the rear seal and the water surface of the SES air cushion do not move under the influence of the air cushion pressure, so the only volume change in response to air pressure is the upward movement of the SES rigid hull (Kaplan et al., 1981; Sorensen & Egeland, 1995): therefore the preliminary rig had rigid walls and pistons, with the vertical motion of the upper piston being the only response to changes in air cushion pressure.

The lower piston was oscillated over a range of frequencies at fixed amplitude, the upper piston with the supported mass being allowed to settle into a steady oscillation after each

change in frequency. The lower piston's driving motor was set to three different speeds, however, the precise speed was not measured.

Observations of the upper piston's motion were made with the aid of an indicator scale mounted to the cylinder's wall. The upper and lower limits of travel were recorded. The observations were repeated with some of the air exit holes closed. A reduced air exit area causes a higher air cushion pressure.

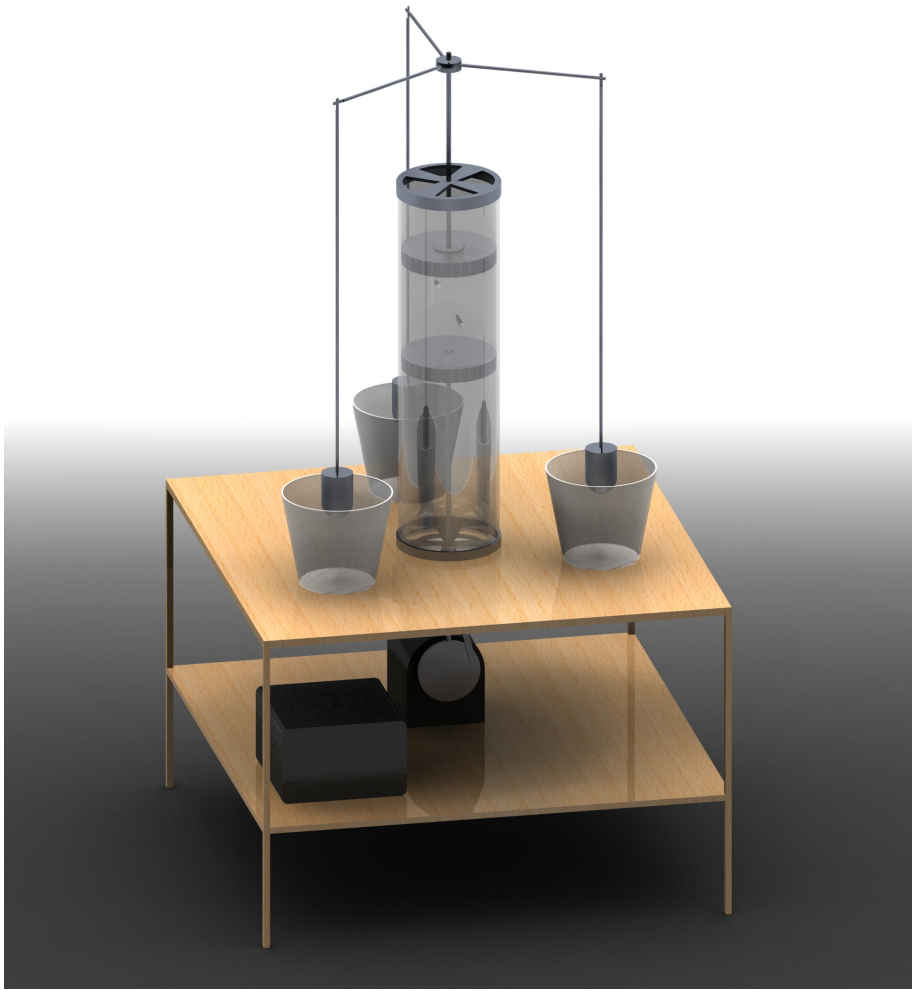


Figure 5.1. Schematic of the preliminary rig.

5.2.3. Results

Magnitudes of the upper piston oscillations are shown in Fig. 5.2 At low frequencies, the upper piston's displacement had approximately the same magnitude as the lower piston displacement (1cm peak to peak). As the forcing frequency increased, the amplitude of the supported mass displacement reduced. The increase in air cushion pressure had very little observable effect.

The upper piston's starting position was recorded for each combination of forcing frequency and air exit area (the static equilibrium point, or 'hover' point). The mid-point of the oscillations of the upper piston was calculated as the mean of the upper and lower

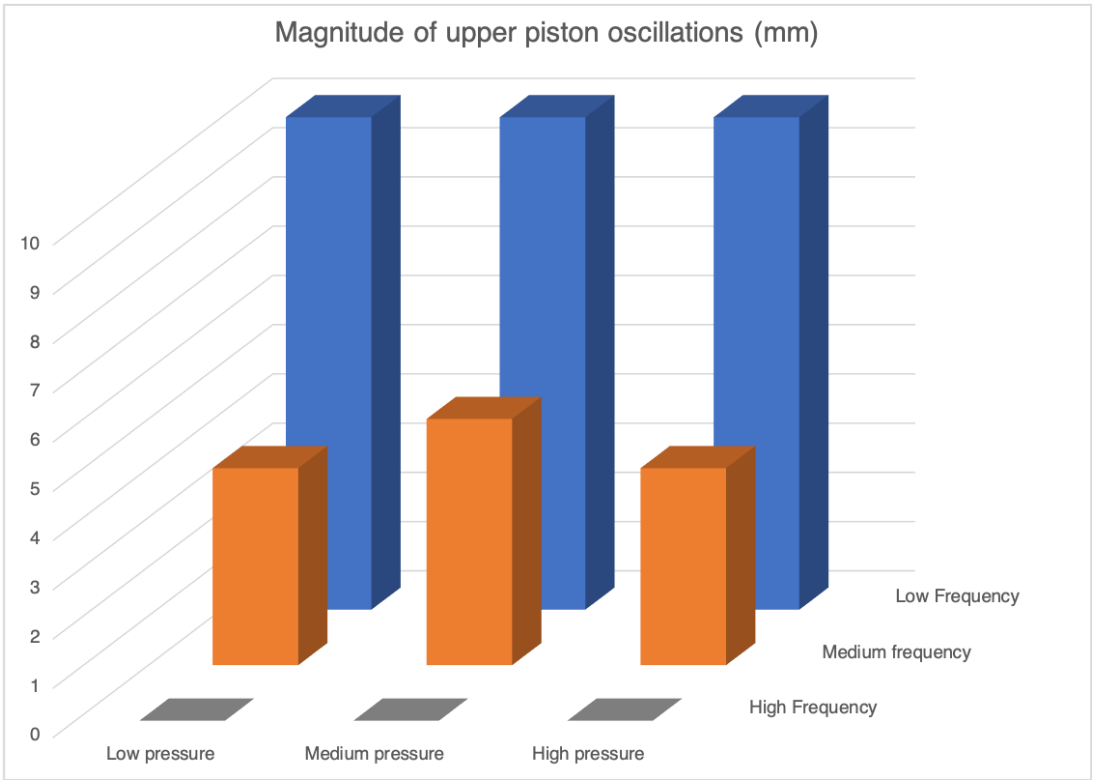


Figure 5.2. Forced oscillation magnitude from preliminary experiment.

limits of the upper piston motion. It was expected that the upper piston would oscillate about the hover point regardless of the conditions. Instead, the upper piston rose to a new mean position as frequency of forcing increased (Fig. 5.3). The hover point increased as the air exit area was made smaller, resulting in higher air cushion pressure since the laboratory air supply maintained a constant air volume flow rate into the air cushion regardless of the changes in air cushion pressure. In an air cushion system with a fixed air exit area, hover can only be achieved if a secondary support force, dependent on hover height, is present. In this experimental rig, the buoyancy from the floats in the water receptacles reduced as the upper piston was lifted by higher air cushion pressure, until a new static equilibrium between the upper piston mass, the air cushion pressure and the buoyancy force was reached. In this experiment, as the frequency of the forced oscillations of the air cushion volume increased, the mean displacement of the upper piston also increased: it appeared to 'hover' at a higher mean height compared to the static equilibrium condition.

5.2.4. Discussion

The first aim of the preliminary experiment was to gain experience in the design and construction of air cushion systems. Based on the preliminary experiment the following five conclusions were made, affecting the design of subsequent experiments.

1. An air cushion system with a low natural frequency is required for subsequent experiments, so that experiments can include controlled forcing oscillations above the natural frequency to investigate potential resonance of an air cushion system.

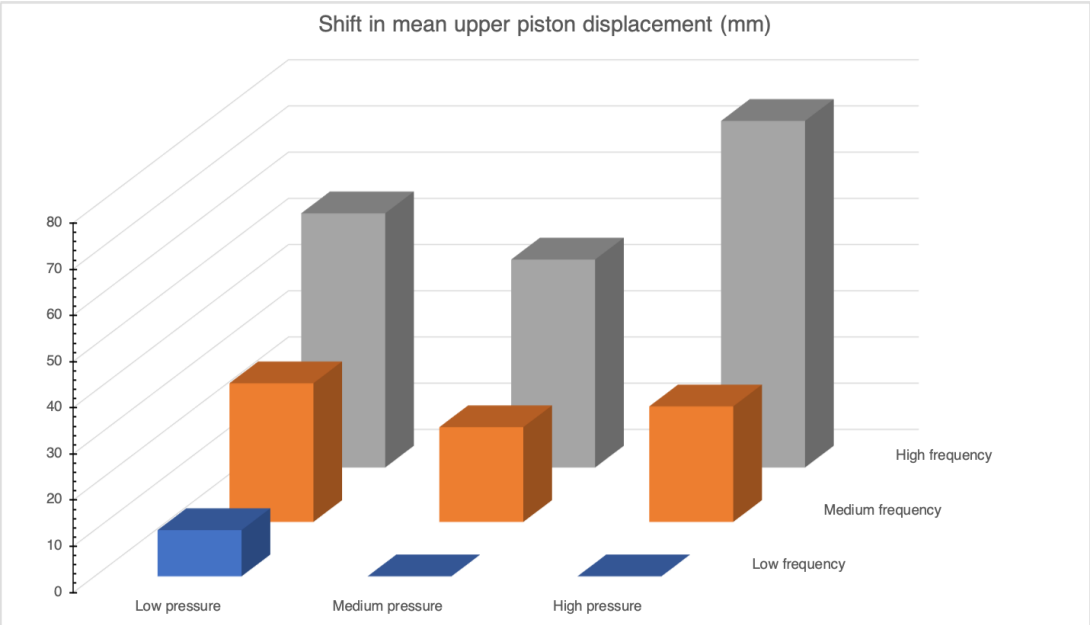


Figure 5.3. Mean of forced oscillations from the preliminary experiment

Forcing an air cushion system at high frequencies will require impractically robust and accurate forcing mechanisms.

2. Using water for buoyancy is impractical, primarily due to secondary effects – such as sloshing in the water receptacle – potentially affecting the results.
3. Pistons constrained to move vertically are impractical, due to the challenges of both realising constraints and sealing the pistons simultaneously in a low pressure system.
4. The forcing (lower) piston caused a flow of air outside of the air cushion, forcing air movement in the local atmosphere. It was unclear if this was affecting the air flow rate into or out of the air cushion.
5. The connection between the floats and the supported mass had some flexibility, which may have introduced another dynamic effect to the motion of the supported mass.

The second aim of the preliminary experiment was to explore whether air cushion systems show evidence of air compressibility. Based on the preliminary experiment the following observations were made.

The upper piston's oscillations change in amplitude as the frequency of forcing changes, supporting the broad hypothesis that there is 'springiness' in the system. However, the springiness may be due to water dynamic effects, or the flexibility of the struts connecting the upper piston with the floats, so the results of the preliminary experiment are inconclusive regarding the hypothesis that the air cushion system acts as a damped mass-spring system. The decrease of upper piston motion amplitude with increasing forcing frequencies contraindicates the hypothesis that the preliminary rig has a resonant frequency – unless the natural frequency of the system is much lower than could be expected for the air cushion by itself.

An unexpected result occurred: the mean of the supported mass oscillations changed with frequency. This phenomenon has not been described in any of the available literature. A conference paper by Doctors (Doctors (1976)) mentions in passing that air can be

'accumulated' in the air cushion system, but no experiments were done in that study, only simulations based on the mathematical modelling. None of Doctor's simulations addressed the 'accumulation' of air. Although the preliminary rig differs from a practical SES in several ways, it is plausible that this phenomenon occurs on practical SESs. In the case of the preliminary rig, the phenomenon may have been caused by one or any combination of the following three phenomena. Firstly, the air in the air cushion not being pushed out by the falling supported mass as quickly as the air cushion volume is being changed by the forcing piston. Secondly, reflected water waves under the floats causing a local maximum in water surface height, forcing the supported mass to a higher point. Thirdly, the descending forcing piston driving air from the atmospheric side of the piston to the air cushion side of the piston. Refer to Sec. 5.3 for the first research question that was developed n response to this observation.

The physical phenomenon of the changing mean height of the forced oscillations cannot be modelled using linear mathematics, indicating that the full, non-linear and coupled, mathematical model published in Kaplan et al. (1981) warrants further investigation.

The observation of a shift in mean supported mass displacement is considered to be relevant to understanding how SES dynamics may affect the practical application of SESs. If a shift in the mean height of forced oscillations could occur on a practical SES, it may manifest as the hulls being lifted further out of the water by the air cushion and could conceivably lead to air being ingested into the water-jet water intakes: a phenomenon that has been reported in the industry literature as being of practical significance (Faltinsen, 2005a). As no observations of this phenomenon have been reported in the available literature, and it has possible practical significance to the application of SESs, further investigation within this research project is warranted.

5.2.5. Concluding remarks

Practical considerations were associated with the design of the main experimental apparatus: make the apparatus sufficiently large so that natural frequencies can drop low enough to enable forced oscillations above the natural frequency practical; remove free-surface buoyancy water from the experimental apparatus; and seek alternatives to pistons sliding vertically. The experimental apparatus used for the preliminary experiment was deemed unsuitable for further development because: the elevated natural frequency of the small air volume would necessitate an impractically high forcing frequency at and above resonance; the sloshing water may introduce unwanted dynamic effects, the motion of the pistons may affect the air flow into the air cushion and the flexible links between the floats and the supported mass may introduce unwanted dynamics. In addition, the observation of an increase in the mean displacement of the supported mass at higher forcing frequencies was unexpected and the further investigation of this phenomenon should be included in the research objectives. The preliminary experiment was ambiguous on the question whether the air cushion system could be forced to resonate, which should be further investigated. It was decided to develop a larger experimental apparatus that could be forced at a range of frequencies that spanned its natural frequency. The new apparatus sought to isolate the air cushion compressibility from any hydrodynamic effect and minimise any dynamics due to flexibility of the experimental apparatus itself that was not justified as being similar to the dynamics of the SES.

5.3. Research Questions and Hypotheses

The overall goal of this experimental program is to investigate the effect of air compressibility on the heave dynamics of a practical Surface Effect Ship.

After a critical review of the literature (Chapter 4), and the completion of a preliminary, qualitative experiment (reported in Sec. 5.2), five research questions are posed concerning the dynamics of a mass-plenum system. The five research questions are listed below, along with associated hypotheses, and a brief descriptive prediction arising from each hypothesis. The descriptive predictions are subsequently made quantitatively, using an adopted mathematical model and its numerical solution. Each research question, hypothesis and prediction is given a unique identifier to aid referencing in subsequent discussion[1].

Question QA: Does the time-wise mean displacement of the supported mass increase when a mass-plenum system experiences oscillations to its plenum volume?

- **Hypothesis HA-1:** The combination of the air density rate of change and the plenum volume rate of change leads to changes of the mean operating point of the supported mass.
- **Prediction PA-1:** When a heave-pressure system's volume is forced to oscillate, the mean of the heave motions increase as the disturbance frequency increases towards the resonant frequency.
- **Prediction PA-2:** The magnitude of any time-wise mean displacement changes is affected by the air exit area.

Question QB: Can resonance be induced in a mass-plenum system?

- **Hypotheses HB-1:** Air compressibility acts as a spring, giving the mass-plenum system a natural frequency.
- **Hypothesis HB-2:** A secondary pressure-induced plenum volume change behaves as an additional spring acting in series, modifying the mass-plenum system's natural frequency.
- **Prediction PB-1:** A step-change to the plenum volume will induce oscillations of the supported mass at its damped frequency.
- **Prediction PB-2:** Forcing oscillations of the plenum volume near the damped frequency will induce large oscillations (i.e. resonance) of the supported mass.
- **Prediction PB-3:** Forcing oscillations of the plenum volume at higher frequencies than the damped frequency will induce smaller magnitude oscillations of the supported mass.
- **Prediction PB-4** Forcing oscillations of the plenum volume at lower frequencies than the damped frequency will induce smaller magnitude oscillations of the supported mass.

Question QC: Does the magnitude of the plenum volume have a significant effect on the damped frequency of a mass-plenum system?

- **Hypothesis HC-1:** Under the same load, large plenum volumes compress further than small plenum volumes, and therefore are less 'stiff'.

[1]Each research question is denoted QA, QB, etc. The hypotheses related to each aim are denoted HA-1, HA-2, etc. where HA-1 denotes the first hypothesis related to research question QA.

Hypothesis HC-2: Large plenum volumes are more likely to have elastic pressure-volume dynamics because their confining structures are less 'stiff'.

Prediction PC-1: Increasing the plenum volume will lower the damped frequency.

Question QD: Does the air exit area have a significant effect on the damping of a mass-plenum system?

Hypothesis HD-1: The air flow through an exit area comprising a set of regular round holes acts as quasi-steady flow through a single round orifice of the same combined area.

Hypothesis HD-2: A greater variation in air flow exiting the plenum arising from a larger exit area will reduce the amount of air compression, damping the oscillations.

Hypothesis HD-3: The air exit area does not have significant effect on the rate that the supported mass returns to equilibrium after a plenum volume disturbance.

Prediction PD-1: A greater exit area will tend to damp the oscillations of the supported mass following a transient volume disturbance.

Prediction PD-2: A greater exit area will not reduce the falling time of the supported mass after a transient change to the plenum volume

Prediction PD-3: A greater exit area will tend to reduce the magnitude of resonant oscillations

Question QE: How sensitive is a mass-plenum system to elastic changes in plenum volume?

Hypothesis HE-1: The elastic pressure-induced changes to plenum volume can be modelled as displacement of a massless plenum wall, opposed by a linear spring.

Hypothesis HE-2: Small changes in the plenum volume due to pressure will have a significant effect on the damped frequency

Prediction PE-1: When observing free oscillations of the supported mass, only one frequency will have significant energy

Prediction PE-2: The overall damped frequency of the experimental plenum-mass system will be lower than the natural frequency of an ideal rigid-volume mass-air oscillator, due to the presence of an elastic volume-pressure dynamic.

5.3.1. Experimental factors, resultants and measurands

To investigate these research hypotheses, it was necessary to use experimental apparatus that allowed a plenum volume to be disturbed in either a transient or periodic way. The current experimental program seeks to vary the following experimental factors:

1. plenum height (with length and width fixed and cuboid form)
2. volume flow rate of air entering the plenum
3. leakage area allowing air to exit the plenum
4. frequency of a periodic volume disturbance to the plenum
5. a single, rapid change in plenum volume

Variations in these experimental factors will determine the following resultants:

1. natural frequency of the air support system

2. damping ratio of the air support system
3. mean displacement of the oscillating supported mass

The measurands that allow results to be found:

1. displacement of the supported mass, recorded as a time series
2. displacement of the mechanism forcing oscillations to the plenum volume, recorded as a time series

5.4. Physical analogue of a typical SES

5.4.1. Overview

The SES was used as a basis for an experimental apparatus, with elements of the SES system finding a physical analogue in the elements of the experimental apparatus (Fig. 5.4). In this section, the research significance of elements of the SES are discussed, and then the physical analogue used for each element in the experimental apparatus is described.

It will be shown that an experimentally practical mass-plenum system that is an analogue to an SES comprises:

1. A chamber of air above atmospheric pressure (plenum)
2. A mass support system representing buoyancy, such as a linear spring
3. A mass supported mostly by the air pressure of the plenum and partially by a buoyancy force
4. A plenum volume that changes proportionally to the displacement of the supported mass
5. A fixed air exit area in the plenum boundary
6. Air supplied to the plenum at a constant volume flow rate
7. The capability for a controlled forced periodic change to the plenum volume, representing wave action
8. Resistance to the motion of the supported mass, acting to damp the supported mass's motions
9. A secondary source of plenum volume changes in response to plenum pressure changes, representing elasticities of the plenum seals and the water surface

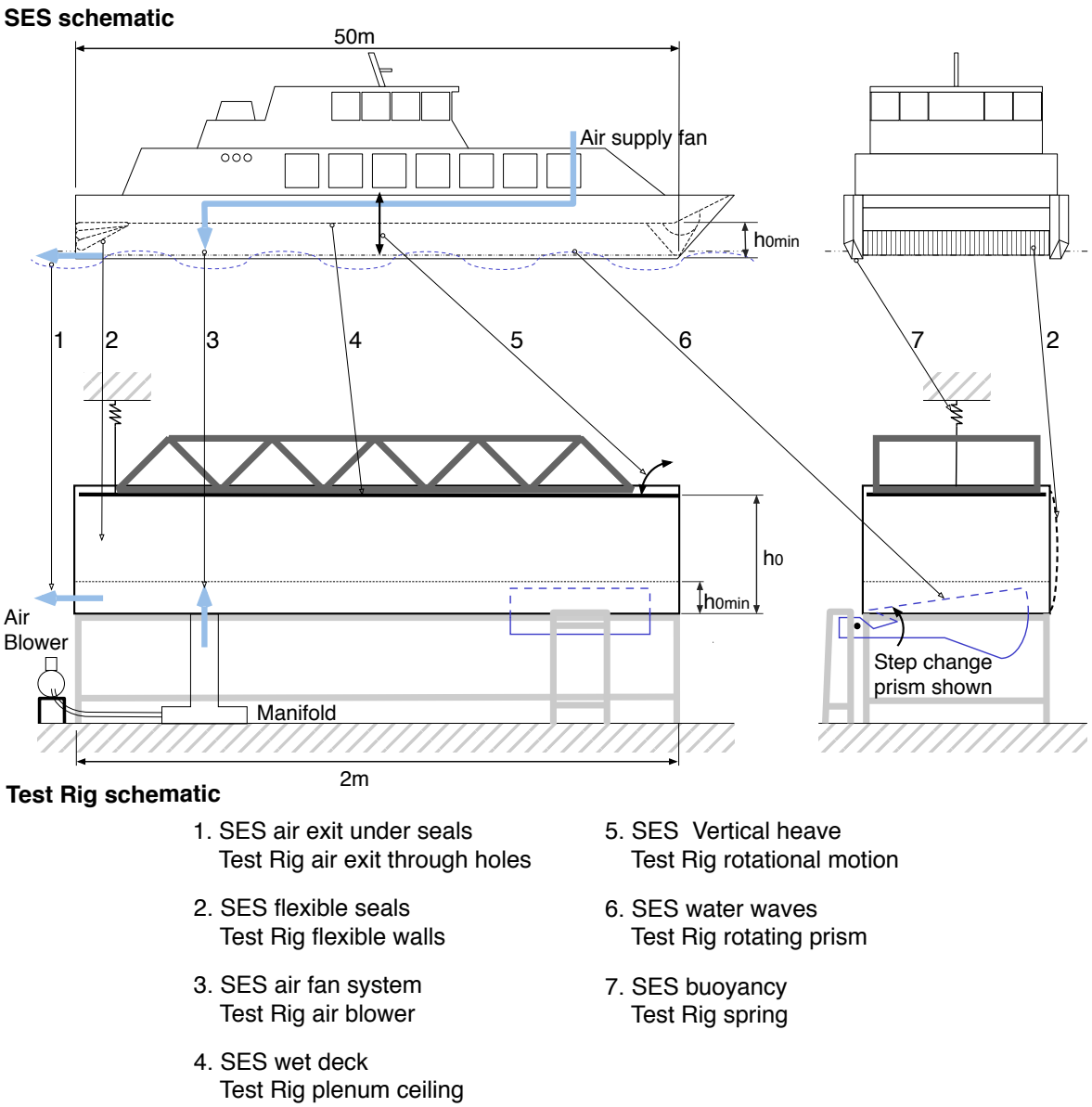


Figure 5.4. SES and analogue of SES experimental rig used for experimental investigations

5.4.2. Air cushion

On a SES, the air cushion is a void or chamber contained by the rigid hull on top and the rigid side hulls on either side, the water surface at the bottom and flexible, inflated, seals at the front and rear. As the seals are flexible and the water surface is mobile, the air cushion volume can change as the seals move and water surface move, responding to air cushion pressure and interactions with the water surface.

The forced changes in air cushion volume due to water waves passing through the air cushion chamber will be discussed in Sec. 5.4.3. The air pressure in the SES air cushion will be discussed in Sec. 5.4.5. The change in air cushion volume due to heave motions of the SES will also be discussed in Sec. 5.4.5.

The experimental air cushion dimensions had the same aspect ratio as a typical SES and the height was used as an experimental variable. A practical SES air cushion is shaped

to best interact with the water surface in two ways. Firstly, the air cushion acts as a patch of pressure passing over the water surface, causing waves. The energy expended in creating waves is the principal resistance to forward motion (wave making drag) and is therefore of practical interest. The aspect ratio of the air cushion has an influence on the wave making drag and is usually optimised to design an efficient SES. A typical aspect ratio is a length three to four times the width. Secondly, it is desirable to minimise the instances of the water waves so the height of the air cushion is designed to raise the rigid under-hull surface ('wet deck') clear of waves passing through the air cushion. A height of one to three metres is typical. While the aspect ratio of the air cushion may be similar when comparing different designs of SES, the air cushion height will vary depending on the height of waves the SES is expected to encounter during operation. An air cushion designed for research must take into account types of volume changes that are found in practical applications. The research air cushion should be the same length to width ratio as a typical SES. The height can be made adjustable, both to cover the range of cushion heights found in practice, and also to provide a simple means of changing the overall volume of the air cushion while maintaining a typical length to width ratio. The air cushion volume is of interest as an experimental variable because of the practical question of designing larger SESs to have better seakeeping. According to the available literature, SESs with the larger air cushion volumes have lower natural frequencies, adversely affecting their seakeeping. The experimental air cushion was built with proportions consistent with the dimensions of typical SESs.

The experimental air cushion was made as large as practical, in order to make the effects of air compressibility readily observable. If the experimental air cushion volume is too small, the natural frequency rises to a value that would be impractical for the operation of volume-forcing mechanisms. Practical considerations such as material standard sizes, workshop and laboratory doorway sizes, and laboratory space dictated an upper size of the experimental rig. The SES field trials reported in Sorensen and Egeland (1995) used a 25 m long SES with a known air cushion width and height. The minimum height (h_{0min}: see Fig. 5.4)) of the air plenum was made to be dimensionally similar to the Sorensen et al. SES, making it 200 mm, the maximum height of the air plenum was 1.000×10^3 mm. The experimental rig air plenum was thus sized to make the natural frequency as observable as possible while being similar to a practical SES studied by Sorensen et al.

An SES air cushion has flexible boundaries. Previous experiments reported in the available literature use either water or flexible seals on the experimental apparatus (or use instruments on real SESs operating on the open water), but previous prediction of SES behaviour have neglected the effect of air cushion boundary flexibility. The walls of the experimental air cushion were designed to incorporate a modest flexibility to better replicate the dynamics of the SES air cushion, following the precedence of experiments reported in the available literature.

A smaller version of the experimental rig was built as a conceptual rig, in order to observe the sensitivity of the mass-plenum system to plenum flexibility Appendix G. The observations made using the conceptual rig confirmed that air compressibility could be expected, and that the natural frequency of the mass-plenum system could be predicted more accurately if plenum volume flexibility could be accommodated in the predictive model. For constructional simplicity, the conceptual rig was only capable of step-changes to the (single sized) plenum volume, not the oscillating and mean volume changes required by this experimental program.

For modelling purposes, it was assumed that flexible plenum walls and seals were effectively massless, so the effect of their flexibility would be to lower the mass-plenum natural frequency, rather than to introduce a second natural frequency of vibrating plenum walls – which would occur if the plenum wall mass was significant. This experimental program will include the wall flexibility as a factor when predicting the behaviour of the mass-plenum system, and the assumption of massless walls will be validated by attempting to observe higher-frequency motions of the supported mass that would arise from independently vibrating walls. The flexibility of the walls was found experimentally and included in the simulations used to predict the supported mass behaviour.

5.4.3. Water waves

Water waves interact with the SES in three ways: changing the volume of the air cushion; immersing the side-hulls, leading to buoyancy, viscous drag and wave-making drag (both horizontally and vertically); and being pushed down by the air cushion pressure – the primary source of wave-making drag – changing the air cushion volume. In the available literature concerning SES vertical motion dynamics, it is usually assumed that the water surface is unperturbed by the air cushion pressure (Kaplan et al., 1981; Sorensen & Egeland, 1995). The buoyancy force, typically contributing between 10%-20% of the vessel mass support (Butler, 1985; Kaplan et al., 1981; Lavis & Spaulding, 1991), is necessary to achieving hover for an SES and will be discussed below. The viscous and wave-making drag in the vertical direction, caused by vertical motions of the side-hulls relative to the water surface, are relatively small compared to the air cushion pressure force, but will act to dampen vertical motions of a SES. The water wave disturbance to the air cushion volume is critical to the vertical dynamics of the SES.

A plenum system suitable for research into SES vertical dynamics must have three characteristics:

1. The ability to force changes to the plenum volume in controlled ways
2. Some resistance to vertical motions proportional to vertical velocity (discussed below)
3. An equivalent force to the buoyancy force (discussed below)

There are two reasons why water seals and buoyancy were not used as part of the experimental apparatus:

1. If contained in a way that allows for water waves, sloshing and reflecting of waves from the walls of a container will have an unwanted extra effect on the experiments
2. Water density and viscosity cannot be scaled in proportion to the physical size of the experimental plenum compared to a full-size SES, magnifying both the desired and undesired effects of water on the plenum system

Two different rigid rotating prisms were designed and built to be forced into the plenum chamber of the experimental apparatus; physical analogues for the forced changes in air cushion volume due to water waves passing through the air cushion space. The first prism was large and could be quickly forced into the plenum space, coming to a rapid halt at a fixed position, creating a step-change in the volume. The prism and mechanism were made as stiff as possible, so that any natural frequency of the prism would be much higher than expected for the air compression phenomenon. A mechanism prevented the prism from being forced back out of the plenum space by the plenum air pressure, so

that a further change in plenum volume due to plenum pressure was not introduced to the experiment. The large size of the prism allowed the change in volume to be adjusted simply by adjusting the angle of sweep, a small angle being preferred to keep unwanted dynamic effects to a minimum. The second prism was moved by a crank mechanism driven by a speed-controlled electric motor, allowing the plenum volume to be oscillated at pre-determined frequencies. The second prism was smaller than the first prism and the angle of sweep could not be adjusted. The second prism was constructed very lightly and very rigidly, to again keep unwanted extra degrees of freedom of the experimental apparatus to a minimum. By using rigid, moving prisms, water could be eliminated from the experimental apparatus, but the primary effect of waters waves, the forced changes to air cushion volume, has a physical analogue in the experimental apparatus.

Both prisms were large, compared to the plenum chamber, so a significant response could be generated for measurement. The prisms were not sized to replicate the size of typical waves, since the typical magnitudes of SES vertical motions in response to typical water waves was outside of the scope of the research aims.

5.4.4. Air exit area

The air from a SES air cushion exits under the front and rear seals. As discussed in Sec. 4.5.3, it is assumed in the available literature that the seals track the surface of the water waves and therefore the exit area is fixed. Some studies have incorporated the effect of variable air exit area (Steen & Faltinsen, 1995). The present research is investigating the possible accumulation of air in the plenum and it is hypothesized that the rate of air exiting the plenum chamber could have a significant effect. Therefore, the experimental apparatus was designed and built to have a constant air exit area, that could be altered as an experimental variable.

The air exit area was realized as a series of round holes, clustered near each other in one end of the plenum chamber. Each hole could be effectively sealed by screwing in a machine screw.

As the plenum chamber had long seams and the plenum chamber could experience some stress due to air pressure and the motion of the supported mass, it was possible that parasitic air leakage could occur. A second set of air exit holes was used to compensate for parasitic air leakage area; holes were closed as necessary to achieve similar supported mass hover heights between series of experimental runs. This adjustment was less intrusive than opening up the plenum chamber completely to reseal all the seams from the inside. The value of the air exit area term in the mathematical model was adjusted to allow for any remaining parasitic air leakage area that could not be adjusted on the experimental rig.

5.4.5. Vessel heave motions

Instead of a simulated twin hull hovering on a cushion of air, a more controlled motion was sought for the experimental apparatus. To this end, only the ceiling of the experimental apparatus plenum chamber was allowed significant movement in response to the plenum pressure. To simplify the motion and make it more practical to build and operate, the ceiling of the plenum chamber was allowed to move in a single degree of freedom: rotation about one end, instead of the two principal degrees of freedom, heave and pitch, of a SES. The entire plenum ceiling was stiffened and made heavier by the addition of a welded steel

tube truss. The mechanism is dubbed the 'heave deck' (Figs. 5.7 and 5.8). As the motion is rotational, the rotational inertia of the heave deck about its point of rotation was found (Sec. 6.2.2).

The research air cushion should change volume in response to air cushion pressure. Allowing the rigid air cushion ceiling to move vertically is the most obvious physical analogue, but this involves effectively sealing sliding surfaces and constraining the motion to act only vertically, which is difficult without introducing unwanted Coulomb or hydrodynamic friction. A rotating ceiling simplifies the sealing and motion constraints considerably. As the research aims only include the first mode of vibration, in which the air pressure in the air cushion can be considered to change uniformly, the centre of pressure on the rotating air cushion ceiling can be assumed to fixed in position, so the rotating rigid air cushion ceiling will react in a similar way to a vertically moving rigid air cushion ceiling.

The mass of the heave deck was not scaled against the mass of an SES, instead it was chosen to give a low air cushion pressure, which also reduces the expected natural frequency due to air compressibility.

The rotating plenum ceiling was made as stiff as possible, to force its own natural frequencies to be higher than the natural frequencies being investigated during plenum air compression. The stiffness was achieved by building a truss structure, welded from square tube steel. A sheet of stiff plywood was added to the bottom, fastened to the truss by screws at close spacing.

The displacement of the plenum ceiling was measured using a laser interferometer mounted above the plenum ceiling and attached to the plenum walls, so that relative motion could be measured. The laser interferometer was mounted at the end furthest from the axis of rotation, so that the motion could be magnified and instrumentation errors minimised. The rotational angles were less than 15°, so the lateral motion of the point being measured was negligible compared to the vertical component, however the angle of rotation was always found by trigonometric analysis in any calculations or simulations to maximise accuracy.

The welded steel truss had significant mass and it was unnecessary to add any mass to get the plenum chamber to operate in the desired pressure range.

The axis of rotation was realised by using heavy-duty hinges. Any secondary degrees of freedom in the hinges was negligible due to the long length of the plenum ceiling and the small angles of rotation.

5.4.6. Buoyancy

The SES is partially supported by buoyancy forces arising from the immersion of the side-hulls in the water. The buoyancy force is typically around 20% of the total supporting forces, with the air cushion pressure supporting the rest of the SES mass. As the SES moves relative to the water surface, the immersion of the side-hulls changes and therefore the buoyancy force is dependent on the relative motion of the SES and the water surface. At extreme motions, the side-hulls may lift clear of the water and the buoyancy drops to nothing. The buoyancy can only act upwards.

Buoyancy can act in ways that would unnecessarily complicate the experimental research. The water waves may interact with the side-hulls independently from the water wave interaction with the air cushion, such as when a single large wave travels from one side of

the SES to the other. This type of more complicated water and side-hull interaction was eliminated in the design and building of the experimental apparatus.

The experimental apparatus used a single spring, mounted above the plenum ceiling, to partially support the mass of the plenum ceiling. The spring was arranged to act in tension through a short wire cable that could go slack if the plenum ceiling moved excessively in the vertical direction, thus the spring force could drop to zero, in a similar fashion to SES buoyancy. The flexible wire cable also prevented the spring from acting in compression, similar to the buoyancy on the SES always acting upwards.

The length of the wire cable could be altered with an adjusting screw, allowing the mechanism to be set to fully support the plenum ceiling when the plenum chamber was at atmospheric pressure ('off-cushion'). The displacement of the plenum ceiling was measured both before and after the plenum was pressurised ('on-cushion') and, given the spring stiffness, the supported mass and the position of the spring relative to the centre of pressure was known, the plenum pressure could be calculated. The plenum ceiling acted as a very large and hence very sensitive pressure sensor.

The effect of buoyancy on the SES is represented in the experimental mass-plenum system by a linear spring.

5.4.7. Sealing

Both the plenum ceiling and the prism used to force plenum volume changes move, and require air tight seals that allow the motion. The need for controlling the air exit area has already been discussed (Sec. 5.4.4. While the Preliminary Rig allowed the air to exit the plenum past the forcing piston and the supported piston (Sec. 5.2.2), this design concept conflicted with the need to control the air exit area. The movement of the air past the moving rigid objects had the potential to induce external flows that may have altered the rate of air volume flow exiting the air plenum. Mathematically modelling possible external flows would have added unnecessary complexity to the analysis of the experimental apparatus.

To seal the plenum and allow motion in a practical and effective way, rolling membrane seals were used. In essence, the plenum seal was a large bag of a flexible polymer (polyethylene) that would not stretch significantly in use. The bag was sealed to the plenum walls around the moving object and the plenum air pressure was allowed to push the bag against the moving object. The bag had enough slack to 'balloon' around the moving object and this compliance allowed the flexible seal to easily roll back and forth as the rigid object moved.

Small inspection cameras were used to observe the rolling seals from inside the plenum chamber[2], confirming the seals rolled easily and the polymer membrane was not placed under sufficient stress to force any observable permanent deformation.

Because the inflated roll of polymer membrane that surrounded the plenum ceiling could act on both the plenum walls and the plenum ceiling as it moved, it was capable of creating a resistance to the plenum ceiling motion. This was used to partially represent the resistance to SES vertical motions of hydrodynamic forces (Sec. 5.4.9).

Effective plenum sealing enables the control of the air exit area and the assumption that the air exit area is fixed.

[2]Video from inspection cameras and of operation of the experimental rig is available on request.

5.4.8. Air supply

A typical SES uses 'Rotating Diffuser' fans, a special type of cross-flow fan, to provide air (Lavis & Spaulding, 1991). Published research into hovercraft lift systems investigates the influence of the fan, ducting and intermediary plenum on the heave dynamics of hovercraft (Sec. 4.5.2).

Investigations published in the available literature on SES use a simplified model of a fan directly feeding into the air cushion. It is common to characterise fan performance by plotting a 'performance curve' (Fox et al., 2004, p.505) or 'characteristic curve' (Fox et al., 2004, p.543) of the downstream air pressure versus the air volume flow rate. The simplified model assumes a small range of air cushion pressures and linearises a negative relationship (negative slope of the characteristic curve) between air volume flow rate and air cushion pressure about an operating point. The same numerical relationship is used by several researchers with no stated justification (Sec. 4.5.2).

A negative slope of the fan characteristic curve will tend to prevent accumulation of air in the cushion, by reducing the flow of air into the plenum as the air plenum pressure rose, so experimental apparatus designed for current research needs a flat fan characteristic slope to ensure that the accumulation phenomenon is present for observation. If reasons for using a steeply negative fan characteristic are found valid, then it would be possible to determine if the air accumulation could always be prevented in practical SESs.

The air supply fan and duct was tested for sensitivity of the air volume flow rate to downstream duct pressure. The fan and duct were configured to enable the duct pressure downstream of the fan and upstream of the bag, to be adjusted by inserting flat plates containing accurately drilled holes ('orifice plate') across the mouth of the duct. The pressure increase in the duct due to the orifice plate was measured with a digital manometer. For each size of orifice, the time taken to inflate a large bag was measured with a manual timing device. The runs were repeated several times for each orifice size. At low duct pressure, similar to the air pressure expected in the plenum of the experimental rig (in the order of 300 Pa), the fan and duct was insensitive to downstream air pressure, therefore it was assumed that the slope of the fan characteristic curve was flat at the operating point.

If peak plenum pressures are subsequently found to be an order of magnitude higher, then the fan characteristic becomes significantly negative. This might happen during sudden transient changes in the plenum volume, or at high frequency oscillations of the plenum volume, where the mean pressure is expected to be higher than the hover pressure, as well as with sudden changes in plenum volume creating high peak pressures. In this case, a quadratic mathematical model of the fan characteristic might be preferable, with a flat slope near zero pressure and with a significant negative slope at higher pressures.

The experimental apparatus used a blower with a fixed speed electric motor and a centrifugal fan, in parallel with a throttled, high pressure laboratory air supply (Fig. 5.9) for commissioning tests intended to check for over-pressure shortcomings in the apparatus. This combination delivered a nearly constant air flow and was capable of much higher pressures than those predicted for the plenum. The blower delivers in the order of 35 litres per second ($35 \times 10^{-3}\,\mathrm{m^3\,s^{-1}}$) at atmospheric pressure.

An industrial hot wire anemometer and a vane anemometer were used to measure the air speed in the centreline of the supply duct, and to provide mutual verification. The rotary vane anemometer was used to monitor air speed on the centreline of the supply duct during the experiments. Due to the turbulent nature of the airflow and the relatively

slow response time of the rotary vane anemometer, compared to the period of air pressure oscillations observed, the centreline speed was not used to estimate the instantaneous air volume flow rate.

5.4.9. Hydrodynamic forces

The vertical motion of the SES side-hulls relative to the water surface creates hydrodynamic forces. The first force is a viscous resistance due to the flow of water past the surface of the side-hull. The second hydrodynamic force is a wave-making resistance. Both of these forces will be proportional to the rigid side-hull vertical velocity and oppose motion, which has the effect of damping out oscillations of the SES hull due to the air compressibility in the air cushion.

With the water removed from the experimental apparatus (Secs. 5.4.3 and 5.4.6) neither of these hydrodynamic forces are present in the experimental apparatus, however, if the experimental apparatus is to be analogous to a SES air cushion, then some damping is required.

The plenum ceiling has three interactions that will act to damp motions: friction in the hinge mechanism, air drag on the oscillating plenum ceiling and pressure from the rolling seals on the plenum ceiling. The friction in the hinges is observable when no plenum pressure present. When the rotational inertia of the plenum ceiling was determined experimentally, the effect of the friction in the mechanism was observable and an equivalent friction was calculated from the measurement of the decline of the oscillations of the plenum ceiling with time (Chapter 6). A simulation of plenum ceiling motion for the concept rig (Appendix G) showed that air drag on the plenum ceiling would be trivial for the amplitudes being monitored, so this factor was ignored for the main experiments.

The resistance due to the rolling seal could be observed in two ways. Firstly, the plenum ceiling was unable to completely return to the static equilibrium position after any displacement, the offset between the at rest position before and after a plenum ceiling displacement was proportional to the resistance due to the rolling seals. Secondly, the greater damping of the plenum ceiling when the plenum was under pressure, compared to the motion of the plenum ceiling when the plenum was not pressurized.

The accomodation in the mathematical model of the resistance due to the rolling seal dynamics is discussed in Sec. 5.6.1. The values for the two types of resistance were found experimentally (Secs. 6.4.1 and 6.4.4).

5.4.10. Summary

By systematically examining the SES air cushion system, a physical analogue of the system was abstracted, forming the basis for a mass-plenum system suitable for experimental use. All of the principal phenomena of the SES that are of interest are included and isolated from higher-order hydrodynamic effects that are to be eliminated in the present research. A practical mass-plenum experimental apparatus was built, as detailed in the following section.

5.5. Experimental rig

In this section the mass-plenum experimental designed and built by the candidate with support from academic supervisors is described. Table 5.2 summarises the numerical values for the main parameters of the system. Section 5.7 discusses the environmental influences. Section 5.8 contains a brief description of the measurement system. The mathematical model adopted for the system is developed in Sec. 5.6.

The air support experimental rig design strategy used was to construct an experimental apparatus with the following characteristics:

The air plenum experimental rig comprised four sub-systems (Fig. 5.5):

1. The air plenum chamber including air exit orifices.
2. The supported mass (heave deck).
3. The air supply into the air plenum.
4. The mechanism for disturbing the volume of the air plenum.

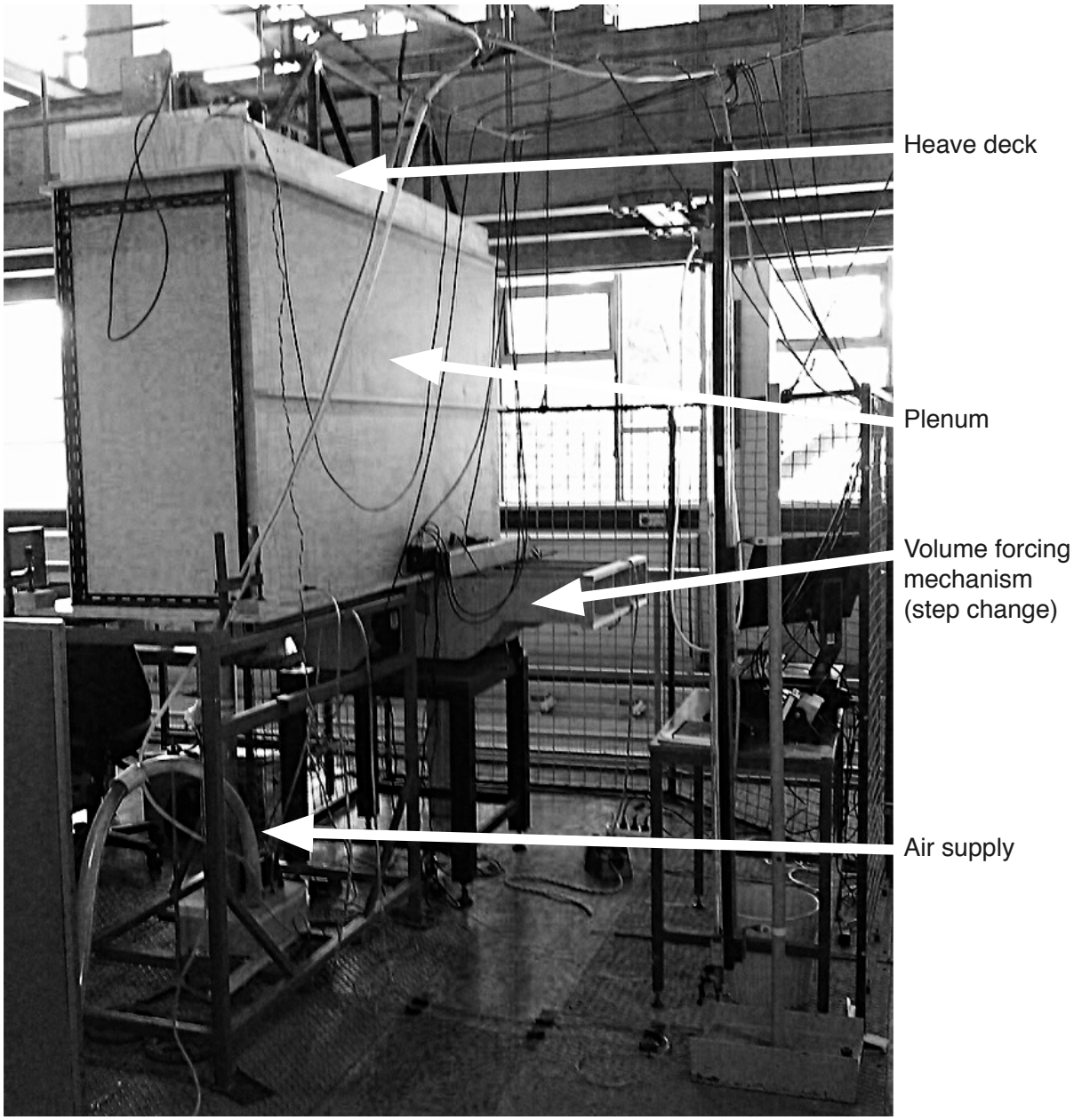


Figure 5.5. Air plenum experimental rig general arrangement. Photograph taken by the author in the Michell Laboratory, The University of Melbourne.

The air plenum is a void contained by plywood walls, stiffened with ribs. The air plenum is reinforced with steel angle, allowing the heave deck sub-assembly to be directly supported by the air plenum walls. The air plenum is kept mechanically isolated from the volume forcing mechanism, the only contact is by flexible film used as an air seal. The air plenum was kept isolated from environmental vibrations using rubber pads and being mounted on a solid and stiff concrete floor.

The experimental rig was initially configured with a step-change volume forcing mechanism for a series of run-in experiments, to find the natural frequency, to determine rig-specific parameters and to validate the mathematical model. The experimental rig was then reconfigured with an oscillating volume changing mechanism (Fig. 5.10). For these experiments, two extra stiffening braces were added to each side of the plenum chamber

walls to help maintain sealing and stability during the higher inertial loads of forcing the heave deck to oscillate at frequencies at and above the natural frequency.

The air exit area was realised as two sets of round holes drilled into one end of the plenum chamber (Fig. 5.6). The holes could be sealed and opened using machine screws. One set was used to set the base level of air exit area (the larger holes arranged horizontally), if parasitic air leakage was detected and could not be sealed, the holes could be closed to restore the required air exit area. The second set of holes were opened and closed to control air exit area as an experimental factor.

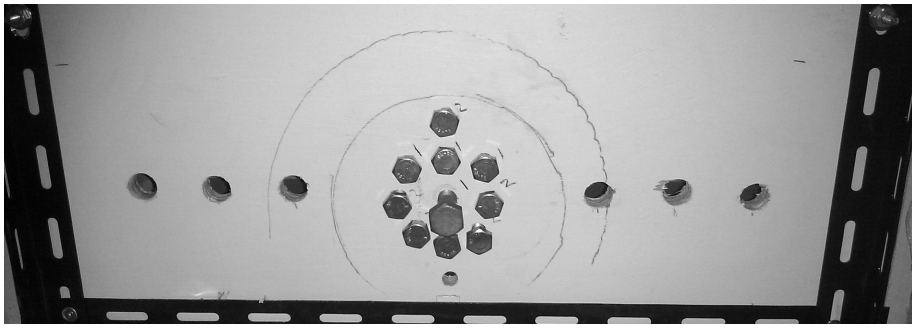


Figure 5.6. Series of regular holes used to control air exit area. Photograph taken by the author in the Michell Laboratory, The University of Melbourne.

The sub-assembly that realised the support of a mass by the air cushion was termed the 'heave deck' as it resembled the deck of a practical SES and replicated the heave motion that was the primary focus of the experimental program. The heave deck sub-assembly (Fig. 5.7) comprised the rigid rotating deck, stiffened by a welded steel truss, hinged at one end to a sub-frame and supported at the other end by an extension spring. The entire sub-frame could be slid up and down inside the plenum chamber, and then bolted into position at the required height, thus allowing plenum height to be an experimental variable. The sub-frame was sealed by screwing through the walls of the plenum to clamp the two surfaces, and then running duct tape along the inside seam.

The rotating deck was sealed to the sub-frame by using a large polypropylene bag (Fig. 5.8), sealed to the sub-frame and laying across the pressure side surface of the heave deck. Plenum air pressure acted to push it against the deck surface, and in a neat fold around the perimeter of the heave deck. When the heave moved, the seal could roll back and forth, avoiding sliding and pinching. When under the pressure, the bag seal would apply some pressure to the edges of the heave deck and the sub-frame walls, creating some extra resistance to the motion of the heave deck. This extra resistance was impractical to predict theoretically, so it was found experimentally (Chapter 6).

The air was supplied by an electric blower, supplemented by air from the laboratory supply. A manifold was used to combine the two air sources and the air was delivered into the plenum chamber by a straight length of tube, 150 mm in diameter (Fig. 5.9). For the initial series of run-in experiments, air taps in the manifold and plenum chamber were connected to a manometer to monitor the pressure difference, this was not used for experimental measurements. The laboratory supply was used in the initial series of run-in experiments, but not for the main set of experiments, which only used the blower as an air source.

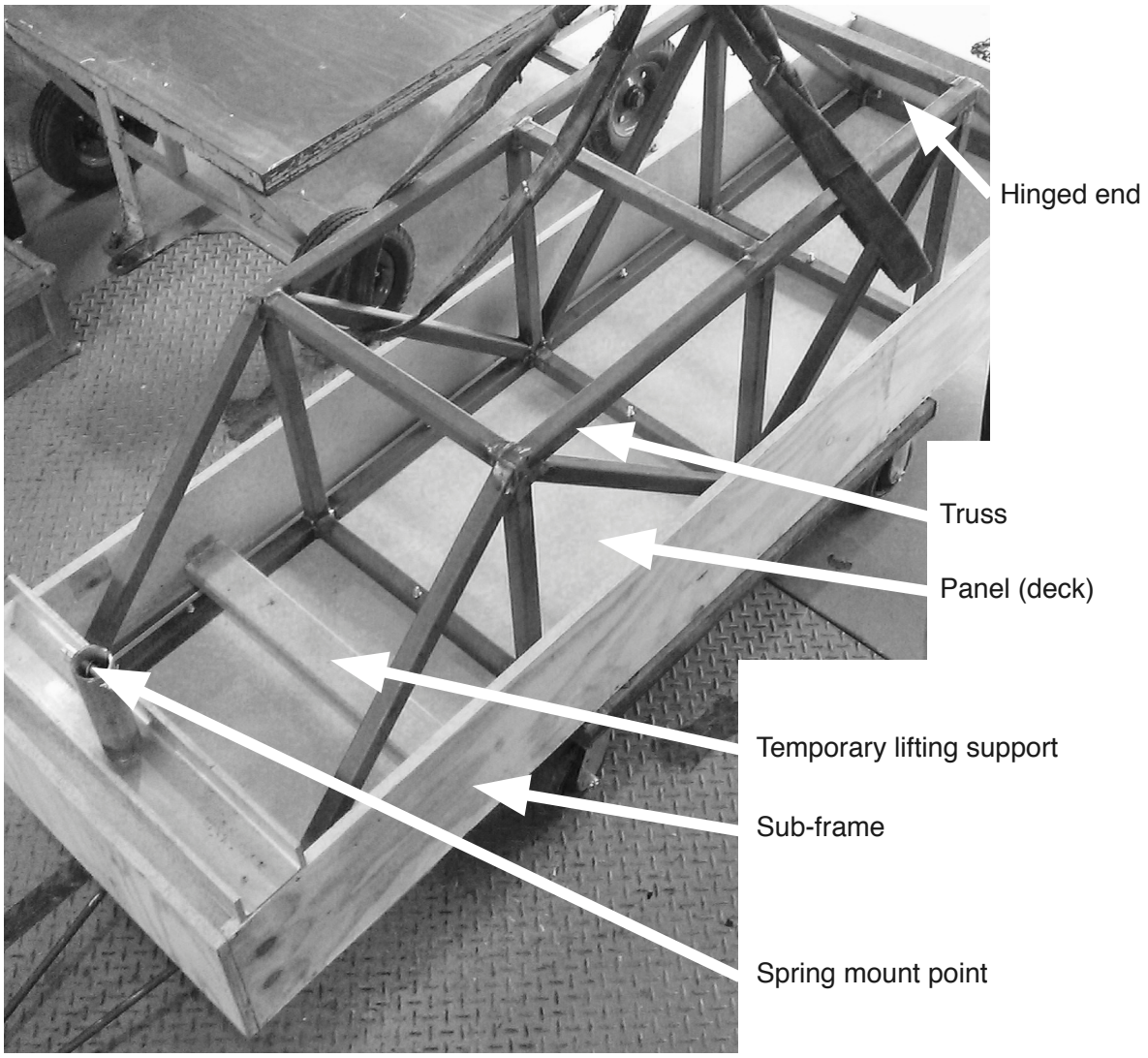


Figure 5.7. Heave deck sub-assembly before installation, seen from above. Photograph taken by the author in the Michell Laboratory, The University of Melbourne.

The volume forcing mechanisms—both for step-changes and oscillatory changes—were based on the principle of rotating a prism into the plenum chamber (Fig. 5.10). The step-change mechanism was sealed using a bag seal operating on similar principles to the sealing of the heave deck. The step-change mechanism was used at a much smaller range of motion than shown in Fig. 5.10, to keep the motion of the heave deck within the range of the measuring sensor.

The mechanism used to force oscillations of the plenum volume used a crank (re-purposed from a small internal combustion engine) to drive a rocker, to which was joined a flap made of Nida-Core honeycomb board, faced with glass fibre, a component with very high stiffness but low mass, strengthened with aluminium ribs (Figs. 5.11 and 5.12). The flap was made stiff and light so that it did not introduce another natural frequency into the system within the range used to investigate the air compressibility effects. The frequency of oscillations could be altered by varying the speed of the electric motor driving the mechanism (Fig. 5.13). The crank mechanism was repurposed from a small internal combustion engine, which had the benefit using components with small variation and

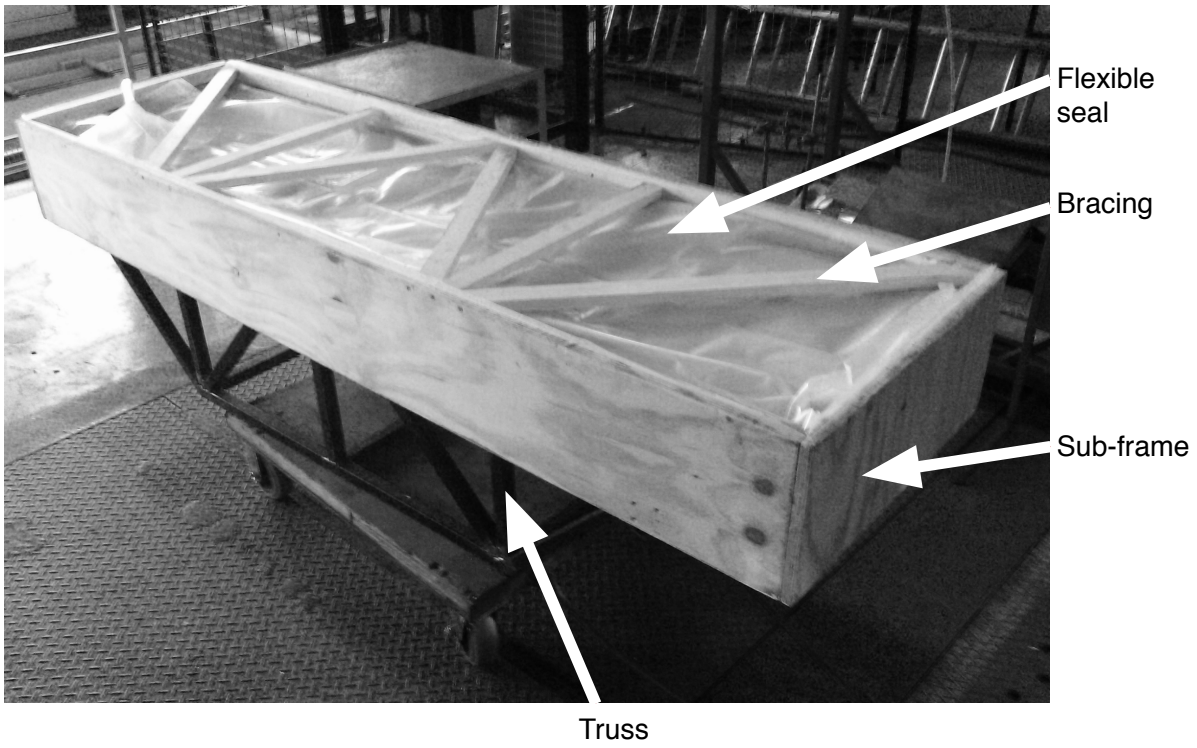


Figure 5.8. Heave deck sub-assembly before installation, seen from below. Photograph taken by the author in the Michell Laboratory, The University of Melbourne.

joints with minimal internal movement. The crank mechanism used did not produce an ideal sinusoidal motion. Therefore, the displacement of the flap was measured using a laser interferometer: the recorded time history could be used to drive the numerical simulation used to predict the system behaviour.

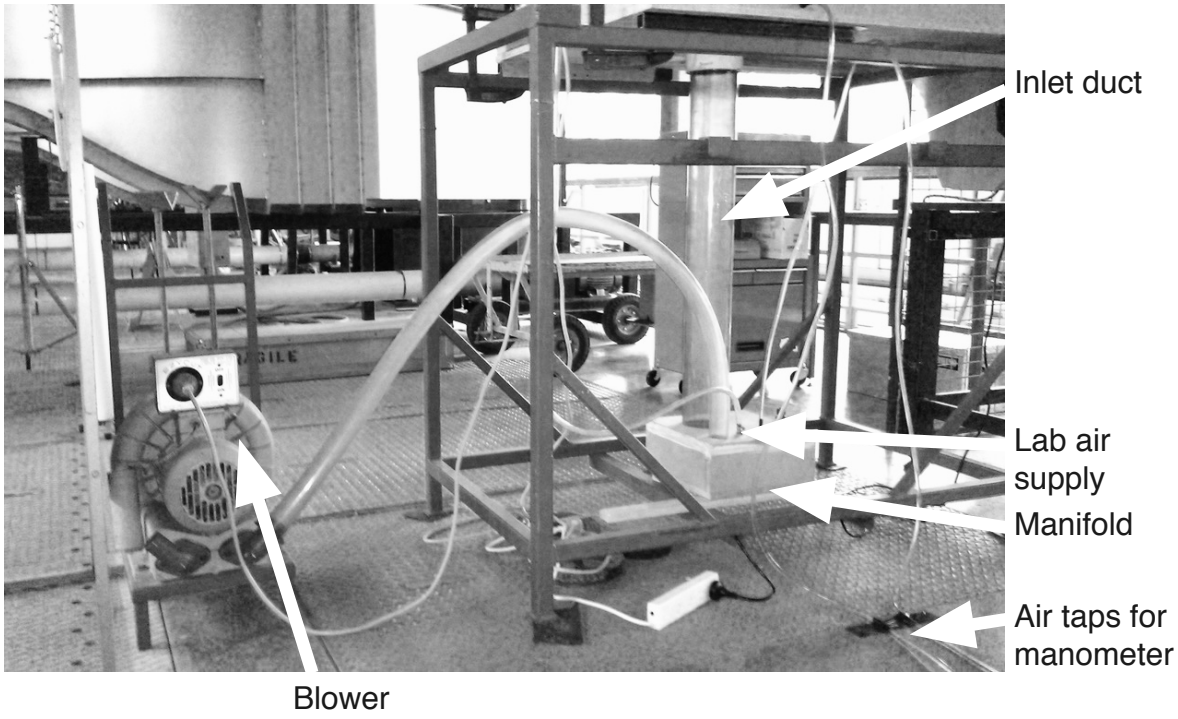


Figure 5.9. Experimental rig air supply sub-system. Photograph taken by the author in the Michell Laboratory, The University of Melbourne.

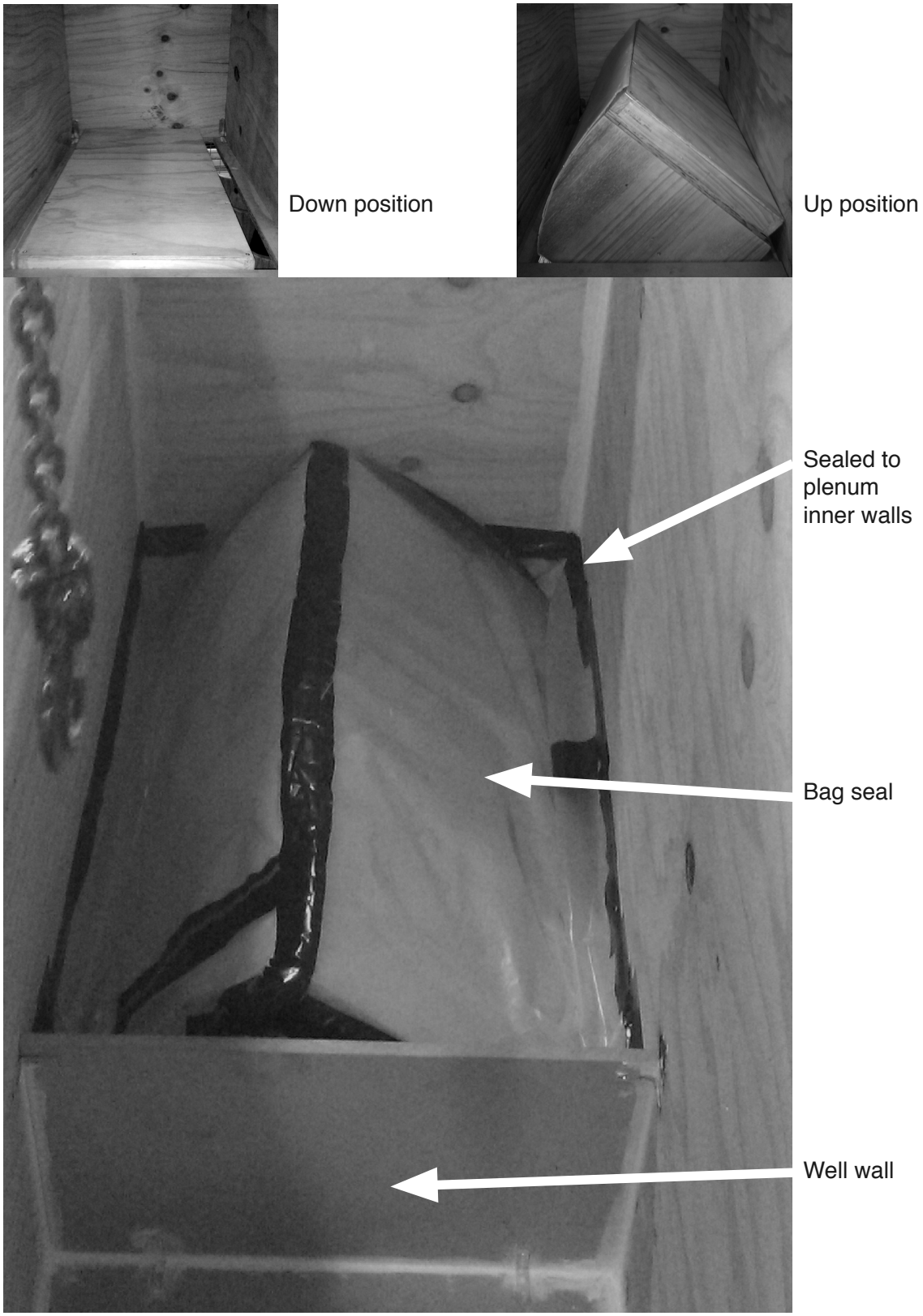


Figure 5.10. Rotating prism mechanism to force step-changes of the plenum volume. Photograph taken by the author in the Michell Laboratory, The University of Melbourne.

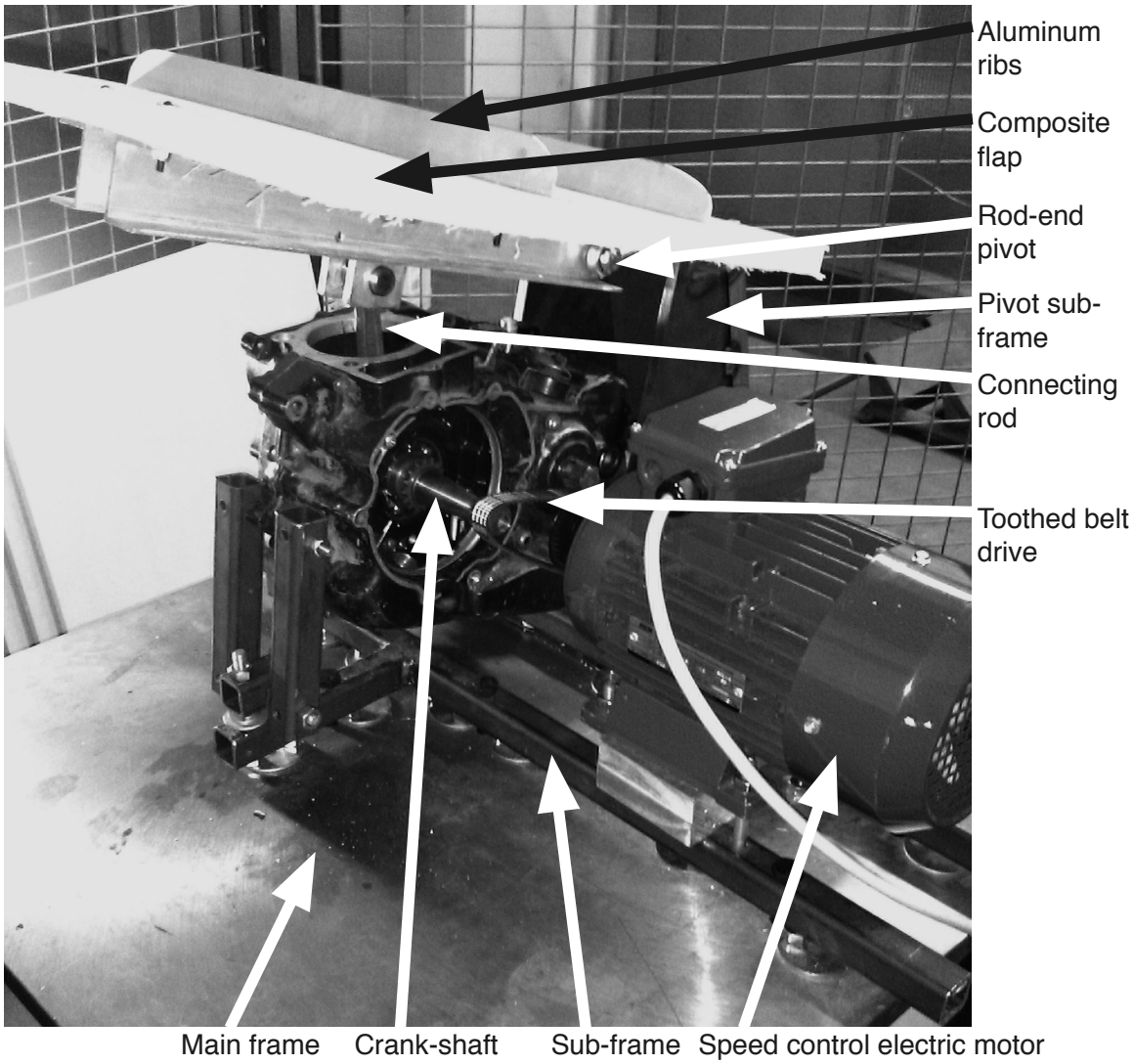


Figure 5.11. Mechanism to force oscillations of the plenum volume, before installation. Photograph taken by the author in the Michell Laboratory, The University of Melbourne.

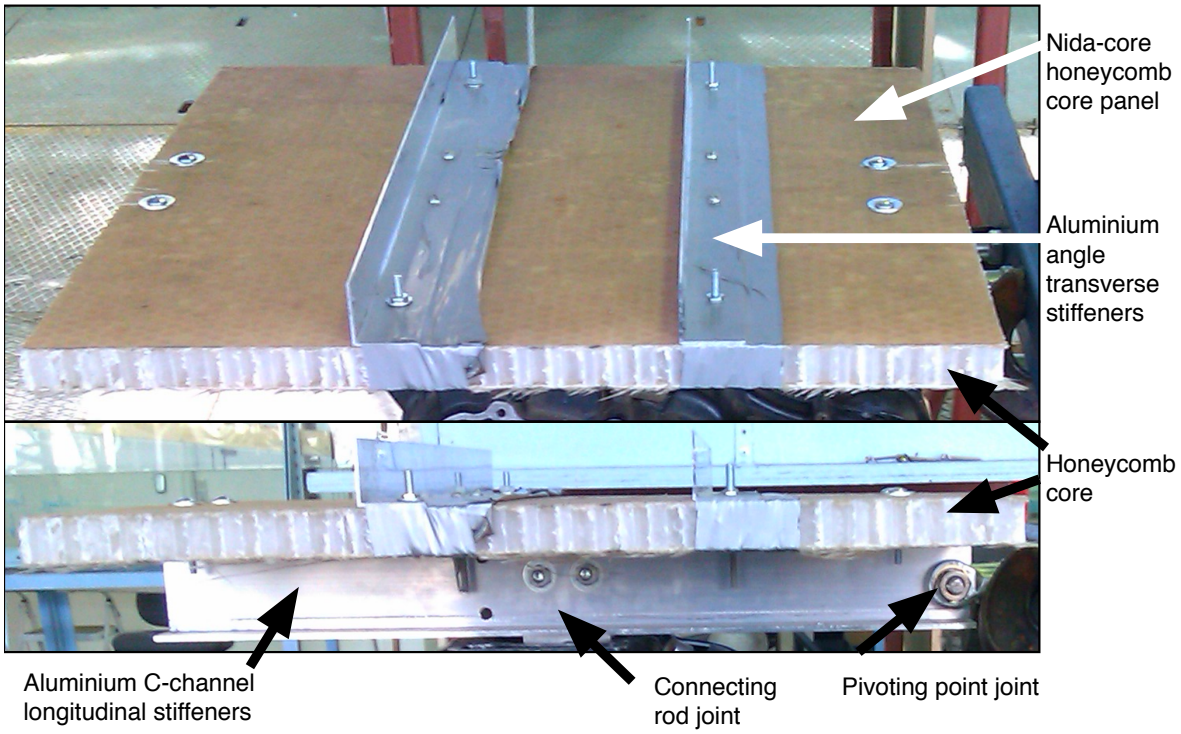


Figure 5.12. Volume oscillating flap detail, before installation. The main flap component is a Nida-core honeycomb cored composite panel, with glass fibre faces. This material was selected for its very high stiffness to mass ratio. Photographs taken by the author in the Michell Laboratory, The University of Melbourne.

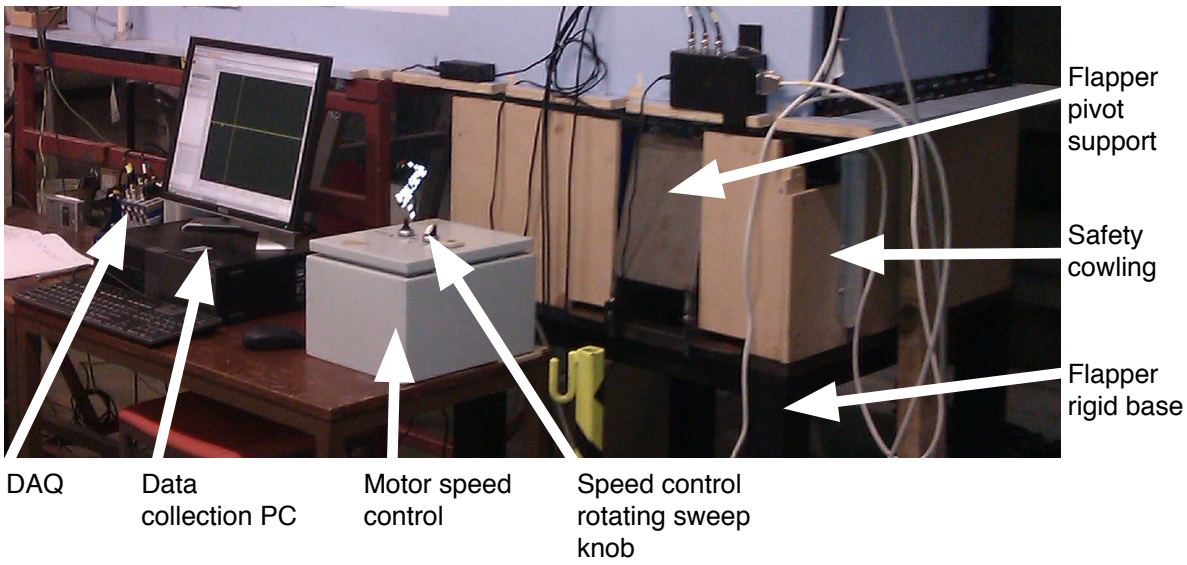


Figure 5.13. Volume oscillating change mechanism installed. The forcing frequency was controlled by an industrial motor speed control unit. Precise forcing frequency was calculated from measurement of the flapper displacement as a time-series. Photographs taken by the author in the Michell Laboratory, The University of Melbourne.

5.6. Mathematical model of the experimental rig

This section discusses the mathematical modelling of the experimental rig. The mathematical model accommodates seven phenomena:

1. The motions of the supported mass under the influence of gravity, plenum air pressure, a spring, Coulomb friction and velocity dependent resistance (Sec. 5.6.1).
2. The continuity of air mass through the plenum volume (Sec. 5.6.2).
3. The air volume flow rate into the plenum (Sec. 5.6.3).
4. The air volume flow rate exiting the plenum (Sec. 5.6.4).
5. The compressibility of the air in the plenum (Sec. 5.6.5).
6. The variations in the plenum volume due to: forced changes to the plenum volume, the motions of the heave deck and flexibility of the plenum volume boundaries (Sec. 5.6.6).
7. The combined effects of the air density and plenum volume rates of change (Sec. 5.6.7).

Taking the Laplace transform of the system equations (Sec. 5.6.8), enabled them to be programmed in the Simulink environment of MATLAB. The use of the Simulink environment of the MATLAB software to solve the mathematical model is described in Sec. 5.9.

5.6.1. Heave deck equation of motion

The motion of the heave deck is governed by Newton's Second Law of Motion, as applied to a rotating body. Refer to Fig. 5.14 for definitions of mathematical terms for the geometry of the mass-plenum system. A general system of coordinates is defined to be non-translating and non-rotating at point O, with coordinate θ, the rotational angle of the Heave Deck, defined as anticlockwise positive rotation from the horizontal about point O. The product of the rotational acceleration and the rotational inertia is equal to the sum of the torques about point O Eq. (5.1).

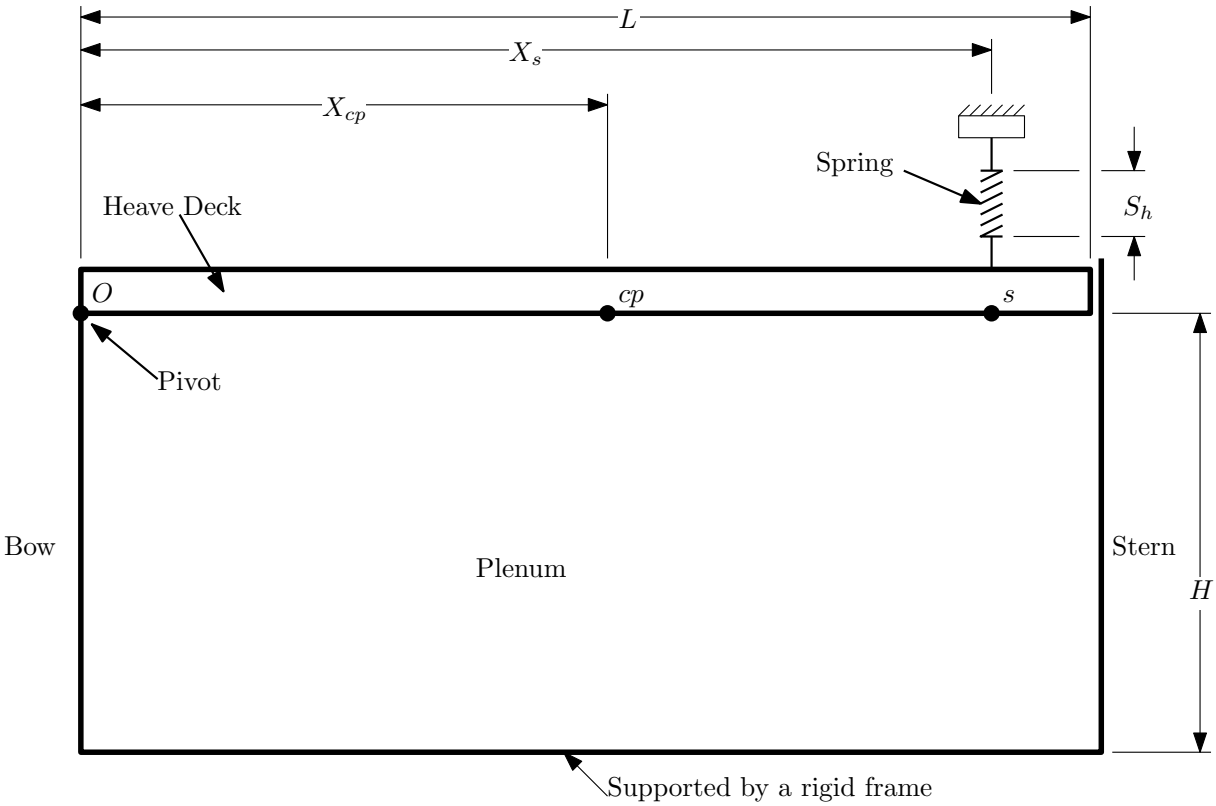


Figure 5.14. Experimental rig heave deck schematic

$$I\ddot{\theta} = \sum T \tag{5.1}$$

where:

- I is the moment of inertia of the rotating object, $\mathrm{kg\,m^{-2}}$.
- $\ddot{\theta}$ is the angular acceleration of the rotating object, $\mathrm{rad\,s^{-2}}$.
- T is the torque applied to the system, $\mathrm{N\,m}$.

The heave deck is assumed to be stiff, of a known and fixed rotational inertia and perfectly pivoted about one end, with a centre of gravity coinciding with the geometric centre. The parameters are defined in Fig. 5.14. This mathematical model includes five forces acting on the heave deck:

1. The force of gravity, acting through the centre of gravity.
2. The spring force, acting at the point where the spring is mounted.
3. A dry friction (Coulomb friction), acting through the centre of gravity.
4. A velocity dependent resistance (damping), acting through the centre of gravity.
5. The plenum air pressure, acting through the centre of pressure.

The heave deck is mathematically modelled at both static equilibrium (hover) and for the general dynamics. The hover state mathematical model is used to calculate the operating conditions of the experimental rig (particularly the plenum pressure at hover). The mathematical model of the general dynamics is used for the numerical solution.

5.6.1.1. Gravity

The weight of the heave deck acts downward through the geometric centre of the heave deck. The mass of the heave is directly measured and denoted as M. The gravitational constant is denoted g. The weight-related torque on the heave deck through the pivot point O is denoted T_M and is the product of the force and the moment arm, length X_{cp}, as shown in Eq. (5.2).

$$T_M = -MgX_{cp} \tag{5.2}$$

5.6.1.2. Spring force

The spring was supported above the heave deck and was mounted so that it could only act in tension. Upward motion of the heave thus reduces the spring force and downward motion of the heave deck increases the spring force. If the upward displacement of the heave deck is sufficient, the spring force reduces to zero and remains zero until the downward motion of the heave deck is sufficient to place the spring in tension again. The initial spring elongation when it supports the heave deck is denoted Δl_o. A local system of coordinates placed at point 's' on Fig. 5.14 when heave deck is supported by the pivot point and the spring is defined so that vertical motion is denoted 'y_s'. The vertical motion is very small compared to the distance from s to point O, therefore horizontal motion of the spring attachment point is neglected. The spring force is given by Eq. (5.3), where the spring stiffness is denoted k.

$$F_s = \begin{cases} k(\Delta l_o - y_s), & \text{if } y_s < \Delta l_o; \\ 0, & \text{if } y_s \geq \Delta l_o; \end{cases} \tag{5.3}$$

The torque on the heave deck due to the spring force is the product of the force and the moment arm is given by Eq. (5.4).

$$T_s = F_s X_s \tag{5.4}$$

The spring could be in one of four states, depending on how the heave deck is supported. Firstly, the spring could be slackened off so that the heave deck was supported by the pivot point and the hard stops at the free end, in this state the spring was not under any tension, this is denoted with the subscript i. Secondly, the spring could be placed under sufficient tension to raise the heave deck clear of the hard stops, with no plenum pressure, this is described as 'off-cushion' and denoted by subscript o. Thirdly, the heave deck could be supported by static plenum pressure, described as the 'hover' condition and denoted by subscript h. Lastly, the heave deck could be supported by dynamic plenum pressure, for this state, no subscript is used.

When off-cushion, the sum of moments about the pivot point is given by Eq. (5.5). When the heave deck is at rest, $\sum M_0 = 0$ and manipulation of Eq. (5.5) gives the off-cushion spring extension Eq. (5.6).

$$\sum M_0 = k\Delta l_0 X_s - MgX_{cp} \tag{5.5}$$

$$\Delta l_0 = \frac{MgX_{cp}}{kX_s} \tag{5.6}$$

The vertical displacement of point s can be expressed in terms of the distance between the pivot point and the point s and the angle of rotation Eq. (5.7). Because the heave deck rotates through a small angle, and the vertical displacement of the heave deck at point s is very small compared to the distance between the pivot point and point s, the tangent function can be approximated by Eq. (5.8) and the vertical displacement of point s can be expressed as Eq. (5.9).

$$y_s = X_s \tan(\theta) \tag{5.7}$$

$$\tan(\theta) \approx \theta \quad \text{for, } \theta \ll 1 \tag{5.8}$$

$$y_s = X_s \theta \tag{5.9}$$

5.6.1.3. Dry friction

The Coulomb friction was only observed when the plenum was pressurised. The narrow gap between the moving heave deck and the sub-frame is completely filled with the flexible seal when the plenum is pressurised. The pressure pushes against the heave deck and plenum, leading to rubbing between the seal and plenum wall. The Coulomb friction is independent of the displacement and velocity of the heave deck, but it always opposes motion. It was observed (Fig. 5.19) that the heave deck came to rest at a higher point after being disturbed by a step-change to the plenum volume. As the mass and plenum pressure remain the same before and after the step-change to the plenum volume, and the force from the spring extension is proportional to the heave deck displacement, it is evident that the friction force (F_c) acting perpendicularly at the centre of the heave deck, can be found from the change in resting positions of the heave deck at the spring (y_c) and the spring rate, k Eq. (5.10).

$$F_c = -k \frac{y_c}{2} \frac{X_s}{X_{cp}} \tag{5.10}$$

For the general case, the force due to Coulomb friction can be expressed as Eq. (5.11).

$$F_c = C_c \frac{\dot{\theta}}{\left|\dot{\theta}\right|} \tag{5.11}$$

5.6.1.4. Velocity dependent resistance

Decaying oscillations of the heave deck were observed when the plenum was not pressurised, and again when the plenum was pressurised. The decaying of the heave deck oscillations was quicker when the plenum was pressurised. It was hypothesised that a velocity dependent heave deck resistance (F_v) acting perpendicularly through the centre of the heave deck was present, and it was dependent on the plenum air pressure. Similar velocity dependent resistances are in effect on SESs, such as the hydrodynamic forces from the side-hulls, therefore it was acceptable to include F_v in the experimental rig modelling. However,

the causes of F_v are very likely to be specific to the experimental rig[3], so no further investigation into the causes was completed. An estimate of F_v was calculated based on the measurements of the heave deck oscillations rate of decay (Sec. 5.10). As F_v was observed to be dependent on the plenum height (the plenum height is set by moving the position of the heave deck within the (plenum chamber), F_v was estimated at each plenum height. The velocity dependent heave deck resistance was mathematically modelled in the same way a general damping force is modelled, using a coefficient C_v,

$$F_v = C_v\dot{\theta} \tag{5.12}$$

5.6.1.5. Dynamic plenum pressure

The dynamic plenum pressure (p) is the plenum pressure at static equilibrium (hover pressure, p_h) plus any change in the plenum air pressure (Δp) as shown in (5.13). The plenum pressure is a gauge pressure.

$$p = p_h + \Delta p \tag{5.13}$$

Following the convention in Kaplan et al. (1981), a non-dimensional term is defined for excess pressure (μ), allowing the heave deck equation of motion to be expressed in dynamic and equilibrium terms. The excess pressure can be expressed in three convenient forms.

$$\mu = \frac{p - p_h}{p_h} \tag{5.14}$$

$$(p - p_h) = \mu p_h \tag{5.15}$$

$$p = \mu p_h + p_h \tag{5.16}$$

The force the plenum air pressure exerts on the heave deck (F_p) is the product of the plenum air pressure and the area of the heave deck Eq. (5.17). The heave deck moves through a sufficiently small angle that the area of the heave deck can always be considered as normal to the plenum air pressure. The plenum air pressure acts through the heave deck centre of pressure, which is coincident to the geometric centre of the heave deck. The torque the plenum air pressure exerts on the heave deck (T_p) is given by Eq. (5.18).

$$F_p = pA \tag{5.17}$$

$$T_p = pAX_{cp} \tag{5.18}$$

[3]Possible causes of the velocity dependent heave deck resistance are viscous resistance occurring in the lubrication oil of the hinges, or from the effects of the flexible polymer seal rubbing against itself, interfering with itself or rubbing against the plenum walls. Polymers often do not follow da Vinci's empirical law for kinetic friction (Ohanian, 1989, pp.135-137)

5.6.1.6. Static equilibrium (hover)

The heave deck is stationary when at hover, the dry friction[4] is assumed to be negligible compared to the other forces and the sum of the vertical forces on the heave deck (including the vertical reaction force at the pivot R_{yh}), is given by Eq. (5.19). The sum of the moments on the heave deck about the pivot point at hover is given by Eq. (5.20).

$$\sum F_{yh} = Ma = 0 = R_{yh} + p_h A + \Delta l_h k - mg \tag{5.19}$$

$$\sum M_{0h} = I\ddot{\theta} = 0 = p_h A X_{cp} - MgX_{cp} + X_s k(\Delta l_h) \tag{5.20}$$

From Eq. (5.20) it can be seen that the weight of the heave deck (Mg) can be expressed in terms of the pressure and spring force.

$$MgX_{cp} = p_h A X_{cp} + X_s k(\Delta l_h) \tag{5.21}$$

Given that the mass of the heave deck is known, the initial displacement of the heave deck will give the initial plenum pressure Eq. (5.22).

$$p_h = \frac{MgX_{cp} - X_s k(\Delta l_h)}{AX_{cp}} \tag{5.22}$$

The plenum air pressure will have some dependency on atmospheric conditions (pressure and density), mainly due to the air blower supplying slightly different flow rates of air in different atmospheric conditions. The plenum static equilibrium pressure p_h must be calculated for each unique condition before dynamic analysis can be done. When possible, experimental runs were grouped together over a short period of time to minimise the influence of changing atmospheric conditions. Because the heave deck is very large and the laser interferometer sensor measuring the heave deck displacement has a fine resolution, the heave deck acts as a very sensitive pressure sensor for static pressure.

5.6.1.7. Heave deck dynamic equation of motion

The equation of motion for the heave deck is derived by taking the sum of moments about the pivot point (5.23). For simplicity, only the case of the spring remaining extended ($y_s < \Delta l_o$) is shown.

$$I\ddot{\theta} = pAX_{cp} + k(\Delta l_o - y_s)X_s - MgX_{cp} - C_v\dot{\theta}X_{cp} - C_c\frac{\dot{\theta}}{\left|\dot{\theta}\right|}X_{cp} \tag{5.23}$$

The reduction in extension of the spring, y_s, can be expressed in terms of θ using Eq. (5.9) to give the final form of the heave deck equation of motion Eq. (5.24). This is the form used to program the Simulink model, as shown in Sec. 5.9, Fig. 5.16.

[4]If the heave deck has been completely off-cushion, then risen to the hover height solely due to plenum pressurisation, then the dry friction has opposed the motion and is keeping the heave deck slightly below the theoretical hover height. The experimental procedure was to lift the heave deck manually and let it drop, where it would come to rest at a slightly higher point. This was done to maintain consistency in the experimental measurements.

$$I\ddot{\theta} = pAX_{cp} + k(\Delta l_o - \theta X_s)X_s - MgX_{cp} - C_v\dot{\theta}X_{cp} - C_c\frac{\dot{\theta}}{\left|\dot{\theta}\right|}X_{cp} \tag{5.24}$$

5.6.2. Continuity of air mass through the plenum

The basic continuity equation for the mass of air in the air cushion (m_a) is:

$$\frac{dm_a}{dt} = \frac{d}{dt}(\rho V) \tag{5.25}$$

For the experimental rig plenum, this can be expressed in terms of the volume flow rate of air into and out of the plenum, and the right hand terms expanded, to give:

$$\rho_a(Q_{out} - Q_{in}) = \rho\frac{dV}{dt} + V\frac{d\rho}{dt} \tag{5.26}$$

The principal terms in Eq. (5.26) will be expanded in turn in the following sections.

5.6.3. Air volume flow rate into the plenum

The first term in Eq. (5.26), that is, ($\rho_a Q_{in}$) concerns the air flow in to the air cushion and can be expressed in terms of the static equilibrium air flow (which is the hover condition) and the fan characteristic:

$$\rho_a Q_{in} = \rho_a Q_h + \rho_a\left(\frac{\delta Q}{\delta p}\right)p_h\mu \tag{5.27}$$

By definition, the air volume flow rate at hover is in equilibrium, $Q_{in} = Q_{out} = Q_h$, assuming that the air density in the plenum is the same at atmospheric air density and applying a simple model of air volume flow rate through an orifice:

$$Q_h = A_{Lh}c_n\sqrt{(2p_h/\rho_a)} \tag{5.28}$$

Let:

$$K_2 = \rho_a c_n\sqrt{(2p_h/\rho_a)} \tag{5.29}$$

Therefore:

$$\rho_a Q_h = K_2 A_{Lh} \tag{5.30}$$

$$\rho_a Q_{in} = K_2 A_{Lh} + \rho_a\left(\frac{\delta Q}{\delta p}\right)p_h\mu \tag{5.31}$$

The effect of the plenum air pressure on the volume flow rate of air into the plenum is deemed to be insignificant, due to the flat fan characteristic. The air blower was tested to confirm this. The blower was arranged to supply air into a known flexible volume through a duct. The time taken to inflate the flexible volume was measured. A constriction in the duct was changed to create a duct pressure that the blower had to work against. An industrial manometer was used to measure the static air pressure across the duct

constriction. At a static air pressure similar to the static equilibrium pressure of the mass-plenum system, the volume flow rate of the air was unaffected. Therefore the fan characteristic slope (relating the volume flow rate to the pressure difference across the inlet duct) was set to zero Eq. (5.32).

$$\left(\frac{\delta Q}{\delta p}\right) = 0 \tag{5.32}$$

$$\rho_a \left(\frac{\delta Q}{\delta p}\right) p_h \mu = 0 \tag{5.33}$$

$$\rho_a Q_{in} = K_2 A_{Lh} \tag{5.34}$$

Table 5.1 lists the factors relevant to the air flow into the plenum. The actual volume flow rate of the air into the plenum was found by measuring the air speed along the centreline of the inlet duct and modifying by an estimated factor (from the Moody chart) for the flow through a turbulent duct (Munson et al., 1990, pp. 492-504). The air inlet duct had a constant and known cross-sectional area.

Table 5.1. Parameters for the air flow into the plenum

Term	Symbol
Q_{in}	volume flow rate of air into the plenum
v_{in}	air flow velocity, measured in the duct, on the centreline
A_{duct}	cross-sectional area of the duct

$$Q_{in} = v_{in} A_{duct} \tag{5.35}$$

The generally accepted value for orifice coefficient of a sharp edged orifice, such as used in this experimental rig, is $c_n = 0.61$ (Munson et al., 1990, p. 126). Equation (5.36) was used to validate the estimates for the turbulent flow volume flow rate based on the centreline air velocity, given that all other parameters were measurable. A further validation was done by timing the inflation of a bag of known volume use the air supply system.

$$v_{in} A_{duct} = \rho_a c_n A_{e0} \sqrt{\frac{2p_h}{\rho_a}} \tag{5.36}$$

As the air volume flow rate into the plenum is constant, it does not explicitly appear as a block in the Simulink block diagram described in Sec. 5.9.

5.6.4. Air volume flow rate exiting the plenum

The second term in Eq. (5.26), that is, $(\rho_a Q_{out})$, describes the mass flow rate of air out of the plenum. Applying the simple model of air volume flow rate through an orifice, allowing for instantaneous changes in cushion pressure, p. The air exit area A_e is fixed.

$$\rho_a Q_{out} = \rho_a c_n A_L \sqrt{\frac{2p}{\rho_a}} \tag{5.37}$$

The air exit area A_e on the experimental rig was fixed and comprised a non-varying part (A_{e0}) and part that was used as an independent variable (A_{eE}). Before each experimental run A_{eE} was changed to a predetermined area. For some experimental runs during the commissioning tests (Sec. 6.3) unplanned parasitic air leakage was detected. The parasitic air leakage area (A_L) was added to the other components of A_e Eq. (5.38), for the main experiments (Sec. 6.5), the parasitic air leakage area was eliminated and $A_L = 0$.

$$A_e = A_{e0} + A_{eE} + A_L \tag{5.38}$$

The instantaneous pressure, in terms of non-dimensional pressure perturbation and hover pressure is given by:

$$p = \mu p_h + p_h \tag{5.39}$$

Therefore, Eq. (5.37) can be rewritten as:

$$\rho_a Q_{out} = \rho_a c_n A_e \sqrt{\frac{2\mu p_h + p_h}{\rho_a}} \tag{5.40}$$

simplifying Eq. (5.40) gives:

$$\rho_a Q_{out} = \rho_a c_n A_e \sqrt{2} \sqrt{\frac{p_h(\mu + 1)}{\rho_a}} \tag{5.41}$$

5.6.5. Air compressibility

Turning now to the second right-hand term of Eq. (5.26), that is $V {}^{d\rho}/_{dt}$. The adiabatic pressure-density law is used in Kaplan et al. (1974, equation 8):

$$\frac{p}{\rho^\gamma} = \frac{p + p_a}{\rho^\gamma} = \frac{p_a + p_0}{\rho_a^\gamma} = \text{constant} \tag{5.42}$$

The non-linear adiabatic gas law is expressed in terms of μ and linearised in several papers: Kaplan et al. (1974), Doctors (1978) and Kaplan et al. (1981):

$$\begin{aligned} \rho &= \rho_h \left[1 + \frac{1}{1 + ({}^{p_a}/_{p_0})} \mu \right]^{\frac{1}{\gamma}} \\ &\approx \rho_a \left[1 + \frac{1}{\gamma(1 + ({}^{p_a}/_{p_h}))} \mu \right] \end{aligned} \tag{5.43}$$

This was checked by repeating the mathematical derivation

$$
\begin{aligned}
\frac{p+P_a}{\rho^\gamma} &= \frac{p_0+p_a}{\rho_h^\gamma} \\
\frac{p+P_a}{p_0+p_a} &= \frac{\rho^\gamma}{\rho_h^\gamma} \\
\frac{p+P_a+p_0-p_0}{p_0+p_a} &= \frac{\rho^\gamma}{\rho_h^\gamma} \\
1+\frac{p-p_0}{p_0+p_a} &= \frac{\rho^\gamma}{\rho_h^\gamma} \\
1+\frac{p_0\mu}{p_0\left(1+{}^{p_a}/_{p_0}\right)} &= \frac{\rho^\gamma}{\rho_h^\gamma} \\
1+\frac{\mu}{\left(1+{}^{p_a}/_{p_0}\right)} &= \frac{\rho^\gamma}{\rho_h^\gamma} \\
\rho_h^\gamma\left[1+\frac{\mu}{\left(1+{}^{p_a}/_{p_0}\right)}\right] &= \rho^\gamma \\
\rho_h\left[1+\frac{\mu}{\left(1+{}^{p_a}/_{p_0}\right)}\right]^{\frac{1}{\gamma}} &= \rho
\end{aligned}
\tag{5.44}
$$

The linearisation is done by applying the Taylor series and neglecting higher order terms Eq. (5.45) about the value $\mu = 0$ (a Maclaurin series) Eq. (5.46). The published Eq. (5.43) uses ρ_a whereas the equation should use the term ρ_h. The density of the air within the plenum should be greater than the atmospheric air density, but the difference will not be large as the pressure difference is not large. The derived equation Eq. (5.46) will be used for analysis in the current research program.

$$
f(x) = f(a) + (x-a)f'(a) \tag{5.45}
$$

$$
\begin{aligned}
& & \rho(\mu) &= \rho_h\left[1+\frac{\mu}{\left(1+{}^{p_a}/_{p_0}\right)}\right]^{1/\gamma} \\
\text{therefore} & & \rho(0) &= \rho_h\left[1+\frac{0}{\left(1+{}^{p_a}/_{p_0}\right)}\right]^{1/\gamma} = \rho_h \\
\text{derivative} & & \rho'(\mu) &= \frac{\rho_h}{\gamma\left(1+{}^{p_a}/_{p_0}\right)}\left[\frac{\mu}{\left(1+{}^{p_a}/_{p_0}\right)}+1\right]^{-1/\gamma} \\
\text{therefore} & & \rho'(0) &= \frac{\rho_h}{\gamma\left(1+{}^{p_a}/_{p_0}\right)}\left[\frac{0}{\left(1+{}^{p_a}/_{p_0}\right)}+1\right]^{-1/\gamma} \\
& & \rho'(0) &= \frac{\rho_h}{\gamma\left(1+{}^{p_a}/_{p_0}\right)} \\
\text{Taylor series} & & \rho(\mu) &\approx \rho_h + \frac{\rho_h\mu}{\gamma\left(1+{}^{p_a}/_{p_0}\right)} \\
& & \rho(\mu) &\approx \rho_h\left[1+\frac{\mu}{\gamma\left(1+{}^{p_a}/_{p_0}\right)}\right]
\end{aligned}
\tag{5.46}
$$

5.6.6. Variations in plenum volume

The first right hand term of Eq. (5.26), that is $\rho^{dV}/_{dt}$, accomodates the changes of plenum volume with time. Kaplan et al. (1974) also use a relation for the change in cushion volume with time:

$$\frac{dV}{dt} = -A\dot{z} + Ax_{cp}\dot{\theta} + \frac{d}{dt}(V_{waves}) \tag{5.47}$$

For the experimental rig, the volume can be forced (wave volume pumping) but there is only one degree of freedom, the rotation of the heave deck. Taking ϕ as the rotation of the wave volume pump and A_p as the area swept by the wave volume pump and assuming that the plan-form area of the plenum is the same as the area of the heave deck (A), then we derive the equation for the instantaneous volume of the plenum.

$$V = Ah - V_{waves} + Ax_{cp}\theta \tag{5.48}$$

The wave volume pump consists of a revolving plate, width of w, outer radius of r_2 and inner radius of r_1, the volume pumped is given by:

$$V_{waves} = \frac{w}{2}(r_2^2 - r_1^2)\phi(t) \tag{5.49}$$

$$\frac{dV}{dt} = Ax_{cp}\dot{\theta} - \frac{d}{dt}(V_{waves}) \tag{5.50}$$

$$\frac{d}{dt}(V_{waves}) = \frac{w}{2}(r_2^2 - r_1^2)\dot{\phi}(t) \tag{5.51}$$

To simplify the equations, a constant (V_{unit}) is defined indicate the unit swept volume of the wave volume pump:

$$V_{unit} = \frac{w}{2}\left(r_2^2 - r_1^2\right) \tag{5.52}$$

$$\frac{d}{dt}(V_{waves}) = V_{unit}\dot{\phi}(t) \tag{5.53}$$

$$V_{waves} = V_{unit}\phi(t) \tag{5.54}$$

$$V = Ah - V_{unit}\phi(t) + Ax_{cp}\theta \tag{5.55}$$

$$\frac{dV}{dt} = Ax_{cp}\dot{\theta} - V_{unit}\dot{\phi} \tag{5.56}$$

Analysis of the air plenum system indicated that the damped frequency of the system is very sensitive to dynamic volume changes. While the air plenum chamber was constructed as stiff as practical, the large size of the walls presented to the air plenum pressure made it possible for small changes in air plenum volume due to instantaneous pressure, especially if, as predicted, the time-wise mean air pressure would increase at high frequencies of forced air plenum volume oscillations, which would result in instantaneous pressures being significantly higher than the static equilibrium air plenum pressure.

It was decided to adopt a simple model of the 'volumetric stiffness' of the air plenum chamber. It was assumed that instantaneous air plenum pressure would act on a surface area A_V equivalent to the two longer side walls, which are the length of the plenum L and the height of the plenum h_0:

$$A_V = 2h_0L \tag{5.57}$$

The virtual displacement of the wall z_V was assumed to be uniform across the wall and to be resisted by a linear spring:

$$z_V = \frac{\mu p_h}{k_p} \tag{5.58}$$

The stiffness of this linear spring k_p would have to be found experimentally. The volume change due to wall flexibility V_V is simply the virtual displacement of the wall:

$$V_V = z_V A_V \tag{5.59}$$

5.6.7. Combined effect of density and volume changes

The first term of the right hand side of Eq. (5.26) is the derivative of the product of density and volume ($^{d(\rho V)}/_{dt}$). The density has been discussed in Sec. 5.6.5 and the plenum volume has been discussed in Sec. 5.6.6. The derivative is taken by applying the product rule Eq. (5.26) which results in two terms. The $\rho\, ^{dV}/_{dt}$ term can be expanded by substituting Eq. (5.46) and Eq. (5.56):

$$\rho\frac{dV}{dt} = \rho_h\left[1 + \frac{\mu}{\gamma(1 + (p_a/p_h))}\right] \times \left[Ax_{cp}\dot{\theta} - V_{unit}\dot{\phi}\right] \tag{5.60}$$

multiplying out:

$$\rho\frac{dV}{dt} = \rho_h Ax_{cp}\dot{\theta} - \rho_h V_{unit}\dot{\phi} + \frac{\rho_h\mu Ax_{cp}\dot{\theta}}{\gamma(1 + (p_a/p_h)} - \frac{\rho_h\mu V_{unit}\dot{\phi}}{\gamma(1 + (p_a/p_h))} \tag{5.61}$$

If Kaplan et al. (1981) is followed, two terms are neglected, apparently because all coupled terms were presumed negligible, although the rationale for dropping these terms is not given in the cited paper.

$$\rho\frac{dV}{dt} \approx \rho_h Ax_{cp}\dot{\theta} - \rho_h V_{unit}\dot{\phi} + \cancel{\frac{\rho_h\mu Ax_{cp}\dot{\theta}}{\gamma(1 + (p_a/p_h)}} - \cancel{\frac{\rho_h\mu V_{unit}\dot{\phi}}{\gamma(1 + (p_a/p_h))}} \tag{5.62}$$

Now consider the second right hand term of Eq. (5.26), $V\, ^{d\rho}/_{dt}$. The derivative of Eq. (5.43) (the linearised version):

$$\frac{d\rho}{dt} = \frac{d}{dt}\left[\rho_h + \frac{\rho_h}{\gamma(1 + (p_a/p_h))}\mu\right] = \frac{\rho_h\dot{\mu}}{\gamma(1 + (p_a/p_h))} \tag{5.63}$$

The instantaneous volume of the plenum is given by Eq. (5.55). Therefore, the fully developed term $V\, ^{d\rho}/_{dt}$ is given by Eq. (5.64).

$$V\frac{d\rho}{dt} = [Ah - V_{unit}\phi(t) + Ax_{cp}\theta] \times \left[\frac{\rho_h\dot{\mu}}{\gamma(1 + (p_a/p_h))}\right] \tag{5.64}$$

Multiplying out gives:

$$V\frac{d\rho}{dt} = \frac{Ah\rho_h\dot{\mu}}{\gamma(1+(p_a/p_h))} - \frac{V_{unit}\phi\rho_h\dot{\mu}}{\gamma(1+(p_a/p_h))} + \frac{Ax_{cp}\theta\rho_h\dot{\mu}}{\gamma(1+(p_a/p_h))} \tag{5.65}$$

Kaplan et al. (1974) assumed that terms that are product of derivatives can be neglected. However, all terms containing the rate of change of the volume will be retained in this mathematical model, to allow investigation of the effects of the rate of change of the plenum volume, particularly on the change in mean displacement of the supported mass when the plenum volume is oscillated at higher frequencies. A solution of a SES dynamics mathematical model which includes the coupled terms Eq. (5.65) was not found in the available literature, and as such, this is a novel contribution of the research reported in this thesis.

The final form of the right hand side of Eq. (5.26) includes five terms that are products of functions of time Eq. (5.66).

$$\begin{aligned}\rho\frac{dV}{dt} + V\frac{d\rho}{dt} = &\left[\rho_a Ax_{cp}\dot{\theta} - \rho_a V_{unit}\dot{\phi} + \frac{\rho_a\mu Ax_{cp}\dot{\theta}}{\gamma(1+(p_a/p_h)} - \frac{\rho_a\mu V_{unit}\dot{\phi}}{\gamma(1+(p_a/p_h))}\right] + \dots \\ &\left[\frac{Ah\rho_a\dot{\mu}}{\gamma(1+(p_a/p_h))} - \frac{V_{unit}\phi\rho_a\dot{\mu}}{\gamma(1+(p_a/p_h))} + \frac{Ax_{cp}\theta\rho_a\dot{\mu}}{\gamma(1+(p_a/p_h))}\right]\end{aligned} \tag{5.66}$$

To simplify the manipulation of Eq. (5.66), constants are defined as follows.

$$K_1 = \rho_a Ax_{cp} \tag{5.67}$$

$$K_2 = \rho_a V_{unit} \tag{5.68}$$

$$K_3 = \gamma\left(1 + \frac{p_a}{p_h}\right) \tag{5.69}$$

$$K_4 = Ah\rho_h \tag{5.70}$$

Substituting the defined constants into Eq. (5.66) gives:

$$\rho\frac{dV}{dt} + V\frac{d\rho}{dt} = K_1\dot{\theta} - K_2\dot{\phi} + \frac{K_4\dot{\mu}}{K_3} + \frac{K_1\mu\dot{\theta}}{K_3} - \frac{K_2\mu\dot{\phi}}{K_3} - \frac{K_2\phi\dot{\mu}}{K_3} + \frac{K_1\theta\dot{\mu}}{K_3} \tag{5.71}$$

Four terms in Eq. (5.71) are products of functions of t: when paired together, they are recognisable as the result of the product rule being applied to another function of t.

$$\frac{K_1\mu\dot{\theta}}{K_3} + \frac{K_1\dot{\mu}\theta}{K_3} = \frac{K_1}{K_3}\frac{d(\mu\theta)}{dt} \tag{5.72}$$

$$-\frac{K_2\mu\dot{\phi}}{K_3} - \frac{K_2\dot{\mu}\phi}{K_3} = -\frac{K_2}{K_3}\frac{d(\mu\phi)}{dt} \tag{5.73}$$

5.6.8. System model adopted for experiment

The final mathematical model of the plenum pressure includes modelling the exiting air volume flow rate as dependent on the instantaneous pressure in the plenum and including the two coupled terms of Eq. (5.61) see Eqs. (5.34), (5.41) and (5.66).

$$K_8\sqrt{K_9} - K_8\sqrt{K_9(\mu+1)} = K_1\dot{\theta} - K_2\dot{\phi} + \frac{K_4\dot{\mu}}{K_3} + \ldots \\ \frac{K_1\mu\dot{\theta}}{K_3} - \frac{K_2\mu\dot{\phi}}{K_3} - \frac{K_2\phi\dot{\mu}}{K_3} + \frac{K_1\theta\dot{\mu}}{K_3} \quad (5.74)$$

Applying the Laplace transform gives:

$$K_8\sqrt{K_9} - K_8\sqrt{K_9(\mu+1)} = K_1\theta s - K_2\phi s + \frac{K_4\mu s}{K_3} + 2\frac{K_1\mu\theta s}{K_3} - 2\frac{K_2\mu\phi s}{K_3} \quad (5.75)$$

This system of equations, formulated in terms of the Laplace variable, is in a convenient form for encapsulating as a block diagram, which is the form used to program a numerical solution in the Simulink environment of the MATLAB software. The numerical solution will be discussed in Sec. 5.9.

The experimental rig parameter values that could be directly measured are in Table 5.2. Seven of the experimental rig parameter values required experimental quantification Secs. 6.2 and 6.4.

Table 5.2. Numerical values of the parameters used in the mathematical model of the heave deck initial value problem.

Parameter	Value	Units
I	61.12	$\mathrm{kg\,m}$
X_{cp}	1.00	m
C_o	934.675×10^{-3}	dimensionless
C_f	135	dimensionless
W	600×10^{-3}	m
L	2.000	m
k	7.04×10^3	$\mathrm{N\,m^{-1}}$
X_s	1.899	m
A_1	10.4412×10^{-3}	$\mathrm{m^2}$
A_{L1}	1.7012×10^{-3}	$\mathrm{m^2}$
A_{L2}	2.0051×10^{-3}	$\mathrm{m^2}$
A_{L3}	2.3867×10^{-3}	$\mathrm{m^2}$
S_h	38.5×10^{-3}	m
V_1	5.3	$\mathrm{m\,s^{-1}}$

5.7. Environmental and random factors

This section discusses the environmental factors most likely to affect the experimental program and the steps that were taken to minimise their impact.

The atmospheric conditions of pressure, humidity and temperature could have affected the experiment if their effects were unmitigated. The density of the air being drawn into the system is dependent on atmospheric conditions. The efficiency of the blower feeding air into the plenum is affected by atmospheric conditions. The expulsion of air from the experimental rig to the atmosphere is affected by atmospheric conditions.

Where possible, the order of experiments was randomised by reference to the random number generator available at www.random.org. Changing the plenum height involved unsealing and resealing the plenum chamber, so all runs planned for a particular plenum height were done in a group; the order of runs within the group being random. Wherever possible, a set of experimental runs was completed over a short period of time to minimise variability in the atmospheric conditions.

At the start of every experimental session, and then at regular intervals afterwards, the atmospheric conditions were measured and recorded. Atmospheric pressure was found by referring by the local readings from the Bureau of Meteorology. Temperature and humidity were found locally using a digital thermometer and hygrometer located in the laboratory.

Atmospheric conditions had the potential to affect the experimental results, but a combination of randomised experimental factors, monitoring atmospheric conditions in order to detect extremes and completing sets of experiments in similar atmospheric conditions minimised the impact.

5.8. Measurement system

A custom measurement system was designed and built for this experimental program. The primary sensor used was a laser interferometer, to measure the displacement of the heave deck (Table 5.3).

Table 5.3. Laser interferometer characteristic parameters and values

Parameter	Value
Measuring range	400 mm
Linearity	700 µm
Resolution	600 µm

A dedicated Data Acquisition system (DAQ) was used, taking a voltage signal from the laser interferometer and sampling at 25 kHz a high enough sampling rate to allow for accurate sensing of the expected natural frequency, forcing frequency and any unexpected higher frequencies (such as spatially varying air pressure). The DAQ was used to record time series data.

A smaller laser interferometer was used to measure the displacement of the oscillating flap used to force plenum volume changes. This sensor had a range of 20 mm, linearity of 40 µm and a dynamic resolution of 10 µm at 750 Hz.

During commissioning tests, the small laser interferometer and an accelerometer were also used to measure the heave deck displacement and acceleration, to validate the measurements made by the primary sensor.

5.9. Numerical solution of the mathematical model

The mathematical model of the experimental rig (Sec. 5.6) was solved using the Simulink environment of MATLAB software. Equation (5.75) can be expressed in block diagram form directly within the Simulink environment of MATLAB software, allowing the system of equations to be solved numerically. The full block diagram is shown in Fig. 5.15 with some blocks shown as summary blocks. Details of the summary blocks are shown in subsequent figures (Figs. 5.16 to 5.18).

The Simulink model is programmed to respond to a pure sine wave, modelling the displacement of the plenum volume forcing 'flapper'. The Simulink model was also programmed to alternatively respond to a data file containing a time-series of the flapper displacement represented in the block diagram as a data file input block and a switch element on the signal path respectively (Fig. 5.15).

The flapper displacement, the heave deck angular displacement and the displacement of the flexible plenum walls are used to calculate the changes in plenum volume (gains K1, K2, K15, K12 and K13 in Fig. 5.15). The changes in the plenum volume result in a change of plenum pressure, calculated in block $^{K3}/_{K4}$. The exit air flow acts as a feedback loop responding to the plenum pressure and directly affecting the plenum pressure, described in more detail below. The flexible plenum walls also respond to the plenum pressure, forming another feedback loop via the change in plenum volume (gains K12 and K13 in the diagram). The plenum pressure is also fed back to the coupled volume and pressure sub-system, described in more detail below. The heave deck responds to the changes in plenum volume (Heave Deck EoM block in the diagram) and the angular displacement of the heave deck is fed back to calculate its effect on the plenum volume as well as being fed back into the couple volume and pressure sub-system. The displacement of the heave deck at the sensor position is calculated and forms the output of the system. The results of the Simulink model are fed to a visual display in real time during running and to computer file.

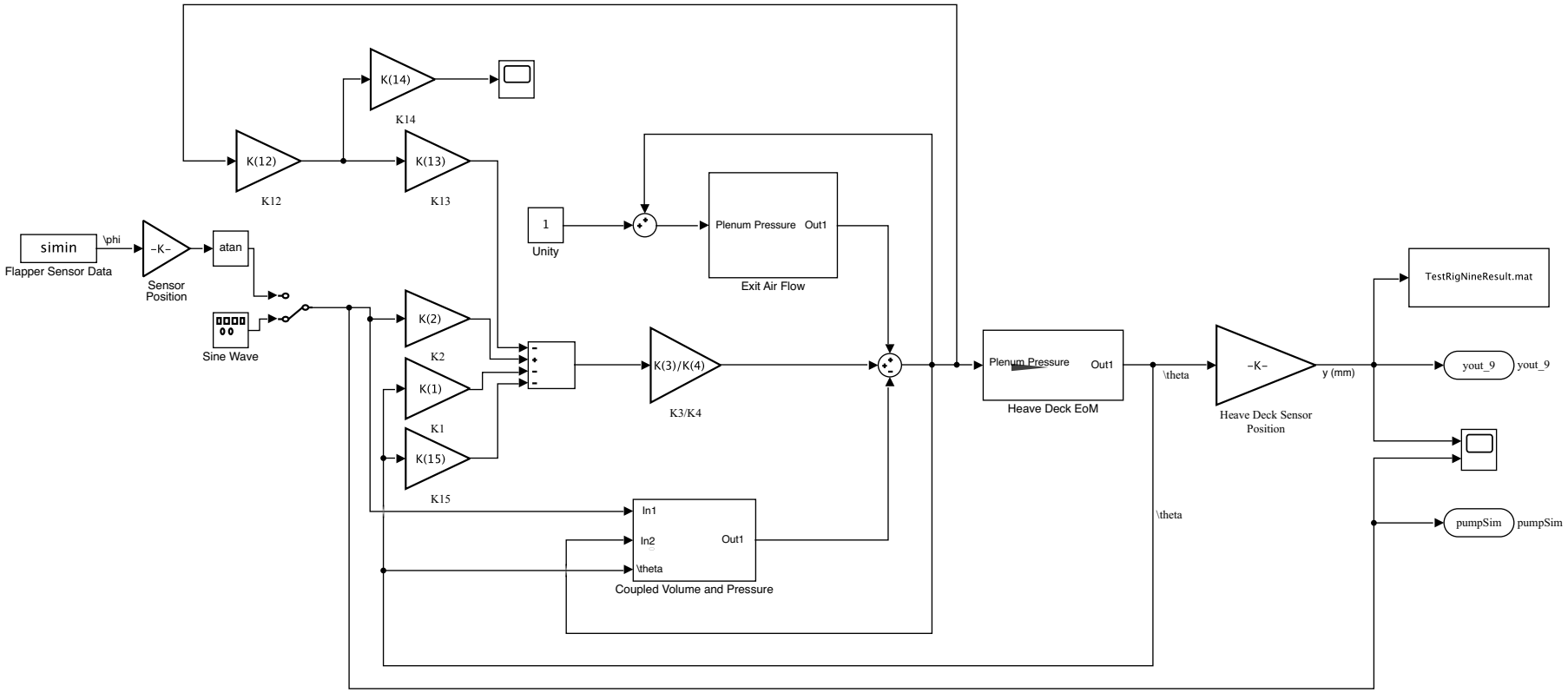


Figure 5.15. Overall mathematical model of the experimental rig expressed in block diagram form within the Simulink environment of MATLAB. Section 5.6 contains details of the associated mathematical model. The three main sub-systems (heave deck, coupled volume and pressure and exit air flow) are represented by summary blocks in this diagram and the details are shown in Figs. 5.16 to 5.18.

The heave deck equation of motion (Sec. 5.6.1) is shown in the Simulink block diagram form in Fig. 5.16. The equation of motion Eq. (5.24) is used. The Coulomb friction and the velocity dependent heave deck resistance are modelled in a combined block, a standard block of the Simulink library (the 'Coulomb and Viscous Friction' block). The heave deck equation of motion for the case where the spring becomes completely slack is not shown in Eq. (5.24), but it is modelled in the Simulink model. The limits of the spring extension incorporated in the Simulink block diagram using a 'Saturation' block.

The air mass continuity through the plenum, discussed in Secs. 5.6.2 to 5.6.5, is shown in its Simulink block diagram form in Fig. 5.17. The Simulink environment enables the rapid computation of the square-root, absolute and saturated elements of the mathematical model, using standard blocks from the Simulink library.

The cross-product terms described in Sec. 5.6.7 are best solved numerically and are the principal reason for using Simulink to solve the experimental rig mathematical model. The Simulink block diagram for the mathematical model described in Sec. 5.6.7 is shown in Fig. 5.18.

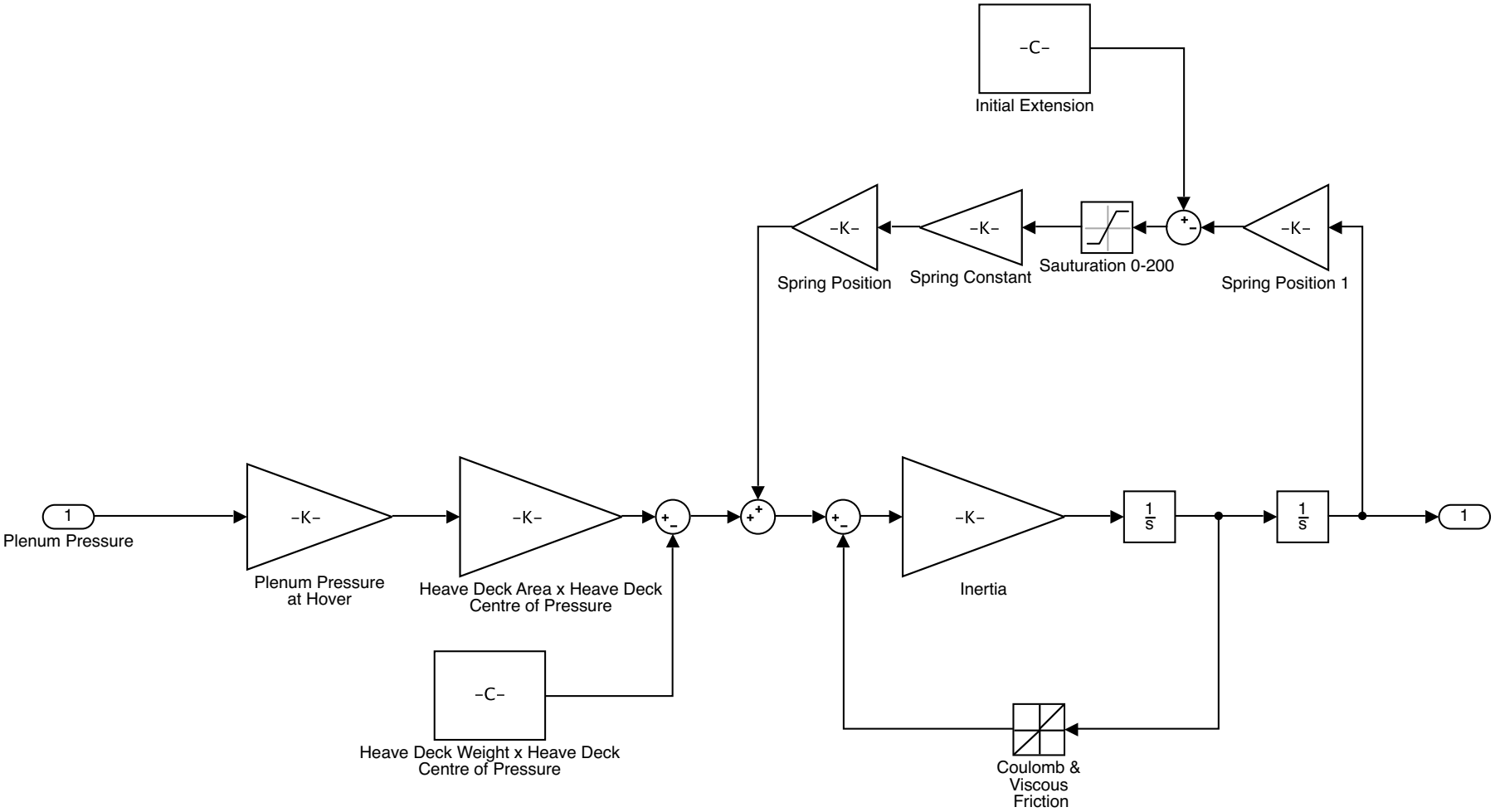


Figure 5.16. The experimental rig supported mass equation of motion, expressed as a block diagram within the Simulink environment of MATLAB. Section 5.6.1 contains details of the associated mathematical model.

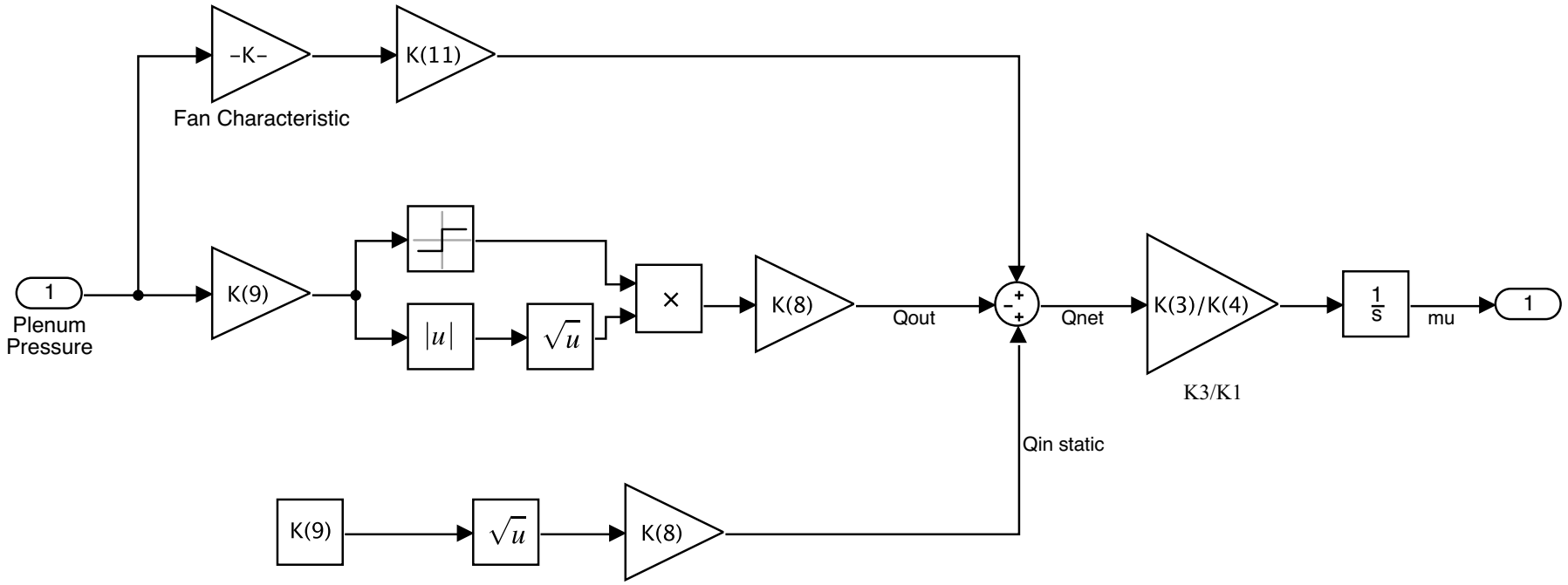


Figure 5.17. The experimental rig plenum volume air mass continuity expressed as a block diagram within the Simulink environment of MATLAB. Sections 5.6.2 to 5.6.5 contains details of the associated mathematical model.

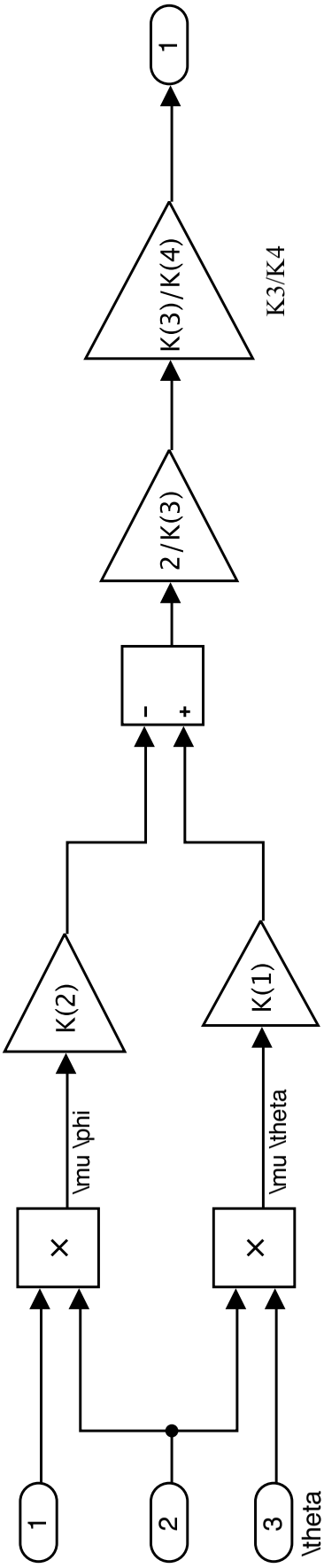


Figure 5.18. The experimental model air density and plenum volume rates of change expressed as a block diagram within the Simulink environment of MATLAB. Section 5.6.7 contains details of the associated mathematical model.

The mathematical model was solved numerically. The numerical solution of the mathematical model was carried out by coding the mathematical model as a Simulink model in the software package MATLAB Relase 2018b. The Simulink model was solved using the Runge-Kutta numerical solver with a fixed step. Various solvers available in Simulink were trialled and the Runge-Kutta numerical solver was computationally efficient and provided consistent solutions (comparing numerical solutions at neighbouring forcing frequencies).

The forcing function used in the numerical model was a pure sine function. The mechanism used to oscillate the plenum volume was a simple crank-rocker mechanism, which does not produce a pure sine wave displacement. The actual displacement of the forcing mechanism will have a slightly different velocity profile to a pure sine wave. A study of this characteristic was undertaken by using the actual forcing mechanism displacement time history in the numerical solution to the mathematical model. There was an observable but not significant effect on the projected heave deck displacements. A pure sine wave oscillation was therefore used in the numerical solution to the mathematical model as its frequency could readily be changed and was free of any measurement errors.

The numerical solution to the mathematical model was found for a range of forcing frequencies. The numerical solution was found at 50 increments of the frequency range. The frequency range was set at 1 Hz to 10 Hz, this being the approximate range of the experimental forcing. The experimental results are plotted as a dashed line on the results reported in Chapter 6.

In summary:

1. The mathematical model was solved numerically in the Simulink environment of the software package MATLAB.
2. The numerical solution used the Runge-Kutta solver with a fixed step.
3. The numerical solution adopted a sinusoidal plenum volume forcing function.
4. The plenum wall flexibility specific to each height of plenum found during the commissioning tests was used in the numerical solutions.
5. The plenum was stiffened slightly after the commissioning tests.
6. The plenum chamber was re-sealed after the commissioning tests and the numerical solutions assumed that there was no parasitic air leakage.
7. The Coulomb friction for each combination of plenum height and air exit area found during the commissioning tests was used in the numerical solution.
8. The mean velocity-dependent heave deck resistance from the final commissioning test runs was used in the numerical solution.
9. The numerical solution was repeated at 50 frequencies, at equal intervals, between 1 Hz and 10 Hz, for each combination of plenum height and air exit area.

5.10. Coupled oscillation and steady decline motions

Commissioning tests of the experimental rig (Secs. 6.3 and 6.4) provided insight into the multi-facted behaviour of the mass-plenum system. The motion of the heave deck is influenced by two dominant phenomena, which are inevitably coupled. Heave deck motion analysis must accommodate both phenomena. A typical time history for the heave deck displacement following a step-change to the plenum volume is shown in Fig. 5.19. Two features have been annotated. The first, shown by a green line, is a general decay in the heave deck position as it returns to the hover displacement, slowed by the need to force air out of the plenum. In Fig. 5.19, an exponential curve has been fitted to the data, starting at the peak of heave deck displacement. The second feature is the oscillation of the heave deck as the 'springiness' in the system allows for oscillation. The fitted curve has been subtracted from the heave deck displacement time history and the result has been plotted as the red line. This red line is an approximation of the oscillating portion of the heave deck response. The decay in oscillation magnitude is due to damping in the system.

The decay in position and the decay in oscillations are coupled and neither can be isolated from the other in this system. The decay in displacement can be made larger compared to the decay in oscillations by setting up an experiment the heave deck released from a large initial displacement. The oscillations will tend to be the same magnitude, whereas the decay in displacement starts from a larger magnitude and takes much longer. Conversely, a very small step-change in the air plenum volume leads to a small initial displacement and hence a quicker decay in displacement, which tends to emphasise the decay in oscillations. Neither decay can be completely removed from the system.

The presence of both the decay in displacement and the decay in oscillations leads to the time period between successive peaks in displacement becoming progressively shorter. The early peaks, added to the high displacement, tend to shift slightly earlier; as the decay in displacement decreases, the peaks in the oscillations become closer to their true position in time. As the oscillations decay and become less pronounced, finding the time of the peak becomes slightly more difficult. To find the period of the oscillations, the mean of the set of periods between successive peaks was found: this was practical, but will lead to a very small under-estimation of the period, hence an over-estimation of the damped frequency. In Fig. 5.19, an approximate value for the natural frequency has been found by calculating the power spectrum of the isolated oscillating portion of the heave deck response, shown as the lower set of axes in the plot. Lower frequencies have been ignored, the maximum power is at 5.51 Hz, about 10% higher than the natural frequency calculated from the period between successive peaks (5 Hz).

The decay in displacement resists analytic treatment. An expression for the decay in displacement can be derived, but the expression is intractable and cannot be successfully solved by Computer Algebra Systems (CAS).

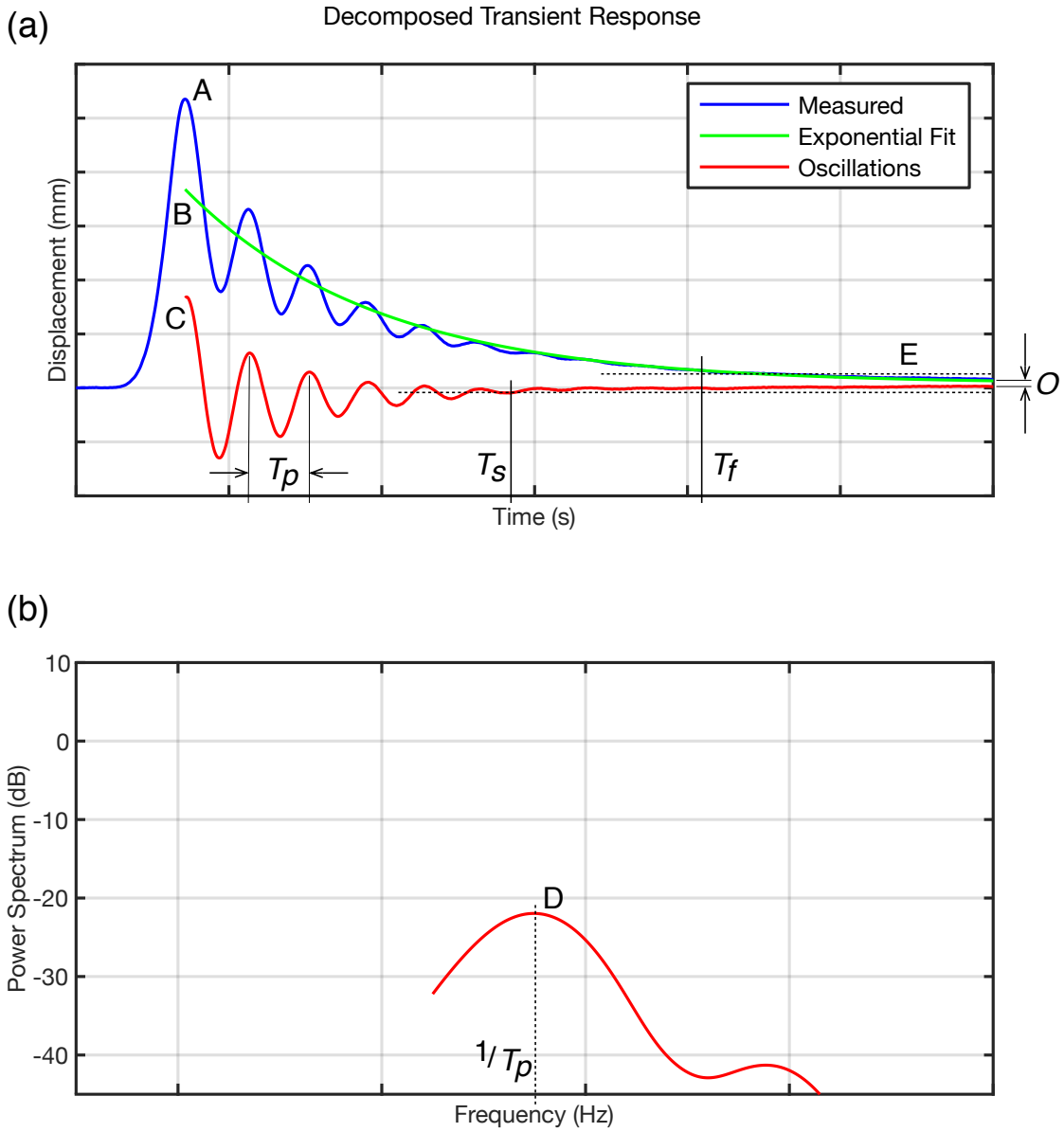


Figure 5.19. Analysis of supported mass motions in response to step-change of the plenum volume. Top: Deck displacement data. Bottom: Power spectrum analysis of the deck displacement data. The parameters shown on the plot and the analysis that enabled their calculation is discussed in Fig. 6.2 and Sec. 6.3.

5.11. Concluding remarks

After a preliminary experiment that offered intriguing results, a new research question (QA) was developed and added to questions arising from the literature review. A set of hypotheses was postulated so that the research questions could be addressed experimentally.

By abstracting the SES air lift system and developing a physical analogue of the SES air lift system, an experimental apparatus was designed and built. The experimental apparatus is different from equivalent experimental apparatus previously reported in the available literature in seven ways. The experimental apparatus:

1. is capable of air compressibility effects at observable levels
2. is capable of significant rates of change of plenum chamber volume and significant rates of change of air mass in the plenum chamber so the coupled effects are observable
3. does not use water as an element, thus eliminating unwanted hydrodynamic effects
4. allows a simple form of motion damping to be used, avoiding the need to reproduce the hydrodynamic damping of the SES in the laboratory
5. can provide a fixed air exit area, eliminating the unwanted air exit area dynamics
6. minimises the air blower pressure-flow dynamic, allowing it to be removed from the analysis
7. allows a simple form of the relationship between plenum pressure and secondary plenum volume changes to be used for analysis

The mathematical model of the theoretical system—an air plenum with constant and compressible through flow, forced changes in volume and pressure-dependent volume changes—was developed by the author and transformed into block diagram form so that it could be numerically solved using the Simulink package of MATLAB, enabling quantified predictions of the experimental rig behaviour based on the incorporated hypotheses. Experimental rig parameter values will be found experimentally (Chapter 6) by conduiting commissioning tests using the experimental rig in its plenum volume forced step-change configuration. The main experimental program is then completed, using the experimental rig in its plenum volume forced oscillation configuration, with quantified theoretical predictions produced using the Simulink model (Chapter 6).

6. Experimental results and analysis

6.1. Introduction

This chapter reports on the results of the experiments completed to test the hypotheses raised in this research program (Sec. 5.3). Sections 6.2 to 6.4 report the results of experiments done to find experimental rig parameter values and characteristics. These experiments were completed using the experimental rig in the plenum volume forced step-change configuration. Section 6.5 reports the main experiment results, which used the experimental rig in the plenum volume forced oscillations configuration.

Section 6.2 quantifies experimental rig sub-system parameter values: stiffness of the buoyancy analogue spring and heave deck rotational inertia.

Section 6.3 presents the commissioning tests to experimentally find three characteristics of the experimental rig behaviour: the damped frequency (Sec. 6.3.1); the settling time (Sec. 6.3.2); and defining and determining a characteristic that is distinctive to the mass-plenum system, i.e. the falling time (Sec. 6.3.3). The commissioning test is done with the experimental rig in the plenum volume forced step-change configuration (Sec. 5.5). To find these three characteristics of the experimental rig behaviour, the data gathered is analysed using a decomposition of the supported mass time-series (Sec. 6.3).

Section 6.4 determines four experimental rig parameter values by analysing the data gathered in the commissioning test using a method of curve fitting. The four parameter values found using this method are: dry (Coulomb) friction (Sec. 6.4.1), parasitic air leakage area (Sec. 6.4.2), the lumped parameter for plenum chamber stiffness (Sec. 6.4.3) and velocity-dependent heave deck resistance (Sec. 6.4.4).

Section 6.5 contains the main forced oscillating experimental results of the research program, that is, results associated with the displacement of the heave deck when the plenum volume is forced to oscillate over a range of discrete frequencies. The experiment was repeated for several values of plenum height and air exit area to investigate the robustness and variability of results. Section 6.5.4.1 presents the results of an experiment conducted at one plenum height and one air exit area, with both parameters set at the mid-point of the range of available values in the test rig. Section 6.5.4.2 presents the results of the experiment being repeated at greater and lesser values of the air exit area. Section 6.5.4.3 presents results at greater and lesser values of the plenum height. Section 6.5.5 presents an overview of the results and discusses the identification of outlying results.

A summary of the experimental results is provided in Sec. 6.6.

6.2. Experimental rig parameter values—part one

The spring stiffness and the heave deck rotational inertia of the experimental rig were found experimentally, directly, and in isolation from the rest of the experimental rig. This section reports the experiments conducted to find these two parameter values.

6.2.1. Spring stiffness

The spring stiffness is an important characteristic of the plenum and heave deck system. The value of the spring stiffness facilitates the calculation of the plenum pressure, once the heave deck displacement is known. A commercial spring was chosen (Model C-259 from Century Springs, Los Angeles, U.S.A. — specification information in Table 6.2). As the manufacturer did not provide the precise elastic modulus of the material, the spring stiffness was found experimentally. The spring was loaded with known masses and the resultant spring length was measured (Table 6.1). Subtracting the extended spring length from the original unloaded spring length gives the spring extension (Table 6.1). The spring stiffness was found using linear regression (Table 6.2).

The spring was plastically stretched before use (by suspending a mass of 75 kg from the spring), to remove the set that the spring was manufactured with. The spring was intended to be completely unloaded during the cycle of the heave deck moving in response to pressure changes in the plenum, therefore the spring set would be an unwanted discontinuity when mathematically modelling the plenum pressure and heave deck system.

Table 6.1. Spring stiffness experimental results

Mass (kg)	Load (N)	Spring length (mm)	Spring extension (mm)
0.0	0.0	122.0	0.0
5.03	49.4	127.0	5.0
11.55	113.2	137.0	15.0
15.89	155.7	144.5	22.5
32.60	319.5	168.5	46.5

Table 6.2. Parameters and values for the spring used in the experimental rig

Spring parameter	Value	Notes
Material	Piano wire	The Elastic Modulus was not provided by the manufacturer.
Wire diameter	3.048 mm	
Coil outer diameter	20.65 mm	
Manufactured length	101.6 mm	The furthest extents of the coil, not including the hooks on the end
Stretched length	122.0 mm	After spring was permanently stretched with 75 kg load by the author to remove manufactured 'set'
Spring stiffness (k)	6.71 N mm^{-1}	Experiment completed by the author

6.2.2. Heave deck rotational inertia

The motion of the heave deck in response to plenum pressure is significantly dependent on the rotational inertia of the heave deck. The rotational inertia of the heave deck was found experimentally. A typical time history of the heave deck displacement following the lift and release of the heave deck is shown in Fig. 6.1.

After finding the spring stiffness, k, it was possible to then find the rotational inertia from the natural period of the heave deck and spring system. The heave deck was positioned within the experimental rig, but the plenum was not closed, so that the plenum pressure remained atmospheric. The heave deck was held at a steady displacement and released. The heave deck oscillated, with the oscillations decaying until the heave deck came to rest. The observed settling time of the heave deck (approximately 2.5 sec) was long compared to the period of the observed motions (approximately 300×10^{-3} sec), indicating a system with low damping. The experiment was repeated 48 times, with varying initial displacements.

The decay of the oscillations of the heave deck free motions is an indication of the damping in the system. The value of the damping ratio (ζ) was calculated from the experimental measurements by finding the reduction in the magnitude of successive peaks (y_1 and y_2) in the displacement time history Eq. (6.1) (Meriam & Kraige, 2008, p.608).

$$\zeta = \frac{\delta}{\sqrt{(2\pi)^2 + \delta^2}} \tag{6.1}$$

where

$$\delta = \ln\left(\frac{y_1}{y_2}\right) \tag{6.2}$$

The heave deck returns to the same height after oscillations cease, indicating that the damping is dependent on the motion of the heave deck, and hence is not due to Coulomb friction. One possible type of motion-dependent resistance is aerodynamic drag. However, the velocity of the heave deck is low and the aerodynamic resistance is also low. The hinges were lightly oiled throughput the experimental program and the presence of the oil makes it possible that viscous forces in the oil activated by rotations in the hinges led to a viscous friction being present in the system. Also, the flexible polyethylene seal was able to rub against itself or interfere with itself in the narrow gap between the heave deck and its cowling, these phenomena may result in a velocity-dependent resistance on the heave deck. The precise nature of the velocity-dependent resistance on the heave deck has no direct relevance to the current topic of investigation. The standard deviation of the damping ratio is substantial (Table 6.3) so it can be expected that some scatter of replicated results may occur in practice.

Table 6.3. Heave deck parameters and values

Parameter	Symbol	Value	Standard deviation
Rotational inertia	I_0	$61.1\,\mathrm{kg\,s^2}$	4.5
Natural frequency	ω_n	$3.25\,\mathrm{Hz}$	0.13
Damping ratio	ζ	0.07	0.01
Mass	m	$52.5\,\mathrm{kg}$	
Off-pressure spring extension	Δl_0	$37.8 \times 10^{-3}\,\mathrm{m}$	

The observed period (p, see Fig. 6.1) of the free oscillations is directly related to the damped frequency (ω_d) as in Eq. (6.3). The natural frequency (ω_n) is dependent on ω_d and ζ Eq. (6.4). These relationships were used to calculate the natural frequency (Table 6.3).

$$\omega_d = \frac{2\pi}{p} \tag{6.3}$$

$$\omega_n = \frac{\omega_d}{\sqrt{1-\zeta^2}} \tag{6.4}$$

Because the heave deck was designed to only rotate through small angles (θ), the spring extension (Δl) can be expressed in terms of the distance from the axis of rotation to the spring (X_s), see Eq. (6.5). The moment on the heave deck due to the spring force is the product of Δl with X_s: this allows the equation of motion to be found by applying Newton's second law Eq. (6.6). The equation of motion can be expressed in terms of ω_n Eq. (6.7), which gives an equation for ω_n in terms of I Eq. (6.8). Rearranging gives the rotational inertia of the heave deck (I) in terms of k, X_s and ω_n Eq. (6.9). Using Eq. (6.9), the heave deck rotational inertia was calculated from the experimental results (Table 6.3).

$$\Delta l \approx X_s\theta \tag{6.5}$$

$$I\ddot{\theta} = k \cdot X_s\theta \cdot X_s = k{X_s}^2\theta \tag{6.6}$$

$$\text{let} \quad \ddot{\theta} + {\omega_n}^2\theta = 0 \tag{6.7}$$

$$\text{giving} \quad \omega_n = \sqrt{\frac{k{X_s}^2}{I}} \tag{6.8}$$

$$\text{therefore} \quad I = \frac{k{X_s}^2}{{\omega_n}^2} \tag{6.9}$$

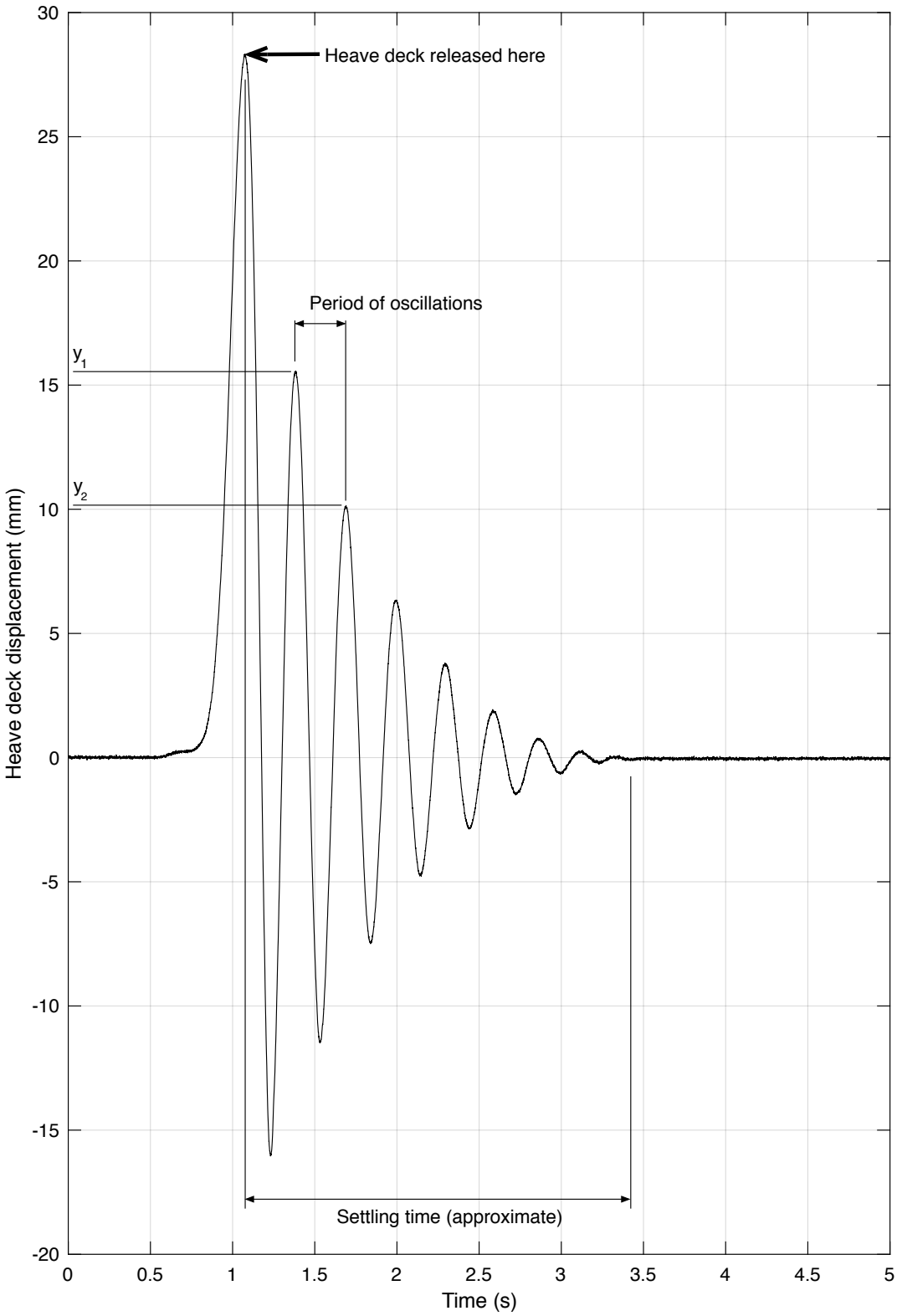


Figure 6.1. Mass-plenum system supported mass displacement time-series, during the raising to a fixed point (marked on the plot), sudden release and free oscillations. The period and decay of the oscillations can be used to find the supported mass rotational inertia and the resistance experienced by the supported mass. Values y_1 and y_2 are used in Eq. (6.2) to calculate the damping of the system.

6.3. Experimental rig dynamic characteristics

The characteristics of the experimental rig's response to a forcing of the plenum volume were required in order to confirm the experimental rig's suitability for plenum volume oscillation experiments. A commissioning test was completed by observing the mass-plenum system response to a forced step-change of the plenum volume at a number of combinations of experimental rig plenum height (H_0), air exit area (A_e) and air supply duct centreline air velocity (V_s). The insight gained was used to refine the main experimental method, especially the range of forcing frequencies to be used, the range of plenum heights to be used, the range of air exit areas to be used and whether it was necessary to vary the air supply volume flow rate.

The response of the mass-plenum system to a forced step-change to plenum volume can be characterised by three parameters of the response, when the plenum volume is subject to a forced step-change.

1. The damped frequency.
2. The settling time of the oscillations.
3. The time taken for the heave deck to fall back to the initial 'hover' displacement — denoted in this thesis as the 'falling time'.

The damped frequency is readily observed and is a dominant characteristic of the system dynamics. For linear, second-order, dynamic systems, the damped frequency is a sufficient predictor of resonance when the system is subjected to periodic forcing. The mass-plenum system is not linear, nor is it second-order. The author sought to investigate if a damped frequency can be observed and if that damped frequency can then be related to the dynamics of the mass-plenum system when it is subjected to periodic actuation.

The settling time of the system is commonly defined as the time it takes for the oscillatory response of a system to decay to within 2% or 5% of its final, steady state, value (Ogata, 1990, pp.268-269). However, the parameter can be defined as any proportion of the final value, which is useful to maintain a high signal to noise ratio for measurements completed on non-ideal systems. A value of 10% was used for the mass-plenum system analysis, to separate the oscillations of the supported mass from underlying trends. For a linear, second-order, dynamic system, the settling time value can be related to the mathematical 'damping' term in the mathematical model, therefore knowing the settling time enables prediction of the dynamic behaviour of a linear second-order system. For the non-linear mass-plenum system, there is no direct relationship between the settling time and the mathematical damping of the system, however, it will be shown that there is a relationship between settling time and the mass-plenum system response to a periodic forcing.

The falling time is distinctive to the non-linear mass-plenum system, defined here as the time it takes for the supported mass to return to within 2% of the final steady-state displacement, which is close to the original steady state position of the supported mass (the initial 'hover' height).

Figure 6.2 shows a typical experimental result from the experiment, overlaid with subsequent computational analysis. The configuration the test rig corresponds to the settings of the three available variables, that is, plenum height, air exit area and air volume flow rate into the plenum.

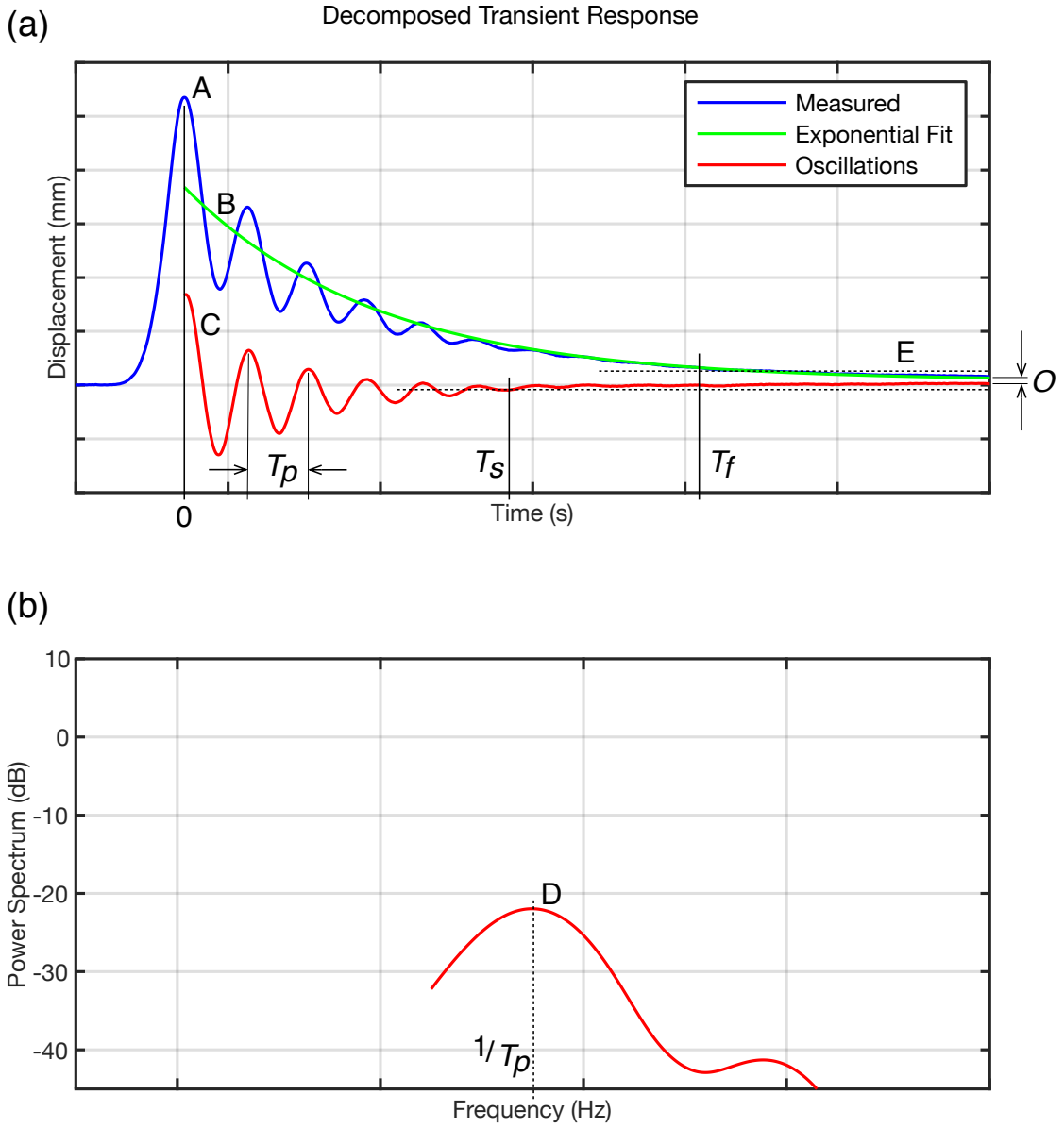


Figure 6.2. Decomposition of the mass-plenum response to a step-change in plenum volume. **Top (a):** The time history (A) of the supported mass has been overlaid with a dual-term exponential function, fitted to the data from the time of the first peak through to the end of the sample, the resulting curve (B) is then subtracted from (A) to give a new set of data (C), approximately representing the oscillating portion of the system response. The oscillating portion can be analysed to find the period (T_p) and the settling time (T_s). The original time-history of the supported mass displacement is further analysed to find the overall 'falling time' (T_f), a characteristic that is distinctive to the non-linear mass-plenum system. The offset (O) between the original position of the supported mass and its final resting position (E) is directly proportional to any Coulomb friction present in the system.
Bottom (b): To investigate if the approximate oscillating portion of the signal can be treated as a single frequency signal, the power spectrum of the approximate oscillating portion is found. The frequency of peak power is shown at (D).

The time history of the heave deck displacement shows two distinct features: a steady decline after the initial peak in displacement and decaying oscillations of the heave deck. An analysis was completed that sought to fit an exponential curve to the data, from the moment of the peak displacement through to the end of the time history. The fitted exponentially decaying curve is shown as a green line and labelled (B) in Fig. 6.2. The characteristic form of the trend in the experimental data is most sensitive to the air exit area. The fitted exponentially decaying curve was subtracted from the heave deck displacement time history and the remainder is an approximation of the oscillations time history and is shown as a red line and labelled (C) in Fig. 6.2.

Both the time history of the heave deck displacement and the fitted exponentially decaying curve asymptote to a displacement that is higher than the position at which the heave deck started (denoted (O) in Fig. 6.2). The difference in static displacement is due to a resistance on the heave deck that is constant — resistance that can be mathematically modelled by Coulomb's law (Sec. 5.6.1).

The transient response of the mass-plenum system shows damped oscillations. The damping is dominated by a velocity-dependent resistance acting on the heave deck; at least part of this resistance is due to forcing air through the air exit areas. The frequency of the damped oscillations is dependent on the compression of the air within the plenum and also the flexibility of the plenum walls.

The approximation of the oscillations time history (red line in Fig. 6.2, top plot) was further analysed by applying a power spectrum analysis (Fig. 6.2, bottom plot). The power spectrum analysis can be used to disclose the presence of resonance in a signal and estimate the frequency at which the resonance occurs (Leaver & Thomas, 1974, p.87). In Fig. 6.2, a peak in the power spectral density has been found (D), the frequency at which this peak occurs is approximately $1/T_p$. To improve the accuracy of the power spectrum analysis, only frequencies between 4 Hz and 400 Hz were considered, with a frequency resolution of 1.75 Hz and the analysis limited to power levels over −50 dB. Frequencies lower than 4 Hz were excluded as the results of the analysis were dominated by the underlying trend of the approximation of the oscillations time history; some of the underlying trend remains in the data because the two-exponent curve does not account for all of the non-oscillating behaviour of the mass-plenum system. The power spectrum analysis would indicate the presence of a second resonance in the mass-plenum system by another peak in power of similar magnitude to the maximum peak. The power spectrum analyses did not indicate the presence of any other resonant frequencies.

The decomposed signal for every experiment is included in Appendix E. The power spectrum analysis has been omitted from each plot as it only confirms that there is a single resonant frequency in each experimental result.

General observations available from these experimental runs and subsequent analysis:

1. The falling time of the mass-plenum system is very slow, it is the equivalent of many natural cycles.
2. The settling time of the mass-plenum system is non-trivial, this is clearly an under-damped system as several oscillations can occur before being damped out.
3. The mathematical decomposition does not necessarily correspond with any physical decomposition. The exponential decline of the heave deck has an exponent that is a function of several test rig parameters. The mathematical decomposition uses two fixed exponent terms as the basis of the curve fitting. It can be seen that some trend stills persists in the red line.

The experimental runs were analysed using the following steps:

1. The raw sensor data was filtered to reduce noise, then mirrored and shifted so that it started at zero (blue line, Fig. 6.2, top plot).
2. An exponential curve was fitted to the data (green line,Fig. 6.2, top plot), with the domain starting at the peak and continuing to 3 seconds.
3. The exponential curve was subtracted from the sensor data, to give the oscillation time history (red line,Fig. 6.2, top plot).
4. The peaks of the oscillation time history (red line) were found, the average period was found and the damped frequency calculated.
5. The damping ratio of the oscillation time history (red line) was found from the decay of the successive peaks.
6. The settling time of the sensor data (blue line) was found and denoted the 'falling time'
7. The settling time of the oscillating time history (red line) was found and denoted the 'settling time'.
8. This experimental procedure was done for thirty experimental conditions, each condition being the combination of the plenum height, the air supply volume flow rate and the air exit area.
9. Random experimental conditions were selected for repetition of the experiment. If an experiment was repeated, the mean of the results was used.

Plots of the results are presented and discussed in Secs. 6.3.1 to 6.3.3.

6.3.1. Estimating system damped frequency

An estimate of the damped frequency of the test rig system was required so that the experiment investigating the resonance of the system could be designed to force the plenum volume at frequencies higher than the damped frequency of the system. The actuating mechanism in the forced oscillating experiments was subsequently designed to be capable of operating in the range 1 Hz to 10 Hz. The most reliable means of setting the forcing frequency necessitated working through the range of operation in 1 Hz increments. It was desirable to measure the system response at two frequencies above the damped frequency and at two frequencies below the damped frequency. Therefore, it was necessary to determine if the damped frequency of the system was between 3 Hz to 8 Hz. The experimental parameter with most influence on the damped frequency was the plenum height—which was the active plenum volume variable given that the width and length of the plenum were fixed. An alternative means of ensuring the natural frequency would lie beneath the practical upper limit for the equipment was to add mass to the heave deck, but this option, demonstrated in a concept rig (Appendix G) was found to be unnecessary with the experimental rig. The height of the plenum could be varied in the range 297 mm to 1.100×10^3 mm. The lowest setting for the plenum height (297 mm) was of particular interest as it produced a plenum chamber of approximately the same height, width and length ratio as the SES which was the subject of study of Sorensen and Egeland (1994). The small plenum height was thought likely to result in a high damped frequency, which may have been outside the range of the plenum volume forcing mechanism. Increasing the plenum height was the main control to ensure the damped frequency was within the range of the plenum volume pumping mechanism. Varying the plenum height as an experimental factor also allowed the experiments to be repeated for different experimental factors, increasing the confidence in the experimental results. Determining if the damped frequency of the mass-plenum system lay in the range 3 Hz to 8 Hz, and stayed in that range as the plenum height was varied, was the principal reason to estimate damped frequency.

The value of the damped frequency parameter should be partly dependent on the flexibility of the plenum walls. It had already been determined that only one peak frequency was present in the response of the mass-plenum system (Sec. 6.3), indicating that the plenum flexibility does not act as a second resonating element of the system. The experimental estimation of the plenum flexibility will be described in Sec. 6.4.3.

It was expected that the air exit area may vary due to the wear and tear experienced by seals and seams during the experiments. As the air supply volume flow rate was held constant during the experiments, varying the air exit area had the effect of lowering the plenum air pressure. According to Kaplan et al. (1981) (see discussion in Sec. 4.7.3), the natural frequency is sensitive to the plenum height Eq. (4.49). However, the natural frequency is insensitive to the plenum pressure . The damping of the mass-plenum system is also sensitive to plenum height Eq. (4.50), but insensitive to the plenum pressure. It follows that the damped frequency is sensitive to the plenum height but insensitive to the air exit area. The assertion that the damped frequency of the mass-plenum system is insensitive to variations in the air exit area was tested in this experiment by varying the air exit area.

The air volume flow rate into the plenum of the experimental rig was thought likely to vary slightly due to natural fluctuations in atmospheric air pressure and air density. The

variations in air supply volume flow rate have an effect on the plenum pressure (as air exit area is held constant). The work of Kaplan et al. (1981) indicated that the natural frequency should be insensitive to the air supply volume flow rate Eq. (4.49). Kaplan et al. (1981) asserts that the damping of the mass-plenum system is sensitive to changes in the air supply volume flow rate, with higher values of air supply volume flow rate resulting in lower damping ratio values Eq. (4.50). The damping ratio has an effect on the damped frequency, higher values of the damping ratio lower the value of the damped frequency. The sensitivity of the damped frequency to changes in the air supply volume flow rate was tested by varying the air supply volume rate during this experiment. The air flow through the air supply duct was turbulent (Fox & McDonald, 1998, pp.330-333). For the purposes of this experiment, the air supply duct centreline velocity (V_a) was taken as being directly proportional to the air supply volume flow rate.

This experiment was repeated for five values of the plenum height (292 mm, 445 mm, 605 mm, 802 mm and 1.143×10^3 mm), two values of the air supply duct centreline air velocity (5.49 m s^{-1} and 6.75 m s^{-1}) and three values of the air exit area (570×10^{-6} m^2, 820×10^{-6} m^2 and 1.20×10^{-3} m^2)—a total of thirty experimental conditions. Multiple repetitions were done at a random selection of conditions.

In this research, the damped frequency was calculated from the experimental data using two distinct methods to enable a validation comparison:

Method (1): *Inspect the supported mass displacement time-series and find the time and magnitude of the local maxima (peaks).* See Fig. 6.2, top plot, for an illustration of this method of analysis. The elapsed time (period) between each successive peak is the inverse of the damped frequency. The presence of the underlying exponential trend affects the time of each peak, therefore it is more accurate to find the peaks after the underlying exponential trend is subtracted from the supported mass time-series. Noise in the signal can affect the accuracy of the location of each peak, therefore it is more accurate to find several peaks and find the mean period between successive peaks. The oscillations decay after several oscillations, with later oscillations diminishing to the point where the noise in the signal obscures the location of the peak. The number of peaks found was therefore limited to three, to avoid the effects of noise in the signal.

Method (2): *Find the power spectrum of the supported mass time-series.* See Fig. 6.2, bottom plot, for an illustration of this method of analysis. The power spectrum is applied after the underlying exponential trend is subtracted from the supported mass time-series, as the high displacement and very slow decay of the underlying exponential trend distorts the interpretation of the power spectrum analysis. The oscillations of interest also decay relatively quickly, with only two to five oscillations being significant compared to the noise in the signal. The power spectrum was applied across one second of the supported mass time-series so that the oscillations of interest had high power compared to the noise in the signal. A limit to the frequencies to be detected (between 4 Hz to 400 Hz) was also applied so that high frequency noise could be filtered out. The background noise was small in magnitude compared to the oscillations of interest, but at a constant level, whereas the oscillations of interest quickly decayed. The power spectrum analysis was designed to be applied to signals where the various oscillating components are present throughout the time period of the signal being analysed. Even though the oscillations in this experiment decay, the oscillations are sufficiently long-lived to be considered persistent across the time of the measurement sample.

The experiment was conducted at all thirty experimental conditions, each condition being a unique combination of plenum height (H_0), air exit area (A_e) and air supply duct centreline air velocity (V_s). Sixteen experimental conditions were randomly selected and the experiment repeated up to six times at the selected condition, a list of the experimental conditions and the runs done at each condition is included in Appendix E. Several conditions had more than one repetition. Every experiment was analysed using both Method (1) and Method (2).

Method (2) was found to be in reasonable agreement with Method (1) furthermore, Method (2) indicated that only one frequency was dominant in the response at every condition. Method (2) has greater opportunity for uncertainty as it uses pre-determined 'bins' of frequency ranges (Leaver & Thomas, 1974), therefore the value for the damped frequency found by Method (1) was used as the experimental result. Plots of every experimental measurement, overlaid with the exponential and oscillating fitted curves (described in Sec. 6.3) and grouped by experimental condition are included in Appendix E. The mean of the damped frequency for all repetitions at each condition was calculated (or the single experimental result as the case may be). It was found that the experimental results at the highest value of the plenum height (1.14 m) had excessive experimental scatter, most likely due to structural instability of the experimental rig at this height. This height was excluded from further analysis and use, nonetheless, the experimental results for this height are included in Appendix E. The remaining experimental results were plotted (Fig. 6.3). The mean result across all conditions at each plenum height was also plotted.

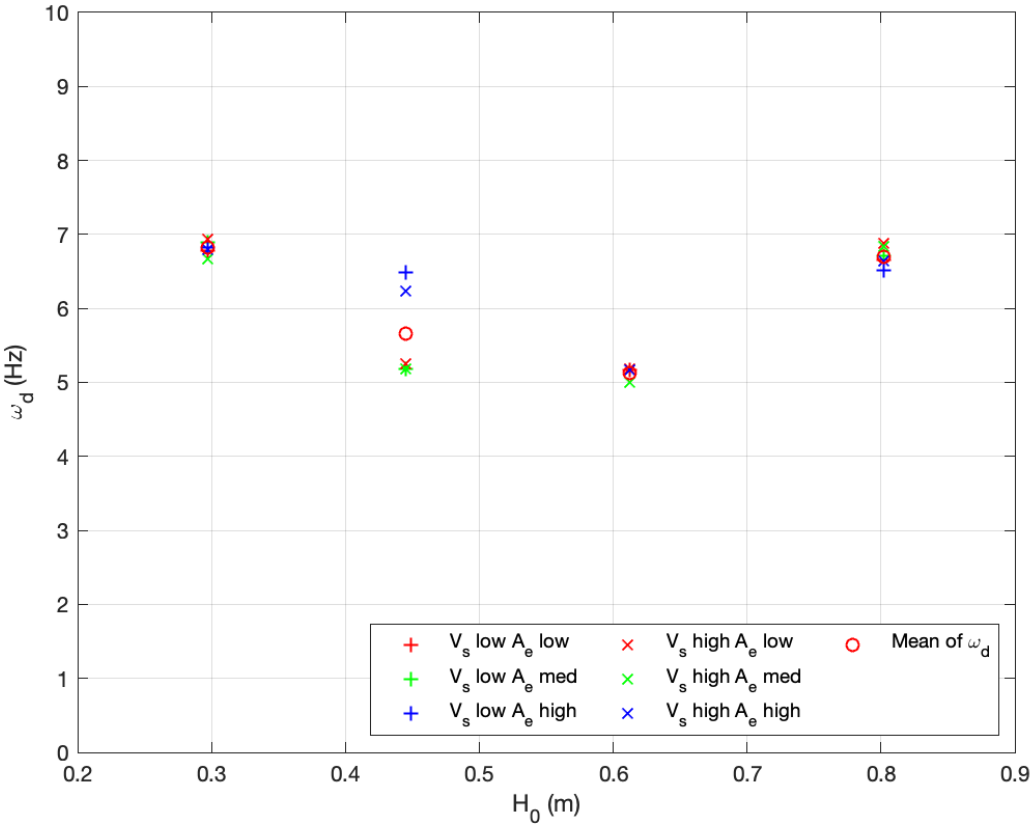


Figure 6.3. The mass-plenum system damped frequency (ω_d) plotted against the plenum height (H_0). All combinations of the plenum air exit area (A_e) and air supply duct centreline are velocity (V_s) are included and marked. The mean damped frequency at each height is marked with a red circle. For low plenum heights, the damped frequency decreases with increasing plenum volume, consistent with the air compressibility and plenum flexibility being dependent on plenum volume and height. The result at H_0=800 $\times$ 10^{-3} m is higher than the trend and is consistent with the plenum flexibility changing as the plenum walls become taller. Fewer satisfactory results were found for H_0=445 $\times$ 10^{-3} m and the experimental scatter is high. These results confirm that ω_d is in the desired range of 3 Hz to 8 Hz regardless of H_0 and that ω_d is insensitive to variations of A_e and V_s.

All of the results were within the range 5 Hz to 7 Hz. The trend for the results between H_0 = 297 mm to 610 mm is a linear downward trend, which is consistent with Eq. (4.49). The results at H_0 = 800 mm are not consistent with the trend of the other results, nor with Eq. (4.49). It is likely that either the plenum flexibility or the velocity-dependent heave deck resistance is different at this plenum height. This will be discussed further in sections Secs. 6.4.3 and 6.4.4.

The results at H_0 = 297 $\times$ 10^{-3} m and H_0 = 610 $\times$ 10^{-3} m had little variation, regardless of variations in A_e or V_s. The results at H_0 = 800 $\times$ 10^{-3} m also had small variation. This supports the assertion that the damped frequency is insensitive to variations in A_e and V_s. The result at H_0 = 445 $\times$ 10^{-3} m had a variation of over 1.3 Hz, most likely due to

abnormal interference within the flexible polyethylene seals. The seals were subsequently relaid to mitigate the risk of this happening in other experiments.

The experiment confirmed that the damped frequency was in the required range of 3 Hz to 8 Hz for all settings of the plenum height. Also, it was confirmed that the damped frequency is insensitive to variations in the air exit area and the air supply volume flow rate. The results for H_0=800 mm did not follow the trend of the results at the other three plenum heights, and this experimental result supports the assertion that plenum flexibility or velocity-dependent heave deck resistance or both are not constant for all values of the plenum height.

6.3.2. Estimating settling time

This section reports on the estimation of the damping of the oscillatory component of the mass-plenum system response to forced changes to the plenum volume. It was necessary that the mass-plenum system remained under-damped throughout the main experiment, to ensure consistency of the results. By further analysis of the data gathered during the commissioning test described in Sec. 6.3.1, the sensitivity of the mass-plenum system damping to changes in plenum height, air exit area and air supply volume flow rate could be investigated.

The damping of a system has a strong effect on the settling time of a system, the time it takes for oscillations to decay to a pre-determined proportion of the steady state system response (Ogata, 1990, pp.266) as discussed in Sec. 6.3.1. The settling time can be directly observed from the oscillatory portion of the decomposed heave deck displacement time-series (Fig. 6.2). If the settling time is longer than the oscillation period, then the system is under-damped.

The same data gathered during the commissioning test (Sec. 6.3.1) and already analysed for damped frequency, (Sec. 6.3.1), was further analysed to find the settling time. The full set of commissioning test runs are included in Appendix E. The results are presented in Fig. 6.4.

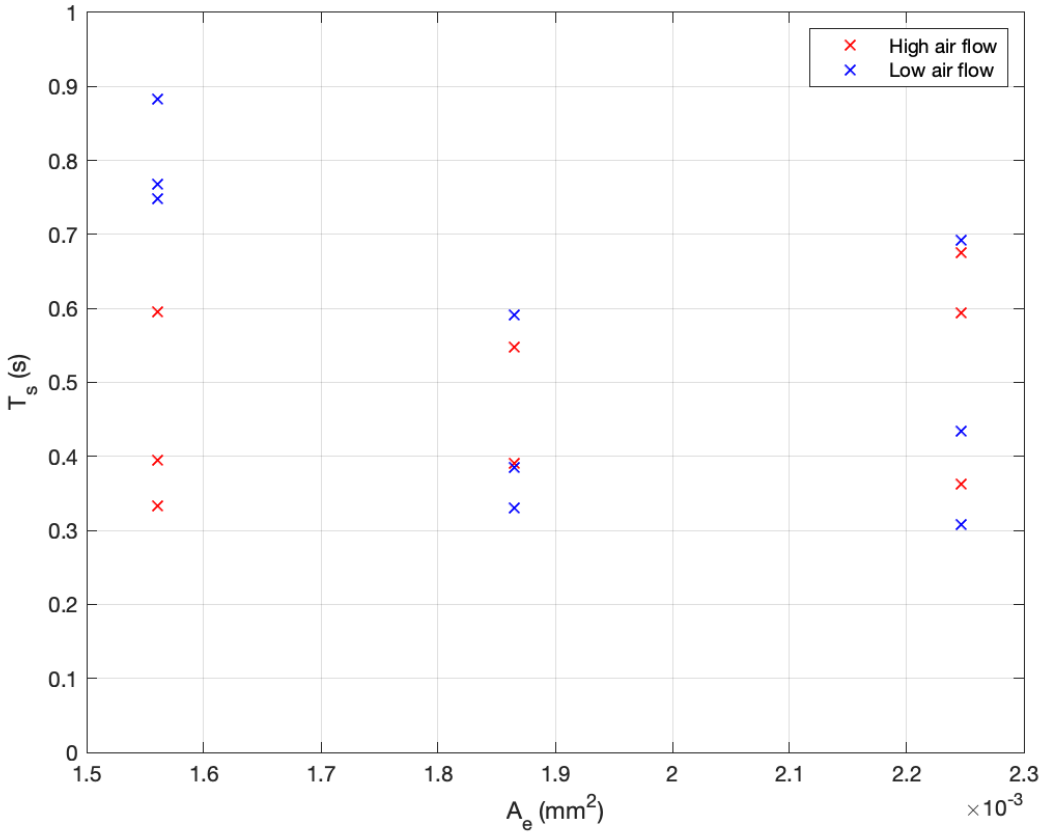


Figure 6.4. Mass-plenum settling time (T_s) plotted against air exit area (A_e). All six combinations of air supply duct centreline air velocity (V_s) and plenum height (H_0) are included at each of the three values for A_e. T_s is insensitive to A_e, but a high degree of experimental scatter is apparent.

The results show that T_s was always in the range 100 ms to 900 ms. This range of T_s is always greater than the damped period (Sec. 6.3.1).

The experimental scatter exceeds the effect of A_e. Further analysis of the relation between H_0 and V_s on T_s showed no strong dependency between any of the experimental factors and T_s. One possible cause of the variability of T_s is the velocity-dependent heave deck resistance (discussed in Sec. 6.4.4 below), including the effect of randomly occurring interference within the fold of the flexible polyethylene rolling seal.

The mass-plenum system settling time, T_s was always greater than the damped period of the mass-plenum system ($T_p = {}^1/\omega_d$), therefore the mass-plenum system was always under-damped. Some variation in T_s due to random factors can be expected during the main experiment.

6.3.3. Estimating falling time

The underlying exponential trend of the supported mass time-series (Fig. 6.2) is characterised as the time it takes to reach a value within 2% of the final value. In this thesis, this is referred to as the 'falling time' to distinguish it from the settling time of the oscillations of the supported mass. The symbol used for falling time is T_f.

The same data gathered during the commissioning test (Sec. 6.3.1) and analysed in Secs. 6.3.1 and 6.3.2 was analysed again to find the falling time. The results, plotted against air exit area (A_e) are shown in Fig. 6.5. The measurements were taken for thirty different combinations of plenum height (H_0), air supply duct centreline air velocity (V_s) and A_e. All the results are shown, with the two settings for V_s distinguished by colour. The falling time is insensitive to H_0, so the measurements taken at different settings of H_0 are not distinguished on the plot. A summary of the T_s results are given in Table 6.4.

Table 6.4. Experimental rig falling time (T_f) results summary

Parameter	Value (s)
Mean	1.61
Standard deviation	0.55
Minimum	1.43
Maximum	2.31

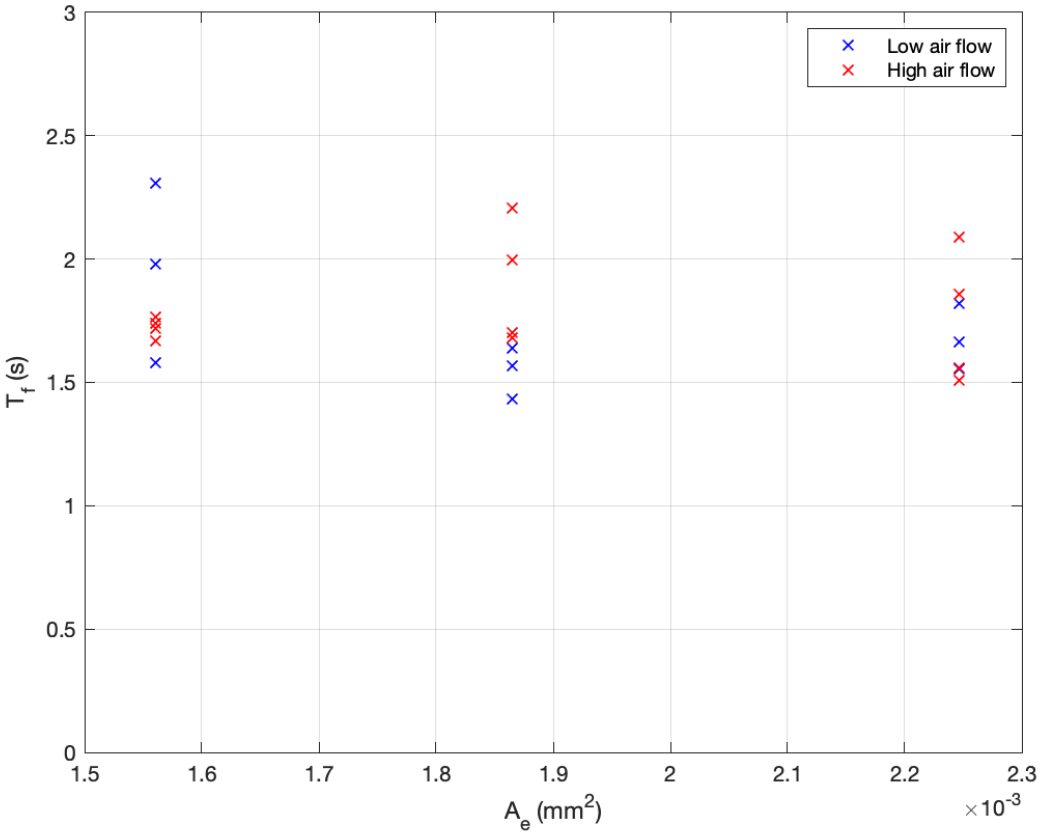


Figure 6.5. Experimental rig falling time T_f plotted against the air exit area (A_e). Each plotted point corresponds to a distinct combination of A_e, plenum height (H_0) and the centreline velocity of the air supply (V_s). Values of V_s are distinguished by colour. The different values of H_0 are not distinguished. The experimental scatter is over a larger range than the correlation to A_e. As such, T_f is assumed to be insensitive to the experimental factors.

Figure 6.5 shows that there is no strong correlation between T_f and any of the experimental variables. The associated experimental scatter (illustrated by Fig. 6.5) and mathematically represented by the standard deviation being significant compared to the mean (Table 6.4) is likely due to variations in the velocity-dependent heave deck resistance. This is discussed in Sec. 6.4.4.

The falling time for the experimental rig will be further discussed when compared to the results of the main experiment in Sec. 6.5.

6.4. Experimental rig parameter values—part two

Additional experimental rig parameters were found using a curve fitting method. Four experimental rig parameter values were found, in the following sequence, before the main experiment could commence. The sections where the parameters were first introduced are included in parentheses.

(A) Coulomb friction factor, C_c (Sec. 5.6.1)
(B) parasitic air leakage, A_L (Sec. 5.6.4)
(C) stiffness of the flexible plenum, k_V (Sec. 5.6.6)
(D) velocity-dependent resistance to the heave deck motion factor, C_v (Sec. 5.6.1.4)

The four parameters were found by fitting a curve to the data gathered during the commissioning tests (Sec. 6.3). The same data was also used in Secs. 6.3.1 to 6.3.3 to find other experimental rig parameter values. The fitted curve was generated using the Simulink model (Sec. 5.9). The curve generated by the Simulink model has four distinct features, each of which was strongly dependent on one of the parameters that was to be found. This is illustrated using a detailed example of curve fitting to a commissioning test result in Fig. 6.6.

All four parameters are included in the mathematical model, derived from mechanical principles (Sec. 5.6). The mathematical modelling of the mass-plenum system has general acceptance in the field (Doctors, 2018; Faltinsen, 2005a). The Simulink model is derived directly from the mathematical model (Sec. 5.9) and is required to solve the set of non-linear equations making up the mathematical model (Sec. 5.6.8). The Simulink model does not use any customised or unique elements that require further validation. The Simulink itself was validated by comparing its results to results found by another numerical solution, independently derived and programmed (Appendix G) using the commercial spreadsheet software 'Excel' (the 'spreadsheet numerical model'). The spreadsheet numerical model was in turn tested by comparing its results to data gathered during trials of a concept rig. The concept rig operated on the same mechanical principles as the experimental rig, but was much smaller. A report of concept rig trials is included in Appendix G.

The highly coupled nature of the supported mass motions (Sec. 5.10) make it impractical to isolate these four parameters, making it necessary to find the parameters from the same set of data. The quantifying of each parameter is discussed in more detail in Secs. 6.4.1 to 6.4.4 below. A full set of the curve fitted plots are included in Appendix F.

6.4.1. Dry (Coulomb) friction

Dry friction in the heave deck mechanism (Figs. 5.7 and 5.8) results in a constant force that opposes its direction of motion, mathematically modelled using Coulomb's law of friction (Sec. 5.6.1). Dry friction results in the final resting position of the heave deck being offset from the starting position during a step-change plenum volume experimental run. The magnitude of the offset was found analytically to be directly related to the force due to the dry friction Eq. (5.10).

Dry friction on the heave deck was not observed during heave deck mechanism tests with no plenum pressure above atmospheric (Fig. 6.1). Therefore, it is postulated that dry friction is due to the plenum air pressure causing sliding contact between surfaces in

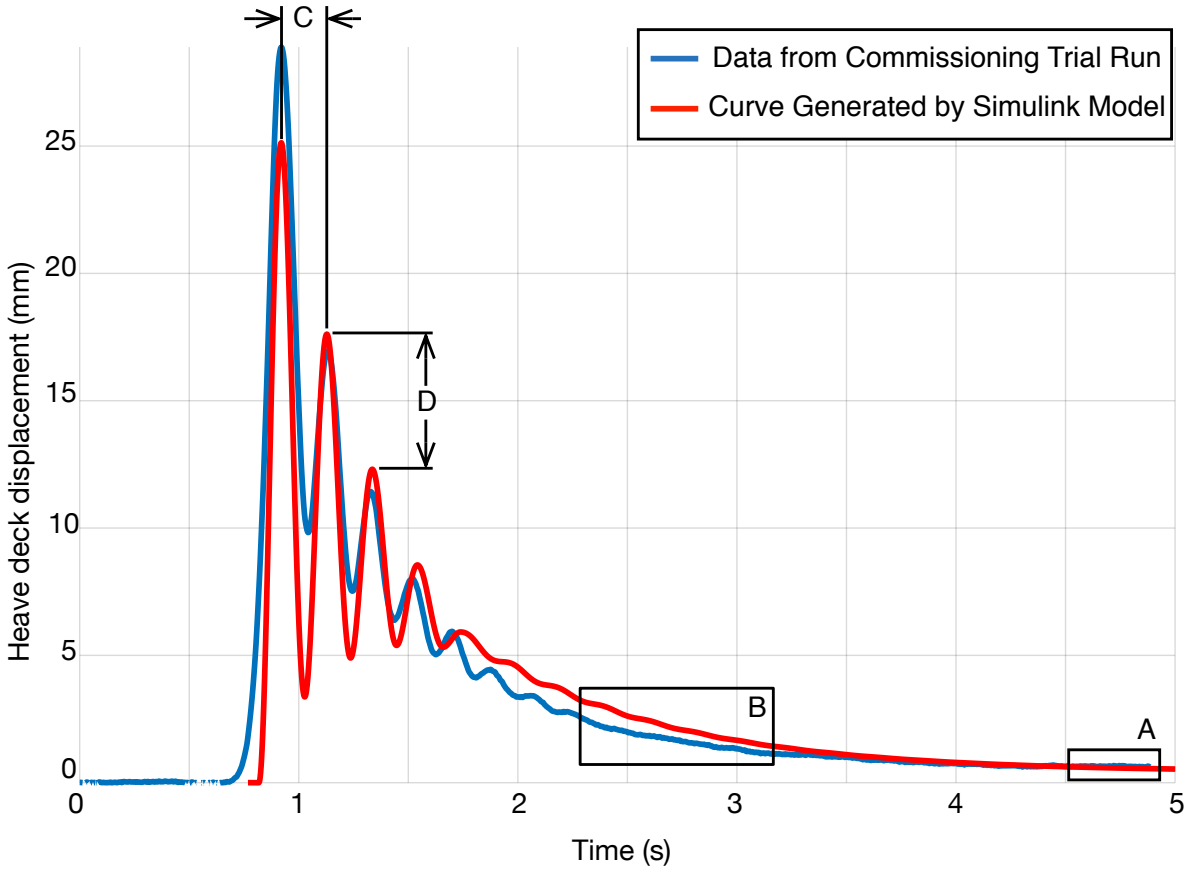


Figure 6.6. Example of curve fitting to a commissioning test result. The blue line is data from one commissioning trial run (Sec. 6.3). The red line is a curve generated using the Simulink model (Sec. 5.9). The shape of the generated curve in region (A) is most sensitive to the Coulomb friction force (F_c). The shape of the generated curve in region (B) is most sensitive to the parasitic air leakage (A_L). The vertical distance between successive peaks of the generated curve (D) is most sensitive to the velocity-dependent heave deck resistance force (F_v). The horizontal distance between successive peaks (C) is most sensitive to the plenum flexibility (k_V).

the heave deck mechanism. Further investigation into the causes of the dry friction in the experimental rig is outside the scope of this thesis.

In the commissioning test data, the effect of dry friction can be isolated by analysing the portion of the data where the oscillations have completely decayed and the heave deck has completed its fall back to a stationary position, as shown by region (A) in Fig. 6.6.

The values found of the Coulomb friction factor using the curve fitting method, for twenty-nine of the thirty conditions[1] are tabulated in Appendix F. All of the generated curves and their fit to the commissioning test data are available in Appendix F.

The Coulomb friction factor (C_c) values were in the range 2 N to 20 N. These values are small when compared to the values for the velocity-dependent heave deck resistance (C_v) (220 N s rad^{-1} to 1.900×10^3 N s rad^{-1}) at velocities encountered during the experiments. The velocity of the heave deck during oscillations is in the range 2 rad s^{-1} to 24 rad s^{-1}, resulting in F_v forces in excess of 440 N. At these respective values of C_c and C_v, C_c has no effect on the damping of the heave deck oscillations, however, C_v has a substantial effect on the damping of the heave deck oscillations. As such, the dry friction had a negligible impact on the supported mass damped frequency, settling time and falling time.

The main experiment was conducted for nine different experimental rig conditions, each condition being a combination of the plenum height and the air exit area. The value of C_c used for each condition was the mean of the values of C_c for the same combination of H_0 and A_e. The nine conditions of the main experiment (and the corresponding values of H_0 and A_e) are tabulated with the values of C_c in Table 6.5.

6.4.2. Parasitic leakage

During the commissioning tests, there was some evidence of air escaping through seams that were not fully sealed[2]. The effect of this 'parasitic air leakage' was to make the falling time (Sec. 6.3.3) faster.

The total area through which the parasitic air leakage was escaping the plenum chamber could be isolated by analysing the region of the supported mass displacement time-series where the oscillations had significantly decayed, but the supported mass was still falling back to the hover region, region (B) in Fig. 6.6. The value of A_L was found by adding an extra air leakage area term (A_L) to the Simulink model and varying the term until the curve generated by the Simulink model fitted the commissioning test data allowed. The values of A_L are tabulated in Appendix F.

During reconfiguration of the experimental rig for the main experiment, the plenum chamber seams were strengthened and better caulking was done. The effect of this amelioration was observed to increase the hover height of the supported mass compared to similar conditions for the commissioning tests. An extra air exit area of known dimensions was introduced to the plenum chamber to return the plenum chamber to hover pressures similar to the ones used during the commissioning tests, As such, the value of A_L was set to zero for the main experiment, whereas the value of A_e was set to the new, measured, value. This is tabulated in Table 6.5.

[1] The data for condition twenty-five had insufficient integrity to be analysed.

[2] Air leaks were detected manually and using indicators made from paper streamers.

6.4.3. Plenum stiffness

The plenum flexibility was included as an analogue to the flexibility inherent in the Surface Effect Ship system through the presence of the water surface and flexible air cushion seals (Sec. 5.4). Plenum stiffness (k_p) results from flexure of the chamber's wall panels and floor, and rolling seal motions under the influence of the plenum (near) instantaneous pressure changes. Further investigation of the causes of the plenum stiffness of the experimental rig is outside the scope if this thesis.

It was found in Sec. 6.3.1, through the use of the power spectrum analysis, that significant periodic motions of the supported mass occur at only one frequency. This supported hypothesis HE-1 (Sec. 5.3) that plenum flexibility could be modelled as a massless flexibility of the plenum walls (Sec. 5.6.6).

The effect of k_p on the supported mass displacement time-series can be isolated by considering the period between successive peaks, labelled (C) in Fig. 6.6. The value for k_p at each condition of the commissioning experiment was found by fitting a curve generated by the Simulink model to the data gathered during the commissioning test. The relevant values for A_L and C_c were retained in the Simulink model for this curve fitting. The results for every condition are tabulated in Appendix F. The value of k_p was unaffected by variations in A_e and V_s. The value of k_p varied between $25 \times 10^3\,\mathrm{Pa\,mm^{-1}}$ to $90 \times 10^3\,\mathrm{Pa\,mm^{-1}}$ (the results for $H_0 = 1.143\,\mathrm{m}$ were disregarded, as discussed in Sec. 6.3).

The relevant values for k_p (Table 6.5) were incorporated into the Simulink model for use in the main experiment (Sec. 6.5), during which the Simulink model was extrapolated to model the forced oscillations of the experimental rig plenum volume.

6.4.4. Velocity-dependent heave deck resistance

A velocity-dependent heave deck resistance factor (C_v) to the supported mass motion was included in the mathematical model (Sec. 5.6.1) as an analogue to the viscous resistance to motion that an actual SES experiences as the side hulls move in and out of the water due to air cushion pressure variation. For the mass-plenum system, the heave deck mechanism has several possible velocity-dependent resistance sources, including viscous friction in the hinge lubricating oil, the sliding of layers of the polyethylene rolling seals against each other and interference between the layers of the polyethylene rolling seal. The actual contribution of individual velocity-dependent resistance sources is outside the scope of the current research and, as such, the overall effect of the velocity-dependent resistance was treated as a lumped parameter, the value of which was estimated by varying the value of the parameter in the mathematical model until the numerical solution to the mathematical model fitted the data gathered during commissioning.

The velocity-dependent resistance to the supported mass motion was greater when the plenum was pressurised, compared to the earlier experiment to find the heave deck's rotational inertia. As the velocity-dependent resistance is dependent on the plenum pressure, the value of this parameter was found at several different mass-plenum operating conditions (Fig. 6.7). The value of C_v was not significantly dependent on the values of A_e and V_s. While C_v was found to change when air pressure was in the plenum, the range of pressures in the plenum that were used in the trials did not have a significant effect on the actual value of C_v. The value of C_v was found to be influenced by the passage of time, and the values found for C_v in Fig. 6.7 are presented chronologically.

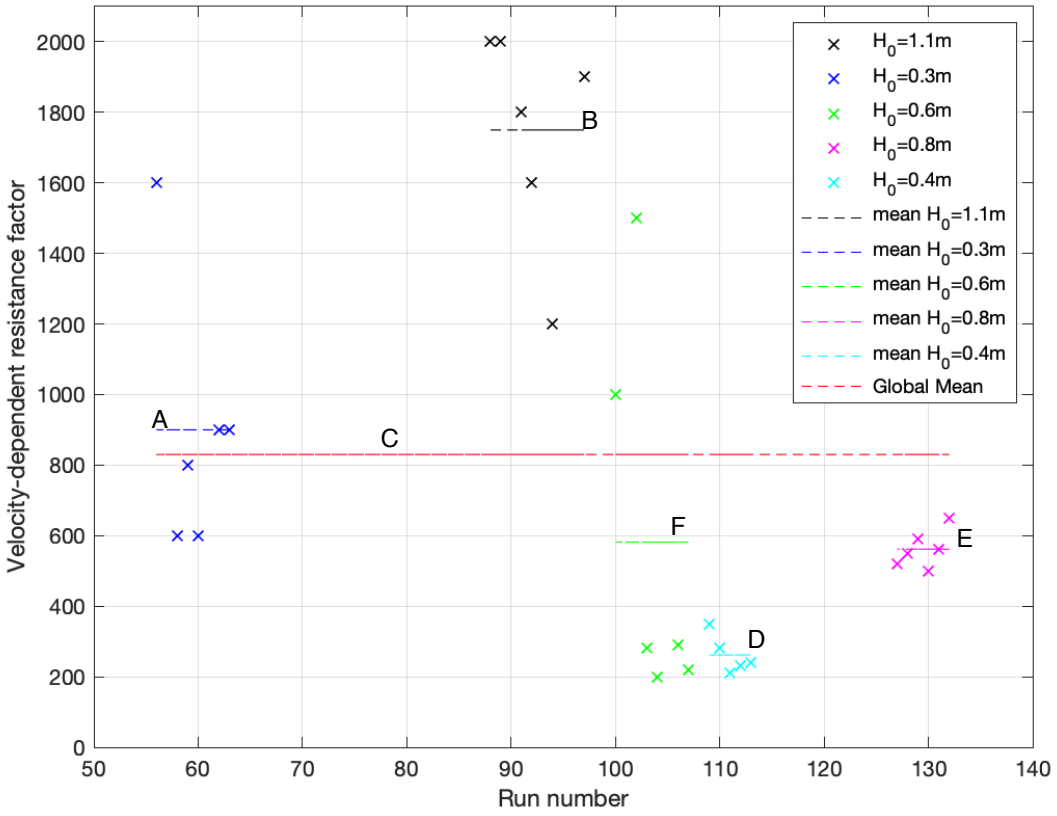


Figure 6.7. Velocity-dependent heave deck resistance factor C_V, found using curves from the Simulink model fitted to the commissioning test data, plotted chronologically. Each plotted point has a unique combination of the plenum height (H_0), the air exit area (A_e) and the centreline velocity of the air supply (V_s). The mean of each group of runs done at the same plenum height (H_0) is plotted, shown in the legend and indicated by points (A, B, D, E, F), along with the global mean of all the test runs (C). The velocity-dependent heave deck resistance was minimised after growing to levels that affected the viability of the results (B), by adjusting the clearance of the heave deck and the arrangement of the flexible rolling seal. These adjustments took several runs to 'bed down', affecting the results (F). The bedded down adjustments reduced both the experimental scatter and the mean of C_v (D, E). The mean of the final group (E), at $H_0 = 800 \times 10^{-3}$ m was used in the Simulink model for C_v.

During early trials, some experimental scatter was observed for C_v (Fig. 6.7), which was addressed by re-aligning the heave deck and reinstalling the polyethylene film rolling seal so that any unexpected interference in the rolling seal (due to bunching up of the flexible film) would be minimised. Later test runs showed a reduction in both the magnitude and scatter of C_v results. The final value of C_v was taken as the mean of the final group of results at $H_0 = 800 \times 10^{-3}\,\mathrm{m}$ (Table 6.5 point E). Variation in the velocity-dependent heave deck resistance was a potential source of experimental scatter during the main experiment.

6.4.5. Summary of experimental rig parameter values

For each value of the plenum height (H_0), a single value for the plenum stiffness (k_p) and velocity-dependent resistance factor (C_v) to the heave deck motion has been found. These values provide the best match across a range of experimental rig configurations, with the air exit area (A_e) and the air supply duct centreline air velocity (V_s) being the associated independent variables. The repeated matching of the predicted behaviour with the experimental rig observations indicates that the values for the parameters are generally correct. The mathematical modelling of the phenomena characterised by the parameters is based on fundamental mechanical principles and are not arbitrary mathematical constructs (Sec. 5.6). The experimental rig parameters values found at this stage of the experimental program are retained for use in the main experiment, where good correspondence between the numerical solutions and the experimental results were found, even though the experimental rig had been reconfigured to include extra strengthening and stiffening of the plenum chamber and the method of forcing the plenum volume was changed from a step-change mechanism to an oscillating mechanism. As such, there is a high confidence that the experimental rig parameter values found by matching numerical solutions to experimental rig test results have produced repeatable and validated results.

Different values for the Coulomb friction, from experimental run to experimental run, were accommodated, although the magnitude range of Coulomb friction was at least an order of magnitude smaller than the velocity-dependent resistance and, as such, the Coulomb friction had an insignificant effect on the damped frequency and damping of the supported mass motions.

The parasitic leakage area varied between experimental runs. The parasitic leakage area was eventually removed from the experimental rig before it was reconfigured for the main forced oscillation experiments.

The values of the parameters found in this section are tabulated in Table 6.5. These values were used in the Simulink model during the main experiment.

Table 6.5. Experimental mass-plenum rig characteristics and parameter values used for the main experiment. The condition numbers (first column) are the unique combinations of plenum height (H_0) and air exit area (A_e) that were used for the main experiment. The parameters found by curve fitting to the commissioning test data are: plenum stiffness (k_p), parasitic air leakage area (A_L), dry (Coulomb) friction factor (C_c) and velocity-dependent resistance factor (C_v). Sec. 6.3 reports on the experimental method and discusses the results. The full set of parameter values found during the commissioning test are included in Appendix F. The curves generated from the parameter values are also shown fitted to commissioning test data in Appendix F.

Condition #	H_0 (m)	A_e (m^2 10^{-3})	k_p ($N\,m^{-1}$ 10^3)	A_L (m^2)	C_c N	C_v $N\,s\,rad^{-1}$ 10^3
1	0.297	0.57	90.0	0	10	0.55
2	0.297	0.82	90.0	0	8	0.55
3	0.297	1.20	90.0	0	10	0.55
4	0.605	0.57	25.0	0	6	0.55
5	0.605	0.82	25.0	0	6	0.55
6	0.605	1.20	25.0	0	6	0.55
7	0.802	0.57	90.0	0	4	0.55
8	0.802	0.82	90.0	0	9	0.55
9	0.802	1.20	90.0	0	4	0.55

6.5. Main experimental results with forced plenum oscillations

This section discusses the results for the main experiment of this thesis using the experimental rig in its configuration that incorporates forced oscillations of the plenum volume. The main experiment addresses the research questions and hypotheses detailed in Sec. 5.3.

Research question QA asks whether the supported mass time-wise mean displacement changes when the plenum volume is forced to oscillate. It was postulated in hypothesis HA-1 that the rate of change of the plenum volume and the rate of change of the air density are the factors that lead to the change in the time-wise mean of the supported mass position. The mathematical model, and hence the Simulink model, incorporates the rate of change of the plenum volume and the rate of change of the air density in the plenum, including non-linear terms that have not been previously included in models in the available literature. The experimental rig was built so that the rate of change of the plenum volume can be used as an experimental factor through the mechanism of forcing the plenum volume over a range of frequencies, with higher forcing frequencies being equivalent to more rapid changes in the plenum volume. In Sec. 6.5.4, the predictions of the supported mass motions produced by the Simulink model will be compared to measurements of the supported mass motions over a range of forcing frequencies, providing a robust test of hypothesis HA-1. The prediction PA-1 can now be made quantitatively by the Simulink mode, that the time-wise mean of the supported mass will increase as the plenum is forced to resonate near the damped frequency, and will be tested in Sec. 6.5.4.1. Prediction PA-2 concerns the affect of the air exit area on the magnitude of the time-wise mean of the supported mass motions. In Sec. 6.5.4.2, the experiment of Sec. 6.5.4.1 is repeated for different values of the air exit area, testing prediction PA-2.

Research question QB asks 'Can resonance be induced in a mass-plenum system?' Hypothesis HB-1 asserted the air compressibility acts as a spring. It was predicted in PB-1 that forcing a step-change to the plenum volume would induce oscillations of the supported mass, and this prediction was supported by the results of the commissioning test (Sec. 6.3.1), by which the damped frequency was found. Prediction PB-2 is that when the plenum volume is forcibly oscillated at a frequency near to the damped frequency, resonant behaviour will be observed, i.e. amplified oscillations of the supported mass, this will be tested by the experiments discussed in Secs. 6.5.4.1 to 6.5.4.3. Prediction PB-3 concerns the reduction in supported mass motion magnitude when the plenum is forced at higher frequencies than the damped frequency and prediction PB-4 concerns the reduction in in supported mass motion magnitude when the plenum is forced at lower frequencies than the damped frequencies. Both of these prediction will be tested by the experiments reported in Secs. 6.5.4.1 to 6.5.4.3, as the forcing frequency is varied from below the damped frequency to above the damped frequency. Hypothesis HB-2 is concerned with the effect of plenum flexibility on the damped frequency. Hypothesis HB-2 has already been supported by sensitivity tests done on the concept rig (conclusion three in Appendix G) and the commissioning tests done on the experimental rig when it was in the plenum volume forced step-change configuration (Sec. 6.4.3). Both of those tests indicated that the plenum flexibility reduced the damped frequency and did not introduce a secondary natural frequency.

Research question QC is concerned with the effect of plenum volume on the damped frequency. Hypothesis HC-1 is that larger air volumes will be less stiff and HC-2 is that taller plenum walls will also be less stiff. Evidence supporting HC-2 has already been found through the test on the concept rig for the sensitivity of the damped frequency to plenum flexibility (conclusion three in Appendix G). Furthermore, evidence supporting HC-2 has already been found by the commissioning test on the experimental rig in the plenum volume forced step-change configuration, for the sensitivity of the damped frequency to changes in plenum volume (Sec. 6.4.3). Prediction PC-1 is that the damped frequency will reduce as the plenum volume is increased, the quantified predictions produced by Simulink for several values of the plenum height (and hence plenum volume) will be compared to the experimental results in Sec. 6.5.4.3.

Research question QD is concerned with the effect of air exit area on the damping of the mass plenum system. Hypothesis HD-1 is that the set of regular round holes in the plenum chamber will act as a single orifice, this is incorporated into the mathematical model (Sec. 5.6.4) and hence the Simulink model (Sec. 5.9). Hypothesis HD-2 is that a greater air exit area will damp the mass-plenum system, leading to predictions PD-1 and PD-3, that the supported mass oscillations will decay more rapidly and be of small magnitude as the air exit area is increased. These predictions will compared to experimental results in Sec. 6.5.4.2. Hypothesis HD-3 is that the greater air exit area does not have an effect on the supported mass returning to its equilibrium position, leading to prediction PD-3, that the falling time will be insensitive to the air exit area. Prediction PD-3 has been compared to experimental results in Sec. 6.3.3 and found to be in agreement, which is evidence supporting hypothesis HD-2.

Research question QE is concerned with the sensitivity of the mass-plenum system damped frequency to plenum flexibility. Hypothesis HE-1 was that plenum flexibility would act as a 'springy' and massless plenum wall, which was incorporated into the mathematical modelling (Sec. 5.6.6) and hence into the Simulink model. Hypothesis HE-1 leads to prediction PE-1, that there will only be one resonant frequency, which was compared to the results of commissioning tests done on the experimental rig when it was in the plenum volume forced step-change configuration (Sec. 6.4.3). Prediction PE-1 was found to be in good agreement with the commissioning test results. Hypothesis HE-2 was that the mass-plenum system damped frequency is sensitive to changes in plenum flexibility, leading to prediction PE-2, that the damped frequency can be lowered through the effects of plenum flexibility. Evidence supporting hypothesis HE-2 has already been found through the sensitivity tests on the concept rig (Appendix G) and the commissioning tests done on the experimental rig when it was in the plenum volume forced step-change configuration (Sec. 6.4.3). In Secs. 6.5.4.1 to 6.5.4.3, the effect of plenum flexibility on the mass-plenum damped frequency is further discussed after presentation of the main oscillating plenum volume experimental results.

Section 6.5.1 reports the scope of the reconfiguration of the experimental rig, to make it suitable for forced oscillations of the plenum volume. The method for setting the forcing frequency for each experimental run is reported in Sec. 6.5.2. Section 6.5.3 summarises the method for analysis of the experimental data.

Section 6.5.4 contains the results for the mean displacement of the supported mass and the magnitude of the supported mass, explaining the salient features of the results. The first set of results is at a plenum height and air exit area in the middle of the range of available settings, with the independent variable being the frequency at which the plenum

volume is forced. The directly observed time history of the supported mass displacement is analysed to give the mean supported mass displacement and the magnitude of the supported mass displacement. These two results are plotted in alignment against the forcing frequency for convenient review and associated discussion.

Several results of individual trials at high forcing frequencies do not follow the trend of the results at other forcing frequencies, these are noted in Secs. 6.5.4.1 to 6.5.4.3. These results of individual trials are further discussed in Sec. 6.5.5.

6.5.1. Reconfiguration of experimental rig to enable forced oscillations of the plenum volume

The test rig was reconfigured to to enable forced oscillations to the plenum volume (Fig. 5.11). The forced oscillations, particularly those planned at higher frequencies than the natural frequency, were predicted to result in much higher dynamic loads due to the oscillating heave deck, so the plenum chamber was stiffened with two additional ribs along the outside of the plenum chamber, to ensure safety and longevity with an associated small increase in the experimental rig plenum stiffness. The value for the plenum stiffness used in the Simulink model was not changed and it was expected that the experimental rig would be slightly stiffer (with a higher damped frequency) than predicted by the Simulink model.

During the reconfiguration, the plenum chamber was re-sealed so that the seams would better withstand the high dynamic loads of the forced oscillations. As reported in Sec. 6.4.2, pre-experiment checks indicated that the model of parasitic air leakage area could be removed from the Simulink model for the main experiment.

The rolling seal on the heave deck was checked for damage and the adhesive tape holding it in place was replaced. The rolling seal was checked for free running before the experiments were done.

6.5.2. Frequency of the forcing

The actual frequency of forcing was found from the time history of the forcing mechanism displacement. The control of the forcing frequency was achieved by an industrial AC motor speed control with a continuous sweep (Fig. 5.13). To allow for small variations in the motor speed, the actual frequency of the forcing motion was found by analysing the time-history of the forcing flapper displacement. The frequency of forcing was changed in approximately 1 Hz increments over a range of 1 Hz to 10 Hz. The natural frequencies for the rig configurations were typically in the region of 5 Hz.

The frequencies at which the peak mean heave deck displacement and peak magnitude of the heave deck oscillations occur, can only be interpolated from the experimental data as the measurements are made at 1 Hz intervals. The experimental results have a range of possible peak frequencies higher than the quantitative prediction of the peak frequency—which was expected as the plenum had been stiffened since the plenum wall flexibility was found. At each frequency there was some experimental scatter, consistent with experimental scatter observed during the step-change commissioning test.

6.5.3. Experimental analysis

The two measurands of the experiment are time histories of: the straight-line displacement of the heave deck at a known point at a significant distance from the axis of rotation (the same location as for the step-change experiments); and the displacement of the rotating volume forcing flap, at a known distance from the axis of rotation (Fig. 6.8). For the forcing flap, the restricted range of the laser interferometer dictated that the point of measurement be relatively close to the axis of rotation. Both time-series are measured simultaneously, synchronised by using the same data acquisition system (DAQ) for both.

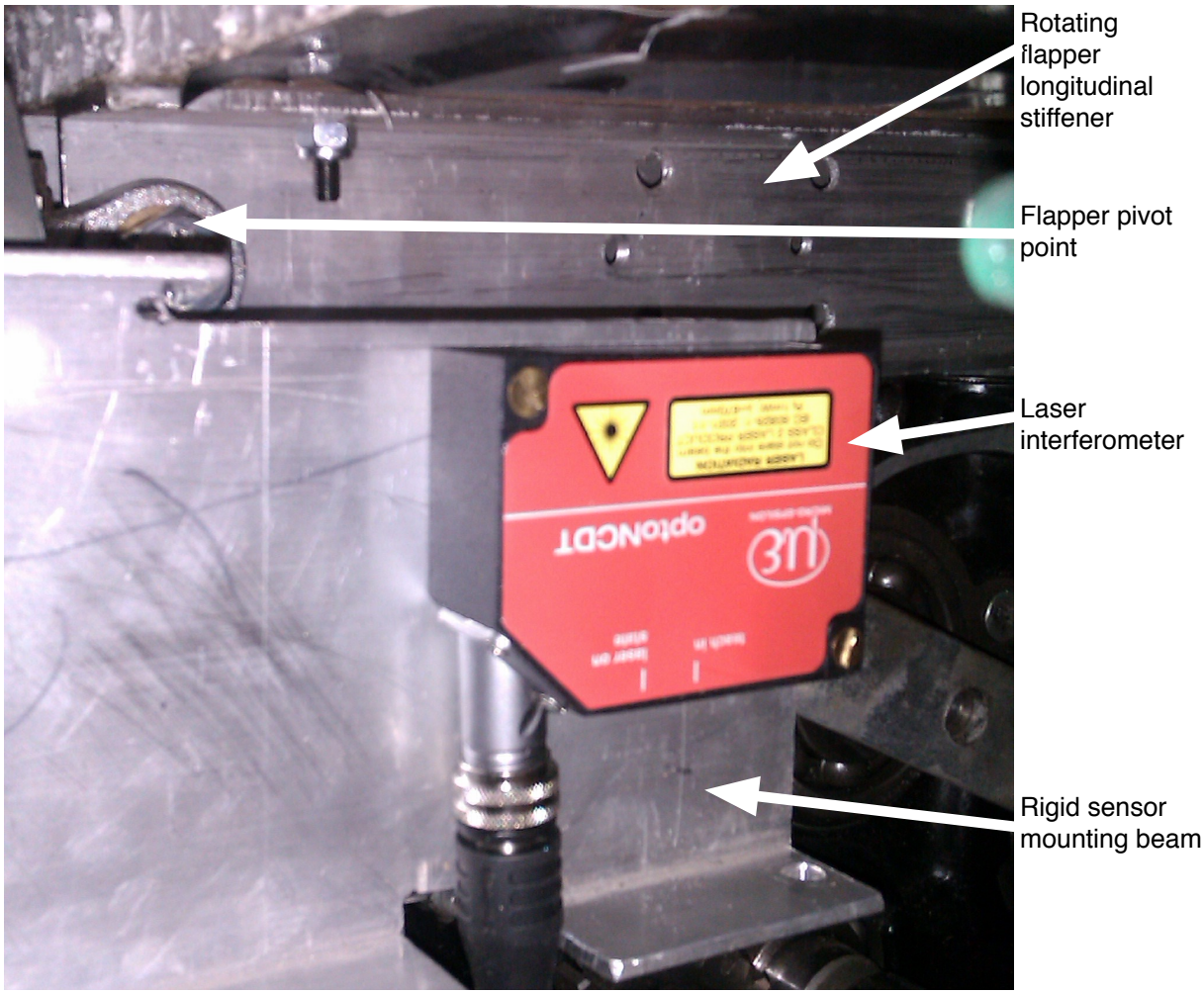


Figure 6.8. Flapper sensor position. The sensor is a laser interferometer with limited range. It is mounted on a rigid beam close to the flapper pivot point so that the range of flapper motion lies within the range of the sensor.

The laser interferometers used were capable of a resolution of 10 µm for dynamic measurements and a sampling frequency of 25 kHz.

At each forcing frequency, the experimental rig was allowed to settle over a period of 2-3 minutes into a dynamic equilibrium, as transients from the change in forcing frequency were significant. The measurements were taken for a sample time of 15 s and the full sample was used for analysis. A shorter sample time (2 s) is used in plots in this thesis to make the graphs clearer to read within the restricted page width (Fig. 6.9). In this

thesis, the displacement time-series data has also been analysed and graphed to identify dominant frequencies in both the forcing flap and supported mass motion, each called a 'power spectrum plot'. A full set of power spectrum plots is included in Appendix H, only a graphical representation of the data is included as each time-series that is plotted comprises 25,000 points per second of time and the power spectrum is most clearly represented graphically. The results presented in Secs. 6.5.4.1 to 6.5.4.3 were prepared from the results of the power spectrum plots.

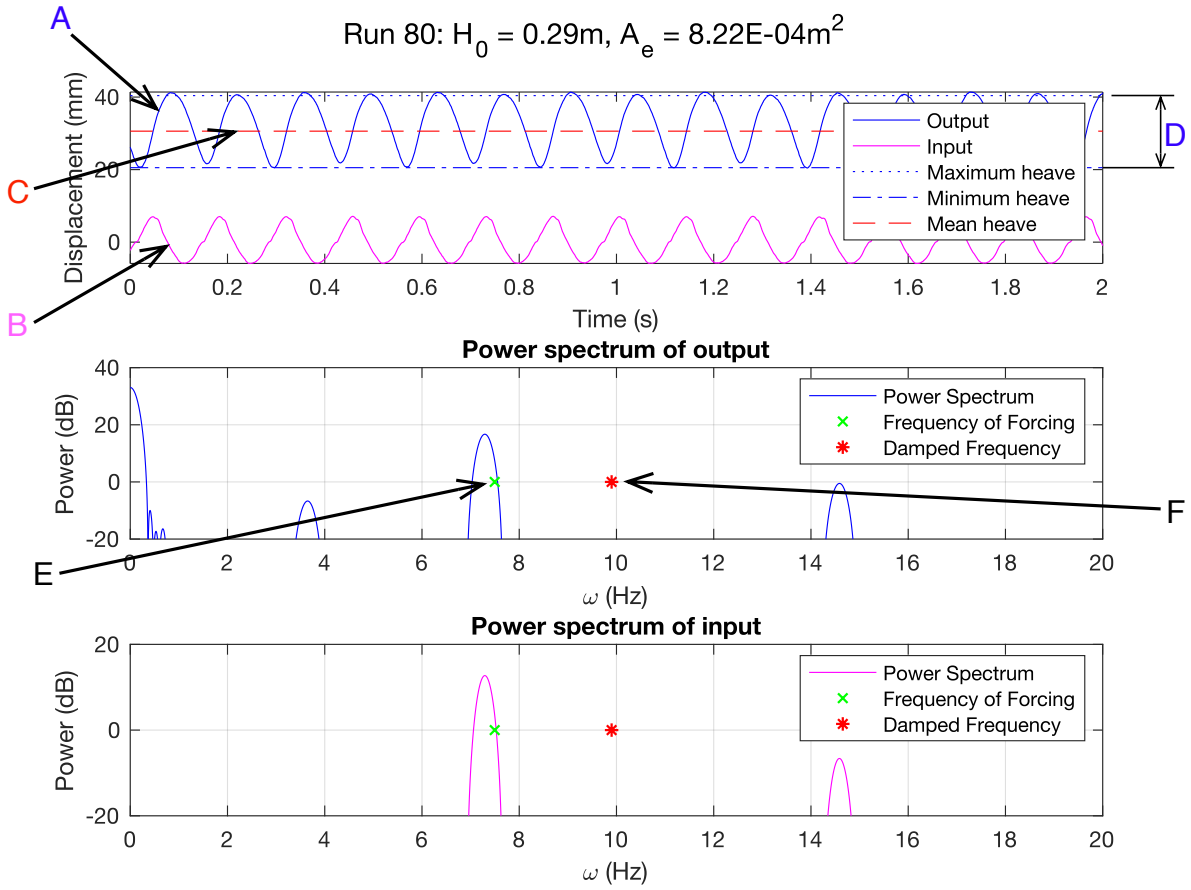


Figure 6.9. Example measurands from experiment showing analysis to find results. The supported mass displacement time series (A) and the forcing flap displacement time series (B) are shown on the upper axes of the plot. A 2 s sample of the 15 s time series is plotted. The arithmetic mean of the supported mass displacement series is calculated (C). The mean peak-to-peak magnitude of the supported mass displacement time series is calculated (D). This example is taken from an experimental run at forcing frequency (ω_f) shown by location E. The predicted damped frequency for this combination of H_0 and A_e is shown by F.

The mean of all the maxima of the supported mass displacement in the sample was calculated. The mean of all the minima of the supported mass displacement in the sample was calculated. The difference between these two numbers was taken as the mean displacement of the supported mass for the experimental run. The alternative methods of calculating the mean displacement had limitations: finding the mean of all the data points

did not account for the partial cycles present in the sample time; and finding the mean of the global maximum and the global minimum did not take account of any outliers in the measurement.

The volume swept by the heave deck was found, for both the mean position of the heave deck and the magnitude of the heave deck motions. The heave deck swept volume was divided by the forcing volume so that the results could be compared for different plenum volumes.

It is convenient to convert the displacements into the equivalent swept volumes as it simplifies a qualitative understanding of the magnitudes of motions involved. If the plenum was sealed and compressibility was negligible, the conservation of mass within the plenum implies that the swept volume of the resultant motions must equal the swept volume of the forcing motions. It also follows that the mean resultant motion of a sealed plenum will be zero, as the reduction in plenum volume by the volume forcing mechanism will be matched by a corresponding increase in plenum volume.

The experimental results are a sample 15 s long, after allowing 2 min to 3 min of operation to pass unsampled to allow the transient effects to fully decay. Thus, there are approximately 15 cycles sampled at the lowest forcing frequency of approximately 1 Hz and up to 150 cycles sampled at the highest forcing frequency of approximately 10 Hz.

The mean displacement of the heave deck is used to calculate the swept volume — this is the net gain in plenum volume over the analysed period.

The magnitude (peak to peak) of the heave deck motion was used to calculate the swept volume of the heave deck motions. The heave deck motion occurs both above and below the mean position, therefore the maximum swept volume of the heave deck is the mean swept volume plus half of the dynamic swept volume, and the minimum swept volume is the mean swept volume minus half the dynamic swept volume.

For convenient reference, the two non-dimensional expressions describing the supported mass motions are given symbols. The ratio of the mean of the supported mass displacement, expressed as a volume, to the volume swept by the forcing mechanism is denoted by S_v. The ratio of the volume swept by the oscillations of the supported mass (subtracting the mean of the oscillating displacements) to the volume swept by the forcing mechanism is denoted by O_v. These terms are used to label the result plots presented in the following sections. To make it clear that these are non-dimensional terms, the units are presented as $^{\mathrm{m}^3}/_{\mathrm{m}^3}$.

6.5.4. Principal experimental results

The experimental results are plotted over the numerical model predictions. For convenience, the two parameters calculated from the same measurand at each value of the forcing frequency (ω_f) is contained in each plot using two sets of axes; the first set of axes is for S_V plotted against ω_f, the second set of axes is for O_V plotted against ω_f. The phase angle (ϕ) between the supported mass motion and the flapper motion is plotted on the third set of axes, with the experimental results plotted over the numerical model predictions.

There are two experimental factors, H_0 and A_e, each set to one of three values, giving nine combinations of experimental factors (Table 6.6). Five of these combinations are presented in the body of this thesis, with all nine experimental results included in Appendix H. The five combinations of the experimental factors are sufficient to give insight to the sensitivity of the experimental results to the two experimental factors.

Table 6.6. The nine combinations of the two experimental factors, with the combinations presented in the body of the thesis shown in **bold type**.

	$A_e = 570 \times 10^{-6}\,\mathrm{m}^2$	$A_e = 820 \times 10^{-6}\,\mathrm{m}^2$	$A_e = 1.207 \times 10^{-3}\,\mathrm{m}^2$
$H_0 = 290 \times 10^{-3}\,\mathrm{m}$	Condition 1	**Condition 2**	Condition 3
$H_0 = 600 \times 10^{-3}\,\mathrm{m}$	**Condition 4**	**Condition 5**	**Condition 6**
$H_0 = 810 \times 10^{-3}\,\mathrm{m}$	Condition 7	**Condition 8**	Condition 9

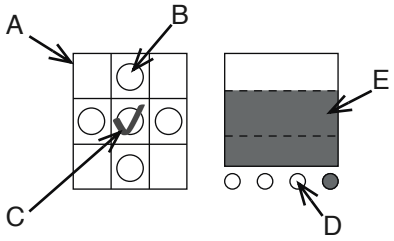


Figure 6.10. Icon representing which condition is relevant to the presented results. The left side grid (A) represents the nine possible conditions, where H_0 corresponds to the vertical axis and A_e corresponds to the horizontal axis. The circles (B) in the cells indicate the conditions that will be discussed in the main body of the thesis. The tick on a circle (C) indicates the current condition. The pictorial part of the icon represents the plenum height by a shaded area (E) and open air exit areas by open circles (D).

An icon of the style introduced in Fig. 6.10 is included on each plot to assist the reader to identify the condition at which the results were obtained. The icon refers to Table 6.6, indicating the relevant condition with a tick in a grid, corresponding to the location in Table 6.6. The icon also contains a representation of the plenum chamber, with H_0 indicated by a shaded portion. The final part of the icon is a series of circles representing A_e, with open circles shown proportional to the A_e. There is always a fixed portion of the total A_e, so four circles are used in the icon, the first circle representing the fixed portion of the total A_e.

At each condition, several forcing frequencies were selected at random for repetition, which are shown as extra points on the plots (rather than an average), acknowledging that the repetition procedure of the experiments can lead to small variations of the forcing frequency.

6.5.4.1. Experimental result at mid-range of experimental factors

Condition Five is approximately at the mid-range for the experimental factors: plenum height (H_0) and the air exit area (A_e). The experimental result for the condition at the middle of the available range of experimental factors is presented first (Fig. 6.11), so that results presented subsequently can provide insight into the sensitivity of the mass-plenum system to the experimental factors. The experimental result at each frequency is plotted in Fig. 6.11 and the predictions of mass-plenum system behaviour made using the numerical model is plotted as a dashed line.

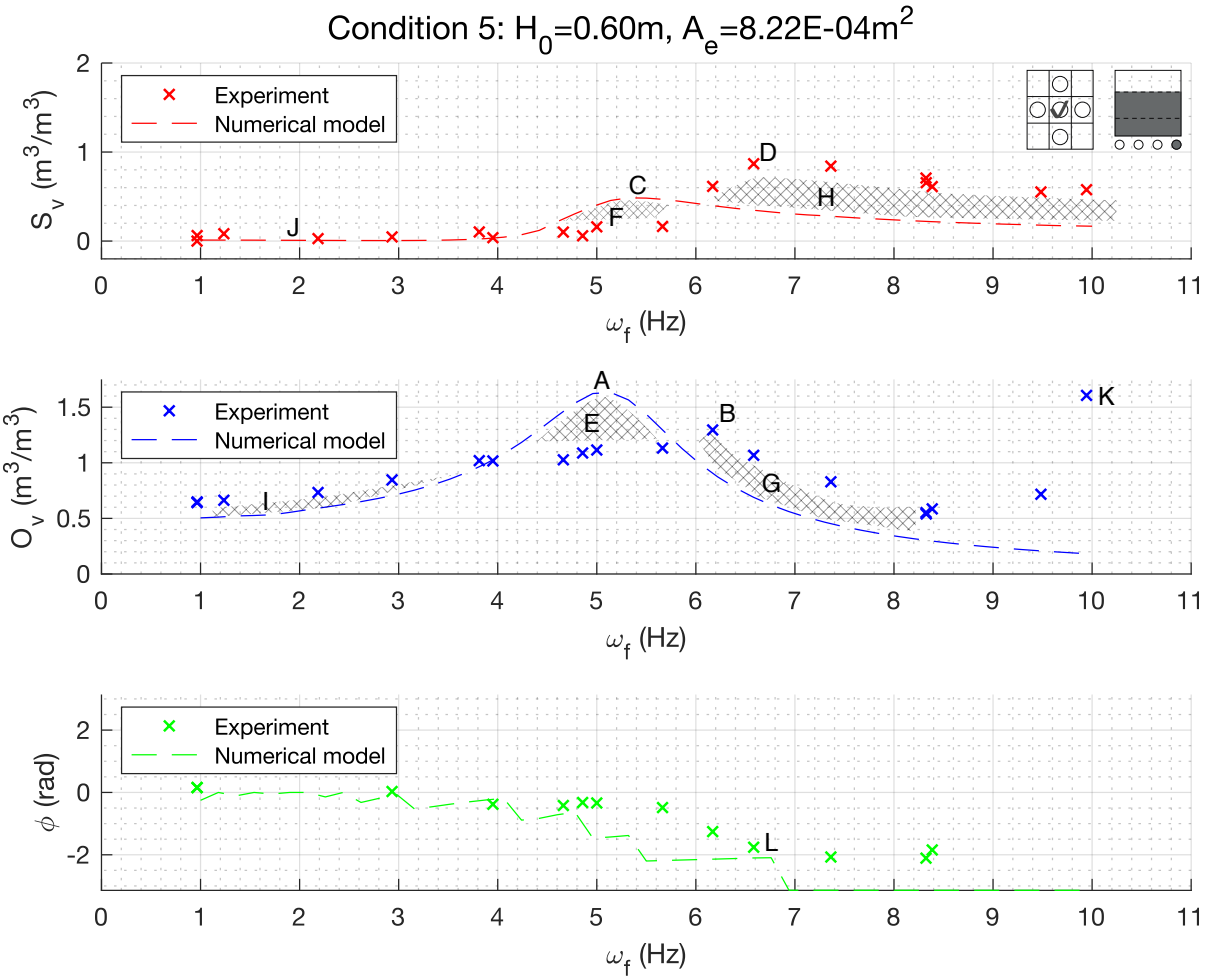


Figure 6.11. Results for main experiment at Condition Five. Overall result for forced oscillations experiment compared to prediction with plenum height (H_0) and air exit area (A_e) set to $H_0 = 600 \times 10^{-3}$ m and $A_e = 820 \times 10^{-6}$ m^2, this is near the middle of the ranges for both H_0 and A_e.

Referring to Fig. 6.11. For Condition Five, the frequency at which the magnitude of the response (O_V) peaks in the numerical solution (A, ω_d) is at approximately 5.2 Hz. The maximum (B) is at approximately 6.2 Hz. Interpolation indicates that the frequency at which is at peak magnitude is probably in the range 5.4 Hz to 6.0 Hz. From the numerical solution, the frequency at which the mean of the supported mass displacement (S_V) is a maximum (C) is approximately 5.4 Hz, slightly higher than the predicted ω_d. The peak in S_V corresponds with an increase in the phase shift (ϕ), point L on the plot. The frequency at which the experimental observations of the S_V was at a maximum (D) is approximately 6.6 Hz. If the experimental results were interpolated, the frequency of the maximum of would most probably be in the range 6.2 Hz to 6.6 Hz. The numerical solution over-predicts O_V near ω_d, but it is likely that parasitic phenomena inherent in the experimental rig are triggered by the high energy in the system at this forcing frequency, reducing the energy available to move the supported mass. The numerical solution also over-predicts S_V near ω_d (F). At frequencies higher than ω_d (G), the numerical solution under-predicts O_V and S_V (H), this is partially explained by the lower ω_d predicted by the

numerical solution (the stiffer plenum walls on the experimental rig). At low frequencies (I), the numerical solution under-predicts O_V, this is expected as the stiffer experimental rig plenum walls will force the energy from the forcing mechanism into the motions of the supported mass. The shift in mean supported mass displacement (S_V) at lower frequencies (J) is negligible and consistent with the predictions made using the numerical solution; this is interesting as it indicates that the slow falling time of the supported mass observed during transient changes to the plenum volume, do not affect the ability of the supported mass to track the plenum forcing volume, this is consistent with the presence of a reduction in plenum volume when the plenum forcing mechanism increases the plenum volume. At very high frequencies, approaching $2\omega_d$, there is an anomalous result for the magnitude of the supported mass motion (K). This is discussed in Sec. 6.5.5.

The experimental results for Condition Five confirms that an increase of the mean supported mass displacement (S_V) occurs when the plenum volume is forced at frequencies above the damped frequency. This is a unique result, not found elsewhere in the available literature. The increase of S_V begins below ω_d and peaks just after ω_d (point D in Fig. 6.11), but remains significantly above zero at frequencies above the peak (region H in Fig. 6.11). The increase of S_V corresponds with an increased lag (more negative phase angle, ϕ) between the flapper motion and supported mass motion occurring over the same range of ω_f (Fig. 6.11, point L). This phenomenon was also observed in the preliminary experiment. In subsequent sections of this thesis it will be shown that this phenomenon was observed for all the experimental conditions used in the experiments. This result supports hypothesis HA-1 that the supported mass is lifted to higher mean displacements when the plenum volume is oscillated at higher frequencies.

Over the frequency range of 1 Hz to 5 Hz, the change in the supported mass time-wise mean is close to zero. This range of forcing frequencies equate to forcing periods of 1 s to 200×10^{-3} s, which is always faster than the falling time (T_f) (Sec. 6.3.3). This comparison of T_f with the value of S_V indicates that the downstroke of the plenum forcing flapper does generate a pressure reduction that is sufficient to 'suck' the supported mass to below its starting position. This is in contrast to the non-zero value of S_V at forcing frequencies above approximately 5 Hz, where the supported mass is no longer 'sucked' down to the starting position. The higher forcing frequencies correspond to faster rates of change of the plenum volume, affirming hypothesis HA-1.

In the plot of O_V against ω_f in Fig. 6.11, the peak magnitude occurs in the region of the predicted ω_d, then decreases at higher frequencies. Near ω_d, the motions of the supported mass are larger than the motions of the forcing flapper. In other words, the ratio of the swept volume of the supported mass to the swept volume of the forcing flapper is greater than unity. This behaviour, and the change in ϕ over the same frequency range, is similar to the forced vibration of a single-degree-of-freedom system under harmonic excitation when the system damping ratio is between 0.5 and 1 (Meriam & Kraige, 2008, pp.623-624). This behaviour supports the hypothesis that resonance can be induced in the mass-plenum system, and will be discussed in Chapter 7. Section 6.5.5 will examine the time-series for the supported mass displacement measurement and the forcing mechanism displacement measurement plotted on the same time scale.

At a very high forcing frequency, approximately double ω_d, an anomalous result for the magnitude of the supported mass motion was observed (Fig. 6.11, note K) (Sec. 6.5.5).

The experimental observations have a good overall agreement with the predictions from the numerical model, and by association, the underlying mathematical model. Sections 6.5.4.2 and 6.5.4.3, will discuss the results from subsequent experiments for varied plenum height and air exit area.

There were five observed behaviours:

1. The numerical model under-predicts the frequency of peak supported mass oscillation magnitude (Fig. 6.11, notes A and B)
2. The numerical model under-products the frequency of peak supported mass increase in mean displacement (Fig. 6.11, notes C and D)
3. The numerical model under-predicts O_V at $\omega_f < \omega_d$ (Fig. 6.11, note I) and at $\omega_f > \omega_d$ (Fig. 6.11, note G)
4. The numerical model under-predicts the increase in S_V at $\omega_f > \omega_d$ (Fig. 6.11, note H)

None of these five observed behaviours prevent the experimental results from being used to investigate the research hypothesis. It is plausible that all of these five observed behaviours are the result of two phenomena that are specific to the experimental rig and are not inherent in the type of mass-plenum system being investigated These observed behaviours lie outside the aims of this thesis and will not be investigated further. The two underlying phenomena that are the hypothesised cause of the five observed behaviours are:

1. The plenum structure is stiffer than estimated during the commissioning trials. Some work on the plenum sealing and structural integrity was required after the plenum forcing mechanism was reconfigured to produce oscillating forcing of the plenum volume and could not subsequently be used to find a plenum stiffness factor (used in the numerical model) using a step-change of the plenum volume. This extra stiffness will act to increase the magnitude of the supported mass motions, compared to the prediction from the numerical model.
2. At $\omega_f \approx \omega_d$ the mass-plenum system experiences high energy motions that could possibly activate parasitic extra motions within the mass-plenum system (e.g. opening of seals, stretching of polymer film used for sealing). The parasitic phenomena will tend to decrease the magnitude of the supported mass motions when activated.

The two hypothesised underlying phenomena are specific to the experimental rig and are not general to the type of mass-plenum system being investigated. as such, they will not be discussed further in this thesis.

6.5.4.2. Experimental results at varying air exit area

Repeating the experiment reported in Sec. 6.5.4.1 at two different sizes of air exit area (A_e), increases confidence in the results of Sec. 6.5.4.1. How the air exit area influences the dynamics of the mass-plenum system is of interest for two reasons. Firstly, the results of the commissioning tests (Sec. 6.3) showed that the rate that the supported mass fell back to the hover position was dependent on the air exit area. Secondly, in Sec. 5.6.4, the mathematical model of the mass-plenum system assumes that the air flow exiting the plenum changes instantly in response to changes in the plenum pressure (the assumption of quasi-steady, incompressible air flow through an orifice). Varying the air exit area while keeping the air supply to the plenum at a fixed volume flow rate tests the sensitivity of the change in mean displacement of the supported mass to the relative ease by which air can be expelled from the plenum. Changing the air exit area, while keeping air supply at a constant value, has the effect of changing the plenum pressure at hover.

Two sets of experimental results are presented to investigate the sensitivity of the results to varying air exit area. Both sets of experimental results have the same plenum height as Condition Five (Fig. 6.11). The first set of experimental results is for the combination of plenum height and air exit area denoted Condition Six (Fig. 6.12), with the air exit area increased, compared to Condition Five (Fig. 6.11). The second set of experimental results is at Condition Four (Fig. 6.13), with the air exit area reduced compared to Condition Five (Fig. 6.11).

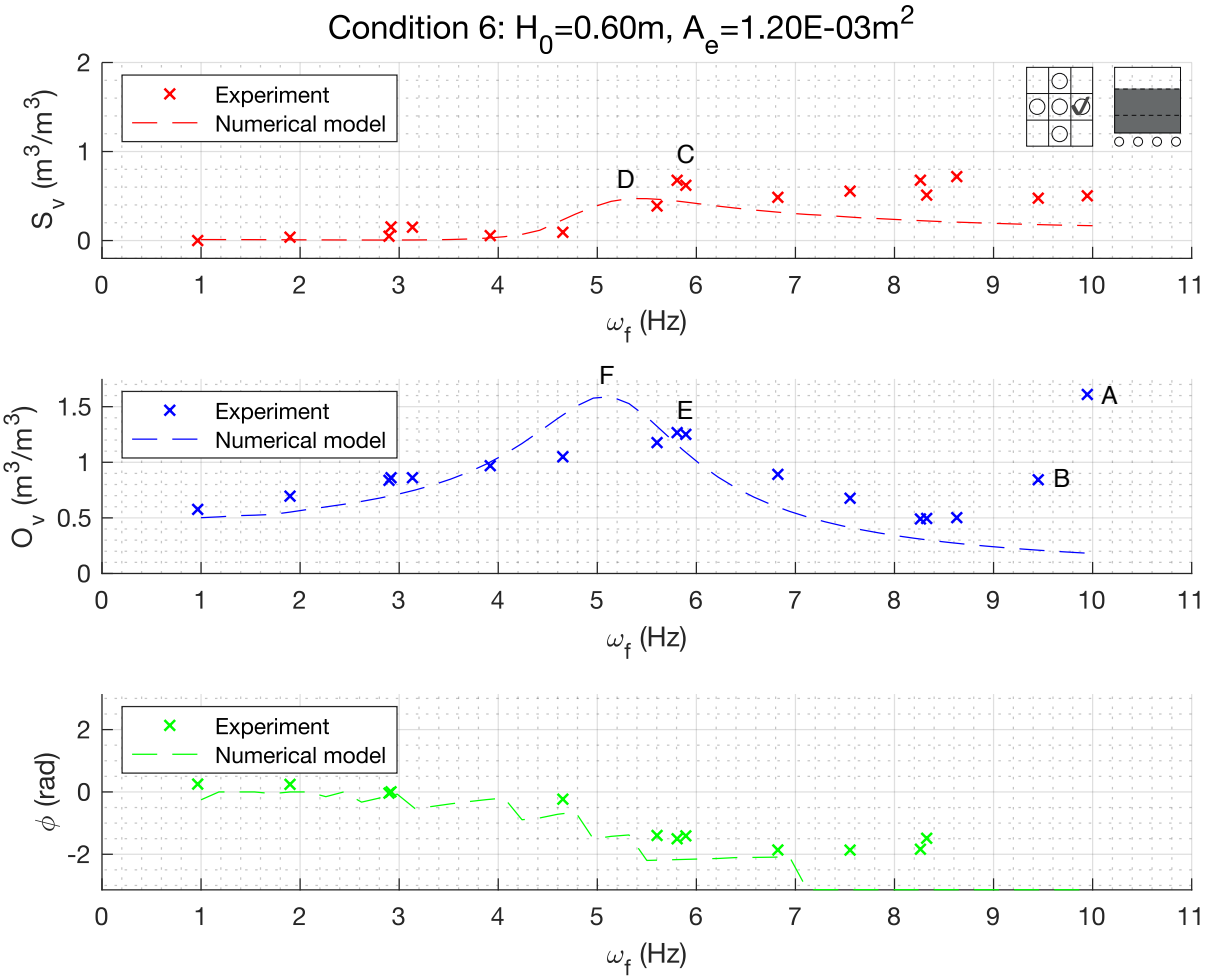


Figure 6.12. Condition Six results. Plenum height (H_0) is the same as Condition Five. Air exit area (A_e) is larger than Condition Five.

Referring to Fig. 6.12. At Condition Six, the salient characteristics of the results are similar to Condition Five (Fig. 6.11), with the frequency of peak change in for the experimental observations (C) at a higher than predicted by the numerical model (D) and the frequency of peak (E) also at a higher than predicted by the numerical model (F). This set of experimental results is a successful repetition of the principal experiment. There is a marked discrepancy in the predicted magnitude compared to the experimental observation at point (A). A similar, but smaller discrepancy is observed at point (B). These points are investigated in Sec. 6.5.5.

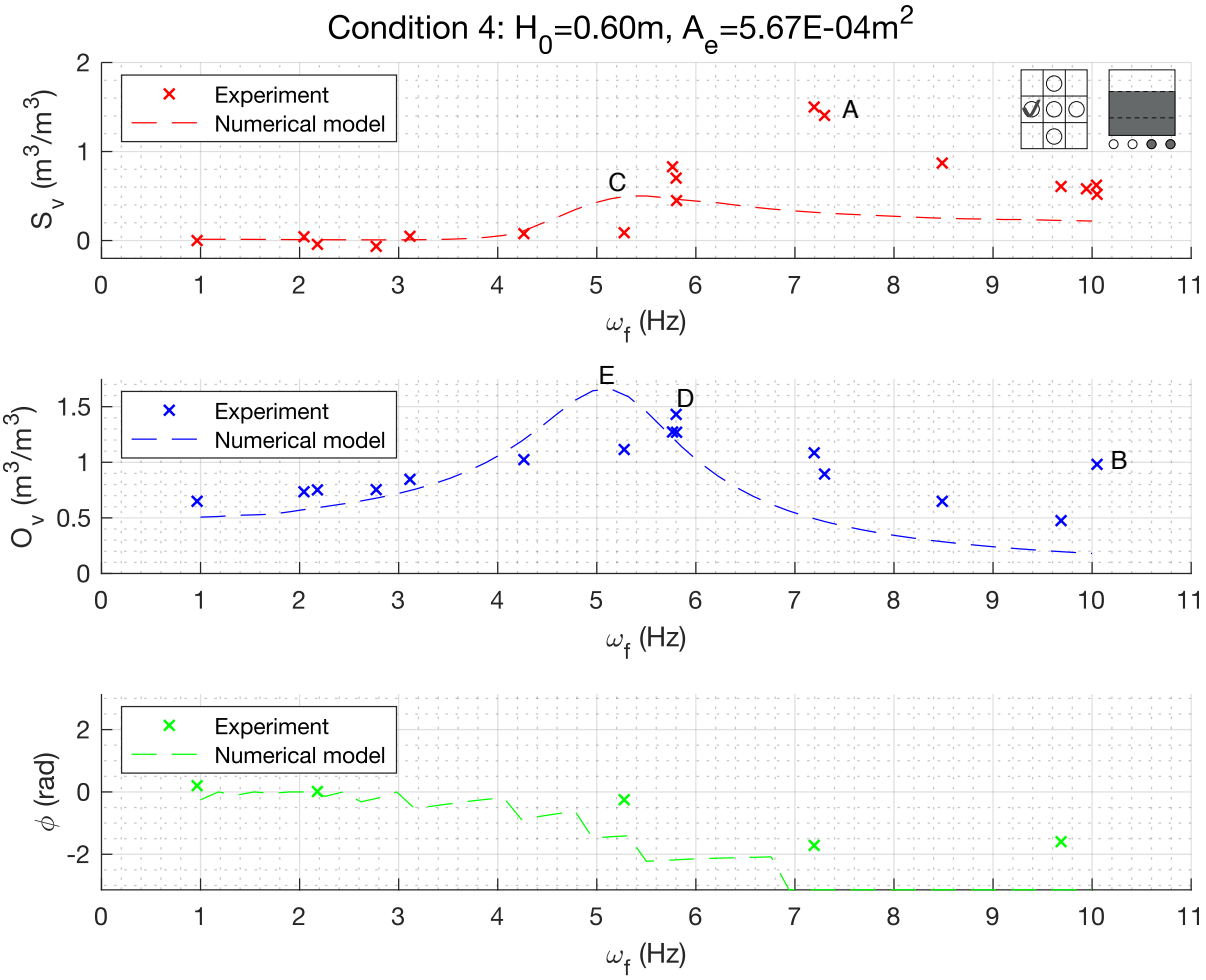


Figure 6.13. Condition Four results. Plenum height (H_0) is the same as Condition Five (Fig. 6.11). Air exit area (A_e) is smaller than Condition Five.

Referring to Fig. 6.13. At Condition Four, the salient features of the results are similar to Condition Five (Fig. 6.11). Two of the results (A), which appear to be the peak magnitudes of S_V, are at a higher frequency than predicted by the numerical model (near ω_d, C). The two points are also of a greater magnitude than predicted by the numerical model. This is different from the observations in Fig. 6.11 and Fig. 6.12. The two results at (A) are considered anomalous. The observed peak of O_V (D) occurs at a value of ω_f that is higher than predicted by the numerical model (near ω_d, E). This is similar to the observations in Fig. 6.11 and Fig. 6.12. There is a discrepancy between the predicted magnitude and the experimental observation at point (B), which is further investigated in Sec. 6.5.5.

The general agreement of the experimental results with the predictions made with the numerical model is similar to Condition Five (Sec. 6.5.4.1). The repetition of the results makes it unlikely that the results of the experiment at Condition Five are anomalous. The predictions of the numerical model consistently under-predict the magnitude of the supported mass oscillations and the change in the mean supported mass displacement. The under-prediction is less than an order of magnitude and the predictions and experimental

results follow the same trend, making it unlikely that the numerical model is missing a significant factor.

Smaller air exit areas (such as in Fig. 6.13, when compared to Fig. 6.12) act to increase the magnitude of the supported mass oscillations and to increase the change in the mean supported mass displacement. This is consistent with the smaller air exit area acting to restrict the flow of air out of the plenum volume, resulting in higher plenum pressure acting on the supported mass.

At a forcing frequency of approximately 7.2 Hz, there are discrepancies in the predicted magnitude of motion compared to the experimentally observed magnitudes of motion (Fig. 6.13, note A). The change in the mean displacement of the supported mass is much higher than the numerical model predicts, and much higher than the general under-prediction that was noted in Sec. 6.5.4.1.

At forcing frequencies greater than 9 Hz, approaching double the damped frequency, the magnitude of the supported mass oscillations is much greater than that predicted by the numerical model (Fig. 6.12 note A and B, Fig. 6.13 note B) and also much greater than the trend of the experimental results. This also occurred at Condition Five (Fig. 6.11, note K). These results will be discussed in Sec. 6.5.5.

6.5.4.3. Experimental results at varying plenum height

The plenum height (H_0) has a significant effect on the mass-plenum system damped frequency (ω_d), primarily due to the volume of air available for compression, and also because the plenum boundary flexibility has a dependency on the plenum wall height Sec. 6.4.3. Repeating the experiment discussed in Sec. 6.5.4.1 at varying plenum height enables the relationship between the supported mass motions and ω_d to be investigated. The volume swept by the plenum volume forcing mechanism remained fixed as H_0 is varied, so the proportion of the plenum volume that is forcibly oscillated is also varied. The ratio between the volume being forced and the air exit area remains the same as previous sets of experiments at the same air exit area.

Two sets of results are presented to investigate the sensitivity of the experimental results to H_0. Both sets of results are at the same air exit area (A_e) as the set of results at Condition Five (Sec. 6.5.4.1). One set of results is at a higher H_0 (Fig. 6.14) and one set of results is at a lower H_0 (Fig. 6.15).

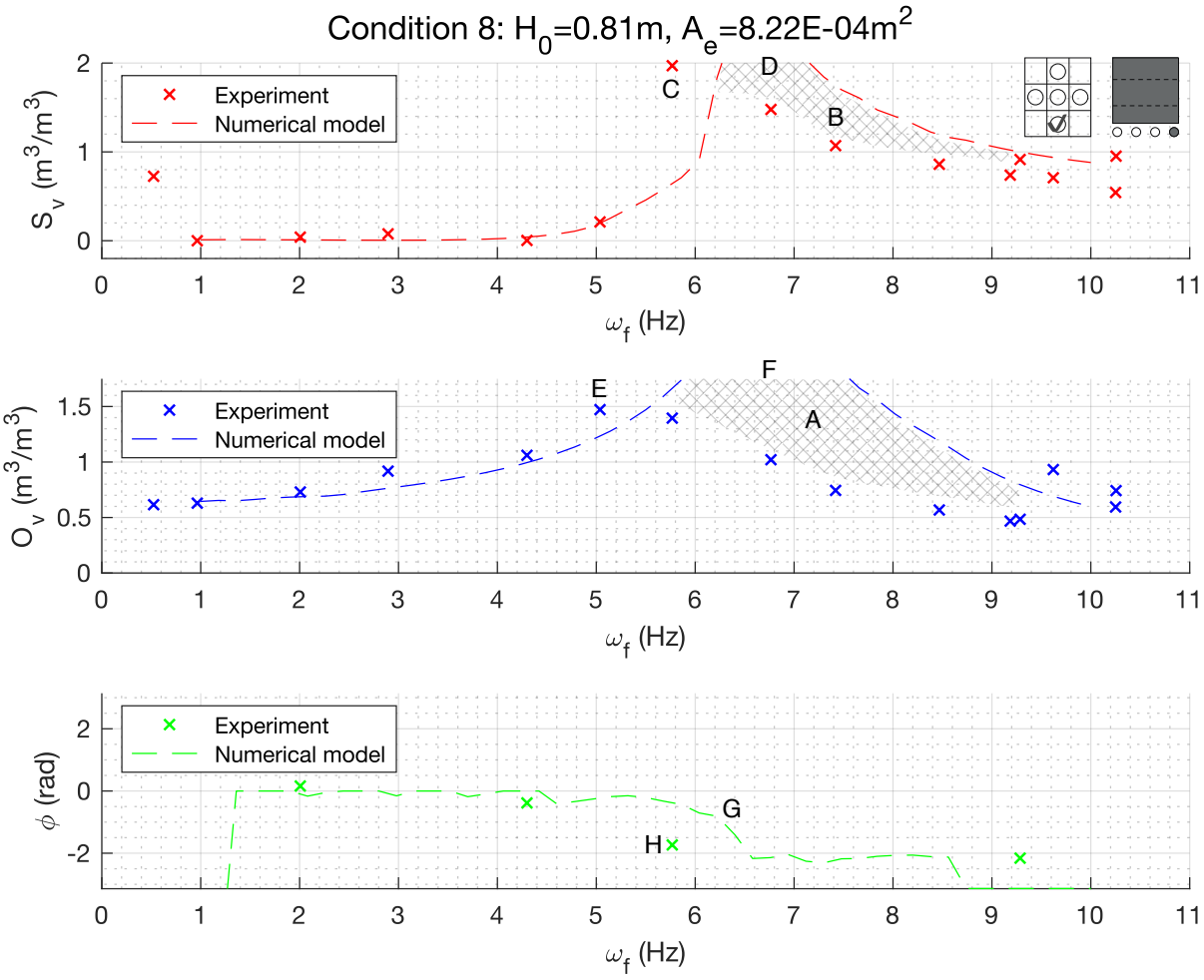


Figure 6.14. Experimental results at Condition Eight. Air exit area (A_e) is the same as Condition Five (Fig. 6.11), plenum height (H_0) is higher than Condition Five. Refer to Fig. 6.11 for identification of the salient points.

Referring to Fig. 6.14. At Condition Eight, the general trends of the numerical model predictions and the experimental observations are consistent with the experimental results at Condition Five (Fig. 6.11). The numerical model predicts that the magnitude of the supported mass oscillations (O_V) occurs at a forcing frequency (ω_f) of approximately 6.5 Hz, whereas the highest was observed at approximately 5 Hz. The numerical model over-predicts O_V at $\omega_f > \omega_d$, though this may be related to the over-prediction of ω_d. The numerical model predicts that the maximum change in mean supported mass displacement (S_V) will occur at a higher ω_f than experimentally observed. The numerical model over-predicts the change in S_V at $\omega_f > \omega_d$. The mismatch between the predictions made by the numerical model and the experimental observations are consistent with the plenum boundary flexibility being different from that measured during the commissioning tests, which is expected. The peak S_V (C) occurs at a higher frequency than the peak O_V (E), consistent with the results at Conditions Five, Six and Four (Figs. 6.11 to 6.13). The peak S_V occurs at a ω_f where the phase angle (ϕ) is greater than $\pi/2$ (H), which is consistent with the previous results at Conditions Five, Six and Four (Figs. 6.11 to 6.13). The large plenum volume has a lower ω_d, enabling the experimental rig to force the plenum volume at frequencies more than $2\omega_d$. The magnitude of O_V at approximately 9.5 Hz is higher than the prediction of the numerical model and the trend of the experimental results in that region, a similar discrepancy was observed at Conditions Five, Six and Four (Figs. 6.11 to 6.13). However, O_V at approximately 10.25 Hz is lower than the result at 9.5 Hz and is closer to the values predicted by the numerical model. These discrepancies will be discussed in Sec. 6.5.5.

The predicted damped frequency (ω_d) at Condition Eight (Fig. 6.14) is higher than was experimentally observed: the predicted frequency of the peak magnitude of O_V (Fig. 6.14, point F) is at a higher frequency than the highest observed O_V (Fig. 6.14, point E). A similar result occurred for the change in S_V (compare Fig. 6.14, point D with Fig. 6.14, point C). The over-prediction of ω_d is consistent across all results for $H_0 = 800 \times 10^{-3}$ m (see Appendix H, Figs. H.8 and H.10). The *over-prediction* of ω_d is a different result than the *under-prediction* of ω_d seen at $H_0 = 600 \times 10^{-3}$ m. It is likely that the taller plenum walls have a different mode of vibration than the shorter plenum walls at the other values of H_0. This behaviour will not be investigated further, for the same reasons discussed in Sec. 6.5.4.1.

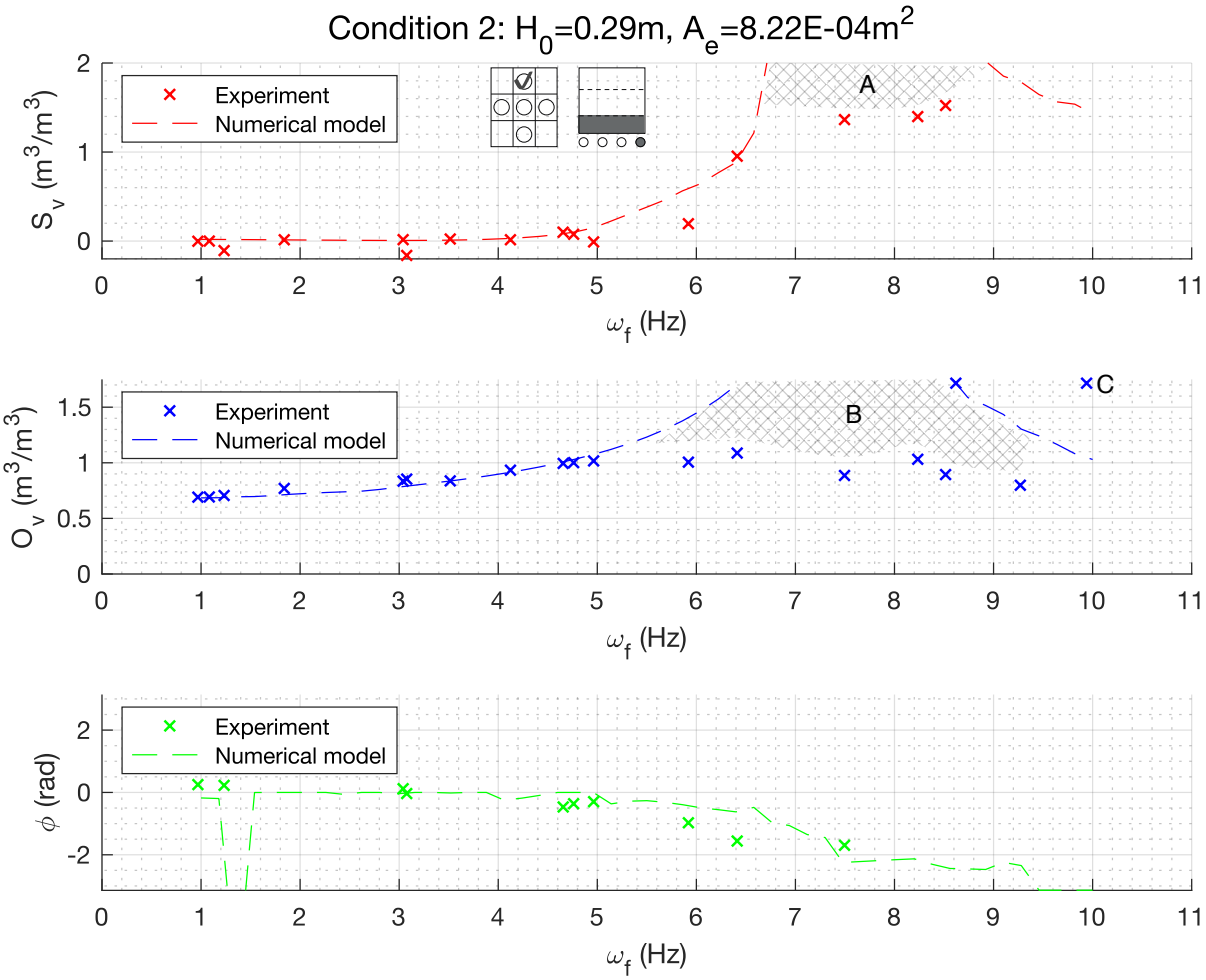


Figure 6.15. Experimental results at Condition Two. Air exit area (A_e) is the same as Condition Five, plenum height (H_0) is less than Condition Five (Fig. 6.11).

Referring to Fig. 6.15. At Condition Two, the volume being forced is a large proportion of the plenum volume. The numerical model predicts a much larger change in mean supported mass displacement (S_V) near the damped frequency (ω_d) than experimentally observed (region A). Similarly, the numerical model predicts a greater magnitude of supported mass oscillations (O_V) than was experimentally observed (region B). For both S_V and O_V, no distinct peak occurs in the experimental observations. At the highest value of the forcing frequency (ω_f), O_V is higher than predicted by the numerical model and also higher than the general trend of O_V results at nearby values of ω_f (C). This observation will be discussed further in Sec. 6.5.5.

At the lowest value of H_0 (Fig. 6.15) the experimental results do not have a clear peak, so no conclusions as to the accuracy of the predicted value of ω_d can be drawn. There are larger over-predictions of S_V and O_V in the region near ω_d. The swept volume of the forcing flapper is a substantial fraction the plenum volume, so it is to be expected that the predicted motions will be substantial, because a smaller portion of the forced volume changes can result in the compression of the air in the plenum volume. It is also reasonable

to assume that potential parasitic phenomena will have a greater effect at this condition due to the large amount of energy that must be dissipated at resonant conditions. The parasitic phenomena has the effect of reducing the experimental observations more than was observed at other experimental conditions. The comparison of experimental conditions and the predictions of the numerical model are consistent for the other two experiments at $H_0 = 290 \times 10^{-3}\,\mathrm{m}$, with a similar absence of a distinct peak in the experimental observations and a significant over-prediction of S_V and O_V. The differences in predictions compared to experimental results will not be investigated further, for the reasons given in Sec. 6.5.4.1.

Changing the plenum height has the predicted effect on ω_d, after allowing for differences in the plenum flexibility lumped parameter found during the commissioning tests. The range of values used for H_o was sufficient for observable differences in the mass-plenum system ω_d. The predictions of the mass-plenum system behaviour made using the numerical model are in good agreement with the experimental results over the range of values for H_0.

6.5.5. Direct comparison of flapper and supported mass time-series

Deeper insight can be gained into the mass-plenum dynamics by directly comparing the time histories of the heave deck displacement and the plenum volume forcing mechanism displacement (Fig. 6.16). To allow for convenient understanding, three sets of axes are included in each plot: a sample of the heave deck displacement and forcing mechanism displacements measured at a particular forcing frequency (ω_f), plenum height (H_0) and air exit area (A_e) are plotted on coincident axes of displacement in millimetres versus the elapsed time. The second set of axes is the power spectrum analysis of the heave deck displacement time history, with the forcing frequency and the predicted natural frequency shown for reference. The third set of axes is the power spectrum analysis of the forcing mechanism time history. In this thesis, this type of plot will be called a 'power spectrum plot'. A full set of power spectrum plots is included in Appendix H, only a graphical representation of the data is included as each time-series that is plotted comprises 25,000 points per second of time and the power spectrum is most clearly represented graphically. The displacement of the plenum volume forcing mechanism (Fig. 6.16 note B) is not directly related to the displacement of the supported mass (Fig. 6.16 note A), direct comparison of relative magnitude is done by comparing the respective swept volumes, as in Sec. 6.5.4. The first comparison of flapper and supported mass time-series is presented to illustrate the typical features of data and power spectrum analysis and aid interpretation of the other figures in this section. The result is from Condition Five (Sec. 6.5.4.1) and is at a low forcing frequency (Fig. 6.16).

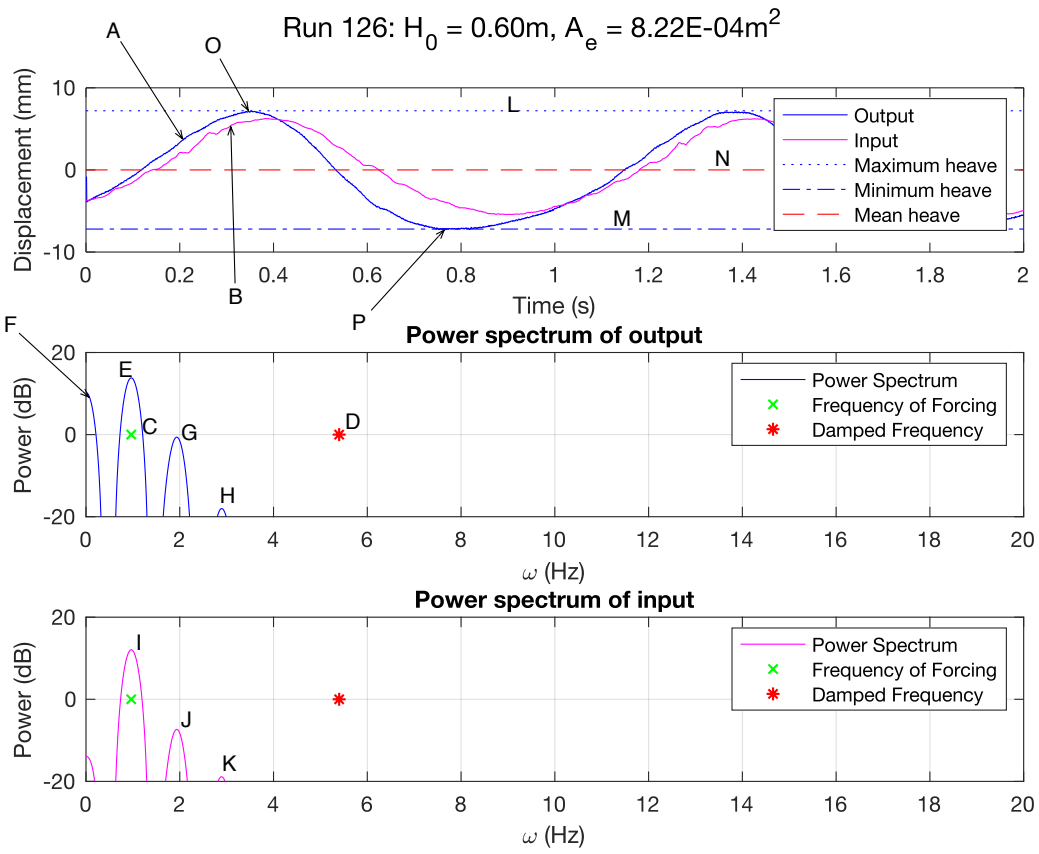


Figure 6.16. Power spectrum analysis of main experiment run 126. This plot illustrates the analysis of the experimental measurements and several observations that aid insight into mass-plenum system operation.

Referring to Fig. 6.16. For experimental run 126, the plot shows the first two seconds of the measurements of the supported mass vertical displacement (A) and the plenum volume forcing mechanism vertical displacement (B). The measurements are taken when the forcing frequency (ω_f, C) is approximately 1 Hz. The predicted damped frequency ω_d, based on the measurements taken in the commissioning tests (Sec. 6.3), is approximately 5.5 Hz (D). A peak in the power spectrum of the supported mass time-series corresponds to (E), and corresponds to a peak in the power spectrum the plenum forcing mechanism (I). A peak in the power spectrum of the supported mass at very low frequency (F) indicates either oscillations at very low frequencies, or an increase in the mean displacement of the supported mass. Further peaks in the supported mass power spectrum (G and H) correspond to peaks in the flapper power spectrum (J and K), indicating that the supported mass is responding to motions of the flapper, and no other significant motions are being excited in the mass-plenum system. The peak at point J is approximately double the frequency of ω_f at point I, and is consistent with small motions in the crank's bearing, with the motions occurring twice each cycle of the flapper mechanism. Examination of the time-series of the flapper (B) shows evidence of some extra motions of the flapper, such as small motions in the bearings of the driving mechanism. The supported mass time-series

was analysed to find all the maxima and minima, and the mean of the maxima (line L) and the mean of the minima (line M) were calculated. The mean of the supported mass displacement was found by taking the mean of the maxima and minima combined (line N), the mean of the entire time-series would be skewed unless the samples spanned an exact number of cycles. The slope of the supported mass displacement plot varies as the supported mass approaches and departs a maxima (O) compared to when the supported mass approaches and departs a minima (P).

An examination of the power spectrum plots for a ω_f of approximately half the damped frequency (ω_d) as in Fig. 6.17 and approximately equal to (Fig. 6.18) allows the change in the mean displacement of the supported mass (Fig. 6.17 note E, Fig. 6.18 note F) and mass-plenum system resonance (Fig. 6.18) to be illustrated. The power spectrum plots in Figs. 6.17 and 6.18 enable comparison with power spectrum plots later in this section that illustrate unanticipated large magnitude heave deck oscillations.

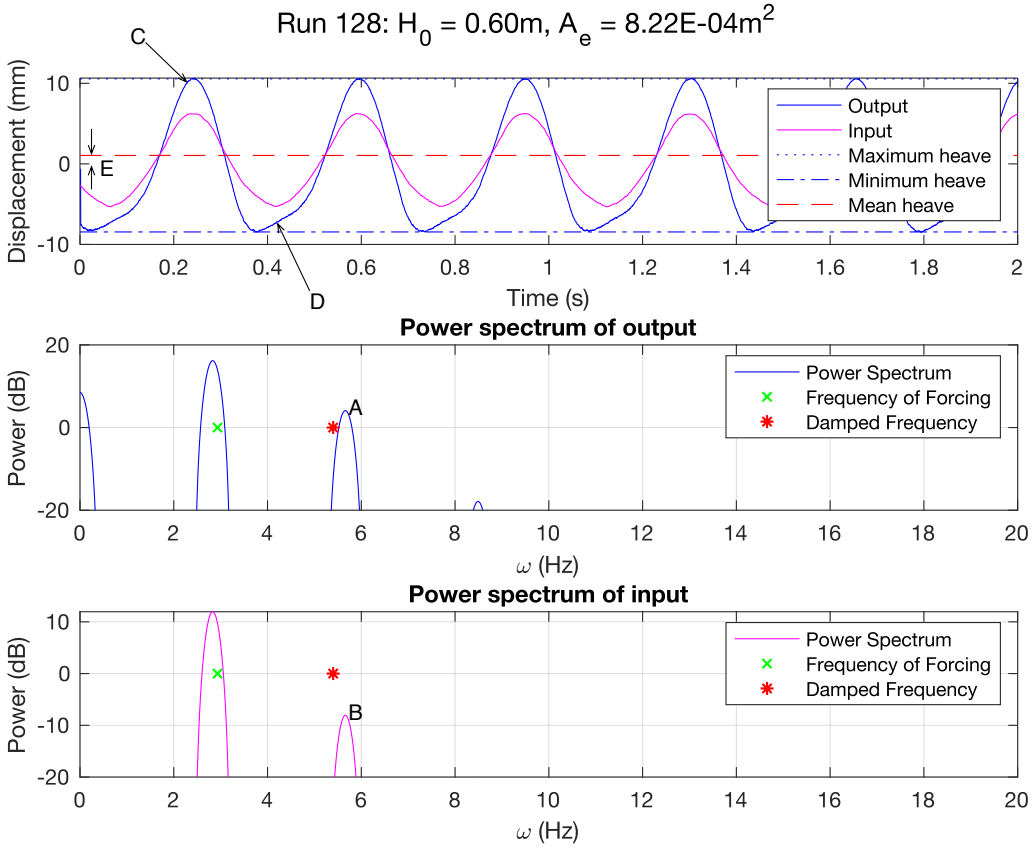


Figure 6.17. Power spectrum analysis of main experiment run 128. This Run illustrates the onset of the increase in mean supported mass displacement.

Referring to Fig. 6.17. For the experimental run 128, the forcing frequency (ω_f) is approximately 3Hz, with another peak in the power spectrum of the output observable at approximately 5.5 Hz (A), corresponding to a peak in the power spectrum of the flapper

(B). This is consistent with either a secondary motion of the flapper mechanism (evidence of which was observed in Fig. 6.16, point J) or the onset of resonance, where the supported mass starts being excited at its damped frequency (ω_d) when ω_f is a rational fraction of ω_d. Examination of the supported mass time-series at the maxima (C) and the minima (D) shows that the path of the supported mass is not symmetric, with a significant flat portion of the path apparent near (D). The timing of the supported mass motion also shows significant asymmetry, with the maxima slightly lagging the maxima of the flapper path, but the minima significantly leading the minima of the flapper path. The change in the mean displacement of the supported mass is also observable (E).

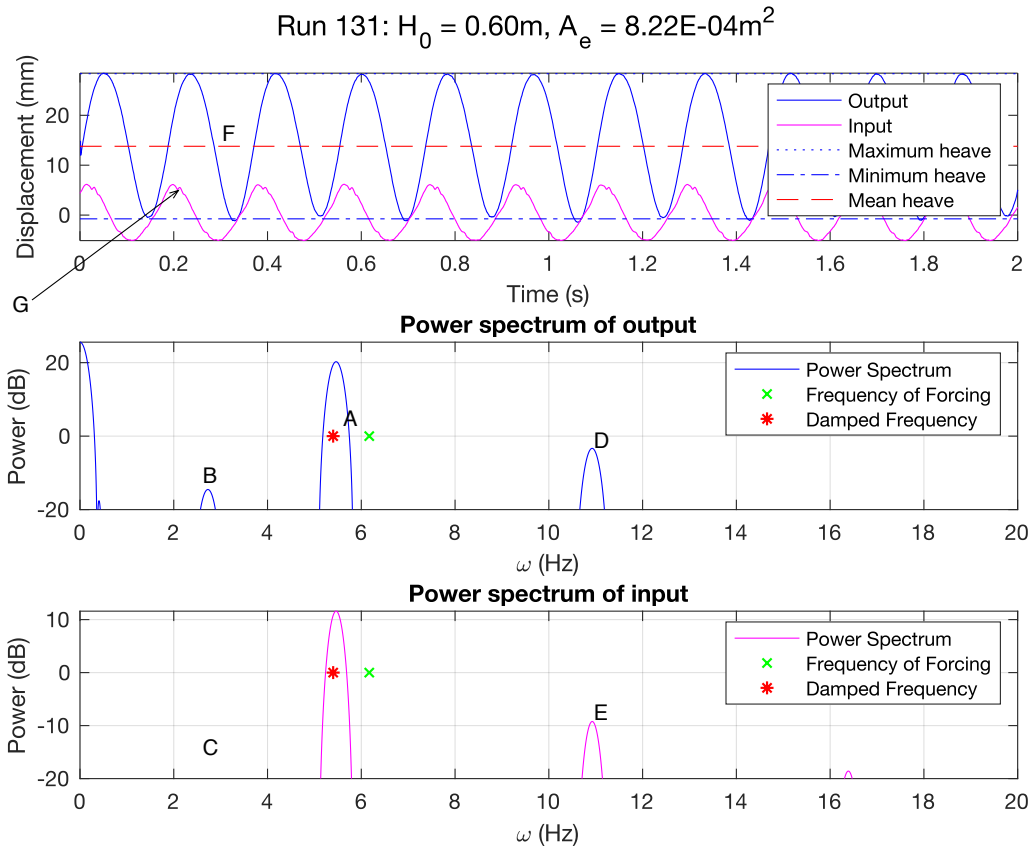


Figure 6.18. Power spectrum analysis of main experiment run 131. The flapper and supported mass time-series, with power spectrum analysis of each time-series, for a case of forcing near the damped frequency.

Referring to Fig. 6.18. For the experimental run 131, the mass-plenum system volume is forced at a frequency near the damped frequency of the system (A). The supported mass motions are large compared to the forcing of the plenum volume, corresponding to resonant behaviour. The motion of the supported mass has a component at a frequency approximately half the forcing frequency (B), which does not correspond to any frequencies detected in the forcing mechanism motions (C), and which is consistent with tones of the damped frequency being excited. Examination of the supported mass time-series shows

that the minima vary from the overall mean of the minima, alternating between higher and lower, which corresponds to a frequency of half the motion frequency. There is a higher frequency component to the supported mass motion (D), which corresponds to a frequency found in the analysis of the forcing mechanism motion (E), which is approximately double the forcing frequency. A similar phenomenon was observed at other forcing frequencies (Figs. 6.16 and 6.17) and is consistent with small motions in the bearings of the forcing mechanism links. The mean of the supported mass motion has increased significantly (F). The time-series of the flapper displacement reveals small deviations from the general path taken by the flapper (G), corresponding to the higher frequencies of motion found in the power spectrum analysis of the time-series. The flapper is potentially responding to the supported mass motion and the subsequent plenum pressure changes. The deviations at point G are consistent with the flapper being forced down by its own crank mechanism, as well as being 'sucked' upwards by the still rising supported mass. If the flapper is not perfectly stiff, then relative motion is possible between the location where the crank mechanism is joined to the flapper and the location that the laser sensor detects the flapper motion.

Examining the power spectrum plots as ω_f approaches $2\omega_d$ reveals mass-plenum system behaviour that was not predicted by the Simulink model, as first discussed in Sec. 6.5.4, identifying larger than predicted oscillations at high values of ω_f. The behaviour is first apparent as alternating large and small magnitude cycles of the supported mass, as ω_f approaches $2\omega_d$, shown in Fig. 6.19, for which A_e is set at approximately the middle of the available range, and shown again in Fig. 6.20 when A_e is set at the maximum of the available range, and again in Fig. 6.21 when A_e is set at the minimum of the available range.

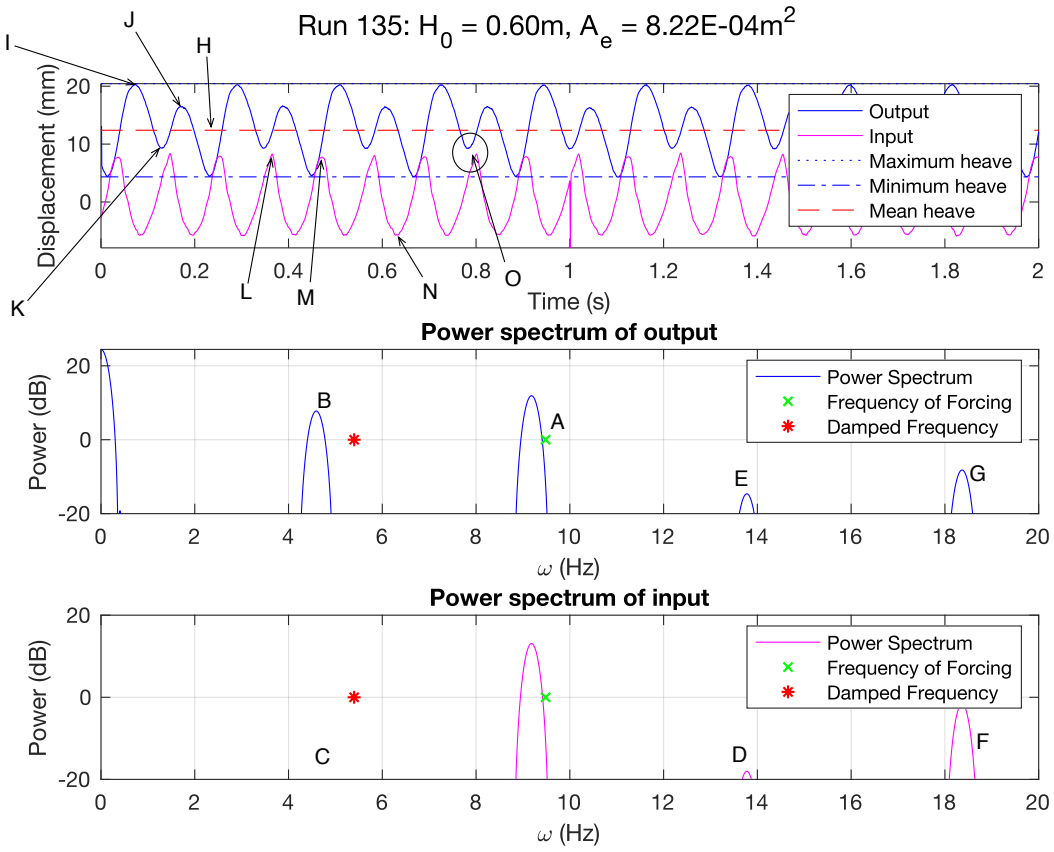


Figure 6.19. Power spectrum analysis of main experiment run 135. The input flapper and supported mass time-series, with a power spectrum analysis of each time-series, for a case of forcing at nearly double the damped frequency (ω_d).

Referring to Fig. 6.19. For experimental run 135, the plenum height (H_0) and the air exit area (A_e) are set to the middle value of the available range. The supported mass has a significantly large motion at the forcing frequency (ω_f), shown by the power spectrum analysis (A). A second motion with a frequency approximately half ω_f and smaller than ω_d is apparent (B), which has been excited independent of any significant motions of the input flapper at that frequency, shown by an absence of power at that frequency in the power spectrum analysis of the flapper motion (C). The flapper had motion at approximately 13.5 Hz (D), which is approximately $1.5\omega_f$ and corresponds to a motion of the supported mass at the same frequency (E), and this may be a response of the flapper to the supported mass motion, rather than vice versa. A more significant motion in the flapper occurs at approximately $2\omega_f$ (F), which is consistent with previous results, and corresponds to the motion of the supported mass at that frequency (G). The mean of the supported mass displacement is significantly elevated (H), so much so that the 'Minimum Heave' line now lies completely above the hover position (0 on the displacement axis). There is significant variation in the maxima and minima of the supported mass path (Output line on Displacement plot). Only the extreme maxima (e.g. point I) have been used to calculate the 'Maximum Heave' line, similar for the minima, the magnitude and the mean are

calculated from the Maximum Heave and Minimum Heave lines. Lower maxima (e.g. point J) and higher minima (e.g. point K) occur on every second cycle, this behaviour was not anticipated during the development of the research questions, cannot be mathematically modelled using linear expressions and was not predicted by the Simulink model. This behaviour is also apparent in Figs. 6.20 and 6.21 and becomes more pronounced in Figs. 6.22 and 6.23. The phase between the flapper and supported mass (O) is such that the flapper peaks before the supported mass can reach the Minimum Heave displacement, forcing the supported mass to travel upwards again. The flapper path ('Input') also shows cyclical variations, sharp peaked maxima (L) alternate with smooth peak maxima (M) and the flapper minima are a flat peak. The displacement of the flapper is not measured at the crank mechanism link to the flapper, but at a point closer to the pivot point and off the crank line of action, slight flexibility in the flapper allows for small motions at the point of measurement that are not necessarily at the link between the flapper and the crank mechanism.

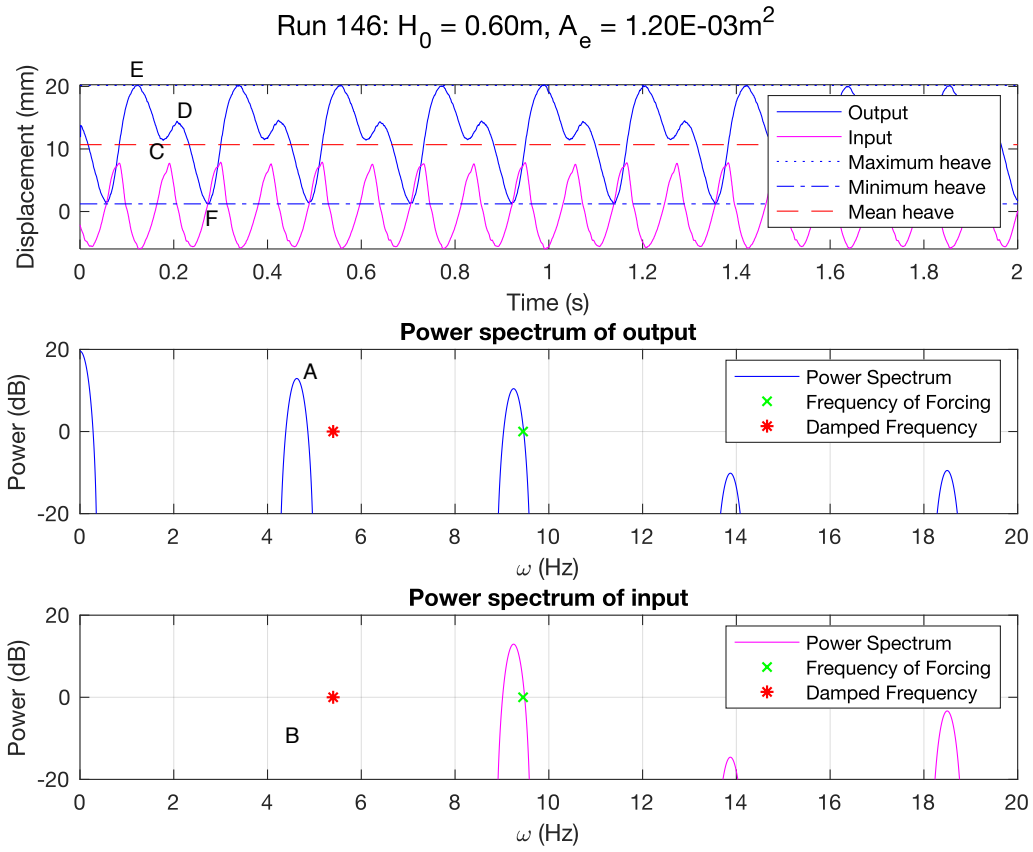


Figure 6.20. Power spectrum analysis of main experiment run 146. The flapper and supported mass time-series, with power spectrum analysis of each time-series, for a case of forcing at nearly double the damped frequency (ω_d).

Referring to Fig. 6.20. For experimental run 146, the plenum height (H_0) is set to the middle value of the available values, the air exit area (A_e) is set to largest area in the available values. Similar to Fig. 6.19, the supported mass has a motion at a frequency approximately half the forcing frequency (ω_f), seen at (A). The flapper has no significant motion at that frequency (B). Similar to Fig. 6.19, the supported mass path has small magnitude cycles (C) alternating with larger magnitude cycles (F). The minima of the smaller magnitude cycles are all greater than the mean of the supported mass motion (C), with the mean being calculated as half way between the larger magnitude maxima (E) and minima (F). The alternating cycles are asymmetric and the supported mass is displaced above the mean for longer periods of time than it is displaced below the mean.

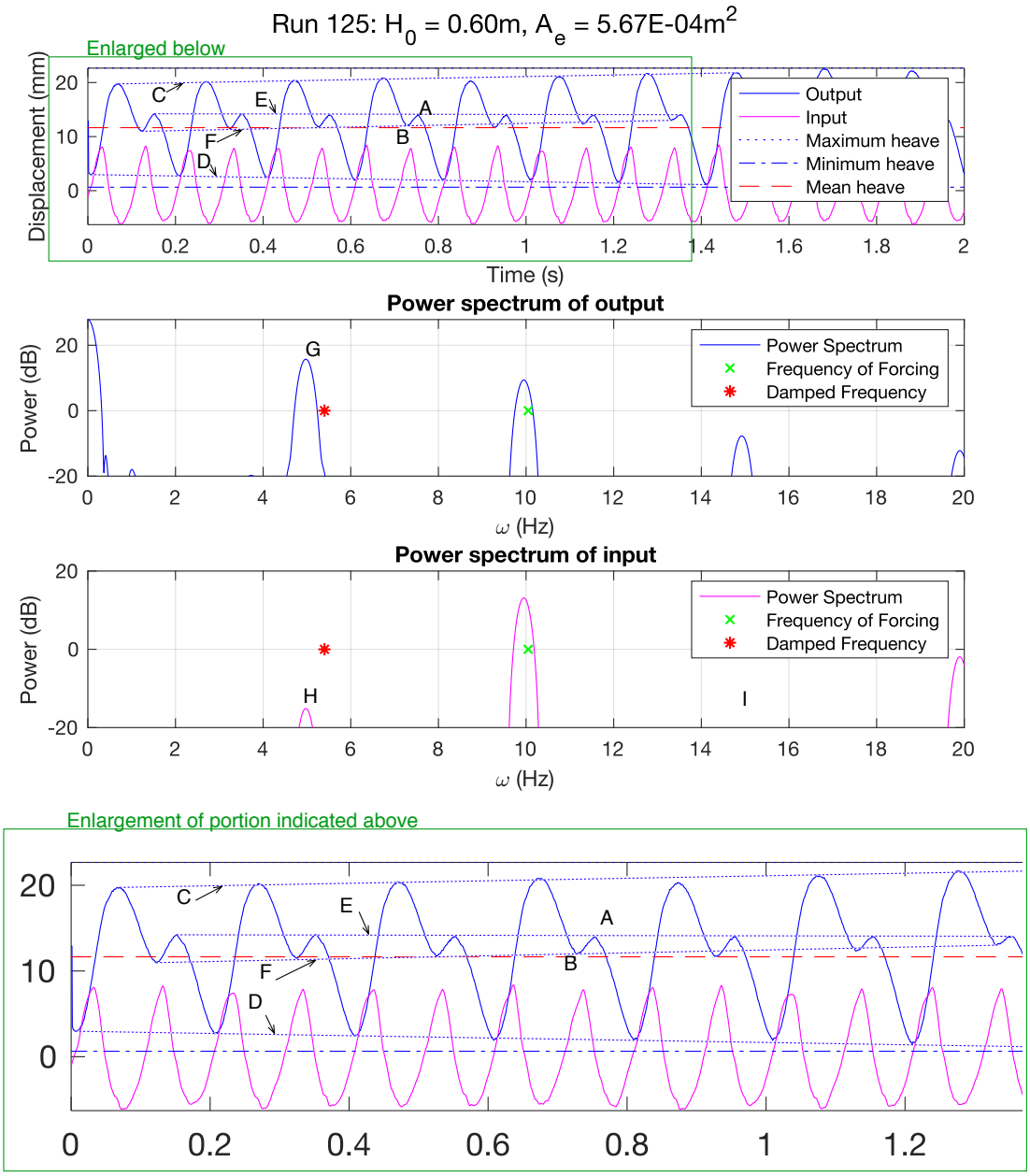


Figure 6.21. Power spectrum analysis of main experiment run 125. The input flapper and supported mass time-series, with power spectrum analysis of each time-series, for a case of forcing at nearly double the damped frequency (ω_d).

Referring to Fig. 6.21. For experimental run 125, the plenum height (H_0) is set to the middle value of the available values, the air exit area (A_e) is set to smallest area of the available values. The forcing frequency (ω_f) is slightly higher than for Figs. 6.19 and 6.20, facilitating the observation of a new transitional behaviour. An enlargement of a portion the time-series plots has been added to the power spectrum plot. Similar to Fig. 6.19, the supported mass has a motion at a frequency approximately half ω_f. Similar to Figs. 6.19

and 6.20, small magnitude cycles (e.g. the local maxima at A and the local minima at B) alternate with larger magnitude cycles. This plot is of a two-second typical data sample, with data being recorded a significant time after the experimental rig was set running at this ω_f, allowing initial transients to decay. A new transient is observable, the maxima of the large magnitude cycles are increasing (trend line C) and the minima of the large cycles are also deceasing (trend line D). Therefore, the overall magnitude of the cycles is increasing. The 'Maximum heave', 'Minimum heave' and 'Mean heave' are all calculated for the full fifteen seconds of recorded data. The maxima of the small magnitude cycles are approximately steady (trend line E), but the minima of the small magnitude cycles are increasing in overall displacement (trend line F), making the small magnitude cycles decay in magnitude with time. The power of the lower frequency cycles (G) has increased, compared to Figs. 6.19 and 6.20. For the first time, an effect on the flapper motion is apparent, with motion at a frequency approximately $1/2\omega_f$ found in the power spectrum analysis (H). The flapper motions at $1.5\omega_f$, seen in Figs. 6.19 and 6.20, are no longer seen in the power spectrum (I).

Examining the power spectrum plots for $\omega_f \approx 2\omega_d$ reveals a significant escalation of the unexpected mass-plenum system behaviour shown in Figs. 6.19 to 6.21 and first discussed in Sec. 6.5.4. In Sec. 6.5.4 several experimental results at high ω_f were highlighted as being much larger than predicted by the numerical model, and also much larger than the local trend (for example, Fig. 6.11 note K, Fig. 6.12 notes A and B, Fig. 6.13 note B). The observed behaviour is large magnitude cycles of the supported mass at a frequency half of ω_f. This behaviour is illustrated in Fig. 6.22 when A_e is set at the middle value of the available values and shown again in Fig. 6.23 when A_e is set at the maximum value of the available values.

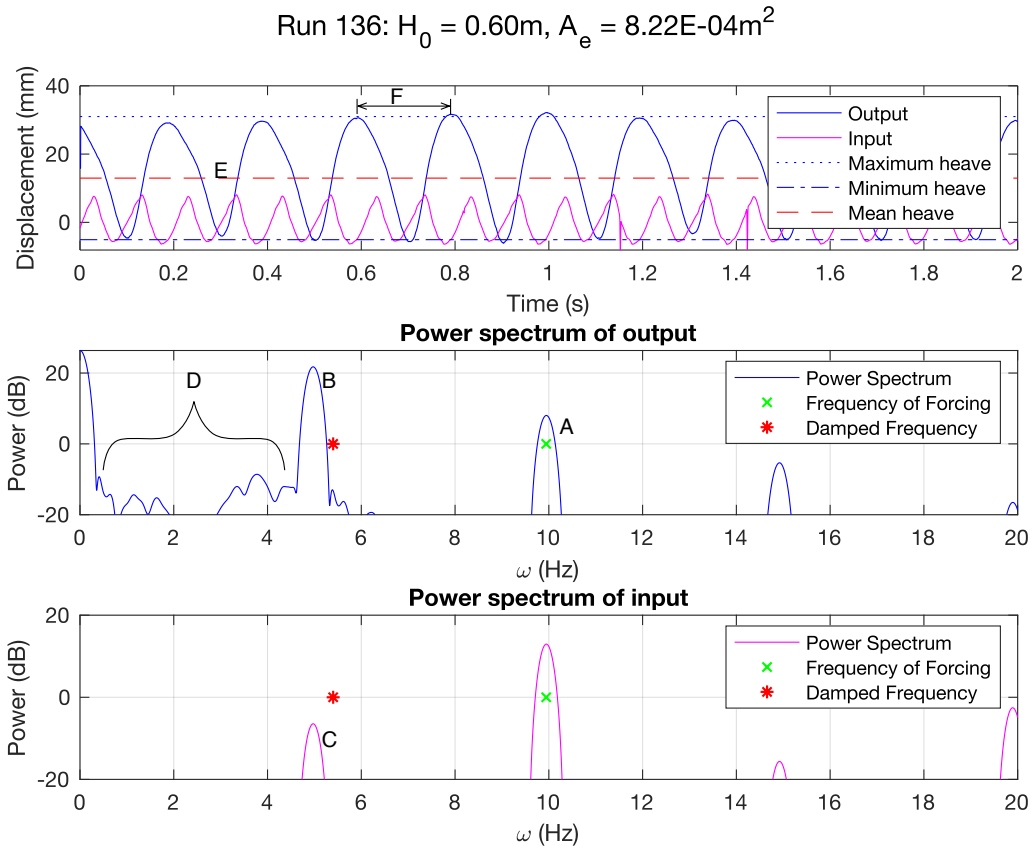


Figure 6.22. Power spectrum analysis of main experiment run 136. The input flapper and supported mass time-series, with power spectrum analysis of each time-series, for a case of forcing at approximately double the damped frequency (ω_d).

Referring to Fig. 6.22. For experimental run 136, the plenum height (H_0) and air exit area (A_e) are each set to the middle value of the available values. The forcing frequency (ω_f) is slightly higher than for Figs. 6.19 to 6.21, facilitating the observation of a new steady-state behaviour. This is the experimental result in Fig. 6.11 note K. The period of the supported mass motions (F) is approximately double the period of the flapper motions (ω_f), allowing the input to directly excite ω_d. The supported mass has significant motions at ω_f (A), but the motions at $\omega \approx \omega_f/2$ are larger, as shown by the larger power at $\omega \approx \omega_f/2$ on the power spectrum analysis (B). There are substantial motions of the flapper at $\omega \approx \omega_f/2$ (C), but it is highly likely that these are a secondary motion of the flapper at the point of measurement, in response to the motions of the supported mass. There are supported mass motions at several other frequencies at low range (D). The mean of the supported mass motions is elevated (E), maintaining a similar mean position to figures Figs. 6.19 to 6.21. The phenomena where the large magnitude oscillations grow and the small magnitude oscillations decay (Fig. 6.21), appears to reach a stage where the supported mass path presents as an oscillation with $\omega \approx \omega_f/2$ (F). The power spectrum analysis indicates the motions at other frequencies are still significant (A, D).

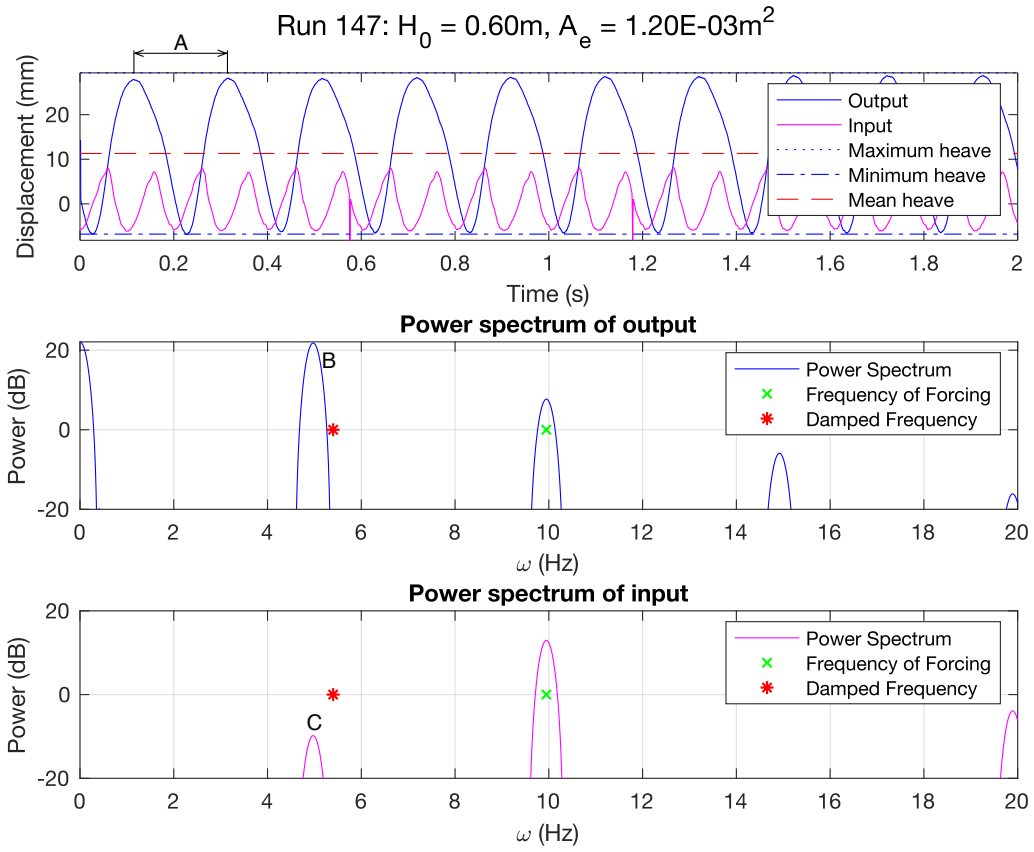


Figure 6.23. Power spectrum analysis of main experiment run 147. The input flapper and supported mass time-series, with power spectrum analysis of each time-series, for a case of forcing at approximately double the damped frequency (ω_d).

Referring to Fig. 6.23. For the experimental run 147, the plenum height (H_0) is set to the middle value of the available values, the air exit area (A_e) is set to largest area in the available range. This is the experimental result in Fig. 6.12 note A. As with Fig. 6.22, the period of the supported mass motions (A) appears to be approximately double the period of the flapper motions. This increased period corresponds to the frequency of the largest motions of the supported mass being $\omega \approx {}^{\omega_f}/_2$ (B). There are other significant frequencies present in the supported mass motions, at ω_f, $\omega \approx 1.5\omega_f$ and $\omega \approx 2\omega_f$. The flapper has a motion at $\omega \approx {}^{\omega_f}/_2$, which may be in response to the motions of the supported mass, which is not observed at other values of ω_f and may be an extra degree-of-freedom of the mass-plenum system, rather than a forcing mechanism of the supported mass motions at $\omega \approx {}^{\omega_f}/_2$.

The phenomenon underlying the large oscillations of the supported mass that was not predicted by the Simulink model and marked in Fig. 6.11 note K, Fig. 6.12 notes A and B, and Fig. 6.13 note B, appear to be the excitation of the natural mode of vibration of the mass-plenum system when $\omega_f \approx 2\omega_d$ (Figs. 6.22 and 6.23). The excitation of the dominant mode of vibration can be seen to be developing in Fig. 6.21. The excited natural mode

of vibration of the mass-plenum system is so pronounced that the path of the supported mass appears to be a single frequency periodic wave of ω_d, however, motions at ω_f are detected using the power spectrum analysis (Fig. 6.22 note A).

At low frequencies of excitation, the path of the supported mass is not symmetric about its mean (Fig. 6.17). The asymmetry of the supported mass path becomes more pronounced as the dominant mode of vibration becomes excited as ω_f approaches $2\omega_d$ (Figs. 6.19 to 6.21).

The motion of the flapper consists of a dominant oscillation at ω_f and also a secondary oscillation at $\omega \approx 2\omega_f$ (e.g. Fig. 6.16 note G, Fig. 6.19 note F). Secondary oscillations are likely due to motions within the joints of the crank mechanism that drives the flapper (Fig. 5.11). The supported mass responds to the secondary frequency of the driven flapper. The flapper was made from a very stiff and light Nida-core honeycomb panel. The crank mechanisms was a repurposed crank mechanism from a small internal combustion engine. As such, it is reasonable to assert that the flapper mechanism was designed and made to minimise secondary motions.

The flapper develops a secondary oscillation at $\omega \approx {}^{\omega_f}/_2$ when $\omega_f \approx 2\omega_d$ (Fig. 6.22 note C and Fig. 6.23 note C). The secondary oscillation is not present at any other value of ω_f, not even at nearby frequencies (Fig. 6.19 note C, Fig. 6.20 note B). This secondary oscillation of the flapper corresponds to the very large oscillation of the supported mass at the same frequency. The secondary oscillation is consistent with the flapper developing a new motion under the influence of the high pressure fluctuations in the plenum volume — the supported mass is moving at twice the period as the flapper, with the supported mass moving down and reducing the plenum volume at the same time as the flapper is driven up, also reducing the plenum volume, resulting in higher plenum air pressure. As this secondary oscillation of the flapper only appears at very high plenum air pressures, it is assumed to be a symptom of the flapper flexing under the combined effect of the high plenum air pressure, and the driving crank mechanism. The secondary motion of the flapper may be acting to create an additional degree-of-freedom of the mass-plenum system, and it may be contributing to the very large supported mass oscillations. Further investigation of the causes of the secondary motion of the flapper lies outside the scope of this thesis.

The numerical model does not predict large magnitude oscillations of the supported mass near $\omega_f \approx 2\omega_d$. It is plausible that the superposition of the supported mass excited oscillations with the flapper secondary motion is resulting in a large supported mass motion. The numerical model assumes a perfectly stiff flapper, so it cannot predict any flapper flexion effects on the system. The flapper flexion phenomenon was only observed at the extreme plenum air pressures, the flapper flexion is ignored for most of the frequency range being investigated. Investigating the reason why the numerical model does not predict this phenomenon is outside the scope of this thesis as it is not directly relevant to the current research aims. The experimental results are in good agreement with the predictions made by the numerical model, over the range $1 \leq \omega_f \leq 1.5\omega_d$.

6.6. Concluding remarks

Two experimental rig parameters were found experimentally, before the experimental rig was commissioned: the supporting spring stiffness and the heave deck rotational inertia (Sec. 6.2).

Three experimental rig parameters were found experimentally during the commissioning test: the mass-plenum damped frequency (ω_d), the supported mass settling time (T_s) and the supported mass falling time (T_f). These three parameters were found from the experimental data, in part by decomposing the path of the supported mass through fitting an exponential function to the data, then subtracting the exponential function from the experimental data to remove the underlying trend (Sec. 6.3). The commissioning test used a plenum volume forcing mechanism that effected a step-change of the plenum volume.

Four further experimental rig parameters were found from the experimental data, by including parameters in the Simulink model and then fitting the curves from the Simulink model to the experimental data. The four parameters found this way were: the Coulomb friction factor (C_c) representing the dry friction acting on the heave deck, the parasitic air leakage area (A_L), a plenum stiffness factor (k_p) and a velocity dependent heave deck resistance factor (C_v). The plenum stiffness factor was a lumped parameter representing the sources of plenum boundary flexibility such as plenum wall flexing and heave deck rolling seal elastic expansion. The method used and the results were discussed in Sec. 6.4.

The experimental rig was reconfigured so that the plenum volume could be forcibly oscillated across a range of frequencies (Secs. 6.5.1 and 6.5.2). The measurements taken during experimental runs gave a time-series for the supported mass displacement and the displacement of the plenum volume forcing mechanism (flapper). The experimental measurements were analysed to give the magnitude of the supported mass oscillations (O_V), the mean of the supported mass oscillations (S_V), and the phase angle (ϕ) between the supported mass motions and the plenum volume forcing mechanism motions (Sec. 6.5.4).

The first oscillating plenum volume experiment was conducted at the middle of the available range of plenum heights and air exit areas (Sec. 6.5.4.1). The experimental results showed that the supported mass increases its mean displacement as the frequency of plenum volume forcing is increased, this was in agreement with the predictions from the Simulink model. This result was consistent with observations first made during the qualitative preliminary experiment (Sec. 5.2). This result is a novel contribution to the field of air cushion dynamics, as no experimental observations of this phenomenon were found in the available literature. At the damped frequency of the mass-plenum system, the magnitude of the supported mass oscillations are amplified compared to the magnitude of the plenum volume forcing mechanism motions—a characteristic of resonant behaviour. The mass-plenum system magnitude and phase angle frequency response is similar to that of a single-degree-of-freedom damped system, including attenuation of the response above the damped frequency and a change of phase angle to $-\pi$ in the region of the damped frequency. In the available literature, this behaviour has not been experimentally confirmed for a mass-plenum system with a fixed air exit area. As such, this experimental result is a novel contribution.

The oscillating plenum volume experiment was repeated with varying air exit area (Sec. 6.5.4.2). The mass-plenum system was sensitive to changes in the air exit area and continued to behave as predicted by the Simulink model. The mass-plenum system observed behaviour continued to be consistent with the results of the first experiment,

different ideasconfirming that the behaviour observed in the first experiment (Sec. 6.5.4.1) was characteristic of the mass-plenum system behaviour.

The oscillating plenum volume experiment was repeated with varying plenum height (Sec. 6.5.4.3). The mass-plenum system was sensitive to changes in the plenum height, most significantly the damped frequency changed. The experimental results were consistent with the predictions made using the Simulink model.

At very high forcing frequency, approaching $\omega_f = 2\omega_d$, the magnitude of the supported mass oscillations are much larger than predicted by the numerical model and much larger than the local trend in the experimental results. This was investigated further by examining, in detail, the supported mass and flapper time-series (Sec. 6.5.5). It was found that large motions of the supported mass at ω_d occur and are sufficiently dominant that the supported mass motions appear as an oscillation at ω_d. The flapper was found to have an additional motion at ω_d, which only occurs near $\omega_f = 2\omega_d$, which is consistent with the flapper responding to the plenum pressures, rather than the motion being associated with the oscillating input motion. The unpredicted high supported mass oscillations may be an effect of the combined motions of the flapper and supported mass. As the numerical model does not predict this large oscillation near $\omega_f = 2\omega_d$, the numerical model is only considered applicable over the range $1 \leq \omega_f < 1.5\omega_d$.

The experimental results are in good agreement with the numerical model predictions, over the applicable frequency range of the numerical model. The results support the research hypotheses, and this will be discussed in detail in Chapter 7.

7. Conclusions and recommendations

7.1. Introduction

This thesis investigated issues associated with fast ship-based freight carriage opportunities in South East Asian open waters. Formal design tools were used to complete a systematic review. The review found that an SES vessel had the potential to facilitate this opportunity. The practicalities of the SES platform were investigated. There were gaps in the SES platform performance capabilities that were investigated, again making use of formal design tools to support a systematic approach. This review lead to the author identifying several salient questions that were worthy of an original research program.

The author, again made use of formal design principles, to design, develop, assess, and test, using limited resources and budget, all the experimental apparatuses used in this research, in particular the main experimental rig. This approach facilitated the creation of a working experimental rig on the first (prototyped) iteration. The experimental rig required minimal changes after the commissioning phase. The experimental rig functioned as expected on the first run, both in its forced step change of the plenum volume configuration, and the forced oscillation of the plenum volume configuration.

The mathematical model of the experimental rig's mass-plenum system had several non-linear aspects that could not be neglected, linearised or simplified. This complex and complicated mathematical model was solved by developing a Simulink model in the MATLAB computational environment. The author made use of computer software development principles to successfully develop computational scripts totalling in excess of 2,900 lines of code in the MATLAB development environment. A substantial Simulink model was developed, with each stage of the software and Simulink development process done with code testing and validation to give successful computational outcomes in support of the research. Development of the Simulink model involved integrating of each block of the model one at a time and assessing the output of the Simulink model. The smooth and accurate functioning of the computational scripts and Simulink model enabled repeated detailed analysis of the experimental results and comparison with quantified predictions of the experimental rig.

In the remaining sections of this chapter:

Section 7.2 The five research questions reported in Sec. 5.3 are addressed.
Section 7.3 The novel contributions of this research are stated.
Section 7.4 The applicable range of the Simulink model is stated.
Section 7.5 Practical applications of the research work are discussed.
Section 7.6 Topics that may provide the basis for further work are discussed.
Section 7.7 Final conclusions are stated.

7.2. Research questions and hypotheses

All of the hypotheses postulated in Sec. 5.3 were affirmed by the experimental program reported in this thesis.

Question QA: Does the time-wise mean displacement of the supported mass increase when a mass-plenum system experiences oscillations to its plenum volume?

Hypothesis HA-1: The combination of the air density rate of change and the plenum volume rate of change leads to changes of the mean operating point of the supported mass.

Hypothesis HA-1 was affirmed by the experimental results (Sec. 6.5.4) being in agreement with the predictions made by the Simulink model. The Simulink model modelled the effects of both the air density rate of change and the plenum volume rate of change.

Question QB: Can resonance be induced in a mass-plenum system?

Hypotheses HB-1: Air compressibility acts as a spring, giving the mass-plenum system a natural frequency.

Hypothesis HB-2: A secondary pressure-induced plenum volume change behaves as an additional spring acting in series, modifying the mass-plenum system's natural frequency.

Hypothesis HB-1 was affirmed by measurements taken during the commissioning test (Sec. 6.3.1) and the experimental results (Sec. 6.5.4). Hypothesis HB-2 was affirmed by incorporating a plenum chamber stiffness factor which lowered the natural frequency, reported in Sec. 6.4.3.

Question QC: Does the magnitude of the plenum volume have a significant effect on the natural frequency of a mass-plenum system?

Hypothesis HC-1: Under the same load, large plenum volumes compress further than small plenum volumes, and therefore are less 'stiff'.

Hypothesis HC-2: Large plenum volumes are more likely to have elastic pressure-volume dynamics because their confining structures are less 'stiff'.

Hypothesis HC-1 was affirmed by the experimental results reported in Sec. 6.5.4.3. Hypothesis HC-2 was affirmed by accommodating the plenum stiffness reported in Sec. 6.4.3.

Question QD: Does the air exit area have a significant effect on the damping of a mass-plenum system?

Hypothesis HD-1: The air flow through an exit area comprising a set of regular round holes acts as quasi-steady flow through a single round orifice of the same combined area.

Hypothesis HD-2: A greater variation in air flow exiting the plenum arising from a larger exit area will reduce the amount of air compression, damping the oscillations.

Hypothesis HD-3: The air exit area does not have a significant effect on the rate that the supported mass returns to equilibrium after a plenum volume disturbance.

Hypothesis HD-1 was affirmed by results reported in Sec. 6.5.4. Hypothesis HD-2 was affirmed by experimental results reported in Sec. 6.5.4.2. Hypothesis HD-3 was affirmed by experimental results reported in Sec. 6.3.3.

Question QE: How sensitive is a mass-plenum system to elastic changes in plenum volume?

Hypothesis HE-1: The elastic pressure-induced changes to plenum volume can be modelled as displacement of a massless plenum wall, opposed by a linear spring.

Hypothesis HE-2: Small changes in the plenum volume due to pressure will have a significant effect on the damped frequency

Hypothesis HE-1 was affirmed by experimental results reported in Secs. 6.3.1 and 6.4.3. Hypothesis HE-2 was affirmed by experimental results reported in Secs. 6.3.1, 6.4.3 and 6.5.4.

7.3. Novel contributions

The research reported in this thesis makes several novel contributions. The research programme:

1. Investigated the change in the supported mass time-wise mean displacement when the plenum volume is forced to oscillate.
2. Developed a unique experimental rig that isolated the effects of air compressibility by:
   a) removing a water surface from the system
   b) holding the air exit area constant
   c) being sufficiently large for the air compression effects to be observable
3. Investigated the coupled parameters of the air cushion systems neglected in Kaplan et al. (1981).
4. Investigated the significance of the non-linear terms that were linearised in Kaplan et al. (1981).
5. Explored a systematic and rational investigation of the practical uses of advanced marine vehicles to Southeast Asia, using methods that enable an informed selection of research questions.

7.4. Applicable range of the experimental findings

The numerical model was confirmed over the range $1 \leq \omega_f \leq 1.5\omega_d$, the nominated applicable range of the numerical model used in this thesis. No experiments were conducted with forcing frequencies below 1 Hz. Experimental results higher than this range differed from the predictions made by the numerical model (Sec. 6.5.5), which is most likely due to the experimental rig not functioning according the theory in the numerical model at very high oscillating plenum volume energies. The numerical model is consistent with the experimental results within the stated range of operation. Because the experimental data became more scattered at higher frequencies, caution should be used when considering an extrapolation from the Simulink model introduced in this thesis.

For the purposes of this experiment, the air supply system could be assumed to provide steady and constant air mass flow rate into the plenum. Caution should be used when making the same assumption for larger practical air supply systems.

7.5. Practical applications of this research

The experimental confirmation of the predicted increase of supported mass displacement when the plenum volume is oscillated at higher frequencies has practical implications. A practical SES will encounter water waves that must be assumed to contain motions over a wide range of frequencies (though many will be at insignificant power). It is therefore possible that a practical SES will encounter plenum volume forcing that could induce an increase in the supported mass displacement, practically observed as an increase in the dynamic hover height of the SES. This may, in turn, impact the sealing of the air cushion, both at the flexible seals at bow and stern, and with the rigid side hulls. The flexible seals may be lifted clear of the water, leading to sudden increases in air exit area—with unknown but likely deleterious impact on the SES heave and pitch dynamics. It is also plausible that the side-hulls may lift relative to the water surface enough to expose water inlets for the propulsion system, resulting in the sudden ingestion of air.. This may adversely impact upon the performance and may damage the water-jet mechanisms.

The research reported in this thesis has found that a non-linear mathematical model of the SES accommodates the phenomenon of a change of mean supported mass displacement when the plenum volume is forcibly oscillated at higher frequencies (Sec. 7.2), analogous to water waves passing through a SES air cushion at high speeds (Sec. 5.4.3). Furthermore, the research reported in this thesis has found that the damped frequency of a mass-plenum system is sensitive to flexibility of the plenum boundaries (Sec. 7.2), analogous to the flexibility of the water surface and cushions seals forming the boundaries of a SES air cushion (Sec. 5.4.2). The findings of the research reported in this thesis creates the opportunity for design work on an innovative SES automatic regulating system system that accommodates the mean increase in SES hover height and the effects of air cushion boundary flexibility.

7.6. Further work

From the research reported in this thesis, several new research questions arise, specifically associated with the effects on the mass-plenum dynamics of:

1. a flexible water surface (responsive the plenum pressure) bounding the plenum
2. flexible seals (responsive to the plenum pressure)
3. air supply mass flow rate (responsive to plenum air pressure)
4. varying air exit area (as a forced parameter)
5. varying air exit area (responsive to the plenum pressure)

It would be of practical interest to investigate how the mean hover height of a practical SES operating in open water varies in real conditions, in particular, investigating the effect of mean hover height on air ingestion into the water-jets of practical SESs.

It would be of interest to further investigate the SES dynamics at forcing frequencies near the mass-plenum system damped frequency, and at, or near double the damped

frequency, especially if a study could either eliminate or theoretically accommodate all secondary flexibility effects.

7.7. Concluding remarks

This thesis has successfully explored the dynamics of a mass-plenum system, using a novel experimental rig and a validated numerical model to investigate the increase in mean displacement of the supported mass when the plenum volume is oscillated at a range of frequencies.

Because the research reported in this thesis has identified physical parameters that contribute to disadvantageous ride dynamics of the SES concept when used for freight transport in South East Asian seas (Chapter 3), it is anticipated that, following further refinement, useful design tools have the potential to be developed for this promising type of commercial ship.

Bibliography

AJTP Information Centre. (2012). *Water transport 2012* (AJTP Information Centre, Ed.). Asean Japan Transportation Partnership. Retrieved September 5, 2015, from http://www.ajtpweb.org/statistics/compareasean/Water_Transport/Water_Transport_2012

ASEAN. (2013). *Selected key indicators* (ASEAN Statistics, Ed.). ASEAN. www.asean.org/images/2015/January/selected_key_indicators/

ASEAN. (2015, September 9). *Asean member states* (ASEAN, Ed.). ASEAN. Retrieved July 27, 2015, from www.asean.org/asean/asean-member-states

Auestad, O., Gravdahl, J., Sorensen, A., & Espeland, T. (2014, August 24). Motion compensation system for a free floating surface effect ship (E. Boje & X. Xia, Eds.). In E. Boje & X. Xia (Eds.), *Proceedings of the 19th ifac world congress, 2014*. Proceedings of the 19th IFAC World Congress, 2014, Cape Town, South Africa, International Federation of Automatic Control. International Federation of Automatic Control. Cape Town International Convention Centre. https://doi.org/10.3182/20140824-6-ZA-1003.01019

Australasia. (2014). *Australasia* (J. Everett-Heath, Ed.). Oxford University Press. Retrieved September 9, 2015, from www.oxfordreference.com.ezp.lib.unimelb.edu.au/view/10.1093/acref/9780191751394.001.0001/acref-9780191751394-e-484

Bertin, D., Bittanti, S., & Savaresi, S. M. (2000). Decoupled cushion control in ride control systems for air cushion catamarans. *Control Engineering Practice*, 191–203.

Bles, W., Bos, J. E., de Graaf, B., Groen, E., & Wertheim, A. H. (1998). Motion sickness: Only one provocative conflict? *Brain Research Bulletin*, *47*(5), 481–487.

Boccotti, P. (2000). *Wave mechanics for ocean engineering* [Knovel Release Date: Feb 7, 2008]. Elsevier.

Bos, J. E., Damala, D., Lewis, C., Ganguly, A., & Turan, O. (2007). Susceptibility to seasickness. *Ergonomics*, *50*(6), 890–901.

Bowersox, D. J., Closs, D. J., & Cooper, M. B. (2007). *Supply chain logistics management* (2nd ed.). Boston, Mass. : McGraw-Hill/Irwin.

Butler, E. A. (1985). The surface effect ship [ISI Document Delivery No.: ADS88 Times Cited: 2 Cited Reference Count: 109 AMER SOC NAVAL ENG INC]. In *Modern ships & craft* (pp. 200–258). ISI Document Delivery No.: ADS88 Times Cited: 2 Cited Reference Count: 109 AMER SOC NAVAL ENG INC. Naval Engineers Journal. %3CGo%20to%20ISI%3E://A1985ADS8800013

Central Intelligence Agency. (2009a). *Southeast asia* (Central Intelligence Agency, Ed.). Central Intelligence Agency. https://www.cia.gov/library/publications/the-world-factbook/maps/refmap_southeast_asia.html

Central Intelligence Agency. (2009b). The world factbook 2009 (Central Intelligence Agency, Ed.). Central Intelligence Agency. https://www.cia.gov/library/publications/the-world-factbook/index.html

Christopher, M. (2000). The agile supply chain: Competing in volatile markets. *Industrial Marketing Management*, *29*(1), 37–44. http://www.sciencedirect.com/science/article/B6V69-3YDGKGP-5/2/d1779ecb57bb4b37da6d8674f6e8d3da

Christopher, M. (2001). An integrated model for the design of agile supply chains. *International Journal of Physical Distribution & Logistics Management*, *31*(4), 235–246.

Christopher, M. (2004). Creating agile supply chains in the fashion industry. *International Journal of Retail & Distribution Management*, *32*(8/9), 367–376.

Christopher, M. (2005). *Logistics and supply chain management : Creating value-added networks* (3rd ed.). Harlow, England ; New York : Financial Times Prentice Hall.

Christopher, M. (2006). A taxonomy for selecting global supply chain strategies. *International Journal of Logistics Management*, *17*(2), 277–287.

Clausing, D. (1994). *Total quality development : A step-by-step guide to world class concurrent engineering*. New York.

Comstock, J. P. (1967). *Principles of naval architecture. written by a group of authorities. editor: John p. comstock* (1939 ed. edited by H. E. Rossell.). New York, Society of Naval Architects; Marine Engineers.

Conolly, J. E. (1974). Standards of good seakeeping for destroyers and frigates in head seas. *Marine Vehicles*.

Coyle, J. J., Langley Jr., C. J., Gibson, B. J., Novack, R. A., & Bardi, E. J. (2009). *Supply chain management : A logistics perspective* (8th ed.). Mason, OH ; Australia : South-Western Cengage.

Davis, M. R., & Holloway, D. S. (2003). The influence of hull form on the motions of high speed vessels in head seas. *Ocean Engineering*, *30*(16), 2091–2115. https://doi.org/10.1016/s0029-8018(03)00045-3

Davis, M. R., Watson, N. L., & Holloway, D. S. (2004). Measurement and prediction of wave loads on a high-speed catamaran fitted with active stern tabs. *Marine Structures*, *17*(7), 503–535. https://doi.org/10.1016/j.marstruc.2005.01.003

de Osés, F., & Castells, M. (2008). Heavy weather in european short sea shipping: Its influence on selected routes. *The Journal of Navigation*, *61*(01), 165–176.

Dieter, G. E., & Schmidt, L. C. (2009). *Engineering design* (4th). Boston, McGraw-Hill Higher Education.

Doctors, L. J. (1976). The effect of air-compressibility on the nonlinear motion of an air-cushion vehicle over waves (Office & N. Research, Eds.). In Office & N. Research (Eds.), *Proceedings, eleventh symposium on naval hydrodynamics*. Eleventh Symposium on Naval Hydrodynamics, London, England.

Doctors, L. J. (2018). *Hydrodynamics of high-performance marine vessels* (2nd, Vol. 2). Doctors, L.J.

Doctors, L. J. (1978). Hydrodynamic power radiated by a heaving and pitching air-cushion vehicle. *Journal of Ship Research*, *22*(2), 67–79.

Eggington, W. J., & Kobitz, N. (1975). Domain of the surface-effect ship. *Transactions - Society of Naval Architects and Marine Engineers*, (11).

Ellery, D. (2009, September 17). *Private email*.

Faltinsen, O. M. (1991). Speed loss and operational limits of high-speed marine vehicles. *High Speed Marine Transportation - Proceedings*.

Faltinsen, O. M. (1993). On seakeeping of conventional and high-speed vessels. *Journal of Ship Research*, *37*(2), 87–101.

Faltinsen, O. M. (2005a). *Hydrodynamics of high-speed marine vehicles* (1st). Cambridge, Cambridge University Press.

Faltinsen, O. M. (2005b). Seakeeping, stability and manoeuvring of high-speed marine vehicles. *Proceedings of the 7th Symposium on High Speed Marine Vehicles, 2005 Conference, HSMV 2005*, *2005*, 5–17.

Fang, C.-C., & Chan, H.-S. (2007). An investigation on the vertical motion sickness characteristics of a high-speed catamaran ferry. *Ocean Engineering*, *34*(14-15), 1909–1917.

Fox, R., & McDonald, A. (1998). *Introduction to fluid mechanics* (5th). New York, John Wiley & Sons, Inc.

Fox, R., McDonald, A., & Pritchard, P. (2004). *Introduction to fluid mechanics* (Sixth Edition). New Jersey, John Wiley & Sons, Inc.

Franklin, G. F., Powell, J. D., & Emami-Naeini, A. (2010). *Feedback control of dynamic systems* (6th). Upper Saddle River, Pearson.

Graham, T. A., & Sullivan, P. A. (2002). Pitch-heave dynamics of a segmented skirt air cushion. *Journal of Ship Research*, *46*(2), 121–137.

Graham, T. A., Sullivan, P. A., & Hinchey, M. J. (1983). Heave stiffness hysteresis measurements on a large scale air cushion (C. A. C. T. Society, Ed.). In C. A. C. T. Society (Ed.), *Seventeenth canadian symposium on air cushion technology preprints*. Seventeenth Canadian Symposium on Air Cushion Technology, Ottawa, Canadian Air Cushion Technology Society. Canadian Air Cushion Technology Society.

Graham, T. A., Sullivan, P. A., & Hinchey, M. J. (1985). Skirt material effects on air cushion dynamic heave stability. *Journal of Aircraft*, *22*(2), 101–109.

Harrison, A., & van Hoek, R. (2008). *Logistics management and strategy. competing through the supply chain* (3rd Edition). Harlow, Prentice Hall.

Hinchey, M. J. (1982). *Heave stability of air cushion vehicles hovering over deep water* (Technical Note No. 236) [Compilation and indexing terms, Copyright 2009 Elsevier Inc. 1983030034844]. University of Toronto, Institute for Aerospace Studies. Compilation and indexing terms, Copyright 2009 Elsevier Inc. 1983030034844.

Hinchey, M. J. (1983). Overview of utias research on the dynamic stability of air cushion vehicles. *Canadian Aeronautics and Space Journal*, *29*(4), 371–390.

Hinchey, M. J., & Sullivan, P. A. (1977). *Duct effects on the dynamic fan characteristics of air cushion systems* (Technical Note No. 211) [Compilation and indexing terms, Copyright 2009 Elsevier Inc. 1978050003085]. University of Toronto, Institute for Aerospace Studies. Compilation and indexing terms, Copyright 2009 Elsevier Inc. 1978050003085.

Hinchey, M. J., & Sullivan, P. A. (1981). Theoretical study of limit cycle oscillations of plenum air cushions. *Journal of Sound and Vibration*, *79*(1), 61–77.

Hinchey, M. J., & Sullivan, P. A. (1984). Hovercraft heave stability. *Canadian Aeronautics and Space Journal*, *30*(2), 130–151.

Hirata, N., & Faltinsen, O. M. (2000). Computation of cobblestone effect with unsteady viscous flow under a stern seal bag of a ses. *Journal of Fluids and Structures*, *14*(7), 1053–1069.

Holthuijsen, L. H. (2007). *Waves in oceanic and coastal waters* [551.4630151 HOLT]. Cambridge : Cambridge University Press.

Hrovat, D., & Margolis, D. (1981). An experimental comparison between semi-active and passive suspensions for air-cushion vehicles. *International Journal of Vehicle Design*, *2*(3), 308–321.

Hullender, D., Wormley, D., & Richardson, H. (1972). Active control of vehicle air cushion suspensions. *Journal of Dynamic Systems, Measurement, and Control*, (March), 41–49.

Instefjord, C. J., Skomedal, N. G., & Kjer, T. (1996). The oskoy class mcmv. *Dawn of a New Era*, (2).

International Maritime Organization. (1995). *International code of safety for high-speed craft (hsc code): Resolution msc.36(63) adopted on 20 may 1994*. IMO.

Jet Propulsion Laboratory. (1999). *Significant wave height cycle 235 30-jan-1999 - 09-feb-1999* (NASA, Ed.). Jet Propulsion Laboratory. ftp://podaac.jpl.nasa.gov/pub/sea_surface_height/topex_poseidon/images/cycle_images/1999/

Jonsson, P. (2008). *Logistics and supply chain management*. Maidenhead [England] : McGraw-Hill Higher Education ;

Kaplan, P., Bentson, J., & Davis, S. (1981). Dynamics and hydrodynamics of surface-effect ships. *SNAME Transactions*, *89*, 211–247.

Kaplan, P., Schneider, J., & Goodman, T. (1974). Motions of air cushion vehicles (acv) in waves, Mechanical Engineering Publications Limited for the Institution of Mechanical Engineers. Institution of Mechanical Engineers.

Kinsman, B. (1965). *Wind waves: Their generation and propagation on the ocean surface*. Englewood Cliffs, Prentice-Hall.

Korvin-Kroukovsky, B. V. (1961). *Theory of seakeeping*. New York, The Society of Naval Architects; Marine Engineers.

Lagoudis, I. N. (2006). Ranking of factors contributing to higher performance in the ocean transportation industry: A multi-attribute utility theory approach. *Maritime Policy & Management*, *33*(4), 345–369.

Lagoudis, I. N., Lalwani, C. S., Naim, M. M., & King, J. (2002). Defining a conceptual model for high-speed vessels. *International Journal of Transport Management*, *1*(2), 69–78.

Lavis, D. R., & Forstell, B. G. (2008). The cost of requirements and emerging technologies. *Naval Engineers Journal*, *120*(1), 59–76.

Lavis, D. R., & Spaulding, K. B. (1991). Surface effect ship (ses) developments worldwide [Chapter 2]. *Naval Engineers Journal*, *103*(5), 39–83.

Leary, M., & Burvill, C. (2007). Enhancing the quality function deployment conceptual design tool. *Journal of Mechanical Design, Transactions of the ASME*, *129*(7), 701–708.

Leaver, R., & Thomas, T. (1974). *Analysis and presentation of experimental results*. The MacMillan Press LTD.

Margolis, D., Tylee, J., & Hrovat, D. (1975). Heave mode dynamics of a tracked air cushion vehicle with semiactive airbag secondary suspension. *Journal of Dynamic Systems Measurement and Control-Transactions of the ASME*, (December), 399–407.

Massel, S. R. (1996). *Ocean surface waves : Their physics and prediction* (1st ed.). Singapore : World Scientific.

Matsumura, T., Yamashita, S., & Ohba, N. (2006). Dynamic performance of a 140m ses in simulations, model tests and sea trial: An introduction to recent development of the techno super liner. *Australian Journal of Mechanical Engineering*, *3*(2), 91–102.

Matsuo, H., & Matsuo, K. (1980). Effects of fan, ducting and powerplant characteristics on the cushion stability of air cushion vehicles. *Journal of Aircraft*, *18*(5).

Meriam, J., & Kraige, L. (2008). *Engineering mechanics* (Sixth Edition SI version).

Munson, B., Young, D., & Okiishi, T. (1990). *Fundamentals of fluid mechanics*.

Oehlmann, H. (1991). Prediction of resistance of surface effect ships (H. Holden Kjell O., Ed.). In H. Holden Kjell O. (Ed.), *International conference on fast sea transportation*, Trondheim.

Ogata, K. (1990). *Modern control engineering* (2nd) [629.8 OGAT]. Englewood Cliffs, Prentice Hall.

Ohanian, H. (1989). *Physics* (2nd Edition Expanded, International Student Edition.). W.W. Norton & Company, Inc.

O'Hanlon, J. F., & McCauley, M. E. (1975). Motion sickness incidence as a function of the frequency and acceleration of vertical sinusoidal motion. *Journal of Sound and Vibration*, *41*(4), 521–521.

Partnership, A.-J. T. (2012). *Water transport 2012* (A.-J. T. Partnership, Ed.). www.ajtpweb.org/statistics/compareasean/Water_Transport/Water_Transport_2012

Phillips, S. J. (Ed.). (2007). *Jane's high-speed marine transportation 2007-2008* (40th). Jane's Information Group Limited.

Pozzi, A., Manzo, F., & Luchini, P. (1993). Compressible flow in a hovercraft air cushion. *American Institute of Aeronautics and Astronautics Journal*, *31*(3), 528–533.

Pugh, S. (1991). *Total design : Integrated methods for successful product engineering*. Wokingham, Addison-Wesley Pub.

Pustoshny, A. V., & Rusetsky, A. A. (2006). Naval and commercial fast ship development experience and further prospects [Reviewed paper originally presented at the Eighth International Conference on Fast Sea Transportation (FAST05), St Petersburg, Russia, 2005.]. *Australian Journal of Mechanical Engineering*, *3*(2), 79–90.

Reynolds, A. (1971). Research note: A linear theory for the heaving response of a hovercraft moving over regular waves. *Journal Mechanical Engineering Science*, *14*(2), 147–150.

Reynolds, A. (1974). A nonlinear theory for a hovercraft moving over regular waves. *Journal Mechanical Engineering Science*, *16*(5), 310–316.

Reynolds, A., & Brooks, B. (1977). The roles of skirt planform and deflection in hovercraft response. *Journal Mechanical Engineering Science*, *19*(1), 1–11.

Reynolds, A., West, R., & Brooks, B. (1972). Heaving and pitching response of a hovercraft moving over regular waves. *Journal Mechanical Engineering Science*, *14*(5), 340–352.

Sariöz, K., & Narli, E. (2005). Effect of criteria on seakeeping performance assessment. *Ocean Engineering*, *32*(10), 1161–1173.

Shaw, R. (1982). *Wave energy - a design challenge*. Chichester, Ellis Horwood Limited.

Sorensen, A., & Egeland, O. (1994). Ride control of surface effect ships using distributed control. *Control Engineering Practice*, *2*(6), 915–922.

Sorensen, A., & Egeland, O. (1995). Design of ride control system for surface effect ships using dissipative control. *Automatica*, *31*, 183–199.

Southeast Asia. (2008). *Southeast asia* (O. U. Press, Ed.). Oxford University Press. www.oxfordreference.com/views/ENTRY.html

Standards Australia. (2001). *Evaluation of human exposure to whole-body vibration - general requirements (as 2670.1-2001)* (Standards Australia, Ed.; tech. rep.) [First published

as part of AS 2670-1983. Revised and redesignated in part as AS 2670.1-1990 and AS 2670.3-1990. AS 2670.1-1990 and AS 2670.3-1990 revised, amalgamated and redesignated as AS 2670.1-2001.]. First published as part of AS 2670-1983. Revised and redesignated in part as AS 2670.1-1990 and AS 2670.3-1990. AS 2670.1-1990 and AS 2670.3-1990 revised, amalgamated and redesignated as AS 2670.1-2001. Standards Australia International.

Steen, S., & Faltinsen, O. M. (1995). Cobblestone oscillations of an ses with flexible bag aft seal, *39*(1), 25–41.

Sugai, K., & Yamaguchi, M. (1991a). Research and development program of techno-superliner (K. Holden, Ed.). In K. Holden (Ed.), *Fast '91: Proceedings from the first international conference on fast sea transportation, norway*, Trondheim, Tapir Forlag.

Sugai, K., & Yamaguchi, M. (1991b). Research and development program of techno-superliner.

Sullivan, P. A., Charest, P. A., & Ma, T. (1994). Heave stiffness of an air cushion vehicle bag-and-finger skirt. *Journal of Ship Research*, *38*(4), 302–307.

Sullivan, P. A., Hinchey, M. J., & Green, G. M. (1982). A review and assessment of methods for prediction of the dynamic stability of air cushions. *Journal of Sound and Vibration*, *84*(3), 337–358.

Sullivan, P. A., Walsh, C., & Hinchey, M. J. (1993). Kelvin-helmholtz wave generation beneath hovercraft skirts. *Journal of Sound and Vibration*, *163*(2), 275–282.

Sweet, L., & Richardson, H. (1976). The pitch-heave dynamics of transportation vehicles. *Journal of Sound and Vibration*, *47*(4), 615–615.

Sweet, L., Richardson, H., & Wormley, D. (1975). Plenum air cushion/compressor-duct dynamic interactions. *Journal of Dynamic Systems, Measurement, and Control*.

Tatinclaux, J. (1975). On the wave resistance of surface-effect ships. *Transactions - Society of Naval Architects and Marine Engineers*, (3).

Tupper, E. (2004). *Introduction to naval architecture*. Elsevier.

Ulstein, T., & Faltinsen, O. M. (1998). Cobblestone effect on surface effect ships. *Ship Technology Research*, *43*(2), 78–90.

Vassalos, D., Xie, N., Jasionowski, A., & Lee, B. S. (2007). Dynamic stability of the air-lifted catamaran. *Proceedings of the Institution of Mechanical Engineers, Part M (Journal of Engineering for the Maritime Environment)*, *221*(M4), 137–46.

Vesely, W., Dugan, J., Fragola, J., Minarick III, J., & Railsback, J. (2002, August 1). *Fault tree handbook with aerospace applications* (Government Document). NASA Office of Safety and Mission Assurance.

Vesely, W., Goldberg, F., Roberts, N., & Haasl, D. (1981, January 1). *Fault tree handbook* (Government Document). U.S. Nuclear Regulatory Commission. http://www.nrc.gov/reading-rm/doc-collections/nuregs/staff/sr0492/sr0492.pdf

Wertheim, A. H., Bos, J. E., & Bles, W. (1998). Contributions of roll and pitch to sea sickness. *Brain Research Bulletin*, *47*(5), 517–524.

Young, I., & Holland, G. (1996). *An atlas of the oceans' wind and wave climate* (lst ed. 1996.). New York, N.Y. : Pergamon.

Appendices

A. Significant Wave Height Data

This presents the available significant wave height data made publicly available from the TOPEX/POSEIDON or GEOSAT satellite missions of the Jet Propulsion Laboratory, NASA (Jet Propulsion Laboratory, 1999).

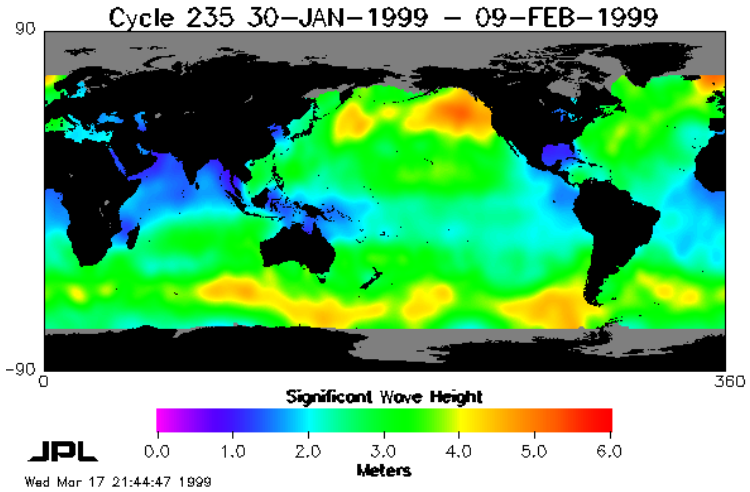


Figure A.1. Significant wave height January 30-February 9 1999 (Jet Propulsion Laboratory, 1999)

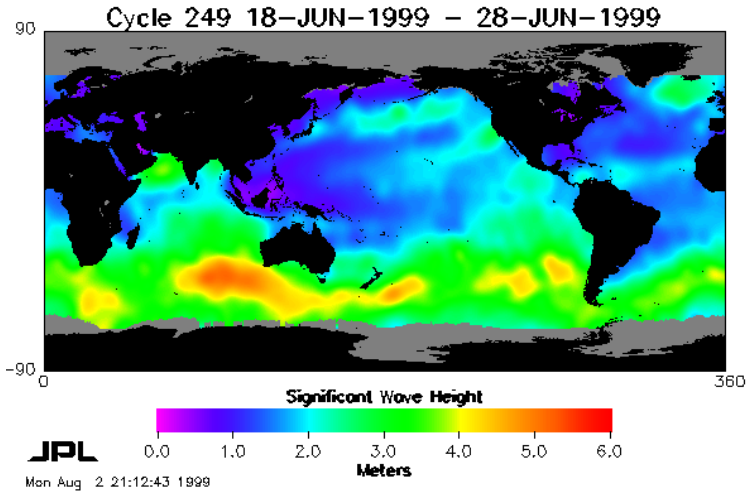


Figure A.2. Significant wave height June 18-28 1999 (Jet Propulsion Laboratory, 1999)

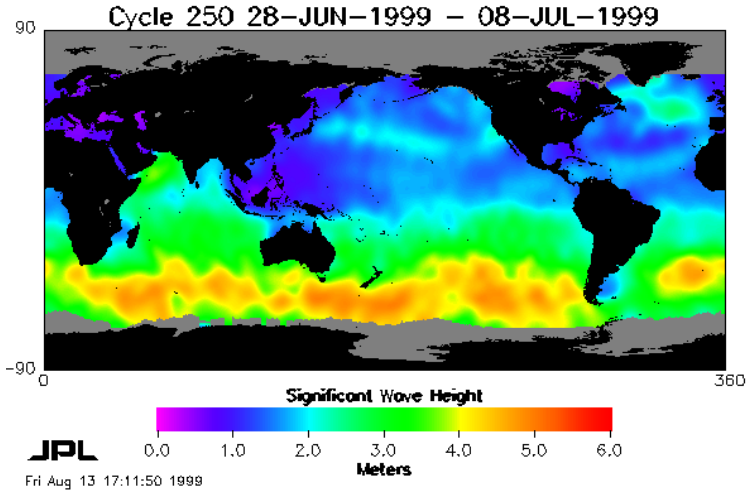


Figure A.3. Significant wave height June 28-July 8 1999 (Jet Propulsion Laboratory, 1999)

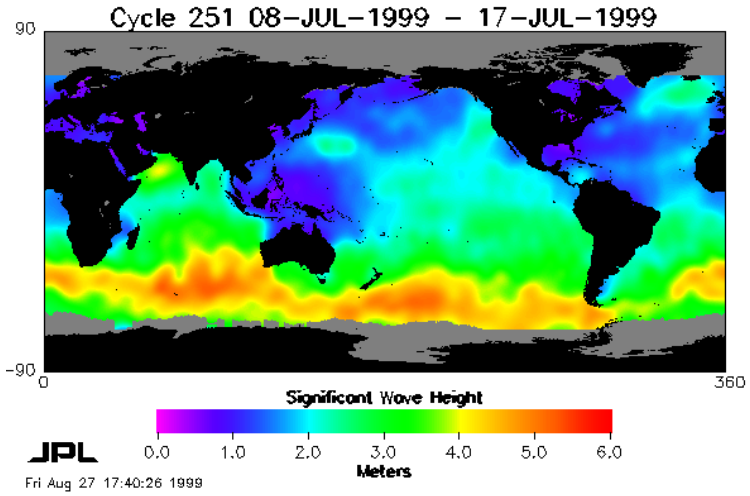


Figure A.4. Significant wave height July 8-17 1999 (Jet Propulsion Laboratory, 1999)

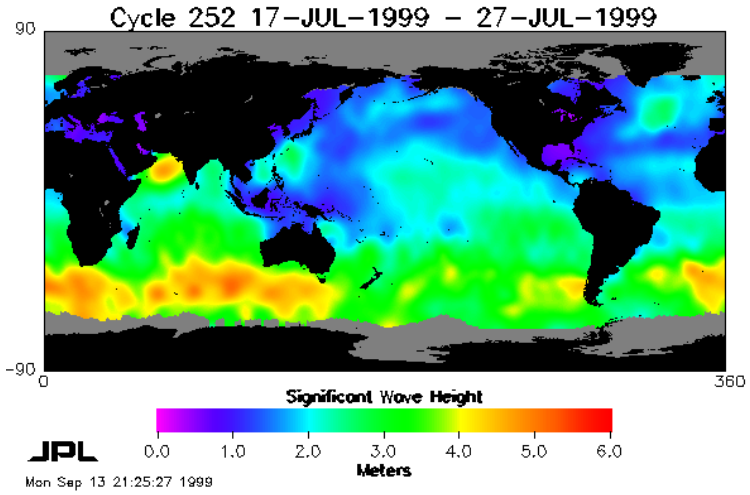


Figure A.5. Significant wave height July 17-27 1999 (Jet Propulsion Laboratory, 1999)

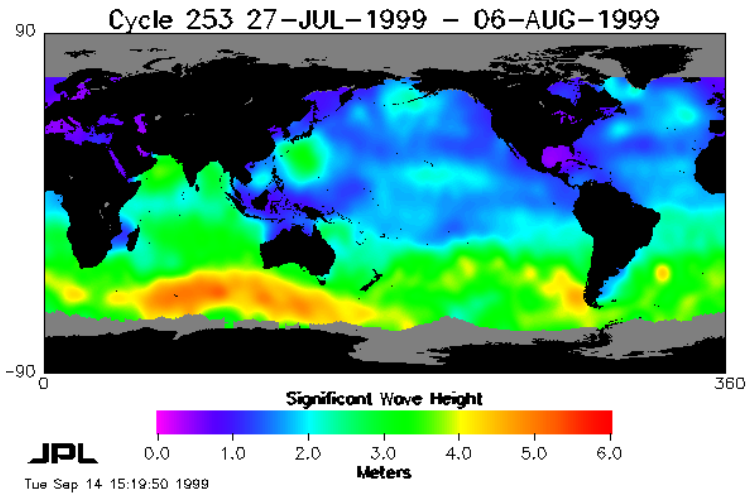


Figure A.6. Significant wave height July 27-August 6 1999 (Jet Propulsion Laboratory, 1999)

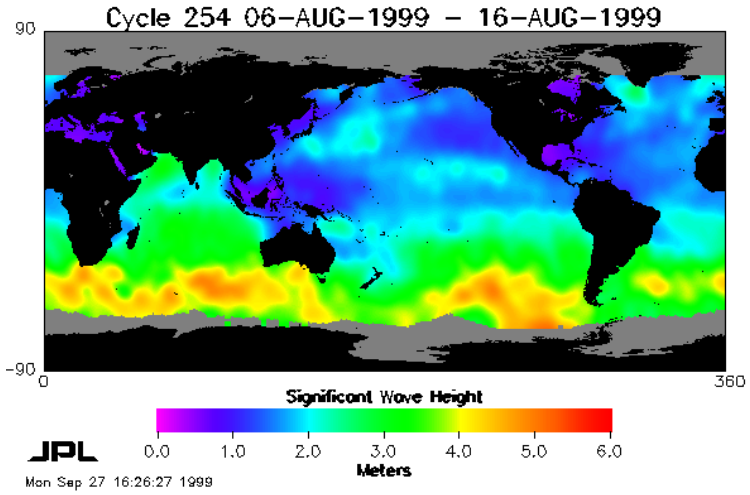


Figure A.7. Significant wave height August 6-16 1999 (Jet Propulsion Laboratory, 1999)

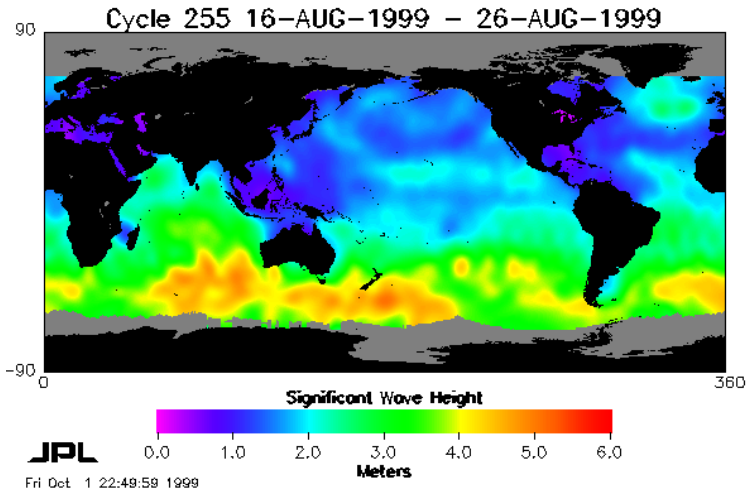


Figure A.8. Significant wave height August 16-26 1999 (Jet Propulsion Laboratory, 1999)

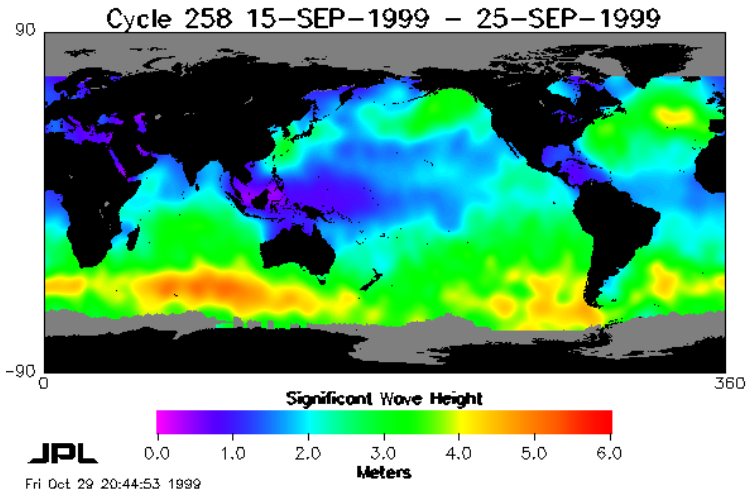


Figure A.9. Significant wave height September 15-20 1999 (Jet Propulsion Laboratory, 1999)

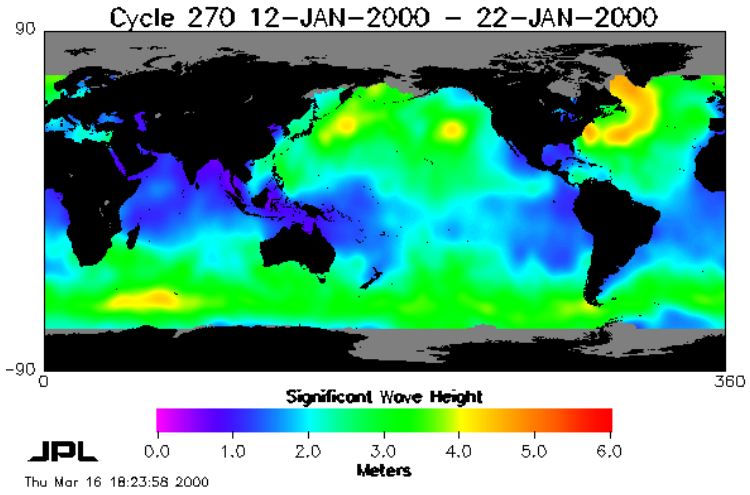


Figure A.10. Significant wave height January 11-22 2000 (Jet Propulsion Laboratory, 1999)

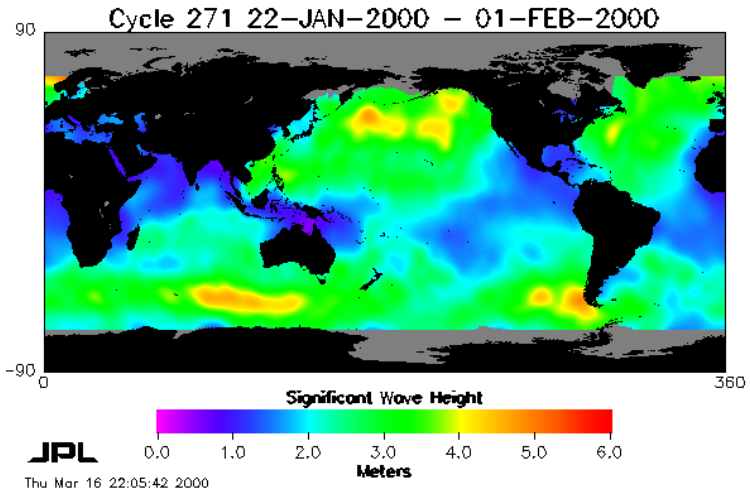


Figure A.11. Significant wave height January 23-February 2000 (Jet Propulsion Laboratory, 1999)

B. Conceptual design tool data

Full analysis of the Customer Requirements (CRs), Engineering Attributes (EAs) and Failure Modes (FMs) found in the available literature is given in Table B.1. The method used is described in Sec. 3.5.

Table B.1. Engineering Attributes, Customer Requirements and Failure Modes sourced and categorised.

Source Text	Type	Source	Year	Page	System	Sub-System	Type of EA	Final Title	Notes
Damage Control	CR	Butler 1985	1985	203	Hull	Centrebody		Damage Control	
Machinery Accomodation volume	CR	Butler 1985	1985	204	Hull	Sidehulls			
Crew protection	CR	Butler 1985	1985	203	Hull			Crew protection	
Enclosed volume	CR	Butler 1985	1985	204	Hull			Gross Tonnage	
shallow propulsor draft	CR	Butler 1985	1985	228	Propulsion	Propulsor		Accessibility	
protection against damage due to impact with debris	CR	Butler 1985	1985	228	Propulsion	Propulsor		Accessibility	
protection against damage due to impact with docking facilities	CR	Butler 1985	1985	228	Propulsion	Propulsor		Accessibility	
Handling characteristics	CR	Butler 1985	1985	203	Propulsion			Manoeuvrability	
Maneuvering	CR	Butler 1985	1985	203	Propulsion			Manoeuvrability	
Draft	CR	Eggington & Kobitz 1975	1975	278	SES			Accessibility	
Payload Stowage Capability	CR	Eggington & Kobitz 1975	1975	278	SES			Gross Tonnage	
Maneuvering	CR	Eggington & Kobitz 1975	1975	278	SES			Manoeuvrability	
Payload	CR	Eggington & Kobitz 1975	1975	278	SES			Payload	
Passenger accessibility	CR	Eggington & Kobitz 1975	1975	278	SES				
Ride Quality	CR	Eggington & Kobitz 1975	1975	282	SES			Ride Comfort	
Design Speed	CR	Butler 1985	1985	200	SES			Speed	
Ship Motions	CR	Butler 1985	1985	202	SES			Ride Comfort	
Well Deck	CR	Butler 1985	1985	202	SES				
operational flexibility	CR	Butler 1985	1985	203	SES			Accessibility	
Seakeeping	CR	Butler 1985	1985	204	SES			Seakeeping	
speed	CR	Butler 1985	1985	204	SES			Speed	
Beaching	CR	Butler 1985	1985	204	SES				
Boarding accessibility	CR	Butler 1985	1985	205	SES			Accessibility	
Dock accessibility	CR	Butler 1985	1985	205	SES			Accessibility	

continued...

continued from previous page

Source Text	Type	Source	Year	Page	System	Sub-System	Type of EA	Final Title	Notes
Low speed maneuverability	CR	Butler 1985	1985	205	SES			Manoeuvrability	
Capital cost	CR	Butler 1985	1985	207	SES			Capital Cost	
Habitability	CR	Butler 1985	1985	208	SES			Ride Comfort	
useful payload	CR	Butler 1985	1985	216	SES			Payload	
Calm Water speed	CR	Butler 1985	1985	216	SES			Speed	
emergency maneuverability	CR	Butler 1985	1985	218	SES			Manoeuvrability	
Stability	CR	Butler 1985	1985	218	SES			Stability	
satisfactory roll motion	CR	Butler 1985	1985	223	SES			Ride Comfort	
lateral stability in a seaway	CR	Butler 1985	1985	223	SES			Seakeeping	
cost of fabrication	CR	Butler 1985	1985	224	SES			Capital Cost	
motions	CR	Butler 1985	1985	224	SES			Ride Comfort	
ship reliability	CR	Butler 1985	1985	224	SES			ship reliability	
stability	CR	Butler 1985	1985	224	SES			stability	
structural weight	CR	Butler 1985	1985	224	SES				
operational profile	CR	Butler 1985	1985	225	SES				Military
Capital cost	CR	Butler 1985	1985	227	SES			Capital Cost	
Maneuverability	CR	Butler 1985	1985	227	SES			Manoeuvrability	
vulnerability	CR	Butler 1985	1985	227	SES			vulnerability	Military
speed range	CR	Butler 1985	1985	227	SES			Speed	
manoeuvrability at low speed	CR	Butler 1985	1985	228	SES			Manoeuvrability	
Habitability	CR	Butler 1985	1985	238	SES			Ride Comfort	
mission capability	CR	Butler 1985	1985	238	SES				Military
high speeds (over 40 knots)	CR	Lavis & Spaulding 1991	1991	57	SES			Speed	
maximum continuous speed obtainable in calm water and still air	CR	Lavis & Spaulding 1991	1991	58	SES			Speed	
docking limits	CR	Lavis & Spaulding 1991	1991	59	SES			Accessibility	
costs	CR	Lavis & Spaulding 1991	1991	59	SES			Operating Cost	
acceptable ride quality	CR	Lavis & Spaulding 1991	1991	59	SES			Ride Comfort	
hull volume	CR	Lavis & Spaulding 1991	1991	67	SES			Gross Tonnage	
payload	CR	Lavis & Spaulding 1991	1991	68	SES			Payload	
cost	CR	Lavis & Spaulding 1991	1991	78	SES			Capital Cost	
comfort	CR	Lavis & Spaulding 1991	1991	78	SES			Ride Comfort	
cabin accomodation space	CR	Lavis & Spaulding 1991	1991	78	SES			Ride Comfort	
speed	CR	Lavis & Spaulding 1991	1991	78	SES			Speed	
shallow draft	CR	Lavis & Spaulding 1991	1991	79	SES			Accessibility	
payload	CR	Lavis & Spaulding 1991	1991	79	SES			Payload	
shock attenuation	CR	Lavis & Spaulding 1991	1991	79	SES			shock attenuation	Military
platform stability	CR	Lavis & Spaulding 1991	1991	79	SES			Seakeeping	
seakeeping	CR	Lavis & Spaulding 1991	1991	79	SES			Seakeeping	

continued...

continued from previous page

Source Text	Type	Source	Year	Page	System	Sub-System	Type of EA	Final Title	Notes
speed	CR	Lavis & Spaulding 1991	1991	79	SES			Speed	
helicopter support	CR	Lavis & Spaulding 1991	1991	79	SES				Military
reliability	CR	Lavis & Spaulding 1991	1991	81	SES			reliability	
payload	CR	Sugai & Yamaguchi 1991	1991	672	SES			Payload	
seaworthiness	CR	Sugai & Yamaguchi 1991	1991	672	SES			seaworthiness	
speed	CR	Sugai & Yamaguchi 1991	1991	672	SES			Speed	
stability	CR	Sugai & Yamaguchi 1991	1991	674	SES			stability	
structural safety	CR	Sugai & Yamaguchi 1991	1991	675	SES			structural safety	
acquisition costs	CR	Instefjord et al. 1996	1996	18	SES			Capital Cost	
availability	CR	Instefjord et al. 1996	1996	18	SES			Availability	
repairability	CR	Instefjord et al. 1996	1996	18	SES			Repairability	
maintainability	CR	Instefjord et al. 1996	1996	18	SES			Maintainability	
Habitability	CR	Instefjord et al. 1996	1996	18	SES			Ride Comfort	
arrangements and habitability	CR	Instefjord et al. 1996	1996	18	SES			Ride Comfort	
favourable shock load levels	CR	Instefjord et al. 1996	1996	18	SES			favourable shock load levels	Military
safety and redundancy	CR	Instefjord et al. 1996	1996	18	SES			safety and redundancy	
shock loads	CR	Instefjord et al. 1996	1996	18	SES			shock loads	Military
seakeeping	CR	Instefjord et al. 1996	1996	18	SES			Seakeeping	
speed	CR	Instefjord et al. 1996	1996	18	SES			Speed	
enclosed volume	CR	Instefjord et al. 1996	1996	18	SES			Gross Tonnage	
acoustic signature	CR	Instefjord et al. 1996	1996	18	SES				Military
magnetic signature	CR	Instefjord et al. 1996	1996	18	SES				Military
NBCD/survivability	CR	Instefjord et al. 1996	1996	18	SES				Military
future growth	CR	Instefjord et al. 1996	1996	18	SES				
IR signature	CR	Instefjord et al. 1996	1996	18	SES				Military
radar signature	CR	Instefjord et al. 1996	1996	18	SES				Military
EMI/EMC	CR	Instefjord et al. 1996	1996	18	SES				Military
sonar performance	CR	Instefjord et al. 1996	1996	18	SES				Military
payload integration	CR	Instefjord et al. 1996	1996	18	SES				Military
speed	CR	Pustoshny & Rusetsky 2006	2006	82	SES			Speed	
construction cost	CR	Pustoshny & Rusetsky 2006	2006	88	SES			Capital Cost	
operation cost	CR	Pustoshny & Rusetsky 2006	2006	88	SES			Operating Cost	
propeller diameter restrictions	CR	Pustoshny & Rusetsky 2006	2006	89	SES			Accessibility	
sufficent cargo capacities	CR	Pustoshny & Rusetsky 2006	2006	89	SES			Payload	

continued...

continued from previous page

Source Text	Type	Source	Year	Page	System	Sub-System	Type of EA	Final Title	Notes
sufficient passenger capacities	CR	Pustoshny & Rusetsky 2006	2006	89	SES			Payload	
Habitability	CR	Pustoshny & Rusetsky 2006	2006	89	SES			Ride Comfort	
comfort	CR	Pustoshny & Rusetsky 2006	2006	89	SES			Ride Comfort	
high speed for continuous operation	CR	Pustoshny & Rusetsky 2006	2006	89	SES			Speed	
trip time	CR	Matsumura et al. 2006	2006	91	SES			Trip time	
maximum cargo payload	CR	Matsumura et al. 2006	2006	92	SES			Payload	
maximum passenger number	CR	Matsumura et al. 2006	2006	92	SES			Payload	
maximum speed	CR	Matsumura et al. 2006	2006	92	SES			Speed	
gross tonnage	CR	Matsumura et al. 2006	2006	92	SES			Gross Tonnage	
required accomodation volume	CR	Matsumura et al. 2006	2006	93	SES			Gross Tonnage	
seaworthiness	CR	Matsumura et al. 2006	2006	93	SES			Seakeeping	
frequency distribution of wave height on route	CR	Matsumura et al. 2006	2006	93	SES			Seakeeping	
worst intended significant wave height	CR	Matsumura et al. 2006	2006	93	SES			Seakeeping	
speed range in terms of Froude number	CR	Matsumura et al. 2006	2006	93	SES			Speed	
required machinery volume	CR	Matsumura et al. 2006	2006	93	SES				
sea trial speed in a seaway	CR	Matsumura et al. 2006	2006	98	SES			Speed	
cost	CR	Lavis & Forstell 2008	2008	59	SES			Capital Cost	
ship life-cycle cost	CR	Lavis & Forstell 2008	2008	59	SES			Ship Life-Cycle cost	
payload	CR	Lavis & Forstell 2008	2008	59	SES			Payload	
seakeeping	CR	Lavis & Forstell 2008	2008	59	SES			Seakeeping	
speed	CR	Lavis & Forstell 2008	2008	59	SES			Speed	
cargo safety in a seaway	CR	Lavis & Forstell 2008	2008	61	SES			Cargo Safety	
passenger comfort in a seaway	CR	Lavis & Forstell 2008	2008	61	SES			Ride Comfort	
ship's structural integrity in a seaway	CR	Lavis & Forstell 2008	2008	61	SES			ship's structural integrity in a seaway	
mission performance in a seaway	CR	Lavis & Forstell 2008	2008	61	SES			Seakeeping	
crew comfort in a seaway	CR	Lavis & Forstell 2008	2008	61	SES			Seakeeping	
continue operations in adverse environmental conditions	CR	Lavis & Forstell 2008	2008	61	SES			Seakeeping	
enclosed volume	CR	Lavis & Forstell 2008	2008	64	SES			Gross Tonnage	
expected wave height	CR	Lavis & Forstell 2008	2008	65	SES			Seakeeping	
expected seaway modal period	CR	Lavis & Forstell 2008	2008	65	SES			Seakeeping	

continued...

continued from previous page

Source Text	Type	Source	Year	Page	System	Sub-System	Type of EA	Final Title	Notes
expected sea spectrum	CR	Lavis & Forstell 2008	2008	65	SES			Seakeeping	
expected wind speed	CR	Lavis & Forstell 2008	2008	65	SES			Seakeeping	
percentage of time operating in mission profile segment	CR	Lavis & Forstell 2008	2008	65	SES			Seakeeping	
required ship speed	CR	Lavis & Forstell 2008	2008	65	SES			Speed	
ride quality	CR	Lavis & Forstell 2008	2008	71	SES			Ride Comfort	
seakeeping	CR	Lavis & Forstell 2008	2008	71	SES			Seakeeping	
speed performance in a seaway	CR	Lavis & Forstell 2008	2008	71	SES			Seakeeping	
maximum beam constraint	CR	Lavis & Forstell 2008	2008	72	SES			Accessibility	
maximum draft constraint	CR	Lavis & Forstell 2008	2008	72	SES			Accessibility	
Appendage drag	EA	Lavis & Spaulding 1991	1991	64	Hull	Appendages			
transverse structural strength	EA	Butler 1985	1985	203	Hull	Centrebody			
bow slamming strength	EA	Butler 1985	1985	203	Hull	Centrebody			
longitudinal strength	EA	Butler 1985	1985	203	Hull	Centrebody			
Fin lift	EA	Butler 1985	1985	218	Hull	Control			
Inward banking moment	EA	Butler 1985	1985	218	Hull	Control			
Rudder Size	EA	Butler 1985	1985	218	Hull	Control			
Rudder spacing	EA	Butler 1985	1985	219	Hull	Control			
Rudder inclination	EA	Butler 1985	1985	219	Hull	Control			
Sidehull Deadrise Angle	EA	Eggington & Kobitz 1975	1975	272	Hull	Sidehulls			
Sidehulls drag	EA	Eggington & Kobitz 1975	1975	273	Hull	Sidehulls	PM	Sidehull Drag	
Sidehull drag coefficient	EA	Eggington & Kobitz 1975	1975	282	Hull	Sidehulls			
Propulsion Accomodation	EA	Butler 1985	1985	200	Hull	Sidehulls	PM	Machinery Accomodation volume	
Hull wetted area	EA	Butler 1985	1985	202	Hull	Sidehulls	DM	Sidehull Wetted Area	
Off cushion sidehull bouyancy	EA	Butler 1985	1985	202	Hull	Sidehulls	DV	Sidehull Displacement	
Machinery Accomodation volume	EA	Butler 1985	1985	202	Hull	Sidehulls	PM	Machinery Accomodation volume	
producibility	EA	Butler 1985	1985	202	Hull	Sidehulls	PM	Producibility	
Roll stability	EA	Butler 1985	1985	202	Hull	Sidehulls	PM	Roll Stability	
On cushion sidehull drag	EA	Butler 1985	1985	202	Hull	Sidehulls	PM	Sidehull Drag	
sidehull drag	EA	Butler 1985	1985	202	Hull	Sidehulls	PM	Sidehull Drag	
Yaw stability	EA	Butler 1985	1985	202	Hull	Sidehulls	PM	Yaw Stability	
bow stem strength	EA	Butler 1985	1985	202	Hull	Sidehulls			
Sidehull keel strength	EA	Butler 1985	1985	202	Hull	Sidehulls			
lower hull deadrise angles	EA	Butler 1985	1985	202	Hull	Sidehulls			
aero-hydrodynamic drag	EA	Butler 1985	1985	202	Hull	Sidehulls			
wave wetting	EA	Butler 1985	1985	202	Hull	Sidehulls			

continued...

continued from previous page

Source Text	Type	Source	Year	Page	System	Sub-System	Type of EA	Final Title	Notes
Spray sheet wetting	EA	Butler 1985	1985	202	Hull	Sidehulls			
waterjet inlet cavitation	EA	Butler 1985	1985	202	Hull	Sidehulls			
waterjet inlet loss of power	EA	Butler 1985	1985	202	Hull	Sidehulls			
Propellor Immersion	EA	Butler 1985	1985	203	Hull	Sidehulls			
Buoyancy fraction	EA	Butler 1985	1985	203	Hull	Sidehulls			
tankage accomodation	EA	Butler 1985	1985	204	Hull	Sidehulls	DV	Tankage Accomodation	
Off cushion wetdeck height	EA	Butler 1985	1985	204	Hull	Sidehulls	DV	Off Cushion Wetdeck Height	
Draft	EA	Butler 1985	1985	204	Hull	Sidehulls	DV	On-Cushion Draft	
Sidehull internal volume	EA	Butler 1985	1985	204	Hull	Sidehulls	PM	Machinery Accomodation volume	
off cushion sidehull resistance	EA	Butler 1985	1985	204	Hull	Sidehulls			
Sidehull deck area	EA	Butler 1985	1985	204	Hull	Sidehulls			
Displacement	EA	Butler 1985	1985	205	Hull	Sidehulls	DV	Sidehull Displacement	
Off cushion freeboard	EA	Butler 1985	1985	205	Hull	Sidehulls			
Damaged stability	EA	Butler 1985	1985	205	Hull	Sidehulls			
off cushion wetted surface area	EA	Butler 1985	1985	205	Hull	Sidehulls			
Sidehull drag	EA	Butler 1985	1985	212	Hull	Sidehulls	PM	Sidehull Drag	
Sidehull skin friction drag	EA	Butler 1985	1985	213	Hull	Sidehulls			
Residual drag	EA	Butler 1985	1985	214	Hull	Sidehulls			
Frictional drag	EA	Butler 1985	1985	214	Hull	Sidehulls			
Roll stability	EA	Butler 1985	1985	218	Hull	Sidehulls	PM	Roll Stability	
sidehull length	EA	Butler 1985	1985	218	Hull	Sidehulls			
Sidehull Deadrise Angle	EA	Butler 1985	1985	218	Hull	Sidehulls			
displacement-length ratio	EA	Butler 1985	1985	222	Hull	Sidehulls			
fine sidehull lines	EA	Butler 1985	1985	222	Hull	Sidehulls			
hull form	EA	Butler 1985	1985	222	Hull	Sidehulls			
draft	EA	Butler 1985	1985	227	Hull	Sidehulls	DV	On-Cushion Draft	
sidehull geometry	EA	Butler 1985	1985	227	Hull	Sidehulls			
Structural stern width	EA	Butler 1985	1985	228	Hull	Sidehulls			
sidehull width	EA	Butler 1985	1985	228	Hull	Sidehulls			
sidehull stern width	EA	Butler 1985	1985	228	Hull	Sidehulls			
sidehull restoring moments	EA	Butler 1985	1985	228	Hull	Sidehulls			
sidehull damping	EA	Lavis & Spaulding 1991	1991	58	Hull	Sidehulls			
sidehull displacement	EA	Lavis & Spaulding 1991	1991	60	Hull	Sidehulls	DV	Sidehull Displacement	
sidehull forward entry fineness	EA	Lavis & Spaulding 1991	1991	60	Hull	Sidehulls			
sidehull flare	EA	Lavis & Spaulding 1991	1991	60	Hull	Sidehulls			
sidehull outer deadrise angle	EA	Lavis & Spaulding 1991	1991	60	Hull	Sidehulls			
sidehull internal haunch volume	EA	Lavis & Spaulding 1991	1991	60	Hull	Sidehulls			
keel flat width	EA	Lavis & Spaulding 1991	1991	60	Hull	Sidehulls			

continued...

continued from previous page

Source Text	Type	Source	Year	Page	System	Sub-System	Type of EA	Final Title	Notes
sidehull length to beam ratio	EA	Lavis & Spaulding 1991	1991	60	Hull	Sidehulls			
sidehull hull-borne beam-to-draft ratio	EA	Lavis & Spaulding 1991	1991	60	Hull	Sidehulls			
sidehull gap ratio	EA	Lavis & Spaulding 1991	1991	60	Hull	Sidehulls			
sidehull prismatic coefficient	EA	Lavis & Spaulding 1991	1991	60	Hull	Sidehulls			
sidehull block coefficient	EA	Lavis & Spaulding 1991	1991	60	Hull	Sidehulls			
sidehull displacement/length ratio	EA	Lavis & Spaulding 1991	1991	60	Hull	Sidehulls			
sidehull deadrise angle amidships	EA	Lavis & Spaulding 1991	1991	60	Hull	Sidehulls			
sidehull wave making drag	EA	Lavis & Spaulding 1991	1991	64	Hull	Sidehulls	PM	Sidehull Drag	
sidehull frictional drag	EA	Lavis & Spaulding 1991	1991	64	Hull	Sidehulls	PM	Sidehull Drag	
Spray drag	EA	Lavis & Spaulding 1991	1991	64	Hull	Sidehulls			
structural weight / total ship weight	EA	Butler 1985	1985	224	Hull	Structural	PM		
simplicity of structure	EA	Butler 1985	1985	224	Hull	Structural			
structural reliability for single largest lifetime loading	EA	Butler 1985	1985	225	Hull	Structural	PM	structural reliability for single largest lifetime loading	
structural reliability for cumulative lifetime fatigue loading	EA	Butler 1985	1985	225	Hull	Structural	PM	structural reliability for cumulative lifetime fatigue loading	
Structural Material	EA	Butler 1985	1985	226	Hull	Structural			
Structural Weight	EA	Butler 1985	1985	226	Hull	Structural			
Longitudinal stiffness	EA	Butler 1985	1985	226	Hull	Structural			
longitudinal strength	EA	Butler 1985	1985	226	Hull	Structural			
Overall Length	EA	Eggington & Kobitz 1975	1975	269	Hull		DV	Length	
Overall Height	EA	Eggington & Kobitz 1975	1975	269	Hull				
Aerodynamic Drag	EA	Eggington & Kobitz 1975	1975	273	Hull				
Appendage drag	EA	Eggington & Kobitz 1975	1975	273	Hull				
Gross Weight	EA	Eggington & Kobitz 1975	1975	275	Hull		PM	Full Load Displacement	
Planform	EA	Butler 1985	1985	200	Hull				
Beam	EA	Butler 1985	1985	202	Hull		DV	Beam	
Off cushion wet deck height	EA	Butler 1985	1985	202	Hull		DV	Off Cushion Wetdeck Height	
Draft	EA	Butler 1985	1985	202	Hull		PM	On-Cushion Draft	
Superstructure aerodynamic drag	EA	Butler 1985	1985	203	Hull				
Deck area	EA	Butler 1985	1985	204	Hull		DV	Deck Area	
Block coefficient	EA	Butler 1985	1985	204	Hull		DV	Sidehull Block Coefficient	

continued...

continued from previous page

Source Text	Type	Source	Year	Page	System	Sub-System	Type of EA	Final Title	Notes
Aerodynamic Drag	EA	Butler 1985	1985	212	Hull				
longitudinal centre of gravity position	EA	Butler 1985	1985	218	Hull		DM	longitudinal centre of gravity position	
L/B ratio	EA	Eggington & Kobitz 1975	1975	268	Lift	Cushion	DV	L/B Ratio	
Cushion Height	EA	Eggington & Kobitz 1975	1975	269	Lift	Cushion	DV	Cushion Height	
Cushion wavemaking drag	EA	Eggington & Kobitz 1975	1975	273	Lift	Cushion	PM	Cushion Wavemaking Drag	
Cushion air flow rate	EA	Eggington & Kobitz 1975	1975	281	Lift	Cushion	DV	Cushion Air Flow Rate	
Cushion pressure	EA	Butler 1985	1985	202	Lift	Cushion	DM	Cushion Pressure	
Cushion Area	EA	Butler 1985	1985	202	Lift	Cushion	DV	Cushion Area	
Cushion Height	EA	Butler 1985	1985	202	Lift	Cushion	DV	Cushion Height	
L/B ratio	EA	Butler 1985	1985	202	Lift	Cushion	DV	L/B Ratio	
Cushion pressure	EA	Butler 1985	1985	212	Lift	Cushion	DM	Cushion Pressure	
Wavemaking drag	EA	Butler 1985	1985	212	Lift	Cushion	PM	Cushion Wavemaking Drag	
Wavemaking drag to lift ratio	EA	Butler 1985	1985	213	Lift	Cushion	PM	Wavemaking Drag to Lift Ratio	
hump speed	EA	Butler 1985	1985	228	Lift	Cushion	DM	Hump Speed	
thrust at hump speed	EA	Butler 1985	1985	228	Lift	Cushion			
cushion height	EA	Lavis & Spaulding 1991	1991	60	Lift	Cushion	DV	Cushion Height	
ratio of cushion height to cushion beam amidships	EA	Lavis & Spaulding 1991	1991	60	Lift	Cushion	PM	Cushion Height to Cushion Beam Ratio	
center of cushion area position	EA	Lavis & Spaulding 1991	1991	61	Lift	Cushion			
total cushion airflow rate	EA	Lavis & Spaulding 1991	1991	63	Lift	Cushion	DV	Cushion Air Flow Rate	
cushion wavemaking drag	EA	Lavis & Spaulding 1991	1991	64	Lift	Cushion	PM	Cushion Wavemaking Drag	
air fan inlet bellmouth geometry	EA	Lavis & Spaulding 1991	1991	63	Lift	Ducts			
air fan inlet shroud geometry	EA	Lavis & Spaulding 1991	1991	63	Lift	Ducts			
air fan inlet shroud-bellmouth clearance	EA	Lavis & Spaulding 1991	1991	63	Lift	Ducts			
Heave Damping	EA	Butler 1985	1985	220	Lift	Fan	PM	Heave motion attenuation	
Slope of the lift fan curve	EA	Butler 1985	1985	220	Lift	Fan			
fan type	EA	Butler 1985	1985	234	Lift	Fan			
fan rpm	EA	Butler 1985	1985	234	Lift	Fan			
pressure rise	EA	Butler 1985	1985	234	Lift	Fan			
airflow	EA	Butler 1985	1985	235	Lift	Fan			
fan wheel angular velocity	EA	Butler 1985	1985	235	Lift	Fan			
fan blade diameter	EA	Butler 1985	1985	235	Lift	Fan			
fan blade tip speed	EA	Butler 1985	1985	235	Lift	Fan			
total fan adiabatic head	EA	Butler 1985	1985	235	Lift	Fan			
absolute pressure at fan discharge	EA	Butler 1985	1985	235	Lift	Fan			
absolute pressure at fan inlet	EA	Butler 1985	1985	235	Lift	Fan			
fan flow coefficient	EA	Butler 1985	1985	235	Lift	Fan			

continued...

continued from previous page

Source Text	Type	Source	Year	Page	System	Sub-System	Type of EA	Final Title	Notes
fan pressure coefficient	EA	Butler 1985	1985	235	Lift	Fan			
fan speed coefficient	EA	Butler 1985	1985	235	Lift	Fan			
fan diameter coefficient	EA	Butler 1985	1985	235	Lift	Fan			
fan state-of-the-art efficiency	EA	Butler 1985	1985	235	Lift	Fan			
fan aerodynamic efficiency	EA	Butler 1985	1985	235	Lift	Fan			
fan stability characteristics	EA	Butler 1985	1985	235	Lift	Fan			
fan combatibility with variable geometry ride control system	EA	Butler 1985	1985	235	Lift	Fan			
fan mass	EA	Butler 1985	1985	237	Lift	Fan			
bandwidth for fan geometry variations	EA	Butler 1985	1985	237	Lift	Fan			
fan fatigue life	EA	Butler 1985	1985	237	Lift	Fan			
duct occupied volume	EA	Butler 1985	1985	238	Lift	Fan			
air fan efficiency	EA	Lavis & Spaulding 1991	1991	63	Lift	Fan			
fan pressure-flow characteristic	EA	Lavis & Spaulding 1991	1991	63	Lift	Fan			
fan flow capacity	EA	Lavis & Spaulding 1991	1991	63	Lift	Fan			
fan volute size	EA	Lavis & Spaulding 1991	1991	63	Lift	Fan			
fan volute shape	EA	Lavis & Spaulding 1991	1991	63	Lift	Fan			
fan cut-off lip configuration	EA	Lavis & Spaulding 1991	1991	63	Lift	Fan			
fan noise	EA	Lavis & Spaulding 1991	1991	63	Lift	Fan			
Slope of the lift fan curve	EA	Lavis & Spaulding 1991	1991	63	Lift	Fan			
fan space occupied	EA	Lavis & Spaulding 1991	1991	63	Lift	Fan			
fan weight	EA	Lavis & Spaulding 1991	1991	63	Lift	Fan			
Fuel Efficiency	EA	Butler 1985	1985	203	Lift	Lift Engine	PM	Fuel Efficiency	
control system's bandwidth	EA	Butler 1985	1985	221	Lift	RCS	PM	Control System Bandwidth	
cushion in-flow	EA	Butler 1985	1985	221	Lift	RCS			
cushion out-flow	EA	Butler 1985	1985	221	Lift	RCS			
control law coefficients	EA	Butler 1985	1985	221	Lift	RCS			
control power	EA	Butler 1985	1985	221	Lift	RCS			
actuator motions	EA	Butler 1985	1985	221	Lift	RCS			
ride control system stability	EA	Butler 1985	1985	222	Lift	RCS	PM	Ride control system satbility	
ride control system performance	EA	Butler 1985	1985	222	Lift	RCS			
vent valve motions	EA	Butler 1985	1985	222	Lift	RCS			
Bow Seal Stiffness	EA	Eggington & Kobitz 1975	1975	272	Lift	Seals			
Seal Material Thickness	EA	Eggington & Kobitz 1975	1975	273	Lift	Seals			
Seal drag	EA	Eggington & Kobitz 1975	1975	273	Lift	Seals			
Seal Drag in seaway	EA	Eggington & Kobitz 1975	1975	279	Lift	Seals			
Seal compliance in a seaway	EA	Eggington & Kobitz 1975	1975	279	Lift	Seals			

continued...

continued from previous page

Source Text	Type	Source	Year	Page	System	Sub-System	Type of EA	Final Title	Notes
Seal tear strength	EA	Eggington & Kobitz 1975	1975	280	Lift	Seals			
Elastomer abrasion resistance	EA	Eggington & Kobitz 1975	1975	280	Lift	Seals			
Seal saewater degradation resistance	EA	Eggington & Kobitz 1975	1975	280	Lift	Seals			
Seal joint adhesion	EA	Eggington & Kobitz 1975	1975	280	Lift	Seals			
Seal fabric to elastomer adhesion	EA	Eggington & Kobitz 1975	1975	280	Lift	Seals			
Stern seal responsiveness	EA	Eggington & Kobitz 1975	1975	281	Lift	Seals			
Seal leakage	EA	Eggington & Kobitz 1975	1975	281	Lift	Seals			
Seal air flow rate	EA	Eggington & Kobitz 1975	1975	281	Lift	Seals			
Seal contact area	EA	Eggington & Kobitz 1975	1975	282	Lift	Seals			
Seal drag coefficient	EA	Eggington & Kobitz 1975	1975	282	Lift	Seals			
Air Leakage	EA	Butler 1985	1985	200	Lift	Seals			
Stern seal flow gap	EA	Butler 1985	1985	203	Lift	Seals			
Seal drag	EA	Butler 1985	1985	212	Lift	Seals			
Seal skin friction drag	EA	Butler 1985	1985	213	Lift	Seals			
pitch stability	EA	Butler 1985	1985	240	Lift	Seals			
seal air leakage	EA	Butler 1985	1985	240	Lift	Seals			
seal lift	EA	Butler 1985	1985	240	Lift	Seals			
seal drag	EA	Butler 1985	1985	240	Lift	Seals			
seal wetting	EA	Butler 1985	1985	240	Lift	Seals			
seal viscous draf	EA	Butler 1985	1985	240	Lift	Seals			
seal wave making drag	EA	Butler 1985	1985	240	Lift	Seals			
roll stability	EA	Butler 1985	1985	240	Lift	Seals			
seal related cushion area change	EA	Butler 1985	1985	240	Lift	Seals			
sealing efficiency	EA	Butler 1985	1985	241	Lift	Seals			
seal free edge length	EA	Butler 1985	1985	241	Lift	Seals			
seal fabric	EA	Butler 1985	1985	242	Lift	Seals			
seal wear rate	EA	Butler 1985	1985	242	Lift	Seals			
seal fabric water permeability	EA	Butler 1985	1985	242	Lift	Seals			
seal fabric air permeability	EA	Butler 1985	1985	242	Lift	Seals			
seal fabric mass	EA	Butler 1985	1985	242	Lift	Seals			
seal fabric motion damping	EA	Butler 1985	1985	242	Lift	Seals			
seal fabric to cord adhesion	EA	Butler 1985	1985	242	Lift	Seals			
seal structural strength	EA	Butler 1985	1985	242	Lift	Seals			
seal fatigue life	EA	Butler 1985	1985	242	Lift	Seals			
seal peel resistance	EA	Butler 1985	1985	243	Lift	Seals			
seal intralamina bond strength	EA	Butler 1985	1985	243	Lift	Seals			
seal fabric durability	EA	Butler 1985	1985	243	Lift	Seals			
seal fabric strength	EA	Butler 1985	1985	243	Lift	Seals			
seal finger size	EA	Butler 1985	1985	244	Lift	Seals			
seal finger strength	EA	Butler 1985	1985	244	Lift	Seals			

continued...

continued from previous page

Source Text	Type	Source	Year	Page	System	Sub-System	Type of EA	Final Title	Notes
number of seal fingers	EA	Butler 1985	1985	244	Lift	Seals			
seal finger radius	EA	Butler 1985	1985	244	Lift	Seals			
seal finger length	EA	Butler 1985	1985	244	Lift	Seals			
seal finger redundancy	EA	Butler 1985	1985	244	Lift	Seals			
seal finger weight	EA	Butler 1985	1985	244	Lift	Seals			
seal compliance	EA	Lavis & Spaulding 1991	1991	61	Lift	Seals			
seal responsiveness	EA	Lavis & Spaulding 1991	1991	61	Lift	Seals			
seal drag	EA	Lavis & Spaulding 1991	1991	61	Lift	Seals			
seal finger redundancy	EA	Lavis & Spaulding 1991	1991	61	Lift	Seals			
restoring moments during slamming	EA	Lavis & Spaulding 1991	1991	61	Lift	Seals			
bow seal bag presssure	EA	Lavis & Spaulding 1991	1991	61	Lift	Seals			
bow seal finger to water surface exterior angle	EA	Lavis & Spaulding 1991	1991	61	Lift	Seals			
bow seal finger wetted length	EA	Lavis & Spaulding 1991	1991	61	Lift	Seals			
bow seal finger drag	EA	Lavis & Spaulding 1991	1991	61	Lift	Seals			
bow seal finger recovery time after deflection	EA	Lavis & Spaulding 1991	1991	61	Lift	Seals			
seal fabric stiffness	EA	Lavis & Spaulding 1991	1991	61	Lift	Seals			
seal fabric shear resistance	EA	Lavis & Spaulding 1991	1991	61	Lift	Seals			
ratio of finger depth to cushion depth	EA	Lavis & Spaulding 1991	1991	62	Lift	Seals			
bow seal finger life	EA	Lavis & Spaulding 1991	1991	62	Lift	Seals			
bow seal finger depth-to-width ratio	EA	Lavis & Spaulding 1991	1991	62	Lift	Seals			
bow seal bag inflated radius	EA	Lavis & Spaulding 1991	1991	62	Lift	Seals			
bow seal bag inflated pressure	EA	Lavis & Spaulding 1991	1991	62	Lift	Seals			
stern seal pressure	EA	Lavis & Spaulding 1991	1991	62	Lift	Seals			
Seal drag	EA	Lavis & Spaulding 1991	1991	64	Lift	Seals			
Ventral Fin Lift	EA	Eggington & Kobitz 1975	1975	272	Lift				
Lift Power	EA	Eggington & Kobitz 1975	1975	273	Lift		DV	Lift Power	
Air momentum drag	EA	Eggington & Kobitz 1975	1975	273	Lift				
Lift System efficiency	EA	Eggington & Kobitz 1975	1975	281	Lift		PM	Lift System Efficiency	
Lift system duct efficiency	EA	Eggington & Kobitz 1975	1975	281	Lift				
Lift fan efficiency	EA	Eggington & Kobitz 1975	1975	281	Lift				
Lift Power	EA	Butler 1985	1985	200	Lift		DV	Lift Power	
Lift air supply rate	EA	Butler 1985	1985	203	Lift				
on cushion wetdeck height	EA	Butler 1985	1985	204	Lift		DV	Cushion Height	

continued...

continued from previous page

Source Text	Type	Source	Year	Page	System	Sub-System	Type of EA	Final Title	Notes
large sea motion reduction	EA	Butler 1985	1985	204	Lift		PM	Large wave motion attenuation	
Lift system capacity	EA	Butler 1985	1985	205	Lift		DM	Lift System capacity	
On cushion freeboard	EA	Butler 1985	1985	205	Lift		DV	On Cushion Freeboard	
Lift Power	EA	Butler 1985	1985	212	Lift		DV	Lift Power	
Cushion air flow rate	EA	Butler 1985	1985	212	Lift				
lift power	EA	Butler 1985	1985	222	Lift		DV	Lift Power	
number of fans	EA	Butler 1985	1985	234	Lift				
total airflow	EA	Butler 1985	1985	234	Lift				
wave pumping cushion air leakage	EA	Butler 1985	1985	241	Lift				
Propulsive power	EA	Butler 1985	1985	212	Propulsion	Engine	DV	Installed Power	
Total Ship Shaft Horsepower	EA	Butler 1985	1985	216	Propulsion	Engine	DV	Installed Power	
engine matching	EA	Butler 1985	1985	227	Propulsion	Engine			
engine power-torque-rpm limits	EA	Butler 1985	1985	228	Propulsion	Engine			
horsepower level	EA	Butler 1985	1985	228	Propulsion	Engine			
Propulsor spacing	EA	Butler 1985	1985	219	Propulsion	Propulsor			
Propulsor efficiency	EA	Butler 1985	1985	226	Propulsion	Propulsor			
Propulsor volume	EA	Butler 1985	1985	226	Propulsion	Propulsor			
Propulsor noise	EA	Butler 1985	1985	226	Propulsion	Propulsor			
Propulsive Efficiency	EA	Butler 1985	1985	227	Propulsion	Propulsor	PM	Propulsive Efficiency	
propeller pitch	EA	Butler 1985	1985	227	Propulsion	Propulsor			
submerged disk area	EA	Butler 1985	1985	228	Propulsion	Propulsor			
effective propeller disk area	EA	Butler 1985	1985	228	Propulsion	Propulsor			
air ingestion probability	EA	Butler 1985	1985	228	Propulsion	Propulsor			FM
propulsor broaching probability	EA	Butler 1985	1985	228	Propulsion	Propulsor			FM
waterjet inlet draft	EA	Lavis & Spaulding 1991	1991	58	Propulsion	Propulsor			
Cross-flow of air to waterjet inlet	EA	Lavis & Spaulding 1991	1991	60	Propulsion	Propulsor			
waterjet inlet recovery	EA	Lavis & Spaulding 1991	1991	75	Propulsion	Propulsor			
waterjet pump efficiency	EA	Lavis & Spaulding 1991	1991	75	Propulsion	Propulsor			
waterjet nozzle efficiency	EA	Lavis & Spaulding 1991	1991	75	Propulsion	Propulsor			
waterjet inlet broching frequency	EA	Lavis & Spaulding 1991	1991	75	Propulsion	Propulsor			
waterjet inlet submergence	EA	Lavis & Spaulding 1991	1991	75	Propulsion	Propulsor			
Propulsor efficiency	EA	Pustoshny & Rusetsky 2006	2006	82	Propulsion	Propulsor			
Drivetrain simplicity	EA	Butler 1985	1985	203	Propulsion	Transmission			
Power transmission volume	EA	Butler 1985	1985	228	Propulsion	Transmission			
shaft loading	EA	Butler 1985	1985	228	Propulsion	Transmission			
Transmission gear ratio	EA	Butler 1985	1985	228	Propulsion	Transmission			
Installed Power	EA	Eggington & Kobitz 1975	1975	268	Propulsion		DV	Installed Power	

continued...

continued from previous page

Source Text	Type	Source	Year	Page	System	Sub-System	Type of EA	Final Title	Notes
Thrust	EA	Eggington & Kobitz 1975	1975	268	Propulsion				
Thrust	EA	Eggington & Kobitz 1975	1975	273	Propulsion				
Waterjet pump headrise	EA	Eggington & Kobitz 1975	1975	280	Propulsion				
Waterjet flow rate	EA	Eggington & Kobitz 1975	1975	280	Propulsion				
Waterjet inlet ram recovery	EA	Eggington & Kobitz 1975	1975	280	Propulsion				
Propulsive Efficiency	EA	Eggington & Kobitz 1975	1975	281	Propulsion		PM	Propulsive Efficiency	
Propulsion Efficiency	EA	Butler 1985	1985	200	Propulsion		PM	Propulsive Efficiency	
Thrust available to weight	EA	Butler 1985	1985	214	Propulsion				
thrust contribution to pitching moment	EA	Lavis & Spaulding 1991	1991	61	Propulsion				
Total Drag	EA	Eggington & Kobitz 1975	1975	273	SES		PM	Total resistance	
First Cost/Capacity*Speed	EA	Eggington & Kobitz 1975	1975	275	SES		PM	First Cost/Capacity*Speed	
Installed Power/-Capacity*Speed	EA	Eggington & Kobitz 1975	1975	275	SES		PM	Installed Power/-Capacity*Speed	
Fuel Weight Fraction	EA	Eggington & Kobitz 1975	1975	278	SES		PM	Fuel Weight Fraction	
Stopping distance	EA	Eggington & Kobitz 1975	1975	278	SES		PM	Stopping Distance	
Range	EA	Eggington & Kobitz 1975	1975	282	SES		CT	Range	
Specific Power SHP/Ton.Knot	EA	Eggington & Kobitz 1975	1975	282	SES		PM	Specific Power SHP/Ton.Knot	
Total Drag/Gross Weight	EA	Eggington & Kobitz 1975	1975	282	SES		PM	Total Drag/Gross Weight	
Longitudinal Stability	EA	Butler 1985	1985	200	SES		PM	Pitch motion attenuation	
Panama Canal	EA	Butler 1985	1985	202	SES		CT	Panama Canal width	
Transverse stability	EA	Butler 1985	1985	202	SES		PM	Transverse stability	
Sea state	EA	Butler 1985	1985	202	SES		PM	Design sea state	
Required Speed	EA	Butler 1985	1985	202	SES		PM	Design Speed	
Resistance	EA	Butler 1985	1985	202	SES		PM	Total resistance	
Range	EA	Butler 1985	1985	204	SES		CT	Range	
Volume efficiency	EA	Butler 1985	1985	204	SES		PM	Payload	
Total powering requirements	EA	Butler 1985	1985	205	SES		DV	Installed Power	
Hull slamming threshold	EA	Butler 1985	1985	205	SES		PM	Hull Slamming Threshold	
Stability	EA	Butler 1985	1985	205	SES		PM	Static Stability	
tons-per-inch immersion	EA	Butler 1985	1985	205	SES				
moment-to-trim	EA	Butler 1985	1985	205	SES				
heave motions	EA	Butler 1985	1985	206	SES		PM	Heave motion attenuation	
pitch motions	EA	Butler 1985	1985	206	SES		PM	Pitch motion attenuation	
Roll motions	EA	Butler 1985	1985	206	SES		PM	Roll motion attenuation	
Operating cost	EA	Butler 1985	1985	207	SES		PM	Operating Cost	
Endurance	EA	Butler 1985	1985	208	SES		CT	Range	
Service power	EA	Butler 1985	1985	212	SES		DV	Installed Power	
Lightship weight	EA	Butler 1985	1985	216	SES		PM	Lightship Weight	
vertical centre of gravity position	EA	Butler 1985	1985	218	SES		DM	VCG Height	
3-degree single amplitude limit	EA	Butler 1985	1985	222	SES		PM	Ride Comfort	

continued...

continued from previous page

Source Text	Type	Source	Year	Page	System	Sub-System	Type of EA	Final Title	Notes
RMS heave accelerations	EA	Butler 1985	1985	222	SES		PM	RMS Heave accelerations	
SES pitch motions	EA	Butler 1985	1985	222	SES		PM	Pitch motion attenuation	
pitch damping	EA	Butler 1985	1985	222	SES		PM	Pitch motion attenuation	
weight distribution	EA	Butler 1985	1985	222	SES				
centre of gravity height	EA	Butler 1985	1985	224	SES		DM	VCG Height	
total ship size	EA	Butler 1985	1985	224	SES		DV	Length	
resistance	EA	Butler 1985	1985	224	SES		PM	Total resistance	
heave stiffness	EA	Butler 1985	1985	224	SES		PM	Heave motion attenuation	
heave damping	EA	Butler 1985	1985	224	SES		PM	Heave motion attenuation	
total ship weight	EA	Butler 1985	1985	224	SES		PM	Lightship Weight	
roll stiffness	EA	Butler 1985	1985	224	SES		PM	Roll motion attenuation	
roll damping	EA	Butler 1985	1985	224	SES		PM	Roll motion attenuation	
static roll stability	EA	Butler 1985	1985	224	SES		PM	Roll Stability	
range	EA	Butler 1985	1985	227	SES		CT	Range	
endurance	EA	Butler 1985	1985	227	SES		CT	Range	
L/B ratio	EA	Butler 1985	1985	227	SES		DV	L/B Ratio	
ship size	EA	Butler 1985	1985	227	SES		DV	Length	
fuel economy	EA	Butler 1985	1985	227	SES		PM	Fuel Efficiency	
top speed	EA	Butler 1985	1985	227	SES		PM	Maximum Speed	
cruise speeds	EA	Butler 1985	1985	227	SES		PM	Design Speed	
resistance curve	EA	Butler 1985	1985	227	SES		PM	Total resistance	
range	EA	Butler 1985	1985	228	SES		CT	Range	
endurance	EA	Butler 1985	1985	228	SES		CT	Range	
mitigtaion of effect of rough seas on craft motions	EA	Lavis & Spaulding 1991	1991	57	SES		PM	Heave motion attenuation	
craft resistance to forward motion at high speed	EA	Lavis & Spaulding 1991	1991	57	SES		PM	Total resistance	
Cushion pressure	EA	Lavis & Spaulding 1991	1991	58	SES		DM	Cushion Pressure	
sidehull wetted surface area	EA	Lavis & Spaulding 1991	1991	58	SES		DM	Sidehull Wetted Area	
Cushion air flow rate	EA	Lavis & Spaulding 1991	1991	58	SES		DV	Cushion Air Flow Rate	
lift power	EA	Lavis & Spaulding 1991	1991	58	SES		DV	Lift Power	
total installed horsepower per ton	EA	Lavis & Spaulding 1991	1991	58	SES		PM	Installed Power/-Ton	
ratio of cushion height to significant wave height	EA	Lavis & Spaulding 1991	1991	58	SES		PM	Cushion Height to Significant Wave Height Ratio	
cushion wave drag	EA	Lavis & Spaulding 1991	1991	58	SES		PM	Cushion Wave-making Drag	
sidehull time-average draft	EA	Lavis & Spaulding 1991	1991	58	SES		PM	On-Cushion Draft	
pitch motions	EA	Lavis & Spaulding 1991	1991	58	SES		PM	Pitch motion attenuation	
Propulsive Efficiency	EA	Lavis & Spaulding 1991	1991	58	SES		PM	Propulsive Efficiency	
sidehull drag	EA	Lavis & Spaulding 1991	1991	58	SES		PM	Sidehull Drag	
design speed Froude number	EA	Lavis & Spaulding 1991	1991	58	SES		PM	Design Speed Froude Number	

continued...

continued from previous page

Source Text	Type	Source	Year	Page	System	Sub-System	Type of EA	Final Title	Notes
weight sensitivity	EA	Lavis & Spaulding 1991	1991	58	SES		PM	Weight Sensitivity	
construction limits	EA	Lavis & Spaulding 1991	1991	59	SES		CT	Capital Cost	
payload-deck area	EA	Lavis & Spaulding 1991	1991	59	SES		DV	Deck Area	
cushion area	EA	Lavis & Spaulding 1991	1991	59	SES		DV	Cushion Area	
Cushion breadth	EA	Lavis & Spaulding 1991	1991	59	SES		DV	Cushion Width	
cushion length	EA	Lavis & Spaulding 1991	1991	59	SES		DV	Cushion Length	
cushion length-to-beam ratio	EA	Lavis & Spaulding 1991	1991	59	SES		DV	L/B Ratio	
overall craft size	EA	Lavis & Spaulding 1991	1991	59	SES		DV	Length	
wave-making drag of the cushion	EA	Lavis & Spaulding 1991	1991	59	SES		PM	Cushion Wave-making Drag	
rms vertical acceleration at the centre of gravity	EA	Lavis & Spaulding 1991	1991	59	SES		PM	RMS Heave accelerations	
rms vertical acceleration at the bow	EA	Lavis & Spaulding 1991	1991	59	SES		PM	RMS vertical accelerations at bow	
dynamic stability	EA	Lavis & Spaulding 1991	1991	59	SES		PM	Dynamic stability	
static stability	EA	Lavis & Spaulding 1991	1991	59	SES		PM	Static Stability	
total drag of the craft	EA	Lavis & Spaulding 1991	1991	59	SES		PM	Total resistance	
freeboard to beam ratio overall	EA	Lavis & Spaulding 1991	1991	60	SES		DM		
cushion height-to-beam overall	EA	Lavis & Spaulding 1991	1991	60	SES		DM		
VCG height-to-beam overall	EA	Lavis & Spaulding 1991	1991	60	SES		DM		
cushion pressure to length ratio	EA	Lavis & Spaulding 1991	1991	60	SES		DM		
cushion length-to-beam ratio	EA	Lavis & Spaulding 1991	1991	60	SES		DV	L/B Ratio	
wet-deck clearance off-cushion	EA	Lavis & Spaulding 1991	1991	60	SES		DV	Off-Cushion Wet Deck Height	
draft off-cushion	EA	Lavis & Spaulding 1991	1991	60	SES		PM	Off-Cushion Draft	
space for machinery installation in sidehulls	EA	Lavis & Spaulding 1991	1991	60	SES		PM	Machinery Accomodation volume	
pitching	EA	Lavis & Spaulding 1991	1991	60	SES		PM	Pitch motion attenuation	
on cushion wet-deck slamming incidence	EA	Lavis & Spaulding 1991	1991	60	SES		PM	Slamming Incidence	
off-cushion wet-deck slamming incidence	EA	Lavis & Spaulding 1991	1991	60	SES		PM	Slamming Incidence	
lift during bow submergence	EA	Lavis & Spaulding 1991	1991	60	SES		PM		
pounding	EA	Lavis & Spaulding 1991	1991	60	SES				
sidehull dynamic lift during turning	EA	Lavis & Spaulding 1991	1991	60	SES				
waterjet inlet accomodation	EA	Lavis & Spaulding 1991	1991	60	SES				

continued...

continued from previous page

Source Text	Type	Source	Year	Page	System	Sub-System	Type of EA	Final Title	Notes
cushion density	EA	Lavis & Spaulding 1991	1991	60	SES				
craft heave stiffness	EA	Lavis & Spaulding 1991	1991	61	SES		PM	Heave motion attenuation	
craft pitch stiffness	EA	Lavis & Spaulding 1991	1991	61	SES		PM	Pitch motion attenuation	
trim angle	EA	Lavis & Spaulding 1991	1991	61	SES				
rough water stability	EA	Lavis & Spaulding 1991	1991	62	SES		PM	Heave motion attenuation	
rough water drag	EA	Lavis & Spaulding 1991	1991	62	SES		PM	Seaway Resistance	
vessel heave stability	EA	Lavis & Spaulding 1991	1991	63	SES		PM	Heave motion attenuation	
installed power per ton knot	EA	Lavis & Spaulding 1991	1991	66	SES		PM	Specific Power SHP/Ton.Knot	
Lightship weight	EA	Lavis & Spaulding 1991	1991	66	SES		PM	Lightship Weight	
installed power	EA	Lavis & Spaulding 1991	1991	67	SES				
total electrical load	EA	Lavis & Spaulding 1991	1991	67	SES				
disposable load	EA	Lavis & Spaulding 1991	1991	68	SES		PM	Deadweight	
fuel load	EA	Lavis & Spaulding 1991	1991	68	SES		PM	Fuel Load	
full-load displacement	EA	Lavis & Spaulding 1991	1991	68	SES		PM	Full Load Displacement	
magnitude and frequency of vertical accelerations	EA	Lavis & Spaulding 1991	1991	68	SES		PM	Heave motion attenuation	
amplitude and period of heave motions	EA	Lavis & Spaulding 1991	1991	68	SES		PM	Heave motion attenuation	
amplitude and period of pitch motions	EA	Lavis & Spaulding 1991	1991	68	SES		PM	Pitch motion attenuation	
amplitude and period of roll motions	EA	Lavis & Spaulding 1991	1991	68	SES		PM	Roll motion attenuation	
course-keeping in a seaway	EA	Lavis & Spaulding 1991	1991	68	SES		PM	Yaw Stability	
magnitude and frequency of longitudinal accelerations	EA	Lavis & Spaulding 1991	1991	68	SES		PM	Surge motion attentuation	
magnitude and frequency of lateral accelerations	EA	Lavis & Spaulding 1991	1991	68	SES		PM	Sway motion attenuation	
frequency of propulsor broaching	EA	Lavis & Spaulding 1991	1991	68	SES		PM		
frequency of shipping water on deck	EA	Lavis & Spaulding 1991	1991	68	SES		PM	Green water on deck incidence	
shock induced strcutural loads	EA	Lavis & Spaulding 1991	1991	68	SES		PM		
vibration induced structural loads	EA	Lavis & Spaulding 1991	1991	68	SES		PM		
intact hullborne stability	EA	Lavis & Spaulding 1991	1991	70	SES		PM	Static Stability	
on-cushion heave stability	EA	Lavis & Spaulding 1991	1991	71	SES		PM	Heave motion attenuation	
on-cushion pitch stability	EA	Lavis & Spaulding 1991	1991	71	SES		PM	Pitch motion attenuation	

continued...

continued from previous page

Source Text	Type	Source	Year	Page	System	Sub-System	Type of EA	Final Title	Notes
on-cushion roll stability at high speed	EA	Lavis & Spaulding 1991	1991	71	SES		PM	Roll Stability at speed	
on-cushion roll stability at hover	EA	Lavis & Spaulding 1991	1991	71	SES		PM	Roll Stability at hover	
roll stability in turning	EA	Lavis & Spaulding 1991	1991	71	SES		PM	Roll Stability during turn	
roll stability in beam seas	EA	Lavis & Spaulding 1991	1991	71	SES		PM	Roll Stability	
damaged hull-borne stability	EA	Lavis & Spaulding 1991	1991	71	SES		PM	Static Stability	
directional (yaw) stability	EA	Lavis & Spaulding 1991	1991	71	SES		PM	Yaw Stability	
cost per passenger mile	EA	Lavis & Spaulding 1991	1991	78	SES		PM	Operating Cost / Passengers*Miles	
seasickness incidence	EA	Lavis & Spaulding 1991	1991	78	SES		PM	Seasickness Incidence	
passenger discomfort incidence	EA	Lavis & Spaulding 1991	1991	78	SES		PM	Passenger Discomfort Incidence	
cabin noise	EA	Lavis & Spaulding 1991	1991	78	SES		PM	Cabin Noise	
rms acceleration	EA	Lavis & Spaulding 1991	1991	78	SES		PM	RMS acceleration	
roll period	EA	Lavis & Spaulding 1991	1991	78	SES		PM	Roll Period	
deck area	EA	Lavis & Spaulding 1991	1991	79	SES		DV	Deck Area	
enclosed volume	EA	Lavis & Spaulding 1991	1991	79	SES		PM	Gross Tonnage	
range	EA	Sugai & Yamaguchi 1991	1991	672	SES		CT	Range	
hull surface area near waterline	EA	Sugai & Yamaguchi 1991	1991	674	SES		DM		
engine power	EA	Sugai & Yamaguchi 1991	1991	674	SES		DV	Installed Power	
structural weight	EA	Sugai & Yamaguchi 1991	1991	674	SES		PM	Lightship Weight	
hull form resistance	EA	Sugai & Yamaguchi 1991	1991	674	SES		PM	Sidehull Drag	
propulsion system power	EA	Sugai & Yamaguchi 1991	1991	675	SES		DV	Installed Power	
maintainance cost	EA	Sugai & Yamaguchi 1991	1991	675	SES		PM	Maintenance Cost	
hull weight	EA	Sugai & Yamaguchi 1991	1991	675	SES		PM	Lightship Weight	
propulsion system reliability	EA	Sugai & Yamaguchi 1991	1991	675	SES		PM		
range	EA	Instefjord et al. 1996	1996	18	SES		CT	Range	
endurance	EA	Instefjord et al. 1996	1996	18	SES		CT	Range	
large beam	EA	Instefjord et al. 1996	1996	18	SES		DV	Beam	
deck area	EA	Instefjord et al. 1996	1996	18	SES		DV	Deck Area	
wetted surface area	EA	Instefjord et al. 1996	1996	18	SES		PM	Sidehull Drag	
important system reducndancy	EA	Instefjord et al. 1996	1996	18	SES		PM		
propulsion power	EA	Instefjord et al. 1996	1996	19	SES		DV	Installed Power	
cushion wavemaking resistance	EA	Instefjord et al. 1996	1996	19	SES		PM	Cushion Wavemaking Drag	
vessel weight	EA	Instefjord et al. 1996	1996	19	SES		PM	Lightship Weight	

continued...

continued from previous page

Source Text	Type	Source	Year	Page	System	Sub-System	Type of EA	Final Title	Notes
weight sensitivity	EA	Instefjord et al. 1996	1996	19	SES		PM	Weight Sensitivity	
fan characteristic	EA	Instefjord et al. 1996	1996	19	SES				
displacement	EA	Pustoshny & Rusetsky 2006	2006	82	SES		PM	Displacement	
full-speed resistance	EA	Pustoshny & Rusetsky 2006	2006	82	SES		PM	Total resistance	
propulsor size	EA	Pustoshny & Rusetsky 2006	2006	82	SES				
sidewall width	EA	Pustoshny & Rusetsky 2006	2006	82	SES				
seal reliability	EA	Pustoshny & Rusetsky 2006	2006	82	SES				
design simplicity	EA	Pustoshny & Rusetsky 2006	2006	88	SES		PM	Producibility	
draught	EA	Pustoshny & Rusetsky 2006	2006	88	SES		PM	Producibility	
frictional resistance	EA	Pustoshny & Rusetsky 2006	2006	88	SES		PM	Sidehull Drag	
lift-drag ratios	EA	Pustoshny & Rusetsky 2006	2006	88	SES		PM		
residual resistance coefficient	EA	Pustoshny & Rusetsky 2006	2006	89	SES		PM	Cushion Wavemaking Drag	
friction coefficient	EA	Pustoshny & Rusetsky 2006	2006	89	SES		PM	Sidehull Drag	
displacement Froude number	EA	Pustoshny & Rusetsky 2006	2006	89	SES		PM	Displacement Froude Number	
stability	EA	Pustoshny & Rusetsky 2006	2006	89	SES		PM	Static Stability	
dynamics in rough seas	EA	Pustoshny & Rusetsky 2006	2006	89	SES		PM		
acceleration loads in rough seas	EA	Pustoshny & Rusetsky 2006	2006	89	SES		PM		
static loading ($V/L\hat{3}$)	EA	Pustoshny & Rusetsky 2006	2006	89	SES				
hull length-beam ratios	EA	Pustoshny & Rusetsky 2006	2006	89	SES				
Endurance	EA	Matsumura et al. 2006	2006	92	SES		CT	Range	
cushion borne ratio	EA	Matsumura et al. 2006	2006	92	SES		DM	Cushion Pressure	
breadth moulded	EA	Matsumura et al. 2006	2006	92	SES		DV	Beam	
propulsion maximum continuous output	EA	Matsumura et al. 2006	2006	92	SES		DV	Installed Power	
length overall	EA	Matsumura et al. 2006	2006	92	SES		DV	Length	
length of design waterline	EA	Matsumura et al. 2006	2006	92	SES		DV	Length	
lift machinery maximum continuous output	EA	Matsumura et al. 2006	2006	92	SES		DV	Lift Power	
design draft moulded off-cushion	EA	Matsumura et al. 2006	2006	92	SES		DV	Off-Cushion Draft	
dead weight	EA	Matsumura et al. 2006	2006	92	SES		PM	Deadweight	
depth moulded	EA	Matsumura et al. 2006	2006	92	SES		PM	Off-Cushion Draft	
design draft moulded on-cushion	EA	Matsumura et al. 2006	2006	92	SES		PM	On-Cushion Draft	
round-trip fuel oil volume requirement	EA	Matsumura et al. 2006	2006	93	SES		PM	Fuel Load	

continued...

continued from previous page

Source Text	Type	Source	Year	Page	System	Sub-System	Type of EA	Final Title	Notes
heave response amplitude operator	EA	Matsumura et al. 2006	2006	94	SES		PM	Heave motion attenuation	
ISO2631-1(ISO 1997)	EA	Matsumura et al. 2006	2006	96	SES		CT	Limits on vibration exposure for humans	
crash stop horizontal accleration for 2000 HSC	EA	Matsumura et al. 2006	2006	97	SES		CT	Limit on horizontal acceleration in a crash stop	
comfort in terms of motion sickness incidence	EA	Matsumura et al. 2006	2006	97	SES		PM	Ride Comfort	
average of the significant accelerations in the public spaces	EA	Matsumura et al. 2006	2006	97	SES		PM	Heave motion attenuation	
vertical accelerations due to roll	EA	Matsumura et al. 2006	2006	97	SES		PM	Roll motion attenuation	
maximum horizontal acceleration	EA	Matsumura et al. 2006	2006	98	SES		CT	Limit on horizontal acceleration in a crash stop	
range	EA	Lavis & Forstell 2008	2008	59	SES		CT	Range	
ship length/beam ratio	EA	Lavis & Forstell 2008	2008	59	SES		DV	L/B Ratio	
ship length	EA	Lavis & Forstell 2008	2008	59	SES		DV	Length	
ship displacement	EA	Lavis & Forstell 2008	2008	59	SES		PM	Displacement	
ship draft	EA	Lavis & Forstell 2008	2008	59	SES		PM	On-Cushion Draft	
shaft power	EA	Lavis & Forstell 2008	2008	63	SES		DV	Installed Power	
manning	EA	Lavis & Forstell 2008	2008	63	SES		PM	Manning	
total drag	EA	Lavis & Forstell 2008	2008	63	SES		PM	Total resistance	
equipment weight	EA	Lavis & Forstell 2008	2008	63	SES				
equipment occupied volume	EA	Lavis & Forstell 2008	2008	63	SES				
equipment occupied deck area	EA	Lavis & Forstell 2008	2008	63	SES				
deck area	EA	Lavis & Forstell 2008	2008	64	SES		DV	Deck Area	
total fuel load	EA	Lavis & Forstell 2008	2008	64	SES		PM	Fuel Load	
lightship weight	EA	Lavis & Forstell 2008	2008	64	SES		PM	Lightship Weight	
hull surface frictional resistance	EA	Lavis & Forstell 2008	2008	65	SES				
wetted surface area	EA	Lavis & Forstell 2008	2008	65	SES				
hull material frictional resistance	EA	Lavis & Forstell 2008	2008	66	SES				
ship propulsive coefficient	EA	Lavis & Forstell 2008	2008	66	SES				
total installed power	EA	Lavis & Forstell 2008	2008	68	SES		DV	Installed Power	
cushion beam	EA	Lavis & Forstell 2008	2008	71	SES		DV	Cushion Width	
cushion height	EA	Lavis & Forstell 2008	2008	71	SES		DV	Cushion Height	
cushionborne stability	EA	Lavis & Forstell 2008	2008	71	SES		PM	Static Stability	
available engine power constraint	EA	Lavis & Forstell 2008	2008	73	SES		CT	Available Engine Power Constraint	
cushion width	EA	Lavis & Forstell 2008	2008	73	SES		DV	Cushion Width	

continued...

continued from previous page

Source Text	Type	Source	Year	Page	System	Sub-System	Type of EA	Final Title	Notes
cushion length	EA	Lavis & Forstell 2008	2008	73	SES		DV	Length	
full-load gross weight	EA	Lavis & Forstell 2008	2008	73	SES		PM	Full Load Displacement	
RO-RO vehicle lanes	EA	Lavis & Forstell 2008	2008	73	SES				
High speed rudder failure	FM	Butler 1985	1985	219	Hull	Control			
Roll instability	FM	Eggington & Kobitz 1975	1975	271	Hull	Sidehulls		Roll Instability	
Hull damage during collision with submerged object	FM	Eggington & Kobitz 1975	1975	277	Hull	Sidehulls		Hull Damage due to collision	
structural failure due to slamming in head seas	FM	Butler 1985	1985	224	Hull	Structural			
off-cushion bow slamming loads	FM	Butler 1985	1985	241	Hull				
Plow-in in chop	FM	Eggington & Kobitz 1975	1975	269	Lift	Cushion		Plough In	
Air cushion vent during turn	FM	Eggington & Kobitz 1975	1975	271	Lift	Cushion		Cushion Vent During Turn	
Cobblestone Effect	FM	Butler 1985	1985	220	Lift	Cushion		Cobblestoning	
fan failure	FM	Lavis & Spaulding 1991	1991	63	Lift	Fan			
lift engine failure	FM	Lavis & Spaulding 1991	1991	63	Lift	Lift Engine			
speed loss during RCS operation	FM	Butler 1985	1985	222	Lift	RCS			
Seal Fatigue	FM	Eggington & Kobitz 1975	1975	273	Lift	Seals		Seal Fatigue	
Seal abrasion	FM	Eggington & Kobitz 1975	1975	273	Lift	Seals		Seal Abrasion	
Seal damage due to collision with submerged object	FM	Eggington & Kobitz 1975	1975	277	Lift	Seals		Seal damage duye to collision	
wear of finger seals due to flagellation	FM	Butler 1985	1985	242	Lift	Seals			
flutter and erosion	FM	Butler 1985	1985	242	Lift	Seals			
abrasion	FM	Butler 1985	1985	242	Lift	Seals			
foreign object damage	FM	Butler 1985	1985	242	Lift	Seals			
impact with the ship's structure	FM	Butler 1985	1985	242	Lift	Seals			
wear at load concentration points	FM	Butler 1985	1985	242	Lift	Seals			
seal trailing edge intralamina bond failure	FM	Butler 1985	1985	242	Lift	Seals			
seal trailing edge intralamina bond erosion	FM	Butler 1985	1985	242	Lift	Seals			
seal finger delamination due to friction between adjacent fingers	FM	Butler 1985	1985	243	Lift	Seals			
rear seal wear failure due to abrasion with sidehull	FM	Butler 1985	1985	243	Lift	Seals			
seal failure due to snag	FM	Butler 1985	1985	243	Lift	Seals			
seal crack initiation due to snag	FM	Butler 1985	1985	243	Lift	Seals			

continued...

continued from previous page

Source Text	Type	Source	Year	Page	System	Sub-System	Type of EA	Final Title	Notes
seal puncture due to contact with wet deck	FM	Butler 1985	1985	243	Lift	Seals			
seal wear at load concentration points	FM	Butler 1985	1985	243	Lift	Seals			
bow seal finger scooping whilst movng astern	FM	Lavis & Spaulding 1991	1991	61	Lift	Seals			
bow finger extending outwards unsupported	FM	Lavis & Spaulding 1991	1991	61	Lift	Seals			
bow seal finger slow recovery from large deflections	FM	Lavis & Spaulding 1991	1991	62	Lift	Seals			
bow seal finger temporary hang-ups after large deflections	FM	Lavis & Spaulding 1991	1991	62	Lift	Seals			
bow seal collapse	FM	Lavis & Spaulding 1991	1991	62	Lift	Seals			
bow seal tuck-under	FM	Lavis & Spaulding 1991	1991	62	Lift	Seals			
wear and tear of the rubber bow and stern seals	FM	Instefjord et al. 1996	1996	23	Lift	Seals			
on-cushion bow slamming loads	FM	Butler 1985	1985	241	Lift				
High speed propulsion failure	FM	Butler 1985	1985	219	Propulsion	Propulsor			
Machinery Corrosion	FM	Eggington & Kobitz 1975	1975	269	SES			Machinery Corrosion	
Excessive Motions in rough water	FM	Eggington & Kobitz 1975	1975	270	SES			Excessive Motions	
Excessive accelerations in rough water	FM	Eggington & Kobitz 1975	1975	270	SES			Excessive Accelerations	
Overturn	FM	Eggington & Kobitz 1975	1975	271	SES			Capsize	
Loss of speed in a seaway	FM	Eggington & Kobitz 1975	1975	274	SES			Added Resistance in Seaway	
Top speed reduction due to weight growth	FM	Butler 1985	1985	206	SES			Overweight	
excessive power requirements due to longitudinal centre of gravity shift	FM	Butler 1985	1985	207	SES				
high frequency and high amplitude vertical accelerations	FM	Butler 1985	1985	207	SES			Excessive Accelerations	
Capsize	FM	Butler 1985	1985	218	SES			Capsize	
encounter period tunes with natural pitch perido	FM	Butler 1985	1985	222	SES				
slamming due to synchronous pitching	FM	Butler 1985	1985	222	SES				
slamming when wave heights exceed wet deck height	FM	Butler 1985	1985	223	SES				

continued...

continued from previous page

Source Text	Type	Source	Year	Page	System	Sub-System	Type of EA	Final Title	Notes
shipping of green water	FM	Butler 1985	1985	223	SES				
speed reduction in a seaway	FM	Lavis & Spaulding 1991	1991	68	SES				
roll/yaw oscillation in high speed turns	FM	Lavis & Spaulding 1991	1991	71	SES				
high-level accelerations	FM	Sugai & Yamaguchi 1991	1991	674	SES				
fragilation of seals	FM	Sugai & Yamaguchi 1991	1991	674	SES				
fatigue failure of hull	FM	Sugai & Yamaguchi 1991	1991	675	SES				
propeller cavitation	FM	Pustoshny & Rusetsky 2006	2006	89	SES				
propulsor vibration	FM	Pustoshny & Rusetsky 2006	2006	89	SES				
wet-deck slamming	FM	Matsumura et al. 2006	2006	93	SES				
air suction into the water-jets	FM	Matsumura et al. 2006	2006	93	SES				
air leakage from the cushion due to low draft	FM	Matsumura et al. 2006	2006	93	SES				
significant discomfort due to high-frequency vertical oscillations	FM	Matsumura et al. 2006	2006	93	SES				
propulsor broaching due to bow-down trim	FM	Lavis & Spaulding 1991	1991	61					
out-of-trim condition	FM	Lavis & Spaulding 1991	1991	61					
reduction in directional stability due to bow-down trim	FM	Lavis & Spaulding 1991	1991	61					
manueuvrability reduction due to bow-up trim	FM	Lavis & Spaulding 1991	1991	61					
increased vertical accelerations in a seaway due to bow-up trim	FM	Lavis & Spaulding 1991	1991	61					

C. Failure Mode and Effects Analyses

The results of the Failure Mode and Effects Analysis for the bow finger seals is given in Table C.1. The results of the Failure Mode and Effects Analysis for the stern bag seals is given in Table C.2. The method for the analyses is given in Sec. 3.7.

Table C.1. Surface Effect Ship Bow Seal Fingers FMEA

Function	Failure Mode	Effects of Failure	Causes of Failure	Detection	S1	O1	D1	RPN1	Mitigation	S2	O2	D2	RPN2
Sealing air cushion	flaking off seal surface	increased leakage rate, adjacent seals expand to partially fill gap	flagellation motions causing fatigue	visual inspection during scheduled maintenance	3	10	3	90	periodic replacement of individual fingers	3	1	3	9
Sealing air cushion	puncture of seal	increased leakage rate, adjacent seals expand to partially fill gap	striking a hard object in the water	visual inspection during scheduled maintenance	3	9	2	54	none suggested	3	9	2	54
Sealing air cushion	fatigue fracture	increased leakage rate, adjacent seals expand to partially fill gap	wave tracking flexure	visual inspection during scheduled maintenance	3	3	3	27	periodic replacement of individual fingers	3	1	3	9
Sealing air cushion	collapse	increased air flow rate, exceeding air supply capacity	large deflection forcing fingers into high pressure area	loss of hover height	8	3	9	216	adjust bag to support fingers better	3	1	7	21
Sealing air cushion	delamination	increased leakage rate, adjacent seals expand to partially fill gap	friction bewteen adjacent fingers	visual inspection during scheduled maintenance	3	5	2	30	periodic replacement of individual fingers	3	1	2	6
Sealing air cushion	erosion of fabric at tips	increased leakage rate, adjacent seals expand to partially fill gap	flutter of tips	visual inspection during scheduled maintenance	3	9	2	54	periodic replacement of individual fingers	3	2	2	12
Sealing air cushion	extension outwards	increased air flow rate, exceeding air supply capacity	cushion pressure blows seal outwards	loss of hover height	8	3	9	216	Restraining straps on fingers	2	1	6	12
Sealing air cushion	fatigue crack propogation	increased leakage rate, adjacent seals expand to partially fill gap	wear at load concentration points	visual inspection during scheduled maintenance	3	3	3	27	periodic replacement of individual fingers	3	1	3	9
Sealing air cushion	interference with water	high resistance forces in an unbalanced mode	water impinges during backwards motion	change in ship motion	4	5	7	140	none suggested	4	5	7	140
Sealing air cushion	intralamina bond erosion	increased leakage rate, adjacent seals expand to partially fill gap	high accelerations of finger tips	visual inspection during scheduled maintenance	3	8	5	120	periodic replacement of individual fingers	3	1	5	15
Sealing air cushion	intralamina bond failure	increased leakage rate, adjacent seals expand to partially fill gap	fatigue failure of bond	visual inspection during scheduled maintenance	3	8	2	48	periodic replacement of individual fingers	3	1	2	6
Sealing air cushion	fracture of seal fingers, due to wear of the seal surface	increased leakage rate, adjacent seals expand to partially fill gap	water abrasion	visual inspection during scheduled maintenance	3	4	2	24	periodic replacement of individual fingers	3	1	2	6

Table C.2. Surface Effect Ship Stern Bag Seal FMEA

Function	Failure Mode	Effects of Failure	Causes of Failure	Detection	S1	O1	D1	RPN1	Mitigation	S2	O2	D2	RPN2
Sealing air cushion	Puncture	increased air flow rate, exceeding air supply capacity	striking a hard object in the water	visual inspection at service	3	6	2	36	periodic replacement of stern seal bag	1	6	2	12
Sealing air cushion	Puncture	increased air flow rate, exceeding air supply capacity	Striking wet deck	visual inspection at service	3	2	2	12	periodic replacement of stern seal bag	1	2	2	4
Sealing air cushion	fatigue fracture at sides	increased air flow rate, exceeding air supply capacity	repeated striking of sidehullls	visual inspection at service	3	3	3	27	periodic replacement of stern seal bag	1	2	2	4
Sealing air cushion	fatigue fracture at joints	increased air flow rate, exceeding air supply capacity	periodic loads at attchment points	visual inspection at service	3	3	3	27	periodic replacement of stern seal bag	1	2	3	6

D. MATLAB code

D.1. Setup experimental rig properties

The measurements of the experimental rig are loaded into the workspace using the following script. Parameter values that must be calculated from the experimental rig measurements are calculated in the same script. The script is organised logically by the sub-systems and components of the experimental rig. The units of each value is both noted in the comments and incorporated into the variable name to mitigate the risk of computation errors due to the mismatch of units.

```
,
%% initialize Test Rig Properties
%
% Loads the measured, assumed and calculated static properties of the test
% rig, based on the spreadsheet of measurements. These are common to all
% experimental runs
%
% All parameters with units have the unit as a suffix for the varaible
% name, all units are in the singular. Division is indicated by 'Per',
% multiplication has no word, ^2 is 'Square' and ^3 is 'Cubic'. The item is
% named first, then the parameter, then the dimension, then the unit. E.g.
% heaveDeckPivotPointXMetre is the heave deck item, the pivot point is the
% parameter, x is the dimension and metre is the unit.
%
% initializeTestRigProperties

% Paul Minty 2012-04-04

% EDIT 20181014 - added oscillating flapper dimensions

% Last edit 20180916 - the transient flapper angle was corrected and the
% assumption that the air supply duct centreline speed was the same as the
% are-mean air velocity was also corrected.

%clear;
% clc;
%format short eng;

%% Global Constants
GRAVITATIONAL_CONSTANT_METRE_PER_SECOND_SQUARED = 9.81;
AIR_SPECIFIC_GAS_CONSTANT_JOULES_PER_KILOGRAM_PER_KELVIN = 287.04;
ICE_MELTING_POINT_KELVIN = 273.15;
SPECIFIC_HEAT_AIR = 1.4; %gamma
GAS_CONSTANT_AIR = 2.869E2;
STANDARD_ATMOSPHERIC_PRESSURE = 101325;

atmosPressureStaticNewtonPerSquareMetre = STANDARD_ATMOSPHERIC_PRESSURE; % assumed standard
    atmosphere for general analysis

%% Atmospheric Conditions
atmosAirDensityKilogramPerCubicMetre = atmosPressureStaticNewtonPerSquareMetre/(
    AIR_SPECIFIC_GAS_CONSTANT_JOULES_PER_KILOGRAM_PER_KELVIN * (ICE_MELTING_POINT_KELVIN + 20)
    ); %ideal gas law at 20 degree celcius

%% Physical Dimensions

heaveDeckLengthMetre =  2.0E+0; %       m       +-0.5   mm      measured directly from the
    pivot point to the tip of the heave deck      Measurand       22/02/2012      Static
heaveDeckWidthMetre = 471.0E-3; %       m       +-1     mm      measured directly across the
    effective surface of the heave deck         Measurand       22/02/2012      Static
heaveDeckAreaSquareMetre =      heaveDeckLengthMetre * heaveDeckWidthMetre; %   m^2
                    Calculated from the length and width of the heave deck  Parameter
    22/02/2012      Static
heaveDeckCentreOfPressureMetre = heaveDeckLengthMetre / 2; % m half way down the heave deck

heaveDeckPivotPointXMetre = 6.0E-3; %   m       0.5     mm      measured from the plenum wall
        Measurand       22/02/2012      Static
heaveDeckPivotPointZMetre =     1.1E+0; %       m       0.5     mm      Directly measured
            Measurand       22/02/2012      Static

heaveDeckRestZMetre =   1.1E+0; %       m       0.5     mm      Directly measured
    Measurand       22/02/2012      Static
initalDisplacementMilimetre = 15.4E+0; %        mm                      measured using MEL
    sensor with inlet flow approximately 5.2 m/s Parameter      21/02/2012      Static
```

```
pivotPointYMetre = -42.0E-3; %                                                  22/02/2012
pivotPointZMetre = -65.5E-3; % m        0.5     mm relative to the plenum floor directly
    measured        Measurand       22/02/2012      Static
56
plenumHeightMetre = 1.1E+0; %   m       0.5     mm      Measured at mid-point   Measurand
            22/02/2012      Static
plenumLengthMetre = 2.1E+0; %   m       0.5     mm      Measured directly       Measurand
            22/02/2012      Static
plenumWidthMetre = 593.0E-3; %  m       0.5     mm      Measured directly       Measurand
            22/02/2012      Static

61  thicknessPlenumFlooringMetre    = 15.0E-3; %    m       0.5     mm      thickness of MDF
    planking floor Measurand        22/02/2012      Static
thicknessPlenumWallMetre = 17.0E-3; %   m       0.5     mm      thickness of plywood
    Measurand       22/02/2012      Static

wellWallHeightMetre = 350.0E-3; %       m       0.5     mm      height of well wall from floor
     Measurand      22/02/2012      Static

66  %% Sensor Positions

accelerometerPositionXMetre = 936.0E-3; %       m       0.5     mm      measured from the pivot
     point of the heave deck Measurand      22/02/2012      Static
accelerometerPositionYMetre =   67.0E-3; %      m       0.5     mm      measured from the mid-
    point of the heave deck   Measurand      22/02/2012      Static
accelerometerPositionZMetre =   47.0E-3; %      m       0.5     mm      Above surface of heave
    deck wood       Measurand       22/02/2012      Static
71  displacementSensorOnePositionXMetre =   380.5E-3; % m   0.5     mm      measured from the pivot
     point of the heave deck Measurand      22/02/2012      Static
displacementSensorOnePositionYMetre =   291.5E-3; %    m       0.5     mm      measured from
    the mid-point of the heave deck   Measurand      22/02/2012      Static
displacementSensorOnePositionZMetre =   50.0E-3; %      m       0.5     mm      Measured from
    plate surface     Measurand       22/02/2012      Static
displacementSensorTwoPositionXMetre = 1.9E+0; % m       0.5     mm      measured from the pivot
     point of the heave deck Measurand      22/02/2012      Static
displacementSensorTwoPositionYMetre = 92.0E-3; %        m       0.5     mm      measured from
    the mid-point of the heave deck   Measurand      22/02/2012      Static
76  displacementSensorTwoPositionZMetre = 367.0E-3; %      m       0.5     mm      Measured from
    plate surface     Measurand       22/02/2012      Static


%% Spring Support

81  springCoilDiameterMilimetre = 20.7E+0; %        mm                      Outside diameter
             Manufacturer Data      8/11/2011       Static
springCoils = 24.0E+0; %        coils                   the number of coils     Measurand
            8/11/2011       Static
springExtensionInitialMeasuredMetre = 45E-3; % m initial extension, fully supporting the heave
    deck measured 2012-05-23
springExtensionInitialMetre = 38.5E-3; % m initial extension, fully supporting the heave deck
    calculated 2013-11-20
springLengthMilimetre = 101.6E+0; %     mm                      Length of unloaded spring
            Manufacturer Data       8/11/2011       Static
86  springPositionXMetre = 1.899; % m       0.5     mm      location of the ring from heave deck
    pivot       Measurand       22/02/2012      Static
springPositionYMetre = 35.0E-3; %       m       0.5     mm      location of the ring from the
    middle of heave deck      Measurand       22/02/2012      Static
springWireDiameterMilimetre = 3.0E+0; % mm                      Diameter of the wire
    Manufacturer Data       8/11/2011       Static

springConstantExptNewtonPerMetre = 7.04E+3; %   N/m                     estimated from
    experiment      Parameter               Calculate
91  springConstantManufNewtonPerMetre = 6.9E+3; %   N/m                     Calculated from
    manufacturer's data     Parameter               Calculate

%% Heave Deck Parameters
heaveDeckPeriodSecond = 0.327; % s period of natural oscillations due to spring support from
    experiment 23
heaveDeckMassKilogram = 52.5; % kg measured on balance 2012-05-23
96  heaveDeckRotationalInertiaKilogramMetre = 61.12; % kg.m^2 from experiment 23.
frictionCoefficient = 219.18; % from experiment 23

%% Air Supply

101 manifoldHeightMetre = 130.0E-3; %       m       0.5     mm      outside height  Measurand
            22/02/2012      Static
manifoldLengthMetre = 300.0E-3; %       m       0.5     mm      outside (walls 15 mm thick)
          Measurand       22/02/2012      Static
manifoldVolumeCubicMetre = -5.1E+0; %   m^3                     inside volume   Parameter
            22/02/2012      Calculate
manifoldWidthMetre = 300.0E-3; %        m       0.5     mm      outside (walls 15 mm thick)
          Measurand       22/02/2012      Static
inletDuctDiameterMetre = 115.3E-3; %    m       0.02    mm      measured using digital calipers
     Measurand      9/12/2011       Static
106 inletDuctLengthMetre = 936.0E-3; %      m       0.5     mm      from outside of plenum to
    outside of manifold   Measurand       22/02/2012      Static
inletDuctPositionXMetre = 1.8E+0; %     m       0.5     mm      from plenum inside bow wall
          Measurand       22/02/2012      Static
inletDuctPositionYMetre = -49.5E-3; %   m       0.5     mm      from centreline of plenum
            Measurand       22/02/2012      Static
% inletAirSpeedBlowerMetrePerSecond =   5.0E+0; %       m/s                     hand held
    anemometer, fan only  Measurand       9/12/2011       Static
inletAirSpeedBlowerMetrePerSecond =     4.0E+0; %       m/s                     hypothesised
    reduced air speed, fan only       Measurand       9/12/2011       Static
111 % inletAirSpeedBlowerTankMetrePerSecond = 6.2E+0; %     m/s                     hand held
    anemometer, with lab air supply and fan       Measurand       9/12/2011       Static
```

```
inletAirSpeedBlowerTankMetrePerSecond = 5.2E+0; %       m/s                     hypothesised
    reduced air speed, with lab air supply and fan      Measurand       9/12/2011       Static


%% Air leakage
nStaticLeakageHoles = 6; % assume that other uncontrolled leakage becomes the equivalent of
    these holes
staticLeakageHoleDiameterMetre = 19.0E-3; % Diameter of one static leakage hole in metres
staticLeakageAreaSquareMetres = pi() * (staticLeakageHoleDiameterMetre/2)^2 *
    nStaticLeakageHoles; % the total static leakage area in metres

%% Inputs

transientFlapperLowerAngleDegree = 300.0E-3; %  degrees                 from horizontal (
    digital level) Measurand        22/02/2012      Static
transientFlapperLowerAngleRadian =  transientFlapperLowerAngleDegree * 2 * pi() /360; % radians
    , angle from horizontal in radian
transientFlapperMassKilogram    = 20.9E+0; %    kg                      on Michell lab balance,
     all rotating parts      Measurand       14/10/2011      Static
transientFlapperMomentArmLengthMetre    = 600.0E-3; %   m       0.5     mm      distance from
    pivot to far edge of the transient flapper      Measurand       22/02/2012      Static
transientFlapperPlanformAreaSquareMetre = 404.5E-3; %   m^2                     calculated from
     length and width       Parameter               Calculate
transientFlapperTotalSweptVolumeCubicMetre = 955.0E-3; % m^3 total volume swept by the flapper
    itself, through a complete rotation
transientFlapperSweptVolumeCubicMetre   = 110.4E-3; %   m^3                     calculated from
     plan form area and rotation of a solid  Parameter               Calculate
% transientFlapperUpperAngleDegree =    41.9E+0; %      degrees                 from horizontal
     (digital level) Measurand       22/02/2012      Static
transientFlapperUpperAngleDegree =      4.6E+0; %       degrees         corrected       from
    horizontal (digital level) Measurand        22/02/2012      Static
transientFlapperUpperAngleRadian =      (transientFlapperUpperAngleDegree/360) * 2 * pi(); %
        radian                  from horizontal (digital level) Measurand       22/02/2012
          Static
transientFlapperSweptAngleRadian = transientFlapperUpperAngleRadian -
    transientFlapperLowerAngleRadian; % radian, travelled angle for step input
transientFlapperWidthXMetre =   903.0E-3; %     m       0.5     mm      Measured directly
          Measurand       22/02/2012      Static
transientFlapperPositionZMetre = 40.0E-3; %     m       0.5     mm      measured from plenum
    floor Directly measured     Measurand       22/02/2012      Static
transientFlapperLengthMetre = 448.0E-3; %       m       0.5     mm      measured directly
          Measurand               Static
transientFlapperUnitSweptVolumeCubicMetre = (transientFlapperWidthXMetre/2)*(
    transientFlapperMomentArmLengthMetre^2 - (transientFlapperMomentArmLengthMetre-
    transientFlapperLengthMetre)^2); % m^3 multiply by the swept angle to get swept volume


oscillatingFlapperLowerAngleDegree = -7.0; %    degrees         6.98    from horizontal (
    digital level) Measurand        22/02/2012      Static
oscillatingFlapperLowerAngleRadian =  oscillatingFlapperLowerAngleDegree * 2 * pi() /360; %
    radians, angle from horizontal in radian
oscillatingFlapperMassKilogram  = 0.6; %        kg                      on Michell lab balance,
     all rotating parts      Measurand       14/10/2011      Static
oscillatingFlapperUpperAngleDegree =    7.0; %  degrees 6.98    corrected       from horizontal
     (digital level) Measurand       22/02/2012      Static
oscillatingFlapperUpperAngleRadian =    (oscillatingFlapperUpperAngleDegree/360) * 2 * pi(); %
      radian                    from horizontal (digital level) Measurand       22/02/2012
    Static
oscillatingFlapperSweptAngleRadian = oscillatingFlapperUpperAngleRadian -
    oscillatingFlapperLowerAngleRadian; % radian, travelled angle for step input
oscillatingFlapperWidthXMetre = 0.45; % m       0.5     mm      0.450 CAD       Measurand
          22/02/2012      Static
oscillatingFlapperLengthMetre = 0.45; % m       0.5     mm      0.450 CAD       Measurand
                Static
oscillatingFlapperPositionZMetre = 40.0E-3; %   m       0.5     mm      measured from plenum
    floor Directly measured     Measurand       22/02/2012      Static
oscillatingFlapperPlanformAreaSquareMetre       = oscillatingFlapperLengthMetre*
    oscillatingFlapperWidthXMetre; %        m^2                     calculated from length and
     width      Parameter               Calculate
oscillatingFlapperMomentArmLengthMetre = 0.45; % same as the width, pivot point is on the edge
oscillatingFlapperTotalSweptVolumeCubicMetre = ...
pi() * oscillatingFlapperWidthXMetre^2 * oscillatingFlapperLengthMetre; % m^3 total volume
    swept by the flapper itself, through a complete rotation
oscillatingFlapperSweptVolumeCubicMetre = ...
oscillatingFlapperSweptAngleRadian/(2*pi()) * oscillatingFlapperTotalSweptVolumeCubicMetre; %
      m^3                   calculated from plan form area and rotation of a solid
    Parameter               Calculate
oscillatingFlapperUnitSweptVolumeCubicMetre = (oscillatingFlapperWidthXMetre/2)*(
    oscillatingFlapperMomentArmLengthMetre^2 - (oscillatingFlapperMomentArmLengthMetre-
    oscillatingFlapperLengthMetre)^2); % m^3 multiply by the swept angle to get swept volume
oscillatingFlapperSensorPositionMetre = 0.0925; % 0.0925 calculated from crank radius and known
      maximum angle
% calculate pumped volume for non-dimensional treatment
pumpedVolumeCubicMetres = oscillatingFlapperSweptAngleRadian *
    oscillatingFlapperUnitSweptVolumeCubicMetre;



%% Assumed Parameters

delQdelp = -140; % assumed same as SES fan
leakageAreaOrificeCoefficient = 0.61; % 0.61 assumed value for the orifice coefficient see
    Munson, 1990, p 126.

%% Measurement System Parameters
% rotaryEncoderSamplingPeriodSecond = 5 / 100;
```

```
% rotaryEncoderSamplingRateHertz = 1 / rotaryEncoderSamplingPeriodSecond;
% displacementSamplingPeriodSecond = 5 / 125000;
% displacementSamplingRateHertz = 1 / displacementSamplingPeriodSecond;
```

D.2. Step change experiment results

An experiment was done using a step change to the plenum volume. The heave deck displacement time history was analysed to give experimental rig parameters.

```
  ,
% Experiment 25 results
% use this to analyse the full set of experiment 25 runs, showing the
% dependence of frequency and damping on leakage area, heave deck height
% and air flow rate.
% Plots step responses on top of each other and also calculates the damped frequncy
% and damping ratio.
% expt25Results

% Paul Minty 2013-09-05

%% Set up working space
close all;
clear;
clc;
format short eng;
disp('Analysing Experiment 25 - Transient Response...');
%cd('/Users/paulminty/Dropbox/Unimelb/MATLAB/Test Rig Analysis/exp25');
disp('Current dirtectory is set to:');
pwd
disp('Initializing the test rig properties...');
initializeTestRigProperties;
load ./vars/experiment25DisplacementSensor1Milimetre.mat;
%load ./vars/experiment25DisplacementSensor2Milimetre.mat;
load ./vars/experiment25RotaryEncoder.mat;
load ./vars/experiment25AnemometerMeanMetrePerSecond.mat;
%inletDuctDiameterMetre = 115.3E-3; %   m       0.02    mm      measured using digital calipers
    Measurand       9/12/2011       Static
experiment = 25;
sensor = 1; % 1 is 1st laser (long), 2 is second laser (short), 3 is accelerometer


%% set up the runs to analyse

% iRun = [11, 19, 55, 63, 65, 73, 75, 83, 85, 86, 87]; % includes outliers
% with high heave deck friction
%iRun = [55, 63, 65, 73, 75, 83, 85, 86, 87]; % acceptable condition 7 runs

%iRun = [56, 61, 66, 76]; % condition 10, air flow rate
%iRun = [88]; % condition 1, cushion height
%iRun = [57, 62, 72, 77, 82]; % condition 8, leakage area

% Set the number of conditions to be analysed, and the possible repetitons
nRepetitions = 9; % the maximum number of repitions that will be analysed, across any conditions
nConditions = 30; % the number of conditions that will be analysed

% setup vector with only good runs, use with intersect to filter results
goodRuns = [55 56 57 58 59 60 62 63 65 66 68 69 103 104 105 106 107 109 110 111 112 113 114 115 116 118
    119 120 121 123 124 125 126 127 128 129 130 131 132 133 134 135 136 137];


% set up a populated matrix, then fill with run numbers
% 20190810 the runs with too much damping have been omitted. see file
% 'EXP25_All_Runs' for same structure with all runs included.
iRun = NaN(nRepetitions,nConditions);
%iRun(1,1) = 88;                 % condition 1
%iRun(1:2,2)= [89,95];          % condition 2 [89,95,96];
%iRun(1:2,3) = [90,97];          % condition 3
%iRun(1,4) = 91;                 % condition 4
%iRun(1,5) = 92;                 % condition 5
%iRun(1:2,6) = [93,94];          % condition 6
iRun(1:3,7) = [55, 63, 65]; % acceptable condition 7 runs
iRun(1:2,8) = [57, 62]; % condition 8, leakage area [57, 62, 72, 77, 82];
iRun(1:2,9) = [59, 69]; % condition 9 [59,69,79];
iRun(1:2,10) = [56, 66]; % condition 10, air flow rate [56, 61, 66, 71, 76];
iRun(1:2,11) = [58,68];          % condition 11
iRun(1,12) = [60];           % condition 12 [60,70,74,80,84];
iRun(1,13) = [107];           % condition 13 [98,107];
%iRun(1,14) = 100;           % condition 14
%iRun(1,15) = 102;           % condition 15
iRun(1:2,16) = [105,106];           % condition 16
iRun(1,17) = [104];           % condition 17
iRun(1,18) = 103;           % condition 18
iRun(1:4,19) = [118,124,128,134];           % condition 19
iRun(1:4,20) = [120,125,130,135];           % condition 20
iRun(1,21) = [132];           % condition 21
iRun(1:2,22) = [119,129];           % condition 22
iRun(1:2,23) = [121,131];           % condition 23
iRun(1:6,24) = [123,126,127,133,136,137];           % condition 24
```

```
%iRun(1,25) = 108;          % condition 25
iRun(1,26) = [110];          % condition 26
iRun(1:3,27) = [112,115,116];          % condition 27
iRun(1,28) = 109;          % condition 28
iRun(1,29) = 111;          % condition 29
iRun(1:2,30) = [113,114];          % condition 30


% analysis parameters
% Settling Time threshold
ST = 0.1; %(within 10% of the final value)

% pre-allocate arrays
sensorHover = zeros(137,1);
naturalFrequencyPower = NaN(nRepetitions,nConditions);
exponentFitA = NaN(nRepetitions,nConditions);
exponentFitB = NaN(nRepetitions,nConditions);
naturalFrequencyCondition = NaN(1,nConditions);
naturalFreqPowHeight = NaN(1,5);
naturalFreqPeaksCondition = NaN(1,nConditions);
hoverShiftFriction = NaN(nRepetitions,nConditions);
fallingTime = NaN(1,nConditions);
settlingTime = NaN(1,nConditions);
heaveDeckHeightMetre = NaN(1,nConditions);
nominalAirFlowSpeedMetresPerSecond = NaN(1,nConditions);
meanAirFlowSpeedMetresPerSecond = NaN(1,nConditions);
meanAirVolumeFlowRateCubicMetresPerSecond = NaN(1,nConditions);
leakageCondition = NaN(1,nConditions);
leakageAreaSquareMetre = NaN(1,nConditions);
conditionIndex = 1:30;


for j = [7:13 16:24 26:nConditions] % skip condition 25 as no data available [1:24 26:nConditions]
disp(['Running condition ', num2str(j),' of ',num2str(nConditions)]);



%% Does the core experiment analysis
% initiate the result arrays so they do not grow in the loop
omegaNatu = NaN(1,length(iRun));
dampingRatio = NaN(1,length(iRun));
height = NaN(1,length(iRun));
naturalFrequencyHertz = NaN(1,length(iRun));
dampedFrequencyHertz = NaN(1,length(iRun));
%stepResponseTimeHistory = zeros(125000,length(iRun));
dampedFrequencyRadPerSec = NaN(1,length(iRun));

% set up a common time vector to plot all the step responses
% conincidentally
samplePeriod = 1/25000; % seconds
sampleLength = 5; % seconds
outputTimeVector(:,1) = (0:samplePeriod:sampleLength-samplePeriod);

%% do the analysis on each run in turn
for i = 1:nRepetitions
if isfinite(iRun(i,j))
run = iRun(i,j);

disp(['Repetition: ',num2str(i),' of possible ',num2str(nRepetitions),'. Run: ',num2str(iRun(i,j))]);
runConditions = lookuprunconditions(run);

output = openoutput(sensor,run); % specify the sensor to open and the run to analyse
rotaryEncoder = experiment25RotaryEncoder(:,run);
%output = laserRun120;

% prepare the raw data for analysis by mirror, truncate, smooth and create
% time arrays
% [cutTimeInput,smoothCutInput,cutTimeOutput,smoothCutOutput,finalOutput] = alignStepResponsePeaks(
    rotaryEncoder,output);
[cutTimeInput,smoothCutInput,cutTimeOutput,smoothCutOutput,finalOutput,sensorHoverTemp] =
    truncatestepdata(rotaryEncoder,output);

% Analyse using the peaks of the response curve
%[zeta,dampedFrequencyRadPerSec(i),dampedFrequencyHertz(i),omegaNatu(i),naturalFrequencyHertz(i),
    timePeaks,peaks] = rampresponseonpeaks(cutTimeOutput,smoothCutOutput,experiment,run,runConditions.
    condition);
%[dampingRatio,dampedFrequencyRadPerSec,dampedFrequencyHertz,naturalFrequen
%cyRadPerSec,naturalFrequencyHertz,timePeaks,peaks]

%plotrampresponse(cutTimeOutput,smoothCutOutput,timePeaks,peaks,experiment,run,runConditions.condition,
    dampedFrequencyRadPerSec,zeta,omegaNatu);

% log the sensor reading at hover to get the hover pressure for each run
sensorHover(run) = sensorHoverTemp;

% Analyse using a step response approach and build simple arrays
stepResponseParameters = stepinfo(smoothCutOutput,cutTimeOutput,finalOutput,'SettlingTimeThreshold',ST)
    ;
riseTime(i) = stepResponseParameters.RiseTime;
fallingTime(i) = stepResponseParameters.SettlingTime;
settlingMin(i) = stepResponseParameters.SettlingMin;
settlingMax(i) = stepResponseParameters.SettlingMax;
overshoot(i) = stepResponseParameters.Overshoot;
undershoot(i) = stepResponseParameters.Undershoot;
peak(i) = stepResponseParameters.Peak;
peakTime(i) = stepResponseParameters.PeakTime;
```

```
169
    % Calculate the damping ratio based on the peak overshoot
    dampingRatio(i) = dynamicsfromstepresponse(stepResponseParameters);
    % Comment the following line to turn off the individual run plots
174 %plotstepresponse(sensor,cutTimeInput,smoothCutInput,cutTimeOutput,smoothCutOutput,dampedFrequencyHertz
        (i),dampingRatio(i),stepResponseParameters,timePeaks,peaks,experiment,run,runConditions.condition)
        ;
    stepResponseTimeHistory(:,i) = makeToLength(smoothCutOutput(:,1),125000);

    % assign the results from each repetition to an array for later averagring

179

    %% Isolate the oscillating portion to do stepinfo analysis and power
    % spectrum and find natural frequency and damping
    % isolate the oscillating portion
184 % report to user
    fprintf('\tDoing Power Spectrum Analysis of run %i...',run);
    %% find the peak so we can do power spectrum on oscillating portion only
    [peakHeave,iPeakHeave] = max(smoothCutOutput);
    % find the shift due to Coulomb friction
189 hoverShiftFriction(j,i) = mean(smoothCutOutput(end-500:end));
    % fit an exponential function to the data
    exponentFit = fit(cutTimeOutput(iPeakHeave:end)',smoothCutOutput(iPeakHeave:end),'exp2');
    exponentFitA(i,j) = exponentFit.a;
    exponentFitB(i,j) = exponentFit.b;
194 exponentFitC(i,j) = exponentFit.c;
    exponentFitD(i,j) = exponentFit.d;
    exponentTimeSeries = exponentFit.a * exp(exponentFit.b*(cutTimeOutput(iPeakHeave:end))) + ...
    exponentFit.c * exp(exponentFit.d*(cutTimeOutput(iPeakHeave:end))) + hoverShiftFriction(j,i);
    % subtract from time series to get oscillating portion
199 osciTimeSeries = smoothCutOutput(iPeakHeave:end) - exponentTimeSeries';
    % mirror and shift the oscillating portion to analyse as a step response
    normOTS = max(osciTimeSeries) - osciTimeSeries;
    % find a final value, remove noise by taking mean of final second
    finalOTS = mean(normOTS(end-25000:end));
204 % calculate an explicit settling threshhold for plotting
    settlingLimit = ST * max(normOTS)/2;
    clear finalOTSLine upperSettlingLimitLine lowerSettlingLimitLine;
    finalOTSLine(1:length(osciTimeSeries)) = finalOTS;
    upperSettlingLimitLine = finalOTSLine + settlingLimit;
209 lowerSettlingLimitLine = finalOTSLine - settlingLimit;
    % do the stepinfo analysis - built in by Matlab
    oscillatingStepInfo = stepinfo(normOTS,cutTimeOutput(1:length(normOTS)),finalOTS,'SettlingTimeThreshold
        ',ST);
    settlingTime(i) = oscillatingStepInfo.SettlingTime;

214 %% find the damped frequency and damping from the peaks, using our custom
    % script
    [zeta(i),dampedFrequencyRadPerSec(i),dampedFrequencyHertz(i),omegaNatu(i),naturalFrequencyHertz(i),
        timePeaks,peaks] = oscillationcharacteristics(cutTimeOutput(iPeakHeave:end),osciTimeSeries,
        experiment,run,runConditions.condition);
    % mirror the peaks so they can be plotted on the step result graph
    normPeaks = max(osciTimeSeries) - peaks;
219
    %% do the power spectrum analysis on the oscillating portion
    % limit to the first second of the oscillating portion so that noise is
    % minimised
    [pxx,f] = pspectrum(osciTimeSeries(1:25000),25000,'FrequencyLimits',[4 400],'Leakage',0.85,'
        FrequencyResolution',1.75,'MinThreshold',-50);
224 % find the index of the frequency with maximum power
    [powerMax,I] = max(pxx);
    % with the index, report the corresponding frequency
    naturalFrequencyPower(i,j) = f(I);

229
    %% plot the data to check the stepinfo result, show settling time,
    % successive peaks and the power spectrum analysis
    F = figure(1000+run);
    sgtitle(sprintf('Analysis of run %i ',run));
234 subplot(2,1,1);
    % plot oscillations
    plot(cutTimeOutput(1:length(normOTS)),normOTS);
    xlim([0 2.5]);
    hold on;
239 % plot peaks
    plot(timePeaks,normPeaks,'bx');
    % plot settling threshold and final value
    plot(cutTimeOutput(1:length(normOTS)),finalOTSLine,'r--');
    plot(cutTimeOutput(1:length(normOTS)),upperSettlingLimitLine,'r:');
244 plot(cutTimeOutput(1:length(normOTS)),lowerSettlingLimitLine,'r:');
    stem(oscillatingStepInfo.SettlingTime,upperSettlingLimitLine(1),'r');
    % create a label to identify run
    foo(1) = {['Experimental condition: ',num2str(runConditions.condition,'%i')]};
    foo(2) = {['H_0 = ',num2str(runConditions.heaveDeckHeight,'%5.1f'),' mm']};
249 foo(3) = {['V_a = ',num2str(runConditions.meanAirFlowSpeedMetresPerSecond,'%2.1f'),' m.s^-1']};
    foo(4) = {['A_e = ',num2str(runConditions.leakageArea,'%4.1f'),' mm^2']};
    % put label on graph
    text(1,0.7*max(normOTS),foo(1:4),'FontSize',10,'FontName','Helvetica');
    grid on;
254 xlabel('t (s)');
    ylabel('y (mm)');
    hold off;
    % second plot is the power spectrum
```

```
    subplot(2,1,2);
259 % plot the power spectrum found earlier
    plot(f,pow2db(pxx));
    % only plot from 1Hz to 10Hz
    xlim([4 10]);
    % only plot from -45dB to 10dB
264 % ylim([-45 10]);
    grid on;
    xlabel('\omega (Hz)');
    ylabel('Power (dB)');
    % label with frequency, easy comparison to frequency from periods
269 text(14,1.1*pow2db(powerMax),['\omega_pmax',sprintf(' = %3.2E',naturalFrequencyPower(i,j))]);
    % plotting finished
    fprintf(' done.\n \tSaving figure...');
    % setup filename
    filename2 = 'StepOscillating';
274 %save the figure as a MATLAB file
    figureFileName = ['./output/',filename2,'/figure',filename2,num2str(run)];
    savefig(figure(F),figureFileName,'compact');
    pdfFileName = ['./output/',filename2,'/figure',filename2,num2str(run)];
    pngFileName = ['./output/',filename2,'/figure',filename2,num2str(run)];
279 svgFileName = ['./output/',filename2,'/figure',filename2,num2str(run)];
    % print the figure as a landscape PDF for reviewing
    print(figure(F),pdfFileName,'-dpdf','-fillpage');
    print(figure(F),pngFileName,'-dpng');
    print(figure(F),svgFileName,'-dsvg');
284 %close(F)
    fprintf(' done.\n');

    %% plot the decomposition
    % get some run conditions to label graph
289 runConditions = lookuprunconditions(run);
    % set up the graph labelling
    %foo(1) = {['Smoothing: ', num2str(smoothFactor)]};
    foo(1) = {['Experimental condition: ',num2str(runConditions.condition,'%i')]};
    foo(2) = {['H_0 = ',num2str(runConditions.heaveDeckHeight,'%5.1f'),' mm']};
294 foo(3) = {['V_a = ',num2str(runConditions.meanAirFlowSpeedMetresPerSecond,'%2.1f'),' m.s^-1']};
    foo(4) = {['A_e = ',num2str(runConditions.leakageArea,'%4.1f'),' mm^2']};
    %foo(5) = {['\omega_d: ', num2str(dampedFrequencyHertz(i),'%3.2G'),' Hz']};
    % plot figures showing original data and analysis
    F = figure(run);
299 filename = 'stepDecomposition';
    % first plot is the time history and the approximate components
    % plot time history
    plot(cutTimeOutput,smoothCutOutput,'b')
    title(sprintf('Decomposition of run %i ',run));
304 hold on;
    % limit to first 2.5 seconds, all oscilaltions decayed by then
    xlim([0 2.5]);
    % plot the exponential fit
    plot(cutTimeOutput(iPeakHeave:end),exponentTimeSeries,'g');
309 % plot the oscillations from the exponential fit
    plot(cutTimeOutput(iPeakHeave:end),osciTimeSeries,'r')
    % label so that the conditions can be identified
    text(1,15,foo,'FontSize',10,'FontName','Helvetica');
    legend('Measured', 'Exponential Fit', 'Oscillations','Location','East');
314 grid on;
    xlabel('t (s)');
    ylabel('y (mm)');
    hold off;
    fprintf(' done.\n \tSaving figure...');
319 %save the figure as a MATLAB file
    figureFileName = ['./output/',filename,'/figure',filename,num2str(run)];
    savefig(figure(F),figureFileName,'compact');
    pdfFileName = ['./output/',filename,'/figure',filename,num2str(run)];
    pngFileName = ['./output/',filename,'/figure',filename,num2str(run)];
324 svgFileName = ['./output/',filename,'/figure',filename,num2str(run)];
    % print the figure as a landscape PDF for reviewing
    print(figure(F),pdfFileName,'-dpdf','-fillpage');
    print(figure(F),pngFileName,'-dpng');
    print(figure(F),svgFileName,'-dsvg');
329 %close(F)
    fprintf(' done.\n');

    end % condition is infinite
    end
334
    %% the individual runs for each condition is over
    % find the mean of the repeats at each condition
    % two methods are used: power spectrum and successive peaks
    naturalFrequencyCondition(j) = mean(naturalFrequencyPower(:,j),'omitnan');
339 naturalFreqPeaksCondition(j) = mean(dampedFrequencyHertz,'omitnan');
    fprintf('\nNatural frequency for condition %i from power spectrum: %3.2GHz \n',runConditions.condition,
        naturalFrequencyCondition(j));
    % exponential fit coefficient A
    exponentFitAMean(j) = mean(exponentFitA(:,j),'omitnan');
    exponentFitBMean(j) = mean(exponentFitB(:,j),'omitnan');
344 fprintf('Exponent coefficient A: %3.2G. Exponent coefficient B: %3.2G. \n',exponentFitAMean(j),
        exponentFitBMean(j));
    % mean of power spectrum most powerful frequency for height 1145mm
    naturalFreqPowHeight(5) = mean(naturalFrequencyCondition(1:6),'omitnan');
    naturalFreqPowHeightMatrix(:,5) = naturalFrequencyCondition(1:6);
    naturalFreqPeaksHeightMatrix(:,5) = naturalFreqPeaksCondition(1:6);
349 % mean of power spectrum most powerful frequency for height 297mm
    naturalFreqPowHeight(1) = mean(naturalFrequencyCondition(7:12),'omitnan');
    naturalFreqPowHeightMatrix(:,1) = naturalFrequencyCondition(7:12);
```

```
    naturalFreqPeaksHeightMatrix(:,1) = naturalFreqPeaksCondition(7:12);
    % mean of power spectrum most powerful frequency for height 600mm
354 naturalFreqPowHeight(3) = mean(naturalFrequencyCondition(13:18),'omitnan');
    naturalFreqPowHeightMatrix(:,3) = naturalFrequencyCondition(13:18);
    naturalFreqPeaksHeightMatrix(:,3) = naturalFreqPeaksCondition(13:18);
    % mean of power spectrum most powerful frequency for height 800mm
    naturalFreqPowHeight(4) = mean(naturalFrequencyCondition(19:24),'omitnan');
359 naturalFreqPowHeightMatrix(:,4) = naturalFrequencyCondition(19:24);
    naturalFreqPeaksHeightMatrix(:,4) = naturalFreqPeaksCondition(19:24);
    % mean of power spectrum most powerful frequency for height 400mm
    naturalFreqPowHeight(2) = mean(naturalFrequencyCondition(25:30),'omitnan');
    naturalFreqPowHeightMatrix(:,2) = naturalFrequencyCondition(25:30);
364 naturalFreqPeaksHeightMatrix(:,2) = naturalFreqPeaksCondition(25:30);

    %% find the mean of the time histories and the statistics
    alignedOutputMatrix = alignStepResponsePeaks(stepResponseTimeHistory);
    clear stepResponseTimeHistory;
369
    %% Calculates the overall results for the core experiment

    % open up the data that describes the run conditions
    load ./vars/experimentalConditions.mat expConditions;
374 load ./vars/runs.mat runs;
    load ./vars/experiment25AnemometerMeanMetrePerSecond.mat experiment25AnemometerMeanMetrePerSecond;

    % build the factors arrays
    % from the run number, look up the condition number
379 condition = runs(run,2);

    % lookup the run number in the matrix of mean air speeds, then retrieve
    % the corresponding air speed
    A = experiment25AnemometerMeanMetrePerSecond(:,1);
384 iARun = find(A == run);

    % set up the data structure 'runConditions'
    runConditions.condition = condition;
    runConditions.heaveDeckHeight = expConditions.heaveDeckHeight(condition);
389 runConditions.nominalAirFlowSpeedMetresPerSecond = expConditions.nominalAirFlowSpeedMetresPerSecond(
        condition);
    runConditions.meanAirFlowSpeedMetresPerSecond = experiment25AnemometerMeanMetrePerSecond(iARun,2);
    runConditions.leakageCondition = expConditions.leakageCondition(condition) + 1;
    runConditions.leakageArea = expConditions.leakageArea(runConditions.leakageCondition,2);

394 % calculate a non-dimensional parameter for the experimental factors

    runConditions.piTemp = ...
    runConditions.leakageArea / ...
    (runConditions.meanAirFlowSpeedMetresPerSecond * runConditions.heaveDeckHeight);
399
    % create simple arrays of the experimental factors
    heaveDeckHeightMetre(condition) = expConditions.heaveDeckHeight(condition)/1000;
    nominalAirFlowSpeedMetresPerSecond(condition) = expConditions.nominalAirFlowSpeedMetresPerSecond(
        condition);
    meanAirFlowSpeedMetresPerSecond(condition) = experiment25AnemometerMeanMetrePerSecond(iARun,2);
404 meanAirVolumeFlowRateCubicMetresPerSecond(condition) = meanAirFlowSpeedMetresPerSecond(condition) * pi
        () * (inletDuctDiameterMetre/2)^2;
    leakageCondition(condition) = expConditions.leakageCondition(condition) + 1;
    % Air leakage
    leakageAreaSquareMetre(condition) = expConditions.leakageArea(runConditions.leakageCondition,2)/(1E6) +
         staticLeakageAreaSquareMetres;

409 % save the experimental factors to file for later plotting
    save ./vars/experimentalFactors.mat heaveDeckHeightMetre...
    meanAirVolumeFlowRateCubicMetresPerSecond leakageAreaSquareMetre;

    % close the conditions and factors variabales to save some memory
414 clear expConditions;
    clear runs;
    clear experiment25AnemometerMeanMetrePerSecond;

    % means and standard deviations of the calculate results
419 % damping ratio - from the rampresponseonpeaks of the oscillating portion
    meanZeta(runConditions.condition) = roundn(mean(zeta,'omitnan'),-5);
    stdZeta(runConditions.condition) = roundn(std(zeta),-5);
    % damping ratio from the stepinfo
    meanDampingRatio(runConditions.condition) = roundn(mean(dampingRatio,'omitnan'),-5);
424 stdDampingRatio(runConditions.condition) = roundn(std(dampingRatio),-5);
    meanDampedFrequencyRadPerSec(runConditions.condition) = roundn(mean(dampedFrequencyRadPerSec,'omitnan')
        ,-2);
    stdDampedFrequencyRadPerSec(runConditions.condition) = roundn(std(dampedFrequencyRadPerSec),-2);
    meanDampedFrequencyHertz(runConditions.condition) = roundn(mean(dampedFrequencyHertz,'omitnan'),-2);
    stdDampedFrequencyHertz(runConditions.condition) = roundn(std(dampedFrequencyHertz),-5);
429
    % save the frequency and damping to file for later plotting
    save ./vars/experimentalFrequncyDamping.mat meanDampingRatio stdDampingRatio...
    meanDampedFrequencyRadPerSec stdDampedFrequencyRadPerSec...
    meanDampedFrequencyHertz stdDampedFrequencyHertz;
434
    %means and standard deviations of the stepinfo generated results
    meanRiseTime(runConditions.condition) = roundn(mean(riseTime,'omitnan'),-3);
    stdRiseTime(runConditions.condition) = roundn(std(riseTime,'omitnan'),-3);
    % settling time - stepinfo of oscillating portion
439 meanSettlingTime(runConditions.condition) = roundn(mean(settlingTime,'omitnan'),-3);
    stdSettlingTime(runConditions.condition) = roundn(std(settlingTime,'omitnan'),-3);
    meanSettlingMin(runConditions.condition) = roundn(mean(settlingMin,'omitnan'),-3);
    stdSettlingMin(runConditions.condition) = roundn(std(settlingMin,'omitnan'),-3);
```

```
    meanSettlingMax(runConditions.condition) = roundn(mean(settlingMax,'omitnan'),-3);
444 stdSettlingMax(runConditions.condition) = roundn(std(settlingMax,'omitnan'),-3);
    meanOvershoot(runConditions.condition) = roundn(mean(overshoot,'omitnan'),-3);
    stdOvershoot(runConditions.condition) = roundn(std(overshoot,'omitnan'),-3);
    meanUndershoot(runConditions.condition) = roundn(mean(undershoot,'omitnan'),-3);
    stdUndershoot(runConditions.condition) = roundn(std(undershoot,'omitnan'),-3);
449 meanPeak(runConditions.condition) = roundn(mean(peak,'omitnan'),-3);
    stdPeak(runConditions.condition) = roundn(std(peak,'omitnan'),-3);
    meanPeakTime(runConditions.condition) = roundn(mean(peakTime,'omitnan'),-3);
    stdPeakTime(runConditions.condition) = roundn(std(peakTime,'omitnan'),-3);
    % falling time - stepinfo of the measured signal
454 meanFallingTime(runConditions.condition) = roundn(mean(fallingTime,'omitnan'),-3);
    stdFallingTime(runConditions.condition) = roundn(std(fallingTime,'omitnan'),-3);

    % save the stepinfo results to file for later plotting
    save ./vars/experimentalStepinfo.mat meanRiseTime stdRiseTime...
459 meanSettlingTime stdSettlingTime meanSettlingMin stdSettlingMin...
    meanSettlingMax stdSettlingMax meanOvershoot stdOvershoot...
    meanUndershoot stdUndershoot meanPeak stdPeak meanPeakTime stdPeakTime...
    meanFallingTime stdFallingTime meanZeta stdZeta;


464
    % build strings for inclusion on plots
    strMeanDampingRatio = sprintf('%4.2e',meanDampingRatio(runConditions.condition));
    strStdDampingRatio = sprintf('%4.2e',stdDampingRatio(runConditions.condition));
    strMeanDampedFrequencyRadPerSec = sprintf('%4.2e',meanDampedFrequencyRadPerSec(runConditions.condition)
        );
469 strStdDampedFrequencyRadPerSec =sprintf('%4.2e',stdDampedFrequencyRadPerSec(runConditions.condition));
    strMeanDampedFrequencyHertz =sprintf('%4.2e',meanDampedFrequencyHertz(runConditions.condition));
    strStdDampedFrequencyHertz =sprintf('%4.2e',stdDampedFrequencyHertz(runConditions.condition));

    end
474
    %% put all the results into one table for convenience and consistency
    resultsTable = table(conditionIndex,heaveDeckHeightMetre,leakageAreaSquareMetre,
        meanAirVolumeFlowRateCubicMetresPerSecond,meanFallingTime,meanSettlingTime,
        naturalFrequencyCondition,naturalFreqPeaksCondition,meanZeta);
    % plot conditions to refer to
    figure(888);
479 subplot(3,1,1);
    plot(resultsTable.conditionIndex,resultsTable.heaveDeckHeightMetre,'x');
    ylabel('H_0 (m)');
    xticks(0:30);
    subplot(3,1,2);
484 plot(resultsTable.conditionIndex,resultsTable.leakageAreaSquareMetre,'x');
    ylabel('A_e (mm^2)');
    xticks(0:30);
    subplot(3,1,3);
    plot(resultsTable.conditionIndex,resultsTable.meanAirVolumeFlowRateCubicMetresPerSecond,'x');
489 ylabel('V_s (m.s^-1)');
    xlabel('Condition number');
    xticks(0:30);
    % assign conditions to various experimental factors, use intersetion and
    % union to select the set to plot
494 % plenum heights
    height300 = 7:12;
    height400 = 25:30;
    height600 = 13:18;
    height800 = 19:24;
499 height1000 = 1:6;
    heightMatrix = [height300,height400,height600,height800,height1000];
    % air exit areas
    exitAreaLow = [1 2 7:3:28];
    exitAreaMed = [3 4 8:3:29];
504 exitAreaHigh = [5 6 9:3:30];
    exitAreaMatrix = [exitAreaLow,exitAreaMed,exitAreaHigh];
    % air supply volume flow rates
    airSpeedLow = [1:2:5 7:9 13:15 19:21 25:27];
    airSpeedHigh = [2:2:6 10:12 16:18 22:24 28:30];
509 airSpeedMatrix = [airSpeedLow,airSpeedHigh];

    % vector assigning conditions to Al and Vf
    airLowAlLow = intersect(exitAreaLow,airSpeedLow);%[7 13 19];
    airLowAlMed = intersect(airSpeedLow,exitAreaMed);%[13 26 20];
514 airLowAlHig = intersect(airSpeedLow,exitAreaHigh);%[9 27 21];
    airHigAlLow = intersect(airSpeedHigh,exitAreaLow);%[10 28 16 22];
    airHigAlMed = intersect(airSpeedHigh,exitAreaMed);%[11 29 17 23];
    airHigAlHig = intersect(airSpeedHigh,exitAreaHigh);%[12 30 18 24];

519
    %% plot the natural frequency versus plenum height
    filename = 'stepFreqDampedVersusHeight';
    plenumHeightRange = [0.297 0.445 0.612 0.802 1.1435];
    F = figure(200);
524 plot(resultsTable.heaveDeckHeightMetre(:,airLowAlLow),...
    resultsTable.naturalFrequencyCondition(:,airLowAlLow),...
    'r+','DisplayName','V_s low A_e low');
    %title('Observed damped frequency (from power spectrum analysis)');
    xlabel('H_0 (m)');
529 ylabel('\omega_d (Hz)');
    hold on;
    plot(resultsTable.heaveDeckHeightMetre(:,airLowAlMed),...
    resultsTable.naturalFrequencyCondition(:,airLowAlMed),...
    'g+','DisplayName','V_s low A_e med');
534 plot(resultsTable.heaveDeckHeightMetre(:,airLowAlHig),...
    resultsTable.naturalFrequencyCondition(:,airLowAlHig),...
```

```
    'b+','DisplayName','V_s low A_e high');
    plot(resultsTable.heaveDeckHeightMetre(:,airHigAlLow),...
    resultsTable.naturalFrequencyCondition(:,airHigAlLow),...
539 'rx','DisplayName','V_s high A_e low');
    plot(resultsTable.heaveDeckHeightMetre(:,airHigAlMed),...
    resultsTable.naturalFrequencyCondition(:,airHigAlMed),...
    'gx','DisplayName','V_s high A_e med');
    plot(resultsTable.heaveDeckHeightMetre(:,airHigAlHig),...
544 resultsTable.naturalFrequencyCondition(:,airHigAlHig),...
    'bx','DisplayName','V_s high A_e high');
    plot(plenumHeightRange,...
    naturalFreqPowHeight,...
    'ro','DisplayName','Mean of \omega_d');
549 ylim([0 10]);
    lgd = legend('Location','Southeast');
    lgd.NumColumns = 3;
    grid on;
    hold off;
554 fprintf(' done.\n \tSaving figure...');
    %save the figure as a MATLAB file
    figureFileName = ['./output/',filename,'/figure',filename,num2str(run)];
    savefig(figure(F),figureFileName,'compact');
    pdfFileName = ['./output/',filename,'/figure',filename,num2str(run)];
559 pngFileName = ['./output/',filename,'/figure',filename,num2str(run)];
    svgFileName = ['./output/',filename,'/figure',filename,num2str(run)];
    % print the figure as a landscape PDF for reviewing
    print(figure(F),pdfFileName,'-dpdf','-fillpage');
    print(figure(F),pngFileName,'-dpng');
564 print(figure(F),svgFileName,'-dsvg');
    %close(F)
    fprintf(' done.\n');


569 %% plot the power spectrum natural frequency for various heights
    %close all;

    figure(300);
    hold on;
574 plot(plenumHeightRange,naturalFreqPowHeight,'ro','DisplayName','Mean of \omega_d');
    plot(plenumHeightRange,naturalFreqPowHeightMatrix,'bx','DisplayName','PowerSpectrum');
    plot(plenumHeightRange,naturalFreqPeaksHeightMatrix,'g*','DisplayName','Peaks');
    grid on;
    %title('Dominant Frequency from Power Spectrum')
579 xlabel('H_0 (m)');
    ylabel('\omega_d (Hz)');
    %legend;
    xlim([0 1.2]);
    ylim([0 12]);
584 hold off;

    %% plot the 4 key results against condition number as a check
    % falling time
    % settling time
589 % damped frequency
    % damping ratio of oscillating portion

    figure(500);
    subplot(4,1,1);
594 plot(resultsTable.conditionIndex,resultsTable.meanFallingTime,'bx');
    grid on;
    xlim([0 30]);
    ylim([0 2.5]);
    ylabel('T_f (s)');
599 subplot(4,1,2);
    plot(resultsTable.conditionIndex,resultsTable.meanSettlingTime,'bx');
    grid on;
    xlim([0 30]);
    ylim([0 1]);
604 ylabel('T_s (s)');
    subplot(4,1,3);
    plot(resultsTable.conditionIndex,resultsTable.naturalFrequencyCondition,'bx','DisplayName','Power
        method');
    hold on;
    plot(resultsTable.conditionIndex,resultsTable.naturalFreqPeaksCondition,'rx','DisplayName','Peaks
        method');
609 grid on;
    xlim([0 30]);
    ylim([0 18]);
    ylabel('\omega_d (Hz)');
    hold off;
614 subplot(4,1,4);
    plot(resultsTable.conditionIndex,resultsTable.meanZeta,'bx');
    grid on;
    xlim([0 30]);
    ylim([0 0.5]);
619 ylabel('\zeta');
    xlabel('Condition Number');

    %% plot the settling time, falling time and damping against the leakage area
    % resultsTable = table(conditionIndex,heaveDeckHeightMetre,leakageAreaSquareMetre,
        meanAirVolumeFlowRateCubicMetresPerSecond,meanFallingTime,meanSettlingTime,
        naturalFrequencyCondition,naturalFreqPeaksCondition,meanZeta);
624


    figure(600);
    subplot(4,1,1);
```

```
    plot(resultsTable.leakageAreaSquareMetre(airSpeedLow), resultsTable.meanFallingTime(airSpeedLow),'bx','
        DisplayName','Low air flow');
629 hold on;
    plot(resultsTable.leakageAreaSquareMetre(airSpeedHigh), resultsTable.meanFallingTime(airSpeedHigh),'rx'
        ,'DisplayName','High air flow');
    legend;
    ylabel('T_f (s)');
    ylim([0 3]);
634 grid on;
    hold off;
    subplot(4,1,2);
    plot(resultsTable.leakageAreaSquareMetre(airSpeedHigh), resultsTable.meanSettlingTime(airSpeedHigh),'rx
        ','DisplayName','High air flow');
    hold on;
639 plot(resultsTable.leakageAreaSquareMetre(airSpeedLow), resultsTable.meanSettlingTime(airSpeedLow),'bx',
        'DisplayName','Low air flow');
    legend;
    ylabel('T_s (s)');
    ylim([0 1]);
    grid on;
644 hold off;
    subplot(4,1,3);
    plot(resultsTable.leakageAreaSquareMetre, resultsTable.meanZeta,'x');
    ylabel('\zeta');
    ylim([0 0.6]);
649 grid on;
    subplot(4,1,4);
    plot(resultsTable.leakageAreaSquareMetre, resultsTable.naturalFreqPeaksCondition,'rx','DisplayName','
        Peaks method');
    hold on;
    plot(resultsTable.leakageAreaSquareMetre, resultsTable.naturalFrequencyCondition,'bx','DisplayName','
        Power method');
654 legend
    ylabel('\omega_d (Hz)');
    ylim([0 12]);
    xlabel('A_e (mm^2)');
    grid on;
659 hold off;

    %% Figure for falling time versus air exit area
    fprintf('\n Plotting falling time...');
    filename = 'stepFallingTime';
664 F = figure(700);
    plot(resultsTable.leakageAreaSquareMetre(airSpeedLow), resultsTable.meanFallingTime(airSpeedLow),'bx','
        DisplayName','Low air flow');
    hold on;
    plot(resultsTable.leakageAreaSquareMetre(airSpeedHigh), resultsTable.meanFallingTime(airSpeedHigh),'rx'
        ,'DisplayName','High air flow');
    legend;
669 ylabel('T_f (s)');
    xlabel('A_e (mm^2)');
    ylim([0 3]);
    grid on;
    hold off;
674 fprintf(' done.\n \tSaving figure...');
    %save the figure as a MATLAB file
    figureFileName = ['./output/',filename,'/figure',filename,num2str(run)];
    savefig(figure(F),figureFileName,'compact');
    pdfFileName = ['./output/',filename,'/figure',filename,num2str(run)];
679 pngFileName = ['./output/',filename,'/figure',filename,num2str(run)];
    svgFileName = ['./output/',filename,'/figure',filename,num2str(run)];
    % print the figure as a landscape PDF for reviewing
    print(figure(F),pdfFileName,'-dpdf','-fillpage');
    print(figure(F),pngFileName,'-dpng');
684 print(figure(F),svgFileName,'-dsvg');
    %close(F)
    fprintf(' done.\n');

    %% Figure for Settling time versus air exit area
689 fprintf('\n Plotting settling time...');
    filename = 'stepSettlingTime';
    F = figure(800);
    plot(resultsTable.leakageAreaSquareMetre(airSpeedHigh), resultsTable.meanSettlingTime(airSpeedHigh),'rx
        ','DisplayName','High air flow');
    hold on;
694 plot(resultsTable.leakageAreaSquareMetre(airSpeedLow), resultsTable.meanSettlingTime(airSpeedLow),'bx',
        'DisplayName','Low air flow');
    legend;
    ylabel('T_s (s)');
    xlabel('A_e (mm^2)');
    ylim([0 1]);
699 grid on;
    hold off;
    fprintf(' done.\n \tSaving figure...');
    %save the figure as a MATLAB file
    figureFileName = ['./output/',filename,'/figure',filename,num2str(run)];
704 savefig(figure(F),figureFileName,'compact');
    pdfFileName = ['./output/',filename,'/figure',filename,num2str(run)];
    pngFileName = ['./output/',filename,'/figure',filename,num2str(run)];
    svgFileName = ['./output/',filename,'/figure',filename,num2str(run)];
    % print the figure as a landscape PDF for reviewing
709 print(figure(F),pdfFileName,'-dpdf','-fillpage');
    print(figure(F),pngFileName,'-dpng');
    print(figure(F),svgFileName,'-dsvg');
    %close(F)
    fprintf(' done.\n');
```

```
714
    %% Figure for damping versus air exit area
    fprintf('\n Plotting damping...');
    filename = 'stepDamping';
    F = figure(1000);
719 plot(resultsTable.leakageAreaSquareMetre, resultsTable.meanZeta,'x');
    ylabel('\zeta');
    xlabel('A_e (mm^2)');
    ylim([0 0.6]);
    grid on;
724 hold off;
    fprintf(' done.\n \tSaving figure...');
    %save the figure as a MATLAB file
    figureFileName = ['./output/',filename,'/figure',filename,num2str(run)];
    savefig(figure(F),figureFileName,'compact');
729 pdfFileName = ['./output/',filename,'/figure',filename,num2str(run)];
    pngFileName = ['./output/',filename,'/figure',filename,num2str(run)];
    svgFileName = ['./output/',filename,'/figure',filename,num2str(run)];
    % print the figure as a landscape PDF for reviewing
    print(figure(F),pdfFileName,'-dpdf','-fillpage');
734 print(figure(F),pngFileName,'-dpng');
    print(figure(F),svgFileName,'-dsvg');
    %close(F)
    fprintf(' done.\n');

739
    %% save the hover sensor readings for later analysis
    save ./vars/sensorHOver.mat sensorHover;
```

D.3. Simulink model

This Simulink model is described in Sec. 5.9, the Simulink block diagrams are reproduced here for convenience.

The equation Eq. (5.75) can be expressed in block diagram form directly within the Simulink environment of the Matlab software, allowing the system of equations to be solved numerically.

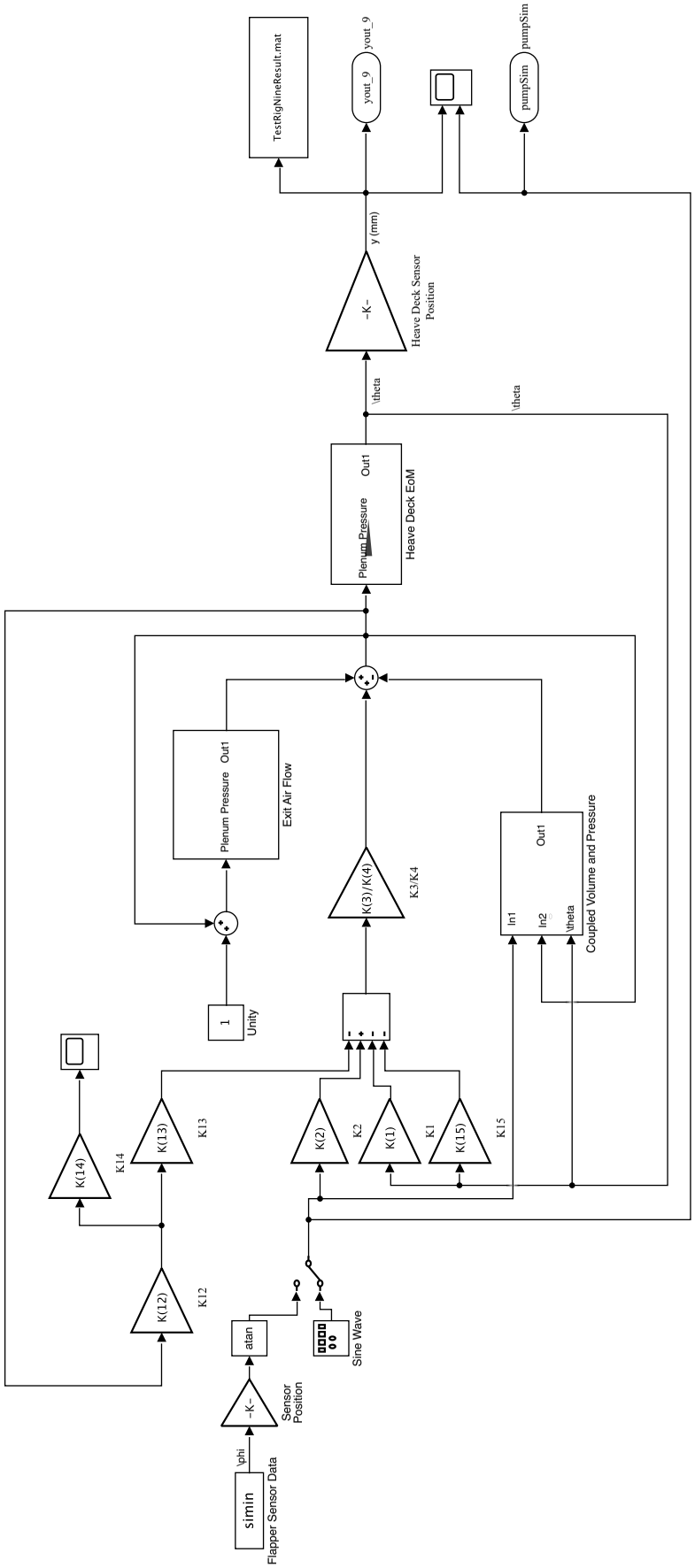


Figure D.1. Overall mathematical model of the experimental rig expressed in block diagram form within the Simulink environment of Matlab.

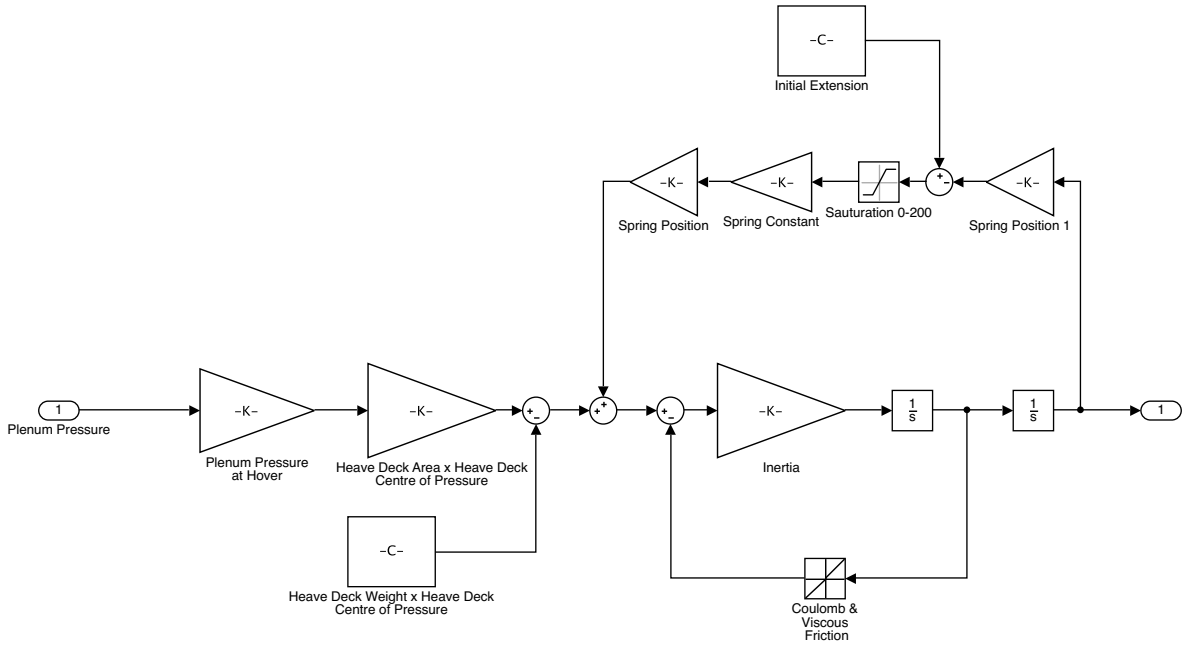


Figure D.2. The experimental rig supported mass equation of motion, expressed as a block diagram within the Simulink environment of Matlab.

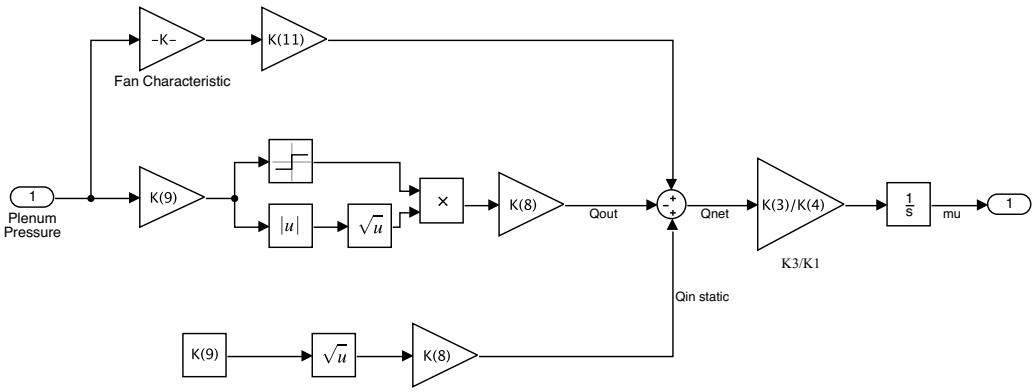


Figure D.3. The experimental rig plenum volume air mass continuity expressed as a block diagram within the Simulink environment of Matlab.

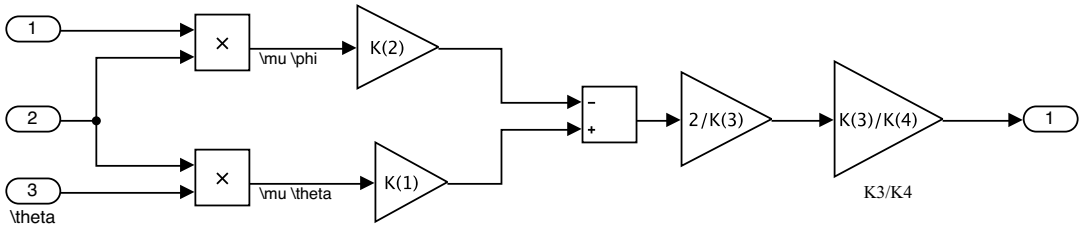


Figure D.4. The experimental model air density and plenum volume rates of change expressed as a block diagram within the Simulink environment of Matlab.

D.4. Parametric curve fitting to step change experimental data

The Simulink model was configured to respond to a step change of the plenum volume. The Simulink model parameters could be systematically varied and the output compared to the experimental data - thus fitting the curve to the experimental data.

```
,
%% runModelElevenStep
% Uses simulation model 11, with provision for plenum flexibility and extra
% friction associated with the rolling seals. The simulation is run using a
% step input. The experimental runs from exp25results are opened and the
% simulation plotted over the top.
% model 11 replaces damping with coulomb and viscous friction


% set up the workspace
clc;
close all;
clear;
format shorteng;
fprintf('\nrun Model Eleven Step');
fprintf('\nrun simulations using Simulink model 11');
fprintf('\nuse a step input and plot over experimental results');
cd('/Users/paulminty/Dropbox/Unimelb/MATLAB/Test Rig Analysis/exp25');
fprintf('Current directory is set to:\n %s\n',pwd);

% mode of analysis
% * do the simulations with the  flexible wall, but no extra friction -
% (stepExpSimVolume)
% * do the simulations with extra friction only - (stepExpSimFriction)
% * keep flexible wall (match frequency) do the simulations with more
% friction - (stepExpSimVolumeFriction)
% * keep flexible wall (match frequency) do the simulations with more
% leakage area - (stepExpSimVolumeExit)



for mode = 8

if mode == 1 % no flexible volume, no fan slope, no seal friction, no leakage
directory = 'stepExpSimNoExtra';
filename = 'NoExtra';
titleText = 'Ideal Simulation';
fanslopeoverride = 0;
plenumFlexSwitch = 0;
extraFrictionSwitch = 0;
exitAreaSwitch = 0;
fprintf('\nMode is no flexible plenum, no fan slope, no extra friction, no leakage\n\n');
elseif mode == 2 % includes only flexible plenum walls
directory = 'stepExpSimVolume';
filename = 'Volume';
titleText = 'Flexible Plenum only';
fanslopeoverride = 0;
plenumFlexSwitch = 1;
extraFrictionSwitch = 0;
exitAreaSwitch = 0;
fprintf('Mode is with flexible plenum only\n');
elseif mode == 3 % includes only friction
directory = 'stepExpSimFriction';
filename = 'Friction';
titleText = 'Friction only';
fanslopeoverride = 0;
plenumFlexSwitch = 0;
extraFrictionSwitch = 1;
exitAreaSwitch = 0;
fprintf('Mode is with friction only\n');
elseif mode == 4 % includes flexible walls and friction
directory = 'stepExpSimVolumeFriction';
filename = 'VolumeFriction';
titleText = 'Flexible Plenum and Friction';
fanslopeoverride = 0;
plenumFlexSwitch = 1;
extraFrictionSwitch = 1;
exitAreaSwitch = 0;
fprintf('Mode is with flexible walls and friction \n');
elseif mode == 5 % includes friction and extra leakage area
directory = 'stepExpSimFrictionExit';
filename = 'FrictionExit';
titleText = 'Friction and Extra Exit Area';
fanslopeoverride = 0;
plenumFlexSwitch = 0;
extraFrictionSwitch = 1;
exitAreaSwitch = 1;
fprintf('Mode is with flexible walls, friction and leakage area \n');
elseif mode == 6 % includes flexible walls, friction and extra leakage area
directory = 'stepExpSimVolumeFricExit';
filename = 'VolumeExit';
titleText = 'Flexible Plenum, Friction and Exit Area';
fanslopeoverride = 0;
```

```
    plenumFlexSwitch = 1;
    extraFrictionSwitch = 1;
    exitAreaSwitch = 1;
87  fprintf('Mode is with flexible walls, friction and leakage area \n');
    elseif mode == 7 % includes extra leakage area
    directory = 'stepExpExit';
    filename = 'Exit';
    titleText = 'Extra Exit Area';
92  fanslopeoverride = 0;
    plenumFlexSwitch = 0;
    extraFrictionSwitch = 0;
    exitAreaSwitch = 1;
    fprintf('Mode is with extra leakage area \n');
97  elseif mode == 8 % includes extra leakage area
    directory = 'stepExpExit';
    filename = 'VolumeVolumeExit';
    titleText = 'Flexible Plenum, Extra Exit Area';
    fanslopeoverride = 0;
102 plenumFlexSwitch = 1;
    extraFrictionSwitch = 0;
    exitAreaSwitch = 1;
    fprintf('Mode is with flexible plenum and extra leakage area \n')
    else
107 fprintf('\n Mode number is incorrect \n');
    error('Incorrect mode number entered');
    end

    fprintf('\nSimulation conditions\n');
112 fprintf('\tMode number: \t\t %i \n',mode);
    fprintf('\tFan slope on?\t\t %i \n',fanslopeoverride);
    fprintf('\tPlenum flex on?\t\t %i \n',plenumFlexSwitch);
    fprintf('\tExtra friction on?\t %i \n',extraFrictionSwitch);
    fprintf('\tExtra area on?\t\t %i \n\n',exitAreaSwitch);
117
    %% RETREIVE THE DATA THAT IS STATIC FOR THE TEST RIG
    % load the test rig invariant parameters

    initializeTestRigProperties;
122 % extraFrictionFactor = 1E0; %1E0
    % frictionCoefficient =  frictionCoefficient + (extraFrictionSwitch * extraFrictionFactor);

    %% OPEN THE DATA FOR THE EXPERIMENTAL RUNS
    % load the data for the experimental runs
127
    fprintf('\nWait, loading experimental data...\n');
    load './vars/exp29Data.mat';
    fprintf('Experimental data loaded.\n');
    % number of experimental runs to consider
132 % there are three plenum heights and three air exit areas
    nCondition = 30;
    % store the nominal flapper angle
    flapperAngleRadian = transientFlapperSweptAngleRadian;

137 %% preallocate for speed

    airExitAreaSquareMetres = NaN(1,nCondition);
    maxHeave = NaN(1,nCondition);
    minHeave = NaN(1,nCondition);
142 frequencyVec = NaN(1,nCondition);
    meanHeight = NaN(1,nCondition);
    checkMean = NaN(1,nCondition);
    lagHeave = NaN(1,nCondition);
    magnitudeHeave = NaN(1,nCondition);
147 frequencyMaxHeaveVec = NaN(1,nCondition);
    heightPlenum = NaN(1,nCondition);
    outlierProportion = NaN(1,nCondition);
    outlierFrequency = NaN(1,nCondition);

152 %% SET ATMOSPHERIC PRESSURE AND AIR DENSITY TO STANDARD ATMOSPHERE
    % this is the same for all of the simulations

    atmosPressureStaticNewtonPerSquareMetre = 101325;
    atmosTemperatureKelvin = 20 + ICE_MELTING_POINT_KELVIN;
157 atmosAirDensityKilogramPerCubicMetre = atmosPressureStaticNewtonPerSquareMetre/...
    (GAS_CONSTANT_AIR * atmosTemperatureKelvin);

    %fprintf('\nAtmospheric Conditions\n');
    %fprintf('\tAtmospheric pressure:    %d N/m^2 \n',atmosPressureStaticNewtonPerSquareMetre);
162 %fprintf('\tAtmospheric air density: %5.4f kg/m^3 \n', atmosAirDensityKilogramPerCubicMetre);


    %% SET THE THEORETICAL PARAMETERS THAT YOU WANT TO SIMULATE

167 % create a matrix of experimental parameters
    conditionMatrix = NaN(30,14);

    % condition number in column 1
    conditionMatrix(:,1) = 1:30;
172 % plenum height in column 2
    conditionMatrix(1:6,2) = 1.143;
    conditionMatrix(7:12,2) = 0.297;
    conditionMatrix(13:18,2) = 0.605;
    conditionMatrix(19:24,2) = 0.802;
177 conditionMatrix(25:30,2) = 0.445;
    % air supply centreline velocity m/s rate in column 3
    conditionMatrix(:,3) = 5.49;
```

```
    conditionMatrix([2:2:6 10:12 16:18 22:24 28:30],3) = 6.75;
    % Air exit area in column 4
182 conditionMatrix(:,4) = 303.9E-6;
    conditionMatrix([1:2 7:3:28],4) = 0.0E-6;
    conditionMatrix([5:6 9:3:30],4) = 685.5E-6;

    % a good step experimental run in column 5
187 conditionMatrix(1:30,5) = [88 89 97 91 92 94 63 57 59 56 58 60 107 100 102 106 104 103 118 120 122 119
        121 123 NaN 110 112 109 111 113];
    conditionMatrix([8 14 20 26],5) = [62 100 125 110];
    conditionMatrix(19:24,5) = [128 130 132 129 131 127];


192 % time of the experimental peak, read from the data manually
    conditionMatrix(1,6) = 0.8868;
    conditionMatrix(2,6) = 0.6581;
    conditionMatrix(3,6) = 0.8217;
    conditionMatrix(4,6) = 0.8375;
197 conditionMatrix(5,6) = 0.7635;
    conditionMatrix(6,6) = 0.2517;
    conditionMatrix(7,6) = 0.7195;
    conditionMatrix(8,6) = 0.4984;
    conditionMatrix(9,6) = 0.6087;
202 conditionMatrix(10,6) = 0.8102;
    conditionMatrix(11,6) = 0.9018;
    conditionMatrix(12,6) = 0.6301;
    conditionMatrix(13,6) = 0.9206;
    conditionMatrix(14,6) = 0.8452;
207 conditionMatrix(15,6) = 0.8633;
    conditionMatrix(16,6) = 1.0210; %0.8121;
    conditionMatrix(17,6) = 0.6624; %0.5279;
    conditionMatrix(18,6) = 0.3566;
    conditionMatrix(19,6) = 0.3648;
212 conditionMatrix(20,6) = 0.8446;
    conditionMatrix(21,6) = 0.4233;
    conditionMatrix(22,6) = 0.5240;
    conditionMatrix(23,6) = 0.8734;
    conditionMatrix(24,6) = 0.4055;
217 conditionMatrix(26,6) = 0.5906;
    conditionMatrix(27,6) = 0.8308;
    conditionMatrix(28,6) = 0.7847;
    conditionMatrix(29,6) = 0.2775;
    conditionMatrix(30,6) = 0.3823;
222
    % set static leakage area - number of very large holes left open
    conditionMatrix(:,7) = 6;
    conditionMatrix(25:30,7) = 5;

227 % set off cushion displacment in column 8
    conditionMatrix(:,8) = 106.24;
    conditionMatrix(1:6,8) = 106.3;
    conditionMatrix(7:12,8) = 105.6;
    conditionMatrix(13:18,8) = 106.4;
232 conditionMatrix(19:24,8) = 106.7;
    conditionMatrix(25:30,8) = 106.2;

    % set on cushion position in column 9
    conditionMatrix(1:6,9) = [88.3 80.0 90.6 84.1 93.8 88.4];
237 conditionMatrix(7:12,9) = [87.6 89.9 93.1 78.0 82.9 87.6];
    conditionMatrix(13:18,9) = [88.9 90.7 94.0 78.8 83.5 88.3];
    conditionMatrix(19:24,9) = [92.2 93.6 96.0 84.5 88.0 91.2];
    conditionMatrix(25:30,9) = [90.0 91.7 94.4 81.2 85.1 88.9];

242 % assign the values into the matrix for later reading

    % setting test rig specific parameters to get step response match
    % plenumStiffness = 6E4; %6E4 column 10
    % parasiticLeakageSquareMetres = 2.5E-3; %2.5E-3 2 metre length, 1mm wide column 11
247 % frictionCoulomb = 9; % 9E0 column 12
    % frictionViscous = 2.2E2; % 2.20E2 column 13
    % inputFlapperFactor = 1.4; % 1.4 scales the input flapper column 14

    % set the current condition for easy trial and error
252 jCondition = [1:24 26:30]; %[8 13 16 17 18 20 26]


    % store the test rig parameters in the condition matrix
    % conditionMatrix(iCondition,10:14)=
257 % [plenumStiffness parasiticLeakageSquareMetres frictionCoulomb frictionViscous inputFlapperFactor]

    conditionMatrix(1,10:14) =  [6.0E5  2.0E-3   8  2.0E3    1.2];
    conditionMatrix(2,10:14) =  [6.0E5  2.0E-3  14  2.0E3    1.2];
    conditionMatrix(3,10:14) =  [6.0E5  2.0E-3   2  1.9E3    1.2];
262 conditionMatrix(4,10:14) =  [6.0E5  2.0E-3  20  1.8E3    1.2];
    conditionMatrix(5,10:14) =  [6.0E5  2.0E-3   3  1.6E3    1.2];
    conditionMatrix(6,10:14) =  [6.0E5  2.0E-3   1  1.2E3    1.2];
    conditionMatrix(7,10:14) =  [9.0E4  1.5E-3  16  9.0E2    1.2];
    conditionMatrix(8,10:14) =  [9.0E4  2.2E-3   6  9.0E2    1.2];%prime H_0=0.297m
267 conditionMatrix(9,10:14) =  [9.0E4  2.2E-3  11  8.0E2    1.2];
    conditionMatrix(10,10:14) = [9.0E4  2.2E-3   6  1.6E3    1.2];
    conditionMatrix(11,10:14) = [9.0E4  2.2E-3   9  6.0E2    1.2];
    conditionMatrix(12,10:14) = [9.0E4  2.2E-3  25  6.0E2    1.2];
    conditionMatrix(13,10:14) = [2.5E4  1.6E-3   6  2.2E2    1.2];
272 conditionMatrix(14,10:14) = [2.5E4  1.2E-3   6  1.0E3    1.2];%prime H_0=0.605m
    conditionMatrix(15,10:14) = [2.5E4  1.8E-3   8  1.5E3    1.2];
    conditionMatrix(16,10:14) = [2.5E4  2.0E-3  10  2.9E2    1.2];
```

```
    conditionMatrix(17,10:14) = [2.5E4  1.2E-3  10  2.0E2    1.2];
    conditionMatrix(18,10:14) = [2.5E4  1.6E-3   6  2.8E2    1.2];%alt H_0=0.605m
277 conditionMatrix(19,10:14) = [9.0E4  3.5E-3   5  5.5E2    1.2];
    conditionMatrix(20,10:14) = [9.0E4  3.0E-3   5  5.0E2    1.2];%prime H_0=0.802m
    conditionMatrix(21,10:14) = [9.0E4  2.0E-3  10  6.5E2    1.2];
    conditionMatrix(22,10:14) = [9.0E4  3.5E-3  12  5.9E2    1.2];
    conditionMatrix(23,10:14) = [9.0E4  3.0E-3   4  5.6E2    1.2];
282 conditionMatrix(24,10:14) = [9.0E4  2.0E-3  16  5.2E2    1.2];
    conditionMatrix(26,10:14) = [2.8E4  2.5E-3  10  2.8E2    1.2];%prime H_0=0.445m
    conditionMatrix(27,10:14) = [2.8E4  0.5E-3   9  2.3E2    1.2];
    conditionMatrix(28,10:14) = [2.8E4  4.0E-3   4  3.5E2    1.2];
    conditionMatrix(29,10:14) = [2.8E4  3.5E-3  10  2.1E2    1.2];
287 conditionMatrix(30,10:14) = [2.8E4  2.5E-3   4  2.4E2    1.2];

    viscousMean(1:6) = mean(conditionMatrix(1:6,13),'omitnan');
    viscousMean(7:12) = mean(conditionMatrix(7:12,13),'omitnan');
    viscousMean(13:18) = mean(conditionMatrix(13:18,13),'omitnan');
292 viscousMean(19:24) = mean(conditionMatrix(19:24,13),'omitnan');
    viscousMean(25:30) = mean(conditionMatrix(25:30,13),'omitnan');

    % conditionMatrix(1:6,13) = viscous(1);
    % conditionMatrix(7:12,13) = viscous(2);
297 % conditionMatrix(13:18,13) = viscous(3);
    % conditionMatrix(19:24,13) = viscous(4);
    % conditionMatrix(25:30,13) = viscous(5);

    legendtext = {'Experiment' 'Simulation'};
302
    % select an experimental run to use data from

    %% INITIATE THE LOOP
    fprintf('\nBeginning loop with conditions, %i.\n',jCondition);
307 for iCondition = jCondition % use jCondition when doing trial and error
    fprintf('\nStart loop, condition value is set to %i\n',iCondition);
    % set the plenum height
    plenumHeight = conditionMatrix(iCondition,2);
    % set the test rig parameters
312 % setting test rig specific parameters to get step response match
    plenumStiffness = conditionMatrix(iCondition,10);
    parasiticLeakageSquareMetres = conditionMatrix(iCondition,11);
    frictionCoulomb = conditionMatrix(iCondition,12);
    frictionViscous = conditionMatrix(iCondition,13);
317 inputFlapperFactor = conditionMatrix(iCondition,14);
    % modify the input volume
    transientFlapperSweptAngleRadian = flapperAngleRadian * inputFlapperFactor;
    % SET THE AIR EXIT AREA
    nStaticLeakageHoles = conditionMatrix(iCondition,7);
322 staticLeakageAreaSquareMetres = pi() * (staticLeakageHoleDiameterMetre/2)^2 * nStaticLeakageHoles;
    airExitAreaSquareMetres(iCondition) = conditionMatrix(iCondition,4)...
    + staticLeakageAreaSquareMetres + (exitAreaSwitch * parasiticLeakageSquareMetres);
    % set the nominal duct inlet speed, modifier of duct centreline
    % velocity
327 ductAirSpeedMetresPerSecond = 0.7 * conditionMatrix(iCondition,3);
    % calculate air supply volume flow rate, assuming turbulent duct flow
    Q_0 = 0.6 * ductAirSpeedMetresPerSecond * inletDuctDiameterMetre^2 * pi();
    % set the experimental run to compare to
    experimentalRun = conditionMatrix(iCondition,5);
332 % set the step time for the simulation
    simStepTime = 0.05;

    % report to user
    fprintf('\nRunning sim for parameter combination %d \n',iCondition);
337 fprintf('\tPlenum height:\t%.2fm \n',plenumHeight);
    fprintf('\tAir exit area:\t%.2Em^2 \n',airExitAreaSquareMetres(iCondition));
    fprintf('\tNominal inlet air speed:\t %.2Em.s^-1 \n',ductAirSpeedMetresPerSecond);
    fprintf('\tNominal air volume flow rate:\t %.2Em^3.s^-1 \n',Q_0);
    fprintf('\tExperimental run number:\t %i \n',experimentalRun);
342 fprintf('\nTest rig parameters\n');
    fprintf('\tPlenum Stiffness: \t %0.2E \n',plenumStiffness);
    fprintf('\tParasitic leakage area: \t %0.2Gm^2 \n',parasiticLeakageSquareMetres);
    fprintf('\tCoulomb friction: \t %0.2G \n',frictionCoulomb);
    fprintf('\tVelocity-dependent resistance: \t %0.2G \n',frictionViscous);
347 fprintf('\tFlapper factor: \t %0.2G \n',inputFlapperFactor);

    %% WORK OUT THE HOVER PLENUM PRESSURE (FROM THE SPRING CHANGE IN LENGTH,
    % CAN VERIFY FROM THE MANOMETER)
    % calculate the hover cushion gauge pressure from the difference in the
352 % spring extensions on and off cushion

    % find the change in spring extension from off cushion to on-cushion
    springExtensionMiliMetres = conditionMatrix(iCondition,8) - ...
    conditionMatrix(iCondition,9);
357 % convert to metres to make consistent
    springExtensionMetres = springExtensionMiliMetres/1000;
    % calculate plenum pressure by finding moments around the pivot point
    plenumPressureHoverNewtonPerSquareMetre = (springExtensionMetres *...
    springConstantExptNewtonPerMetre * springPositionXMetre)/...
362 (heaveDeckAreaSquareMetre * heaveDeckCentreOfPressureMetre);
    % add atmospheric pressure to get an absolute pressure in the plenum
    plenumAbsolutePressureHoverNewtonPerSquareMetre =...
    plenumPressureHoverNewtonPerSquareMetre + atmosPressureStaticNewtonPerSquareMetre;
    % assume plenum is at ambient temperature and calculate the air density
367 plenumDensityHoverKilogramPerCubicMetre = plenumAbsolutePressureHoverNewtonPerSquareMetre/...
    (GAS_CONSTANT_AIR * atmosTemperatureKelvin);
    % report to the user
    fprintf('\nPlenum air conditions...\n');
```

```
    fprintf('\tPlenum hover pressure: %.3G N/m^2 \n',plenumPressureHoverNewtonPerSquareMetre);
372 fprintf('\tPlenum air density:    %.3G kg/m^3 \n',plenumDensityHoverKilogramPerCubicMetre);

    %% Fan Slope

    % assume a basic average air speed in inlet duct
377

    % from experiment on blower flow rate versus duct static pressure
    %Q = Ap^2 + Bp + C;
    A = -0.001306;
382 B = -0.004188;
    C = 0.03497;

    ductPressurePascal = plenumPressureHoverNewtonPerSquareMetre -...
    0.5 * plenumDensityHoverKilogramPerCubicMetre * ductAirSpeedMetresPerSecond^2;
387
    % check for sensitivity to fan characteristic slope
    % fanslopeoverride = 1E-5;
    % fanslopeoverride = 0; % revert to a flat fan slope

392 fanSlope = fanslopeoverride * (2*A*ductPressurePascal + B);
    % report to user
    fprintf('\tInlet duct pressure: %0.3G Pa\n',ductPressurePascal);
    fprintf('\tFan Slope is:\t%0.3G Q/p_h\n',fanSlope);

397 %% Plenum stiffness - a simple model for the flexibilty of the plenum walls

    % plenumStiffness = 3.4E5;

    plenumFlexArea = plenumFlexSwitch * 0.8E0; % arbitrary 0.1m^2 effective flex area
402 plenumVolumeCubicMetres = heaveDeckAreaSquareMetre * plenumHeight;

    %% CALCULATE ALL THE GAINS FOR THE SIMULATION MODEL
    % calculate the gains for the simulation

407 K(1) = plenumDensityHoverKilogramPerCubicMetre * heaveDeckAreaSquareMetre *
        heaveDeckCentreOfPressureMetre;
    K(2) = plenumDensityHoverKilogramPerCubicMetre * transientFlapperUnitSweptVolumeCubicMetre;
    K(3) = SPECIFIC_HEAT_AIR*(1+(atmosPressureStaticNewtonPerSquareMetre/(
        plenumPressureHoverNewtonPerSquareMetre)));
    K(4) = plenumDensityHoverKilogramPerCubicMetre*heaveDeckAreaSquareMetre*plenumHeight;
    K(5) = heaveDeckAreaSquareMetre * heaveDeckCentreOfPressureMetre * (
        plenumPressureHoverNewtonPerSquareMetre);
412 K(6) = springConstantExptNewtonPerMetre * springPositionXMetre^2;
    K(7) = frictionCoefficient;
    K(8) = atmosAirDensityKilogramPerCubicMetre * airExitAreaSquareMetres(iCondition) *
        leakageAreaOrificeCoefficient;
    K(9) = 2*(plenumPressureHoverNewtonPerSquareMetre)/atmosAirDensityKilogramPerCubicMetre;
    K(10) = heaveDeckRotationalInertiaKilogramMetre;
417 K(11) = atmosAirDensityKilogramPerCubicMetre * plenumPressureHoverNewtonPerSquareMetre;
    K(12) = plenumPressureHoverNewtonPerSquareMetre * plenumFlexArea^2  / plenumStiffness;
    K(13) = plenumDensityHoverKilogramPerCubicMetre;
    K(14) = 100 / plenumVolumeCubicMetres;

422 %% RUN THE SIMULATION

    % set the ramp slope
    rampSlope = transientFlapperSweptAngleRadian/0.0001;

427 fprintf('\nRunning simulation... ');
    % setup the simulation to run for 5 seconds (allowing quasi-steady behaviour)
    sim('testRigModelElevenStep.slx',[0 5]);
    fprintf(' finished\n');

432 % calculate shift to align peaks
    % find the index of the peak response
    [Y,I] = max(yout_10(:,1));
    % find the equivalent time from the time vector
    timeSimPeakSecond = tout(I);
437 % find the time offset in seconds
    offsetSecond = conditionMatrix(iCondition,6) - timeSimPeakSecond;

    % % set up the text box
    % textx = 2.5;
442 % texty = max(yout_10(:,1)) * 0.4;
    % % set the lines of text
    % foo(1) = {['Condition: ',num2str(iCondition)]};
    % foo(2) = {['Nominal heave deck height: ',num2str(plenumHeight),' mm']};
    % foo(3) = {['Air volume flow rate: ',num2str(Q_0),' m^3.s^-1']};
447 % foo(4) = {['Air exit area: ',num2str(airExitAreaSquareMetres),' mm^2']};
    %
    %     % plot the simulation output
    %     nFigure = 300 + iCondition;
    %     figure(nFigure);
452 %     subplot(2,1,1);
    %     plot(tout,yout_10(:,1));
    %     grid on;
    %     ylabel('y mm');
    %     xlabel('time s');
457 %     text(textx,texty,foo,'BackgroundColor','white','FontSize',10,'FontName','Helvetica');
    %     subplot(2,1,2);
    %     plot(tout,yout_10(:,2));
    %     grid on;
    %     ylabel('angle rad');
462 %     xlabel('time s');
```

```
%
%
%
%
%
% % export the file to a PDF for inclusion into LaTeX
% %save the figure as a MATLAB file
%
% figureFileName = ['./output/stepSimulation/figureStepSimulation',num2str(iCondition)];
% savefig(figure(nFigure),figureFileName,'compact');
% pdfFileName = ['./output/stepSimulation/pdf/figureStepSimulation',num2str(iCondition)];
% pngFileName = ['./output/stepSimulation/png/figureStepSimulation',num2str(iCondition)];
% svgFileName = ['./output/stepSimulation/svg/figureStepSimulation',num2str(iCondition)];
% % print the figure as a landscape PDF for reviewing
% print(figure(nFigure),pdfFileName,'-dpdf','-fillpage');
% print(figure(nFigure),pngFileName,'-dpng');
% print(figure(nFigure),svgFileName,'-dsvg');
%
% % report to user
% fprintf('\tPlot %i of condition %i saved to files. \n',nFigure,iCondition);
% close(nFigure);



% plot over the experimental value
if not(isnan(experimentalRun))
F = openfig(['./output/stepExperiment/figureStepExperiment',num2str(experimentalRun),'.fig']);
plot((tout+offsetSecond),yout_10(:,1),'r');
title(titleText);
xlim([0 5]);
legend('Experiment','First Peak','Peaks','Simulation');

% export the file to a PDF for inclusion into LaTeX
%save the figure as a MATLAB file

figureFileName = ['./output/',directory,'/figure', filename, num2str(iCondition)];
savefig(figure(F),figureFileName,'compact');
pdfFileName = ['./output/',directory,'/figure',filename,num2str(iCondition)];
pngFileName = ['./output/',directory,'/figure',filename,num2str(iCondition)];
svgFileName = ['./output/',directory,'/figure',filename,num2str(iCondition)];
% print the figure as a landscape PDF for reviewing
print(figure(F),pdfFileName,'-dpdf','-fillpage');
print(figure(F),pngFileName,'-dpng');
print(figure(F),svgFileName,'-dsvg');
%close(F)

% report to user
fprintf('\tExperiment and Simulation plot %i of condition %i saved to files. \n',iCondition,iCondition)
    ;
fprintf('\tPath and figure filename %s \n',figureFileName);
else
fprintf('\tSkipping a run with no plot\n');
end
end
end
%% plot plenum stiffness
F = figure(100);
semilogy(conditionMatrix(:,2),conditionMatrix(:,10),'kx');
grid on;
%title('log plenum stiffness for each H_0');
ylim([1E-1 1E6]);
ylabel('Plenum stiffness factor (N.m^-1)');
xlabel('H_0 (m)');
% export the file to a PDF for inclusion into LaTeX
%save the figure as a MATLAB file
filename = 'stepPlenumStiffness';
figureFileName = ['./output/',filename,'/figure', filename];
savefig(figure(F),figureFileName,'compact');
pdfFileName = ['./output/',filename,'/figure',filename];
pngFileName = ['./output/',filename,'/figure',filename];
svgFileName = ['./output/',filename,'/figure',filename];
% print the figure as a landscape PDF for reviewing
print(figure(F),pdfFileName,'-dpdf','-fillpage');
print(figure(F),pngFileName,'-dpng');
print(figure(F),svgFileName,'-dsvg');
% report to user
fprintf('\tPath and figure filename %s \n',figureFileName);

%% plot velocity-dependent resistance versus height
F = figure(200);
plot(conditionMatrix(:,2),conditionMatrix(:,13),'kx');
hold on;
plot(conditionMatrix(:,2),viscousMean,'r+');
grid on;
%title('log plenum stiffness for each H_0');
ylim([0 2.0E3]);
ylabel('Velocity-dependent resistance factor');
xlabel('H_0 (m)');
hold off;
% export the file to a PDF for inclusion into LaTeX
%save the figure as a MATLAB file
filename = 'stepVelocityDependentResistance';
figureFileName = ['./output/',filename,'/figure', filename];
savefig(figure(F),figureFileName,'compact');
pdfFileName = ['./output/',filename,'/figure',filename];
```

```
pngFileName = ['./output/',filename,'/figure',filename];
svgFileName = ['./output/',filename,'/figure',filename];
% print the figure as a landscape PDF for reviewing
print(figure(F),pdfFileName,'-dpdf','-fillpage');
print(figure(F),pngFileName,'-dpng');
print(figure(F),svgFileName,'-dsvg');
% report to user
fprintf('\tPath and figure filename %s \n',figureFileName);

%% plot velocity-dependent resistance chronologically
viscousGlobalMean(1:30) = mean(conditionMatrix(:,13),'omitnan');
F = figure(300);
plot(conditionMatrix(1:6,5),conditionMatrix(1:6,13),'kx','DisplayName','H_0=1.1m');
hold on;
plot(conditionMatrix(7:12,5),conditionMatrix(7:12,13),'bx','DisplayName','H_0=0.3m');
plot(conditionMatrix(13:18,5),conditionMatrix(13:18,13),'gx','DisplayName','H_0=0.6m');
plot(conditionMatrix(19:24,5),conditionMatrix(19:24,13),'mx','DisplayName','H_0=0.8m');
plot(conditionMatrix(25:30,5),conditionMatrix(25:30,13),'cx','DisplayName','H_0=0.4m');

plot(conditionMatrix(1:6,5),viscousMean(1:6),'k—','DisplayName','mean H_0=1.1m');
plot(conditionMatrix(7:12,5),viscousMean(7:12),'b—','DisplayName','mean H_0=0.3m');
plot(conditionMatrix(13:18,5),viscousMean(13:18),'g—','DisplayName','mean H_0=0.6m');
plot(conditionMatrix(19:24,5),viscousMean(19:24),'m—','DisplayName','mean H_0=0.8m');
plot(conditionMatrix(25:30,5),viscousMean(25:30),'c—','DisplayName','mean H_0=0.4m');

plot(conditionMatrix(:,5),viscousGlobalMean,'r—','DisplayName','Global Mean');
grid on;
%title('log plenum stiffness for each H_0');
ylim([0 2.1E3]);
%xlim([0 400]);
ylabel('Velocity-dependent resistance factor');
xlabel('Run number');
legend;
hold off;
% export the file to a PDF for inclusion into LaTeX
%save the figure as a MATLAB file
filename = 'stepVelocityDependentResistance';
figureFileName = ['./output/',filename,'/figure', filename];
savefig(figure(F),figureFileName,'compact');
pdfFileName = ['./output/',filename,'/figure',filename];
pngFileName = ['./output/',filename,'/figure',filename];
svgFileName = ['./output/',filename,'/figure',filename];
% print the figure as a landscape PDF for reviewing
print(figure(F),pdfFileName,'-dpdf','-fillpage');
print(figure(F),pngFileName,'-dpng');
print(figure(F),svgFileName,'-dsvg');
% report to user
fprintf('\tPath and figure filename %s \n',figureFileName);

%% plot all the parameters

figure(900);
subplot(6,1,1);
plot(conditionMatrix(:,1),conditionMatrix(:,11),'x');
title('Leakage area (m^2)');
grid on;
subplot(6,1,2);
plot(conditionMatrix(:,1),conditionMatrix(:,12),'x');
title('Coulomb friction');
grid on;
subplot(6,1,3);
plot(conditionMatrix(:,1),conditionMatrix(:,13),'x');
title('Viscous friction');
grid on;
subplot(6,1,4);
plot(conditionMatrix(:,1),conditionMatrix(:,14),'x');
title('Input volume scale');
grid on;
subplot(6,1,5);
semilogy(conditionMatrix(:,1),conditionMatrix(:,10),'x');
title('Plenum stiffness');
grid on;
subplot(6,1,6);
plot(conditionMatrix(:,1),conditionMatrix(:,2),'x');
title('Plenum height');
ylabel('H_0 (m)');
xlabel('Condition number');
grid on;
```

D.5. Experimental data analysis for oscillating plenum volume

The following script analyses the experimental data and plots it on the appropriate graphs, ready to be overlaid with the theoretical predictions.

```
,
```

```
%% OscillatingExperimentResults
% Takes the raw time-series data from the oscillating plenum volume
% experiments, calculates mean response (shift) magntidue of response and
% phase of response and plots againts forcing frequency. These results are
% added to by another script that does the numerical solution and plots
% theory against experimental results

% set up the workspace
clc;
close all;
clear;
format shorteng;
fprintf('\nInitiating test rig simulations for an oscillating volume forcing...\n');
cd('/Users/paulminty/Dropbox/Unimelb/MATLAB/Test Rig Analysis/exp29');
fprintf('Current directory is set to:\n %s\n',pwd);


%% RETREIVE THE DATA THAT IS STATIC FOR THE TEST RIG
% load the test rig invariant parameters

initializeTestRigProperties;

%% OPEN THE DATA FOR THE EXPERIMENTAL RUNS
% load the data for the experimental runs

fprintf('\nWait, loading experimental data...\n');
load './vars/exp29Data.mat';
fprintf('Experimental data loaded.\n');
% number of experimental runs to consider
nRun = 167;

%% preallocate for speed

airLeakageAreaSquareMetres = NaN(1,nRun);
maxHeave = NaN(1,nRun);
minHeave = NaN(1,nRun);
frequencyVec = NaN(1,nRun);
meanHeight = NaN(1,nRun);
checkMean = NaN(1,nRun);
lagHeave = NaN(1,nRun);
amplitudeHeave = NaN(1,nRun);
frequencyMaxHeaveVec = NaN(1,nRun);
heightPlenum = NaN(1,nRun);
outlierProportion = NaN(1,nRun);
outlierFrequency = NaN(1,nRun);
minAbsHeave = NaN(1,nRun);
maxAbsHeave = NaN(1,nRun);
magAbsHeave = NaN(1,nRun);
meanAbsHeight = NaN(1,nRun);
phaseAngle = NaN(1,nRun);
% create a main results matrix for later plotting
% run number, frequency ratio, response volume to forced volume ratio, mean volume to
% forced volume ratio, leakage area, PI term for mean, PI term for
% magnitude, phase angle
oscillatingResults = NaN(nRun,9);

% set the list of hand-picked outliers
outliers = [44 47 54 68:72 81:83 94 100 110 136 147 153 163];

% set which peak to use to find the phase
indexPeakPhase = 3;

%% SET THE RUN THAT YOU WANT TO SIMULATE
% identify the experimental run that you want to simulate
% comment out the following line if you want to loop
%iRun = 20;

for condition = 1:9  %1:9 for full set
close all;
%oscillatingResults = NaN(nRun,6);

if condition == 1

% H = 0.292 A_L 0.567E-3
plenumHeight = 0.292; % 0.805 0.292 0.605
%airExitArea = 0.567E-3; % 0.822E-3; 0.567E-3 1.20E-3
%Q_0 = 6.99E-3;
plenumNaturalFrequencyExperimentHertz = 9.9;
plenumNaturalFrequencyOscExpHertz = 6.4;
iRecord = [62:72 95 105];
iRecordOne = iRecord;


elseif condition == 2

% H = 0.292 A_L = 0.822E-3
plenumHeight = 0.292; % 0.805 0.292 0.605
%airExitArea = 0.822E-3; % 0.822E-3; 0.567E-3 1.20E-3
%Q_0 = 9.29E-3;
plenumNaturalFrequencyExperimentHertz = 9.9;
plenumNaturalFrequencyOscExpHertz = 6.4;
iRecord = [73:83 97:99 104 107:109 114];
iRecordTwo = iRecord;


elseif condition == 3
```

```
97
    % H = 0.292 A_L = 1.2E-3
    plenumHeight = 0.292; % 0.805 0.292 0.605
    %airExitArea = 1.20E-3; % 0.822E-3; 0.567E-3 1.20E-3
    %Q_0 = 13.6E-3;
102 plenumNaturalFrequencyExperimentHertz = 9.9;
    plenumNaturalFrequencyOscExpHertz = 6.4;
    iRecord = [84:94 96 100:103 106 110:113];
    iRecordThree = iRecord;

107
    elseif condition == 4

    % H = 0.605 A_L = 0.567E-3
    plenumHeight = 0.605; % 0.805 0.292 0.605
112 %airExitArea = 0.567E-3; % 0.822E-3; 0.567E-3 1.20E-3
    %Q_0 = 5.75E-3;
    iCondition = 67:77;
    iRecord = [115:125 148 153 157 158 163 167];
    iRecordFour = iRecord;
117 plenumNaturalFrequencyExperimentHertz = 5.4;
    plenumNaturalFrequencyOscExpHertz = 6.0;


    elseif condition == 5
122
    % H = 0.605 A_L = 0.822E-3
    plenumHeight = 0.605; % 0.805 0.292 0.605
    %airExitArea = 0.822E-3; % 0.822E-3; 0.567E-3 1.20E-3
    %Q_0 = 8.97E-3;
127 iRecord = [126:136 150 152 154 156 160 162 164 166];
    iRecordFive = iRecord;
    plenumNaturalFrequencyExperimentHertz = 5.4; %6.9
    plenumNaturalFrequencyOscExpHertz = 6.0;

132
    elseif condition == 6

    % H = 0.605 A_L = 1.2E-3
    plenumHeight = 0.605; % 0.805 0.292 0.605
137 % airExitArea = 1.20E-3; % 0.822E-3; 0.567E-3 1.20E-3
    % Q_0 = 13.1E-3;
    iRecord = [137:147 149 151 155 159 161 165];
    iRecordSix = iRecord;
    plenumNaturalFrequencyExperimentHertz = 5.4; %6.9
142 plenumNaturalFrequencyOscExpHertz = 6.0;



    elseif condition == 7
147
    % H = 0.805 A_L = 0.567E-3
    plenumHeight = 0.805; % 0.805 0.292 0.605
    % airExitArea = 0.567E-3; % 0.822E-3; 0.567E-3 1.20E-3
    % Q_0 = 7.93E-3;
152 plenumNaturalFrequencyExperimentHertz = 5.2;
    plenumNaturalFrequencyOscExpHertz = 5.7;
    iRecord = [1:19 43:46 49 51 53:56 59 61];
    iRecordSeven = iRecord;

157
    elseif condition == 8

    % H = 0.805 A_L = 0.822E-3
    plenumHeight = 0.805; % 0.805 0.292 0.605
162 % airExitArea = 0.822E-3; % 0.822E-3; 0.567E-3 1.20E-3
    plenumNaturalFrequencyExperimentHertz = 5.2;
    plenumNaturalFrequencyOscExpHertz = 5.7;
    % Q_0 = 10.3E-3;
    iCondition = 12:22;
167 iRecord = [20:30 42 48 52 58];
    iRecordEight = iRecord;

    elseif condition == 9

172 % H = 0.805 A_L = 1.20E-3
    plenumHeight = 0.805; % 0.805 0.292 0.605
    airExitArea = 1.20E-3; % 0.822E-3; 0.567E-3 1.20E-3
    plenumNaturalFrequencyExperimentHertz = 5.2;
    plenumNaturalFrequencyOscExpHertz = 5.7;
177 % Q_0 = 13.4E-3;
    iRecord = [31:41 50 60];
    iRecordNine = iRecord;


182 else
    error('Wrong condition number entered');
    end


187 % set up a loop that does one leakage area
    %iRecord = [1:19 43:47 49 51 53:57 59 61:72 115:125];


    % set up a loop that only does everythjing
192 % iRecord = 1:167;
```

```
% assign a natural frequency from the transient input results
% for heave deck height 0.297
%     plenumNaturalFrequencyExperimentHertz = 9.9;
%     if heightPlenum(iRun) > 0.297
%         plenumNaturalFrequencyExperimentHertz = 8.2;
%     end
%     if heightPlenum(iRun) > 0.445
%         plenumNaturalFrequencyExperimentHertz = 6.9;
%     end
%     if heightPlenum(iRun) > 0.612
%         plenumNaturalFrequencyExperimentHertz = 6.7;
%     end
%     if heightPlenum(iRun) > 0.802
%         plenumNaturalFrequencyExperimentHertz = 5.2;
%     end


% this is the start point of any loop - end at line 231
for iIndex = 1:length(iRecord)
iRun = iRecord(iIndex);
oscillatingResults(iRun,1) = iRun;

% set up basic vectors for describing experimental runs
heightPlenum(iRun) = exp29Data(iRun).hoverHeightMiliMetres/1000;

% tell the user about the run being done
fprintf('\nExperimental run: %d\n', iRun);
fprintf('\tRun ID:                    %s run %d. \n', exp29Data(iRun).type,exp29Data(iRun).iRun);
fprintf('\t Experimental condition: %d. \n',exp29Data(iRun).condition);
fprintf('\tHover height:              %1.3f m \n', heightPlenum(iRun));
fprintf('\tSmall leakage holes open: %d \n', exp29Data(iRun).leakageHoles);
fprintf('\tMotor speed setting:       %d \n',exp29Data(iRun).motorSpeedSetting);


%% WORK OUT THE ATMOSPHERIC PRESSURE AND AIR DENSITY
% retrieve the atmospheric conditions

atmosPressureStaticNewtonPerSquareMetre = exp29Data(iRun).atmosphericPressurePascals;
atmosTemperatureKelvin = exp29Data(iRun).temperatureAtmosphereCelsius + ICE_MELTING_POINT_KELVIN;
atmosAirDensityKilogramPerCubicMetre = atmosPressureStaticNewtonPerSquareMetre/...
(GAS_CONSTANT_AIR * atmosTemperatureKelvin);

fprintf('\nAtmospheric Conditions\n');
fprintf('\tAtmospheric pressure:    %d N/m^2 \n',atmosPressureStaticNewtonPerSquareMetre);
fprintf('\tAmbient temperature:     %3.1f degrees C \n',exp29Data(iRun).temperatureAtmosphereCelsius);
fprintf('\tAtmospheric air density: %5.4f kg/m^3 \n', atmosAirDensityKilogramPerCubicMetre);

%% WORK OUT THE HOVER PLENUM PRESSURE (FROM THE SPRING CHANGE IN LENGTH,
% CAN VERIFY FROM THE MANOMETER)
% calculate the hover cushion gauge pressure from the difference in the
% spring extensions on and off cushion

% find the change in spring extension from off cushion to on-cushion
springExtensionMiliMetres = exp29Data(iRun).displacmentOffCushionMiliMetres - ...
exp29Data(iRun).displacmentOnCushionMiliMetres;
% convert to metres to make consistent
springExtensionMetres = springExtensionMiliMetres/1000;
% calculate plenum pressure by finding moments around the pivot point
plenumPressureHoverNewtonPerSquareMetre = (springExtensionMetres *...
springConstantExptNewtonPerMetre * springPositionXMetre)/...
(heaveDeckAreaSquareMetre * heaveDeckCentreOfPressureMetre);
% check against the reading taken using a home-built manometer
plenumPressureManometer = exp29Data(iRun).cushionPressurePascals;
% add atmospheric pressure to get an absolute pressure in the plenum
plenumAbsolutePressureHoverNewtonPerSquareMetre =...
plenumPressureHoverNewtonPerSquareMetre + atmosPressureStaticNewtonPerSquareMetre;
% assume plenum is at ambient temperature and calculate the air density
plenumDensityHoverKilogramPerCubicMetre = plenumAbsolutePressureHoverNewtonPerSquareMetre/...
(GAS_CONSTANT_AIR * atmosTemperatureKelvin);
% report to the user
fprintf('\nPlenum air conditions...\n');
fprintf('\tPlenum hover pressure: %.3G N/m^2 \n',plenumPressureHoverNewtonPerSquareMetre);
fprintf('\tPlenum air density:    %.3G kg/m^3 \n',plenumDensityHoverKilogramPerCubicMetre);

%% WORK OUT THE LEAKAGE AREA FROM THE EXPERIMENTAL NOTES ABOUT HOLES THAT ARE OPEN
% find the leakage area from the number of open holes

% the big holes opened up and left open, recorded in notes
nStaticLeakageHoles = exp29Data(iRun).leakageMainHoles;
% Diameter of one static leakage hole in metres
staticLeakageHoleDiameterMetre = 19.0E-3;
% the area of the static leakage area
staticLeakageAreaSquareMetres =...
pi() * (staticLeakageHoleDiameterMetre/2)^2 * nStaticLeakageHoles;
% the number of holes opened for the specific run
nDynamicLeakageHoles = exp29Data(iRun).leakageHoles;
% diameter of smaller leakage holes in metres
dynamicLeakageHoleDiameterMetre = 9.0E-3;
% the total area of small open holes
dynamicLeakageAreaSquareMetres =...
pi() * (dynamicLeakageHoleDiameterMetre/2)^2 * nDynamicLeakageHoles;
% sum to get the total
airLeakageAreaSquareMetres(iRun) =...
```

```
    staticLeakageAreaSquareMetres + dynamicLeakageAreaSquareMetres;
    % add to the results
    oscillatingResults(iRun,5) = airLeakageAreaSquareMetres(iRun);
292 % report to user
    fprintf('\tLeakage area: %.2E m^2 \n',airLeakageAreaSquareMetres(iRun));

    %% CALCULATE THE NATURAL FREQUENCY AND DAMPING
    % uses the expressions published in Kaplan et al (1981)
297 % very simplified from full equations (by Kaplan)
    % left in translation, rather than rotation

    % first constant
    rho_0 = plenumDensityHoverKilogramPerCubicMetre;
302 h_c = heightPlenum(iRun);
    A_c = heaveDeckAreaSquareMetre;
    gamma = 1.4; % adiabatic constant
    p_a = atmosPressureStaticNewtonPerSquareMetre;
    p_0 = plenumPressureHoverNewtonPerSquareMetre;
307
    K1 = KayOne(rho_0, h_c, A_c, gamma, p_a, p_0);
    % second constant
    C_ns = leakageAreaOrificeCoefficient;
    rho_a = atmosAirDensityKilogramPerCubicMetre;
312
    K2 = KayTwo(rho_0, C_ns, p_0, rho_a);

    % third constant
    % assume air volume flow rate through the system is at equilibrium
317 % assume all exit area acts as a single orifice
    % find velocity of escaping air by applying Bernoulli
    airExitVelocityMetresPerSecond = sqrt(2*...
    plenumPressureHoverNewtonPerSquareMetre/...
    plenumDensityHoverKilogramPerCubicMetre);
322 % as the exit is a sharp hole in a plane surface, the orifice coefficient
    % modifies the exit area, giving the volume flow rate

    Q_0 = airExitVelocityMetresPerSecond * leakageAreaOrificeCoefficient * ...
    airLeakageAreaSquareMetres(iRun);
327
    % delQdelp is defined as -140 in the test rig properties

    K3 = KayThree(rho_0, Q_0, p_0, delQdelp);

332 % natural frequency
    A_b = heaveDeckAreaSquareMetre;
    m = heaveDeckMassKilogram;
    h_b = heightPlenum(iRun);

337 omega_n = SESNatFreq(A_b, p_0, m, h_b);
    plenumNaturalFrequencyHertz = omega_n/(2 * pi());


    % damping (of air compression related oscillations)
342 zeta = DampingRatio(K3, omega_n, K1);

    % report to the user
    fprintf('\nThe nominal dynamic characteristics...\n');
    fprintf('\tNatural frequency %.2f Hz or %.2f rad/s \n',plenumNaturalFrequencyHertz,omega_n);
347 fprintf('\tThe damping ratio of oscillations is %.2f \n',zeta);

    %% OPEN THE SENSOR DATA FOR THE FLAPPER

    % set up the time vector
352 timeVec = exp29Data(iRun).timeVector;
    % find the sampling rate
    sampleRate = (length(timeVec)-1)/timeVec(length(timeVec));
    % report to the user
    fprintf('\nThe time and sample rate of the run are:\n');
357 fprintf('\tLength of run:  %2.2f seconds\n',timeVec(length(timeVec)));
    fprintf('\tSample rate: %5.1f samples per second\n',sampleRate);
    % put the flapper sensor reading into a simple vector in memory
    flapperVec = exp29Data(iRun).pumpVector;

362 %% WORK OUT THE FREQUENCY OF THE FORCING (SO IT COULD BE PLOTTED LATER).
    % STORE IN ARRAY.
    % Use findpeaks to find period
    % apply find peaks to get a time series of peaks that are genuine maxima
    [pksFlapper,locFlapper] =...
367 findpeaks(flapperVec,sampleRate,'MinPeakHeight',0.75*max(flapperVec),'MinPeakProminence',0.5);
    % findpeaks(flapperVec,sampleRate,'MinPeakHeight',0.75*max(flapperVec),'MinPeakProminence',0.5);
    % find the mean of the maximum peaks (to check angle and volume)
    maxFlapper = mean(pksFlapper);
    % findpeaks on the minima
372 pksMinFlapper =...
    -1 * findpeaks((-1 * flapperVec),sampleRate,'MinPeakHeight',-0.75*max(flapperVec),'MinPeakProminence'
        ,0.5);
    % find the mean minimum peak magnitude

    minFlapper = mean(pksMinFlapper);
377

    % go through the peaks and find all the times between peaks
    % preallocate for speed
    periodFlapperPeaks = NaN(1,length(locFlapper)-1);
382
    for i = 2:length(locFlapper)
```

```
    periodFlapperPeaks(i-1) = locFlapper(i) - locFlapper(i-1);
    end
    % find the mean time between peaks
387 meanPeriodFlapperPeaksSeconds = mean(periodFlapperPeaks);
    % from the period, find the frequency in Hertz
    meanFrequencyFlapperPeaksHertz = 1/meanPeriodFlapperPeaksSeconds;
    % convert Hertz to Radians per Second
    meanFrequencyFlapperPeaksRadiansPerSecond = 2*pi()*meanFrequencyFlapperPeaksHertz;
392 % put in a vector for plotting for frequency
    frequencyVec(iRun) = meanFrequencyFlapperPeaksHertz;
    % find the ratio of forcing frequency to the natural frequency
    frequencyRatio = meanFrequencyFlapperPeaksHertz/plenumNaturalFrequencyExperimentHertz;
    frequencyRatioOsc = meanFrequencyFlapperPeaksHertz/plenumNaturalFrequencyOscExpHertz;
397 % add the frequency ratio to the result matrix to use as the abscissa
    oscillatingResults(iRun,2) = frequencyRatioOsc;
    % log the actual pumping frequency for plotting
    oscillatingResults(iRun,6) = meanFrequencyFlapperPeaksHertz;

402 % find the volume of the pumping
    pumpedVolumeCubicMetres = oscillatingFlapperSweptAngleRadian *
        oscillatingFlapperUnitSweptVolumeCubicMetre;

    % report to the user
    fprintf('\nThe frequency of the volume forcing is:\n');
407 fprintf('\t%4.2f Hertz \n',meanFrequencyFlapperPeaksHertz);
    fprintf('\t%4.2f rad/sec \n',meanFrequencyFlapperPeaksRadiansPerSecond);
    fprintf('\tNatural frequency %.2f Hz \n',plenumNaturalFrequencyExperimentHertz);
    fprintf('\tFrequency ratio %.2f \n',oscillatingResults(iRun,2));
    fprintf('\tPumped volume %.2G m^3 \n',pumpedVolumeCubicMetres);
412 fprintf('\tMean maximum flapper sensor %.2f mm \n', maxFlapper);
    fprintf('\tMean minimum flapper sensor %.2f mm \n',minFlapper);


    %% CALCULATE THE MEAN HEAVE HEIGHT AND STORE IN ARRAY
417 clear heaveVec pksMaxHeave pksMinHeave meanHeightVec maxHeaveVec minHeaveVec;

    % extract the heave deck sensor data from the data structure and put in a
    % simple array
    heaveVec = (exp29Data(iRun).displacmentOnCushionMiliMetres - exp29Data(iRun).heaveVector);
422 % find the simple linear trend, the DC shift
    meanAbsHeight(iRun) = mean(heaveVec);
    % reset the first element of the heave meassurement to remove
    % measurement artifacts that affect plotting
    heaveVec(1:40) = meanAbsHeight(iRun);
427
    % detrend the heave vector to find maxima, minima and magnitude, this
    % has to be added back in to find the shift
    detrendHeaveVec = heaveVec - meanAbsHeight(iRun);

432 % CALCULATE THE AMPLITUDE OF THE HEAVE OSCILLATIONS AND STORE IN ARRAY
    % use findpeaks to get all the peaks so an average of peaks can be used.

    % simple absolute maximum and minimum
    [minAbsHeave(iRun),maxAbsHeave(iRun)] = bounds(heaveVec);
437 % simple magnitude
    magAbsHeave(iRun) = maxAbsHeave(iRun) - minAbsHeave(iRun);

    % findpeaks on the maxima
    %findpeaks(heaveVec,sampleRate,'MinPeakHeight',0.60*max(heaveVec(50:length(heaveVec))),'
        MinPeakProminence',0.25);
442 %[pksMaxHeave, locMaxHeave] =...
    %     findpeaks(heaveVec,sampleRate,'MinPeakHeight',0.90*max(heaveVec(50:length(heaveVec))),'
        MinPeakProminence',0.25);
    [pksMaxHeave, locMaxHeave] =...
    findpeaks(detrendHeaveVec,sampleRate,'MinPeakHeight',0.75*max(detrendHeaveVec(50:length(heaveVec))),'
        MinPeakProminence',0.25);
    % undo the detrend
447 pksMaxHeave = pksMaxHeave + meanAbsHeight(iRun);
    % find the mean maximum peak magnitude
    maxHeave(iRun) = mean(pksMaxHeave);
    % set a vector for plotting
    %maxHeaveVec(1:length(timeVec)) = maxHeave(iRun);
452 %maxHeaveVec(1:length(timeVec)) = maxAbsHeave(iRun);

    % findpeaks on the minima
    % reflect the heave vector so that findpeaks can work on minima
    reflectHeaveVec = -1 * detrendHeaveVec;
457 pksMinHeave =...
    -1 * findpeaks((reflectHeaveVec),sampleRate,'MinPeakHeight',0.75*max(reflectHeaveVec(50:length(heaveVec
        ))),'MinPeakProminence',0.25);

    % find the mean minimum peak magnitude, add back in the detrend factor
    % now
462 minHeave(iRun) = mean(pksMinHeave) + meanAbsHeight(iRun);
    % set up a vector for plotting
    %minHeaveVec(1:length(timeVec)) = minHeave(iRun);
    %minHeaveVec(1:length(timeVec)) = minAbsHeave(iRun);

467 % find the mean of the entire sample
    meanHeight(iRun) = mean([maxHeave(iRun) minHeave(iRun)]);

    if iIndex == 1
    heaveZero = mean(meanHeight(iRun));
472 end
    meanHeight(iRun) = meanHeight(iRun) - heaveZero;
    % as a check compare the mean of the mean of the peaks to the overall mean
```

```
    checkMean(iRun) = meanAbsHeight(iRun) - mean([maxHeave(iRun) minHeave(iRun)]);
    % set up a vector for plotting
477 meanHeightVec(1:21) = meanHeight(iRun);
    % find the non-dimensional ratio of mean height to cube root of forcing volume
    % begin by finding angle swept in the mean height
    meanAngle = atan(meanHeight(iRun)/(displacementSensorTwoPositionXMetre*1000));
    meanVolume = (meanAngle/(2*pi())) * (pi() * heaveDeckLengthMetre^2 * heaveDeckWidthMetre);
482 meanRatio = meanVolume/pumpedVolumeCubicMetres;
    oscillatingResults(iRun,3) = meanRatio;
    oscillatingResults(iRun,7) = meanRatio * (airLeakageAreaSquareMetres(iRun)/plenumHeight^2);

    % find the absolute magnitude
487 amplitudeHeave(iRun) = maxHeave(iRun) - minHeave(iRun);
    % create two vectors to plot over time-series, adjust for first vector
    % being zero shift
    maxHeaveLine(1:21) = maxHeave(iRun)-heaveZero;
    minHeaveLine(1:21) = minHeave(iRun)-heaveZero;
492 % find the angle swept during oscillation (does not include the mean
    % shift)
    amplitudeAngle = atan(amplitudeHeave(iRun)/(displacementSensorTwoPositionXMetre*1000));
    % find the volume of the oscillation
    amplitudeVolume = (amplitudeAngle/(2*pi())) * (pi() * heaveDeckLengthMetre^2 * heaveDeckWidthMetre);
497 % find the ratio of the heave deck oscillating volume to the pumped
    % volume
    amplitudeRatio = amplitudeVolume/pumpedVolumeCubicMetres;
    % add to the results matrix
    oscillatingResults(iRun,4) = amplitudeRatio;
502 oscillatingResults(iRun,8) = amplitudeRatio * (airLeakageAreaSquareMetres(iRun)/plenumHeight^2);


    % go through the peaks and find all the times between peaks
    % preallocate for speed
507 periodMaxHeave = NaN(1,length(locMaxHeave)-1);

    for i = 2:length(locMaxHeave)
    periodMaxHeave(i-1) = locMaxHeave(i) - locMaxHeave(i-1);
    end
512 % find the mean time between peaks
    meanPeriodMaxHeaveSeconds = mean(periodMaxHeave);
    % from the period, find the frequency in Hertz
    meanFrequencyMaxHeaveHertz = 1/meanPeriodMaxHeaveSeconds;
    % convert Hertz to Radians per Second
517 meanFrequencyMaxHeaveRadiansPerSecond = 2*pi()*meanFrequencyMaxHeaveHertz;
    % put in a vector for plotting for frequency
    frequencyMaxHeaveVec(iRun) = meanFrequencyMaxHeaveHertz;

    % test for outliers
522 outlierProportion(iRun) = abs(frequencyMaxHeaveVec(iRun)- frequencyVec(iRun));
    if outlierProportion(iRun) > 0.6
    outlierFrequency(iRun) = frequencyMaxHeaveVec(iRun);
    else
    outlierFrequency(iRun) = NaN;
527 end

    %% PHASE
    % which peak to work from
    indexPeakPhase = 3;
532 % calculate the time difference between the two peaks
    lagHeave(iRun) = locFlapper(indexPeakPhase) - locMaxHeave(indexPeakPhase);
    % convert from time to angle in radian
    % ratio of lag in seconds to period in seconds multiplied by the angle
    % in a cycle gives phase lag. Same as multiplying the time difference
537 % by the frequency in radians per second.
    phaseAngle(iRun) = lagHeave(iRun) * meanFrequencyMaxHeaveRadiansPerSecond;
    oscillatingResults(iRun,9) = phaseAngle(iRun);

    %% plot the input and output displacements for illustration
542 % find the power spectrum and plot, showing forcing frequency and
    % natural frequency

    % power spectrum of output
    [pyy,fy] = pspectrum(heaveVec,timeVec,'FrequencyLimits',[0 20],'FrequencyResolution',0.25,'Leakage'
        ,0.85,'MinThreshold',-20);
547 % power spectrum of input
    [pxx,fx] =pspectrum((flapperVec-mean(flapperVec)),timeVec,'FrequencyLimits',[0 20],'FrequencyResolution
        ',0.25,'Leakage',0.85,'MinThreshold',-20);

    % plotting
    F = figure(iRun);
552 sgtitle(sprintf('Run %i: H_0 = %.2fm, A_e = %3.2Em^2',iRun,heightPlenum(iRun),
        airLeakageAreaSquareMetres(iRun)));
    subplot(3,1,1);
    plot(timeVec,(heaveVec-heaveZero),'b',timeVec,(flapperVec-mean(flapperVec)),'m');
    xlabel('Time (s)');
    ylabel('Displacement (mm)');
557 legend('Output','Input');
    xlim([0 2]);
    %plot max and min heave
    hold on;
    plot(0:0.1:2,maxHeaveLine,'b:','DisplayName','Maximum heave');
562 plot(0:0.1:2,minHeaveLine,'b-.','DisplayName','Minimum heave');
    % plot mean heave
    plot(0:0.1:2,meanHeightVec,'r--','DisplayName','Mean heave');
    % plot peak analysed for phase
    %plot(locMaxHeave(indexPeakPhase),pksMaxHeave(indexPeakPhase),'bx','DisplayName','Peak Output');
```

```
%plot(locFlapper(indexPeakPhase),(pksFlapper(indexPeakPhase)-mean(flapperVec)),'mx','DisplayName','Peak Input');
hold off;
subplot(3,1,2);
plot(fy,pow2db(pyy),'b','DisplayName','Output');
xlim([0 20]);
grid on;
title('Power spectrum of output');
ylabel('Power (dB)');
xlabel('\omega (Hz)')
hold on;
plot(meanFrequencyFlapperPeaksHertz,0,'gx',plenumNaturalFrequencyExperimentHertz,0,'r*');
hold off;
legend('Power Spectrum', 'Frequency of Forcing', 'Damped Frequency');
subplot(3,1,3);
plot(fx,pow2db(pxx),'m','DisplayName','Input');
xlim([0 20]);
grid on;
title('Power spectrum of input');
ylabel('Power (dB)');
xlabel('\omega (Hz)');
hold on;
plot(meanFrequencyFlapperPeaksHertz,0,'gx',plenumNaturalFrequencyExperimentHertz,0,'r*');
legend('Power Spectrum', 'Frequency of Forcing', 'Damped Frequency');
hold off;

%save the figure as a MATLAB file
figureFileName = ['./output/ExpOscillateResultSpectrum/ExpOscillateResultSpectrum',num2str(iRun)];
savefig(figure(F),figureFileName,'compact');
pdfFileName = ['./output/ExpOscillateResultSpectrum/ExpOscillateResultSpectrum',num2str(iRun)];
pngFileName = ['./output/ExpOscillateResultSpectrum/ExpOscillateResultSpectrum',num2str(iRun)];
svgFileName = ['./output/ExpOscillateResultSpectrum/ExpOscillateResultSpectrum',num2str(iRun)];
% print the figure as a landscape PDF for reviewing
print(figure(F),pdfFileName,'-dpdf','-fillpage');
print(figure(F),pngFileName,'-dpng');
print(figure(F),svgFileName,'-dsvg');
close(F);

% report to user
fprintf('Spectrum plot, figure %i, saved to files\n',iRun);


%report to the user
fprintf('\nThe heave deck motions are characterised...\n');
fprintf('\tHeave deck frequency:                  %3.1f Hz \n',frequencyMaxHeaveVec(iRun));
fprintf('\tmean of MAX heave deck peaks:       %3.1f mm \n',maxHeave(iRun));
fprintf('\tMAX of heaveVec:                       %3.1f mm \n',maxAbsHeave(iRun));
fprintf('\tmean of MIN heave deck peaks:       %3.1f mm \n',minHeave(iRun));
fprintf('\tMIN of heaveVec:                       %3.1f mm \n',minAbsHeave(iRun));
fprintf('\tMean heave deck displacement:          %3.1f mm \n',meanHeight(iRun));
fprintf('\tCheck SHIFT:                           %3.1f mm \n',checkMean(iRun));
fprintf('\tAmplitude of heave deck displacement: %3.1f mm \n',amplitudeHeave(iRun));
fprintf('\tLag between output and input:          %4.3f s \n',lagHeave(iRun));
fprintf('\tPhase angle:                           %4.3f rad \n',oscillatingResults(iRun,9));


end
%% STATISTICAL ANALYSIS OF MEASUREMENTS
% this only works for repeats (same plenum height, same leakage area, same
% frequency)
% does mean, mode, median, standard deviation of all key measurements

% frequency of flapper
meanInputFrequencyVecHertz = mean(frequencyVec,'omitNaN');
modeInputFrequencyVecHertz = mode(frequencyVec);
medianInputFrequencyVecHertz = median(frequencyVec,'omitNaN');
stdInputFrequencyVecHertz = std(frequencyVec,'omitNaN');
errorInputFrequencyVecHertz = stdInputFrequencyVecHertz/sqrt(length(iRecord));
% set up error bars - this has to be full plus and minus values as the data
% may be on either the x-axis or the y-axis
negErrorInputFrequencyVecHertz(1:length(iRecord)) = errorInputFrequencyVecHertz;
posErrorInputFrequencyVecHertz(1:length(iRecord)) = errorInputFrequencyVecHertz;
% report to user
fprintf('\nDescriptive statistics of the input frequency... \n')
fprintf('\tMean:               %.2f \n',meanInputFrequencyVecHertz);
fprintf('\tMode:               %.2f \n',modeInputFrequencyVecHertz);
fprintf('\tMedian:             %.2f \n',medianInputFrequencyVecHertz);
fprintf('\tStandard Deviation: %.2f \n',stdInputFrequencyVecHertz);
fprintf('\tStandard error:     %.2g \n',errorInputFrequencyVecHertz);

% frequency of the heave deck
meanOutputFrequencyVecHertz = mean(frequencyMaxHeaveVec,'omitNaN');
modeOutputFrequencyVecHertz = mode(frequencyMaxHeaveVec);
medianOutputFrequencyVecHertz = median(frequencyMaxHeaveVec,'omitNaN');
stdOutputFrequencyVecHertz = std(frequencyMaxHeaveVec,'omitNaN');
errorOutputFrequencyVecHertz = stdOutputFrequencyVecHertz/sqrt(length(iRecord));
% report to user
fprintf('\nDescriptive statistics of the output frequency... \n')
fprintf('\tMean:               %.2f \n',meanOutputFrequencyVecHertz);
fprintf('\tMode:               %.2f \n',modeOutputFrequencyVecHertz);
fprintf('\tMedian:             %.2f \n',medianOutputFrequencyVecHertz);
fprintf('\tStandard Deviation: %.2f \n',stdOutputFrequencyVecHertz);
fprintf('\tStandard error:     %.2g \n',errorOutputFrequencyVecHertz);

% time mean heave deck displacement
```

```
meanMeanHeaveDeckDisplacement = mean(meanHeight,'omitNaN');
modeMeanHeaveDeckDisplacement = mode(meanHeight);
medianMeanHeaveDeckDisplacement = median(meanHeight,'omitNaN');
stdMeanHeaveDeckDisplacement = std(meanHeight,'omitNaN');
errorMeanHeaveDeckDisplacement = stdMeanHeaveDeckDisplacement/sqrt(length(iRecord));
% set up error bars - this has to be full plus and minus values as the data
% may be on either the x-axis or the y-axis
negErrorMeanHeaveDeckDisplacement(1:length(iRecord)) = errorMeanHeaveDeckDisplacement;
posErrorMeanHeaveDeckDisplacement(1:length(iRecord)) = errorMeanHeaveDeckDisplacement;
% report to user
fprintf('\nDescriptive statistics of the mean heave deck displacement... \n')
fprintf('\tMean:                  %.2f \n',meanMeanHeaveDeckDisplacement);
fprintf('\tMode:                  %.2f \n',modeMeanHeaveDeckDisplacement);
fprintf('\tMedian:                %.2f \n',medianMeanHeaveDeckDisplacement);
fprintf('\tStandard Deviation:    %.2f \n',stdMeanHeaveDeckDisplacement);
fprintf('\tStandard error:        %.2g \n',errorMeanHeaveDeckDisplacement);

% heave deck magnitude
meanHeaveDeckAmplitude = mean(amplitudeHeave,'omitNaN');
modeHeaveDeckAmplitude = mode(amplitudeHeave);
medianHeaveDeckAmplitude = median(amplitudeHeave,'omitNaN');
stdHeaveDeckAmplitude = std(amplitudeHeave,'omitNaN');
errorHeaveDeckAmplitude = stdHeaveDeckAmplitude/sqrt(length(iRecord));
% report to user
fprintf('\nDescriptive statistics of the heave deck magnitude... \n')
fprintf('\tMean:                  %.2f \n',meanHeaveDeckAmplitude);
fprintf('\tMode:                  %.2f \n',modeHeaveDeckAmplitude);
fprintf('\tMedian:                %.2f \n',medianHeaveDeckAmplitude);
fprintf('\tStandard Deviation:    %.2f \n',stdHeaveDeckAmplitude);
fprintf('\tStandard error:        %.2g \n',errorHeaveDeckAmplitude);

% heave deck lag
meanHeaveDecklag = mean(lagHeave,'omitNaN');
modeHeaveDecklag = mode(lagHeave);
medianHeaveDecklag = median(lagHeave,'omitNaN');
stdHeaveDecklag = std(lagHeave,'omitNaN');
errorHeaveDecklag = stdHeaveDecklag/sqrt(length(iRecord));
% report to user
fprintf('\nDescriptive statistics of the heave deck lag... \n')
fprintf('\tMean:                  %.2f \n',meanHeaveDecklag);
fprintf('\tMode:                  %.2f \n',modeHeaveDecklag);
fprintf('\tMedian:                %.2f \n',medianHeaveDecklag);
fprintf('\tStandard Deviation:    %.2f \n',stdHeaveDecklag);
fprintf('\tStandard error:        %.2g \n',errorHeaveDecklag);

% print error bar plot of results versus frequency
x = meanInputFrequencyVecHertz;
y = meanMeanHeaveDeckDisplacement;
xneg = negErrorInputFrequencyVecHertz(1);
xpos = posErrorInputFrequencyVecHertz(1);
yneg = negErrorMeanHeaveDeckDisplacement(1);
ypos = posErrorMeanHeaveDeckDisplacement(1);


% figure(400);
% errorbar(x,y,yneg,ypos,xneg,xpos,'o');
% xlim([0 10]);
% ylim([0 10]);

%% plot the non-dimensional experimental results

fprintf('\nPlotting shift and magnitude for condition %i...',condition);
H = figure;
%foo = ['Experimental results A_L=',num2str(airLeakageAreaSquareMetres(iRun),'%1.2E'),'m^2 H_0=',
    num2str(mean(heightPlenum,'omitnan'),'%1.2E')];
%sgtitle(foo);
% first subplot, mean increase in volume versus frequency ratio
subplot(3,1,1);
hold on;
grid on;
%title('Response mean');
plot(oscillatingResults(iRecord,6),oscillatingResults(iRecord,3),'rx'); %,oscillatingResults(outliers
    ,6),oscillatingResults(outliers,3),'ro'

xlabel('\omega_f (Hz)');
ylabel('S_v (m^3/m^3)');
% second subplot, magnitude versus frequency
subplot(3,1,2);
hold on;
grid on;
%title('Response magnitude');
plot(oscillatingResults(iRecord,6),oscillatingResults(iRecord,4),'bx'); %,oscillatingResults(outliers
    ,6),oscillatingResults(outliers,4),'ro'

xlabel('\omega_f (Hz)');
ylabel('O_v (m^3/m^3)');

subplot(3,1,3);
hold on;
grid on;
%title('Response magnitude');
plot(oscillatingResults(iRecord,6),oscillatingResults(iRecord,9),'gx'); %,oscillatingResults(outliers
    ,6),oscillatingResults(outliers,4),'ro'
ylim([-pi() pi()]);
xlabel('\omega_f (Hz)');
ylabel('\phi (rad)');
```

```
    % save the figure as a Matlab file
757 savefig(H,['./output/figureResultsExp29-CON',num2str(condition)]);
    fprintf(' done.\n');


    end
762
    %% plot all the results (when looped)
    % assign data points to separate series for different leakage areas and
    % plenum heights

767 % dummy x-axis, waiting for frequency based vectors
    runVec = (1:167);

    % plot the key parameters on 3 subplots
    % plot the experimental factors on 3 subplots
772
    % open a unique figure
    figure(170);
    sgtitle('Oscillating Experiment Results');
    hold on;
777 grid on;
    % first subplot of 6 - for mean height
    subplot(6,1,1);
    plot(runVec,meanHeight,'kx',outliers,meanHeight(outliers),'ro',runVec,meanAbsHeight,'b+');
    title('Mean Heave Height');
782 ylabel('R_A (mm)');
    xlabel('Run');
    % second subplot of 6 - for magnitude
    subplot(6,1,2);
    plot(runVec,amplitudeHeave,'kx',outliers,amplitudeHeave(outliers),'ro',runVec,magAbsHeave,'b+');
787 title('Amplitude of heave');
    ylabel('R_M (mm)');
    xlabel('Run');
    grid on;
    % third subplot of 6 - lag
792 subplot(6,1,3);
    plot(runVec,phaseAngle,'kx',outliers,lagHeave(outliers),'ro');
    ylim([-pi() pi()]);
    title('Phase angle from output to input');
    ylabel('rad');
797 xlabel('Run');
    grid on;
    % fourth subplot of 6 - frequency
    subplot(6,1,4);
    plot(runVec,frequencyVec,'kx',runVec,frequencyMaxHeaveVec,'b+',runVec,outlierFrequency,'ro');
802 ylim([0 12]);
    title('Frequency of flapper and heave deck');
    ylabel('\omega_f (Hz)');
    xlabel('Run');
    legend('Input','Output');
807 grid on;
    % fifth subplot of 6 - Leakage Area
    subplot(6,1,5);
    plot(runVec,airLeakageAreaSquareMetres,'kx',outliers,airLeakageAreaSquareMetres(outliers),'ro');
    ylim([0 15E-4]);
812 title('Air Leakage Area');
    ylabel('A_e (m^2)');
    xlabel('Run');
    grid on;
    % sixth subplot of 6 - Plenum Height
817 subplot(6,1,6);
    plot(runVec,heightPlenum,'kx',outliers,heightPlenum(outliers),'ro');
    ylim([0 0.9]);
    title('Plenum Height');
    ylabel('H_0 (m)');
822 xlabel('Run');
    grid on;

    %save the figure as a MATLAB file
    figureFileName = 'figureSummaryExp29';
827 savefig(figure(170),['./output/',figureFileName],'compact');
    pdfFileName = ['./output/pdf/',figureFileName];
    pngFileName = ['./output/png/',figureFileName];
    svgFileName = ['./output/svg/',figureFileName];
    % print the figure as a landscape PDF for reviewing
832 print(figure(170),pdfFileName,'-dpdf','-fillpage');
    print(figure(170),pngFileName,'-dpng');
    print(figure(170),svgFileName,'-dsvg');

    %% plot non-dimensional results across all conditions
837 fprintf('\nPlotting shift and magnitude for all conditions...');
    H = figure(270);
    sgtitle('non-dimensional results');
    % first subplot, mean increase in volume versus frequency ratio
    subplot(2,1,1);
842 hold on;
    grid on;
    %title('Response mean');
    %plot(oscillatingResults(:,2),oscillatingResults(:,7),'bx',oscillatingResults(outliers,2),
        oscillatingResults(outliers,7),'ko');
    plot(oscillatingResults(iRecordOne,2),oscillatingResults(iRecordOne,7),'k+');
847 plot(oscillatingResults(iRecordTwo,2),oscillatingResults(iRecordTwo,7),'kx');
    plot(oscillatingResults(iRecordThree,2),oscillatingResults(iRecordThree,7),'kd');
```

```
plot(oscillatingResults(iRecordFour,2),oscillatingResults(iRecordFour,7),'b+');
plot(oscillatingResults(iRecordFive,2),oscillatingResults(iRecordFive,7),'bx');
plot(oscillatingResults(iRecordSix,2),oscillatingResults(iRecordSix,7),'bd');
plot(oscillatingResults(iRecordSeven,2),oscillatingResults(iRecordSeven,7),'m+');
plot(oscillatingResults(iRecordEight,2),oscillatingResults(iRecordEight,7),'mx');
plot(oscillatingResults(iRecordNine,2),oscillatingResults(iRecordNine,7),'md');
legend('Condition 1', 'Condition 2','Condition 3','Condition 4','Condition 5','Condition 6','Condition
    7','Condition 8','Condition 9');
legend('Location','NorthEastOutside');
xlabel('\omega_f/\omega_n');
ylabel('V_{ave}A_L/V_fh^2');
%ylim([-0.005 0.01]);
% second subplot, magnitude versus frequency
subplot(2,1,2);
hold on;
grid on;
%title('Response magnitude');
%plot(oscillatingResults(:,2),oscillatingResults(:,4),'bx',oscillatingResults(outliers,2),
    oscillatingResults(outliers,4),'ko');
plot(oscillatingResults(iRecordOne,2),oscillatingResults(iRecordOne,4),'k+');
plot(oscillatingResults(iRecordTwo,2),oscillatingResults(iRecordTwo,4),'kx');
plot(oscillatingResults(iRecordThree,2),oscillatingResults(iRecordThree,4),'kd');
plot(oscillatingResults(iRecordFour,2),oscillatingResults(iRecordFour,4),'b+');
plot(oscillatingResults(iRecordFive,2),oscillatingResults(iRecordFive,4),'bx');
plot(oscillatingResults(iRecordSix,2),oscillatingResults(iRecordSix,4),'bd');
plot(oscillatingResults(iRecordSeven,2),oscillatingResults(iRecordSeven,4),'m+');
plot(oscillatingResults(iRecordEight,2),oscillatingResults(iRecordEight,4),'mx');
plot(oscillatingResults(iRecordNine,2),oscillatingResults(iRecordNine,4),'md');
legend('Condition 1', 'Condition 2','Condition 3','Condition 4','Condition 5','Condition 6','Condition
    7','Condition 8','Condition 9');
legend('Location','NorthEastOutside');
xlabel('\omega_f/\omega_n');
ylabel('V_{mag}/V_f');

% save the figure as a Matlab file
fprintf('\n\tprinting...');
figureFileName = 'figureSummaryExp29-NONDIMENSIONAL';
savefig(H,['./output/',figureFileName],'compact');
pdfFileName = ['./output/pdf/',figureFileName];
pngFileName = ['./output/png/',figureFileName];
svgFileName = ['./output/svg/',figureFileName];
% print the figure as a landscape PDF for reviewing
print(H,pdfFileName,'-dpdf','-fillpage');
print(H,pngFileName,'-dpng');
print(H,svgFileName,'-dsvg');
fprintf('\n\tdone.\n');
```

D.6. Theoretical predictions

The following MATLAB script runs the Simulink model using a sine wave input for the plenum volume forcing. The resulting heave deck time-series is analysed and then plotted over the experimental results.

```
,
%% runModelElevenOscillating
% Paul Minty
% last edit 20190927
% Set up sinusoidal inputs, run the simulation, iterate the frequency, end
% up with a plot of amplitude and mean height and phase versus the frequency.

% set up the workspace
clc;
close all;
clear;
format shorteng;
clc;
fprintf('\nrunModelElevenOscillating\n');
fprintf('\tRun simulation Model Eleven Oscillating for varying plenum height and air exit area\n');
fprintf('\tUse an ideal sinusoidal form for the input oscillations\n');
fprintf('\tUses modifications to allow for test rig variations\n');
cd('/Users/paulminty/Dropbox/Unimelb/MATLAB/Test Rig Analysis/exp29');
fprintf('\tCurrent directory is set to: \n\t%s\n',pwd);


% RETREIVE THE DATA THAT IS STATIC FOR THE TEST RIG
% load the test rig invariant parameters
fprintf('\nSetting test rig properties\n');
fprintf('\tWait, running initializeTestRigProperties... ')
initializeTestRigProperties;
fprintf(' done.\n');
% load the data for the experimental runs
fprintf('\tWait, loading /vars/exp29Data.mat...');
load './vars/exp29Data.mat';
fprintf(' done.\n');


% number of experimental conditions to consider
% there are three plenum heights and three air exit areas
```

```
% at each condition there are 10 forcing frequency settings
fprintf('\nSetting up conditions for simulation\n');
nRun = 9;
% preallocate for speed
airLeakageAreaSquareMetres = NaN(1,nRun);
maxHeave = NaN(1,nRun);
minHeave = NaN(1,nRun);
frequencyVec = NaN(1,nRun);
meanHeight = NaN(1,nRun);
checkMean = NaN(1,nRun);
lagHeave = NaN(1,nRun);
magnitudeHeave = NaN(1,nRun);
frequencyMaxHeaveVec = NaN(1,nRun);
heightPlenum = NaN(1,nRun);
outlierProportion = NaN(1,nRun);
outlierFrequency = NaN(1,nRun);
phaseAngleRad = NaN(1,nRun);
phaseAngle = NaN(1,nRun);
% oscillatingResults = NaN(9,5);
% frequencyPumpRatio = NaN(1,51);
% amplitudeRatio = NaN(1,51);
% meanRatio = NaN(1,51);
% phase = NaN(1,51);
fprintf('\tBlank parameter matrices created\n');

% SET ATMOSPHERIC PRESSURE AND AIR DENSITY TO STANDARD ATMOSPHERE
% this is the same for all of the simulations
atmosPressureStaticNewtonPerSquareMetre = 101325;
atmosTemperatureKelvin = 20 + ICE_MELTING_POINT_KELVIN;
atmosAirDensityKilogramPerCubicMetre = atmosPressureStaticNewtonPerSquareMetre/...
(GAS_CONSTANT_AIR * atmosTemperatureKelvin);
fprintf('\tAtmospheric conditions set\n');

% create matrix for test rig parameters this will reset on every run
expParam = NaN(9,9);
% input the parameters that are adopted, these have to be manually edited if parameters change
% plenum height
expParam(1:3,1) = 292E-3;
expParam(4:6,1) = 605E-3;
expParam(7:9,1) = 805E-3;
% exit area
expParam([1 4 7],2) = 567E-6;
expParam([2 5 8],2) = 822E-6;
expParam([3 6 9],2) = 120E-5;
% air volume flow rate - found experimentally
expParam(1:3,3) = [7.93E-3 9.29E-3 13.6E-3];
expParam(4:6,3) = [5.75E-3 15.07E-3 13.1E-3];
expParam(7:9,3) = [7.93E-3 10.3E-3 13.4E-3];

% Coulomb friction - range is 4 - 18
expParam(:,4) = [10 8 10 6 6 6 4 9 4]; %[10 8 10 8 6 6 4 9 4]
% viscous friction - range is 200-600
expParam(:,5) = 5.6E2;
%expParam(1:3,5) = 9.0E2; %[1.0E3 1.4E3 1.8E3]
%expParam(4:6,5) = 5.9E2; %1.2E3 [2.2E2 1.7E3 1.6E3]
%expParam(7:9,5) = 5.8E2; %[6.25E2 7.0E2 8.0E2]
% plenum flexibility (spring constant in N/m)
%expParam(:,6) = 4.5E4; %5.1E4
expParam(1:3,6) = 9.0E4; %[3.4E4 3.6E4 3.8E4]
expParam(4:6,6) = 2.5E4; %1.4E5 [6.0E4 5.0E6 5.0E6]
expParam(7:9,6) = 9.0E4; %[2.0E5 2.3E5 2.8E5]

% parasitic leakage
expParam(:,7) = 0.0E0;
% condition that it matches, this allows multiple theories to be matched to one of the 9 sets
% of experimental results
expParam(:,8) = 1:9;
% initial run for each condition - enables plenum pressure calculation
expParam(1:3,9) = [62 73 84];
expParam(4:6,9) = [115 126 137];
expParam(7:9,9) = [11 20 32];

fprintf('\tExperimental parameters to match 9 experimental runs set\n');

% add extra test rig paremeters using this section
% select the configuration to edit, use slots 10 - whatever to avoid
% over-writing the experimentally determined parameters
% copy this section to create more alternatives
extraCondition = 10;
% this section is a convenient way to edit the matrix of test rig parameters
plenumHeight = 805E-3;
exitArea = 120E-5;
volumeFlowRate = 0.0E-3;
coulombFriction = 0.0E0;
viscousFriction = 2.19E2;
plenumFlexibility = 2.6E5;
parasiticLeakage = 0.0E-3;
initialRun = 137;
% which of the original 9 conditions does this get compared to?
condition = 9;
% apply the parameters to the matrix
expParam(extraCondition,1:9) = [plenumHeight exitArea volumeFlowRate coulombFriction viscousFriction
    plenumFlexibility parasiticLeakage condition initialRun];
fprintf('\tExperimental conditions for alternative %i is set\n',condition);

% select an experimental run to use data from
```

```
    iRun = 19; % run 19 is the best flapper time vector to use
    indexRuns = 0; % set to zero, increments inside loop
132
    % specify which experimental runs to process, use vector for multiple runs
    runConditions = 5; % 1:9 for all [1 3 5] for some, etc.
    fprintf('\nSelected conditions for simulation are:\n');
    fprintf('\t %i\n',runConditions);
137
    %% INITIATE THE LOOP TO DO ALL REQUESTED CONDITIONS
    for i = 1:length(runConditions)
    % find the condition we are going to simulate
    iCondition = runConditions(i);
142 % find which of the experiments we will match
    condition = expParam(iCondition,8);
    % find the initial run to get hover height data from
    iRun = expParam(iCondition,9);
    fprintf('\nThis simulation will be for:\n')
147 fprintf('\tExperimental condition: %i of 9\n',condition);
    fprintf('\tInitial run: %i\n',iRun);

    % SET PLENUM HEIGHT
    plenumHeight = expParam(iCondition,1);
152 fprintf('\tPlenum height %3.2Em \n',plenumHeight);

    % WORK OUT THE LEAKAGE AREA FROM THE EXPERIMENTAL NOTES ABOUT HOLES THAT ARE OPEN
    % find the leakage area from the number of open holes
    % the big holes opened up and left open, recorded in notes
157 nStaticLeakageHoles = exp29Data(iRun).leakageMainHoles;
    % Diameter of one static leakage hole in metres
    staticLeakageHoleDiameterMetre = 19.0E-3;
    % the area of the static leakage area
    staticLeakageAreaSquareMetres =...
162 pi() * (staticLeakageHoleDiameterMetre/2)^2 * nStaticLeakageHoles;
    % the number of holes opened for the specific run
    nDynamicLeakageHoles = exp29Data(iRun).leakageHoles;
    % diameter of smaller leakage holes in metres
    dynamicLeakageHoleDiameterMetre = 9.0E-3;
167 % the total area of small open holes
    dynamicLeakageAreaSquareMetres =...
    pi() * (dynamicLeakageHoleDiameterMetre/2)^2 * nDynamicLeakageHoles;
    % retrieve estimation of parasitic leakage
    parasiticLeakageSquareMetres = expParam(iCondition,7);
172 % sum to get the total
    airLeakageAreaSquareMetres(iRun) =...
    staticLeakageAreaSquareMetres + dynamicLeakageAreaSquareMetres...
    + parasiticLeakageSquareMetres;
    % add to the results
177 oscillatingResults(iCondition,5) = airLeakageAreaSquareMetres(iRun);
    % report to user
    fprintf('\tLeakage area: %.2E m^2 \n',airLeakageAreaSquareMetres(iRun));

    % WORK OUT THE HOVER PLENUM PRESSURE (FROM THE SPRING CHANGE IN LENGTH,
182 % CAN VERIFY FROM THE MANOMETER)
    % calculate the hover cushion gauge pressure from the difference in the
    % spring extensions on and off cushion
    % find the change in spring extension from off cushion to on-cushion
    springExtensionMiliMetres = exp29Data(iRun).displacmentOffCushionMiliMetres - ...
187 exp29Data(iRun).displacmentOnCushionMiliMetres;
    % convert to metres to make consistent
    springExtensionMetres = springExtensionMiliMetres/1000;
    % calculate plenum pressure by finding moments around the pivot point
    plenumPressureHoverNewtonPerSquareMetre = (springExtensionMetres *...
192 springConstantExptNewtonPerMetre * springPositionXMetre)/...
    (heaveDeckAreaSquareMetre * heaveDeckCentreOfPressureMetre);
    % check against the reading taken using a home-built manometer
    plenumPressureManometer = exp29Data(iRun).cushionPressurePascals;
    % add atmospheric pressure to get an absolute pressure in the plenum
197 plenumAbsolutePressureHoverNewtonPerSquareMetre =...
    plenumPressureHoverNewtonPerSquareMetre + atmosPressureStaticNewtonPerSquareMetre;
    % assume plenum is at ambient temperature and calculate the air density
    plenumDensityHoverKilogramPerCubicMetre = plenumAbsolutePressureHoverNewtonPerSquareMetre/...
    (GAS_CONSTANT_AIR * atmosTemperatureKelvin);
202 % report to the user
    fprintf('\tPlenum hover pressure: %.3G N/m^2 \n',plenumPressureHoverNewtonPerSquareMetre);
    fprintf('\tPlenum air density:    %.3G kg/m^3 \n',plenumDensityHoverKilogramPerCubicMetre);

    % set up a sinusoidal volume pumping signal
207 % use run 19 flapper vector as it is the cleanest
    % set up the time vector
    timeVec = exp29Data(19).timeVector;
    % put the flapper sensor reading into a simple vector in memory
    flapperVecMax = max(exp29Data(19).pumpVector);
212 flapperVecMin = min(exp29Data(19).pumpVector);
    flapperVecAmplitude = 1.5 * (flapperVecMax - flapperVecMin)/2;

    % Fan Slope
    % assume a basic average air speed in inlet duct
217 % ductAirSpeedMetresPerSecond = 4;
    % from experiment on blower flow rate versus duct static pressure
    %Q = Ap^2 + Bp + C;
    %     A = -0.001306;
    %     B = -0.004188;
222 %     C = 0.03497;
    %     ductPressurePascal = plenumPressureHoverNewtonPerSquareMetre -...
    %         0.5 * plenumDensityHoverKilogramPerCubicMetre * ductAirSpeedMetresPerSecond^2;
    %     % report to user
```

```
%     fprintf('\tInlet duct pressure: %0.3G Pa\n',ductPressurePascal);
%     fprintf('\tFan Slope is:\t%0.3G Q/p_h\n',fanSlope);
fanSlope = 0;

% Plenum stiffness - a simple model for the flexibilty of the plenum walls
plenumStiffness = expParam(iCondition,6);
plenumFlexArea = 0.8; %heaveDeckLengthMetre * plenumHeight;
plenumVolumeCubicMetres = heaveDeckAreaSquareMetre * plenumHeight;
fprintf('\tPlenum stiffness: %3.2G \n',plenumStiffness);

% SET THE FRICTION COMPONENTS
frictionCoulomb = expParam(iCondition,4);
frictionViscous = expParam(iCondition,5);
fprintf('\tFriction Coulomb: %3.2G \n',frictionCoulomb);
fprintf('\tFriction Viscous: %3.2G \n',frictionViscous);

%ALLOW FOR EXTRA VOLUME IN ROLLING SEAL
sealGapMetre = (plenumWidthMetre - heaveDeckWidthMetre);

% CALCULATE ALL THE GAINS FOR THE SIMULATION MODEL
K(1) = plenumDensityHoverKilogramPerCubicMetre * heaveDeckAreaSquareMetre *
    heaveDeckCentreOfPressureMetre;
K(2) = plenumDensityHoverKilogramPerCubicMetre * oscillatingFlapperUnitSweptVolumeCubicMetre;
K(3) = SPECIFIC_HEAT_AIR*(1+(atmosPressureStaticNewtonPerSquareMetre/(
    plenumPressureHoverNewtonPerSquareMetre)));
K(4) = plenumDensityHoverKilogramPerCubicMetre*heaveDeckAreaSquareMetre*plenumHeight;
K(5) = heaveDeckAreaSquareMetre * heaveDeckCentreOfPressureMetre * (
    plenumPressureHoverNewtonPerSquareMetre);
K(6) = springConstantExptNewtonPerMetre * springPositionXMetre^2;
K(7) = frictionCoefficient;
K(8) = atmosAirDensityKilogramPerCubicMetre * oscillatingResults(iCondition,5) *
    leakageAreaOrificeCoefficient;
K(9) = 2*(plenumPressureHoverNewtonPerSquareMetre)/atmosAirDensityKilogramPerCubicMetre;
K(10) = heaveDeckRotationalInertiaKilogramMetre;
K(11) = atmosAirDensityKilogramPerCubicMetre * plenumPressureHoverNewtonPerSquareMetre;
K(12) = plenumPressureHoverNewtonPerSquareMetre * plenumFlexArea^2  / plenumStiffness;
K(13) = plenumDensityHoverKilogramPerCubicMetre;
K(14) = 100 / plenumVolumeCubicMetres;
K(15) = plenumDensityHoverKilogramPerCubicMetre * sealGapMetre * 0.5 * (heaveDeckLengthMetre +
    heaveDeckWidthMetre) * heaveDeckLengthMetre;

% RUN THE SIMULATION, USING A SINUSOID AS THE INPUT VECTOR

% SETUP THE LOOP TO VARY FREQUENCY
% guess a plenum natural frequency
plenumNaturalFrequencyHertz = 5.5;
%timeVec = 0:(1/250000):30;
lowerFrequency = 1.0;
proportionFrequencyDisplay = 2.0;
proportionFrequencyRun = 2.0;
upperFrequency = 10; %proportionFrequencyRun*plenumNaturalFrequencyHertz;
nSteps = 50 ;
stepFrequency = (upperFrequency-lowerFrequency)/nSteps;
frequencyPumpHertz = lowerFrequency:stepFrequency:upperFrequency;
frequencyPumpRadPerSec = frequencyPumpHertz*2*pi();
% report to the user
fprintf('\tRunning simulations from %.2fHz to %.2fHz\n',lowerFrequency,upperFrequency);
F = waitbar(0,'Simulations running...');

% run the loop for each forcing frequency, doing the simulation
for iFrequency = 1:length(frequencyPumpRadPerSec)
pumpVector = flapperVecAmplitude * sin(frequencyPumpRadPerSec(iFrequency)*timeVec);
meanFrequencyMaxHeaveRadiansPerSecond = frequencyPumpRadPerSec(iFrequency);
% load the volume pump sensor data to drive the simulation with
simin.time = timeVec;
simin.signals.values = (pumpVector/1000);
% setup the simulation to run for 10 seconds (allowing quasi-steady behaviour)
[tout,xout_9,yout_9,pumpSim] = sim('testRigModelElevenOscillating.slx',[0 30]);

% TRIM THE SIMULATION RESULT TO REMOVE THE TRANSIENT
% setup the trimming of data to the final 1/4
iTimeStart = floor(length(yout_9)*0.75);
iTimeEnd = length(yout_9);

% FIND THE MEAN OF THE SIMULATION RESULT AND THE AMPLITUDE
% find the amplitude and mean of the heave deck displacement
maxYout_9 = max(yout_9(iTimeStart:iTimeEnd));
minYout_9 = min(yout_9(iTimeStart:iTimeEnd));
magnitudeYout_9 = maxYout_9 - minYout_9;
meanYout_9 = mean([minYout_9 maxYout_9]);
meanHeight(iFrequency) = meanYout_9;
magnitudeHeave(iFrequency) = magnitudeYout_9;
%% test the finding delay of simulation - phase angle prediction
% this method allows for varying time steps during numerical solution and
% always assumed a delay

% shift all the time-series to start at zero
time = tout(iTimeStart:iTimeEnd)-min(tout(iTimeStart:iTimeEnd));
pumpTime = pumpSim(iTimeStart:iTimeEnd);
heaveTime = yout_9(iTimeStart:iTimeEnd);

% find the amplitude and mean of the pumping, then normalise
ampPump = (max(pumpTime)-min(pumpTime))/2;
meanPump = (max(pumpTime)+min(pumpTime))/2;
pumpNorm = (pumpTime-meanPump)/ampPump;
% find the amplitude and mean of the heave response, then normalise
```

```
ampHeave = (max(heaveTime)-min(heaveTime))/2;
meanHeave = (max(heaveTime)+min(heaveTime))/2;
heaveNorm = (heaveTime-meanHeave)/ampHeave;
% find the peaks of the input and output
[pksPump,locPump] = findpeaks(pumpNorm,'MinPeakProminence',0.9);
[pksHeave, locHeave] = findpeaks(heaveNorm,'MinPeakProminence',0.9);


% calculate from the first peak, assume always a delay
timePumpPeak = time(locPump(1));
if locHeave(1) < locPump(1)
timeHeavePeak = time(locHeave(2));
else
timeHeavePeak = time(locHeave(1));
end
timePumpSecondPeak = time(locPump(2));
timeVector = [timePumpPeak timeHeavePeak timePumpSecondPeak];
% the delay is always the difference (assumed always delay)
delaySecond = timePumpPeak-timeHeavePeak;
% find a period, this is a mathematically calculated time-series
periodPumpSecond = timePumpSecondPeak-timePumpPeak;
% as we assumed a delay, express as ratio of circle
phaseAngleRad(iFrequency) = (delaySecond/periodPumpSecond) * 2 * pi();
phaseAngleDegree = (delaySecond/periodPumpSecond) * 360;
% write a label for the phase
foo(1) = {['Period: ',num2str(periodPumpSecond,'%3.2f'),'s']};
foo(2) = {['Delay: ',num2str(delaySecond,'%3.2f'),'s']};
foo(3) = {['\phi: ',num2str(phaseAngleDegree,'%3.2f'),'deg']};
foo(4) = {['\phi: ',num2str(phaseAngleRad(iFrequency),'%3.2f'),'rad']};
xtext = mean([timePumpPeak timeHeavePeak]);
ytext = 0.6;

% allocate random figure 867 to the phase visulisation
PMF = figure(867);
hold on;
% plot normalised time-series - this makes it easy to see the delay
plot(time,pumpNorm,'DisplayName','Pump norm');
plot(time,heaveNorm,'DisplayName','Heave norm');
% plot all the found peaks
plot(time(locPump),pksPump,'bs','DisplayName','Pump peaks');
plot(time(locHeave),pksHeave,'rs','DisplayName','Heave peaks');
% plot the important peak locations
stem(timeVector,[1.2 1.2 1.2],'g','DisplayName','Critical Peaks');
% configure plot
xlim([0 timePumpSecondPeak * 2]);
text(xtext,ytext,foo);
legend;
grid;
hold off;
% code in a pause so we can look at the plot
%pause;
close(PMF);


%               figure(iFrequency);
%               plot(tout,yout_9,timeVec,pumpVector);
%               legend('Heave deck displacment','Pump displacement');

% report to the user
progress=iFrequency/length(frequencyPumpRadPerSec);
waitbar(progress,F,['Running sim for frequency ',num2str(frequencyPumpHertz(iFrequency),'%.2f'),'Hz']);
%    fprintf('\tSimulation complete for %.2fHz\n',frequencyPumpHertz(iFrequency));
end % looping through forcing frequencies for simulation
% close waitbar
close(F);
% report to use
fprintf('\tFrequency range done\n');

% non-dimensional results

% find the index of the maximum magnitude of heave (natural damped frequency)
[maxMagnitudeHeave,indexMagnitudeHeave] = max(magnitudeHeave);
frequencyNaturalSimulationHertz = frequencyPumpHertz(indexMagnitudeHeave);
% report to user
fprintf('\tActual damped frequency:\t%.2fHz\n',frequencyNaturalSimulationHertz);
frequencyPumpRatio(:,iCondition) = frequencyPumpHertz/frequencyNaturalSimulationHertz;
% find the angle swept during oscillation (does not include the mean
% shift)
amplitudeAngle = atan(magnitudeHeave/(displacementSensorTwoPositionXMetre*1000));
% find the volume of the oscillation
amplitudeVolume = (amplitudeAngle/(2*pi())) * (pi() * heaveDeckLengthMetre^2 * heaveDeckWidthMetre);
% find the ratio of the heave deck oscillating volume to the pumped
% volume
amplitudeRatio(:,iCondition) = amplitudeVolume/pumpedVolumeCubicMetres;
% begin by finding angle swept in the mean height
meanAngle = atan(meanHeight/(displacementSensorTwoPositionXMetre*1000));
meanVolume = (meanAngle/(2*pi())) * (pi() * heaveDeckLengthMetre^2 * heaveDeckWidthMetre);
meanRatio(:,iCondition) = meanVolume/(pumpedVolumeCubicMetres);
% phase angle
phase(:,iCondition) = phaseAngleRad;
%report to user
fprintf('\tNondimensional parameters found\n');

% plot all the results (when looped)
% assign data points to separate series for different leakage areas and
% plenum heights
```

```
% report to user
fprintf('\n\nPlotting results...\n');
% only plot up to the pre-determined proportion of the simulation - do not
% show big discrepancy
upperPlot = floor((proportionFrequencyDisplay/proportionFrequencyRun) * length(frequencyPumpRadPerSec))
    ;
% report the plot range to the user
fprintf('\tPlotting from %.2fHz to %.2fHz... \n',lowerFrequency,upperPlot);

% plot the key parameters on 2 subplots

% parameters are known, setup label for plot
legendtext = {'Experiment' 'Numerical model'};
titletext = {['Condition ',num2str(condition,'%i'),': H_0=',num2str(plenumHeight,'%3.2f'),'m, A_e=',
    num2str(airLeakageAreaSquareMetres(iRun),'%3.2E'),'m^2']};

% open the figure for experimental results
F = openfig(['./output/figureResultsExp29-CON',num2str(condition)]);

% report to user
fprintf('\tExperimental result plot opened\n');

% open a unique figure
figure(F);
sgtitle(titletext);
hold on;
% first subplot of 6 - for mean height
subplot(3,1,1);
title remove;
grid minor;
plot(frequencyPumpHertz,meanRatio(:,iCondition),'r--');
% title('Shift in supported mass displacement');
ylim([-0.2 2]);
xlim([0 11]);
LGD1 = legend(legendtext,'Location','northwest');
ylabel('S_v (m^3/m^3)');
xlabel('\omega_f (Hz)');
% second subplot of 6 - for amplitude
subplot(3,1,2);
title remove;
grid minor;
plot(frequencyPumpHertz,amplitudeRatio(:,iCondition),'b--');
% title('Oscillation magnitude of supported mass displacement');
ylim([0 1.75]);
xlim([0 11]);
LGD2 = legend(legendtext,'Location','northwest');
ylabel('O_v (m^3/m^3)');
xlabel('\omega_f (Hz)');
subplot(3,1,3);
title remove;
grid minor;
plot(frequencyPumpHertz,phase(:,iCondition),'g--');
% title('Oscillation magnitude of supported mass displacement');
ylim([-pi() pi()]);
xlim([0 11]);
LGD3 = legend(legendtext,'Location','northwest');
ylabel('\phi (rad)');
xlabel('\omega_f (Hz)');
orient(figure(F),'portrait');
% report to user
fprintf('\tPlotting of results done\n');


%save the figure as a MATLAB file
figureFileName = ['./output/figureTheoryPrediction-CON',num2str(condition)];
savefig(figure(F),figureFileName,'compact');
pdfFileName = ['./output/pdf/figureTheoryPrediction-CON',num2str(condition)];
pngFileName = ['./output/png/figureTheoryPrediction-CON',num2str(condition)];
svgFileName = ['./output/svg/figureTheoryPrediction-CON',num2str(condition)];
% print the figure as a landscape PDF for reviewing
print(figure(F),pdfFileName,'-dpdf','-fillpage');
print(figure(F),pngFileName,'-dpng');
print(figure(F),svgFileName,'-dsvg');

% report to user
fprintf('\tPlot saved to files. All finished.\n\n');

end % for loop that does all the requested conditions
```

E. Decomposed signal results

This appendix contains the plots of the analysis of the signals done in the experiments to determine the rig dynamic properties. The experiment and analysis are described in Sec. 6.3. The results are grouped by the experimental conditions, each condition being a combination of the plenum height (H_0), the centreline velocity of the air passing through the supply duct (V_a) and the air exit area, labelled in these plots as the extra air exit area (A_e). In the body of the thesis, the air supply centreline velocity is denoted V_s.

Table E.1. Experimental conditions for finding experimental rig dynamic properties. These conditions are discussed in Secs. 6.3 and 6.4. The experimental condition number is denoted '#'. Plenum height is denoted H_0. Air exit area is denoted A_e. Air supply duct centreline velocity is denoted V_a and for the purposes of this experiment is taken as directly proportional to the air supply volume flow rate. In the body of the thesis, the air supply centreline velocity is denoted V_s.

#	H_0 (m)	V_a ($\mathrm{m\,s^{-1}}$)	A_e ($\mathrm{m^2}$)	Experimental runs
1	1.143	5.49	0.57E-3	88
2	1.143	6.75	0.57E-3	89, 95
3	1.143	5.49	0.82E-3	90, 97
4	1.143	6.75	0.82E-3	91
5	1.143	5.49	1.20E-3	92
6	1.143	6.75	1.20E-3	93, 94
7	0.297	5.49	0.57E-3	55, 63, 65
8	0.297	5.49	0.82E-3	57, 62
9	0.297	5.49	1.20E-3	59, 69
10	0.297	6.75	0.57E-3	56, 66
11	0.297	6.75	0.82E-3	58, 68
12	0.297	6.75	1.20E-3	60
13	0.605	5.49	0.57E-3	107
14	0.605	5.49	0.82E-3	100
15	0.605	5.49	1.20E-3	102
16	0.605	6.75	0.57E-3	105, 106
17	0.605	6.75	0.82E-3	104
18	0.605	6.75	1.20E-3	103
19	0.802	5.49	0.57E-3	118, 124, 128, 134
20	0.802	5.49	0.82E-3	120, 125, 130 135
21	0.802	5.49	1.20E-3	119
22	0.802	6.75	0.57E-3	119, 129
23	0.802	6.75	0.82E-3	121, 131
24	0.802	6.75	1.20E-3	123, 126, 127, 133, 136, 137
25	0.445	5.49	0.57E-3	No valid experimental data available.
26	0.445	5.49	0.82E-3	110
27	0.445	5.49	1.20E-3	112, 115, 116
28	0.445	6.75	0.57E-3	109
29	0.445	6.75	0.82E-3	111
30	0.445	6.75	1.20E-3	113, 114

E.1. Experimental condition one

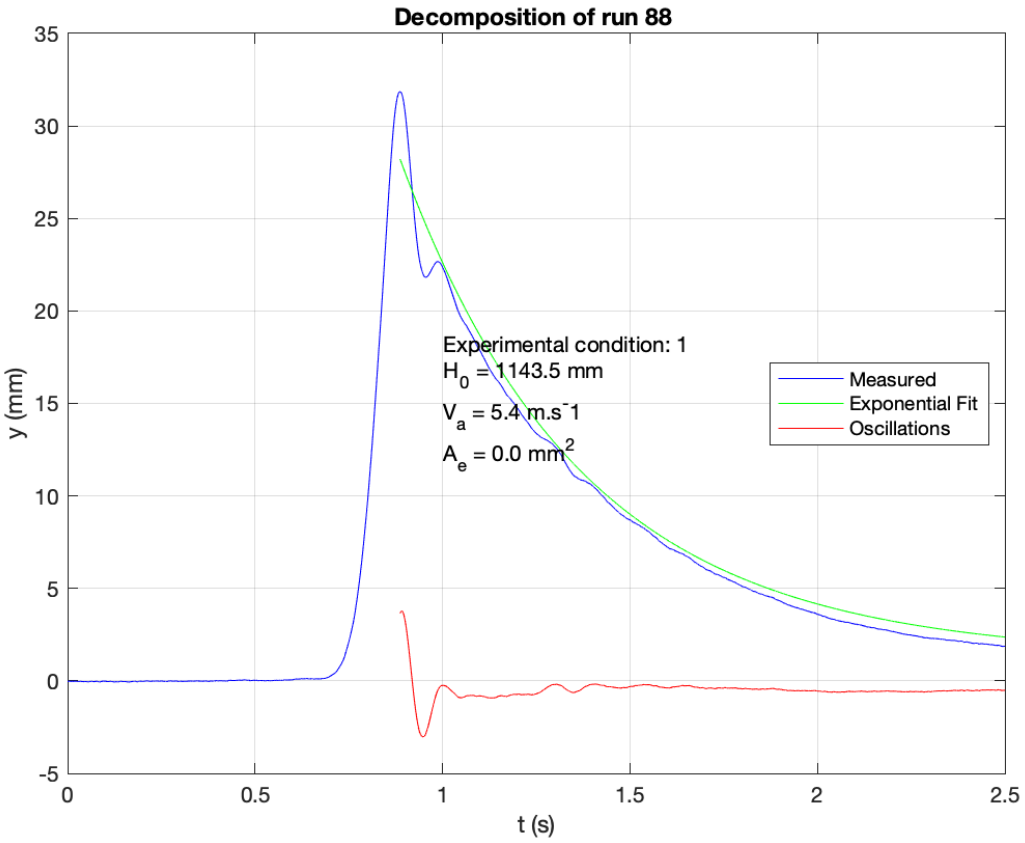


Figure E.1. Decomposition of run 88.

E.2. Experimental condition two

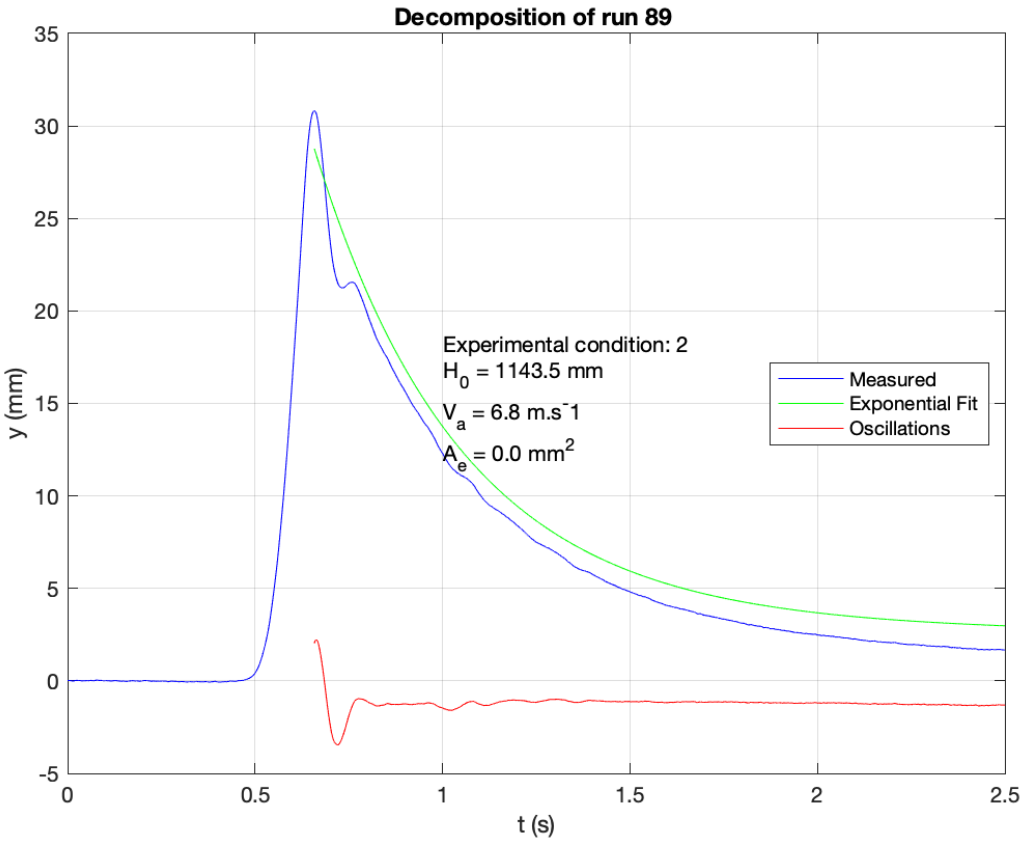


Figure E.2. Decomposition of run 89.

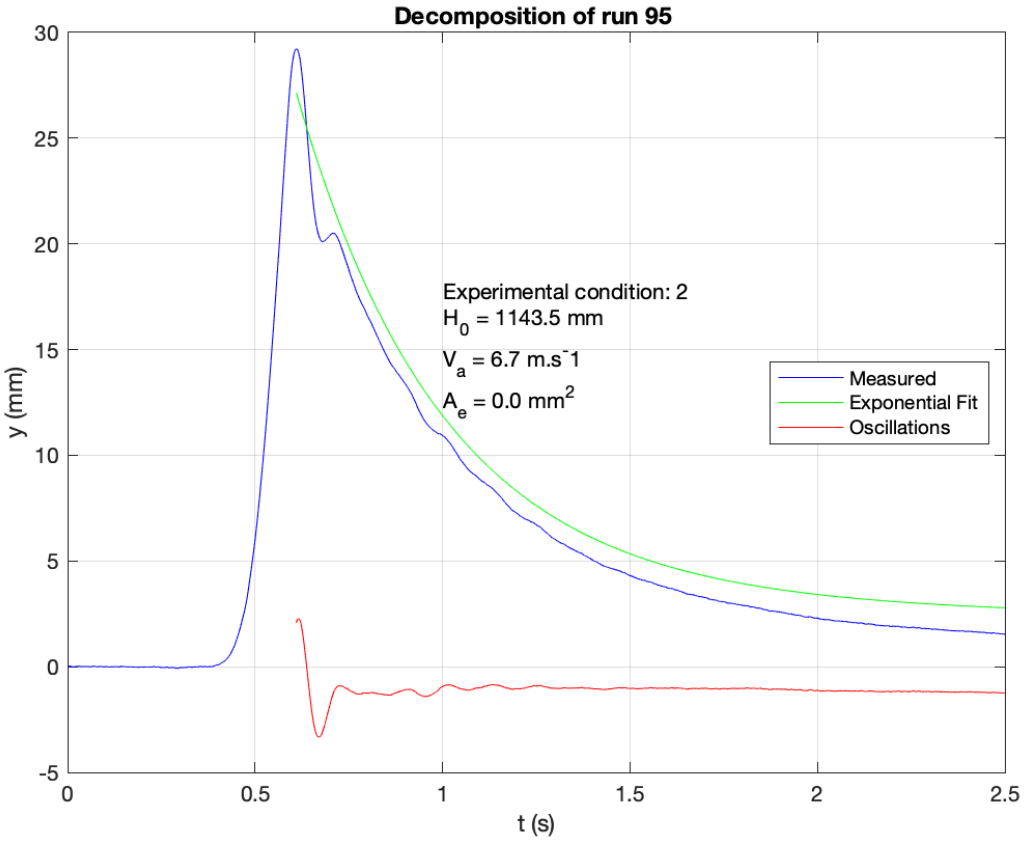


Figure E.3. Decomposition of run 95.

E.3. Experimental condition three

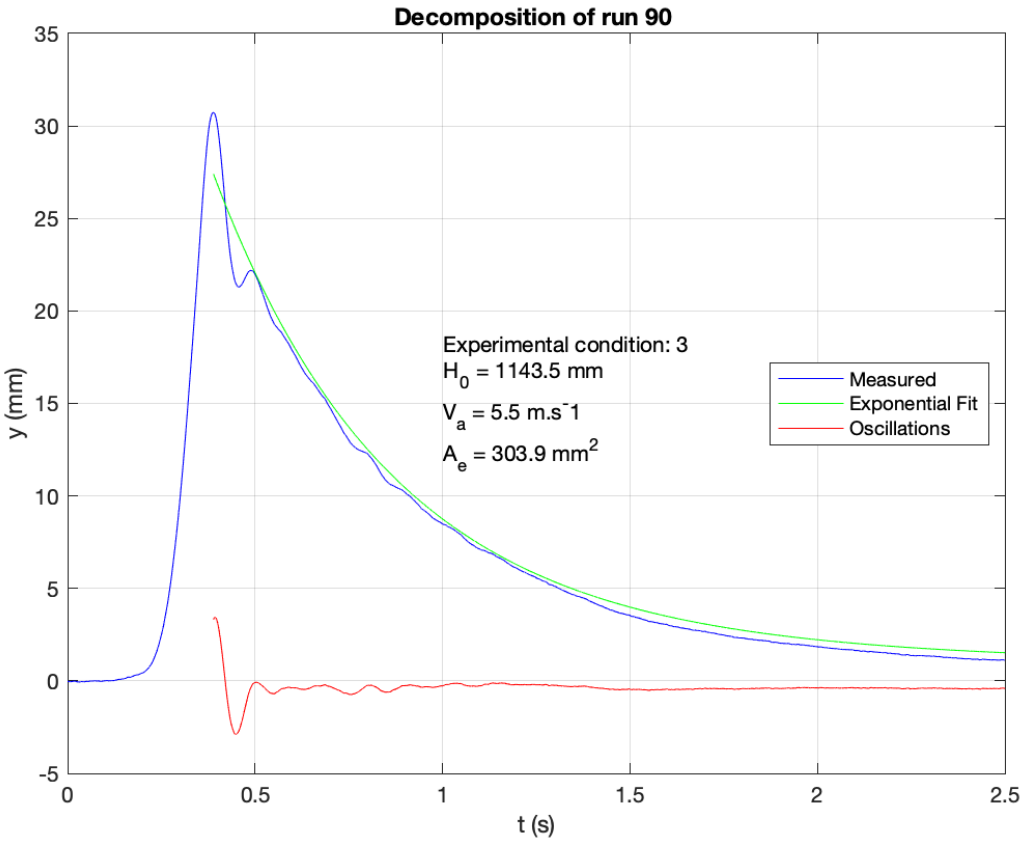


Figure E.4. Decomposition of run 90.

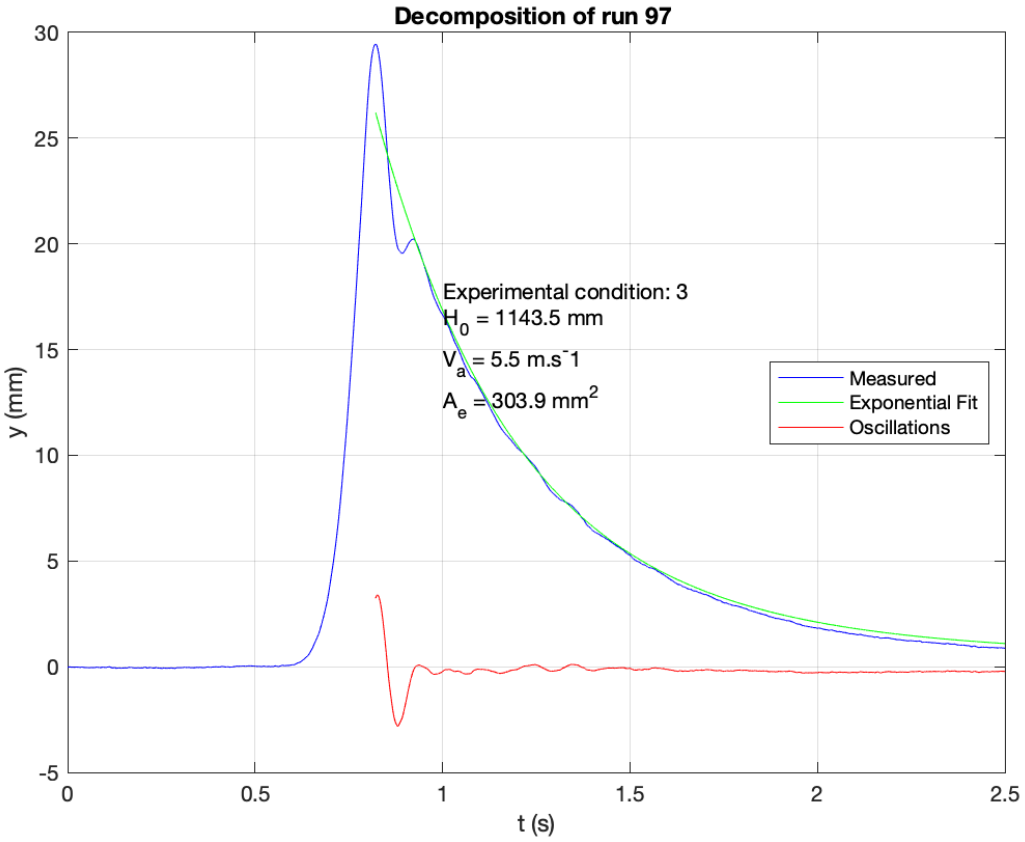


Figure E.5. Decomposition of run 97.

E.4. Experimental condition four

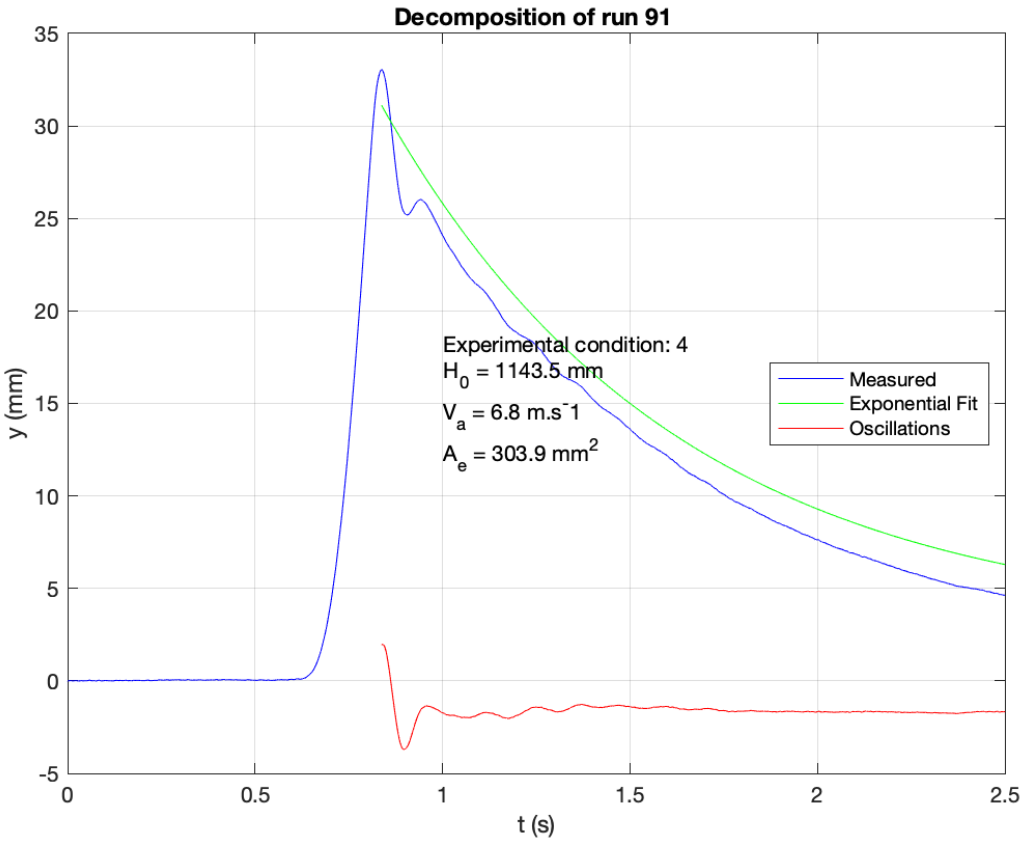


Figure E.6. Decomposition of run 91.

E.5. Experimental condition five

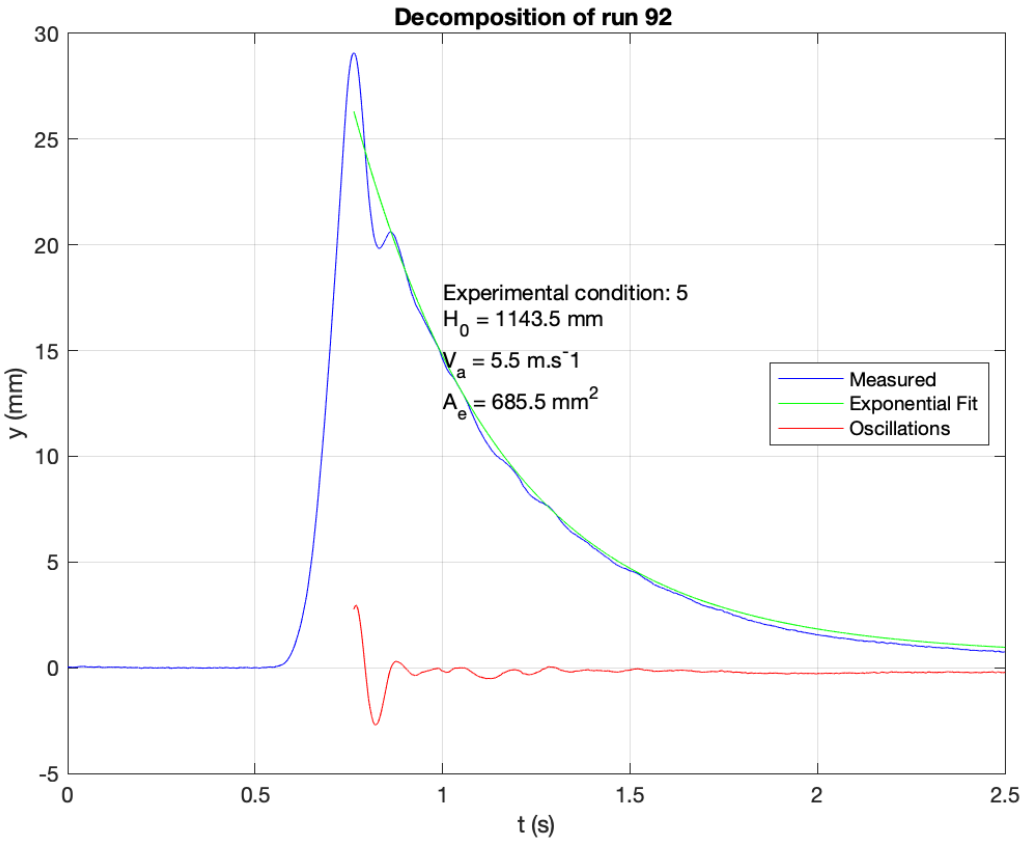


Figure E.7. Decomposition of run 92.

E.6. Experimental condition six

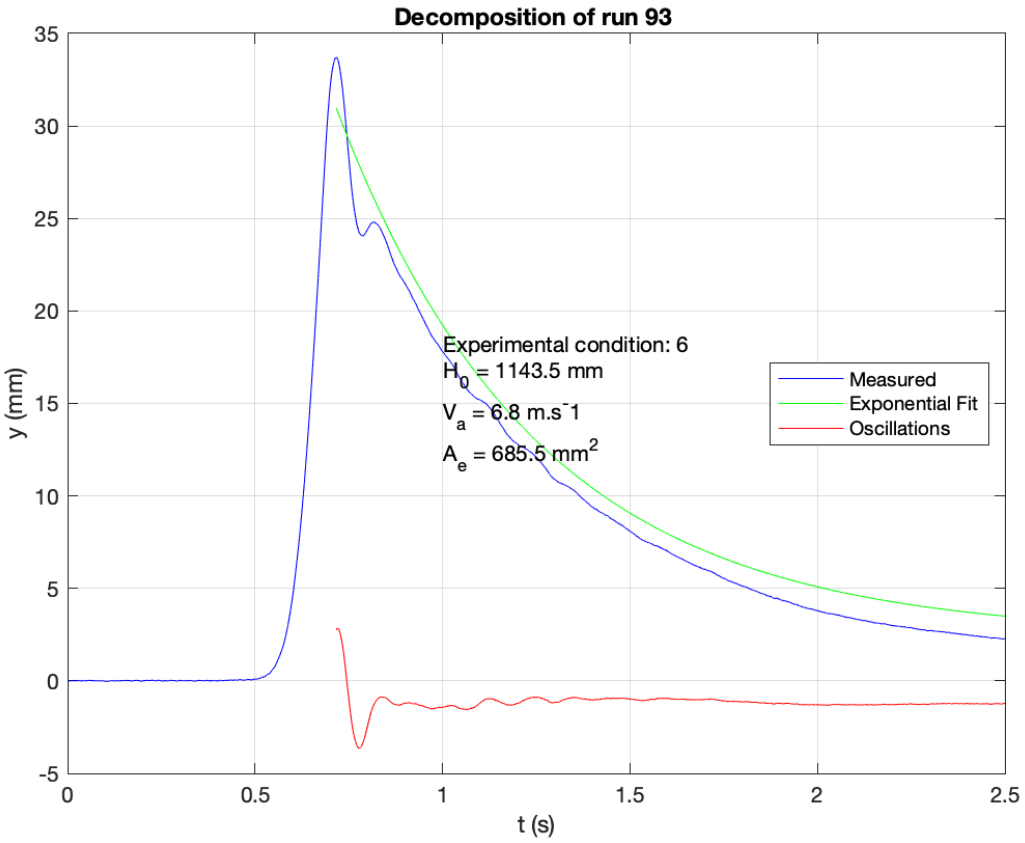


Figure E.8. Decomposition of run 93.

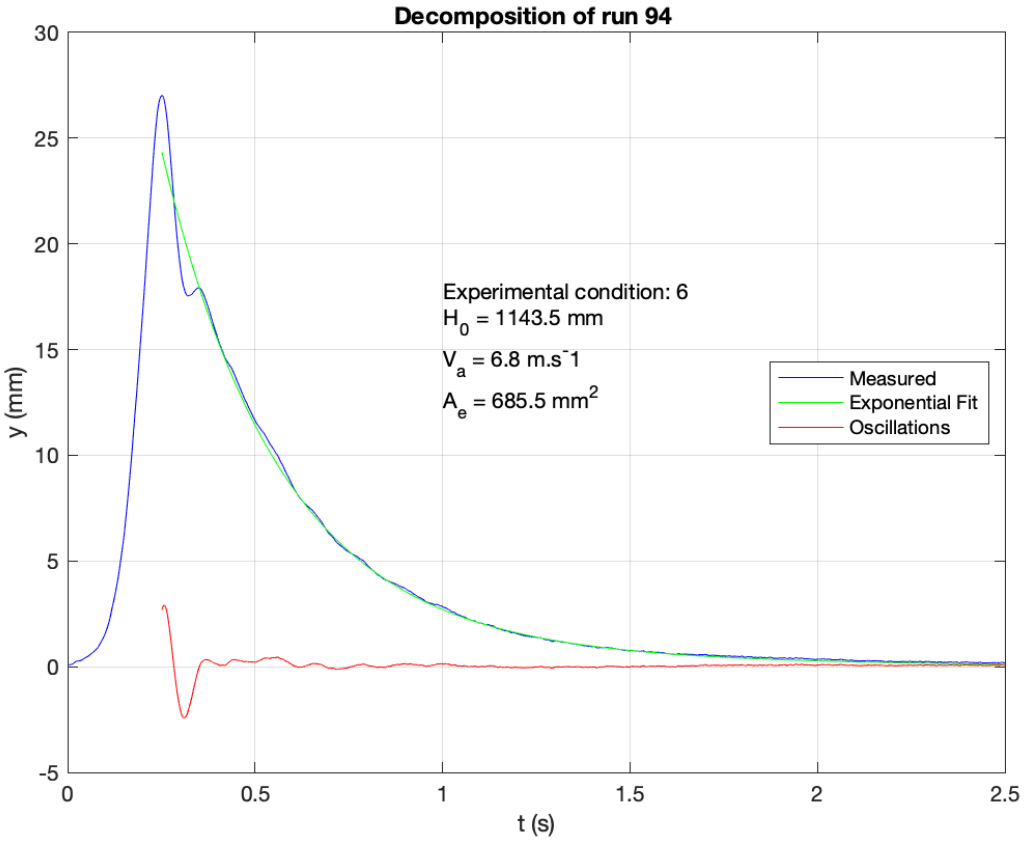


Figure E.9. Decomposition of run 94.

E.7. Experimental condition seven

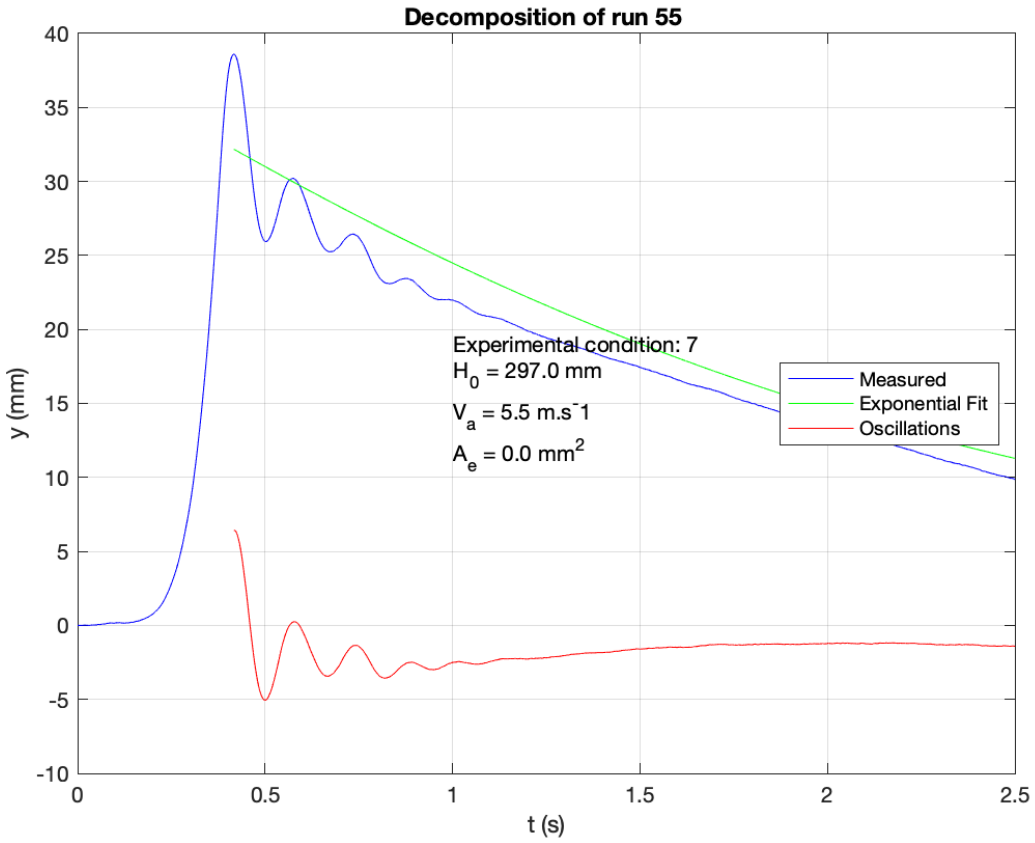


Figure E.10. Decomposition of run 55.

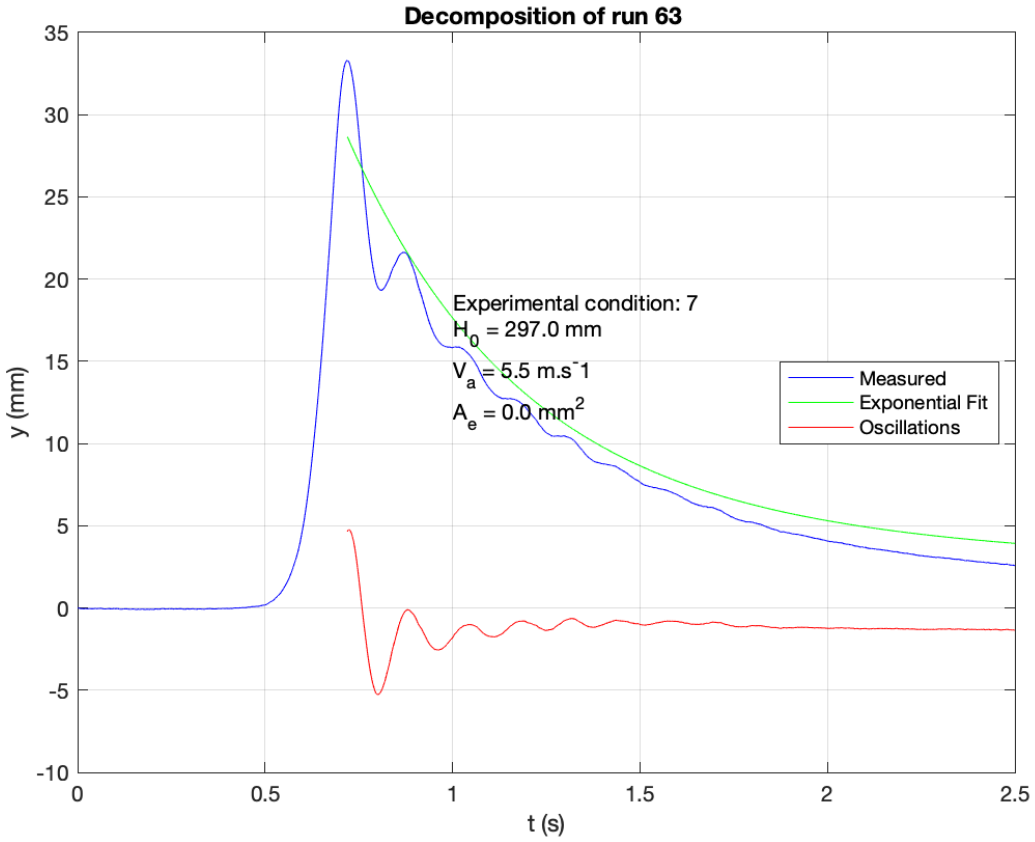


Figure E.11. Decomposition of run 63.

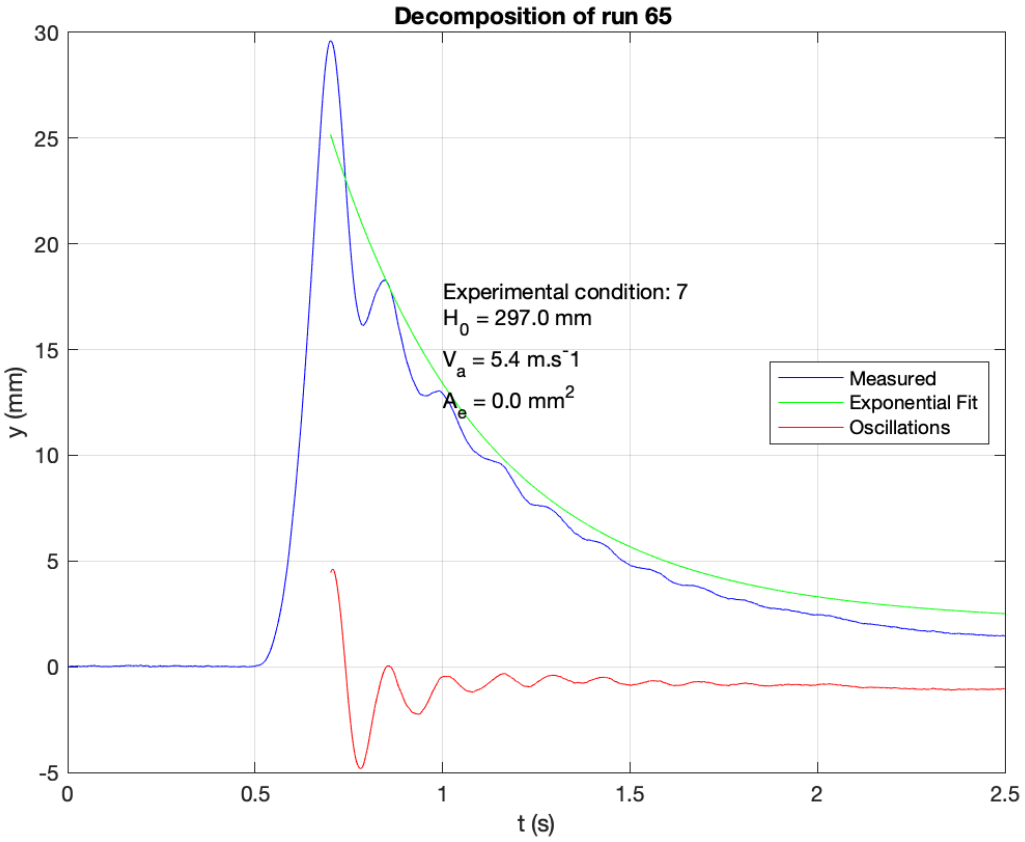


Figure E.12. Decomposition of run 65.

E.8. Experimental condition eight

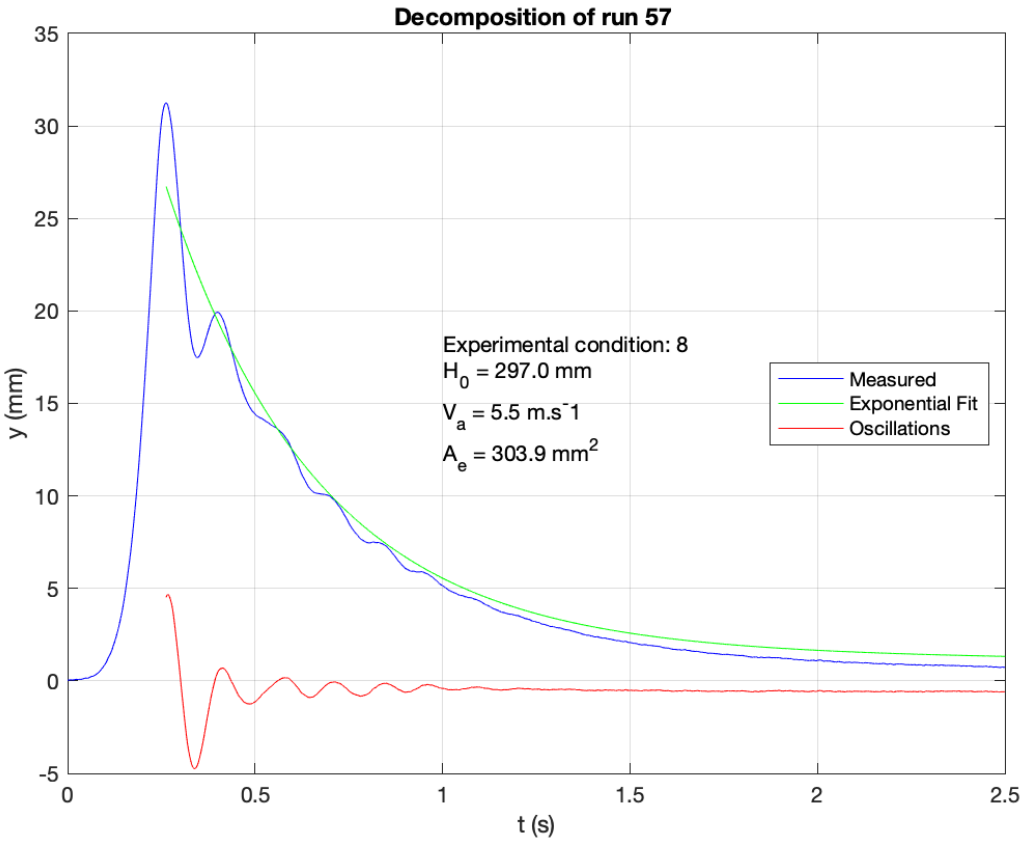


Figure E.13. Decomposition of run 57.

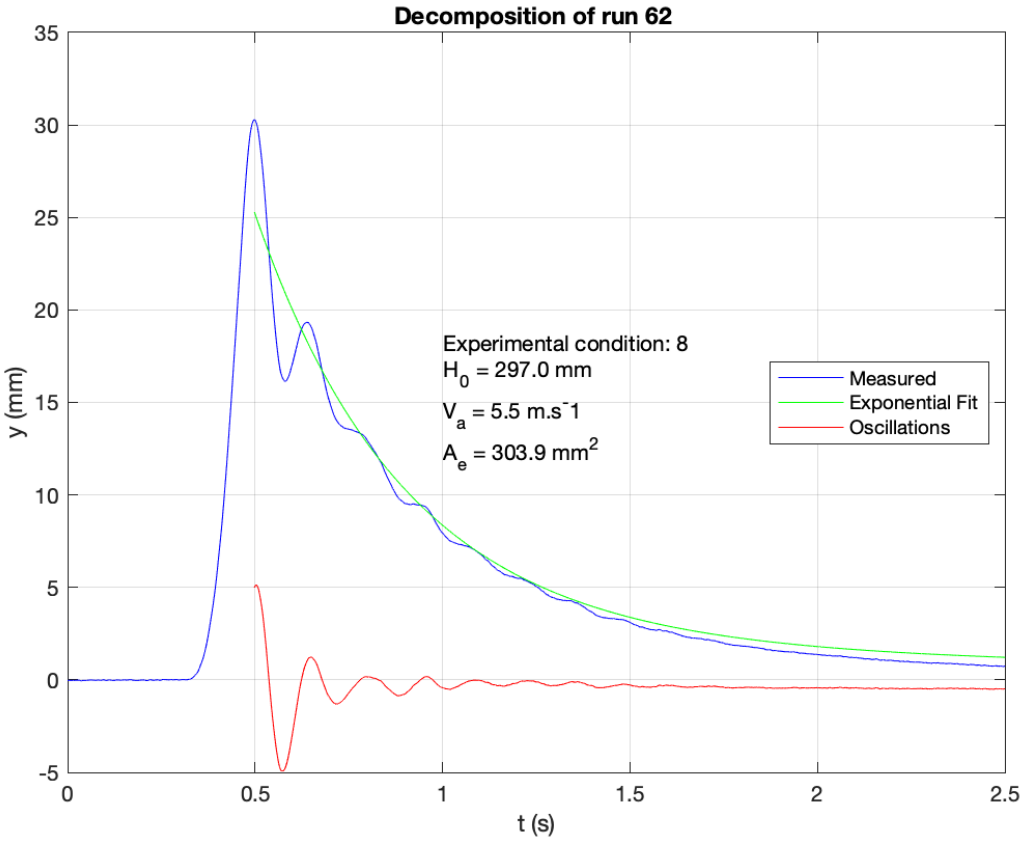


Figure E.14. Decomposition of run 62.

E.9. Experimental condition nine

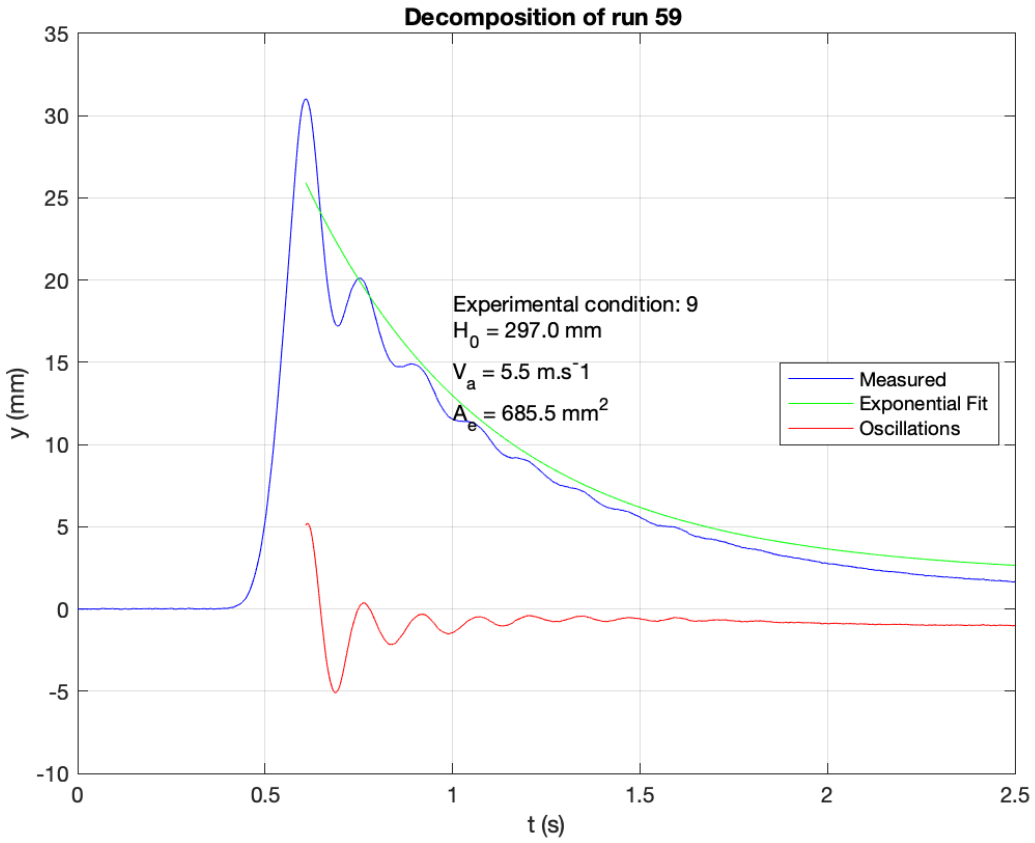


Figure E.15. Decomposition of run 59.

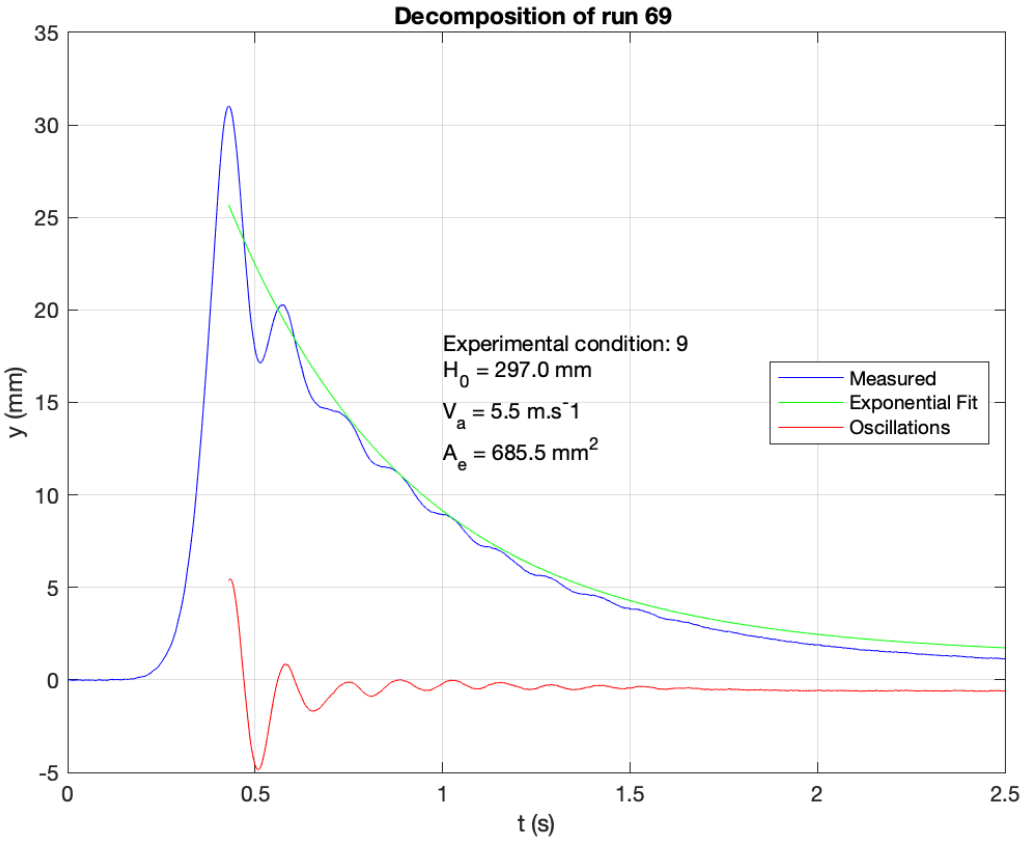


Figure E.16. Decomposition of run 69.

E.10. Experimental condition ten

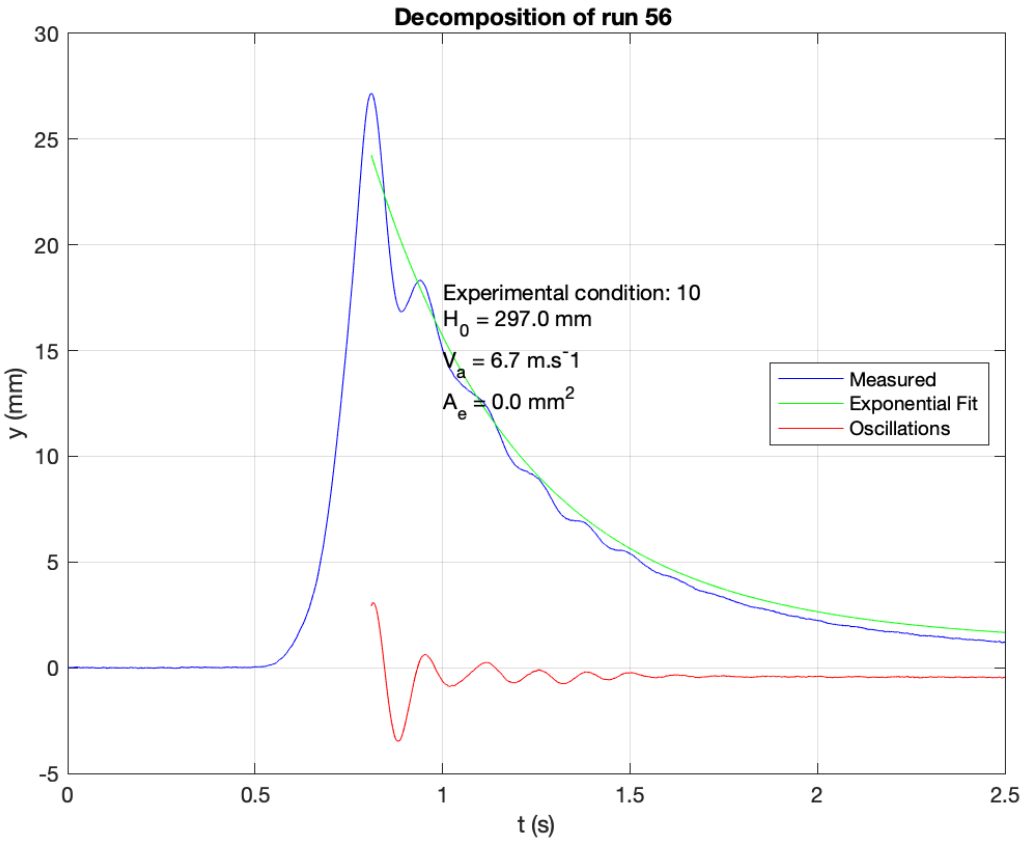


Figure E.17. Decomposition of run 56.

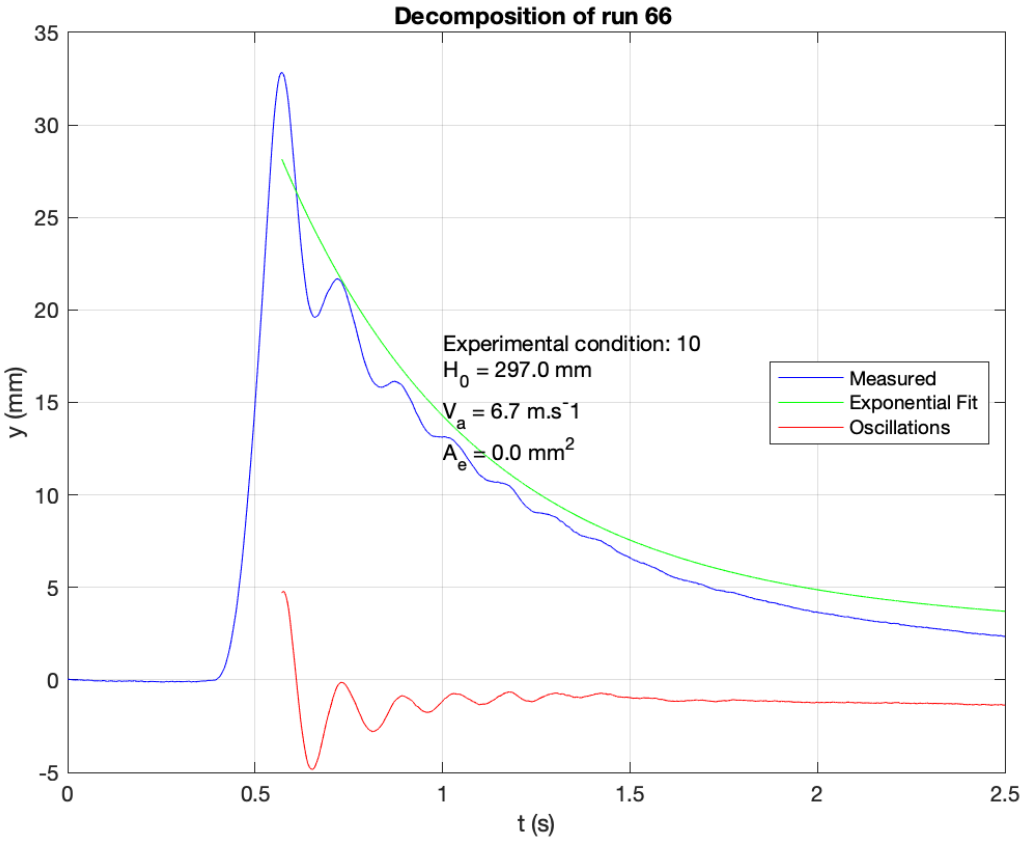


Figure E.18. Decomposition of run 66.

E.11. Experimental condition eleven

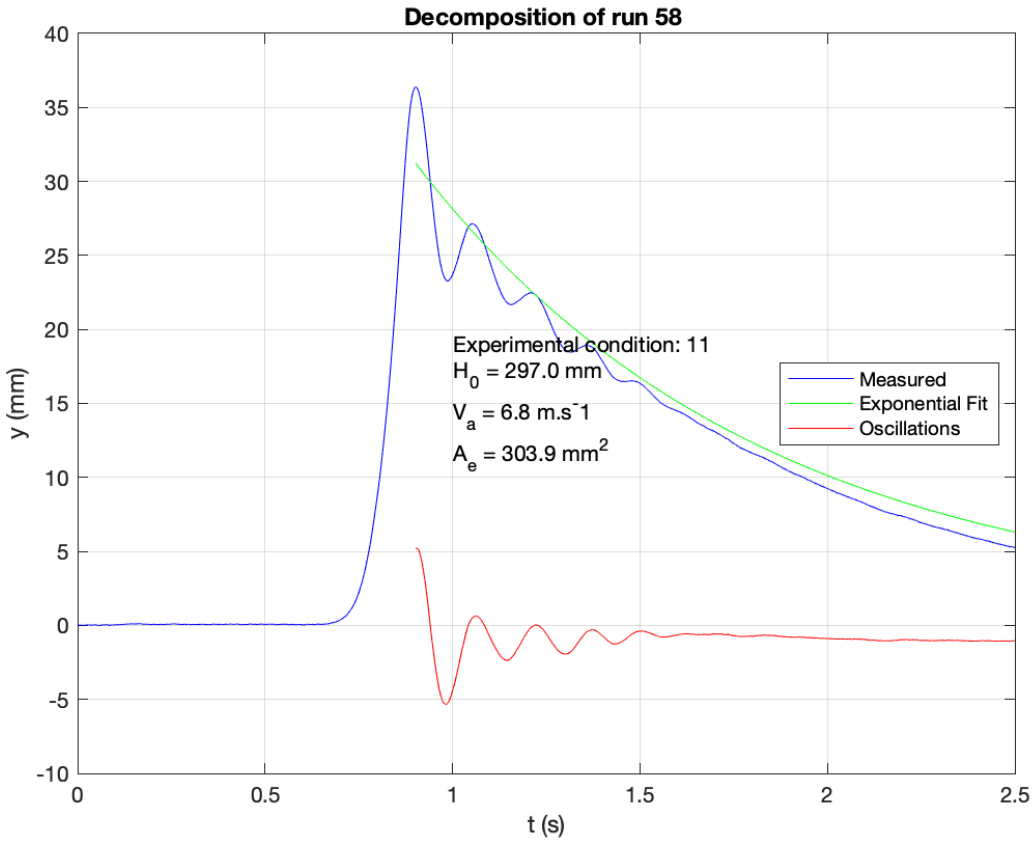


Figure E.19. Decomposition of run 58.

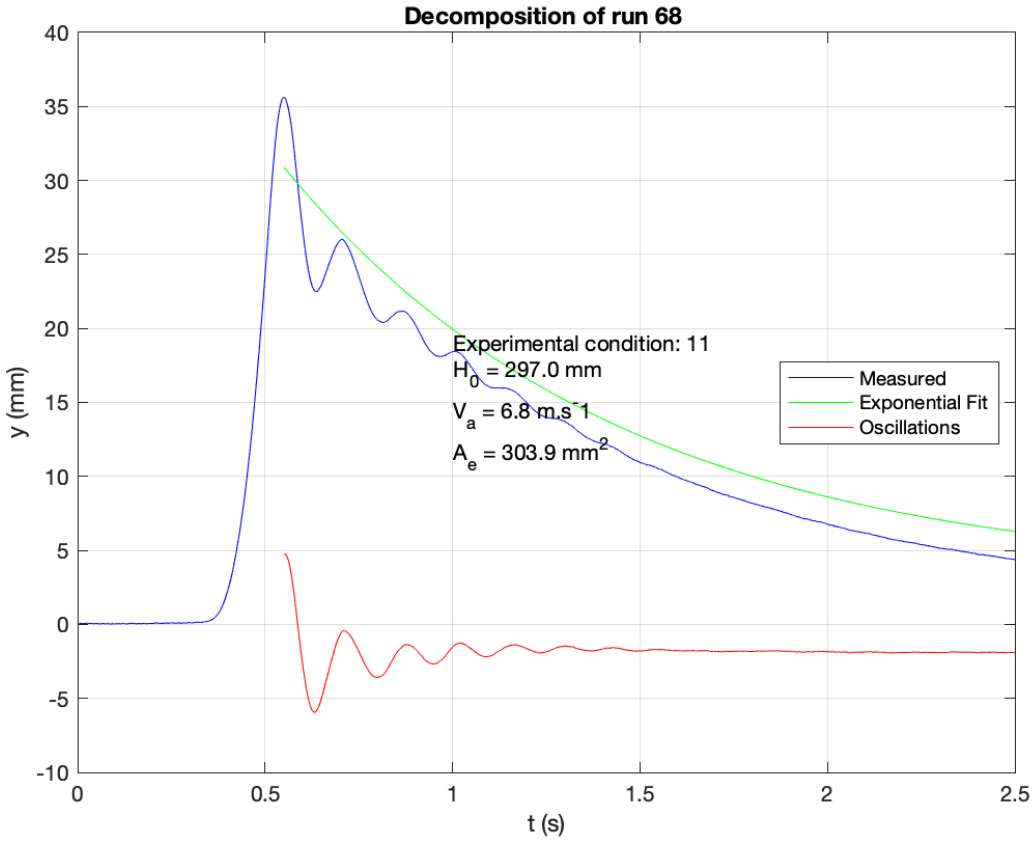


Figure E.20. Decomposition of run 68.

E.12. Experimental condition twelve

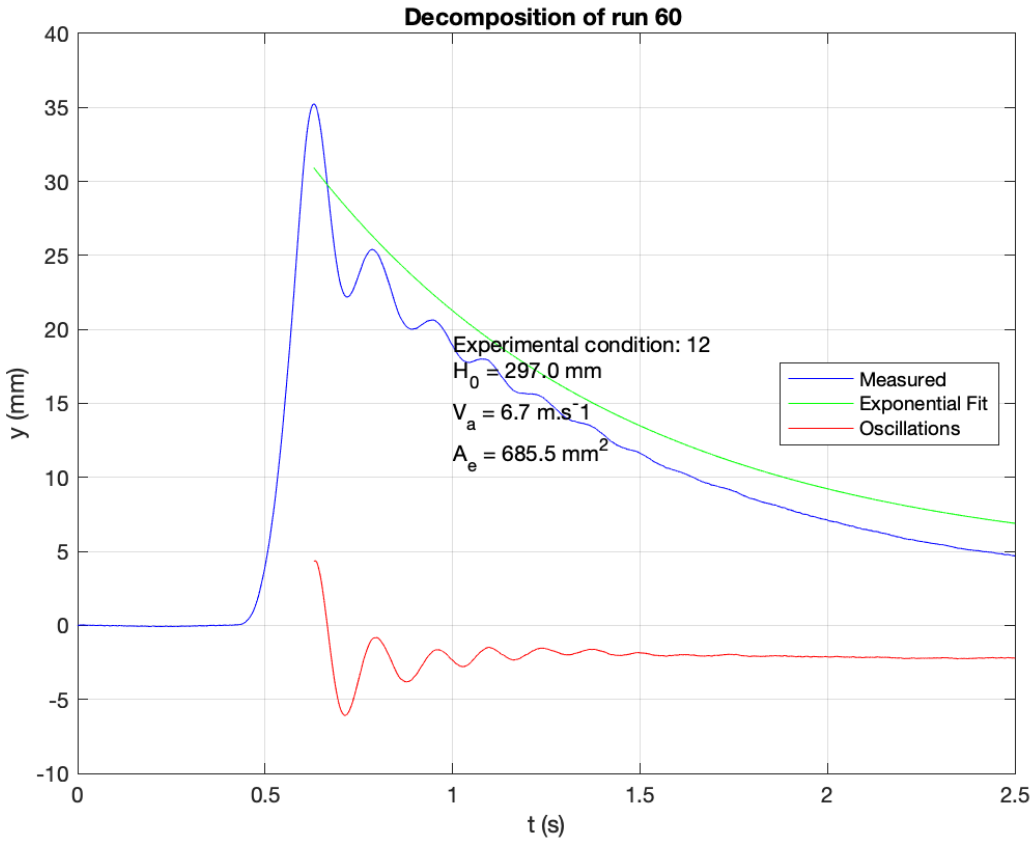


Figure E.21. Decomposition of run 60.

E.13. Experimental condition thirteen

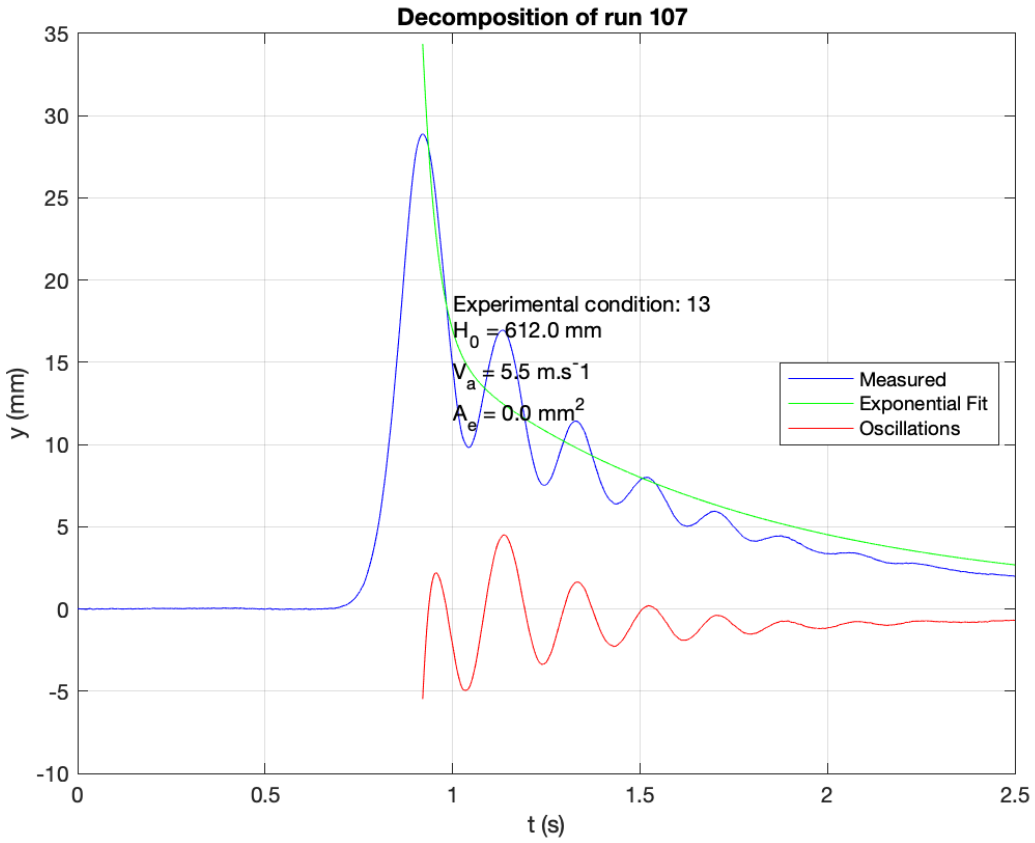


Figure E.22. Decomposition of run 107.

E.14. Experimental condition fourteen

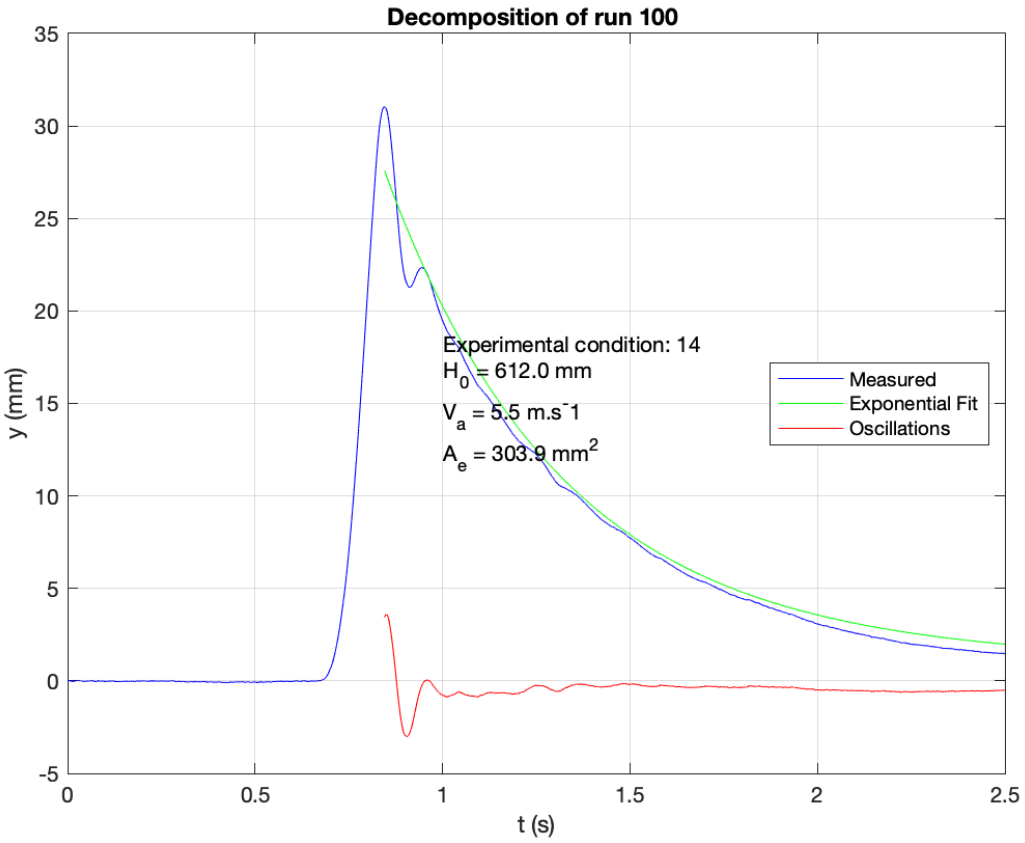


Figure E.23. Decomposition of run 100.

E.15. Experimental condition fifteen

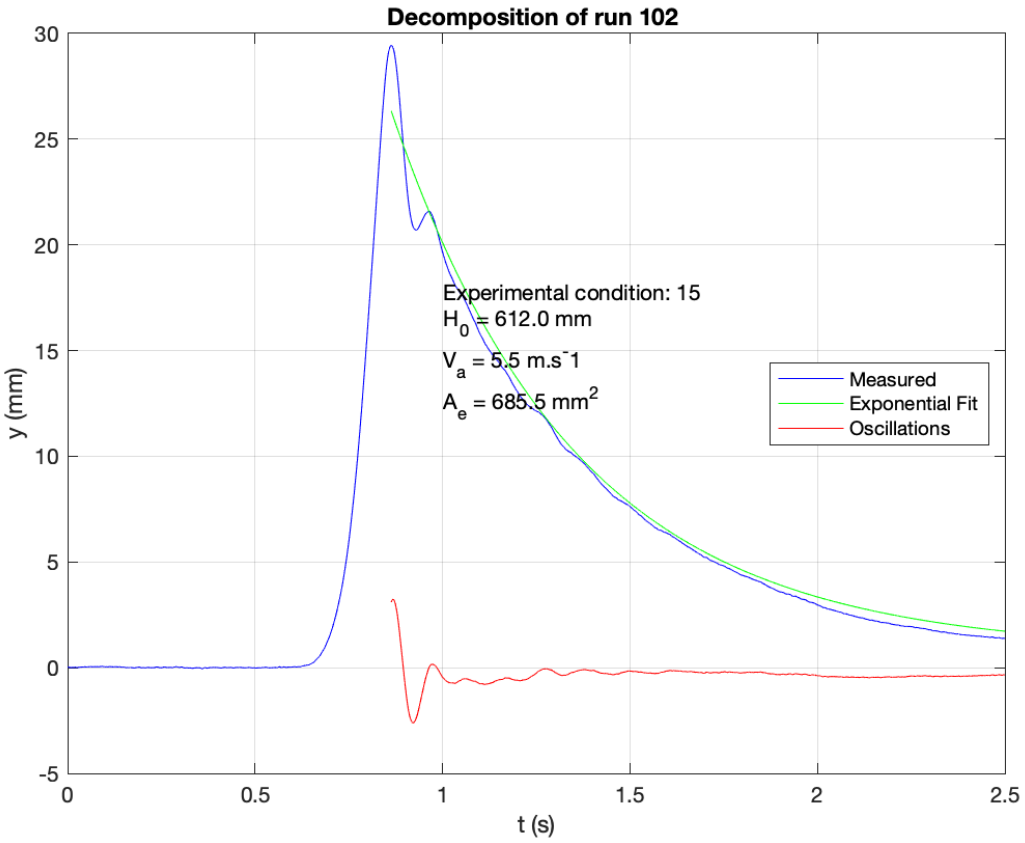


Figure E.24. Decomposition of run 102.

E.16. Experimental condition sixteen

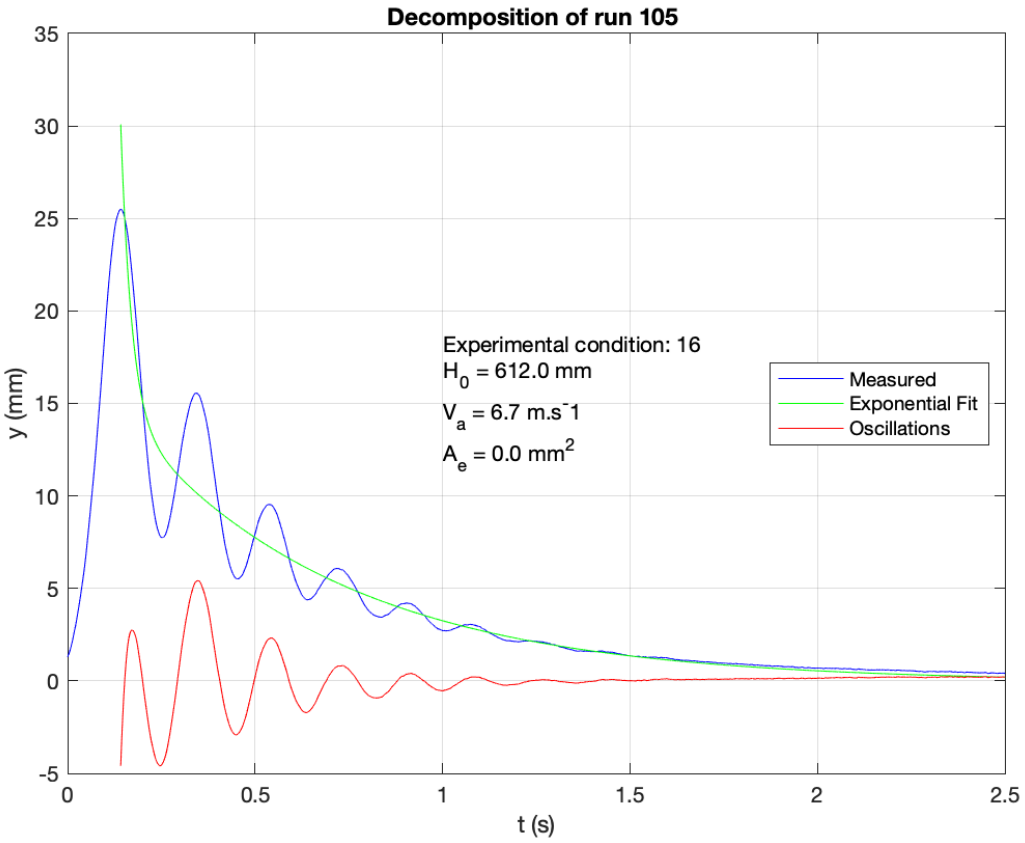


Figure E.25. Decomposition of run 105.

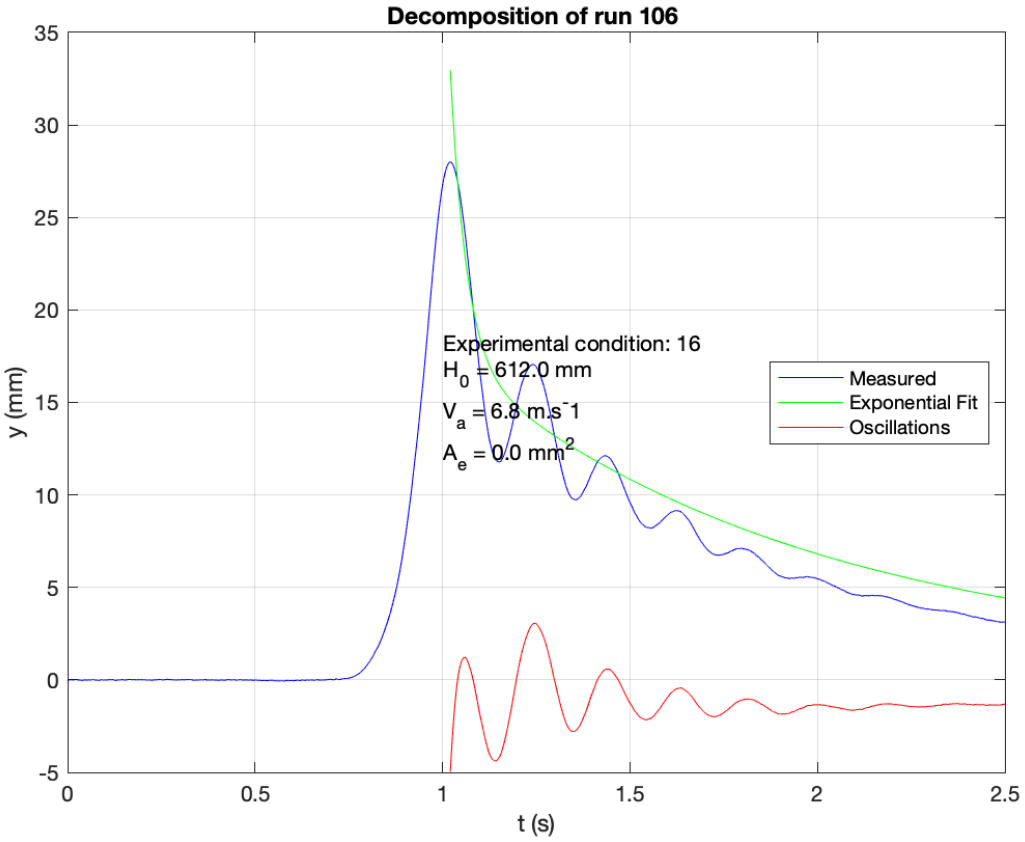


Figure E.26. Decomposition of run 106.

E.17. Experimental condition seventeen

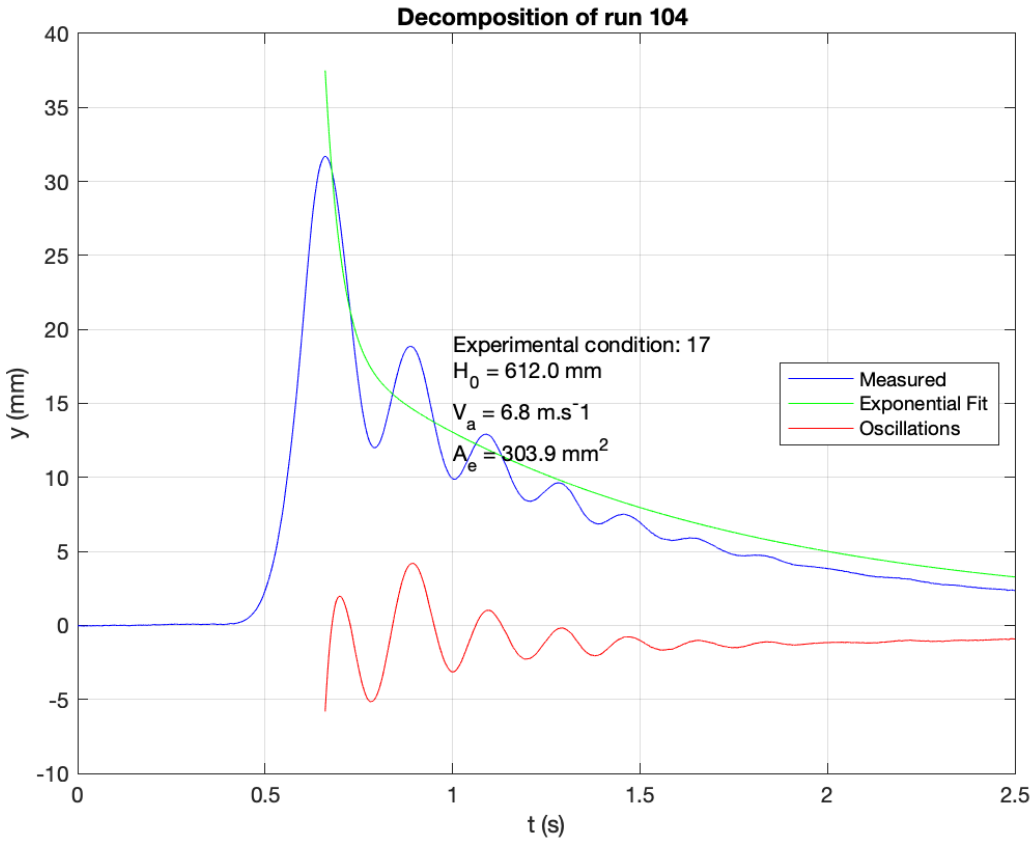


Figure E.27. Decomposition of run 104.

E.18. Experimental condition eighteen

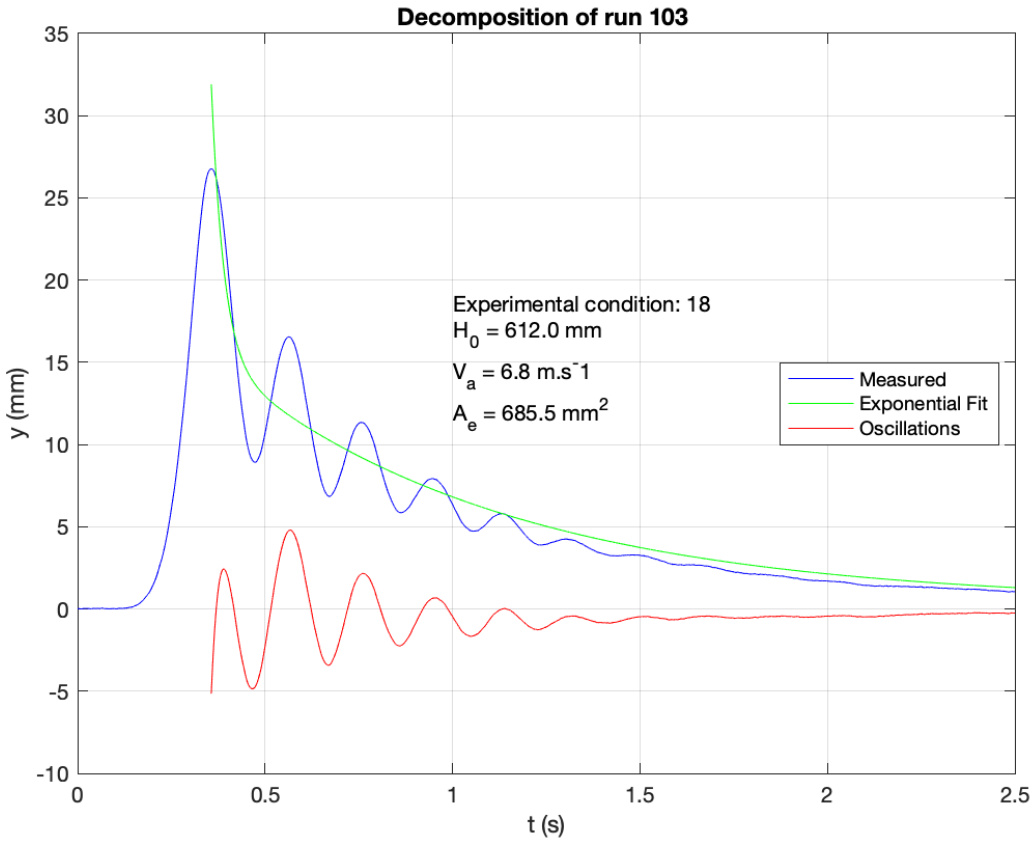


Figure E.28. Decomposition of run 103.

E.19. Experimental condition nineteen

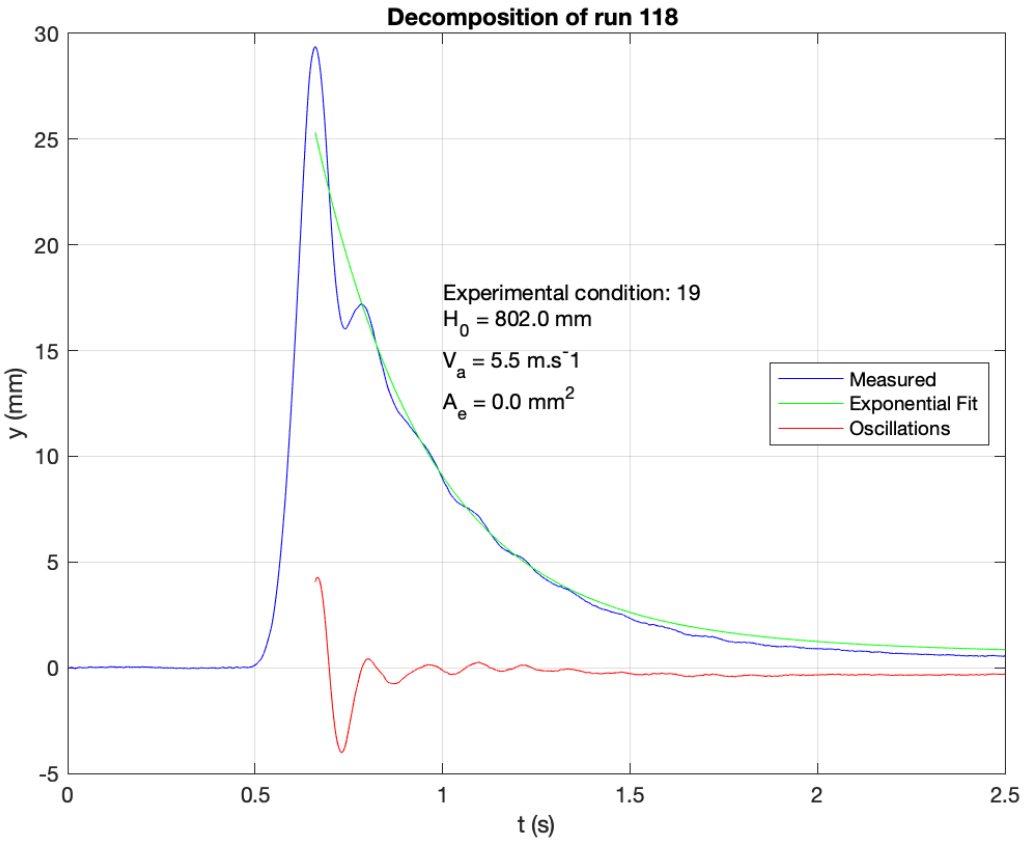


Figure E.29. Decomposition of run 118.

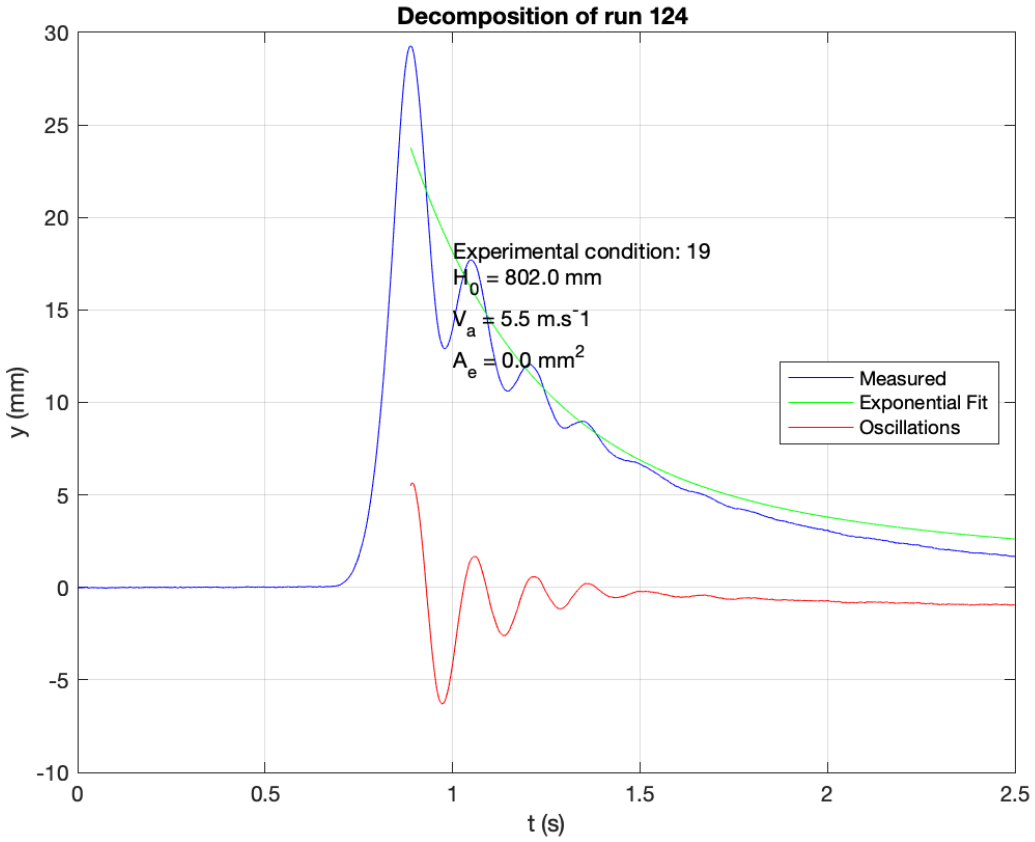


Figure E.30. Decomposition of run 124.

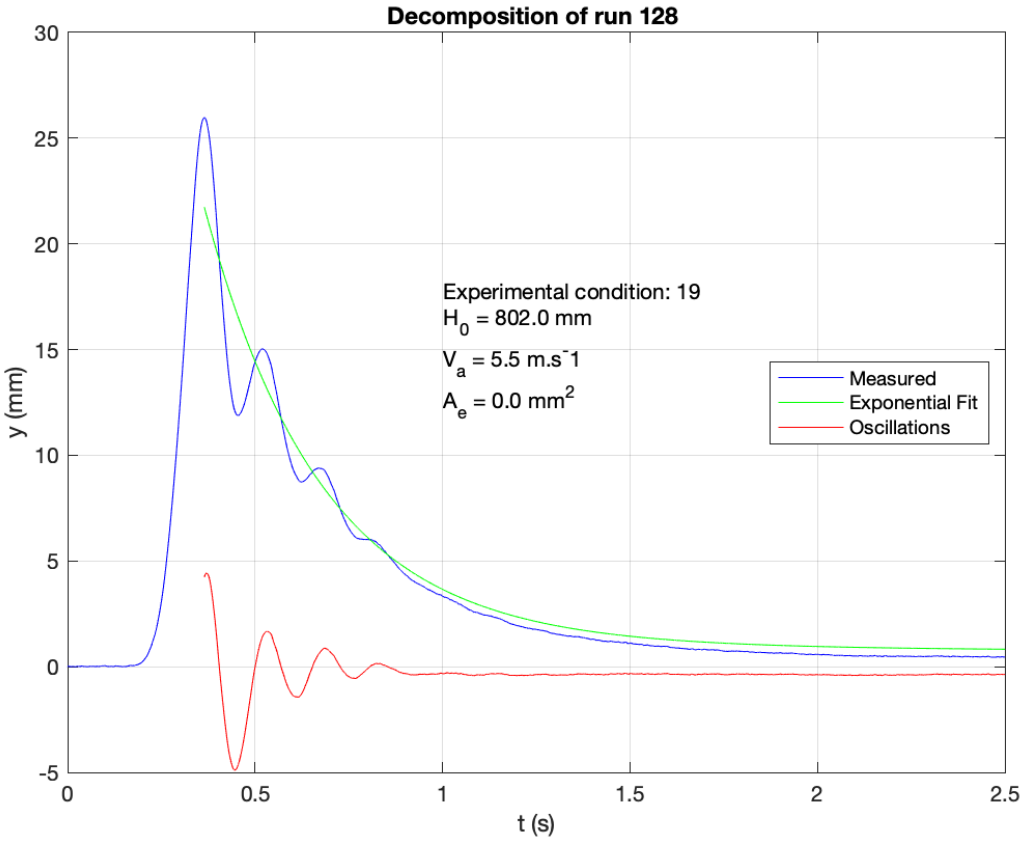


Figure E.31. Decomposition of run 128.

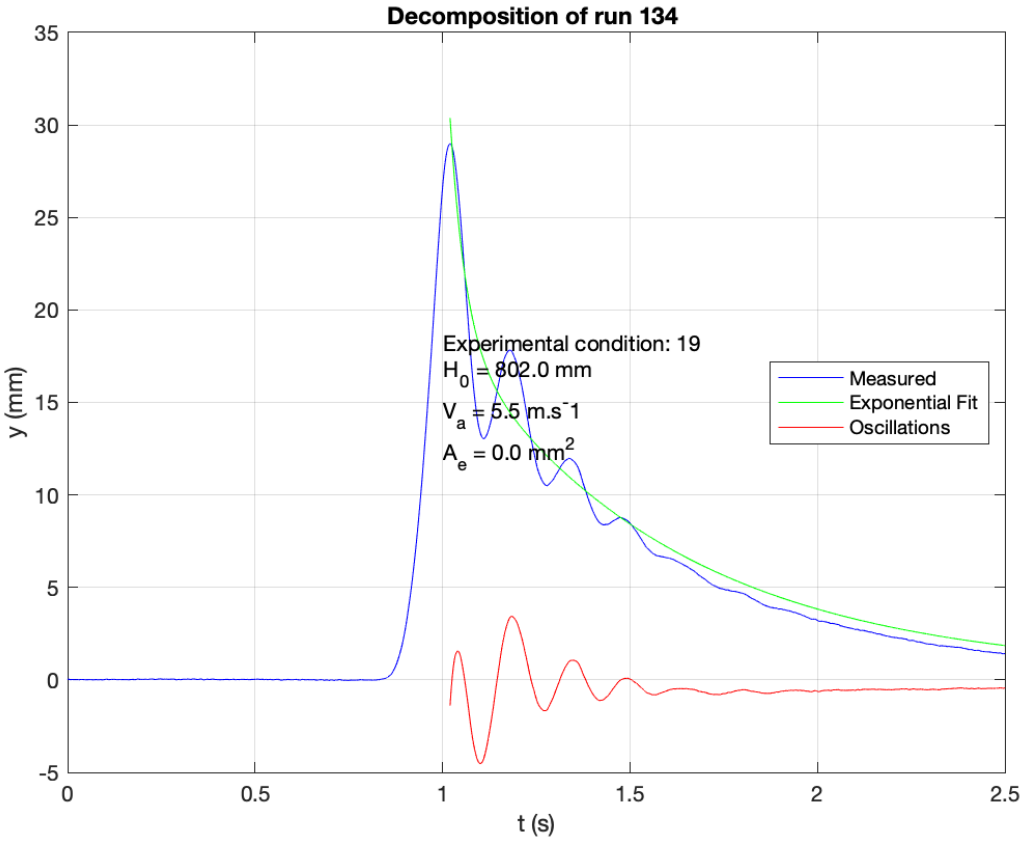


Figure E.32. Decomposition of run 134.

E.20. Experimental condition twenty

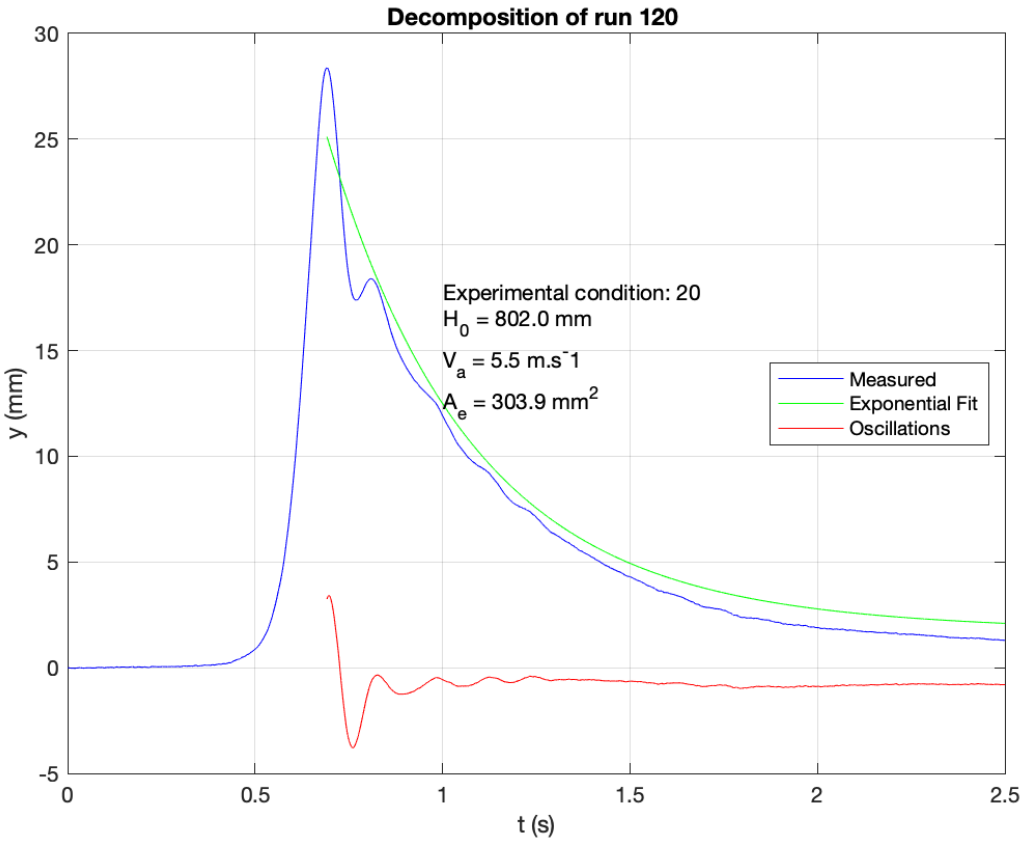


Figure E.33. Decomposition of run 120.

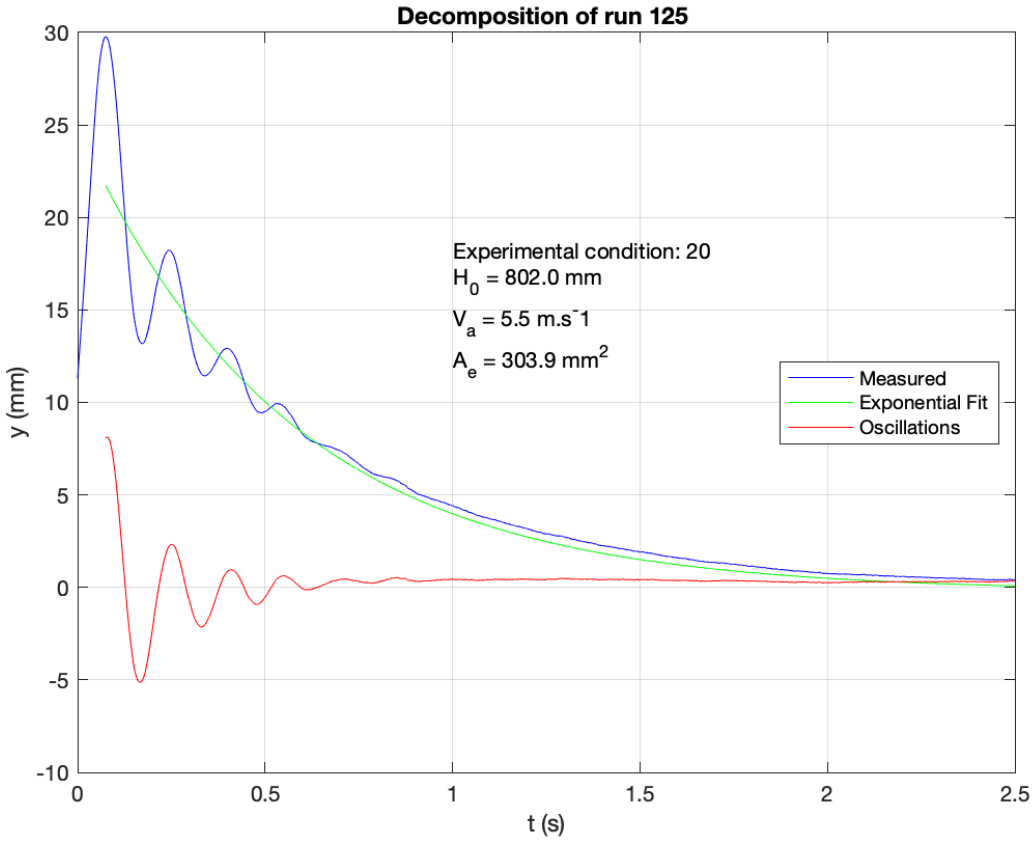


Figure E.34. Decomposition of run 125.

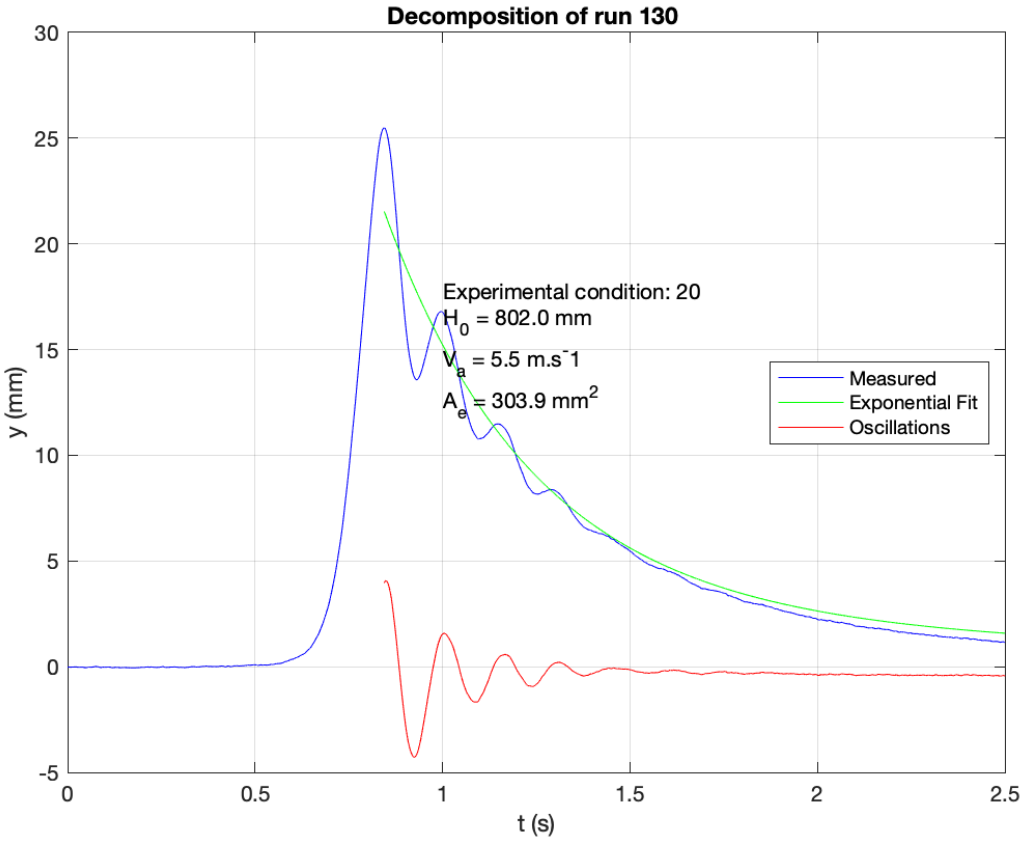


Figure E.35. Decomposition of run 130.

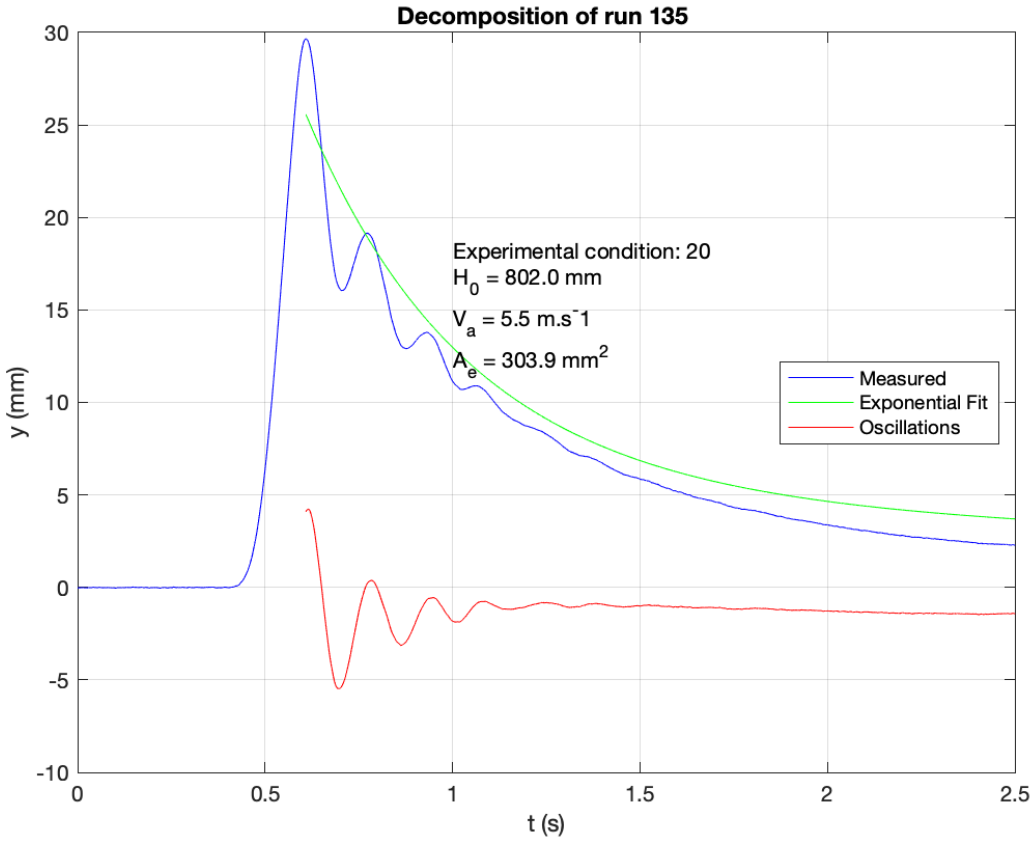


Figure E.36. Decomposition of run 135.

E.21. Experimental condition twenty-one

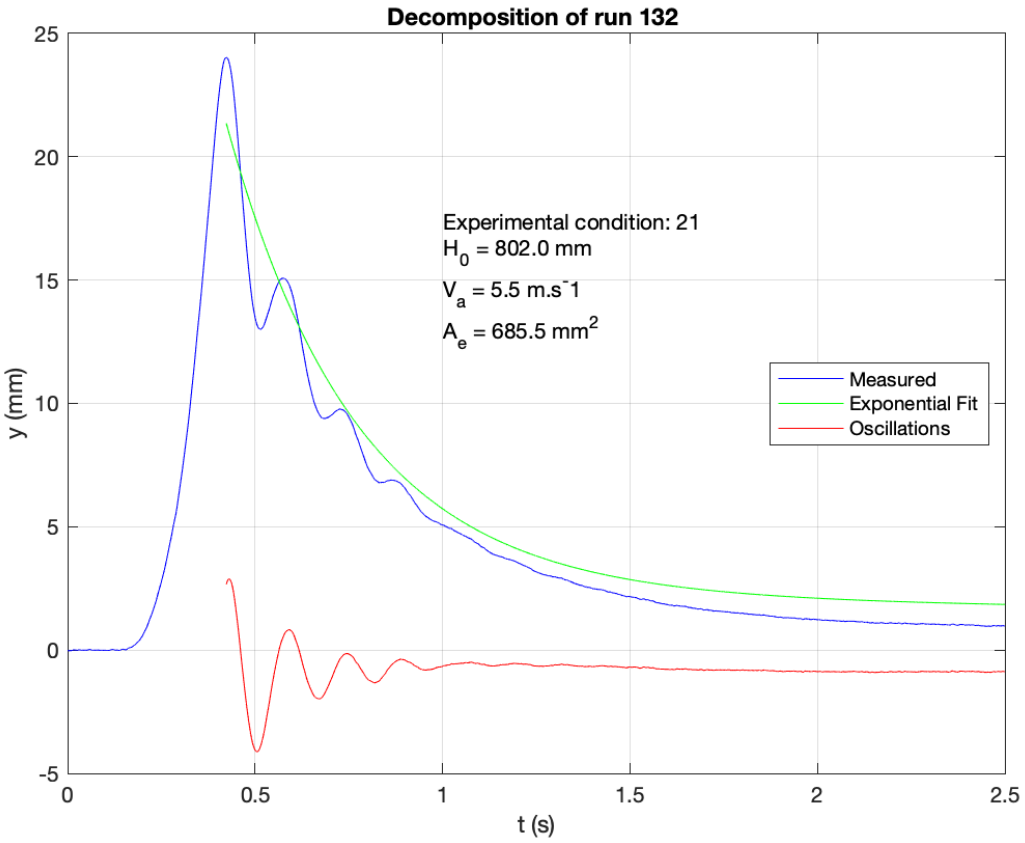


Figure E.37. Decomposition of run 132.

E.22. Experimental condition twenty-two

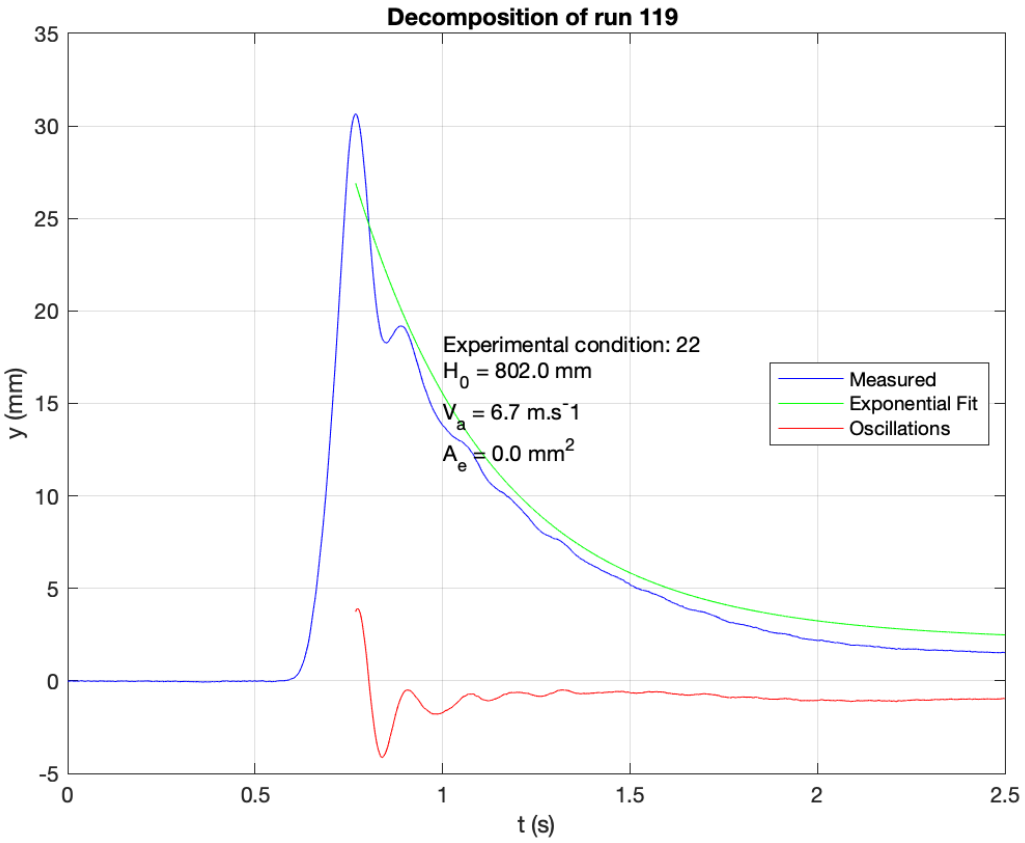


Figure E.38. Decomposition of run 119.

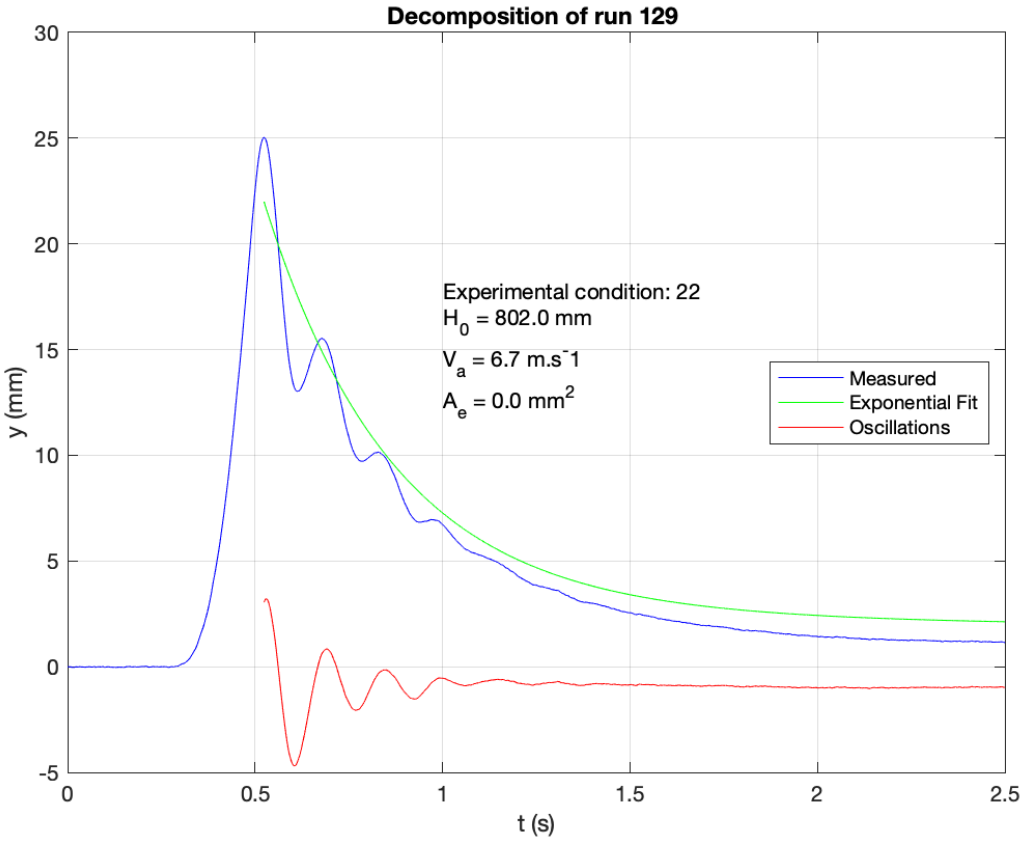


Figure E.39. Decomposition of run 129.

E.23. Experimental condition twenty-three

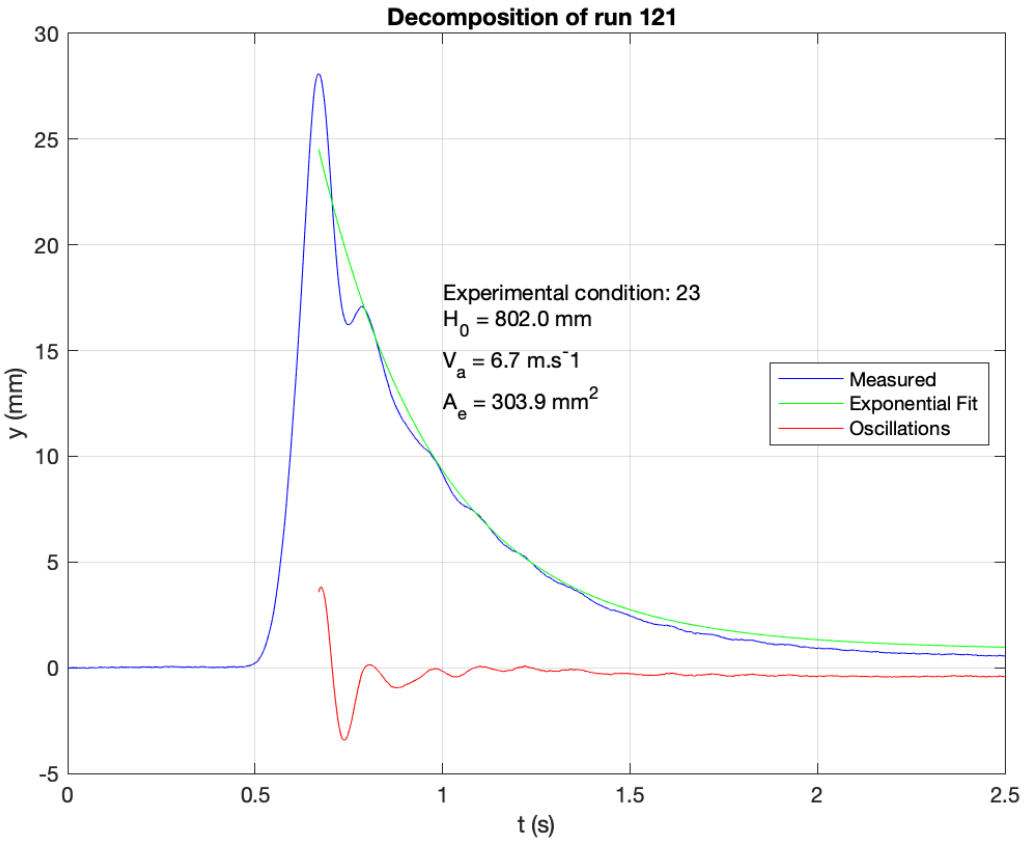


Figure E.40. Decomposition of run 121.

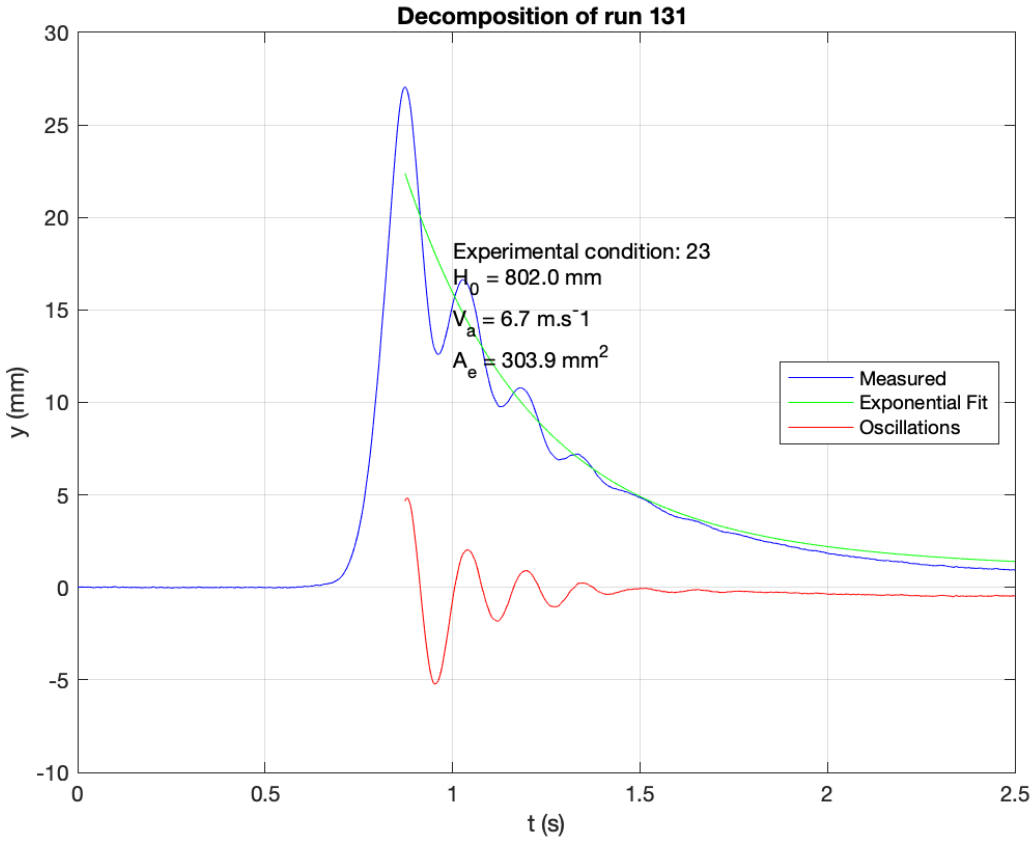


Figure E.41. Decomposition of run 131.

E.24. Experimental condition twenty-four

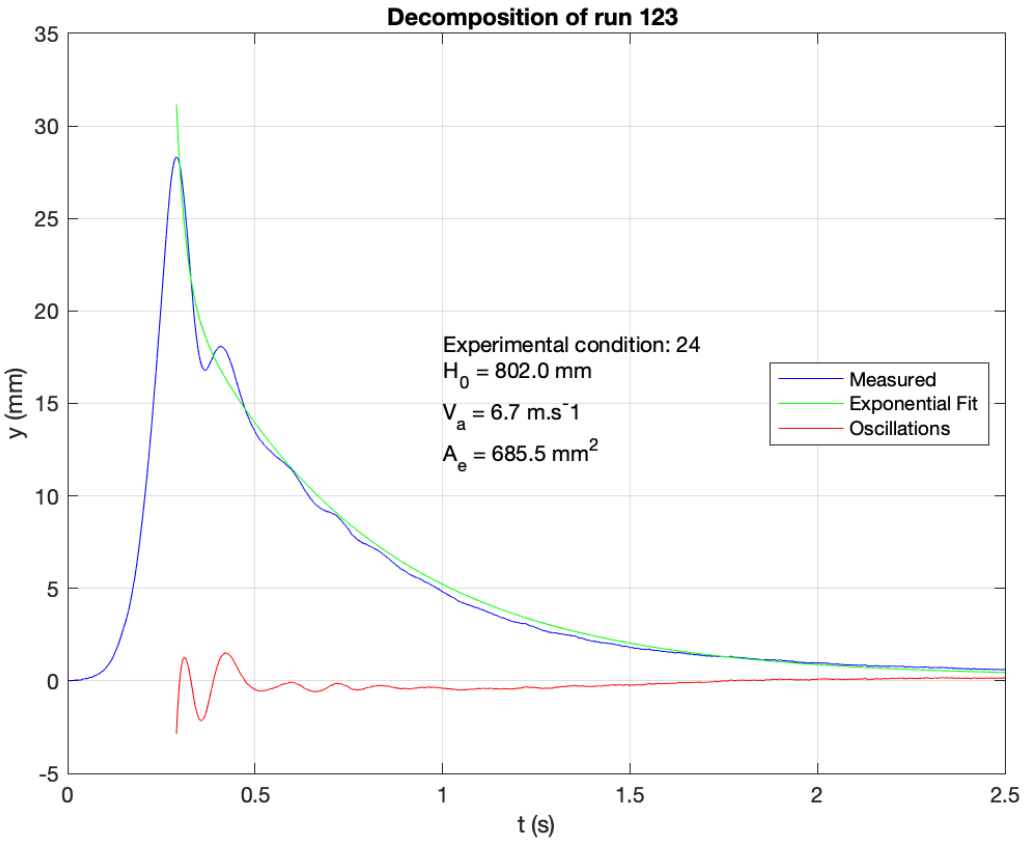


Figure E.42. Decomposition of run 123.

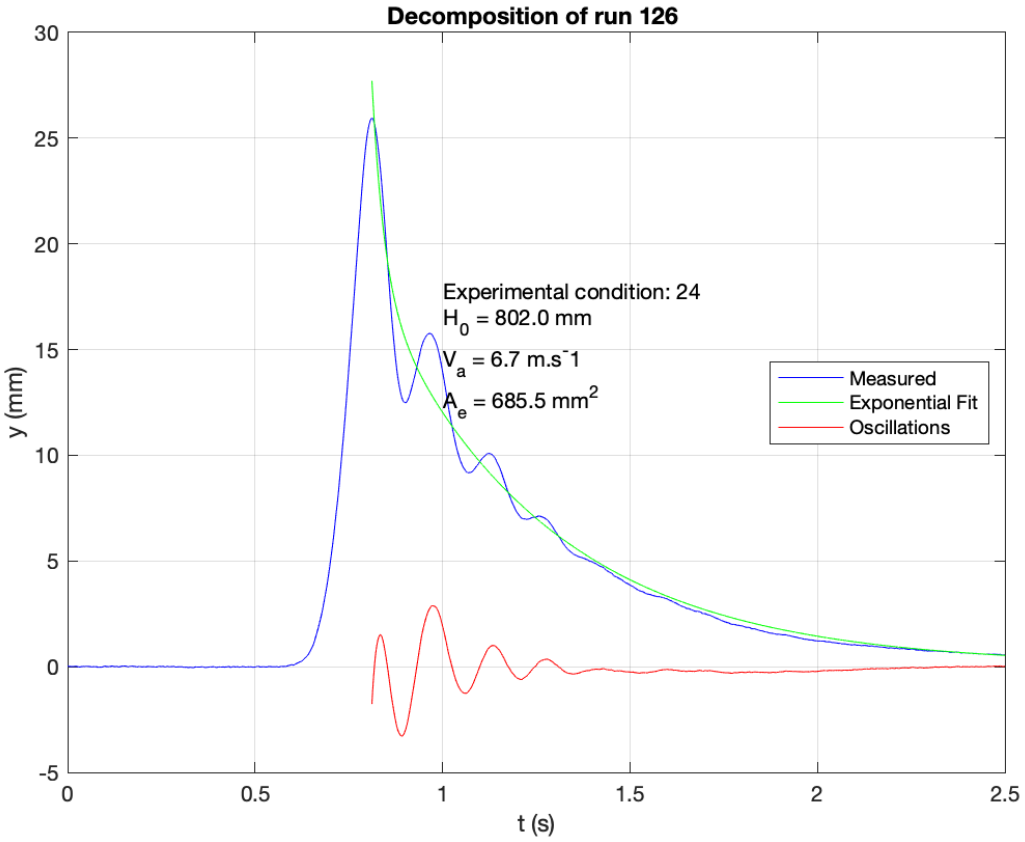


Figure E.43. Decomposition of run 126.

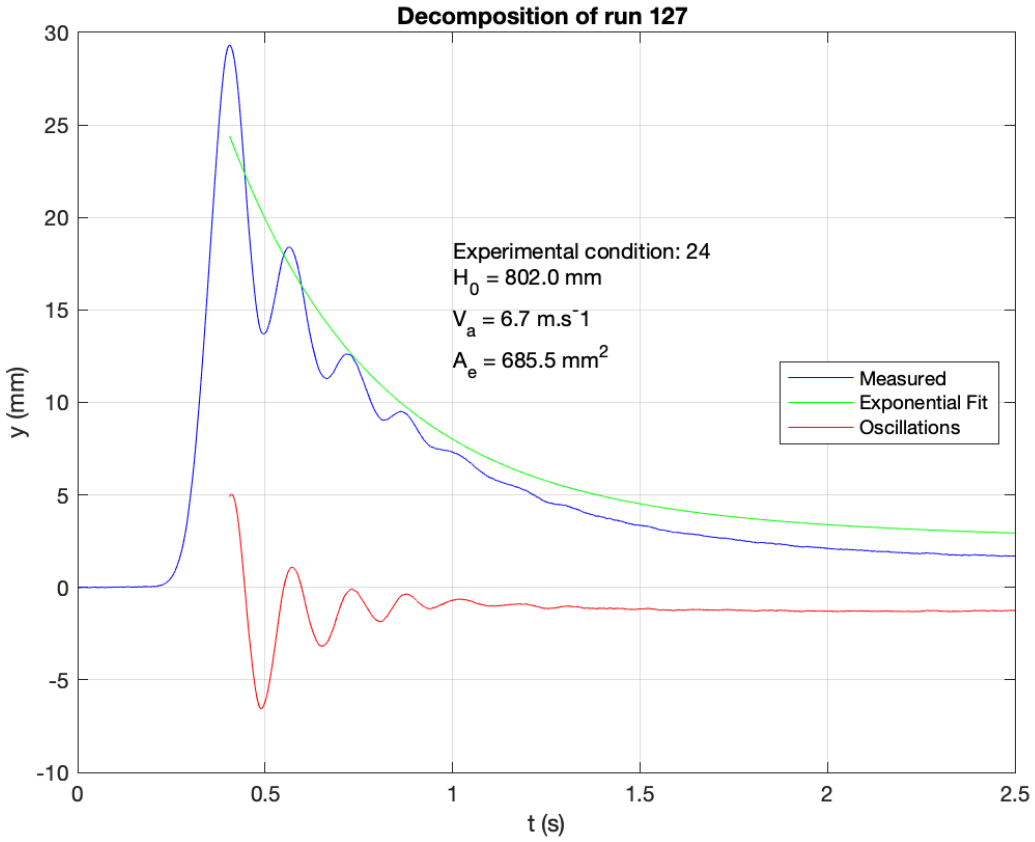


Figure E.44. Decomposition of run 127.

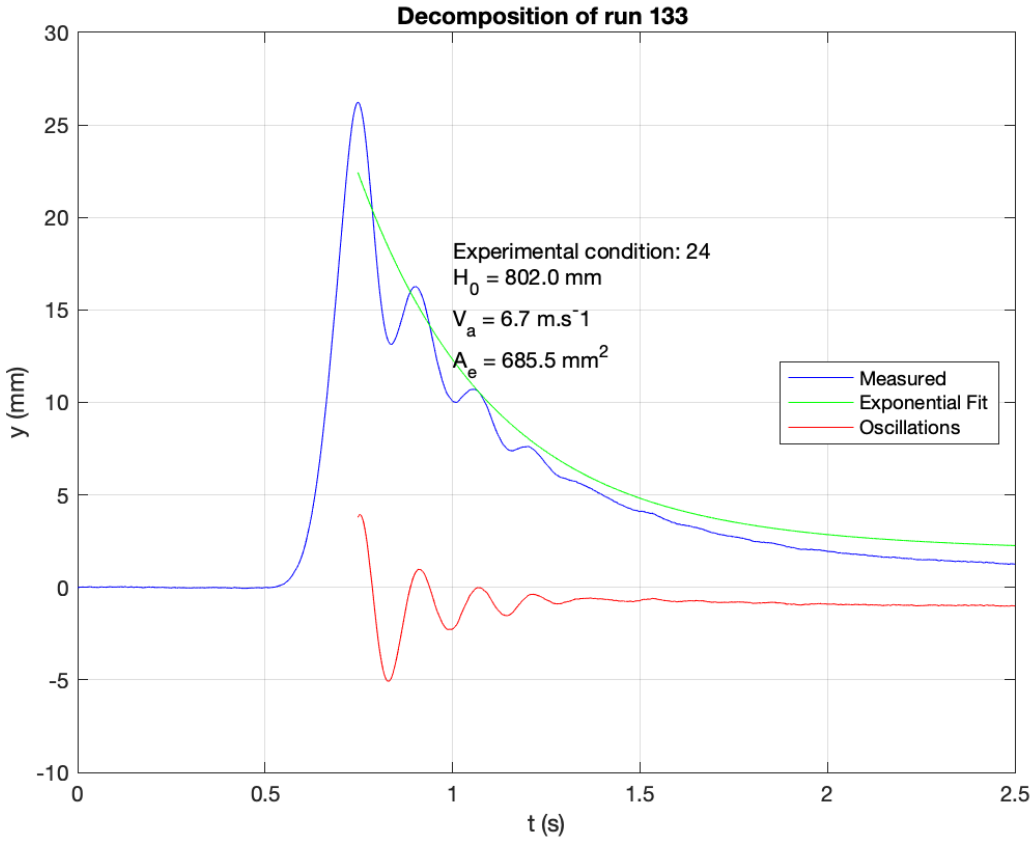


Figure E.45. Decomposition of run 133.

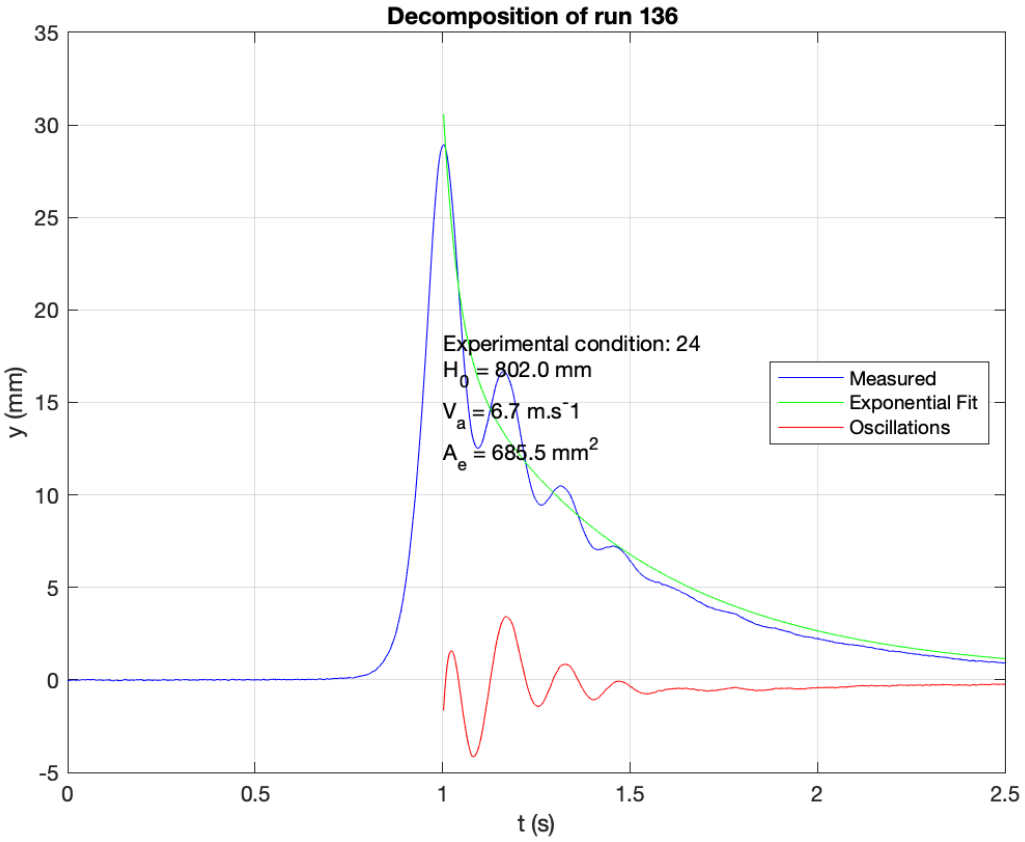


Figure E.46. Decomposition of run 136.

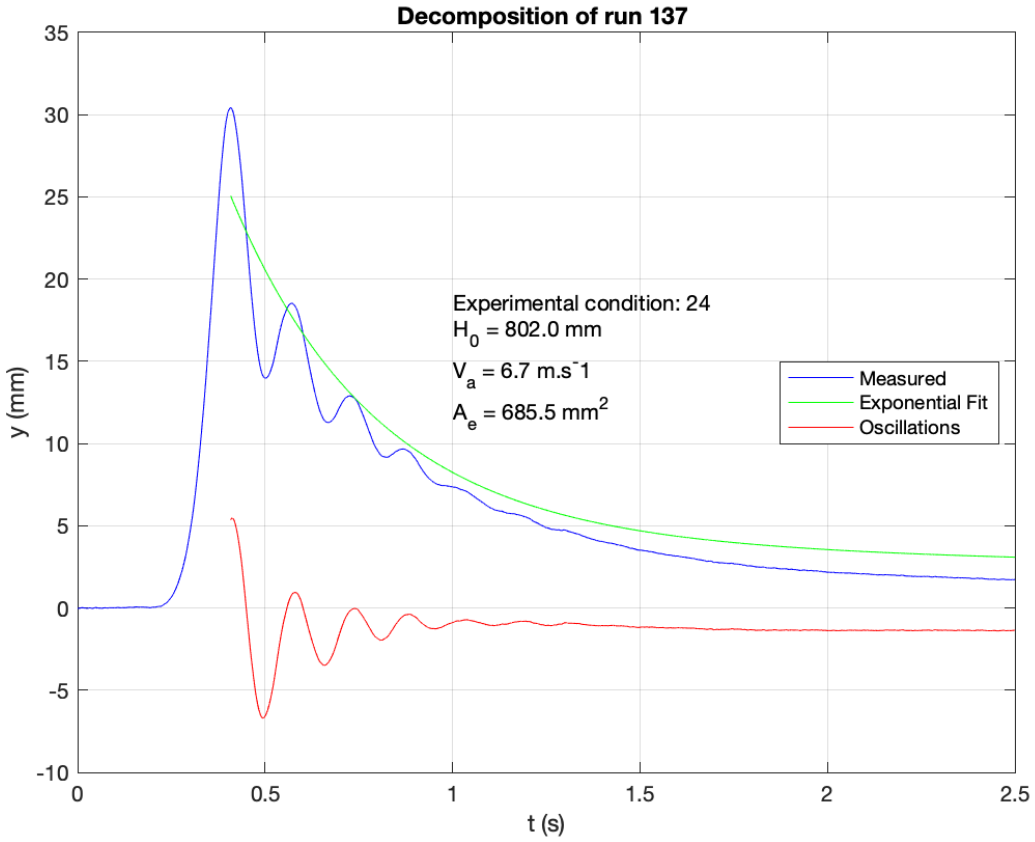


Figure E.47. Decomposition of run 137.

E.25. Experimental condition twenty-five

No valid experimental data available.

E.26. Experimental condition twenty-six

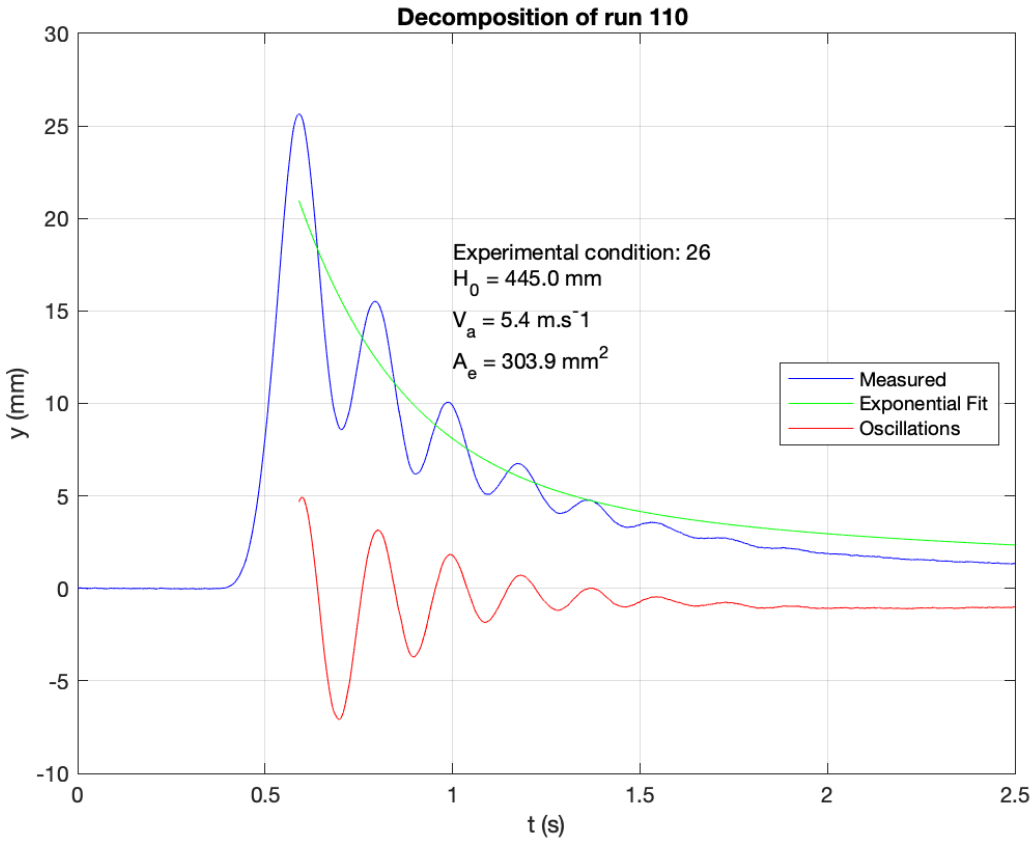


Figure E.48. Decomposition of run 110.

E.27. Experimental condition twenty-seven

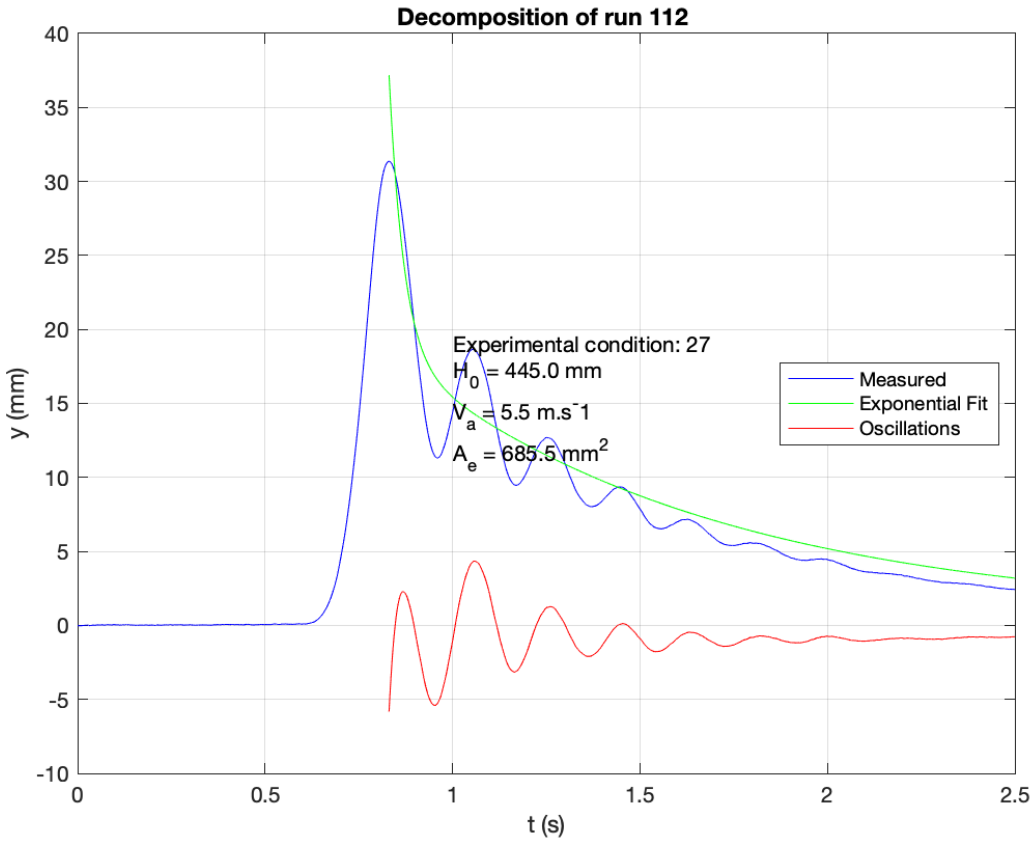


Figure E.49. Decomposition of run 112.

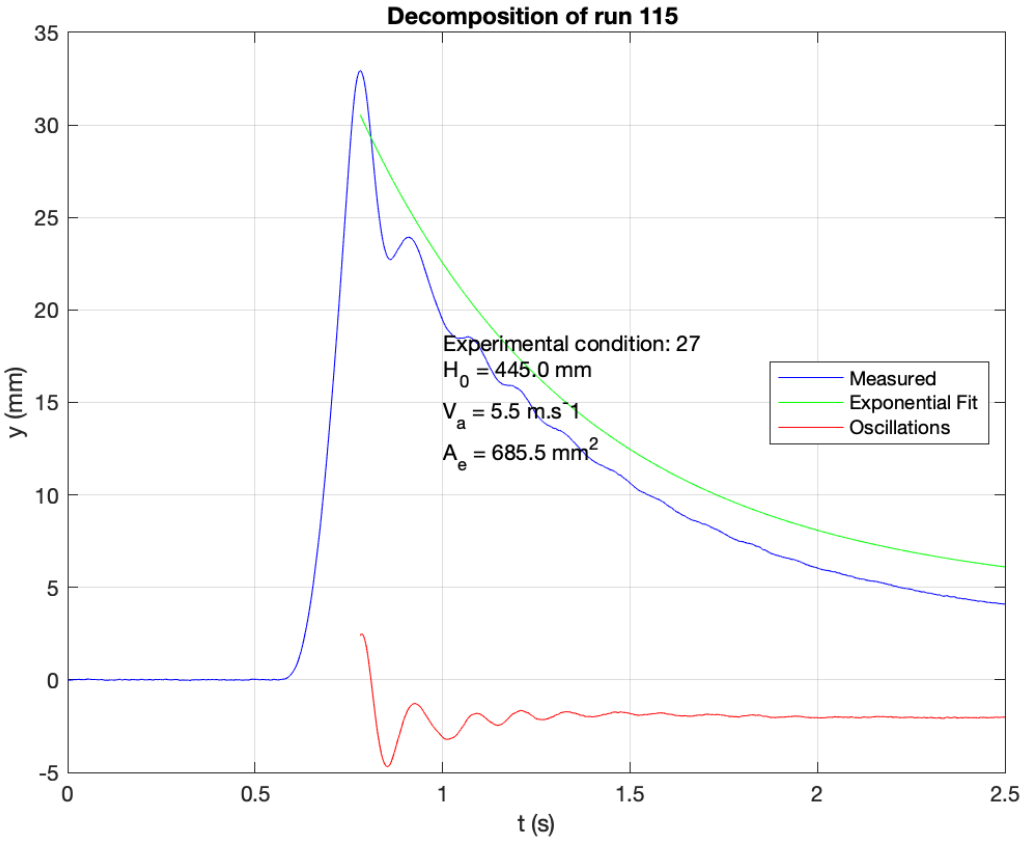


Figure E.50. Decomposition of run 115.

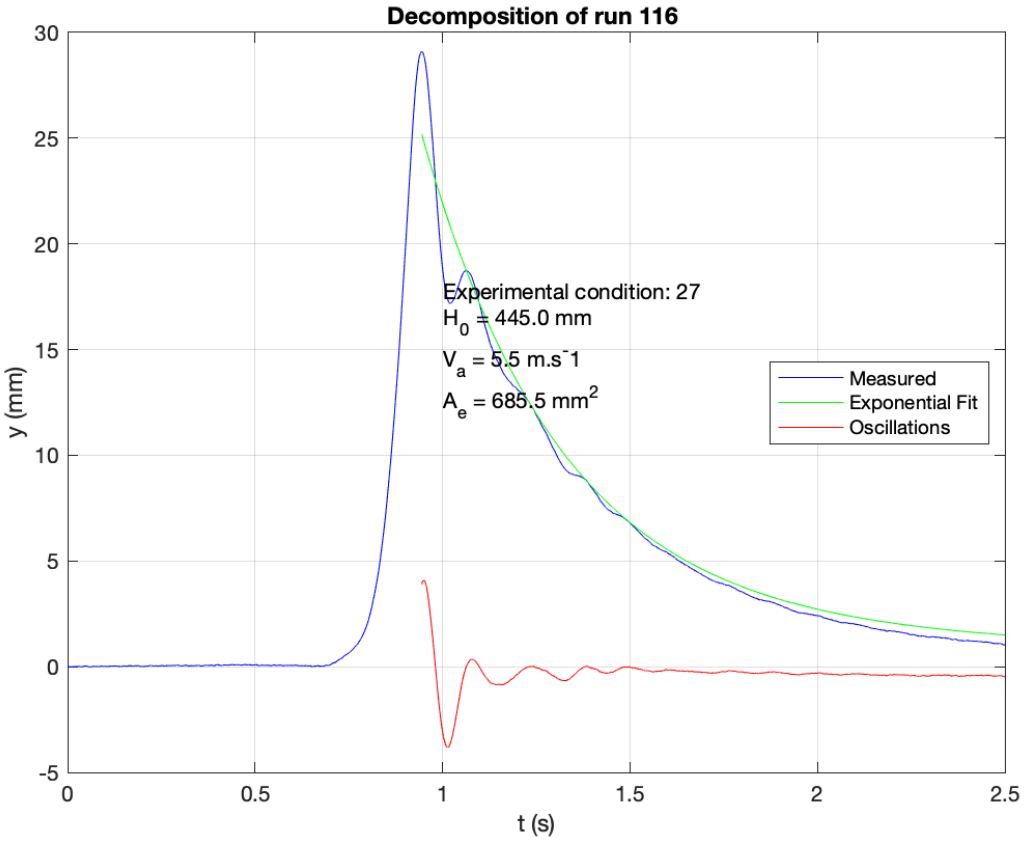


Figure E.51. Decomposition of run 116.

E.28. Experimental condition twenty-eight

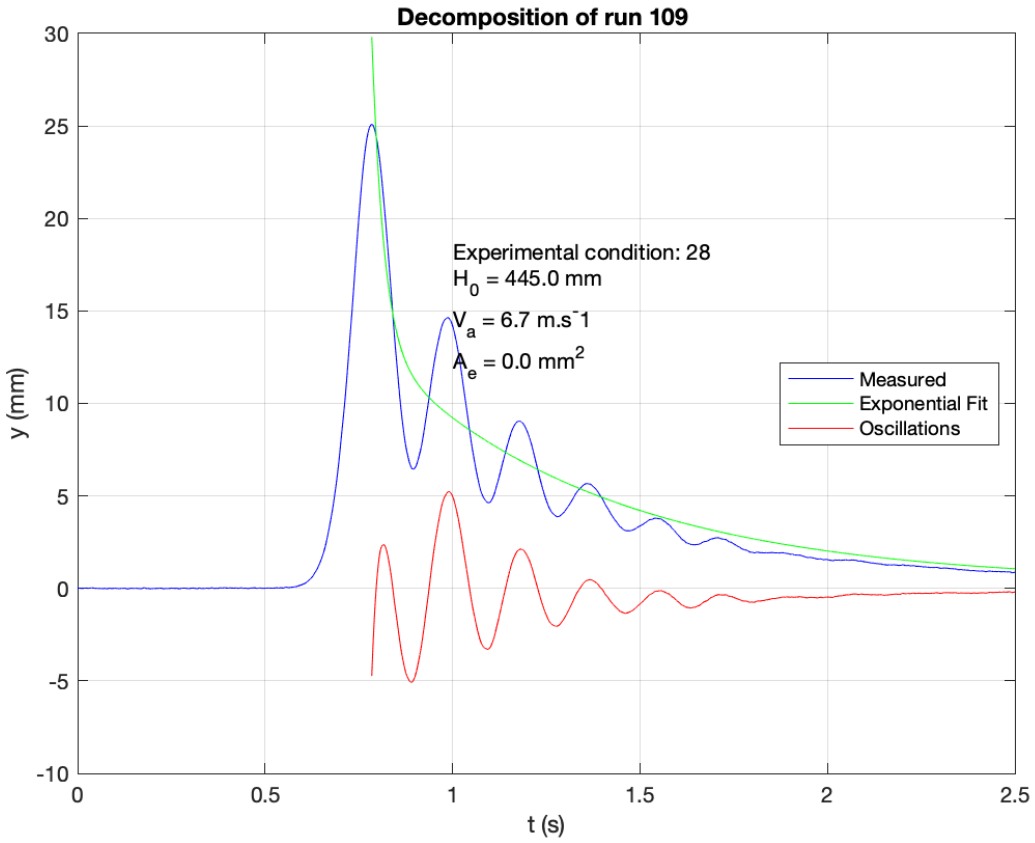


Figure E.52. Decomposition of run 109.

E.29. Experimental condition twenty-nine

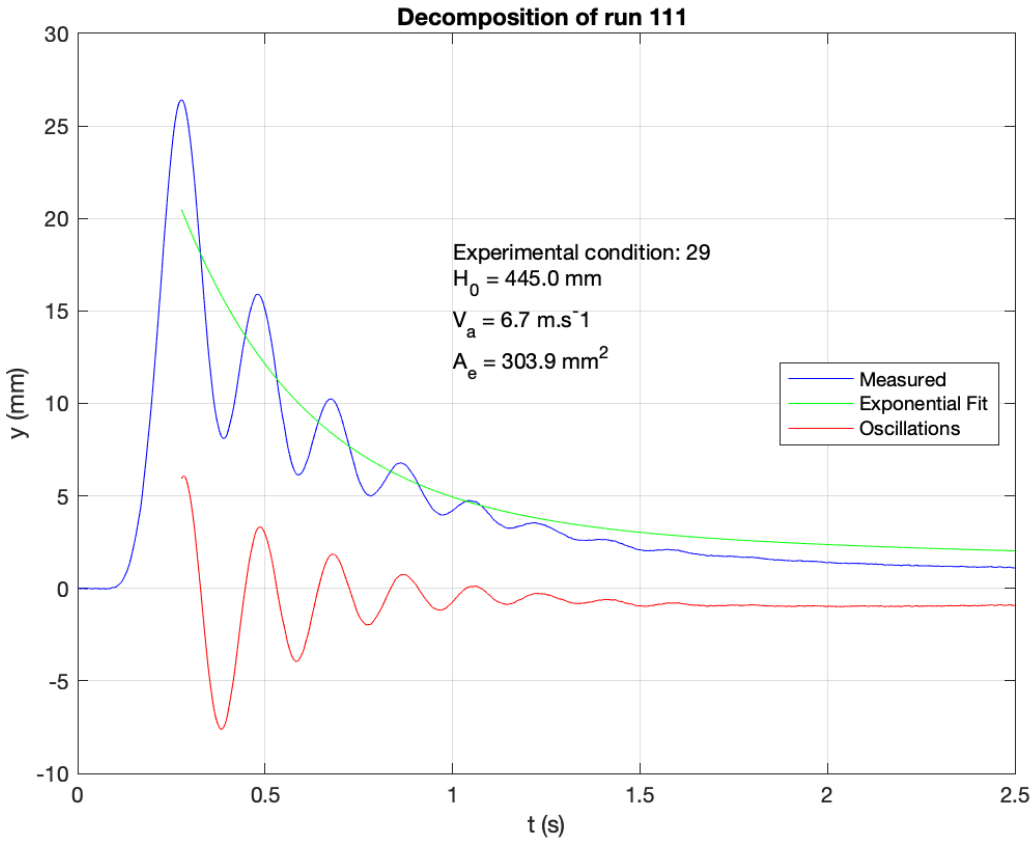


Figure E.53. Decomposition of run 111.

E.30. Experimental condition thirty

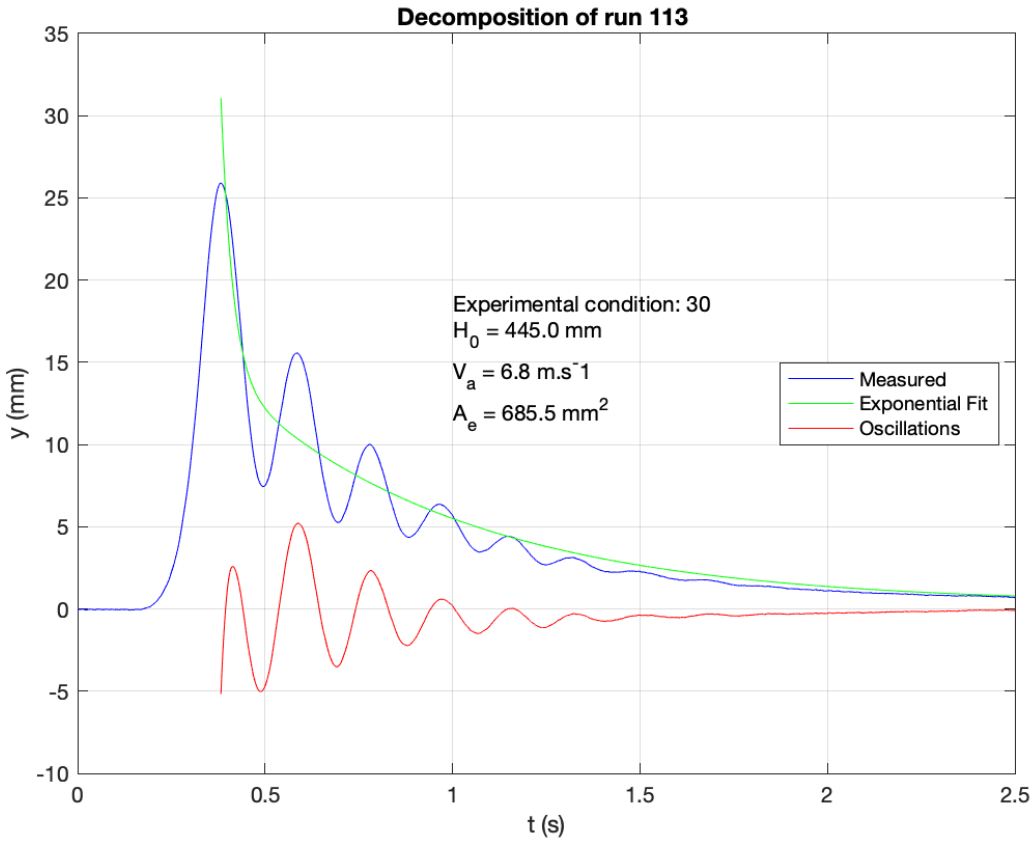


Figure E.54. Decomposition of run 113.

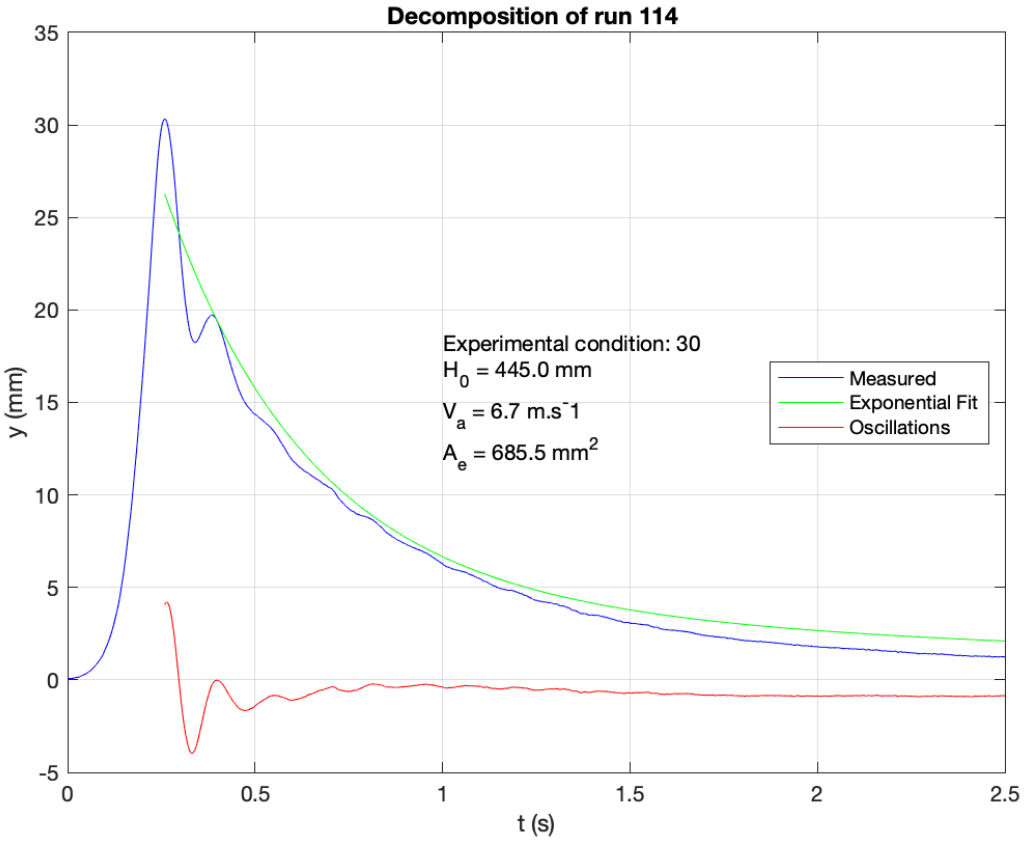


Figure E.55. Decomposition of run 114.

F. Experimental Rig Parameter Estimation Through Curve Fitting

This appendix contains the curve fitting plots discussed in Sec. 6.4. Conditions one to six (Figs. F.1 to F.6) were discarded as the velocity-dependent heave deck resistance was abnormally high and it was concluded that the plenum height for those conditions ($H_0 = 1.143 \times 10^3\,\mathrm{mm}$) caused instability in the experimental rig. No data was available for condition twenty-five. The values used to generate the curves are tabulated in Appendix F.

Table F.1. Experimental mass-plenum rig characteristics and parameter values. The experimental condition (denoted '#') is the unique combination of plenum height (H_0), air supply duct centreline air velocity (V_s), and air exit area (A_e) that were used for the commissioning tests of the experimental rig in the plenum volume forced step change configuration. The hover pressure (h_p) is tabulated to show the effect of the different combinations of V_s and A_e. The parameters found by curve fitting to the commissioning test data are: plenum stiffness (k_p); parasitic air leakage area (A_L); dry (Coulomb) friction coefficient (F_c) and; velocity-dependent resistance coefficient (F_v). Refer to Sec. 6.3 for a report on the method and discussion of the results. The curves generated from these values are shown fitted to commissioning test data in Appendix F.

#	H_0 (m)	V_s ($\mathrm{m\,s^{-1}}$)	A_e ($\mathrm{m^2}$)	p_h ($\mathrm{N\,m^{-2}}$)	k_p ($\mathrm{N\,m^{-1}}$)	A_L ($\mathrm{m^2}$)	C_c N	C_v $\mathrm{N\,s\,rad^{-1}}$
1	1.143	5.49	0.57E-3	255	0.6E6	2E-3	8	1.0E3
2	1.143	6.75	0.57E-3	373	0.6E6	2E-3	14	1.0E3
3	1.143	5.49	0.82E-3	223	0.6E6	2E-3	2	1.0E3
4	1.143	6.75	0.82E-3	315	0.6E6	2E-3	20	1.0E3
5	1.143	5.49	1.20E-3	177	0.6E6	2E-3	3	1.0E3
6	1.143	6.75	1.20E-3	254	0.6E6	2E-3	1	1.0E3
7	0.297	5.49	0.57E-3	255	90E3	1.5E-3	16	0.8E3
8	0.297	5.49	0.82E-3	223	90E3	1.5E-3	6	0.9E3
9	0.297	5.49	1.20E-3	177	90E3	1.5E-3	11	0.9E3
10	0.297	6.75	0.57E-3	392	90E3	1.5E-3	6	1.9E3
11	0.297	6.75	0.82E-3	322	90E3	1.5E-3	9	0.9E3
12	0.297	6.75	1.20E-3	255	90E3	1.5E-3	25	0.9E3
13	0.605	5.49	0.57E-3	248	25E3	1.6E-3	6	0.2E3
14	0.605	5.49	0.82E-3	223	25E3	1.2E-3	6	0.91E3
15	0.605	5.49	1.20E-3	176	25E3	1.8E-3	8	1.5E3
16	0.605	6.75	0.57E-3	392	25E3	2E-3	10	0.34E3
17	0.605	6.75	0.82E-3	325	25E3	1.2E-3	10	0.30E3
18	0.605	6.75	1.20E-3	257	25E3	1.6E-3	6	0.30E3
19	0.802	5.49	0.57E-3	206	90E3	3.5E-3	5	0.55E3
20	0.802	5.49	0.82E-3	186	90E3	3.0E-3	5	0.55E3
21	0.802	5.49	1.20E-3	152	90E3	2.0E-3	10	0.55E3
22	0.802	6.75	0.57E-3	315	90E3	3.5E-3	12	0.55E3
23	0.802	6.75	0.82E-3	265	90E3	3.0E-3	4	0.55E3
24	0.802	6.75	1.20E-3	220	90E3	2.0E-3	16	0.55E3
25	0.445	5.49	0.57E-3	230	-	-	-	-
26	0.445	5.49	0.82E-3	206	28E3	2.5E-3	10	0.30E3
27	0.445	5.49	1.20E-3	167	28E3	0.5E-3	9	0.25E3
28	0.445	6.75	0.57E-3	355	28E3	4.0E-3	4	0.35E3
29	0.445	6.75	0.82E-3	299	28E3	3.5E-3	10	0.22E3
30	0.445	6.75	1.20E-3	246	28E3	2.5E-3	4	0.22E3

No valid experimental data is available for condition twenty-five.

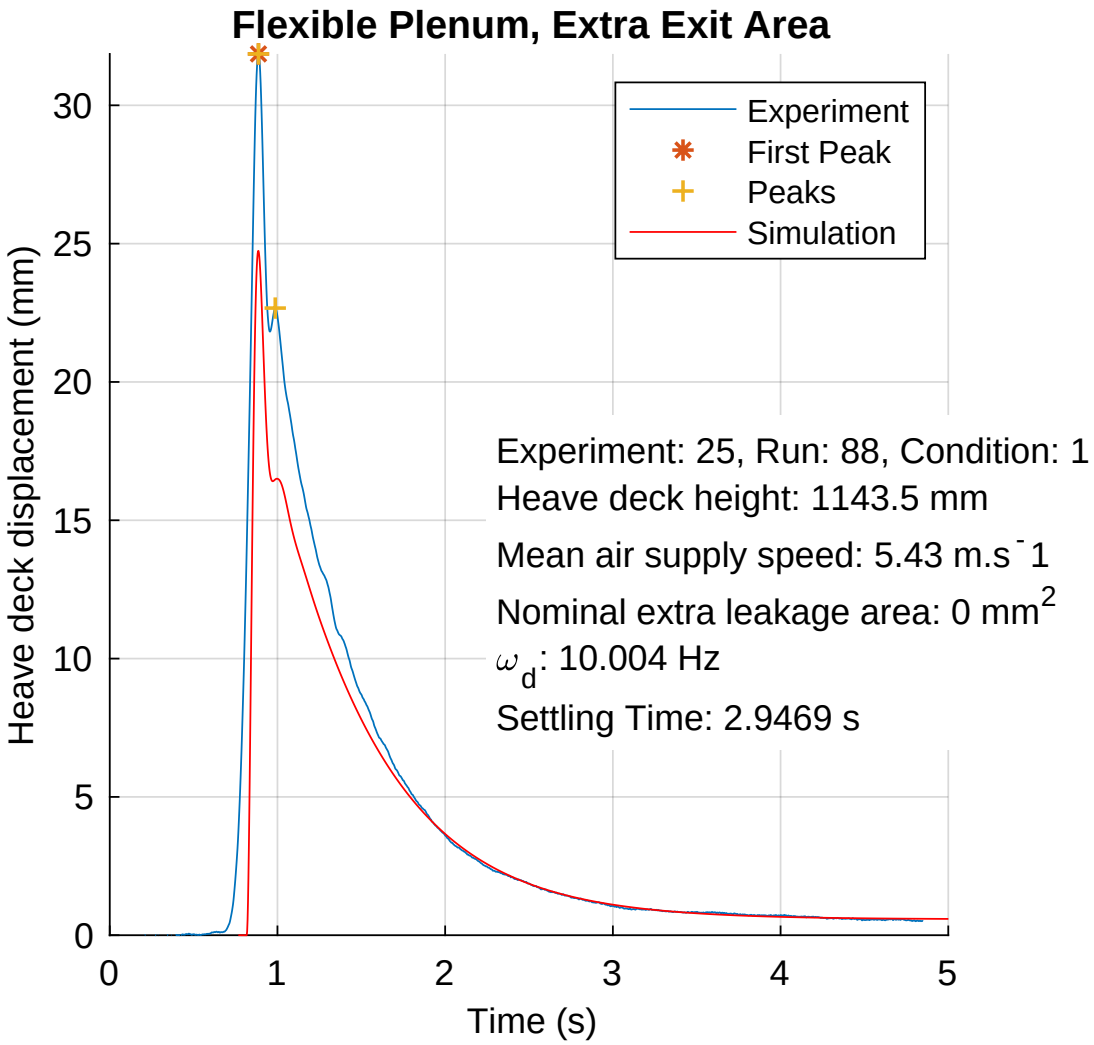


Figure F.1. Curve fitting for condition 1

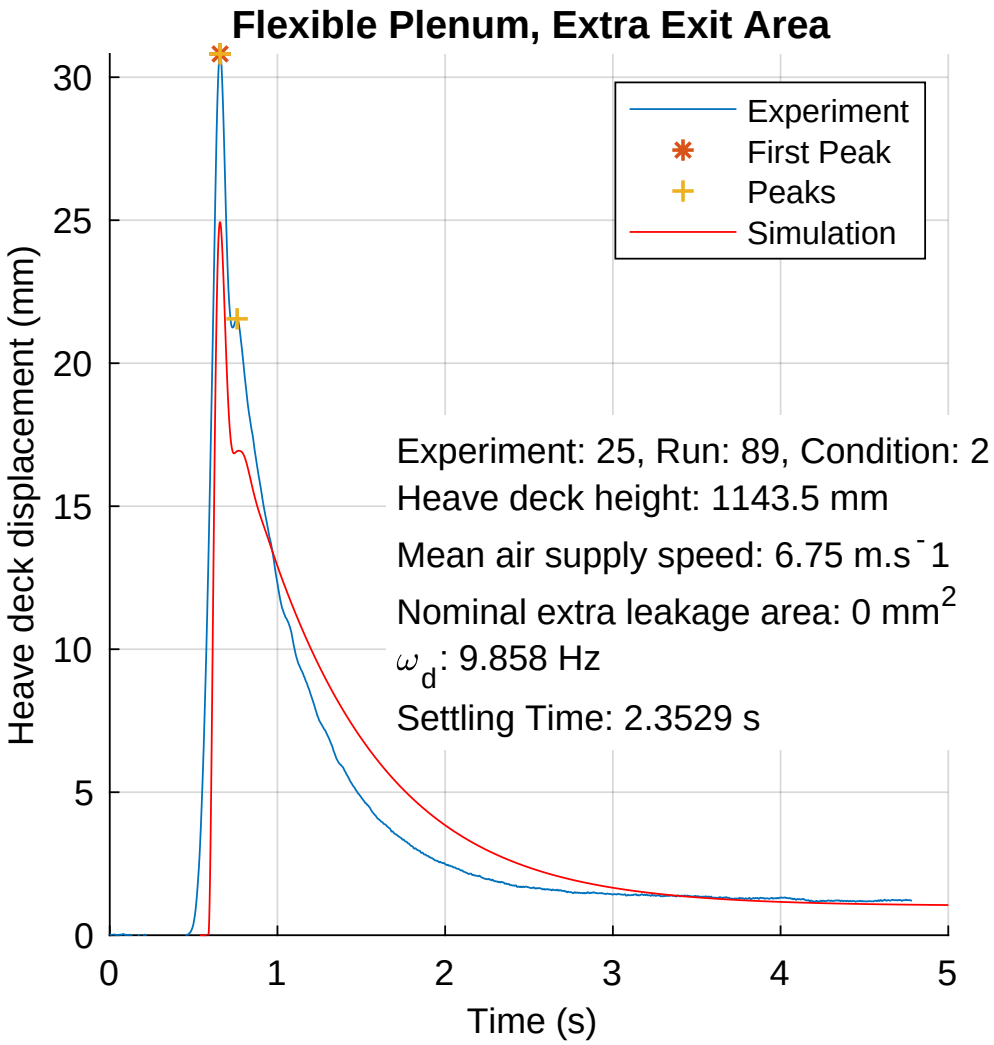


Figure F.2. Curve fitting for condition 2

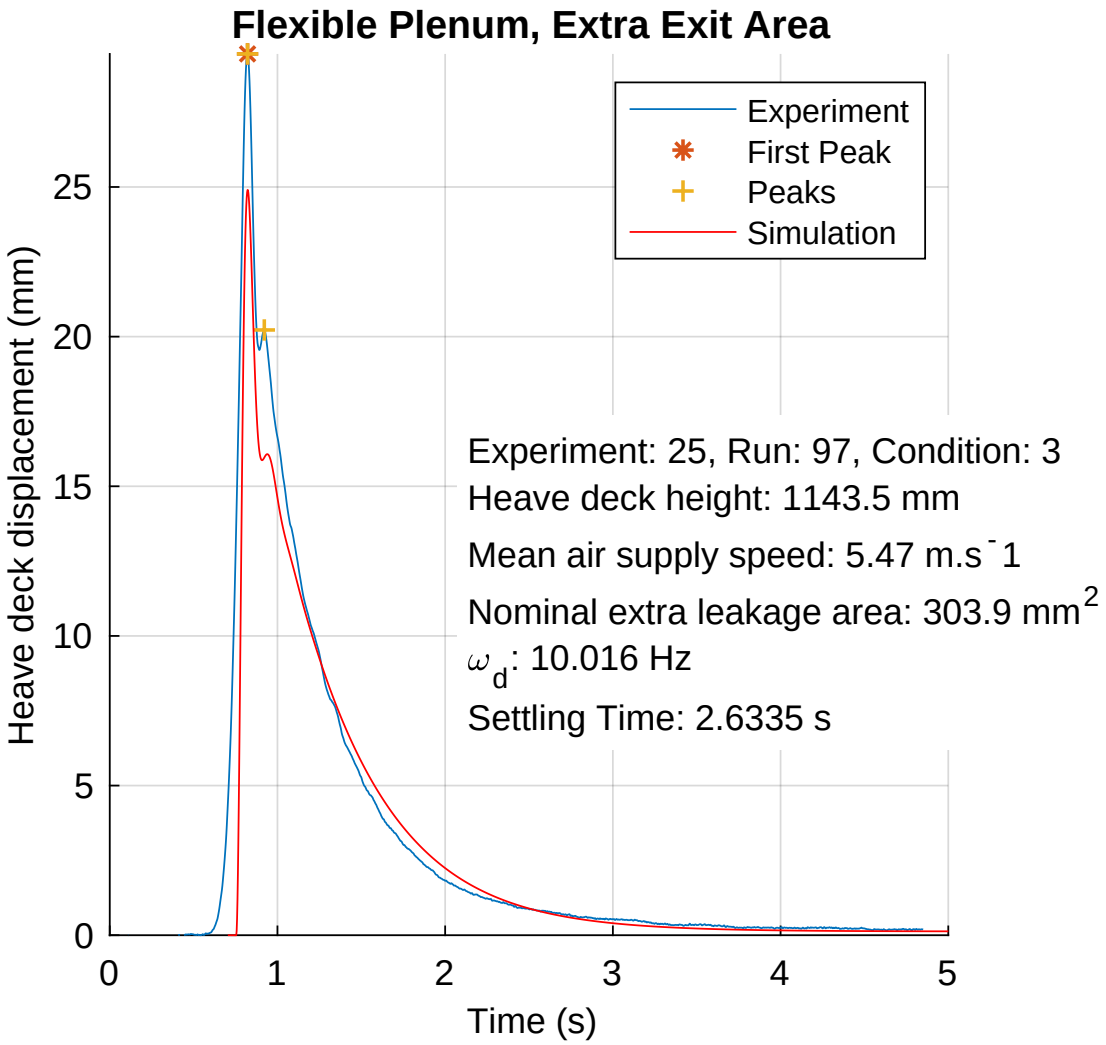


Figure F.3. Curve fitting for condition 3

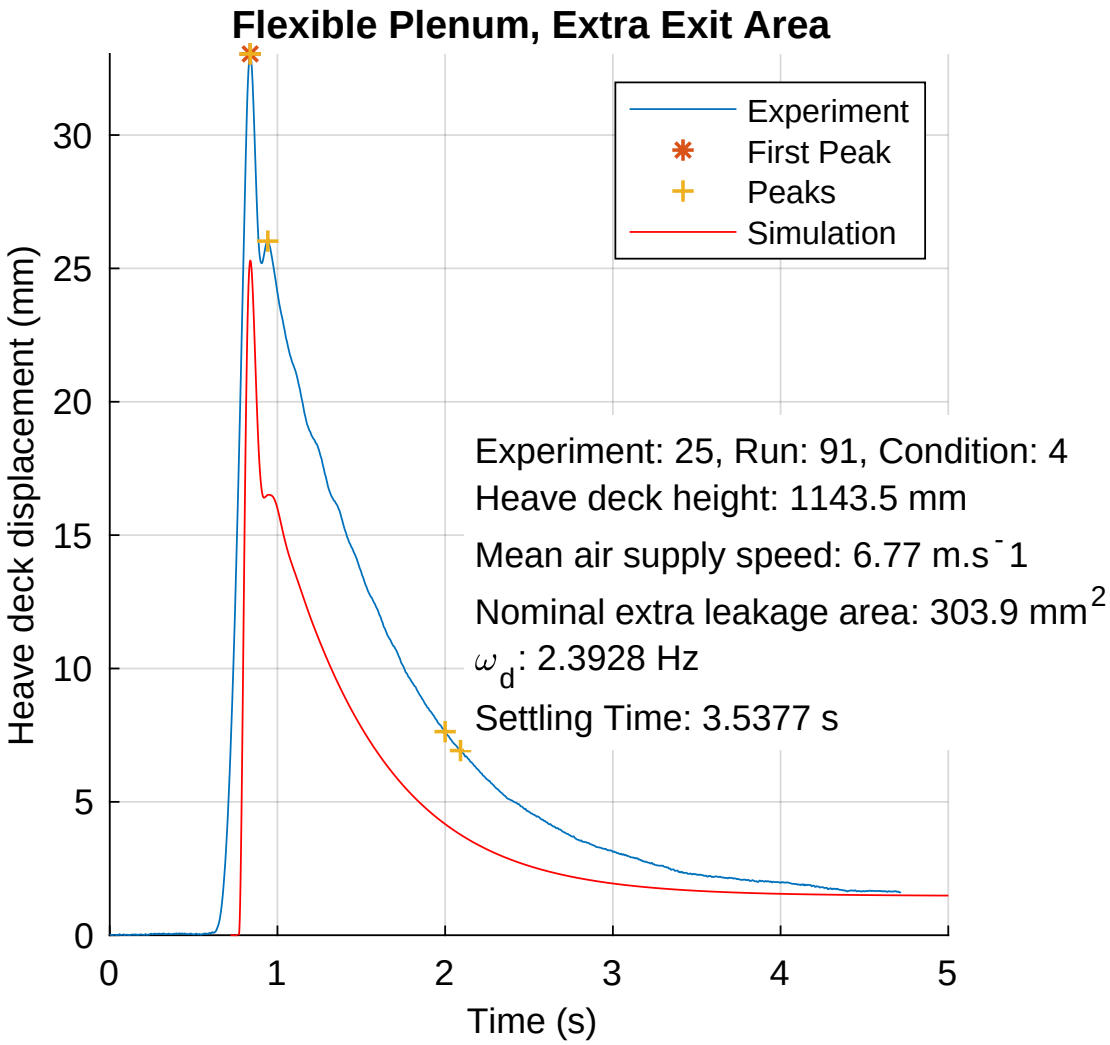


Figure F.4. Curve fitting for condition 4

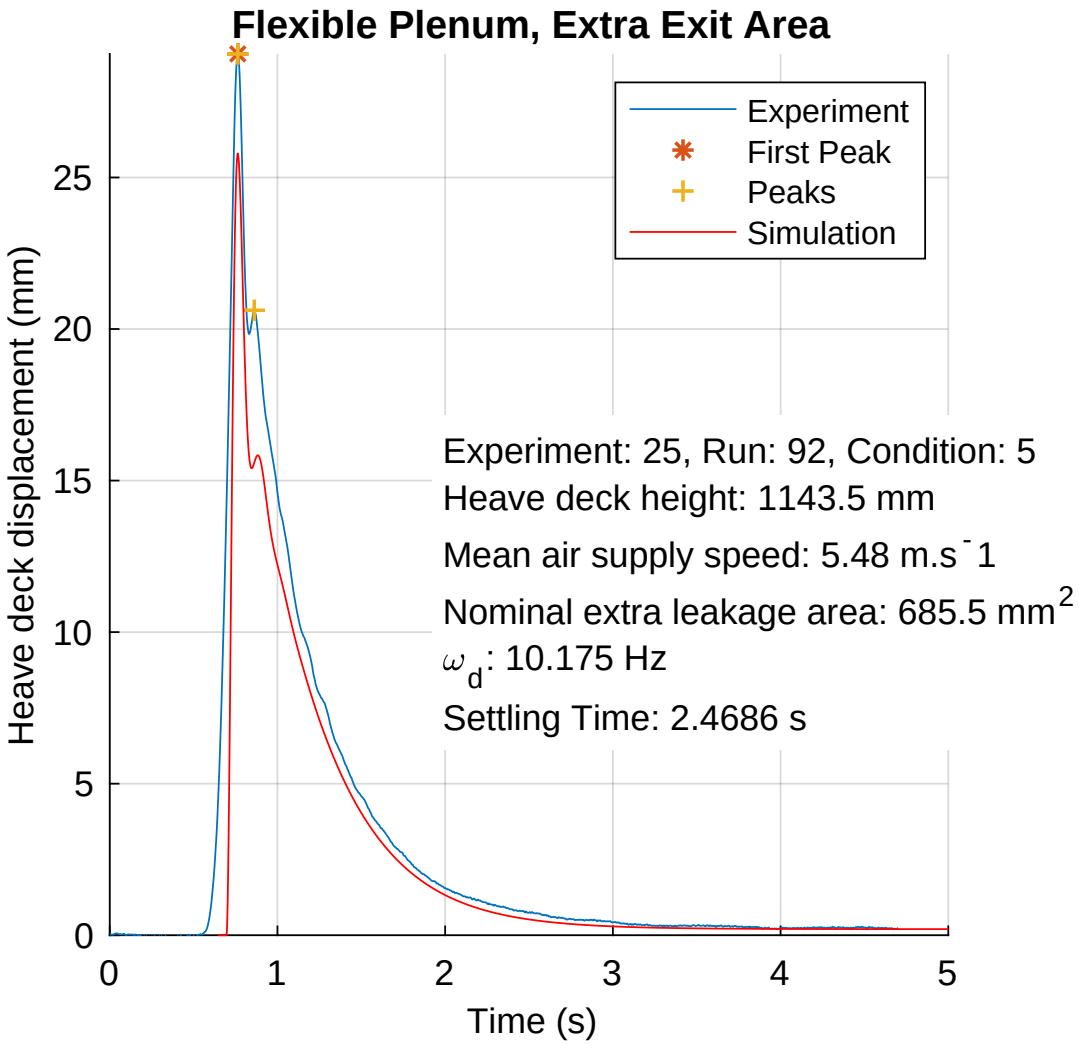


Figure F.5. Curve fitting for condition 5

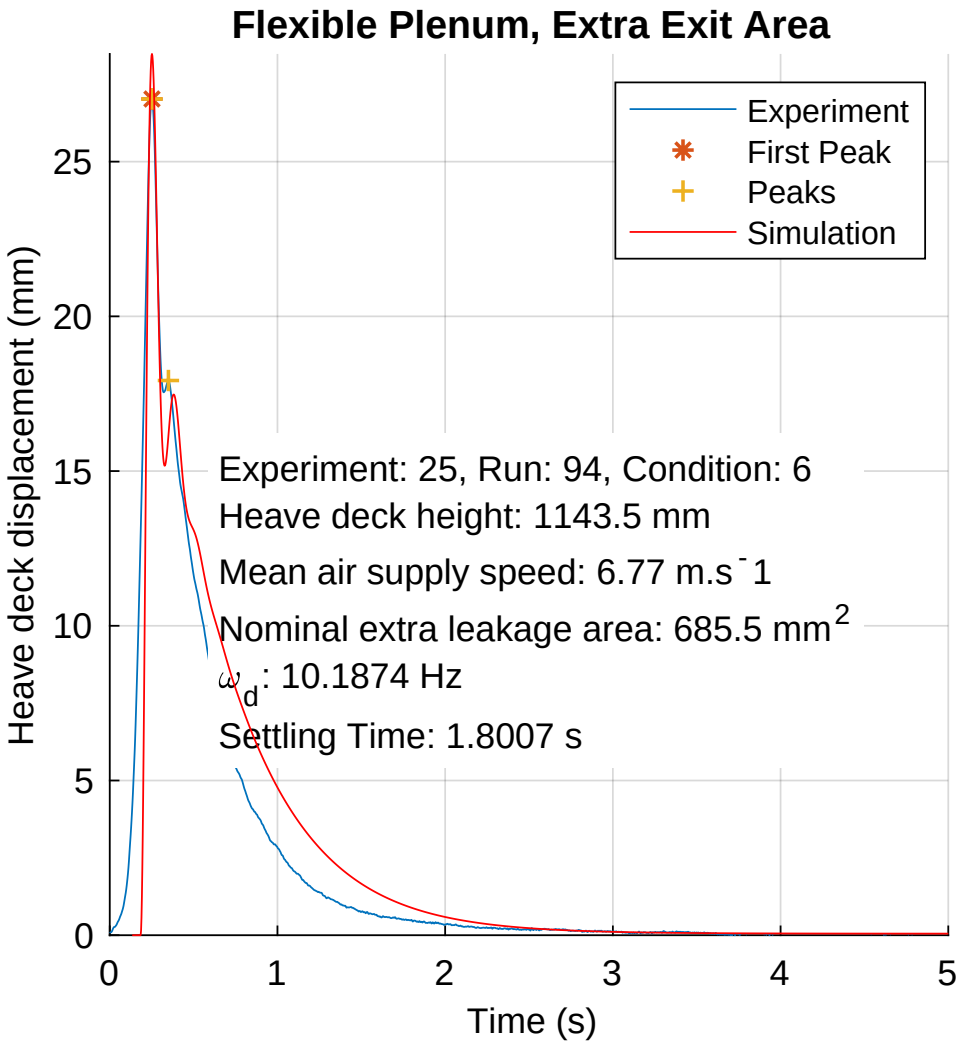


Figure F.6. Curve fitting for condition 6

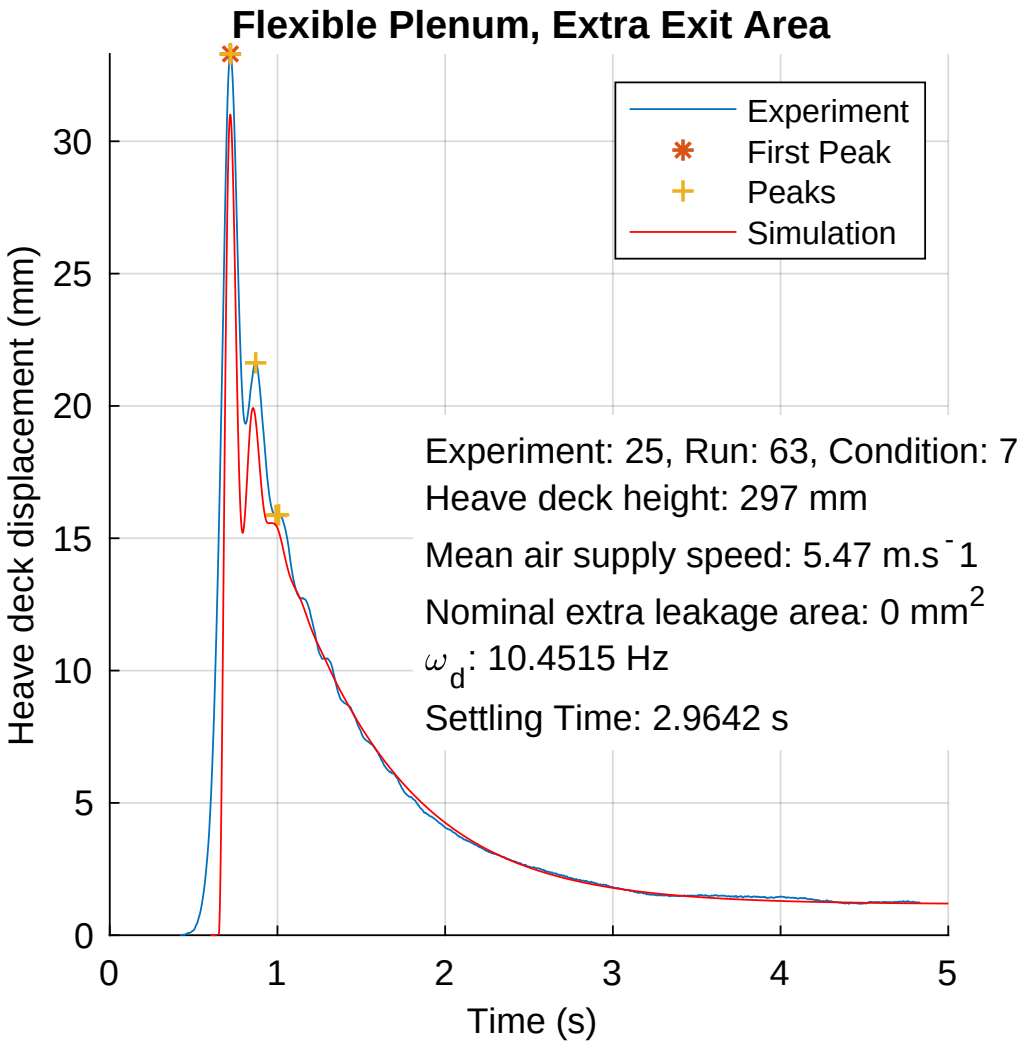


Figure F.7. Curve fitting for condition 7

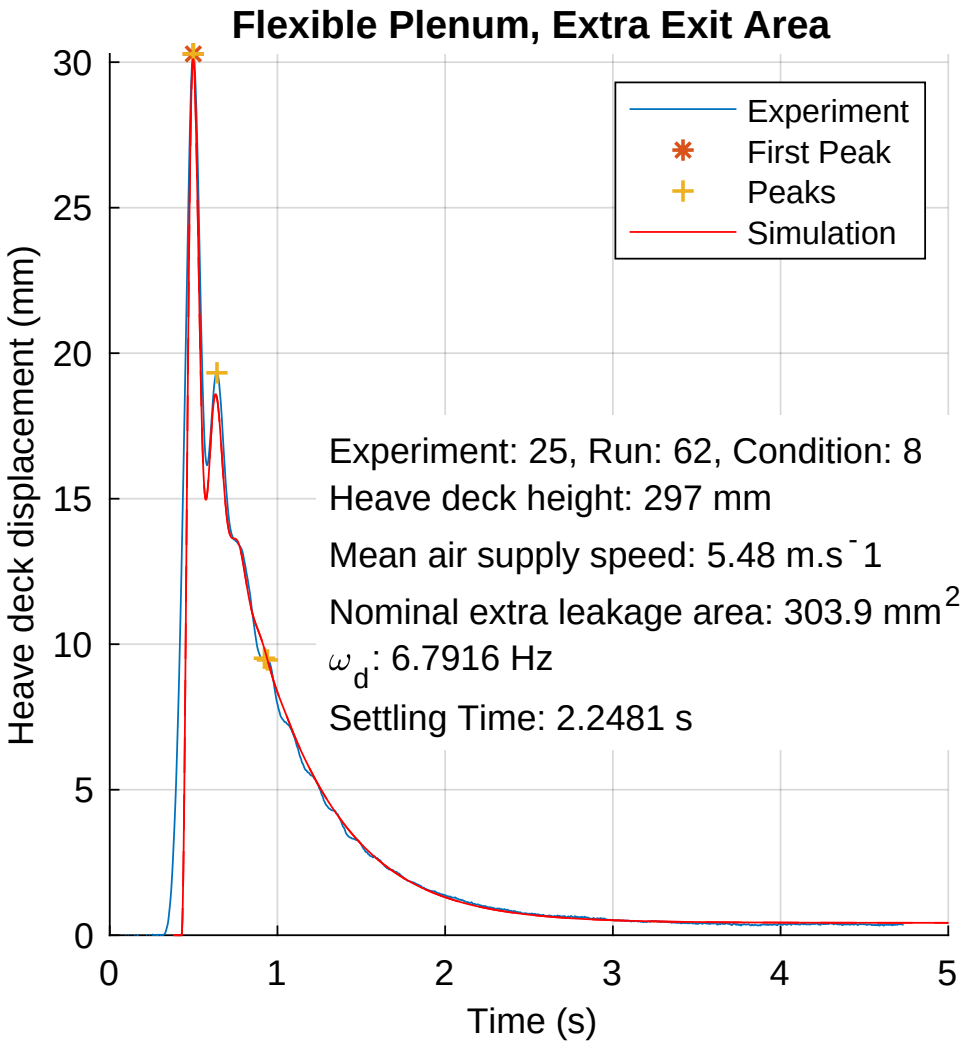


Figure F.8. Curve fitting for condition 8

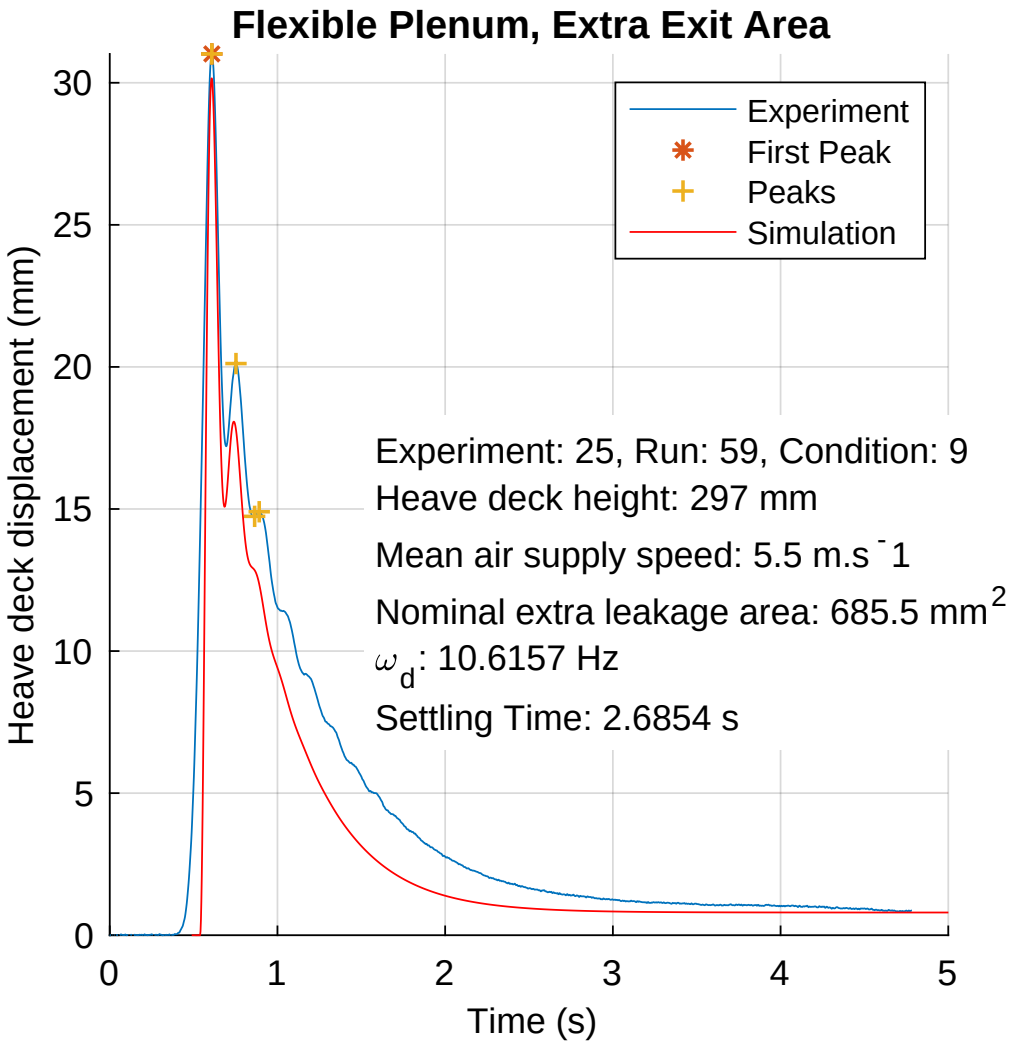


Figure F.9. Curve fitting for condition 9

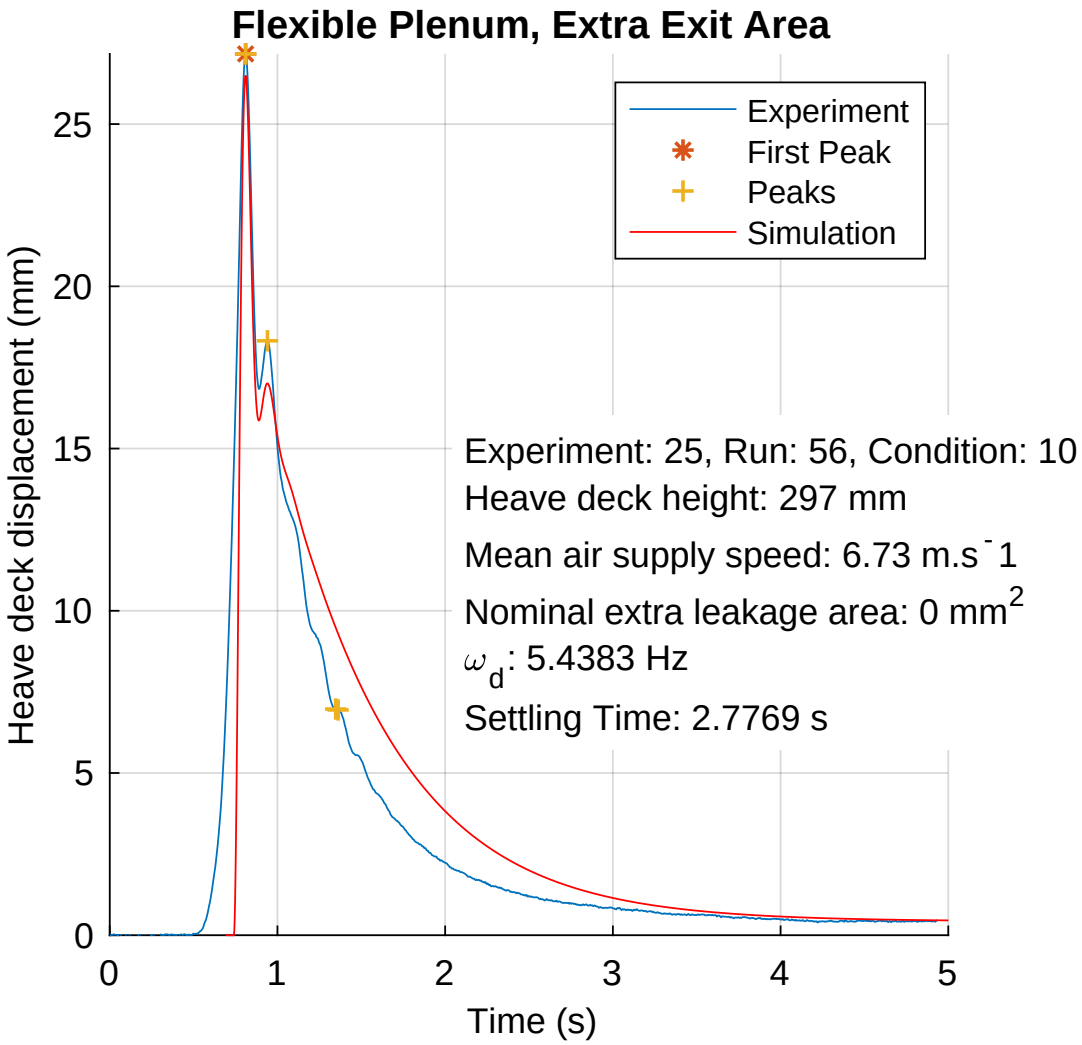


Figure F.10. Curve fitting for condition 10

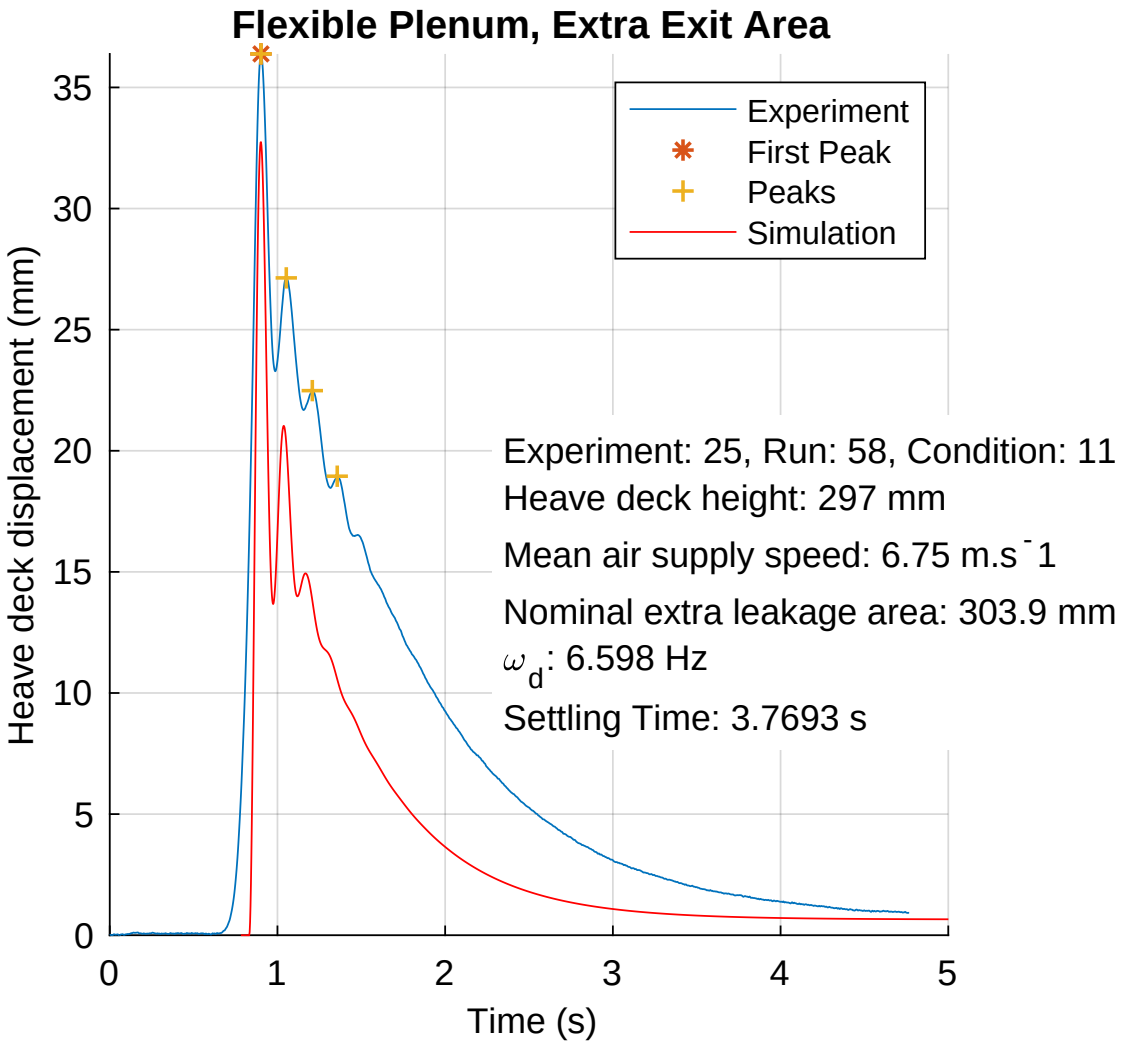


Figure F.11. Curve fitting for condition 11

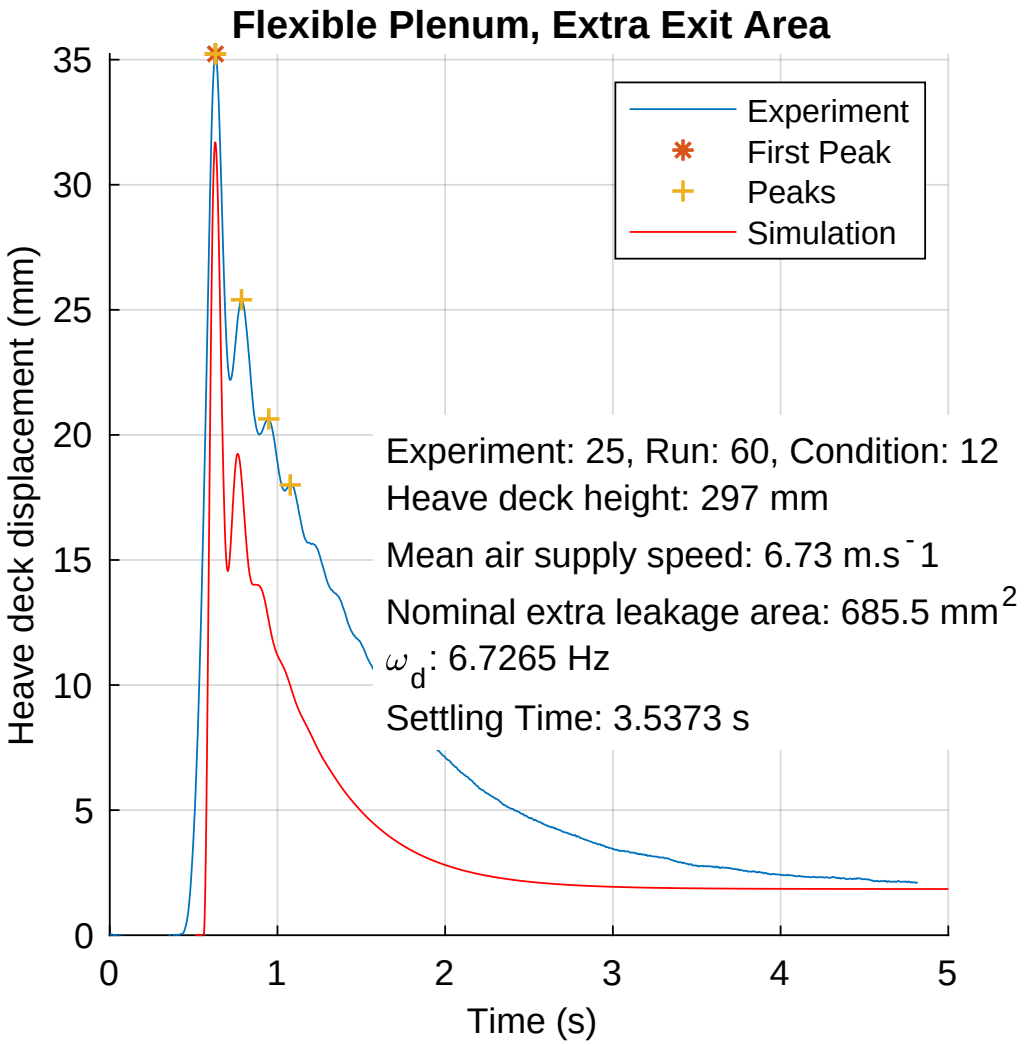


Figure F.12. Curve fitting for condition 12

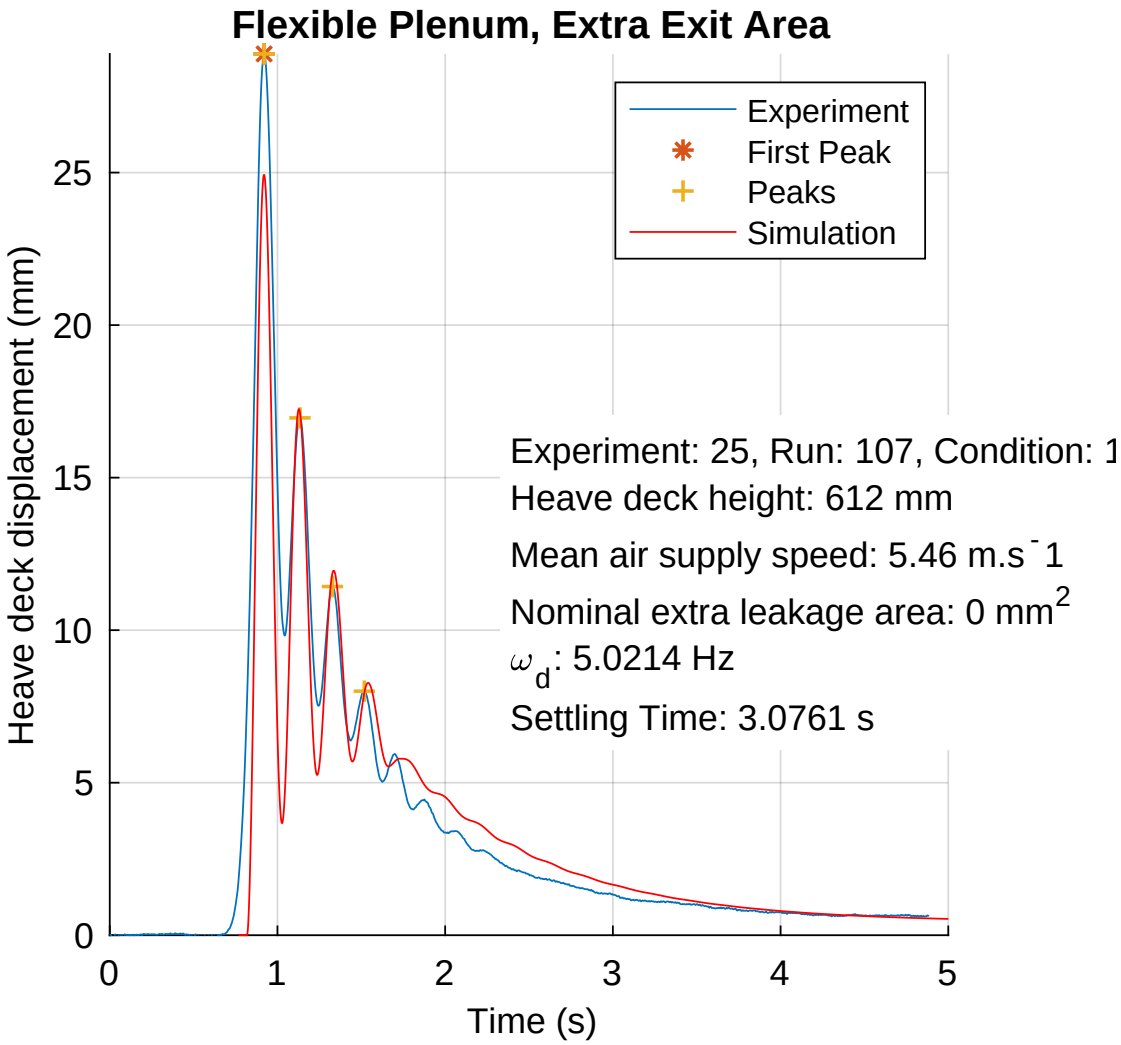


Figure F.13. Curve fitting for condition 13

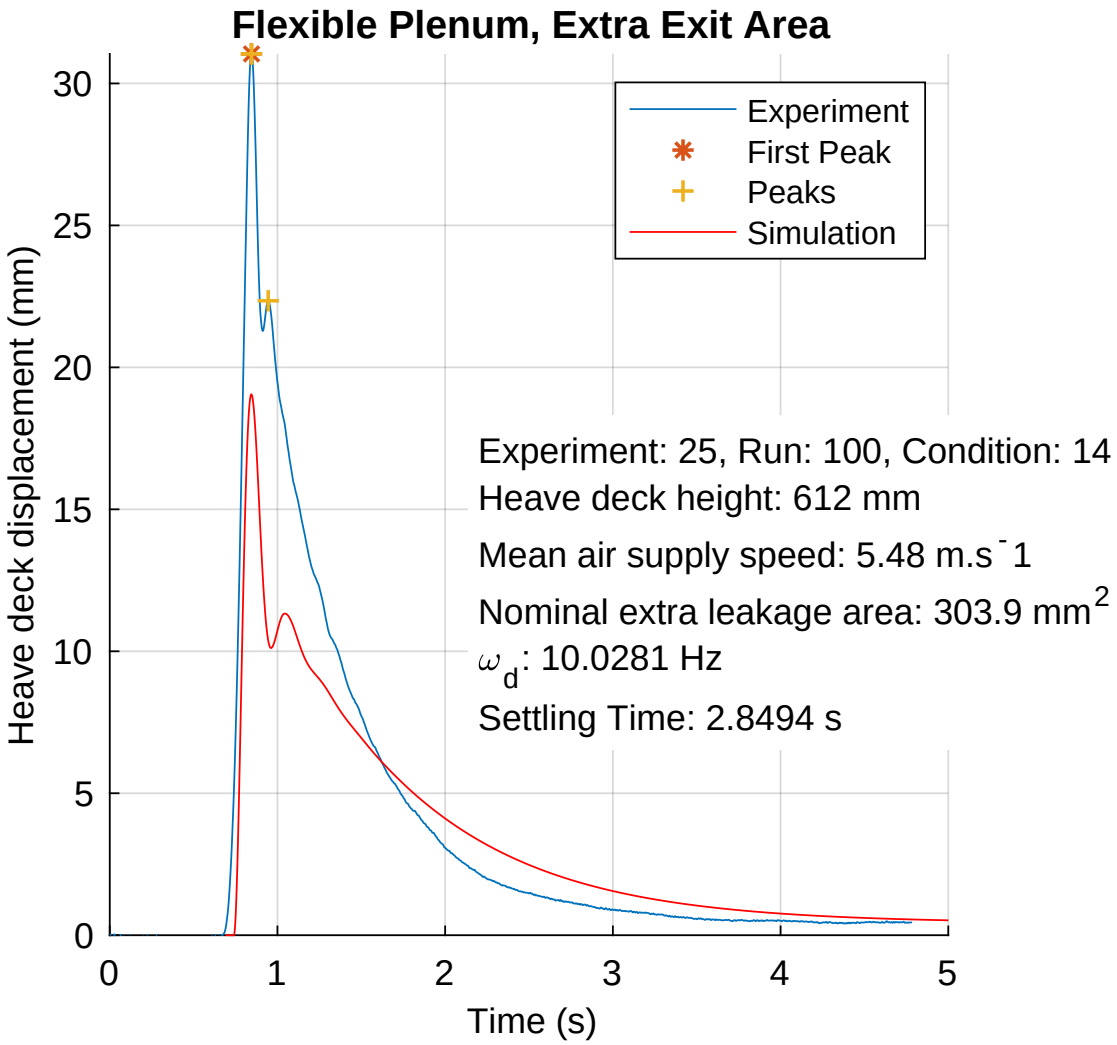


Figure F.14. Curve fitting for condition 14

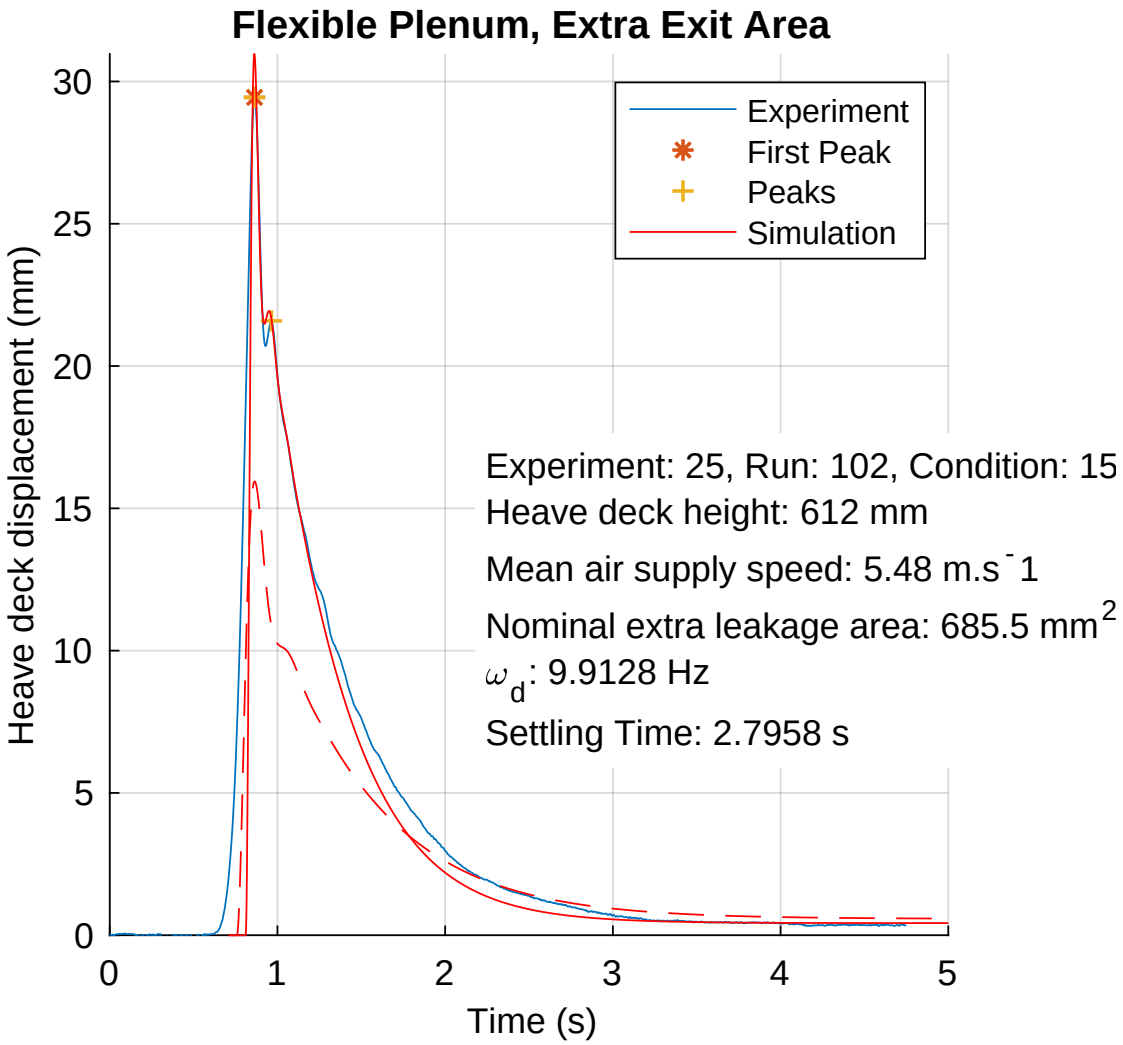


Figure F.15. Curve fitting for condition 15

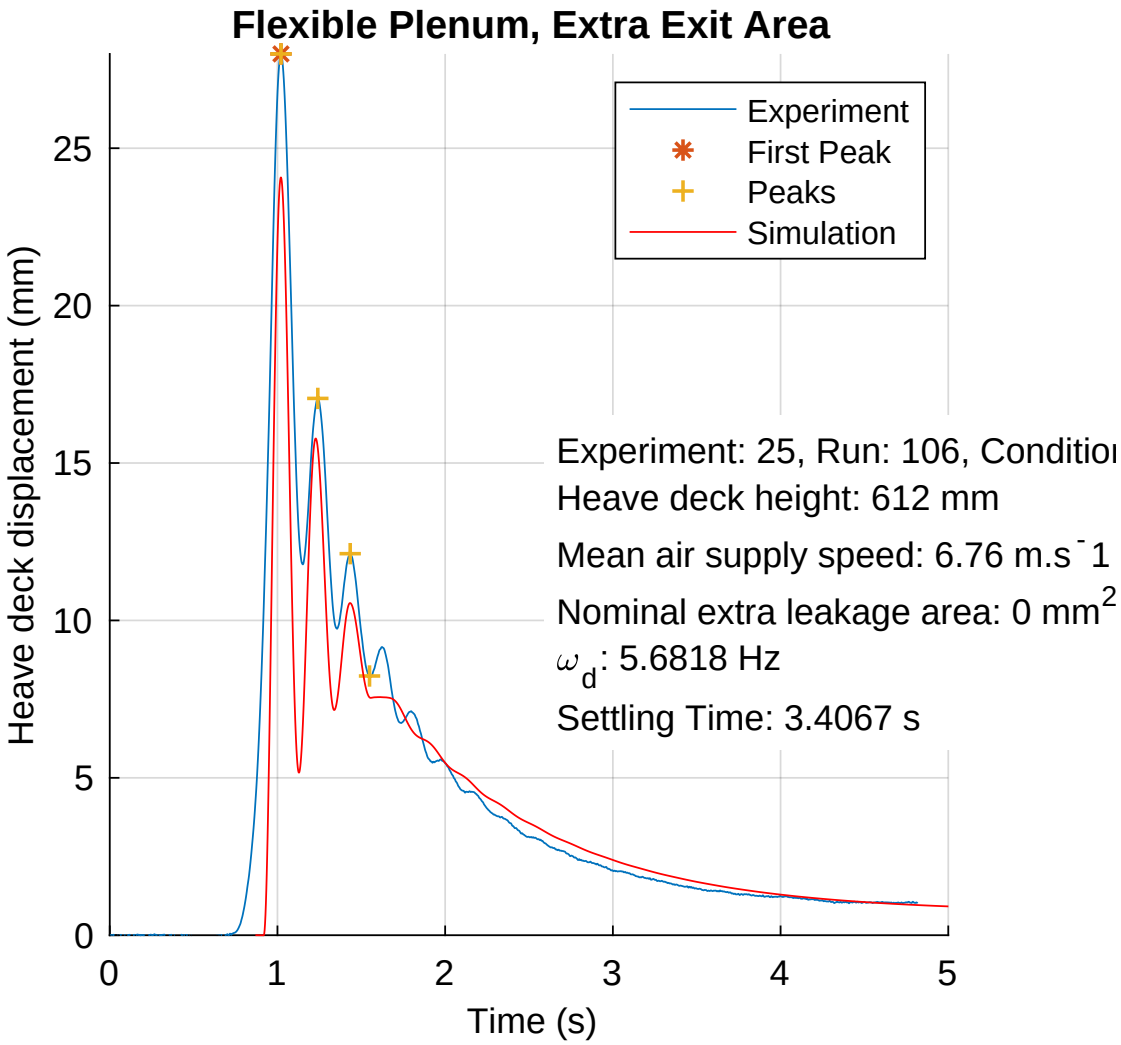


Figure F.16. Curve fitting for condition 16

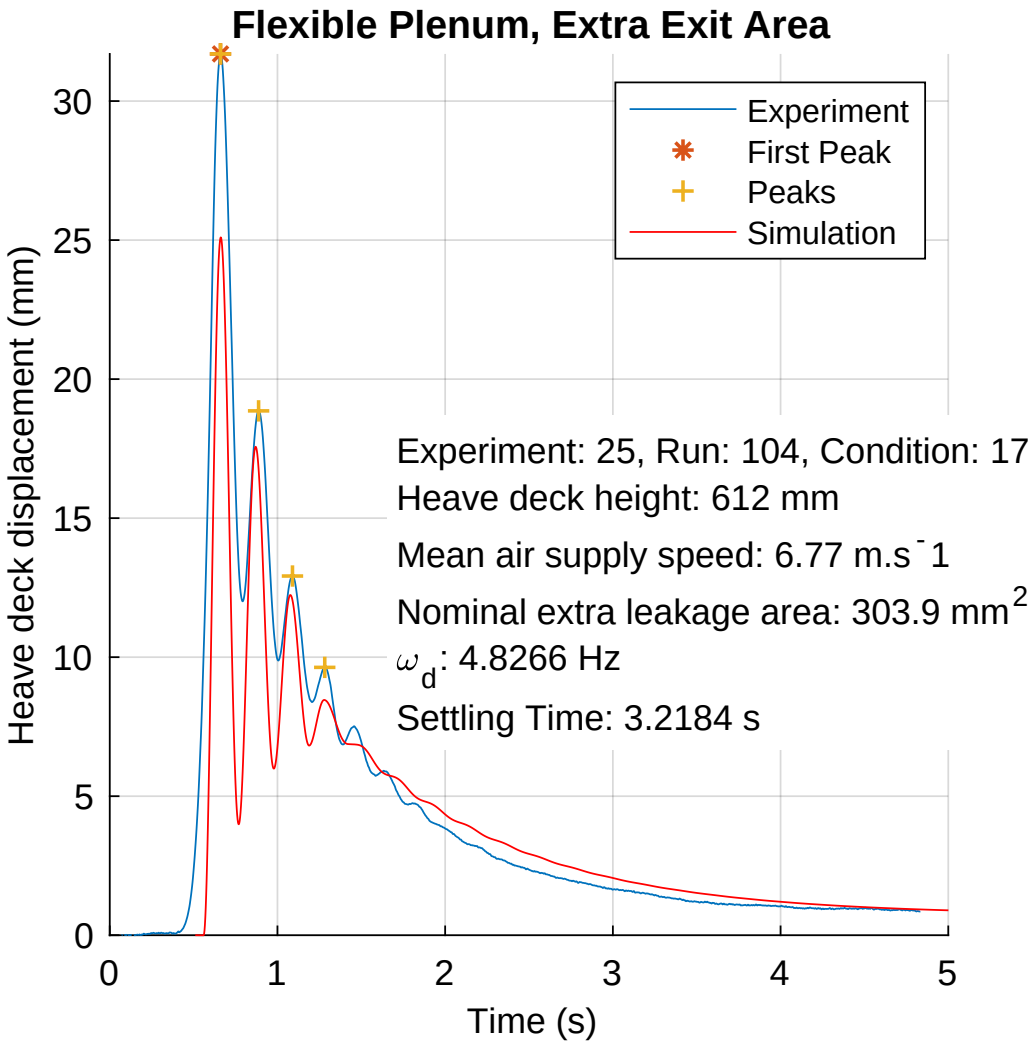


Figure F.17. Curve fitting for condition 17

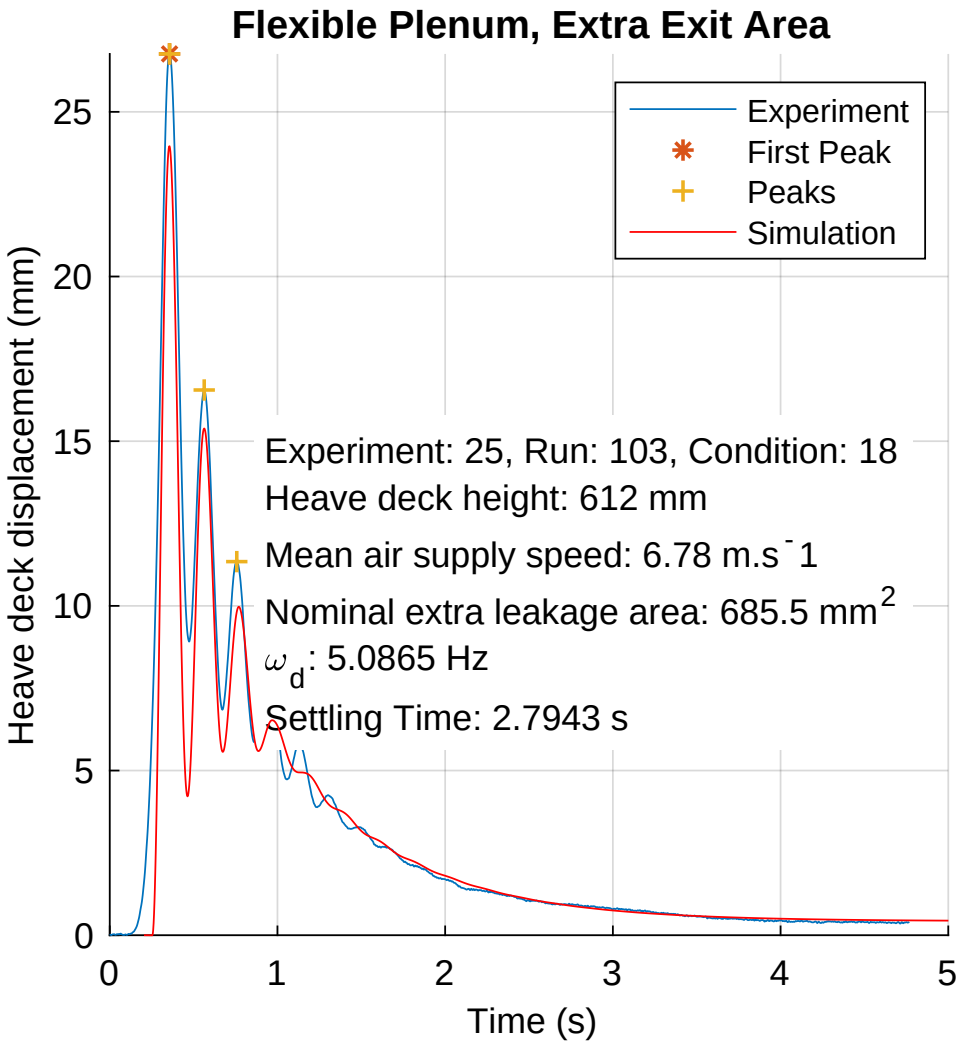


Figure F.18. Curve fitting for condition 18

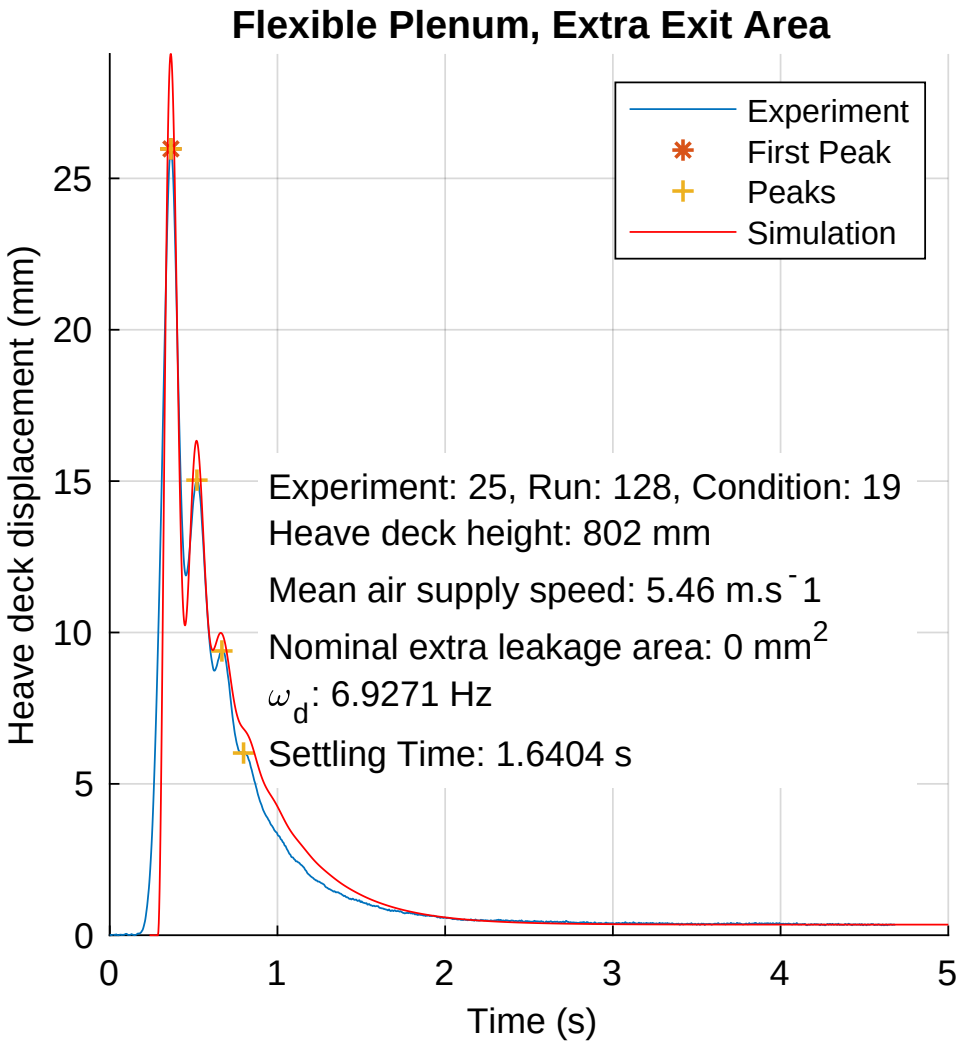


Figure F.19. Curve fitting for condition 19

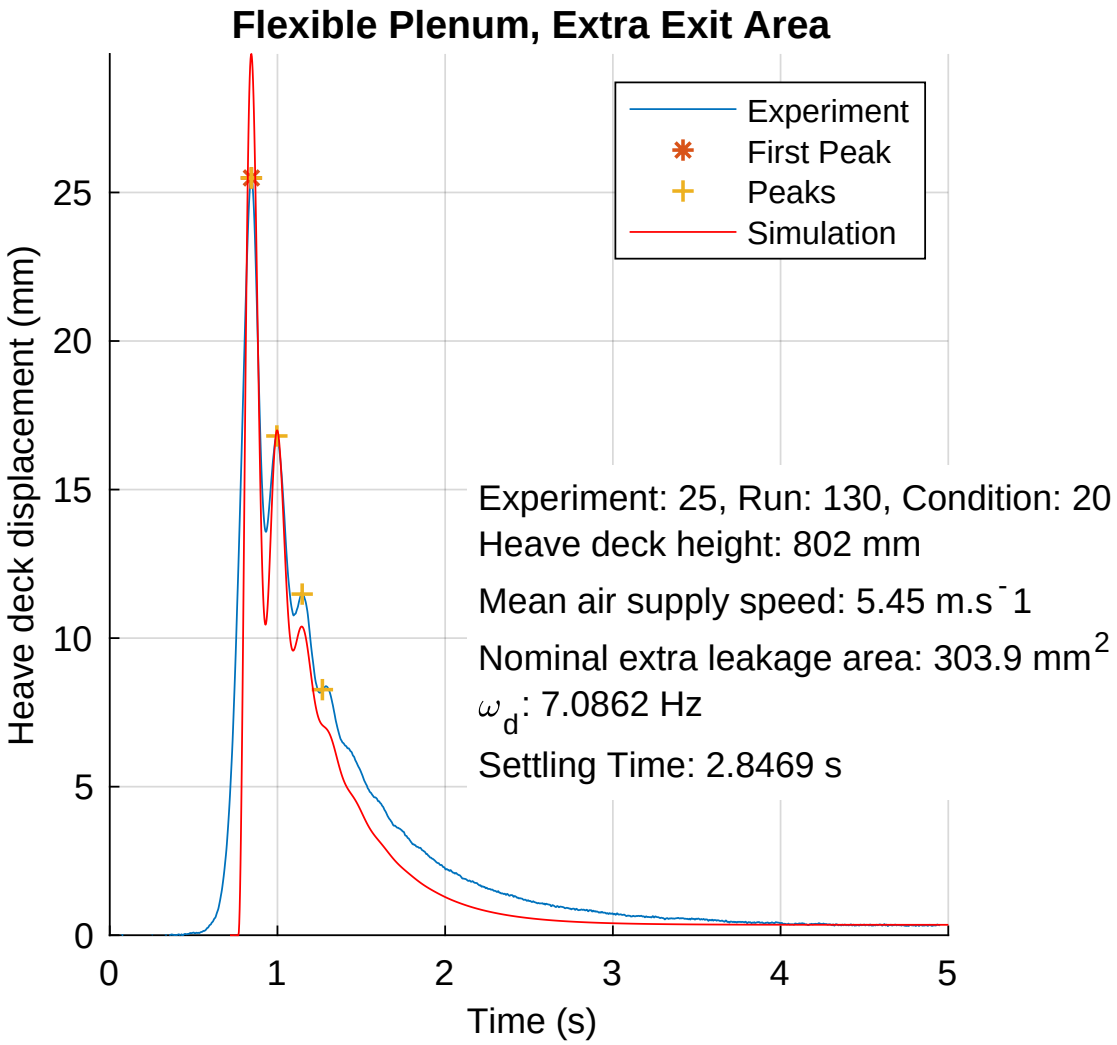


Figure F.20. Curve fitting for condition 20

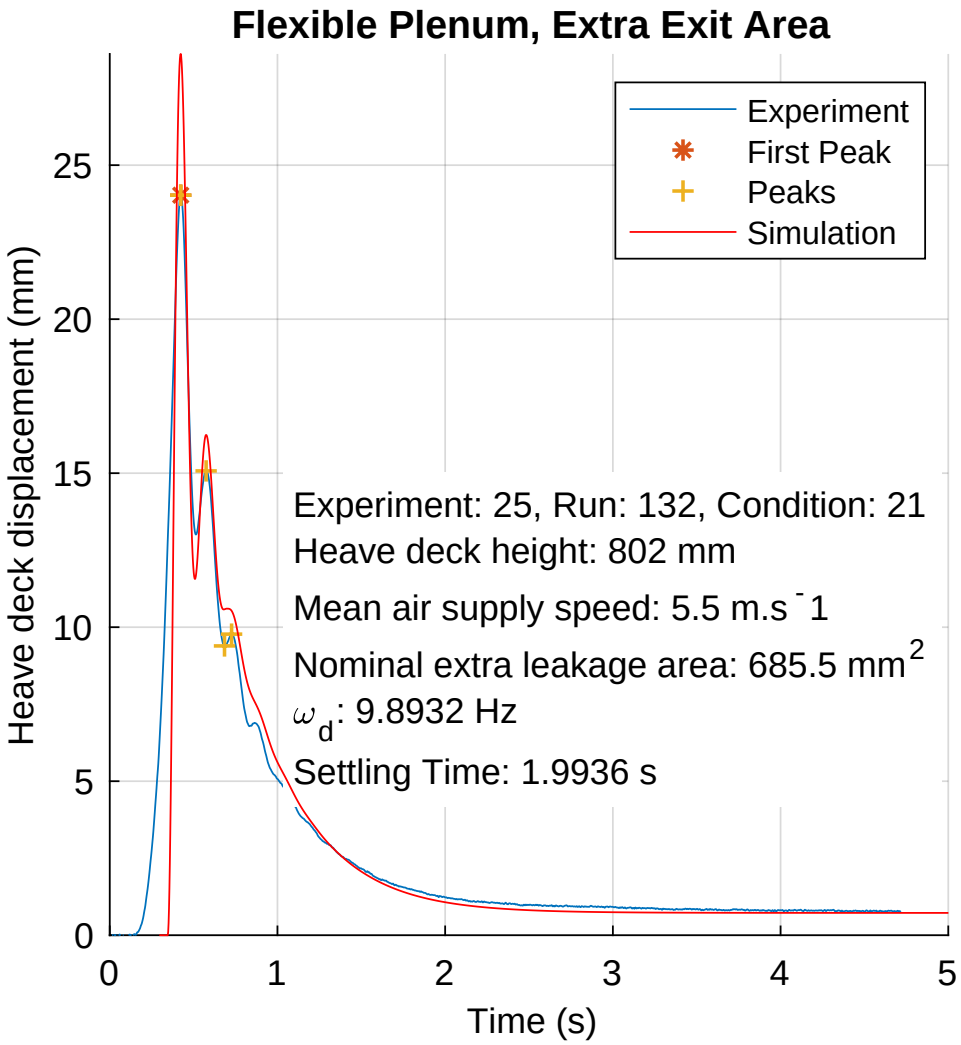


Figure F.21. Curve fitting for condition 21

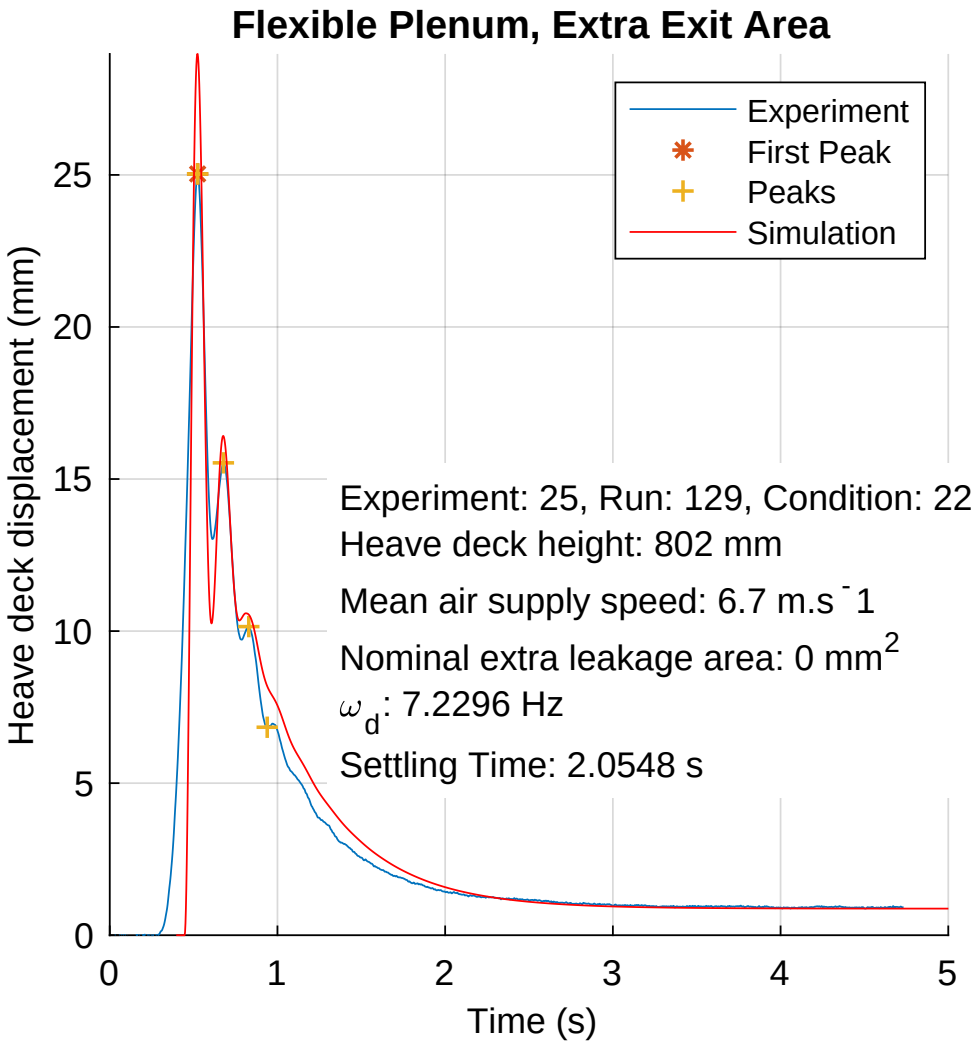


Figure F.22. Curve fitting for condition 22

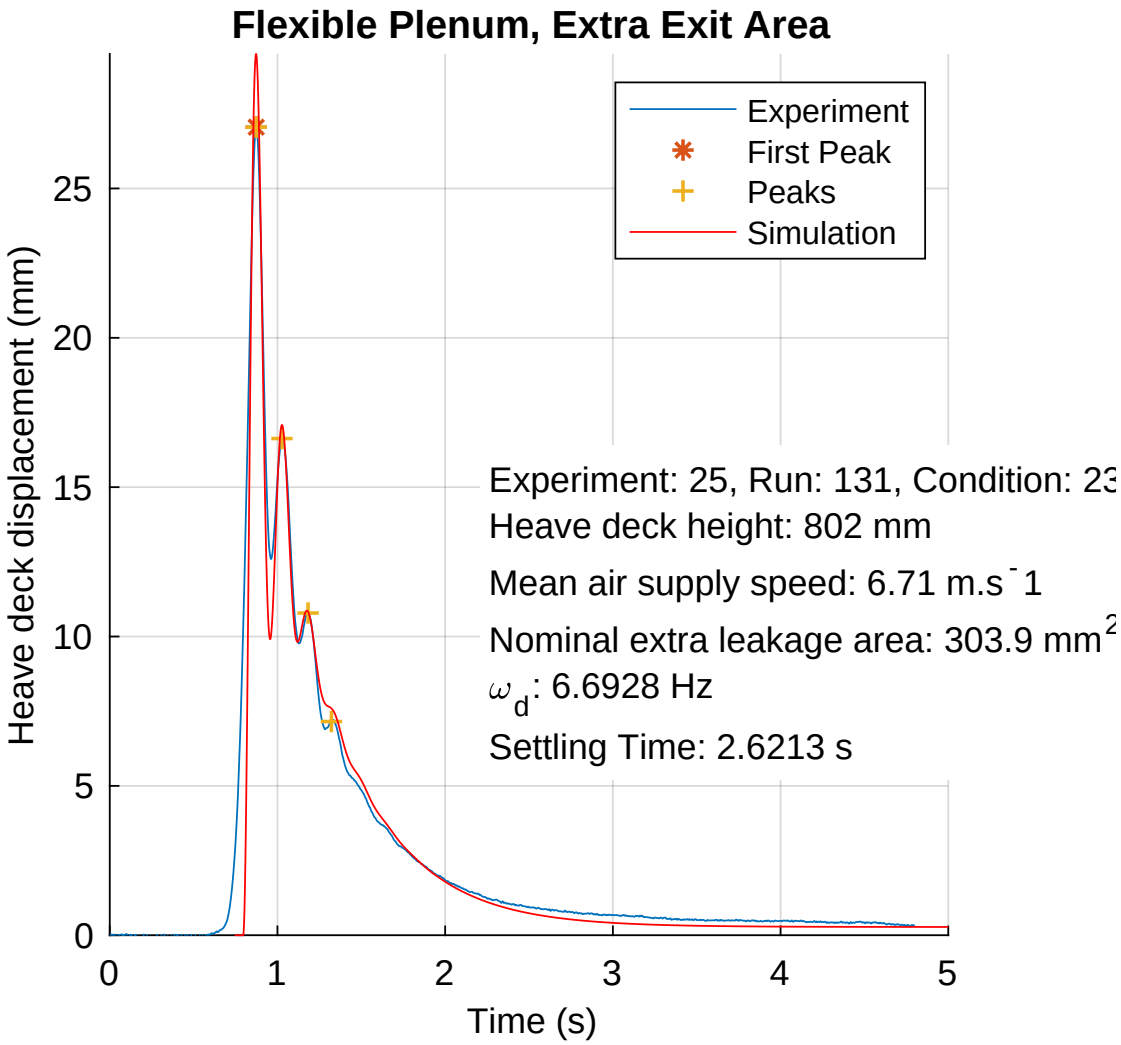


Figure F.23. Curve fitting for condition 23

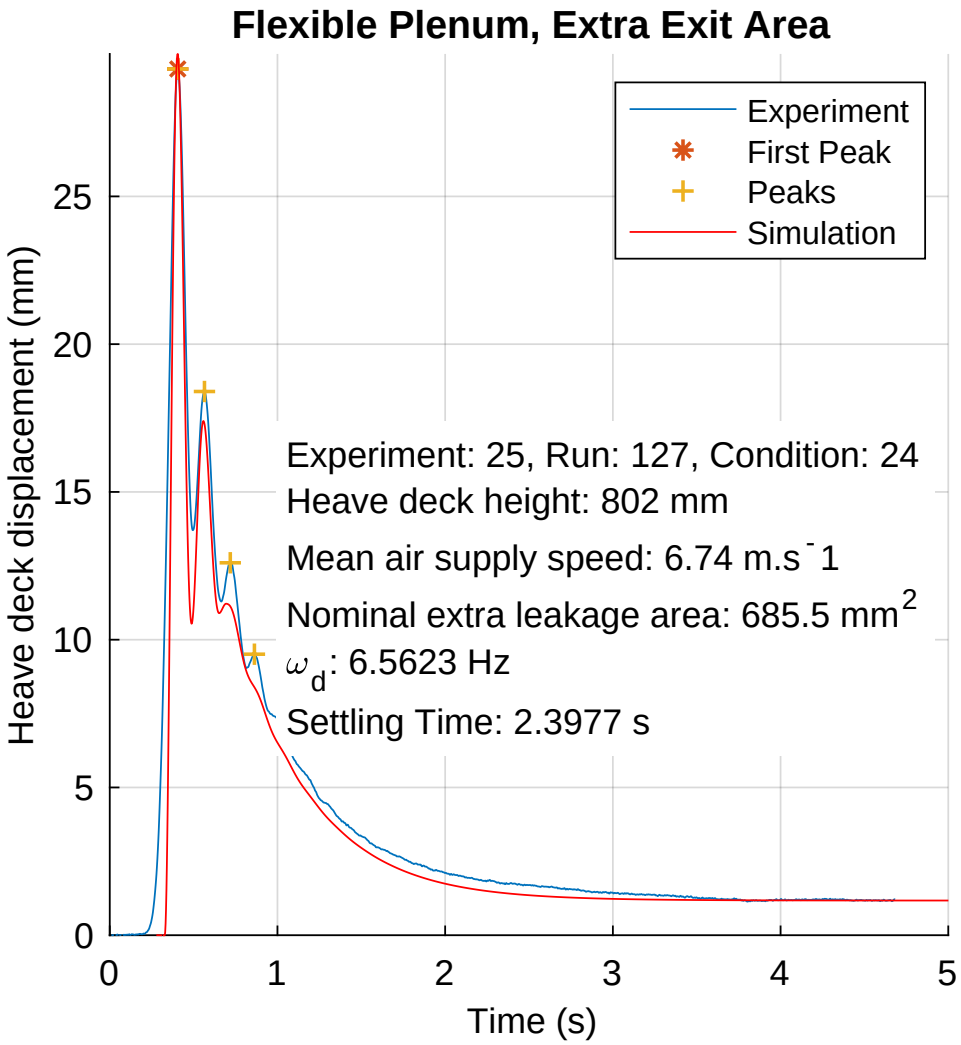


Figure F.24. Curve fitting for condition 24

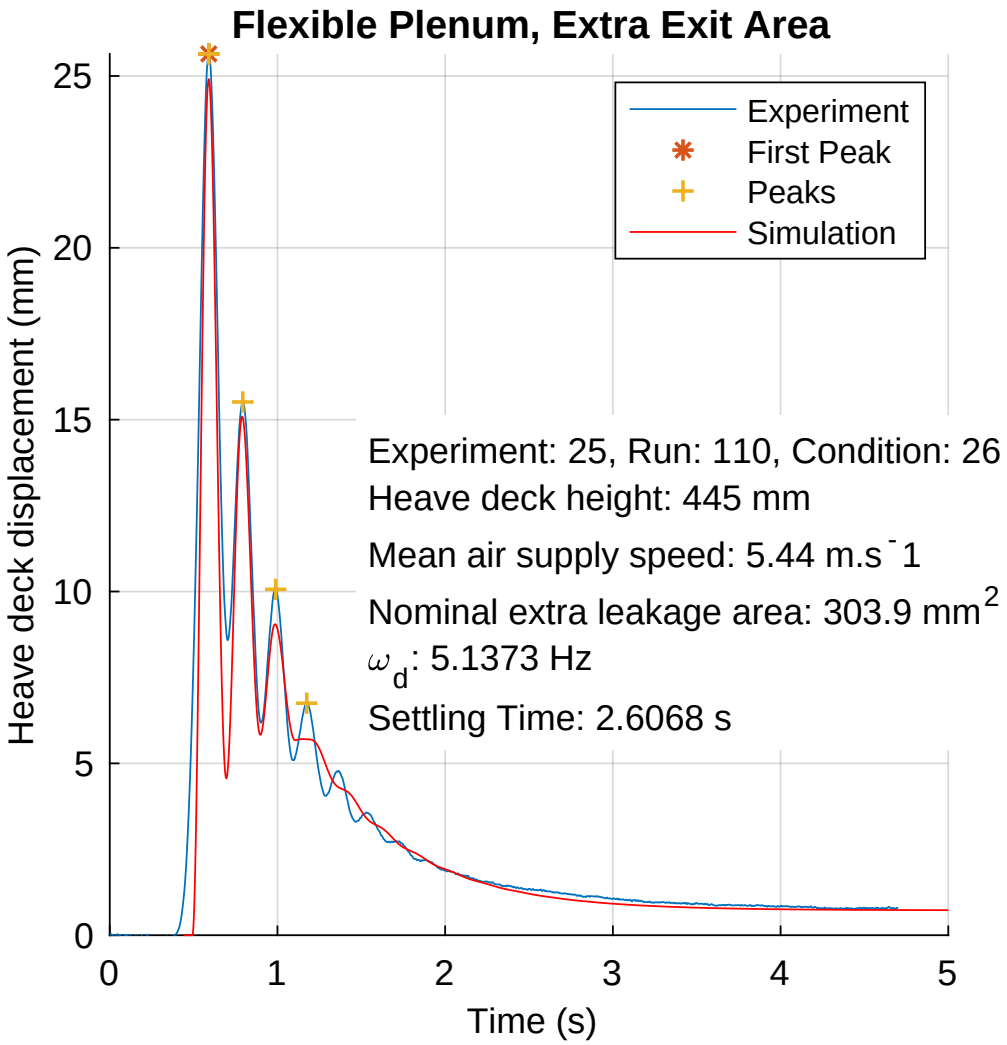


Figure F.25. Curve fitting for condition 26

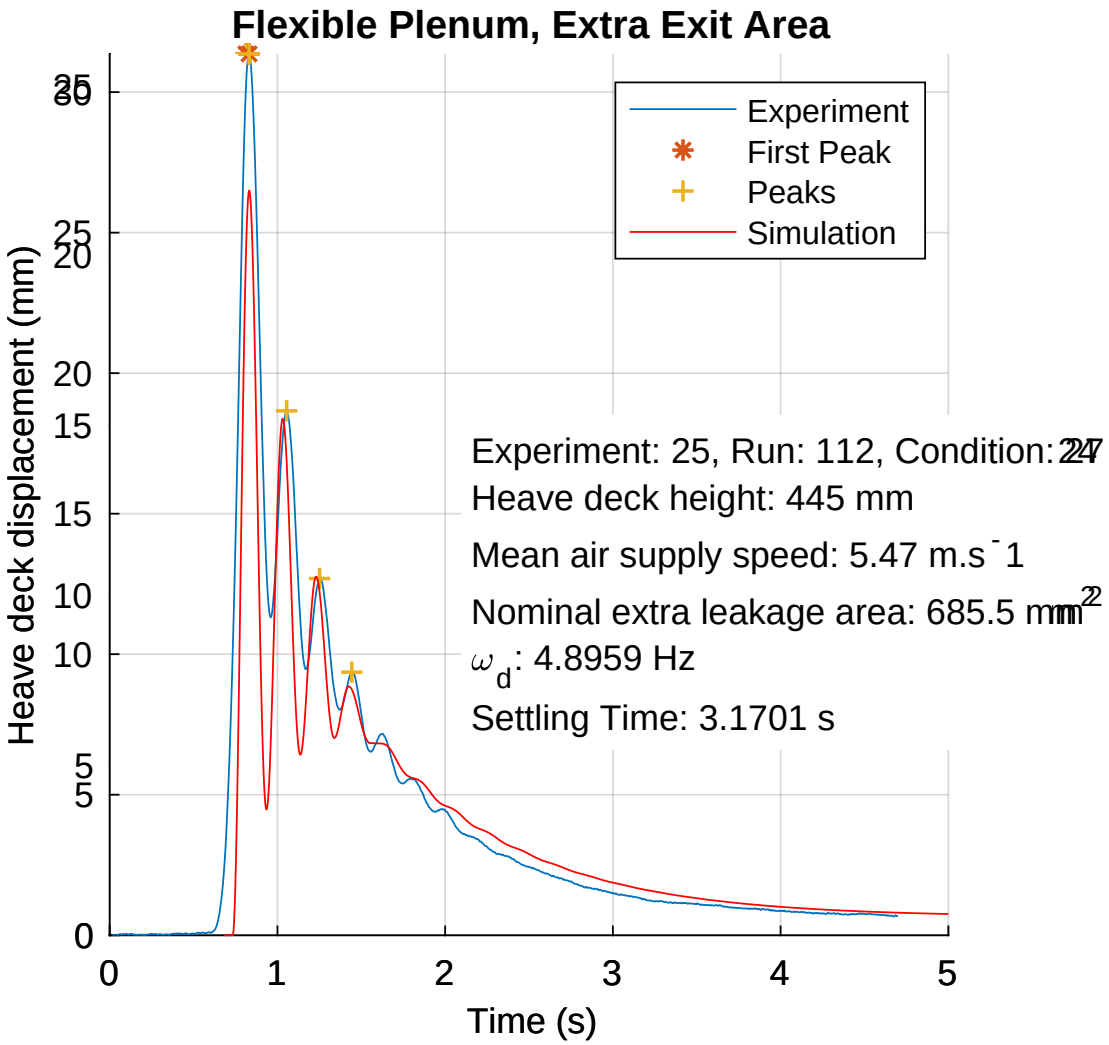


Figure F.26. Curve fitting for condition 27

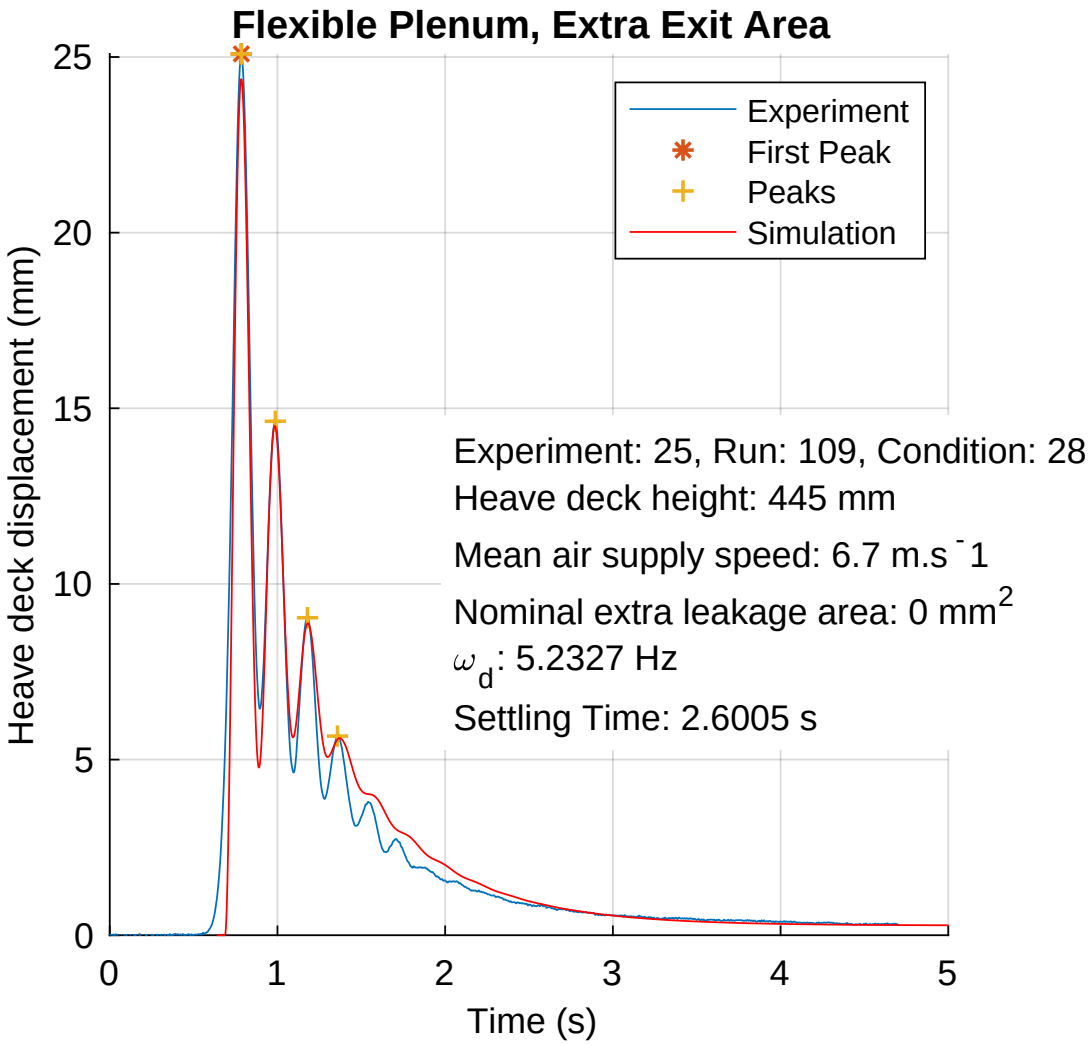


Figure F.27. Curve fitting for condition 28

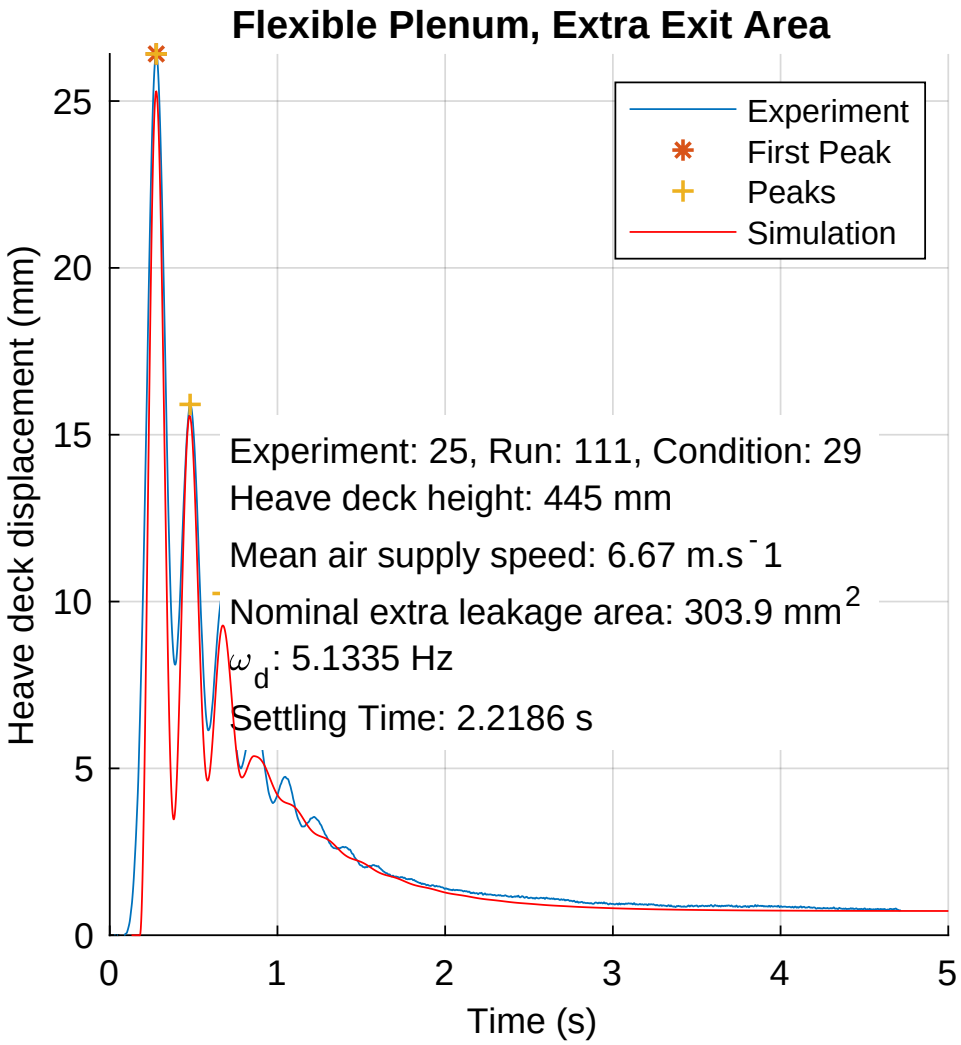


Figure F.28. Curve fitting for condition 29

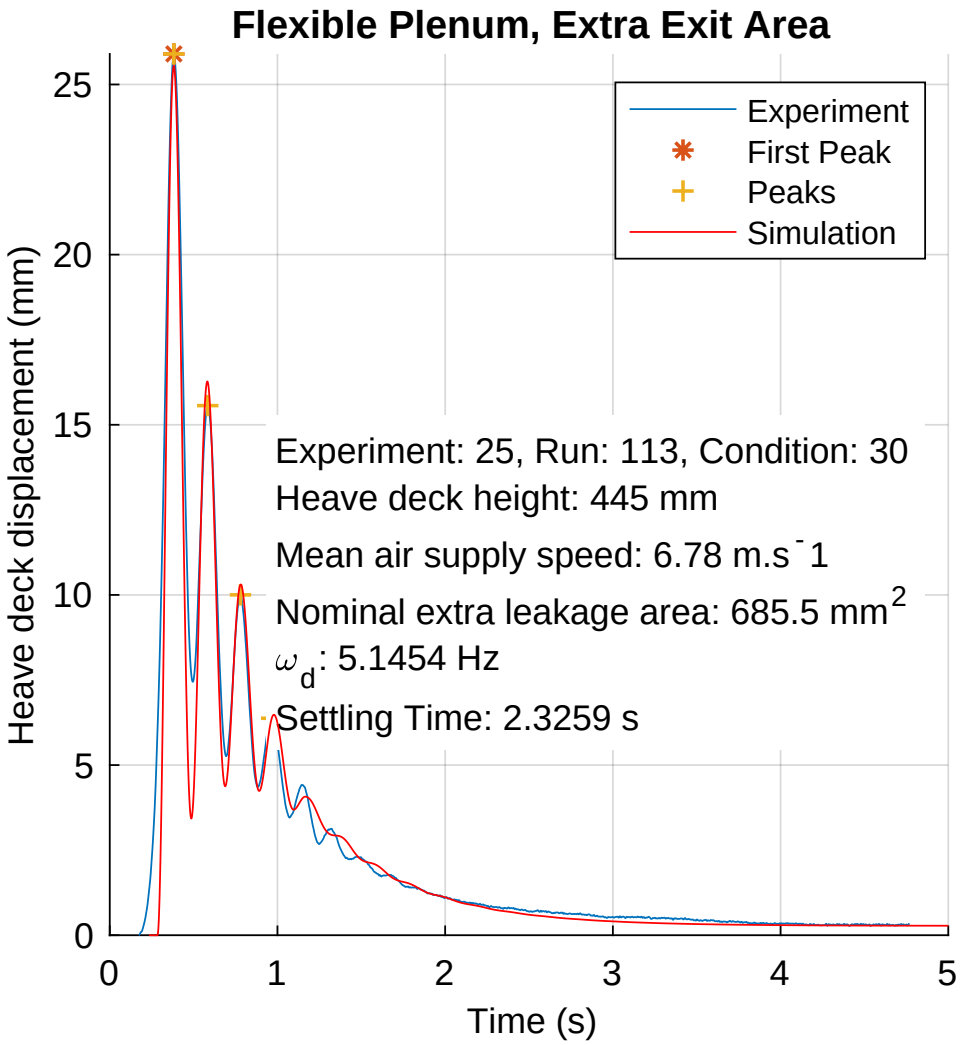


Figure F.29. Curve fitting for condition 30

G. The construction, testing and modelling of a concept rig

A Concept Rig was designed, constructed, tested and modelled by the author and B.W. Field. This Appendix was compiled from the laboratory workbooks of the author and B.W. Field.

G.1. Purpose

A small-scale Concept Rig was designed, built and tested to:

1. Explore technical construction details, such as flexible seals and limitations on the proposed instrumentation
2. Create sample data from a measured set of rig parameters and a transient input
3. Provide validation data for a simplified analytical tool using an alternative computational technique
4. Provide experimental and computational evidence of the sensitivity of some simplifying assumptions in the analytical tool

G.2. Construction images of the Concept Rig



Figure G.1. Starting cabinet (ex-bookcase), internal dimensions: 450 x 404 x 1180 mm



Figure G.2. Cabinet divided approximately 2:1 with a short vertical plate, and the input flap polythene seal installed in the smaller portion



Figure G.3. Input flap installed. Seal guides on the top of the flap.



Figure G.4. Heave deck installed. Air inlet duct in the end of the cabinet. Seal guides still to be installed

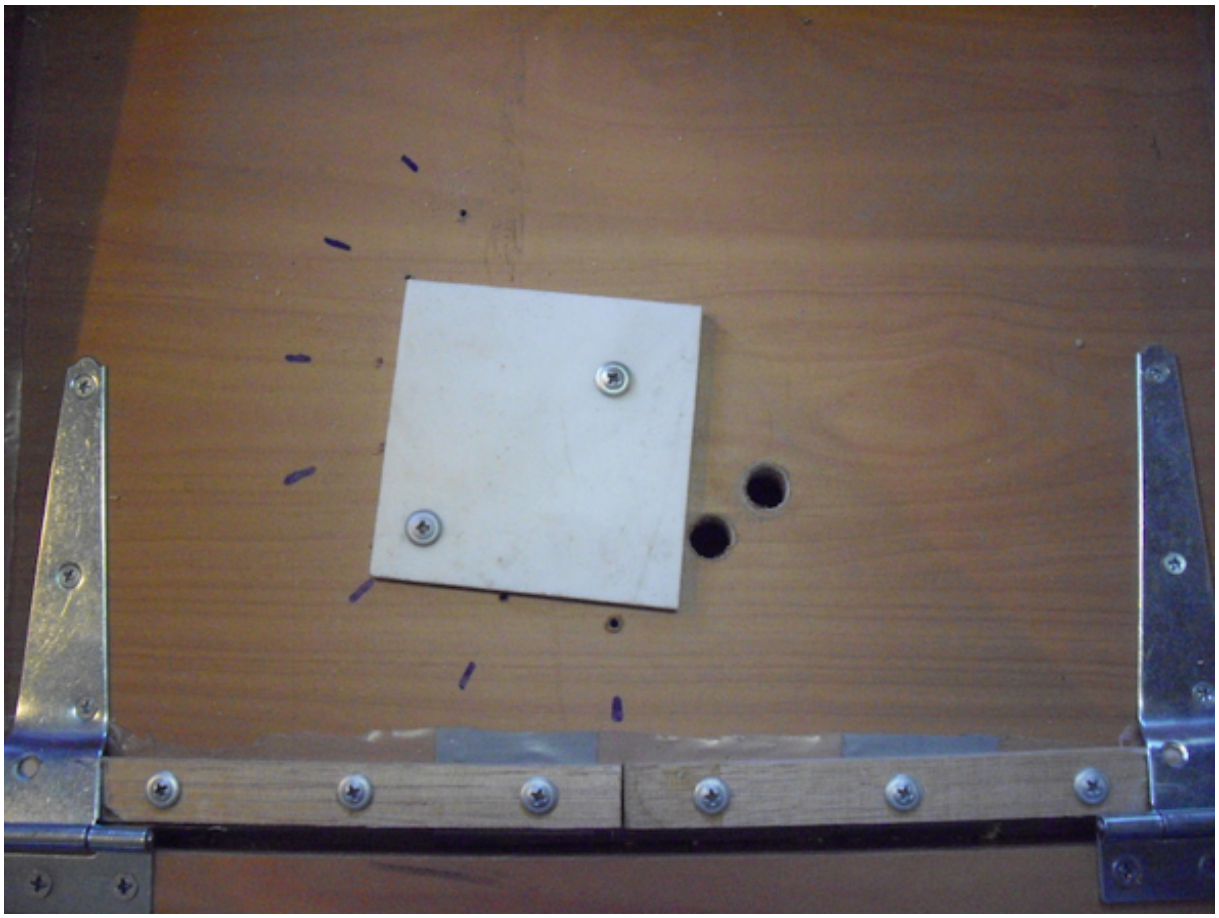


Figure G.5. Air leakage holes in input flap. The square plate can be rotated and re-locked to uncover up to six holes.



Figure G.6. Deck suspension spring, heave deck seal guides and limit stops installed.

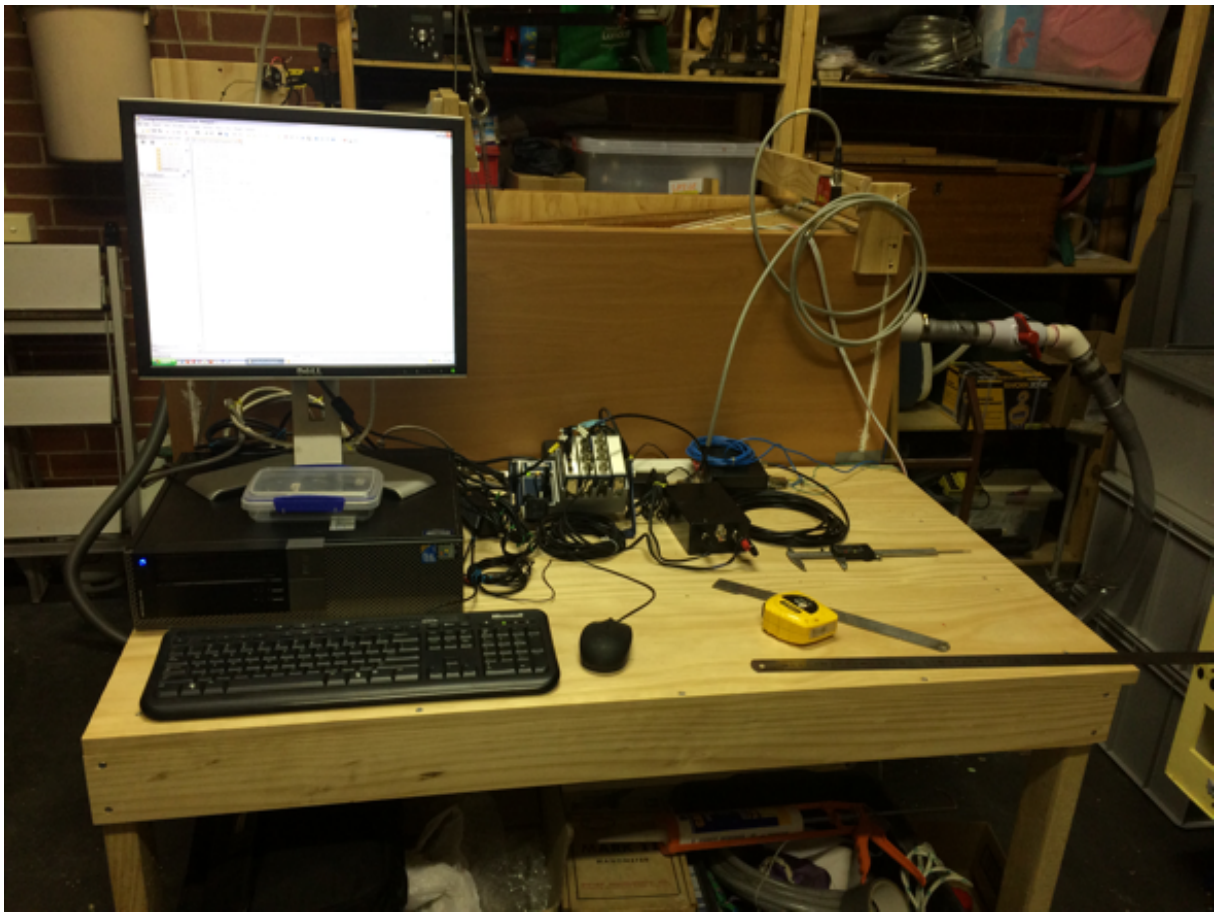


Figure G.7. Test instrumentation. Heave deck sensor at top right. The pivot point of the heave deck is at the far right. Inlet air control on right. Obscured by the PC screen is the input flapper.

G.3. Concept Rig geometric parameters used for modelling

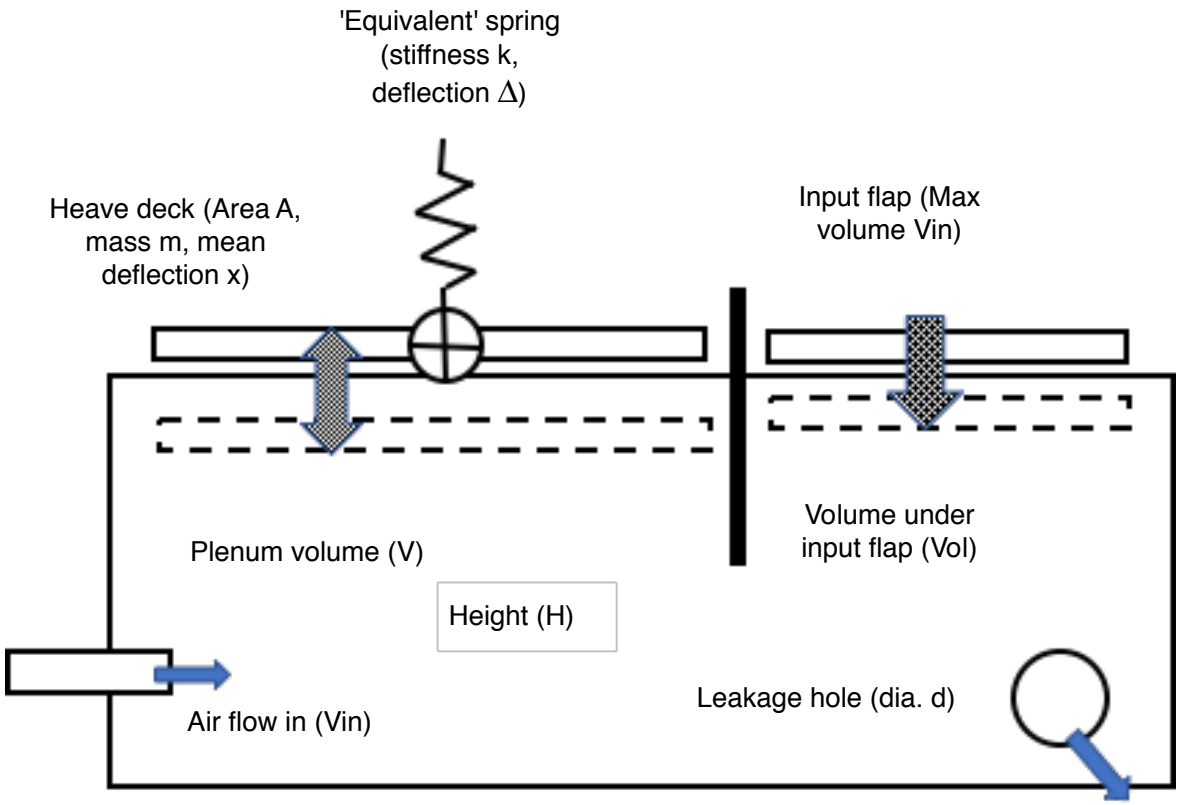


Figure G.8. Concept rig schematic showing geometric parameters used for modelling.

Fixed numerical values:

A $320 \times 10^{-3}\,\mathrm{m}^2$
m $12.0\,\mathrm{kg}$
k $1.340 \times 10^{3}\,\mathrm{N\,m}^{-1}$
V $67.2 \times 10^{-3}\,\mathrm{m}^3$
H $404 \times 10^{-3}\,\mathrm{m}$

Selectable parameters:

n 1 to 1.4 (poly-tropic index)
d $0\,\mathrm{m}$ to $100 \times 10^{-3}\,\mathrm{m}$ (range of leakage diameters)
δt $0\,\mathrm{s}$ to $100 \times 10^{-3}\,\mathrm{s}$ (time interval for numerical calculation)
$V_i(t)$ $0\,\mathrm{m}^3\,\mathrm{s}^{-1}$ to $500 \times 10^{-3}\,\mathrm{m}^3\,\mathrm{s}^{-1}$ (rate at which input flap closes)
V_{in} $0\,\mathrm{m}^3\,\mathrm{s}^{-1}$ to $200 \times 10^{-3}\,\mathrm{m}^3\,\mathrm{s}^{-1}$ (volumetric flow rate from fan)
C_f 300×10^{-3} to 1.0 (discharge coefficient for outlet hole)
C_d 500×10^{-3} to 1.0 (drag coefficient of heave deck)
δs $0\,\mathrm{m}$ to $100 \times 10^{-3}\,\mathrm{m}$ (initial extension of spring)
Friction $0\,\mathrm{N}$ to $50\,\mathrm{N}$ (coulomb friction in the heave deck hinge and seal)
ExtraV $0\,\mathrm{m}$ to $1.000 \times 10^{3}\,\mathrm{m}$ (length of a tube (dia d) representing exit volume

Stiffness 0 to 18 % factor/plenum gauge pressure (p) (increasing H)

Other data:

P_{atm} $101.325 \times 10^3\,\mathrm{N\,m^{-3}}$ (atmospheric pressure)
ρ $1.225\,\mathrm{N\,m^{-3}}$ (air density)

Calculated parameters:

a $\mathrm{m\,s^2}$ (upward acceleration of heave deck)
v_d $\mathrm{m\,s}$ (upward velocity of heave deck)
p Pa (absolute pressure in plenum)
p_{init} Pa (absolute pressure in plenum before inlet flap moves
t s (time since input flap began to move)

Output parameter

x m (upward deflection at centre of heave deck)

G.4. Basis of analysis:

From the dynamics of the heave deck, modelled as a linearly accelerating mass:

1. Net upward vertical force = ma, therefore:
2. Acceleration = (pressure force + spring force – weight - seal friction - air drag) / mass (assuming linear motion), i.e: $a = \frac{(pA+k(s-x)-mx0.981\pm(\mathrm{Friction}+C_dAv_{d2}))}{m}$ (sign of fiction term dependent on direction of motion)
3. Flow out through holes = $V_{out} = 0.785d_2\sqrt{2(p-p_{atm})}$
4. Internal pressure = initial pressure x (initial volume/current volume) ˆn, i.e., $p(t_i) = p_{init}\left(\frac{AH+V+V_{in}-V_{out}+0.785d_2\mathrm{ExtraV}}{(A(H+x)+V(V_{it}t)}\right)^n$ ...
5. v_d = previous velocity + at (assumes constant acceleration in the time interval)
6. x = previous$x + v_dt + 0.5at^2$ (assumes constant acceleration in the time interval)

G.4.1. Approach to numerical solution using Excel spreadsheet

1. Set time (t) to current time (initially zero) $+\delta t$
2. Calculate reduction in volume due to input flap from $V–V_i(t)t$
3. Calculate x from equation 6 (a and v_d initially set to zero)
4. Calculate v_d from equation 5 (a initially set to zero)
5. Calculate pressure in plenum from equations 3 and 4
6. Calculate acceleration of heave deck from equation 2.
7. Cycle back to (1) and repeat for the required number of time intervals.
8. Plot x vs t to see oscillations and decay.

G.5. Result of sample run with Concept Rig

Data:

- Six 12.5 mm holes (equivalent area to one at 31 mm dia).
- Air speed 11 $\mathrm{m\,s^{-1}}$ (approx. $21 \times 10^{-3}\,\mathrm{m^3\,s^{-1}}$ through 50 mm duct).
- Height sensor 94.5 mm from hinge: deck centre is 400 mm from hinge (4.2 times further).

Outcome:

- Peak reached: = 4.76 mm above hover (19.9 mm at centre).
- Two clear peaks.
- Period of oscillation: 160×10^{-3} s.
- Decay to 6 mm at centre in 3.5 s.

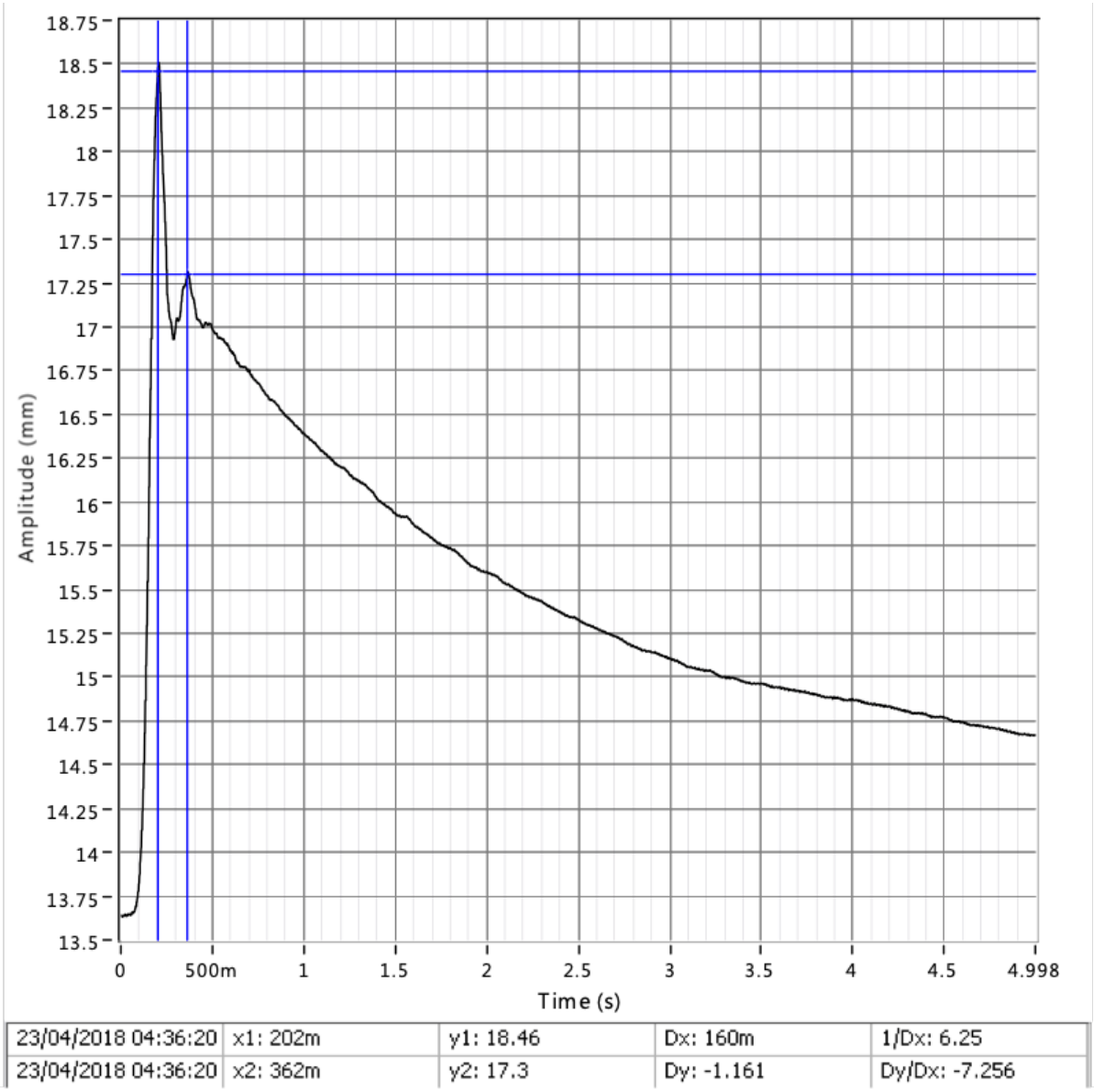


Figure G.9. Concept rig heave deck amplitude plot from sample run. The data is direct readings from the sensor. The initial heave deck zero position is at $\approx 13.6\,\text{mm}$.

G.6. Predicted vibration period for an idealised mass / spring oscillator

The heave deck can be simplified to a mass m (12 kg) supported on an air spring of stiffness k_{air}. The vibration period would then be: period (sec) $= 2\pi\sqrt{m/k_{air}}$.

The stiffness of the air in the plenum can be found from calculating the deflection arising when a unit force is applied to the heave deck area ($320 \times 10^{-3}\,\mathrm{m}^2$), thereby increasing the pressure according to standard gas laws.

- Volume of plenum $V_1 = 198 \times 10^{-3}\,\mathrm{m}^3$
- Atmospheric pressure $= 101.325 \times 10^3\,\mathrm{Pa}$
- Initial pressure with deck floating $p_1 = 101325 + 12 \times {}^{9.8}/_{0.32} = 101.6925 \times 10^3\,\mathrm{Pa}$
- Pressure p_2 with 1 N added to the deck $= 101692.5 + {}^{1}/_{0.32} = 101.695\,625 \times 10^3\,\mathrm{Pa}$
- $V_2 = V_1 {}^{p_1}/_{p_2}$ (Gas law) $= 0.198 \times ({}^{101692.5}/_{101695.625}) = 197.9939 \times 10^{-3}\,\mathrm{m}^3$
- Deflection $x = {}^{(V1-V2)}/_{\text{area}} = {}^{(0.198-0.1979939)}/_{0.32} = 19.0625 \times 10^{-6}\,\mathrm{m}$
- Since this deflection arose from 1 N, $k_{air} = {}^{1}/_{x} = 52.460 \times 10^3\,\mathrm{N\,m^{-1}}$
- Predicted period $= 2\pi\sqrt{{}^{12}/_{52460}} = 95 \times 10^{-3}\,\mathrm{s}$
- This is considerably shorter than the experimentally determined period of $160 \times 10^{-3}\,\mathrm{s}$

G.7. Results of Excel simulations of sample run

G.7.1. Simulation one: data as for sample run

This run shows several important features:

- The deck continues to rise even when the initial spring setting is zero.
- There are multiple oscillations.
- The period of the oscillations is approximately 0.096 sec (the same as that predicted for a linear mass-spring oscillator with no through-air flow).

It is apparent that either the estimate of air flow is too high, or there is additional leakage, other than from the formed holes. The input air flow was estimated from the anemometer reading at the centre of the inlet duct, the known diameter of the duct (50 mm), and an assumed flow profile across the duct. It is recommended that a better means of determining air flow be found (although this factor is not, in itself, important in the model).

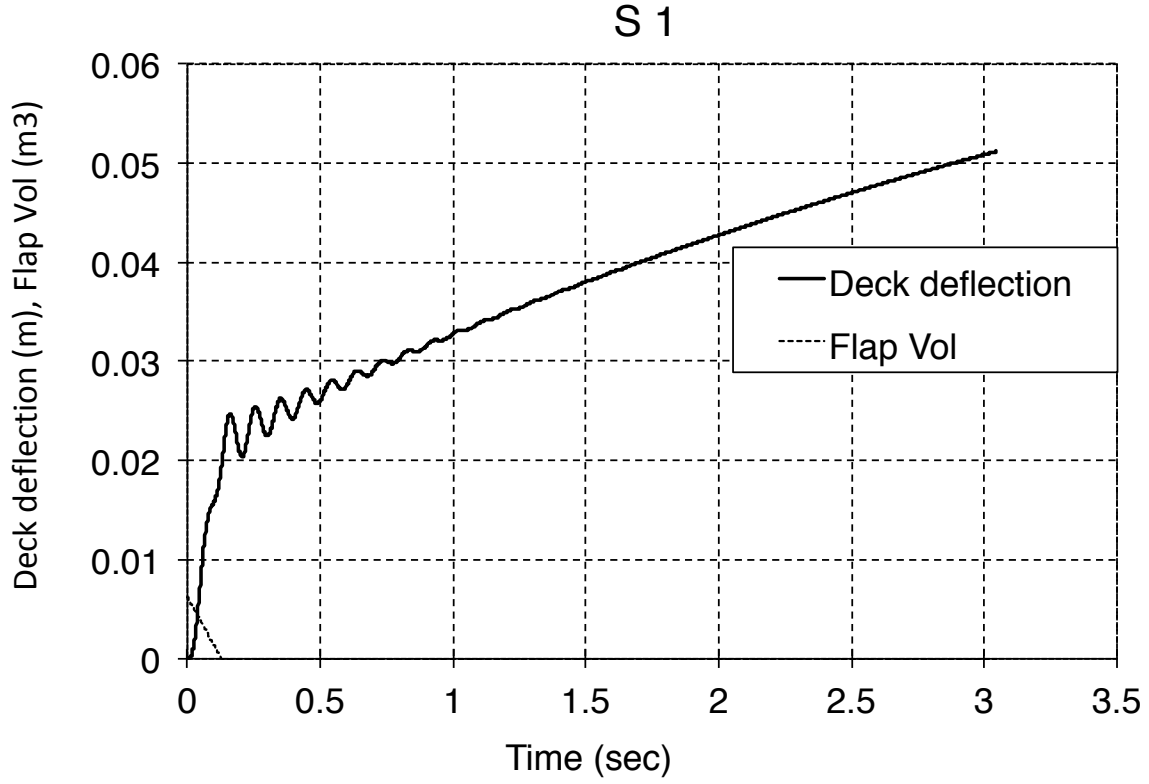


Figure G.10. Concept rig trial simulation one sample run showing an accumulating error.

G.7.2. Simulation two: larger exit hole diameter (44 mm)

This prediction shows the following features:

- The deck rises to the measured height, and decays slightly more rapidly than the experimental result.
- There are two oscillation peaks, as with the experiment.
- The period of the oscillations is 0.092 sec, slightly less than with Simulation 1.

The larger outflow area has had the effect of both allowing the deck to return to hover near to the predicted rate, and to dampen the oscillations.

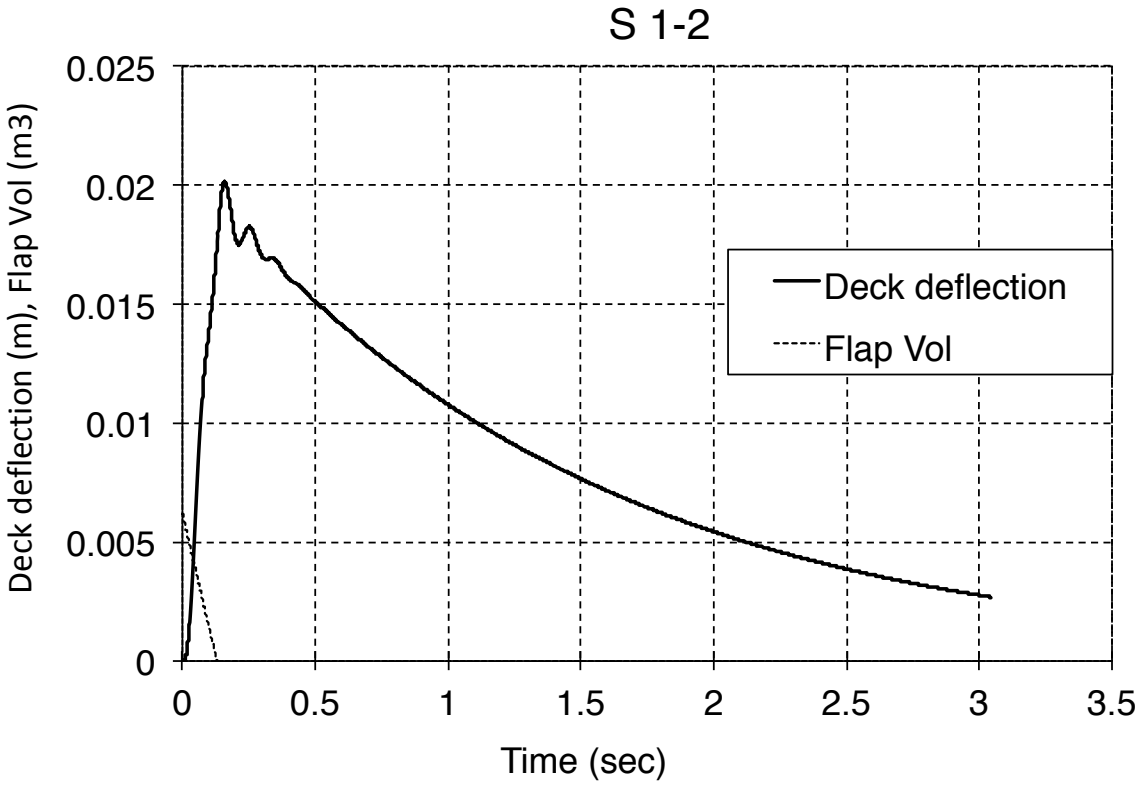


Figure G.11. Concept rig simulation two sample run (larger leakage area).

G.7.3. Simulation three: reduced air flow ($0.01 \mathrm{m}^3\,\mathrm{s}^{-1}$)

This prediction shows the following features:

- The deck rises to the measured height, and decays slightly more rapidly than the experimental result.
- There are multiple oscillation peaks, unlike the experiment.
- The period of the oscillations is 95×10^{-3} s, slightly less than with Simulation 1.

The reduced air flow (approximately 50% of the experimentally measured flow) leads to a good prediction of the heave deck return to hover, but does not create a similar dampening of the oscillations.

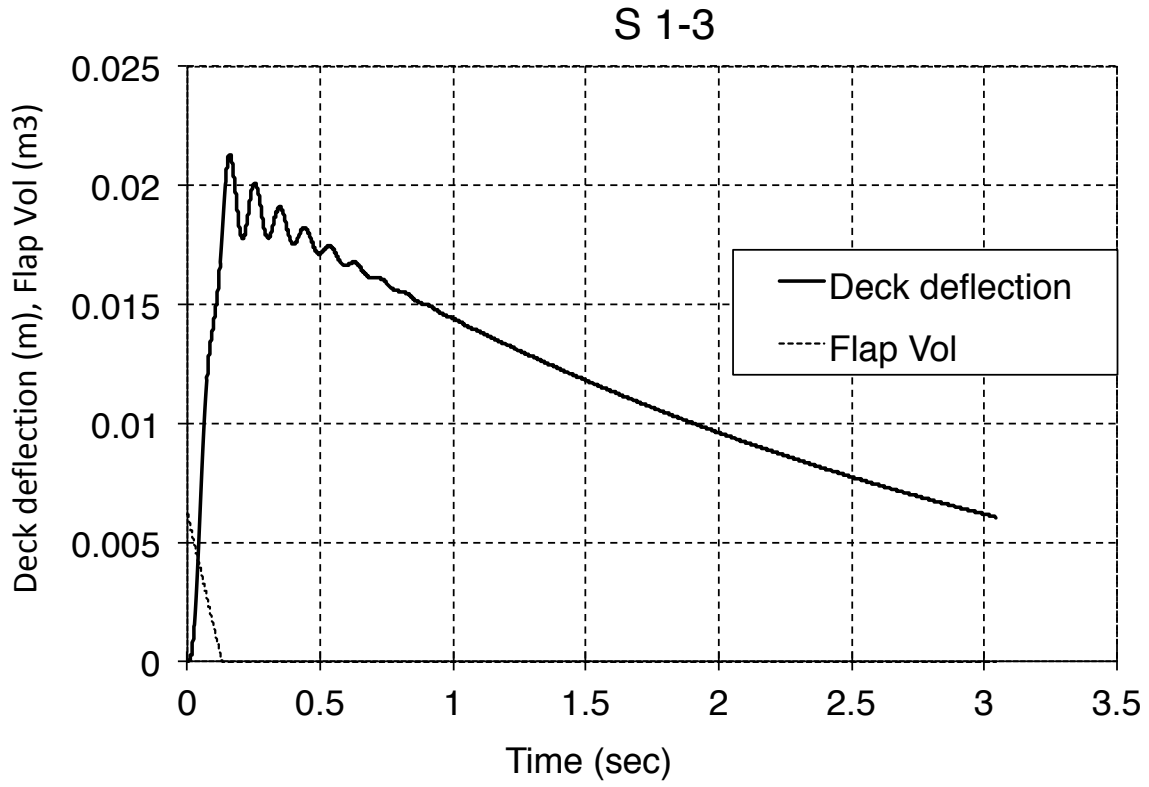


Figure G.12. Concept rig simulation three sample run, showing effects of larger leakage area.

G.7.4. Simulation four: add Coulomb Friction to 44 mm hole (10 N friction)

This run (Fig. G.13) shows the following features:

- The deck rises to the measured height, and decays at about the same rate as the experimental result, to hover at 5 mm above the starting position.
- There are two oscillations, as with the experiment, with a similar difference in the peak magnitudes.
- The period of the oscillations is 85×10^{-3} s.

The coulomb friction has had the effect of dampening the oscillations (after the first) and slowed the return to hover. The magnitude of the friction is not unreasonable.

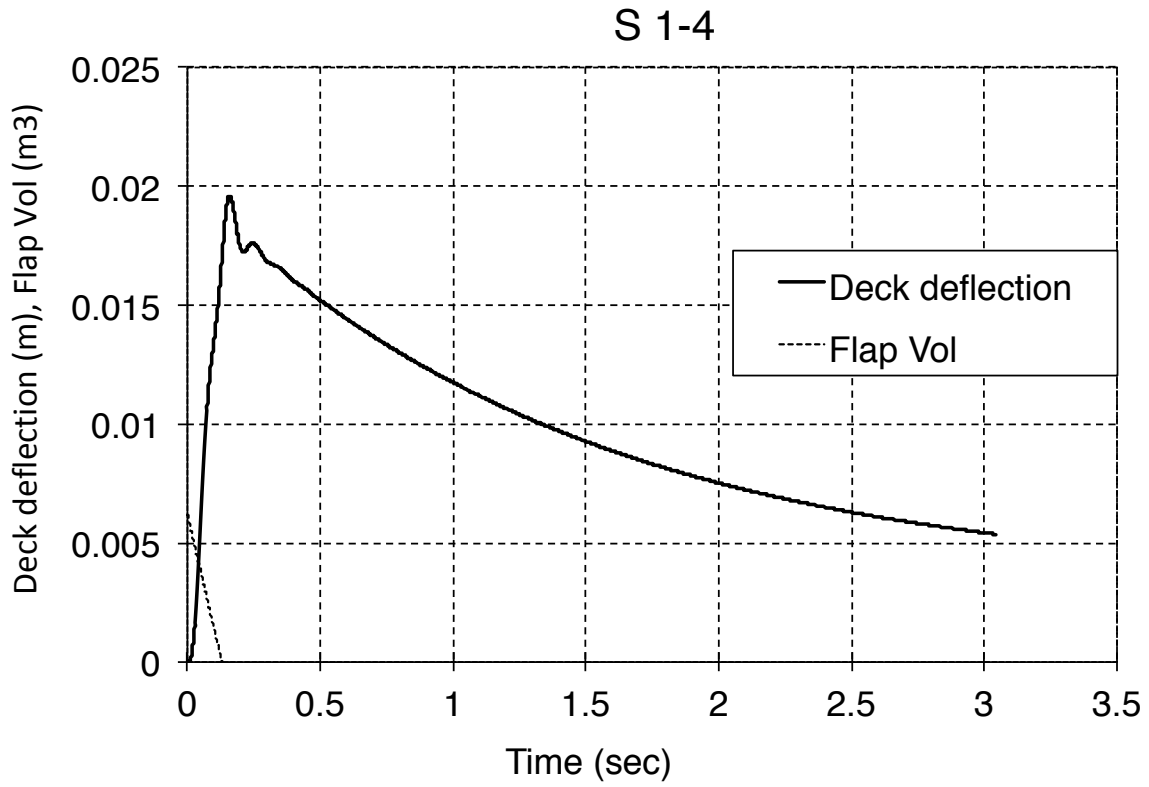


Figure G.13. Concept rig simulation four sample run, showing effects of ladded Coulomb friction.

An extended recording on the Concept Rig heave deck's amplitude showed that after the input flap had been closed and the heave deck had settled back to a hover (some 10 s after the transient input), the heave deck was 4.2 mm higher (Fig. G.14). This indicates that the adjusted coulomb friction of 10 N was realistic.

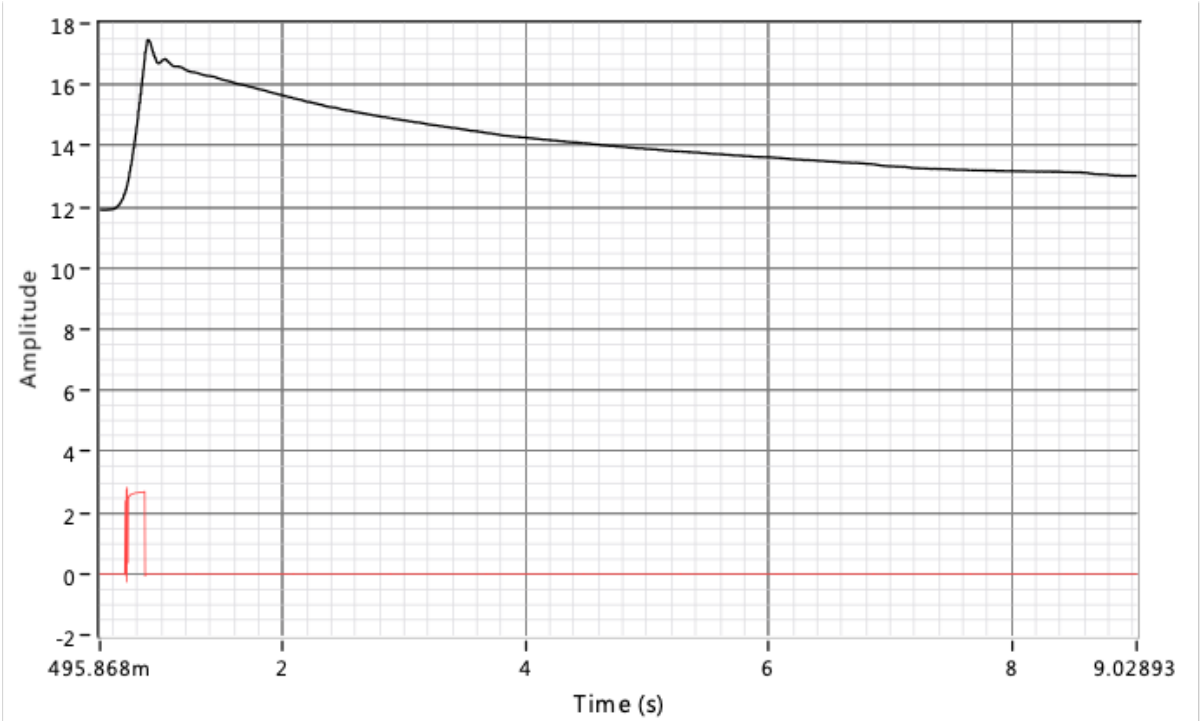


Figure G.14. Concept rig extended-time sample run to identify final heave deck height at sensor.

G.7.5. Simulation five: add extended outlet volume represented by a 300 m long tube

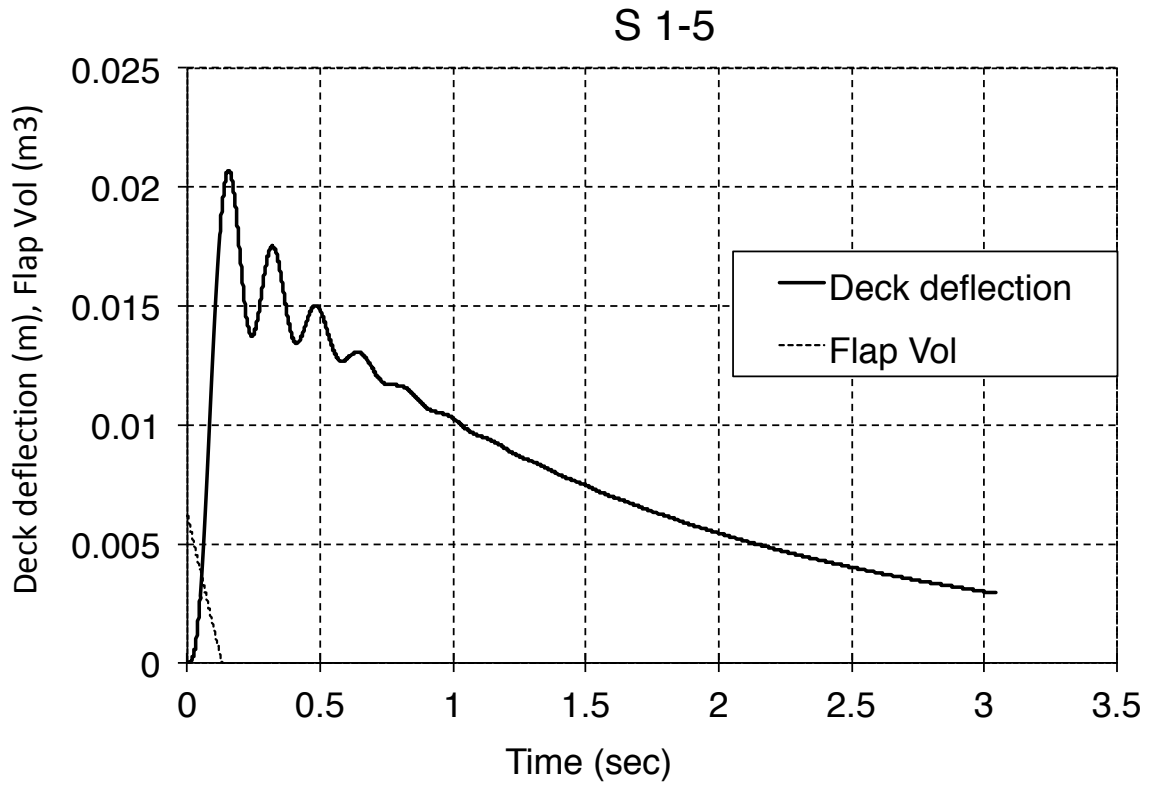


Figure G.15. Concept rig simulation five sample run, showing effects of extra active volume in the air supply duct.

This run shows the following features:

- The deck rises to the measured height, and decays at about the same rate as the experimental result.
- There are many more oscillations than with the experiment.
- The period of the oscillations is 161×10^{-3} s

The larger volume of the plenum (approximately doubling its volume) has brought the period up to the experimental value. However, the additional volume represented by the 'tube' is not realistic, and the reduced damping of oscillations is not consistent with the data.

G.7.6. Simulation six: add flexibility to plenum volume

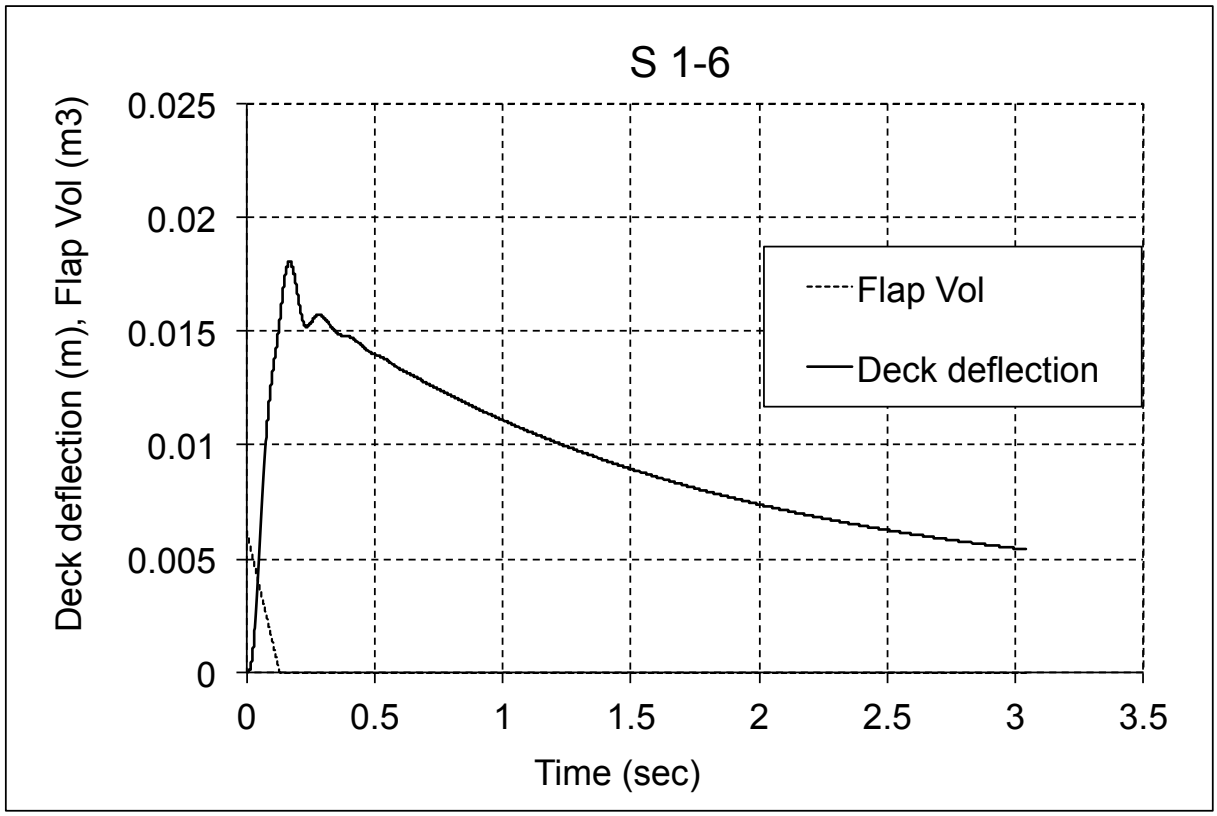


Figure G.16. Concept rig simulation six sample run, adding elastic volume (plenum flexibility) to simulation four.

This run (Fig. G.16) shows the following features:

- The deck rises to the measured height, and decays at about the same rate as the experimental result.
- There are two oscillations, as with the experiment, with a similar difference in the peak magnitudes.
- The period of the oscillations is 121×10^{-3} s.

The Excel spreadsheet becomes unstable if further 'flexibility' is built into the model. The flexibility in the plenum represents about 9% of the volume, and with this figure, the model's graph is a reasonable match to the experimental data.

G.8. Sensitivity study

A series of sensitivity studies was done to investigate the sensitivity of the system to:

- hole size
- spring initial deflection
- discharge coefficient of the air exit area
- speed of flap closure
- aerodynamic drag coefficient of the heave deck

Simulation six was used as the basis for sensitivity studies. The separate parameters were altered by realistic but large magnitudes individually and the simulation prediction was compared with that of Simulation six.

G.8.1. Sensitivity Study one: Hole size from 0 to 60 mm

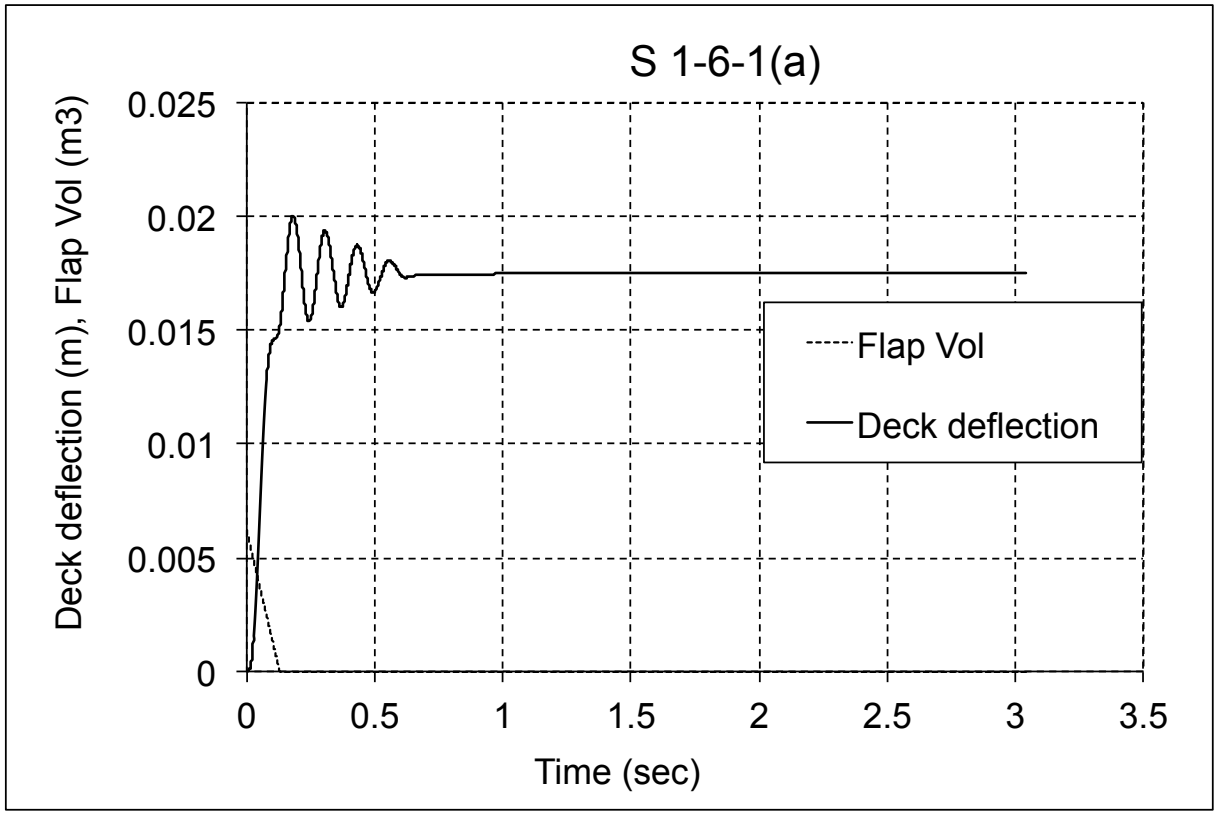


Figure G.17. Sensitivity run 1(a): hole size 0 mm (also zero air flow) Period 128×10^{-3} s.

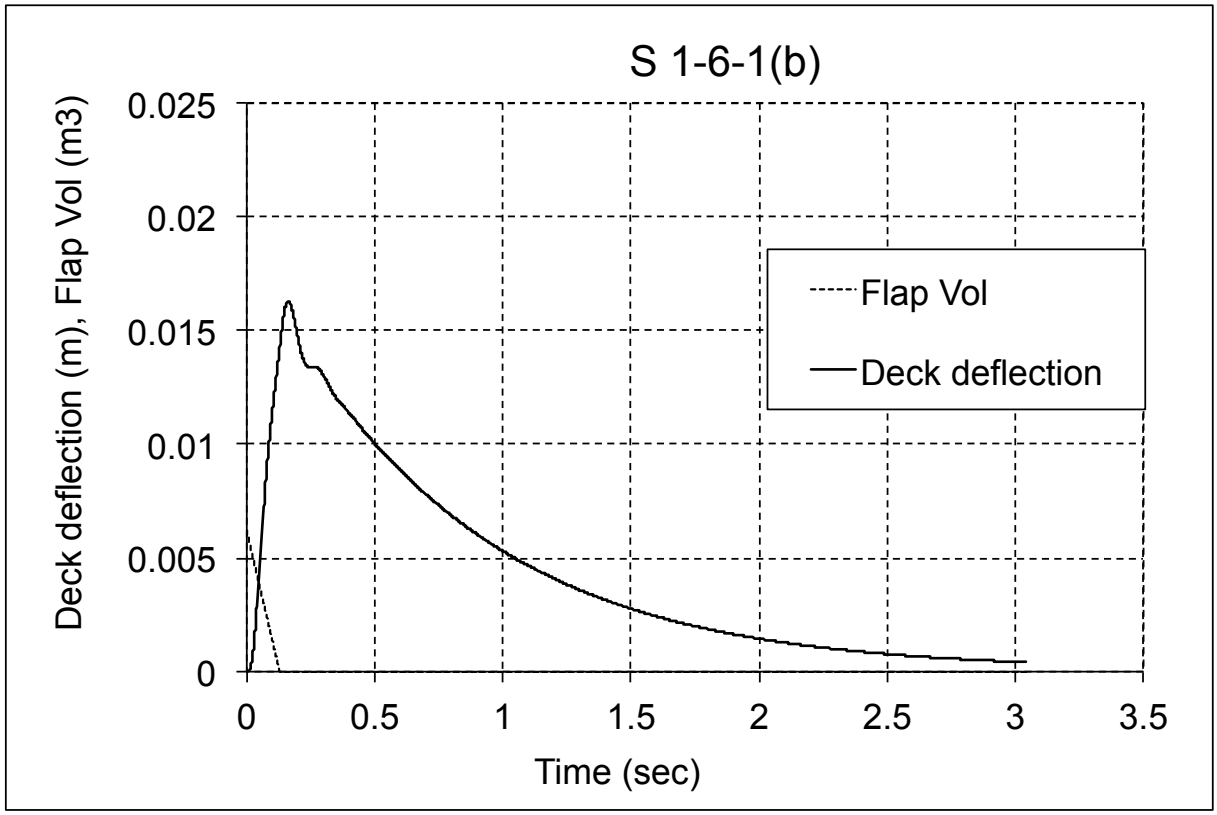


Figure G.18. Sensitivity run 1(b): hole size 60 mm (air flow $37.5 \times 10^{-3}\,\mathrm{m^3\,s^{-1}}$) Period $97 \times 10^{-3}\,\mathrm{s}$.

The size of the leakage/outlet hole has a modest effect on the natural frequency of the oscillations. However, the reliable identification of a second peak with the larger hole makes its measure of period somewhat inaccurate.

An experimental investigation of the sensitivity of the period of oscillation to leakage hole size was conducted. The leakage holes were entirely blanked off and the air flow turned down to a minimum: a small air flow was still required, (at an average duct speed of $2.8\,\mathrm{m\,s^{-1}}$, compared to the earlier speed of $11\,\mathrm{m\,s^{-1}}$). A series of larger holes was bored, and experiments conducted to measure the periods of vibration.

The results are summarised in Table G.1.

Table G.1. Data from concept rig varying air exit area sensitivity test

Run #	Hole ø mm	Hole Area $\mathrm{mm^2}$	Air Speed $\mathrm{m\,s^{-1}}$	Peak height mm	Period s
1	0	0	2.8	19.9	0.129
2	19	284	4.2	18.3	0.14
3	32	804	13.1	14.8	0.13
4	44	1520	23.7	17.6	0.10
5	51	2042	30.5	16.2	0.13

This experiment confirms that the leakage hole size/input air flow rate has a modest effect on the period of the vibrations, with the larger holes and larger air flows associated

with shorter periods. Hole size has a small effect on the peak height reached, as was also shown in the simulation.

A plot of Air Speed vs Hole Area (Fig. G.19) demonstrates a relationship with a non-zero intercept. Extrapolating to zero air flow yields the result that at around $-400\,\mathrm{mm}^2$, there would be no air flow. The figure of $400\,\mathrm{mm}^2$ is therefore an estimate of the leakage area.

Consequently, while the physical holes in Simulations two and six were equivalent to one with 31 mm diameter, having an area of $755\,\mathrm{mm}^2$, the effective total leakage area could have been $755 + 400 = 1155\ \mathrm{mm}^2$. This represents a single hole of equivalent diameter 38 mm. Simulations two and six adopted a 44 mm hole to obtain the reported characteristics. In view of the errors associated with extrapolation, uncertainties over the discharge characteristics of a group of holes, and the instability of the fan and anemometer at very low air speeds in the experiment with blanked off exit holes, the requirement to adopt a 44 mm hole for the simulation seems a reasonable adaptation of the model.

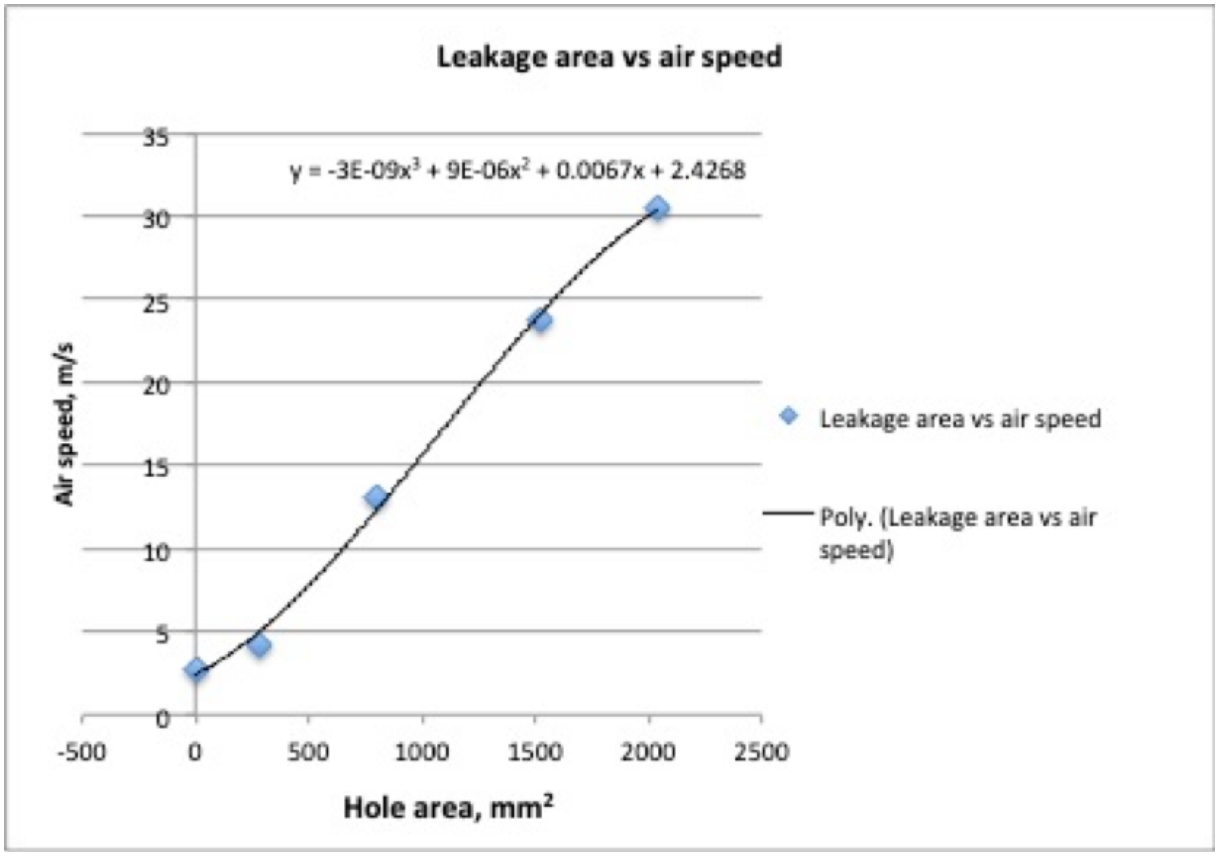


Figure G.19. Plot of leakage area vs air speed. Suggests a parasitic leakage area of $400\,\mathrm{mm}^2$.

G.8.2. Sensitivity study two: Reduced spring deflection (and increased air flow to compensate)

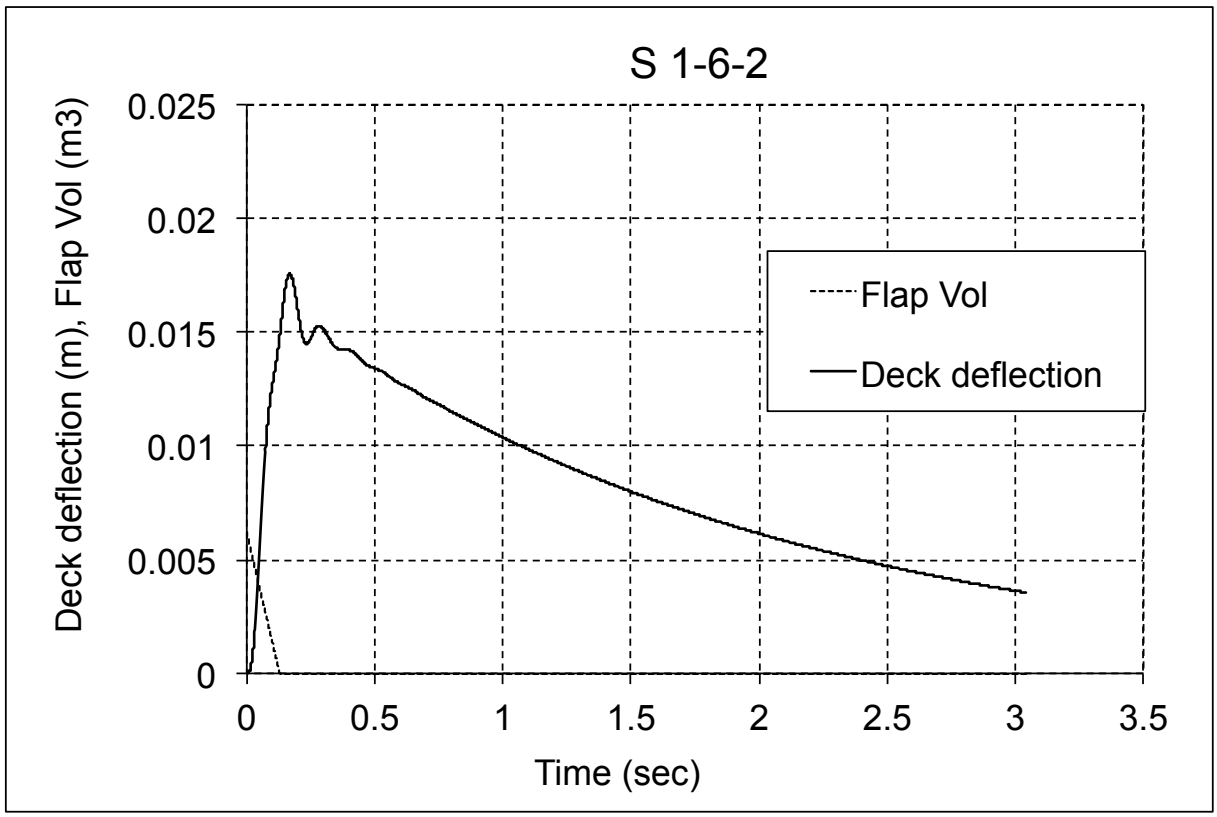


Figure G.20. Sensitivity run two: hole size 44 mm, 20 mm spring deflection. Period 116×10^{-3} s.

The balance between the spring setting and air flow to give a particular hover height has a small effect on the natural frequency. The higher air flow that is needed to support more of the weight at hover lengthens the period slightly. The period has a modest sensitivity to the spring's setting and the associated input flow rate.

G.8.3. Sensitivity study three: altering the discharge coefficient of the leakage hole from 0.8

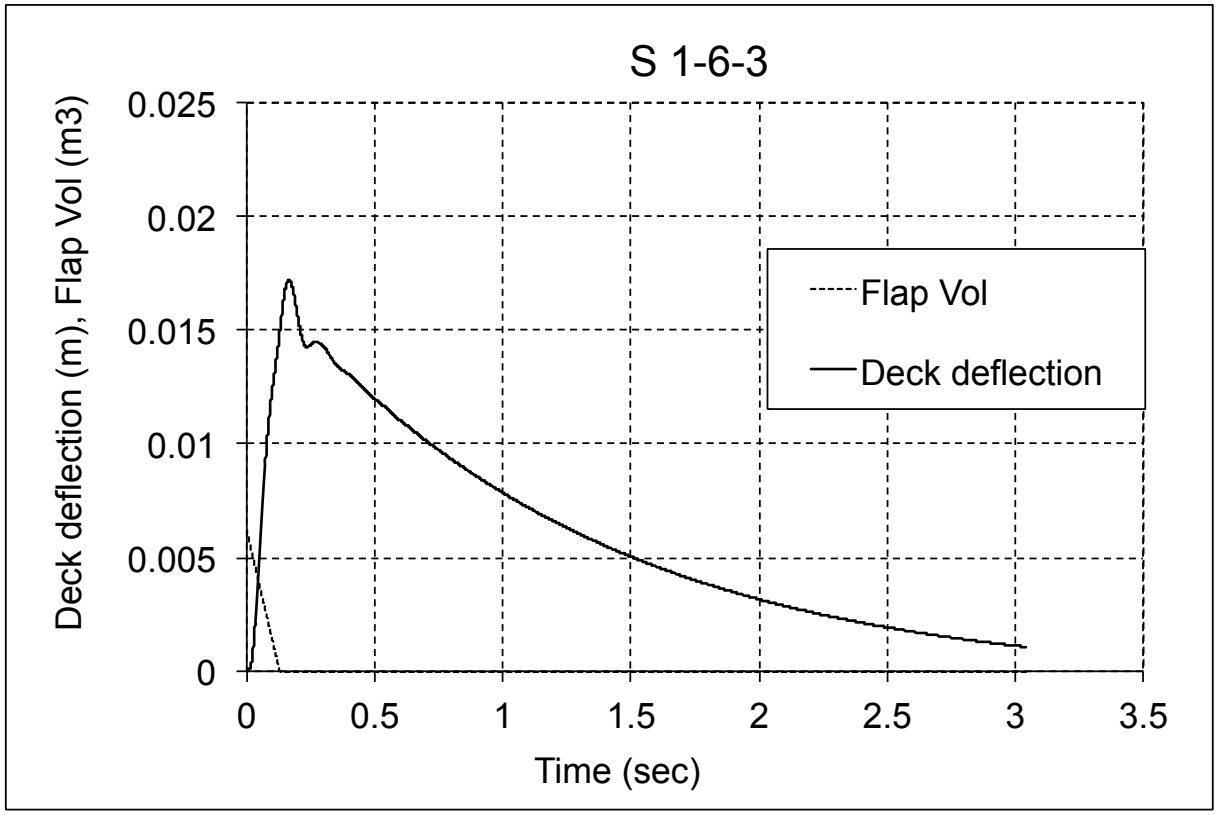


Figure G.21. Sensitivity run three: hole size 44 mm, discharge coefficient 1.0. Period 110×10^{-3} s.

The air is able to discharge more rapidly with the higher coefficient, and the period of the oscillations is slightly shorter. There is a sensitivity to this factor.

G.8.4. Sensitivity study four: Altering the speed at which the input flap closes

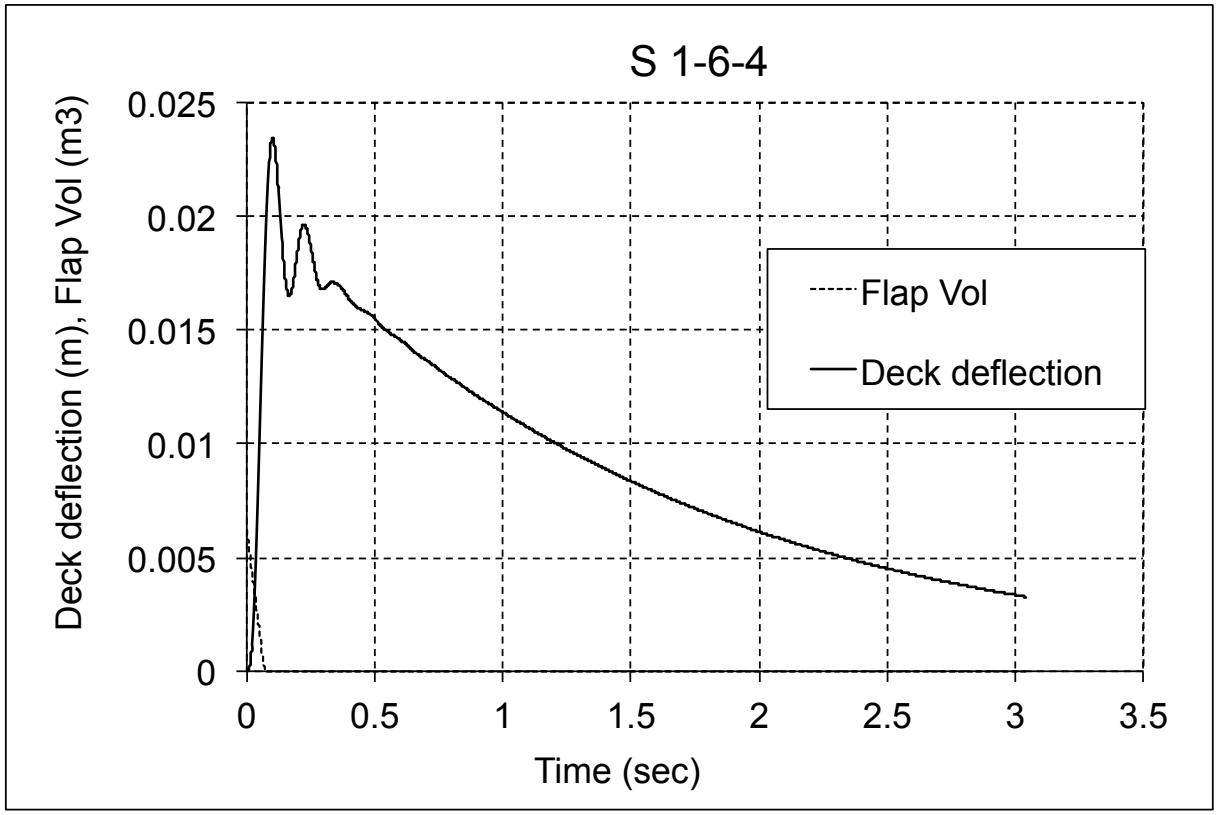


Figure G.22. Sensitivity run four: hole size 44 mm, input flap closed in 60% of the time. Period 120×10^{-3} s.

The heave deck rises to a greater height when the input flap is closed more rapidly (to about 24 mm instead of 19 mm), but the period of the subsequent oscillations remains the same. The initial height reached by the heave deck is sensitive to the speed at which the input flap is closed.

G.8.5. Sensitivity study five: Altering the drag coefficient on the deck

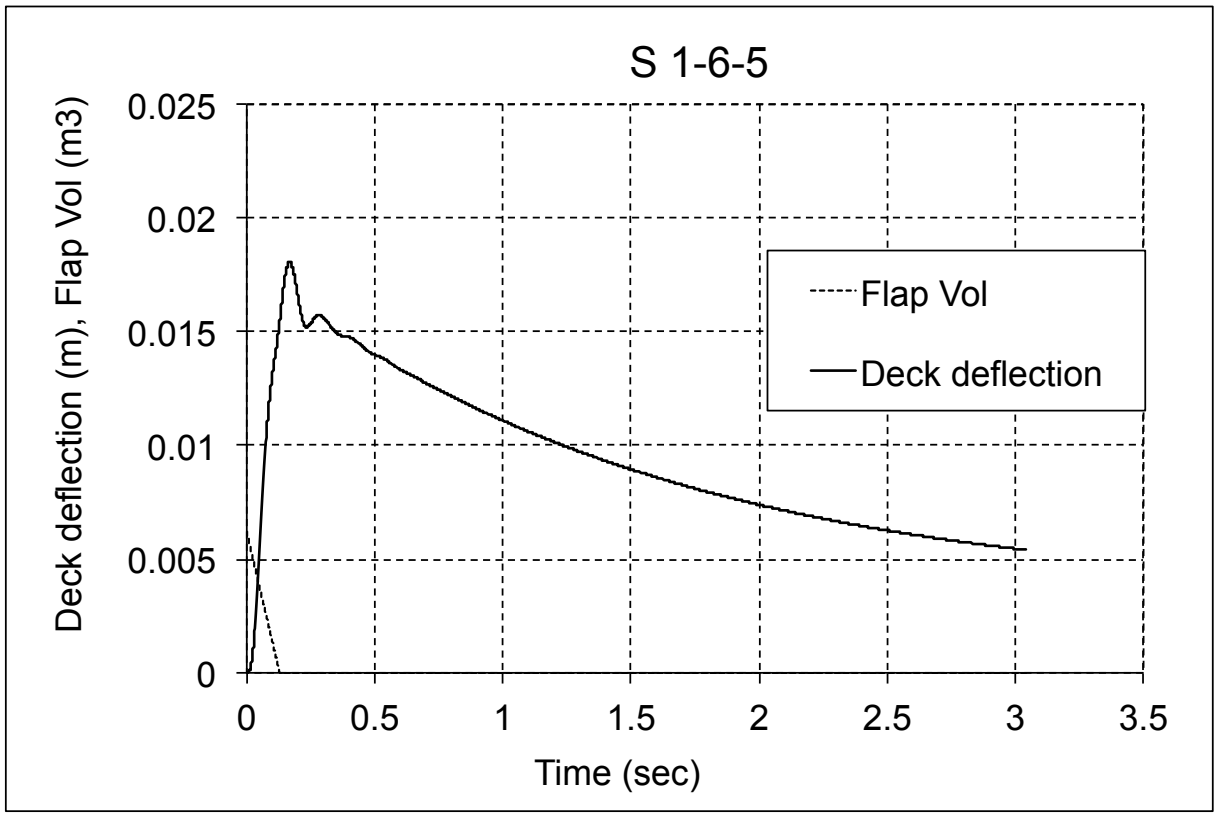


Figure G.23. Sensitivity run four: hole size 44 mm, drag coefficient 0.5 instead of 1.0. Period 121×10^{-3} s.

The graph is indistinguishable from that in Simulation six. The air resistance of the deck has no effect on the vibrating profile.

G.9. Conclusions from concept rig trials

1. The parasitic air leakage area was substantial, and was difficult to quantify, since the air flow measurement, based on a centreline anemometer, also relied on an assumed flow profile. Nevertheless, the unaccounted air flow area of about 400 mm^2 (representing a hole of 22 mm diameter) did not materially affect the critical determination of period of vibration. It did, however, affect the rate at which vibrations decayed.
2. The measured period of vibrations was found to be substantially greater than that which was predicted by the initial, 'idealised' Excel model (and also by analytical modelling).
3. The rig-based parameter that had the most significant effect on the predicted period was the stiffness of the plenum chamber and its flexible parts, such as the seals. It was not plausible to measure such flexibility, but the amount of flexibility did not significantly affect other output parameters such as the rate of decay of vibrations or the rate at which the heave deck returned to hover.

4. A small amount of Coulomb friction added to the heave deck seals caused the vibrations to dampen out more rapidly, but did not appear to affect other experimental parameters, such as period.
5. Since a hover at a chosen 'zero' height can be achieved by several combinations of air flow and spring pre-setting, and since the period is modestly sensitive to the internal pressure, there is a small but scattered relationship between leakage area and period.
6. The period and other parameters have a modest sensitivity to the leakage holes' assumed discharge coefficient. While it is likely that the coefficient can be reasonably well selected for the deliberate holes (being square-cornered holes in a flat plate), this is not the case for any unintended leakage regions, where the geometry is unknown. It is therefore important to limit parasitic leakage from the rig.
7. The speed at which the input flap closes has an effect on the magnitude of the first peak of heave deck motion. For accurate predictions of the heave deck motion, it is necessary for the input flap to close well within the natural period of the subsequent oscillation.

H. Extended experimental results

This appendix contains all of the experimental results for the main experiments. Appendix H.1 has the results in fully analysed form, as discussed in Sec. 6.5.4. Appendix H.2 has partially analysed data from each experimental run, as discussed in Sec. 6.5.5.

H.1. Power spectrum analysis of experimental results

This text is a copy of text in the main body of the thesis, Sec. 6.5.4.

The experimental results are plotted over the numerical model predictions. For convenience, the two parameters calculated from the same measurand at each value of the forcing frequency (ω_f) is contained in each plot using two sets of axes; the first set of axes is for S_V plotted against ω_f, the second set of axes is for O_V plotted against ω_f. The phase angle (ϕ) between the supported mass motion and the flapper motion is plotted on the third set of axes, with the experimental results plotted over the numerical model predictions.

There are two experimental factors, H_0 and A_e, each set to one of three values, giving nine combinations of experimental factors (Table H.1). Five of these combinations are presented in the body of this thesis, with all nine experimental results included in Appendix H. The five combinations of the experimental factors are sufficient to give insight to the sensitivity of the experimental results to the two experimental factors.

Table H.1. The nine combinations of the two experimental factors, with the combinations presented in the body of the thesis shown in **bold type**.

	$A_e = 570 \times 10^{-6}\,\mathrm{m}^2$	$A_e = 820 \times 10^{-6}\,\mathrm{m}^2$	$A_e = 1.207 \times 10^{-3}\,\mathrm{m}^2$
$H_0 = 290 \times 10^{-3}\,\mathrm{m}$	Condition 1	**Condition 2**	Condition 3
$H_0 = 600 \times 10^{-3}\,\mathrm{m}$	**Condition 4**	**Condition 5**	**Condition 6**
$H_0 = 810 \times 10^{-3}\,\mathrm{m}$	Condition 7	**Condition 8**	Condition 9

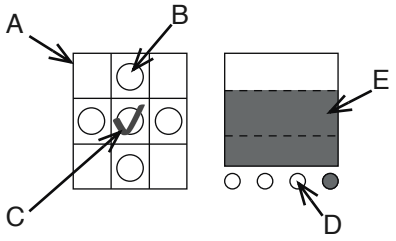


Figure H.1. Icon representing which condition is relevant to the presented results. The left side grid (A) representing the nine possible conditions, where H_0 corresponds to the vertical axis and A_e corresponds to the horizontal axis. The circles (B) in the cells indicate the conditions that will be discussed in the main body of the thesis. The tick on a circle (C) indicates the current condition. The pictorial part of the icon represents the plenum height by a shaded area (E) and open air exit areas by open circles (D).

An icon of the style introduced in Fig. H.1 is included on each plot to assist the reader to identify the condition at which the results were obtained. The icon refers to Table H.1, indicating the relevant condition with a tick in a grid, corresponding to the location in Table H.1. The icon also contains a representation of the plenum chamber, with H_0 indicated by a shaded portion. The final part of the icon is a series of circles representing A_e, with open circles shown proportional to the A_e. There is always a fixed portion of the total A_e, so four circles are used in the icon, the first circle representing the fixed portion of the total A_e.

At each condition, several forcing frequencies were selected at random for repetition, which are shown as extra points on the plots (rather than an average), acknowledging that the repetition procedure of the experiments can lead to small variations of the forcing frequency.

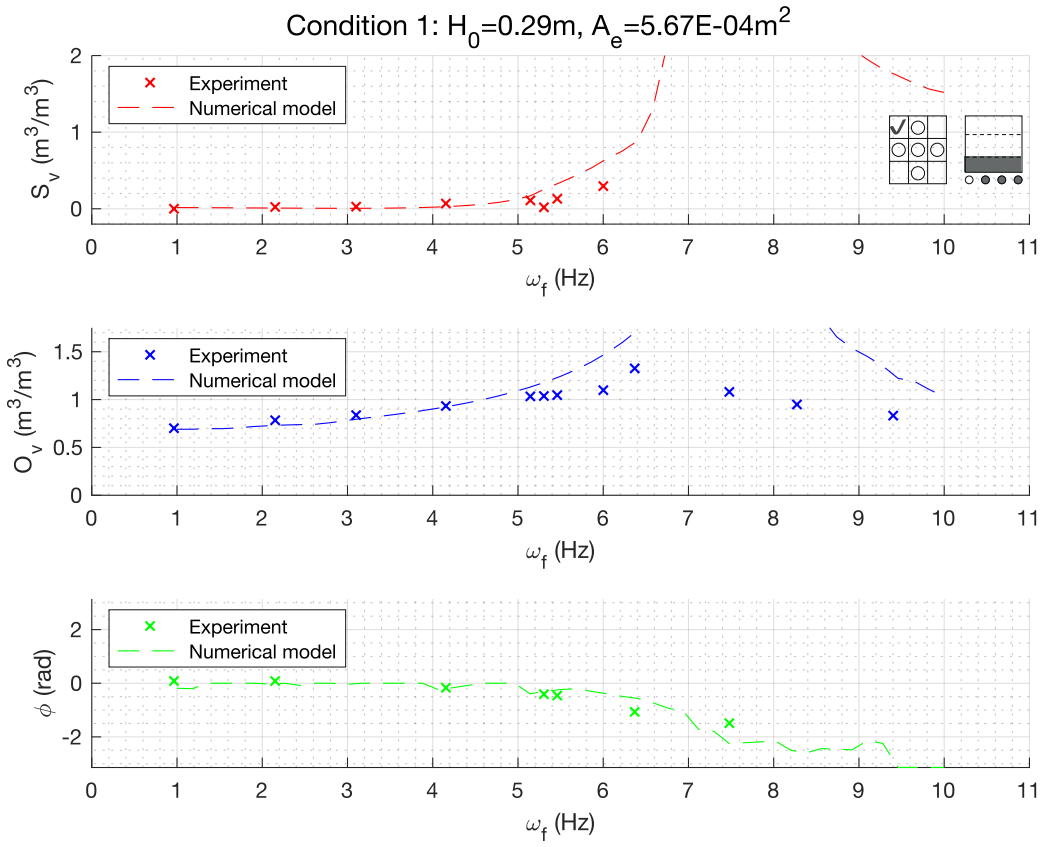


Figure H.2. Experimental results at Condition One.

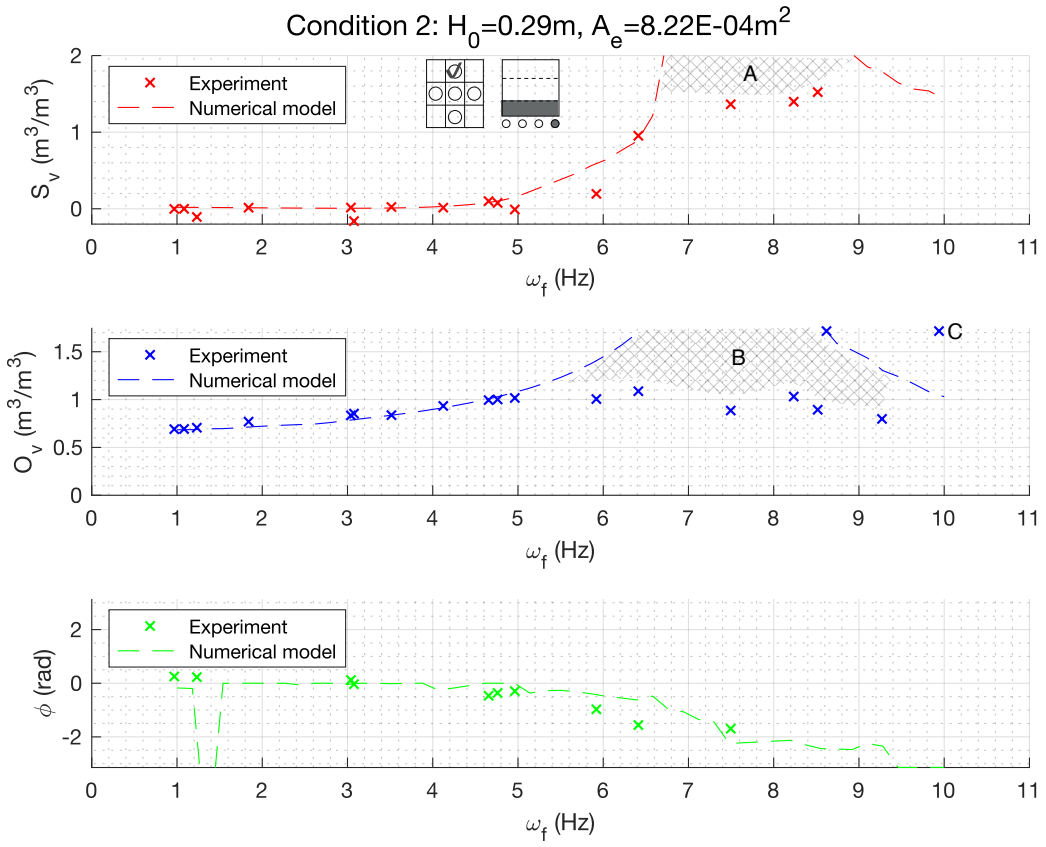


Figure H.3. Experimental results at Condition Two. For full commentary see Fig. 6.15.

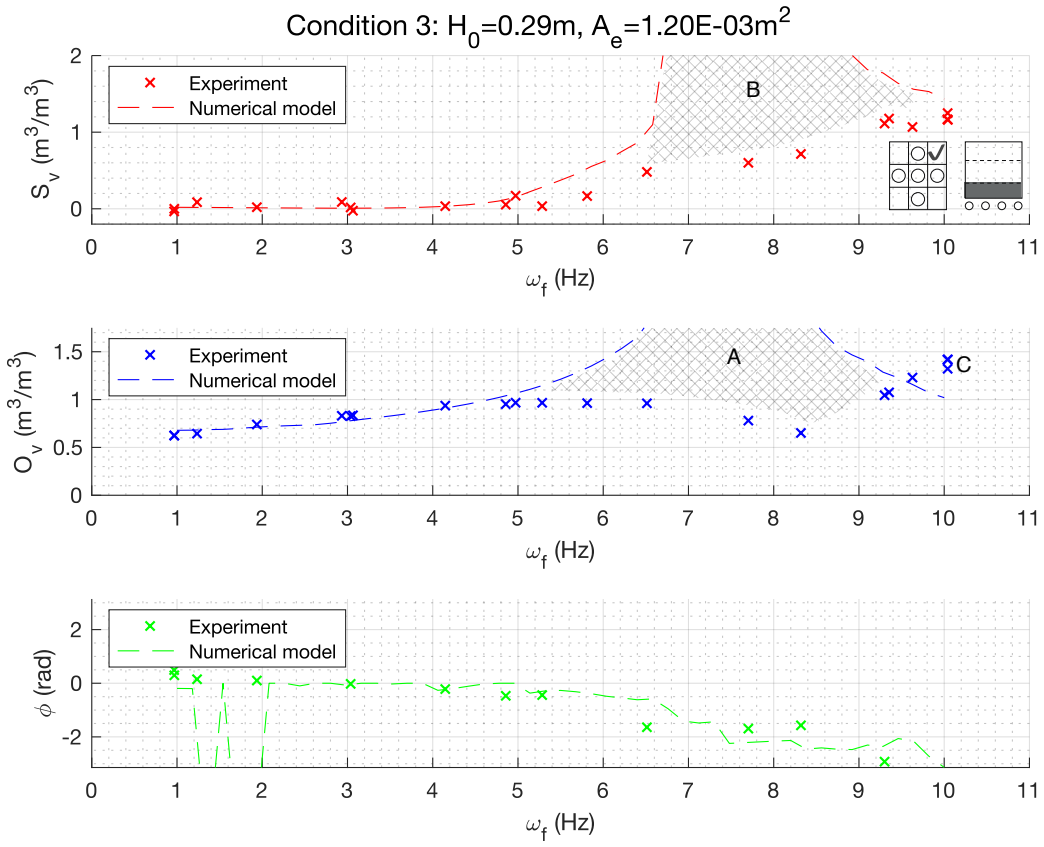


Figure H.4. Experimental results at Condition Three.

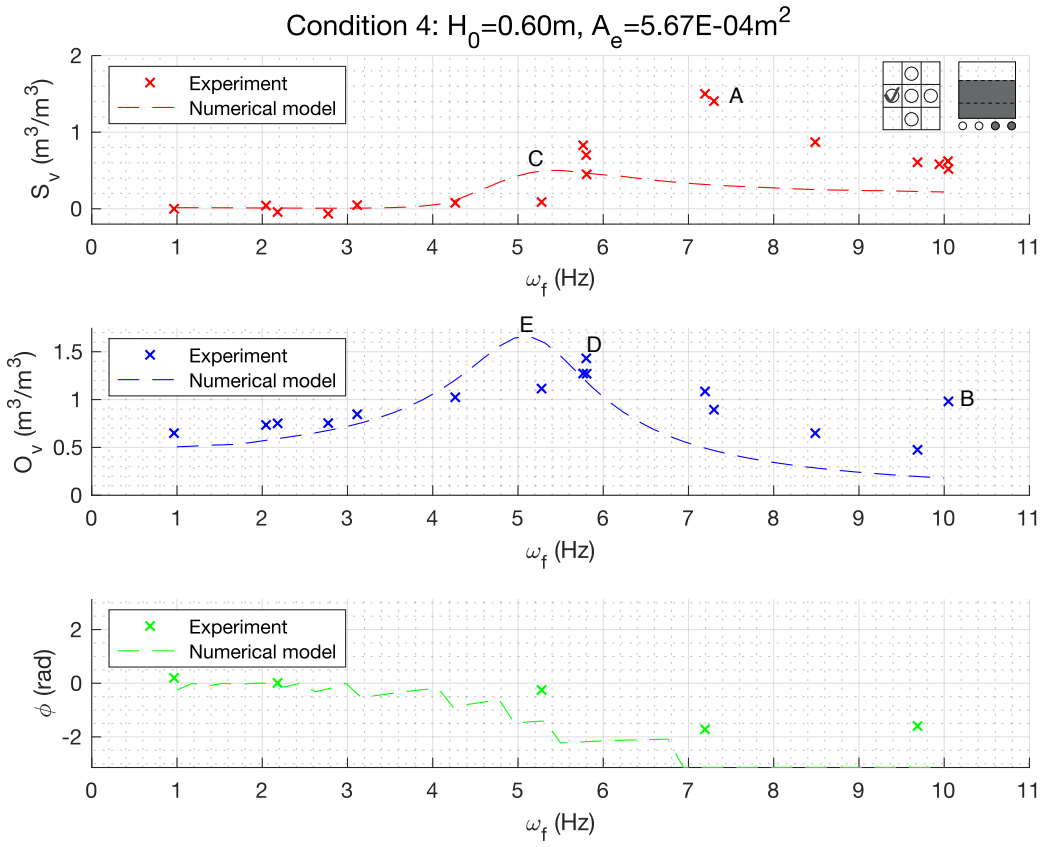


Figure H.5. Experimental results at Condition Four. For full commentary see Fig. 6.13.

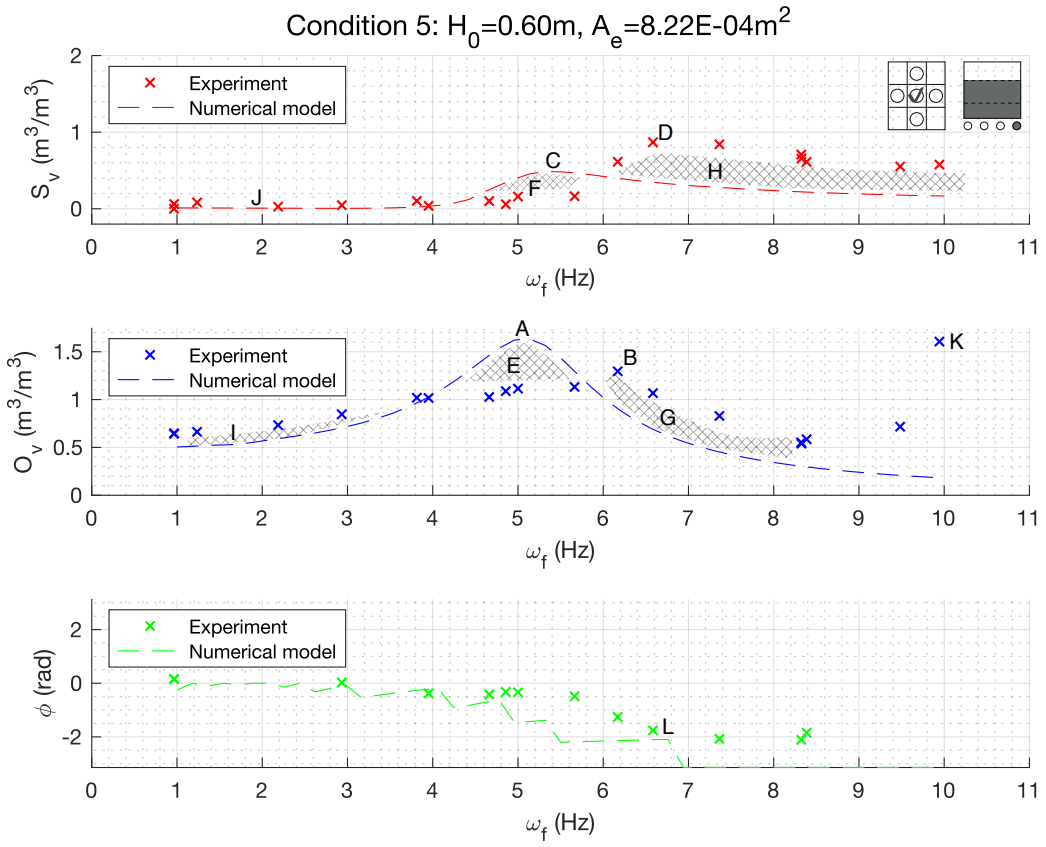


Figure H.6. Experimental results at Condition Five. For full commentary see Fig. 6.11.

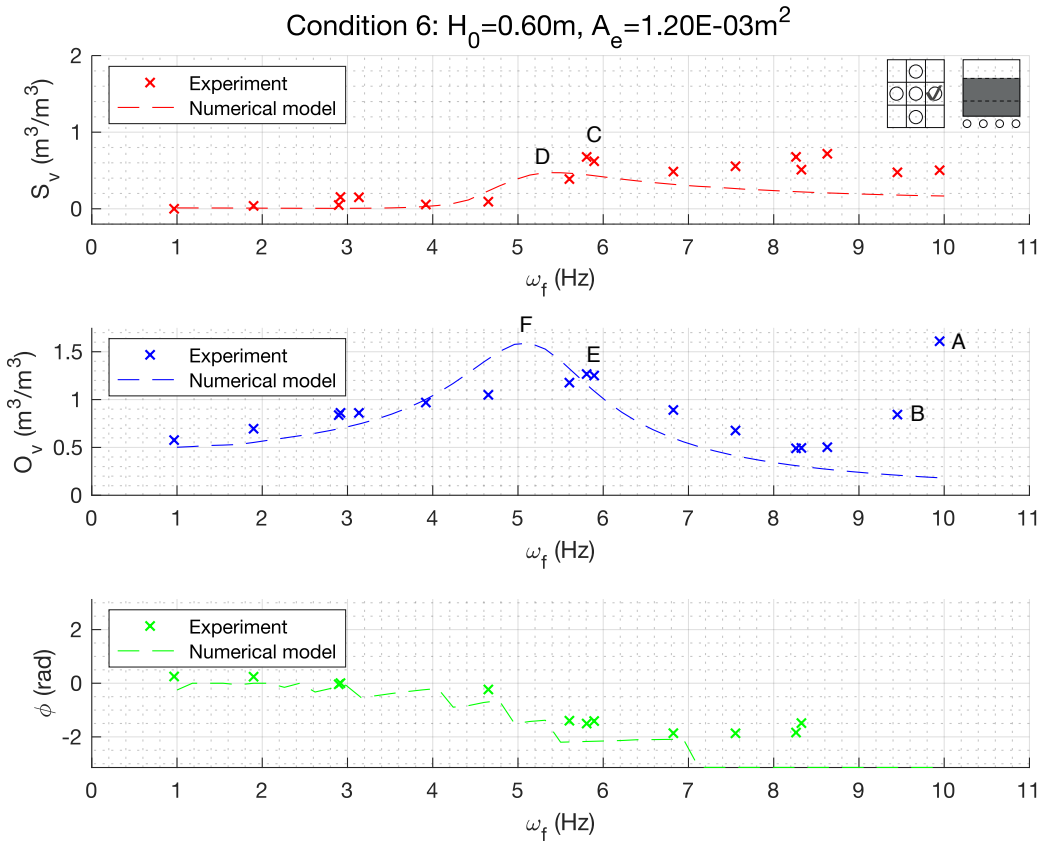


Figure H.7. Experimental results at Condition Six. For full commentary see Fig. 6.12.

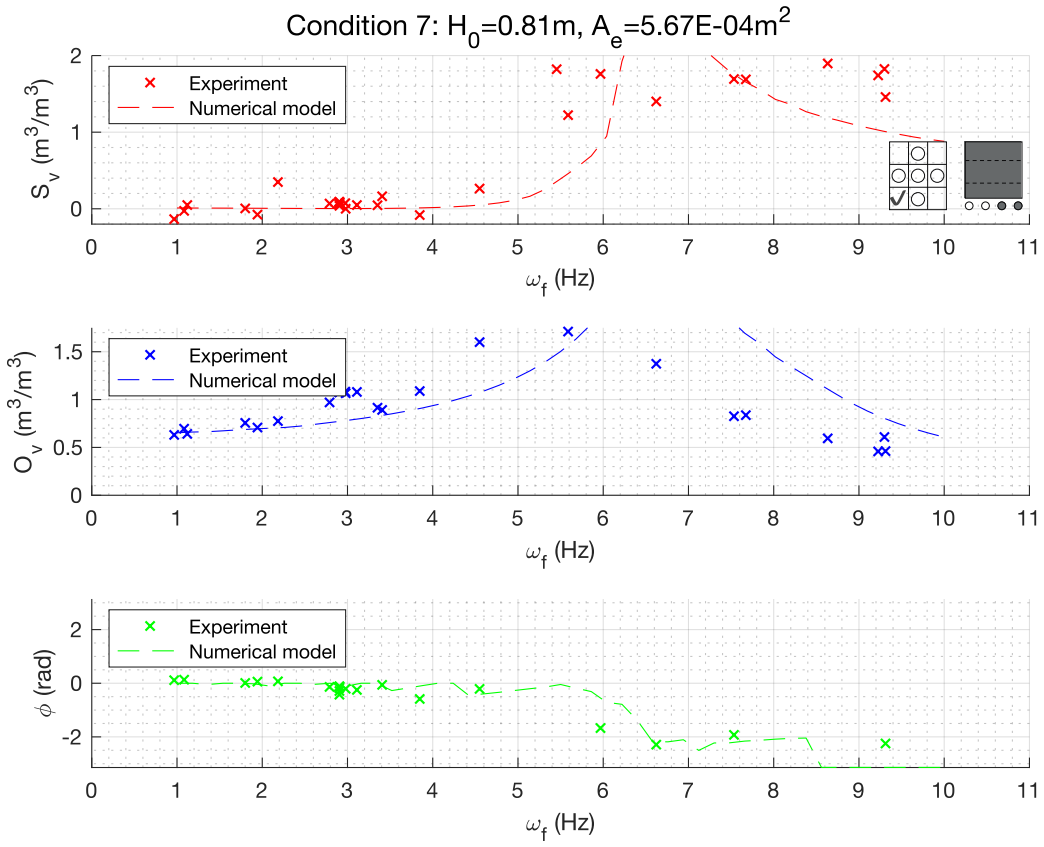


Figure H.8. Experimental results at Condition Seven.

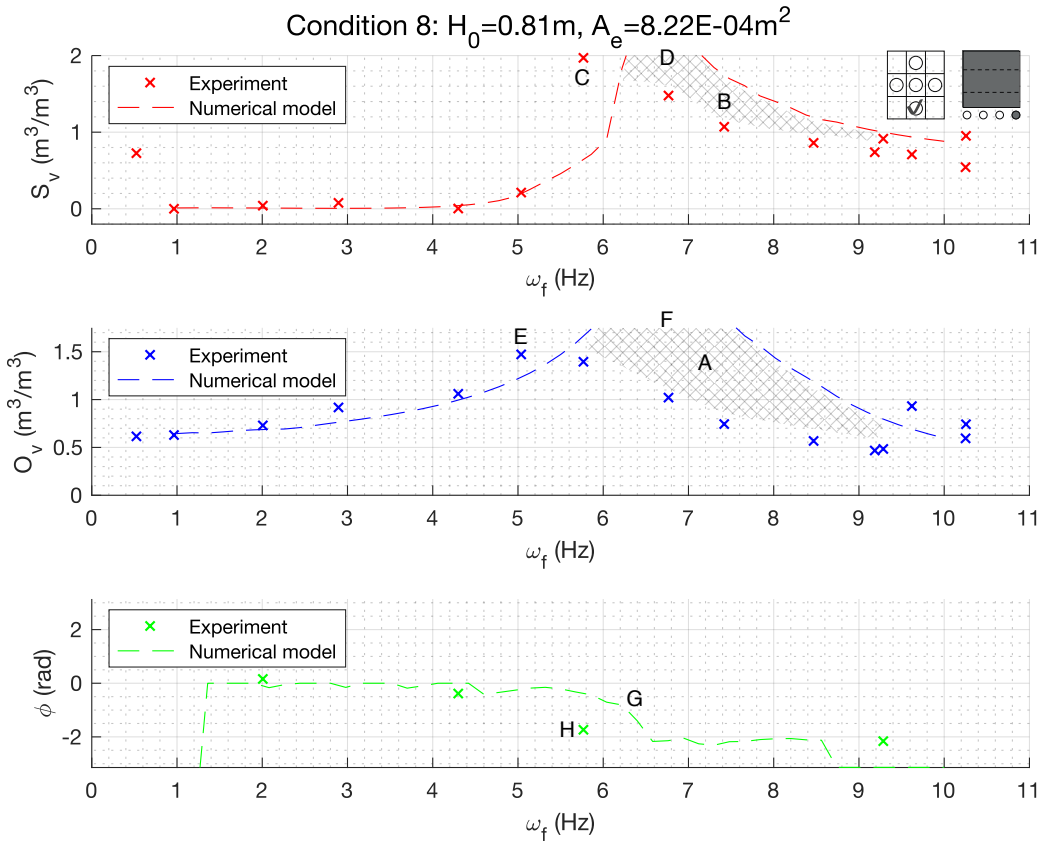


Figure H.9. Experimental results at Condition Eight. For full commentary see Fig. 6.14.

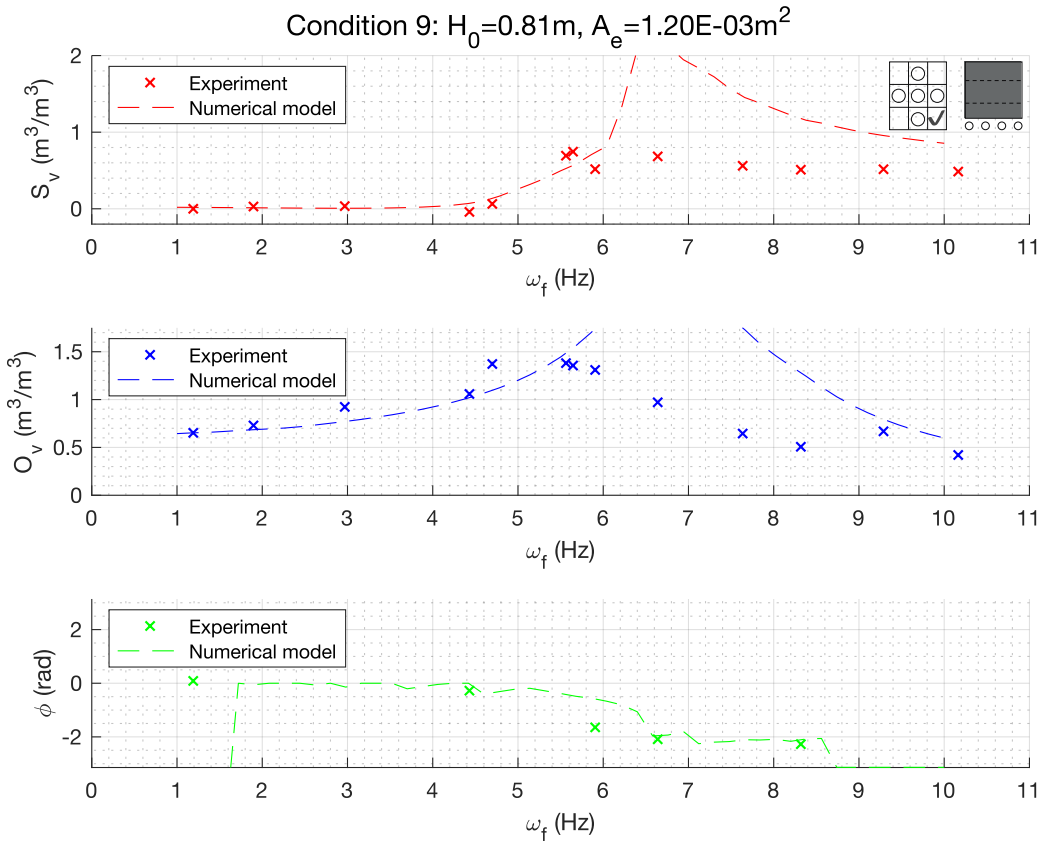


Figure H.10. Experimental results at Condition Nine.

H.2. Input and output time series of experimental results

This section contains partially analysed data from individual experimental runs. See Table H.1 for definitions of the experimental conditions and Table H.2 for a list of run numbers at each condition.

Any and all annotations on the plots are discussed in the main body of the thesis, Sec. 6.5.5.

Table H.2. Main experiment condition numbers (column one), plenum heights (H_0), air exit area (A_e) and run numbers (column four).

Condition #	H_0 m	A_e m^2	Runs #
1	292×10^{-3}	567×10^{-6}	62-72, 95, 105
2	292×10^{-3}	822×10^{-6}	73-83, 97-99, 104, 107-109, 114
3	292×10^{-3}	1.20×10^{-3}	84-94 96 100-103 106 110-113
4	605×10^{-3}	567×10^{-6}	115-125, 148, 153, 157, 158, 163, 167
5	605×10^{-3}	822×10^{-6}	126-136, 150, 152, 154, 156, 160, 162, 164, 166
6	605×10^{-3}	1.20×10^{-3}	137-147, 149, 151, 155, 159, 161, 165
7	805×10^{-3}	567×10^{-6}	1-19, 43-46, 49, 51, 53-56, 59, 61
8	805×10^{-3}	822×10^{-6}	20-30, 42, 48, 52, 58
9	805×10^{-3}	1.20×10^{-3}	31-41, 50, 60

H.2.1. Condition One

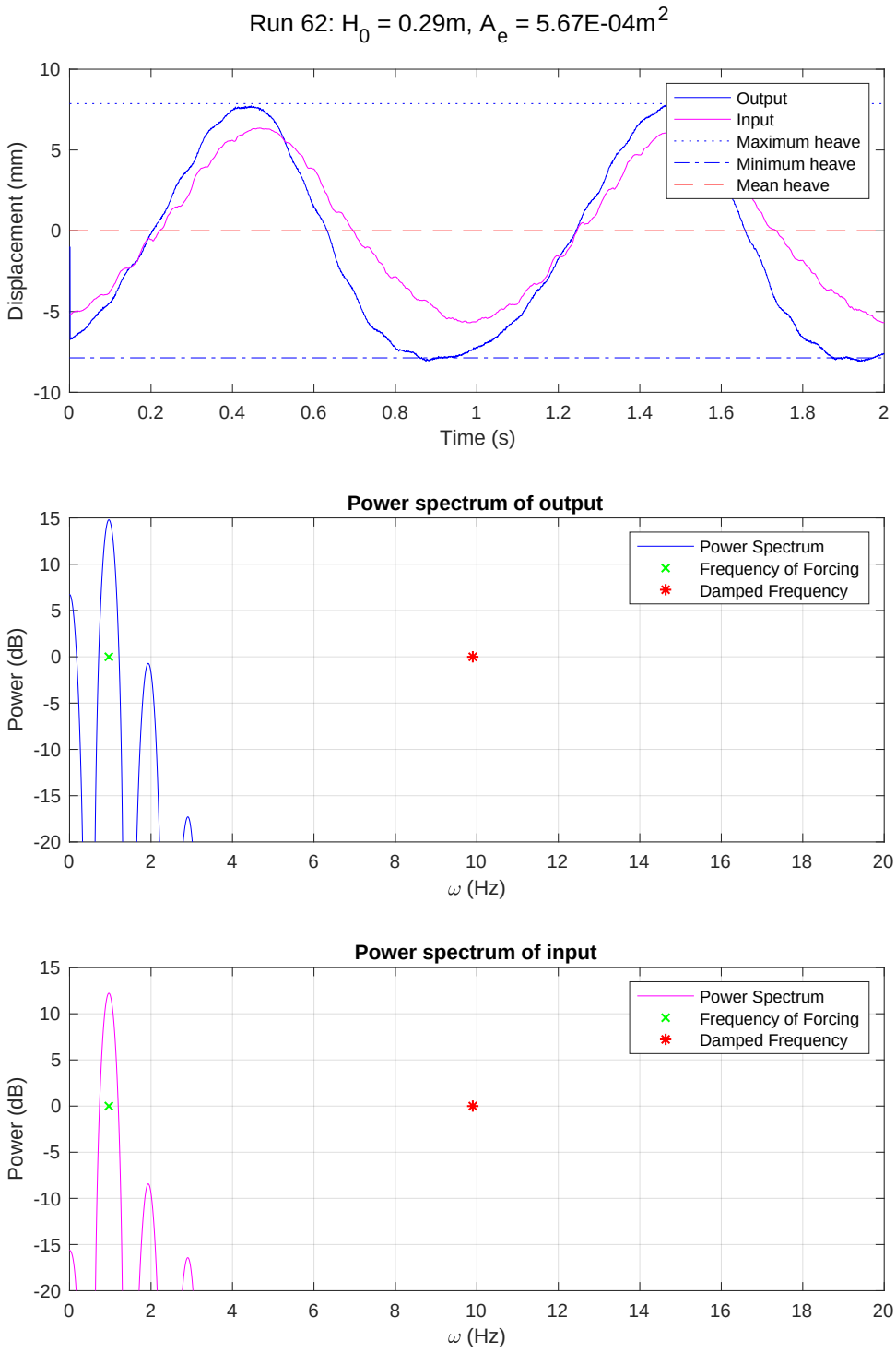


Figure H.11. Experimental trial data for Condition 62

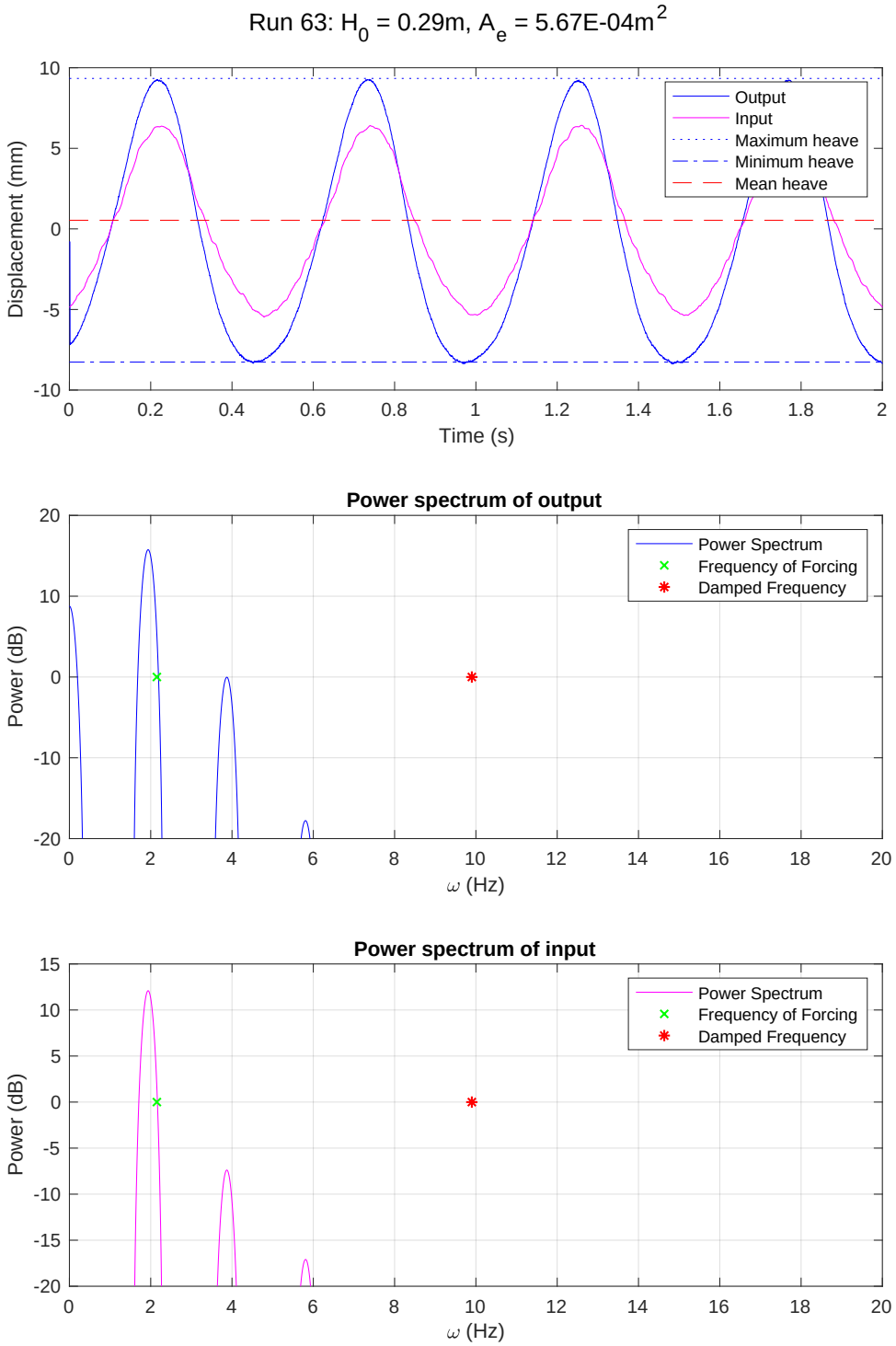


Figure H.12. Experimental trial data for Condition 63

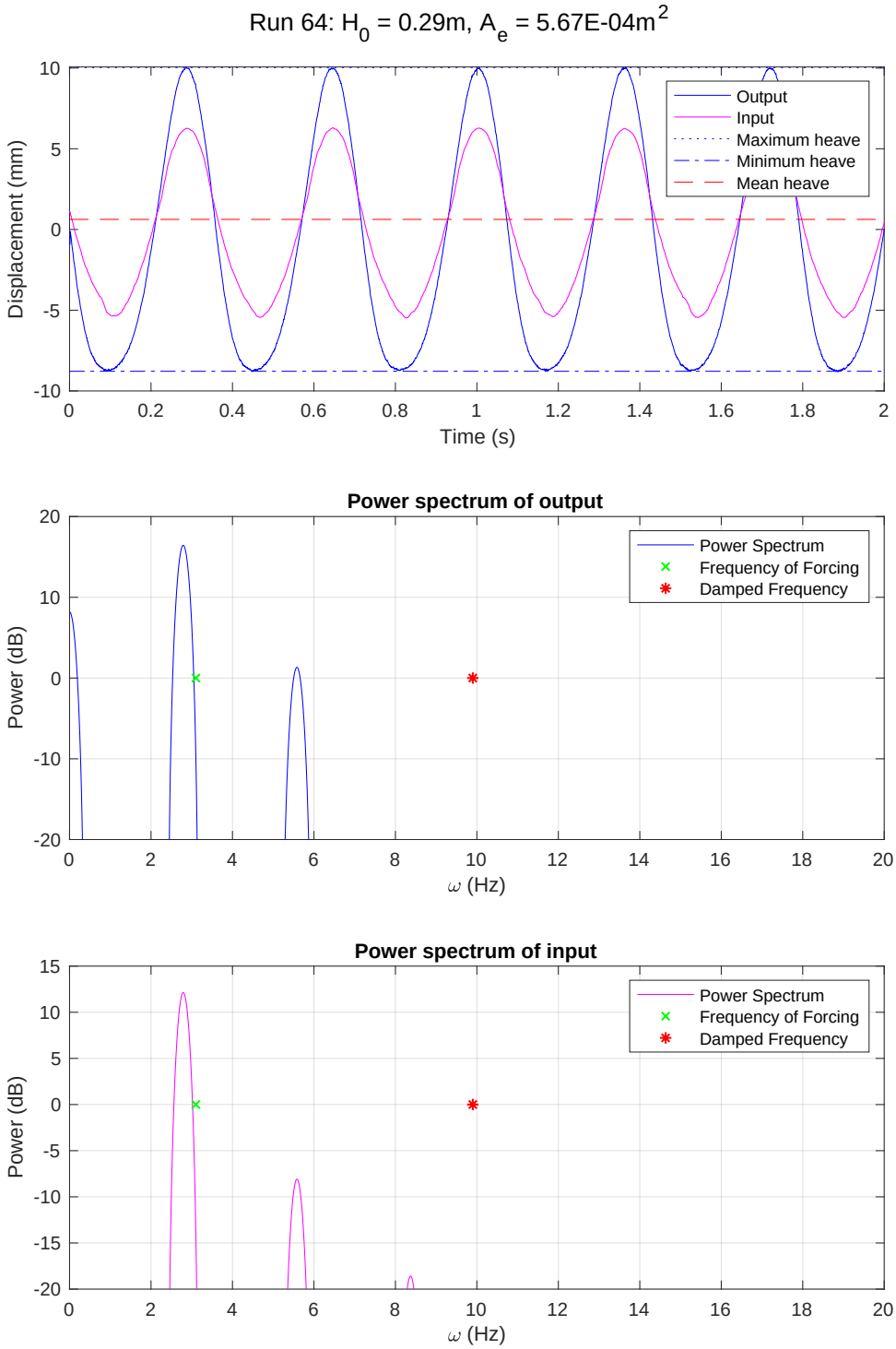


Figure H.13. Experimental trial data for Condition 64

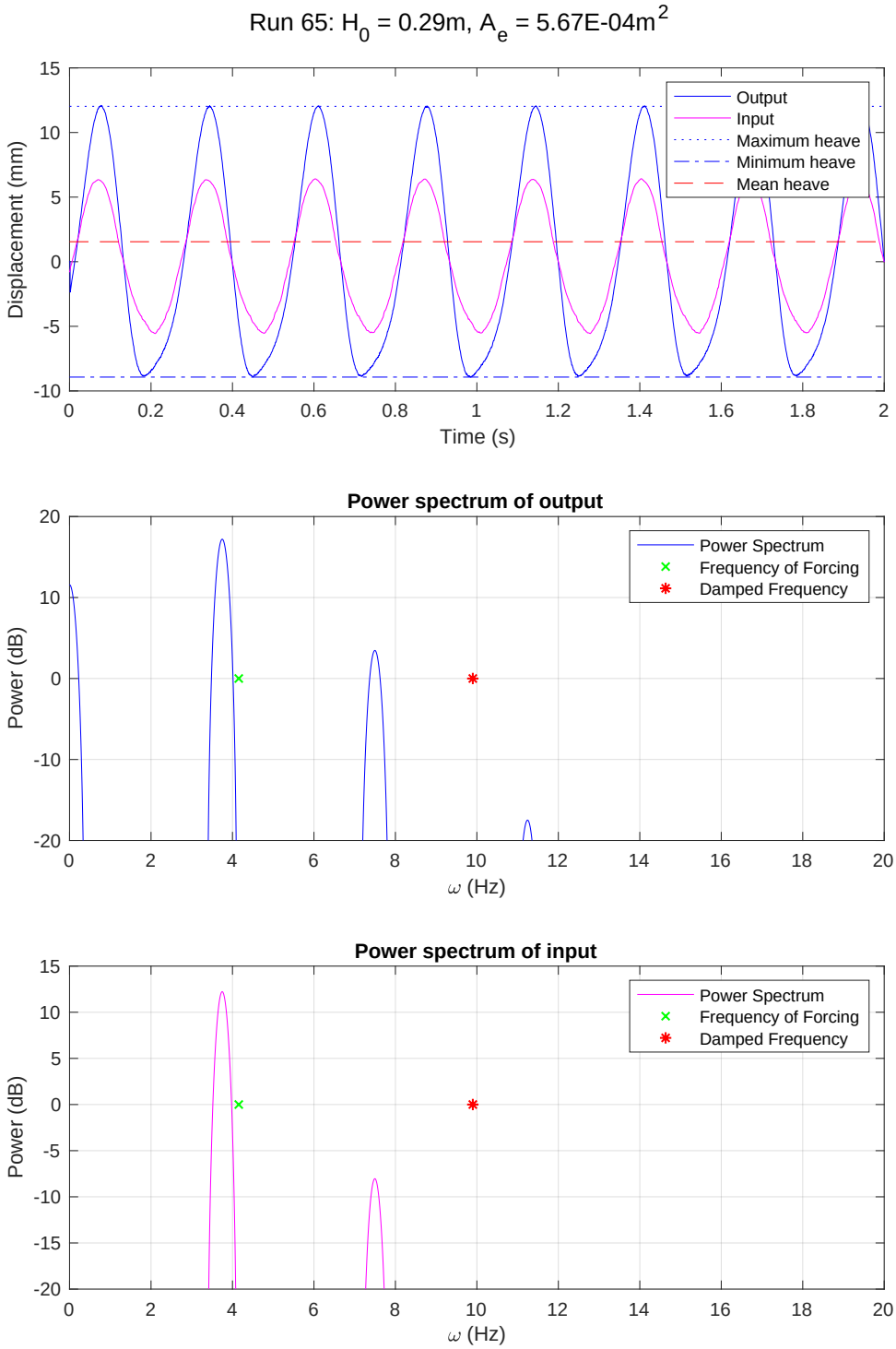


Figure H.14. Experimental trial data for Condition 65

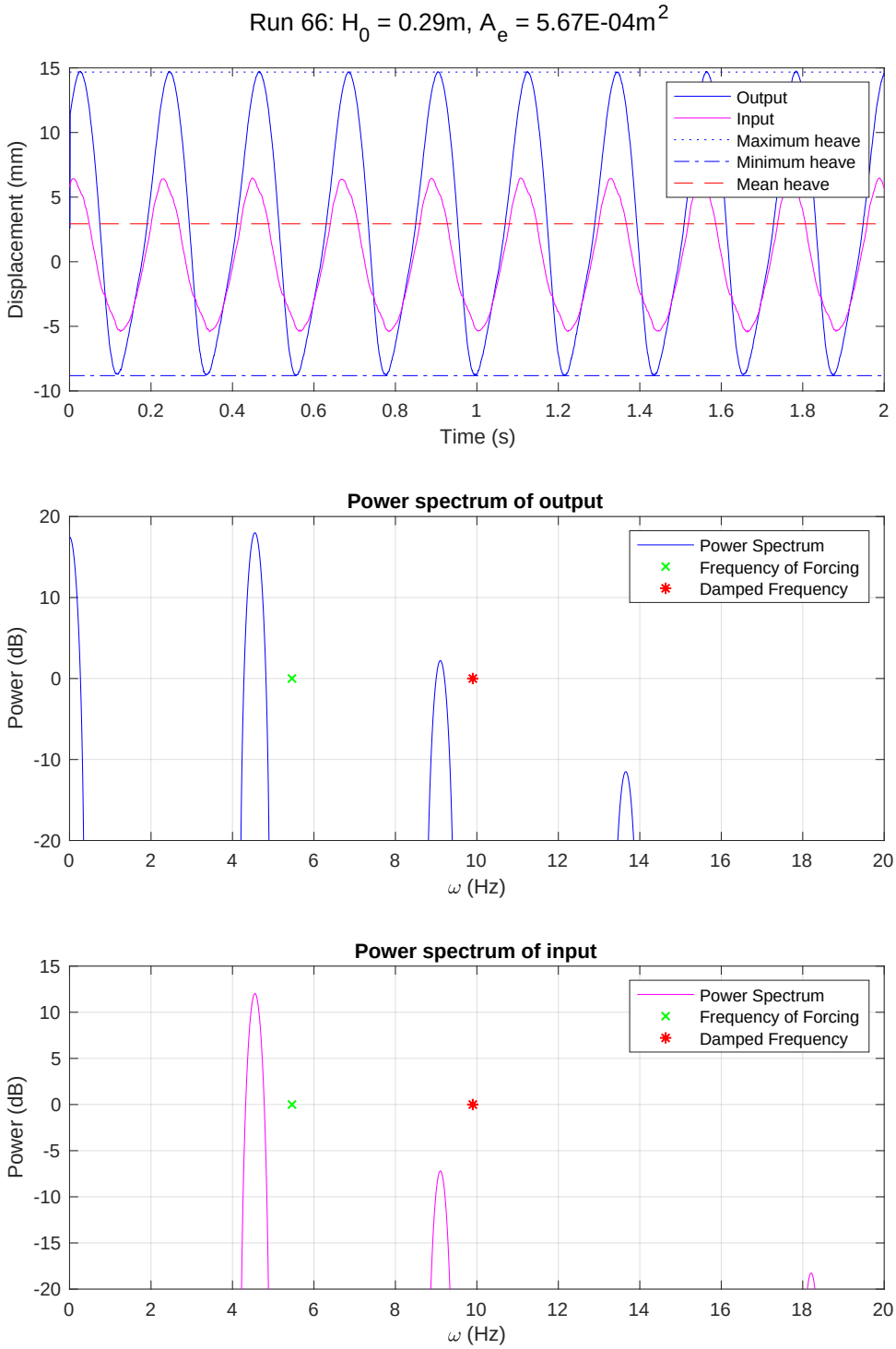


Figure H.15. Experimental trial data for Condition 66

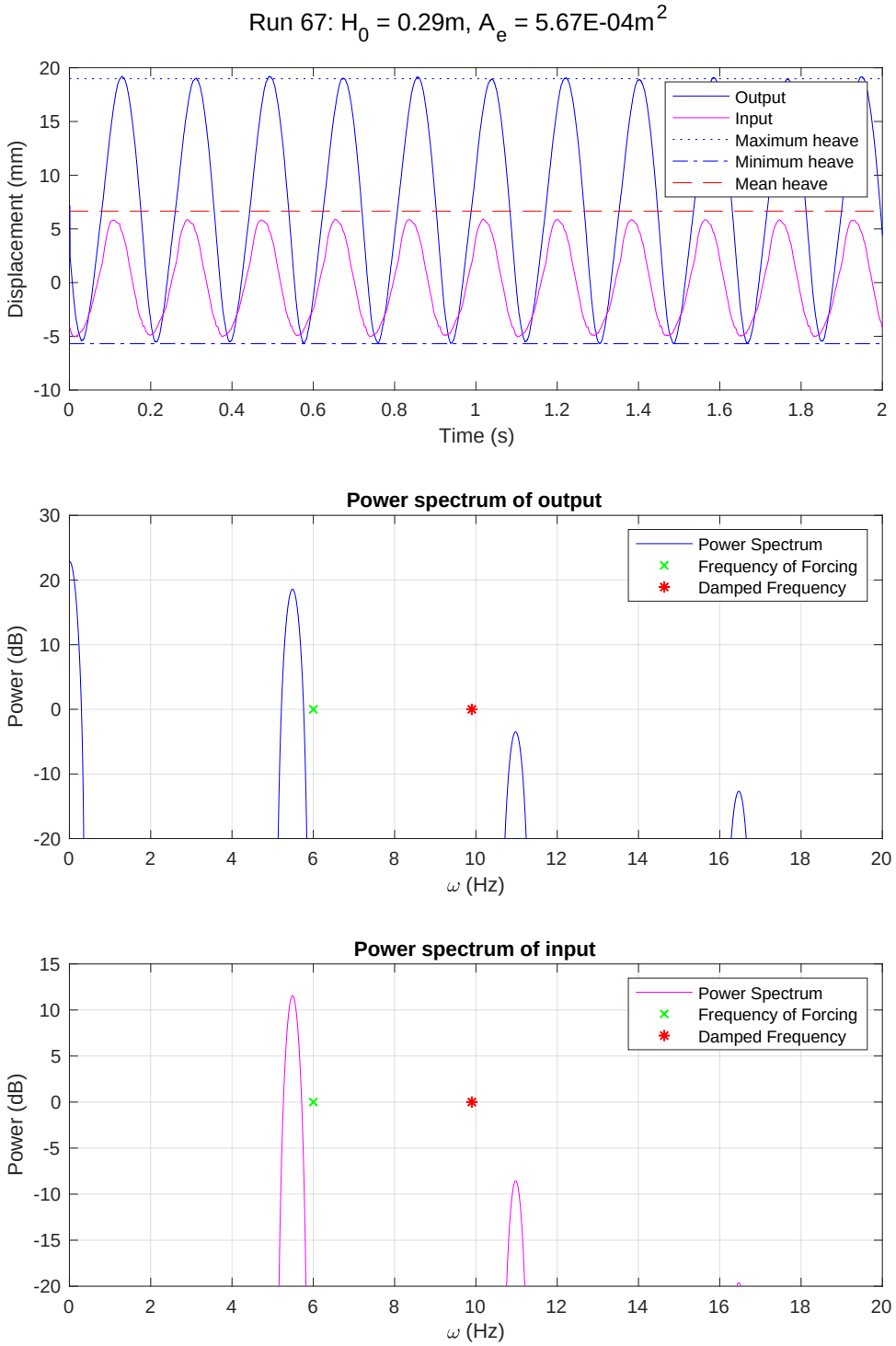


Figure H.16. Experimental trial data for Condition 67

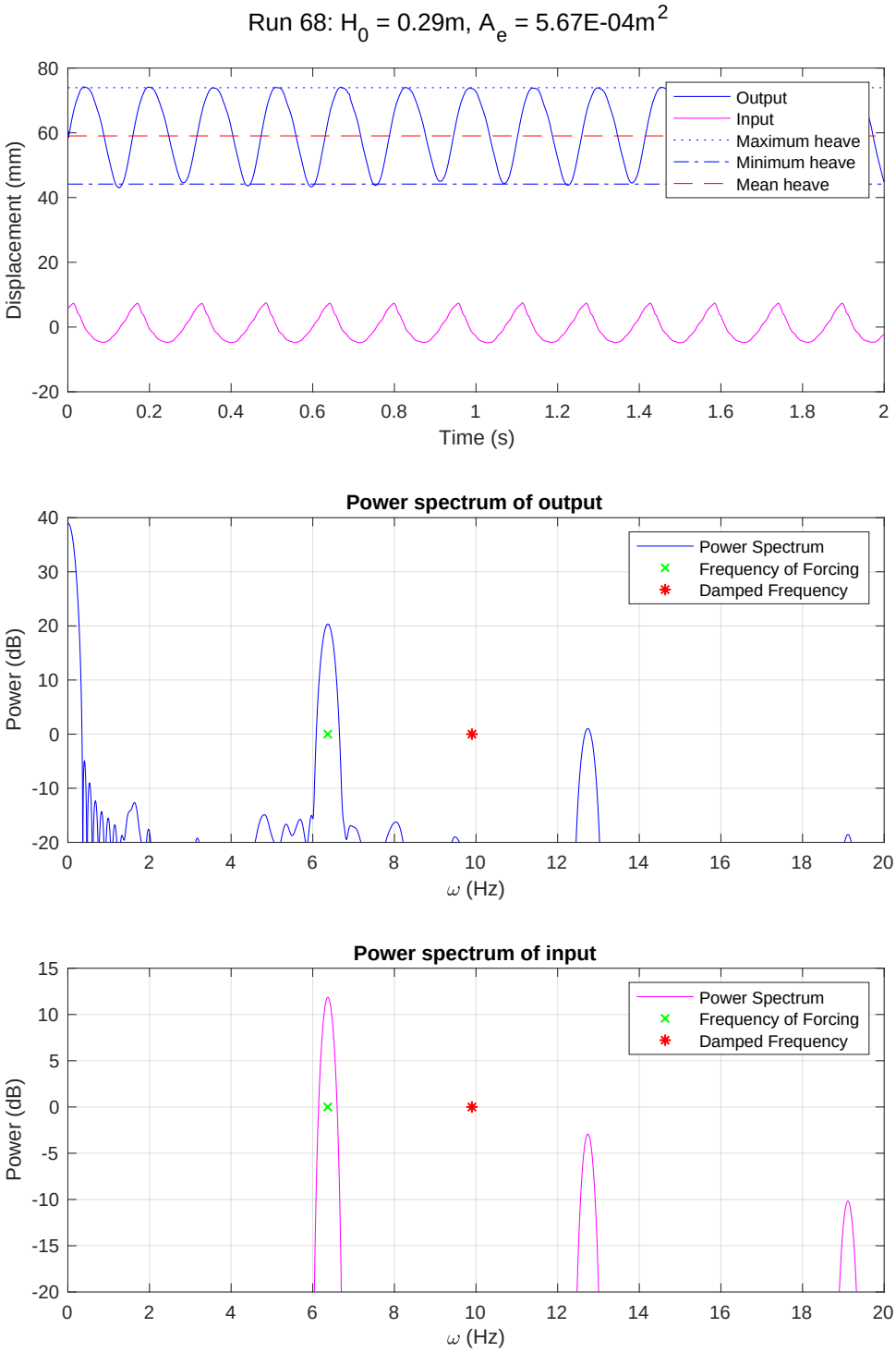


Figure H.17. Experimental trial data for Condition 68

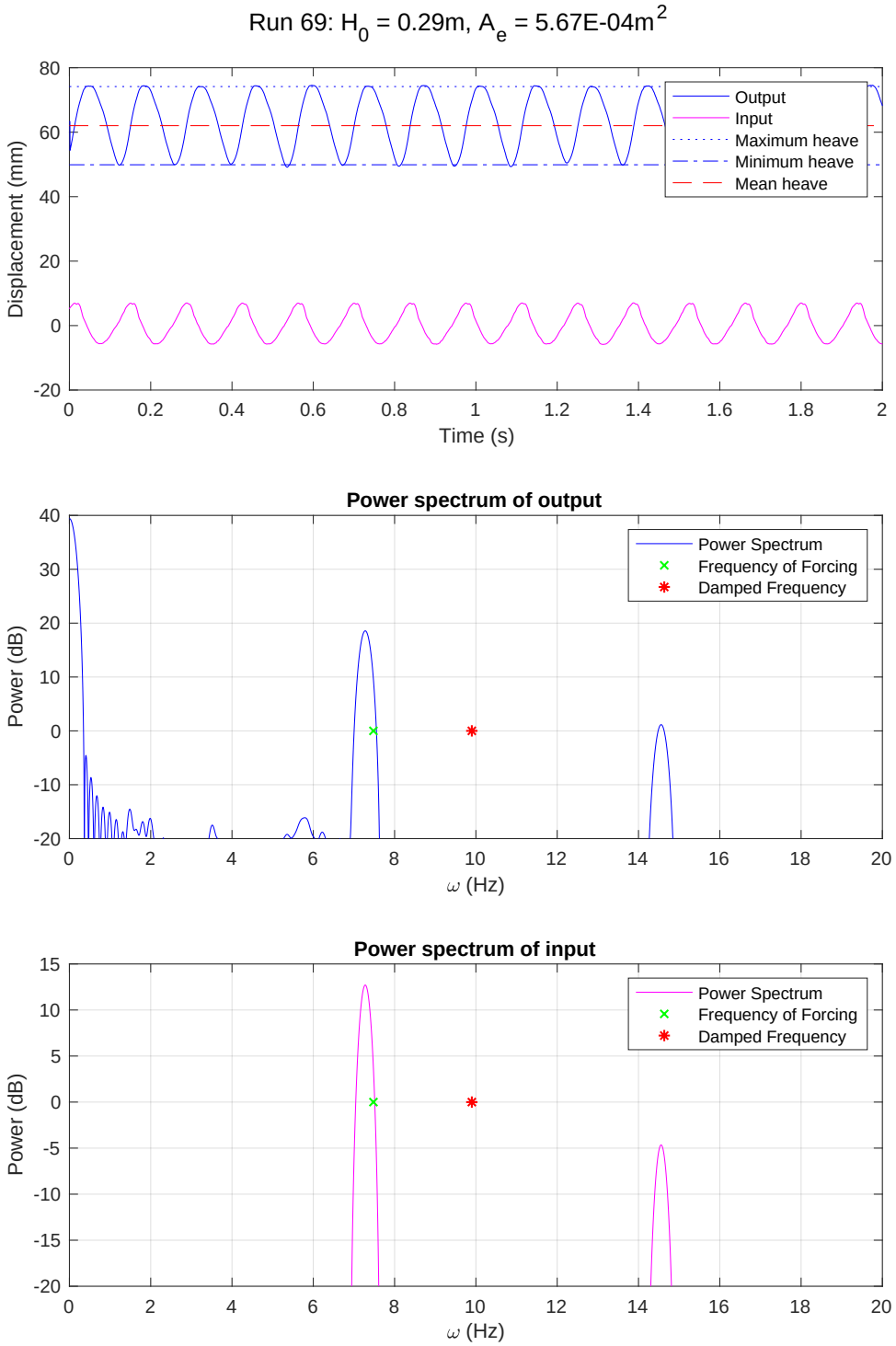


Figure H.18. Experimental trial data for Condition 69

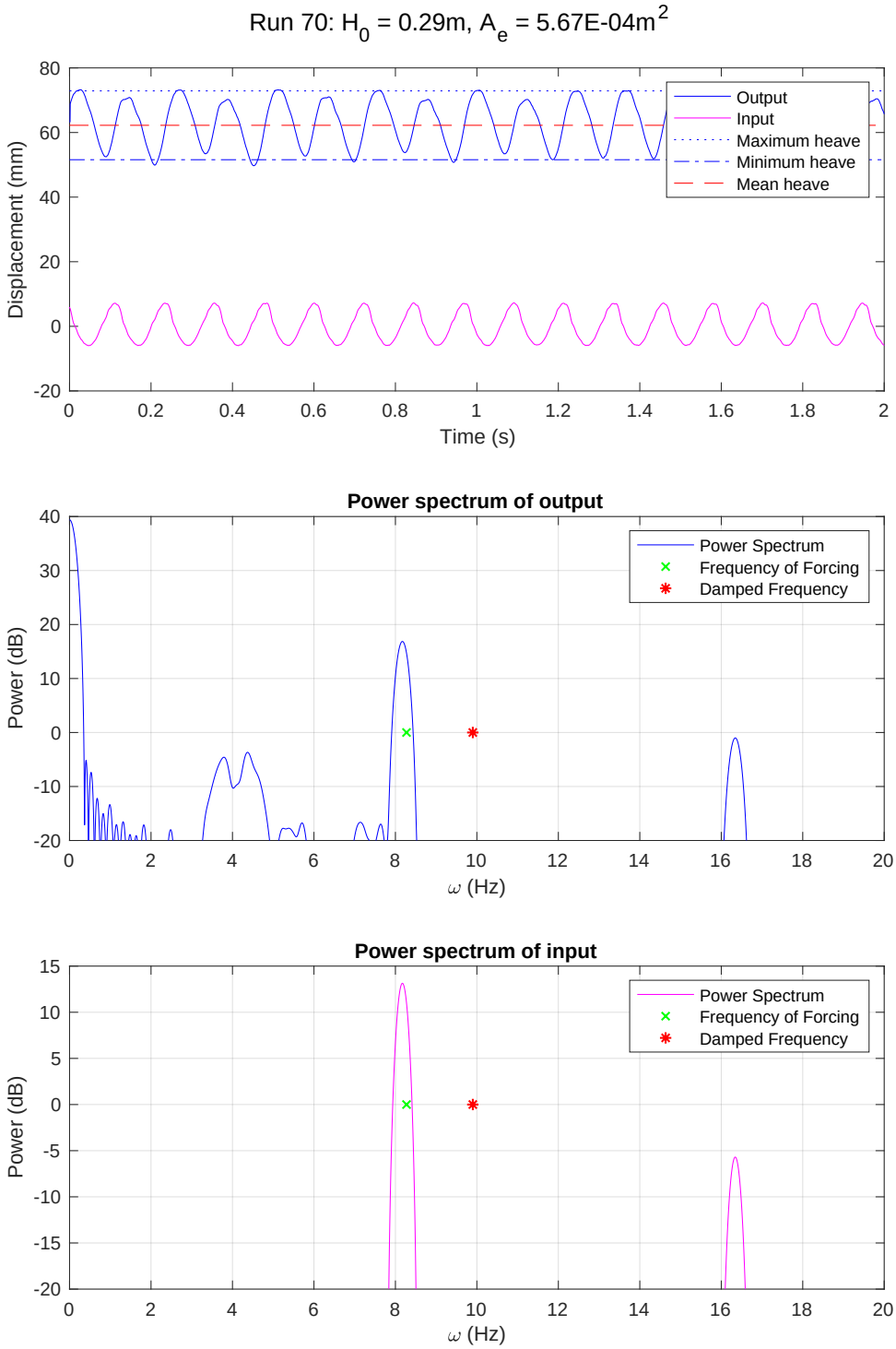


Figure H.19. Experimental trial data for Condition 70

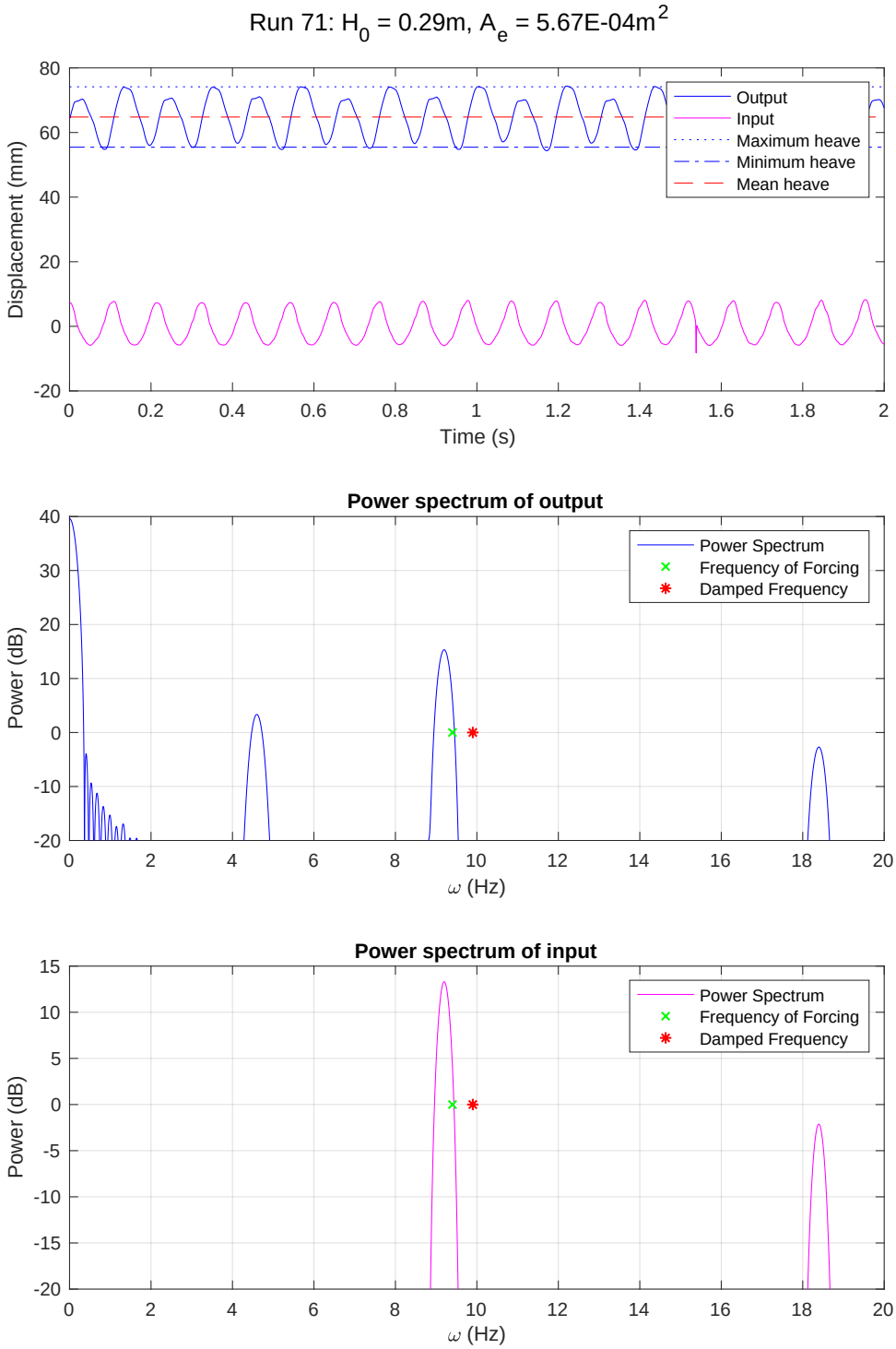


Figure H.20. Experimental trial data for Condition 71

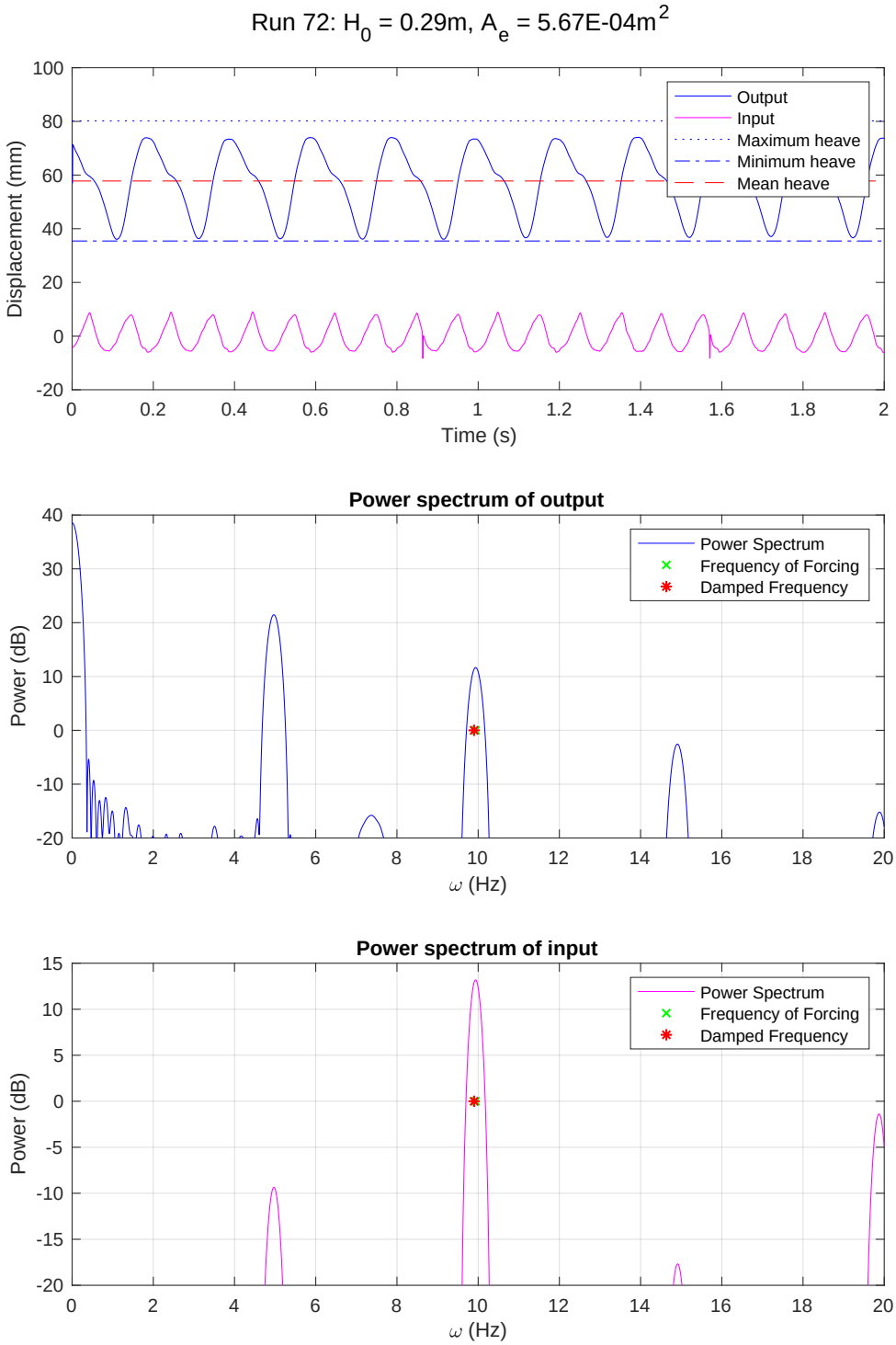


Figure H.21. Experimental trial data for Condition 72

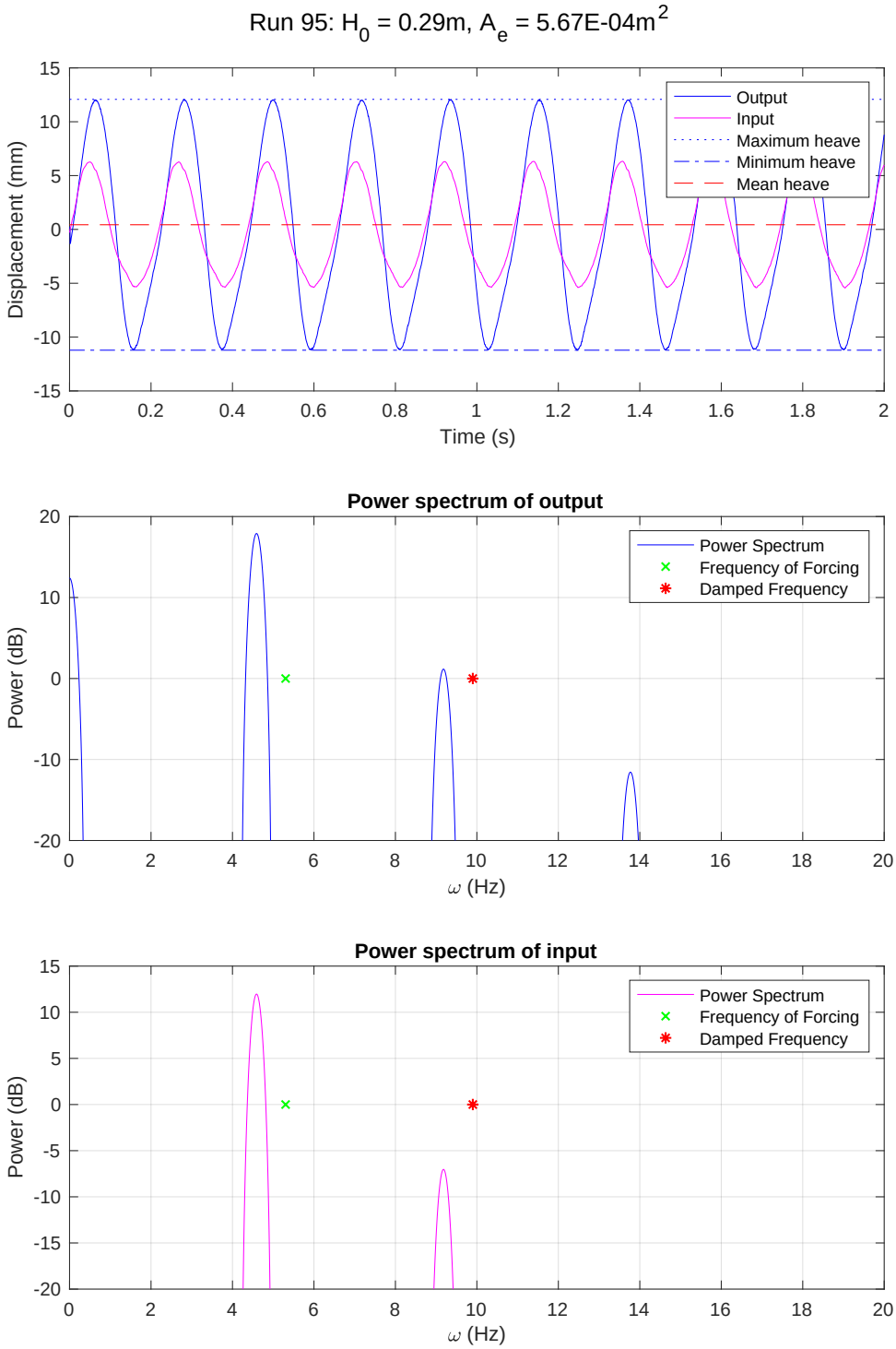


Figure H.22. Experimental trial data for Condition 95

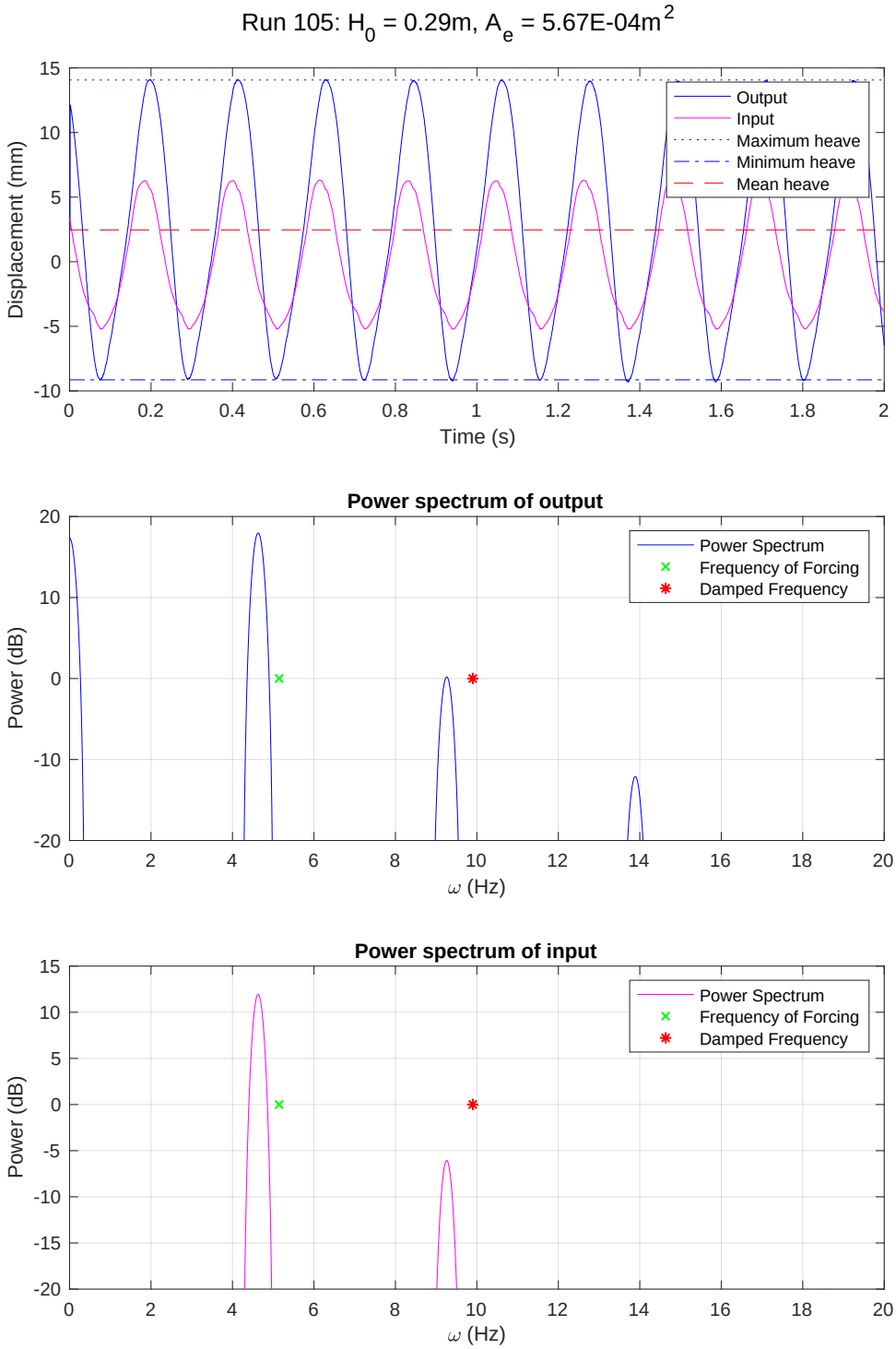


Figure H.23. Experimental trial data for Condition 105

H.2.2. Condition Two

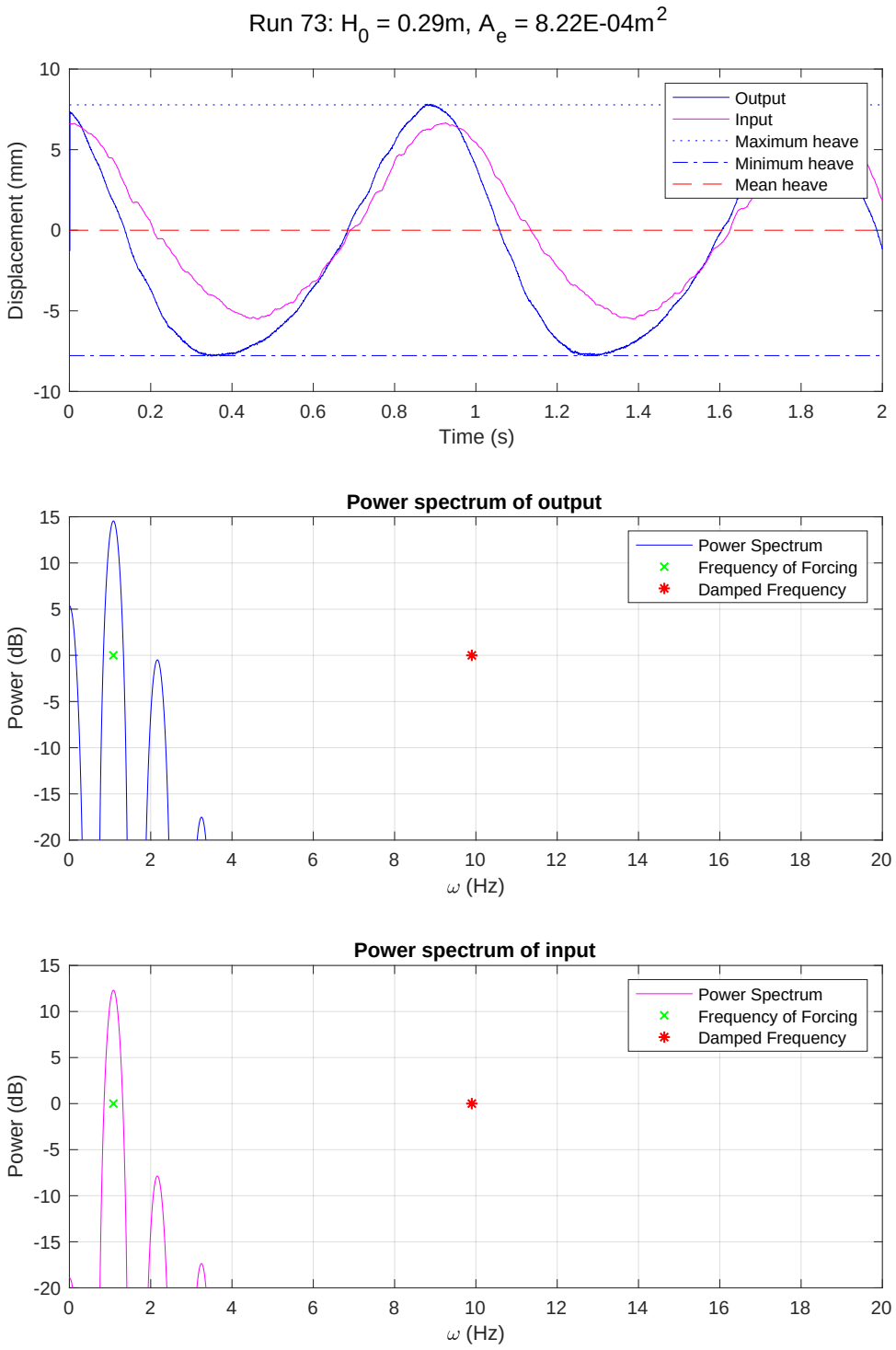


Figure H.24. Experimental trial data for Condition 73

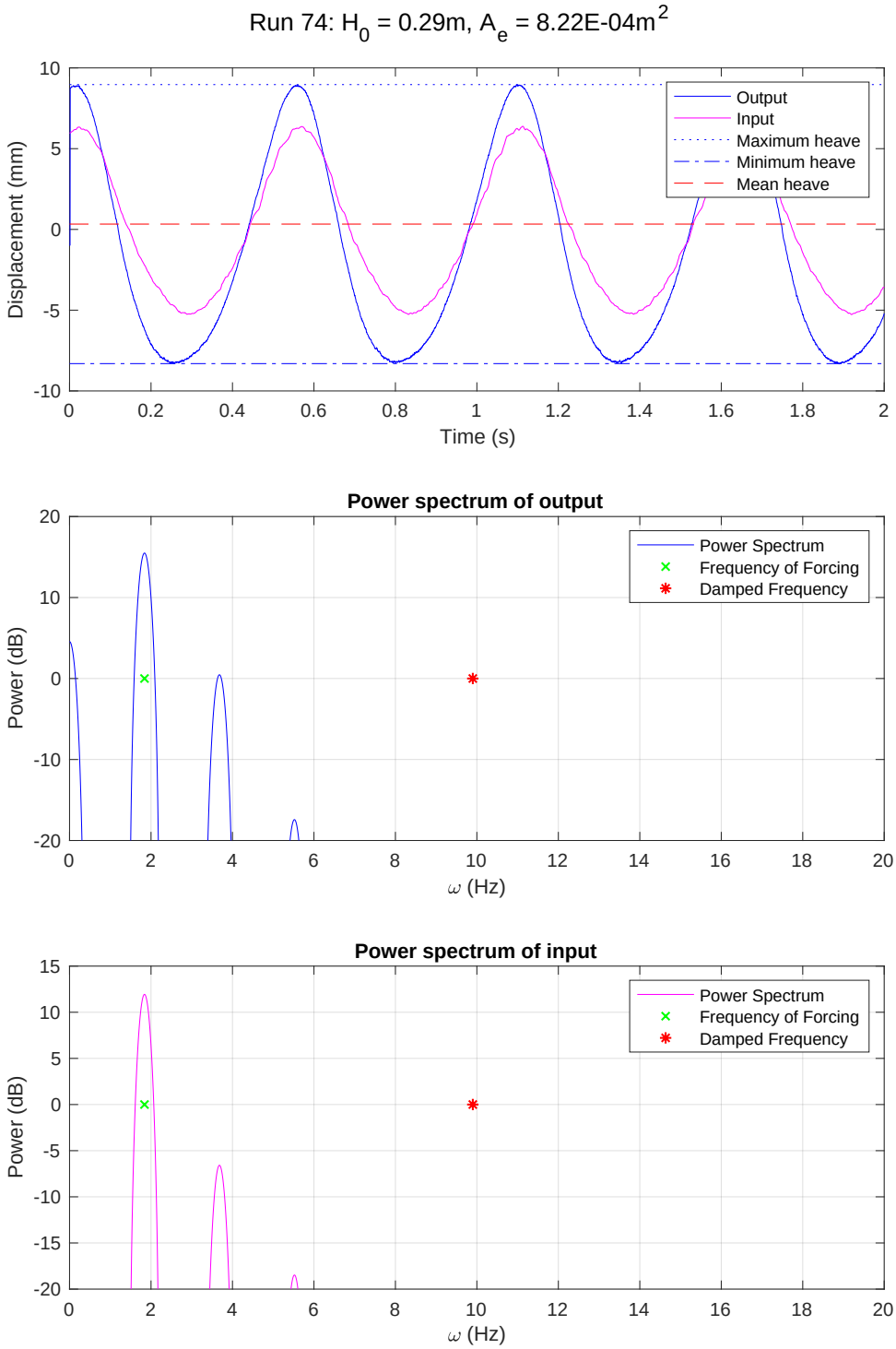


Figure H.25. Experimental trial data for Condition 74

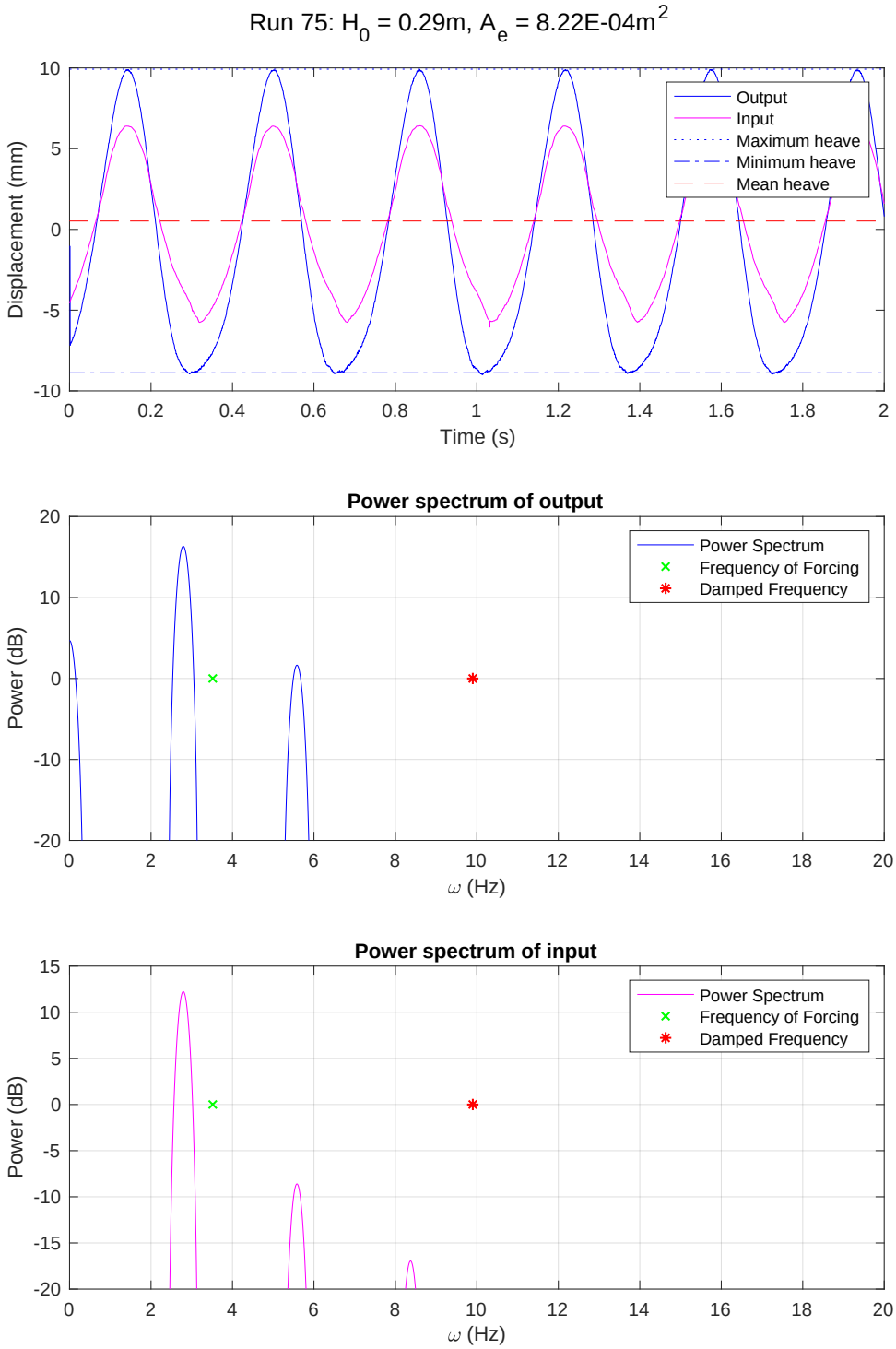


Figure H.26. Experimental trial data for Condition 75

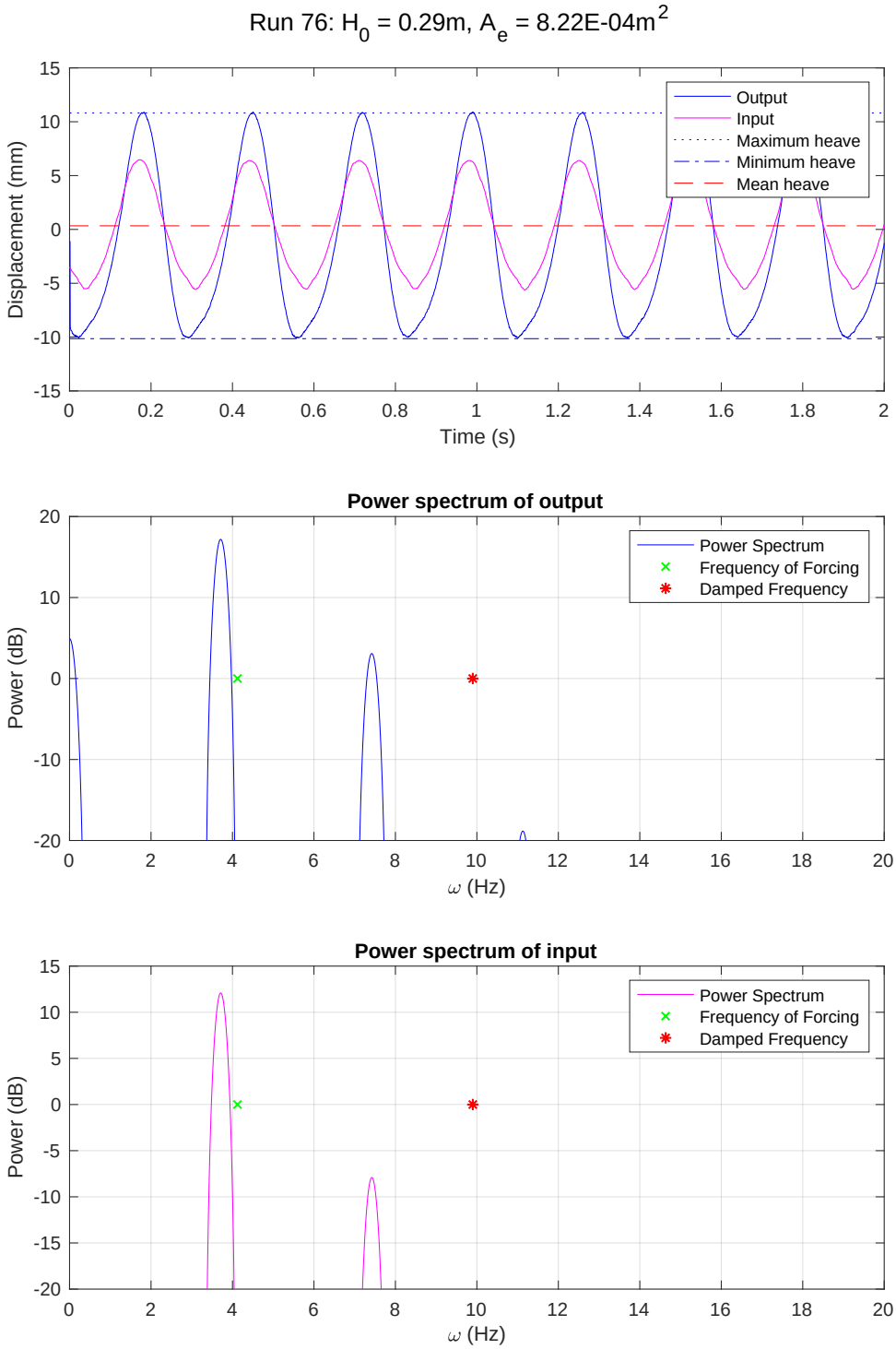


Figure H.27. Experimental trial data for Condition 76

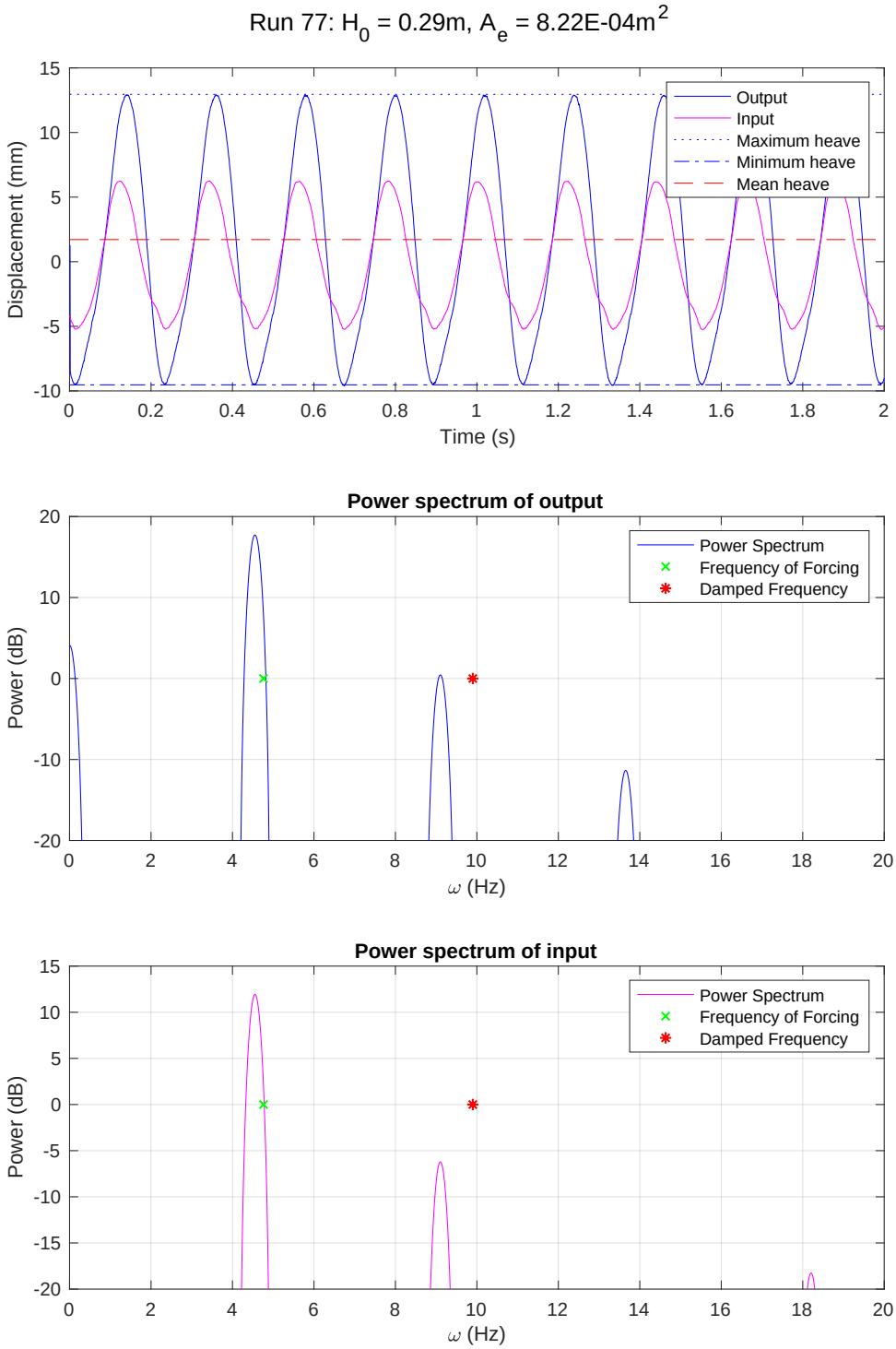


Figure H.28. Experimental trial data for Condition 77

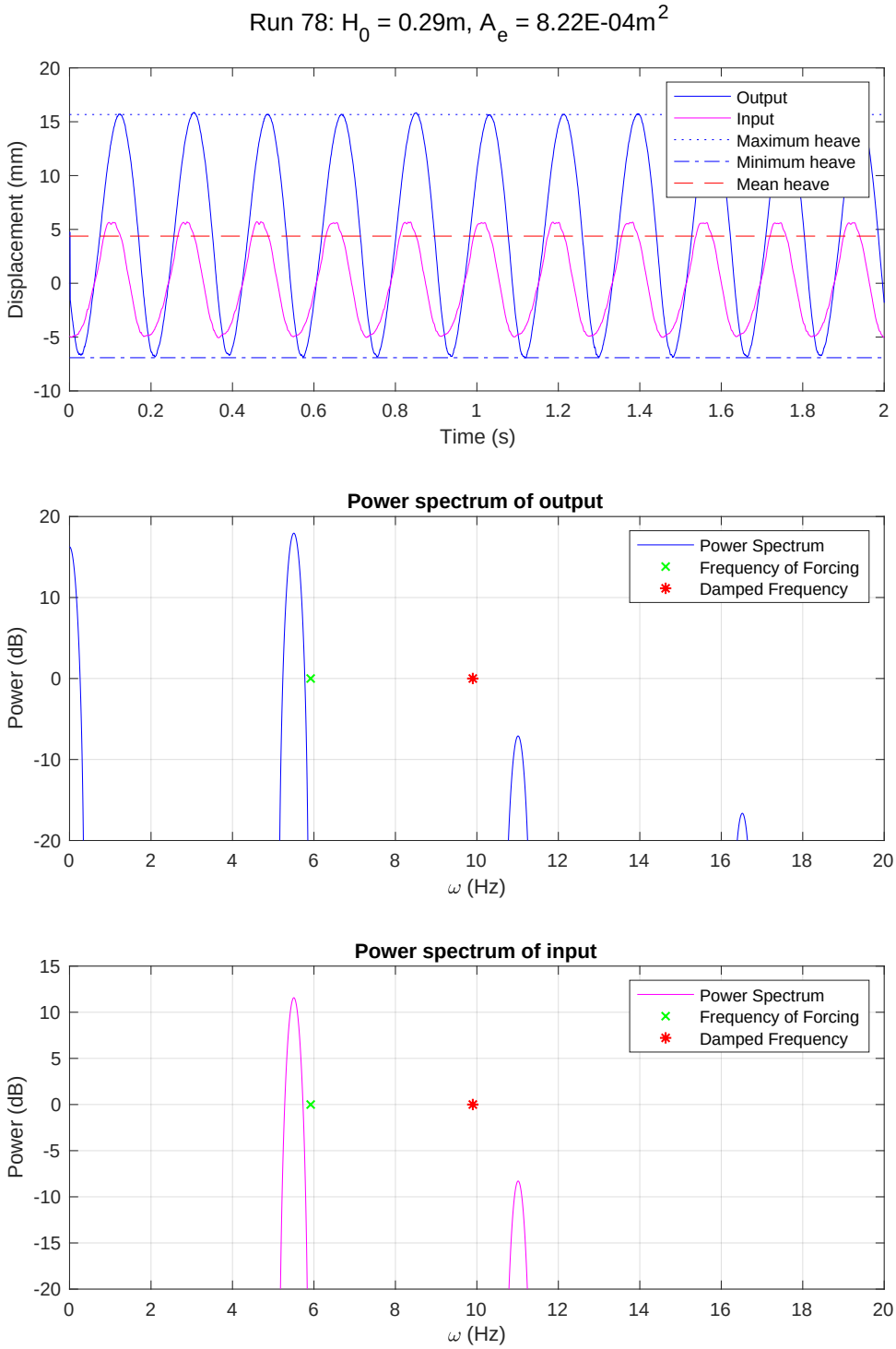


Figure H.29. Experimental trial data for Condition 78

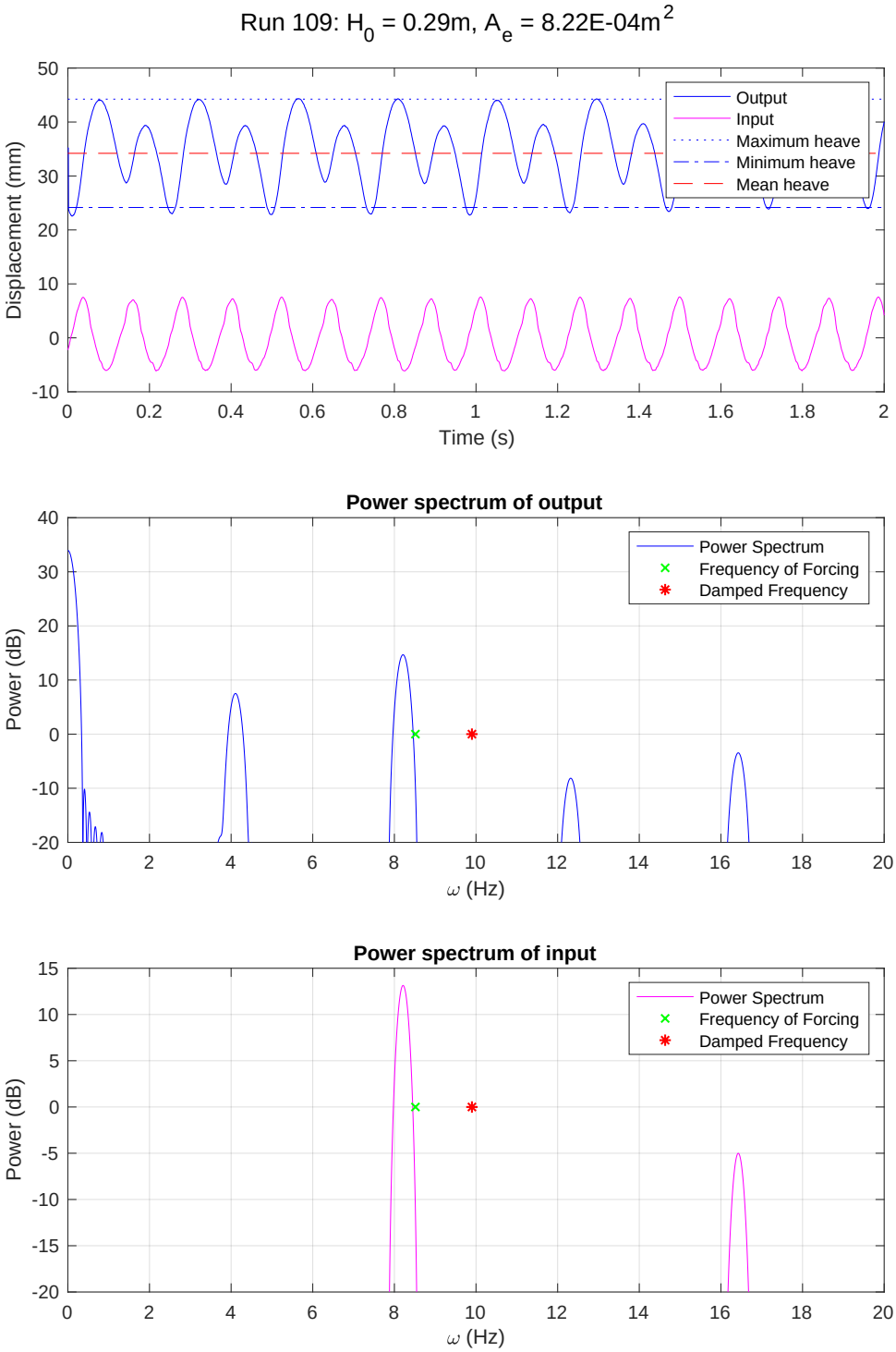


Figure H.30. Experimental trial data for Condition 109

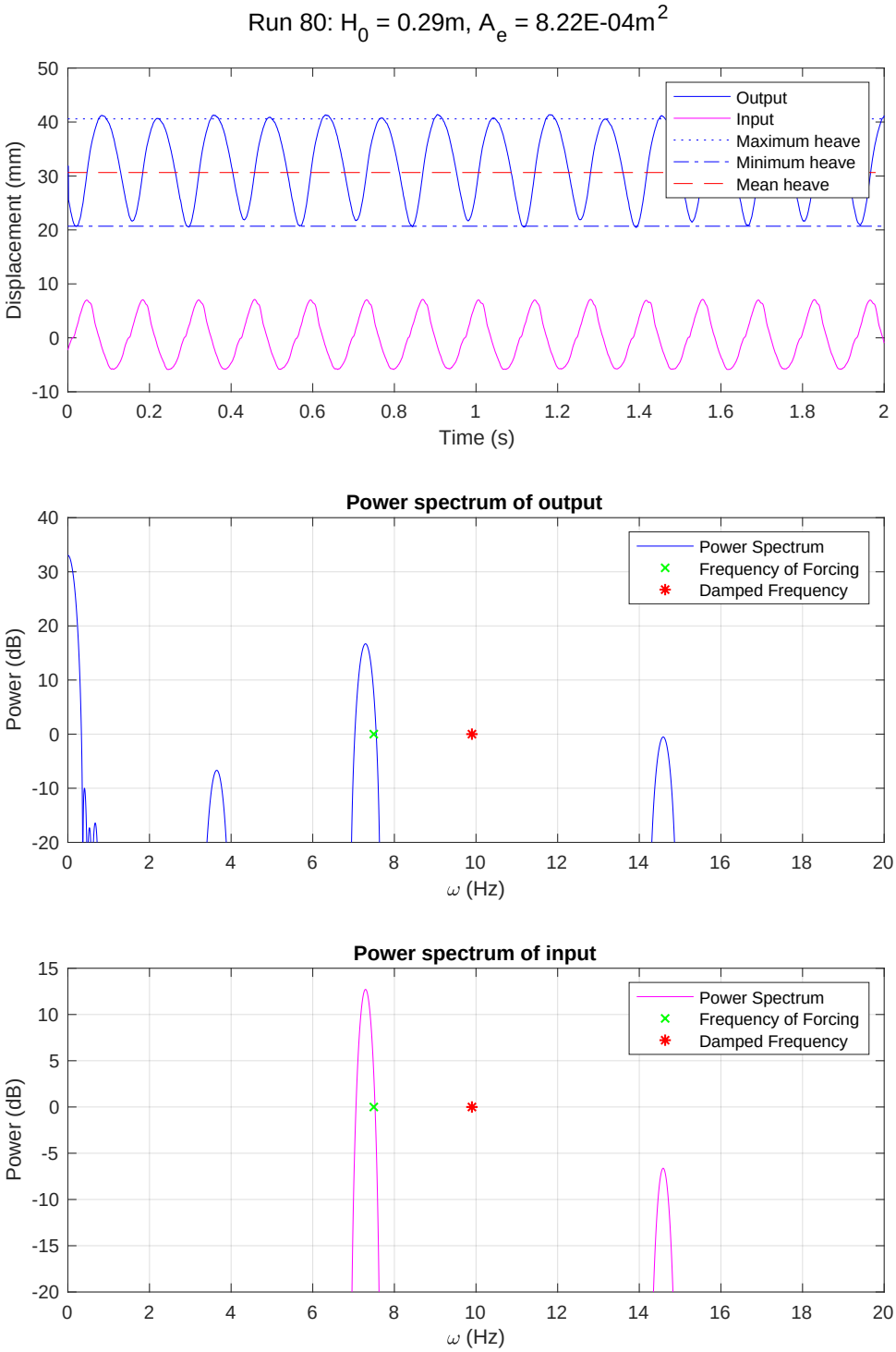


Figure H.31. Experimental trial data for Condition 80

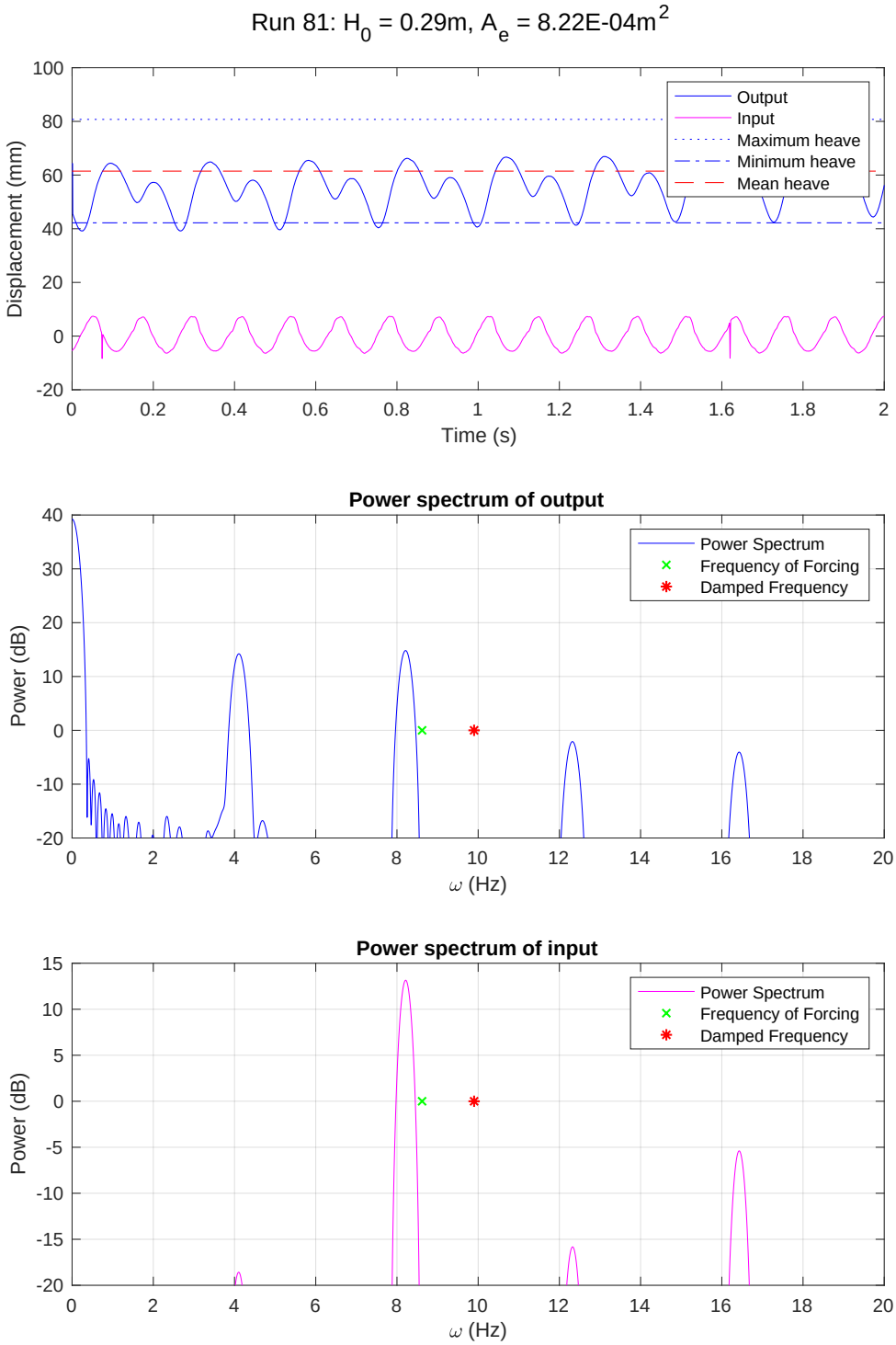


Figure H.32. Experimental trial data for Condition 81

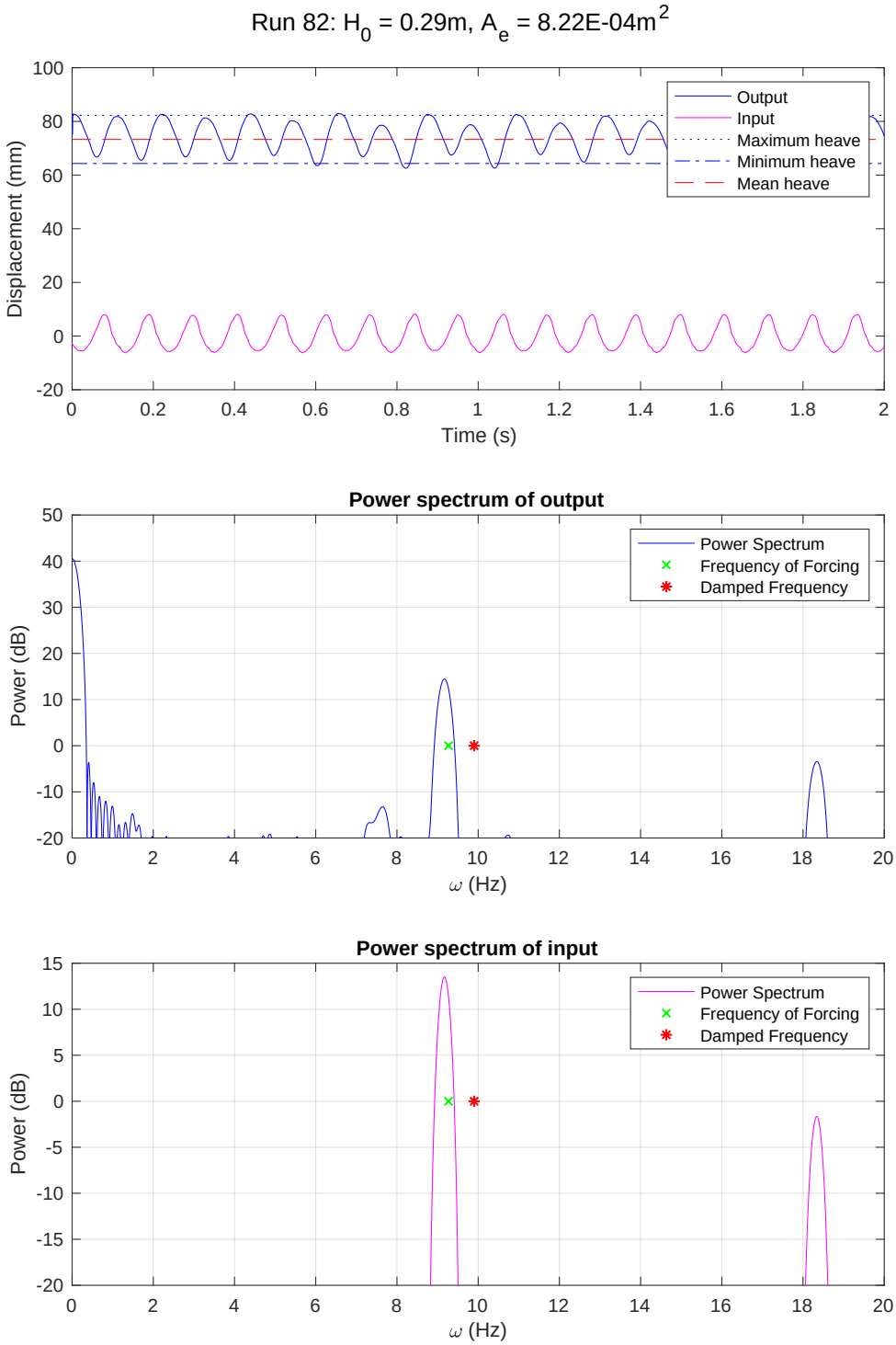


Figure H.33. Experimental trial data for Condition 82

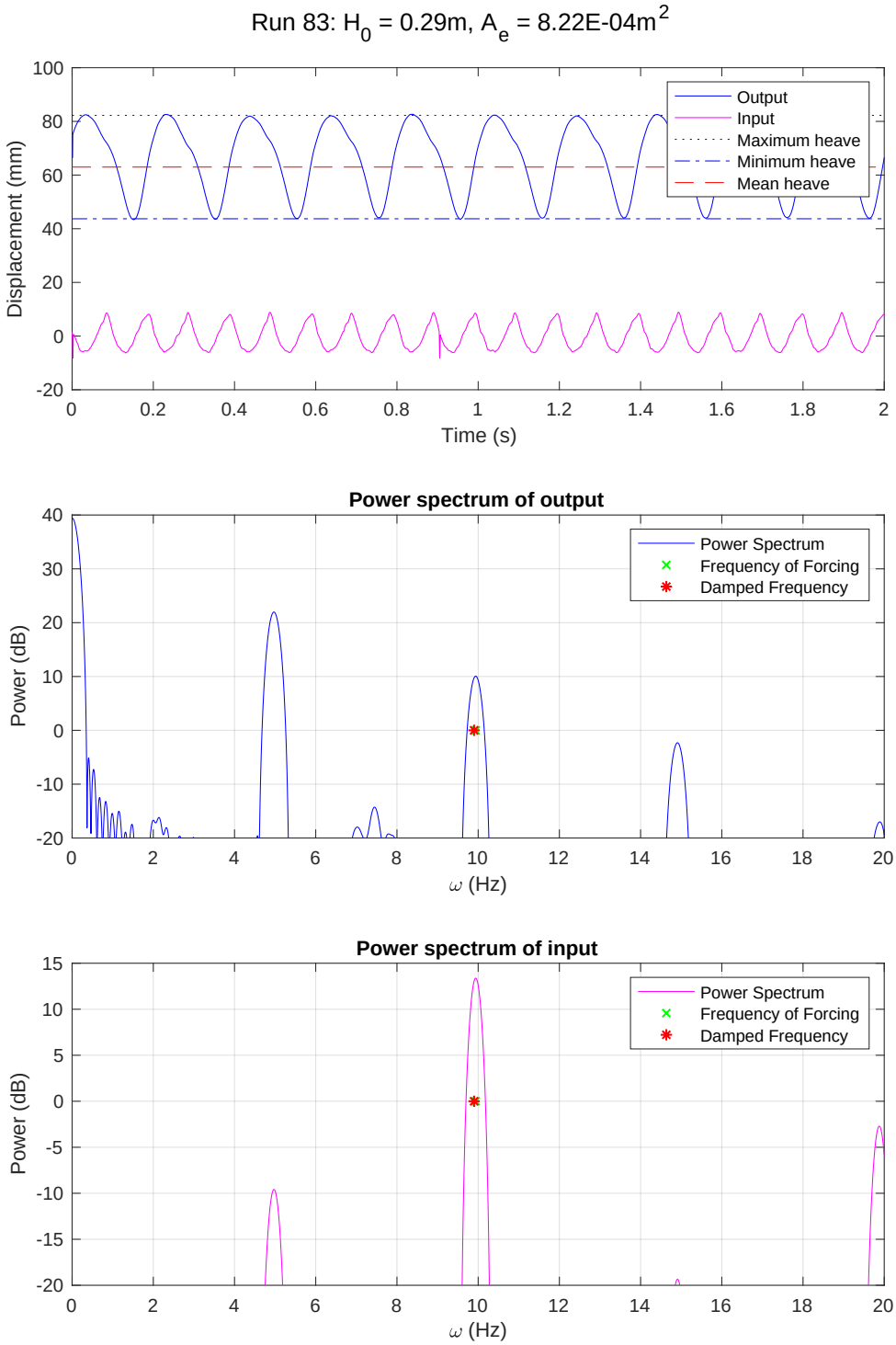


Figure H.34. Experimental trial data for Condition 83

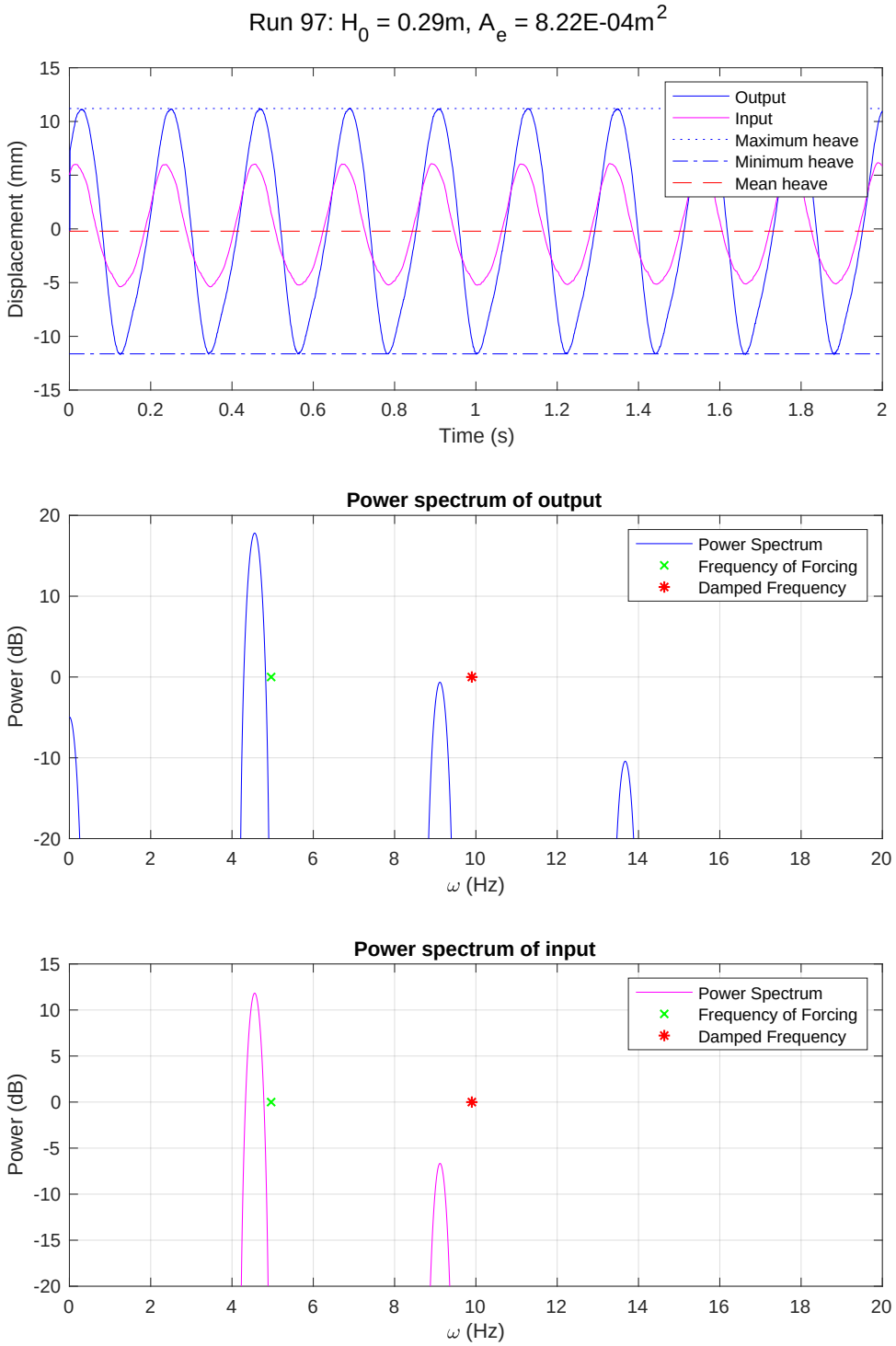


Figure H.35. Experimental trial data for Condition 97

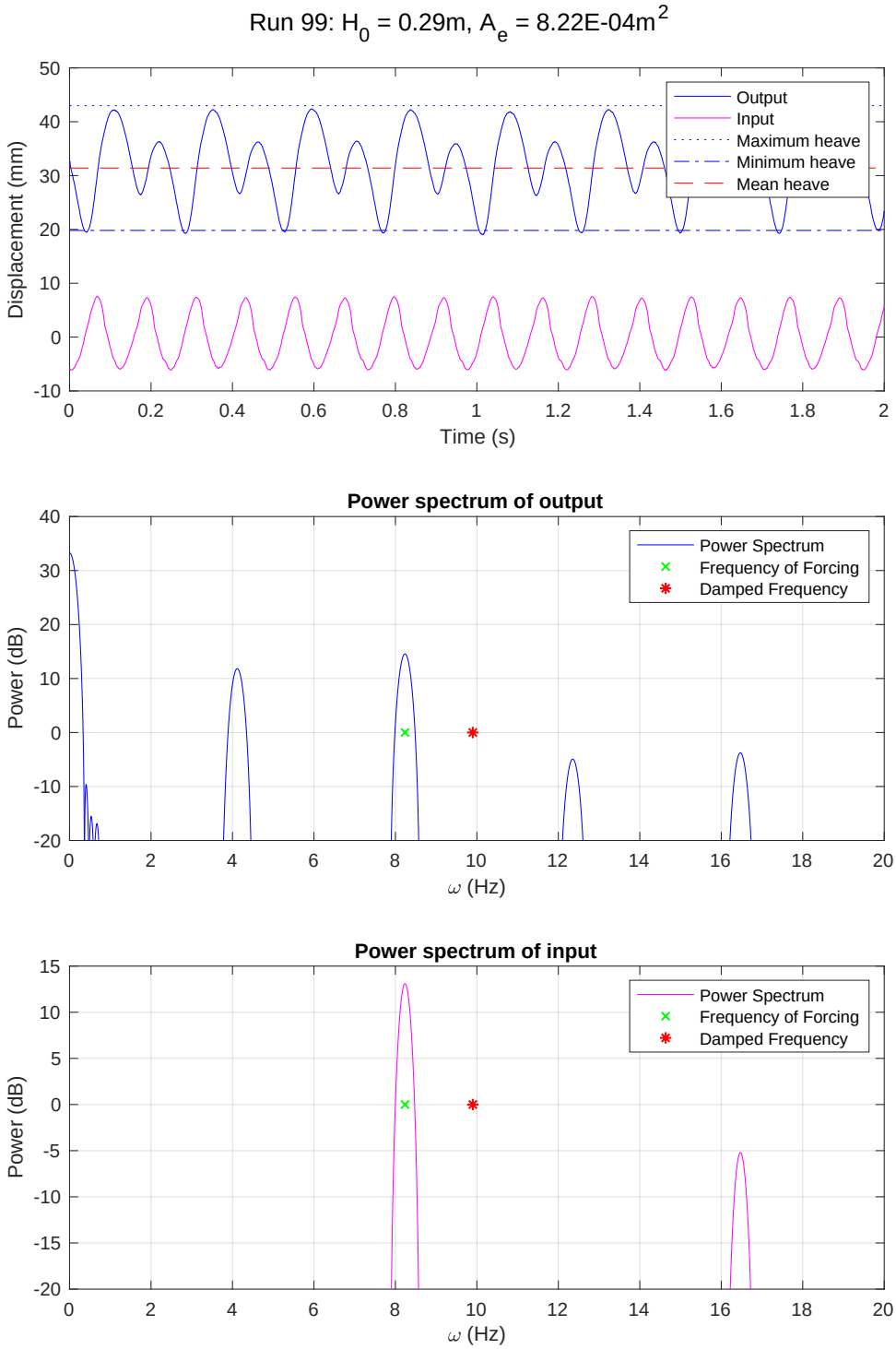


Figure H.36. Experimental trial data for Condition 99

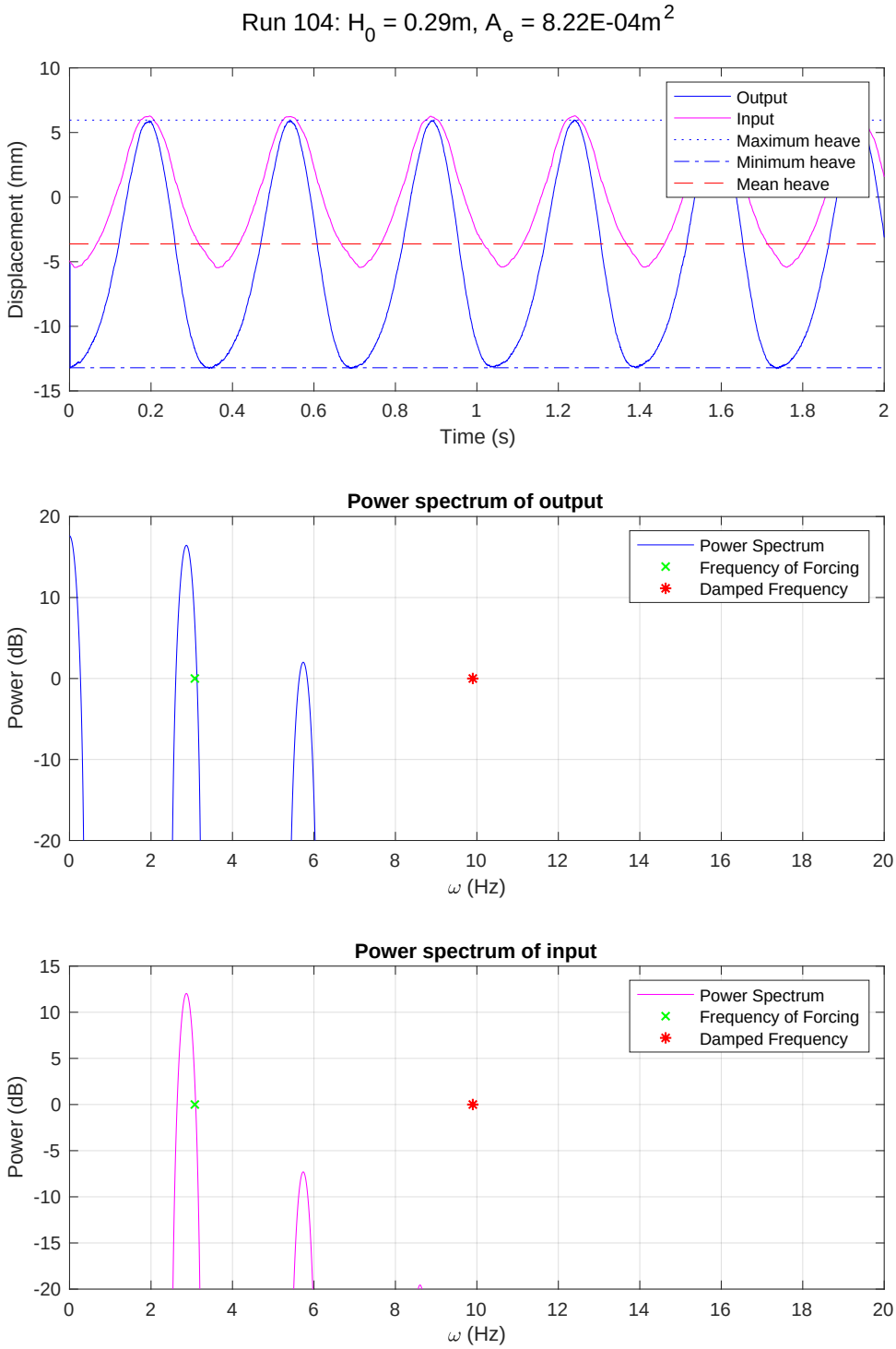


Figure H.37. Experimental trial data for Condition 104

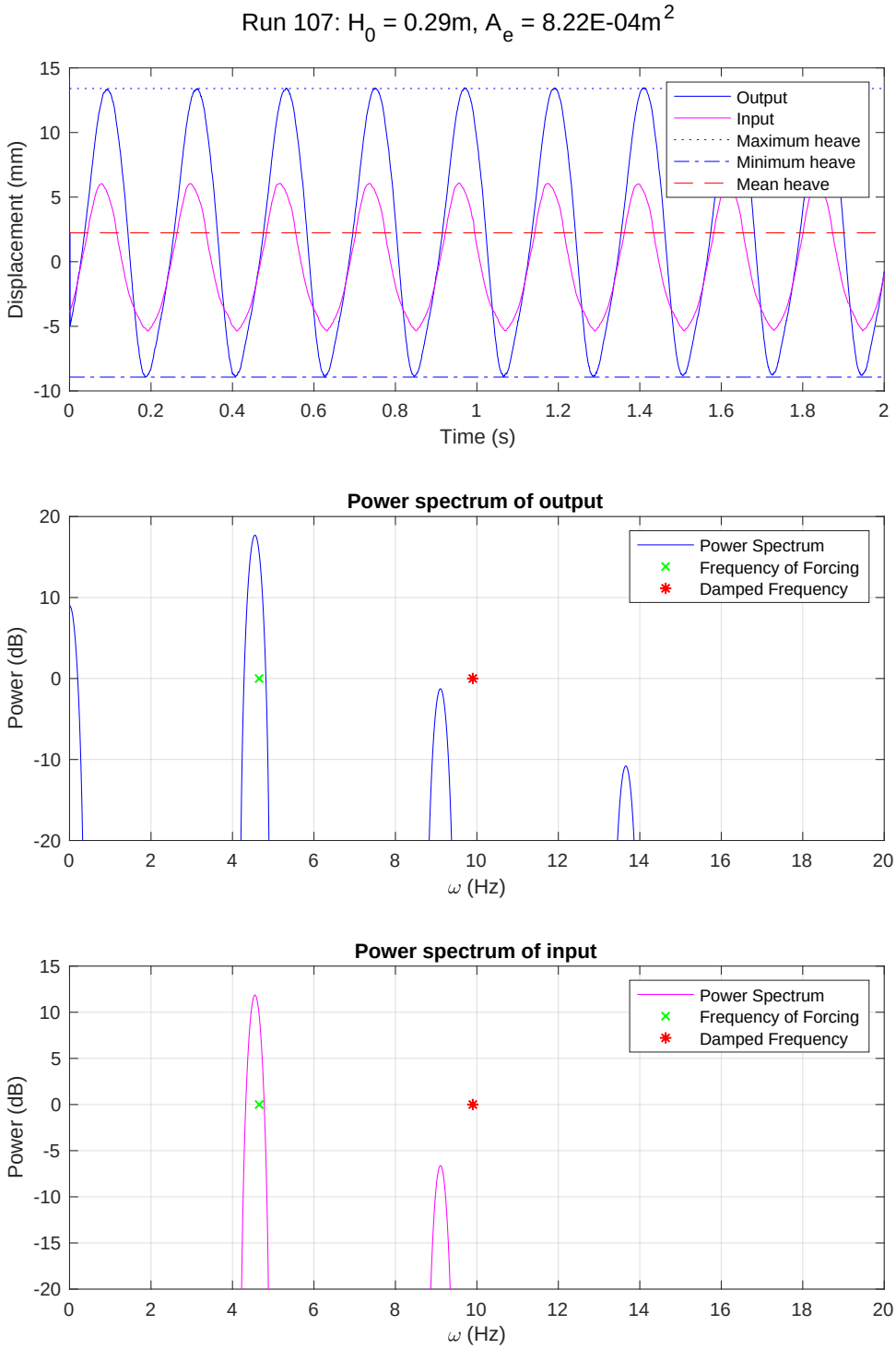


Figure H.38. Experimental trial data for Condition 107

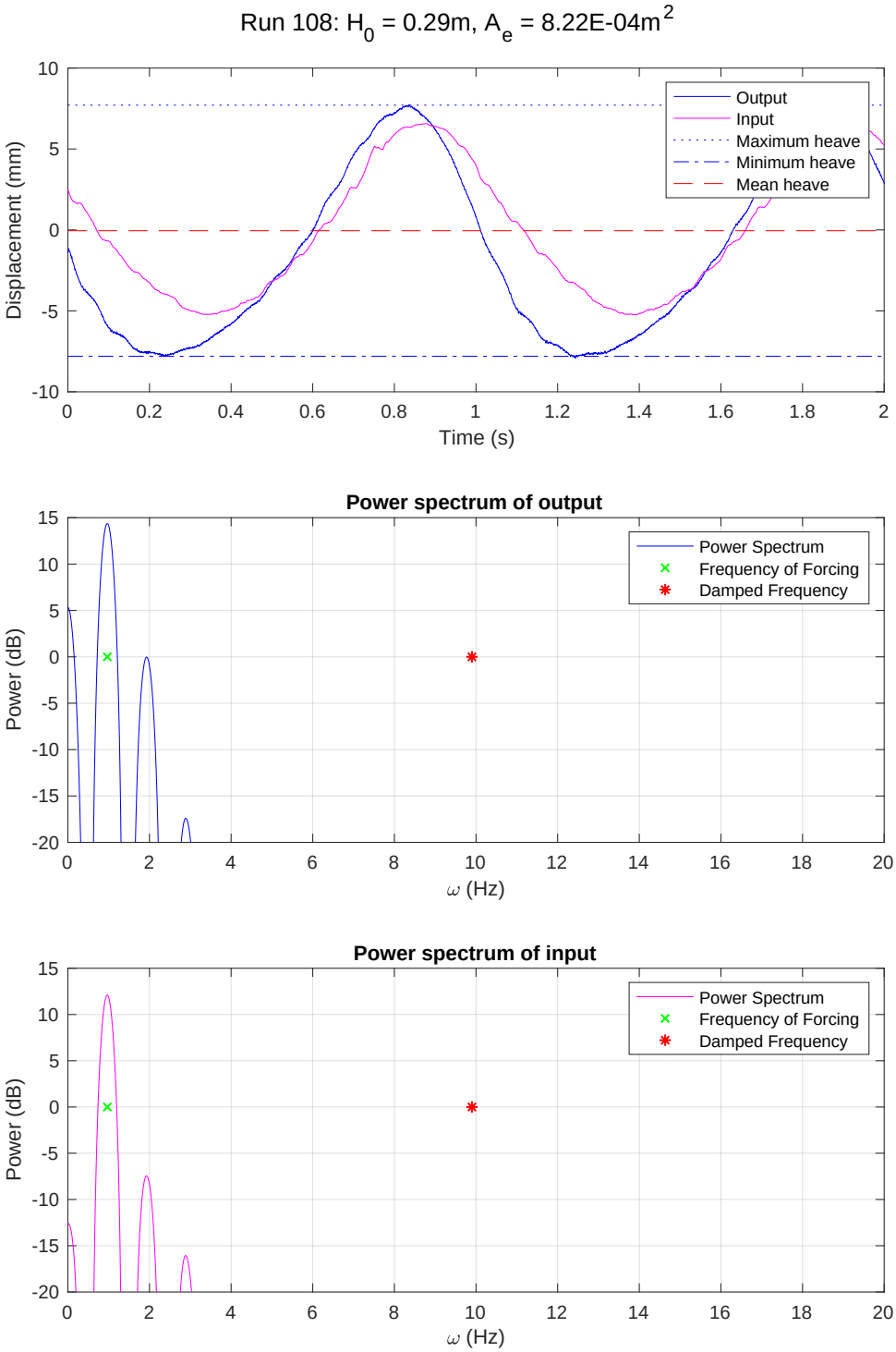


Figure H.39. Experimental trial data for Condition 108

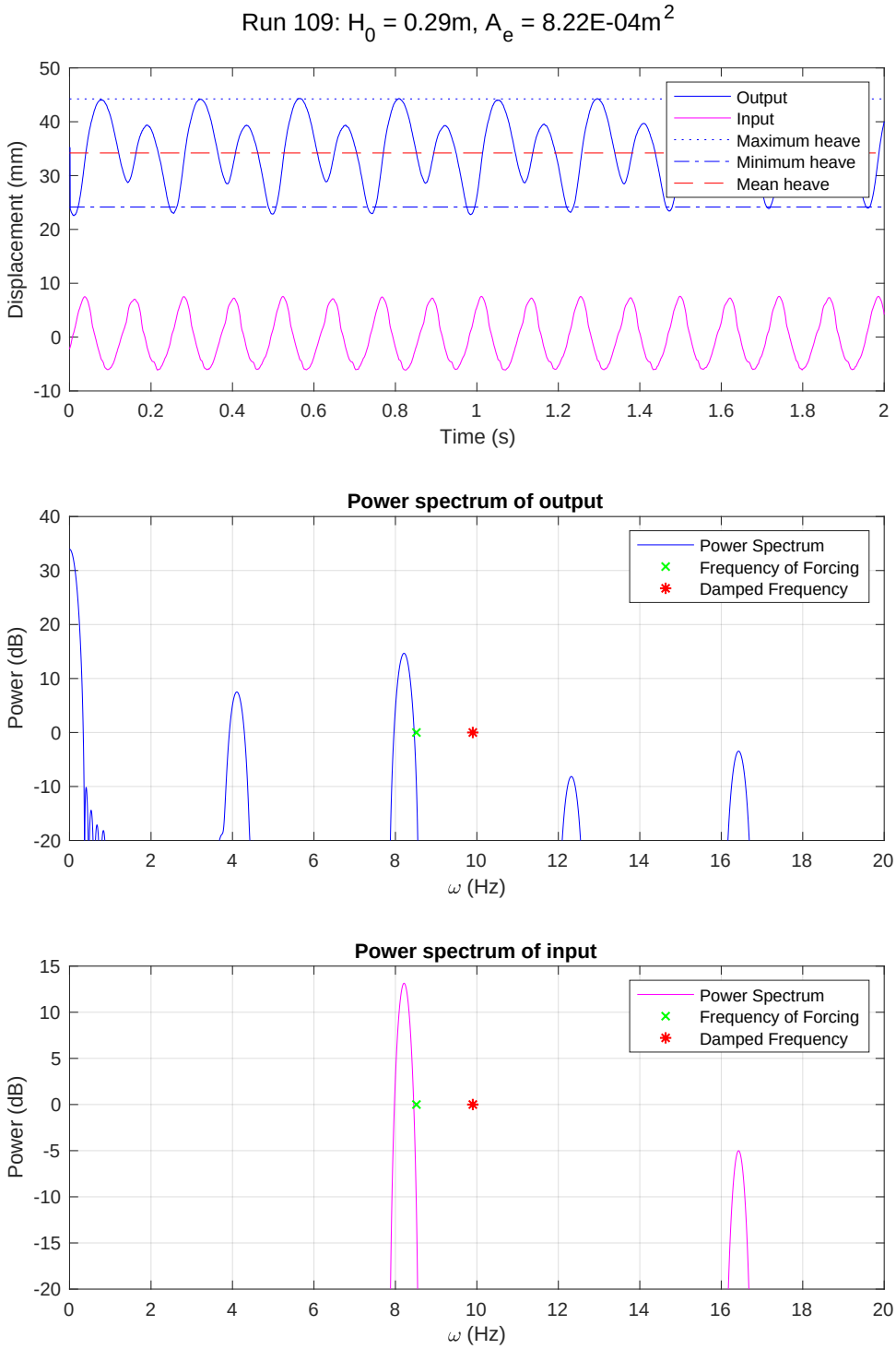


Figure H.40. Experimental trial data for Condition 109

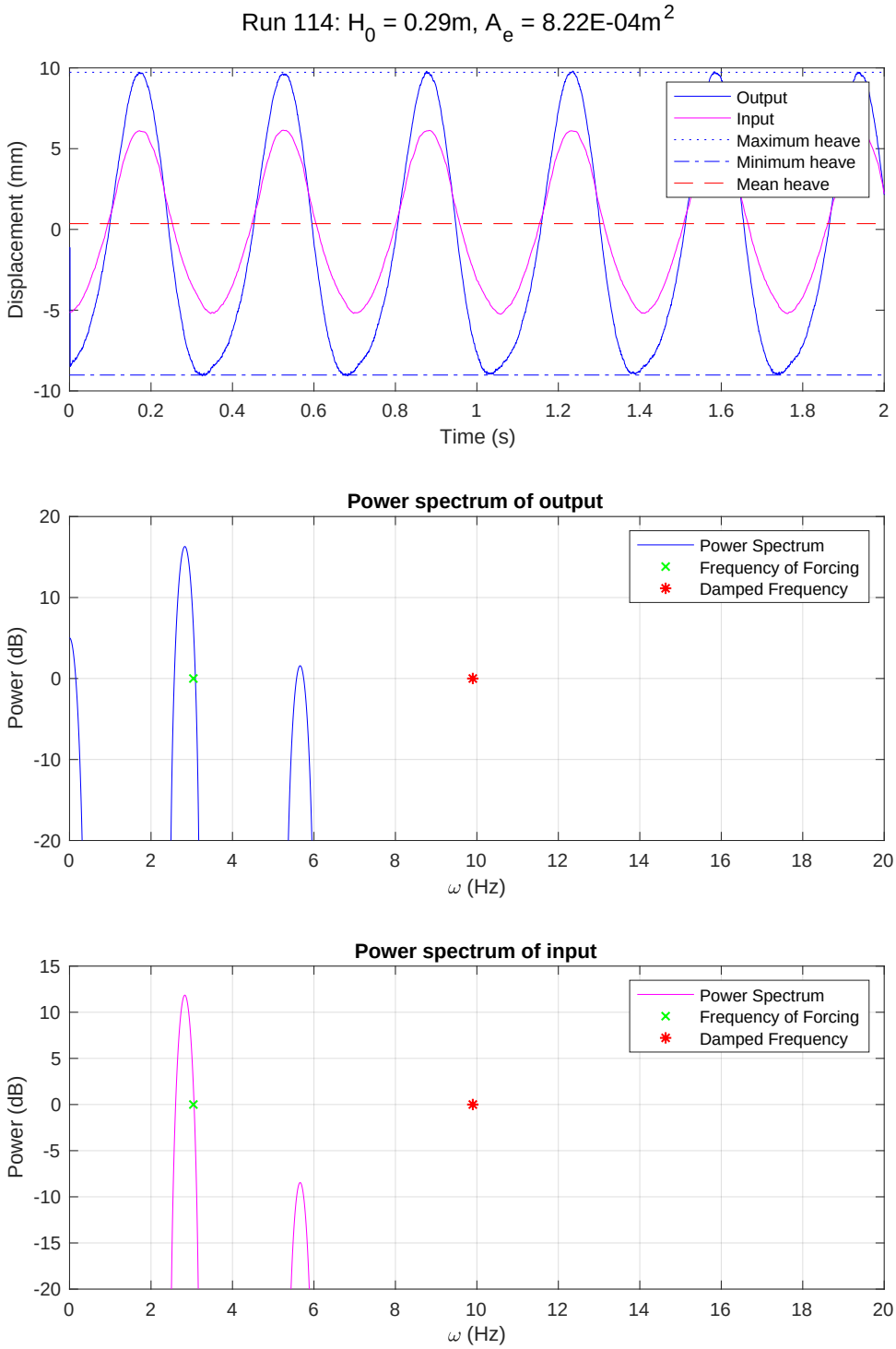


Figure H.41. Experimental trial data for Condition 114

H.2.3. Condition Three

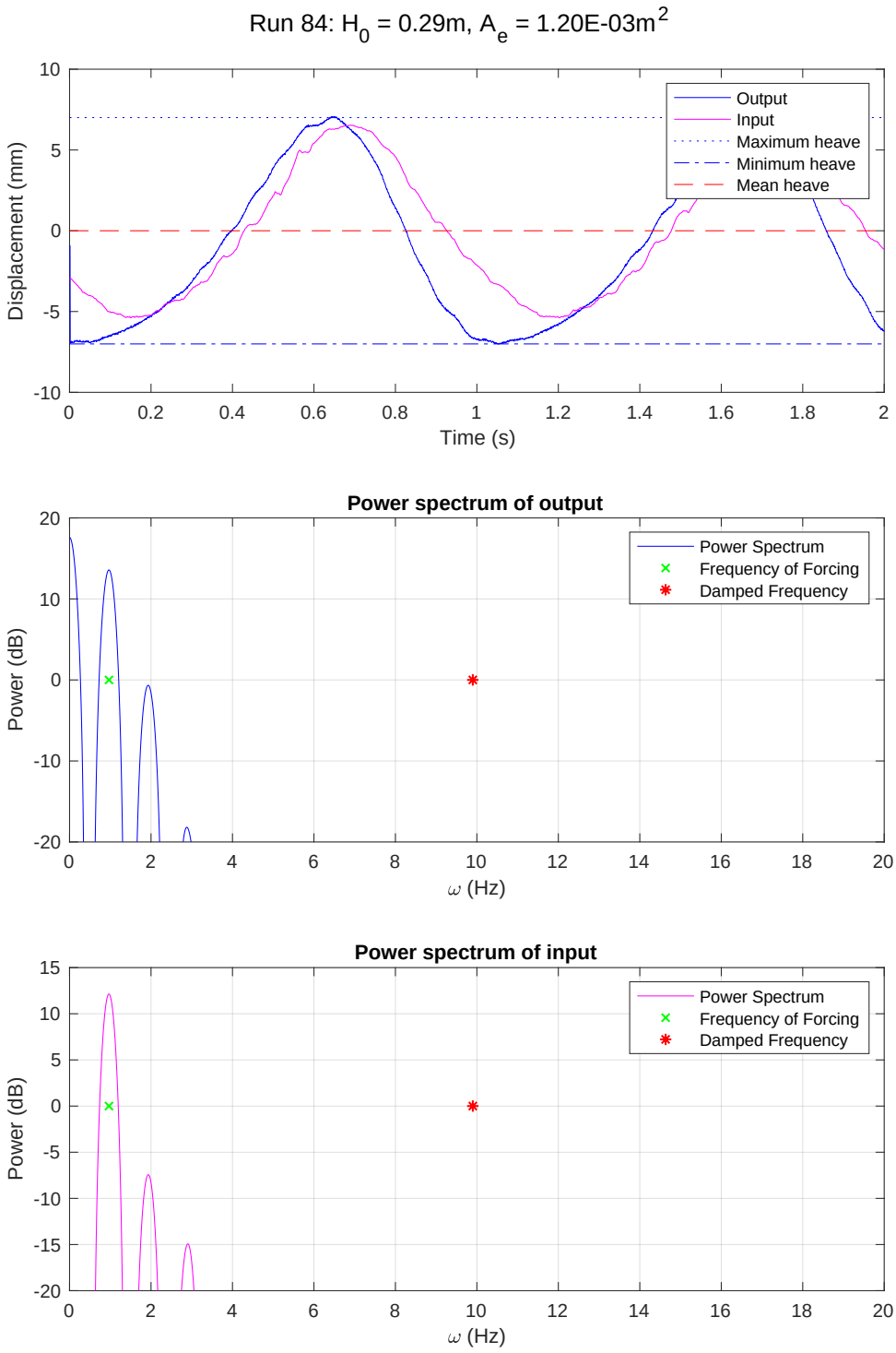


Figure H.42. Experimental trial data for Condition 84

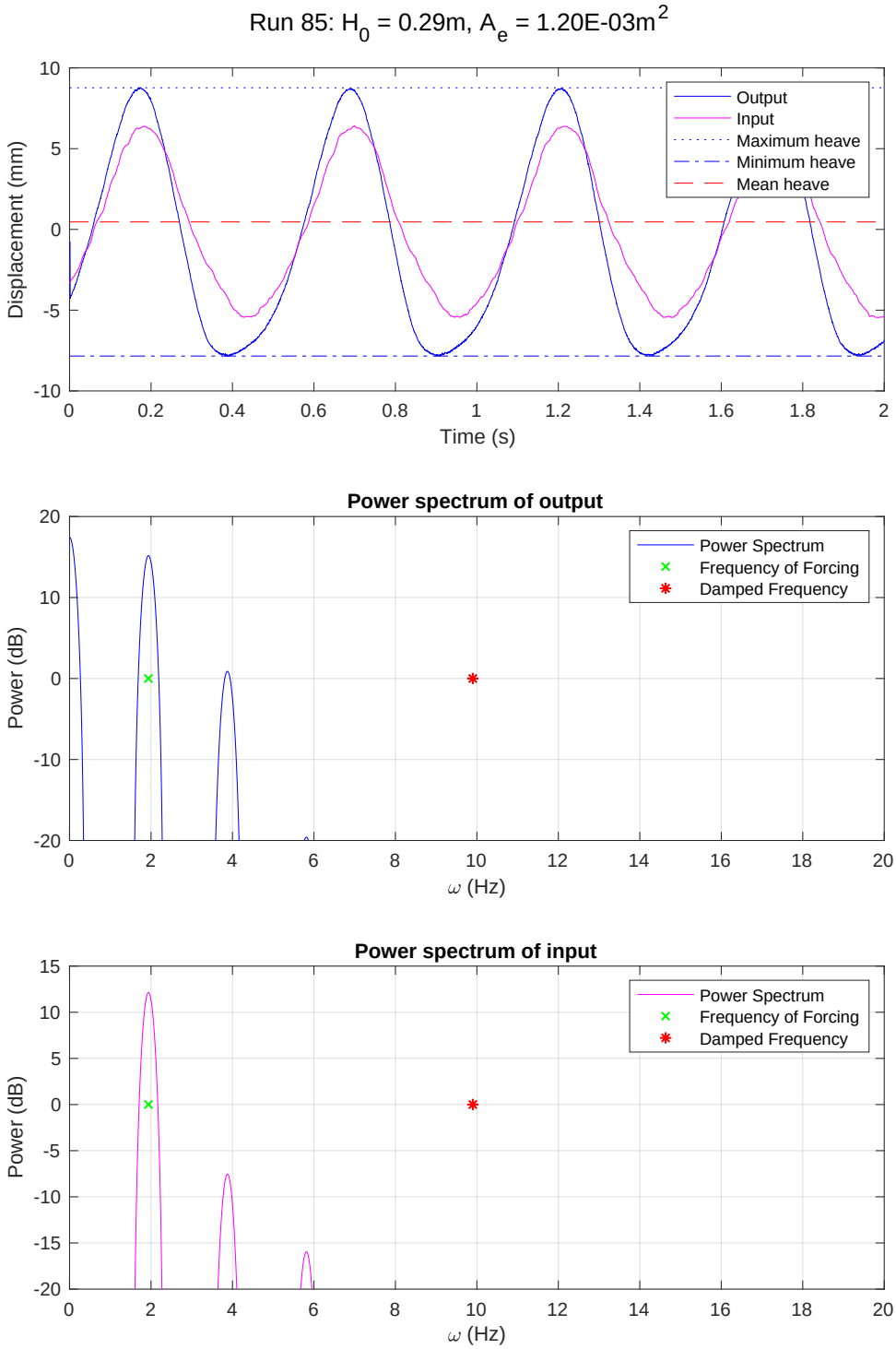


Figure H.43. Experimental trial data for Condition 85

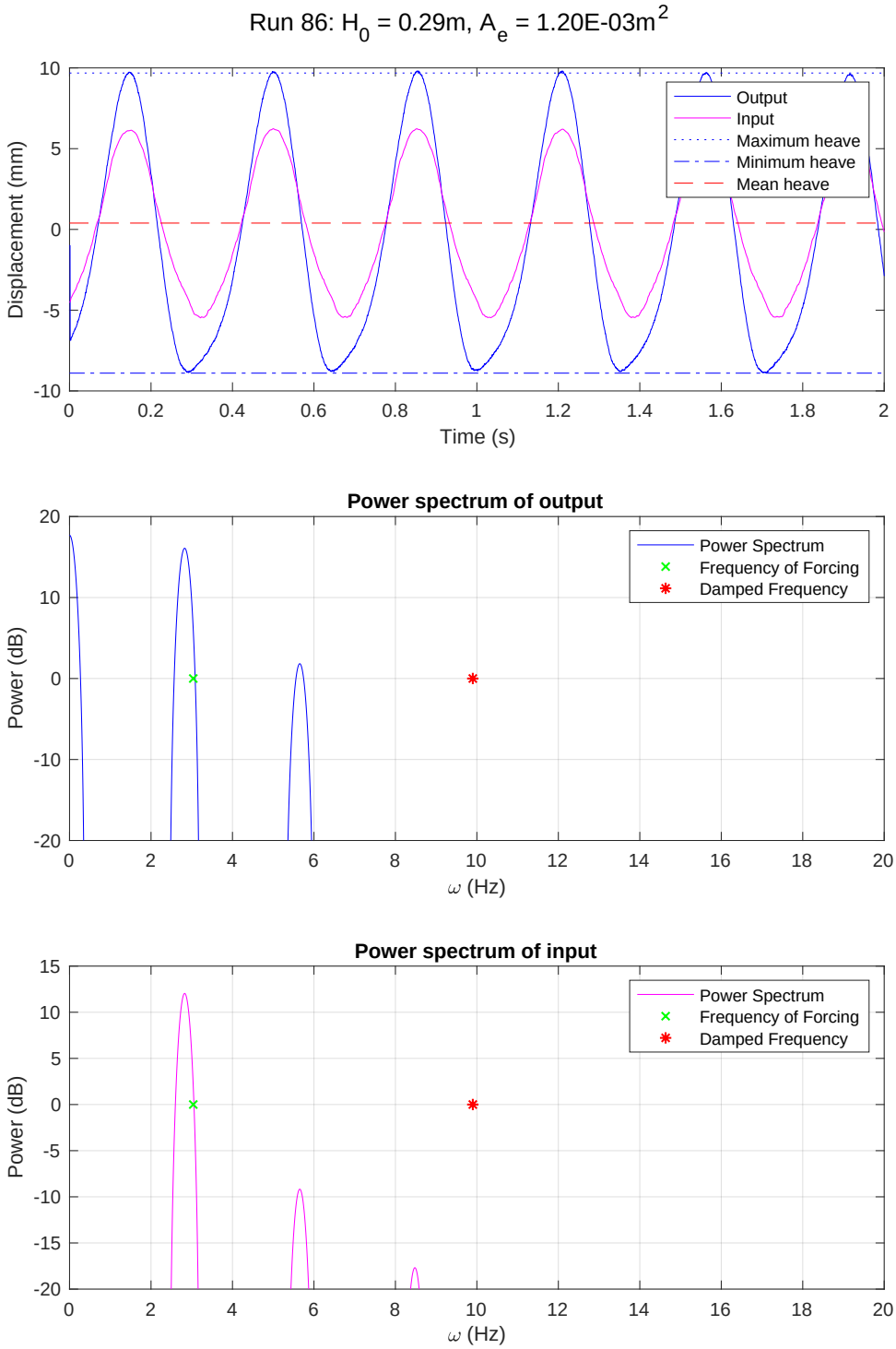


Figure H.44. Experimental trial data for Condition 86

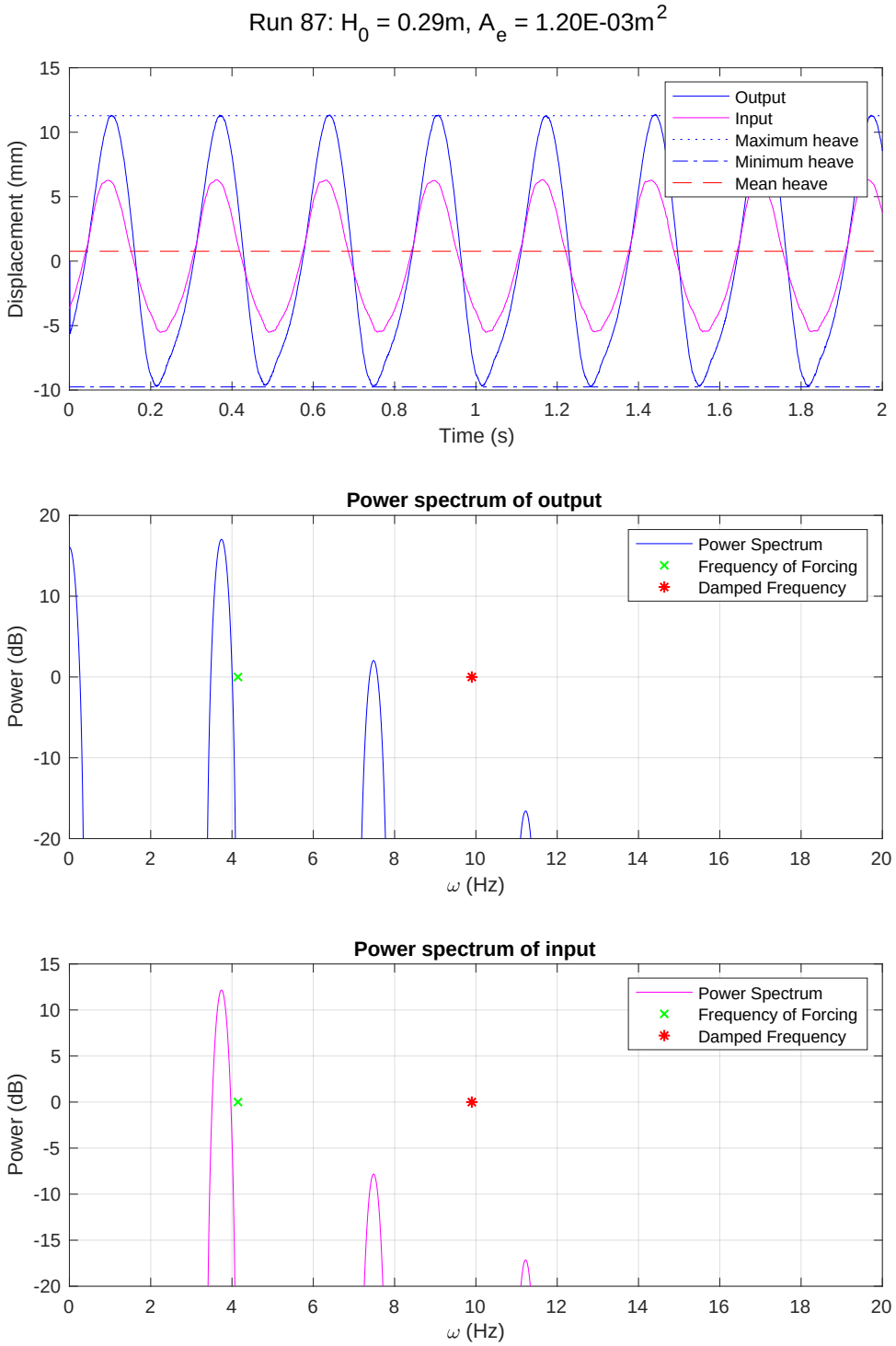


Figure H.45. Experimental trial data for Condition 87

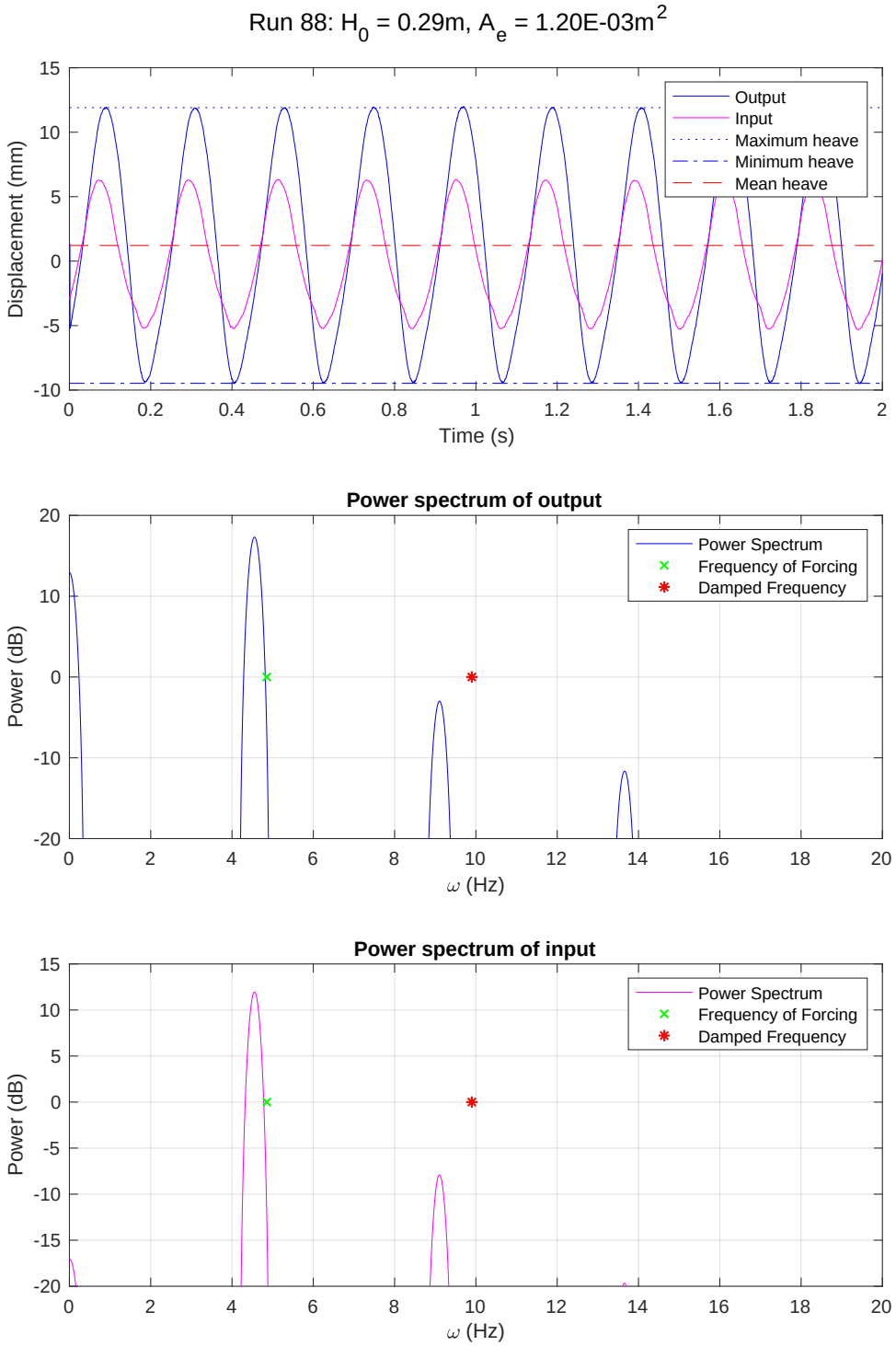


Figure H.46. Experimental trial data for Condition 88

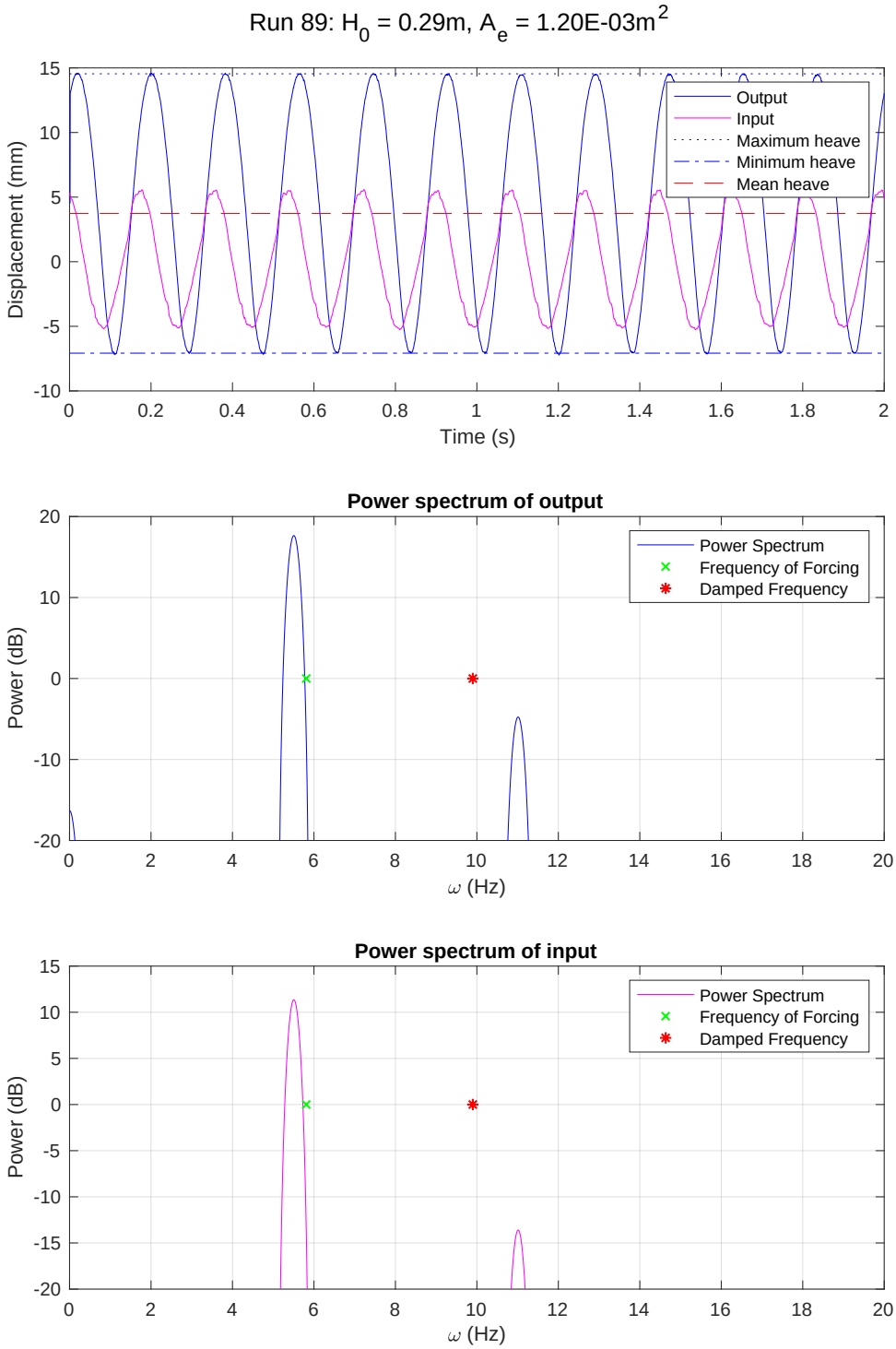


Figure H.47. Experimental trial data for Condition 89

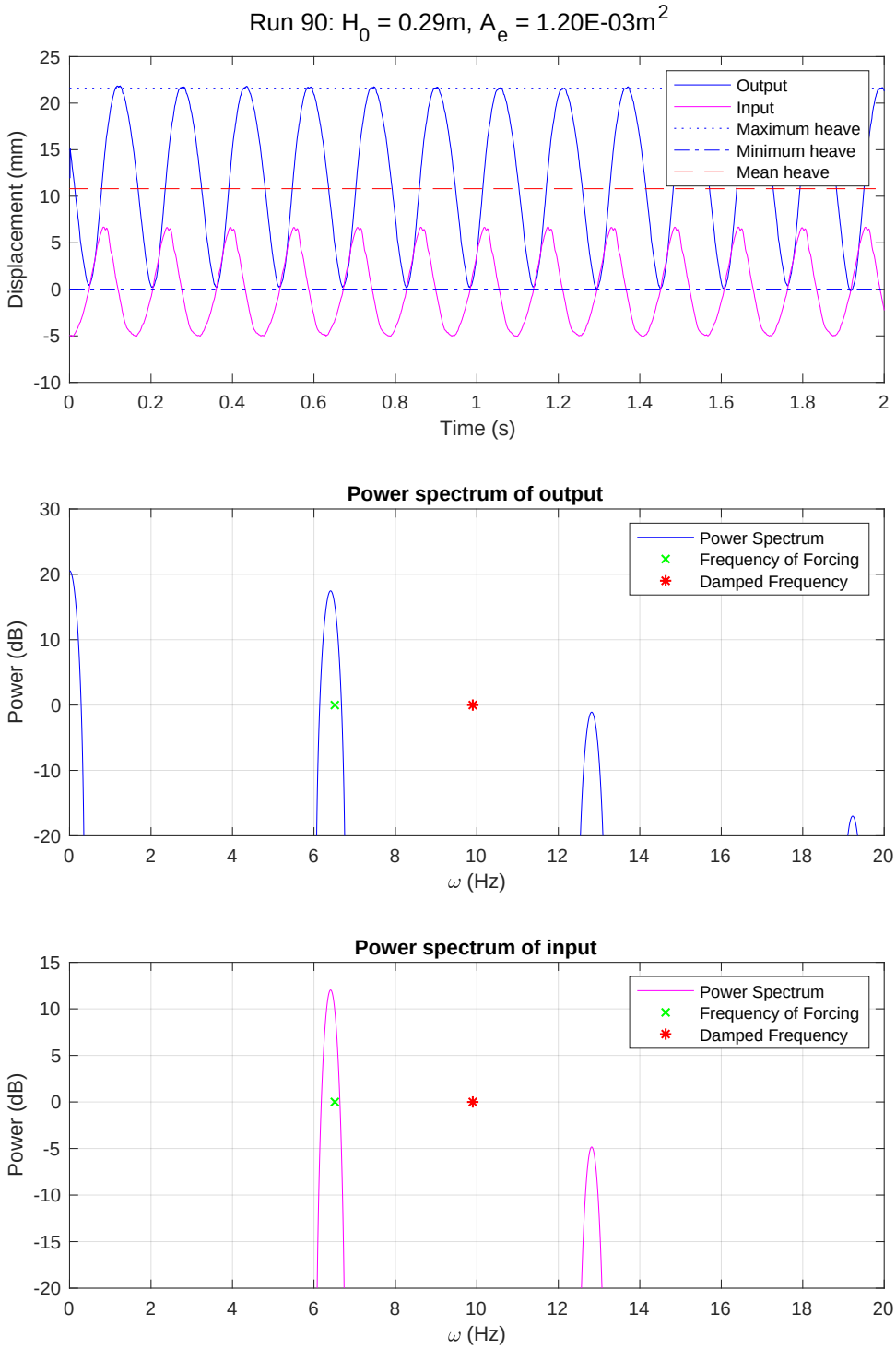


Figure H.48. Experimental trial data for Condition 90

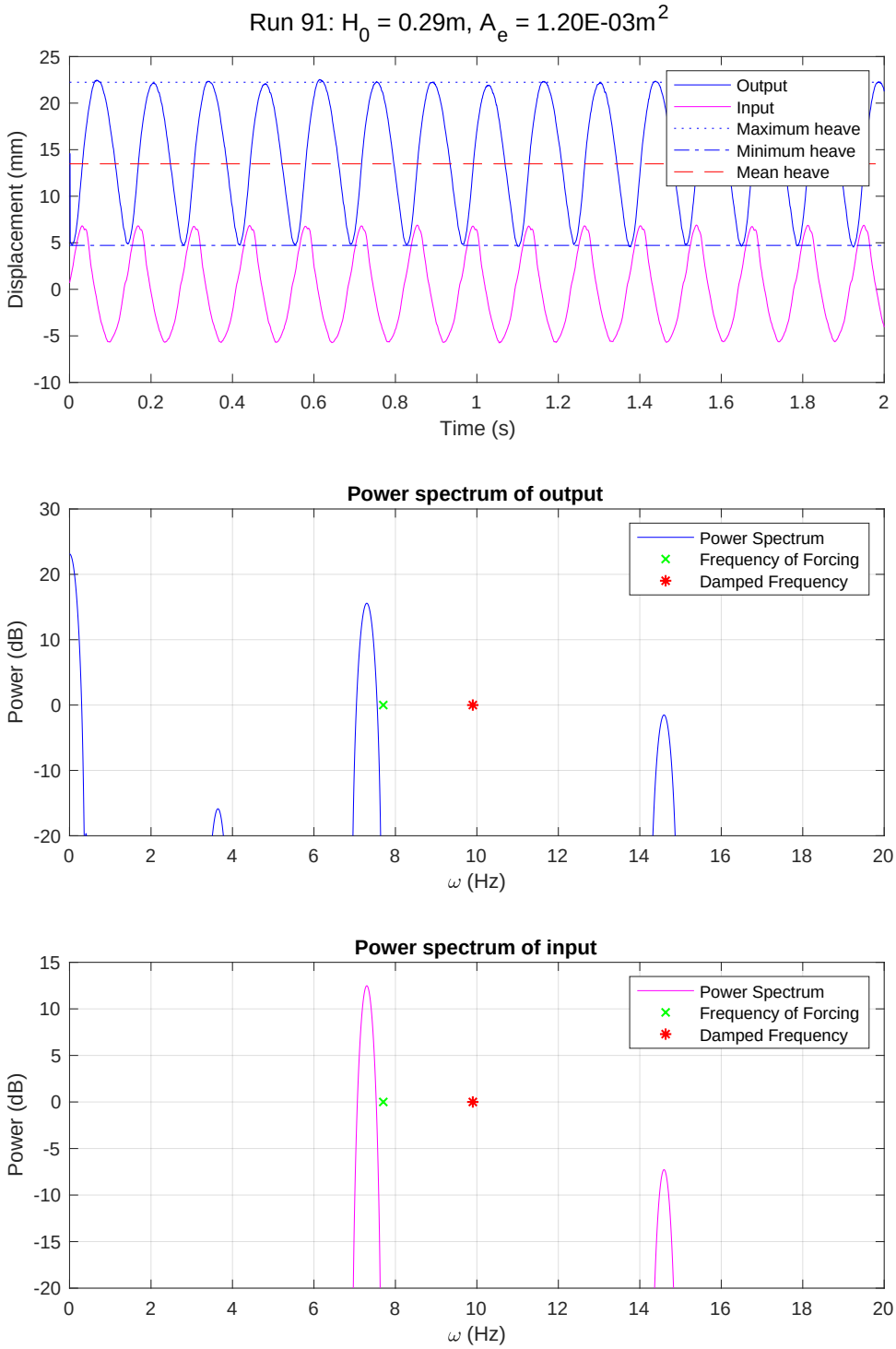


Figure H.49. Experimental trial data for Condition 91

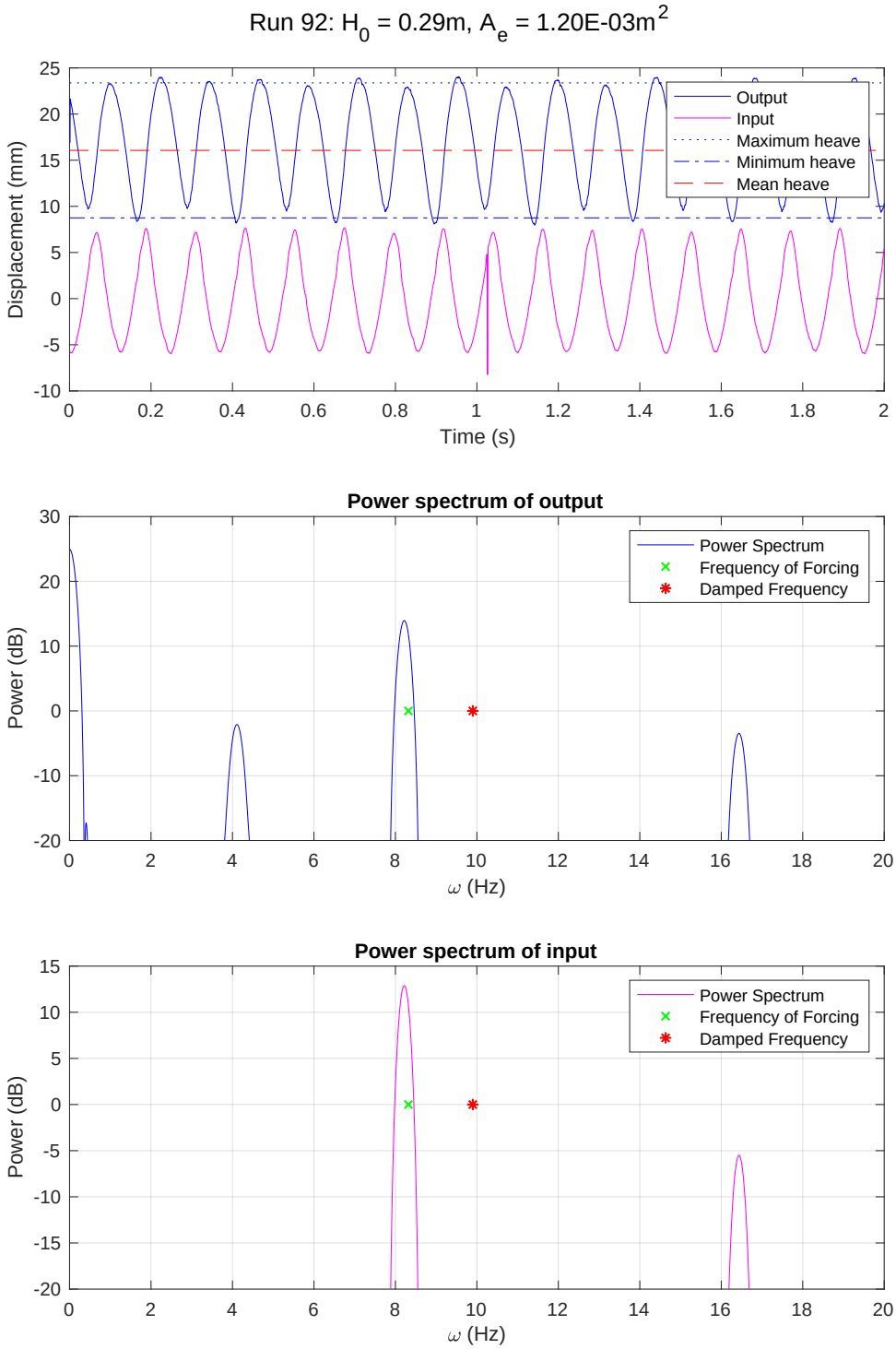


Figure H.50. Experimental trial data for Condition 92

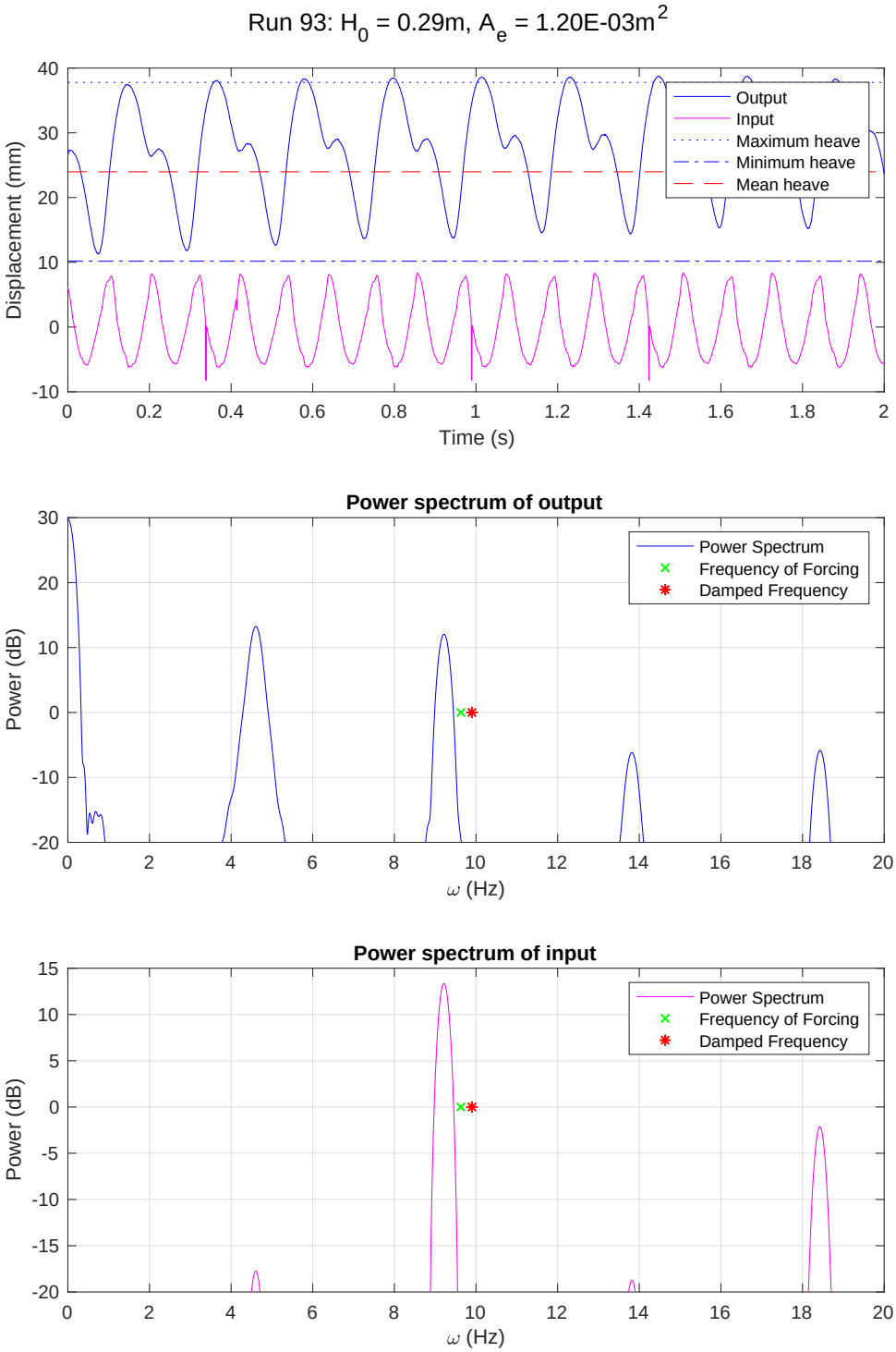


Figure H.51. Experimental trial data for Condition 93

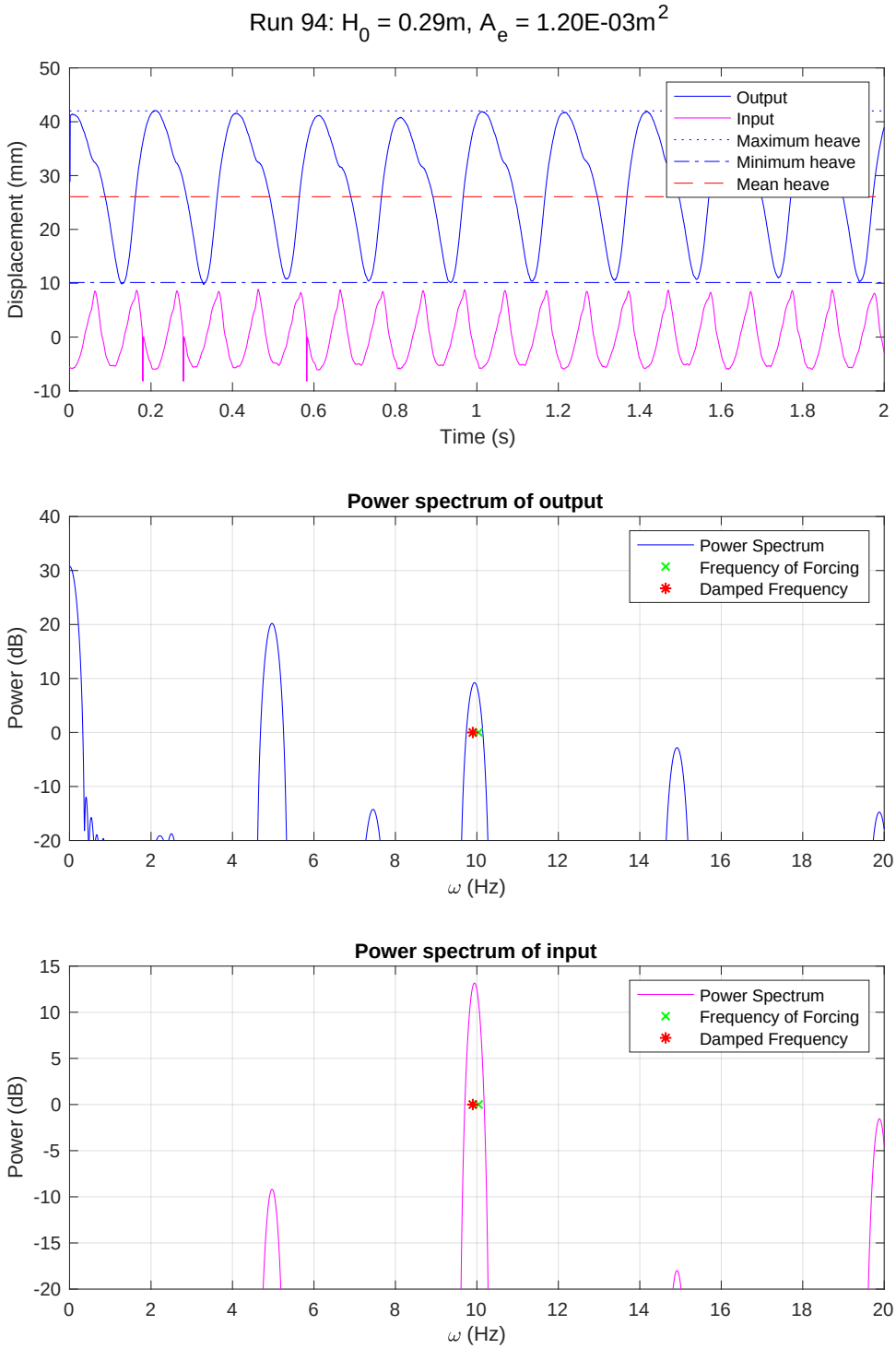


Figure H.52. Experimental trial data for Condition 94

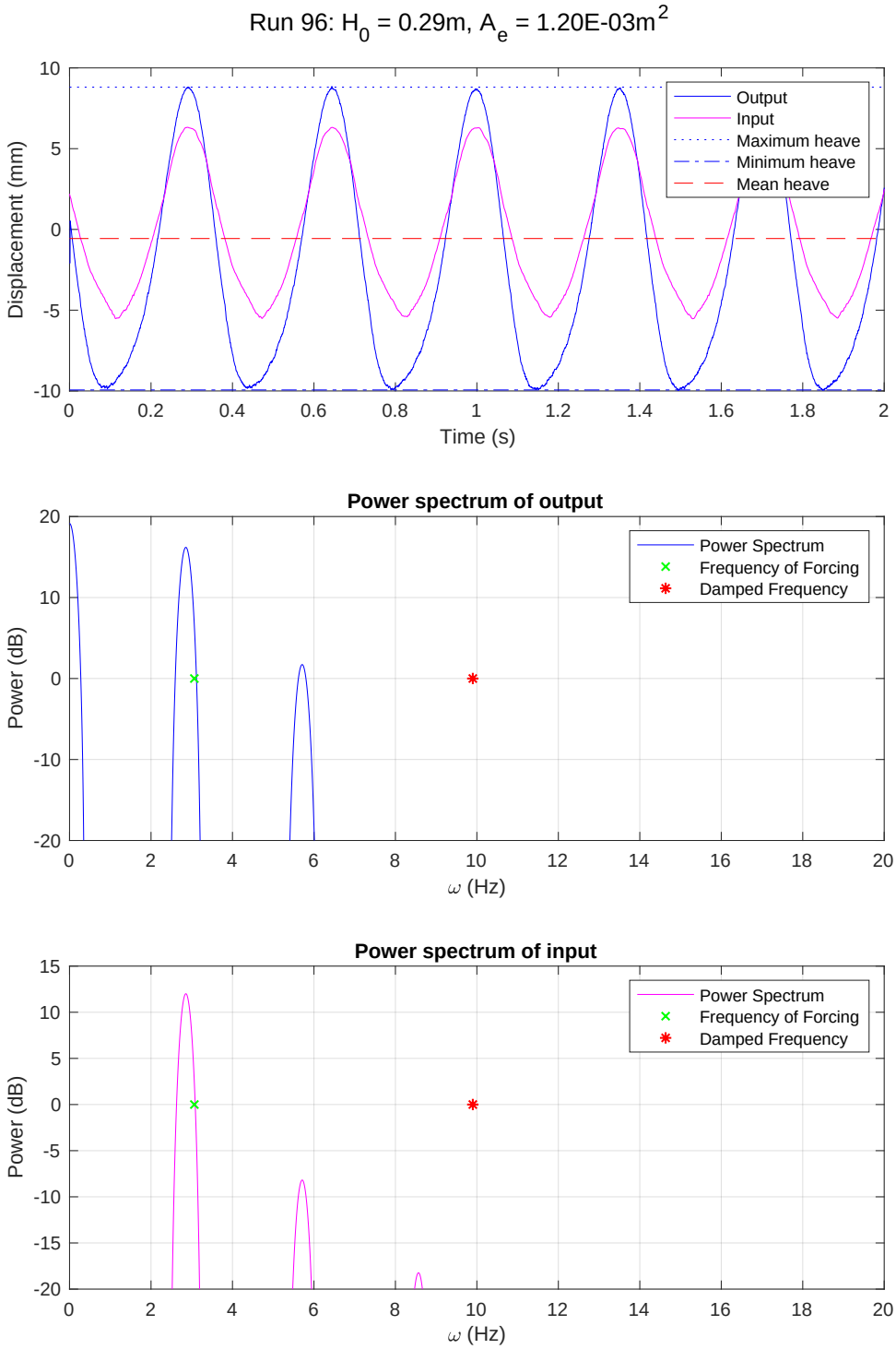


Figure H.53. Experimental trial data for Condition 96

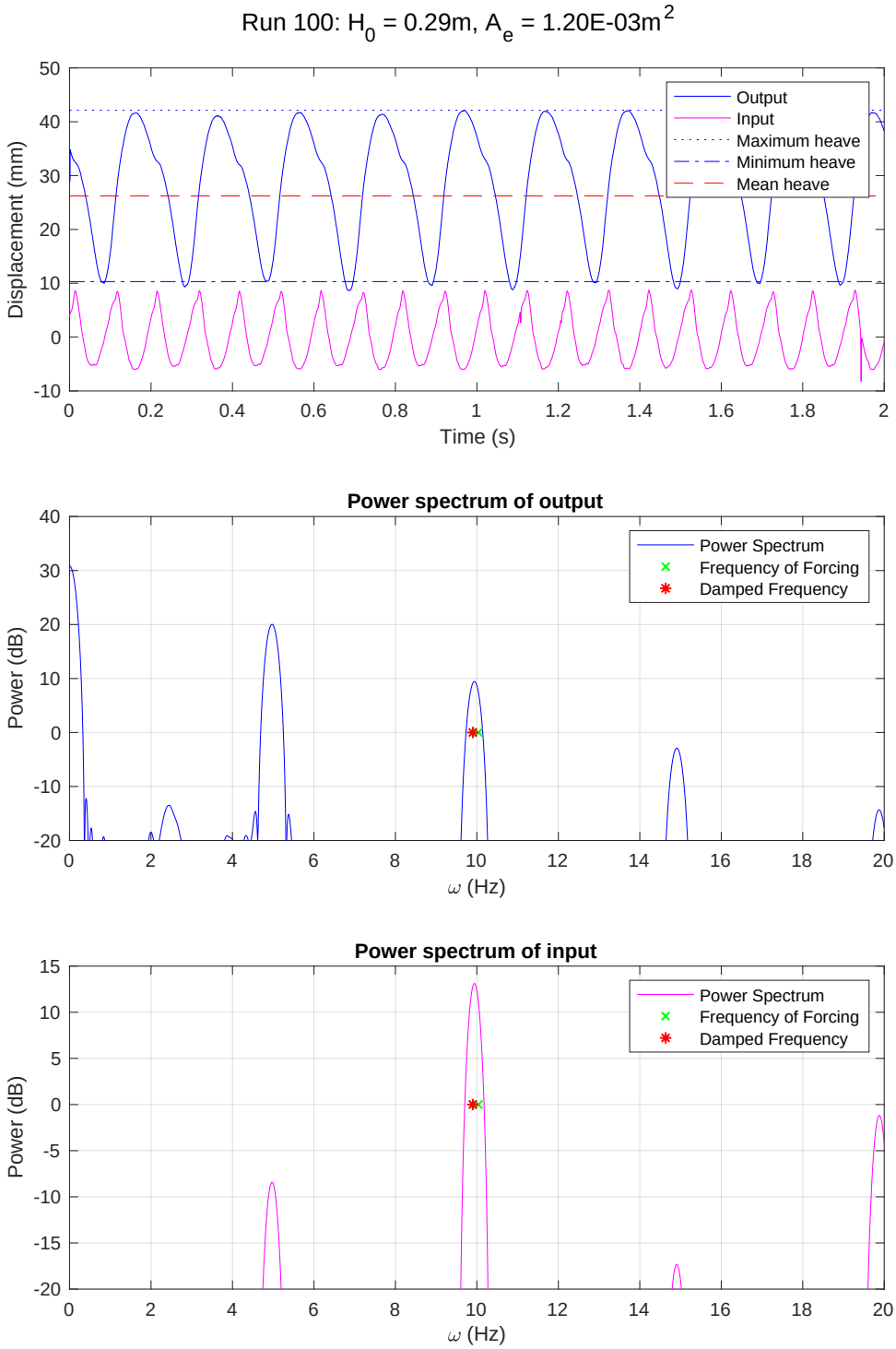


Figure H.54. Experimental trial data for Condition 100

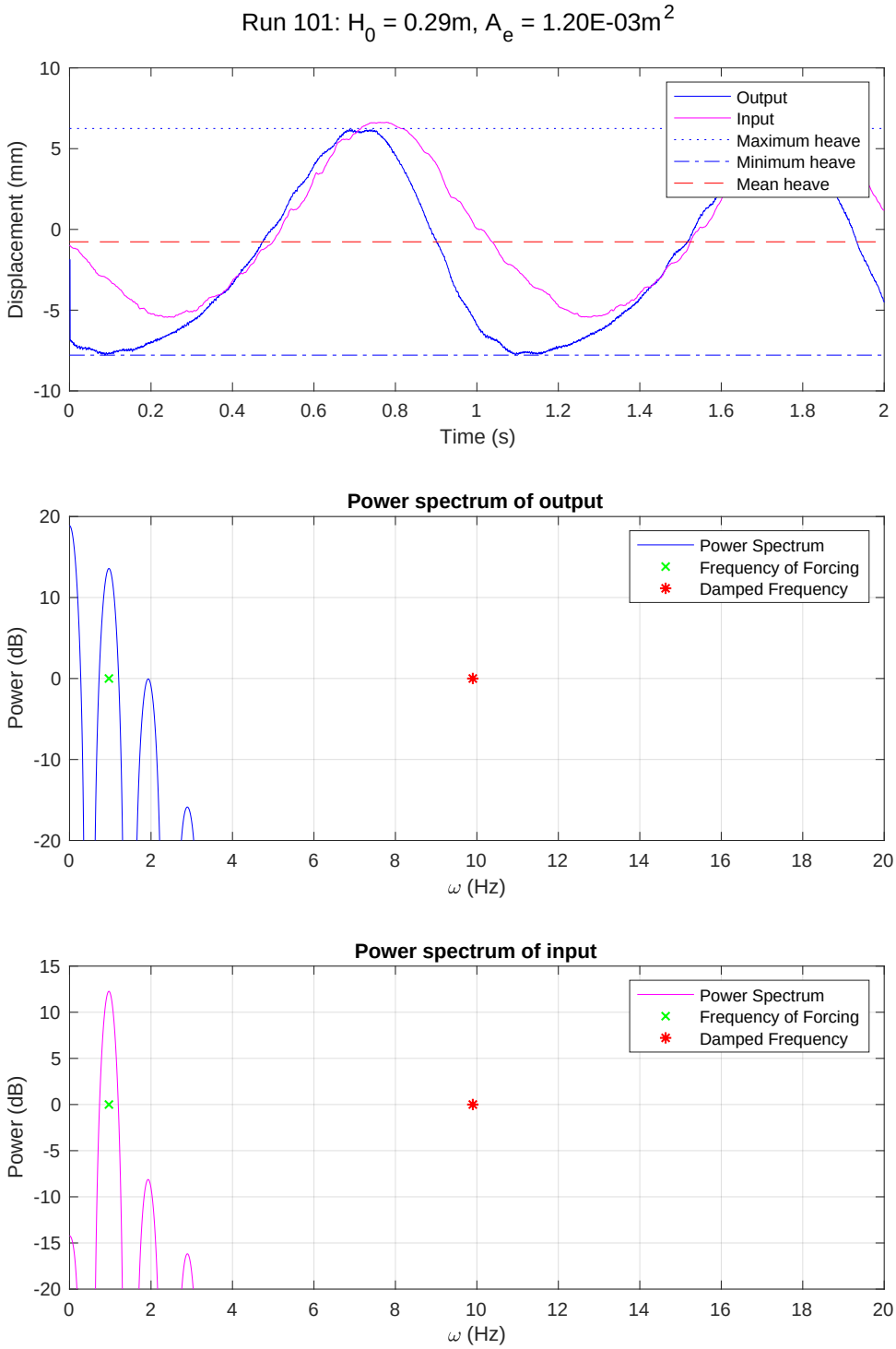


Figure H.55. Experimental trial data for Condition 101

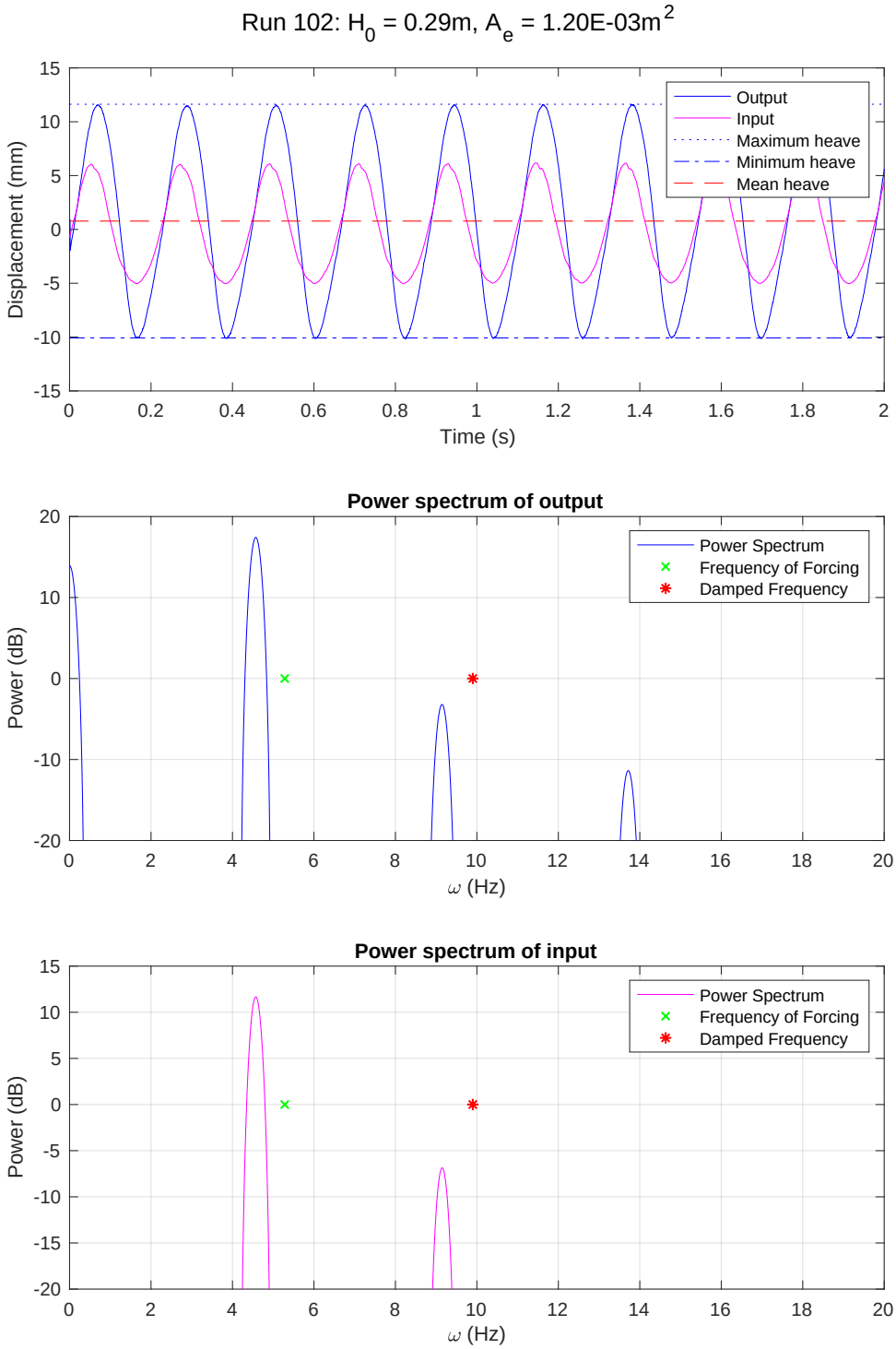


Figure H.56. Experimental trial data for Condition 102

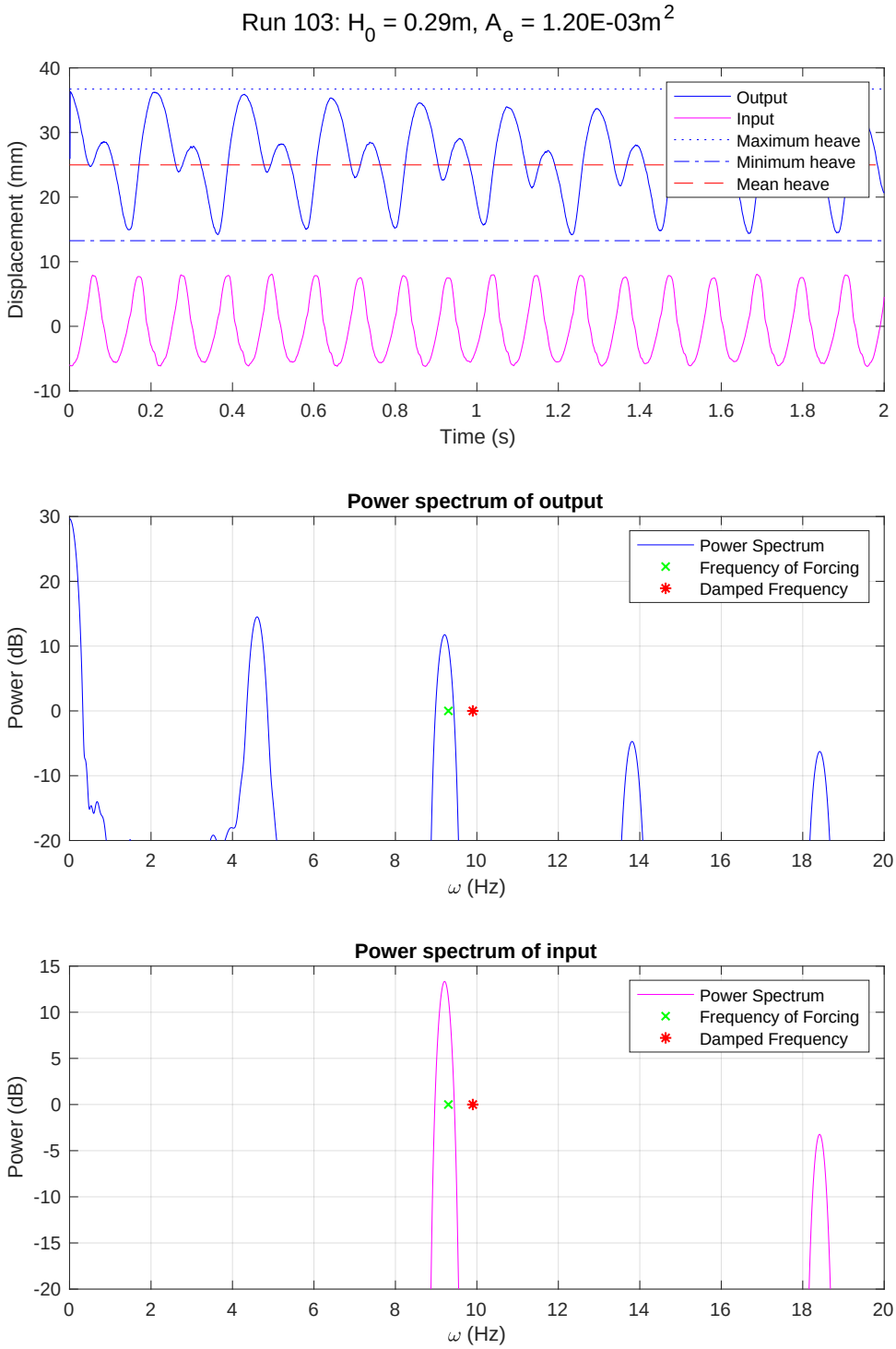


Figure H.57. Experimental trial data for Condition 103

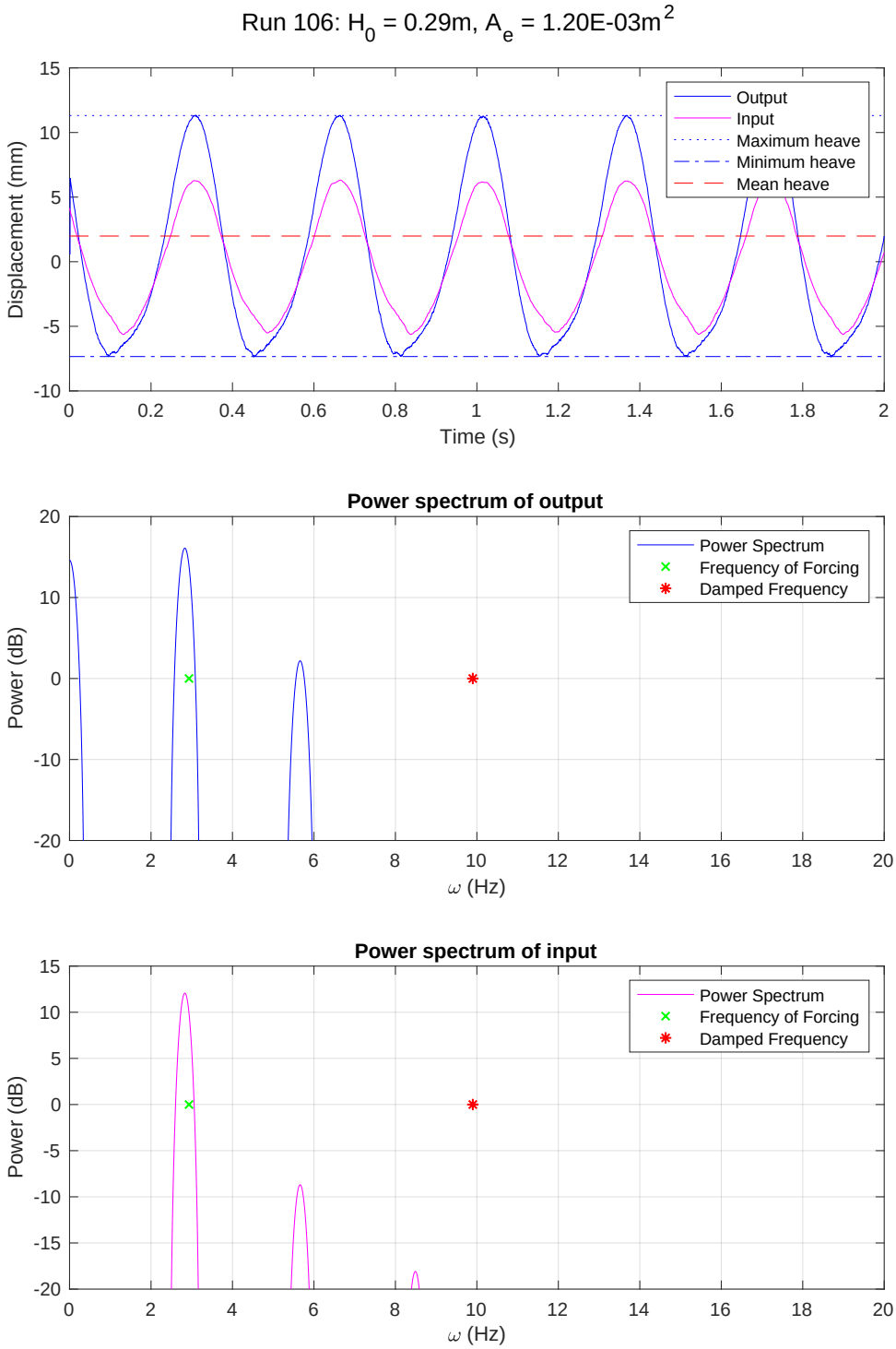


Figure H.58. Experimental trial data for Condition 106

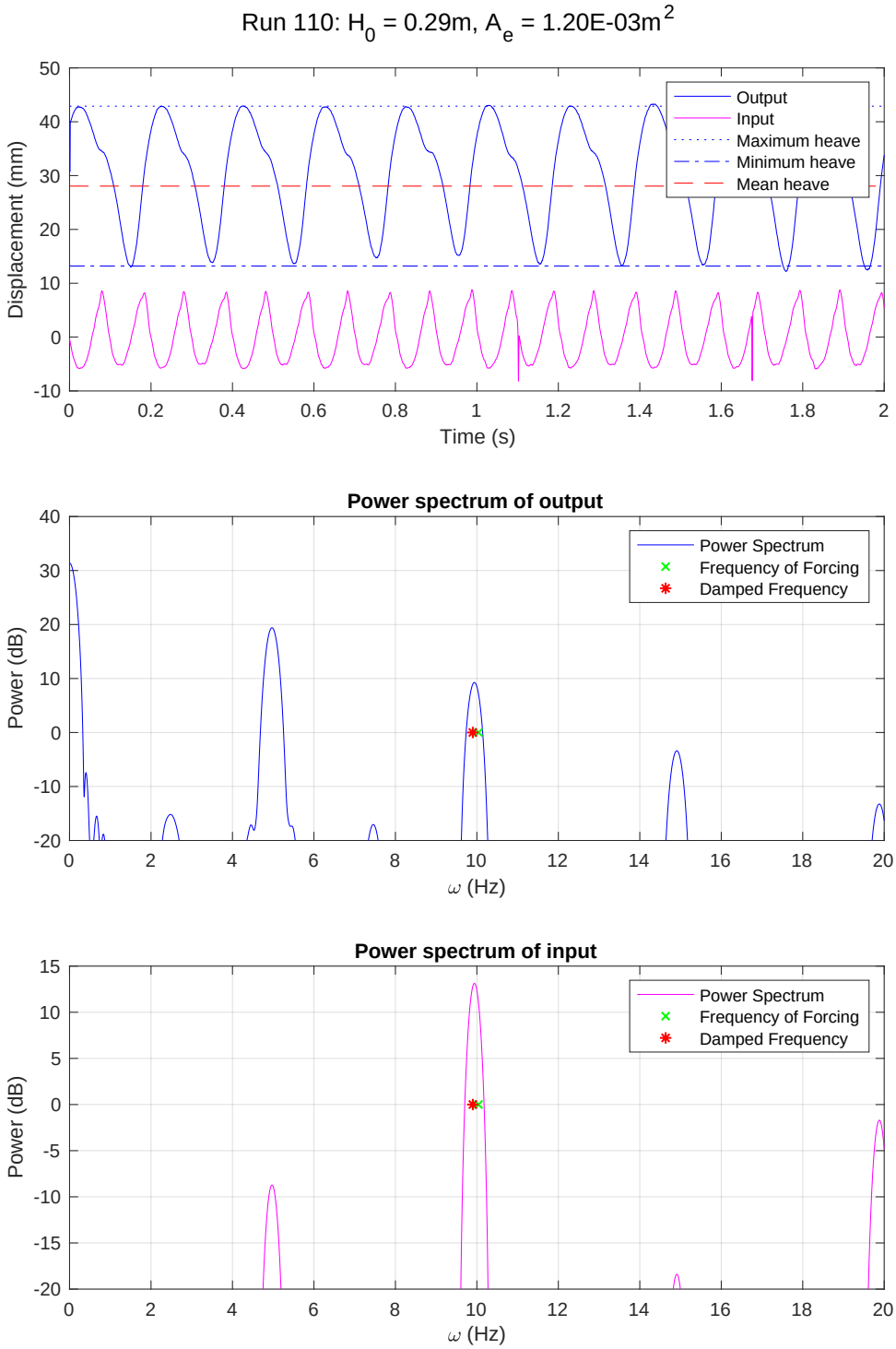


Figure H.59. Experimental trial data for Condition 110

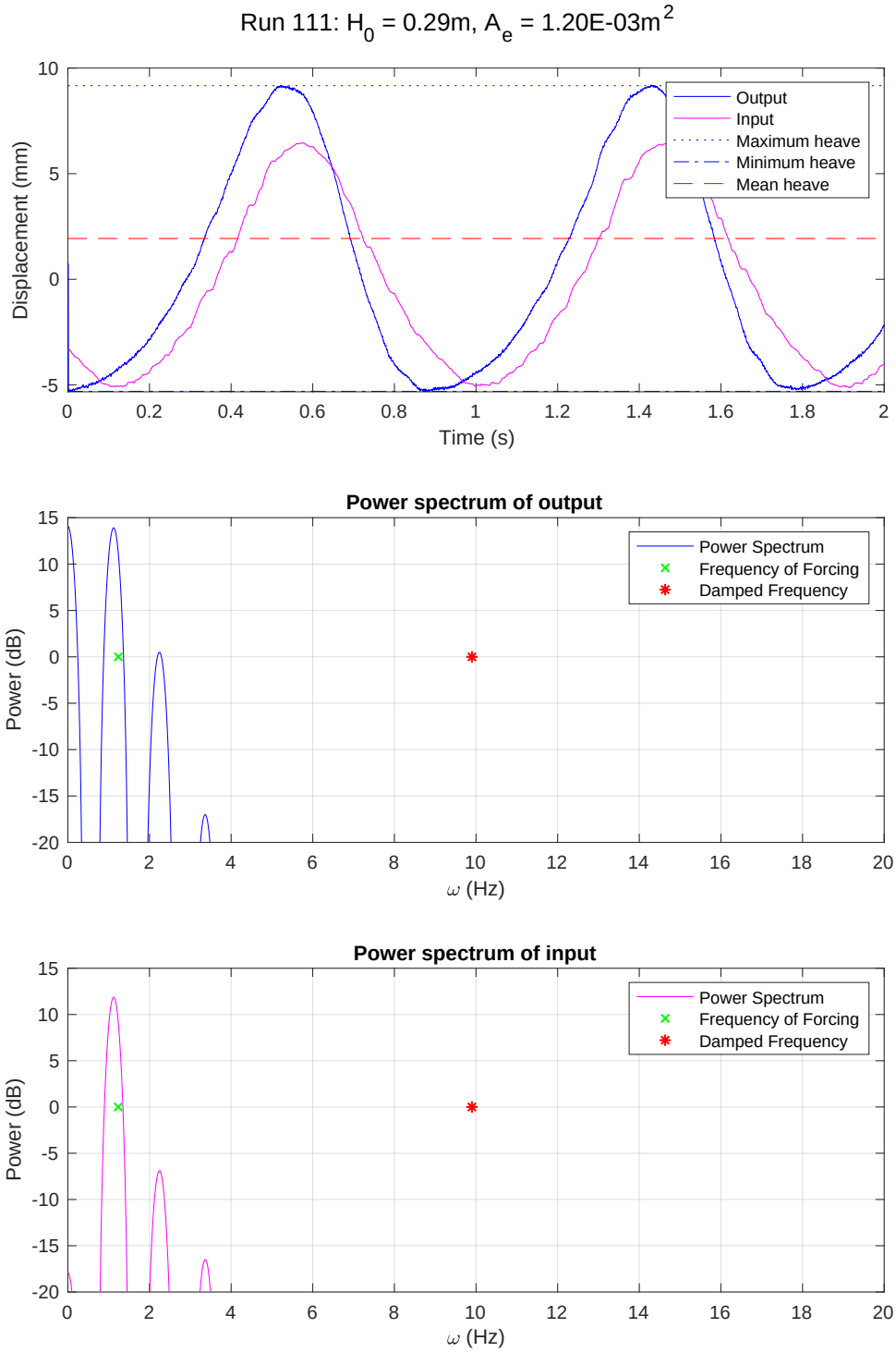


Figure H.60. Experimental trial data for Condition 111

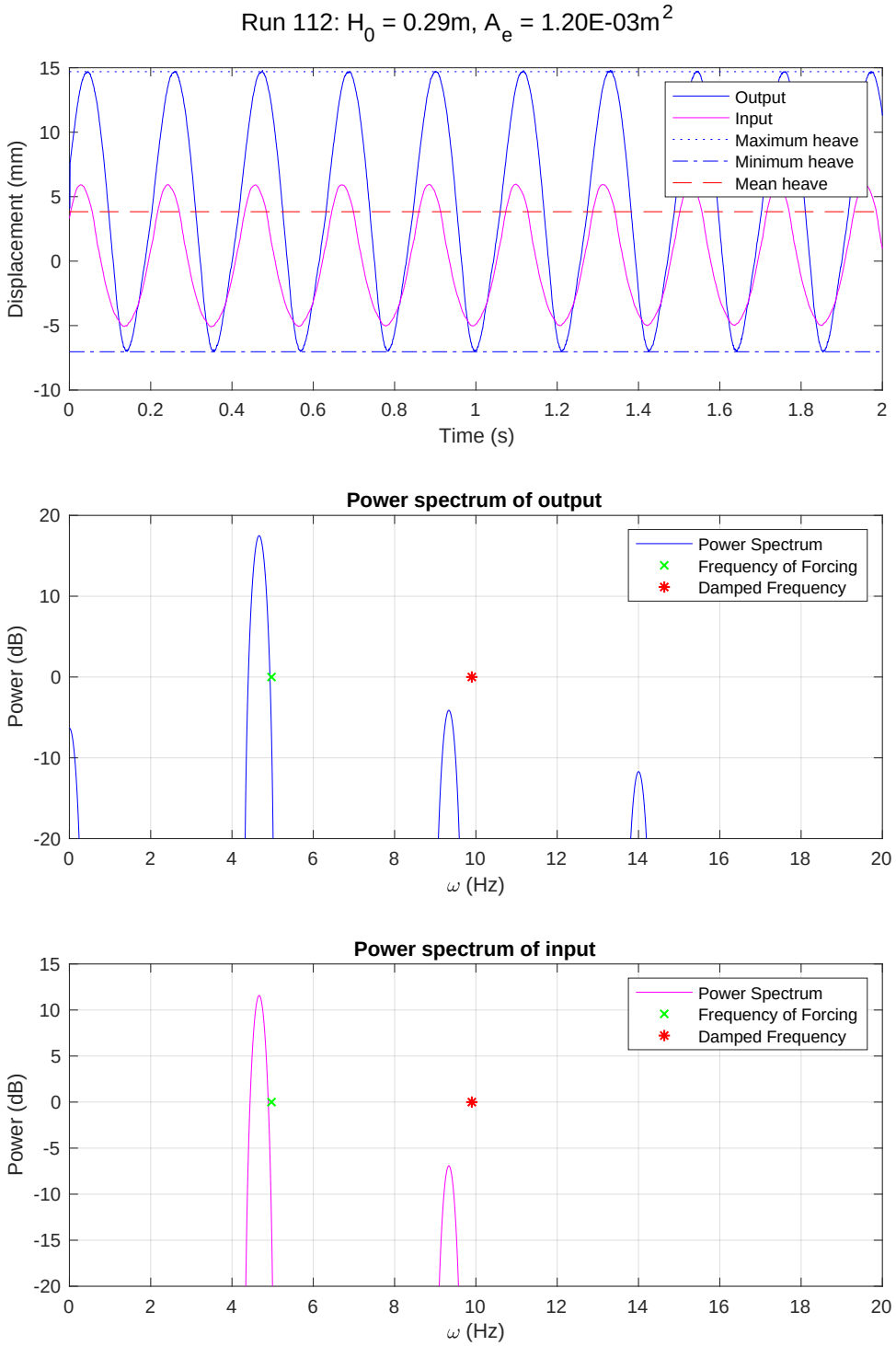


Figure H.61. Experimental trial data for Condition 112

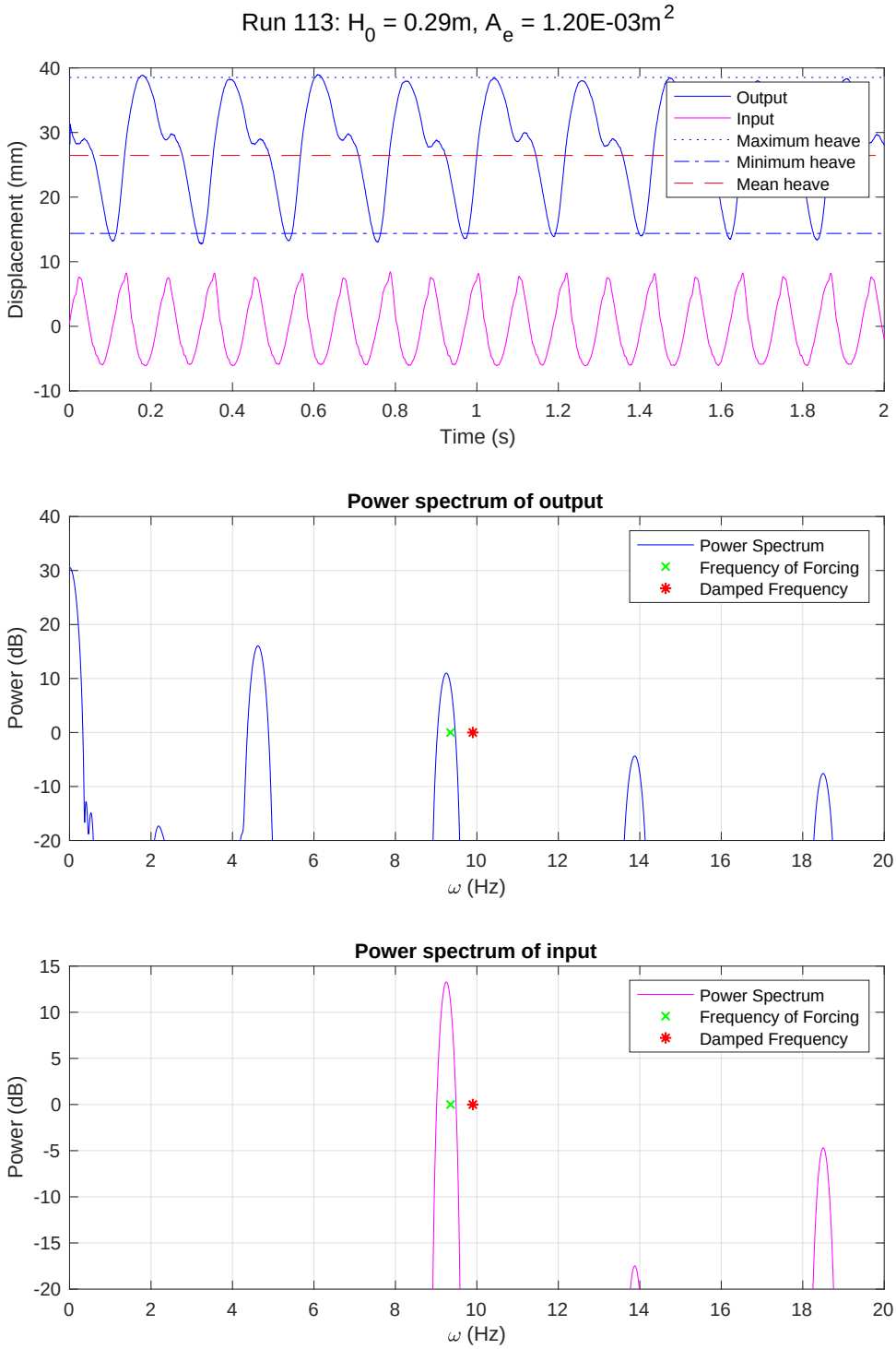


Figure H.62. Experimental trial data for Condition 113

H.2.4. Condition Four

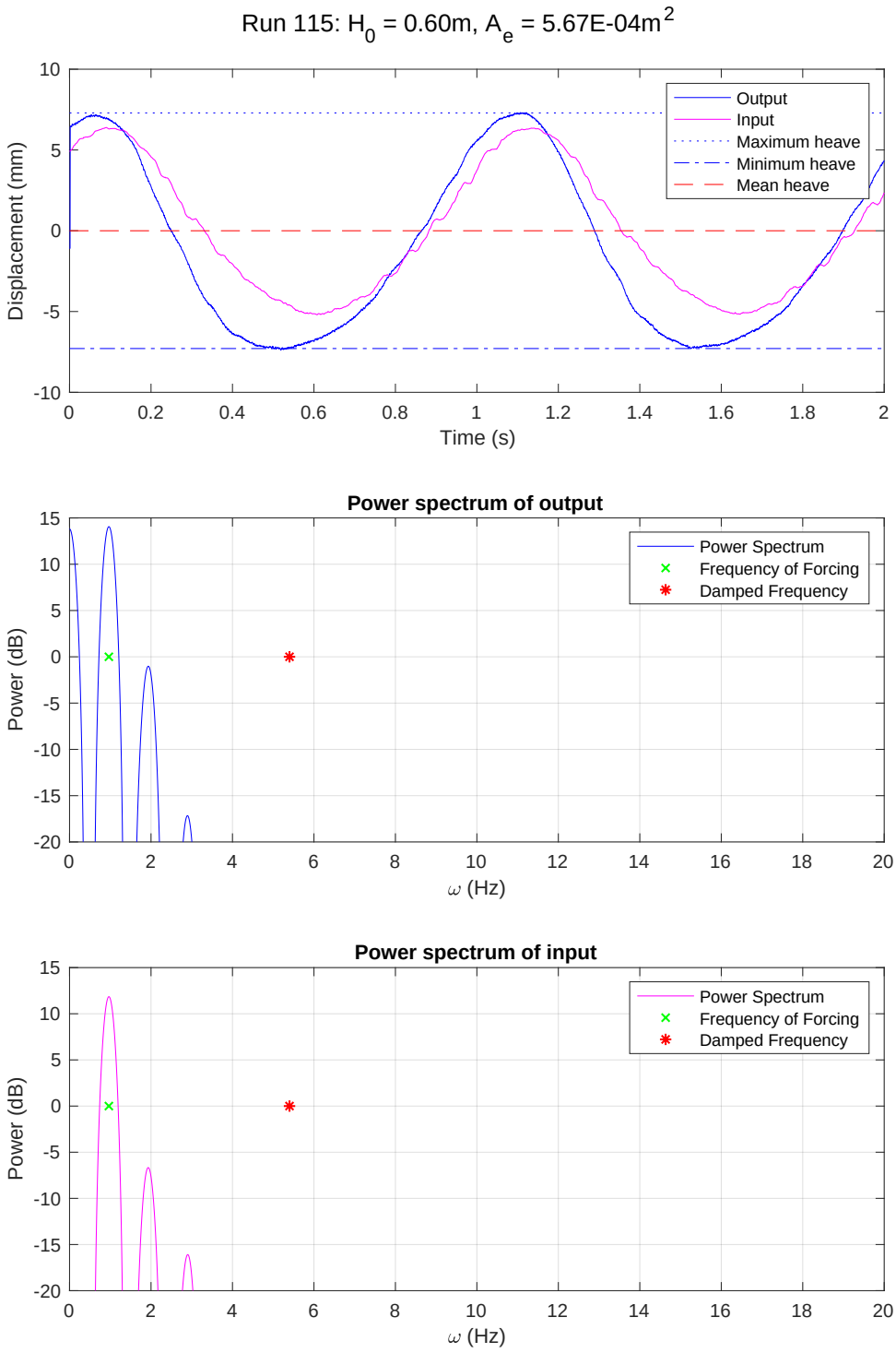


Figure H.63. Experimental trial data for Condition 115

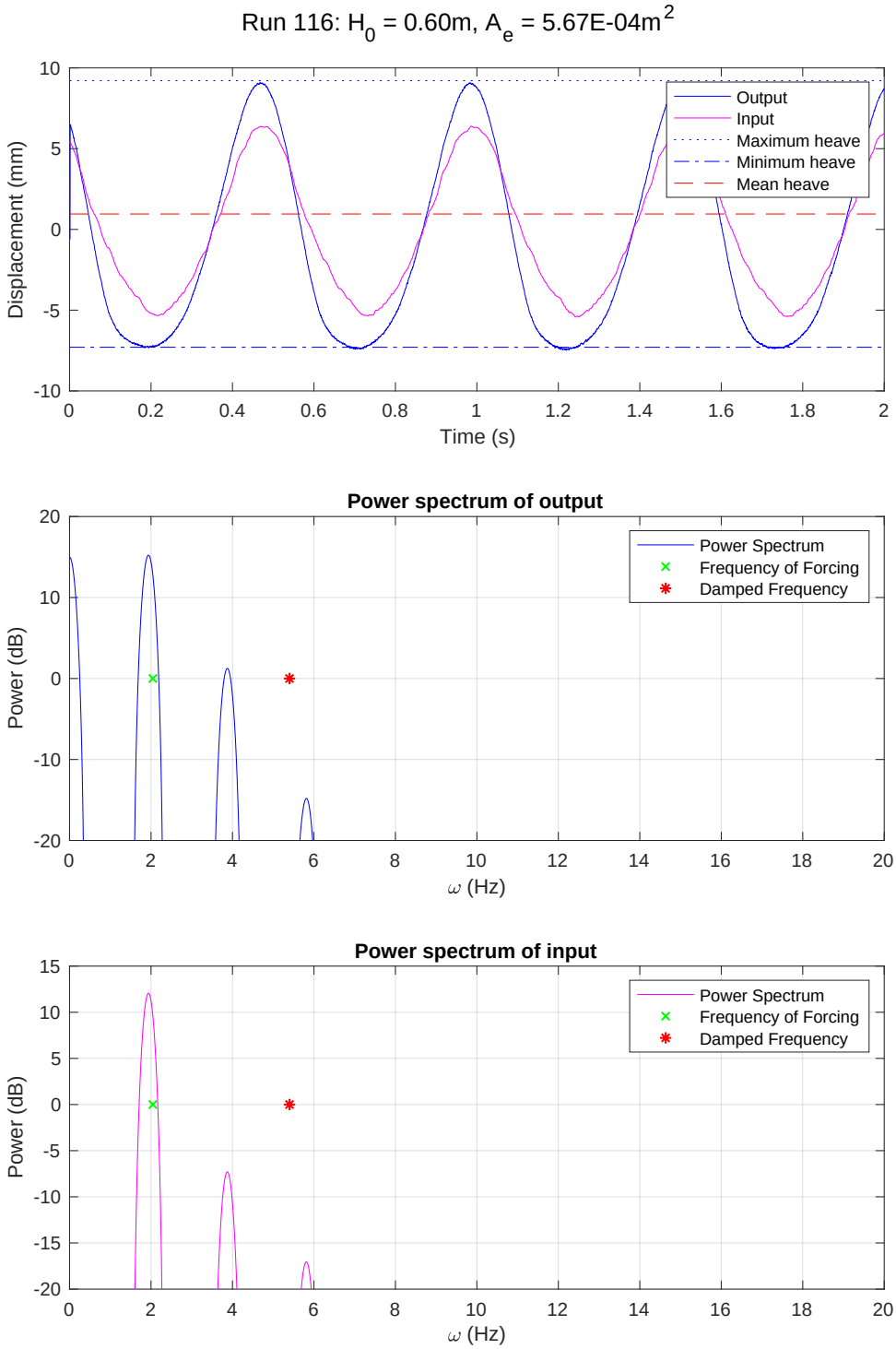


Figure H.64. Experimental trial data for Condition 116

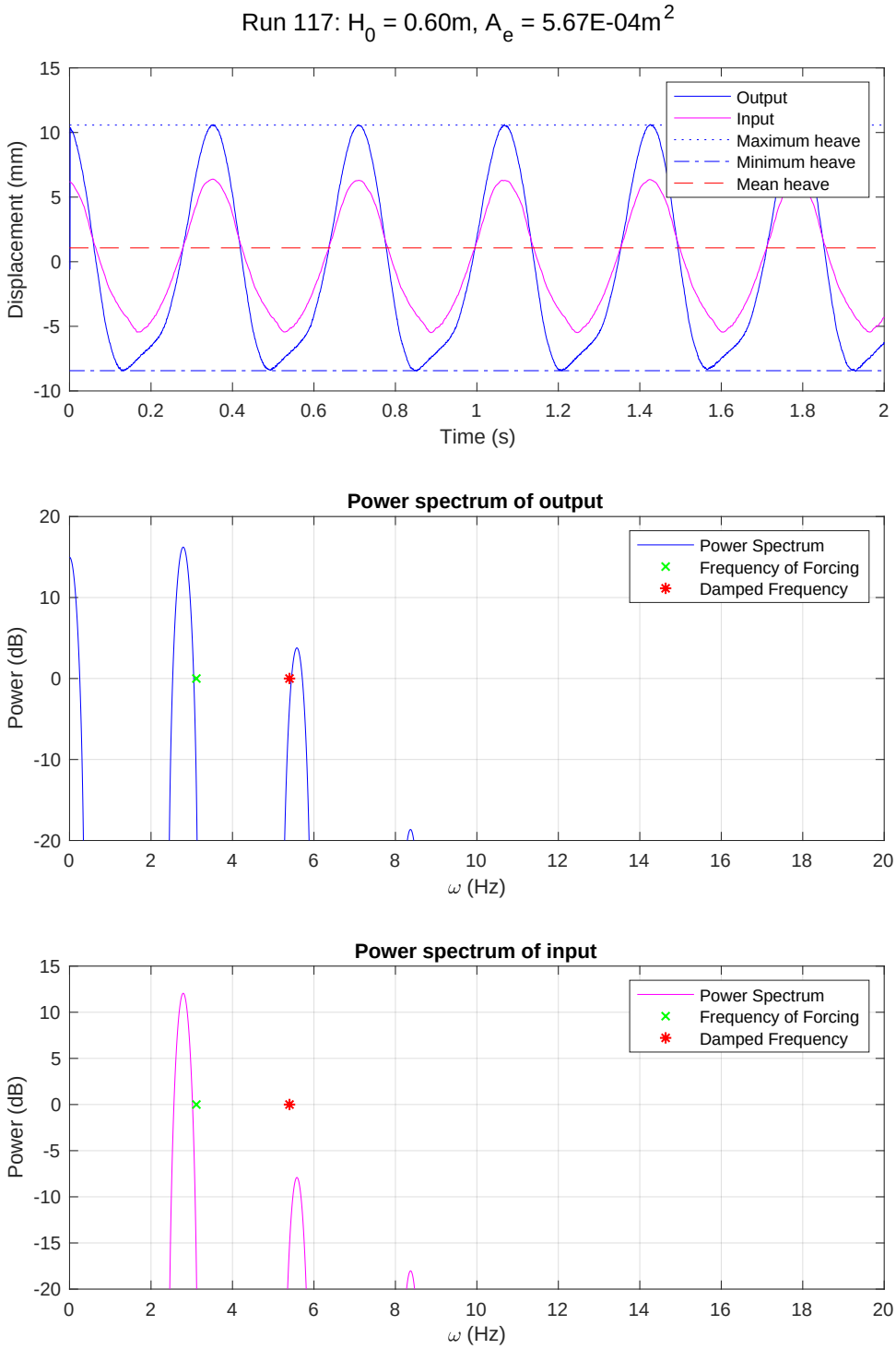


Figure H.65. Experimental trial data for Condition 117

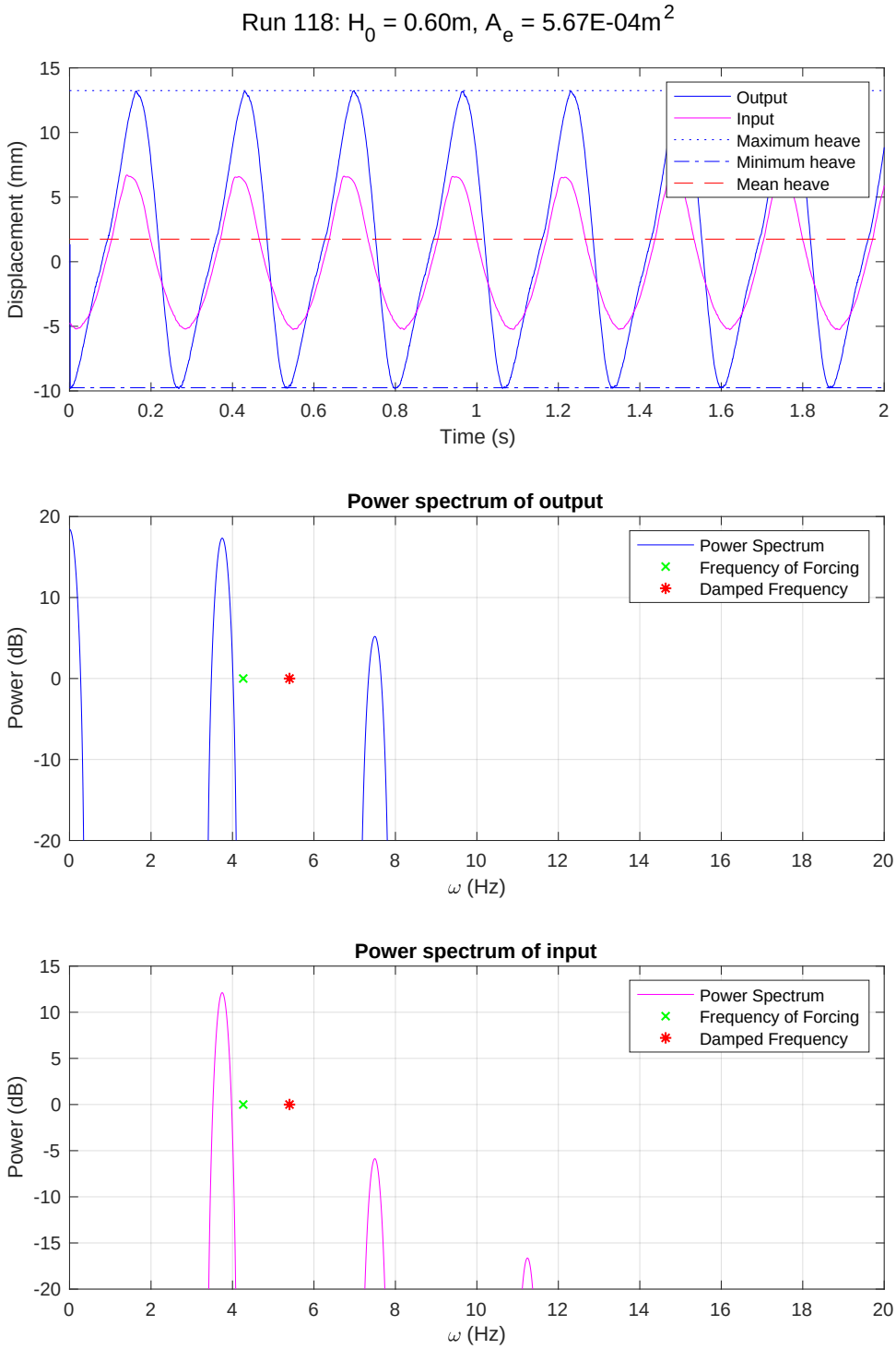


Figure H.66. Experimental trial data for Condition 118

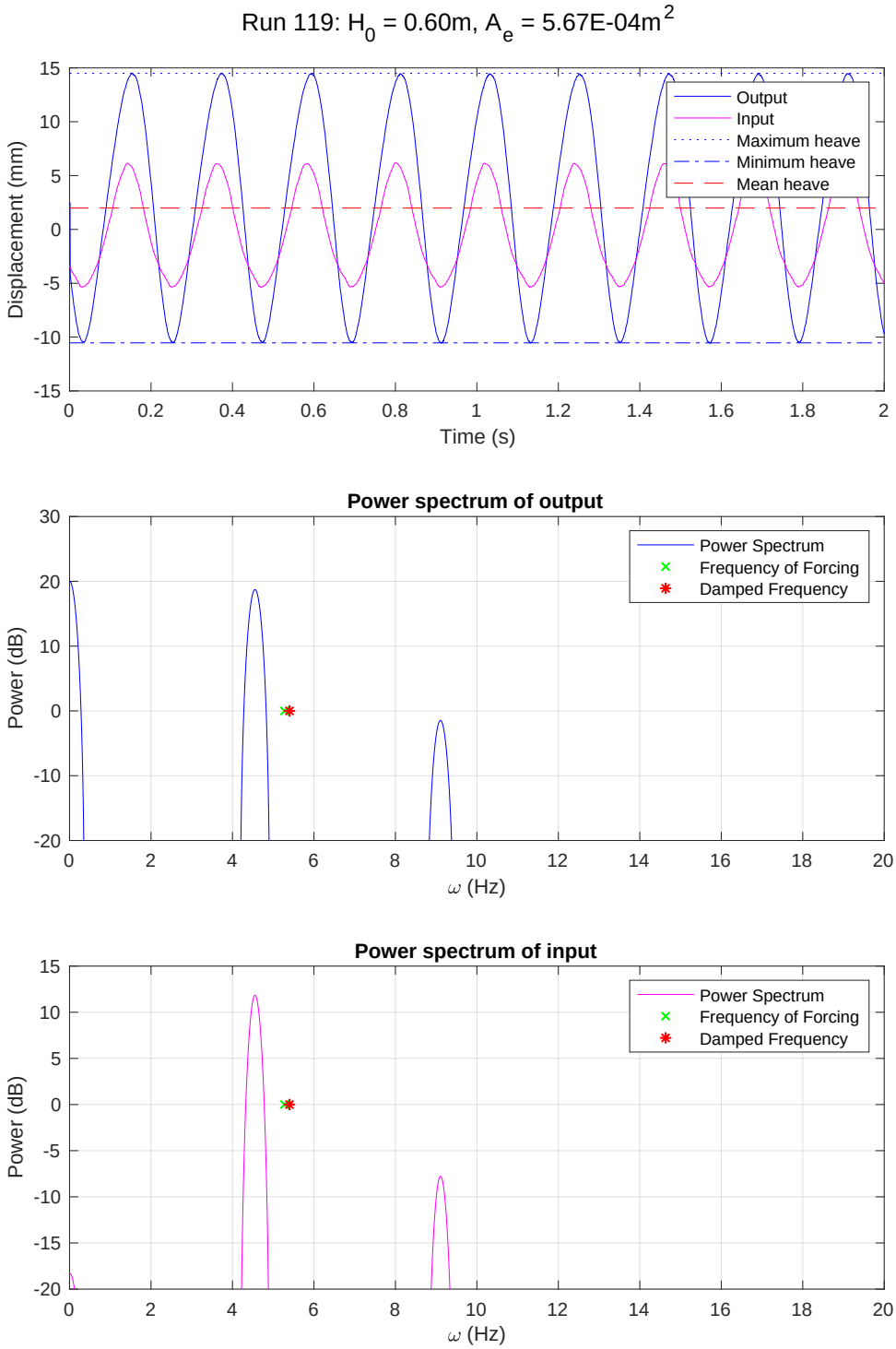


Figure H.67. Experimental trial data for Condition 119

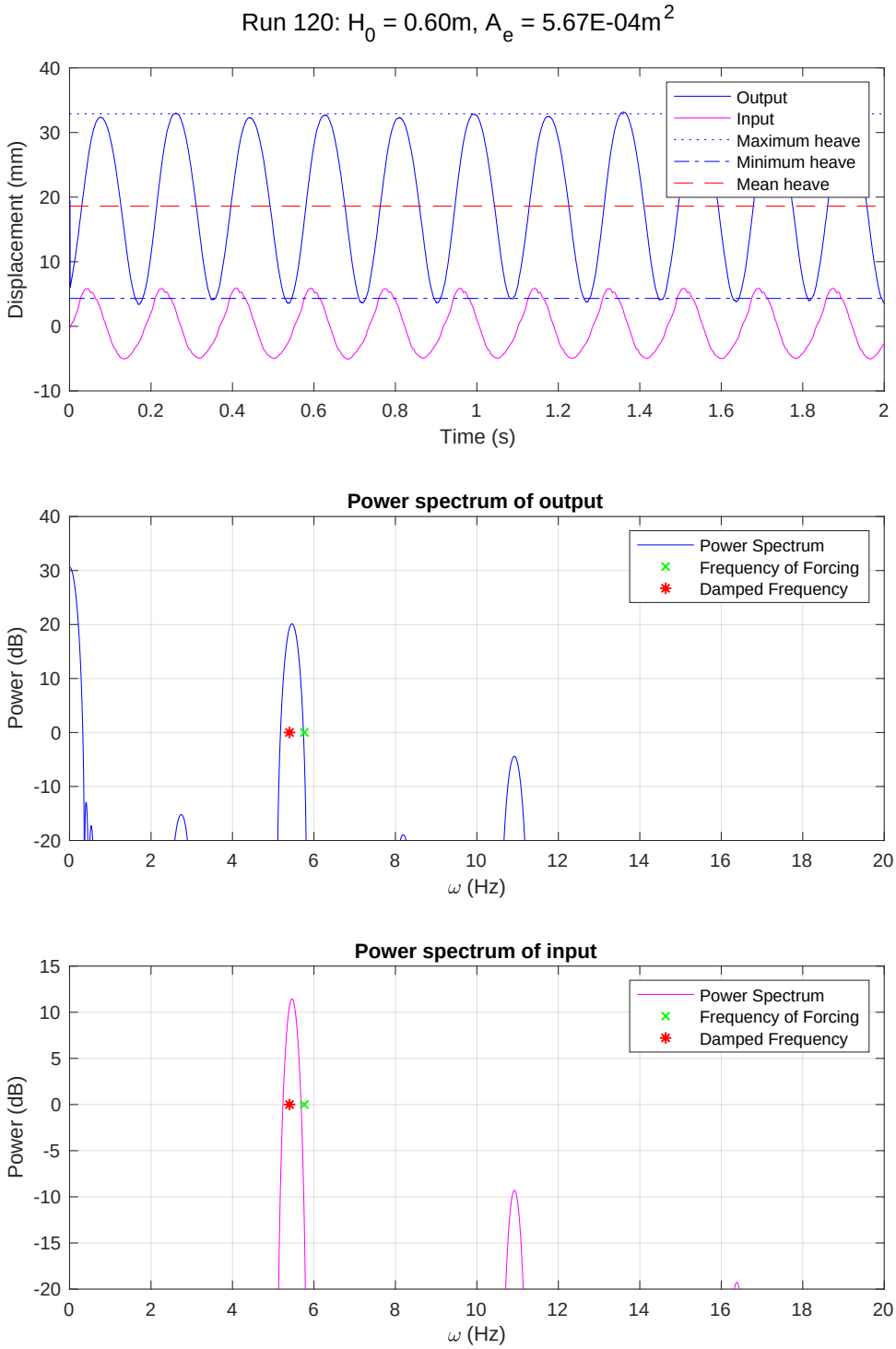


Figure H.68. Experimental trial data for Condition 120

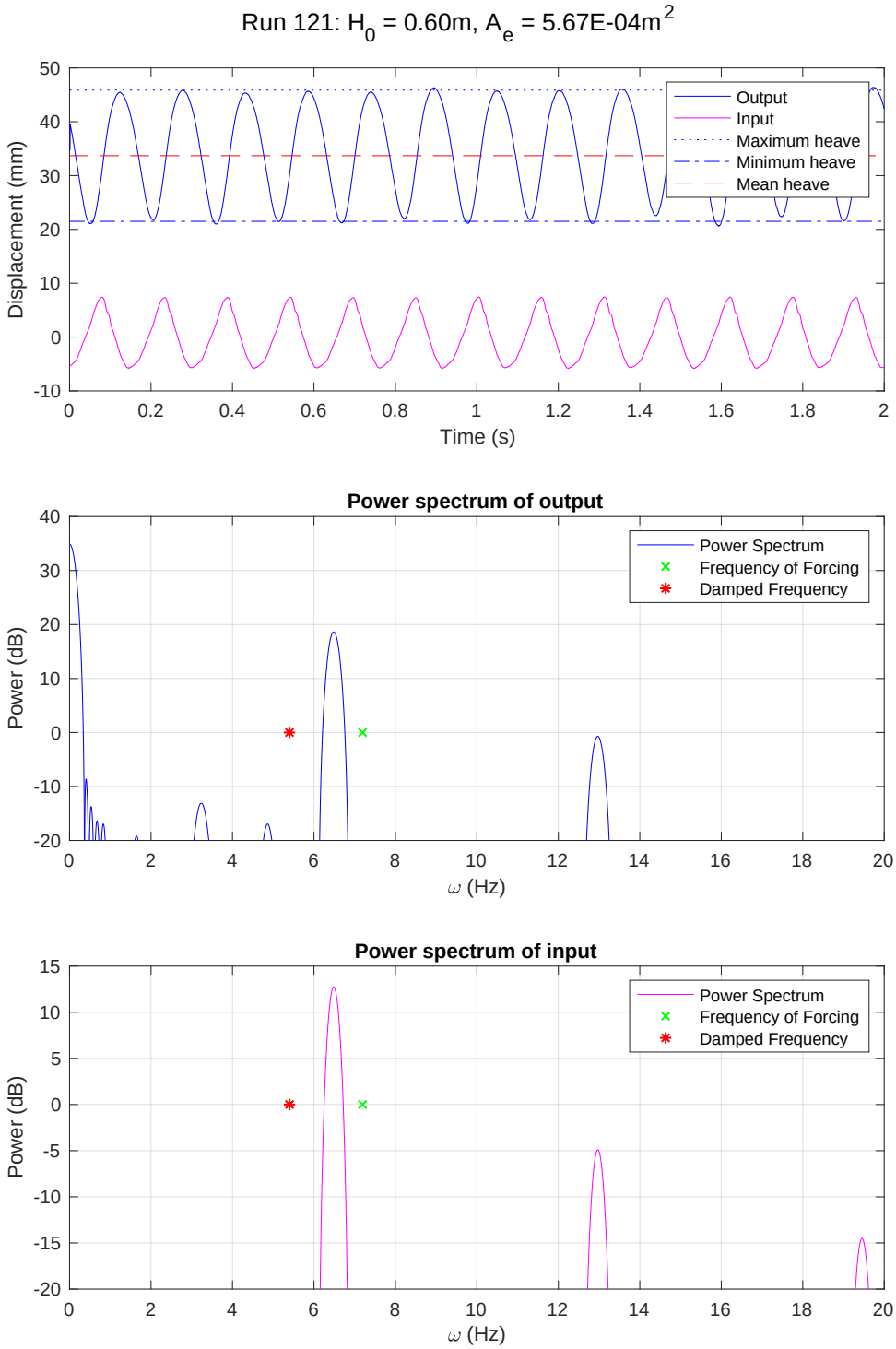


Figure H.69. Experimental trial data for Condition 121

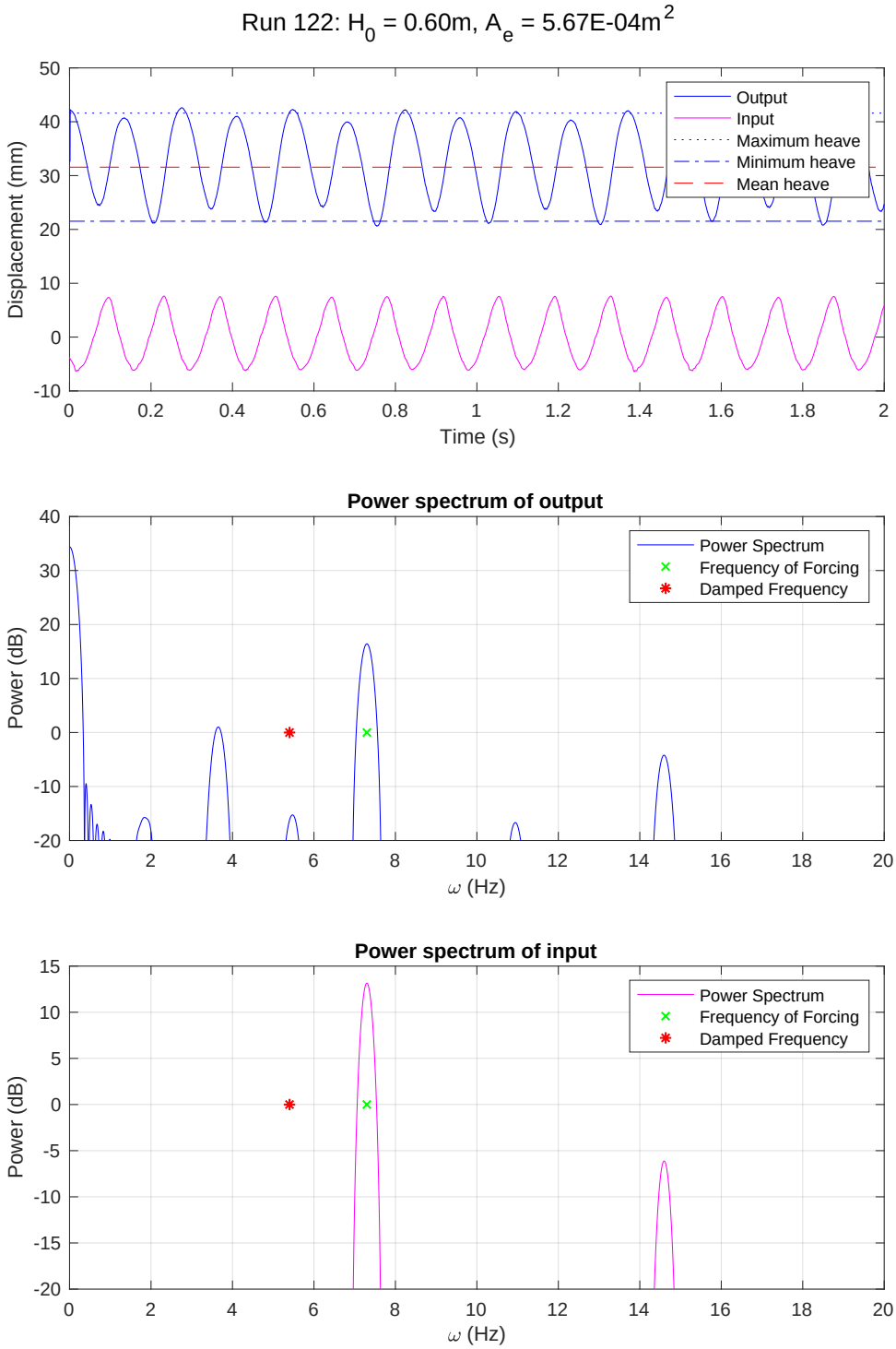


Figure H.70. Experimental trial data for Condition 122

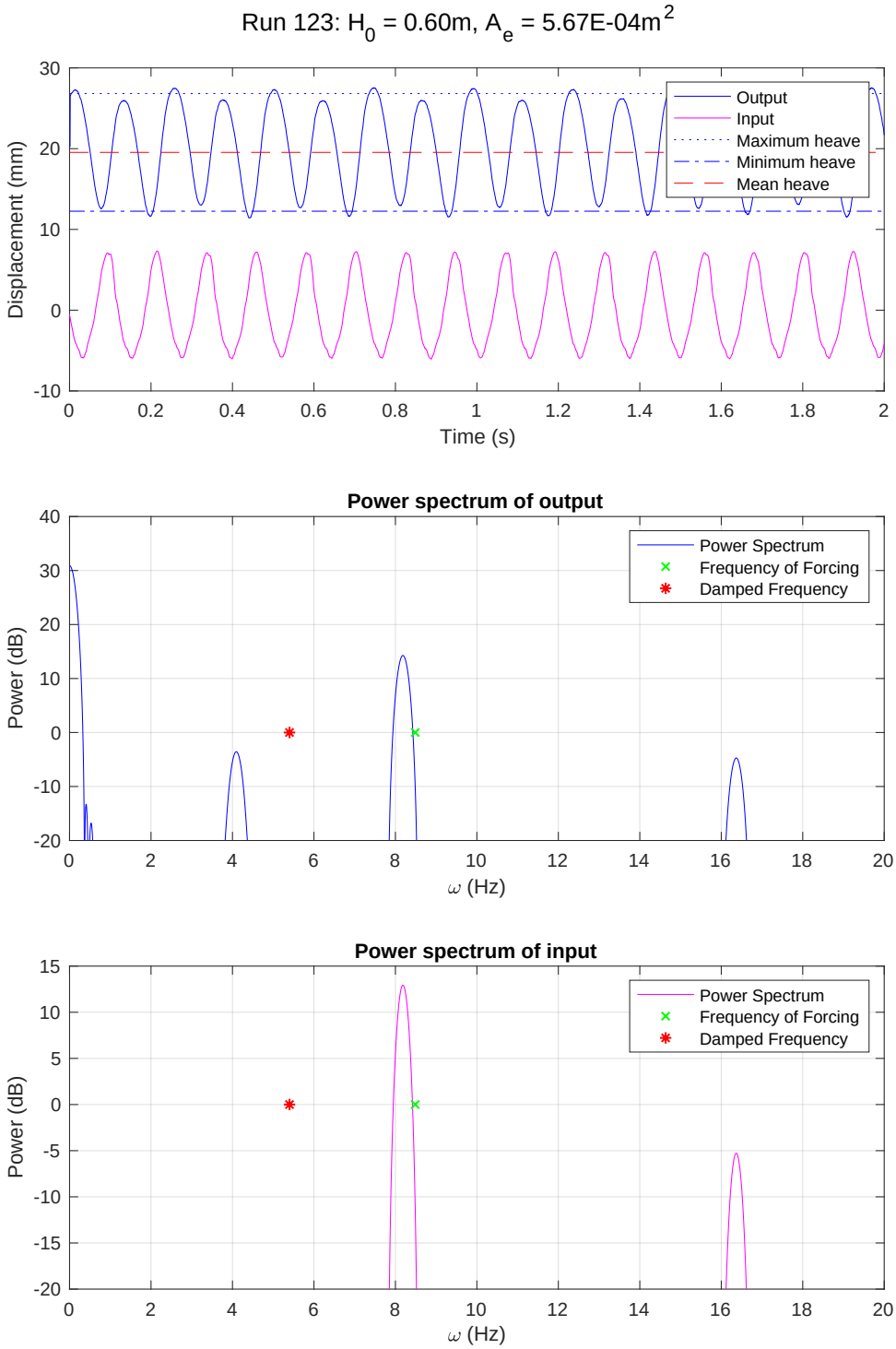


Figure H.71. Experimental trial data for Condition 123

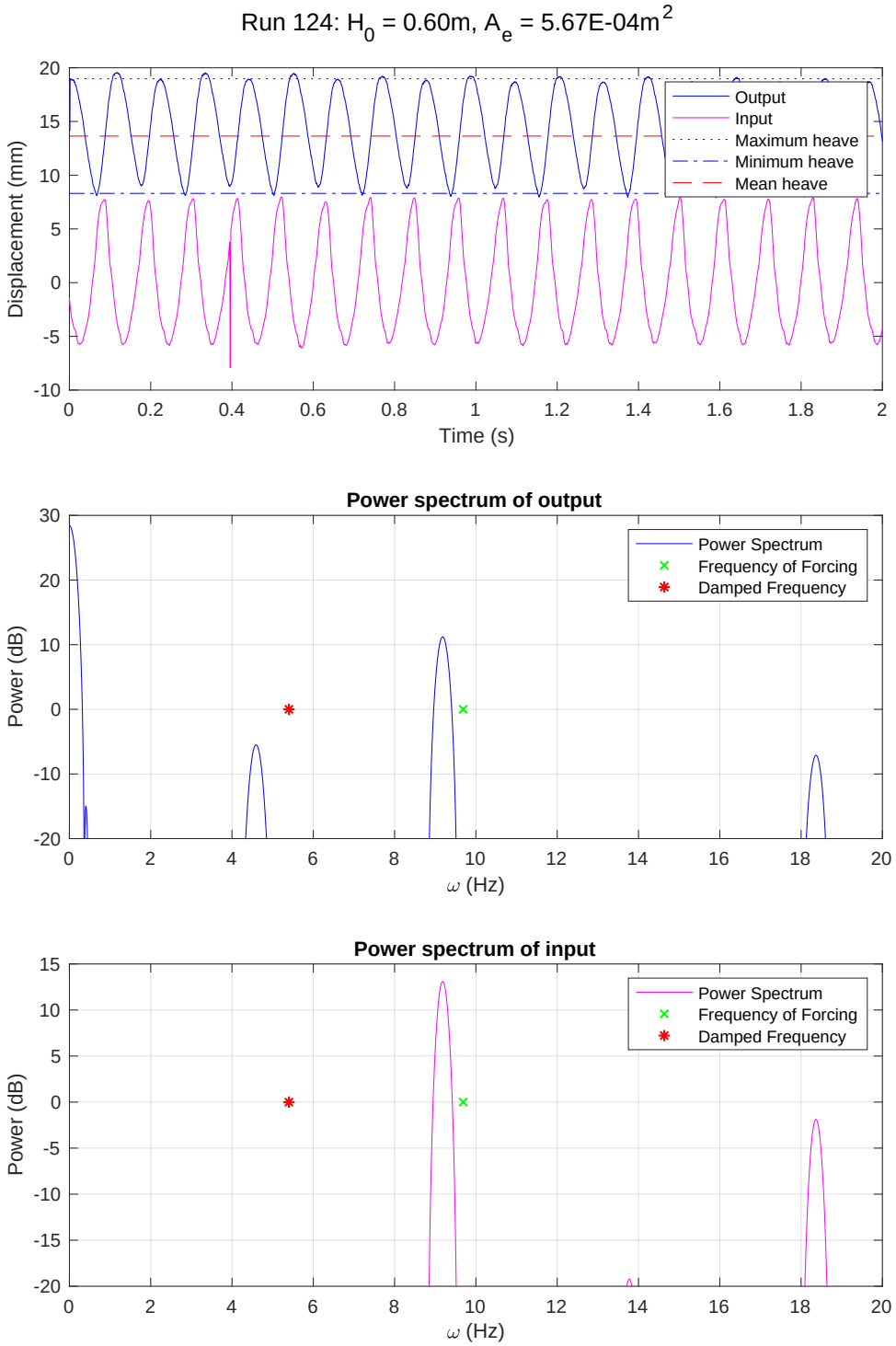


Figure H.72. Experimental trial data for Condition 124

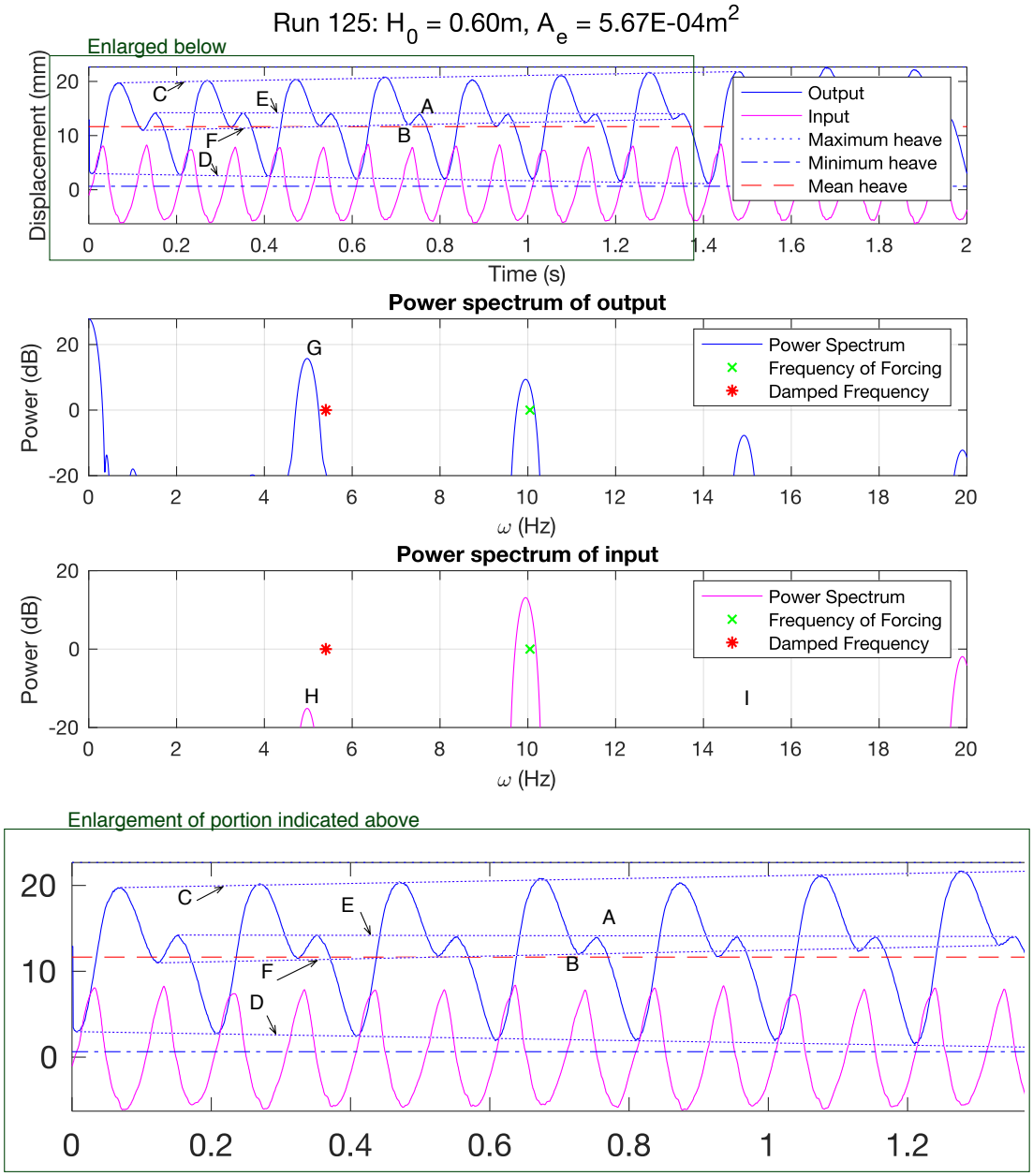


Figure H.73. Experimental trial data for Condition 125

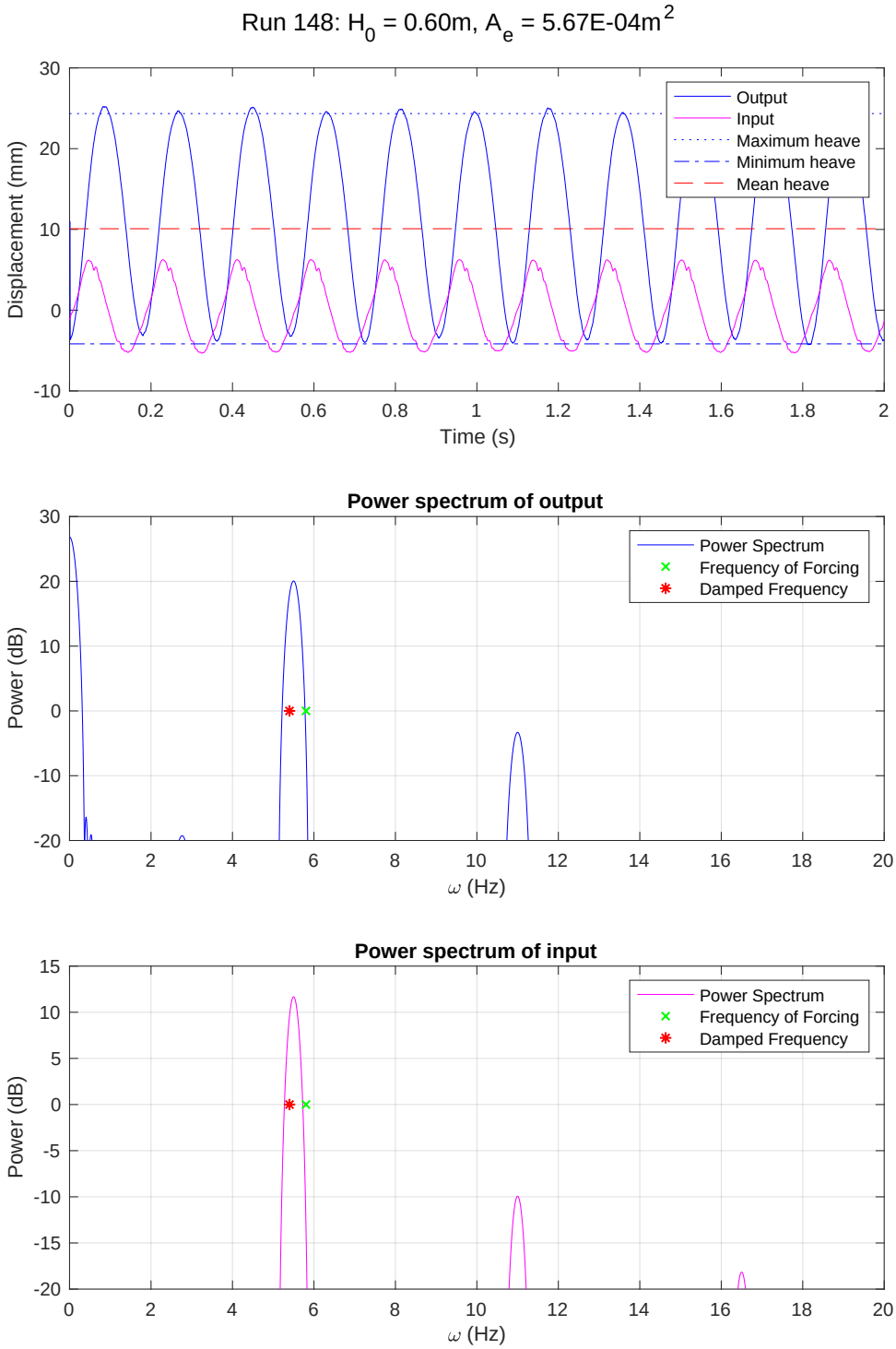


Figure H.74. Experimental trial data for Condition 148

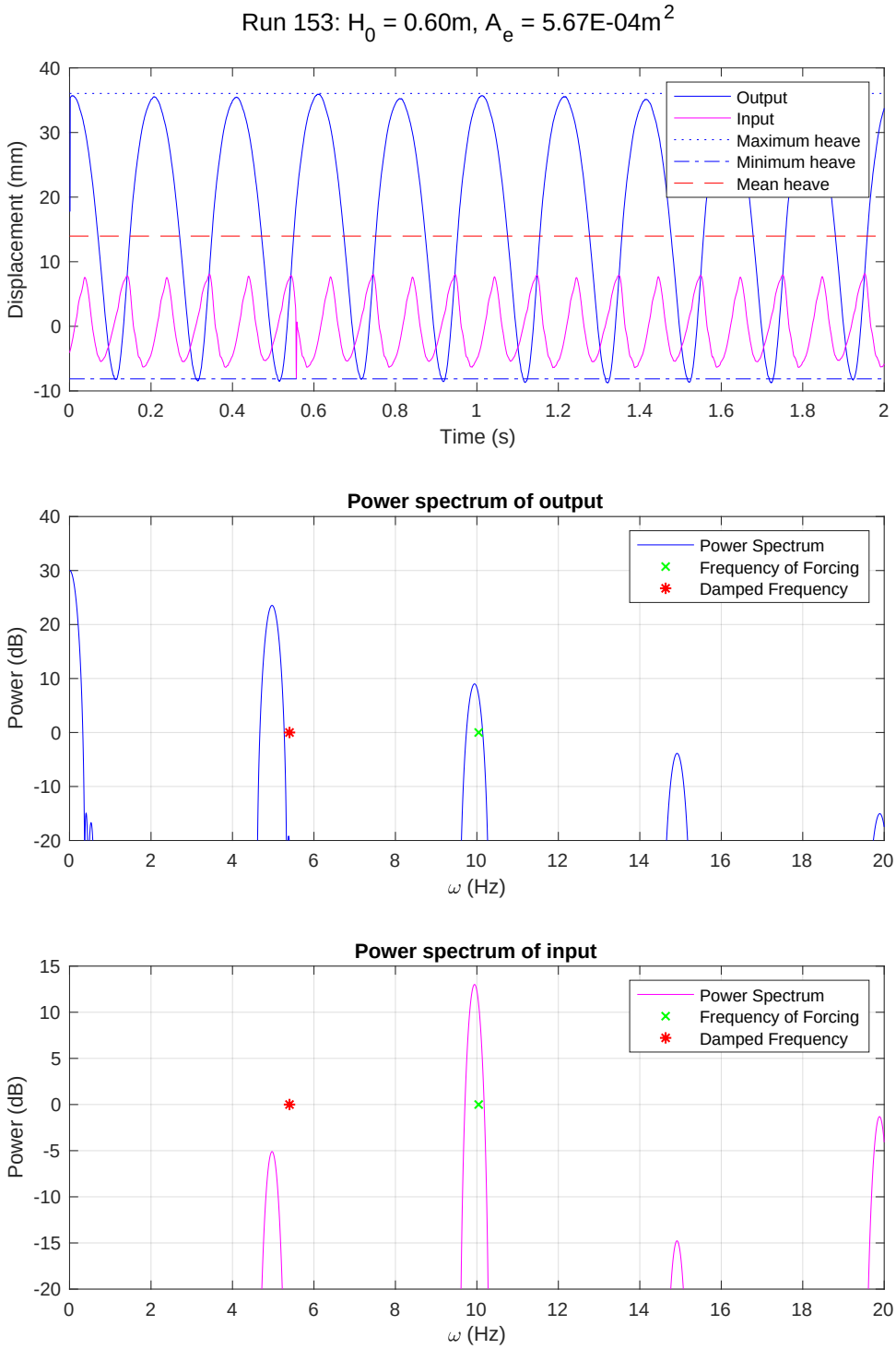


Figure H.75. Experimental trial data for Condition 153

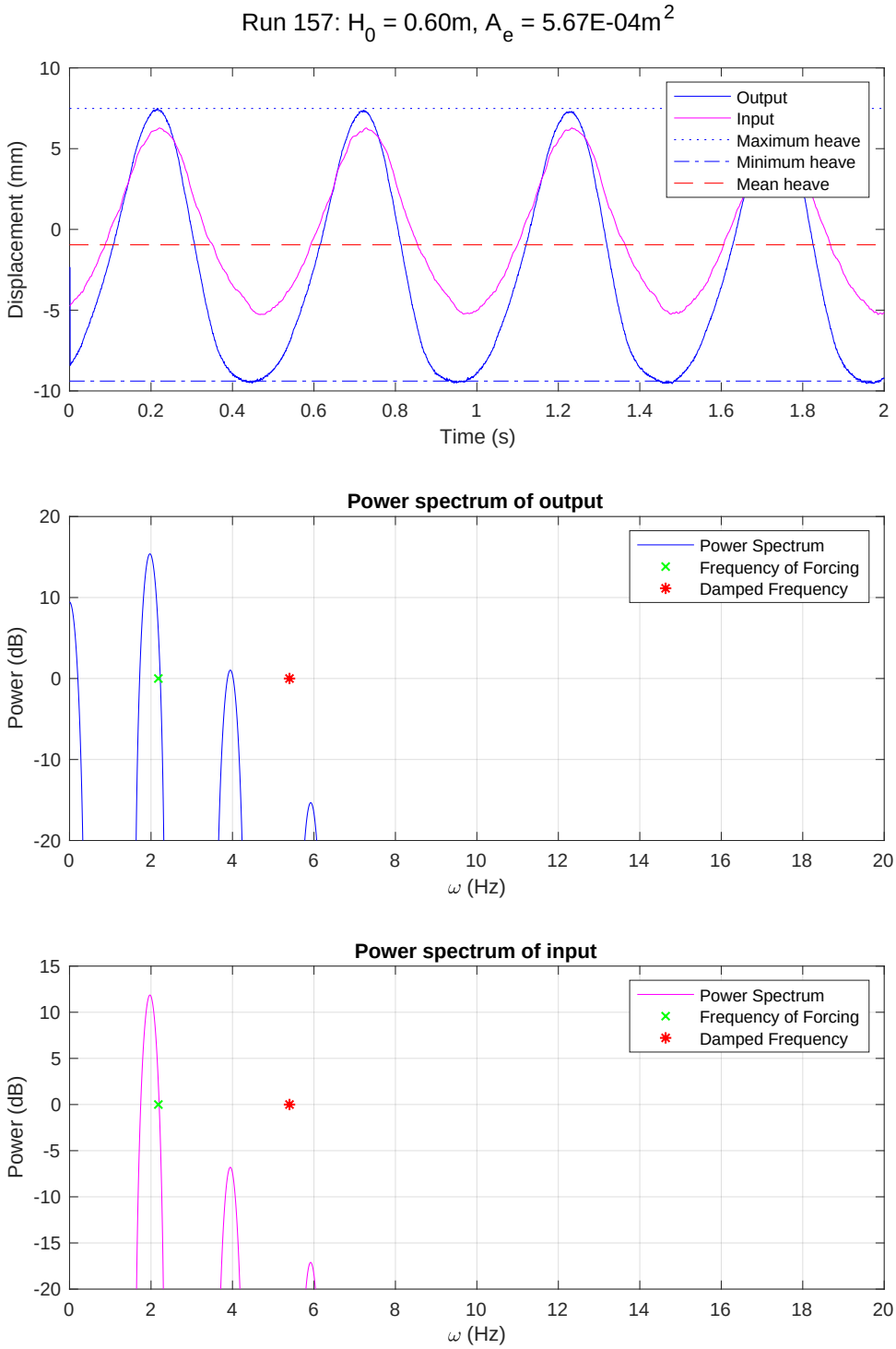


Figure H.76. Experimental trial data for Condition 157

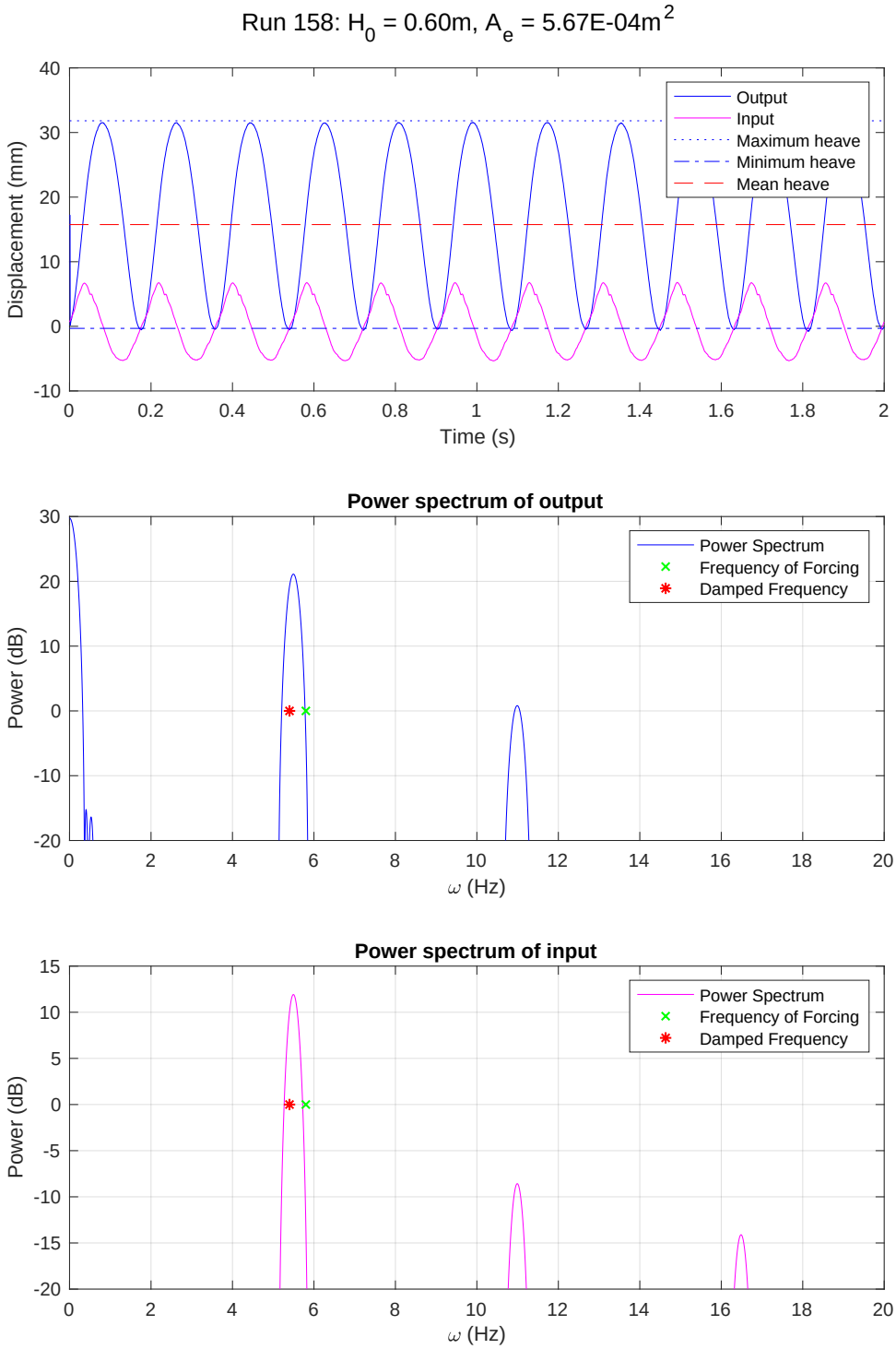


Figure H.77. Experimental trial data for Condition 158

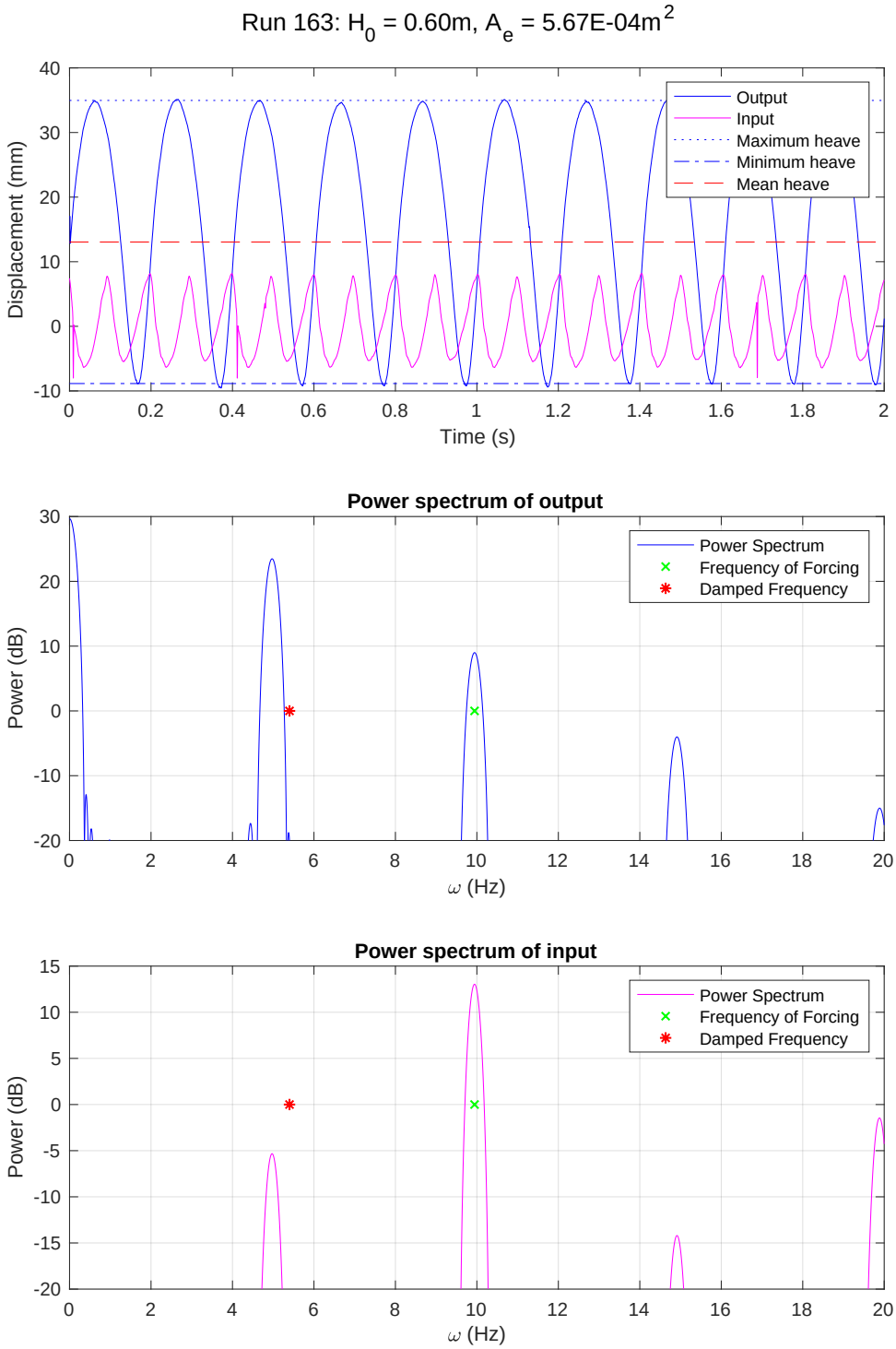


Figure H.78. Experimental trial data for Condition 163

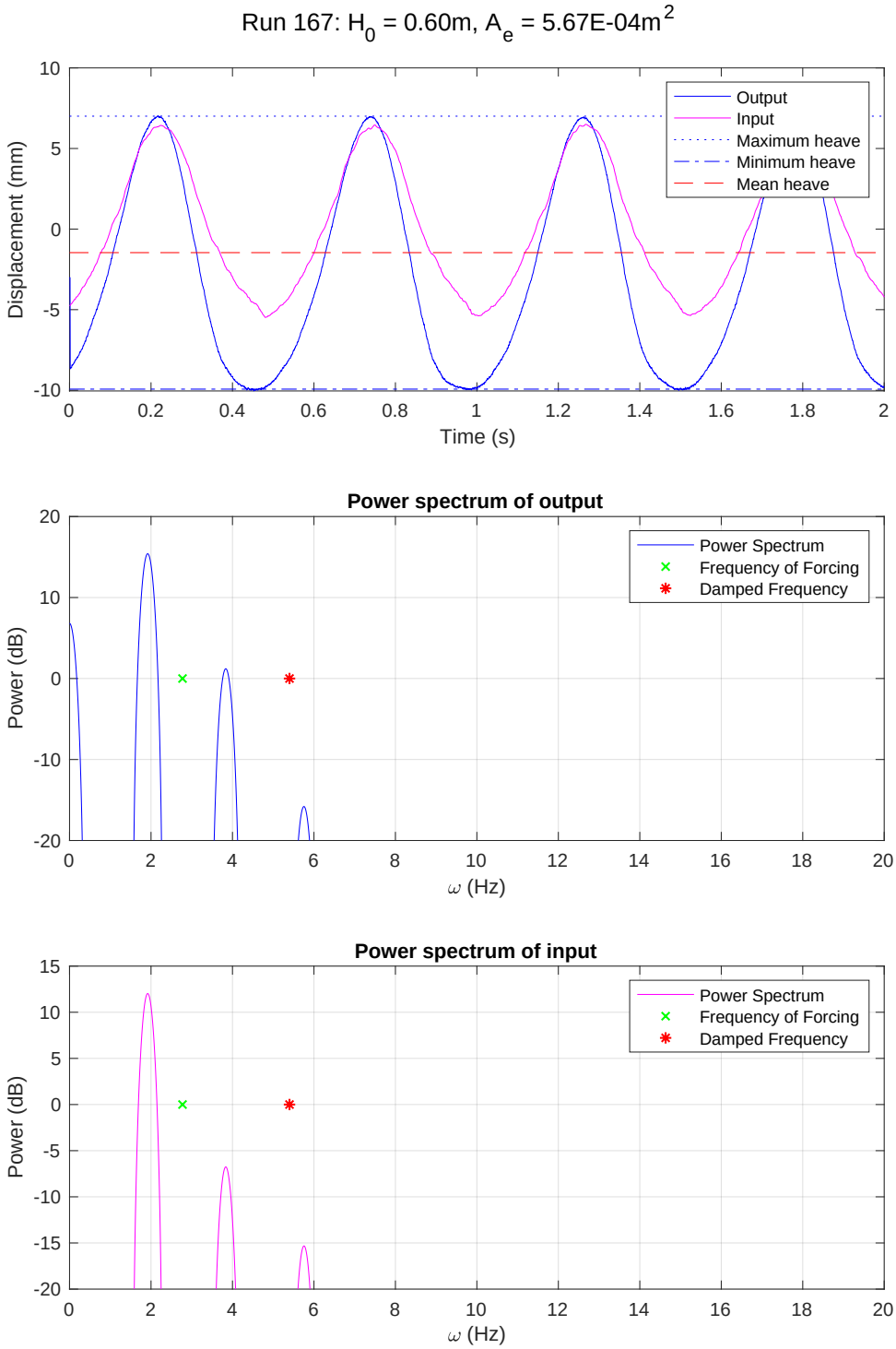


Figure H.79. Experimental trial data for Condition 167

H.2.5. Condition Five

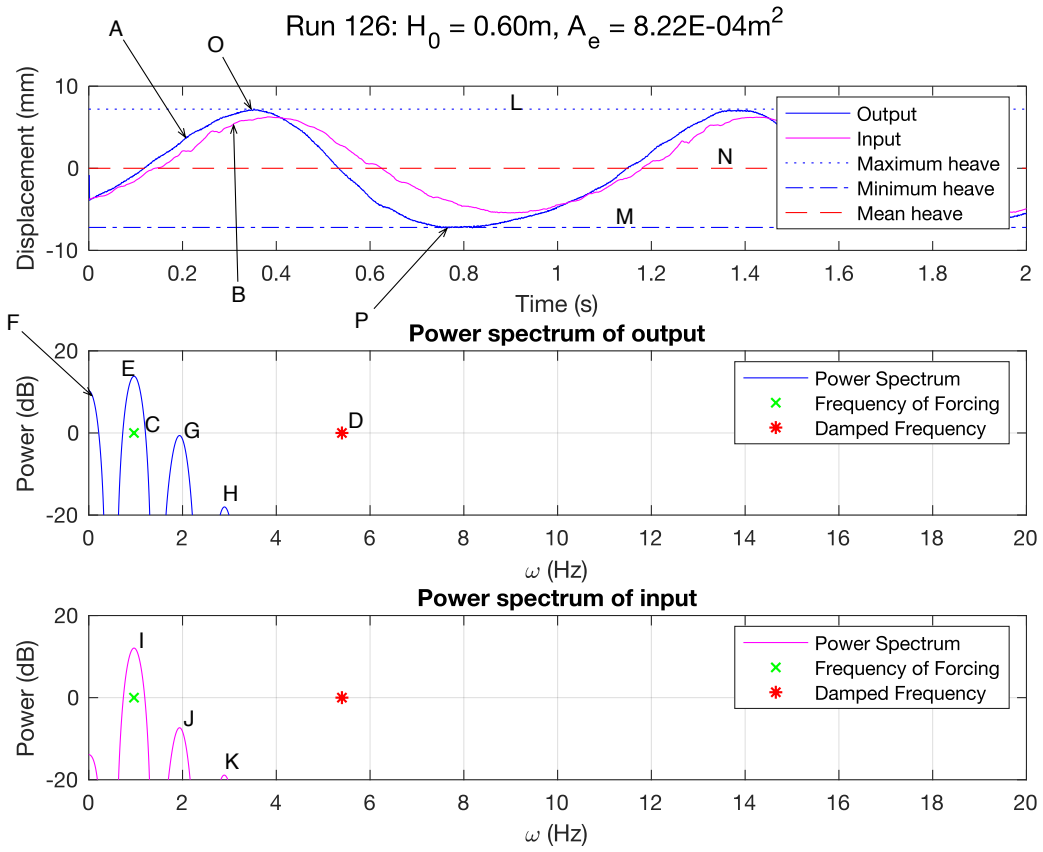


Figure H.80. Experimental trial data for Condition 126

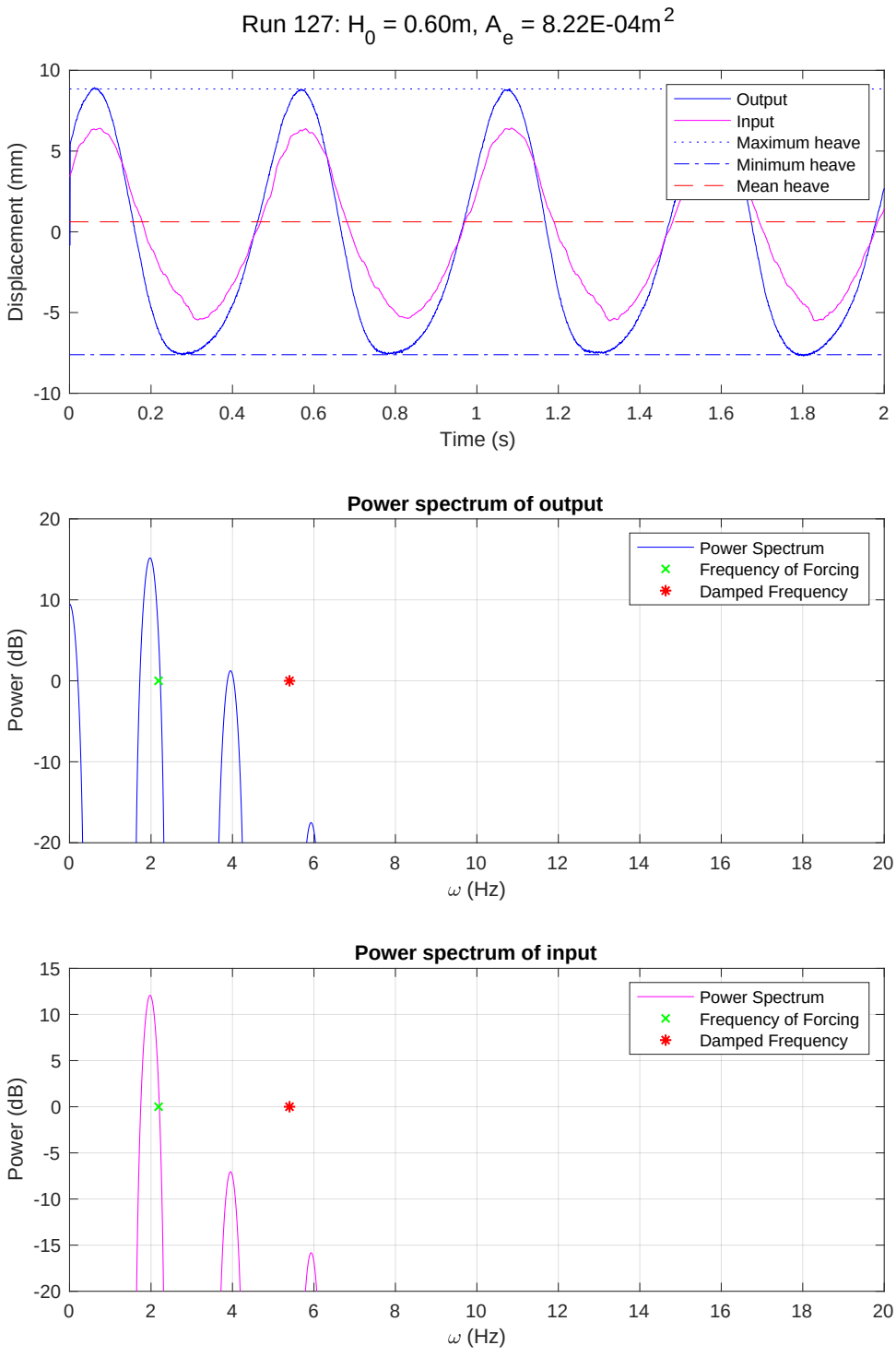


Figure H.81. Experimental trial data for Condition 127

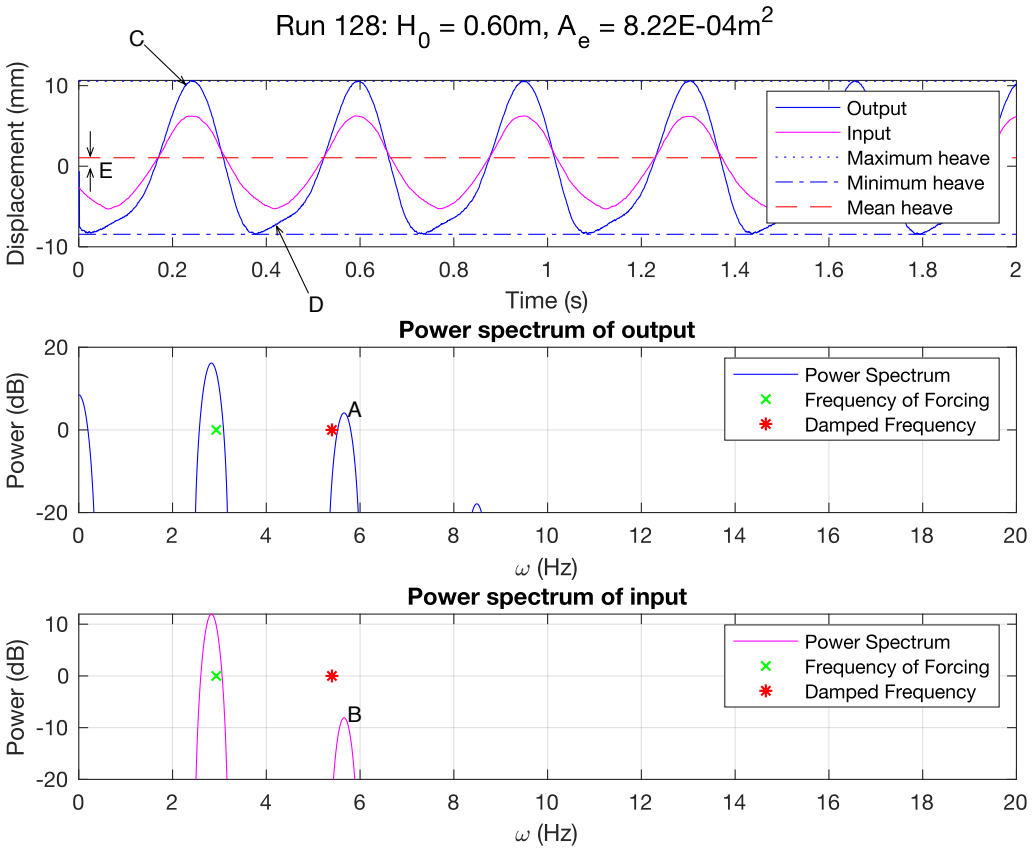


Figure H.82. Experimental trial data for Condition 128

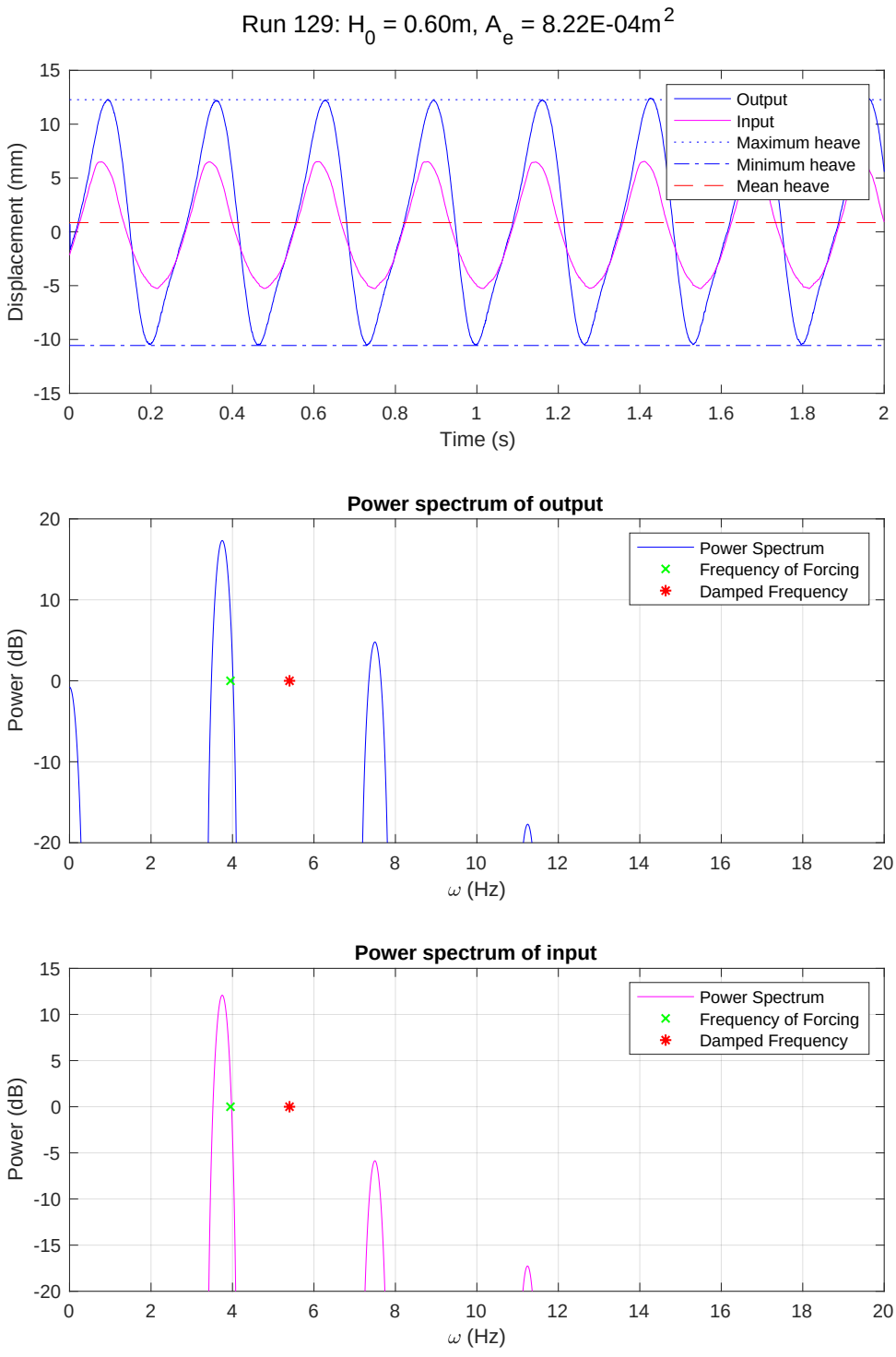


Figure H.83. Experimental trial data for Condition 129

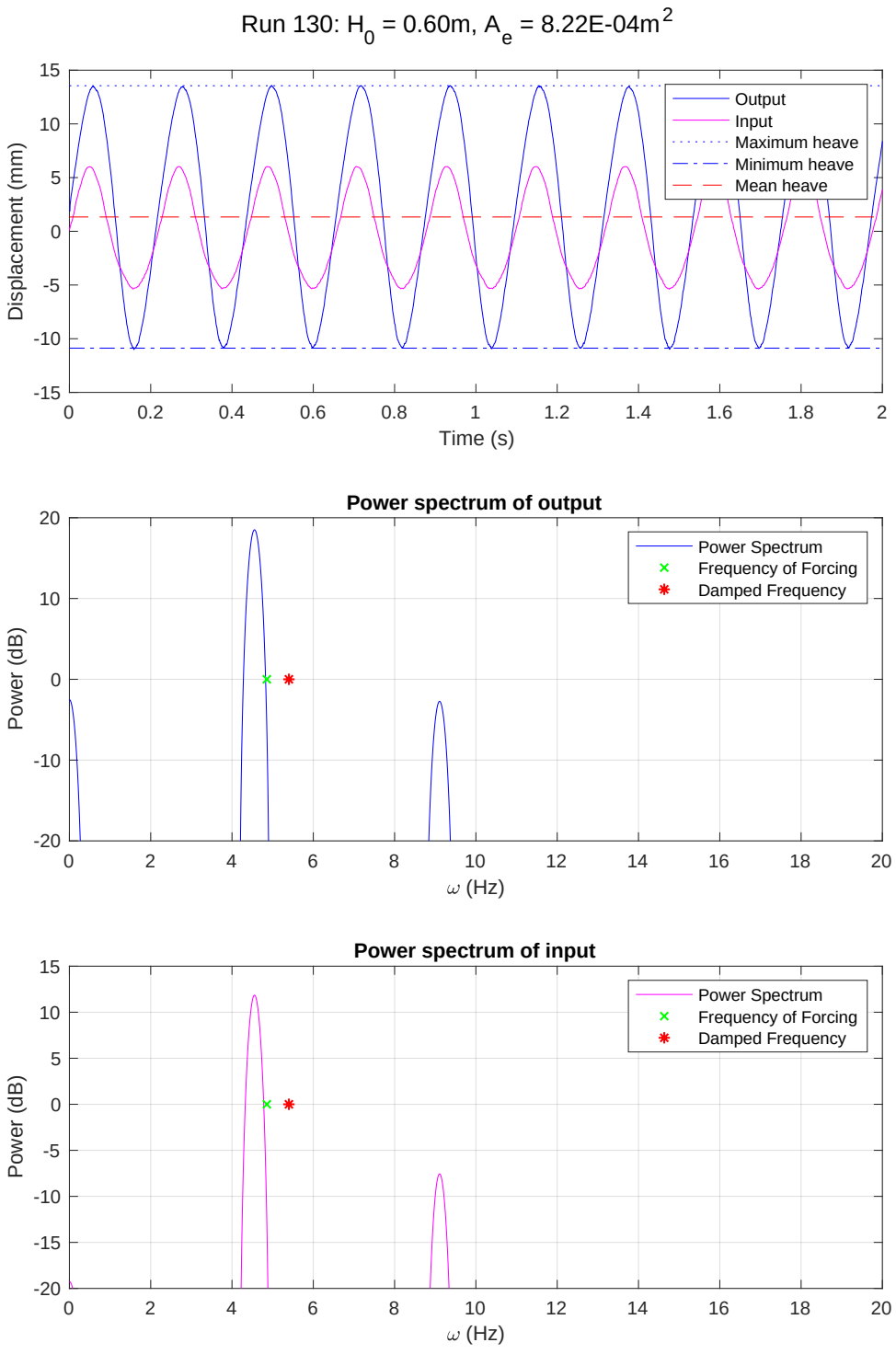


Figure H.84. Experimental trial data for Condition 130

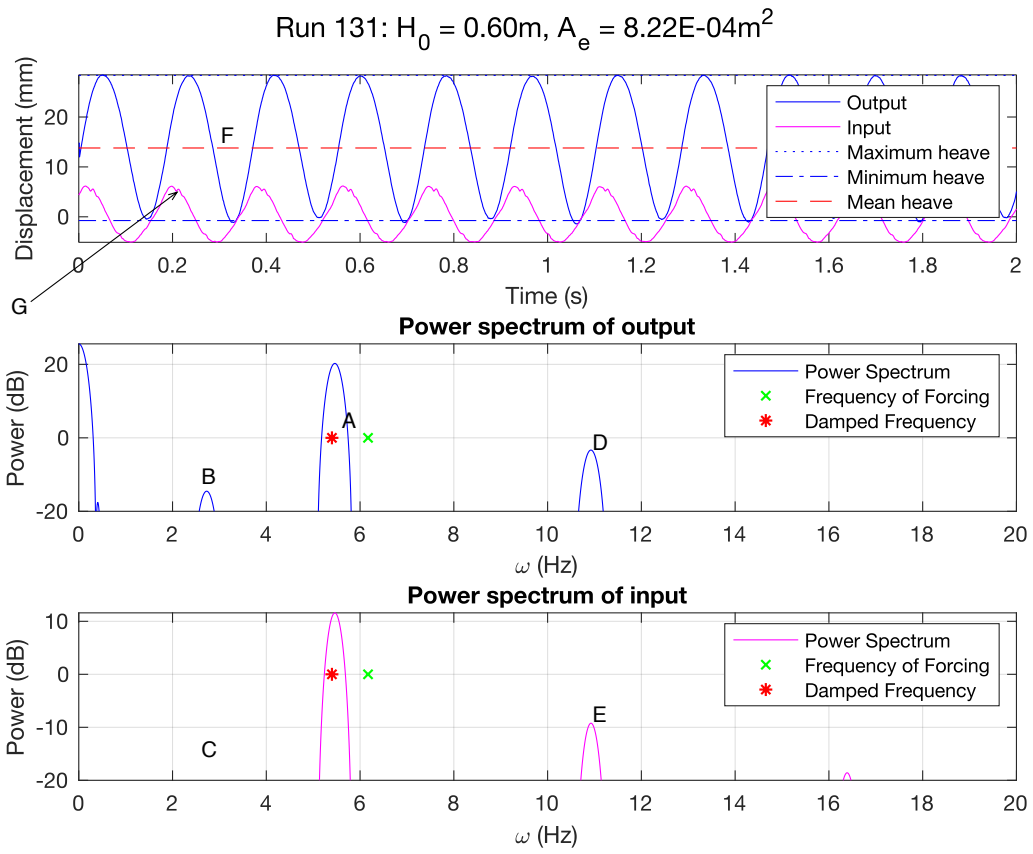


Figure H.85. Experimental trial data for Condition 131

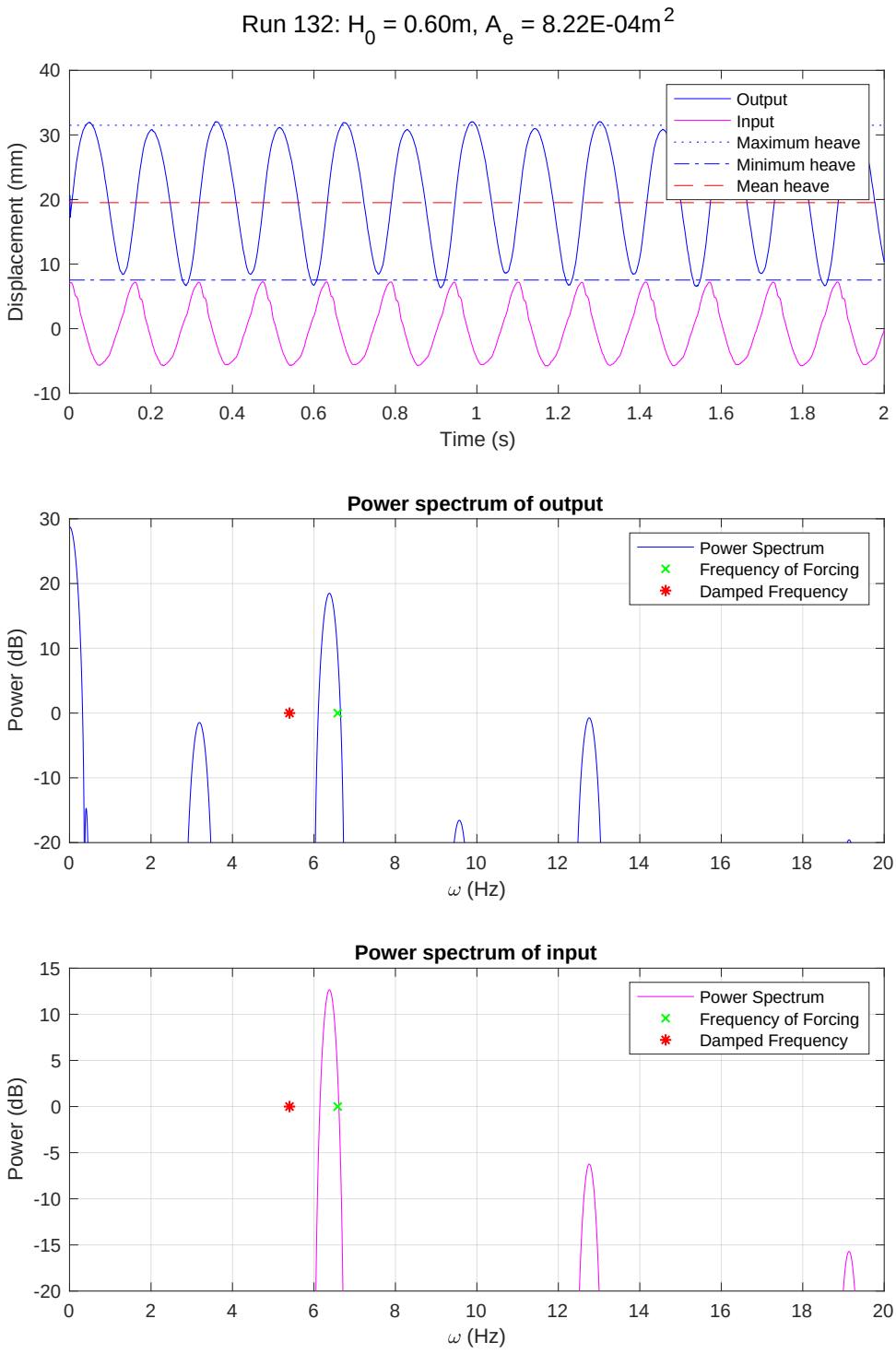


Figure H.86. Experimental trial data for Condition 132

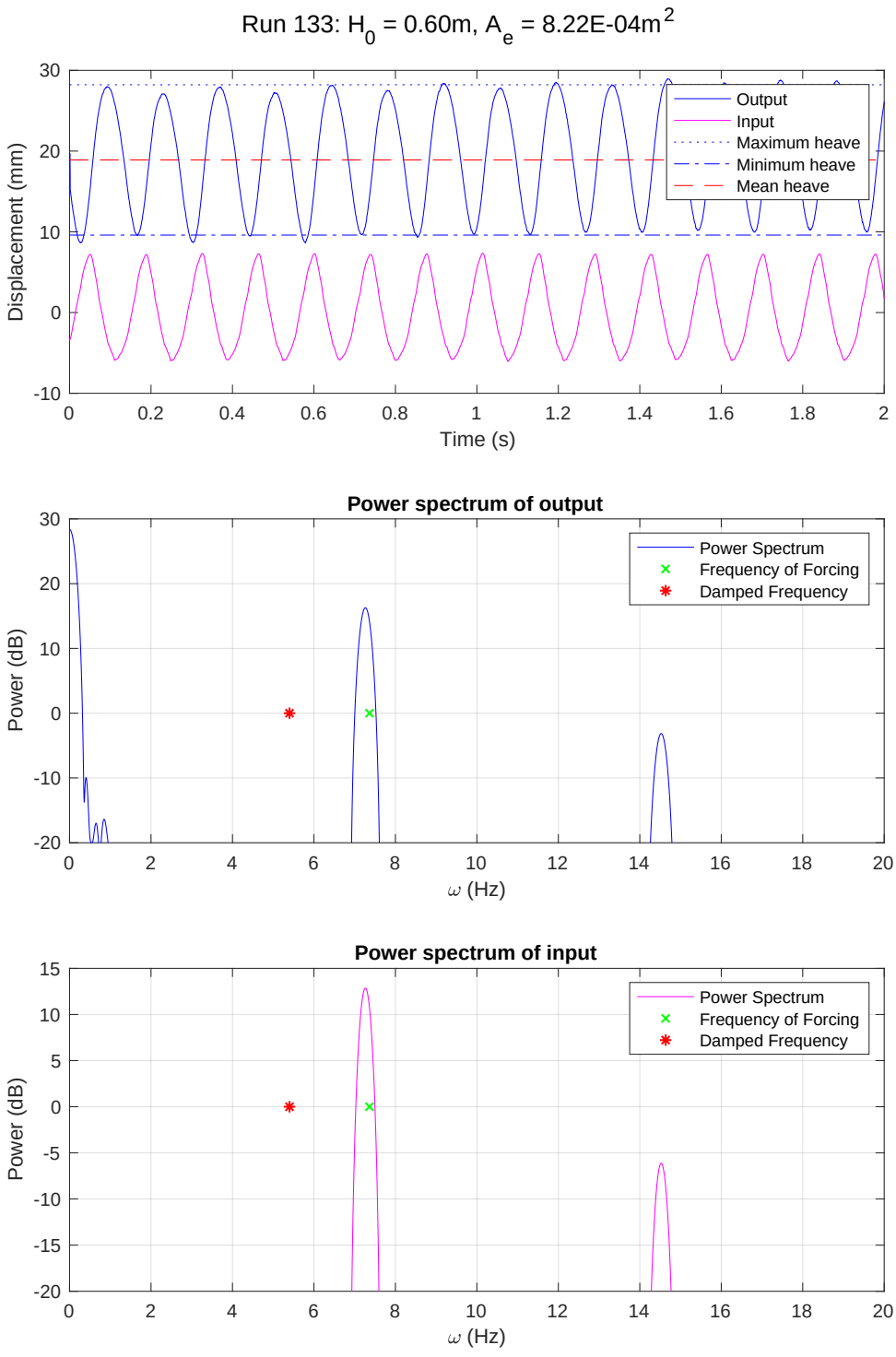


Figure H.87. Experimental trial data for Condition 133

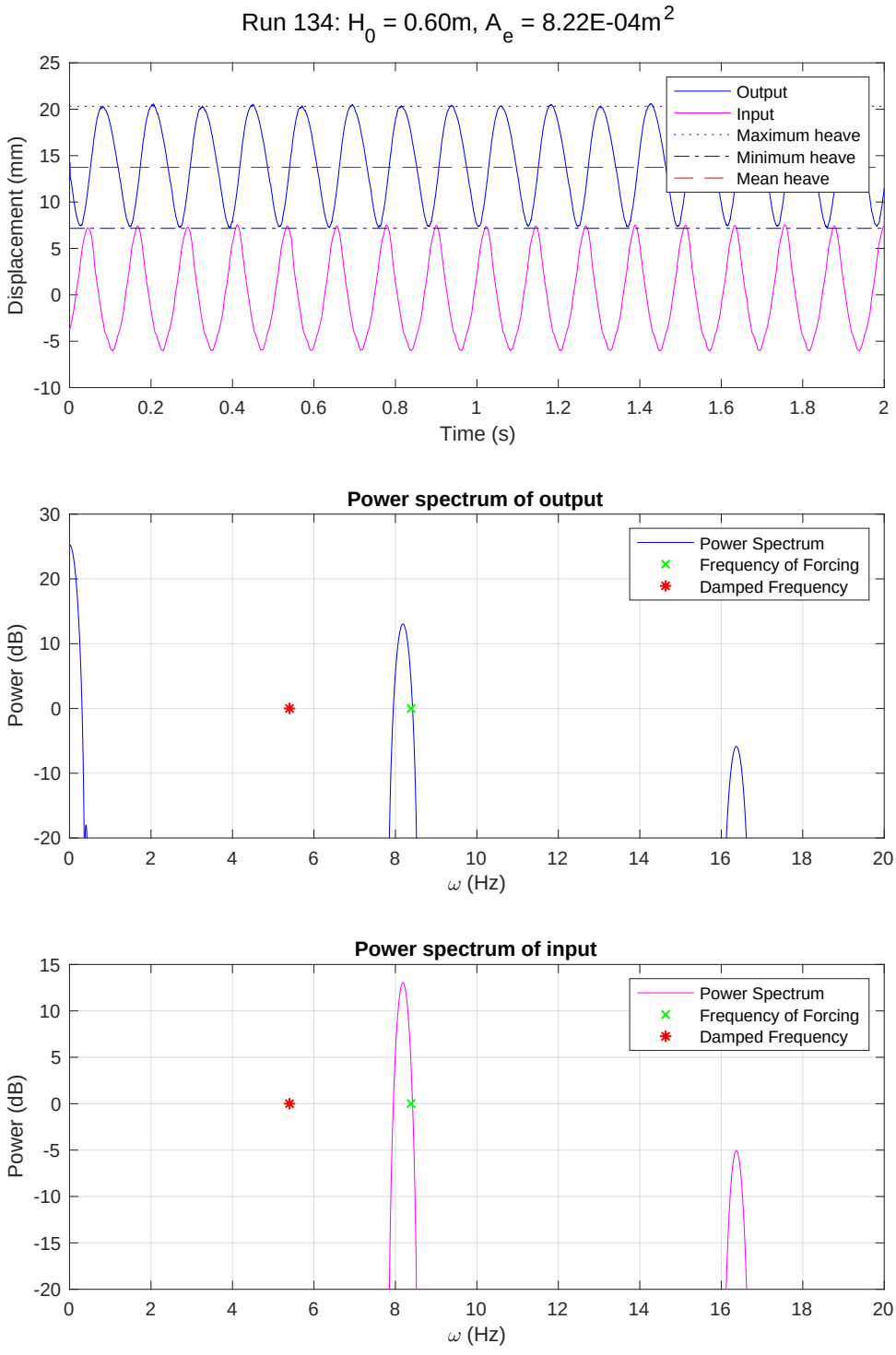


Figure H.88. Experimental trial data for Condition 134

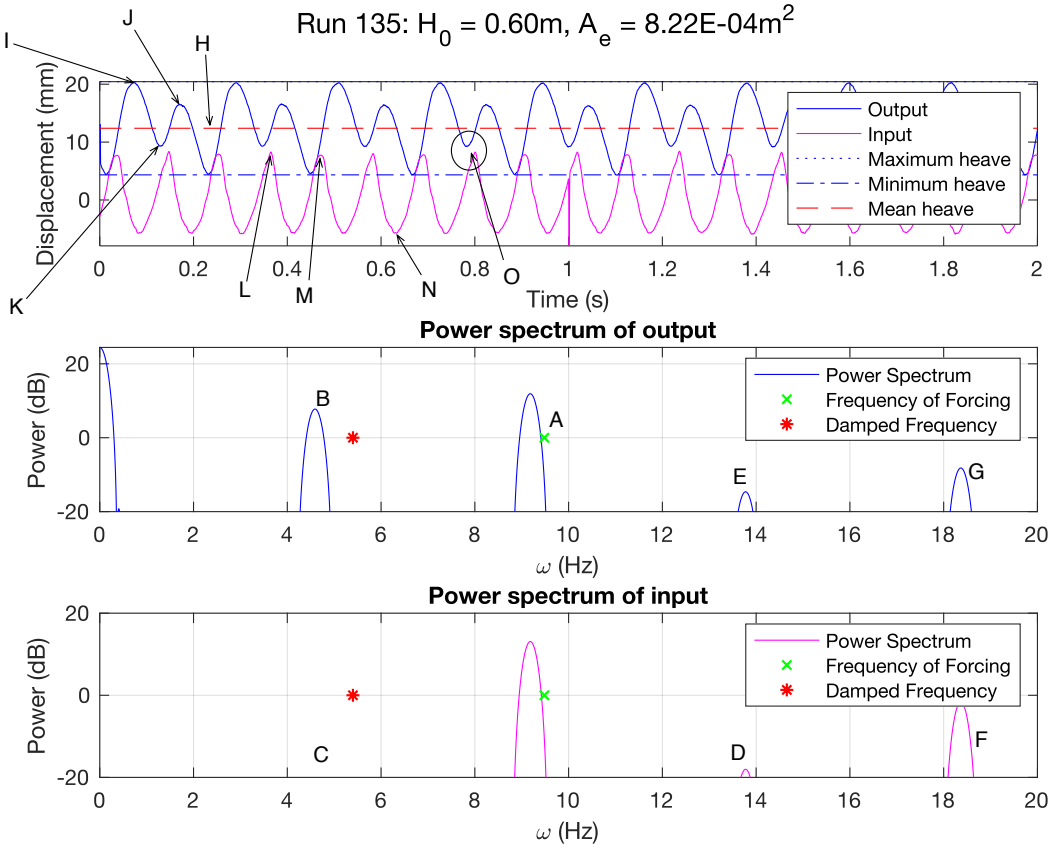


Figure H.89. Experimental trial data for Condition 135

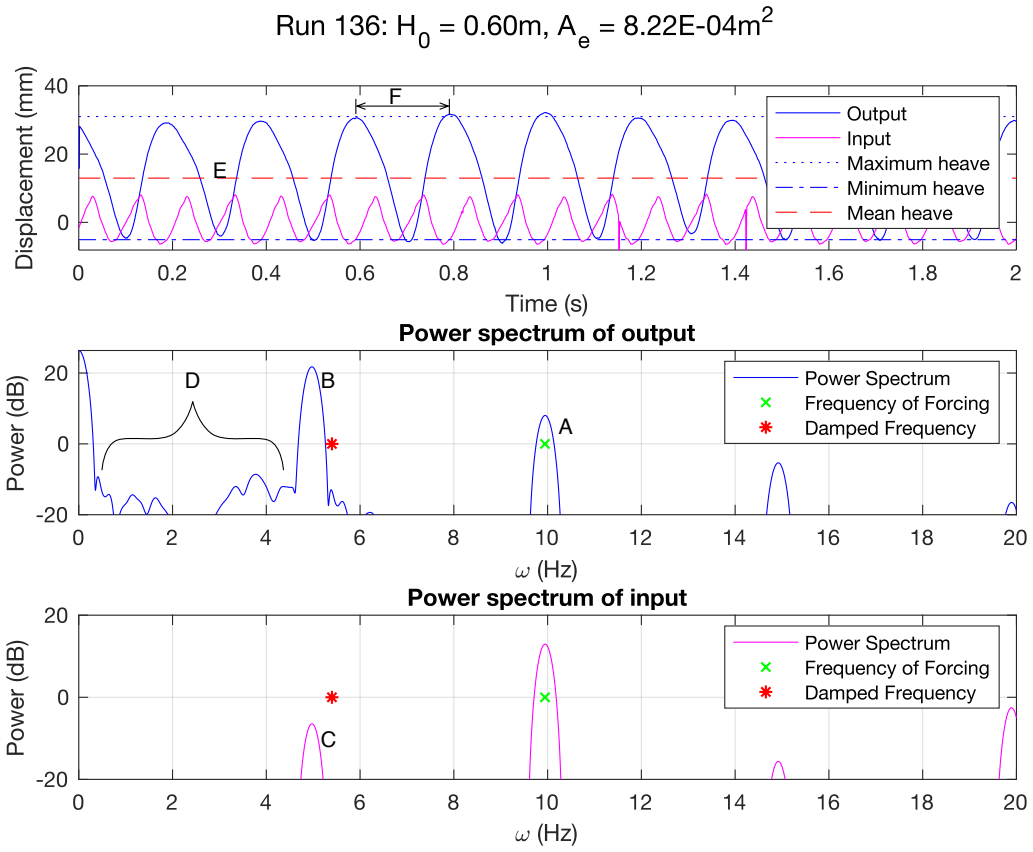


Figure H.90. Experimental trial data for Condition 136

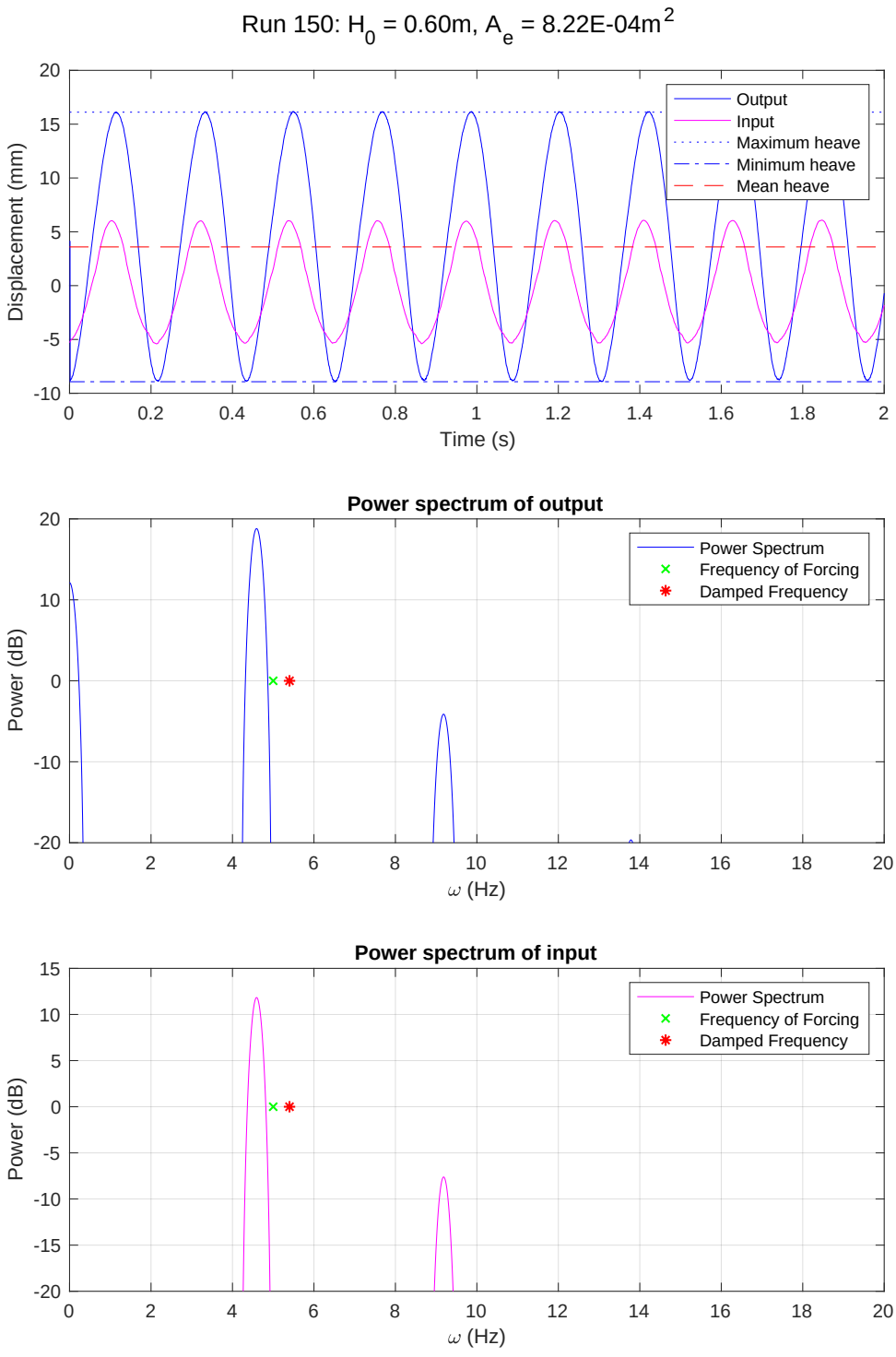


Figure H.91. Experimental trial data for Condition 150

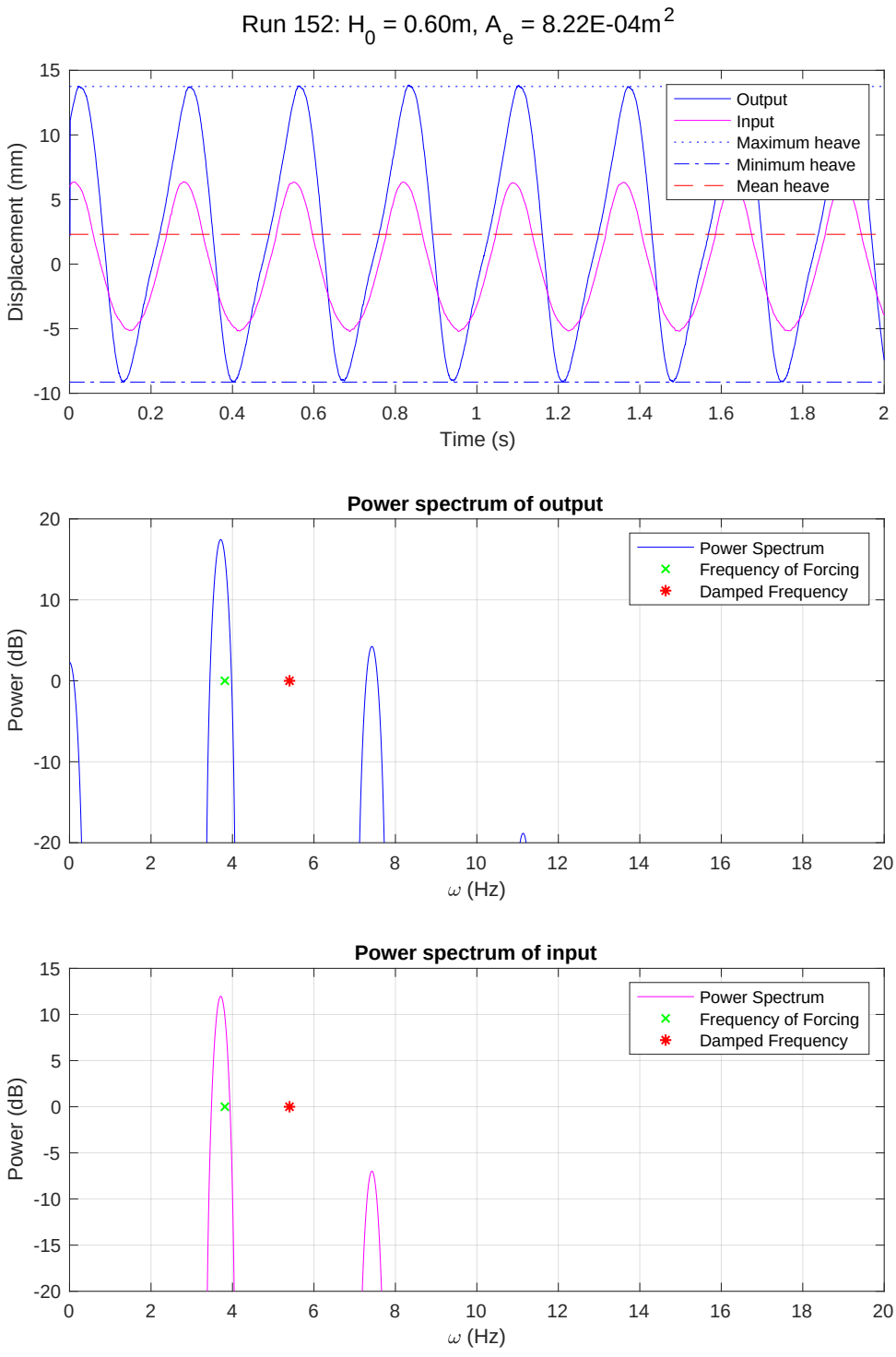


Figure H.92. Experimental trial data for Condition 152

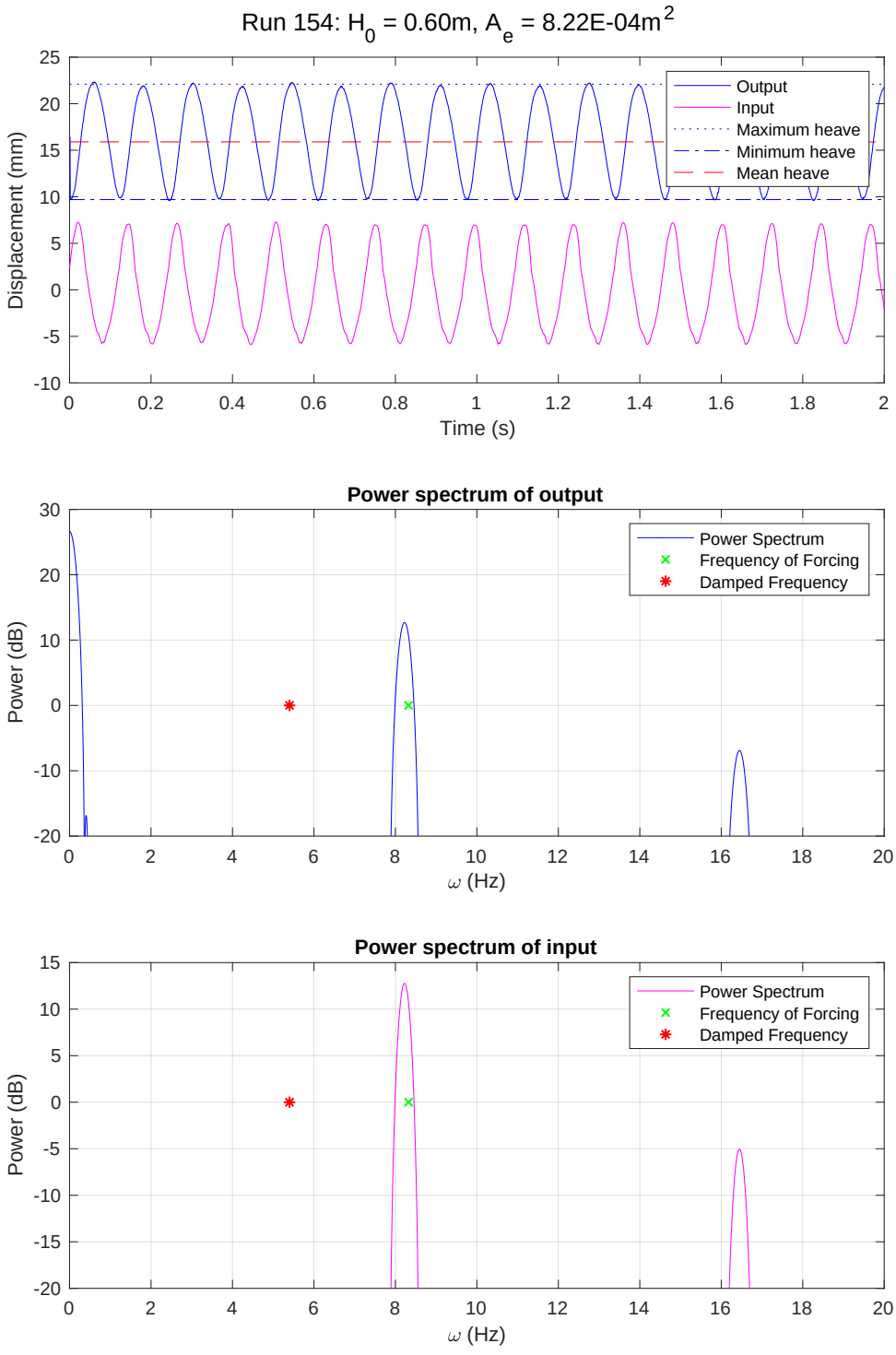


Figure H.93. Experimental trial data for Condition 154

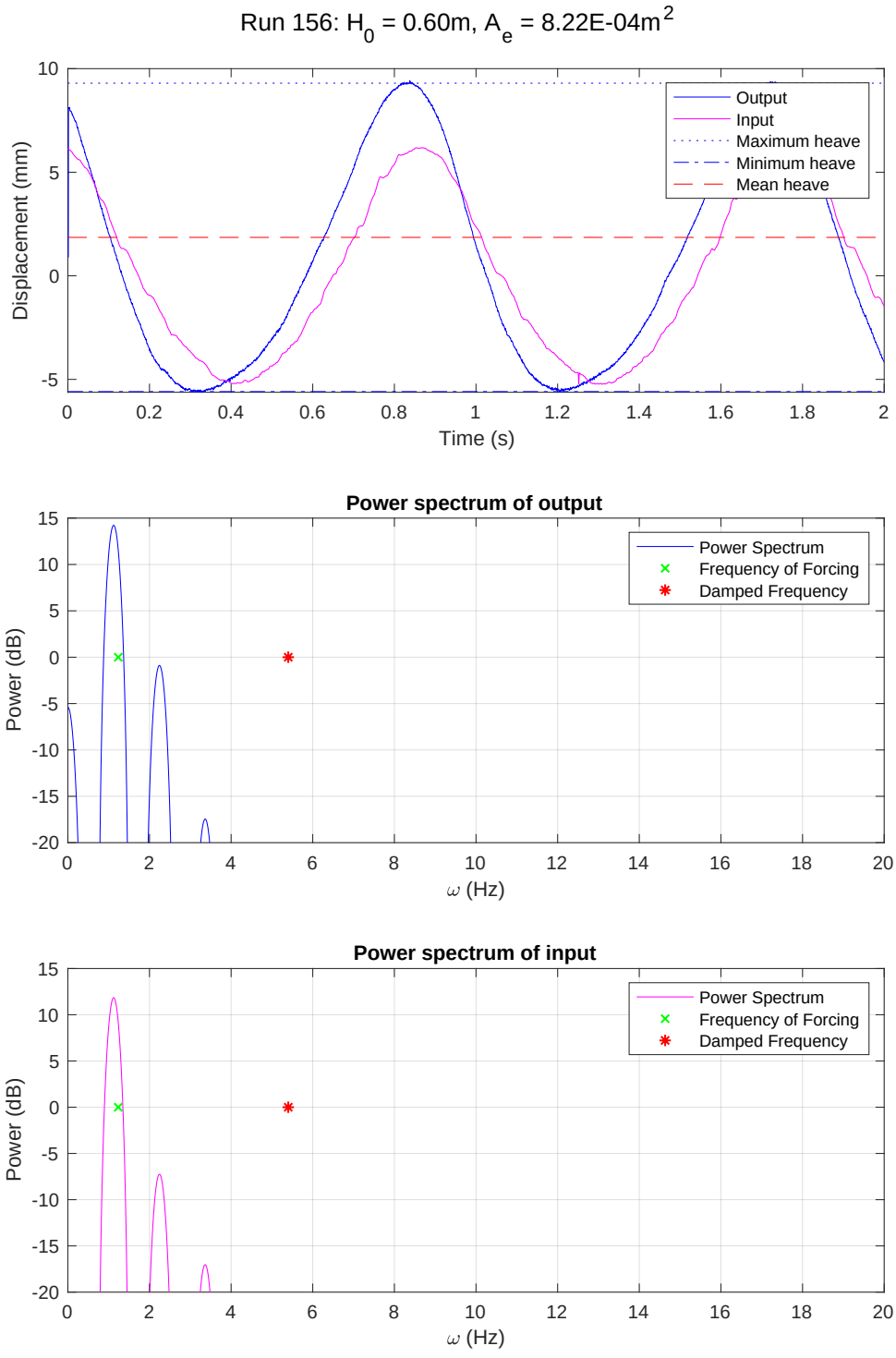


Figure H.94. Experimental trial data for Condition 156

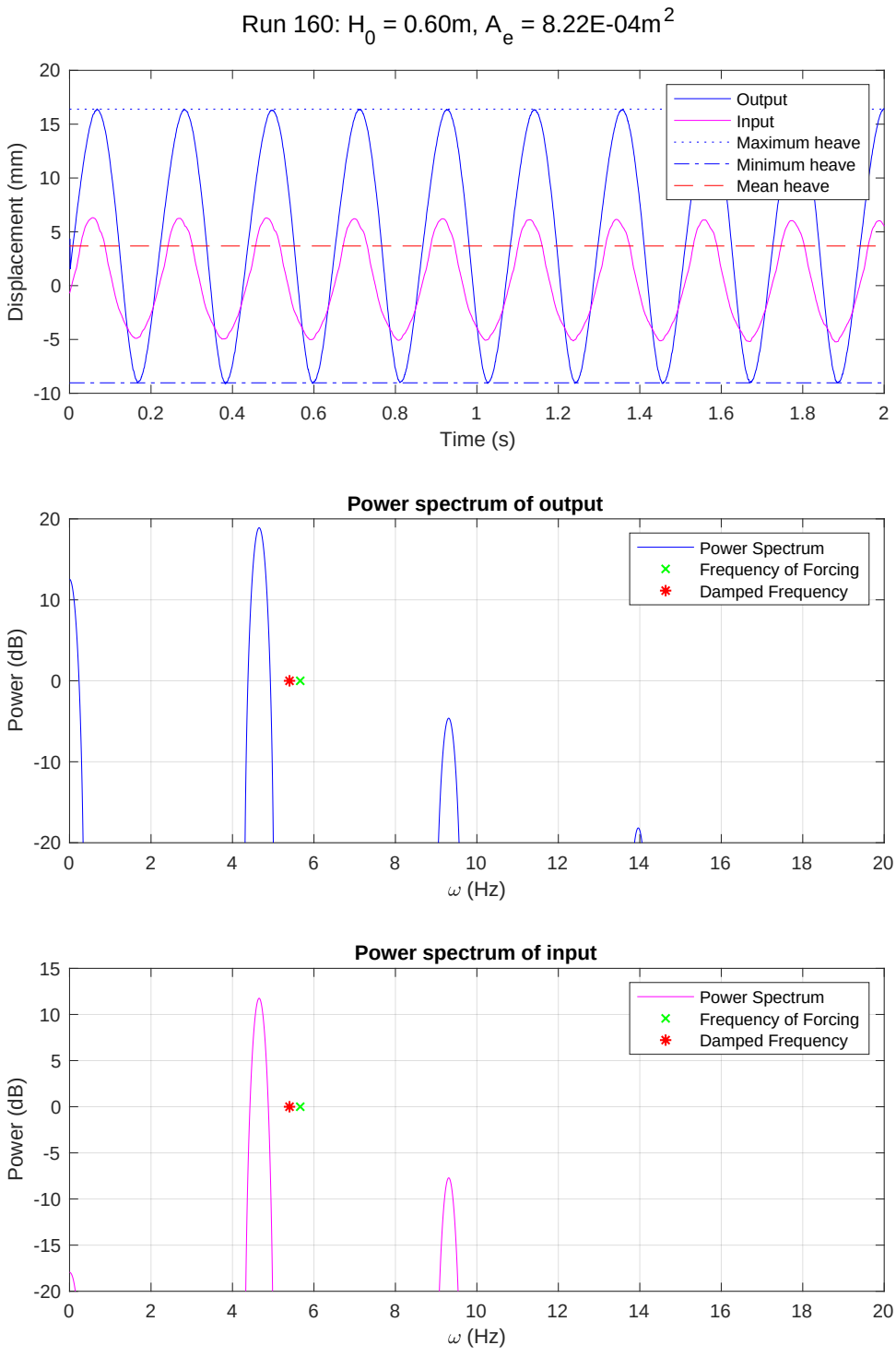


Figure H.95. Experimental trial data for Condition 160

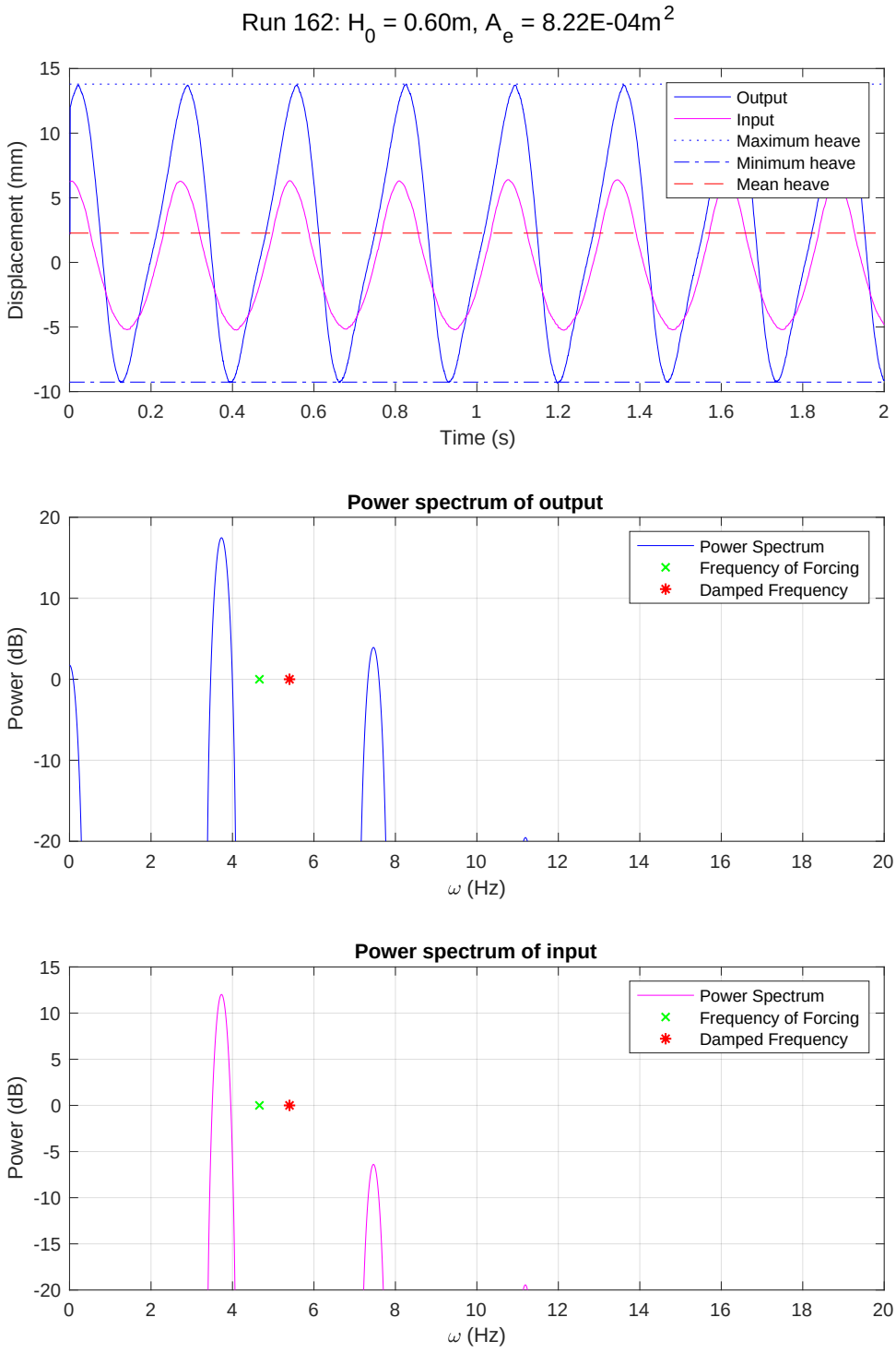


Figure H.96. Experimental trial data for Condition 162

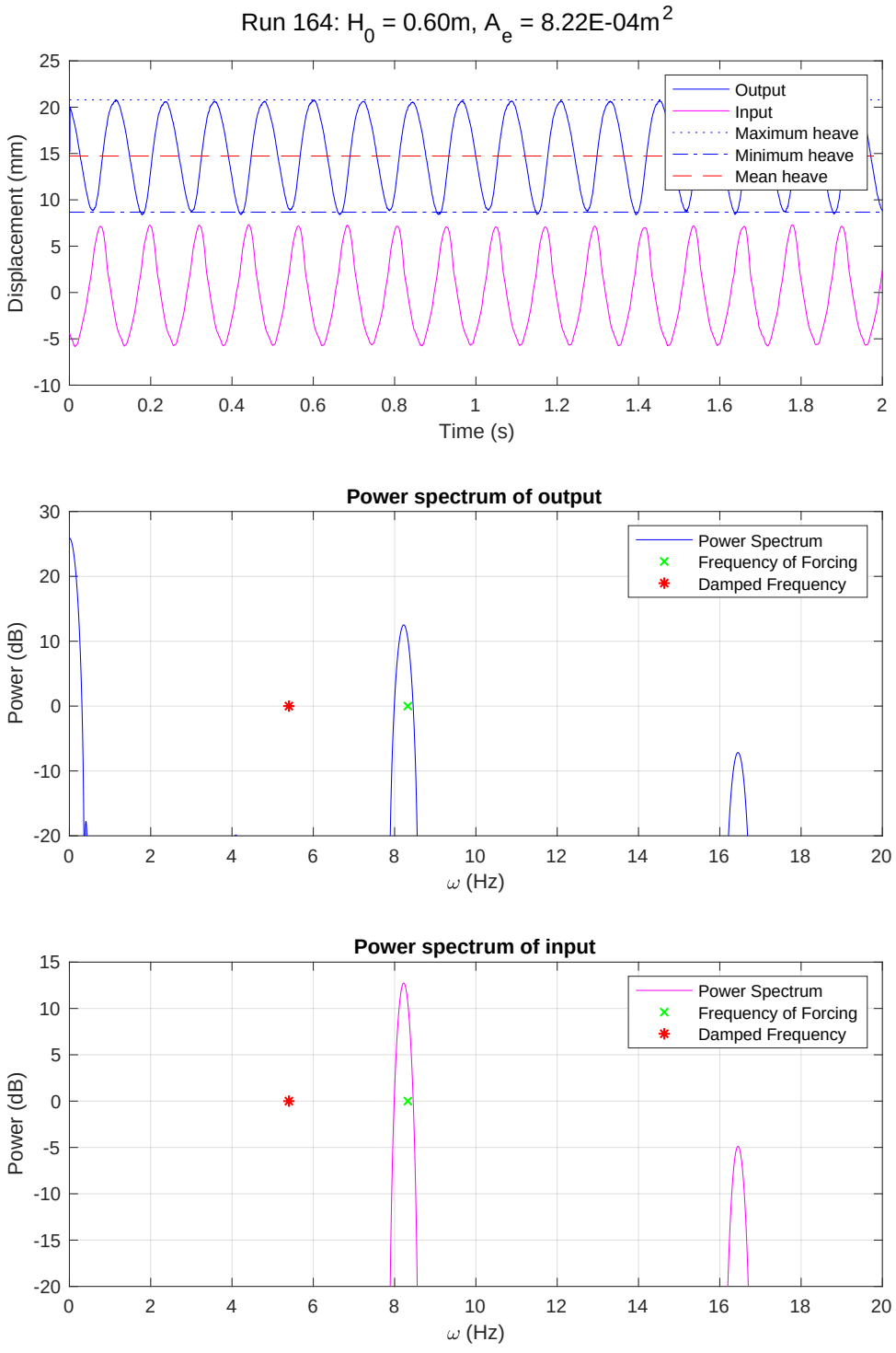


Figure H.97. Experimental trial data for Condition 164

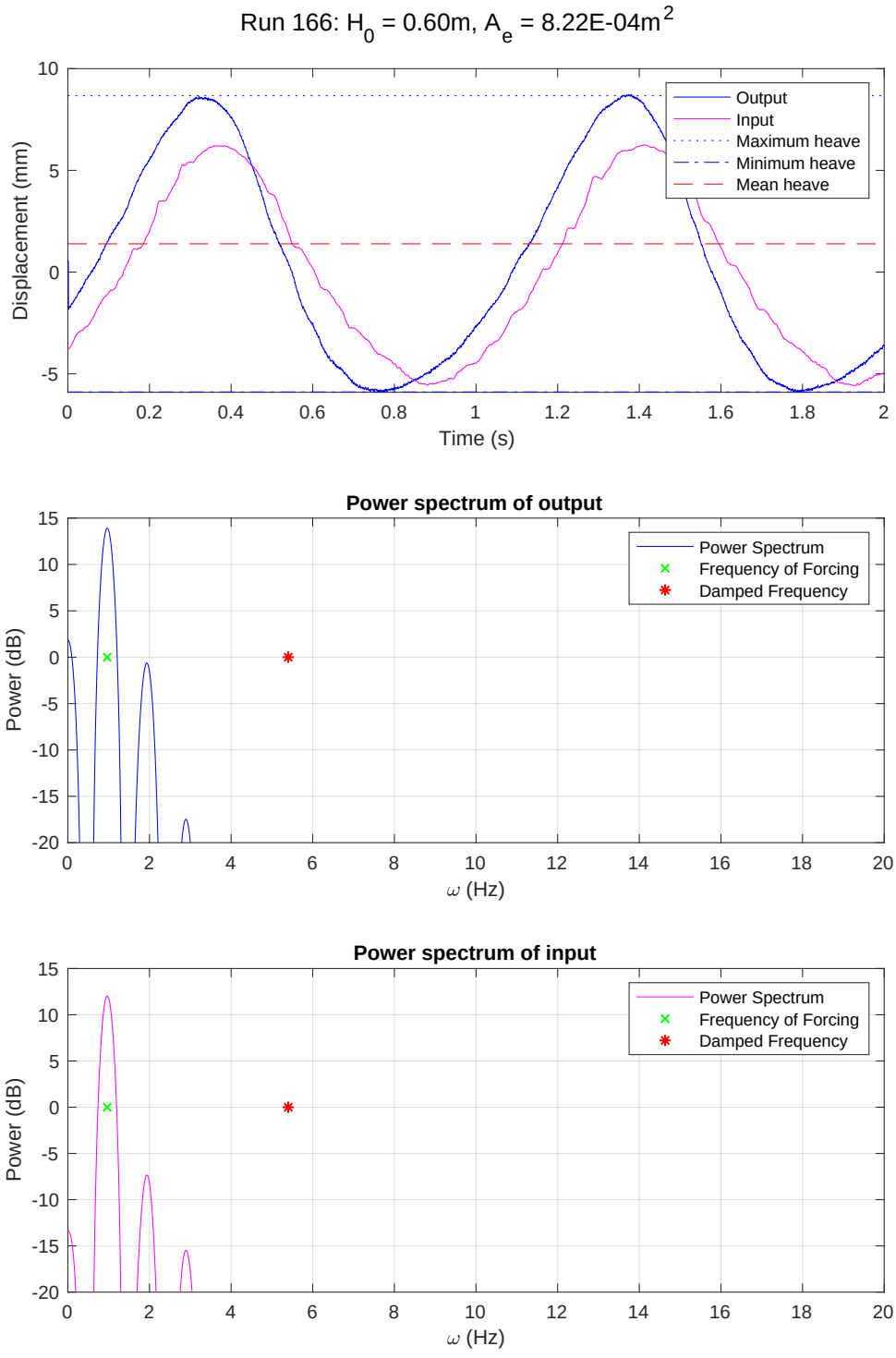


Figure H.98. Experimental trial data for Condition 166

H.2.6. Condition Six

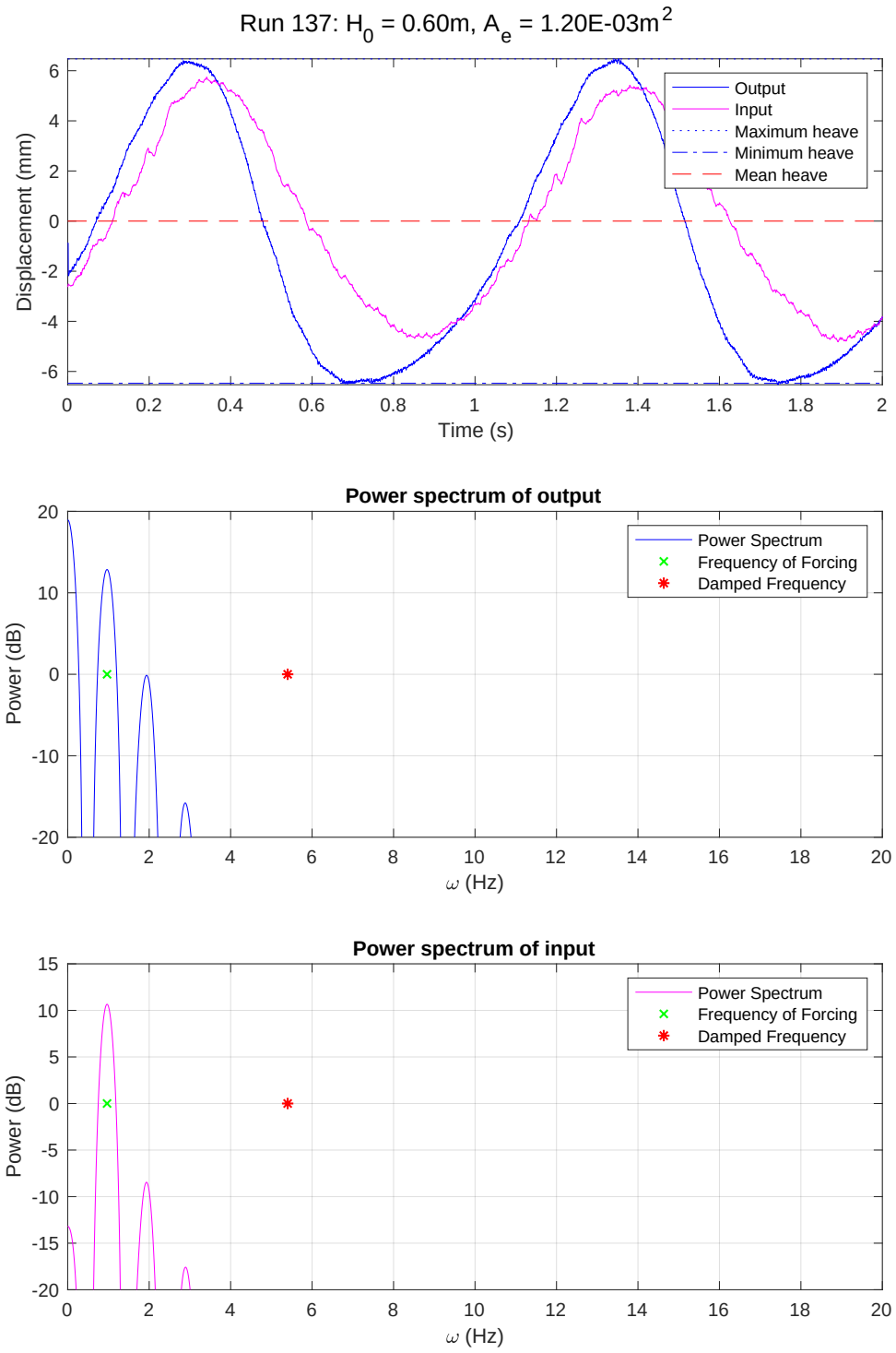


Figure H.99. Experimental trial data for Condition 137

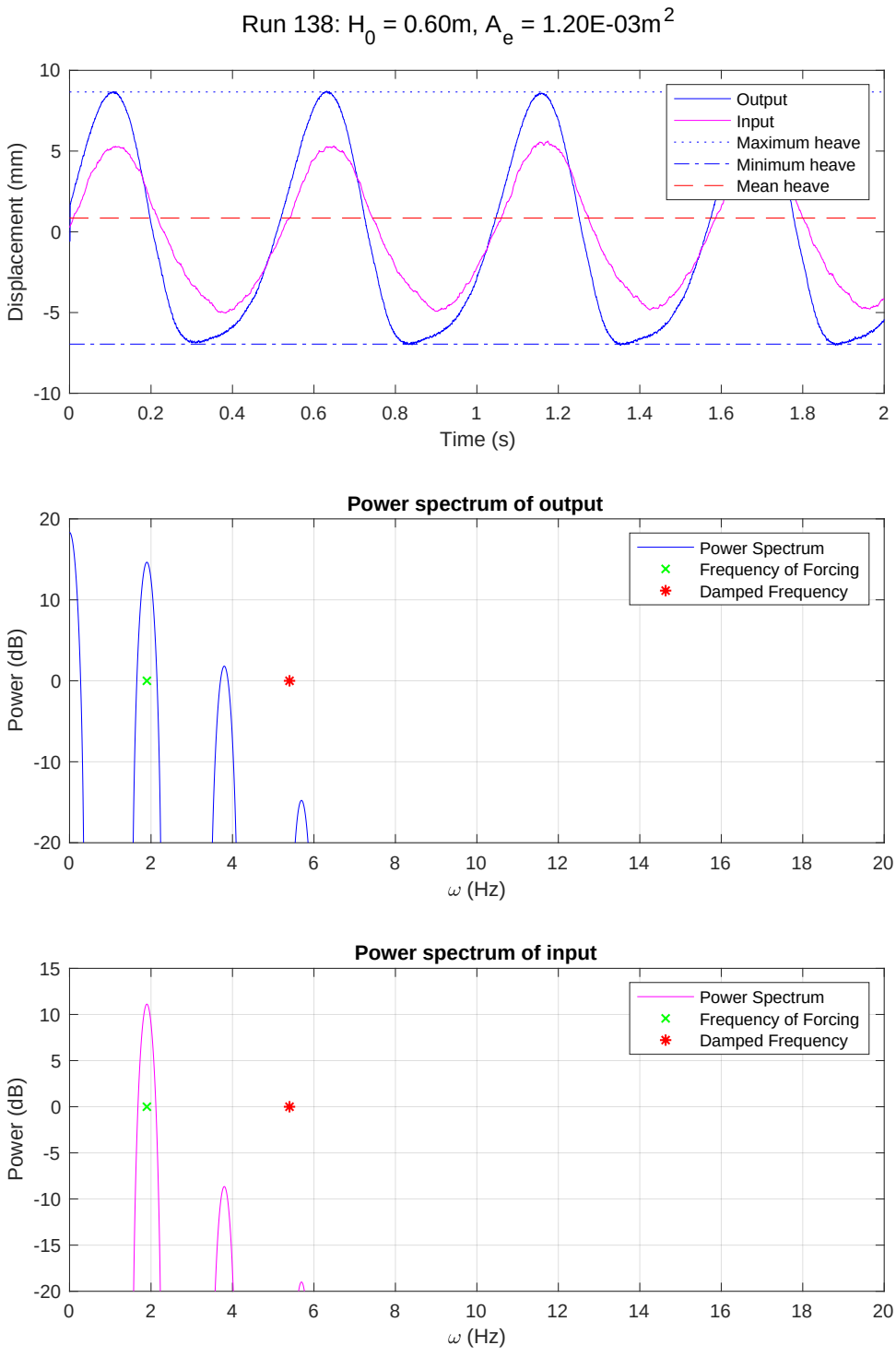


Figure H.100. Experimental trial data for Condition 138

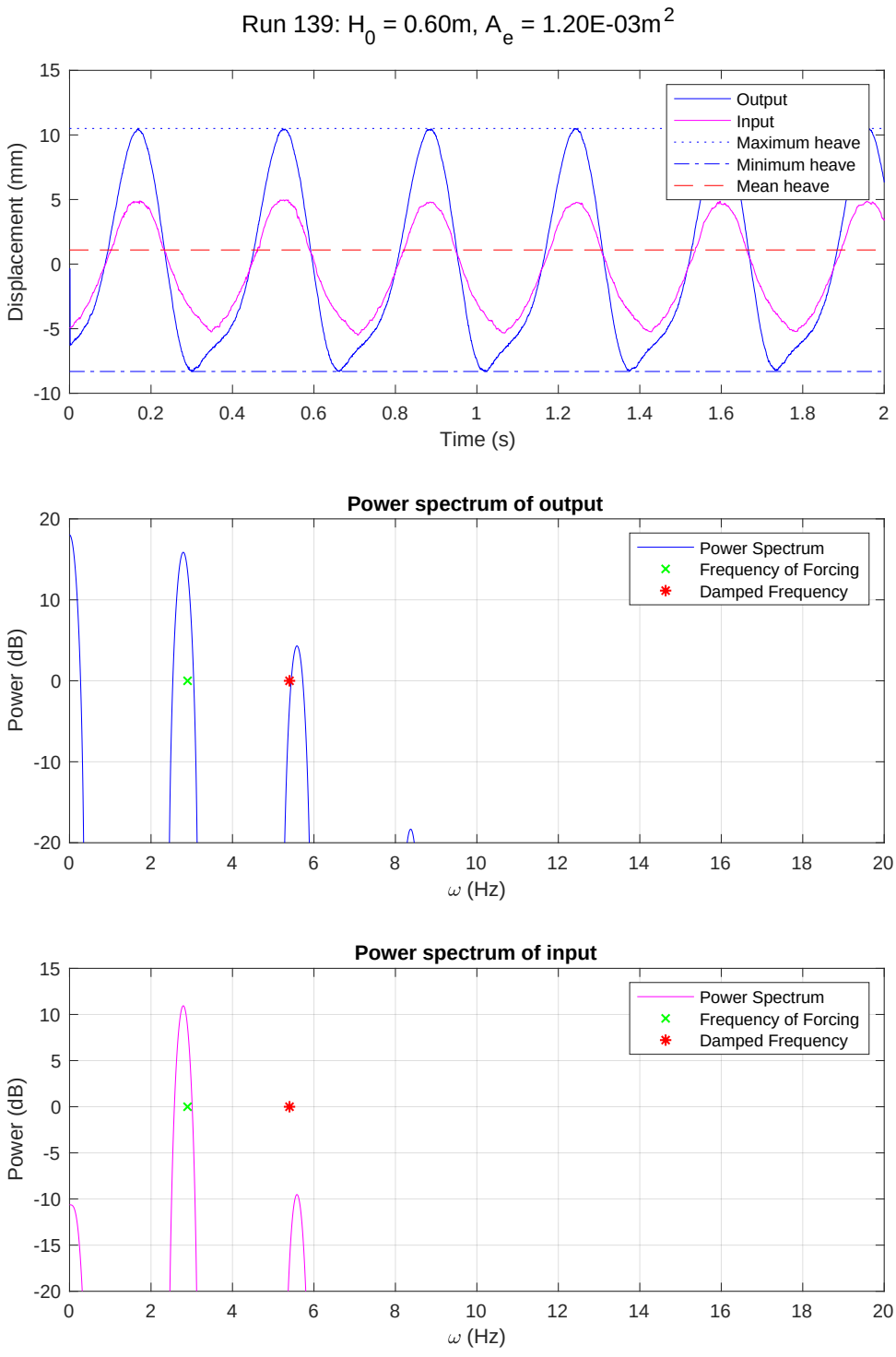


Figure H.101. Experimental trial data for Condition 139

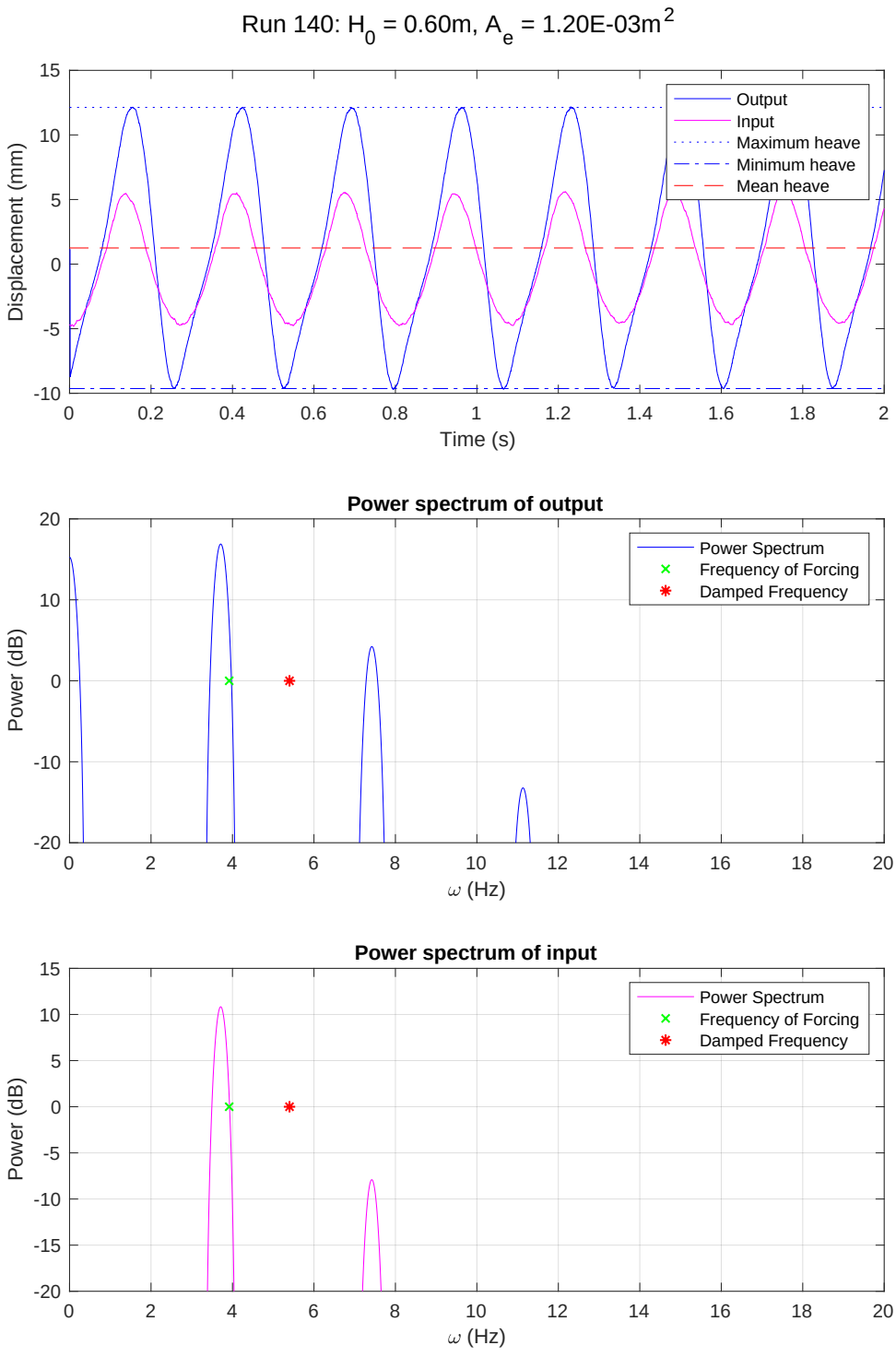


Figure H.102. Experimental trial data for Condition 140

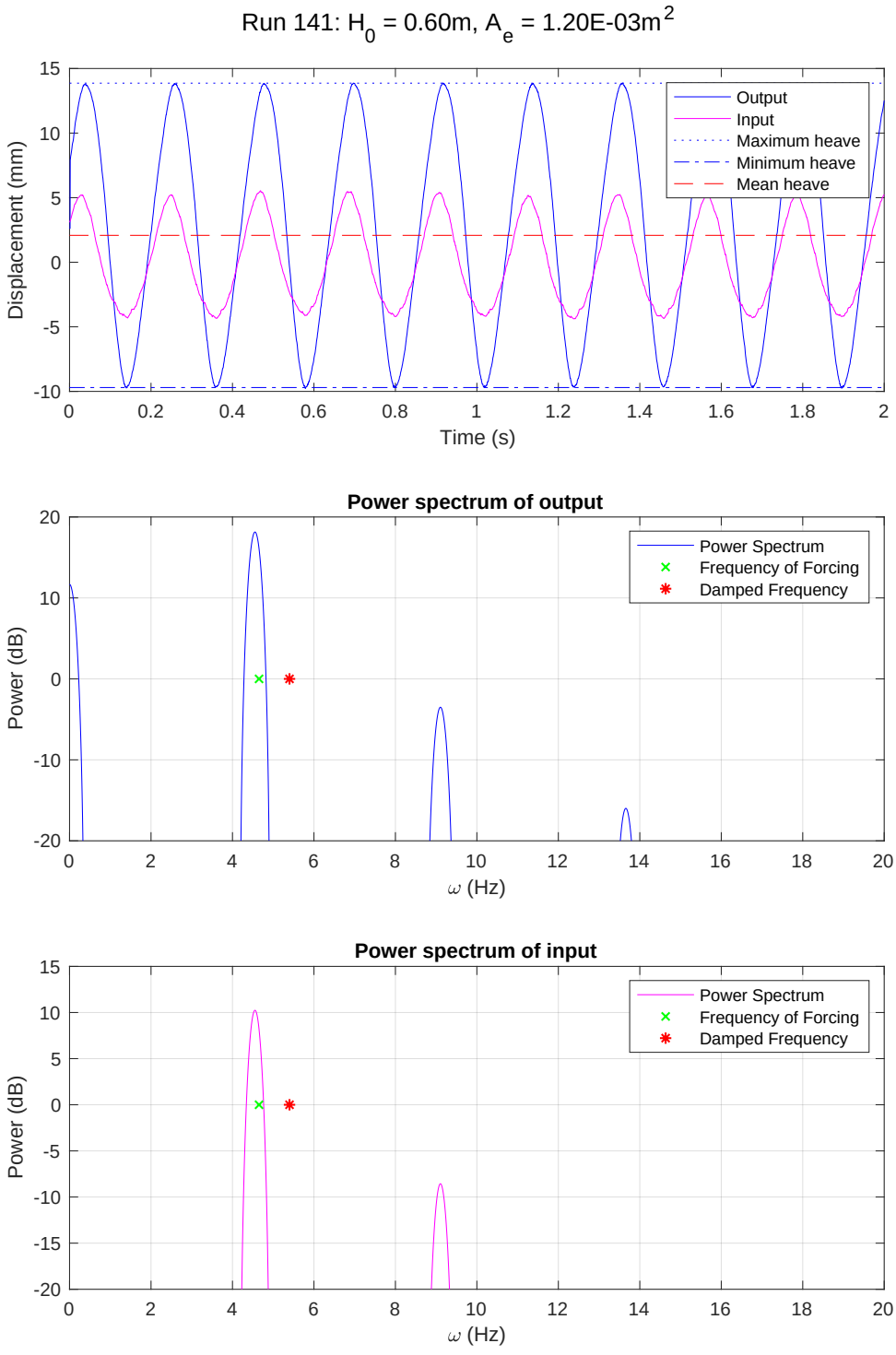


Figure H.103. Experimental trial data for Condition 141

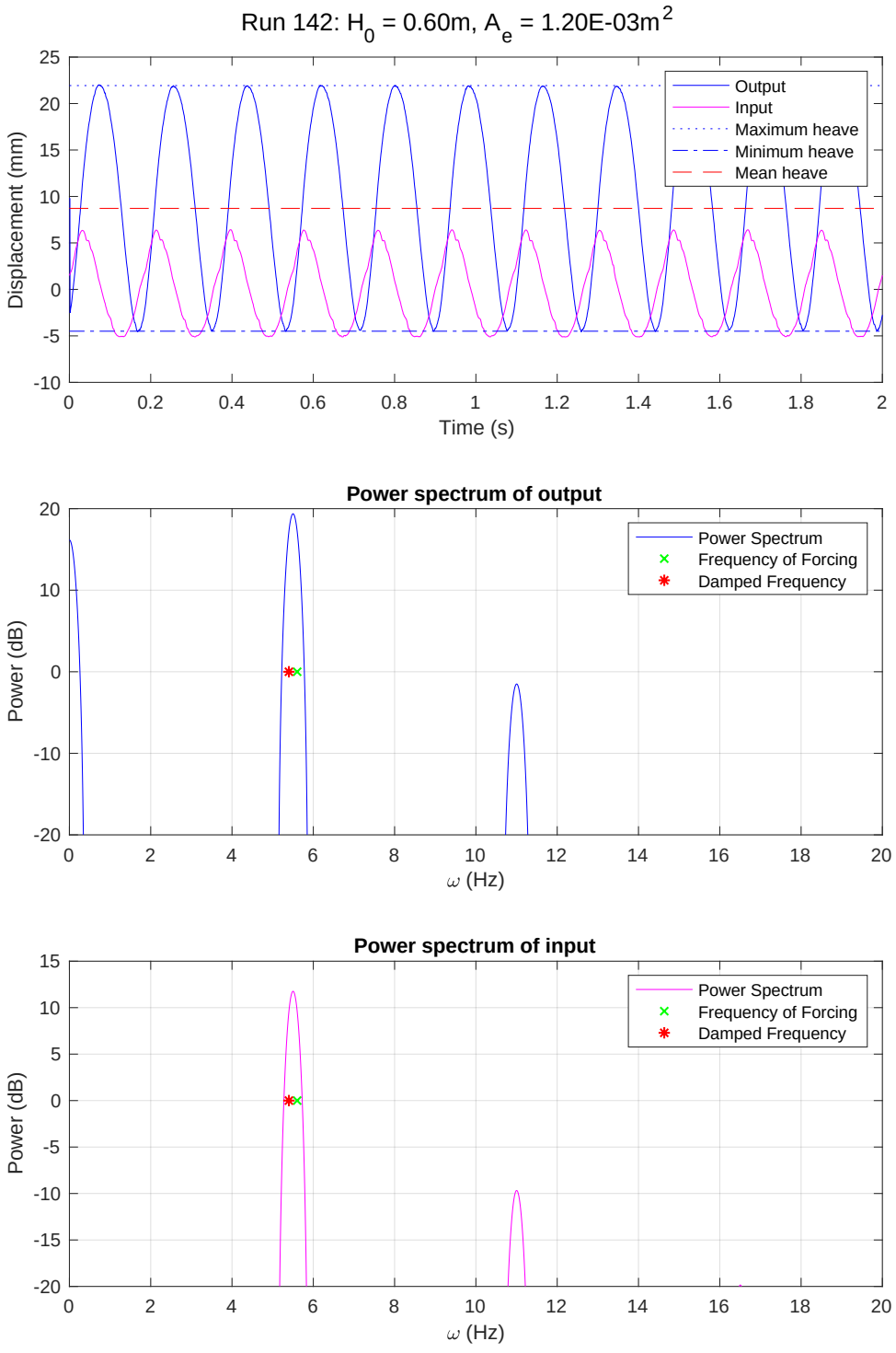


Figure H.104. Experimental trial data for Condition 142

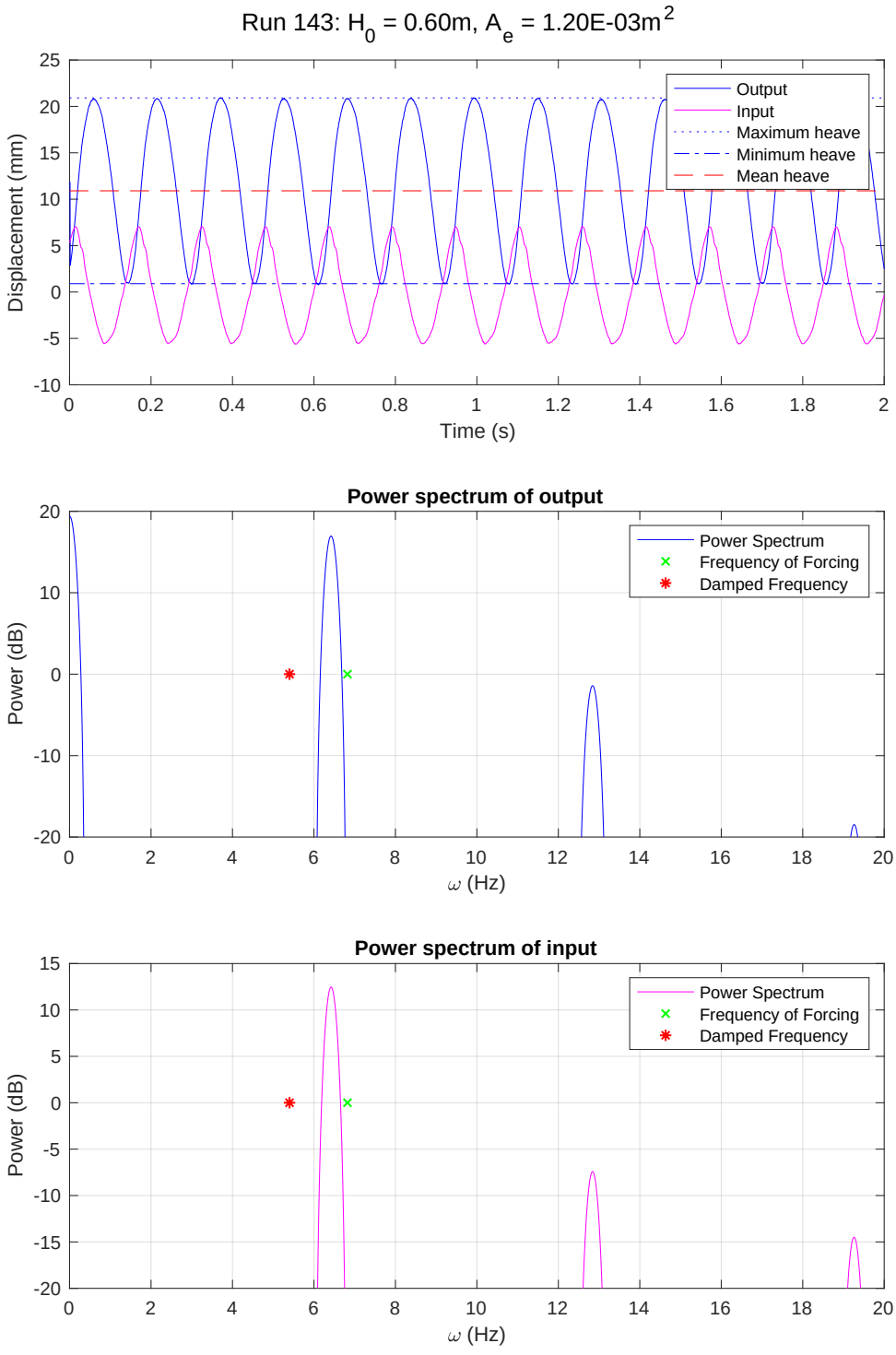


Figure H.105. Experimental trial data for Condition 143

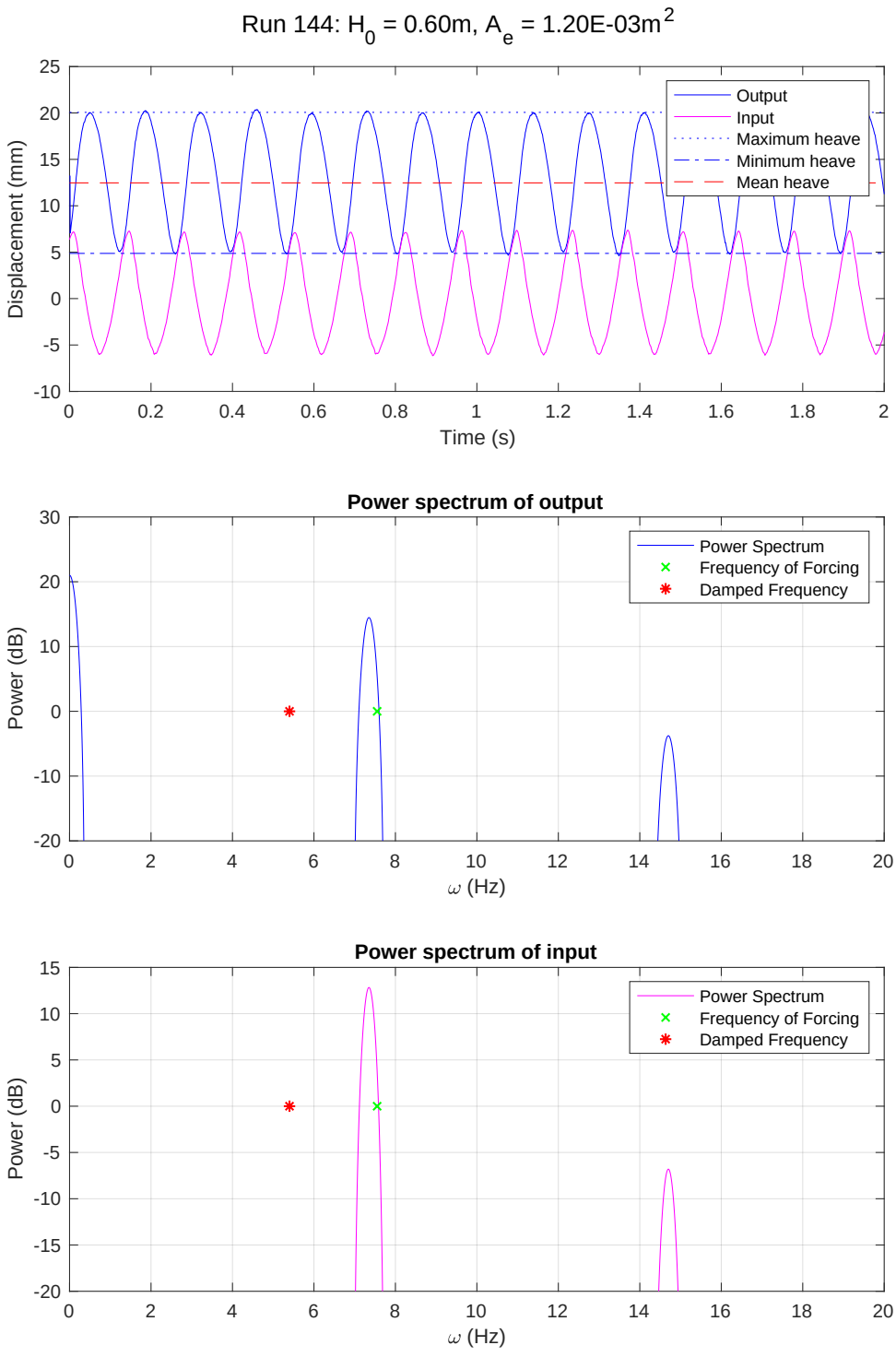


Figure H.106. Experimental trial data for Condition 144

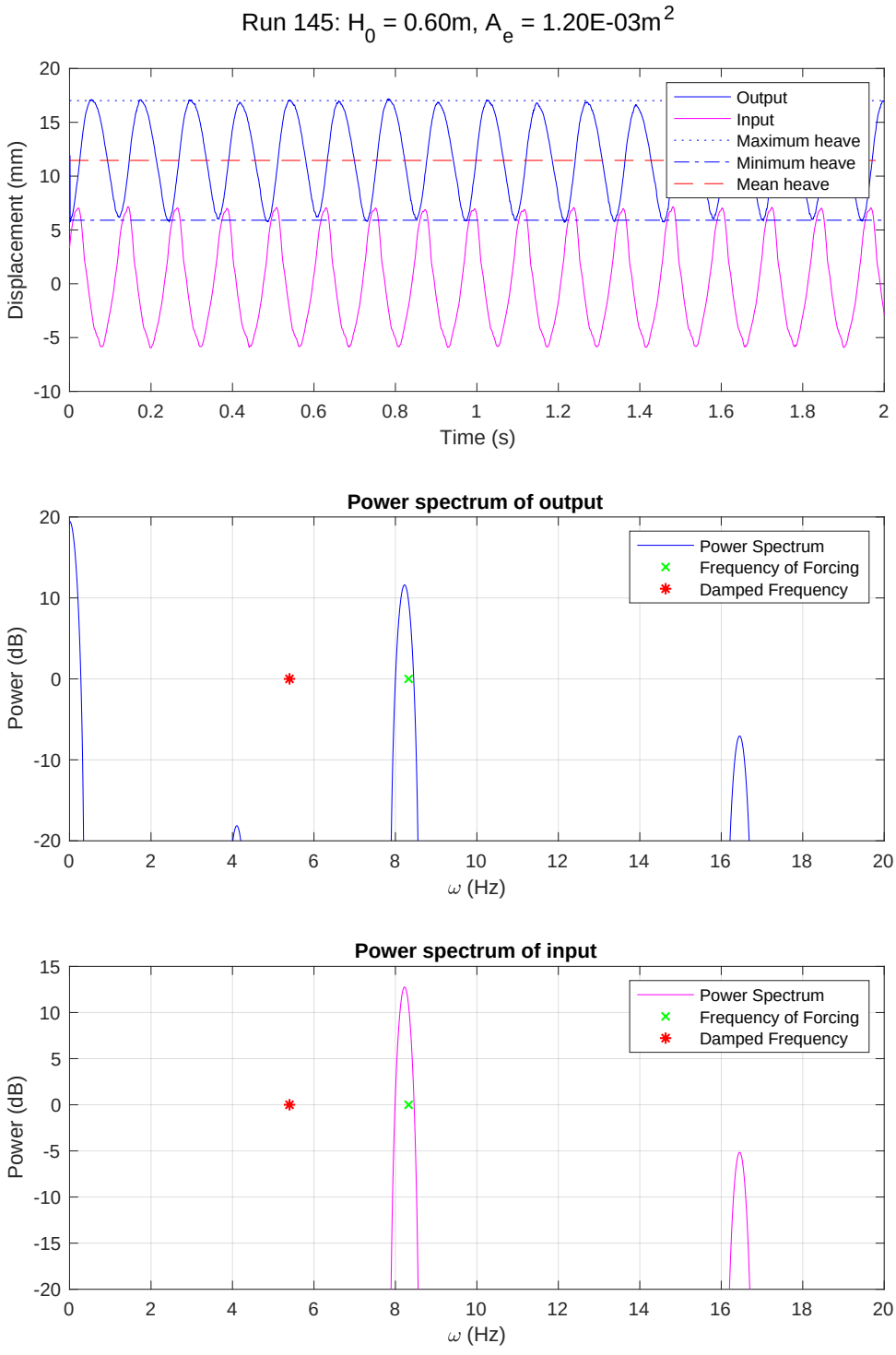


Figure H.107. Experimental trial data for Condition 145

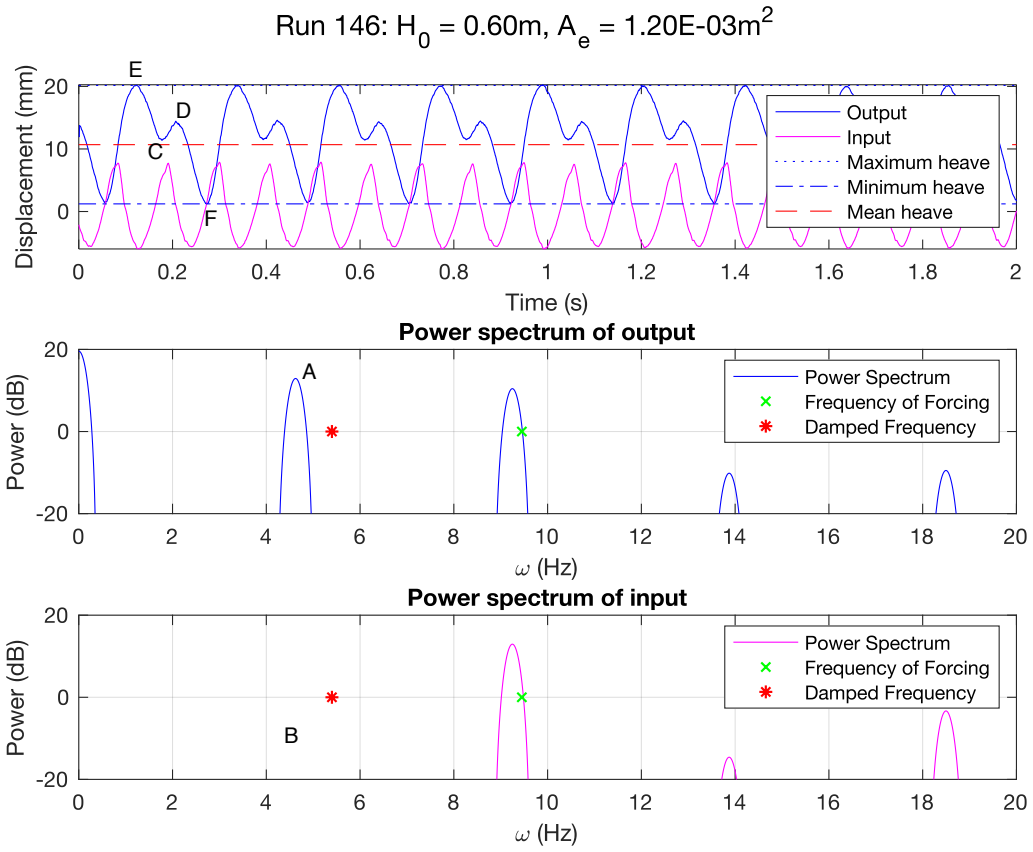


Figure H.108. Experimental trial data for Condition 146

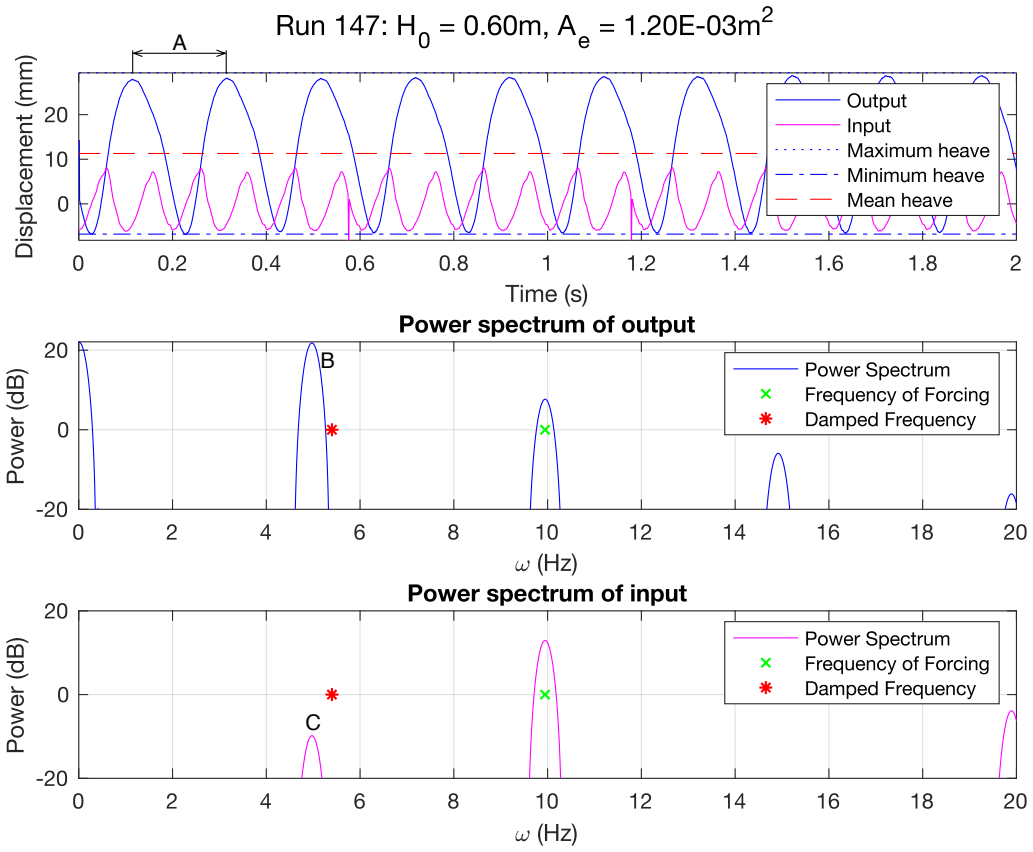


Figure H.109. Experimental trial data for Condition 147

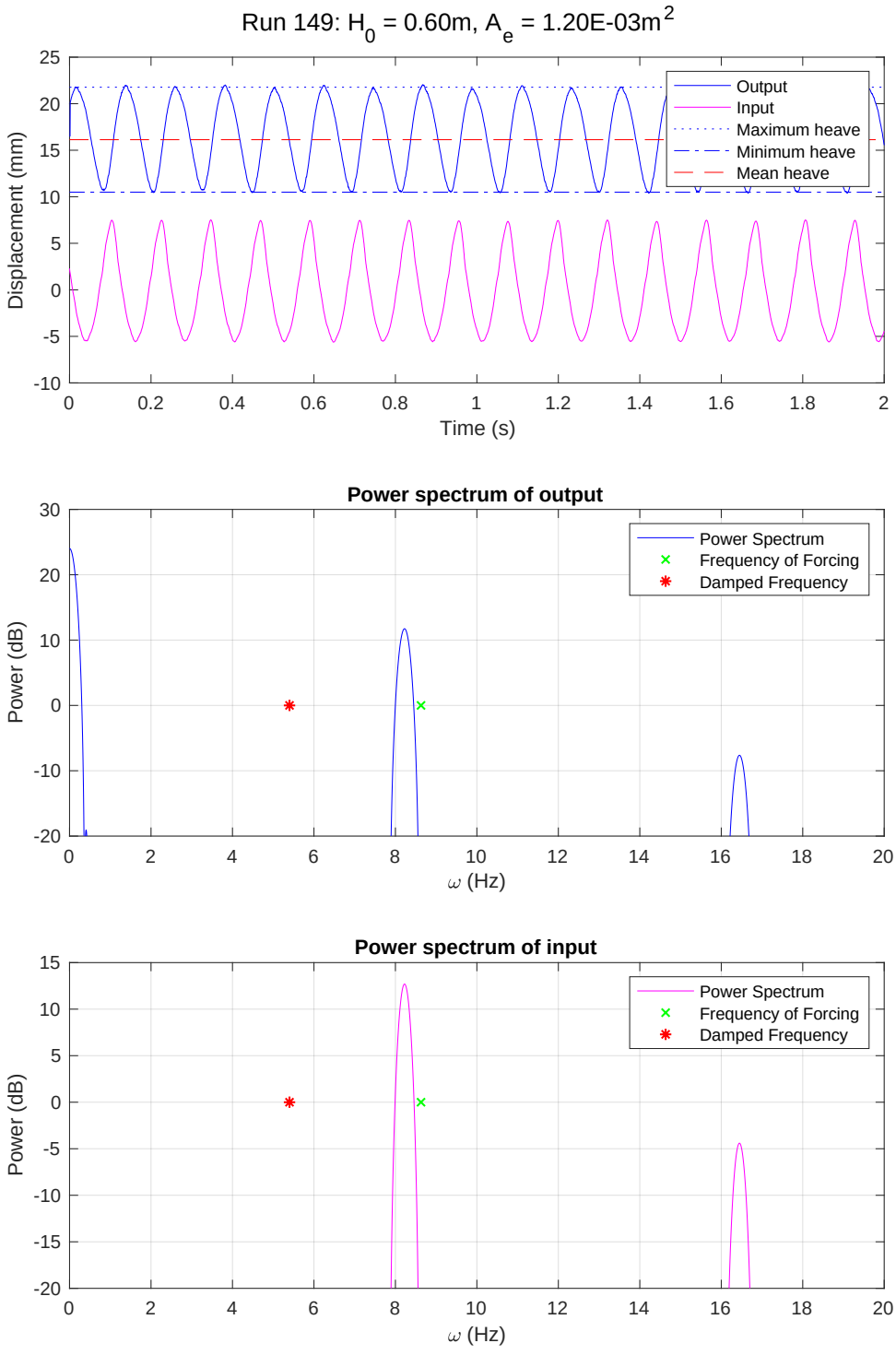


Figure H.110. Experimental trial data for Condition 149

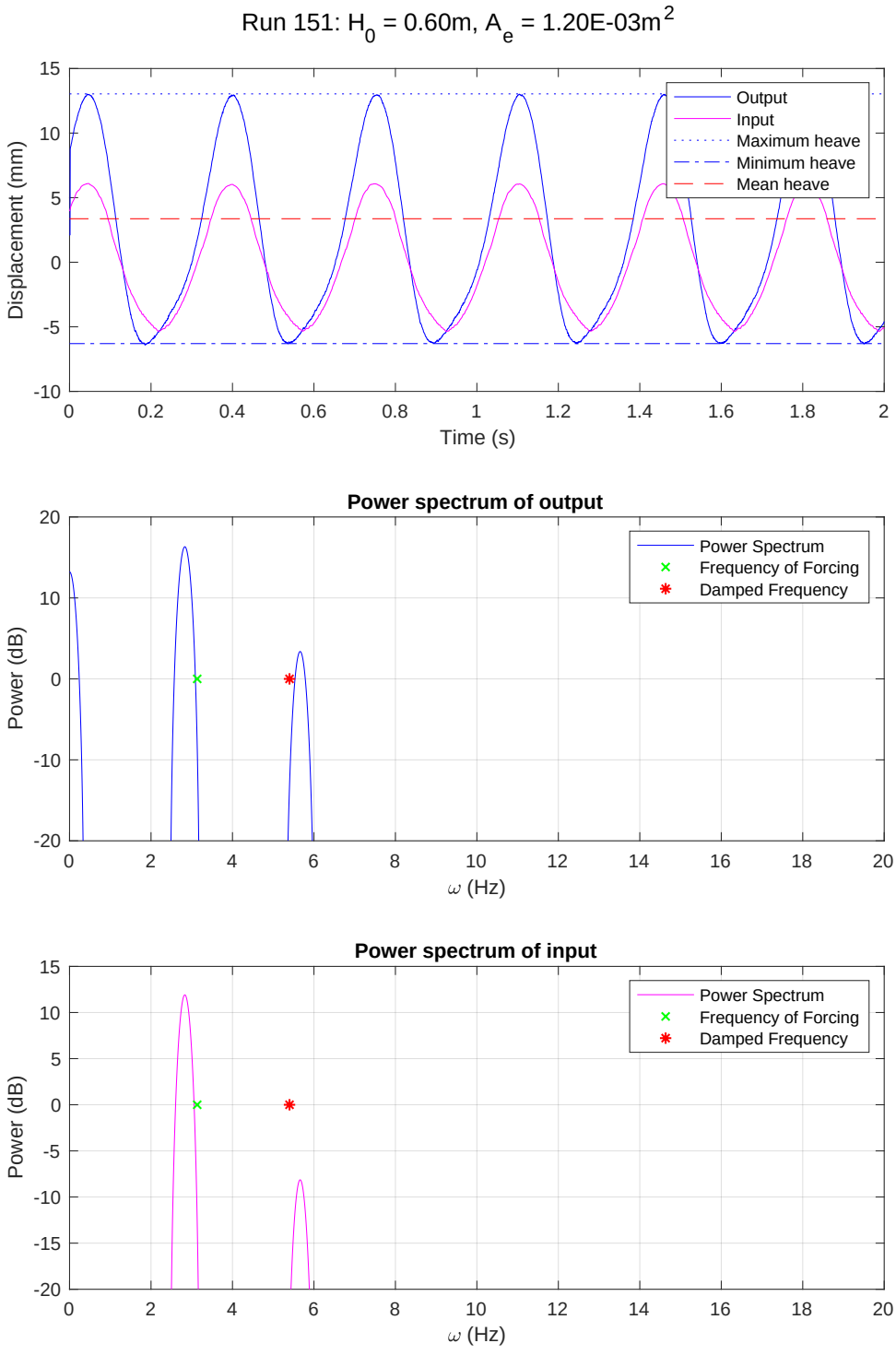


Figure H.111. Experimental trial data for Condition 151

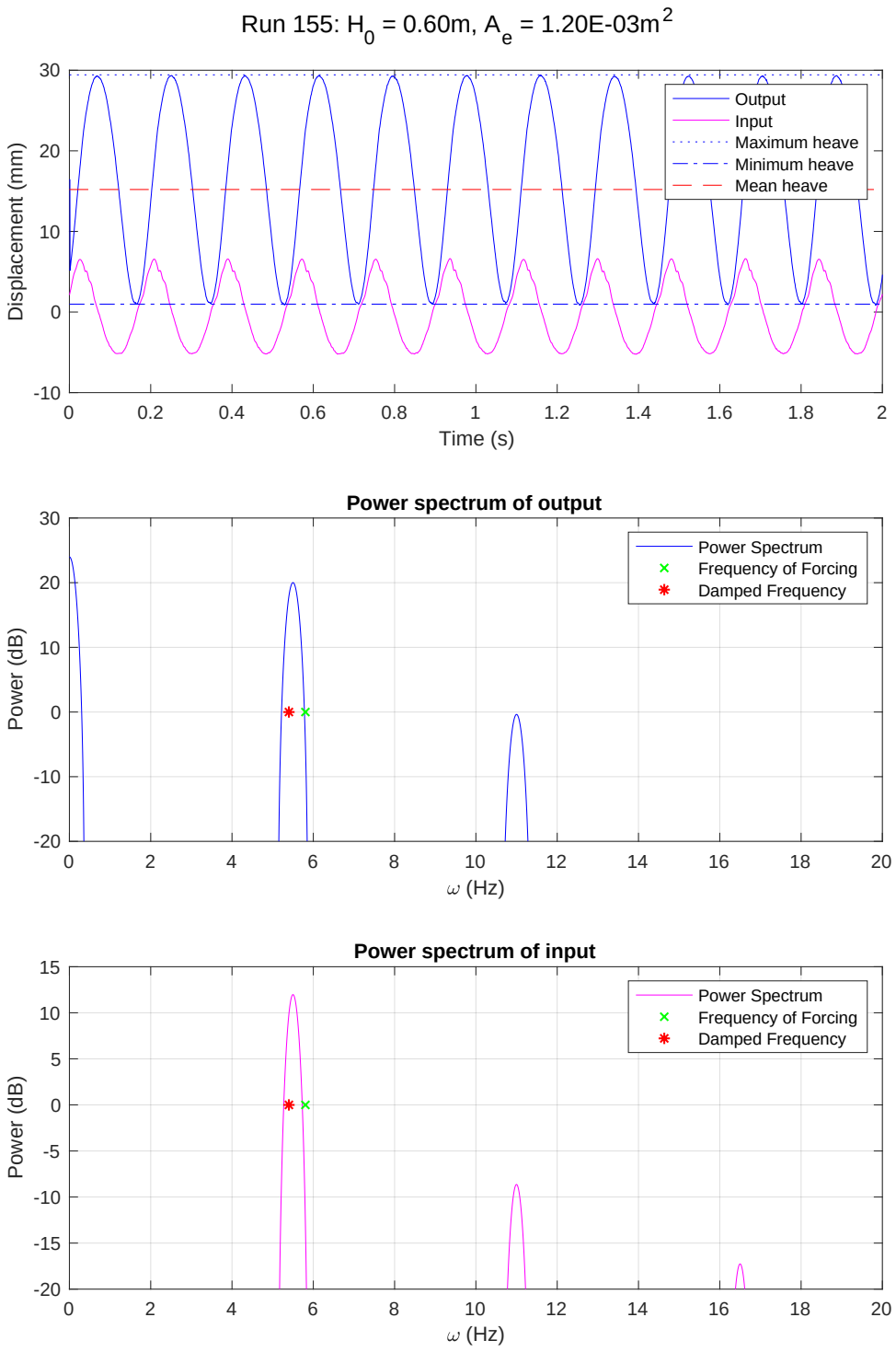


Figure H.112. Experimental trial data for Condition 155

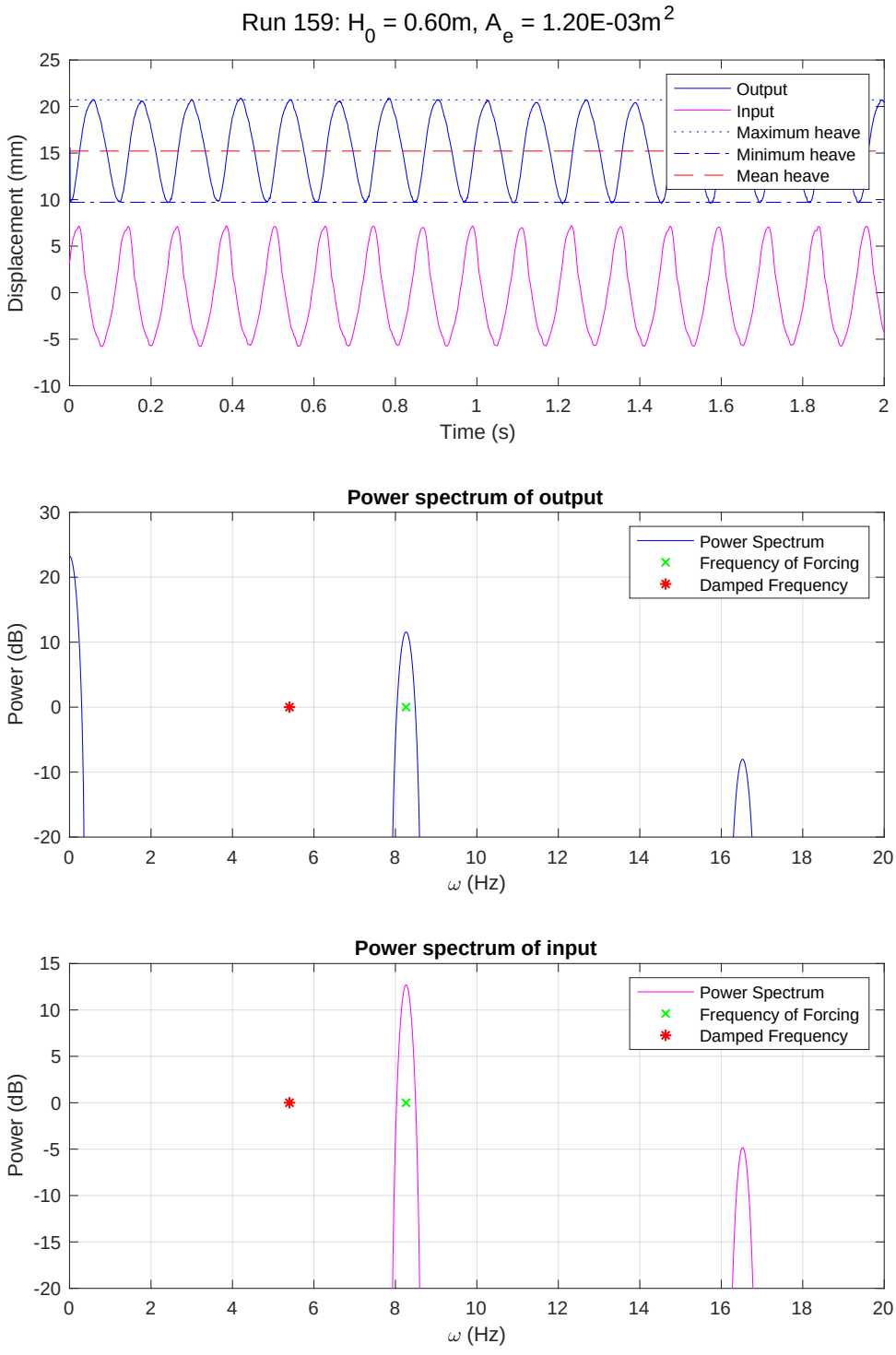


Figure H.113. Experimental trial data for Condition 159

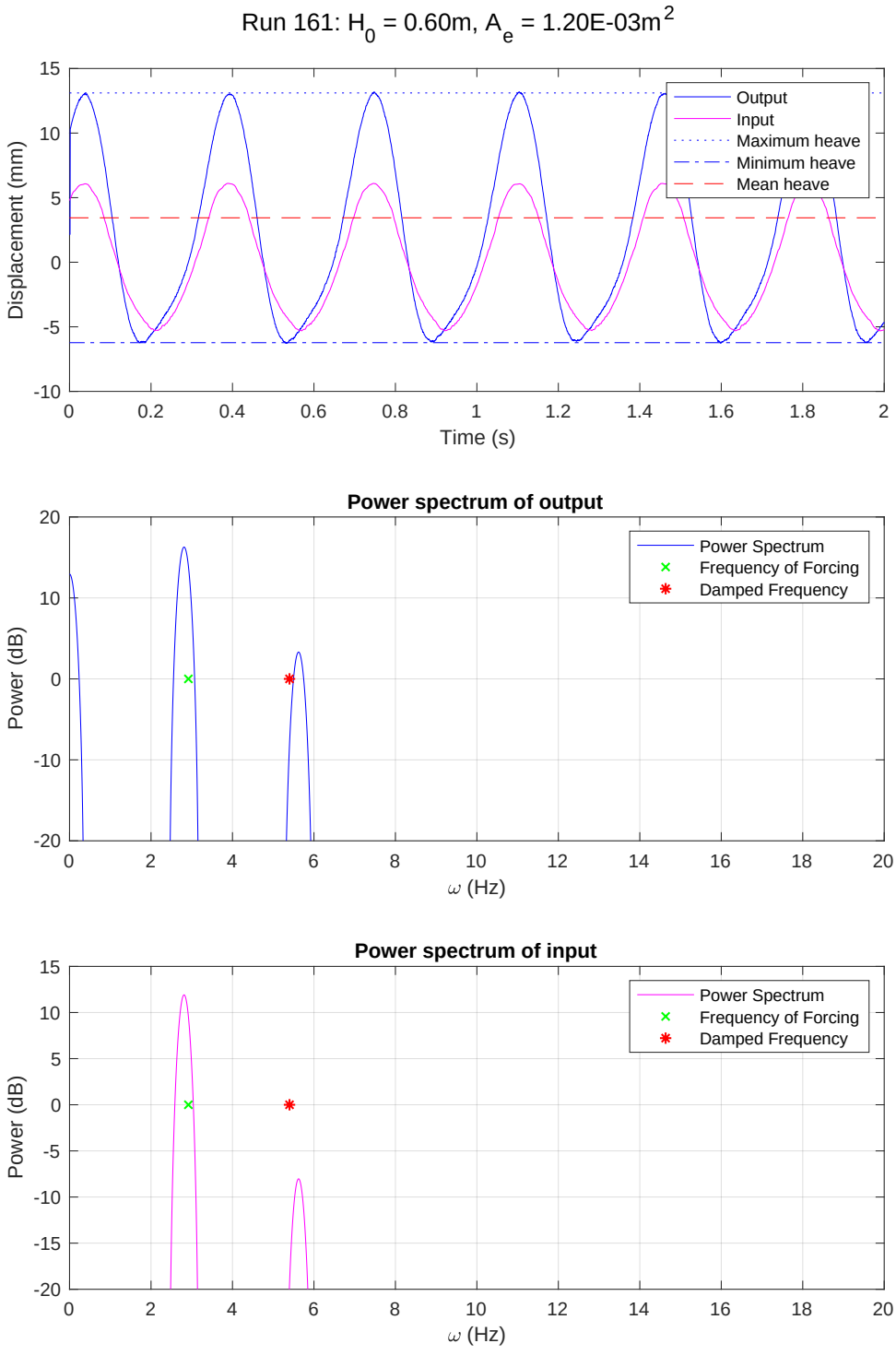


Figure H.114. Experimental trial data for Condition 161

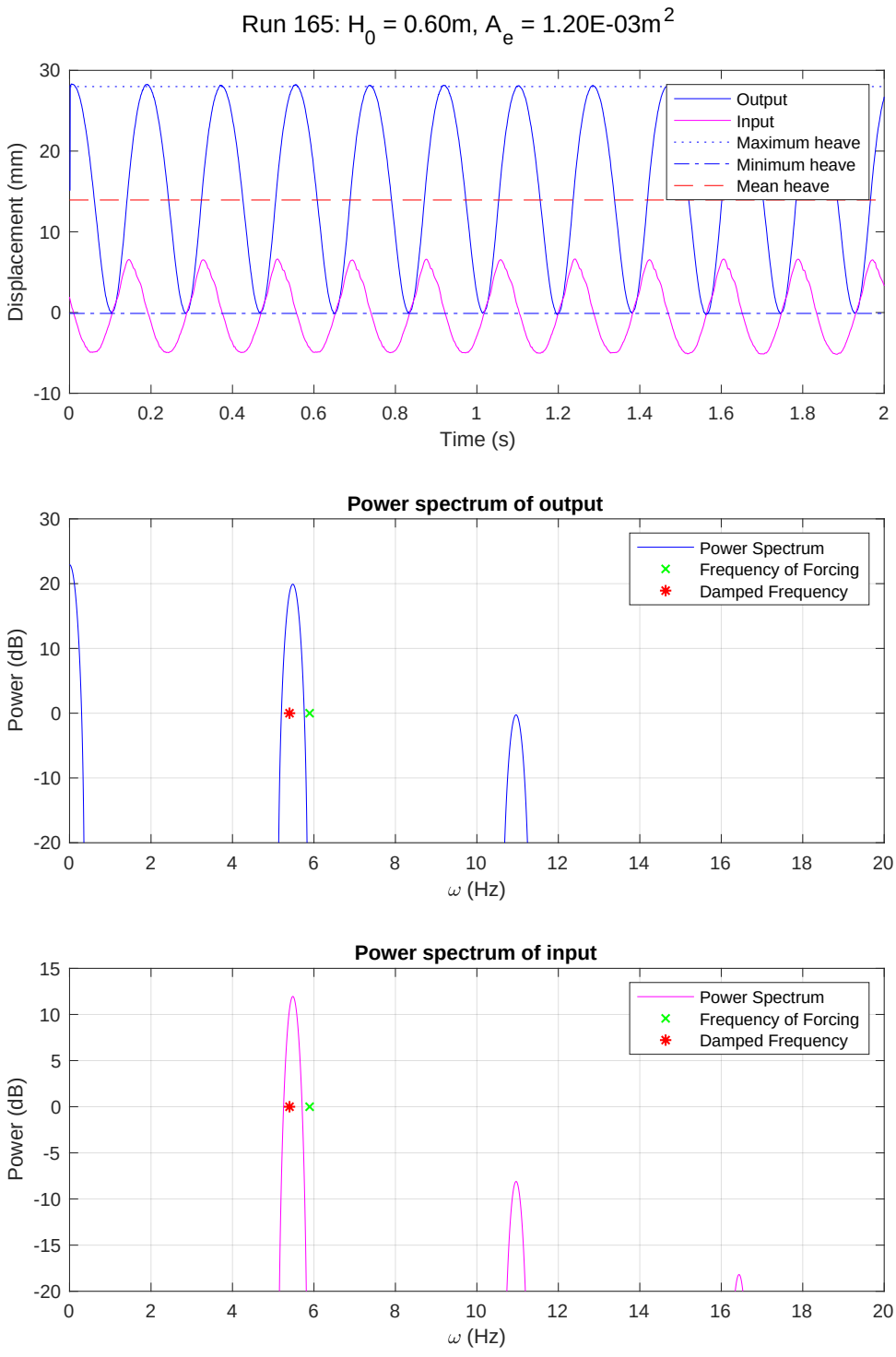


Figure H.115. Experimental trial data for Condition 165

H.2.7. Condition Seven

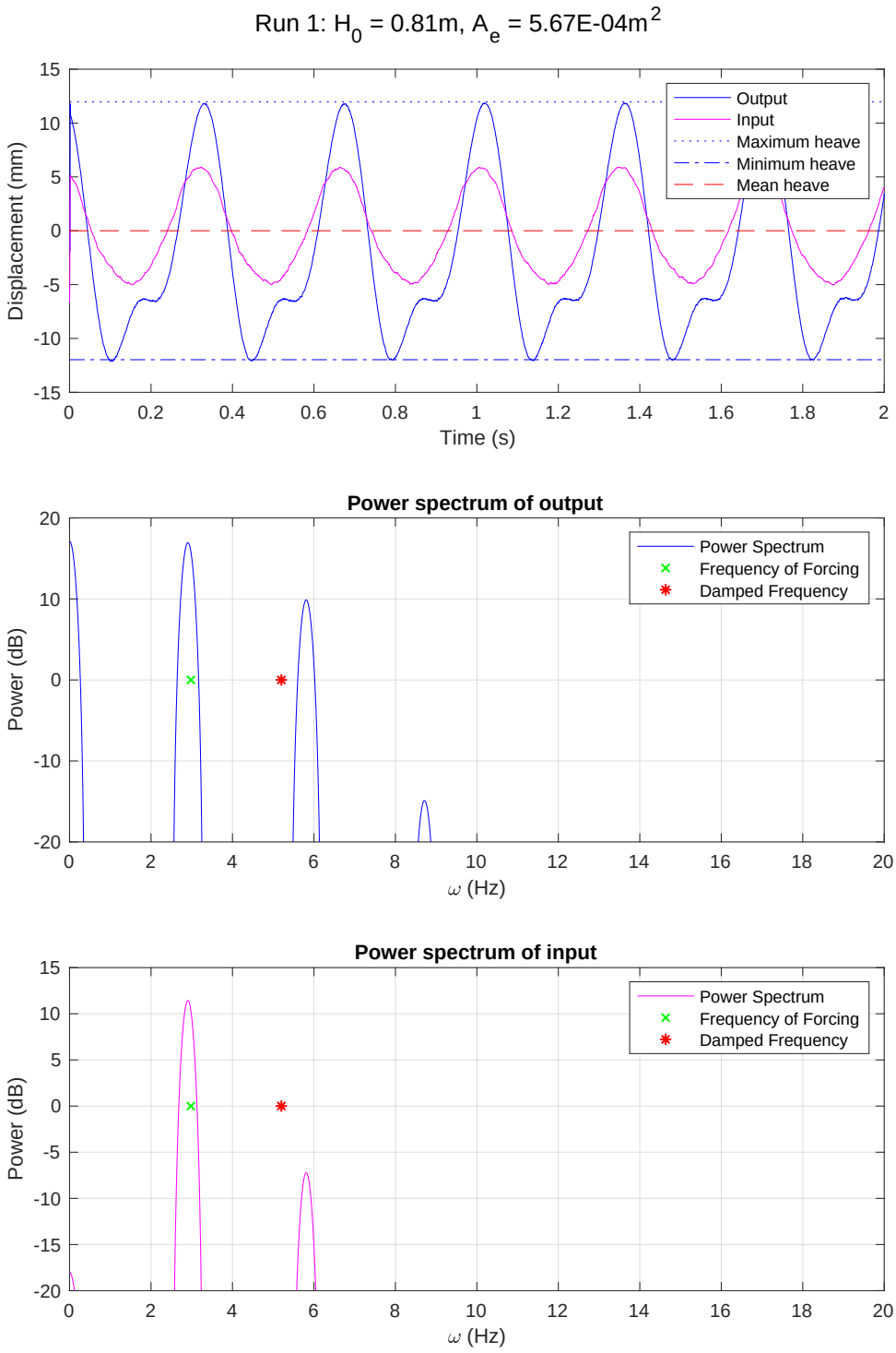


Figure H.116. Experimental trial data for Condition 1

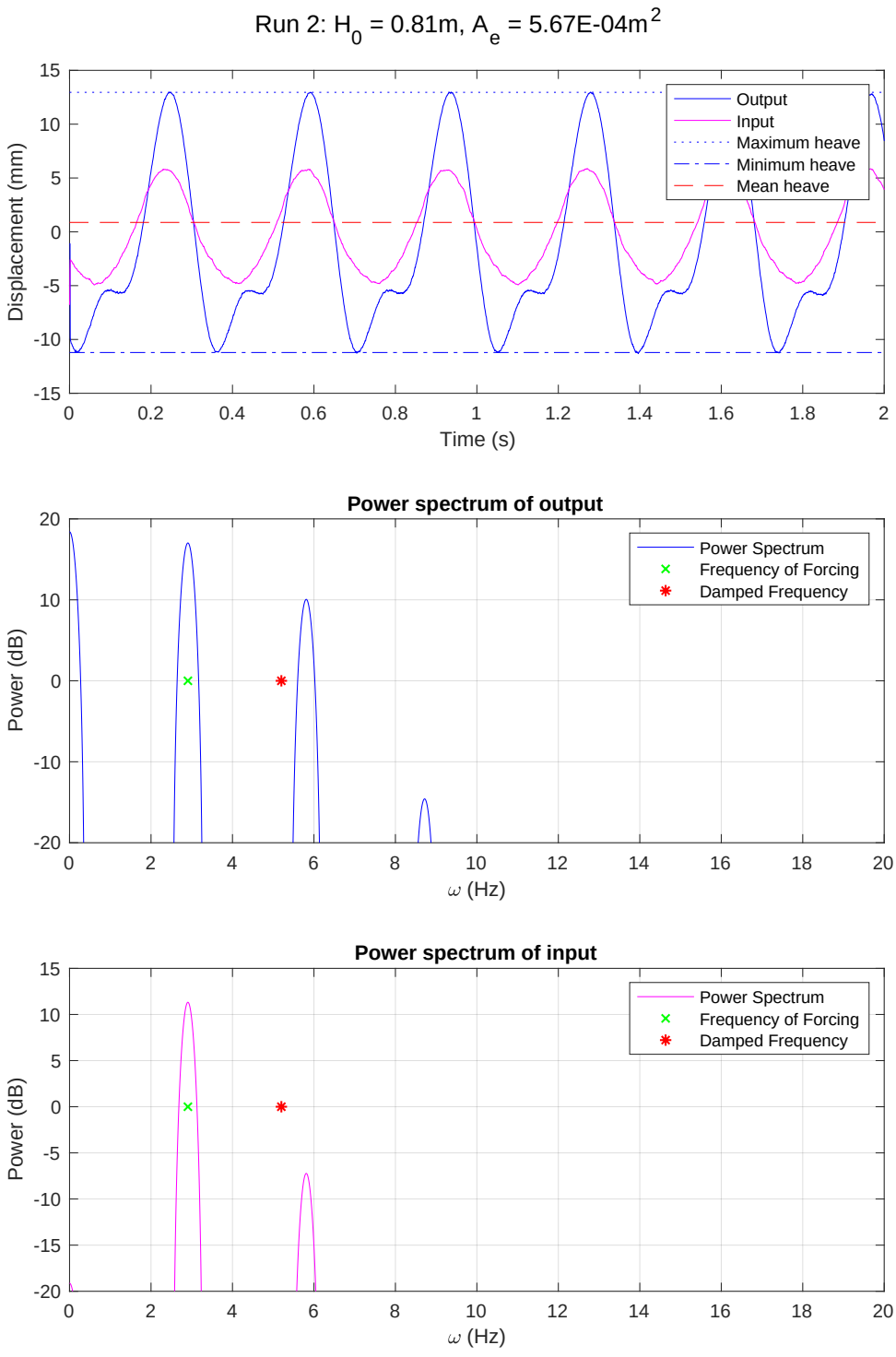


Figure H.117. Experimental trial data for Condition 2

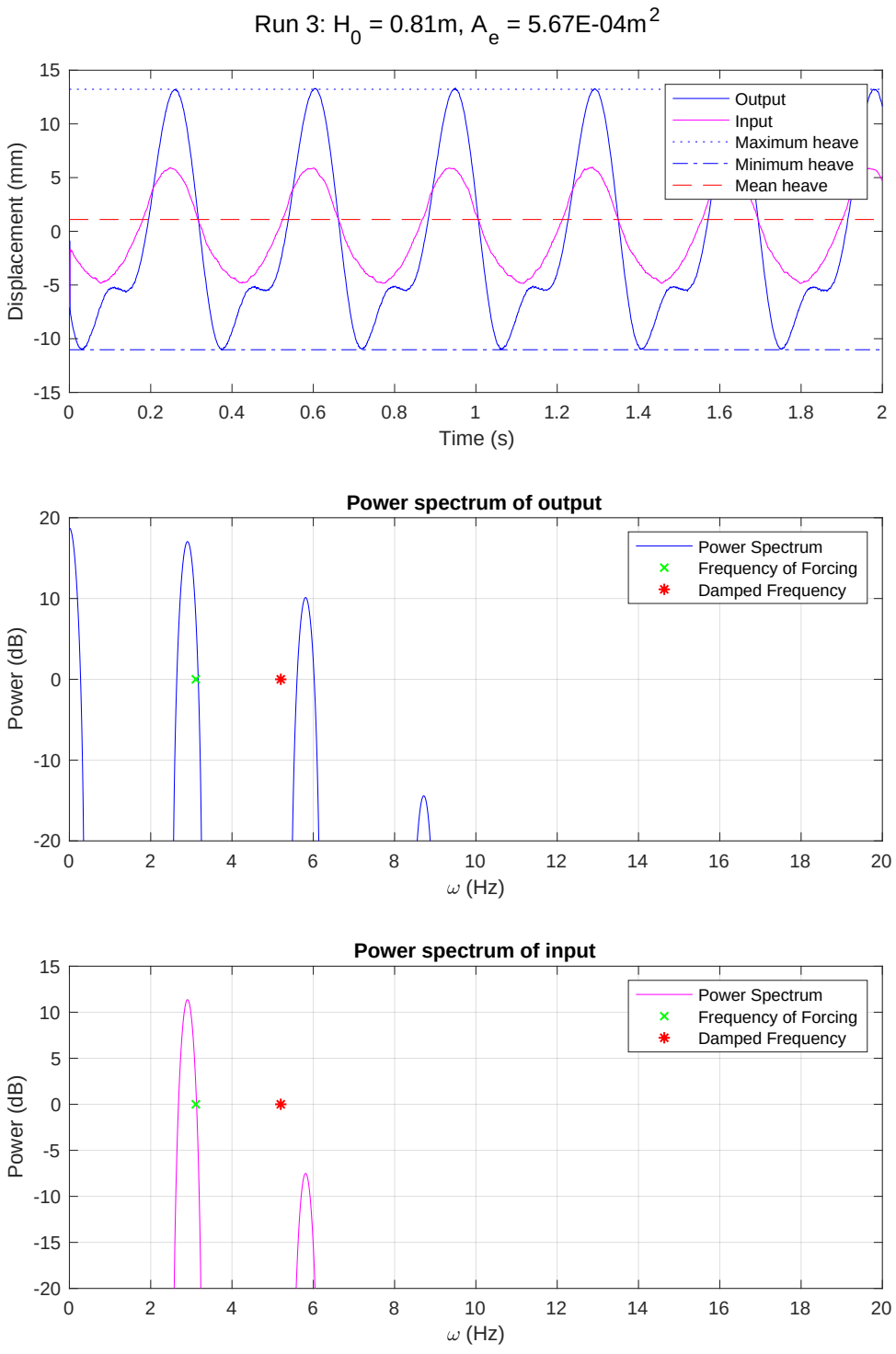


Figure H.118. Experimental trial data for Condition 3

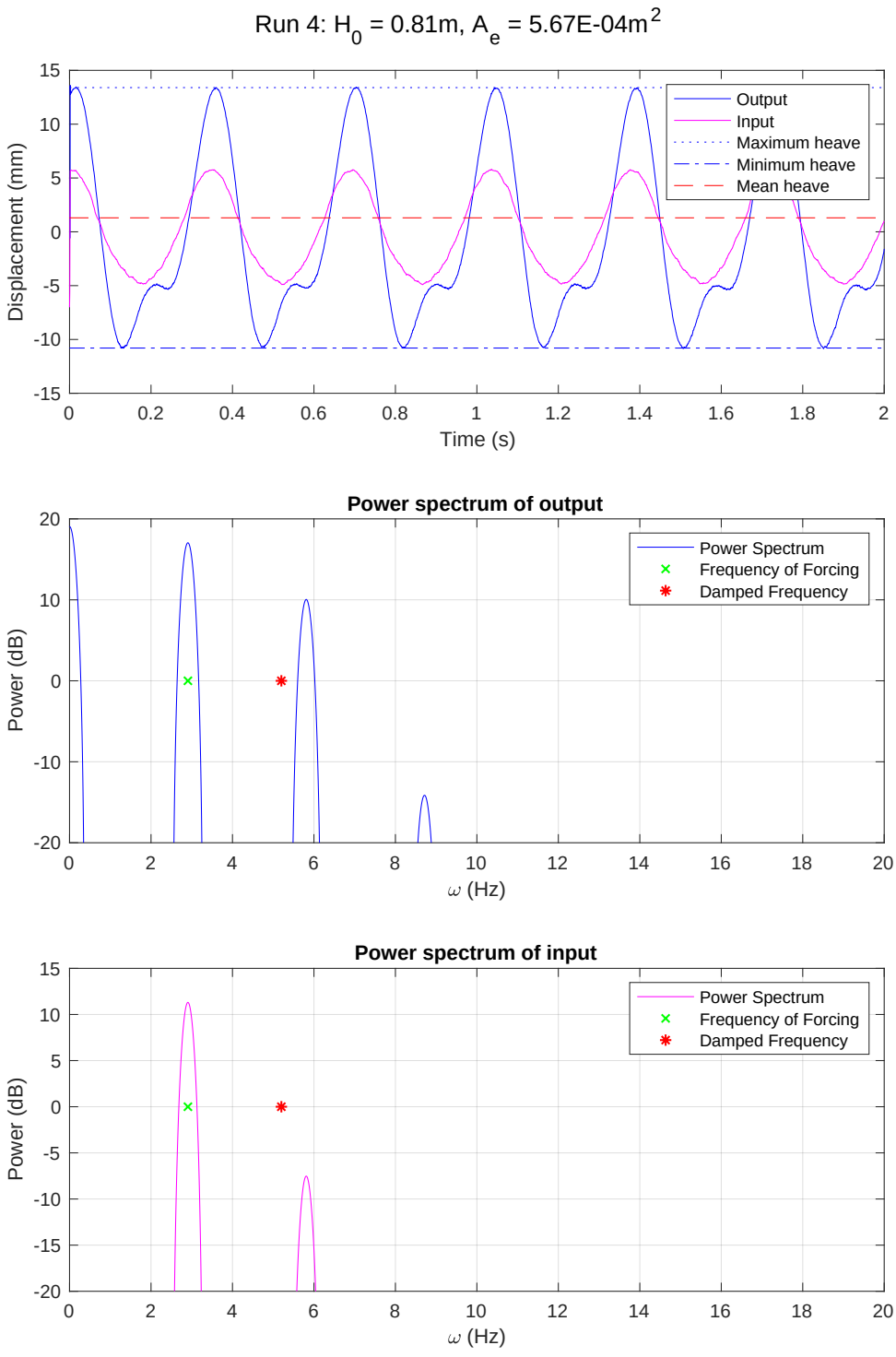


Figure H.119. Experimental trial data for Condition 4

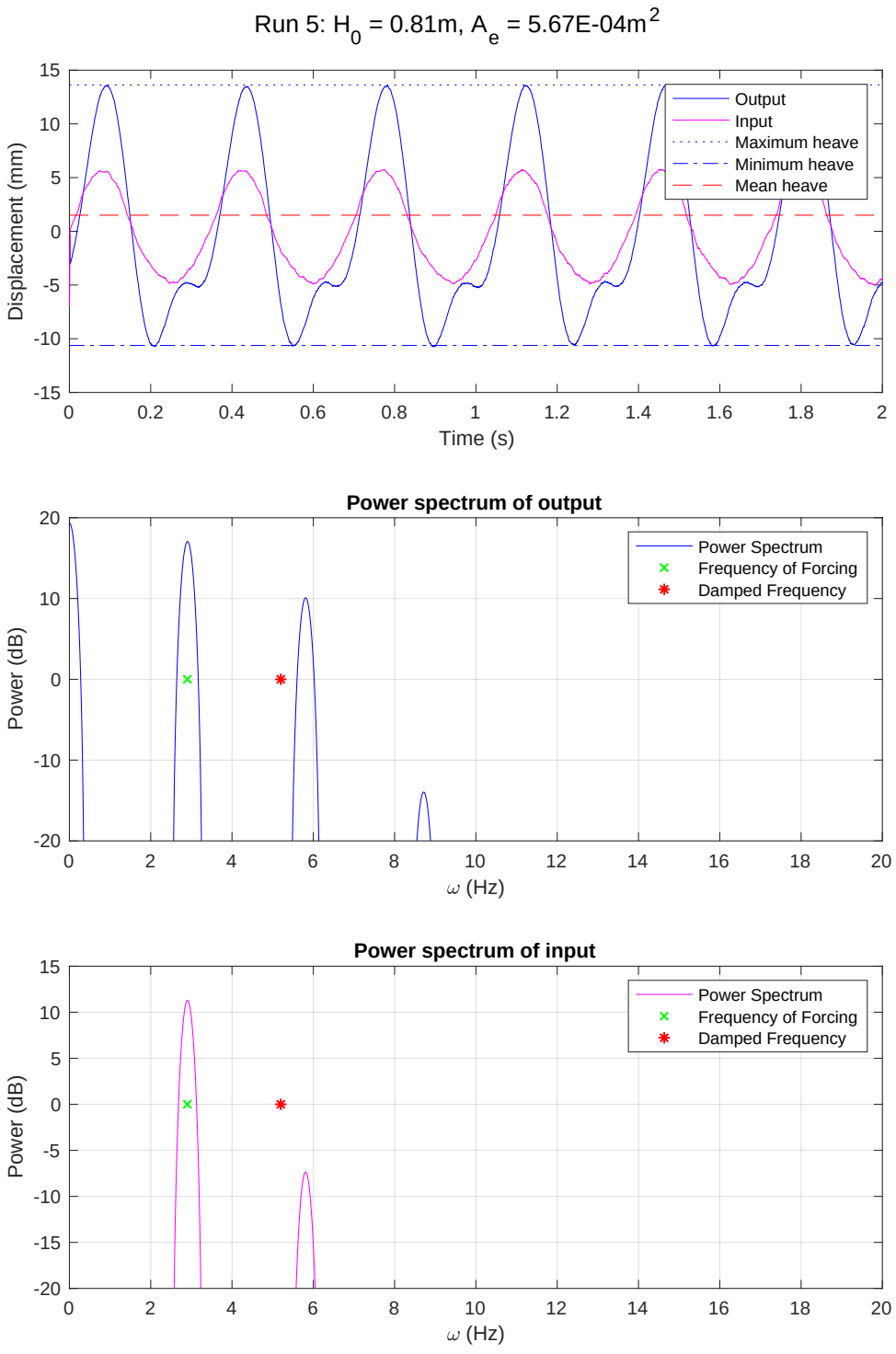


Figure H.120. Experimental trial data for Condition 5

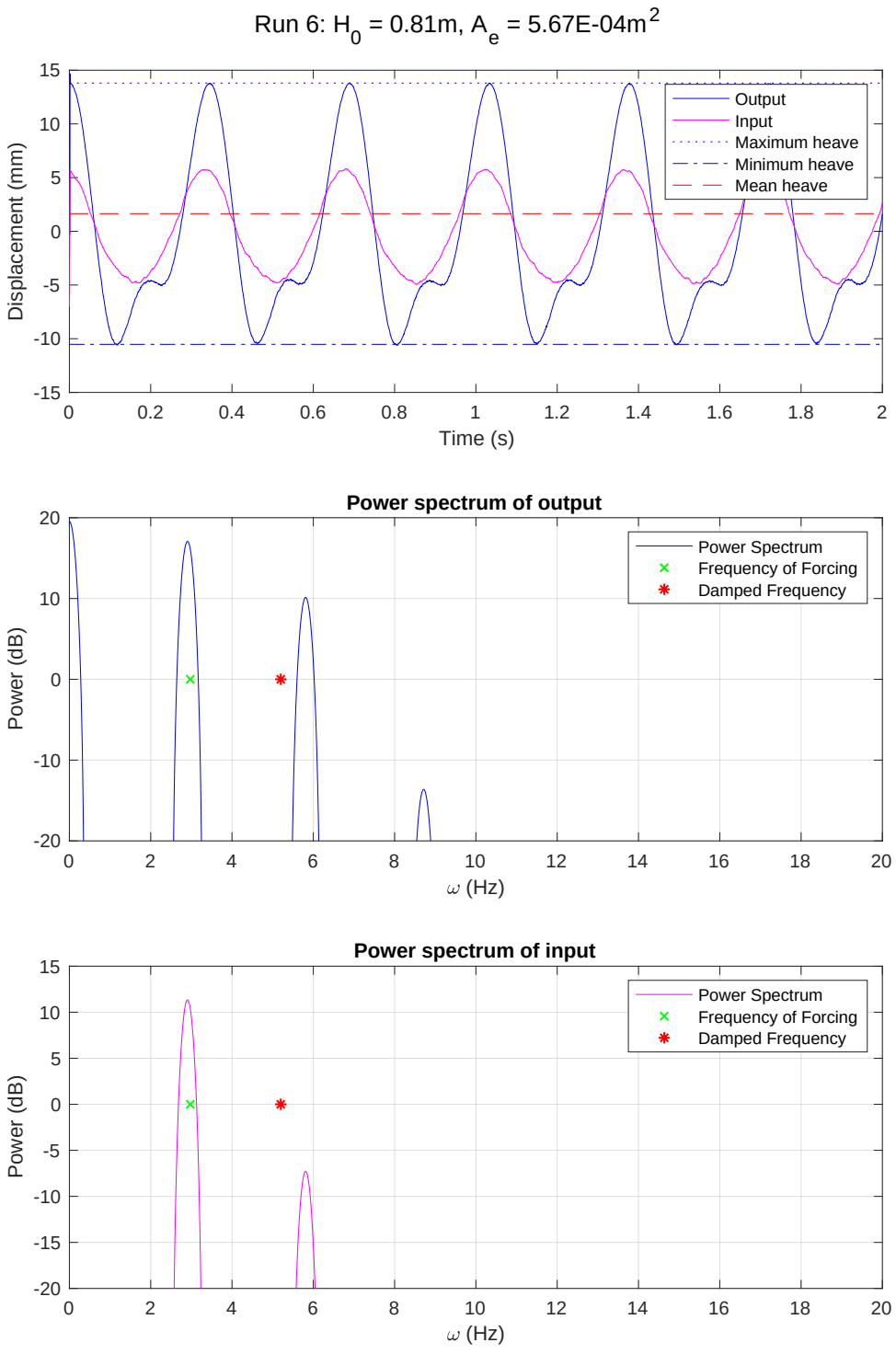


Figure H.121. Experimental trial data for Condition 6

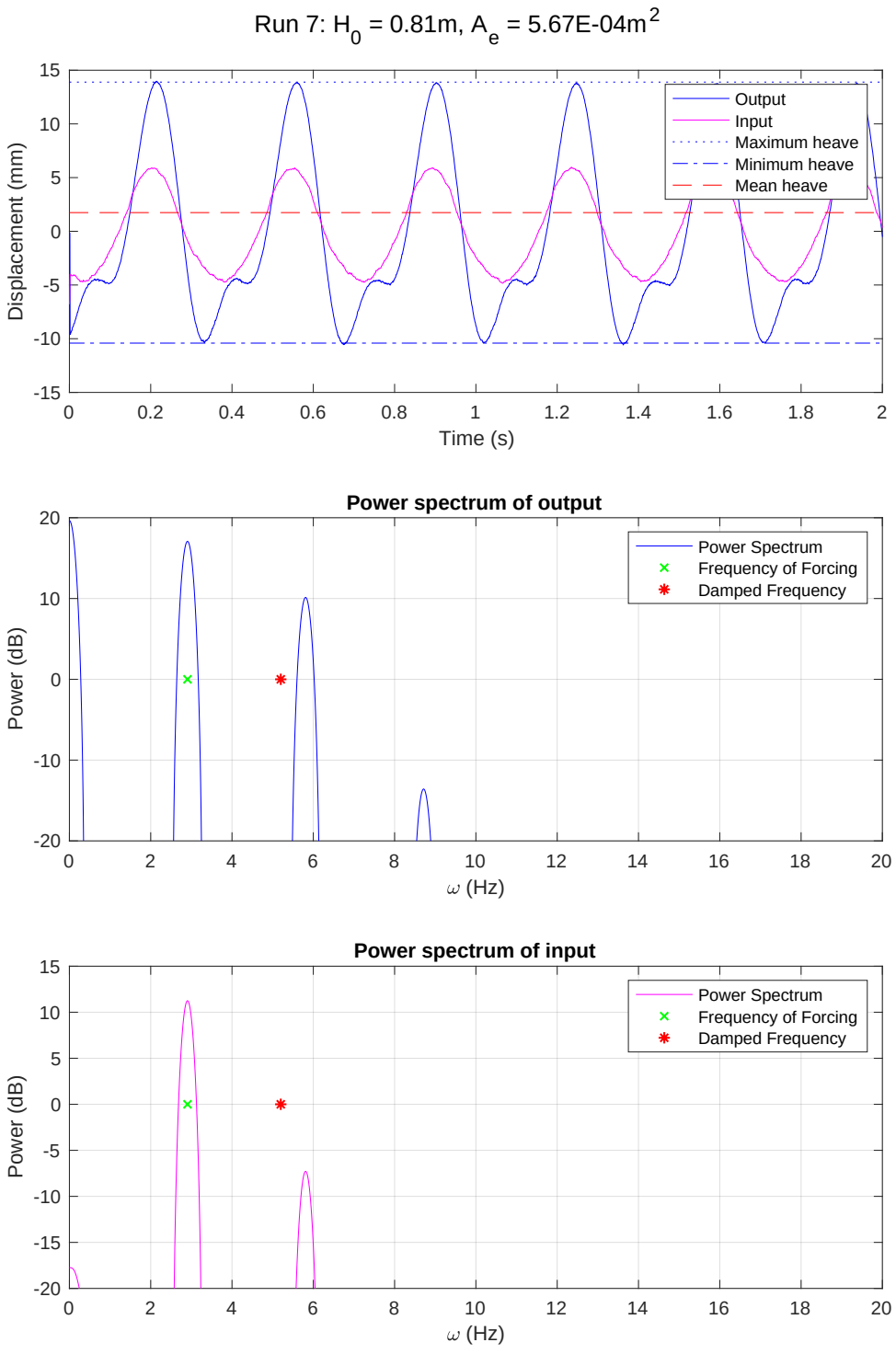


Figure H.122. Experimental trial data for Condition 7

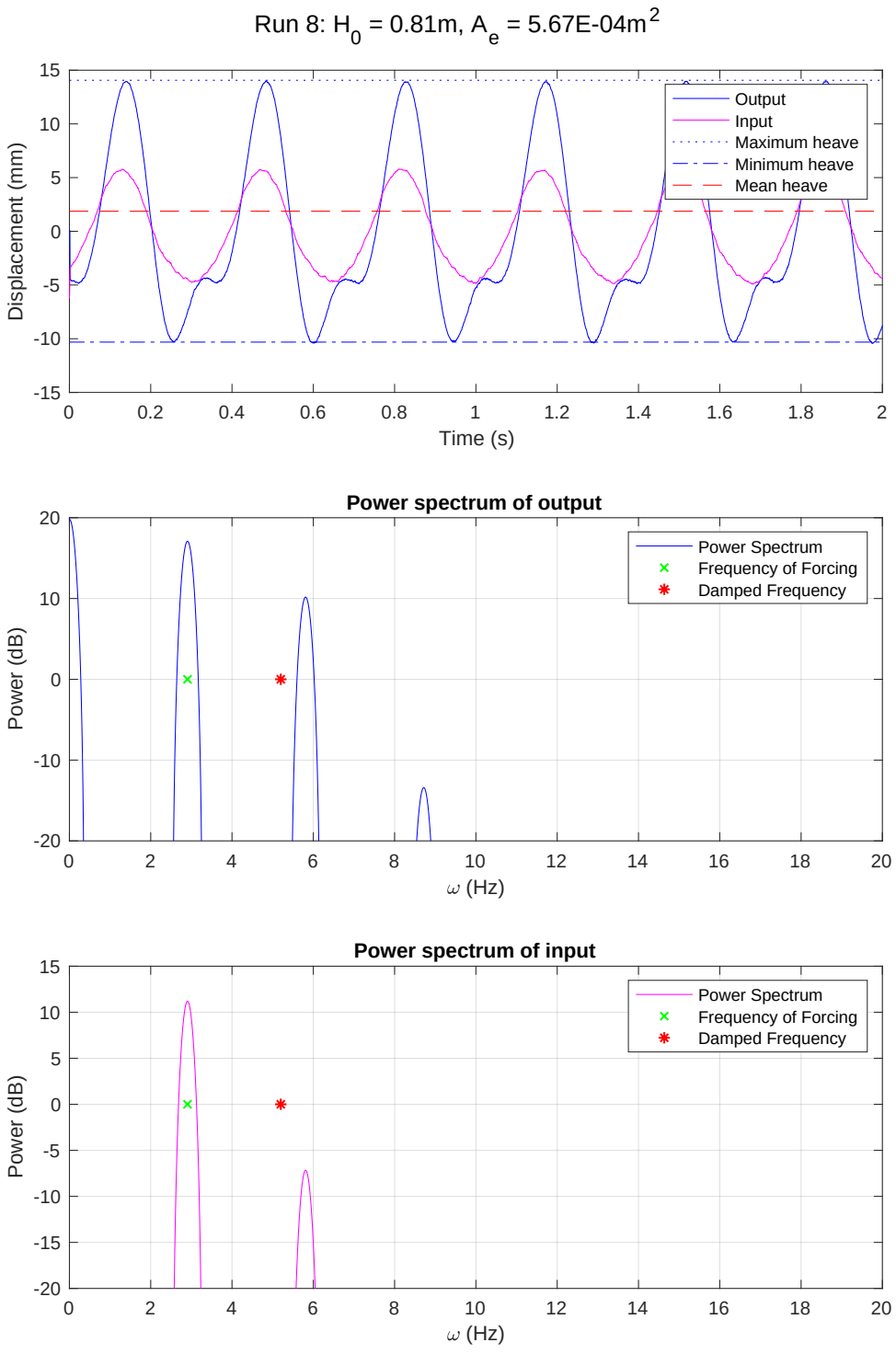


Figure H.123. Experimental trial data for Condition 8

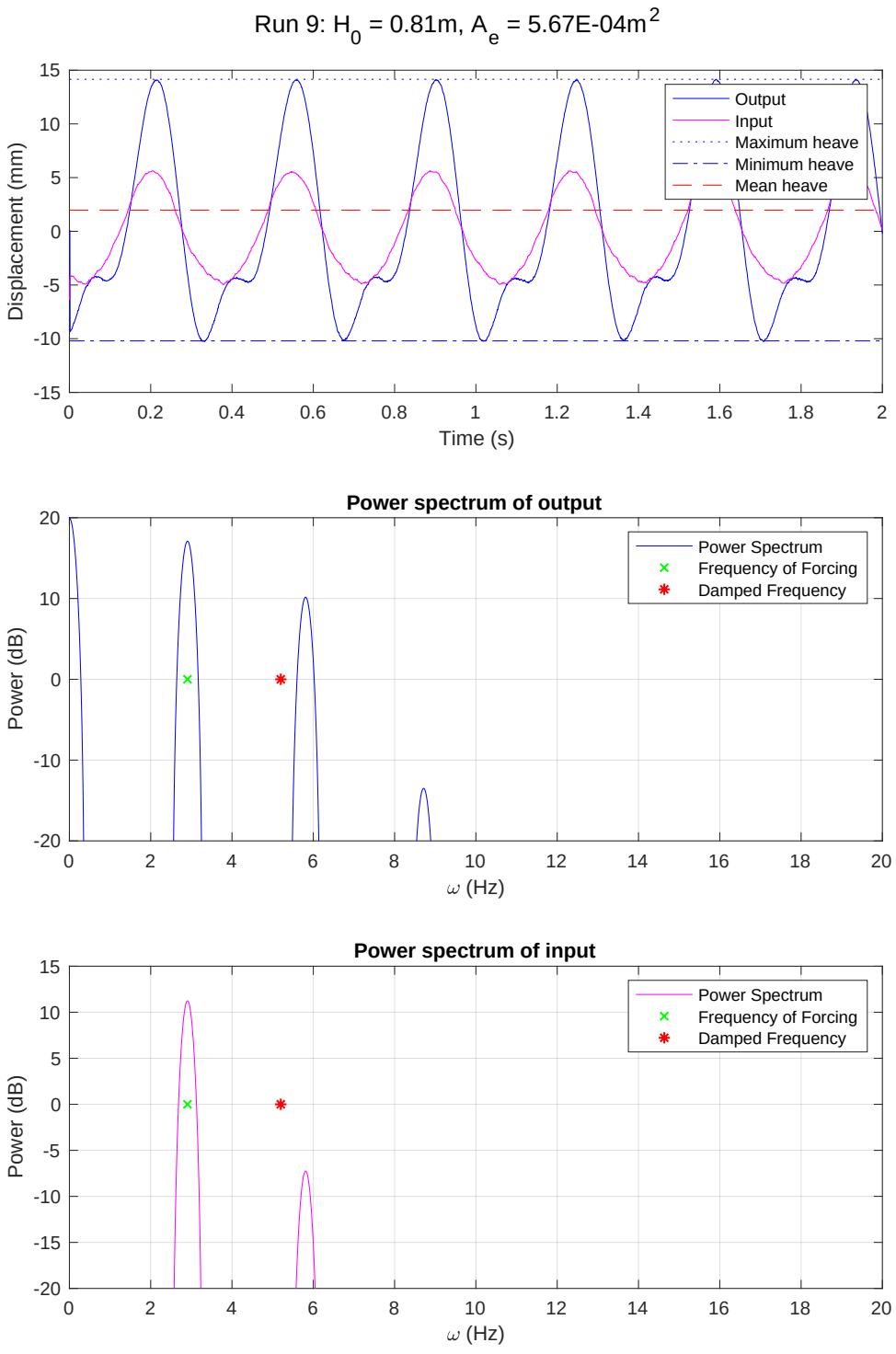


Figure H.124. Experimental trial data for Condition 9

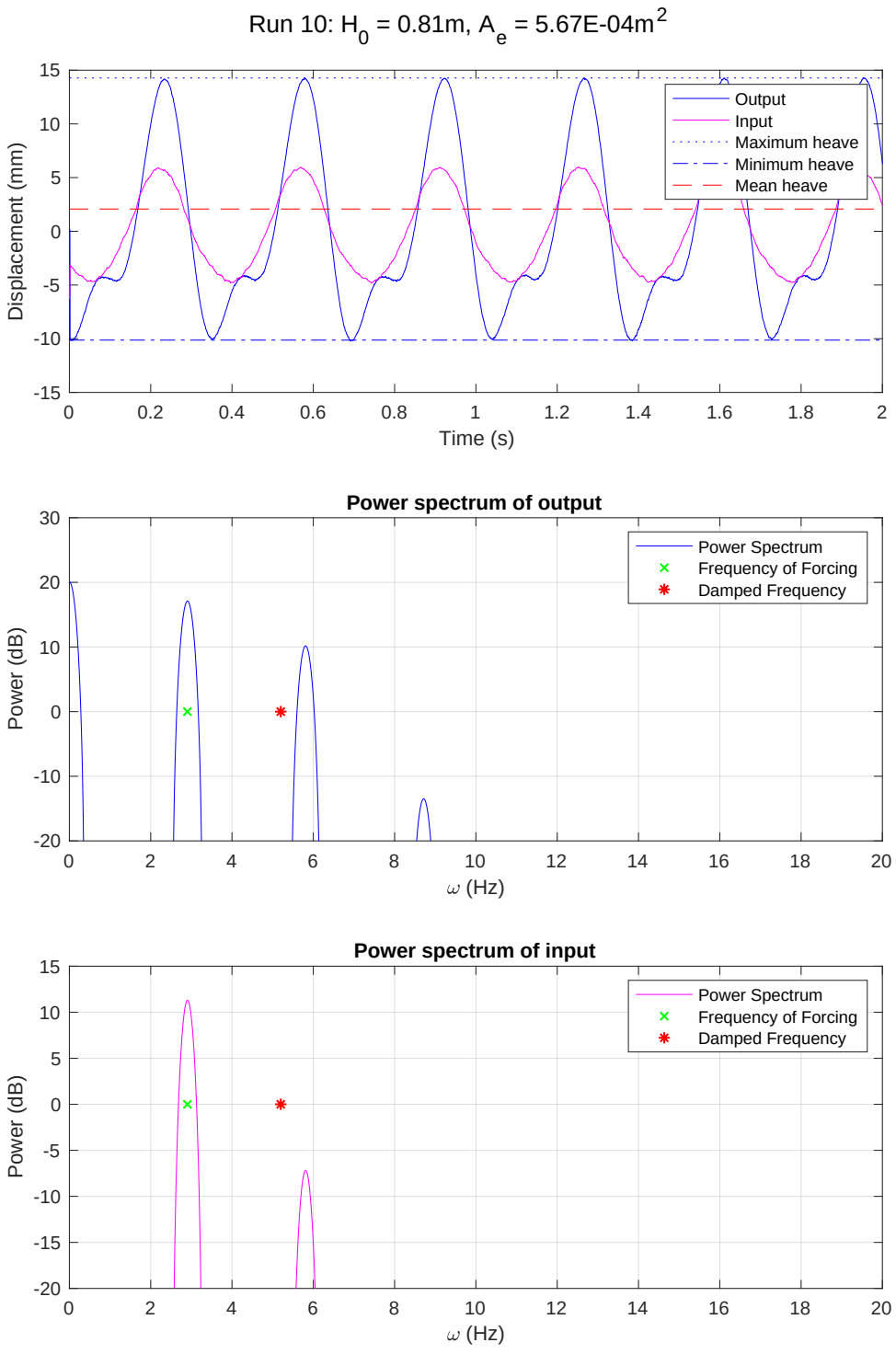


Figure H.125. Experimental trial data for Condition 10

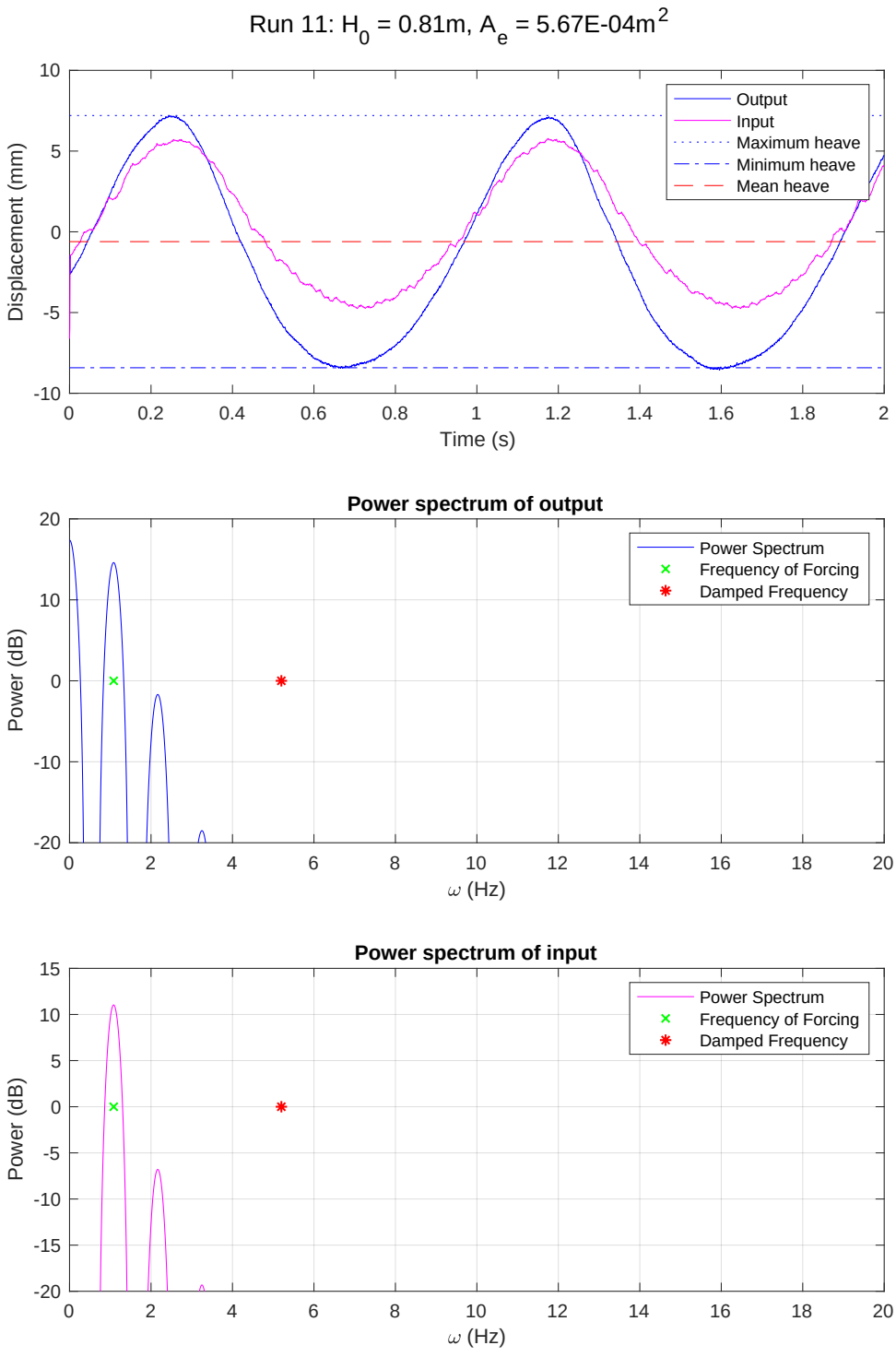


Figure H.126. Experimental trial data for Condition 11

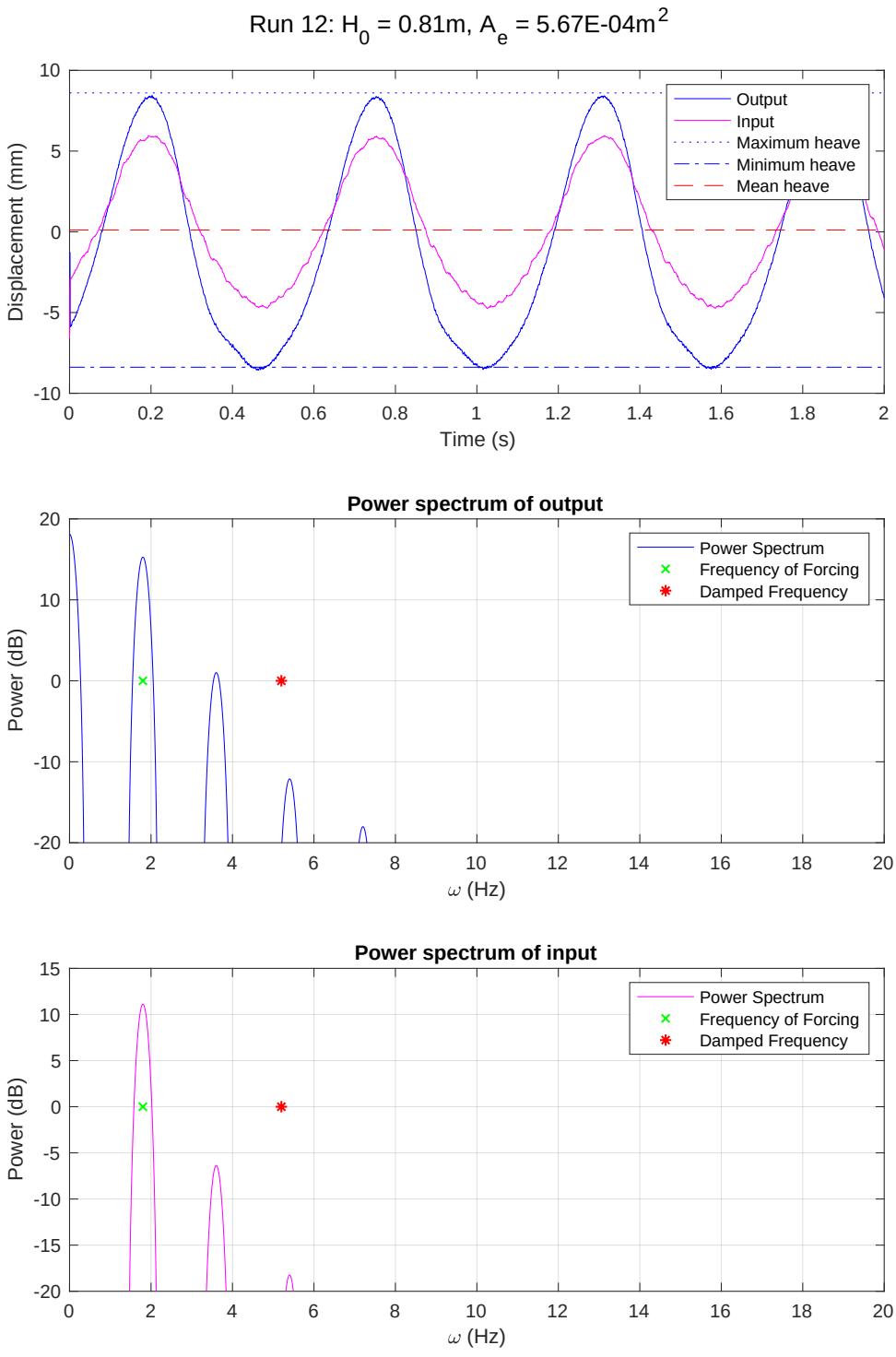


Figure H.127. Experimental trial data for Condition 12

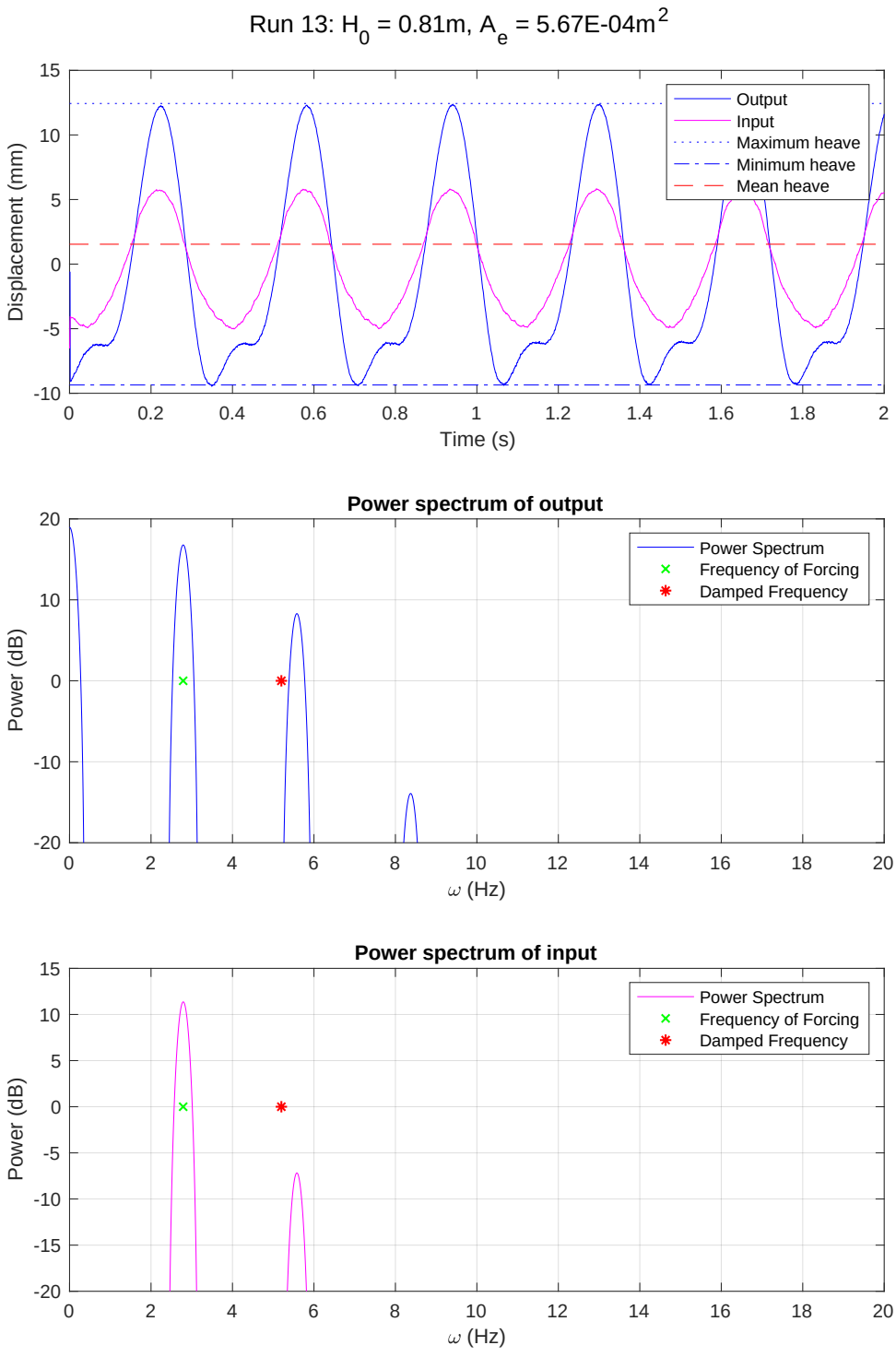


Figure H.128. Experimental trial data for Condition 13

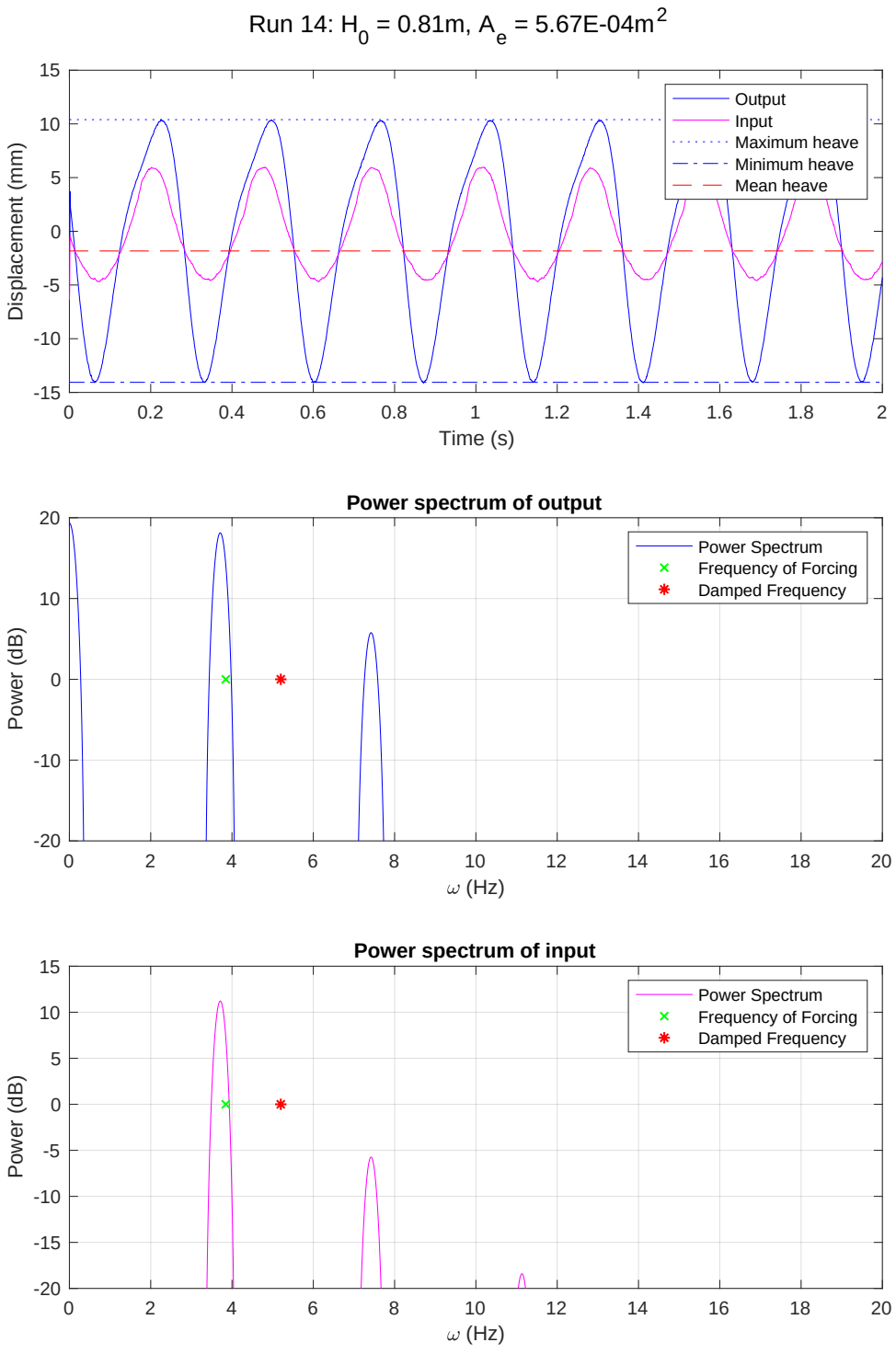


Figure H.129. Experimental trial data for Condition 14

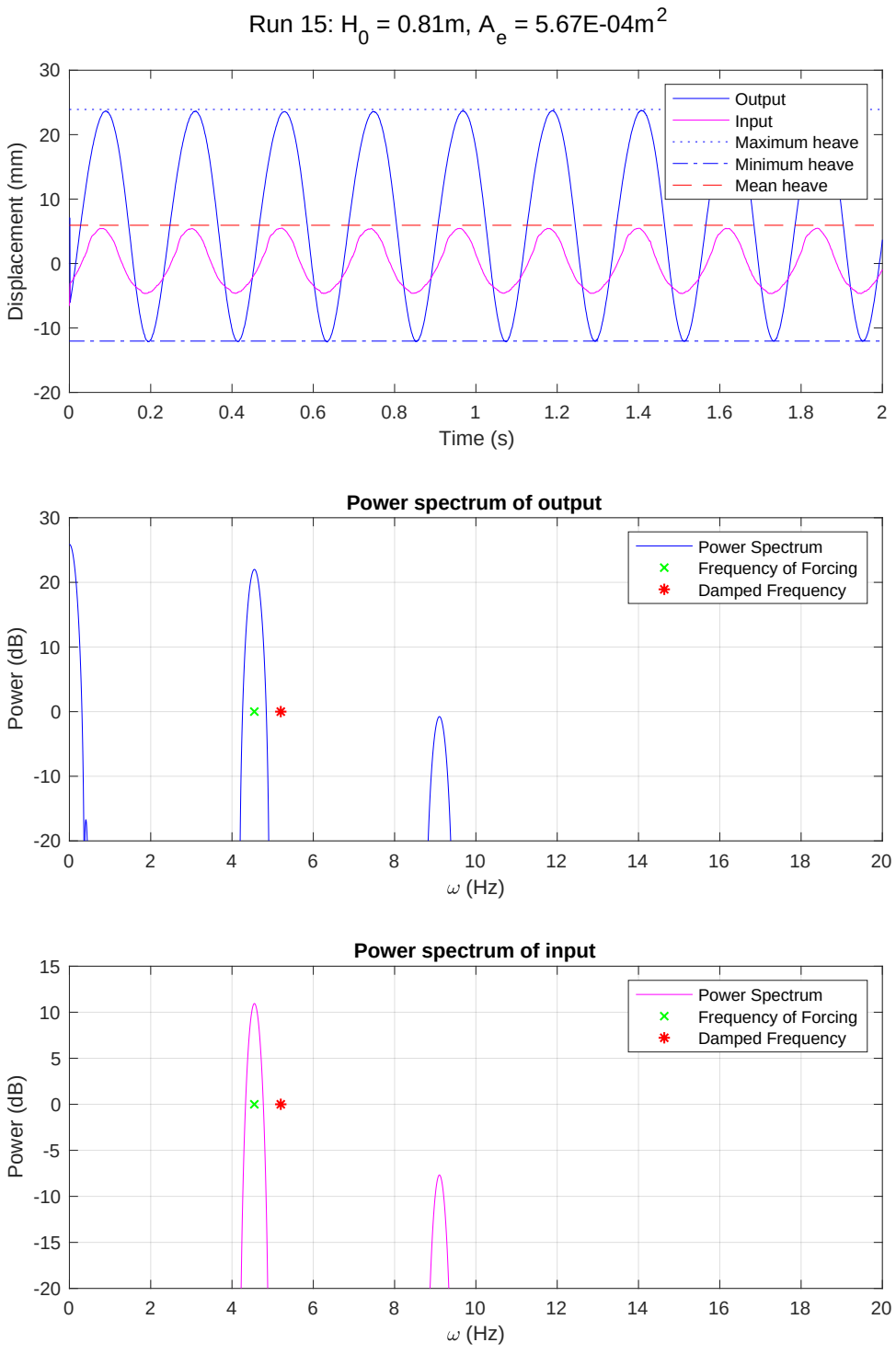


Figure H.130. Experimental trial data for Condition 15

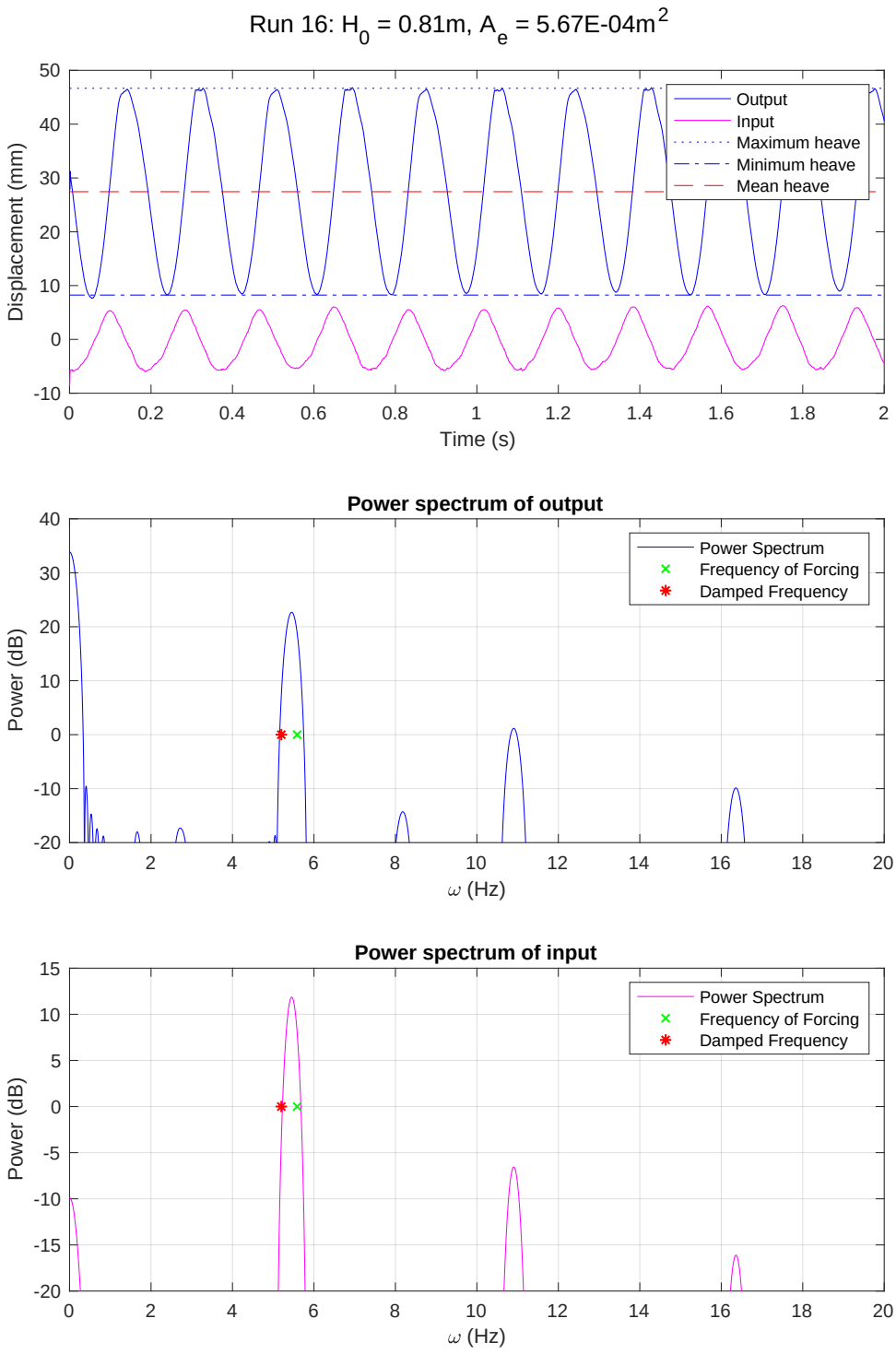


Figure H.131. Experimental trial data for Condition 16

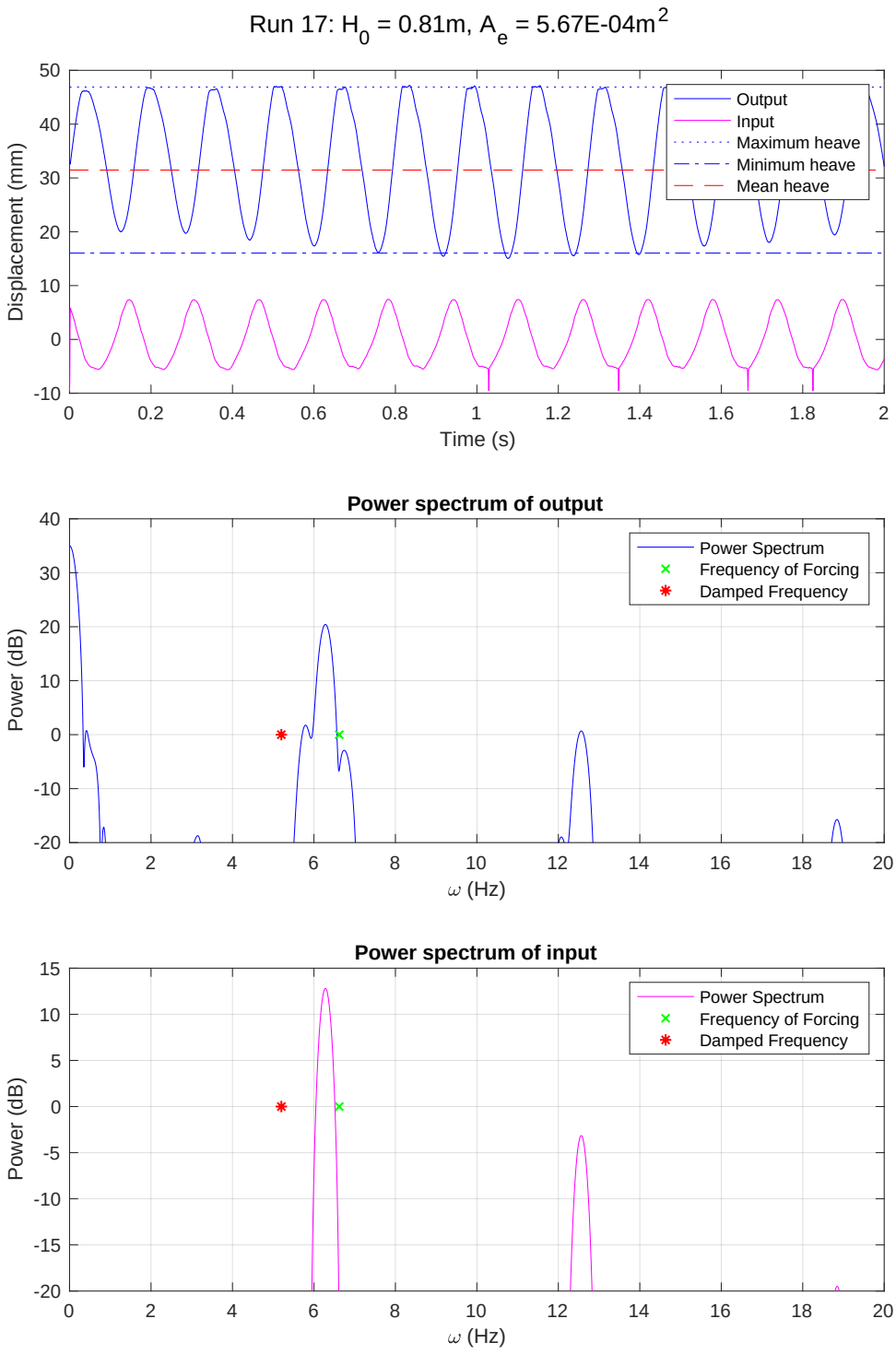


Figure H.132. Experimental trial data for Condition 17

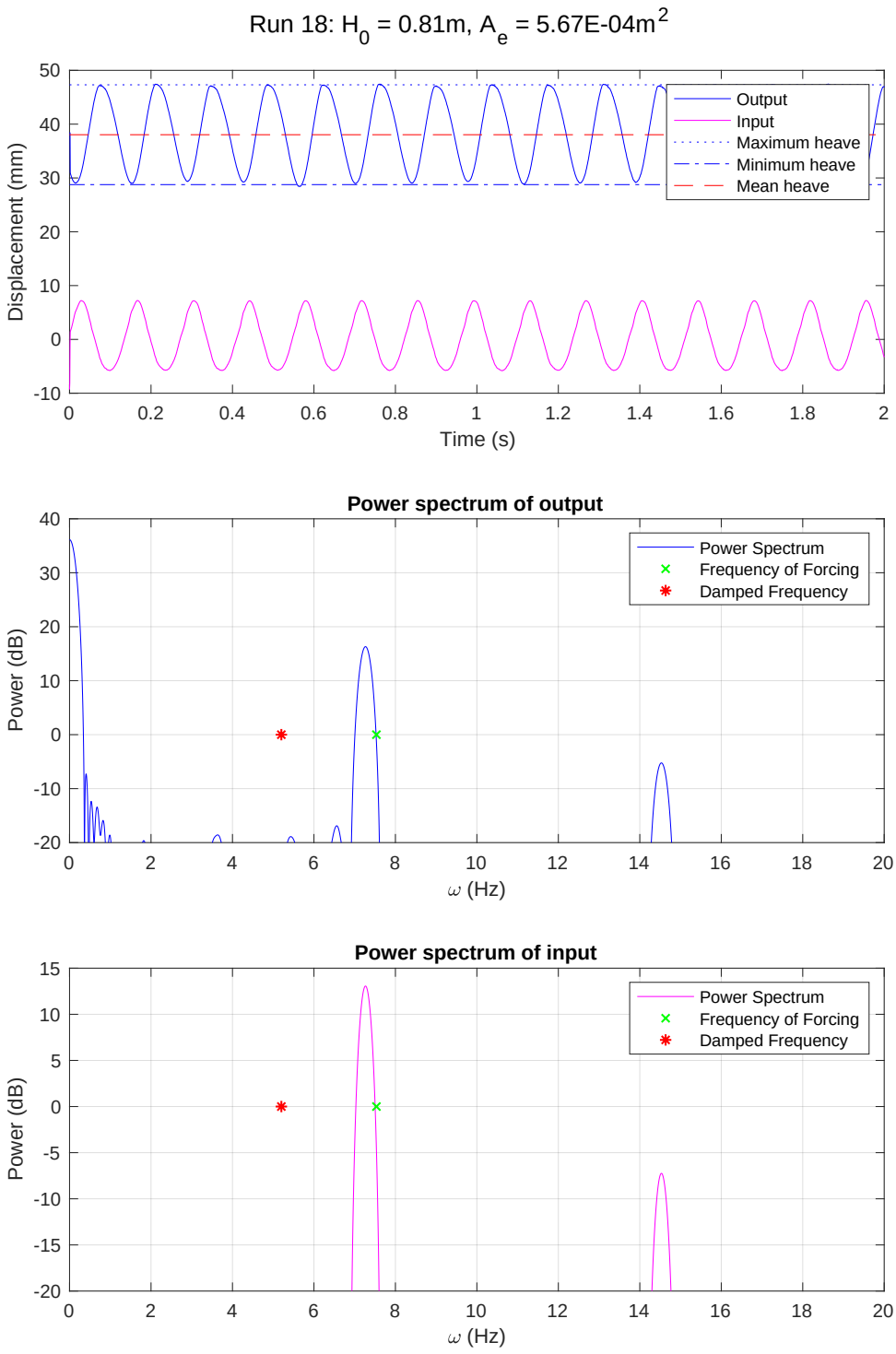


Figure H.133. Experimental trial data for Condition 18

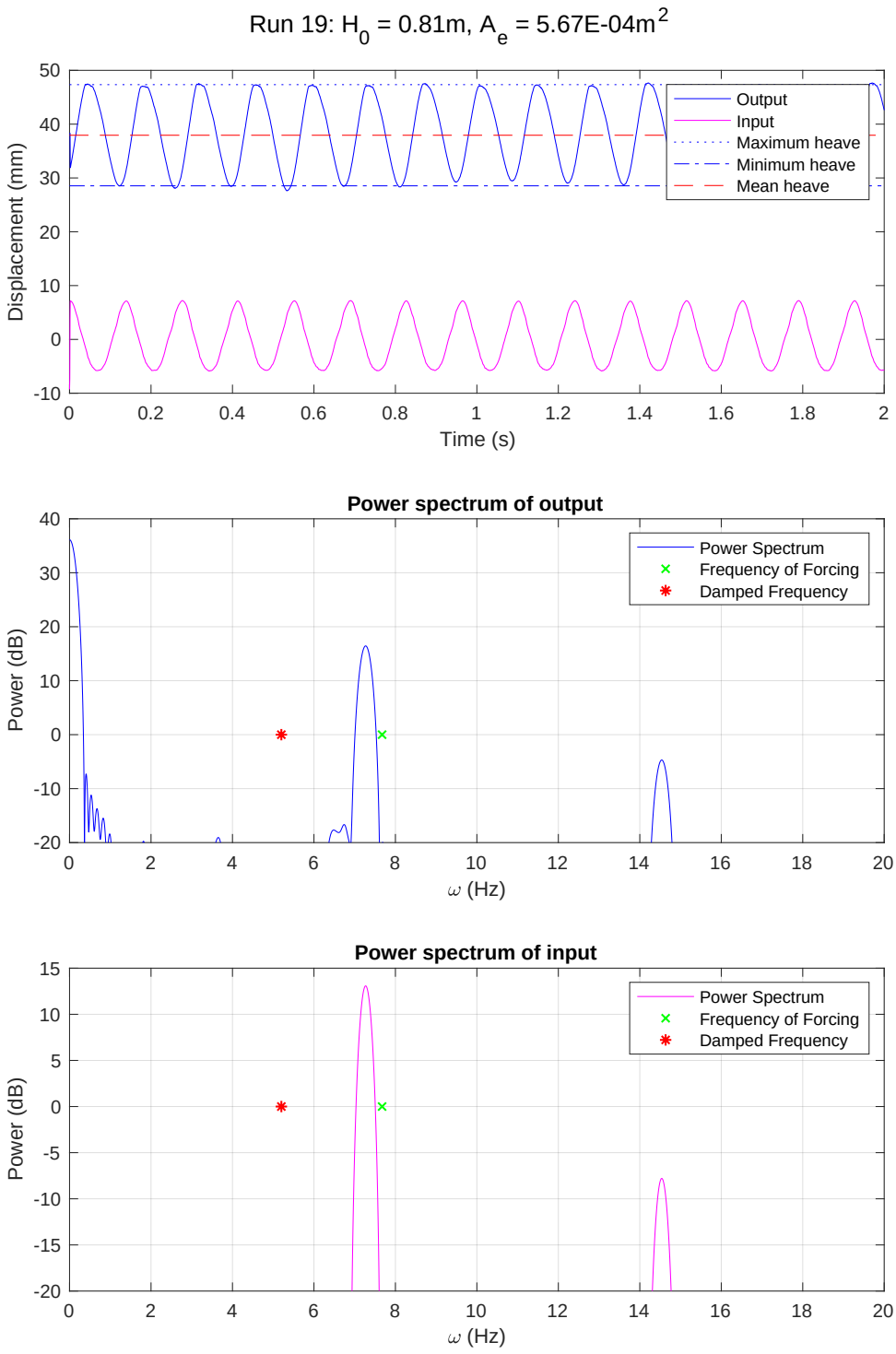


Figure H.134. Experimental trial data for Condition 19

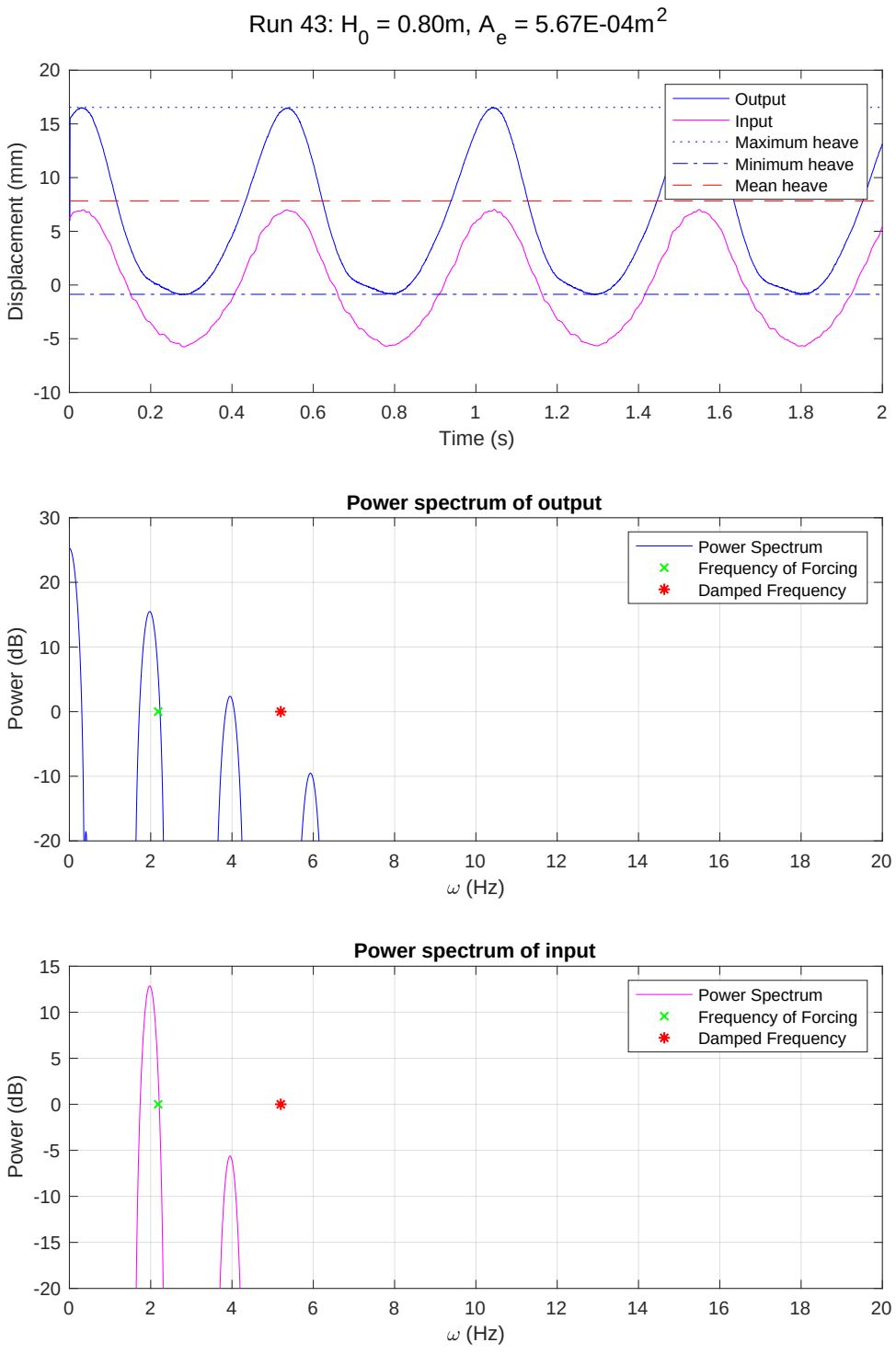


Figure H.135. Experimental trial data for Condition 43

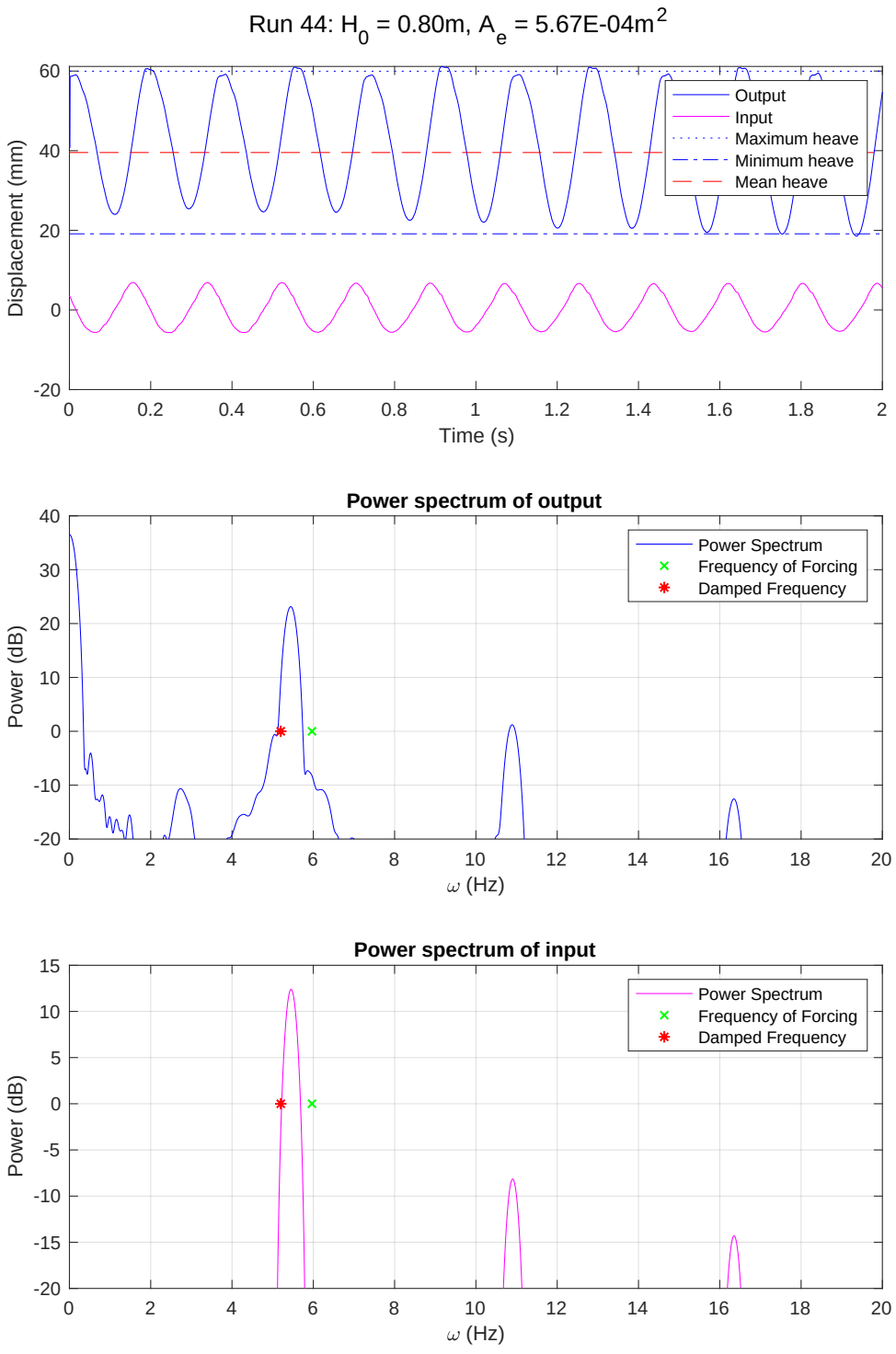


Figure H.136. Experimental trial data for Condition 44

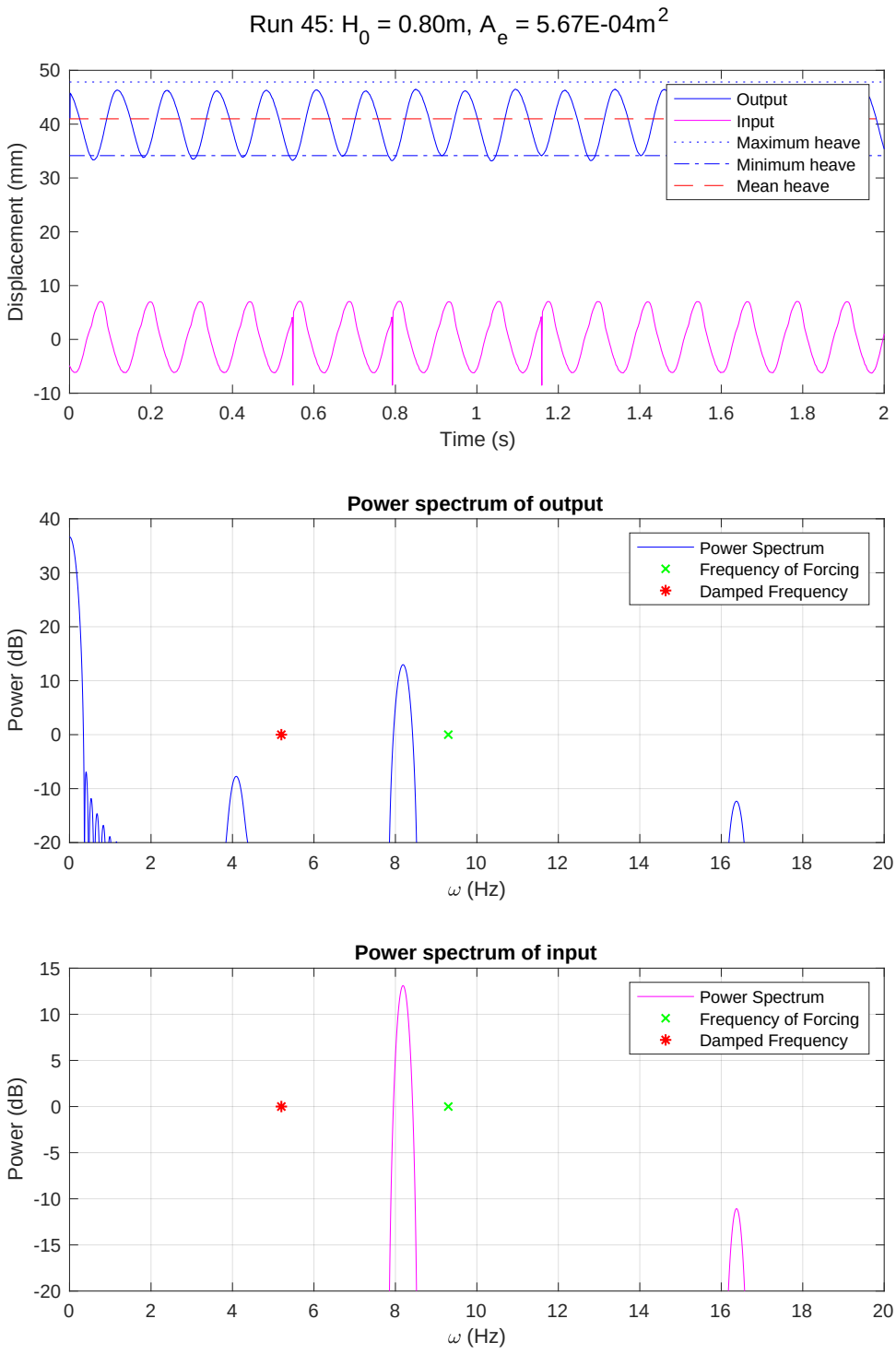


Figure H.137. Experimental trial data for Condition 45

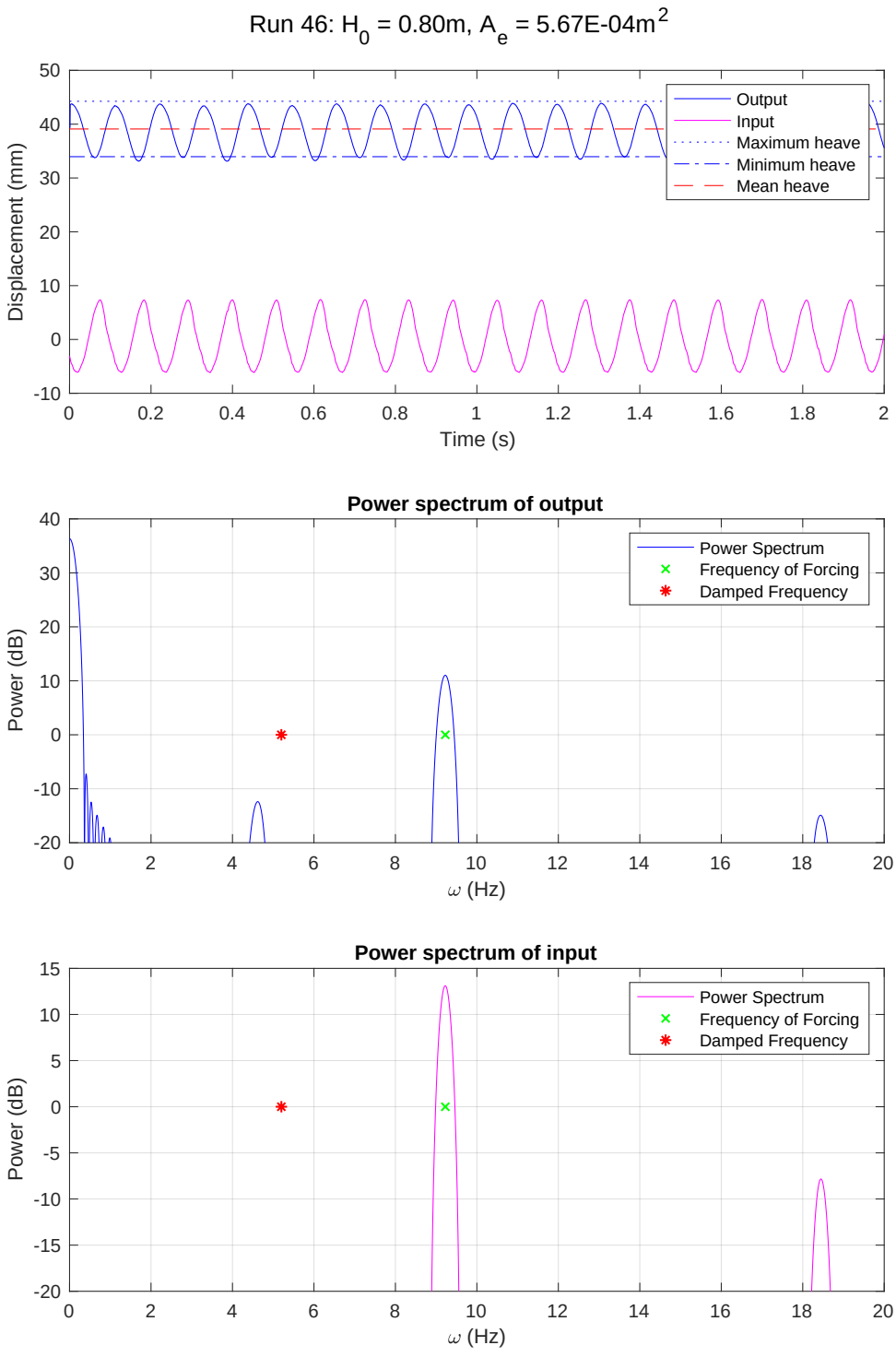


Figure H.138. Experimental trial data for Condition 46

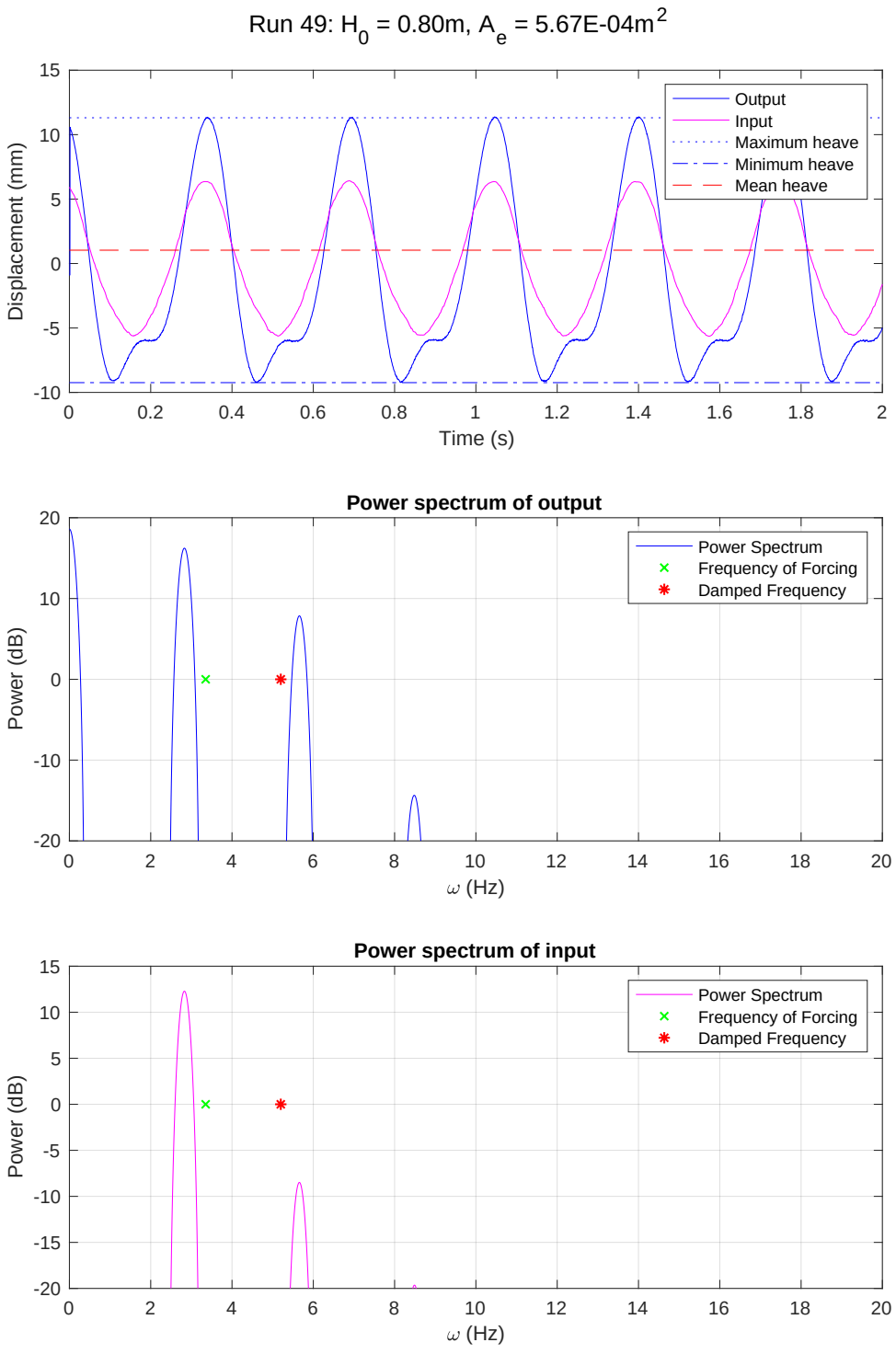


Figure H.139. Experimental trial data for Condition 49

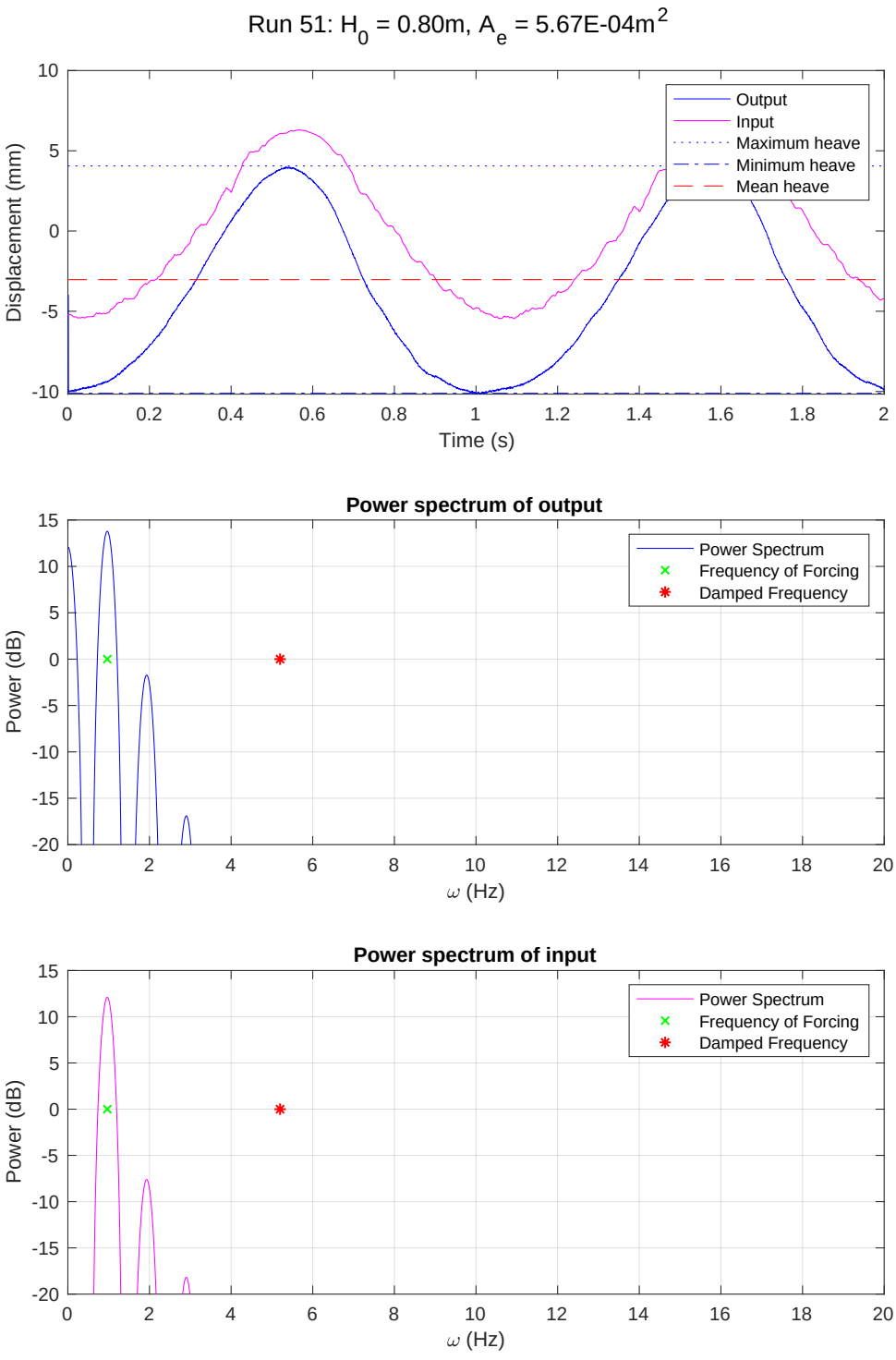


Figure H.140. Experimental trial data for Condition 51

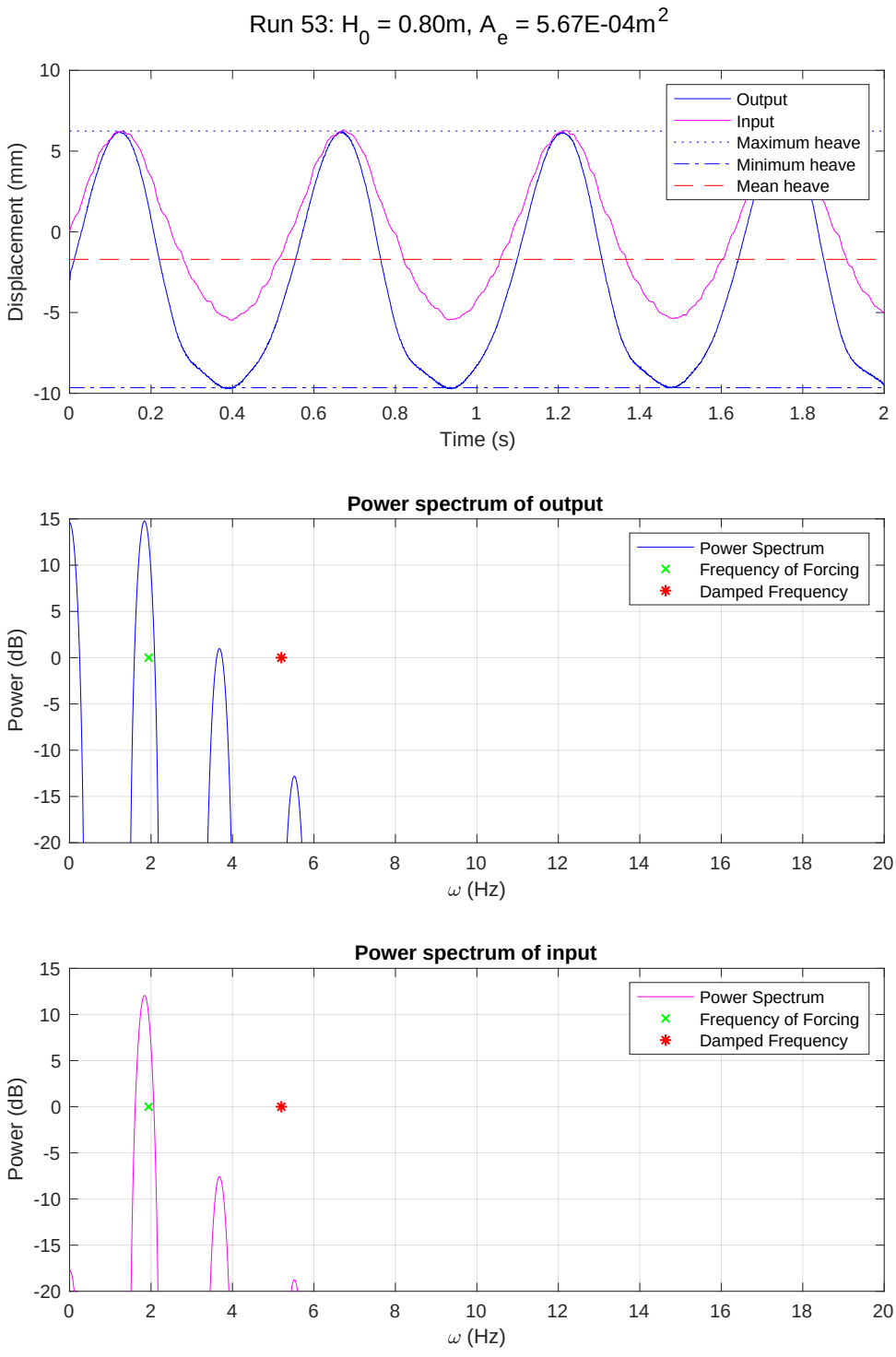


Figure H.141. Experimental trial data for Condition 53

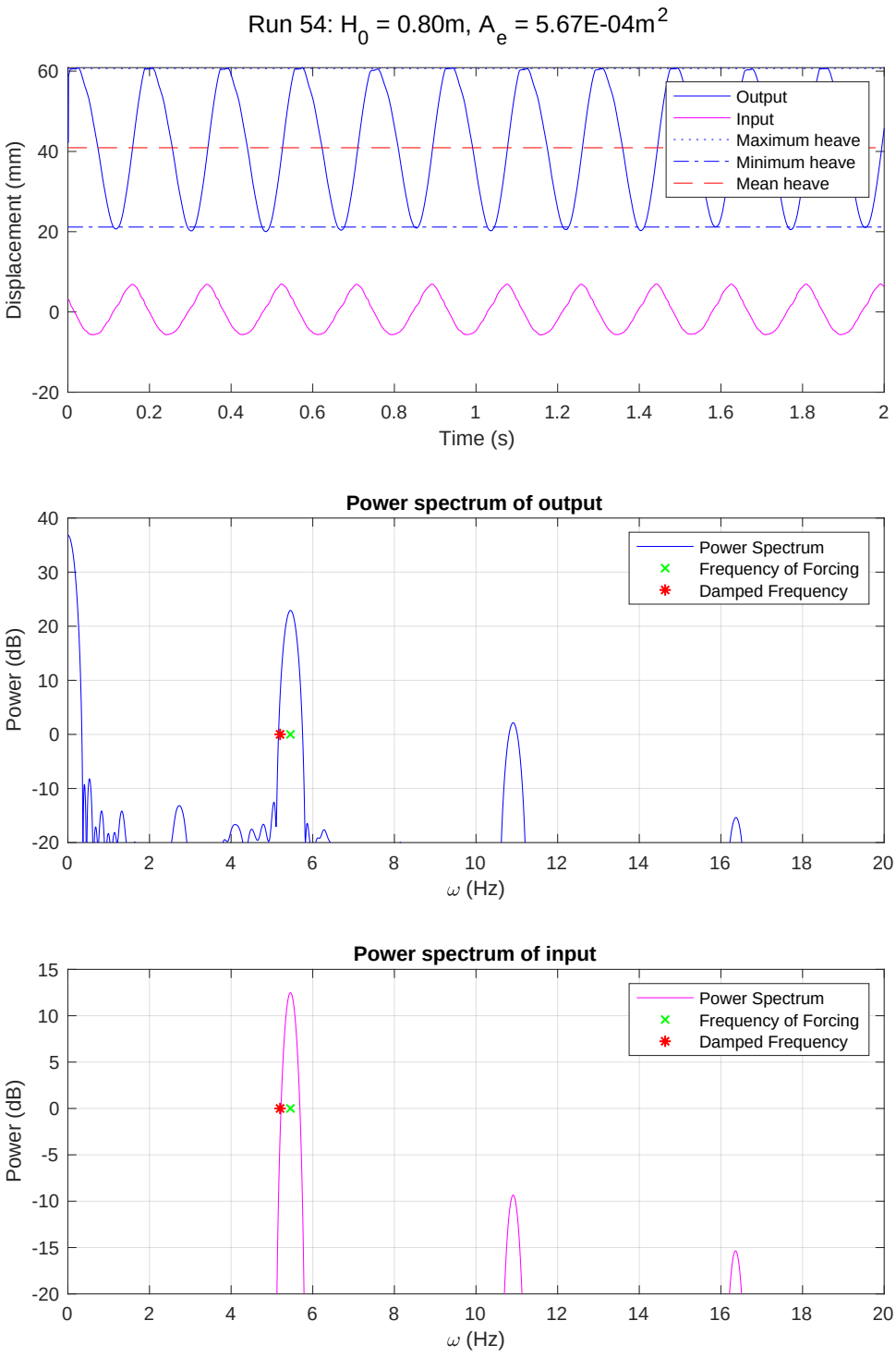


Figure H.142. Experimental trial data for Condition 54

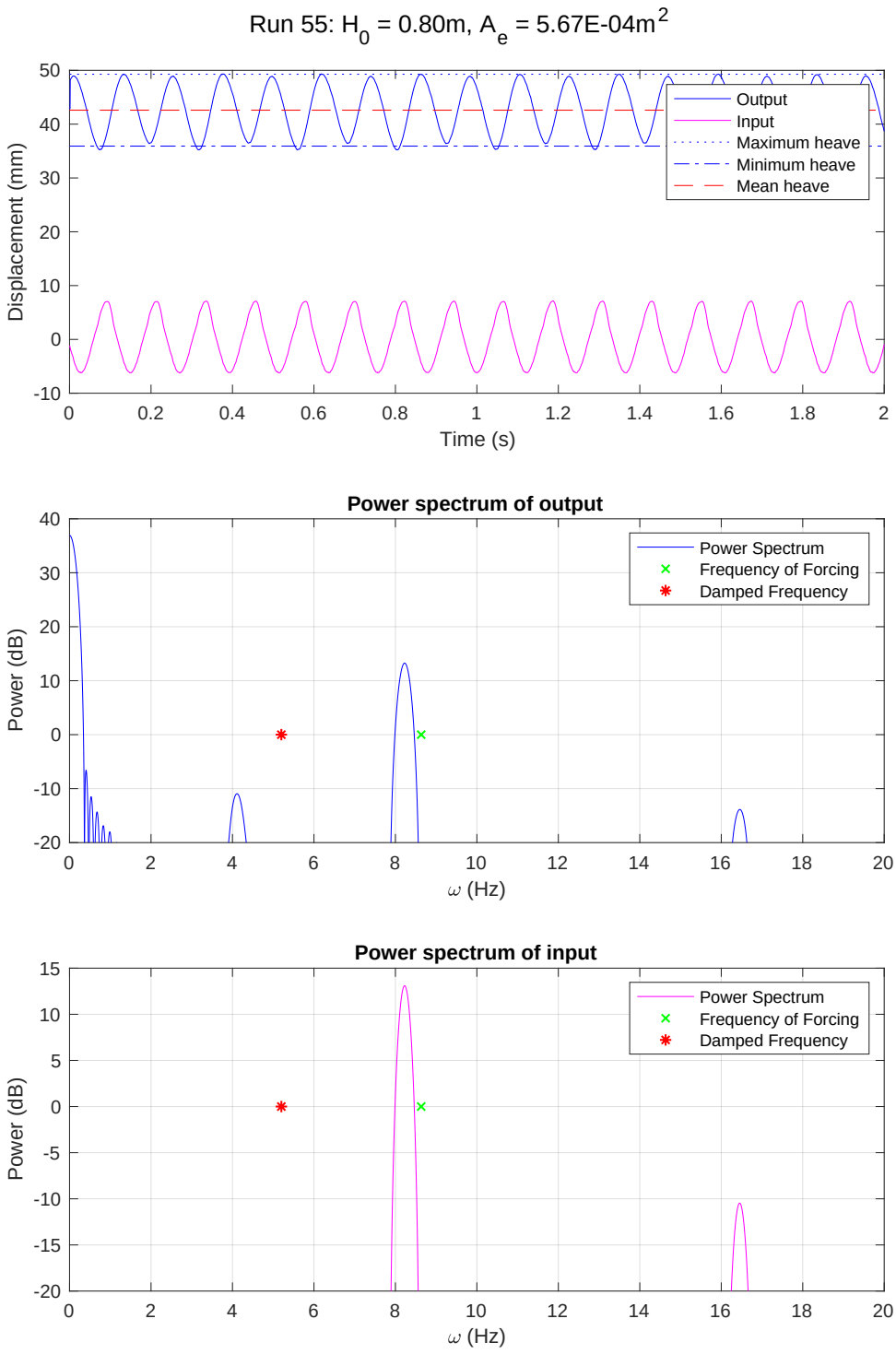


Figure H.143. Experimental trial data for Condition 55

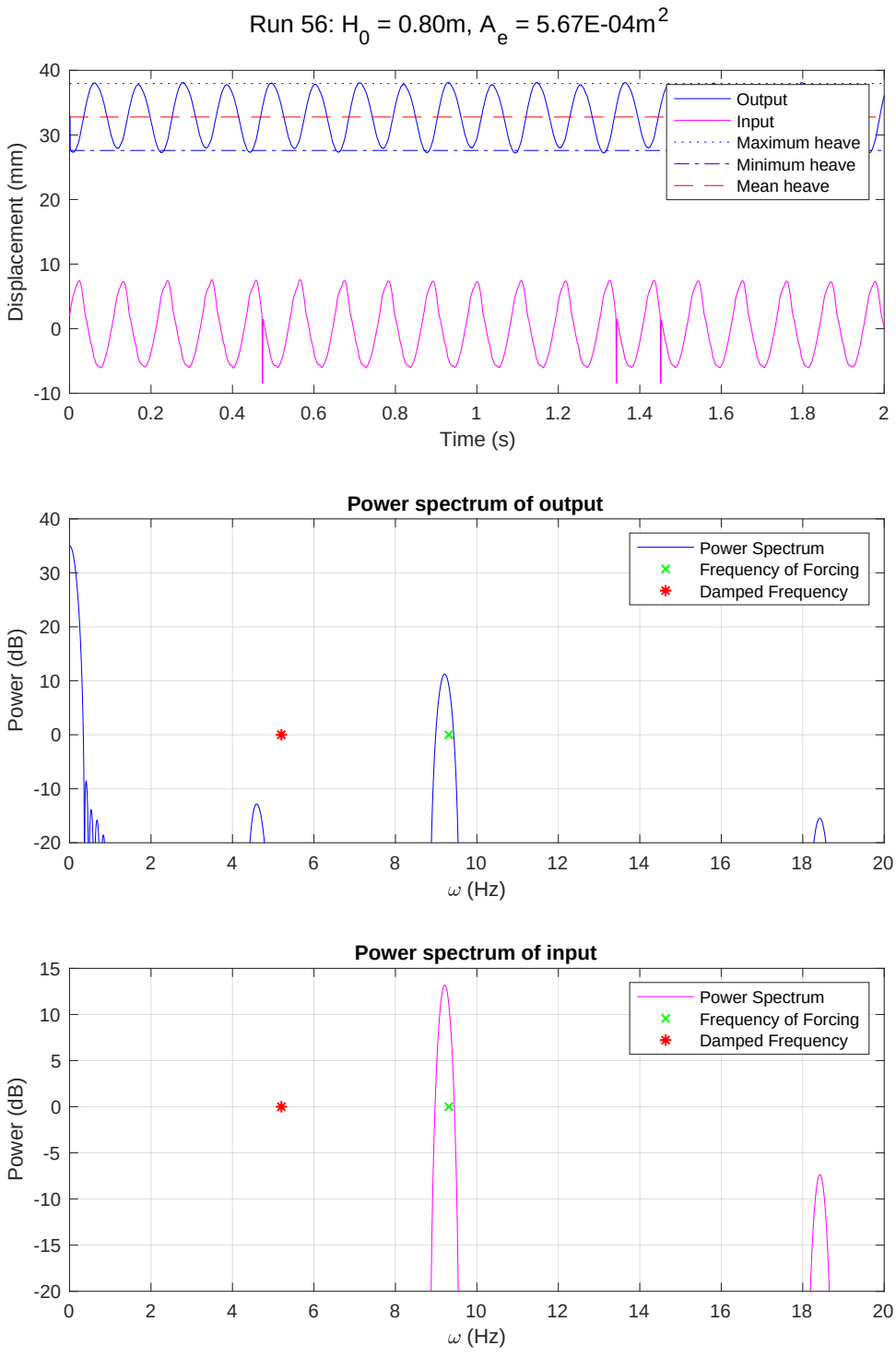


Figure H.144. Experimental trial data for Condition 56

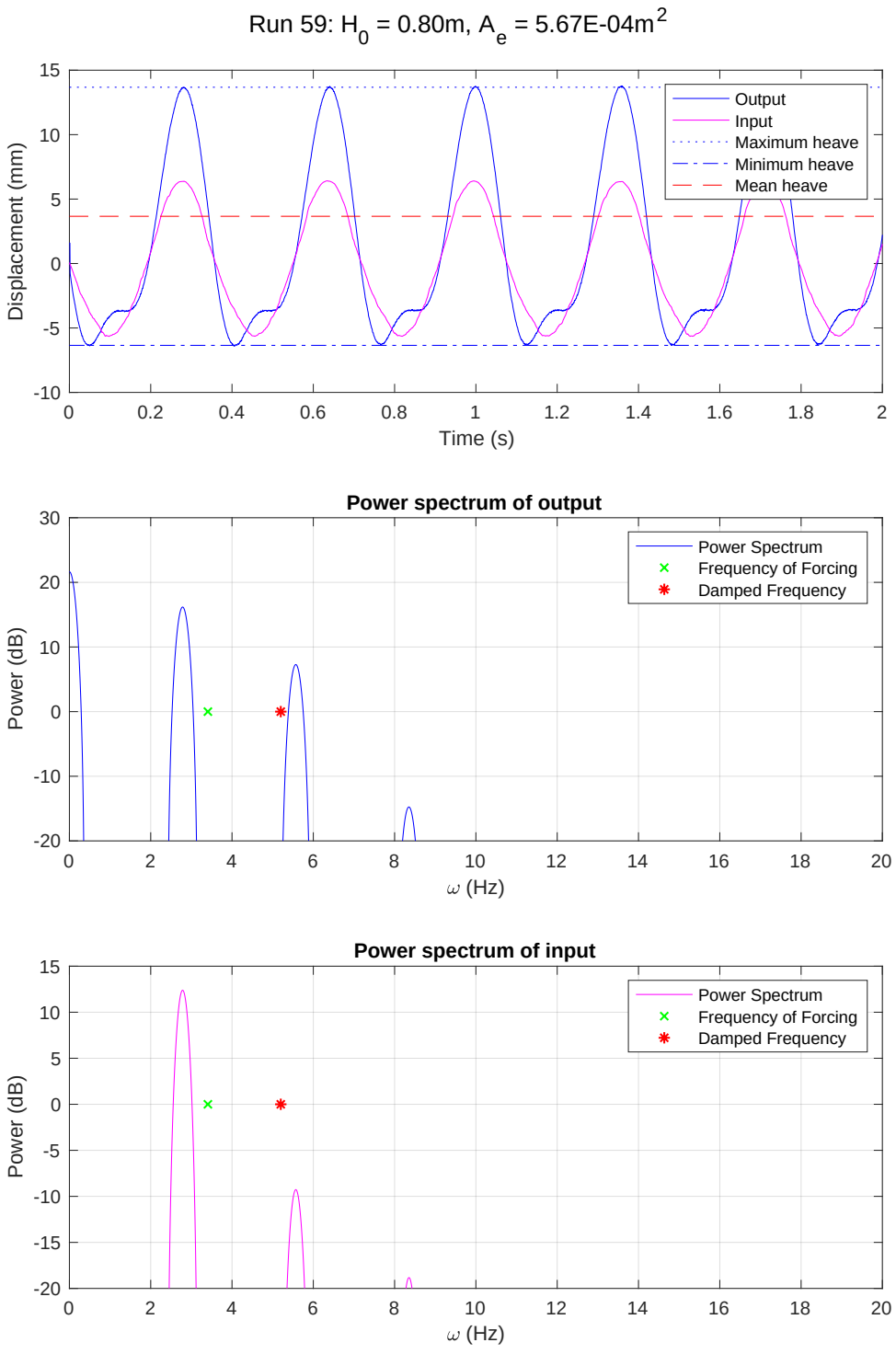


Figure H.145. Experimental trial data for Condition 59

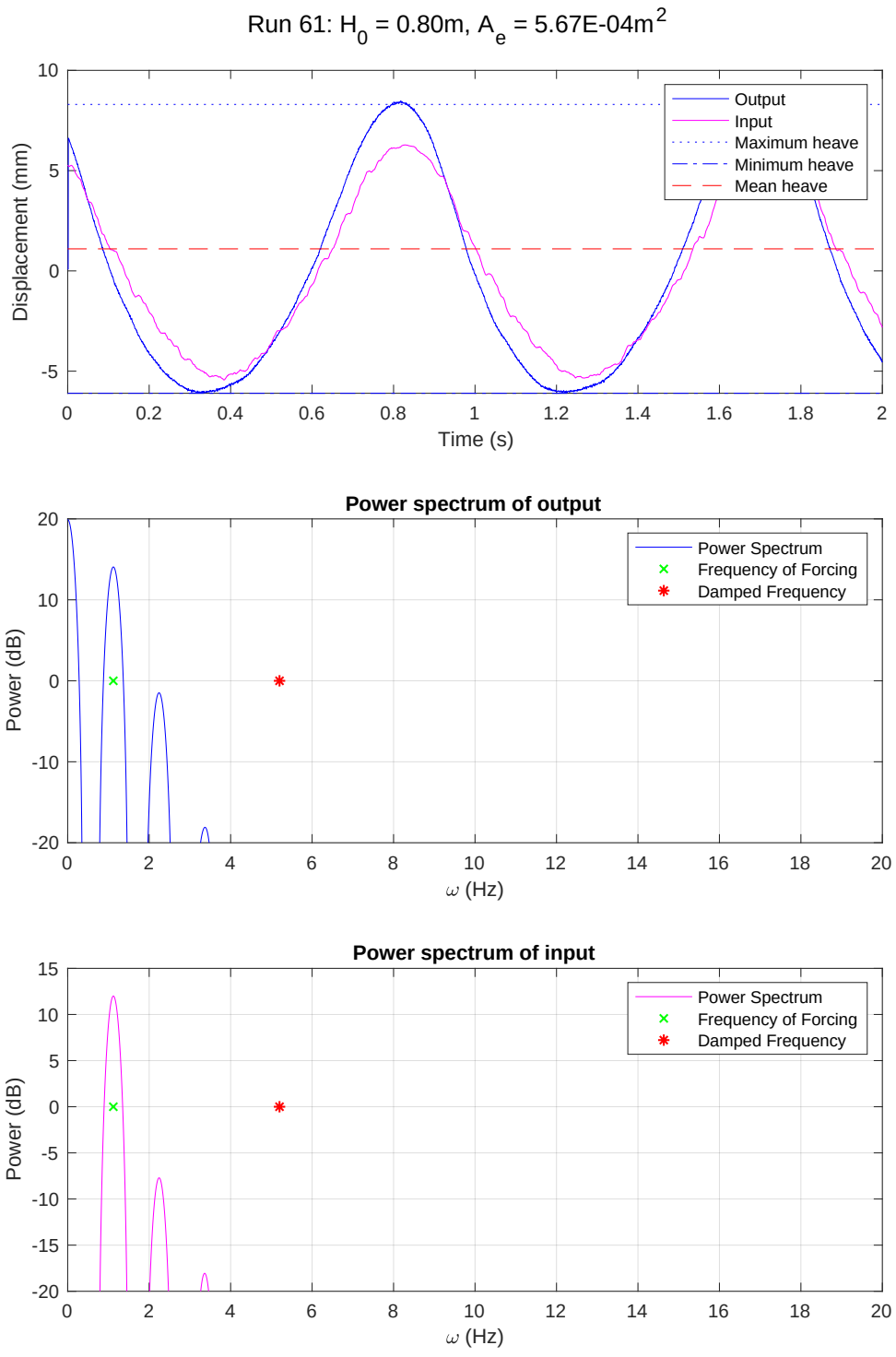


Figure H.146. Experimental trial data for Condition 61

H.2.8. Condition Eight

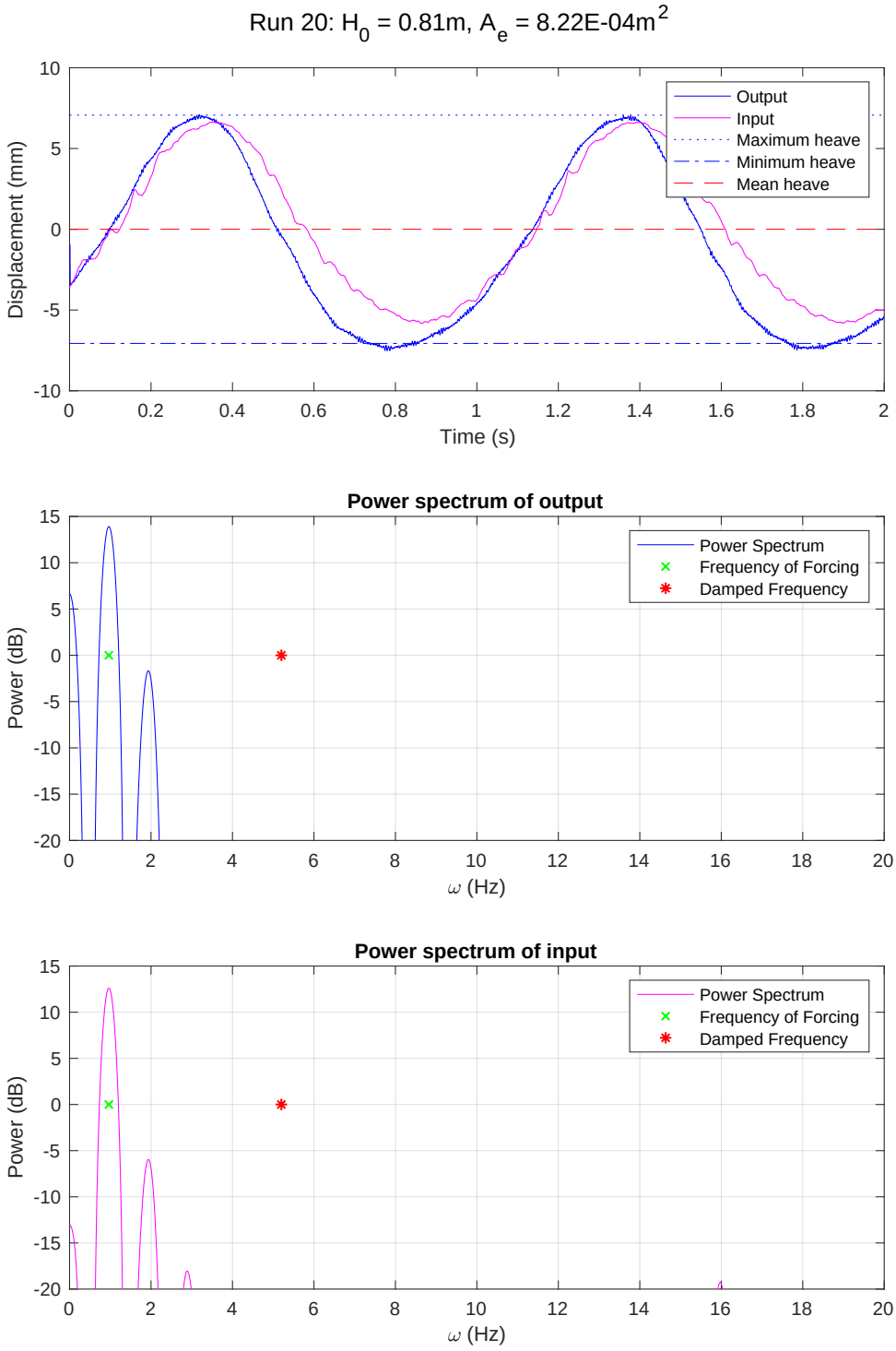


Figure H.147. Experimental trial data for Condition 20

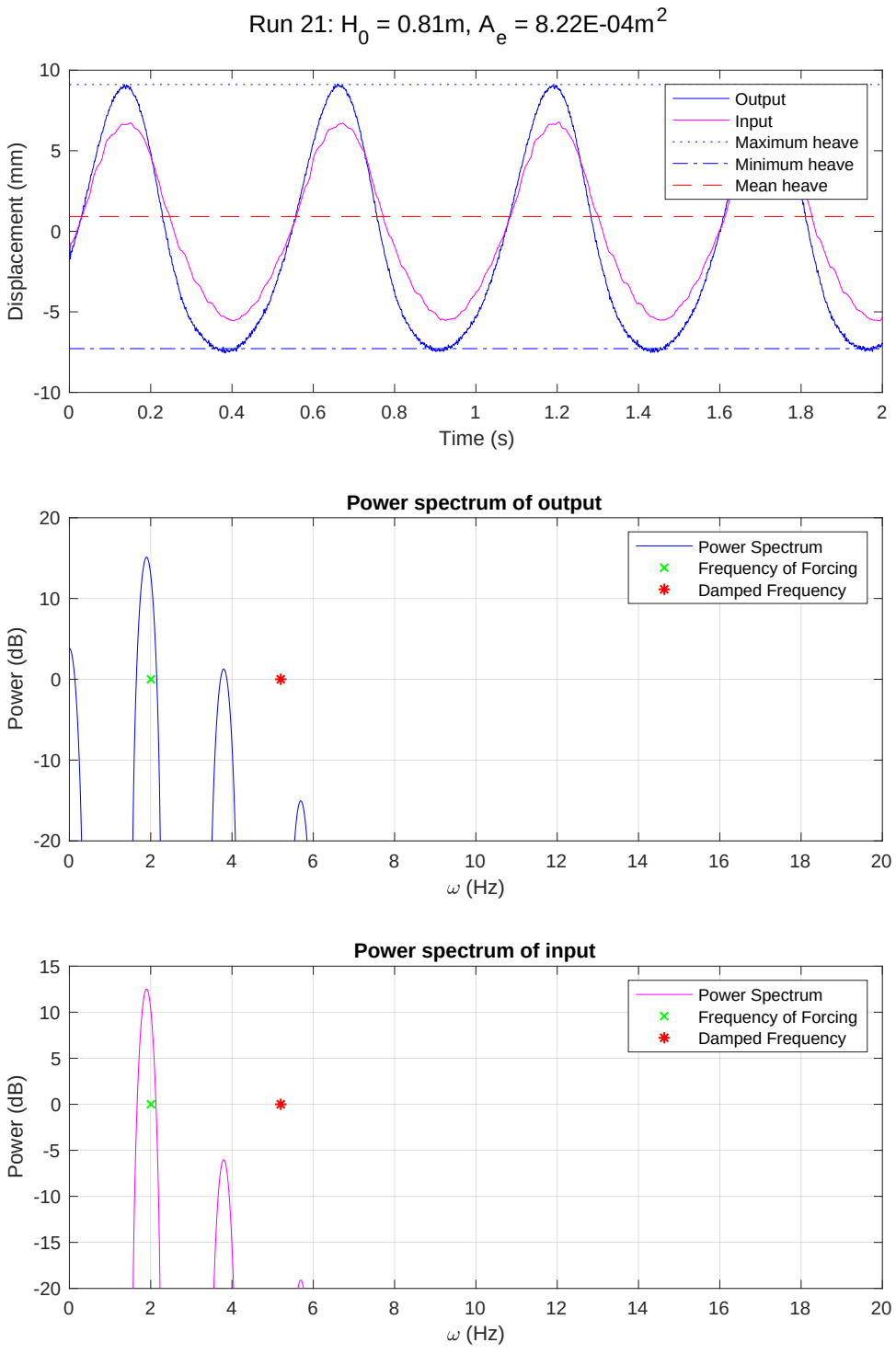


Figure H.148. Experimental trial data for Condition 21

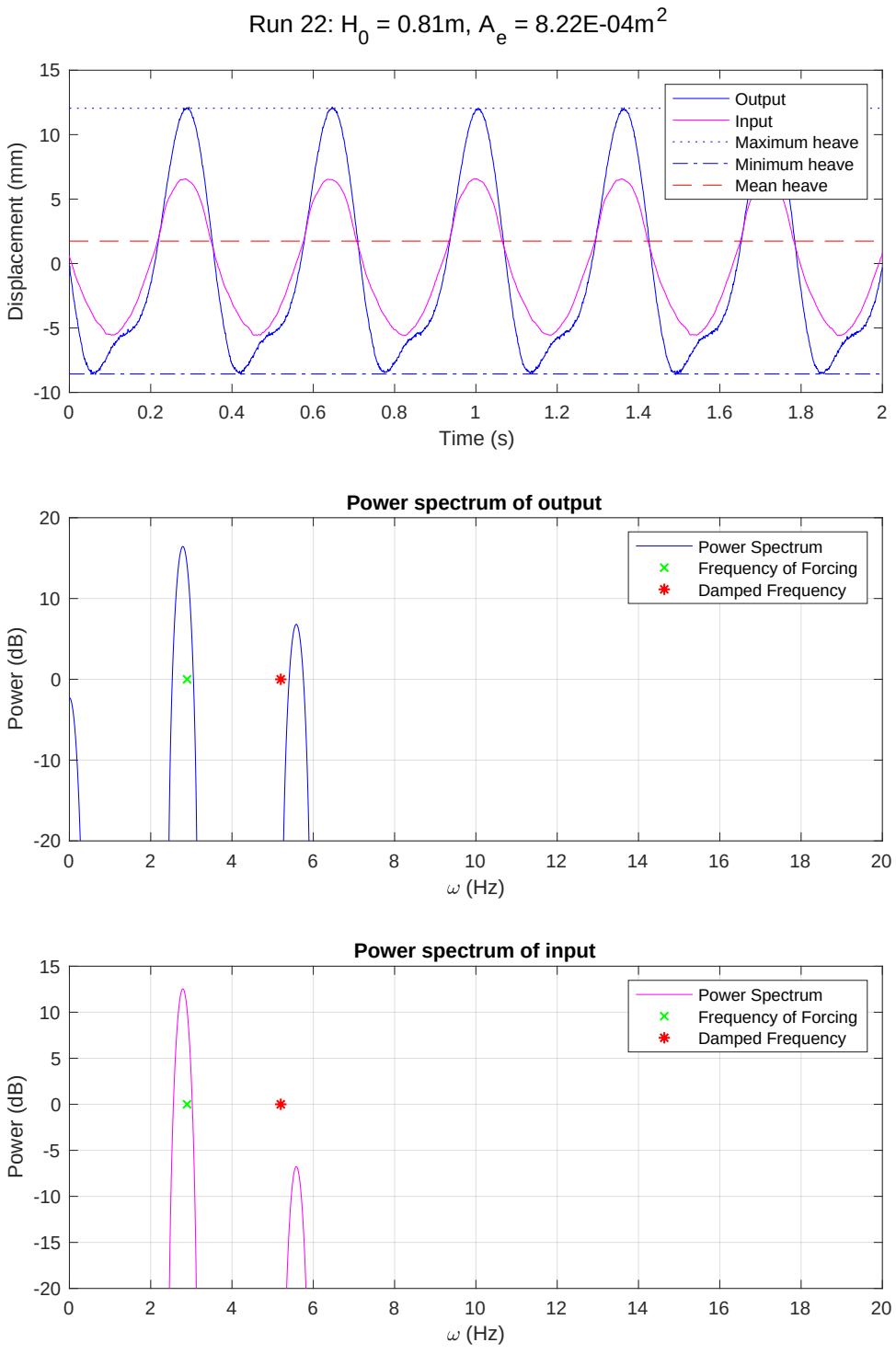


Figure H.149. Experimental trial data for Condition 22

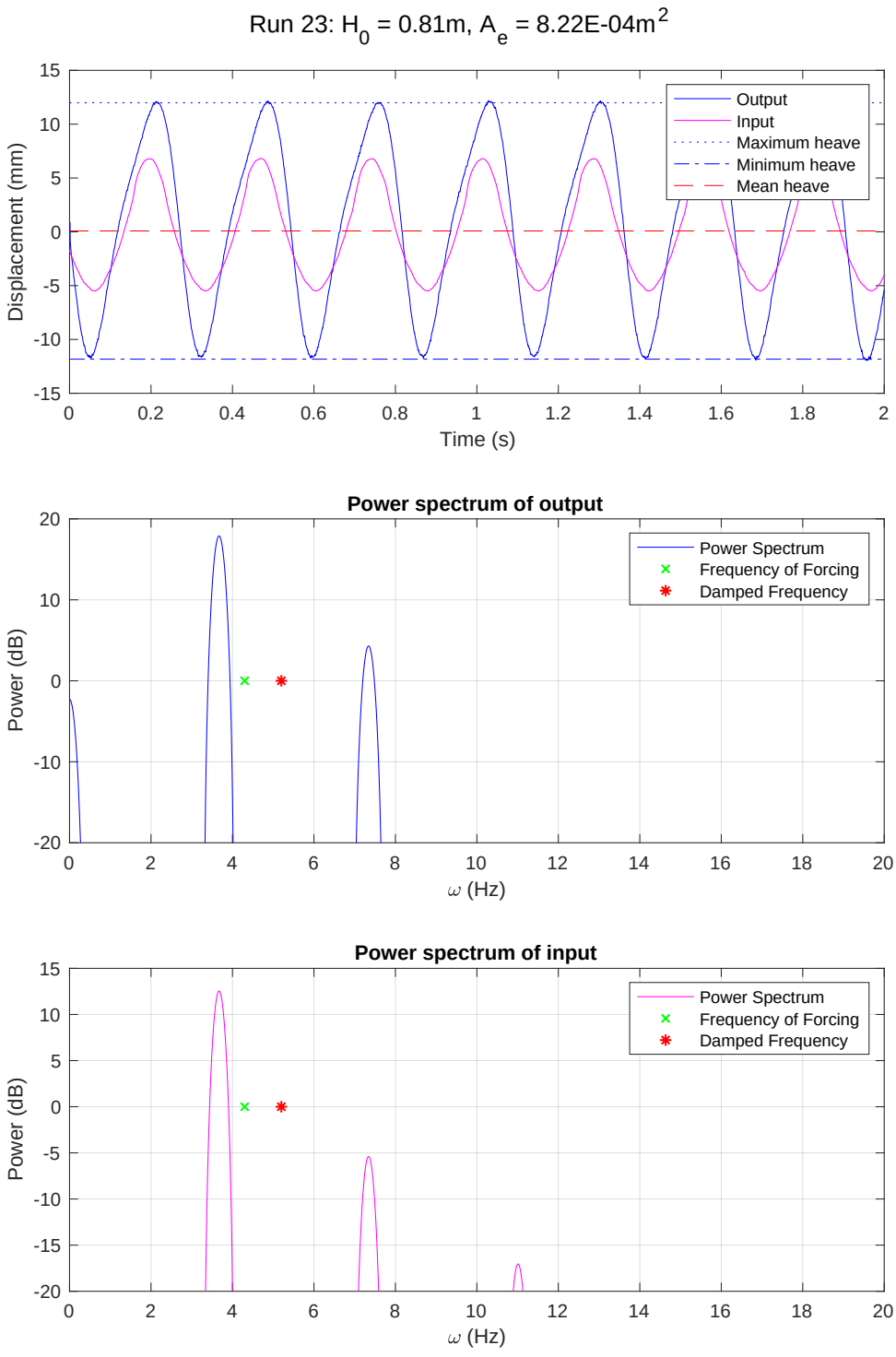


Figure H.150. Experimental trial data for Condition 23

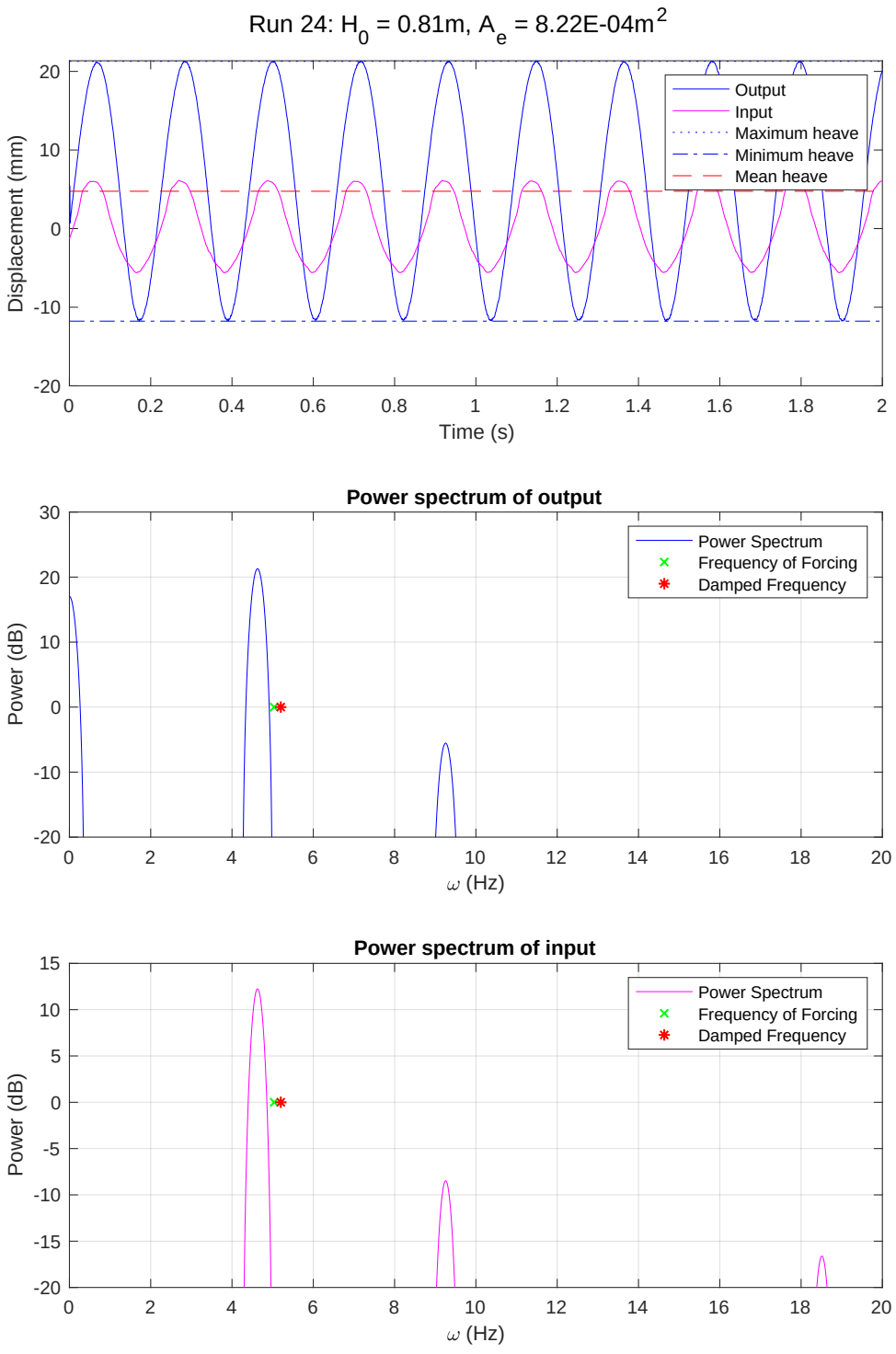


Figure H.151. Experimental trial data for Condition 24

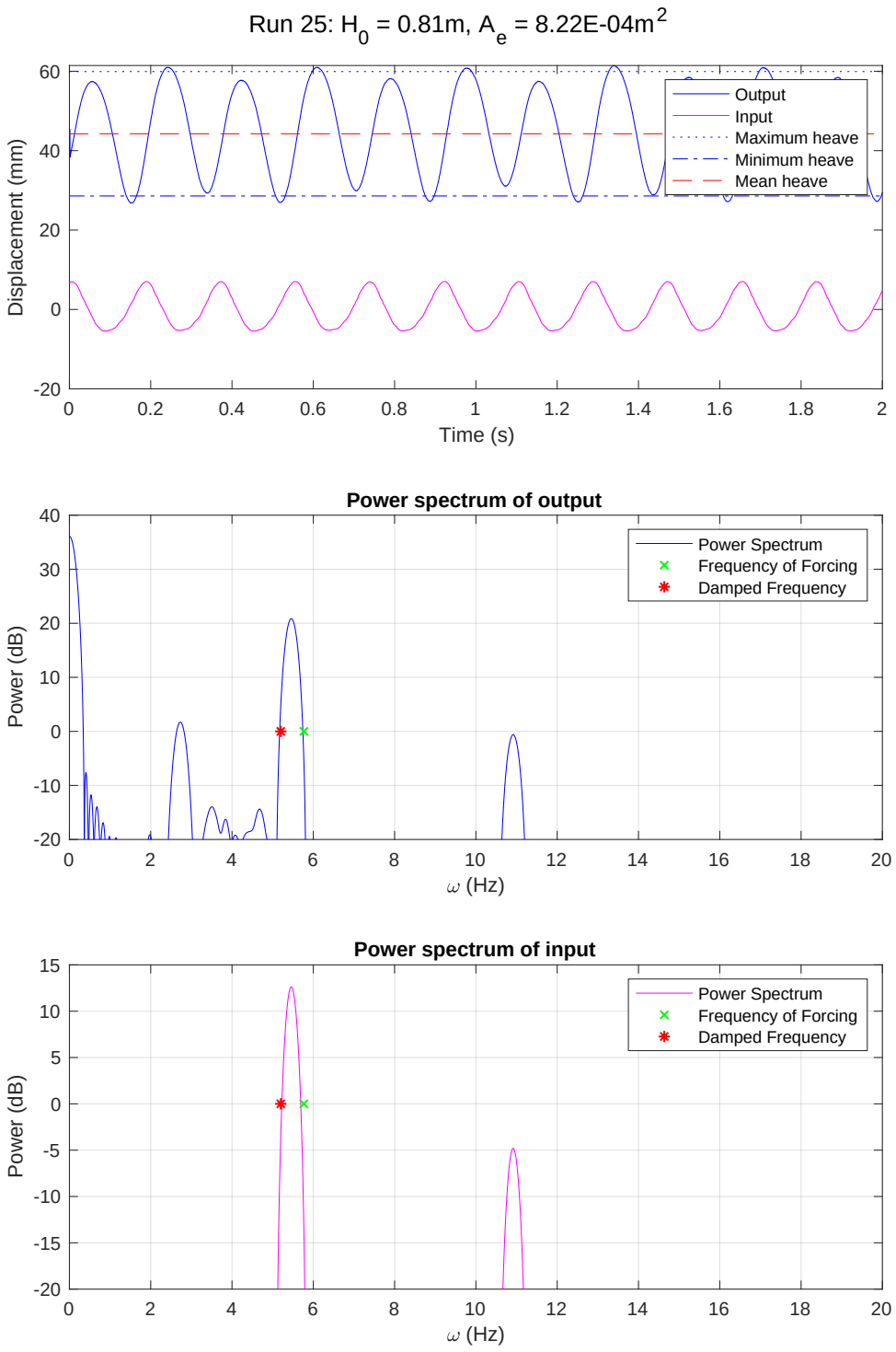


Figure H.152. Experimental trial data for Condition 25

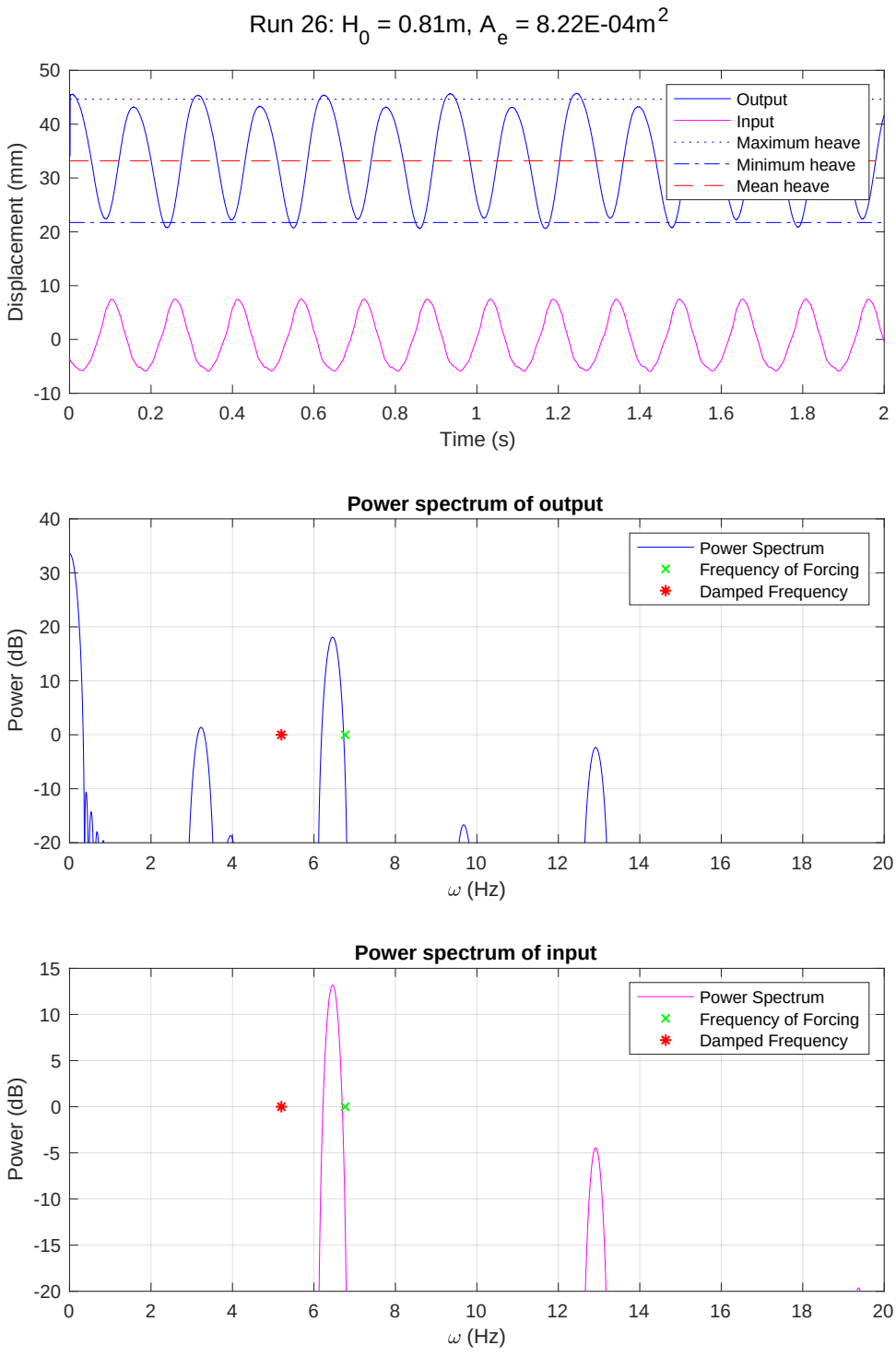


Figure H.153. Experimental trial data for Condition 26

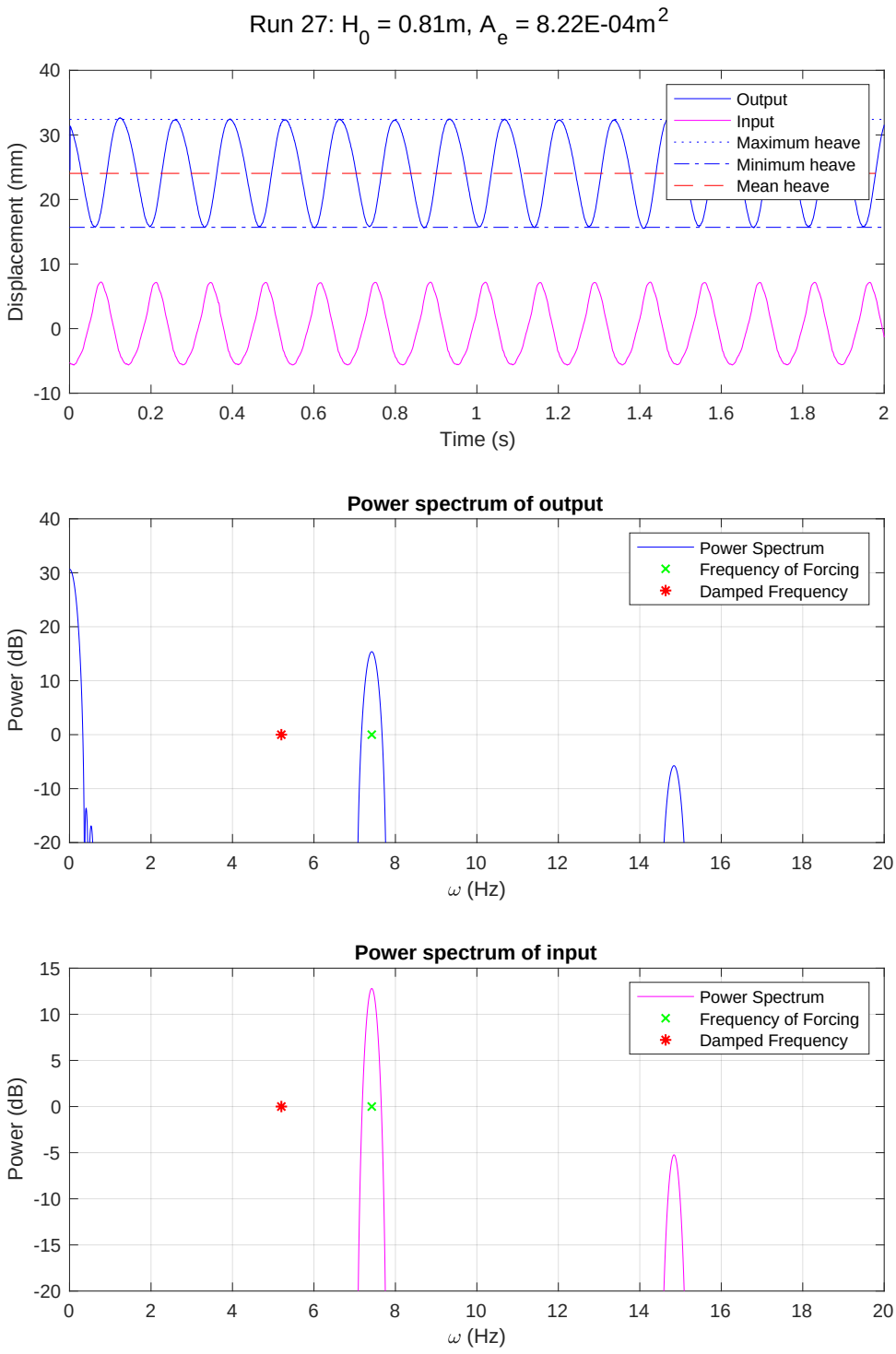


Figure H.154. Experimental trial data for Condition 27

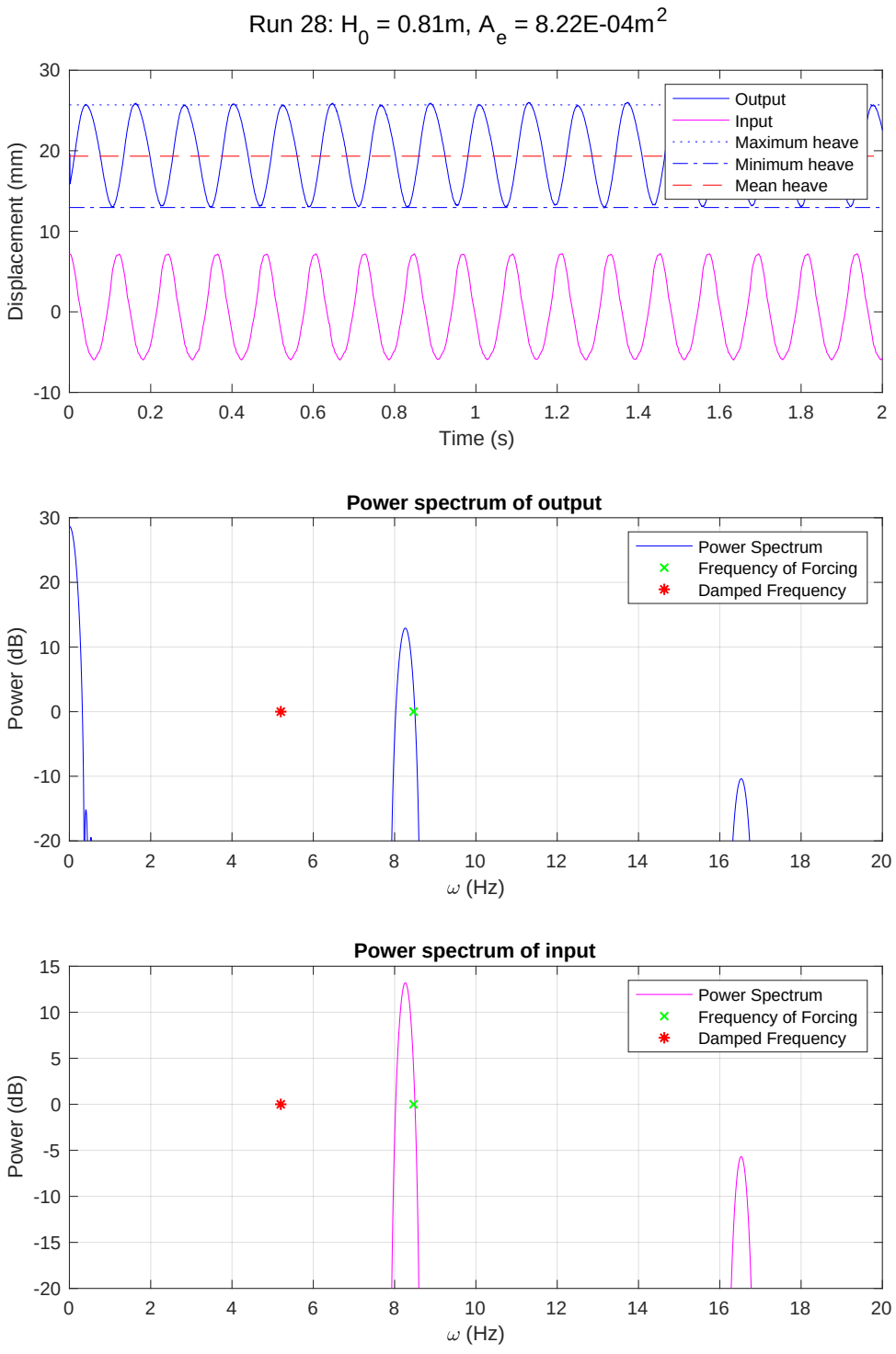


Figure H.155. Experimental trial data for Condition 28

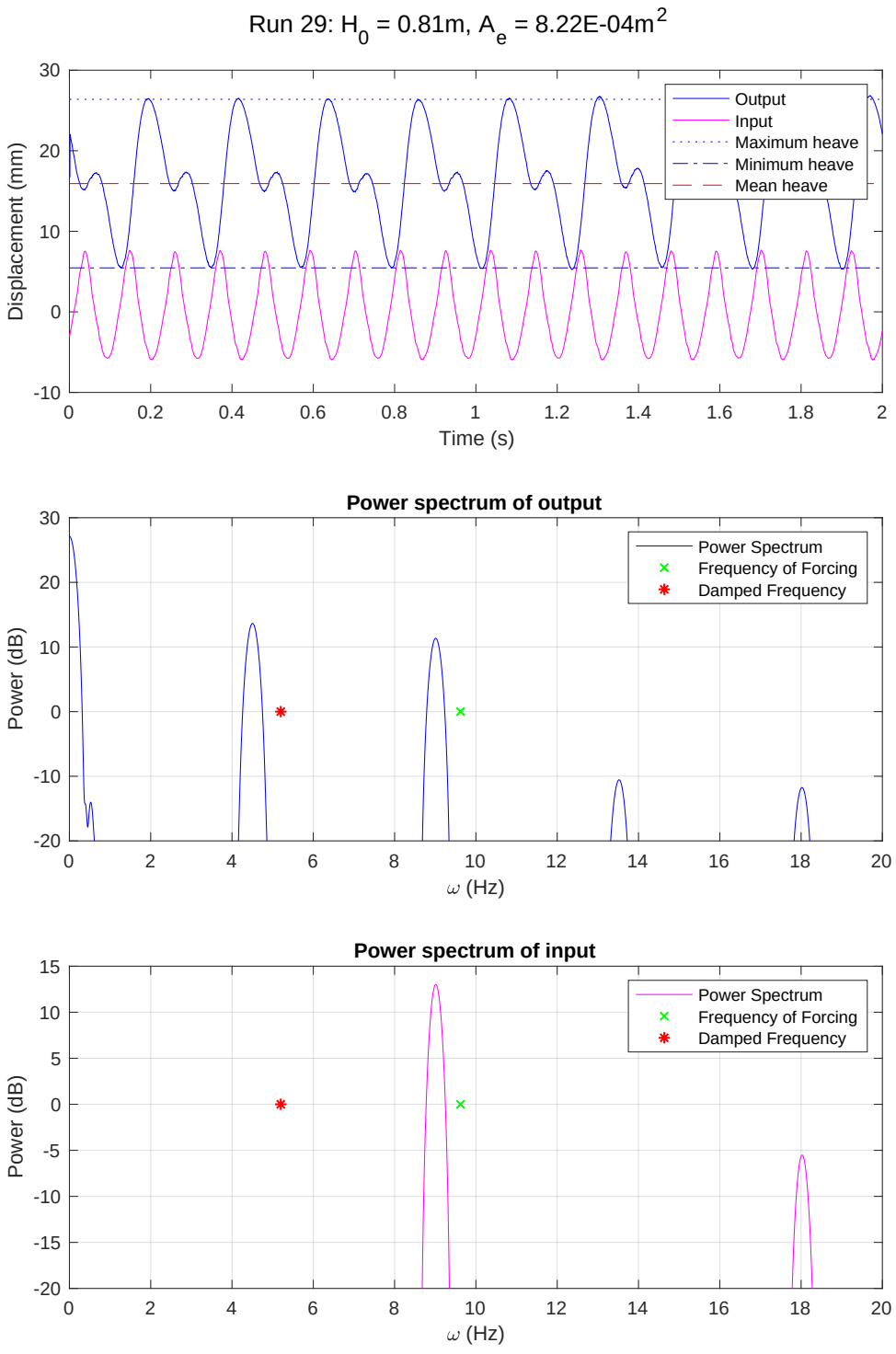


Figure H.156. Experimental trial data for Condition 29

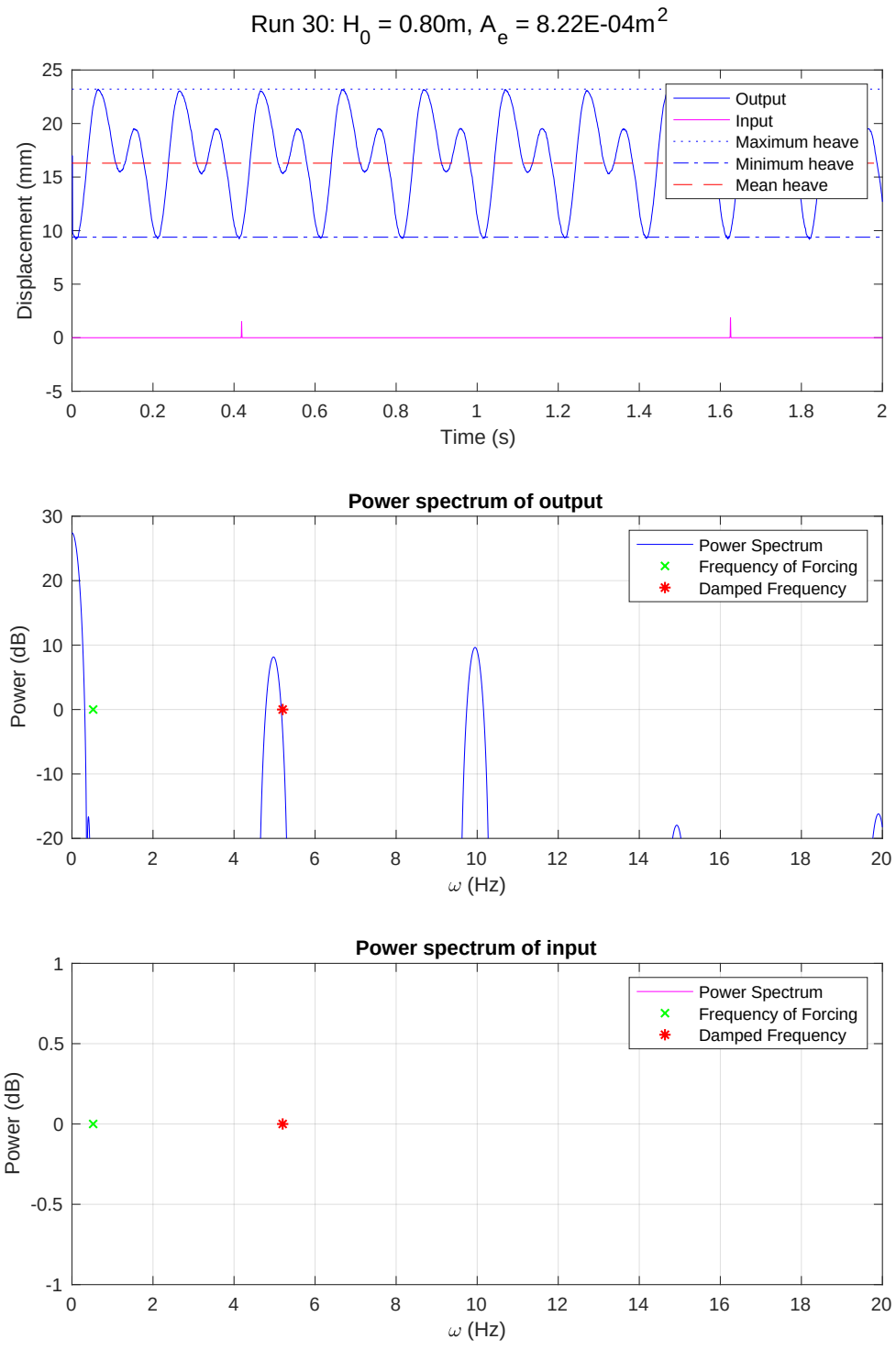


Figure H.157. Experimental trial data for Condition 30

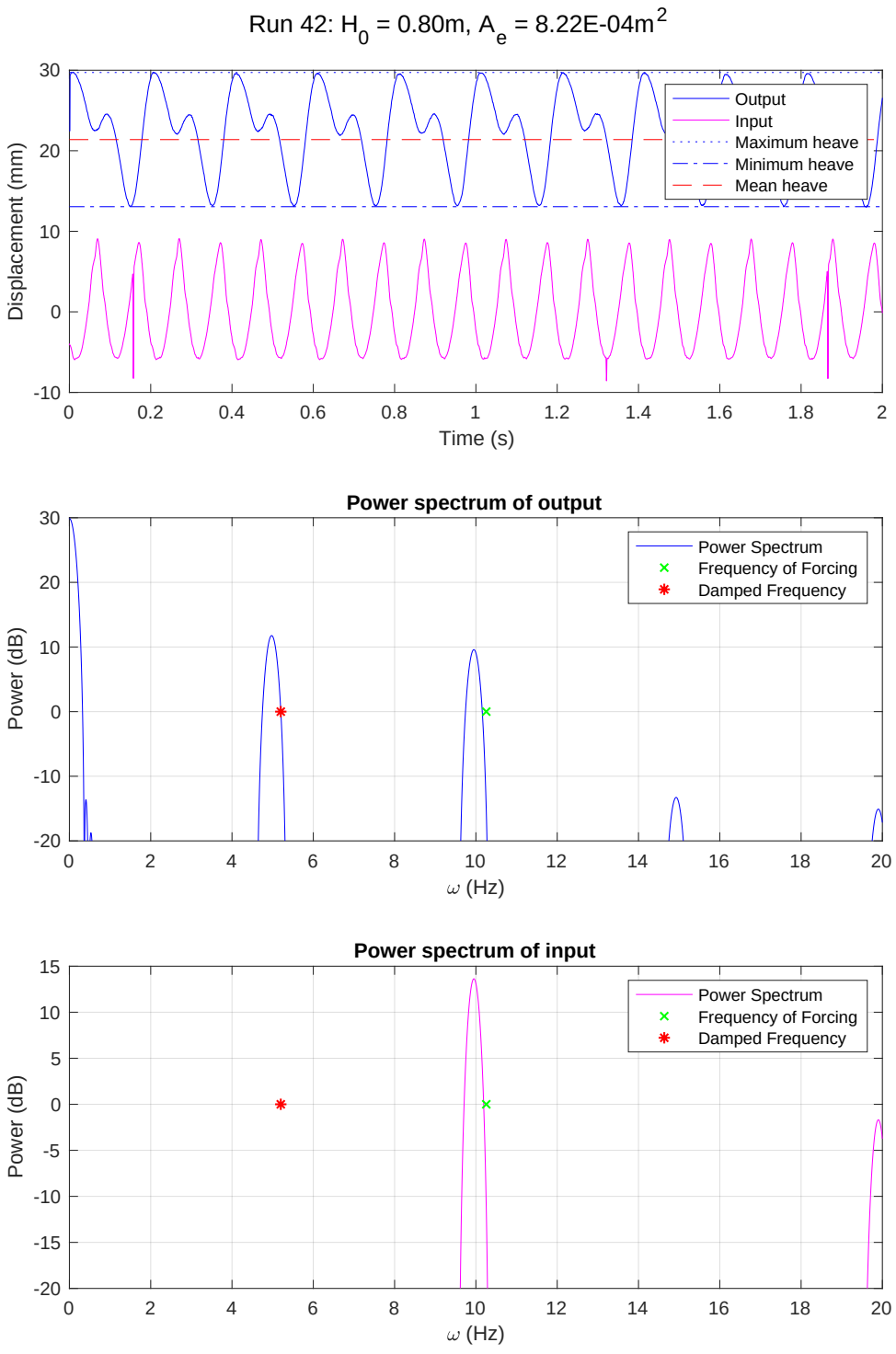


Figure H.158. Experimental trial data for Condition 42

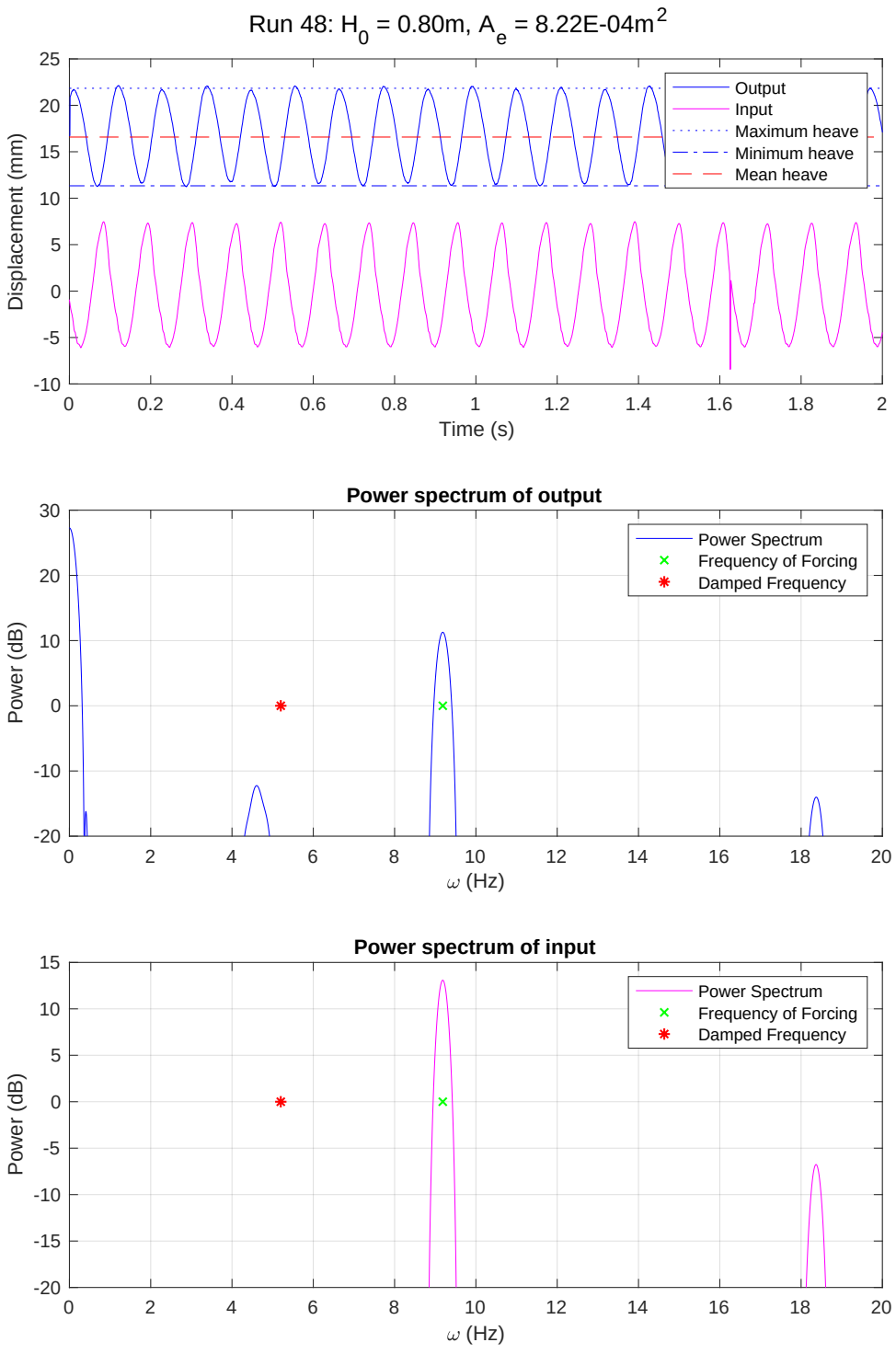


Figure H.159. Experimental trial data for Condition 48

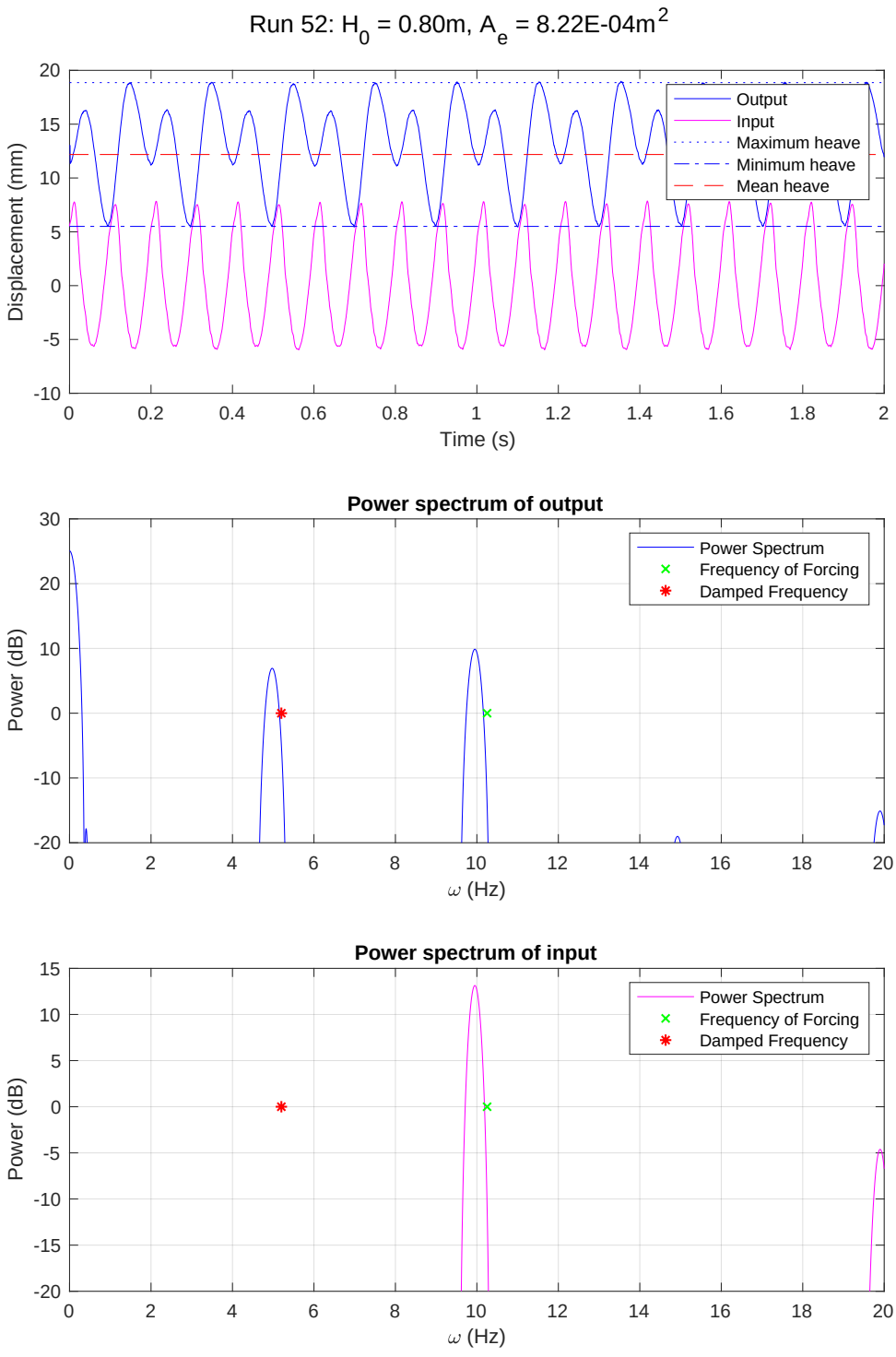


Figure H.160. Experimental trial data for Condition 52

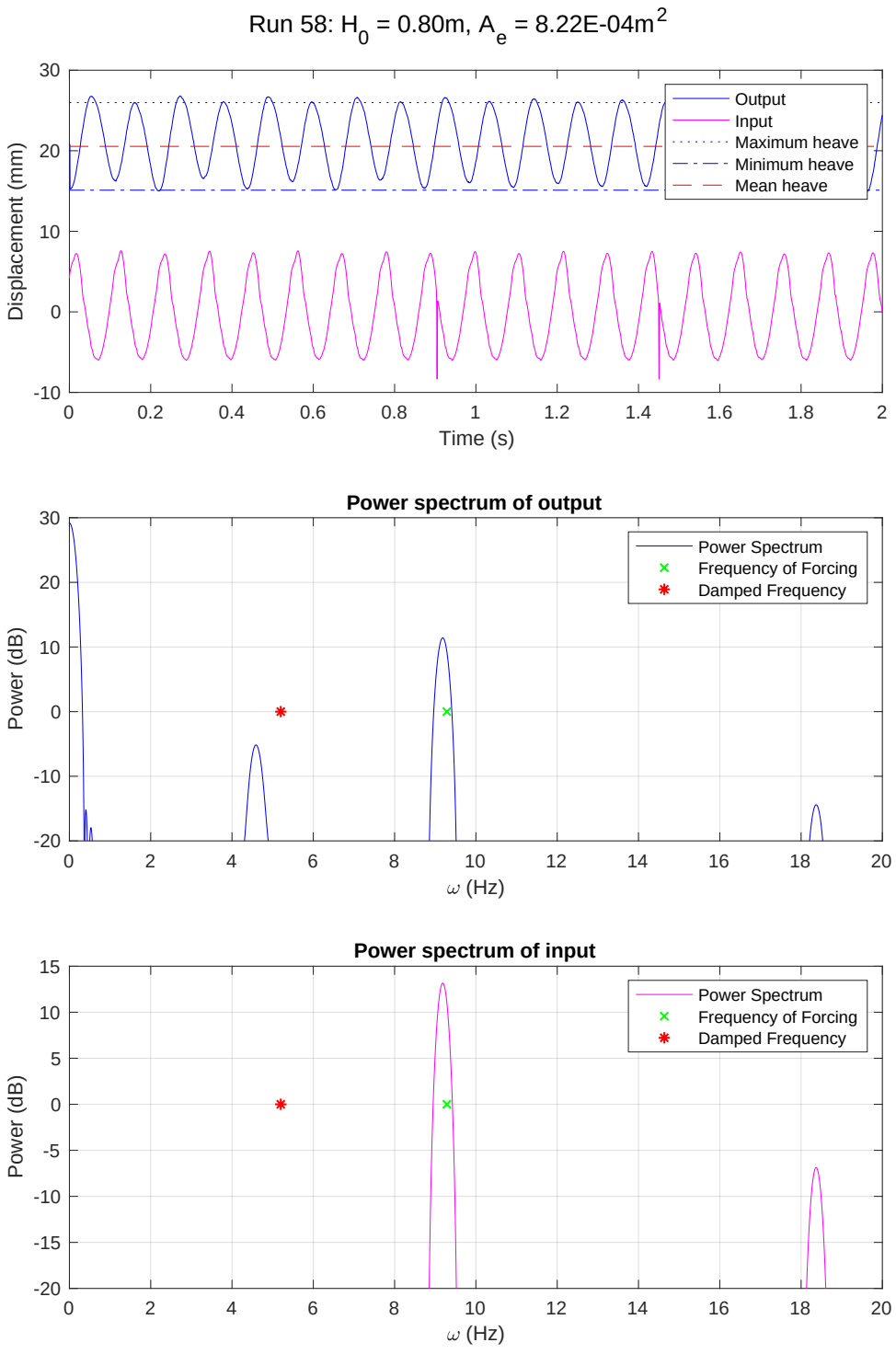


Figure H.161. Experimental trial data for Condition 58

H.2.9. Condition Nine

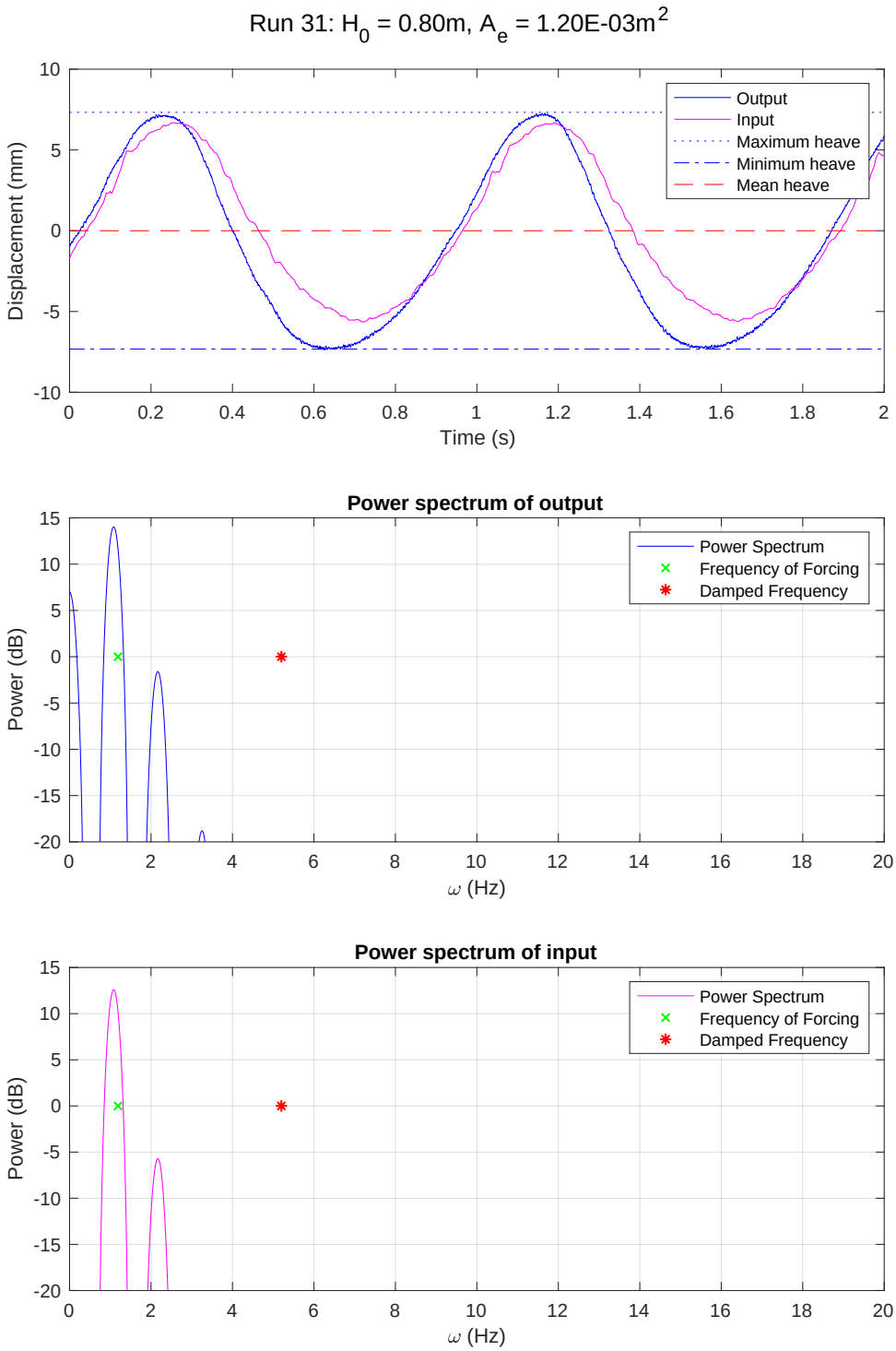


Figure H.162. Experimental trial data for Condition 31

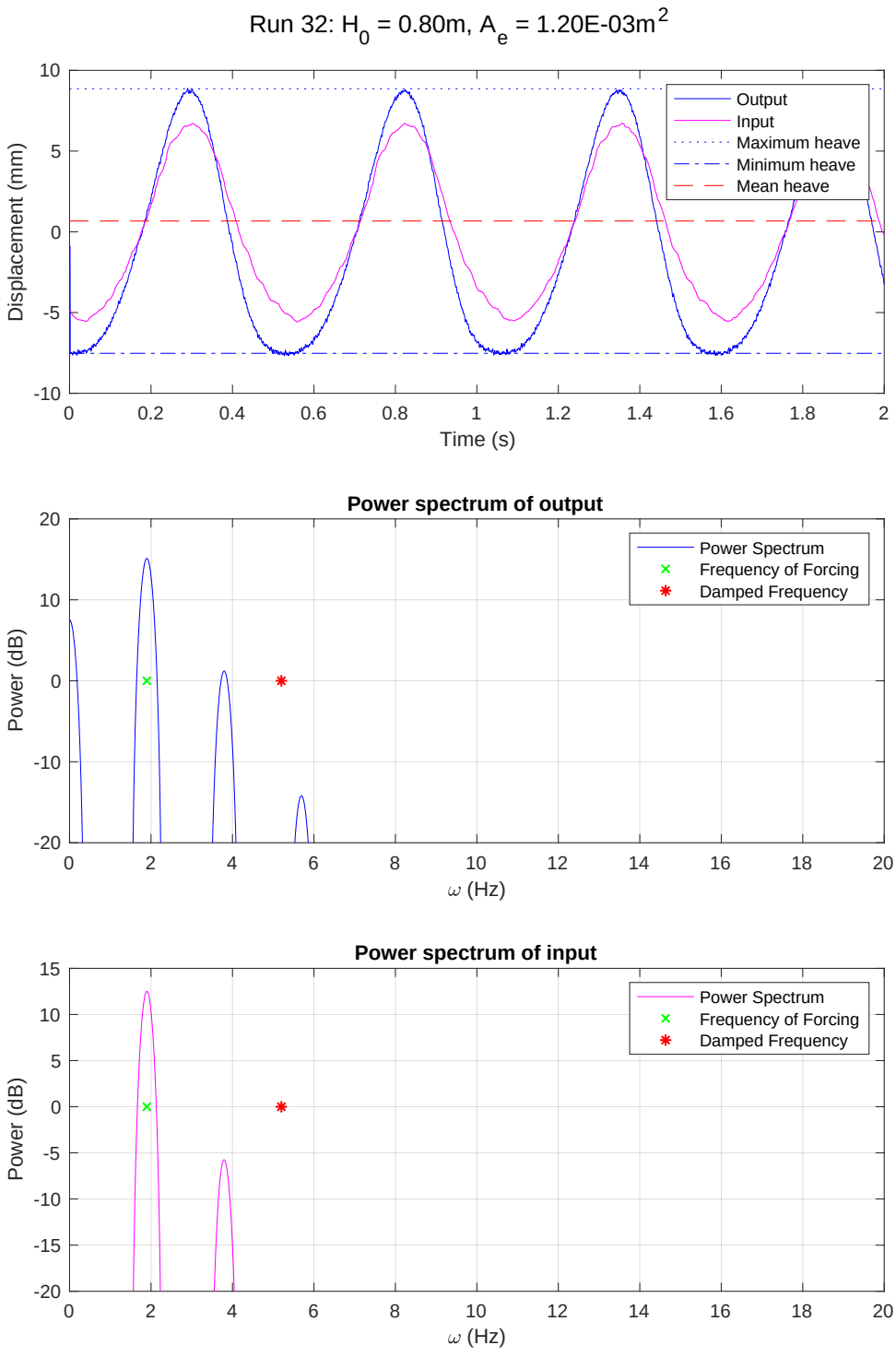


Figure H.163. Experimental trial data for Condition 32

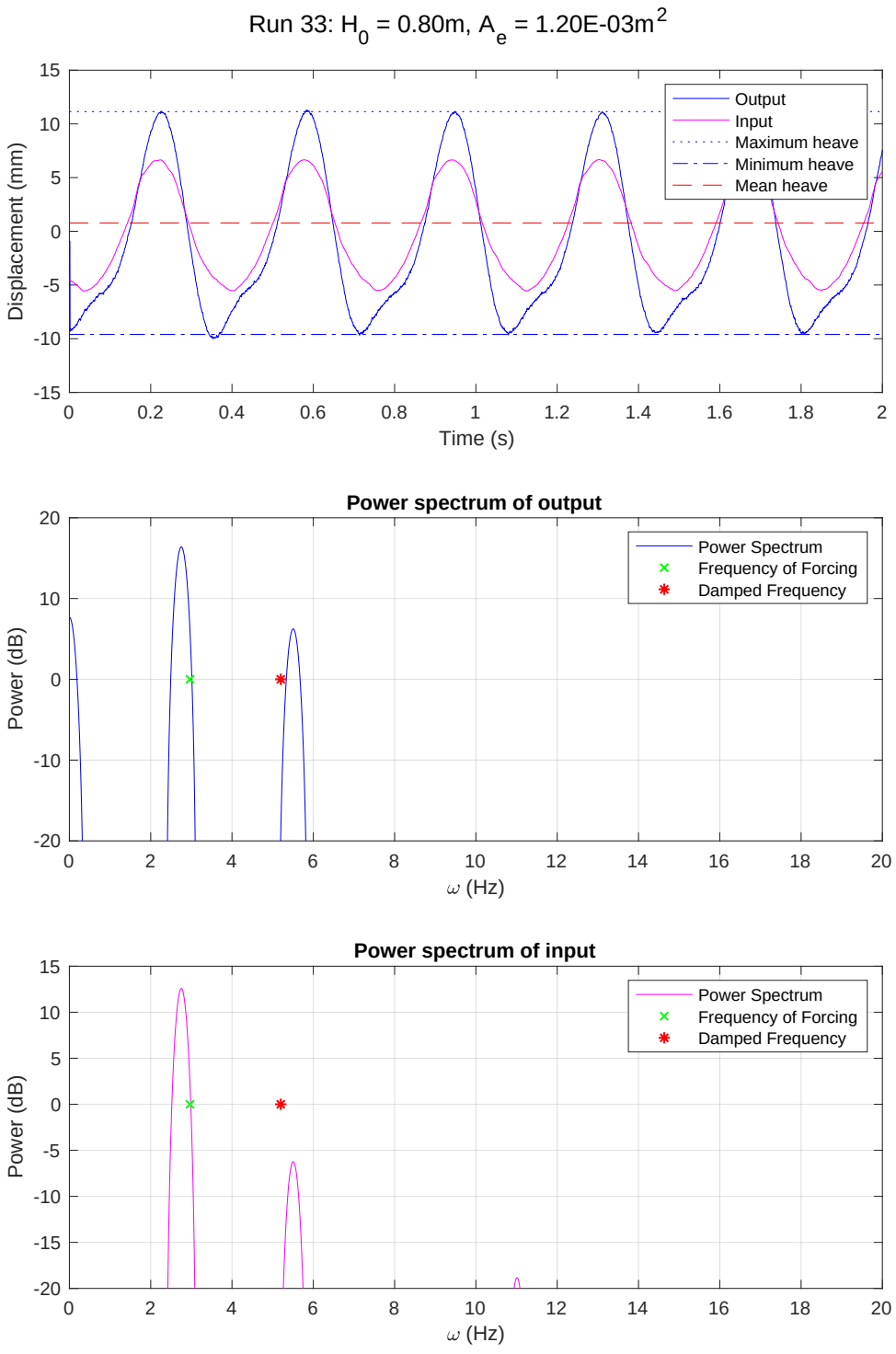


Figure H.164. Experimental trial data for Condition 33

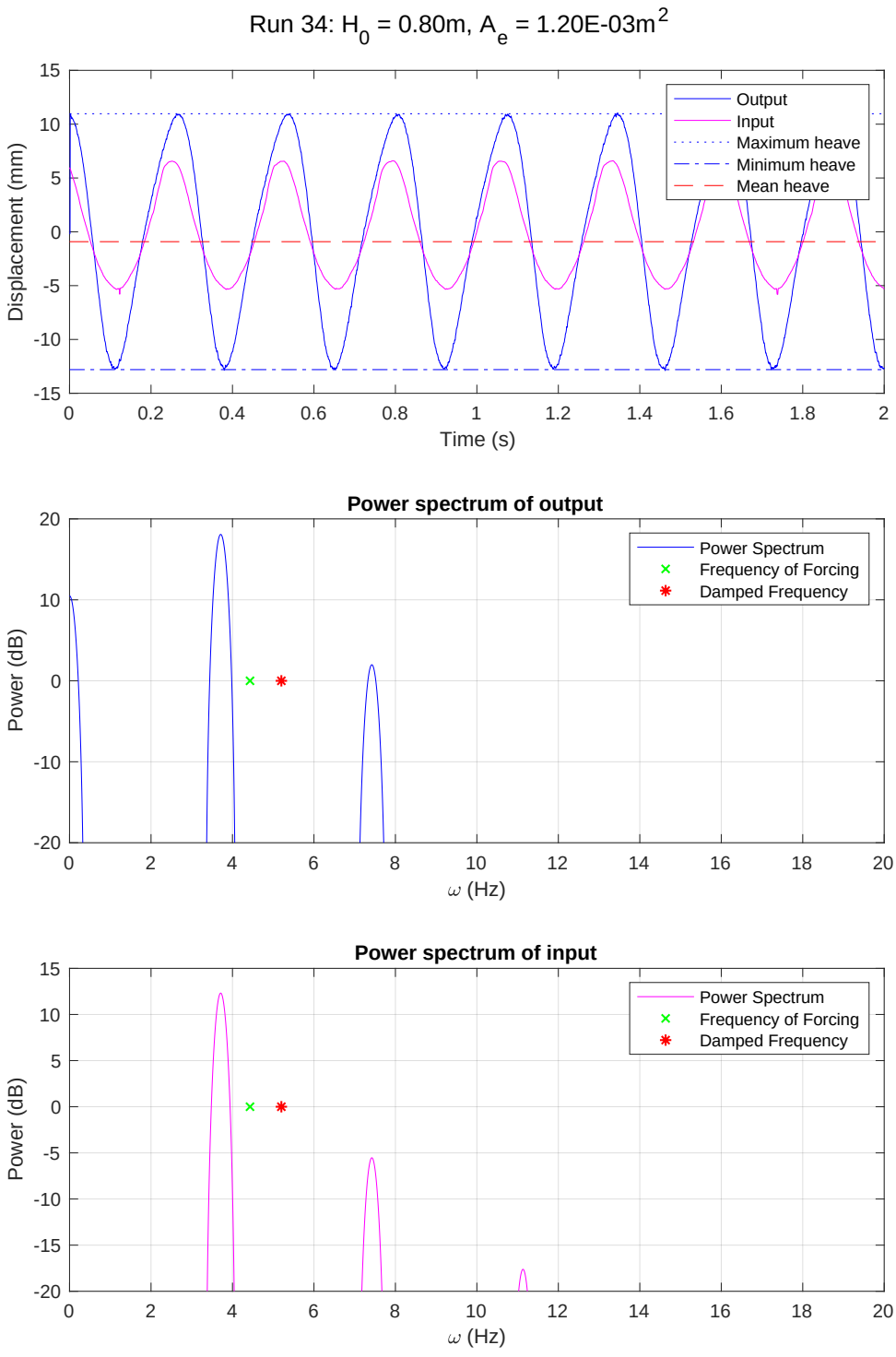


Figure H.165. Experimental trial data for Condition 34

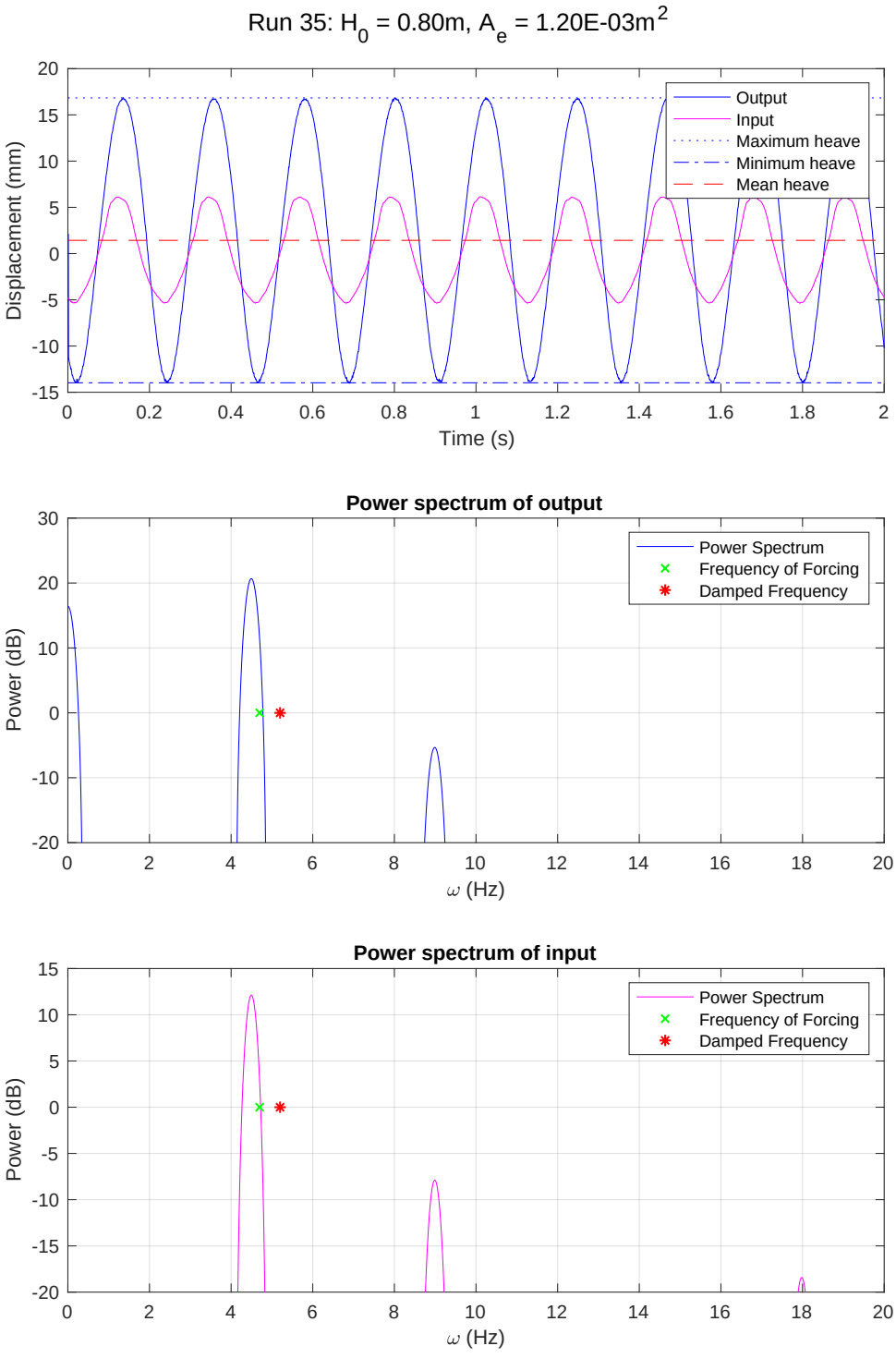


Figure H.166. Experimental trial data for Condition 35

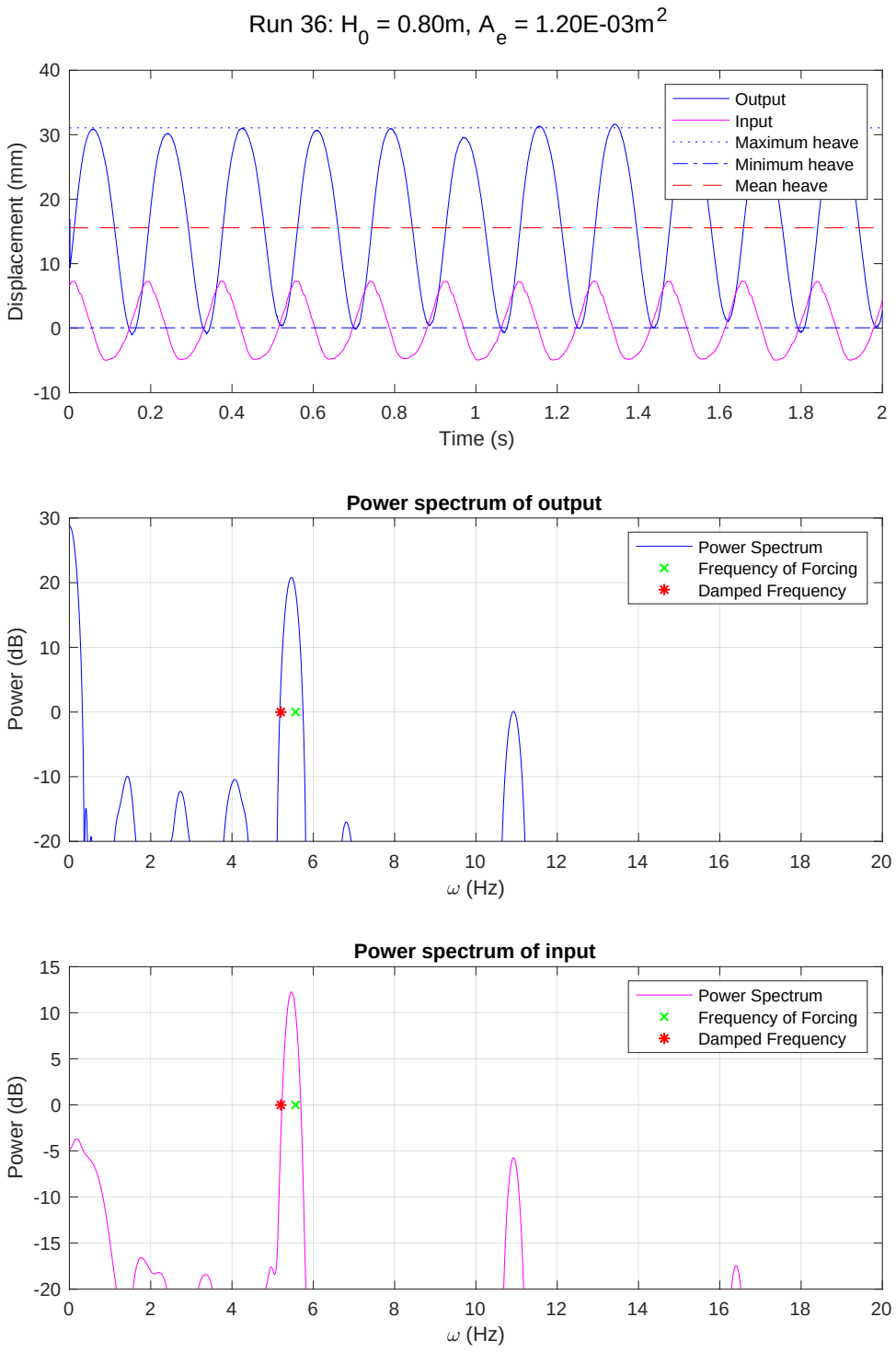


Figure H.167. Experimental trial data for Condition 36

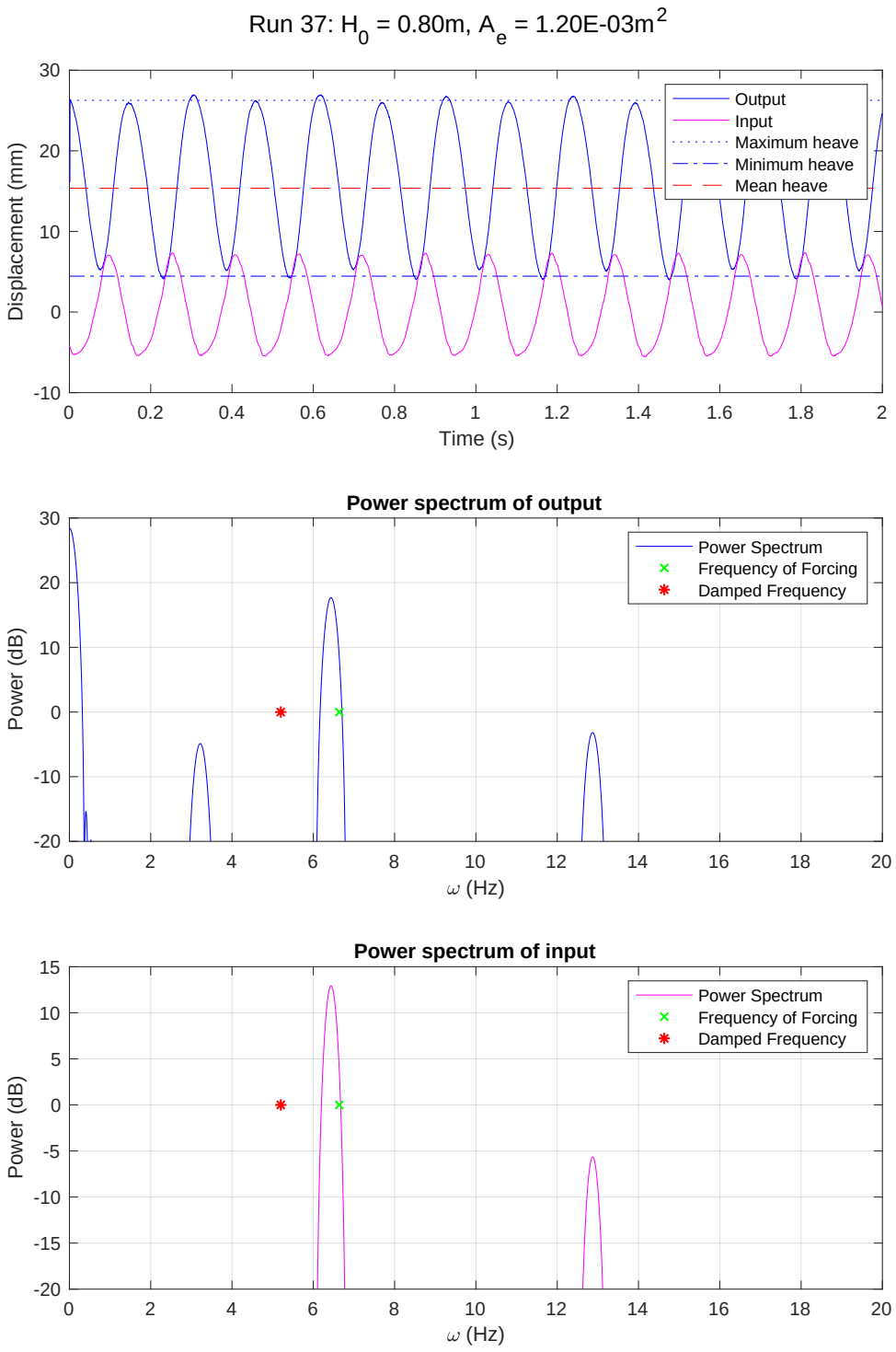


Figure H.168. Experimental trial data for Condition 37

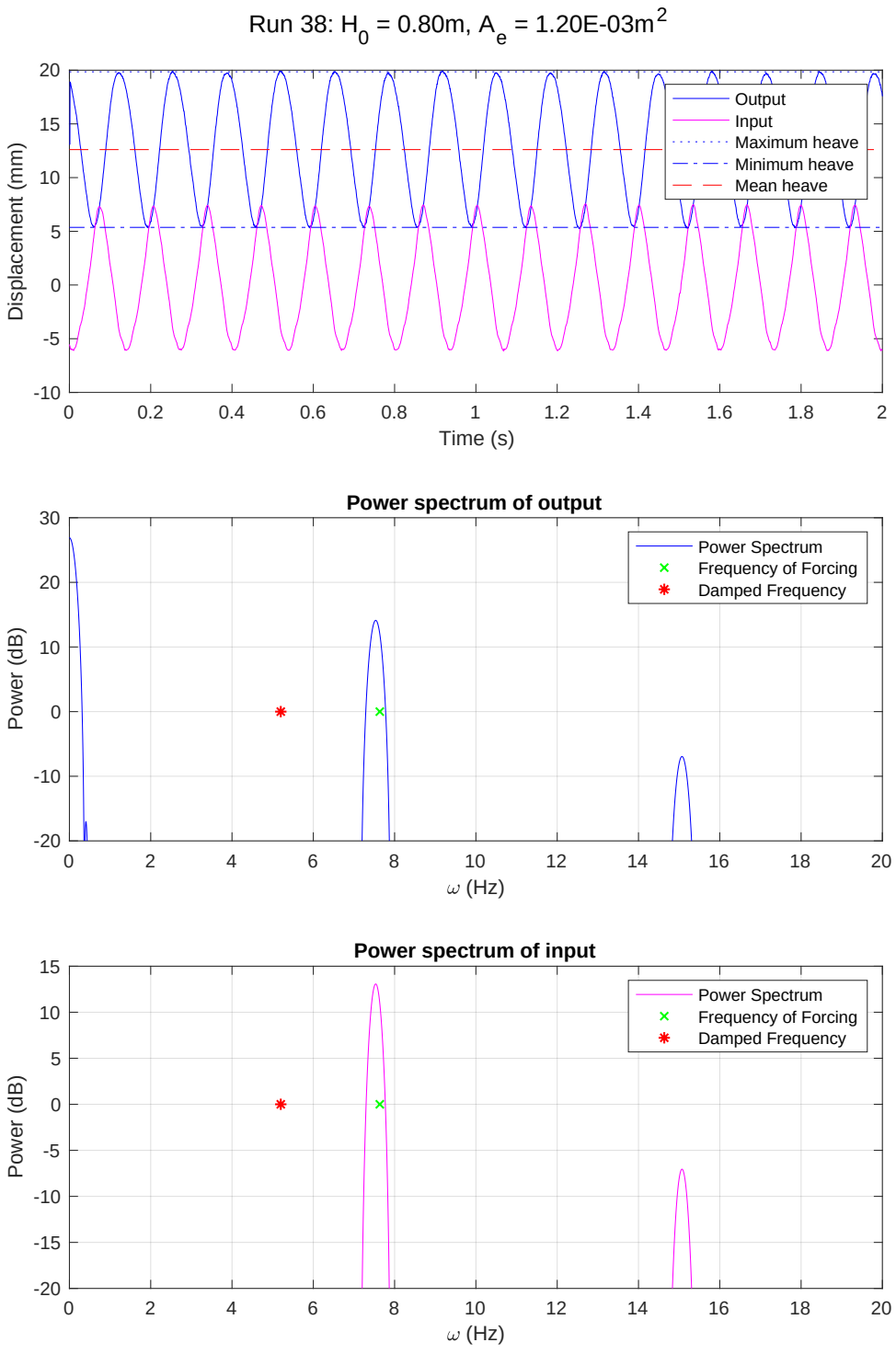


Figure H.169. Experimental trial data for Condition 38

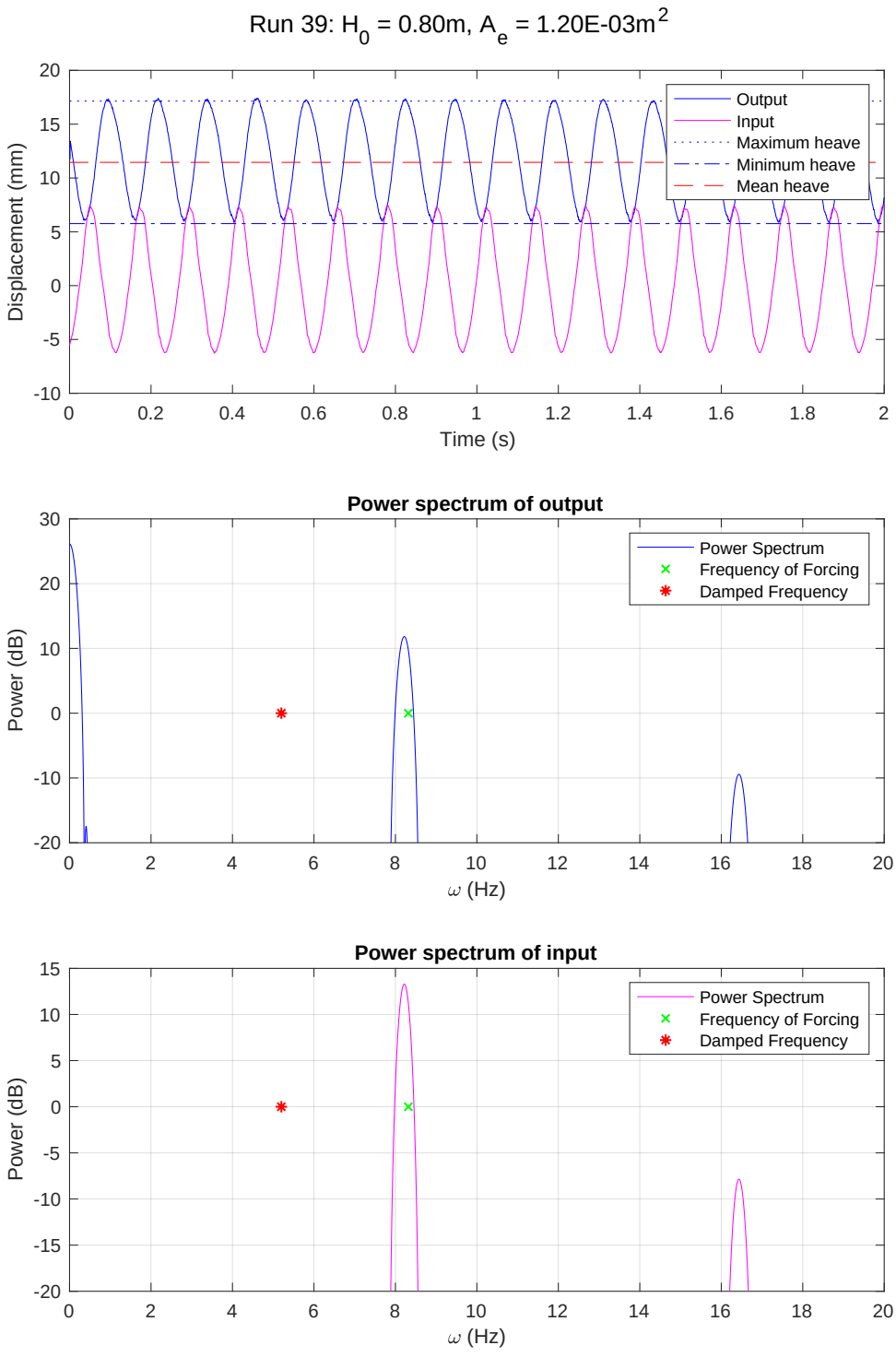


Figure H.170. Experimental trial data for Condition 39

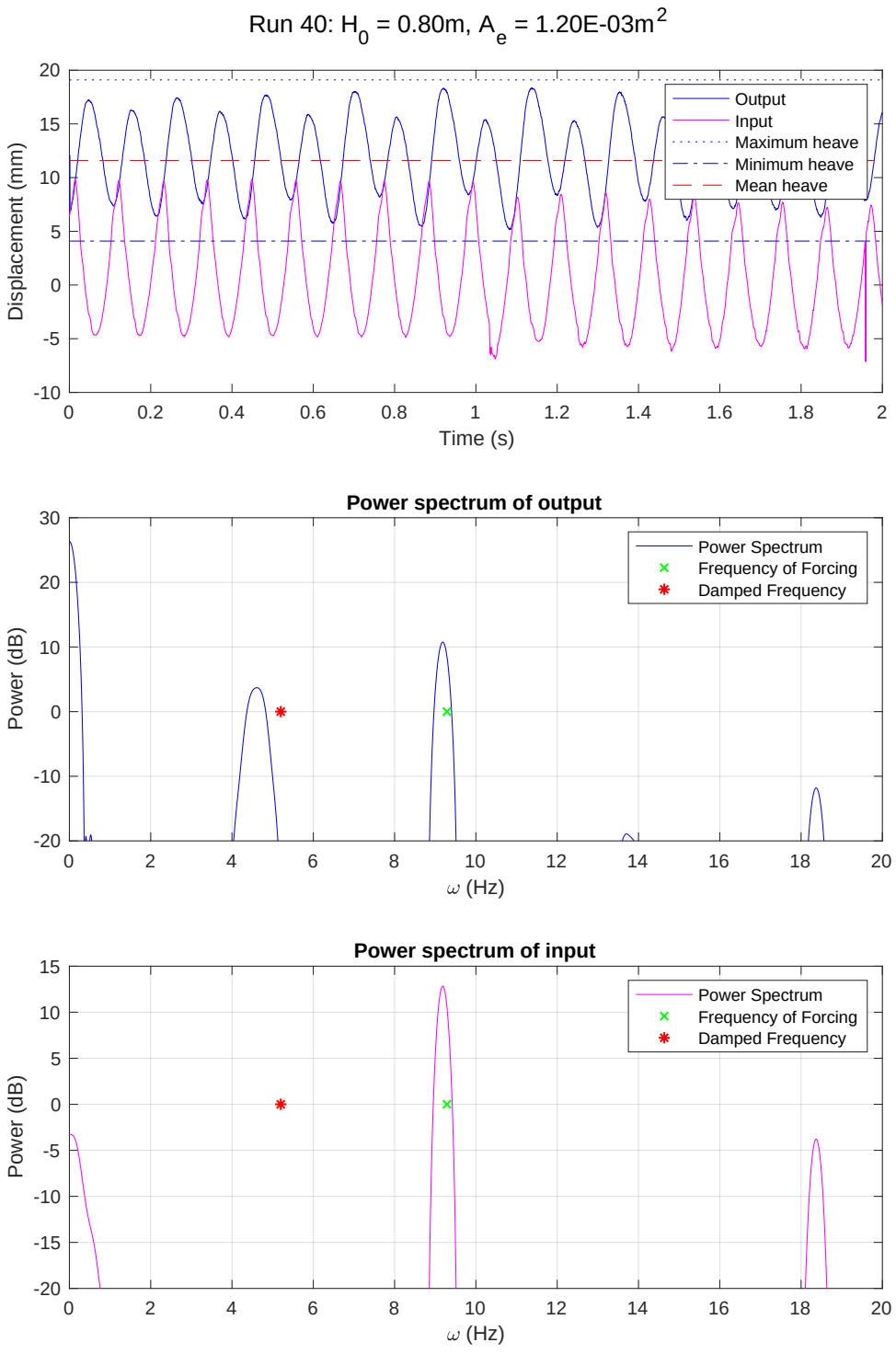


Figure H.171. Experimental trial data for Condition 40

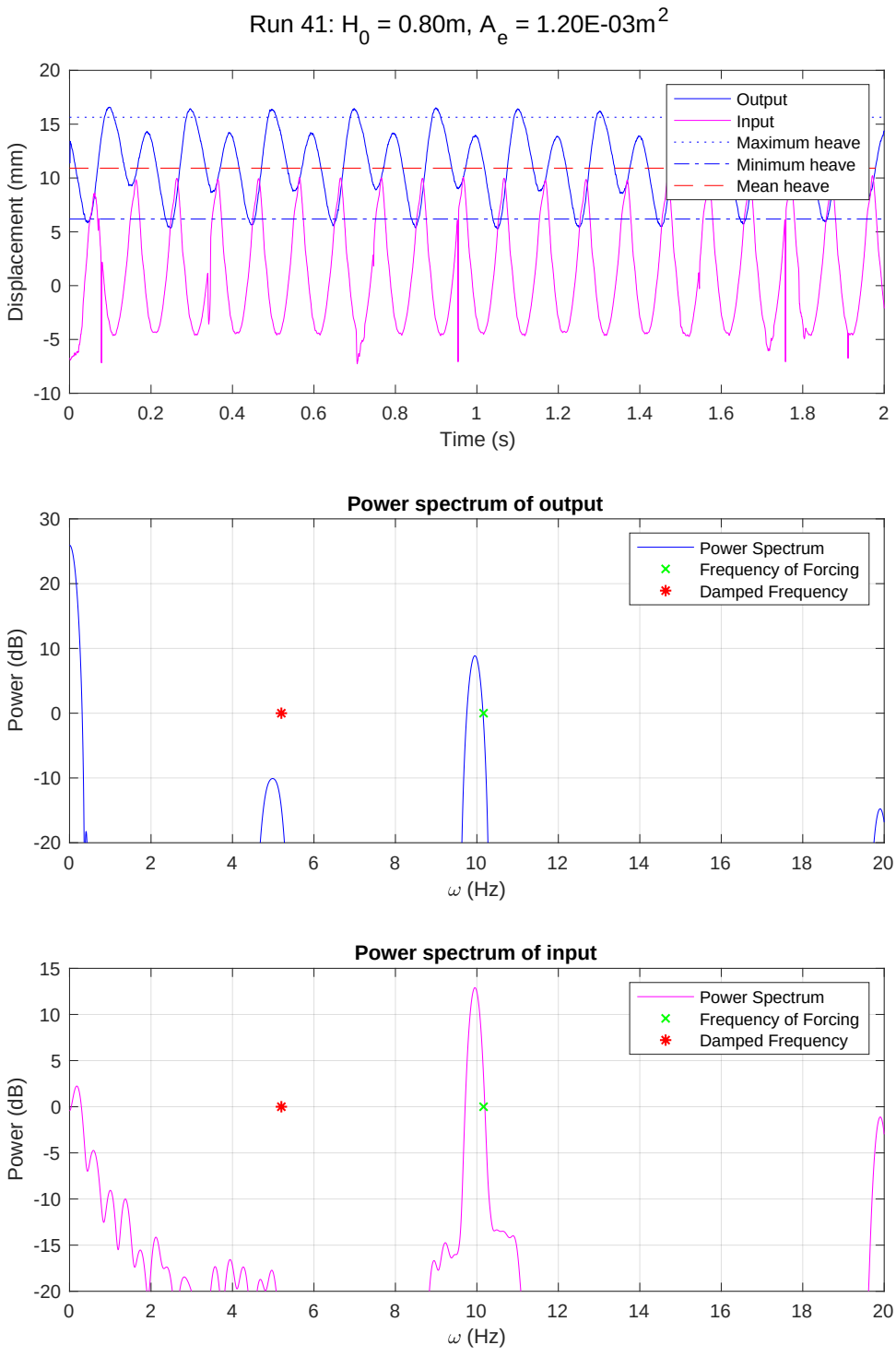


Figure H.172. Experimental trial data for Condition 41

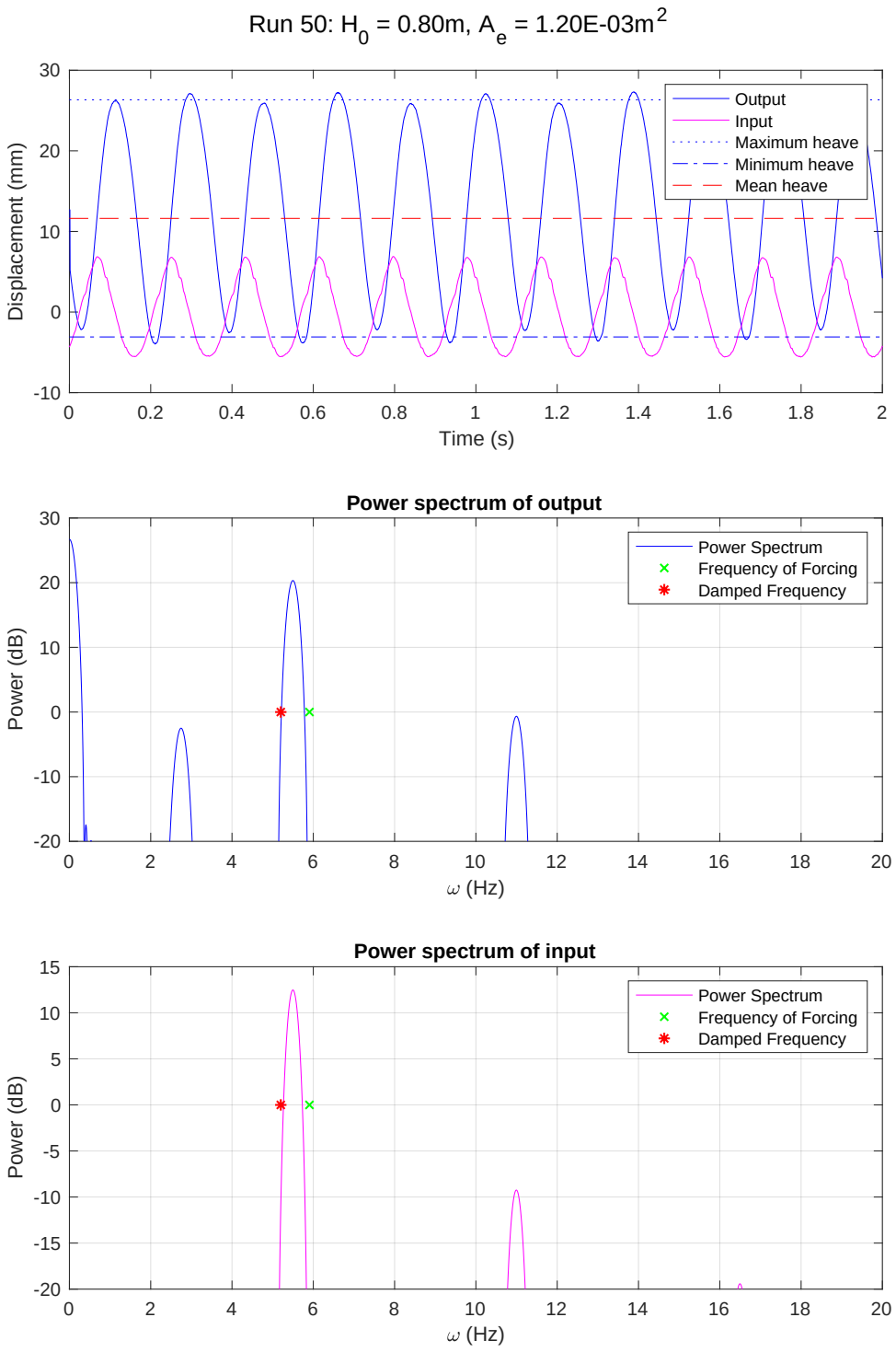


Figure H.173. Experimental trial data for Condition 50

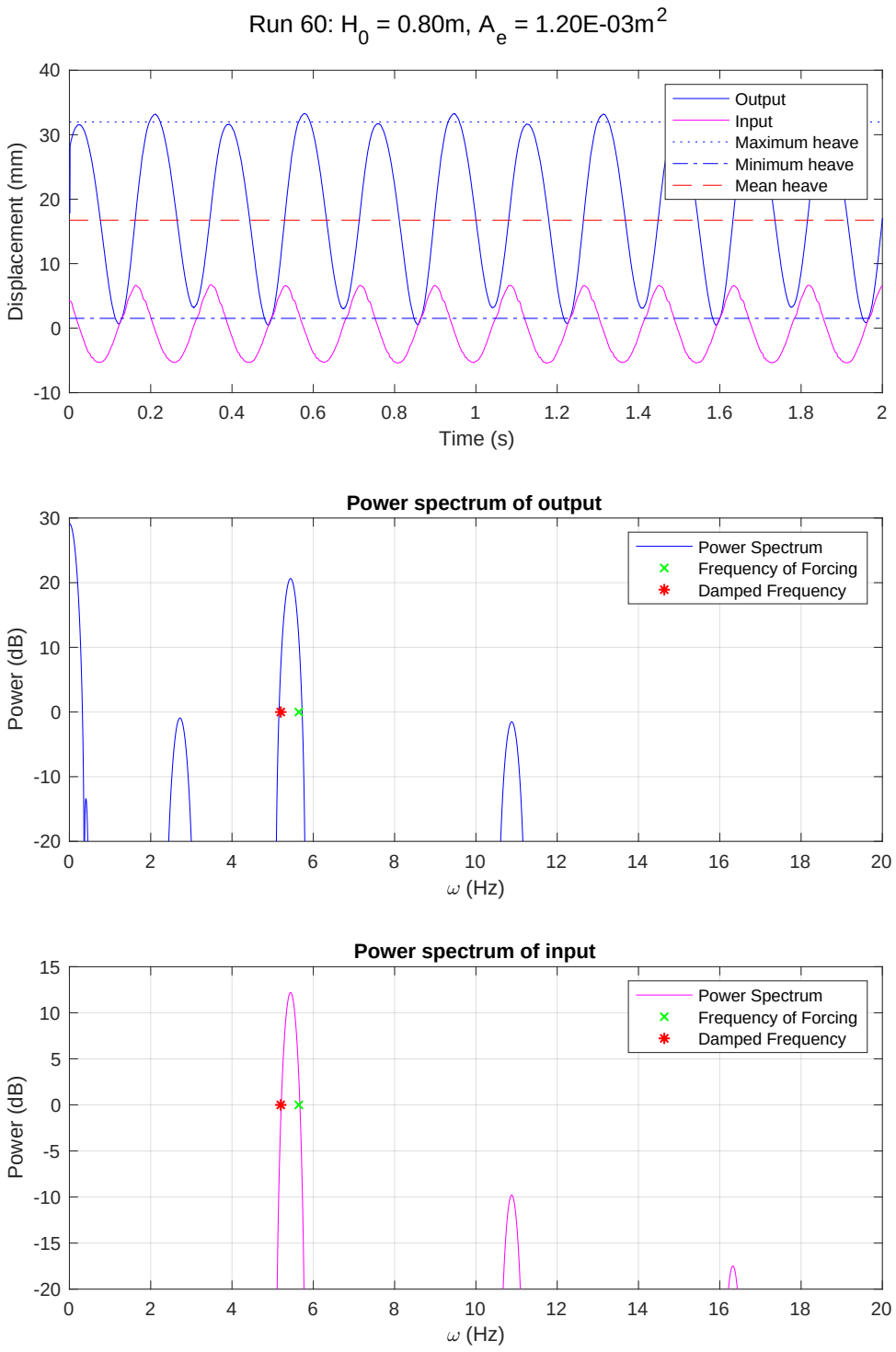


Figure H.174. Experimental trial data for Condition 60